RTU RĒZEKNE

RTU RĒZEKNES AKADĒMIJA
Inženierzinātņu centrs

REZEKNE ACADEMY OF RIGA TECHNICAL UNIVERSITY
Engineering Centre

VIDE.TEHNOLOĢIJA. RESURSI

XVI starptautiskās zinātniski praktiskās konferences rakstu krājums
2025. gada 19.–20. jūnijs

4. SĒJUMS

ENVIRONMENT. TECHNOLOGY. RESOURCES

Proceedings of the 16th International Scientific and Practical Conference
June 19th – 20th, 2025

VOLUME IV

Rēzekne 2025

RTU RĒZEKNES AKADĒMIJA
Inženierzinātņu centrs

REZEKNE ACADEMY
OF RIGA TECHNICAL UNIVERSITY
Engineering Centre

VIDE. TEHNOLOĢIJA. RESURSI

XVI starptautiskās zinātniski praktiskās konferences materiāli
2025.gada 19.-20.jūnijs

4. SĒJUMS

ENVIRONMENT. TECHNOLOGY. RESOURCES

Proceedings of the 16th International Scientific and Practical Conference
June 19th – 20th, 2025

Volume IV

Rezekne
2025

VIDE. TEHNOLOĢIJA. RESURSI. 16. starptautiskās zinātniski praktiskās konferences materiāli. 2025.gada 19.-20. jūnijs. *4.sējums*: RTU Rēzeknes akadēmija, Rēzekne, Latvija, 2025. 510 lpp.

ENVIRONMENT. TECHNOLOGY. RESOURCES. Proceedings of the 16th International Scientific and Practical Conference on June 19-20, 2025. *Volume IV*: Rezekne Academy of Riga Technical University, Rezekne, Latvia, 2025. pp. 510.

16.starptautiskās zinātniski praktiskās konferences "Vide. Tehnoloģija. Resursi" materiālos četros sējumos ir pārstāvēti jaunākie pētījumi vides inženierzinātnē, vides un dabas aizsardzībā, ilgtspējīgā lauksaimniecībā, enerģētikā, materiālzinātnē, mehānikā, metālapstrādē, lāzeru tehnoloģijās, matemātiskajā modelēšanā, elektrotehnikā, vides ekonomikā un vadībā, informācijas tehnoloģijās un sociotehnisko sistēmu modelēšanā, vides izglītībā un ilgtspējīgas attīstības procesos, izglītība inženierzinātnēs, aizsardzības un drošības tehnoloģijās. Krājumā pārstāvēto pētījumu joma ir daudzpusīga un starpdisciplināra, balstīta uz starptautisko zinātnieku kolektīvu sasniegumu rezultātiem. Konferences materiālos iekļauti 317 zinātniskie raksti. Konferences dalībnieki pārstāv 28 valstis.

16.starptautiskās zinātniski praktiskās konferences "Vide. Tehnoloģija. Resursi" norises vieta ir RTU Rēzeknes akadēmija, Rēzekne, Latvija.

Proceedings of the 16th International Scientific and Practical Conference "Environment. Technology. Resources" include recent research in fields of engineering, environmental and nature protection, sustainable agriculture, energy, material science, mechanics, metalworking, laser technologies, mathematical modelling, electrical engineering, environmental economics and management, information technologies and sociotechnical systems modelling, environmental education and sustainable development, education in engineering sciences, defense and security technologies. The research area presented in the proceedings is comprehensive and cross-disciplinary, on the advances of international researchers. The proceedings comprise 317 scientific papers. Conference participants represent 28 countries.

16th International Scientific and Practical Conference "Environment. Technology. Resources." hosted by Rezekne Academy of Riga Technical University, Rezekne, Latvia

https://conferences.rta.lv/index.php/ETR/ETR2025
Link to conference proceedings: http://journals.rta.lv/index.php/ETR

This journal is licensed under
Creative Commons Attribution 4.0 International (CC BY 4.0) License
The author(s) of the paper take responsibility for the content of the paper

Online **ISSN 2256-070X**

Published by **RTU PRESS, 2025**

Scientific Committee Chairman

Dr.sc.ing. Edmunds Teirumnieks, Rezekne Academy of Riga Technical University, Latvia

Scientific Committee Co-Chairmen

Dr. Walter Leal, Hamburg University of Applied Sciences, Germany, Manchester Metropolitan University, United Kingdom
Dr.sc.ing. Andris Martinovs, Rezekne Academy of Riga Technical University, Latvia
Dr.sc.ing. Artis Teilāns, Rezekne Academy of Riga Technical University, Latvia

Scientific Committee

Dr.agr. Aleksandrs Adamovičs, Latvia University of Life Sciences and Technologies, Latvia
PhD Nikolaj Angelov, Technical University of Gabrovo, Bulgaria
PhD Kiril Anguelov, Technical University of Sofia, Bulgaria
PhD Andres Annuk, Estonian University of Life Sciences, Estonia
Dr. agr. Lidiia Antypova, Mykolaiv National Agrarian University, Ukraine
PhD Iluta Arbidane, Rezekne Academy of Riga Technical University, Latvia
PhD Plamen Atanasov, New Bulgarian University, Bulgaria
PhD Todor Balabanov, University of Transport "Todor Kableshkov", Bulgaria
PhD Stefan Bankov, The Ministry of Interior of Bulgaria, Bulgaria
PhD Jānis Bičevskis, University of Latvia, Latvia
PhD Aija Brakovska, Daugavpils University, Latvia
PhD Ģirts Būmanis, Riga Technical University, Latvia
PhD Ivan Byanov, University of Veliko Tarnovo "St. Cyril and St. Methodius", Bulgaria
PhD Hamid Can, Trakya University, Turkey
Dr. hab. Ing. Tadeusz Chrzan, Poltegor Institute, Poland
PhD Dimitar Dimitrov, Todor Kableshkov University of Transport, Bulgaria
PhD Sevdalina Dimitrova, “Vasil Levski” National Military University, Bulgaria
PhD Nadezhda Dimova, New Bulgarian University Department "Economics", Bulgaria
PhD Nikolay Dolchinkov, "Vasil Levski" National Military University, Bulgaria
Dr.hist. Edvins Evarts, Turiba University, Latvia
PhD Vanko Ganev, "Vasil Levski" National Military University, Bulgaria
Dr.sc.ing. Imants Gorbāns, Riga Technical University, Latvia
Dr.sc.ing. Aleksandrs Gorbunovs, Riga Technical University, Latvia
Dr.sc.ing. Pēteris Grabusts, Rezekne Academy of Riga Technical University, Latvia
PhD Grigor Grigorov, “Vasil Levski” National Military University, Bulgaria
PhD Inga Grinfelde, Latvia University of Life Sciences and Technologies, Latvia
PhD Tzvetelin Gueorguiev, Technical University of Gabrovo, Bulgaria
PhD Mart Hovi, Estonian University of Life Sciences, Estonia
PhD Maria Ilcheva, Saint Cyril and Methodius University of Veliko Tarnovo, Bulgaria
Dr. agr. Sofija Jankauskiene, Lithuanian Research Centre for Agriculture and Forestry, Lithuania
PhD Aivars Jermuss, Latvia University of Life Sciences and Technologies, Latvia
Dr.sc.ing. Aivars Kaķītis, Latvia University of Life Sciences and Technologies, Latvia
PhD Sabrina Kalinkova, University of National and World Economy, Bulgaria
Dr.paed. Ilmārs Kangro, Rezekne Academy of Riga Technical University, Latvia
PhD Atis Kapenieks, Riga Technical University, Latvia
Dr. paed. Janis Kapenieks, Riga Technical University, Latvia
PhD Tsanko Karadzhov, Technical University of Gabrovo, Bulgaria
PhD Aivars Kaupuzs, Rezekne Academy of Riga Technical University, Latvia
PhD Stancho Kajkov, “Vasil Levski” National Military University, Bulgaria
PhD Anna Khilya, Vinnytsia Mykhailo Kotsiubynskyi State Pedagogical University, Spain
PhD Georgi Komitov, Agricultural University Plovdiv, Bulgaria
PhD Inga Ļašenko, Riga Technical University, Latvia
Dr.sc.ing. Lyubomir Lazov, Rezekne Academy of Riga Technical University, Latvia
PhD Iveta Linina, Turiba University, Latvia

PhD Lyuboslav Lyubenov, University of Ruse "Angel Kanchev", Bulgaria
Dr.sc.math. Maksims Marinaki, University of Latvia, Latvia
PhD Rumen Marinov, “Vasil Levski” National Military University, Bulgaria
PhD Dilyan Markov, Georgi Rakovski Military Academy, Bulgaria
Dr.sc.ing. Linda Mežule, Riga Technical University, Latvia
PhD Ziedonis Miklašēvičs, Rezekne Academy of Riga Technical University, Latvia
PhD Nikolai Minkovski, University of Forestry, Bulgaria
PhD Penko Mitev, Technical University of Sofia, Bulgaria
Dr.sc.ing. Ivan Mitev, Technical University of Gabrovo, Bulgaria
PhD Marufjon Musaev, Tashkent State Technical University, Uzbekistan
PhD Nikolay Padarev, "Vasil Levski" National Military University, Bulgaria
Dr.sc.ing. Desislava Petrova, Technical University of Gabrovo, Bulgaria
Dr.agr. Liena Poiša, Rezekne Academy of Riga Technical University, Latvia
Dr. agr. Valentīna Pole, IK Tava zeme, Latvia
PhD Dimcho Pulov, Technical University of Gabrovo, Bulgaria
PhD Aurelija Pūraitė, Mykolas Romeris University, Lithuania
Dr. agr. Gundega Putniece, Latvia University of Life Sciences and Technologies, Latvia
PhD Todor Rachovski, Plovdiv University “Paisii Hilendarski”, Bulgaria
Dr.sc.ing. Ādolfs Ruciņš, Latvia University of Life Sciences and Technologies, Latvia
PhD Rashmi Jaymin-Sanchaniya, Riga Technical University, Latvia
PhD Iryna Sarancha, Vinnytsia Mykhailo Kotsiubynskyi State Pedagogical University, Ukraine
PhD Dafinka Sidova, New Bulgaria University, Bulgaria
PhD Inese Skapste, Latvia University of Life Sciences and Technologies, Latvia
Dr.sc.ing. Andris Skromulis, Rezekne Academy of Riga Technical University, Latvia
PhD Krasimir Slavyanov, "Vasil Levski" National Military University, Bulgaria
PhD Nikolay Stefanov, “Vasil Levski” National Military University, Bulgaria
PhD Julija Steinhart, BA School of Banking and Finance, Switzerland
PhD Agrita Švarta, Latvia University of Life Sciences and Technologies, Latvia
PhD Adiljan Suleymanov, Tashkent State Technical University, Uzbekistan
Dr.sc.ing. Artis Teilāns, Rezekne Academy of Riga Technical University, Latvia
Dr.-Ing. Josef Timmerberg, Jade University of Applied Sciences, Germany
Dr.sc.ing. Edmunds Teirumnieks, Rezekne Academy of Riga Technical University, Latvia
PhD Ērika Teirumnieka, Rezekne Academy of Riga Technical University, Latvia
Dr.biol. Rasma Tretjakova, Rezekne Academy of Riga Technical University, Latvia
PhD Dragomir Vassilev, Technical University of Gabrovo, Bulgaria
PhD Valentin Vassilev, South-West University "Neofit Rilski", Bulgaria
PhD Tsanka Zlateva-Petkova, Technical University of Gabrovo, Bulgaria
PhD Anda Zvaigzne, Rezekne Academy of Riga Technical University, Latvia
PhD Rosita Zvirgzdina, Turiba University, Latvia

Organising Committee Chairman

PhD Nikolay Dolchinkov, "Vasil Levski" National Military University, Bulgaria

Organising Committee

Dr.agr. Aleksandrs Adamovičs, Latvia University of Life Sciences and Technologies, Latvia
Dr. agr. Lidiia Antypova, Mykolaiv National Agrarian University, Ukraine
MA Yanitsa Boyanova, “Vasil Levski” National Military University, Bulgaria
Dr.sc.ing. Aleksandrs Gorbunovs, Riga Technical University, Latvia
Dr.sc.ing. Pēteris Grabusts, Rezekne Academy of Riga Technical University, Latvia
Dr.sc.ing. Ēriks Kronbergs, Latvia University of Life Sciences and Technologies, Latvia
Dr.sc.ing. Sergejs Kodors, Rezekne Academy of Riga Technical University, Latvia
Dr. paed. Janis Kapenieks, Riga Technical University, Latvia
PhD Tsanko Karadzhov, Technical University of Gabrovo, Bulgaria
Dr.sc.ing. Lyubomir Lazov, Rezekne Academy of Riga Technical University, Latvia
Dr.sc.ing. Andris Martinovs, Rezekne Academy of Riga Technical University, Latvia

PhD Rumen Marinov, “Vasil Levski” National Military University, Bulgaria
Dr.agr. Liena Poiša, Rezekne Academy of Riga Technical University, Latvia
Dr.sc.ing. Andris Skromulis, Rezekne Academy of Riga Technical University, Latvia
Dr.-Ing. Josef Timmerberg, Jade University of Applied Sciences, Germany
Dr.sc.ing. Artis Teilāns, Rezekne Academy of Riga Technical University, Latvia
Mg.sc.comp. Gundega Teilāne, Rezekne Academy of Riga Technical University, Latvia
PhD Ērika Teirumnieka, Rezekne Academy of Riga Technical University, Latvia

Reviewers

PhD Nikolaj Angelov, Technical University of Gabrovo, Bulgaria
PhD Andres Annuk, Estonian University of Life Sciences, Estonia
PhD Neli Arabadzhieva - Kalcheva, Technical University of Varna, Bulgaria
PhD Iluta Arbidane, Rezekne Academy of Riga Technical University, Latvia
PhD Svetlana Asmuss, University of Latvia, Latvia
PhD Plamen Atanasov, New Bulgarian University, Bulgaria
Dr.sc.ing. Anita Avišāne, Riga Technical University, Latvia
PhD Todor Balabanov, University of Transport "Todor Kableshkov", Bulgaria
PhD Yanka Baneva, Medical University Varna, Bulgaria
Dr.agr. Biruta Bankina, Latvia University of Life Sciences and Technologies, Latvia
PhD Stefan Bankov, The Ministry of Interior of Bulgaria, Bulgaria
PhD Sholpan Bekmukhanbetova, Kazakh Automobile and Road Institute, Kazakhstan
PhD Daniel Berchev, “Vasil Levski” National Military University, Bulgaria
PhD Ansis Ataols Bērziņš, Riga Technical University, Latvia
PhD Jānis Bičevskis, University of Latvia, Latvia
PhD Aija Brakovska, Daugavpils University, Latvia
Dr. Rene Brunsch, Apromace data systems GmbH, Germany
PhD Ģirts Būmanis, Riga Technical University, Latvia
PhD Ivan Byanov, University of Veliko Tarnovo "St. Cyril and St. Methodius", Bulgaria
PhD Basar Caglar, Izmir Institute of Technology, Turkey
Dr.hab.Ing. Tadeusz Chrzan, Poltegor Institute, Poland
PhD Maria Chunchukova, Agricultural University Plovdiv, Bulgaria
PhD Dimitar Dimitrov, "Georgi Benkovski", Bulgarian Air Force Academy, Bulgaria
PhD Dimitar Dimitrov, Todor Kableshkov University of Transport, Bulgaria
PhD Sevdalina Dimitrova, “Vasil Levski” National Military University, Bulgaria
PhD Nadezhda Dimova, New Bulgarian University Department "Economics", Bulgaria
PhD Nikolay Dolchinkov, "Vasil Levski" National Military University, Bulgaria
Dr.hist. Edvins Evarts, Turiba University, Latvia
Dr. agr. Daina Feldmane, Institute of Horticulture, Latvia
PhD Vanko Ganev, "Vasil Levski" National Military University, Bulgaria
PhD Dmitri Goljandin, Tallinn University of Technology, Estonia
Dr.sc.ing. Imants Gorbāns, Riga Technical University, Latvia
PhD Jānis Grabis, Riga Technical University, Latvia
PhD Grigor Grigorov, “Vasil Levski” National Military University, Bulgaria
PhD Inga Grinfelde, Latvia University of Life Sciences and Technologies, Latvia
Dr. agr. Elvyra Gruzdevienė, Flax museum, the branch of Eriskiai Cultural Center of the Panevezys District, Lithuania
PhD Ilze Gudro, Riga Technical University, Latvia
PhD Tzvetelin Gueorguiev, Technical University of Gabrovo, Bulgaria
PhD Mart Hovi, Estonian University of Life Sciences, Estonia
PhD Maria Ilcheva, Saint Cyril and Methodius University of Veliko Tarnovo, Bulgaria
PhD Valery Ivanov, Defense Institute "Professor Tsvetan Lazarov", Bulgaria
Dr. agr. Sofija Jankauskiene, Lithuanian Research Centre for Agriculture and Forestry, Lithuania
PhD Aivars Jermuss, Latvia University of Life Sciences and Technologies, Latvia
PhD Amit Joshi, BA School of Banking and Finance, Latvia
Dr.sc.ing. Aivars Kaķītis, Latvia University of Life Sciences and Technologies, Latvia
PhD Sabrina Kalinkova, University of National and World Economy, Bulgaria

Dr.paed. Ilmārs Kangro, Rezekne Academy of Riga Technical University, Latvia
PhD Veiko Karu, Estonian Business School, Estonia
PhD Aivars Kaupuzs, Rezekne Academy of Riga Technical University, Latvia
PhD Anna Khilya, Vinnytsia Mykhailo Kotsiubynskyi State Pedagogical University, Spain
PhD Andrejs Koliškins, Riga Technical University, Latvia
PhD Georgi Komitov, Agricultural University Plovdiv, Bulgaria
PhD Karīne Laganovska, Latvian University of Biosciences and Technologies, Malnava College, Latvia
PhD Vjaceslavs Lapkovskis, Riga Technical University, Latvia
PhD Inga Ļašenko, Riga Technical University, Latvia
PhD Lazar Lazarov, "Vasil Levski" National Military University, Bulgaria
Dr. Walter Leal, Hamburg University of Applied Sciences, Germany, Manchester Metropolitan University, United Kingdom
Dr.sc.ing. Angel Lengerov, Technical University of Plovdiv, Bulgaria
PhD Iveta Linina, Turiba University, Latvia
Dr.oec. Jelena Lonska, Rezekne Academy of Riga Technical University, Latvia
PhD Slobodan Lubura, University of East Sarajevo, Bosnia and Herzegovina
PhD Lyuboslav Lyubenov, University of Ruse "Angel Kanchev", Bulgaria
PhD Velichko Machev, Todor Kableshkov University of Transport, Bulgaria
Dr.sc.math. Maksims Marinaki, University of Latvia, Latvia
PhD Georgi Marinov, Rakovski National Defence College, Bulgaria
PhD Dilyan Markov, Rakovski National Defence College, Bulgaria
PhD Arturs Medveckis, Liepaja Academy of Riga Technical University, Latvia
Dr.sc.ing. Linda Mežule, Riga Technical University, Latvia
PhD Ziedonis Miklašēvičs, Rezekne Academy of Riga Technical University, Latvia
PhD Roussi Minev, Ruse University, Bulgaria
PhD Nikolai Minkovski, University of Forestry, Bulgaria
PhD Penko Mitev, Technical University of Sofia, Bulgaria
Dr.sc.ing. Ivan Mitev, Technical University of Gabrovo, Bulgaria
PhD Ilie Nuca, Technical University of Moldova, Republic of Moldova
Dr.chem. Sergejs Osipovs, Daugavpils University, Latvia
PhD Nikolay Padarev, "Vasil Levski" National Military University, Bulgaria
PhD Jana Paidere, Daugavpils University, Latvia
Dr.sc.ing. Jeļena Pečerska, Riga Technical University, Latvia
Dr.sc.ing. Desislava Petrova, Technical University of Gabrovo, Bulgaria
PhD Valentina Petrova, Nikola Vaptsarov Naval Academy, Bulgaria
Dr. agr. Valentīna Pole, IK Tava zeme, Latvia
PhD Dimcho Pulov, Technical University of Gabrovo, Bulgaria
PhD Aurelija Pūraitė, Mykolas Romeris University, Lithuania
Dr. agr. Gundega Putniece, Latvia University of Life Sciences and Technologies, Latvia
PhD Todor Rachovski, Plovdiv University "Paisii Hilendarski", Bulgaria
PhD Anton Rassolkin, Tallinn University of Technology, Estonia
Dr.phys. Gita Rēvalde, Riga Technical University, Latvia
Dr.sc.ing. Ādolfs Ruciņš, Latvia University of Life Sciences and Technologies, Latvia
PhD Jolanta Šadauskiene, Kaunas University of Technology, Lithuania
Dr.sc.math. Felikss Sadirbajevs, Daugavpils University, Latvia
PhD Rashmi Jaymin-Sanchaniya, Riga Technical University, Latvia
PhD Iryna Sarancha, Vinnytsia Mykhailo Kotsiubynskyi State Pedagogical University, Ukraine
PhD Zhaneta Savova, National Military University, Bulgaria
Dr.geol. Valdis Segliņš, University of Latvia, Latvia
PhD Dafinka Sidova, New Bulgaria University, Bulgaria
PhD Andrejs Šiškins, Riga Technical University, Latvia
PhD Inese Skapste, Latvia University of Life Sciences and Technologies, Latvia
PhD Krasimir Slavyanov, "Vasil Levski" National Military University, Bulgaria
Dr.-Ing. Bambang Soemardiono, Institut Teknologi Sepuluh Nopember, Indonesia
Dr.geol. Juris Soms, Daugavpils University, Latvia
PhD Nikolay Stefanov, "Vasil Levski" National Military University, Bulgaria

PhD Julija Steinhart, BA School of Banking and Finance, Switzerland
PhD Aina Strode, Rezekne Academy of Riga Technical University, Latvia
PhD Agrita Švarta, Latvia University of Life Sciences and Technologies, Latvia
Dr.sc.ing. Edmunds Teirumnieks, Rezekne Academy of Riga Technical University, Latvia
PhD Plamen Teodosiev, University of Library Studies and Information Technologies, Bulgaria
Dr.biol. Rasma Tretjakova, Rezekne Academy of Riga Technical University, Latvia
PhD Dragomir Vassilev, Technical University of Gabrovo, Bulgaria
PhD Valentin Vassilev, South-West University "Neofit Rilski", Bulgaria
Dr.habil.sc.ing. Janis Viba, Riga Technical University, Latvia
PhD Emil Yankov, Rezekne Academy of Riga Technical University, Latvia
Dr.sc.ing. Imants Zarembo, Rezekne Academy of Riga Technical University, Latvia
PhD Tsanka Zlateva-Petkova, Technical University of Gabrovo, Bulgaria
PhD Anda Zvaigzne, Rezekne Academy of Riga Technical University Academy, Latvia
PhD Rosita Zvirgzdina, Turiba University, Latvia

Secretariat Chairman

PhD Ērika Teirumnieka, Rezekne Academy of Riga Technical University, Latvia

Secretariat Members

Dr.agr. Liena Poiša, Rezekne Academy of Riga Technical University, Latvia
Mg.sc.comp. Gundega Teilāne, Rezekne Academy of Riga Technical University, Latvia

IV SĒJUMS
SATURS
CONTENTS

Engineering Sciences and Production Technologies

Milka Atanasova **17**
INVESTIGATION OF THE MICROSTRUCTURE AND MICROHARDNESS AFTER ELECTRON BEAM WELDING OF AISI 316L STAINLESS STEEL AND LASERFORM MARAGING STEEL

Milka Atanasova **23**
WELDABILITY OF AISI 316L STAINLESS STEEL AND CARBIDIC AUSTEMPERED DUCTILE IRON USING ELECTRON BEAM WELDING TECHNOLOGY

Valeri Bakardzhiev, Sabi Sabev, Konstantin Chukalov **29**
STUDYING INFLUENCE OF 3D PRINTING PARAMETERS OF PETG TO IMPROVE HARDNESS AND MAXIMUM TENSILE STRENGTH

Valeri Bakardzhiev, Sabi Sabev, Konstantin Chukalov **37**
STUDY ABOUT INFLUENCE OF PRINTING SPEED AND LAYER HEIGHT ON DIMENSIONAL ACCURACY OF 3D PRINTED CARBON FIBER-REINFORCED POLYAMIDE PARTS

Iryna Bohashko, Oleksandr Bohashko, Inna Kosmidailo **45**
INDUSTRY 4.0: IMPLEMENTATION OF DIGITAL TECHNOLOGIES TO IMPROVE PRODUCTION AND ECONOMIC EFFICIENCY

Konstantin Chukalov, Valeri Bakardzhiev, Sabi Sabev **53**
STUDY OF INFLUENCE OF 3D PRINTING TEMPERATURE ON SHORE D HARDNESS OF NYLON CF15 CARBON

Konstantin Chukalov, Sabi Sabev, Valeri Bakardzhiev **59**
RESEARCH ON IMPACT RESISTANCE USING FREE-FALLING DART DROP TESTING OF 3D PRINTED PARTS MADE OF ABS AND PETG ACCORDING ASTM D1709

Dimitar Dichev, Borislav Georgiev, Iliya Zhelezharov **65**
ELECTRO-HYDRAULIC SYSTEM OPTIMIZATION THROUGH AN ADVANCED KALMAN FILTER

Dimitar Dichev, Borislav Georgiev, Iliya Zhelezharov **73**
PARAMETER EVALUATION AND CONTROL IN AN ELECTRO-HYDRAULIC SYSTEM USING AN ADVANCED LEAST SQUARES METHOD

Boyan Dochev, Filip Ublekov, Desislava Dimova, Mihail Zagorski, Nikola Tomanov **81**
DEVELOPMENT OF COMPOSITES BASED ON THERMOSETTING POLYMERS (EPOXY, POLYESTER AND VINYLESTER RESINS) WITH CENOSPHERE FILLERS IN DIFFERENT CONCENTRATIONS – 5 WT.%, 10 WT.% AND 15 WT.%

Svetlana Dimitrakieva, Marina Marinova-Stoyanova, Zhulieta Mihaylova **85**
THE ROLE OF THE LEADER IN THE PROCESS OF OVERCOMING COMMUNICATION BARRIERS IN THE NEW ERA OF INDUSTRY 4.0

Svetlana Dimitrakieva, Marina Marinova-Stoyanova, Boris Gramchev **91**
INTEGRATING ARTIFICIAL INTELLIGENCE INTO THE MANAGEMENT DECISION-MAKING PROCESS IN THE NEW ERA OF INDUSTRY 4.0

Petia Gencheva, Iliyan Hutov, Borislav Genov **99**
NUTRITIONAL STRATEGIES AND INNOVATIVE TECHNOLOGIES FOR MAINTAINING THE OPERATIONAL READINESS OF MILITARY PERSONNEL IN EXTREME CONDITIONS

Borislav Georgiev **105**
SIMULATION ANALYSIS OF WIENER AND LOW-PASS FILTRATION IN EHS

Georgi Slavchev Iliev, Hristo Nedev Hristov, Docho Svetlozarov Dimitrov **111**
EXPERIMENTAL STUDY OF THE FREQUENCY CHARACTERISTICS OF AN ELECTROPNEUMATIC TRACKING SYSTEM WITH HIGH SPEED PNEUMATIC VALVES AND PWM CONTROL

Georgi Slavchev Iliev, Hristo Hristov **117**
EXPERIMENTAL INVESTIGATION OF DYNAMIC PROCESSES IN AN ELECTROPNEUMATIC POSITIONING SYSTEM WITH HIGH SPEED VALVES AND PWM

Evgeniy Ivanov, Stefan Parvanov **123**
A STUDY OF THE BOILOVER PHENOMENON. EXPERIMENTAL DETERMINATION OF MASS BURNING RATE AND BOILOVER TIME

Evgeniy Ivanov, Stefan Parvanov **127**
DETERMINING THE RELATIONSHIP BETWEEN THE PARAMETERS TIME TO BOILOVER AND MASS BURNING RATE WITH THE PREVENTION AND RESPONSE STRATEGIES IN PETROLEUM PRODUCT STORAGE TANK FIRES

Nadejda Jeleva, Petya Gencheva **133**
APPROACHES TOWARDS IMPROVING THE SAFETY OF DINITRAMIDES AS ENERGETIC MATERIALS

Tsanko Karadzhov, Borislav Georgiev **139**
SYSTEM FOR TESTING AND DETERMINING THE ACCURACY OF A MECHANICAL WATCH

Kalin Krumov, Hristo Metev **145**
RESEARCH AND MODELING OF THE FINISHING METHOD OF CYLINDRICAL GEAR TEETH THROUGH COLD PLASTIC CALIBRATION

Georgi Karlovski, Petko Naydenov **151**
RESEARCH OF THE SURFACE ROUGHNESS DURING HARD TURNING OF 42CRMOS4 STEEL WITH A QUICK-CHANGE TOOL HOLDER

Desislava Kovacheva, Borislav Stoyanov, Krasimir Drumev, Ivelin Banev, Petar Nikolov **157**
STRUCTURES FOR WOVEN-LIKE KNITTING FABRICS MADE ON CIRCULAR KNITTING MACHINES

Angel Lengerov, Nadya Arabadzhieva, Konstantin Chukalov **161**
ANALYTICAL DETERMINATION OF ERROR FROM STATIC ADJUSTMENT OF BORING HEADS CUTTING PART DURING COMBINED MACHINING OF HOLES

Angel Lengerov, Silvia Salapateva, Konstantin Chukalov **165**
IMPROVEMENT OF DIMENSIONAL ACCURACY ANALYSIS FOR ASSEMBLY OF ENGINEERING PARTS

Inga Lasenko, Andris Martinovs, Artūrs Mačanovskis, Arta Viluma-Gudmona, Sanjay Rajni Vejanand, Sandra Vasilevska, Sai Pavan Kanukuntla **169**
MECHANICAL AND MORPHOLOGICAL PROPERTIES OF PP/PE COMPOSITE FISHING NET ROPES

Angel Lengerov, Nadya Arabadzieva, Silvia Salapateva **181**
DETERMINATION OF AXIAL FORCES OF TOOL ELEMENTS FOR PLASTICALLY STRENGTHENING HOLE MACHINING

Velichko Machev, Vladimir Kamenov, Stefan Stanev, Nikolay Tontchev **185**
INVESTIGATION OF THE TREND BETWEEN THE RESULTS OF THE BARKHAUSEN MAGNETIC NOISE (MBN) METHOD WITH CLASSICAL METHODS FOR ION NITRIDED TESTING OF STEEL, BH11

Marin Jordanov Marinov **189**
COMPUTER GRAFOANALITIC KINEMATICAL ANALYSIS FOR FOUR-BAR LINKAGE MECHANISM

Misho Matsankov **195**
RESEARCH OF ELECTRICITY LOSSES IN ELECTRIC NETWORKS

Vaidotas Matutis, Loreta Savulioniene, Mantas Vanagas, Karolis Bojakovas, Tomas Kasperavicius **201**
RESEARCH OF ELECTRICAL GENERATOR MODEL (STAGE: PHASE DIFFERENCES IMPACT ON GENERATION PROCESSES)

Gulrukh Memonova, Peter Schmidt, Javlon Tursunov, Guljakhon Gofurova **209**
AUTOMATED GROUNDWATER MONITORING SYSTEM WITH REAL-TIME DATA COLLECTION AND ANALYSIS USING LORA AND GSM TECHNOLOGIES

Hristo Metev, Irina Aleksandrova, Nikolay Kolev **217**
MULTI-OBJECTIVE OPTIMIZATION OF CUTTING PARAMETERS FOR CNC TURNING 42CRMO4 HARDENED STEEL USING UTILITY FUNCTION

Hristo Metev, Irina Aleksandrova, Nikolay Kolev **225**
INVESTIGATION OF THE MACHINABILITY OF 42CRMO4+QT STEEL IN TOOL TURNING WITH CARBIDE INSERTS ON CNC MACHINES WITH ROBOTIC POWER SUPPLY

Yuliyan Minchev, Ivaylo Minchev **235**
INFLUENCE OF THE GEOMETRIC ECCENTRICITY OF A GEAR ON THE VIBRATIONS OF A BEVEL GEAR

Yuliyan Minchev, Ivaylo Minchev **239**
ON THE INFLUENCE OF THE ELASTIC ANISOTROPY OF THE PROPELLER ON THE VIBRATIONS OF AZIMUTH THRUSTERS

Petko Naydenov **245**
DETERMING THE COMPENSATING ACTION OF COPPER AFTER SINTERING OF POWDER METALLURGICAL STRUCTURAL STEELS

Neli Nikolova, Desislava Petrova **251**
INVESTMENT ACTIVITY OF SMES IN THE FURNITURE INDUSTRY IN THE REPUBLIC OF BULGARIA

Jekaterina Niktina, Viktors Mironovs, Irina Voronova, Vladimirs Šatrevičs
SELECTION OF MATERIALS USING MULTICRITERIA DECISION MAKING. A CASE STUDY ON CELLULAR MATERIALS **257**

Marija Osipova, Viktors Mironovs, Antons Pacejs, Aleksejs Tatarinovs, Jānis Lungevics, Vjaceslavs Zemcenkovs **265**
PROPERTIES ASSESSMENT OF PERFORATED METAL PLATES FOR MEDICAL USE

Nikolay Iliyanov Padarev **271**
MATHEMATICAL MODEL FOR CALCULATING THE DISPERSION FLOW RATE OF DECONTAMINATION SOLUTIONS FOR CHEMICAL AND RADIOLOGICAL AGENTS WHEN SPRAYED FROM NOZZLES

Stanimir Penchev, Hristian Panayotov **277**
WIND TUNNEL STUDY OF AERODYNAMIC CHARACTERISTICS OF WING WITH ARC SHAPED WINGTIPS

Stanimir Penchev, Hristian Panayotov, Martin Zikyamov **283**
WIND TUNNEL INVESTIGATION OF WAKE CHARACTERISTICS OF A WING WITH WINGLETS

Desislava Petrova **289**
CLASSIFICATION OF MICROMECHANICAL ELEMENTS AND FABRICATION OF BEAM-TYPE MICROMECHANICAL ELEMENTS

Desislava Petrova, Neli Nikolova **297**
INNOVATIVE DEVELOPMENT AND COMPETITIVENESS OF THE INDUSTRIAL SECTOR INBULGARIA

Irena Petrova **305**
MODERN RISK ANALYSIS IN THE PLANNING AND IMPLEMENTATION OF MODERNIZATION PROJECTS IN RAILWAY INFRASTRUCTURE

Desislava Petrova, Tsanka Zlateva-Petkova, Angel Lengerov **309**
ALGORITHM AND FLOWCHART FOR GEOMETRIC MODELING OF MICROCOMPONENTS BASED ON THE CAD SYSTEM "MICROSYS 25"

Desislava Petrova, Tsanka Zlateva-Petkova, Angel Lengerov **315**
METHODOLOGY FOR VARIANT AND GENERATIVE DESIGN OF MICROCOMPONENTS BASED ON THE CAD SYSTEM "MICROSYS 25"

Desislava Petrova **323**
APPLICATION OF ALTERNATIVE APPROACHES FOR INNOVATIVE TECHNOLOGY OBSOLENCENCE IN BULGARIAN ENGINEERING COMPANIES

Dimcho Pulov, Petar Tsvyatkov **329**
PASSIVE ATHERMALIZATION OF LENSES FOR LWIR SPECTRAL RANGE

Rajeev Ralla, Karunamoorthy Rengasamy Kannathasan, Ilgar Jafarli **337**
PROPER ORTHOGONAL DECOMPOSITION TECHNIQUE FOR DIMENSIONAL REDUCTION FOR NUMERICAL SNAPSHOT MATRIX

Adolfs Rucins, Dainis Viesturs **345**
TRENDS IN THE DEVELOPMENT OF THE TRACTOR AND COMBINE FLEET IN LATVIA

Sabi Sabev, Valeri Bakardzhiev, Konstantin Chukalov **351**
INVESTIGATION OF THE INFLUENCE OF PARAMETERS IN 3D PRINTING OF NYLON CF15 CARBON ON LINEAR STRAIN DURING TENSILE CREEP

Sabi Sabev, Konstantin Chukalov **357**
DESIGN AND MANUFACTORING OF A LABORATORY STAND FOR TESTING ACCELERATED TENSILE CREEP OF PLASTICS ACCORDING TO ASTM D6992

Silviya Salapateva, Radostina Mihova **363**
DYNAMIC ALGORITHM FOR DIMENSIONAL SUB-TUNING IN TURNING

Silviya Salapateva, Angel Lengerov **369**
CUTTING MODES IN MULTI-PASS TURNING ON CNC LATHES

Jaymin Vrajlal Sanchaniya, Karunamoorthy Rengasamy Kannathasan, Sanjay Rajni Vejanand, Jay Joshi, Inga Lasenko **375**
EFFECT OF INFILL PATTERN DESIGN ON TENSILE STRENGTH OF FUSED DEPOSITION MODELLED SPECIMENS

Jaymin Vrajlal Sanchaniya, Ilze Liepiņlauska, Andris Skromulis, Inga Lasenko, Karunamoorthy Rengasamy Kannathasan, Sanjay Rajni Vejanand, Liena Poiša **383**
STRENGTHENING INTERFACIAL BONDING IN NANOFIBRE LAMINATED TEXTILE COMPOSITES

Liliya Staneva, Yuliyan Petrov **389**
GENERALIZED NETS AND THEIR APPLICATION IN THE MANAGEMENT OF A RECORDING STUDIO

Ani Stefanova **393**
FLOOD RISK ASSESSMENT AND MANAGEMENT UNDER DIRECTIVE 2007/60/EU: GEODETIC APPROACHES AND DIGITAL TECHNOLOGIES FOR EFFECTIVE PREVENTION

Julija Steinhart **399**
AGILE LEADERSHIP UNVEILED: ESSENTIAL TRAITS

Simeon Tsenkulovski, Petko Naydenov **407**
MODELING THE PENETRATION DEPTH DURING LASER MARKING OF LAYERED REINFORCED COMPOSITES WITH A POLYMER MATRIX

Mirena Todorova, Kostadin Trifonov **413**
DETERMINING THE RELATIVE IMPORTANCE OF INDICATORS OF SUBURBAN PUBLIC TRANSPORT COMFORT BY THE METHOD OF GEOMETRIC MEAN FUZZY-AHP

Mirena Todorova, Mihail Rangelov **419**
MODELING THE TECHNOLOGY OF THE VARNA FERRY COMPLEX OPERATION USING THE QUEUEING THEORY

Tsvetelina Vladimirova, Hristo Katrandjiev, Noncho Dimitrov **425**
RHETORICAL DEVICES IN ADVERTISING SLOGANS: A COMPETITIVENESS VIEWPOINT

Linda Valkovska, Amélie Canon, Anta Sparinska, Olivier dal Zuffo, Ansis Avotins, Martins Marcinkevics **431**
IMPACT OF LIGHT INTENSITY AND LUMINAIRE TYPE ON BASIL YIELD: INSIGHTS FROM A HYDROPONIC URBAN AGRICULTURE SYSTEM

Serhii Yermakov, Taras Hutsol, Oleksandr Hovorov, Pavlo Potapskyi, Serhii Oleksiyko **439**
RATIONALITY OF USING PNEUMATIC LOOSENERS OF VIBRATION ACTION ON PLOW BODIES

Yosif Yosifov **445**
RESEARCH INTO THE POSSIBILITY OF CREATING A WI-FI RADAR FOR DETECTING MOVING FLYING TARGETS IN THE NEARBY AREA OF PROTECTED OBJECTS

Laser Technologies

Arturs Abolins **453**
POTENTIAL LASER PROCESSING PARAMETERS FOR OBTAINING MILK REPELLING SURFACE ON STAINLESS STEEL (AISI 316L)

Nikolay Angelov, Lyubomir Lazov, Erika Teirumnieka, Artis Teilans, Arturs Abolins **459**
NUMERICAL EXPERIMENTS FOR THE LASER MARKING BY OXIDATION, MELTING AND EVAPORATION OF AISI 304 STAINLESS STEEL SAMPLES

Yordan Katsarov **467**
A NEW APPROACH TO DEVELOPING GAMMA-RAY LASER

Lyubomir Lazov, Risham Singh Ghalot, Nikolay Angelov **475**
OPTIMIZATION OF PARAMETERS FOR WHITE AND DARK LASER MARKING OF COPPER AND BRASS PRODUCTS

Lyubomir Lazov, Nikolay Angelov, Erika Teirumnieka, Artis Teilans, Ritvars Revalds **481**
DETERMINATION OF PRELIMINARY OPERATING POWER DENSITY RANGES FOR SOME LASER TECHNOLOGICAL PROCESSES ON AISI 316 STAINLESS STEEL

Jekabs Lapa, Imants Adijāns, Silvija Kukle, Lyubomir Lazov, Ieva Baķe, Uģis Briedis **489**
THE IMPACT OF CO2 LASER TREATMENT ON GRAPHENE-MODIFIED KM2-440 BALLISTIC KEVLAR FABRIC AND ITS PROPERTY CHANGES

Polya Mihaylova, Yulia Varadinova, Georgi Komitov **497**
COMPARATIVE ANALYSIS OF THE EFFECTIVENESS OF THE APPLICATION OF UAV AND CONVENTIONAL GROUND EQUIPMENT FOR PLANT PROTECTION MEASURES IN SUNFLOWER CULTIVATION

Normunds Teirumnieks, Lyubomir Lazov, Emil Yankov, Edmunds Teirumnieks, Prodan Prodanov, Artis Teilans **503**
LASER SURFACE TRANSFORMATION HARDENING WITH HIGH-POWER DIODE LASERS

IV
ENGINEERING SCIENCES AND PRODUCTION TECHNOLOGIES

Environment. Technology. Resources. Rezekne, Latvia
Proceedings of the 16th International Scientific and Practical Conference. 2025. Volume IV, 17-21

Investigation of the Microstructure and Microhardness after Electron Beam Welding of AISI 316L Stainless Steel and LaserForm Maraging Steel

Milka Atanasova
dept. Material science and Mechanical of materials
Technical University of Gabrovo
Center of competence "Smart mechatronic, eco-and energy-saving systems and technologies"
Gabrovo, Bulgaria
matanasova@tugab.bg

***Abstract*—The present study is related to the implementation of Electron Beam Welding of 316L stainless steel blanks obtained by traditional methods of plastic deformation and a blank made of LaserForm Maraging Steel obtained by Additive manufacturing also known as 3D Metal Printing Technology. A microstructural analysis was performed using a Scanning Electron Microscopy (SEM). To determine the chemical distribution at the fusion zone (FZ) an energy dispersive spectroscopy (EDS) was used. Vickers microhardness distribution across the welded seam was investigated in two zones – the first one at 1 mm from the surface and the second one at 3 mm from the surface.**

Keywords— Electron beam welding, microstructure, microhardness.

I. INTRODUCTION

The Electron Beam Welding (EBW) process is a Fusion Welding process as the metal to metal joint forms in liquid or molten state. This type of welding process is also classified as a new welding process as it uses the kinetic energy of fast-moving electrons to fuse two metal pieces at its joint [1].

The advantages of the process, as no edge preparation is necessary, the high welding speed results in narrow welds and heat affected zones with little distortion of the workpiece, short evacuating times can be achieved by adopting the working chamber to suit the number and size of workpieces, simple longitudinal weld seams can be welded as well as complicated three-dimensional components requiring use of programmed welding parameters and workpiece manipulation [2] etc., make it applicable in Aerospace, Automotive, Defense, Semiconductor, Medical, Nuclear, Oil & Gas, Power Generation and a variety of other industries.

On the other hand Additive manufacturing (AM), also known as 3D printing, is a process of joining materials to make objects from 3D model data, usually layer upon layer, as opposed to subtractive manufacturing methodologies. This tool less manufacturing approach can give industry new design flexibility, reduce energy use and shorten time to market. Main applications of additive manufacturing include rapid prototyping, rapid tooling, direct part production and part repairing of plastic, metal, ceramic and composite materials.

The 3d printing technology covering wide range of alloys used in a variety of industries (including aerospace, automotive, dental, jewelry, oil and gas, orthopedics printed electronics, and tooling) [3], [4], [5].

From the above, it is striking that both processes have the same application.

In various publications, data on the application of electron beam welding have been found as:

- technology for welding similar and dissimilar materials[1], [2], [6], [7], [21];
- application of coatings;

Online ISSN 2256-070X
https://doi.org/10.17770/etr2025vol4.8432
© 2025 The Author(s). Published by RTU PRESS.
This is an open access article under the Creative Commons Attribution 4.0 International License.

- modification of the surface layer [8];
- Electron beam cladding [2], [9];
- Alloying [10], [11];
- Hardening [11];
- Electron beam rapid prototyping [12], [13] etc.

The unifying factor that connects all these methods is that they are characteristic only for blanks obtained by classical methods such as casting and plastic deformation, or only for obtaining parts through so-called additive technologies and, in particular, 3D printing with metal powder.

Considering the advantages and disadvantages of both technologies, the question arises: is it possible and what will be obtained by electron beam welding of two dissimilar workpieces, one obtained using traditional technologies, and the other using additive technologies and 3D printing of metal powder.

Scarce information about such welding was found on the Electron Beam Processes Ltd website [14] for an example of an electron beam welded Titanium Additive Manufacturing body with Turned ring from stock bar, which does not provide detailed information about the implementation of the process.

The object of the study is obtaining a monolithic defect-free joint using electron beam welding between two dissimilar workpieces with similar properties, which are products of two fundamentally different technologies.

II. Materials and Methods

A. Materials

The selection of materials for the blanks used (metal powder for 3D printer and metal blank) was made based on the following criteria:

- Specificity of the existing equipment.
- The selected materials must be non-magnetic.
- The materials must have a certain chemical composition, physical and thermal properties.
- Application of the parts obtained by electron beam welding, etc.

316L stainless steel is an austenitic corrosion-resistant steel with excellent weldability, regardless of the welding method used. It is used in food preparation equipment, especially in chloride environments, pharmaceuticals, marine applications, medical implants, including pins, screws and orthopedic implants such as total hip and knee prostheses, etc. [15], [16]. It has a chemical composition listed in Table 1.

Table 1 Composition ranges for 316L stainless steels

Chemical Composition							
Grade	C	Mn	Si	Cr	Mo	Ni	N
Min	-	-	-	16.0	2.00	10.0	-
Max	0.03	2.0	0.75	18.0	3.00	14.0	0.10

On the other hand, LaserForm Maraging Steel (B) is designed for use on the ProX DMP 200 metal printer, producing industrial parts and tool inserts with a combination of high strength and excellent hardness [17].

It is easily heat treatable by an age hardening process, which results in excellent hardness and strength. In terms of subsequent processing, the material shows good weldability and machinability and is corrosion resistant. It is used for: tools and molds for injection molding, die casting and extrusion; high-performance industrial parts, e.g. the manufacturing and automation; high -wear components and aerospace. Its chemical composition and properties are listed in Table 2.

Table 2 Composition ranges for for LaserFormMaraging Steel (B)

Chemical Composition								
Grade	Fe	Ni	Co	Mo	Ti	Si	Mn	C
Min	Bal.	17.0	9.0	4.0	0.9	≥1.0	≥1.0	≥0.03
Max		19.0	11.0	6.0	1.1			

The two selected materials have properties that meet the requirements set out above.

To carry out the experiments are used rectangular blanks with geometric dimensions as follows: width b= 10mm, s= 10mm, l= 30mm, and a ProX DMP 200 3D printer was used to make the blanks from LaserForm Maraging Steel (B).

B. Electron beam welding machine

EBW process was carried out with an Evobeam Cube 400 welding unit manufactured by Evobeam (Fig. 1). In Table 3 was presented Specification of Electron Beam Welding Machine [18],[19],[20].

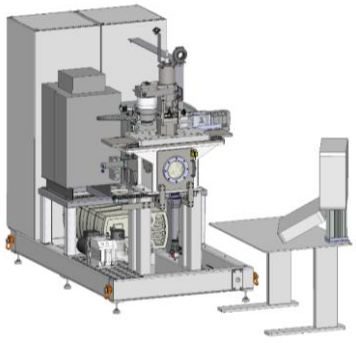

Fig. 1. Evobeam Cube 400 welding unit manufactured by Evobeam.

Table 2 Specification of Electron Beam Welding Machine

Elements	Description
Vacuum chamber	300 x 300 x 300 mm
Chamber pumping system	High Vacuum Turbo-Molecular-pumpset
Electron Beam gun system	High Vacuum Turbo-Molecular-pumpset
Manipulation system	3 mechanical CNC axes: X, Y and C all interpolated; 4 virtual CNC-Axes: IX, IY, IB und IL
Gun vacuum	5.10^{-4} mbar
Accelerating Voltage (U_a)	60 kV
Beam Current (I_f)	0-100 mA
Welding speed (V)	0-2500 mm/min

Based on previous studies related to the EBW process of various materials, the following technological parameters were selected: Accelerating voltage U=60kV, Focusing current I_f=1480mA, Welding speed V= 96mm/min, Beam current I_b= 20mA.

C. Microstructural analysis

To determine the quality of the weld obtained after EBW, a microstructural analysis was performed. A microsection was made from sample using a standard procedure: The test specimen was sanded manually using sandpapers of different sizes from 500 to 2500 mm. It was then polished with DiaMax diamond paste and developed with 4-10% aqueous HF solution for an optimum time of 45 s.

Vickers microhardness was measured along the cross-section of the weld seam in two parallel lines. The first was located at a distance of 1mm from the surface of the weld, and the second (bottom of weld zone) - at a distance of 3mm from the first. A semi-automatic microhardness tester, "ZWICK/ Indentec-ZHVμ-S" (ZwickRoell, Ulm, Germany) with a loading force of 0.5 N was used.

A scanning electron microscope (SEM) was used to determine the distribution of the elements constituting the structure of the obtained compound. An elemental analysis of the composition of the studied sample was performed using energy-dispersive X-ray spectroscopy (EDX).

III. RESULTS AND DISCUSSION

An electron microscope Neophot 32 was used to determine the presence of defects. Fig. 2 shows that there are no defects, there are clearly defined areas characteristic of electron beam welding Fusion Zone (FZ) and Heat Affected Zone (HAZ), and the structure formed in the seam is typical for this type of welding.

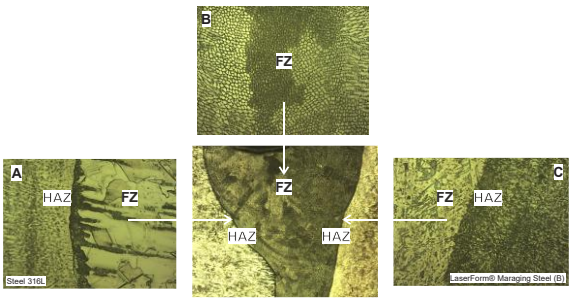

Fig. 2. Weld seam of both materials at x 50 magnification and transition zones at x 500 magnification between: A) 316L steel and weld seam; B) within the weld seam itself and C) weld seam and LaserForm Maraging Steel (B).

To obtain more information about the chemical composition of the studied sample, a straight-line EDX analysis was performed (Fig. 3).

The purpose of performing this analysis is to establish the distribution and concentration of chemical elements (mostly Cr, Ti, Co and Ni) with a predominant percentage content in the main zones HAZ, FZ and in the individual materials of the blanks.

The analysis shows redistribution of chromium. Before welding, it predominates in 316L steel and in LaserForm Maraging Steel (B) it is absent. After welding, its content, albeit a little, is also found in LaserForm Maraging Steel (B).

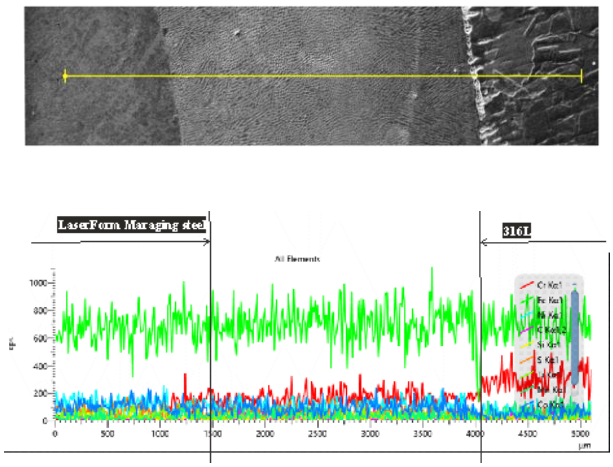

Fig. 3. Line EDX analys in HAZ and FZ of weld.

Fig. 4, Fig. 5 and Fig. 6 present EDX analysis at points located in the HAZ and FZ.

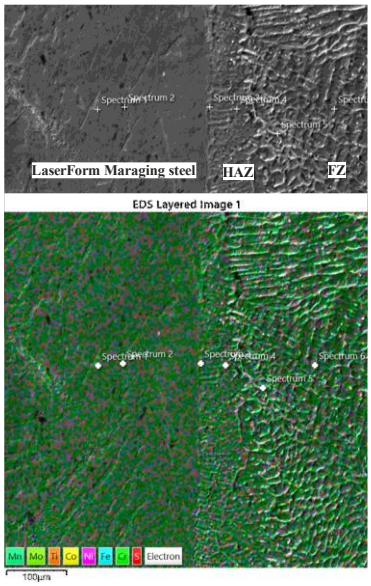

Fig. 4. EDX analys in HAZ and FZ of weld LaserForm Maraging Steel (B).

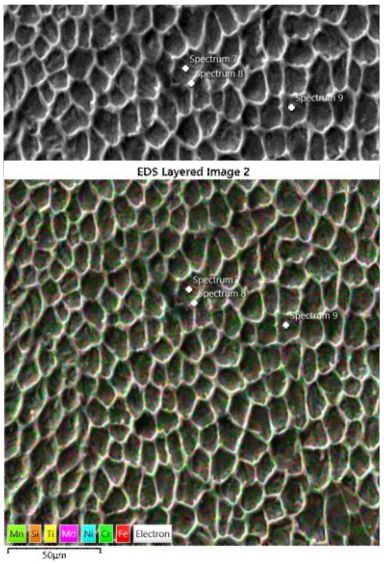

Fig. 5. EDX analys in FZ of weld

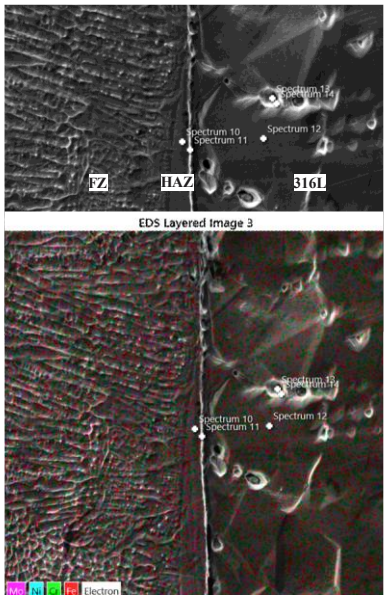

Fig. 6. EDX analys in HAZ and FZ of weld of of AISI 316L Steinless steel.

The microhardness of the used blanks before and after EBW was also measured. The average measured value of microhardness before welding for AISI 316L Stainless steel it is 432 $HV_{0,05}$, and for LaserForm Maraging Steel – 445 $HV_{0,05}$.

Fig. 7 shows the measured microhardness after EBW process.

The figure shows the same nature of the microhardness distribution of the two lines. The FZ and HAZ of the weld are clearly demarcated. There is no higher microhardness value in the weld, as is the case when welding homogeneous or heterogeneous materials. The reason for this is the different technologies used to obtain the blanks.

In the FZ, an average microhardness value of 315.5 $HV_{0,05}$ was measured on the first line and 349.7 $HV_{0,05}$ on the second line.

As expected, higher microhardness values were measured in both HAZ due to the thermal processes that occurred during the process and some elements (e.g. Cr, Ni, Co) from the chemical composition of both materials.

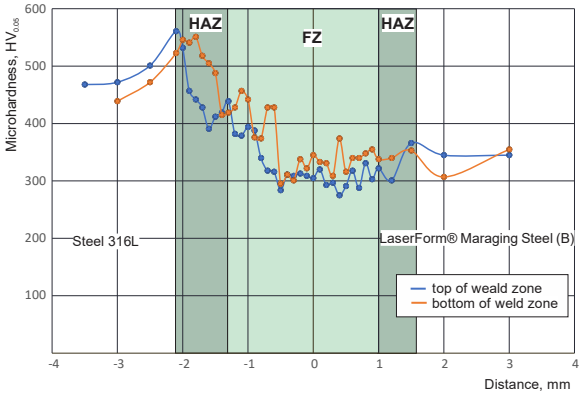

Fig. 7. Vickers microhardness in two parallel lines: the first was located at a distance of 1mm from the surface of the weld, and the second (bottom of weld zone) - at a distance of 3mm from the first.

IV. CONCLUSIONS

In this study, the set goal of obtaining a high-quality, monolithic and defect-free welded joint between blanks obtained by two different technologies (steel 316 L and LaserForm Manganic steel (B)) using electron beam welding was achieved.

The microstructural studies and the measured hardness of a microsection served to prove this. Using an electron microscope, it was found that the resulting weld seam and the areas around it lack defects in the form of pores, voids or cracks. The SEM and EDX analysis established the chemical composition at selected characteristic points of the cross-section of the sample and the homogeneous distribution of the elements with a predominant percentage content, such as Cr, Ti, Co and Ni in both materials.

The measured microhardness (from 315.5 $HV_{0.05}$ near the surface of the section and 349.7 $HV_{0.05}$ at 3mm from it) is also relatively uniform and confirms the presence of a monolithic joint. Compared to that of electron beam welding between homogeneous or dissimilar metals, it has a lower value, but the reason for this is the fact that one of the materials is a product of Additive manufacturing (AM) and 3D printing.

The subject of upcoming research will be determining the optimal mode of electron beam welding as a function of the microstructure and mechanical properties of samples of different materials obtained using different technologies.

ACKNOWLEDGMENTS

This research was funded by the European Regional Development Fund within the OP "Research, Innovation and Digitalization Programme for Intelligent Transformation 2021-2027", Project No. BG16RFPR002-1.014-0005 Center of competence "Smart Mechatronics, Eco- and Energy Saving Systems and Technologies".

REFERENCES

[1] P N Siddharth, C Sathiya Narayanan, "A review on Electron Beam Welding process". Journal of Physics: Conference Series 1706, 2020, http://dx.doi:10.1088/1742-6596/1706/1/012208

[2] M. St. Węglowski, S. Błacha, A. Phillips, "Electron beam welding - Techniques and trends – Review", Vacuum, vol. 130, pp. 72-92, 2016, https://doi.org/10.1016/j.vacuum.2016.05.004

[3] T. Duda, L. V. Raghavan, "3D Metal Printing Technology", IFAC, vol.49, Issue 29, pp. 103-110, 2016, https://doi.org/10.1016/j.ifacol.2016.11.111

[4] https://www.sciaky.com/additive-manufacturing/what-is-ded-3d-printing

[5] C. Körner," Additive manufacturing of metallic components by selective electron beam melting — a review", International Materials Reviews, vol. 61:5, pp. 361-377, 2016, https://doi.org/10.1080/09506608.2016.1176289

[6] Z. Sun, R. Karppi, "The application of electron beam welding for the joining of dissimilar metals: an overview", Journal of Materials Processing Technology, vol. 59, Issue 3,pp 257-267, 1996, https://doi.org/10.1016/0924-0136(95)02150-7

[7] I. Magnabosco, P. Ferro, F. Bonollo, L. Arnberg," An investigation of fusion zone microstructures in electron beam welding of copper–stainless steel", Materials Science and Engineering", vol.424, Issues 1–2, pp. 163-173, 2006, https://doi.org/10.1016/j.msea.2006.03.09

[8] S. Valkov, G. Kotlarski, S. Parshorov, M. Ormanova, B. Stoyanov, F. Padikova, I. Parshorov, "Effect of Electron Beam Surface Modification on the Plasticity of Inconel Alloy 625", Coatings, vol.14(3), pp. 2-12, 2024, https://doi.org/10.3390/14030268

[9] B. Wahlmann, C. Körner, M. Nunn, "Electron beam wire cladding of nickel alloys and stainless steel on a reactor pressure vessel steel", Materials Science and Engineering, vol. 811, 2021, https://doi.org/10.1016/j.msea.2021.141082

[10] P. Petrov, "Electron beam surface remelting and alloying of aluminium alloys", Vacuum, vol. 48, Issue 1, pp. 49-50, 1997, https://doi.org/10.1016/S0042-207X(96)00240-0

[11] S. Valkov, M. Ormanova and P. Petrov, "Electron-Beam Surface Treatment of Metals and Alloys: Techniques and Trends", Metals,Vol. 10(9), 1219, 2020, https://doi.org/10.3390/met10091219

[12] N. S. Nambolan, A. A. Kapil, S., P. S. Joshi, R.. M. Karunakaran, K.P. Bhargava, "Review on electron beam based additive manufacturing", Rapid Prototyping Journal, Vol. 26 No. 3, pp. 485-498, 2020, https://doi.org/10.1108/RPJ-07-2019-0182

[13] H. I. M. Castillo, J. E. P. Torres, "Rapid Prototyping and Manufacturing: A Review of Current Technologies", Proceedings of the ASME 2009 International Mechanical Engineering Congress and Exposition. vol. 4: Design and Manufacturing. Lake Buena Vista, Florida, USA. November 13–19, pp. 609-621, 2009,https://doi.org/10.1115/IMECE2009-11750

[14] EBP Manufacturing Solutions Making Challenging Products Cost Effective https://www.ebpglobal.com/gallery

[15] Shanghai Bozhong Metal Group Co., Ltd https://www.bzstainless.com/316l.html?gad_source=1&gclid=CjwKCAiAhP67BhAVEiwA2E_9gzUqToi_1ESWrbtoZ0HTphtMBRxO_KcSXNWXeb8zIN5CQzVf6IbV-BoCMpMQAvD_BwE

[16] Ounited Performance metals, https://www.upmet.com/sites/default/files/datasheets/316-316l.pdf

[17] 3D Systems Inc, https://www.3dsystems.com/sites/default/files/2019-03/3D-Systems_LaserForm_Maraging%20Steel%20%28B%29_DATASHEET_USEN_2019.03.15_WEB.pdf

[18] M. Atanasova, "Effects of Electron Beam Treatment on Microstructure of Ti6Al4V Alloy", Journal of the Technical University of Gabrovo, vol. 68, pp. 43-48, 2024, doi.org/10.62853/WAWB1418

[19] G. Iliev and H. Hristov, "Modelling and Simulation of Electropneumatic Positioning System Including the Length of Pneumatic Lines", ETR, vol. 3, pp. 106–111, Jan. 2024, http://doi.org/10.17770/etr2023vol3.7186

[20] G. Iliev, "Experimental Study of the Frequency Responses of Electropneutic Positioning System", ETR, vol. 3, pp. 90–94, Jun. 2024, http://doi.org/10.17770/etr2024vol3.8116

[21] I.Mitev, S. Tsenkulovski, "Local Processing of Non-Metal Materials with Concentrated Energy Flow", 14th ISPC "Environment Technology Resources", Rezekne, Latvia, vol. 3, 2023, pp.183÷186,ISSN 1691-5402 print; ISSN 2256-070X online

Environment. Technology. Resources. Rezekne, Latvia
Proceedings of the 16th International Scientific and Practical Conference. 2025. Volume IV, 23-27

Weldability of AISI 316L Stainless Steel and Carbidic Austempered Ductile Iron Using Electron Beam Welding Technology

Milka Atanasova
dept. Material science and Mechanical of materials
Technical University of Gabrovo
Center of competence "Smart mechatronic, eco-and energy-saving systems and technologies"
Gabrovo, Bulgaria
matanasova@tugab.bg

***Abstract*— The aim of this study is to determine the weldability of different materials - AISI 316L stainless steel and carbidic austempered ductile iron (CADI) by electron beam welding (EBW). Welding is performed with different beam current (I_b) of 10 mA and 20 mA, welding speed (V) of 400 mm/min and 1000 mm/min with an offset relative to the stainless steel of 0.2 mm at a constant frequency deviation (Freq). Vickers microhardness is measured in the fusion zone (FZ) and in the heat affected zones (HAZ). The most suitable welding mode is determined in terms of higher microhardness in the FZ with the presence of defects in the weld seam.**

Keywords*— *carbidic austempered ductile iron, electron beam welding, stainless steel, weldability.

I. INTRODUCTION

In recent years, the need to create new materials and designs has arisen. Electron beam processing and, in particular, electron beam welding (EBW) is among those technologies by which monolithic joints are obtained, both between similar and dissimilar metals and their alloys, as well as non-metallic materials [1], [2], [3].

There are publications [4], which describe the application of electron beam processing. This publication indicates the possible combinations of different metals and their alloys depending on any dependence. Weglowski [5] generally presents possible combinations of electron beam weldable materials with the inclusion of some steels and non-ferrous metals.

A trend in agriculture [7], [8] is the effect of Carbidic austempered ductile irons (CADI). Compared to other cast irons, they have greater wear resistance and high toughness at the expense of their high brittleness [9].

Due to the high carbon content of cast irons, their welding is difficult, but not impossible. In practice, conventional welding methods with preheating of cast iron are recommended to reduce residual stresses and deformations [10], [11], [12], [13].

An advantage of electron beam welding is the presence of a concentrated thermal energy effect with a high density, and the vacuum environment allows obtaining a quality weld seam with chemically active and hard-to-melt metals and alloys [14].

In addition to the availability of a suitable machine, it is necessary for the materials to possess the complex characteristic of weldability, which is related to:

- The suitability of the metal for welding, depending on chemical composition, metallurgical method of production, way of making the details, the heat treatment of the metal before the welding process;
- The technological possibilities of welding, expressed by the factors: method of welding; of the parameters of the welding mode; the general technological plan of welding; thermal mode of welding; need for preliminary or accompanying heat treatment; the need for subsequent heat treatment of the joint or the entire welded structure.
- Structural reliability of the welded joint, which is a function of the thickness of the welded material; the shape of the welded joint; the manner and preparation of the joined ends.

Online ISSN 2256-070X
https://doi.org/10.17770/etr2025vol4.8433
© 2025 The Author(s). Published by RTU PRESS.
This is an open access article under the Creative Commons Attribution 4.0 International License.

Weldability is determined by using quantitative and qualitative indicators in terms of whether the welding material is suitable for a specific welded structure, whether the specific parameters of the welding mode are selected and assessing the reliability of the resulting monolithic joint [10], [15], [16].

The aim of the present research is to create a monolithic welded joint between dissimilar materials austenitic stainless steel AISI 316L and CADI by means of EBW. The reason why this combination of materials was chosen is that the chemical composition of 316L austenitic steel contains nickel in the order of 10.0-14.0%. It is known that pure nickel electrodes are used in arc welding of cast iron. This is due to the fact that it takes a significant amount of carbon without changing its properties.

II. MATERIALS AND METHODS

A. Materials

The CADI blanks were obtained according to the methodology proposed in [17]. Castings were obtained using the method of casting from fused patterns, which were then subjected to isothermal quenching in salt baths. Those made of austenitic stainless steel AISI 316L were pre-turned and ground. The chemical composition of the two materials is listed in Table 1.

TABLE 1 CHEMICAL COMPOSITION OF THE USED MATERIALS

Mat.	C, %	Si, %	Mg, %	B, %	Mn, %	Cr, %	Mo, %	Ni, %
CADI	3,5	2,3	0,03	0,13	-	-	-	-
316L	0,03	0,75	-	-	2,0	16,0 - 18,0	2,0 - 3,0	10,0 - 14,0

Fig. 1 shows the dimensions of the blanks used for both materials.

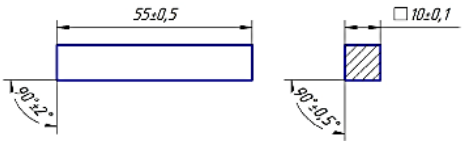

Fig. 1 Geometric dimensions of blanks from CADI and austenitic stainless steel AISI 316L.

B. Electron beam welding

EBW was performed with an Evobeam Cube 400 welding unit manufactured by Evobeam, which has the parameters specified in Table 2.

Various companies that deal with welding cast iron, [19] recommend preliminary cleaning and preheating of the cast iron.

According to [10] the best way to control the cooling rate during welding is to apply preliminary and concomitant heating. Depending on the temperature of the preheating, the following main methods of welding cast iron are distinguished:

- hot welding, with a heating temperature of 600-650 °C;
- semi-hot welding, with a heating temperature of 300-400 °C;
- cold welding - without preheating.

TABLE 2 SPECIFICATION OF ELECTRON BEAM WELDING MACHINE [18]

Elements	Description
Vacuum chamber	300 x 300 x 300 mm
Chamber pumping system	High Vacuum Turbo-Molecular-pumpset
Electron Beam gun system	High Vacuum Turbo-Molecular-pumpset
Manipulation system	3 mechanical CNC axes: X, Y and C all interpolated; 4 virtual CNC-Axes: IX, IY, IB und IL
Gun vacuum	5.10^{-4} mbar
Accelerating Voltage (U_a)	60 kV
Beam Current (I_f)	0-100 mA
Welding speed (V)	0-2500 mm/min

For this reason, two types of welding of dissimilar materials have been made: without and with preheating of the workpieces.

The main parameters in the EBW mode are classified into three main categories [18], [20] are:

- The parameters characteristic to the Electron Beam are Accelerating Voltage (U_a), Beam Current (I_f), Focusing Current (F), Depth of Penetration (H) and Beam Focal Diameter (d_{fo});
- The parameters characteristic to the Welding Joint Features are Welding Speed (v), Welding Width (B), Focal Distance (d_t), Vacuum Pressure (P_s) and Preheating Temperature (T_{pr});
- Other parameters involve Material Type, Thermo-physical and Chemical features of the material and Workpiece Thickness. These parameters do not constitute as being a part of Process Parameters.

Table 3 shows the selected parameters of EBW for the first type of workpieces (without preheating), and in table 4 - for the second type of workpieces (with preheating).

TABLE 3 TECHNOLOGICAL PARAMETERS OF EBW FOR WORCKPIECES WITHAUT PREHEATING

Accelerating voltage U, kV	Welding speed V, mm/min	Beam current I_b, mA	offset	Focusing current I_f,mA
60	1000	10	0,20 (steel)	1530 1510 (surface) 1490
60	1000	20	0,20 (steel)	1510 (surface)
60	600	1	0,20 (steel)	1510 (surface)
60	600	2	0,20 (steel)	1510 (surface)

TABLE 4 TECHNOLOGICAL PARAMETERS OF EBW FOR WORCKPIECES WITH PREHEATING

Sample	Accelerating Voltage U, kV	Focusing current I_f, mA	Welding speed V, mm/min	Beam current, I_b, mA	Offset mm	Radius of oscillation r_{osc}, mm
1	60	1510 (surface)	400	10	0,2 (steel)	0
2			400	20		0
3			400	10		0,15
4			400	20		0,15

The pre-heating of the blanks was carried out in a PEK-4 chamber furnace with the heating mode specified in table 5.

TABLE 5 HEATING MODE FOR CADI AND 316L BLANKS

Preheating, t°C	Retention time in the vacuum chamber after EBW, min	Removal temperature, °C
340	5	90

C. *Microstructure analysis*

To carry out a qualitative and quantitative analysis regarding the monolithic compound created after EBW, a microstructural analysis was carried out, including making a macro- and micro-analysis. For this purpose, all welded samples were cut along the cross-section of the seam and microsections were made using a standard methodology. They were sanded manually using sandpapers of different sizes from 500 to 2500 mm, then polished with DiaMax diamond paste and developed with 4% solution of picric acid in ethyl alcohol. Then an electron microscope was used to determine the depth of the resulting weld seam and the presence of defects. The Vickers microhardness of some of the samples was determined with DURAMIN-40 AC3.

III. RESULTS AND DISCUSSION

A. *For samples without preheating before EBW*

After welding this group of samples and using the modes indicated in Table 3, the following observations were made: for the samples with a current of 1 and 2 mA, no monolithic joint was obtained, and for the remaining samples with a current of 10 mA and 20 mA, a monolithic joint was obtained, but it was of a small depth ranging from 3-5 mm regardless of whether the Focusing current If was above, along and below the surface of the workpiece. This confirms the fact that it is advisable to preheat dissimilar materials before EBW. For these reasons, the need to determine the microhardness of this group of samples is eliminated.

B. *For samples with preheating before EBW*

In the second group of samples, which were subjected to preheating after electron beam welding, a monolithic joint was obtained. After cutting them in cross-section, the expected greatest depth of the weld seam was measured in samples with numbers №2 and №4, for which the magnitude of Beam current was I_b=20mA.

Vickers microhardness was measured near the surface of the weld on all specimens in this group with a loading force of 0.1N (Figure 3). The results obtained are grouped in two figures, as follows: Figure 4 - results of the measured microhardness of welded materials with a Beam current of I_b=10mA and Figure 5 - results of the measured microhardness of welded materials with a Beam current of I_b=20mA.

The figures show that the nature of the microhardness distribution is almost the same. As expected in the HAZ (in green in the figures) the measured microhardness is higher than that of the materials. The heterogeneous measured values are from the CADI side and are due to its composition. The reason for the nature of the microhardness distribution is that the appearance of brittle intermetallic compounds in the HAZ and FZ of the weld seam is possible. The measured maximum values are: for Sample 1 – 450 $HV_{0,1}$, Sample 2 - 422 $HV_{0,1}$, Sample 3 - 360 $HV_{0,1}$ and Sample 4 - 460 $HV_{0,1}$.

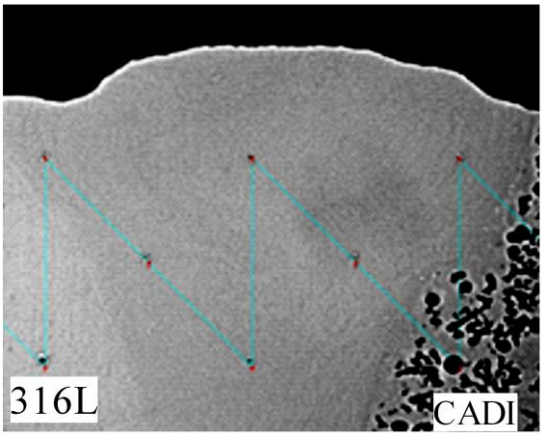

Fig. 2 Vickers microhardness measurement of specimen No. 4.

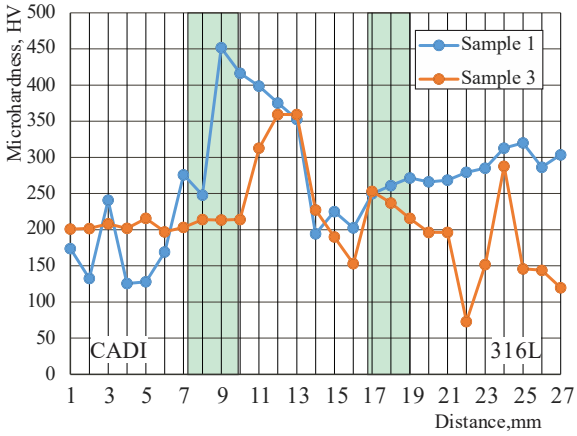

Fig. 3 Measured microhardness of electron beam welded samples with Beam current I_b=10mA.

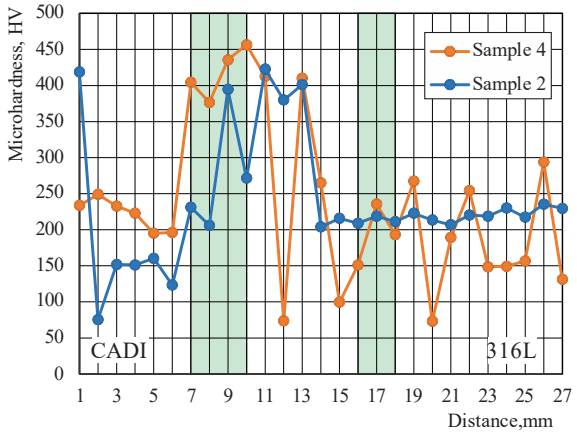

Fig. 4 Measured microhardness of electron beam welded samples with Beam current I_b=20mA.

From the macro analysis made regarding the presence of defects, defects were found only in the form of hollows, which are located near the root of the seam. The Depth of Penetration (H) of the seam was measured, with the largest being 10mm in sample No. 4, which was welded with a Beam current of I_b=20mA but also had oscillation with Radius of oscillation r_{osc}=0.15mm.

IV. CONCLUSIONS

Electron beam welding of dissimilar materials austenitic stainless steel AISI 316L and Carbidic austempered ductile irons (CADI) was performed. Two cases of welding were selected - with and without preheating the workpieces. EBW is performed with different magnitude of Beam current.

The following conclusions and recommendations can be made from the obtained results for electron beam welding of dissimilar materials:

- Despite the fact that a large part of the literature recommends that welding of cast iron be performed with a combination of preheating and the use of conventional welding methods with pure nickel electrodes, a defect-free monolithic joint is obtained, albeit with a small seam depth of penetration H=5 mm at a beam current I_b= 20 mA;
- When preheating the blanks, a monolithic joint is obtained in cases where a oscillation radius r_{osc}=0.15mm is used at beam current of I_b=10mA and I_b=20mA. A maximum depth of penetration 10 mm of the weld seam was achieved at a current of 20 mA.
- In some of the welds obtained in the second case of electron beam welding, a incomplete penetration was formed at the end of the weld. The probable reasons for this are both poor pressing of the parts against each other and insufficient preheating temperature.
- The Vickers microhardness of all samples was measured in both heat affected zones (HAZ) and fusion zone (FZ). In the HAZ it has an average value of 214 $HV_{0,1}$ to 423 $HV_{0,1}$ for CADI and from 257 $HV_{0,1}$ to 274 $HV_{0,1}$ for 316L, and in the FZ - from 336 $HV_{0,1}$ to 401 $HV_{0,1}$.

ACKNOWLEDGMENTS

The author expresses his gratitude to T. Bakalova at Technical University of Liberc for the assistance provided.

This research was funded by the European Regional Development Fund within the OP "Research, Innovation and Digitalization Programme for Intelligent Transformation 2021-2027", Project No. BG16RFPR002-1.014-0005 Center of competence "Smart Mechatronics, Eco- and Energy Saving Systems and Technologies".

REFERENCES

[1] P. Lacki , K. Adamus, "Numerical simulation of the electron beam welding process", Computers & Structures, vol. 89, Issues 11–12, pp 977-985, 2011 https://doi.org/10.1016/j.compstruc.2011.01.016

[2] A Munteanu, "The electron beam welding of dissimilar materials – case study", IOP Conf. Series: Materials Science and Engineering ,vol. 161, https://doi.org/10.1088/1757-899X/161/1/012058

[3] D. Kaisheva, G. Kotlarski, B. Stoyanov, V. Dunchev, M. Ormanova, S. Valkov, "Electron Beam Welding of Dissimilar Metals and Alloys", International Scientific Conference "UNITECH 2022" – Gabrovo, vol.1, pp. 566- 571, 2022.

[4] Z. Sun and R. Karppi,"The application of electron beam welding for the joining of dissimilar metals: an overview", Journal of Materials Processing Technology, vol. 59, Issu 3, pp. 257 -267, 1996, https://doi.org/10.1016/0924-0136(95)02150-7.

[5] M. St. Węglowski, S. Błacha, A. Phillips, "Electron Beam Welding – Techniques and Trends – Review", Vacuum, vol. 130, pp. 72-92, 2016, https://doi.org/10.1016/j.vacuum.2016.05.004.

[6] K. E. Elliott and C.M. Greene, "A Local Adaptive Protocol," Argonne National Laboratory, Argonne, France, Tech. Rep. 916-1010-BB, 1997.

[7] V. Todorov, "Bainite Ductile Cast Iron – Possibilities and Problems", XXIII International scientific and technical conference, Pleven, Year XXIV, Issue 79193, 2016 ISSN: 1310-3946.

[8] K. L. Hayrynen and K. R. Brandenberg," Carbidic Austempered Ductile Iron (CADI) – The New Wear Material", Journal of Materials Engineering and Performance, vol.31, pp. 3409–3417, 2022, https://doi.org/10.1007/s11665-021-06476-8.

[9] S. Laino, J.A. Sikora, R.C. Dommarco, "Development of Wear Resistant Carbidic Austempered Ductile Iron (CADI)", Wear, vol. 265, Issues 1–2, pp. 1-7, 2008, https://doi.org/10.1016/j.wear.2007.08.013.

[10] J. C. Lippold,Welding Metallurgy and Weldability. John Wiley & Sons, 2014.

[11] D.Q. Sun, X.Y. Gu, W.H. Liu, Z.Z. Xuan, "Welding consumable research for austempered ductile iron (ADI)", Materials Science and Engineering,vol. 402, Issues 1–2, pp. 9-15, 2005, https://doi.org/10.1016/j.msea.2005.01.034.

[12] A. O. Alao, A.A. Barnabas, J. Ogbodo, A. A. Akinwande, B.J. Kutelu, "Investigation of Micro-addition of Antimony on the Weldability of Pre-heated Treated at 400°C Carbidic Austempered Ductile Iron (CADI)", International Journal of Advanced Academic Research, vol. 6, Issue 8, pp. 70-79, 2015, https://doi.org/10.46654/ij.24889849.e6820

[13] El-Shennawy M, Abdel-Aleem HA, Ghanem MM, Sehsah AM, "Effect of welding parameters on microstructure and mechanical properties of dissimilar AISI 304/ductile cast iron fusion welded joints", Sci Rep. 14(1), 2024, https://doi.org/10.1038/s41598-024-70050-0

[14] M. Hatate, T. Shiota, N. Abe, M. Amano, T. Tanaka, "Bonding characteristics of spheroidal graphite cast iron and mild steel using electron beam welding process", Vacuum, vol. 73, Issues 3–4, pp. 667-671, 2004, https://doi.org/10.1016/j.vacuum.2003.12.097.

[15] N. Nikov, Weding. Part I. Welding process theory. Varna, 1990

[16] R. K. Bhatnagar, G. Gupta, "A Review on Weldability of Cast Iron", International Journal of Scientific and Engineering Research, vol. 7, Issue 5, pp. 126-131, May-2016, ISSN 2229-5518

[17] G. Raschev, V. Todorov, S. Savov, "Study of the wear resistance of bajnitic cast iron with different carbide phase", International scientific Conference "Unitech 2015", Vol.III, Gabrovo, 2015.

[18] M. Atanasova, "Effects of electron beam treatment on microstructure of Ti6Al4V alloy", Journal of Technical University of Gabrovo, vol.68, pp. 43-48, 2024, doi.org/10.62853/WAWB1418

[19] Pierre-Jean Cunat," The welding of stainless steels". Euro Inox, 2001

[20] I. Mitev, S. Tsenkulovski, "Local Processing of Non-Metal Materials with Concentrated Energy Flow", 14th ISPC "Environment Technology Resources", Rezekne, Latvia, vol. 3, 2023, pp.183÷186, ISSN 1691-5402 (print); ISSN 2256-070X (online)

Environment. Technology. Resources. Rezekne, Latvia
Proceedings of the 16th International Scientific and Practical Conference. 2025. Volume IV, 29-35

Studying Influence of 3D Printing Parameters of PETG to Improve Hardness and Maximum Tensile Strength

Valeri Bakardzhiev
Technical University of Sofia,
Branch Plovdiv
Plovdiv, Bulgaria
bakardzhiev@tu-plovdiv.bg

Sabi Sabev
Technical University of Sofia,
Branch Plovdiv
Plovdiv, Bulgaria
sabi_sabev@tu-plovdiv.bg

Konstantin Chukalov
Technical University of Sofia,
Branch Plovdiv
Plovdiv, Bulgaria
chukalov@tu-plovdiv.bg

***Abstract*— In this article, the main mechanical properties of PETG - hardness and maximum tensile strength, produced with different printing parameters, will be investigated. The experimental results were statistically processed using MiniTab. 13 experimental samples were tested with printing parameters - speed in the range of 40-120 m/min and layer thickness from 0.1 to 0.4 mm. The aim of the article is to investigate in which discrete zone of 3D printing parameters the parts have the highest strength characteristics - hardness and maximum tensile strength.**

Keywords — mechanical properties, optimization, 3D printing, regression analysis,printing parameters, tensile strenght

I. INTRODUCTION

3D printer filament is primary material used to create three-dimensional objects[1]. These filaments are polymers that are melted and extruded through a printer nozzle to build a model layer by layer. Choosing the right filament is critical to the success of any 3D printed part, as different materials offer different mechanical and physical properties.

The most common types of filaments in the field of 3D printing are: PLA, ABS, and PETG. Along with these materials, engineered filaments such as PEEK, PEI, and PC are used in industrial applications due to their thermal stability, chemical resistance, and exceptional strength[2].

II. MATERIALS AND METHODS

PETG (Polyethylene terephthalate glycol) is one of the most popular and versatile filaments for 3D printing[3]. PETG combines some of the best features of PLA and ABS, offering good flexibility, strength and chemical resistance. It is used to create functional parts that need to withstand higher loads than PLA. PETG is the preferred material for applications requiring stiffness and resistance to external loads[4].

Unlike ABS, PETG is easier to print, as it has better adhesion to the 3D printing bed and is less prone to warping. In addition, PETG is resistant to chemicals and UV rays, making it an excellent choice for outdoor applications. PETG is resistant to most chemicals, including oils, acids and alkalis, making it suitable for technical applications.PETG is with good adhesion between layers and minimum deformation during printing.

The experiment was planned using the central composite design[5]. When using such a design, the resulting mathematical regression model provides equal accuracy for all points equally distant from the center of the factor space.The design of experiment was made using Minitab, the values of the speed printing are in the range of 40-120mm/min and the height of the layer are in the range 0.1-0.4mm . The value of α in this two-factor design is 1.41 with a total of 13 trials, with 5 trials in the center of the square, figure 1 shows a drawing of a test specimen[6].

The main parameters under which the samples were printed are the following:

- Material: PetG
- Printing speed range: 40 - 120mm/s
- Extruder temperature range: 235ºC
- Bed temperature: 65ºC
- Layer height range: 0.1 – 0.4mm
- Infill: 100%
- Flow: 103%
- Printing time range: 25- 28min

Online ISSN 2256-070X
https://doi.org/10.17770/etr2025vol4.8410
© 2025 The Author(s). Published by RTU PRESS.
This is an open access article under the Creative Commons Attribution 4.0 International License.

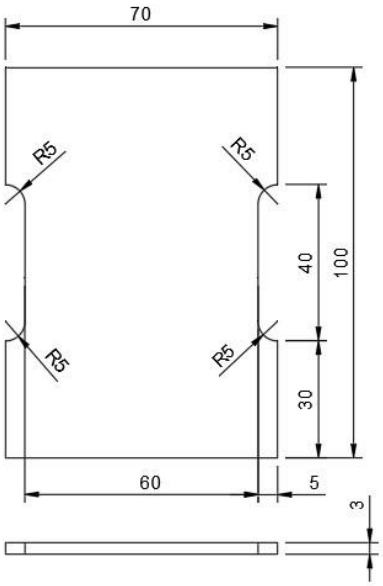

Fig. 1. Test specimen dimensions

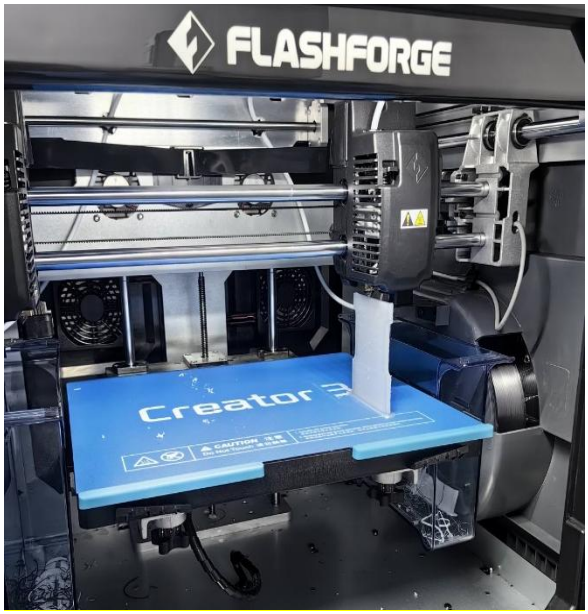

Fig. 2. Vertically printing of the samples

13 samples were printed using a Flashforge Creator 3 3D printer, Fig. 2. The samples were printed vertically to investigate the connection between the layers.

Hardness tests were performed on a calibrated Shore D durometer according to ASTM D2240. The tested material was within the working range of the instrument[7]. The requirements for distances between test runs were met.

Tensile strength tests were performed on a calibrated tensile testing machine operating with a maximum possible force of 10 kN. The selected strain rate was 40 mm/min in order to obtain more precise results[8].

III. RESULTS AND DISCUSSION

The experimental data from Table 1 were processed mathematically and statistically with the MINITAB software product to achieve a math model[9]

TABLE 1 OBTAINED RESULTS

Speed	Layer	F max (kN)	H Shore D
80	0,1	1,44	73,20
52	0,35	1,05	68,93
52	0,14	2,14	74,83
80	0,25	1,61	71,38
108	0,14	1,11	73,63
80	0,25	1,65	73,00
80	0,25	1,60	70,50
80	0,25	1,64	70,60
40	0,25	1,92	72,97
80	0,25	1,64	71,40
108	0,35	1,06	68,55
120	0,25	1,35	71,90
80	0,4	0,47	67,03

For the mathematical description of the objective function (maximum force - F max), the following regression model was obtained[10]:

$$Y_F = b_0 + b_1X_1 + b_2X_2 + b_3X_2^2 + b_4X_1X_2 \quad (1)$$

Table 2 presents the coefficient values. You can use the T-value to determine whether the coefficients are significant. However, the P-value is more commonly used because the threshold for rejecting the null hypothesis does not depend on the degrees of freedom. In our case, the P-value for each coefficient is lower than 0.05, so we can reject the null hypothesis. In other words, the coefficients have a lower p-value and are significant for this model [11].

TABLE 2 COEFFICIENTS

Term	Coef	SE Coef	T-Value	P-Value	VIF
Constant	3,1071	0,0835	37,20	0,000	
Speed	-0,03182	0,00093	-33,98	0,000	13,88
Layer	3,980	0,435	9,15	0,000	42,57
Layer*Layer	-30,167	0,635	-47,49	0,000	22,72
Speed*Layer	0,09789	0,00394	24,83	0,000	44,43

The calculated coefficient of determination R-sq = 99.88%, the adjusted coefficient of determination R-sq(adj) = 99.82% and the predicted coefficient of determination has the value R-sq(pred) = 99.58%(tab.3)[12].

TABLE 3 MODEL SUMMARY

S	R-sq	R-sq(adj)	R-sq(pred)
0,0186151	99,88%	99,82%	99,58%

The P-value for the F-test of the overall significance test is lower than 0.05, which gives us grounds to reject the null hypothesis and conclude that the resulting model provides a good and adequate description of the studied variable(tab.4)[13].

TABLE 4 ANALYSIS OF VARIANCE

Source	DF	Seq SS	Seq MS	F-Value	P-Value
Regression	4	2,09498	0,523746	1511,43	0,000
Speed	1	0,72606	0,726059	2095,27	0,000
Layer	1	0,45369	0,453686	1309,25	0,000
Layer*Layer	1	0,70163	0,701633	2024,78	0,000
Speed*Layer	1	0,21360	0,213604	616,42	0,000
Error	7	0,00243	0,000347		
Lack-of-Fit	3	0,00055	0,000182	0,39	0,769
Pure Error	4	0,00188	0,000470		
Total	11	2,09741			

The Pareto diagram, Fig. 3, arranges the coefficients according to their effect on the desired function from largest to smallest. The diagram also draws a reference line to show where the limit of statistical significance is. It can be seen that the components pass the significance line, therefore they are significant [14].

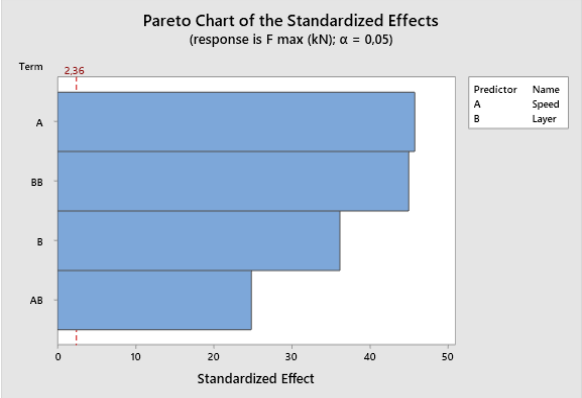

Fig. 3. Pareto diagram

The standard residual is equal to the value of the residual divided by an estimate of its standard deviation. These residuals are useful because raw residuals may not be good indicators of a deviation in the regression model. It is clear from Fig. 4 - 5 that there are no gross errors in this regression model. The analysis of the residuals does not indicate a violation of the assumptions of the regression analysis. From Fig. 5. it is seen that all residuals are in the interval ±2

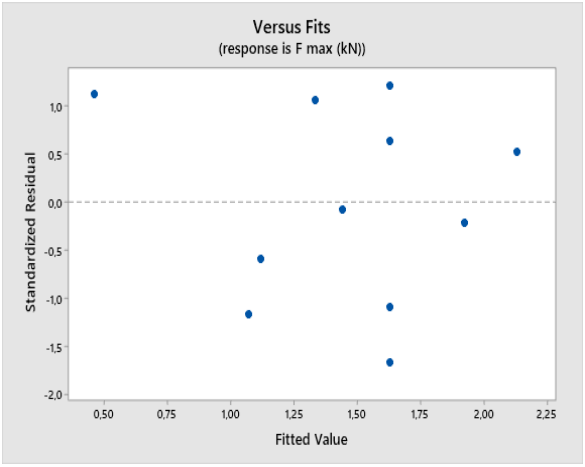

Fig. 4. Standard residuals

The Anderson-Darling (AD) statistical test was used, which measures how well the data follow the chosen distribution[15]. The test was also used to determine the adequacy of the model. The AD test confirmed the normal distribution of the standardized residuals. The calculated AD value of 0.374 is less than the critical value of 0.683 for the sample of 12 observations and the associated p-value of 0.356 of the AD statistic is significantly above the 0.05 level. The lower value of AD compared to the critical value and the P-value ≥ α,confirm a normal probability distribution of the residuals[16]. Therefore, it may be concluded that the regression model is adequate.

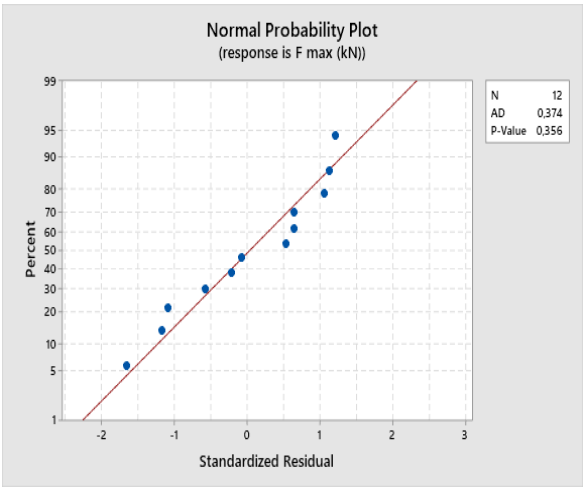

Fig. 5. Standardized residuals

The main effects plots, Fig. 6, show mean values for each predictor variable while holding the other variables in the model constant. Since the lines are not horizontal, main effects are present for velocity and layer. The results of the regression analysis confirm that all main effects are statistically significant[17]. However, because the interaction effects are statistically significant, the main effects plot can be misleading. Therefore, you cannot interpret the main effects without considering interaction effects.

Fig. 6. Main effects plot for F max

The interaction plot, Fig. 7 shows an obvious interaction effect, as the lines are not horizontal, suggesting that the maximum tensile force depends on the speed and layer height when printing.

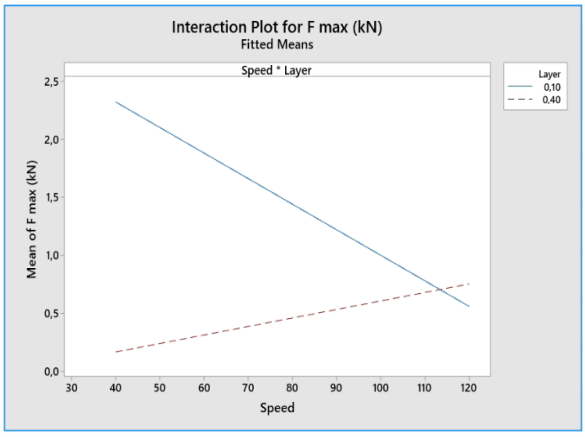

Fig. 7. Interaction plot for F max

For technological reasons, a maximum is sought for the maximum force - F max. Based on a preliminary analysis of the experimental results, 2.4kN was selected as a logical maximum value. A single-parameter optimization was performed and the maximum values for the objective function were found. The data are presented in Tables 5,6,7.

TABLE 5 PARAMETERS

Response	Goal	Lower	Target	Upper	Weight	Importance
F max	Max	0,466667	2,4		1	1

TABLE 6 SOLUTIONS

Solution	Speed	Layer	F max Fit	Composite Desirability
1	40,000	0,130303	2,35094	0,743792
2	40,000	0,100000	2,32220	0,732449
3	40,000	0,100000	2,32220	0,732449
4	119,999	0,258465	1,33824	0,344043

TABLE 7 MULTIPLE RESPONSE PREDICTION

Variable	Setting			
Speed	40			
Layer	0,1303			
Response	**Fit**	**SE Fit**	**95% CI**	**95% PI**
F max	2,3509	0,0213	(2,3006; 2,4013)	(2,2841; 2,4178)

The graphical optimization consists of plotting graphs with lines of constant values for the objective function. The results obtained are presented in Fig. 8 at a speed of 40mm/s and a layer thickness of 0.13mm, obtaining a maximum force of 2.35kN.

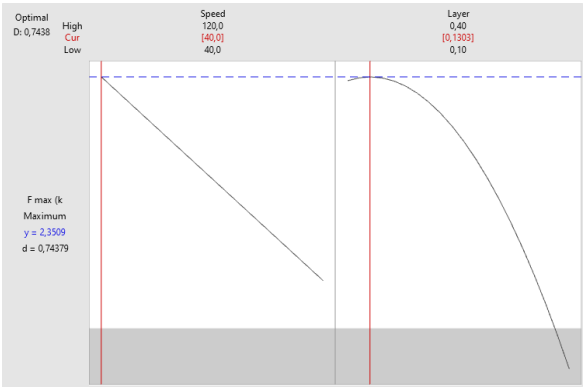

Fig. 8. Fig..8 Optimal solution

The experimental data from Table 1 for hardness (H Shore D) were also processed mathematically and statistically with the MINITAB software product and the following regression model was obtained:

$$Y_D = b_0 + b_1X_1 + b_2X_2 + b_3X_1^2 + b_4X_2^2 \qquad (2)$$

In this case, the P-value for almost every coefficient is lower than 0.05, except for Layer and Layer*Layer, so you can say that these coefficients are insignificant for this model.

TABLE 8 COEFFICIENTS

Term	Coef	SE Coef	T-Value	P-Value	VIF
Constant	81,89	1,97	41,56	0,000	
Speed	-0,1660	0,0395	-4,20	0,004	41,07
Layer	-6,50	8,71	-0,75	0,479	28,12
Speed*Speed	0,000951	0,000244	3,90	0,006	41,12
Layer*Layer	-34,0	17,3	-1,96	0,090	28,19

The calculated coefficient of determination R-sq = 97.06%, the adjusted coefficient of determination R-sq(adj) = 95.37% and the predicted coefficient of determination has the value R-sq(pred) = 90.25% tab.9.

TABLE 9 MODEL SUMMARY

S	R-sq	R-sq(adj)	R-sq(pred)
0,490259	97,06%	95,37%	90,25%

The P-value for the F-test of the overall significance test of the regression model is lower than 0.05, which gives us grounds to reject the null hypothesis and conclude that the resulting model is adequate. There are 2 coefficients with a slightly elevated value above 0.05, these are Speed and Layer*Layer, which do not affect the overall regression.

TABLE 10 ANALYSIS OF VARIANCE

Source	DF	Seq SS	Seq MS	F-Value	P-Value
Regression	4	55,4699	13,8675	57,70	0,000
Speed	1	1,1946	1,1946	4,97	0,061
Layer	1	48,6663	48,6663	202,48	0,000
Speed*Speed	1	4,6813	4,6813	19,48	0,003
Layer*Layer	1	0,9278	0,9278	3,86	0,090
Error	7	1,6825	0,2404		
Lack-of-Fit	4	0,9758	0,2439	1,04	0,509
Pure Error	3	0,7067	0,2356		
Total	11	57,1524			

The Pareto diagram, Fig. 9, arranges the coefficients according to their effect on the objective function from the largest to the smallest[18]. The diagram also draws a reference line to show where the statistical significance limit is. It can be seen that components B and AA pass the significance line, therefore they are significant, and the remaining A and BB are very close to it[19].

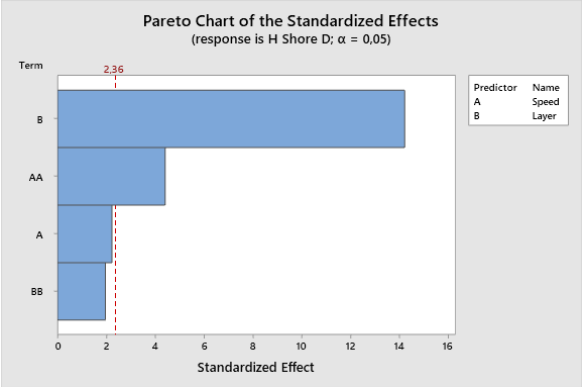

Fig. 9. Pareto chart

From fig.10. it is seen that all standardized residuals are in the interval ±2. The lower value of AD compared to the critical value and P-value ≥ α, confirm a normal probability distribution of the residuals[20]. Therefore, it can be concluded that the regression model is adequate and the null hypothesis can be rejected.

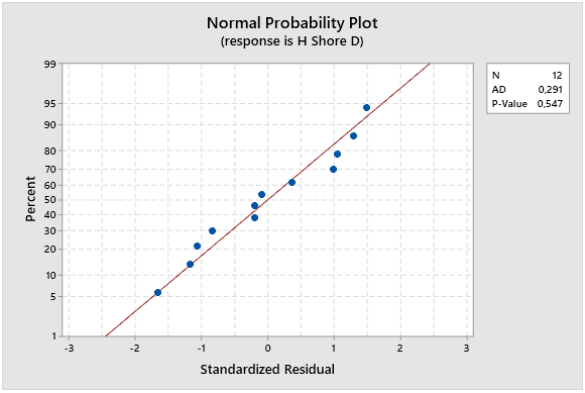

Fig. 10. Standardized residuals

From the diagram of the main effects, Fig. 11, it is seen that the greatest influence on the hardness is the printing layer[21].

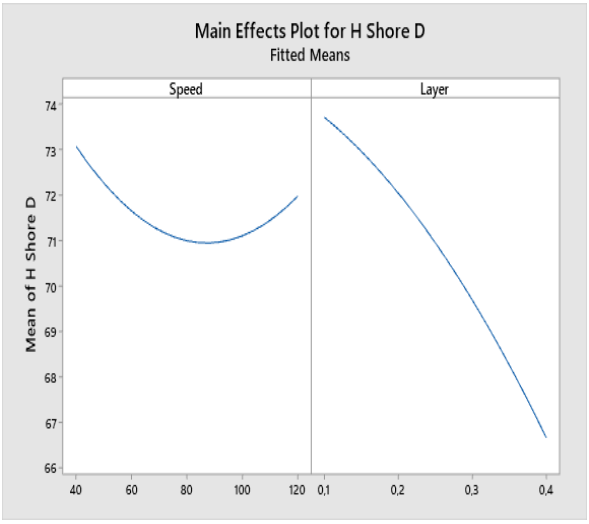

Fig. 11. Main effects plot for hardness Shore D

For technological reasons, a maximum hardness - H Shore D is sought, Table 11. A single-parameter optimization was performed and the maximum values for the objective function were found[22]. The printing modes for 4 values obtained from the hardness optimization are presented in Tables 12,13.

TABLE 11 PARAMETERS

Response	Goal	Lower	Target	Upper	Weight	Importance
H Shore D	Max	67,03	74,83		1	1

TABLE 12 SOLUTIONS

Solution	Speed	Layer	H Shore D Fit	Composite Desirability
1	40,000	0,1000	75,7870	1,00000
2	40,000	0,1618	74,8333	1,00000
3	54,029	0,1000	74,7138	0,98467
4	120,000	0,1000	74,6885	0,98143

TABLE 13 MULTIPLE RESPONSE PREDICTION

Variable	Setting
Speed	40
Layer	0,1

Response	Fit	SE Fit	95% CI	95% PI
H Shore D	75,787	0,543	(74,504; 77,070)	(74,058; 77,516)

The results obtained for the graphical optimization are presented in Fig. 12 at a speed of 40mm/s and a layer thickness of 0.1mm, obtaining a maximum hardness of 75.79 Shore D.

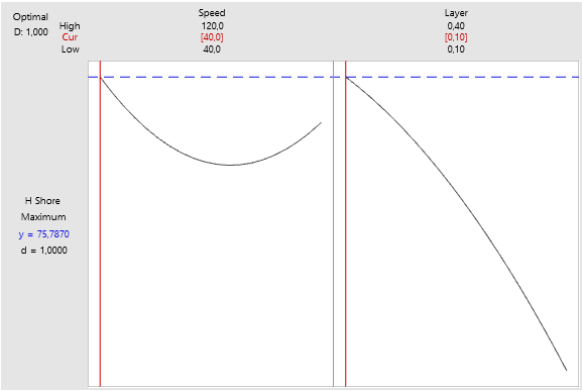

Fig. 12. Graphical presentation of the optimization

Fig. 13 presents a graph of the relationship between tensile strength and hardness.

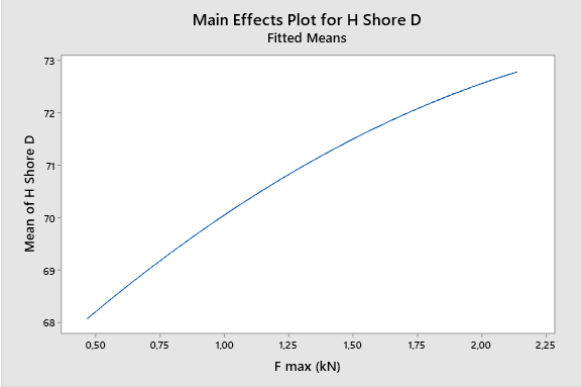

Fig. 13. Main effects plot for Hardness Shore D.

From the analysis of the experimental results, it can be concluded that the tensile strength and hardness decrease when the layer thickness increases. This is due to the higher density of defects[23]. Compared to experimental results of PLA, the decrease in strength characteristics is weaker[24]. Increasing the printing speed reduces the tensile strength because more defects are obtained due to impaired polymerization[25].

IV. CONCLUSIONS

1. From the research it may be concluded that the greatest influence on tensile strength is exerted by the printing speed factor.

2. The tensile strength of the sample is highest at low speed and small height between the layers of 3D printing.

3. From the optimization with obtained 95% probability is clear that at a printing speed of 40mm/s and a 0.13mm layer height, the strength of the sample will be into the confidence interval from 2.30 to 2.40kN.

4. The study of the hardness of the sample shows that only the layer height factor is relevant to the hardness. The printing speed factor can be ignored.

5. The hardness of the sample is highest at small heights of the printed layer.

6. From the optimization with 95% probability is observed that at a printing speed of 40mm/s and a 0.1mm layer height, the hardness of the sample will be into the selected confidence interval from 74.50 to 77.07 Shore.

7. Based on the above conclusions, we can conclude that 3D printing of the PetG material should be performed at the lowest possible printing speeds and the minimum possible height between the layers for maximum tensile strength and maximum hardness.

V. ACKNOWLEDGMENTS

This research was funded by the European Regional Development Fund within the OP " Research, Innovation and Digitalization Programme for Intelligent Transformation 2021-2027 ", Project CoC "Smart Mechatronics, Eco- and Energy Saving Systems and Technologies", No. BG16RFPR002-1.014-0005.

REFERENCES

[1] Y. Li, X. Li and D. Shen, "Existing 3D Printing Technologies", 2024. [Online]. Available: https://doi.org/10.1007/978-981-97-4094-9_2 (Accessed: January 10, 2025).

[2] Y. Xu, "Types and applications of 3D printing", Highlights in Science, Engineering and Technology, vol. 119, pp. 697–702, 2024. [Online]. Available: https://doi.org/10.54097/26ya9h57 (Accessed: January 10, 2025).

[3] M. Nerella, N. U. B. C. Prasad, M. P. Kumar and D. D. P. Reddy, "Performance Evaluation of Carbon Fiber Reinforced with Polyethylene Terephthalate Glycol (PETG) in Additive Manufacturing", E3S Web of Conferences, vol. 588, 2024. [Online]. Available: https://doi.org/10.1051/e3sconf/202458801014 (Accessed: January 10, 2025).

[4] M. Baltic, M. Filipovic, M. Vukcevic, J. Ignjatovic, M. Vujicic, M. Baltic and S. Vukcevic, "PETG as an Alternative Material for the Production of Drone Spare Parts", Polymers, vol. 16, p. 2976, 2024. [Online]. Available: https://doi.org/10.3390/polym16212976 (Accessed: January 10, 2025).

[5] M. Iwundu, "Construction of Modified Central Composite Designs for Non-standard Models", International Journal of Statistics and Probability, vol. 7, pp. 95–95, 2024. [Online]. Available: https://doi.org/10.5539/ijsp.v7n5p95 (Accessed: January 10, 2025).

[6] S. Arhamnamazi, S. B. Mahdavinejad, M. Golzar, M. Sadighzadeh and M. Vossoughi, "Application of Central Composite Design in the Drilling Process of Carbon Fiber-Reinforced Polymer Composite", Applied Sciences, vol. 14, p. 7610, 2024. [Online]. Available: https://doi.org/10.3390/app14177610 (Accessed: January 10, 2025).

[7] C. Ganapathi, S. Prasanna, M. M. Kumar and S. S. P. Raj, "A Study on Shore D Hardness of Areca Husk Fibre Reinforced Polyester Resin Composite: Impact of Fibre Maturity", Materials Science Forum, vol. 1111, pp. 83–88, 2023. [Online]. Available: https://doi.org/10.4028/p-inPOp0 (Accessed: January 10, 2025).

[8] E. Kanlı, A. Altun, C. Kocakulak and Y. Mert, "Effect of Dimensional Differences on Tensile Strength in Tensile Test Specimens", Gazi Journal of Engineering Sciences, vol. 10, pp. 619–631, 2024. [Online]. Available: https://doi.org/10.30855/gmbd.0705AR13 (Accessed: January 10, 2025).

[9] I. S. Nashrudin, Isywatuddiyanah and I. Muzaffar, "Calculation of Parameter Estimation for Two Means Using Minitab," 2024. [Online]. Available: https://doi.org/10.13140/RG.2.2.18935.94881 (Accessed: January 10, 2025).

[10] T. Runkler, "Regression," 2024. [Online]. Available: https://doi.org/10.1007/978-3-658-45951-2_6 (Accessed: January 10, 2025).

[11] N. Zhou, O. Blaha and D. Zelterman, "Distributions and Their Approximations for p-Values", 2024. [Online]. Available: https://doi.org/10.1007/978-3-031-65937-9_16 (Accessed: January 10, 2025).

[12] P. Lecca, "Regression and Variable Selection", 2024. [Online]. Available: https://doi.org/10.1007/978-3-031-74748-9_4 (Accessed: January 10, 2025).

[13] G. Zhao, M. Feng, S. Wang and Y. Xu, "ANOVA F Test of Non-Null Hypothesis", European Journal of Statistics, vol. 4, 2024. [Online]. Available: https://doi.org/10.28924/ada/stat.4.4 (Accessed: January 10, 2025).

[14] D. Funke, D. Hespe, P. Sanders, S. Storandt and C. Truschel, "Pareto Sums of Pareto Sets: Lower Bounds and Algorithms", 2024. [Online]. Available: https://doi.org/10.48550/arXiv.2409.10232 (Accessed: January 10, 2025).

[15] H. Coronel-Brizio, M. Hernández-Murillo and E. R. Hernández-Bautista, "Anderson-Darling and Watson tests for the geometric distribution with estimated probability of success", PLOS ONE, vol. 19, 2024. [Online]. Available: https://doi.org/10.1371/journal.pone.0315855 (Accessed: January 10, 2025).

[16] X. Qu, "Exact Moments of Residuals of Independence", Mathematics, vol. 12, p. 3987, 2024. [Online]. Available: https://doi.org/10.3390/math12243987 (Accessed: January 10, 2025).

[17] M. Finkelstein and B. Levin, "Regression Models", 2024. [Online]. Available: https://doi.org/10.1007/978-1-0716-4156-9_13 (Accessed: January 10, 2025).

[18] R. Ye, Z. Guo, Q. Liu and J. Wang, "Pareto Front Shape-Agnostic Pareto Set Learning in Multi-Objective Optimization", 2024. [Online]. Available: https://doi.org/10.48550/arXiv.2408.05778 (Accessed: January 10, 2025).

[19] A. W. Fodouop Kouam, "Assimilating Mediating and Moderating Variables in Academic Research: Role and Significance", International Journal of Research Publications, vol. 143, pp. 273–278, 2024. [Online]. Available: https://doi.org/10.47119/IJRP1001431220246119 (Accessed: January 10, 2025).

[20] Z. Chen and F. Yao, "Matrix Completion via Residual Spectral Matching", 2024. [Online]. Available: https://doi.org/10.48550/arXiv.2412.10005 (Accessed: January 10, 2025).

[21] C. Andiku, A. M. Tumuhairwe, R. E. Musoke and B. A. Asea, "Additive Main Effects and Multiplicative Interaction and Genotype Main Effect and Genotype by Environment Interaction Effects-Biplot Analysis of Sorghum Grain Yield in Uganda", Journal of Agricultural Science, vol. 12, pp. 98–98, 2024. [Online]. Available: https://doi.org/10.5539/jas.v12n6p98 (Accessed: January 10, 2025).

[22] C.-J. Shih and J.-J. Ding, "A Tutorial of Optimization", 2024. [Online]. Available: https://doi.org/10.13140/RG.2.2.24437.38889 (Accessed: January 10, 2025).

[23] D. Jovanić, E. Desnica and D. Malić, "The Influence of the Layer Height on the Hardness of the TPU Plastic Specimen Made by 3D Printing", pp. 77–83, 2024. [Online]. Available: https://doi.org/10.46793/IIZS24.077J (Accessed: January 10, 2025).

[24] S. Cahyati and Y. Furqon, "The Layer Height Variations Effect on Tensile Strength of 3D Printing Product PLA Material Based", Jurnal Rekayasa Mesin, vol. 13, pp. 647–657, 2022. [Online]. Available: https://doi.org/10.21776/jrm.v13i3.823 (Accessed: January 10, 2025).

[25] J. Loskot, M. Smieško, A. Nováková and J. Šoltés, "Influence of print speed on the microstructure, morphology, and mechanical properties of 3D-printed PETG products", Polymer Testing, vol. 123, 2023.

Environment. Technology. Resources. Rezekne, Latvia
Proceedings of the 16th International Scientific and Practical Conference. 2025. Volume IV, 37-44

Study about Influence of Printing Speed and Layer Height on Dimensional Accuracy of 3D Printed Carbon Fiber-Reinforced Polyamide Parts

Valeri Bakardzhiev
Technical University of Sofia, Branch Plovdiv, Bulgaria
bakardzhiev@tu-plovdiv.bg

Sabi Sabev
Technical University of Sofia, Branch Plovdiv, Bulgaria
sabi_sabev@tu-plovdiv.bg

Konstantin Chukalov
Technical University of Sofia, Branch Plovdiv, Bulgaria
chukalov@tu-plovdiv.bg

***Abstract*—In this article dimensional accuracy of 3D printed parts made of carbon fiber-reinforced polyamide was studied. For this purpose, 8 samples were produced in the shape of a rectangular prism with 2 types of holes - hexagonal and round through holes. The dimensional accuracy of the overall dimensions and the holes was studied. The data was processed statistically.**

Keywords— 3D print,dimensional accuracy

I. INTRODUCTION

In recent years, 3D printing has developed dramatically, as has field of its application. The technology is used in automotive, space technology, medicine, pharmacy, dental industry, etc[1],[2],[3]. The quality of the final product depends mainly on printing parameters[4]. In parallel with development of technology, more and more materials are used that are characterized by high accuracy and quality. Initially used for rapid prototyping, the technology is increasingly used for the production of engineering parts, tools, etc[5]. The use of 3D printing for highly responsible parts has increased requirements for the properties of the parts - mechanical, physical, etc[6]. Along with them, an important characteristic of 3D printed parts is their accuracy, especially for assembled large units[7]. Accuracy depends on both-used materials and the printing parameters. Dimensional accuracy in 3D printing is characterized by the deviation of the real part from the theoretical one, i.e. from the CAD model. An integral part of dimensional accuracy is the precision or repeatability of the obtained dimensions with a certain variation[8].

The most common materials for 3D printing are ABS, PLA, PETG, etc[9]. Carbon fiber reinforced plastics are extremely strong and lightweight materials.They may be considered as a very perspective material[10].

II. MATERIALS AND METHODS

Carbon fiber reinforced polyamide is a filament for 3D printing. It is characterized by high stiffness, heat resistance and adhesion. It is used for bearings and other machine elements.

The purpose of this study is to determine the accuracy of a dimensional chain in 3D printing with this material. It must be proven to what extent this material can be used for engineering tasks.

Preliminary planning was carried out using the Taguchi method in the following steps[11]:

1. Determining the goal or more precisely the target value (dimensional accuracy) for the process.

2. Determining the parameters of the experiment planning. Two factors were selected for this material. The first factor is the 3D printing speed, marked in the figures with the index X1, and the second factor is the height of the print layer, marked in the figures with the index X2. Levels were set within the permissible limits for the used 3D printer model Adventurer 5M Pro. Printing temperature is not included in the listed factors because the material requires a minimum extrusion temperature of 280ºC, which is the maximum for this model of 3D printer. The parameters used when printing the samples shown in Figure 1 are as follows:

Material: Polyamide PA6-CF Carbon

- Printing speed range: 10 - 100mm/s
- Extruder temperature range: 280ºC

Online ISSN 2256-070X
https://doi.org/10.17770/etr2025vol4.8411
© 2025 The Author(s). Published by RTU PRESS.
This is an open-access article under the Creative Commons Attribution 4.0 International License.

- Bad temperature: 105ºC
- Layer height range: 0.15 - 0.4mm
- Infill: 10%
- Number of wall layers: 2 pieces
- Flow: 83%

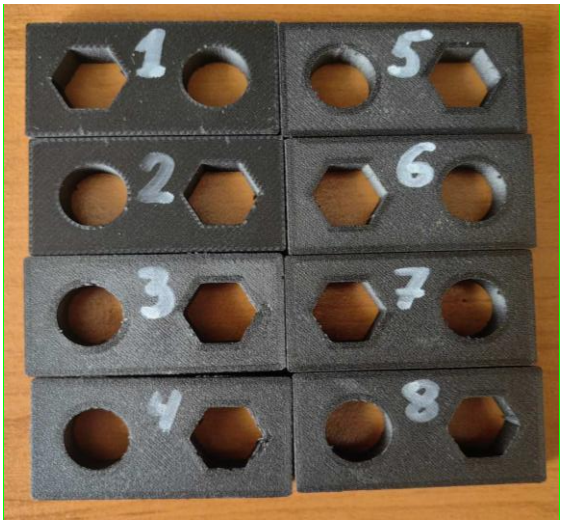

Fig. 1. Test spicemens.

3. Creating an orthogonal array showing the number and conditions for each experiment. Preliminary planning was performed in Minitab, and an orthogonal array was created as shown in Table 1.

TABLE 1 PRINTING PARAMETERS OF THE SAMPLES

Sample	Speed [mm/s]	Layer [mm]
1	10	0,15
2	10	0,15
3	10	0,4
4	10	0,4
5	100	0,15
6	100	0,15
7	100	0,4
8	100	0,4

4. Conducting the experiments specified in the completed orthogonal array and collecting data on the effect on the target. 8 samples of Polyamide PA6-CF were printed. Figure 2 shows a drawing of the sample with the designation of the control dimensions.

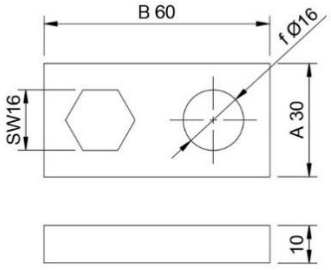

Fig. 2. Dimensions of the samples.

5. Measurement of the test specimens, using micrometres, with a resolution of 0.01 mm. The hole marked “f” with a size of φ16mm, the hexagonal SW with a size of 16mm, the small side of the specimen A with a size of 30mm and the long side of the specimen marked “B” with a size of 60mm were measured. The figures 3,4,5,6 show the measurement process

Fig. 3. Measurement of “f”.

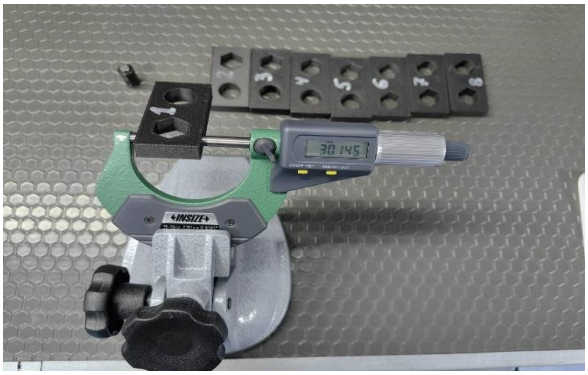

Fig. 4. Measurement of the hexagonal SW.

Fig. 5. Measurement of the dimension A.

Fig. 6. Measurement of the dimension B.

III. RESULTS AND DISCUSSION

The experimental results obtained from the measurement of the dimensions listed in the previous point are shown in table 2.

TABLE 2 EXPERIMENTAL RESULTS

№	Hole f, [mm]	Hexagonal SW [mm]	Size A [mm]	Size B [mm]
1	15,85	15,85	30,15	60,2
2	15,87	15,87	30,18	60,24
3	15,74	15,71	30,35	60,53
4	15,77	15,7	30,37	60,52
5	15,81	15,79	30,14	60,22
6	15,82	15,82	30,13	60,22
7	15,76	15,83	30,12	60,19
8	15,78	15,83	30,11	60,2

We have previously performed a variance statistical analysis to determine parameters.

Range in which the sample values vary :

$$R = Xi_{max} - Xi_{min} \qquad (1)$$

The standard deviation provides information about the deviation of the values in the sample from the arithmetic mean.:

$$S = \sqrt{\frac{\sum(X_i - \bar{X})^2}{n-1}} \qquad (2)$$

The coefficient of variation expresses the dispersion in percentages:

$$V = \frac{S}{\bar{X}} \cdot 100 \qquad (3)$$

From the obtained value of the coefficient of variation, we can say that the sample is relatively homogeneous.

The coefficient of asymmetry can be represented by the following equation[12]:

$$A_s = \frac{m_3}{S^3} \qquad (4)$$

Where:

S- the standard deviation;

m_3- the third central moment

$$m_3 = \frac{\sum(X_i - \bar{X})^3}{n} \qquad (5)$$

The coefficient of kurtosis is determined by the equation[13]:

$$E_x = \frac{m_4}{S^4} - 3 \qquad (6)$$

Where:

m_4- the fourth central moment

$$m_4 = \frac{\sum(X_i - \bar{X})^4}{n} \qquad (7)$$

We have graphically presented a diagram of the normal distribution of the hole measurement result in Figure 7.

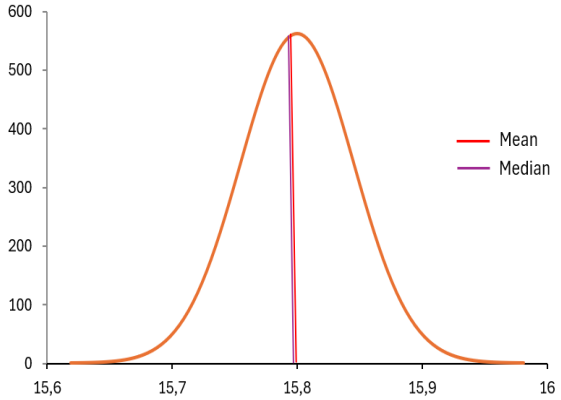

Fig. 7. Normal distribution of measured hole data.

The summary of the statistical approach is presented in tab.3

TABLE 3 STATISTICAL SUMMARY

Summary	Value
Mean	15,8
Standard Error	0,016
Median	15,80
Standard Deviation	0,045
Sample Variance	0,0021
Kurtosis	-1,10
Skewness	0,33
Range	0,13

Since the coefficient of variation is V=0.0021≤10 the sample is uniform. The distribution is symmetric about X the perpendicular, lowered to the abscissa at point , because the coefficient of asymmetry A_s=0.33. The distribution has a reduced kurtosis, because E_x=-1.1<0.

Results of the variational statistical analysis for the hexagonal hole SW 16mm.

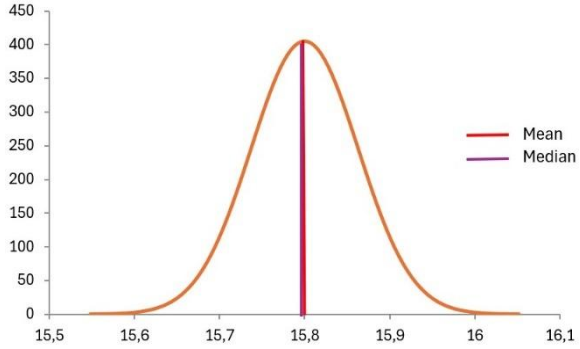

Fig. 8. Normal distribution of measured data for the hexagon.

In the statistical processing of the measured results of the hexagon, the coefficient of variation is V=0.0022≤10, the sample is uniform. The distribution is symmetric about the perpendicular, lowered to the abscissa at point $\bar{X}$, because the coefficient of asymmetry A_s=-0.6. The distribution has a reduced kurtosis, because E_x=-0.91<0.The statistical summary is shown in tab. 4

TABLE 4 STATISTICAL SUMMARY

Summary	Value
Mean	15,8
Standard Error	0,022
Median	15,83
Mode	15,83
Standard Deviation	0,0630
Sample Variance	0,0040
Kurtosis	-0,60
Skewness	-0,91
Range	0,17

Results of the statistical analysis of variance for the hexagon side A 30mm,fig 9,tab.5

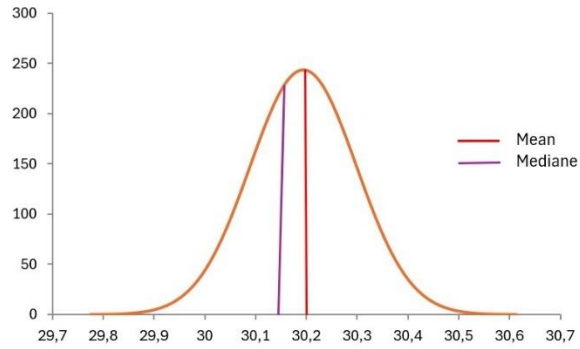

Fig. 9. Normal distribution of measured data for size A.

TABLE 5 STATISTICAL SUMMARY

Summary	Value
Mean	30,19
Standard Error	0,037
Median	30,15
Standard Deviation	0,10
Sample Variance	0,011
Kurtosis	-0,17
Skewness	1,29
Range	0,26

From the statistical analysis for the wall with size A we get, the coefficient of variation is V=0.0011≤10 therefore the sample is uniform. The distribution is asymmetric with a right-extended shoulder, because the coefficient of asymmetry A_s=1.29>0. The distribution has a normal kurtosis, because E_x=-0.17≤0.

Results of the statistical analysis of variation for the hexagonal side B 60mm, fig.10, tab.6

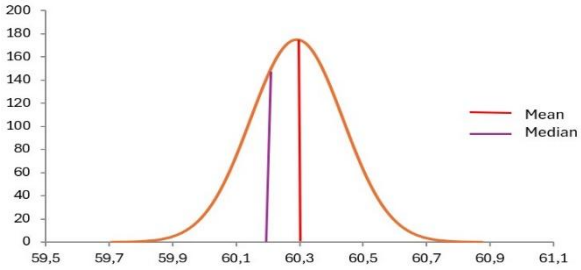

Fig. 10. Normal distribution of measured data for the dimension B

TABLE 6 STATISTICAL SUMMARY

Summary	Value
Mean	60,29
Standard Error	0,052
Median	60,22
Mode	60,2
Standard Deviation	0,15
Sample Variance	0,021
Kurtosis	-0,056
Skewness	1,39
Range	0,34

From the statistical analysis for the wall with size B we obtain, the coefficient of variation is V=0.0021≤10 therefore the sample is uniform. The distribution is asymmetric with a right-skewed shoulder, because the coefficient of asymmetry A_s=1.39>0. The distribution has a normal kurtosis, because Ex=-0.05≤0.

Although the above conclusions have been made, a regression single-factor statistical analysis must be

performed to determine how the factors affect the dimensions accuracy .

The experimental data from table. 2 were processed mathematically and statistically with the MINITAB software product. For the mathematical description of the target function, the following linear regression model was obtained, describing 4 regression equations for each dimension[14]:

$$Y_f = b_0 + b_1X_1 + b_2X_2 + b_3X_1X_2 \qquad (8)$$

TABLE 7 COEFFICIENTS OF FUNCTION "HOLE"

Term	Coef	SE Coef	95% CI	T-Value	P-Value
Constant	15.9320	0.0202	(15.8758; 15.9882)	787.20	0.000
Speed	-0.000900	0.000285	(-0.001691; -0.000109)	-3.16	0.034
Layer	-0.4467	0.0670	(-0.6327; -0.2606)	-6.67	0.003
Speed*Layer	0.002667	0.000943	(0.000049; 0.005284)	2.83	0.047

TABLE 8 COEFFICIENTS OF FUNCTION "HEXAGON"

Term	Coef	SE Coef	95% CI	T-Value	P-Value
Constant	15.9711	0.0178	(15.9216; 16.0207)	894.79	0.000
Speed	-0.001811	0.000251	(-0.002508; -0.001114)	-7.21	0.002
Layer	-0.7000	0.0591	(-0.8641; -0.5359)	-11.85	0.000
Speed*Layer	0.008000	0.000831	(0.005691; 0.010309)	9.62	0.001

Tab. 9 COEFFICIENTS OF DIMENSIONS OBJECTIVE FUNCTION

Term	Coef	SE Coef	95% CI	T-Value	P-Value
Constant	30.0370	0.0185	(29.9857; 30.0883)	1625.78	0.000
Speed	0.001100	0.000260	(0.000378; 0.001822)	4.23	0.013
Layer	0.8756	0.0612	(0.7057; 1.0454)	14.32	0.000
Speed*Layer	-0.009556	0.000861	(-0.011945; -0.007166)	-11.10	0.000

TABLE10 COEFFICIENTS OF FUNCTION DIMENSION "B"

Term	Coef	SE Coef	95% CI	T-Value	P-Value
Constant	60.0150	0.0202	(59.9588; 60.0712)	2965.34	0.000
Speed	0.002200	0.000285	(0.001409; 0.002991)	7.72	0.002
Layer	1.3667	0.0670	(1.1806; 1.5527)	20.40	0.000
Speed*Layer	-0.014667	0.000943	(-0.017284; -0.012049)	-15.56	0.000

Tables 7, 8, 9 and 10 present the coefficient values. We use the T-value to determine whether the coefficients are significant. However, the P-value is used more often, since the threshold for rejecting the null hypothesis does not depend on the degrees of freedom. In our case, the P-value for each coefficient is lower than 0.05, so we can reject the null hypothesis. The coefficients of all 4 regression models are statistically significant.

TABLE11 SUMMARY MODEL OF HOLE

S	R-sq	R-sq(adj)	PRESS	R-sq(pred)
0.015	93.75%	89.06%	0.0036	75.00%

TABLE 12 SUMMARY MODEL OF HEXAGON

S	R-sq	R-sq(adj)	PRESS	R-sq(pred)
0.0132288	97.48%	95.59%	0.0028	89.93%

TABLE13 SUMMARY MODEL OF "A"

S	R-sq	R-sq(adj)	PRESS	R-sq(pred)
0.0136931	99.03%	98.30%	0.003	96.10%

TABLE 14 SUMMARY MODEL OF "B"

S	R-sq	R-sq(adj)	PRESS	R-sq(pred)
0.015	99.40%	98.94%	0.0036	97.58%

From Tables 11 to 15 we can conclude about the coefficient of determination. For the 4 regression equations the coefficient is over 90%. Therefore, over 90% of the values of the model factors directly affect the regression models.

TABLE 16 ANALYSIS OF VARIANCE HOLE

Source	DF	Seq SS	F-Value	P-Value
Regression	3	0.013500	20.00	0.007
Speed	1	0.000450	9.99	0.034
Layer	1	0.011250	44.45	0.003
Speed*Layer	1	0.001800	8.00	0.047
Error	4	0.000900		
Total	7	0.014400		

TABLE 17 ANALYSIS OF VARIANCE HEXAGON

Source	DF	Seq SS	F-Value	P-Value
Regression	3	0.027100	51.62	0.001
Speed	1	0.002450	51.99	0.002
Layer	1	0.008450	140.35	0.000
Speed*Layer	1	0.016200	92.57	0.001
Error	4	0.000700		
Total	7	0.027800		

TABLE 18 ANALYSIS OF VARIANCE DIMENSION A

Source	DF	Seq SS	F-Value	P-Value
Regression	3	0.076238	135.53	0.000
Speed	1	0.037813	17.90	0.013
Layer	1	0.015313	204.93	0.000
Speed*Layer	1	0.023113	123.27	0.000
Error	4	0.000750		
Total	7	0.076988		

TABLE 19 ANALYSIS OF VARIANCE DIMENSION B

Source	DF	Seq SS	F-Value	P-Value
Regression	3	0.148100	219.41	0.000

Speed	1	0.054450	59.67	0.002
Layer	1	0.039200	416.09	0.000
Speed*Layer	1	0.054450	242.00	0.000
Error	4	0.000900		
Total	7	0.149000		

From Tables 16 to 19 we can conclude about the coefficient of determination. For the 4 regression equations the coefficient is over 90%. Therefore, over 90% of the values of the model factors directly affect the regression models.

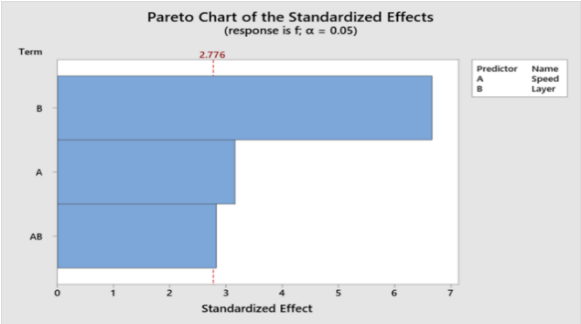

Fig. 11. Pareto diagram hole.

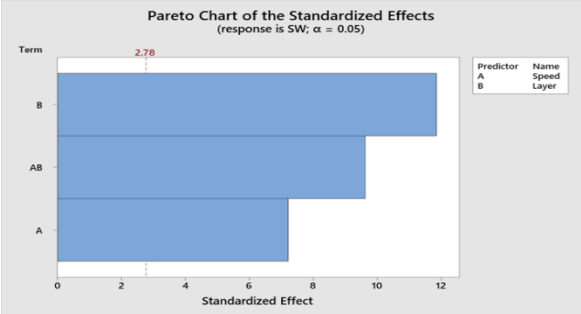

Fig. 12. Pareto diagram hexagon.

The Pareto diagram, Fig. 11 to 14, arranges the coefficients according to their effect on the target function from the largest to the smallest. The diagram also draws a reference line to show where the limit of statistical significance is. It can be seen that the components pass the significance line, therefore they are significant [15].

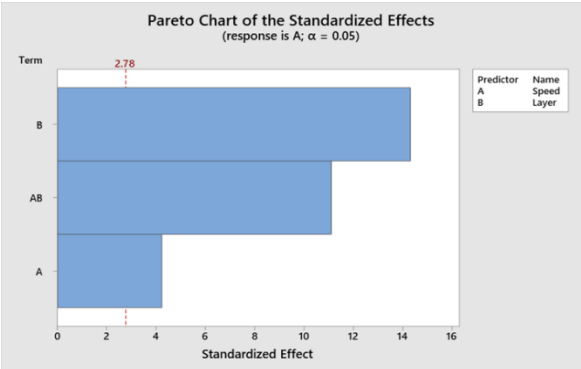

Fig. 13. Pareto diagram of size A.

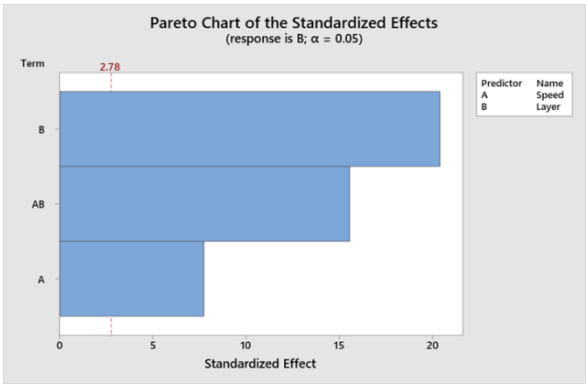

Fig. 14. Pareto diagram of size B.

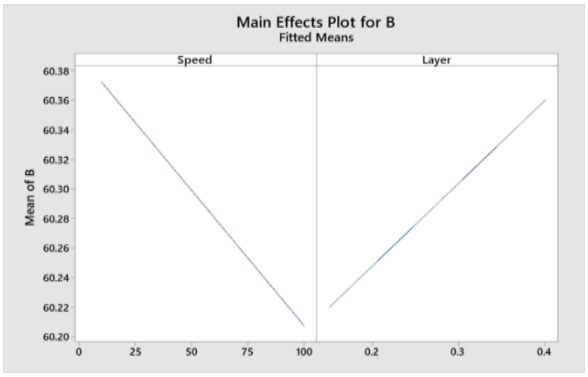

Fig. 15. Main plot "B"

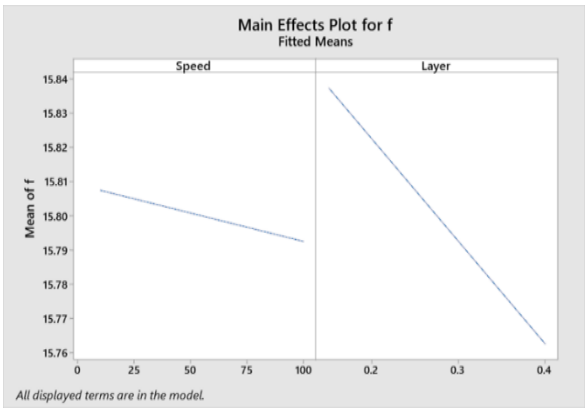

Fig. 16. Main plot f.

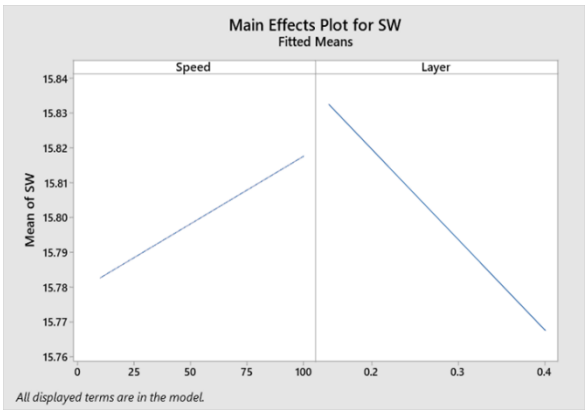

Fig. 17. Main plot SW.

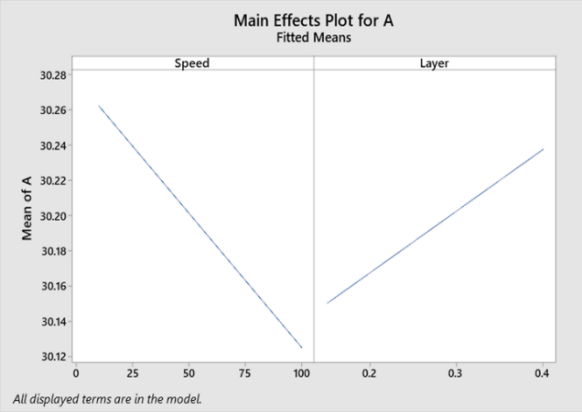

Fig. 18. Main plot A.

Figures 15-18 show the graphs of the influence between each of the factors against the regression equation.

We can explain the different slope in Figure 15 and 16 by the fact that the dimensions are rotational, when printing the size increases towards the inside of the hole and the hexagon, that is, the size decreases. For the outer dimensions, the tension is reversed.

An optimization was performed as shown in Table 16. Based on a preliminary analysis of the experimental results, we have set a certain interval for each of the dimensions

TABLE 16. POSSIBLE SOLUTION

Solution	Speed	Layer	**B Fit**	**A Fit**	**SW Fit**	**f Fit**	**Composite Desirability**
1	100	0.15	60.1375	30.0813	15.85	15.83	0.562381

Variable	**Setting**
Speed	100
Layer	0.15

Response	**Fit**	**SE Fit**	**95% CI**	**95% PI**
B	60.1375	0.0644	(59.9719; 60.3031)	(59.8204; 60.4546)
A	30.0813	0.0423	(29.9725; 30.1900)	(29.8730; 30.2895)
SW	15.8500	0.0356	(15.7585; 15.9415)	(15.6748; 16.0252)
F	15.8300	0.0142	(15.7934; 15.8666)	(15.7600; 15.9000)

From the analysis of the results and statistical work, the optimal option is a low printing speed and low filament thickness, tab.16 High filament thicknesses lead to lower density and greater deviation from dimensional accuracy[16].

The greatest influence on dimensional accuracy is the printing speed, since the printing speed affects the flow of liquid filament[17].

IV. Conclusions

From the obtained results the following conclusions are determined:

1. From the research we can conclude that the greatest influence on the accuracy of the size is the printing speed.

2. The performed variation analysis shows a 95% probability that the size tolerance varies in the range from 0.13 to 0.34mm

3. From the optimization we can say with a 95% probability that at a printing speed of 100mm/s and 0.15mm the samples have the highest size accuracy.

4. The accuracy of the sample dimensions is greatest at small print layer heights and low speeds.

5. The resulting regression model and the subsequent optimization we can say with a 95% probability that at a printing speed of 100mm/s and 0.15mm layer height the accuracy of the sample dimensions will be in the confidence interval for the hole from 15.79 to 15.87; for the hexagon from 15.76 to 15.94; for size A from 29.97 to 30.19 and for size B from 59.97 to 60.30mm.

7. Based on the above conclusions, we can conclude that 3D printing of PA6-CF material should be performed at the lowest possible printing speeds and the minimum possible layer height..

V. ACKNOWLEDGMENTS

This research was funded by the European Regional Development Fund within the OP " Research, Innovation and Digitalization Programme for Intelligent Transformation 2021-2027 ", Project CoC "Smart Mechatronics, Eco- and Energy Saving Systems and Technologies", No. BG16RFPR002-1.014-0005.

REFERENCES

[1] "Pharmacy 3D printing," Biofabrication, vol. 17, 2024. [Online]. Available: https://doi.org/10.1088/1758-5090/ad837a, [Accessed: January 10, 2025].

[2] Y. Xu, "Types and applications of 3D printing," Highlights in Science, Engineering and Technology, vol. 119, pp. 697–702, 2024. [Online]. Available: https://doi.org/10.54097/26ya9h57 , [Accessed: January 10, 2025].

[3] D. Serrano, S. Sánchez, B. Ongoren, I. Yuste, B. Anaya, F. Luciano and A. Kara, "3D printing in personalized medicine," 2024.

[4] H. Mahajan, O. Gule and A. Malpure, "Design and Optimization of 3D Printing Process Parameters," 2024.

[5] M. A. Petrov and T. D. Hung, "Application of 3D-Printing Technologies in Manufacturing of Tools for Microforming of Sheet Metal Blanks," pp. 411–417, 2024. [Online]. Available: https://doi.org/10.25206/978-5-8149-3873-2-2024-411-417, [Accessed: January 10, 2025].

[6] M. A. Rahman, L. Gibbon, M. Z. Islam, E. Hall and C. Ulven, "Adjustment of Mechanical Properties of 3D Printed Continuous Carbon Fiber-Reinforced Thermoset Composites by Print Parameter Adjustments", Polymers, vol. 16, p. 2996, 2024. [Online]. Available: https://doi.org/10.3390/polym16212996, [Accessed: January 10, 2025].

[7] M. Alghauli, S. Almuzaini, R. Aljohani and A. Alqutaibi, "Influence of 3D printing orientations on physico-mechanical properties and accuracy of additively manufactured dental ceramics", Journal of Prosthodontic Research, 2025. [Online]. Available: https://doi.org/10.2186/jpr.JPR_D_24_00092 , [Accessed: January 10, 2025].

[8] A. C. Murariu, A. Sirbu, M. Cocard and I. Duma, "Influence of 3D Printing Parameters on Mechanical Properties of the PLA Parts Made by FDM Additive Manufacturing Process," Engineering

Innovations, vol. 2, pp. 7–20, 2022. [Online]. Available: https://doi.org/10.4028/p-4isiu8, [Accessed: January 10, 2025].

[9] S. O. Eteje, C. Ifuwe and O. Olujimi, "Precision and Accuracy Determination of Horizontal Geodetic Networks Using Least Squares Technique," Caliphate Journal of Science and Technology, vol. 6, pp. 265–272, 2024. [Online]. Available: https://doi.org/10.4314/cajost.v6i3.3, [Accessed: January 10, 2025].

[10] P. Liacouras, E. Huo and D. Mitsouras, "3D Printing Technologies and Materials," 2024. [Online]. Available: https://doi.org/10.1007/978-3-031-42851-7_4, [Accessed: January 10, 2025].

[11] J. Liu, L. He, D. Yang, J. Liang, R. Zhao, Z. Wang, X. Li and Z. Chen, "Effects of Carbon Fiber Content on the Crystallization and Rheological Properties of Carbon Fiber-Reinforced Polyamide 6,", Polymers, vol. 16, p. 2395, 2024. [Online]. Available: https://doi.org/10.3390/polym16172395 , [Accessed: January 10, 2025].

[12] M. Hisam, A. Dar, M. Elrasheed, M. Khan, R. Gera and I. Azad, "The Versatility of the Taguchi Method: Optimizing Experiments Across Diverse Disciplines", Journal of Statistical Theory and Applications, vol. 23, 2024. [Online]. Available: https://doi.org/10.1007/s44199-024-00093-9, [Accessed: January 10, 2025].

[13] A. Aceña Rodríguez, "Prediction of Injuries in Elite Soccer Players with the Analysis of Asymmetries in the CMJ through the use of Machine Learning tools," 2024.

[14] L. Merabet, L. Boucerredj, M. Behim and K. Abderrahmane, "Comparative study of kurtosis and L-kurtosis for bearing fault classification in induction motors," Studies in Engineering and Exact Sciences, vol. 5, e12489, 2024. [Online]. Available: https://doi.org/10.54021/seesv5n3-035, [Accessed: January 10, 2025].

[15] Y. Geng, Q. Li, G. Yang and W. Qiu, "Linear Regression," 2024. [Online]. Available: https://doi.org/10.1007/978-981-97-3954-7_3, [Accessed: January 10, 2025].

[16] D. Funke, D. Hespe, P. Sanders, S. Storandt and C. Truschel, "Pareto Sums of Pareto Sets: Lower Bounds and Algorithms," 2024. [Online]. Available: https://doi.org/10.48550/arXiv.2409.10232, [Accessed: January 10, 2025].

[17] K. M. Agarwal, P. Shubham, D. Bhatia, P. Sharma, H. Vaid and R. Vajpeyi, "Analyzing the Impact of Print Parameters on Dimensional Variation of ABS specimens printed using Fused Deposition Modelling (FDM)", Sensors International, 2022.

[18] A. Solouki, M. R. M. Aliha, A. Makui, M. Choupani and H. Seiti, "Analyzing the effects of printing parameters to minimize the dimensional deviation of polylactic acid parts by applying three different decision-making approaches,", Scientific Reports, vol. 14, article 2767, 2024.

Environment. Technology. Resources. Rezekne, Latvia
Proceedings of the 16th International Scientific and Practical Conference. 2025. Volume IV, 45-51

Industry 4.0: Implementation of Digital Technologies to Improve Production and Economic Efficiency

Iryna Bohashko
Department of germanic languages
Dragomanov Ukrainian State University
Kyiv, Ukraine
23fif.i.bohashko@std.udu.edu.ua

Oleksandr Bohashko
Department of marketing, management and business management
Pavlo Tychyna Uman State Pedagogical University
Uman, Ukraine
bogashko@ukr.net

Inna Kosmidailo
Department of management, finance and information technology
Private Higher Education Establishment «European University»
Kyiv, Ukraine
inna.kosmidailo@e-u.edu.ua

Abstract- **The paper investigates the relationship between Industry 4.0 technologies and the competitiveness of manufacturing enterprises. Industry 4.0, which integrates digital technologies such as artificial intelligence, big data, robotics, and the Internet of Things, is transforming production processes and business models, fostering innovation, and enhancing global competitiveness. The study aims to explore how these technologies influence manufacturing efficiency, flexibility, and product quality, and to identify the main motivations and barriers faced by companies in adopting Industry 4.0 technologies. The research employs several methodologies: systematic literature review - to summarize existing research on Industry 4.0 and its impact on competitiveness, identifying key innovations and trends in manufacturing; bibliometric analysis - analysing scientific publications to map the research landscape, identify influential works, and discern key technological trends in Industry 4.0; survey method - a survey of 100 Ukrainian manufacturing enterprises was conducted to assess the main motivations and barriers for adopting Industry 4.0 technologies. The results show that Industry 4.0 allows companies to significantly improve productivity, reduce costs and adapt to changing market conditions. However, the introduction of new technologies is accompanied by a number of risks, including economic, technical problems, including high initial investments, cyber security, and the need for new skills of employees. The challenges associated with the introduction of these technologies, including financial, technical and organisational costs, as well as problems associated with resistance to change, are considered. The reasons for this resistance are analysed, including personal interests of employees, distrust and uncertainty. Effective methods of managing resistance to change, such as communication, training and active participation of employees in the change process, are proposed. The importance of clear communication, support and skills development for successful technology adoption is emphasised.**

Key words- Automation, Digital transformation, Innovation management, Industry 4.0, Production processes, Productivity, Resource savings,.

I. Introduction

In the context of globalisation and rapid technological change, the modern economy is undergoing a period of transformation, the main feature of which is the rapid development of the latest technologies. Industry 4.0, or the Fourth Industrial Revolution, is the undisputed leader among these changes, as it changes not only production processes but also the way of doing business and creating competitive advantages in global markets. Industry 4.0 technologies, such as automation, artificial intelligence, the Internet of Things, big data and robotics, have a huge potential to increase production efficiency, reduce costs and accelerate time-to-market for new products.

Industry 4.0 has a significant impact on the competitiveness of manufacturing companies, especially in the innovation economy, where technology and innovation have become the main drivers of economic growth. Therefore, the study of the relationship between Industry 4.0 and the competitiveness of companies is extremely important for modern enterprises.

II. Materials and Methods

A variety of methods and materials were used in the course of researching the topic to achieve objective and reliable results.

Online ISSN 2256-070X
https://doi.org/10.17770/etr2025vol4.8460
© 2025 The Author(s). Published by RTU PRESS.
This is an open access article under the Creative Commons Attribution 4.0 International License.

Systematic literature review - this method allows for a detailed analysis of existing research on Industry 4.0, its impact on the competitiveness of enterprises, as well as current innovations within manufacturing companies. It involves the study of articles, books, reports, papers and other publications to systemise and summarise knowledge on the topic. The main stages of a systematic literature review are: identifying the topic and formulating research questions, searching for and selecting publications, analysing and synthesising the data obtained; structuring and summarising knowledge; writing conclusions and practical recommendations for businesses on the implementation of Industry 4.0 technologies.

Bibliometric analysis is a method that combines bibliometric and computational tools to analyse scientific publications. This allows for the estimation of the number of publications on Industry 4.0, identification of the main research areas, key scientific works, and influential authors in this field, as well as the identification of the main trends in the development of technologies in the innovation economy. The main stages of bibliometric analysis include data collection, data processing and analysis, and interpretation of the results. Bibliometrics enables the coverage of a large volume of scientific publications, which makes it possible to draw more accurate conclusions about important trends in the development of technologies and scientific approaches in the field of Industry 4.0.

The survey method is one of the main tools for collecting data in scientific research, in particular in the study of Industry 4.0. During a survey, respondents (the target audience) fill out questionnaires or questionnaires. Surveys in our research can help us find out how representatives of different companies feel about the concept of Industry 4.0, what benefits and challenges they see in implementing these technologies. Questionnaires allow us to interview a large number of respondents, which makes it possible to obtain representative data.

Research materials: scientific publications - articles from scientific journals, books, conference reports describing the theoretical and practical aspects of Industry 4.0; reports of international organisations analysing the implementation of Industry 4.0 technologies in different countries; publications and information from open sources - statistics, materials from company websites, as well as media interviews covering the implementation of Industry 4.0 at enterprises, results of a survey of enterprises.

The use of these methods and materials allows us to form a comprehensive view of the impact of Industry 4.0 on the competitiveness of enterprises and determine how innovative technologies are changing the structure and efficiency of manufacturing companies in the modern economy.

III. Results and discussion

Industry 4.0 (I4) is defined as the use of digital technologies to integrate production processes, enabling greater flexibility, automation and intelligent solutions. It is based on technologies such as:

- *Internet of Things (IoT)*. This is a technology that allows various devices to connect to the Internet and exchange data in real time. It makes it possible to monitor and control production processes remotely, improving efficiency.

- *Artificial intelligence (AI)* and machine learning. AI is used to analyse large amounts of data, predict and optimise production processes. With machine learning, companies can improve their strategies based on automated recommendations.

- *Big data.* Huge volumes of data generated during production processes can be used to make decisions, optimise workflows, and forecast market needs.

- *Robotics.* The use of robots to automate physical tasks in production can improve accuracy, reduce human error, and cut costs.

- *3D printing.* A technology that allows for rapid prototyping of products, which reduces the time and cost of their development [1].

The integration of these technologies into production processes allows companies to significantly increase productivity, product quality and adaptability to changing market conditions.

The innovation economy is an economy that is based on the use of innovative technologies to increase productivity, create new goods and services, and attract new investment. It relies on knowledge, research and development, and the ability of businesses to adapt to rapid change.

Industry 4.0 is one of the key factors driving the development of the innovation economy. Thanks to I4 technologies, businesses can significantly improve their efficiency and create competitive advantages. The competitiveness of an enterprise is its ability to successfully compete in the market, ensuring sustainable growth and profitability. In an innovative economy, companies must constantly introduce new technologies to maintain and increase their market share.

Industry 4.0 is already being actively implemented in various manufacturing sectors. For example, robotic car assembly lines are widely used in the automotive industry, and automated systems for product testing and quality control are used in electronics. In pharmaceuticals, big data is used to forecast demand for medicines and analyse market trends.

Scientists have developed a model [2] based on the literature on organisational motivation, resources/capabilities, and technology acceptance, as shown in Figure 1. The main part of the model examines the influence of external/reactive motives (pressure from competitors, suppliers and customers) and internal/proactive motives (efficiency and expected competitive advantage) on the intention to use I4

technologies, as well as the influence of the latter on the actual use of I4 technologies.

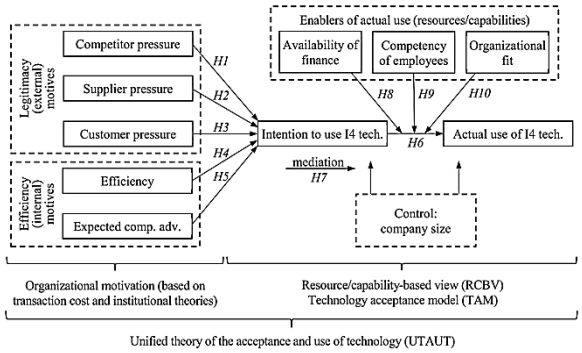

Fig. 1. Model of motivation for organisations to implement Industry 4.0 technologies.

Source: [2]

This study identifies five main groups of motivations for the adoption of I4 technologies: competitor pressure, supplier pressure, consumer pressure, efficiency and expected competitive advantage.

The first three categories - competitor pressure, supplier pressure, consumer pressure - are considered external motivations, as they arise under the influence of external factors, such as changes in the market or consumer needs. At the same time, the last two motives - efficiency and expected competitive advantage - are internal, as their main goal is to improve internal processes and achieve the company's strategic goals. Pressure from competitors, suppliers and consumers can be seen as reactive motives that encourage companies to change under the influence of the external environment. Instead, the desire for efficiency and competitive advantage are defined as proactive motives that focus on internal improvement and achievement of long-term strategic goals [2].

Industry 4.0 offers a wide range of the latest technologies for the digitalisation of business processes, including automation, the Internet of Things, artificial intelligence and big data, which are significantly transforming modern production and management [1]. The introduction of I4 technologies can significantly increase productivity and reduce costs, improve production quality and end-user convenience, as well as increase process transparency and create more sustainable business models. By integrating digital and physical systems, companies can achieve significant improvements in resource savings and develop more flexible organisational structures [4].

The introduction of I4 technologies is accompanied by a number of positive aspects, as illustrated in Figure 2, developed by the authors.

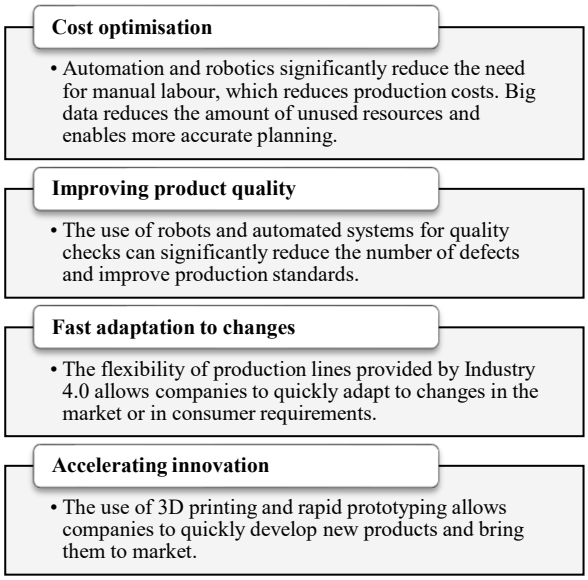

Fig. 2. The role of Industry 4.0 in improving the competitiveness of enterprises.

Efficiency motivations are the basis for the adoption of new technologies in organisations, as process efficiency gains are an important factor in making such decisions [3]. Rationalistic approaches to technology adoption are considered important as organisations expect significant productivity gains, cost reductions and improved performance through innovation. The motivation for technology adoption is based on the desire to improve the overall performance of the company, which is becoming an important factor in ensuring its competitiveness in the context of digital transformation.

On the other hand, the introduction of I4 technologies creates new challenges for organisations. In particular, there are difficulties in ensuring cyber security and data protection, organising new work processes, and adapting staff to new conditions [5]. The need for new skills and qualifications of employees, as well as the creation of an effective infrastructure for digital technologies, are urgent issues that need to be addressed to ensure the successful integration of new solutions. The problems of standardisation and integration of different technologies also remain significant on the way to the full realisation of the potential of I4 [2].

Thus, while the benefits of I4 technologies are clear, organisations must be prepared for the new challenges that arise on the way to their implementation, which includes not only technical but also organisational and human factors that determine the success of digital transformations.

Industry 4.0, or the Fourth Industrial Revolution, is characterised by the integration of digital technologies into production processes, which ensures automation, increased efficiency and flexibility of production. However, the introduction of these technologies is accompanied by a number of risks and challenges that

may affect the success of the transformation of enterprises, as shown by the authors in Table 1.

TABLE 1 RISKS OF IMPLEMENTING INDUSTRY 4.0 TECHNOLOGIES

Type of risk	Risk description
High initial investment	Implementing I4 requires significant financial investments in the latest technologies, which can be burdensome for SMEs.
Uncertainty of economic benefits	Businesses may not have a clear idea of the potential economic benefits of I4, which can lead to excessive investment without a guaranteed return.
Replacement of jobs	Automation and the use of robots may lead to job losses, especially for low-skilled workers, causing social tensions.
Growing gender inequality	The introduction of new technologies may increase gender inequalities, as women are less represented in industries related to I4.
Lack of regulation and standards	An insufficient regulatory framework and lack of common standards can complicate the implementation of I4 and create legal uncertainty for businesses.
Cybersecurity issues	The increase in the number of connected devices and systems increases the risk of cyber-attacks, which can lead to data loss, financial loss and damage to the company's reputation.
Insufficient staff qualifications	Lack of necessary skills and knowledge among employees can complicate the digitalisation process and reduce the effectiveness of new technologies.
Resistance to change	Resistance to change from employees and management can delay or complicate the transformation process.
Integration of new technologies	The difficulty of integrating new digital technologies with existing systems can lead to technical problems and disruptions in production processes.
Dependence on technology providers	Businesses can become dependent on technology providers, which can limit their flexibility.
Increase in e-waste	The rapid development of technology can lead to an increase in the amount of e-waste, which requires effective disposal and recycling systems.
Energy consumption	The use of new technologies can increase energy consumption, which requires the development of efficient and sustainable energy solutions.

Thus, the implementation of I4 is a complex and multifaceted process, accompanied by numerous risks and challenges. For a successful transformation, businesses need to develop risk management strategies, invest in staff development, ensure cyber security, and adapt their organisational structure to new requirements. It is also important to cooperate with government agencies to develop an appropriate regulatory framework and standards that will facilitate the effective implementation of I4.

Given the risks and opportunities that accompany the introduction of new technologies, it is necessary to better understand the main driving forces that determine their integration and use in organisations. Based on studies such as [6], it can be argued that a company's openness to I4 can be measured by two parameters: breadth (the number of technologies integrated into production processes) and depth (the number of stages at which these technologies are used).

Industry 4.0 technologies require deeper scientific expertise and closer integration into the operational structures of companies [2].

The main characteristics of such technologies are interaction through wireless networks, assistance in decision-making at all levels, and strong interdependence between different technological elements. As a result, machines, devices, sensors, and people can interact in real time, creating transparency and allowing participants to access information instantly and make decentralised decisions. In such environments, humans are supported by technology to perform physical and intellectual tasks, while robots perform complex or hazardous operations, thereby reducing health risks and increasing efficiency [7].

At the same time, the integration of I4 involves significant financial, technical and organisational costs, requiring companies to take a strategic approach to planning and adaptation. Thus, the adoption of such technologies should be justified, taking into account not only potential benefits but also possible risks and challenges on the way to implementation.

Industry 4.0 is focused on the integration of digital technologies that fundamentally change the way organisations create value. At the same time, a key feature is the deep interaction between the physical and virtual worlds, which allows for the creation of new business models and optimisation of production processes. Although the technologies underpinning I4 are technocentric, focusing on innovation and technological advancement, their interconnected nature indicates that their potential can only be maximised in the context of inter-organisational value chains, not within individual enterprises [8].

The most important aspects of I4 are the application of technologies that offer a new operating paradigm for industry. They can significantly increase efficiency and productivity, which, in turn, contributes to the creation of so-called ‘smart factories’ through the digitalisation and automation of production processes. Industry 4.0 is based on the principles of integration, decentralisation of decisions, information transparency and technical support at every stage of production [9].

The changes caused by the implementation of the I4 concept should have a positive impact on the competitiveness of enterprises; increase the flexibility of production processes, which generally contributes to the improvement of companies' market positions through increased efficiency.

Based on the results of a survey of 100 Ukrainian industrial enterprises, we assessed the main motivations that encourage companies to implement the I4 concept. The main results of the survey are shown in Figure 3.

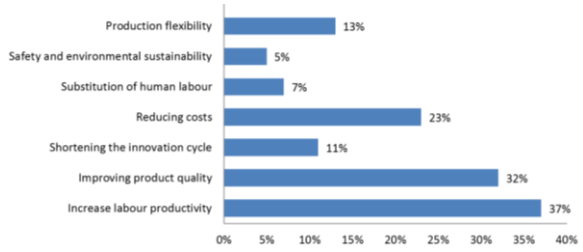

Fig. 3. Motives that encourage companies to implement the Industry 4.0 concept.

As can be seen from Figure 3, the main factors contributing to the implementation of I4 elements in organisations are visualised, with the most common factors for implementing the I4 concept being increase labour productivity, improving product quality, reducing costs, production flexibility and shortening the innovation cycle.

We have already shown that Industry 4.0 offers tremendous benefits for businesses that have managed to implement and adapt the latest technologies into their daily operational processes. But there is always a downside when companies fail to implement Industry 4.0 technologies in their business. We conducted a survey among 100 industrial enterprises in Ukraine to investigate the main barriers to digital transformation. The survey results are shown in Table 2.

TABLE 2 THE MAIN BARRIERS TO THE IMPLEMENTATION OF INDUSTRY 4.0 IN THE PRACTICE OF INDUSTRIAL ENTERPRISES

Main barriers	Disagree	Neutral	Agree
Resistance to change	21%	24%	55%
Lack of qualified personnel	23%	26%	51%
High initial investment	19%	39%	42%
Poor quality of management	17%	33%	50%
Cybersecurity and data risks	42%	27%	31%

The table shows that the majority of respondents consider the factor 'Resistance to change' (55%) to be an important obstacle to the implementation of Industry 4.0 benefits. This is the highest figure among the other reasons. However, there are also significant barriers, such as 'Lack of qualified personnel' (51%) and 'Poor quality of management' (50%), which also hinder digital transformation.

However, despite the potential of I4 technologies, their successful implementation at the industrial level requires consideration of soft factors such as organizational strategies, company structure, corporate culture, and workforce training during the transition to the I4 era [10].

However, even when change appears to be 'rational' or 'positive', it always carries with it an element of uncertainty that can cause emotional discomfort among employees and those involved in the change process. Uncertainty often causes resistance to change, which is a natural human reaction to the loss of stability and the desire to maintain the status quo. When faced with uncertainty, people often try to avoid change, as it allows them to maintain a sense of control and security in the face of new challenges [9].

Kotter and Schlesinger identify four main reasons for resistance to change: personal interests, misunderstanding or lack of trust, different assessments of the situation, and low tolerance for change. According to them, people often resist when they believe that they may lose something that is important to them; when they do not trust those who are implementing the changes; when they do not understand the reasons for the changes and do not believe in their ability to adapt to new conditions. According to other research, resistance can also be the result of uncertainty or fear of future change [11].

However, resistance is not always a purely negative reaction to change. Resistance can be a tool for identifying shortcomings in change plans or information provided, giving the organisation the opportunity to adjust strategies to achieve better results. As a result, the proper management of resistance can lead to significant organisational gains, as it helps to identify weaknesses in the change process.

Thus, effective management strategies, including communication, employee participation in the change process, as well as training and negotiation, contribute to a smoother implementation of the change and increase employee acceptance. As a result, these strategies help to reduce the level of resistance and ensure the successful transition of the organization through the change.

In this context, it is important to consider different approaches to dealing with employee resistance when implementing I4 technologies. Since the implementation of such technologies is often accompanied by significant changes in organizational processes, it is necessary to consider strategies that minimize resistance and ensure the successful adaptation of employees to new conditions. The following will analyse the main methods of managing resistance, in particular through effective communication, employee participation in the change process and providing clear explanations for the implementation of new technologies.

1. Communication. Communication is a key aspect in the process of digital transformation of organizations. Satisfactory communication allows for a positive perception of changes among employees by explaining to them the benefits of the implemented technologies. When employees understand why and how a specific I4 technology is being implemented in the organization, this significantly reduces the level of resistance. Leaders should provide evidence of positive outcomes from the use of technology to confirm its effectiveness and minimize fears that may arise due to uncertainty [9].

According to a study [12], presenting a clear strategy for implementing and using new technologies is another important step to reduce resistance. Employees should be informed in detail about the stages of change and the

possible side effects of implementing new technologies. Unclear communication or lack of information can lead to negative rumors, which can seriously complicate the change process. Therefore, it is important for managers to provide accurate and understandable information, answering employees' questions and explaining all aspects of the change, even if they have certain shortcomings or difficulties. Another important component of an effective communication strategy is constant feedback. Employees should feel that their feedback is important and that they can influence the change processes.

2. Training. Training is a critical factor for the successful implementation of I4 technologies. With the implementation of I4 technologies, there is a need for new technical skills, such as data analysis, data modelling, knowledge of cyber-physical systems, the Internet of Things, and robotic manufacturing. In addition, soft skills, such as the ability to solve problems, work in a team, implement change, and adapt to new conditions, are necessary for the successful application of new technologies [13].

Training provides employees with the opportunity not only to update their knowledge but also to gain experience in using new technologies. In addition, training programs allow them to demonstrate the value of new technologies by providing employees with a clear understanding of their functions and potential opportunities for implementation within the organization. Therefore, investments in training are becoming an important component of the strategy for the successful implementation of I4 in organizations.

Successful implementation of training for I4 requires efforts not only from the industrial sector, but also significant participation from academic institutions. Research institutes and universities should be involved in the development and updating of educational programs that meet the requirements of new technologies. An important aspect is the close cooperation between manufacturing companies and educational institutions to create specialized programs that will contribute to the training of a skilled workforce [9].

3. Participation. To increase employee involvement in the implementation of new technologies, it is important to encourage their active participation in the process. This allows employees not only to understand more deeply the principles of how the technology works, but also to realize its real benefits in the context of expected results. Interaction with new technologies through direct participation helps people develop a more positive attitude towards them and, thus, increase their commitment to innovation.

Furthermore, when employees are involved in the process of developing and implementing technology, they can influence its adaptation to their specific needs and constraints, which contributes to the formation of a sense of ownership and responsibility for innovation.

IV. Conclusions

Industry 4.0, through the integration of digital technologies into production processes, has a powerful impact on the competitiveness of enterprises. However, this process is accompanied by a number of risks, including economic, social, political and technical. For a successful digital transformation, companies need to address cyber security issues, develop risk management strategies, adapt HR policies and develop infrastructure.

The introduction of I4 creates new opportunities for the development of an innovative economy, but requires a comprehensive approach and readiness for challenges. The introduction of I4 technologies opens up new opportunities for organizations, but is accompanied by significant challenges. Assessing a company's openness to these technologies through the parameters of breadth and depth allows you to better understand the scale of integration and the potential of technologies. Industry 4.0 technologies require deep scientific expertise and close integration into companies' operational processes. They provide transparency, increase efficiency and reduce risks for employees. However, successful implementation requires significant investments in technology, as well as consideration of organizational, financial and human factors.

An important aspect is change management, in particular combating employee resistance. Effective change management strategies include communication, training and employee participation in the adaptation process. Through clear communication, providing the necessary knowledge and involving employees in decision-making, the level of resistance can be significantly reduced and ensure the successful implementation of new technologies. Investment in education, cooperation between companies and educational institutions are also key to preparing a skilled workforce. Therefore, to achieve success in the era of I4, it is important to combine technological innovations with an effective management approach, focusing on employee participation and development.

References

[1] I. Bohashko and O. Bohashko, "Development of organisational competencies during transition and adaptation to industry 4.0", Environment. Technology. Resources: Proceedings of the 15 th International Scientific and Practical Conference' 06, 2024, vol. III, pp. 34-38, June 2024. [Online]. Available: https://doi.org/10.17770/etr2024vol3.8134 [Accessed: Feb. 13, 2025].

[2] T. Čater, B. Čater, M. Černe, M. Koman and T. Redek, "Industry 4.0 technologies usage: motives and enablers", Journal of Manufacturing Technology Management, vol. 32, no. 9, pp. 323-345, December 2021. [Online]. Available: https://doi.org/10.1108/JMTM-01-2021-0026 [Accessed: Feb. 13, 2025].

[3] M. Obal, "What drives post-adoption usage? Investigating the negative and positiveantecedents of disruptive technology continuous adoption intentions", Industrial Marketing Management, vol. 63, pp. 42-52, May 2017. [Online]. Available: https://doi.org/10.1016/j.indmarman.2017.01.003 [Accessed: Feb. 13, 2025].

[4] S-V. Buer, J. O. Strandhagen and F. T. S. Chan, "The link between Industry 4.0 and lean manufacturing: mapping current research and establishing a research agenda", International Journal of Production Research, vol. 56, pp. 1-17, March 2018. [Online]. Available: https://doi.org/10.1080/00207543.2018.1442945 [Accessed: Feb. 13, 2025].

[5] T. Zheng, M. Ardolino, A. Bacchetti, M. Perona and M. Zanardini, "The impacts of Industry 4.0: a descriptive survey in the Italian manufacturing sector", Journal of Manufacturing Technology Management, vol. 31, no. 5, pp. 1085-1115, October 2019. [Online]. Available: https://doi.org/10.1108/JMTM-08-2018-0269 [Accessed: Feb. 13, 2025].

[6] G. Buchi, M. Cugno and R. Castagnoli, "Smart factory performance and Industry 4.0", Technological Forecasting and Social Change, vol. 150, 119790, January 2020. [Online]. Available: https://doi.org/10.1016/j.techfore.2019.119790 [Accessed: Feb. 13, 2025].

[7] M. Hermann, T. Pentek and B. Otto, "Design principles for Industry 4.0 scenarios", Proceedings of the Annual Hawaii International Conference on System Sciences' 03, 2016, pp. 3928-3937, March 2016. [Online]. Available: https://doi.org/10.1109/HICSS.2016.488 [Accessed: Feb. 13, 2025].

[8] J. W Veile, M.-C. Schmidt, J. M. Muller and K.-I. Voigt, "Relationship follows technology! How Industry 4.0 reshapes future buyer-supplier relationships", Journal of Manufacturing Technology Management, vol. 32, no. 6, pp. 1245-1266, August 2020. [Online]. Available: https://doi.org/10.1108/JMTM-09-2019-0318 [Accessed: Feb. 13, 2025].

[9] A. Ito, T. Ylipää, P. Gullander, J. Bokrantz, V. Centerholt and A. Skoogh, "Dealing with resistance to the use of Industry 4.0 technologies in production disturbance management", Journal of Manufacturing Technology Management. vol. 32, no. 9, pp. 285-303, June 2021. [Online]. Available: https://doi.org/10.1108/JMTM-12-2020-0475 [Accessed: Feb. 13, 2025].

[10] R. C. Santos and J. L. Martinho, "An Industry 4.0 maturity model proposal", Journal of Manufacturing Technology Management, vol. 31, no. 5, pp. 1023-1043, November 2020. [Online]. Available: https://doi.org/10.1108/JMTM-09-2018-0284 [Accessed: Feb. 13, 2025].

[11] J. Kotter and L. Schlesinger, "Choosing Strategies for Change". Harvard business review. vol. 57, no. 2, 106-14, July 2008. [Online]. Available: https://doi.org/10.1007/978-1-349-20317-8_21 [Accessed: Feb. 13, 2025].

[12] H. S Birkel, J. W Veile, J. M Muller, E. Hartmann and K. I. Voigt, "Development of a riskframework for Industry 4.0 in the context of sustainability for established manufacturers", Sustainability, vol. 11, no. 2, pp. 1-27, January 2019. [Online]. Available: https://doi.org/10.3390/su11020384 [Accessed: Feb. 13, 2025].

[13] M. Pejic-Bach, T. Bertoncel, M. Meško and Ž. Krstić, "Text mining of Industry 4.0 jobadvertisements", International Journal of Information Management, vol. 50, pp. 416-431, February 2020. [Online]. Available: https://doi.org/10.1016/j.ijinfomgt.2019.07.014 [Accessed: Feb. 13, 2025].

Environment. Technology. Resources. Rezekne, Latvia
Proceedings of the 16th International Scientific and Practical Conference. 2025. Volume IV, 53-57

Study of Influence of 3D Printing Temperature on Shore D Hardness of Nylon CF15 Carbon

Konstantin Chukalov
Technical University of Sofia, Branch Plovdiv
Plovdiv, Bulgaria
chukalov@tu-plovdiv.bg

Valeri Bakardzhiev
Technical University of Sofia, Branch Plovdiv
Plovdiv, Bulgaria
bakardzhiev@tu-plovdiv.bg

Sabi Sabev
Technical University of Sofia, Branch Plovdiv
Plovdiv, Bulgaria
sabi_sabev@tu-plovdiv.bg

***Abstract*— This article investigates the influence of 3D printing temperature on the Shore D hardness of Nylon CF 15 Carbon samples. For this purpose, 20 standardized hardness samples were made. The data were statistically processed, and the main values - median, mode, range, maximum, minimum value of the obtained results were derived.**

***Keywords*— 3D printing, Shore D hardness, Carbon fiber reinforced polymers**

I. INTRODUCTION

3D printing is an additive manufacturing technology that creates three-dimensional parts by extruding layer after layer[1]. The technology is used to create models of various shapes, sizes and colors[2]. 3D printing is an increasingly used technology worldwide. The creation of parts is carried out using a CAD model.

The most commonly used materials in 3D printing of plastics are ABS, PLA, Nylon, Polypropylene, ASA, etc[3]. The choice of material is dictated by the requirements for application properties - durability, strength, stiffness, etc. As 3D printing is increasingly used in mechanical engineering, the automotive industry, space technology, food industry, electronics and electrical engineering, the requirements for the performance of 3D printed parts are becoming increasingly higher[4],[5]. In addition to the listed materials, which are generally used for general applications, there are also materials with unique properties that are used for high-tech applications such as TPU, PEEK, CFRP[6].

Hardness is the property of materials to resist plastic deformation caused by an external force. There are various standardized hardness tests according to Brinell, Rockwell, Shore, etc[7].

The Shore test has 12 scales, such as hard rubber and plastics are tested by method D[8]. Indenting foot is Hardened steel rod 1.1 mm – 1.4 mm diameter, with a 30° conical point, 0.1 mm radius tip. The range of results is from 0 to 100 dimensionless units. The test, like other hardness tests, measures the depth of penetration. The essence of the test is to apply a load, wait and record the results. As 3D printed parts are increasingly used for machine elements, it is important to evaluate their performance under friction and erosion[9].

II. MATERIALS AND METHODS

CFRPs (Carbon fiber-reinforced polymers) are composites that represent a polymer matrix with embedded carbon fibers. Nylon CF15 carbon is part of this group. and is characterized by high strength characteristics, light weight, low density, low thermal expansion, wear resistance, etc[10].This material contains carbon fibers with a length of 100 µm in order to improve mechanical properties. The material is used as a structural material for bearings, reinforced parts, gears, etc. It is used in the aerospace industry, automotive, structures, sports equipment, shipbuilding and a number of other technical areas.

The printing parameters are as follows:

- Material- Nylon CF15 Carbon
- 3d printing speed- 350mm/s
- Extruding temperature- 235-265ºC
- Bed temperature- 105ºC
- Layer height- 0,275mm
- Infill- 100%
- 3d printing duration: 15,42мин

The 3D printer used for this study is the Adventurer 5 Mpro, fig.1.

Online ISSN 2256-070X
https://doi.org/10.17770/etr2025vol4.8405
© 2025 The Author(s). Published by RTU PRESS.
This is an open access article under the Creative Commons Attribution 4.0 International License.

Fig. 1. 3d printing process.

The test samples were manufactured according to ISO 868 with dimensions 50x50x6 mm,fig.2. The hardness was measured on a calibrated Shore D testing machine according to the standardized test method ASTM D2240[11]. Before the experimental tests, the accuracy of the device was checked using calibrated plates for hardness - 25, 50, 75 units,fig.3

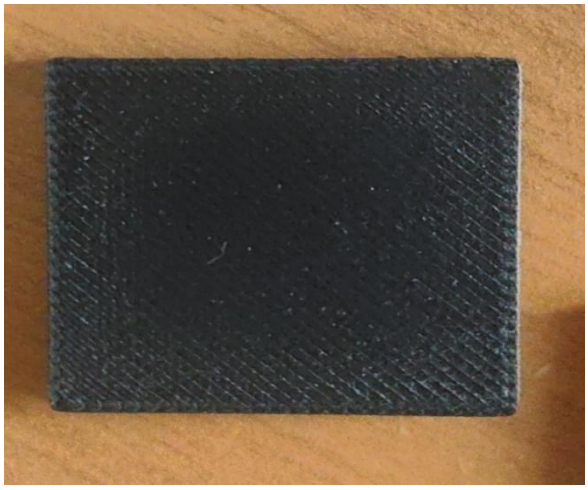

Fig. 2. Standartized hardness sample.

Fig. 3. Shore D hardness tester.

According to the standard, for more accurate results, 5 tests were taken from each sample. The requirements for a distance greater than 5 times the tip diameter between the samples were met, as well as not to measure close to the edges of the part. The parts were not subjected to shock loading for more precise results. After the tests were completed, average values were taken for the 20 samples to perform the regression analysis between the measured hardnesses and the different 3D printing temperatures. 20 test samples were printed with a constant layer height of 0.275mm and a printing speed of 350mm/s. and different printing temperatures. The selected temperature range is from 235 to 2650 degrees, which is recommended according to the material specification. The distribution of the 20 samples by temperature is as follows:

- 10 samples, central temperature – 250° degree
- 2 samples, extremem temperatures – 235° и 265° degree
- 8 the sample - 4 on both sides of the central point, at a selected constant intermediate temperature between the extremes and the central point - 241.1° and 258.9°degree.

III. Results and Discussion

The obtained averaged results and the corresponding 3D printing temperatures are presented in Table 1, fig.4.

Table.1 Avaraged results

Sample Number	Hardness [Shore D]	Temperature [ºC]
1	72,76	241,1
2	71,08	258,9
3	71,88	241,1
4	72,54	258,9
5	72,72	241,1
6	73,38	258,9
7	72,6	241,1
8	73,08	258,9
9	72,34	235
10	62,4	265
11	72,4	250
12	71,18	250
13	71,62	250
14	73,3	250
15	71,62	250
16	73	250
17	72,64	250
18	72,22	250
19	72,26	250
20	71,86	250

Fig. 4. One of the obtained results.

We performed statistical processing of the obtained data to determine the statistical center-Mode, Median, Mean and also Variance, Standard Deviation, etc[12],[13]. Statistical processing of the experimental results was performed in MS Excel and the obtained values are shown in tab.2

TABLE.2 STATISTICAL SUMMARY

Mean	71,79
Standard Error	0,51
Median	72,36
Mode	71,62
Standard Deviation	2,29
Sample Variance	5,25
Range	10,9
Minimum	62,4
Maximum	73,3
Sum	1435,88
Count	20
Confidence Level(95,0%)	1,07
99,7% Low	64,92
99.7% High	78,67
Step	19
Gap	0,72

Regression Equation:

Hardness [Shore D] = 0.28701 Temperature [ºC] (1)

Model Fit: To determine which coefficient is statistically significant, the value in the P-value field is taken. If P-value ≤ α, the null hypothesis is rejected and the coefficient is statistically significant.

If P-value ≥ α, the null hypothesis is accepted and the corresponding coefficient is statistically insignificant. Tables 3,4,5 show that all coefficients and factors are statistically significant.

TABLE.3 COEFFICIENTS

Variable	Coef	SE Coef	T-Value	P-Value	VIF
Temperature [ºC]	0,28701	0,00341	84,19	0,000	1,00

TABLE.4 MODEL SUMMARY

S	R-sq	R-sq(adj)	R-sq(pred)
3,81295	99,73%	99,72%	99,70%

TABLE.5 ANALYSIS OF VARIANCES

Source	DF	Adj SS	Adj MS	F-Value	P-Value
Regression	1	103057	103057	7088,50	0,000
Temperature [ºC]	1	103057	103057	7088,50	0,000
Error	19	276	15		
Lack-of-Fit	4	269	67	133,40	0,000
Pure Error	15	8	1		
Total	20	103333			

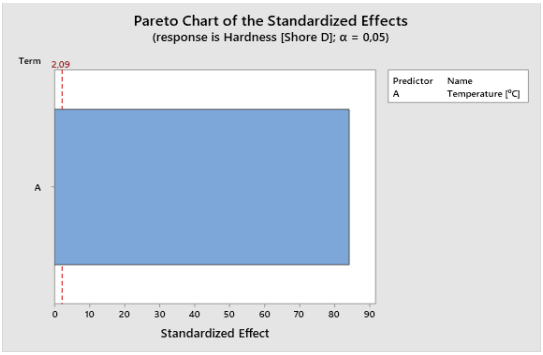

Fig. 5. Standartized effects

The standardized residual, Fig. 5, is equal to the residual value divided by an estimate of its standard deviation.[14,15] These residuals are useful because raw residuals may not be good indicators of bias in the regression model. Analysis of the residuals does not indicate a violation of the assumptions of the regression analysis. From Fig. 5, it is seen that the residual for trial 10 is outside the ±2 interval.

From the analysis of the residuals and the main effect(fig.6,7,8) of the influence of printing temperature on hardness, it may be concluded that there is significant decrease of the the dependent variable above 2600.

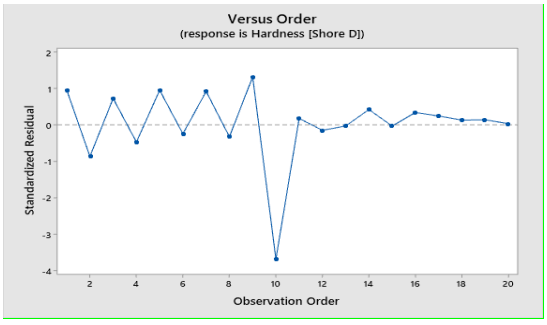

Fig. 6. Standard residuals.

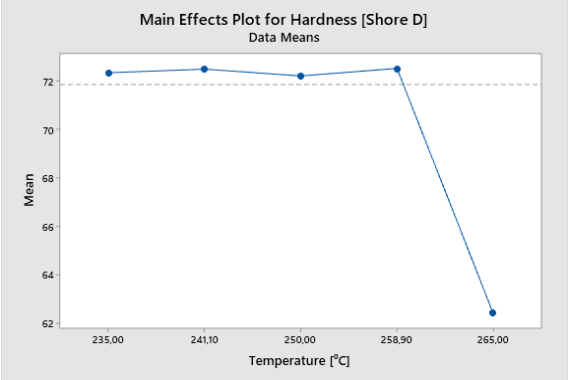

Fig. 7. Main effect plot.

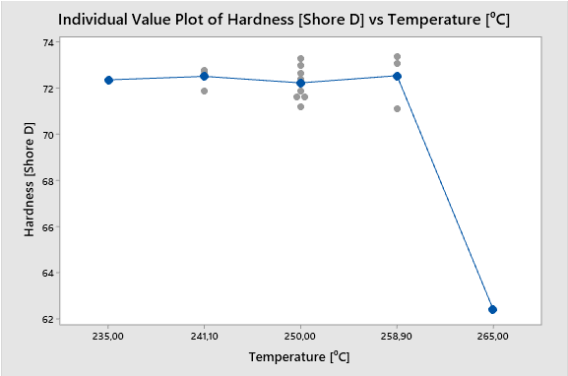

Fig. 8. Individual value plot.

After removing trial 10, the regression analysis was repeated.

Model adequacy: The coefficient of determination R2 = 99.92 was calculated, and the adjusted coefficient of determination has the value R2 adj = 99.92. To check the significance of a value having a Fisher distribution (F-value) was calculated. For its verification, we use P-value, since the threshold for rejecting the null hypothesis does not depend on the degrees of freedom. In our case, the P-value for each coefficient is lower than α=0.05, so we can reject the null hypothesis.

For the coefficient in front of the variable to be significant, the P-value for the Student distribution should be less than α=0.05. This condition is met and the coefficient is significant, tables 6,7,

Hardness [Shore D] = 0,29007 Temperature [ºC](2)

TABLE.6 COEFFICIENTS

Term	Coef	SE Coef	T-Value	P-Value	VIF
Temperature [ºC]	0,29007	0,00192	150,83	0,000	1,00

TABLE.7 MODEL SUMMARY

S	R-sq	R-sq(adj)	R-sq(pred)
2,08990	99,92%	99,92%	99,91%

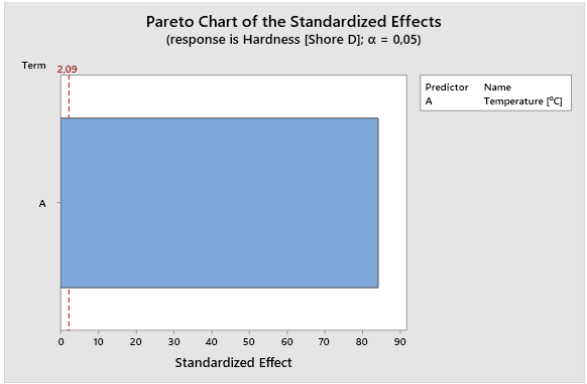

Fig. 9. Analysis of variations

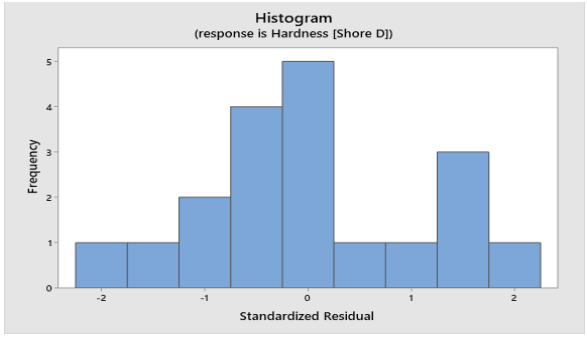

Fig. 10. Standardized residuals.

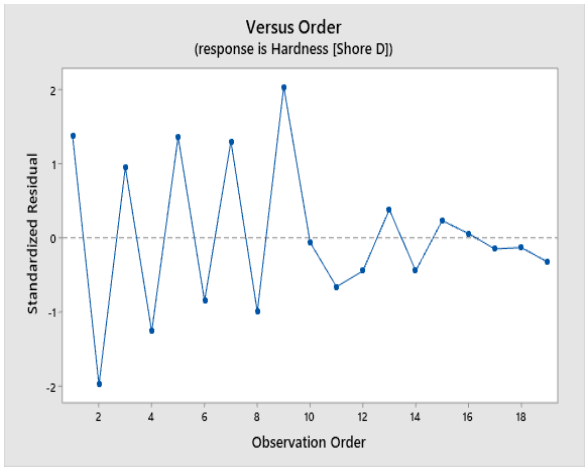

Fig. 11. Observation order

From fig.9,10,11 it may be concluded that in the range of temperature range 235^0-258^o the hardness is almost unchanged, which corresponds to the optimal printing temperature range [16,17]. With an increase in temperature above 260^0, due to physical-chemical processes, the mechanical properties and in particular the hardness is reduced[18]. This is caused by chemical degradation of the polymer and disrupted structure, which leads to a decrease in mechanical properties.

IV. CONCLUSIONS

Temperature in 3D printing is a key parameter for obtaining quality parts. At high temperatures in 3D printing, adhesion improves, but the stability of the polymer is impaired. At high temperatures in 3D printing, adhesion is improved, but the stability of the polymer is impaired. For this reason, it is important to investigate the temperature range for optimal printing temperature. From the study conducted, the following conclusions can be drawn - the optimal temperature for 3D printing of Nylon CF 15 Цarbon is in the range of 235-258^0,in this range the hardness Shore D has a small range within the limits of 71.08-73.3. At printing temperatures above 260^0, hardness decreases due to chemical-physical processes.

V. ACKNOWLEDGMENTS

This research was funded by the European Regional Development Fund within the OP " Research, Innovation and Digitalization Programme for Intelligent Transformation 2021-2027 ", Project CoC "Smart Mechatronics, Eco- and Energy Saving Systems and Technologies", No. BG16RFPR002-1.014-0005.

REFERENCES

[1] J. Ma, "The application of 3D printing in mechanical manufacturing", Applied and Computational Engineering, vol. 117, pp. 44–50, 2025. [Online]. Available: https://doi.org/10.54254/2755-2721/2025.20112. [Accessed: Jan. 5, 2025].

[2] Y. Li, X. Li and D. Shen, "Existing 3D Printing Technologies", Artificial Intelligence in 3D Printing, pp. 77–88, 2024, [Online]. Available: https://doi.org/10.1007/978-981-97-4094-9_2. [Accessed: Jan. 5, 2025].

[3] İ. Karamanli and K. Tahnal, "Optimization of Printing Parameters of PLA and ABS Produced by FFF", Journal of Materials and Mechatronics: A, vol. 5, pp. 286–302, 2024. [Online]. Available: https://doi.org/10.55546/jmm.1566700. [Accessed: Jan.y 5, 2025].

[4] P. Shah, V. Shah, S. Shrestha and P. Mitra, "A Review on 3D Food Printing Technology in Food Processing", Journal of Food Industry, vol. 8, p. 17, 2024. [Online]. Available: https://doi.org/10.5296/jfi.v8i1.22468. [Accessed: Jan. 5, 2025].

[5] J. Zheng, Y. Niu, Z. Song, N. Li and S. Ju, "Application of 3D Printing Technology in Microreactor Fabrication", JOM, vol. 77, 2024. [Online]. Available: https://doi.org/10.1007/s11837-024-06961-0. [Accessed: Jan. 5, 2025].

[6] N. Blessing and K. Extension, "Developing Sustainable Materials for 3D Printing", Research Output Journal of Engineering and Scientific Research, vol. 3, pp. 18–21, 2024. [Online]. Available: https://www.researchgate.net/publication/383873999_Developing_Sustainable_Materials_for_3D_Printing. [Accessed: Jan. 5, 2025].

[7] K. Kriener, K. Sinclair, G. Robison, R. Lala, H. Finley, W. Richardson and M. Midwinter,"Investigating the Reliability of Shore Hardness in the Design of Procedural Task Trainers", Bioengineering, vol. 12, p. 41, 2025. [Online]. Available: https://doi.org/10.3390/bioengineering12010041. [Accessed: Jan. 5, 2025].

[8] A. Adib, J. Pratama, U. Salim, S. Dr, M. Mahardika and B. Arifvianto, "Effect of Core Material Thickness on the Shore Hardness of the Sandwich-Structured Multi-Material 3D-Printed Parts", Applied Mechanics and Materials, vol. 920, pp. 35–42, 2024. [Online]. Available: https://doi.org/10.4028/p-zs9Z6i. [Accessed: Jan. 5, 2025].

[9] A. Voropay, P. Yehorov, G. Gnatenko, S. Povaliaiev and A. Sharapata, "Optimization of Machine Parts Models for 3D Printing", International Journal of 3D Printing Technologies and Digital Industry., vol. 6, 2022. [Online]. Available: https://doi.org/10.46519/ij3dptdi.1187111. [Accessed: Janu. 5, 2025].

[10] H. K. Azad, Dr Rahman and D. Zhu, "Carbon fiber: composites and applications", Synthetic and Mineral Fibers, Their Composites and Applications, vol. 1, pp. 291-319, 2024. [Online]. Available: https://doi.org/10.1016/B978-0-443-13623-8.00010-1. [Accessed: Jan. 5, 2025].

[11] D. Jovanić, E. Desnica and D. Malić, "The Influence of the Layer Height on the Hardness of the TPU Plastic Specimen Made by 3D Printing," in 11th International Conference on Information Science and Information Literacy, vol. 1, pp. 77–83, 2024. [Online]. Available: https://doi.org/10.46793/IIZS24.077J. [Accessed: Jan. 5, 2025].

[12] S. B, "Statistical Measures of Center: A Focus on Mean, Median, and Mode", INTERANTIONAL JOURNAL OF SCIENTIFIC RESEARCH IN ENGINEERING AND MANAGEMENT, vol. 08, pp. 1–5, 2024. [Online]. Available: https://doi.org/10.55041/IJSREM39608. [Accessed: Jan. 5, 2025].

[13] B. Pospelov, R. Meleshchenko, Y. Bezuhla, L. Chubko, R. Kornienko, Y. Kozar, L. Datsenko, O. Bilotil, S. Pysarevskyi and K. Tishechkina, "Revealing the peculiarities of asymmetry and kurtosis coefficients of gas medium parameters in premises during fire", Eastern-European Journal of Enterprise Technologies, vol. 3, pp. 39–47, 2023. [Online]. Available: https://doi.org/10.15587/1729-4061.2023.28074 2. [Accessed: Jan..5, 2025].

[14] A. Adityaningrum, R. Resmawan, A. Brahim, D. Isa, L. Nashar and A. Asriadi, "Robust Least Median of Square Modelling Using Seemingly Unrelated Regression with Generalized Least Square on Panel Data for Tuberculosis Cases", BAREKENG: Jurnal Ilmu Matematika dan Terapan., vol. 18, pp. 2293–2306, 2024. [Online]. Available: https://doi.org/10.30598/barekengvol18iss4pp2293-2306. [Accessed: January 5, 2025].

[15] S. Kumar and P. Rani, "An AI-based Liver Disease Prediction Model based on Pearson Correlation Feature Selection Method", Biomedical and Pharmacology Journal, vol. 17, pp. 2187–2202, 2024. [Online]. Available: https://doi.org/10.13005/bpj/3016. [Accessed: Jan.y 5, 2025].

[16] P. Ozili, "The Acceptable R-Square in Empirical Modelling for Social Science Research", 2023. [Online]. Available: https://doi.org/10.4018/978-1-6684-6859-3.ch009. [Accessed: Janu. 5, 2025].

[17] S. Darmos, "Assessing the p-values of hierarchies", 2025.

[18] O. A. Ulkir, I. Ertugrul, S. Ersoy and B. Yagimli, "The Effects of Printing Temperature on the Mechanical Properties of 3D-Printed Acrylonitrile Butadiene Styrene", Applied Sciences, vol. 14, p. 3376, 2024. [Online]. Available: https://doi.org/10.3390/app14083376. [Accessed: Jan. 5, 2025].

Environment. Technology. Resources. Rezekne, Latvia
Proceedings of the 16th International Scientific and Practical Conference.2025. Volume IV, 59-63

Research on Impact Resistance Using Free-Falling Dart Drop Testing of 3D Printed Parts Made of ABS and PETG According ASTM D1709

Konstantin Chukalov
Technical University of Sofia, Branch Plovdiv
Plovdiv, Bulgaria
chukalov@tu-plovdiv.bg

Sabi Sabev
Technical University of Sofia, Branch Plovdiv
Plovdiv, Bulgaria
sabi_sabev@tu-plovdiv.bg

Valeri Bakardzhiev
Technical University of Sofia, Branch Plovdiv
Plovdiv, Bulgaria
bakardzhiev@tu-plovdiv.bg

***Abstract*—The paper investigates impact resistance of 3D printed ABS and PETG specimens by a falling dart drop. 25 specimens of each material were manufactured in accordance to ASTM D1709 standard, as well as 25 specimens of notched ABS. The test data is processed when 10 cracked and 10 uncracked specimens are available. Dart drop tests are typical for specimens that are manufactured in shape of films. The purpose of the test is to perform an impact from a certain height with a controlled velocity of the falling dart drop.**

Keywords— 3D printing, impact resistance,free-falling dart,mechanical properties

I. Introduction

3D printing is a basic technology for rapid prototyping[1].The application of the technology is increasingly used in mechanical engineering, aerospace engineering, medical applications, etc[2]. .3D printing is a preferred technology because of the following advantages - the ability to create parts with complex geometry, without technological waste, energy efficiency. The most commonly used 3D printing technologies are FDM, SLA, SLS[3].

The most commonly used materials for 3D printing are PLA, ABS[4].In addition to them, other polymers are also used with specific requirements for impact resistance, rigidity, chemical resistance, etc[5].

Impact resistance is classified as a dynamic test method in which the destruction of the sample occurs at high speed[6]. The method can be used on a wide range of materials - metals, plastics, rubbers, etc[7]. The test is a transfer of energy created by a falling wedge or hammer on the test sample, which leads to its destruction. Impact resistance is equal to the work done to break divided by the impact cross-section. There is no dependence on the size of the test pieces, the sizes of the test pieces for testing are determined by different standards. The following conditions are important for impact resistance testing:

- Dimensions of specimen
- Presence of notches, curvatures
- Test temperature
- Mass of the falling dart drop/hammer
- Height of fall of dart drop/hammer
- Geometry of dart drop/hammer

In impact resistance testing, specimens with different notches are used in order to create a stress concentrator. Keyhole, U and V type notches are standardized, with keyhole and U being most often used for brittle materials such as cast iron[8]. The most commonly used methods for impact resistance testing are the Izod method, the Charpy method and the free-falling dart test. The Charpy and Izod methods contain usage of pendulum hammers, and the falling method contains usage of different heads[9]. The load is selected depending on the material and testing conditions in order to guarantee the destruction of the test specimens. Impact resistance tests are extremely important for parts that are subjected to impact loads. In practice, parts obtained by 3D printing are often used as machine elements and structural parts, which determines the importance of testing the impact resistance of parts obtained by this technology[10].

II. Materials and Methods

For this study, filament materials of PetG-(Polyethylene terephthalate glycol) and ABS were selected[11]. The choice was due to the fact that both materials have applications in mechanical engineering parts. PetG has excellent properties for 3D printing, is also easy to mold, has excellent chemical resistance and strength[12]. Its high temperature resistance and lack of

Online ISSN 2256-070X
https://doi.org/10.17770/etr2025vol4.8406
© 2025 The Author(s). Published by RTU PRESS.
This is an open access article under the Creative Commons Attribution 4.0 International License.

pigmentation make it suitable for printing various body parts. The other selected filament is ABS, which is distinguished by heat resistance, good dimensional accuracy and hardness[13]..ABS has a very wide range of applications - pipes, fittings, keyboard keys, in the refrigeration industry, automotive industry, etc[14]. For our study, we will use a Flashforge Adventurer 5M Pro 3D printer from Zhejiang Flashforge 3D Technology Co., Ltd. The 3D printer works using material deposition technology and has the following characteristics:

- X-axis travel-220mm
- Y-axis travel-220mm
- Z-axis travel-220mm
- Nozzle opening- 0.4mm
- Maximum extruder temperature- 270 ºC
- Maximum bad temperature- 110 ºC
- Maximum printing speed – 600mm/s

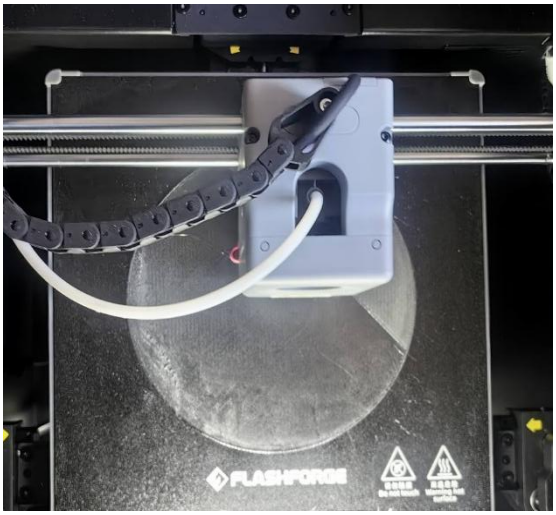

Fig. 1. Process of printing a spicemen from PETG.

The used 3d printing parameters used for the test specimens (fig.1) are:.:

- Materials- PetG and ABS
- Print speed- 200mm/s
- Extruder temperature- 235ºC
- Bed temperature- 60ºC
- Layer height- 0.2mm
- Infill- 100%

25 samples shown were printed from colorless PetG material, as well as 50 from ABS, of which 25 with notches to investigate the impact resistance of the material. The study will expand an accumulate experimental data on the strength of this material and its application in various printed parts. The samples were printed with the same printing parameters outlined above. The test sample was designed according to the available impact resistance test stand, namely with a diameter of 158mm and a thickness of 1.6mm for PetG and 1.2mm for ABS. Approximately 36.5g of filament is used in one test sample. Impact resistance test samples are often made with artificial notches - most often with a U and B shape in order to localize stress concentrators[15]. In plastic products, a U notch is most often used[16]. The notches were made only on the ABS samples. The notch was made by milling the samples. The diameter of the notch is F2 in the middle of the sample. The notch is standardized for plastic products. The notched samples were installed on the stand so that the notches were on the upper side. Before the test, the pneumatic system of the stand was checked, as well as the location of the impact with the falling wedge was checked by marking the central mark. Slippage during fastening is critical for the reliability of the results. The dimensions of the samples are shown in Fig. 2.

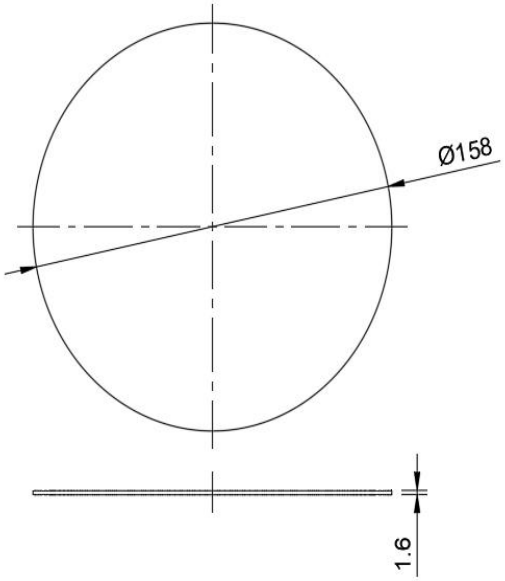

Fig. 2. Spicemens dimensions.

For testing purposes, a calibrated impact resistance using free-falling dart drop machine according to ASTM 1709 Method A was used,fig.3

The height of the dart drop is the standardized 0.66m for ABS and 0.260m for PetG, the tip has a diameter of 38.1mm and a hemispherical head. This method is suitable for testingfilms with a mass of 50 grams or less, which is why it is preferred for testing. Missile weight and incremental weights are calibrated for the purpose of accuracy of the test. The atmospheric conditions for temperature and humidity mentioned in the standard are observed. The dart is positioned vertically above the specimen, during the tests no slippages greater than 0.1mm were detected

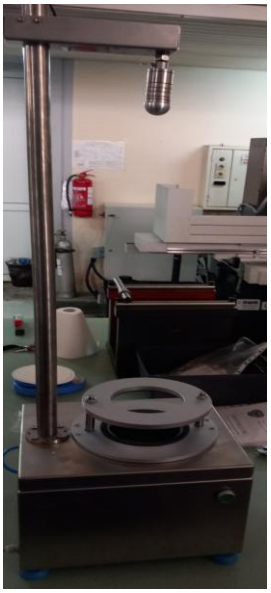

Fig. 3. Free-falling dart drop stand.

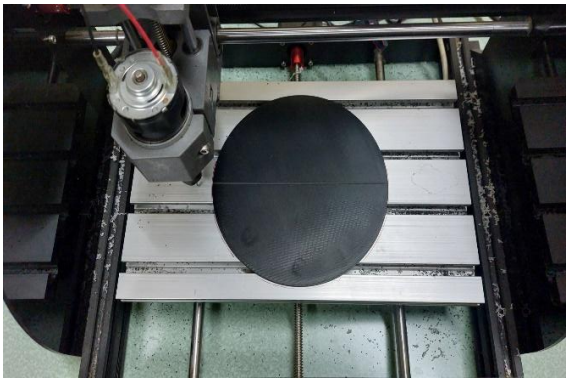

Fig. 4. The engraving router.

The notches were made using an engraving router, Fig. 4. with a 4mm ball nose cutter at a depth of 0.8mm, representing half of the total thickness of the test specimen,fig.6

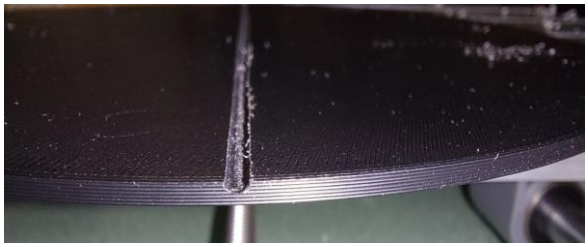

Fig. 5. Notched ABS sample

The results are presented in a table according to the standard, and it is necessary to have 10 broken and 10 unbroken test specimens, Table 1. According to the theoretical data, a weight is selected with which to start the test, and in case of successful breakage, the weight is reduced, if unsuccessful, it is increased by one step. The signs X are used for a broken specimen and O for an unsuccessfully broken specimen. After the end of the test, the impact failure weight is calculated..

III. RESULTS AND DISCUSSION

TAB.1. TEST RESULTS IMPACT RESISTANCE,NOTCHED ABS SAMPLES.

Missle weight [g]	1	2	3	4	5	6	7	8	9	10
120								O		
130	O						X		O	
140		O		O		X				O
150			X		X					
Missle weight [g]	11	12	13	14	15	16	17	18	19	20
120				O		O		O		
130			X		X		X		O	
140		X								X
150	X									

After the tests are completed, failure rates are calculated according to the different missile weights.tab.2

TABLE.2 MISSILE WEIGHT AND % OF FAILURES

Missile weight,g	**% Failure**
130	57
140	50
150	100
∑	207

Failure weight is calculated in several alternative ways according the standard, with similar results, the difference in them being within the statistical error. In this article, the used formula is:

$$W_F = W_L - [\Delta W (S/100-1/2)] \quad (1)$$

where

WF - impact failure weight, g,

DW - uniform weight increment used, g,

WL - lowest missile weight, g,

according to the particular DW used, at which 100 % failure occurred, and S- sum of the percentages of breaks at each missile weight (from a weight corresponding to no failures up to and including WL

$$WF = WL - [DW (S/100 - 1/2)]$$

$$WF=150-[10(207/100-1/2]$$

$$WF=150-15.7$$

$$WF=134.3 \text{ g}$$

The results of ABS without notches are shown in a table 3.

TABLE 3 TEST RESULTS OF ABS SAMPLES WITHOUT NOTCH

Missle weight [g]	1	2	3	4	5	6	7	8	9	10
120		O				O				O
130	X		O		X		O		X	
140				X				X		
Missle weight [g]	11	12	13	14	15	16	17	18	19	20
120				O		O				
130	O		X		X		X		X	O
140		X						X		

Similarly presented are the percentage of the failures according the missile weight,tab.4

TABLE4 MISSILE WEIGHT AND % OF FAILURES

Missile weight,g	**% Failure**
130	64
140	100
∑	164

WF = WL − [DW (S/100 − 1/2)]

WF=140-[10(164/100-1/2]

WF=140-11.4

WF=138.6 g

The PetG results are presented in a table 5. The requirements for 10 destroyed and undestroyed specimens are met.

TABLE 5 TEST RESULTS IMPACT RESISTANCE OF PETG SAMPLES

Missle weight [g]	1	2	3	4	5	6	7	8	9	10
80	O				O		O			
90		O		X		X		O		X
100			X						X	
Missle weight [g]	11	12	13	14	15	16	17	18	19	20
80	O		O		O				O	
90		X		X		O		X		O
100							X			

TABLE 6 MISSILE WEIGHT AND % OF FAILURES

Missile weight,g	**% Failure**
90	60
100	100
∑	160

WF = WL − [DW (S/100 − 1/2)]

WF=100-[10(160/100-1/2]

WF=100-11

WF=89 g

The experimental results show a very small range, which validates them. The results cannot be compared with values obtained from other standard methods, different shapes of the specimens, as well as different geometry of the falling dart drop,fig.6. The test results of the ABS specimens show a notch effect with low sensitivity, which is due to the geometry of the hemispherical head of the dart drop in relation to the width and depth of the notch[16]. No notched specimen failed from a crack initiated by the artificial stress concentrator,fig.7 All notched ABS specimens failed from a crack initiated near the notch and propagated through the notch.[17],fig.7.

Fig. 6. All the tested samples.

Fig. 7. The crack of a notched sample.

IV. Conclusions

The following conclusions can be drawn from the study:

• Impact weight failure was calculated for ABS (with and without notch) and PETG test specimens

• The number and geometry of the specimens was in accordance with the requirements of the standard.

• The results of ABS show a notch effect with little sensitivity to notches in the falling dart drop test.

• The experimental results can be used in strength design of impact resistance at similar thicknesses.

• The cracks of the failed specimens are near the notch

• There is no single specimen that failed due to crack propagation initiated from the notch.

• No critical deviations were observed during the test that would affect the experimental results.

• The specimens had no visible defects that would affect testing

• Due to the specificity of the impact resistance test, data from specimens with other geometries and dimensions, as well as with different thicknesses, cannot be used, which makes such studies applicable in engineering practice.

• The selected materials are increasingly used in mechanical engineering and automotive industry, which necessitates testing of their mechanical properties

V. Acknowledgments

This research was funded by the European Regional Development Fund within the OP "Research, Innovation and Digitalization Programme for Intelligent Transformation 2021-2027", Project CoC "Smart Mechatronics, Eco- and Energy Saving Systems and Technologies", No. BG16RFPR002-1.014-0005.

REFERENCES

[1] Ma, "The application of 3D printing in mechanical manufacturing", Applied and Computational Engineering, vol. 117, pp. 44–50, 2025. [Online]. Available: https://doi.org/10.54254/2755-2721/2025.20112. (Accessed: January 14, 2025).

[2]]Y. Xu, "Types and applications of 3D printing," Highlights in Science, Engineering and Technology, vol. 119, pp. 697–702, 2024. [Online]. Available: https://doi.org/10.54097/26ya9h57. (Accessed: January 14, 2025).

[3] N. Jaiswal and J. Akhtar, "Additive manufacturing (3d printing)," 2024. [Online]. Available: https://doi.org/10.1016/B978-0-443-13774-7.00017-7. (Accessed: January 10, 2025).

[4] D. Pérez, E. Zumba, H. Mazón and J. Llamuca, "Elasticity and plasticity of PLA, PETG, ABS polymers for printing automotive parts," Espirales Revista Multidisciplinaria de Investigación, vol. 8, 2024. [Online]. Available: https://doi.org/10.31876/er.v8i4.875. (Accessed: January 14, 2025).

[5] T. Wajima and K. Yamashita, "Recovery of carbon fiber from carbon fiber reinforced plastics using alkali molten hydroxide," Scientific Reports, vol. 15, 2025. [Online]. Available: https://doi.org/10.1038/s41598-024-84293-4. (Accessed: January 14, 2025).

[6] Y. Wu, Y. Guo, S. Yi, Z. Lv and Z. Fan, "Impact Resistance of Aluminum Foam Composites with Filler and Coating Materials," *Polymers*, vol. 16, p. 3286, 2024. [Online]. Available: https://doi.org/10.3390/polym16233286. (Accessed: January 14, 2025).

[7] Z. Zhang, R. Lu, H. Zhang, L. Bai and Y. Sun, "Research Progress on the Impact Resistance of Basalt Fiber-Reinforced Polymer Composites," Journal of Physics: Conference Series, vol. 2891, p. 082017, 2024. [Online]. Available: https://doi.org/10.1088/1742-6596/2891/8/082017. (Accessed: January 10, 2025).

[8] X. Xueting, T. Wang, Q. Sun, B. Wang, Y. Ge, J. Lang and Y. Yan, "The Effect of Notch and Molecular Weight on the Impact Fracture Behavior of Polycarbonate," Polymers, vol. 16, p. 1072, 2024. [Online]. Available: https://doi.org/10.3390/polym16081072. (Accessed: January 10, 2025).

[9] L. F. De Freitas, F. P. D. Lopes, G. Cosme and N. Simonassi, "Study of Tensile Strength and Izod Impact on Epoxy Matrix Composites Reinforced with Jute Fabric," 2024. [Online]. Available: https://doi.org/10.5151/2594-5327-41345. (Accessed: January 10, 2025).

[10] M. Dębski, M. Magniszewski, J. Bernaczek, Ł. Przeszłowski, M. Gontarz and M. Kiełbicki, "Influence of torsion on the structure of machine elements made of polymeric materials by 3D printing," Polimery, vol. 66, 2021. [Online]. Available: https://doi.org/10.14314/polimery.2021.5.3. (Accessed: January 10, 2025).

[11] K. Mirasadi, D. Rahmatabadi, I. Ghasemi, M. Khodaei, M. Baniassadi and M. Baghani, "Investigating the Effect of ABS on the Mechanical Properties, Morphology, Printability, and 4D Printing of PETG-ABS Blends," Macromolecular Materials and Engineering, vol. 309, 2024. [Online]. Available: https://doi.org/10.1002/mame.202400038. (Accessed: January 14, 2025).

[12] E. Hozdić and E. Hozdić, "Influence of Infill Structure Shape and Density on the Mechanical Properties of FDM 3D-Printed PETG and PETG+CF Materials," Advanced Technologies & Materials, vol. 49, pp. 15–27, 2024. [Online]. Available: https://doi.org/10.24867/ATM-2024-2-002. (Accessed: January 10, 2025).

[13] A. Khledj, H. M. Mohamed, M. Mendas and I. Zidane, "Comparative Analysis of Three Polymers: ABS, PMMA, and ABS/15%PMMA Bilayer in Three-Point Bending," vol. 22, pp. 1–6, 2024.

[14] P. Katiyar, B. Singh, M. Chhabra, N. Kumar and D. Parle, "Analysis of tensile strength of thin ABS specimens 3-D printed in various build orientations for turbomachinery applications," International Journal on Interactive Design and Manufacturing (IJIDeM), pp. 1–13, 2024. [Online]. Available: https://doi.org/10.1007/s12008-024-01869-0. (Accessed: January 14, 2025).

[15] L. Guo, H. Huang, J. Chen and K. Romanov, "Axial behavior of square CFST with local corrosion simulated by artificial notch," Journal of Constructional Steel Research, vol. 174, p. 106314, 2020. [Online]. Available: https://doi.org/10.1016/j.jcsr.2020.106314. (Accessed: January 10, 2025).

[16] S. Cicero, F. Devito, M. Sánchez, S. Arrieta and B. Arroyo, "Notch Effect in Acrylonitrile Styrene Acrylate (ASA) Single-Edge-Notch Bending Specimens Manufactured by Fused Filament Fabrication," Materials, vol. 17, p. 5207, 2024. [Online]. Available: https://doi.org/10.3390/ma17215207. (Accessed: January 10, 2025).

[17] S. Cicero, V. Martinez-Mata, A. Alonso-Estébanez, L. Castañón Jano and B. Arroyo, "Analysis of Notch Effect in 3D-Printed ABS Fracture Specimens Containing U-Notches," Materials, vol. 13, p. 4716, 2020. [Online]. Available: https://doi.org/10.3390/ma13214716. (Accessed: January 10, 2025).

Environment. Technology. Resources. Rezekne, Latvia
Proceedings of the 16th International Scientific and Practical Conference. 2025. Volume IV, 65-71

Electro-Hydraulic System Optimization Through an Advanced Kalman Filter

Dimitar Dichev
Department of Mechanical and Precision Engineering
Technical University of Gabrovo
Center of competence "Smart mechatronic, eco-and energy-saving systems and technologies"
Gabrovo, Bulgaria
dichevd@abv.bg

Borislav Georgiev
Department of Mechanical and Precision Engineering
Technical University of Gabrovo
Center of competence "Smart mechatronic, eco-and energy-saving systems and technologies"
Gabrovo, Bulgaria
gborislav@gbg.bg

Iliya Zhelezharov
Department of Mechanical and Precision Engineering
Technical University of Gabrovo
Center of competence "Smart mechatronic, eco-and energy-saving systems and technologies"
Gabrovo, Bulgaria
izhel@tugab.bg

***Abstract*— This paper presents a mathematical model of the Kalman Extended Filter (EKF) for estimating dynamic states in an electro-hydraulic system. The main goal is to increase the accuracy and stability of estimates in the presence of noise and nonlinearities in the dynamics of the system. EKF combines information from hydraulic motor shaft angular velocity measurements and the pressure difference between its inlet and outlet to provide reliable estimates of basic dynamic system parameters, including the current angular velocity and the moment created by the external load. Simulation studies demonstrate the advantages of the EKF compared to a system without a filter, emphasizing the importance of tuning the covariance matrices Q and R to achieve a balance between response speed and filter stability. The developed model shows high applicability for real electro-hydraulic systems, while offering the possibility of adaptation to other nonlinear dynamic systems.**

Keywords*— Electro-hydraulic system; Extended Kalman Filter (EKF); nonlinear dynamics; optimization algorithm.

I. INTRODUCTION

Electro-hydraulic systems are important components in industrial and mobile technology because they provide high power, flexibility and efficiency. They combine the advantages of electric and hydraulic drives, providing high concentrated power, smooth speed and torque control, as well as the ability to operate under heavy loads [1-4]. In addition, electro-hydraulic systems offer high energy efficiency, thanks to the ability to adjust the pressure and flow rate according to the requirements of the application [5-7].

Thanks to these advantages, electro-hydraulic systems are widely used in various industrial and transport sectors [8-12]. They are used in robotic production lines, heavy construction machinery, aviation and automotive systems, as well as in automated processes in mechatronics [13-20]. Their ability to provide a stable and controlled flow of energy makes them indispensable for tasks requiring high accuracy and reliability [21, 22].

Despite their many advantages, electro-hydraulic systems also have some significant disadvantages that make their optimization and control difficult. One of the main problems is the presence of nonlinearities arising because of variations in pressure, temperature and dynamic loads [23]. These factors lead to non-linear behaviour of the system, which can lead to efficiency losses, instability, and degraded control accuracy. In addition, electro-hydraulic systems are often subject to noise and uncertainties related to sensor measurements and dynamic changes in the operating environment.

To overcome these shortcomings, various methods of data processing and management optimization are applied. Among the most used are different types of Kalman filters, which offer effective algorithms for assessing the state of the system in the presence of noise and uncertainty. The traditional Kalman Advanced Filter (EKF) is widely used in technical systems for processing nonlinear processes, offering reliable state assessment in the presence of noises and uncertainties. However, when the system's nonlinearities are significant, these methods can encounter difficulties related to loss of accuracy and numerical instability.

The present study proposes the use of an extended Kalman filter (EKF) as a method for data processing and control optimization in an electro-hydraulic system. The EKF uses a linear approximation through Jacobian

Online ISSN 2256-070X
https://doi.org/10.17770/etr2025vol4.8416
© 2025 The Author(s). Published by RTU PRESS.
This is an open access article under the Creative Commons Attribution 4.0 International License.

matrices, which allows the evaluation of nonlinear processes through first-order approximation. This article discusses the application of EKF to evaluate and correct the parameters of the electro-hydraulic system and its integration with a PID regulator for optimized control, to minimize errors and improve its efficiency. The main objective of the study is to demonstrate the effectiveness of EKF for signal processing in nonlinear electro-hydraulic systems.

II. MATERIALS AND METHODS

A. Description of the electro-hydraulic system

The electro-hydraulic system has been developed with the aim of providing high-precision motion control through the combined use of hydraulic and electrical components. The main idea behind this system is the transformation of electrical energy into hydraulic, which allows for effective control of the angular velocity and torque of the output shaft. By integrating various sensors and controls, the system can adapt its operation to loads and dynamic changes in conditions.

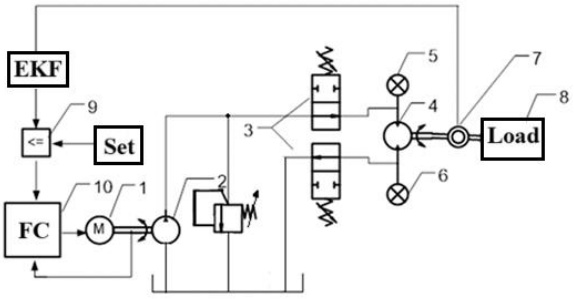

Fig. 1. Structural diagram of the electro-hydraulic system.

The schematic diagram of the electro-hydraulic system is presented in Fig. 1. The induction motor 1 creates a torque on its output shaft, to which the hydraulic pump is connected 2. The pump converts mechanical energy into hydraulic energy, creating a flow of working fluid under a certain pressure. This flow is fed to the hydraulic motor 4, which converts hydraulic energy back into mechanical energy, driving its output shaft and overcoming the external load 8. To measure and control the main quantities, measuring sensors are integrated into the system. Pressure sensors 5 and 6 are located respectively at the inlet and outlet of the hydraulic motor, measuring the created inlet and outlet pressure after energy conversion. In addition, to record the angular velocity of the output shaft of the hydraulic motor, tach generator 7 is installed. The system is controlled by frequency control 10 with a built-in PID regulator, which regulates the supplied voltage and frequency to the induction motor depending on the measured values of angular velocity and pressure. At the same time, the data processing unit 9 receives signals from the Extended Kalman Filter (EKF), which improves the accuracy of current measurements and provides the necessary algorithm for optimized system control.

B. EKF mathematical model for estimating hydraulic motor dynamics

The main goal of the EKF mathematical model is to provide reliable estimates of the angular velocity of the hydraulic motor shaft and of the moment created by the external load, combining information from angular velocity measurements and the pressure difference at the inlet and outlet of the hydraulic motor. Since the system is non-linear, EKF uses a first-order approximation to linearize the equations. The equation defining in nonlinear form the model of dynamics in the system has the following form:

$$x(k+1) = f[x(k), u(k)] + \omega(k), \quad (1)$$

where: $f[x(k), u(k)]$ is a function describing the nonlinear dynamics in the system; $x(k)$ are the values of the state vector in the step k; $\omega(k)$ is the noise defined in the kth step of the dynamic model.

Usually, the vector of control $u(k)$ contains input quantities that affect the dynamics of the system. In the case under consideration, the dynamics of the hydraulic motor is mainly determined by the pressure difference ΔP between its entrance and exit. Since $\Delta P(k)$ directly affects the generated torque, it is taken as a control variable. Thus, the control vector in the EKF model is defined as: $u(k) = \Delta P(k)$. This allows the EKF to use the measured pressure values to correct condition predictions.

To relate the real state in the system to the values of the measured quantities, the EKF is based on the nonlinear form of the measurement equation:

$$y(k) = h[x(k)] + v(k), \quad (2)$$

where: $h[x(k)]$ is the nonlinear relationship between the vector of states and the vector of measurements; $v(k)$ is the noise (errors) in the measurements.

The State Vector $x(k)$ contains the main dynamic variables of the hydraulic motor that EKF needs to evaluate. In the model under consideration, these are the angular velocity of the hydraulic motor shaft $w_l(k)$ and the moment of external load $T_L(k)$. These values determine the dynamics of the system, affect the behaviour of the hydraulic motor and can be set by:

$$x(k) = \begin{bmatrix} w_l(k) \\ T_L(k) \end{bmatrix}. \quad (3)$$

The measurement vector $y(k)$ consists of quantities that are measured directly in the system. In this case, these are the angular velocity of the shaft $w_l(k)$, measured by the tach generator and the pressure difference $\Delta P(k)$, whose current values are determined by the pressure sensors located at the inlet and outlet of the hydraulic motor. These dimensions are used to correct the EKF forecasts, and the vector looks like this:

$$y(k) = \begin{bmatrix} w_l^{meas}(k) \\ \Delta P^{meas}(k) \end{bmatrix}, \quad (4)$$

where: $w_l^{meas}(k)$ is the measured value of the angular velocity of the hydraulic motor shaft in the kth step; $\Delta P^{meas}(k)$ – The measured value of the pressure difference between the inlet and outlet of the hydraulic motor in the kth step.

If we apply an inverse relation to equation (1) and write it from a discrete procedure in continuous time, we get an equation describing the evolution of the state vector $x(t)$

$$\dot{x}(t) = f[x(t), u(t)] + \omega(t). \quad (5)$$

The basic equation for the dynamics of a hydraulic motor is:

$$J_l \cdot \dot{w}_l(t) = T_{hid}(t) - T_L(t) - B_l \cdot w_l(t), \quad (6)$$

where: J_l – Inertial moment of the hydraulic motor shaft; B_l - resistance moment coefficient; $T_L(t)$ – the moment created by the external load; $T_{hid}(t)$ - the torque generated by the hydraulic motor.

The torque generated by the hydraulic motor $T_{hid}(t)$ It depends on the pressure difference between the inlet and outlet of the motor and is proportional to the working volume of the motor. This relationship can be expressed by the following formula:

$$T_{hid}(t) = \frac{V_d}{2 \cdot \pi} \cdot \Delta P(t), \quad (7)$$

where: V_d is the volume of hydraulic fluid that passes through the engine in one full revolution of the shaft.

After substituting (7) in (6), the expression

$$\dot{w}_l(t) = \frac{V_d}{2 \cdot \pi \cdot J_l} \cdot \Delta P(t) - \frac{T_L(t)}{J_l} - \frac{B_l}{J_l} \cdot w_l(t). \quad (8)$$

In the model under consideration, we assume that the load moment $T_L(t)$ changes slowly within short time intervals. This assumption is justified because in most practical applications of hydraulic motors, the external load does not undergo rapid changes in very short intervals. Usually, load changes are due to mechanical loads or external forces that act with smooth dynamics.

As a result, in small time intervals, we can assume that the derivative of the load moment is approximately zero:

$$\dot{T}_L(t) \approx 0. \quad (9)$$

This assumption facilitates mathematical modeling and improves the stability of the EKF by allowing the filter to predict states more efficiently under conditions of smooth load changes.

Thus, the dynamic model of the EKF system is written as:

$$\dot{x}(t) = \begin{bmatrix} \dot{w}_l(t) \\ \dot{T}_L(t) \end{bmatrix} = \begin{bmatrix} \frac{V_d}{J_l \cdot 2 \cdot \pi} \cdot \Delta P(t) - \frac{B_l}{J_l} \cdot w_l(t) - \frac{T_L(t)}{J_l} \\ 0 \end{bmatrix} + \begin{bmatrix} \omega_w(t) \\ \omega_T(t) \end{bmatrix}, \quad (10)$$

Where: $\omega_w(t)$ – noise and errors in the model related to angular velocity dynamics; $\omega_T(t)$ - the noise and errors in the model that occur when determining the external load.

Since EKF works in an iterative structure, it is necessary to bring the matrix equation (10) into discrete time, i.e.

$$w_l(k+1) = w_l(k) + \Delta t \cdot \left[\frac{V_d}{J_l \cdot 2 \cdot \pi} \cdot \Delta P(t) - \frac{B_l}{J_l} \cdot w_l(t) - \frac{T_L(t)}{J_l} \right] + \Delta t \cdot \omega_w(t), \quad (11)$$

$$T_L(k+1) = T_L(k) + \Delta t \cdot \omega_T(t).$$

Equations (11) represent the discrete dynamical model for EKF. In addition, in the discretization of the load torque equation $T_L(k+1)$ the added random component $\omega_T(t)$ is multiplied by Δt, since it derives from its derivative. But the load moment itself $T_L(k)$ it is not multiplied by the discrete of time, because in the model it is assumed that it changes slowly, and its derivative is approximately zero.

To be able to use EKF to estimate the states of the system, it is necessary to define the mathematical relationship between the measured quantities and the real states. This connection allows the filter to adjust its predictions using the available measurement information. In the model under consideration, the measured parameters include the angular velocity of the hydraulic motor shaft and the pressure difference between the inlet and outlet of the motor, which are used to update the states in the EKF. Angular velocity $w_l^{meas}(k)$ is measured by the tach generator and therefore:

$$w_l^{meas}(k) = w_l(k) + v_w(k), \quad (12)$$

where: $v_w(k)$ - noise and errors made in angular velocity measurement.

The pressure difference $\Delta P^{meas}(k)$ is measured by the sensors located at the inlet and outlet of the hydraulic motor, and the relationship with the moment generated by the hydraulic motor is determined by (7), i.e.

$$\Delta P(k) = \frac{2 \cdot \pi}{V_d} \cdot T_{hid}(k), \quad (13)$$

Considering the basic equation for the dynamics of a hydraulic motor (6) and after bringing the dependencies into discrete time, we get:

$$\Delta P^{meas}(k) = \frac{2 \cdot \pi}{V_d} \cdot \left[T_L(k) + J_l \cdot \frac{w_l(k) - w_l(k-1)}{\Delta t} + B_l \cdot w_l(k) \right] + v_P(k), \quad (14)$$

where: $v_P(k)$ is the noise and errors made when measuring pressure differences.

Then, the final form of the measurement model will be:

$$y(k) = \begin{bmatrix} w_l^{meas}(k) \\ \Delta P^{meas}(k) \end{bmatrix} = \begin{Bmatrix} w_l(k) \\ \frac{2 \cdot \pi}{V_d} \cdot \left[T_L(k) + J_l \cdot \frac{w_l(k) - w_l(k-1)}{\Delta t} + B_l \cdot w_l(k) \right] \end{Bmatrix} + \begin{bmatrix} v_w(k) \\ v_P(k) \end{bmatrix}. \quad (15)$$

In this way, the measurement model for EKF relates the measured quantities to the real states, considering both the non-linear dependencies in the system and the influence of noise in the measurements.

In EKF, Jacobian matrices are used to perform linearization of the nonlinear dynamic and measurement model. These matrices represent the local derivatives (gradients) of the respective functions relative to the states of the system. The Jacobian of the dynamic model $F(k)$ describes how small changes in states $x(k)$ affect the prediction of states in the next iteration, i.e.

$$F(k) = \frac{\partial f(x,u)}{\partial x}. \quad (16)$$

In addition, the Jacobian (16) is used to update the state covariance matrix.

For its part, the Jacobian of the measuring model $H(k)$ shows how the measured quantities depend on the current states, and its general form is:

$$H(k) = \frac{\partial h(x)}{\partial x}. \quad (17)$$

It is necessary to note that the matrix $H(k)$ participates in the calculation procedure for specifying the gain in the EKF filter by determining the weight of the measurements in the forecast correction.

The Jacobian matrix $F(k)$ can be presented in an expanded form as follows:

$$F(k) = \frac{\partial f(x,u)}{\partial x} = \begin{bmatrix} \frac{\partial f_1}{\partial w_l} & \frac{\partial f_1}{\partial T_L} \\ \frac{\partial f_2}{\partial w_l} & \frac{\partial f_2}{\partial T_L} \end{bmatrix}, \quad (18)$$

where f_1 is the equation for $w_l(k+1)$ в (11); f_2 is the equation for $T_L(k+1)$ in (11).

After calculating the partial derivatives of (18), the following final form for the matrix is obtained $F(k)$:

$$F(k) = \begin{bmatrix} 1 - \Delta t \cdot \frac{B_l}{J_l} & -\frac{\Delta t}{J_l} \\ 0 & 1 \end{bmatrix}. \quad (19)$$

From (15), the following two components can be determined that are necessary to determine the elements of the Jacobian matrix of the measurement model $H(k)$:

$$h_1 = w_l(k), \quad (20)$$

$$h_2 = \frac{2 \cdot \pi}{V_d} \cdot \left[T_L(k) + J_l \cdot \frac{w_l(k) - w_l(k-1)}{\Delta t} + B_l \cdot w_l(k) \right].$$

This matrix has the following form:

$$H(k) = \frac{\partial h(x)}{\partial x} = \begin{bmatrix} \frac{\partial h_1}{\partial w_l} & \frac{\partial h_1}{\partial T_L} \\ \frac{\partial h_2}{\partial w_l} & \frac{\partial h_2}{\partial T_L} \end{bmatrix}. \quad (21)$$

Then, the full form of the matrix $H(k)$ will be:

$$H(k) = \begin{bmatrix} 1 & 0 \\ \frac{2 \cdot \pi}{V_d} \cdot \left(\frac{J_l}{\Delta t} + B_l \right) & \frac{2 \cdot \pi}{V_d} \end{bmatrix}. \quad (22)$$

Among the elements of the matrix $H(k)$, the calculation of $\frac{\partial h_2}{\partial w_l}$ requires special analysis because it contains a difference between states from two consecutive iterations. In this case, the partial derivative of $J_l \cdot \frac{w_l(k) - w_l(k-1)}{\Delta t}$ to $w_l(k)$ determines the attitude $J_l / \Delta t$, since the derivative of $w_l(k-1)$ is equal to 0, because it is a value from the previous iteration and does not depend on the current state $w_l(k)$.

In the EKF, covariance matrices $Q(k)$ and $R(k)$ are essential for assessing uncertainty in the dynamic and measurement model. They are related to dynamic noise and deviations in the theoretical model, respectively $\omega(k)$ and noise and errors in measurement procedures $v(k)$. The covariance matrix of dynamic noise $Q(k)$ defines the statistical characteristics of the uncertainties in the model related to the dynamics of angular velocity and the moment created by the external load. In general, this matrix has extra diagonal elements that determine the correlation between the individual noise components. In the model under consideration, however, the noises $\omega_w(k)$ and $\omega_T(k)$ are considered uncorrelated because angular velocity dynamics errors and load moment uncertainties originate from different physical sources. This allows simplification of the covariance matrix $Q(k)$, Assuming as diagonal with the following form:

$$Q(k) = \begin{bmatrix} \sigma^2_{\omega_w}(k) & 0 \\ 0 & \sigma^2_{T_L}(k) \end{bmatrix}, \quad (23)$$

where: $\sigma^2_{\omega_w}(k)$ is the variance characterizing uncertainties and random variations in angular velocity dynamics $w_l(k)$, caused by model inaccuracies, nonlinear effects and external interference; $\sigma^2_{T_L}(k)$ is the dispersion that determines the deviations in the dynamics of the load moment $T_L(k)$, which may result from random external influences, changes in mechanical loads or unidentified variations in the characteristics of the system.

In the present paper, the variance $\sigma^2_{\omega_w}(k)$ is calculated dynamically by analysing the differences between measured and predicted angular velocity values in separate time intervals. This involves calculating the mean and standard deviation of these differences, and the variance can be adjusted adaptively as the characteristics of the system change. By analogy, the variance $\sigma^2_{T_L}(k)$ is estimated based on variations in the load time, analysing the deviations between the calculated and real values for different operating modes.

The covariance matrix of the measuring noise $R(k)$ describes the errors and noises made when measuring angular velocity and pressure difference. In this work, it is accepted that measurement errors $v_w(k)$ and $v_P(k)$ are uncorrelated because the tach generator and pressure sensors work on different principles and measure physically independent quantities. Therefore, the matrix $R(k)$ It has the following diagonal view:

$$R(k) = \begin{bmatrix} \sigma^2_{v_\omega}(k) & 0 \\ 0 & \sigma^2_{v_P}(k) \end{bmatrix}, \quad (24)$$

where $\sigma^2_{v_\omega}(k)$ is the variance characterizing errors in angular velocity measurement $w_l(k)$, caused by external interference and errors of the tach generator; $\sigma^2_{v_P}(k)$ is the variance determining the errors in measuring the pressure difference $\Delta P(k)$, which can arise from the sensitivity of sensors, temperature fluctuations, noises in electronic circuits or dynamic effects in the hydraulic system.

In practical applications, the variances of measuring noise $\sigma^2_{v_\omega}(k)$ and $\sigma^2_{v_P}(k)$ can be determined by statistical analysis of measurement results. One of the most common approaches is to calculate the standard deviation of the errors between the repeatedly measured values and their filtered estimates. This method allows adaptive updating of the covariance matrix in real time, which is why it is used in the present work.

In the structure of the Kalman Advanced Filter (EKF), the first step is prediction (Prediction Step of the status):

$$x^-_{k+1} = f(x_k, u_k). \quad (25)$$

In this phase, a prediction of the states of the system for the next iteration is performed using the nonlinear dynamic model. This allows the expected state values to be calculated in advance before making an adjustment based on the new measurements. Mathematically, this step is defined in a general form by equation (1), and for the specific system - by the already derived discretized equations for dynamics (11). For a more compact representation, these equations can be written in matrix form:

$$x^-_{k+1} = \begin{bmatrix} w^-_l(k+1) \\ T^-_L(k+1) \end{bmatrix} = \begin{bmatrix} w_l(k) \\ T_L(k) \end{bmatrix} + \Delta t \cdot \begin{bmatrix} \frac{V_d}{J_l \cdot 2 \cdot \pi} \cdot \Delta P(k) - \frac{B_l}{J_l} \cdot w_l(k) - \frac{T_L(k)}{J_l} \\ 0 \end{bmatrix}. \quad (26)$$

Along with the prediction of states, EKF also calculates the covariance error matrix of the model, which characterizes the uncertainty in the predicted state. This matrix P^-_{k+1} is updated by linear approximation using the Jacobian matrix $F(k)$ and the covariance matrix of dynamic noise $Q(k)$:

$$P^-_{k+1} = F(k) \cdot P_k \cdot F^T(k) + Q(k). \quad (27)$$

Gain $K(k)$ ensures the optimal combination of forecast values and current measurements by calculating according to the following formula:

$$K(k) = P^-_k \cdot H^T(k) \cdot [H(k) \cdot P^-_k \cdot H^T(k) + R(k)]^{-1}, \quad (28)$$

where: $H(k)$ – the Jacobian matrix of the measurement model, defined by (22); $R(k)$ – the covariance matrix of errors and noises allowed in the measurement of angular velocity and pressure difference determined by (24).

The correction of the predicted state is based on the difference between the current values of measured quantities $y(k)$ and their predicted values $h(x^-_k)$:

$$x_{k+1} = x^-_{k+1} + K(k) \cdot [y(k) - h(x^-_k)]. \quad (29)$$

Equation (29) has the following matrix form:

$$\begin{bmatrix} w_l(k+1) \\ T_L(k+1) \end{bmatrix} = \begin{bmatrix} w^-_l(k+1) \\ T^-_L(k+1) \end{bmatrix} + \begin{bmatrix} K_{11}(k) & K_{12}(k) \\ K_{21}(k) & K_{22}(k) \end{bmatrix} \cdot \left\{ \begin{bmatrix} w^{meas}_l(k) \\ \Delta P^{meas}(k) \end{bmatrix} - \begin{bmatrix} w_l(k) \\ \frac{2 \cdot \pi}{V_d} \cdot \left[T_L(k) + J_l \cdot \frac{w_l(k) - w_l(k-1)}{\Delta t} + B_l \cdot w_l(k) \right] \end{bmatrix} \right\}, \quad (30)$$

where $K_{11}(k)$, $K_{12}(k)$, $K_{21}(k)$, $K_{22}(k)$ are values obtained in the kth iteration when solving the matrix equation (28).

After the state correction, the EKF updates the covariance matrix P_{k+1}^{-}, by refining the assessment of state uncertainty after the inclusion of the new measurements:

$$P_{k+1} = [I - K(k) \cdot H(k)] \cdot P_{k+1}^{-}, \quad (31)$$

where: I is the single matrix.

III. Results and Discussion

A. Evaluation of EKF performance based on simulation studies

To evaluate the effectiveness of the developed EKF model, a simulation model was created in the MATLAB/Simulink programming environment. The simulations include the dynamic system of the hydraulic motor, measuring noises, as well as the application of EKF for state assessment. Some of the simulation results are shown in figures 2 and 3.

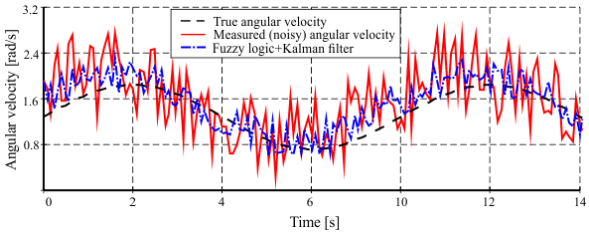

Fig. 2. Fig. 2: Change in the angular velocity of the hydraulic motor shaft with EKF set with preset values of Q and R.

The curves in Fig. 2 represent the change in angular velocity of the hydraulic motor shaft in two operating modes. In the first mode, the system works without turning on the EKF module, and the angular velocity is determined directly from the measured values (red curve). In this case, the noise in the measurements has a significant impact, resulting in deviations from the true value (the black broken curve). In the second mode, EKF is applied, and the resulting filtered value is represented by the blue curve. The figure shows that although the EKF reduces some of the noise, the result is not optimal due to incorrect adjustment of the filter parameters. In this case, the covariance matrices Q and R are selected with preset values, but without additional adjustment to the actual measurements, which limits the efficiency of the filter.

In Fig. Figure 3 shows the results after optimization of the covariance matrices Q and R. In this case, the filtered value (blue curve) is significantly closer to the true angular velocity (black dashed line), while the measurement noise is suppressed. This demonstrates the importance of proper adjustment of dies Q and R on the effectiveness of the EKF. In the optimized configuration, the die Q is tuned to reflect the dynamic uncertainties in the model, and R has been corrected based on empirical data from the measurement system, thus reducing correction errors.

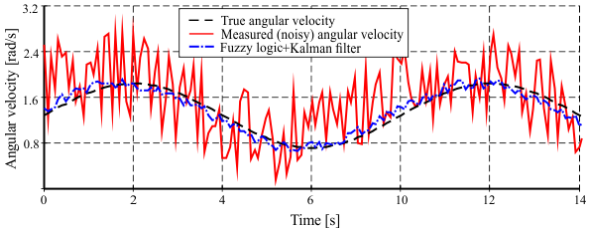

Fig. 3. Fig. 3: Angular velocity change with optimized covariance matrices Q and R in EKF.

Gain also plays an essential role in this iterative process K, which determines to what extent the measured values correct the predicted state. At optimal settings, the gain provides a balance between the predicted and measured values, which greatly improves the accuracy of the estimate. In the first case (Fig. 2) K is not optimally adjusted, resulting in less noise suppression, while in the second case (Fig. 3) an adaptive tuning method was used, resulting in a significantly better match to the actual dynamics of the system.

The results of simulation studies show that EKF can effectively reduce the influence of noise and improve the accuracy of the evaluated parameters, but its effectiveness is highly dependent on the adjustment of the covariance matrices Q and R, as well as the correct choice of gain K.

IV. Conclusions

In this work, a mathematical model of an extended Kalman filter (EKF) has been developed for evaluating dynamic states in an electro-hydraulic system. The main goal is to ensure higher accuracy and stability of estimates in the presence of noise and nonlinearities in the dynamics of the system. The model combines information from angular velocity and pressure difference measurements to provide reliable estimates of this output shaft speed and the torque created by the external load.

Simulation studies have shown that EKF significantly improves the accuracy of the evaluated parameters compared to a system without a filter. Along with this, these studies have shown the importance of tuning covariance matrices Q and R, which directly determine the accuracy and stability of the EKF. By optimizing these matrices, an optimal balance was achieved between the speed of reaction and the stability of the filter.

The practical significance of the developed model is expressed in its applicability for real electro-hydraulic systems, while at the same time it can be adapted for other nonlinear dynamic systems. The results obtained demonstrate the potential of EKF to improve the accuracy and stability of control systems under noise and dynamic load conditions.

Acknowledgment

This research was funded by the European Regional Development Fund under the Operational Program "Scientific Research, Innovation and Digitization for Smart Transformation 2021-2027", Project CoC "Smart

Mechatronics, Eco- and Energy Saving Systems and Technologies", BG16RFPR002-1.014-0005.

REFERENCES

[1] F. Wang, Y. Qiao, H. Zhou, J. Wu, B. Xu, "An Independent Electro-Hydraulic Variable Speed Drive to Improve Energy Efficiency of Electric Wheel Loader Working System, " IEEE Transactions on Vehicular Technology, volume 73, issue 12, 2024, pp. 18250 – 18265. DOI: 10.1109/TVT.2024.3438268

[2] S. Qiao, Y. Hao, L. Quan, L. Ge, L. Xia, " A Novel Electro-Hydraulic Compound Driving System with Potential Energy Regeneration Capability for Lifting Device," IEEE Access, volume 10, 2022, pp. 18248-18256. DOI: 10.1109/ACCESS.2022.3149515

[3] S. Qu, F. Zappaterra, A.Vacca, Z. Liu, E. Busquets, "Experimental Verification of an Electro-Hydraulic Actuation System Driven by an Integrated Electro-Hydraulic Unit," International Journal of Fluid Power, volume 24, issue 2, 2023, pp. 327-360. 10.13052/ijfp1439-9776.2427

[4] T. Ntsiyin, E. Markus, L. Masheane, "A Survey of Energy-Efficient Electro-Hydraulic Control System for Collaborative Humanoid Robots," In IOT with Smart Systems: Proceedings of ICTIS 2021, volume 2, 2022, pp. 65-77. DOI: 10.1007/978-981-16-3945-6_8

[5] Z. Yan, L. Ge, L. Quan, "Energy-Efficient Electro-Hydraulic Power Source Driven by Variable-Speed Motor," Energies, volume 15, issue 13, 2022. DOI: 10.3390/en15134804

[6] D. Padovani, S. Ketelsen, L. Schmidt, "Downsizing the Electric Motors of Energy-Efficient Self-Contained Electro-Hydraulic Systems by Using Hybrid Technologies," In Fluid Power Systems Technology, volume 83754, 2020, September. DOI: 10.1115/FPMC2020-2717

[7] J. Li, L. Kong, H. Liang, W. Li, "Review of Development and Characteristics Research on Electro-Hydraulic Servo System," Recent Patents on Engineering, volume 18, issue 6, pp. 140-154, 2024. DOI: 10.2174/1872212118666230711165517

[8] A. Santos, A. da Silva, C. Felgueiras, F. Pereira, "Increasing Energy Efficiency of Electro-Hydraulic Oil Systems to Reduce Industrial Carbon Emissions,"In International Conference on Energy and Environment Research, 2022, September, pp. 471-480. DOI: 10.1007/978-3-031-43559-1_45

[9] M. Kowalczyk, K. Tomczyk, "Quality of Machined Surface and Cutting Force When Milling NiTi Alloys Materials," volume 17, issue 24, 2024, DOI: 10.3390/ma17246122.

[10] I. Malakov, V. Zaharinov, Choosing an Optimal Size Range of the Product "Pipe Clamp". (Book Chapter). In: Matoušek R., Kůdela J. (eds) Recent Advances in Soft Computing and Cybernetics., ISSN: 14349922, Springer, Cham., Volume 403, 2021, Pages 197-213, DOI: 10.1007/978-3-030-61659-5_17

[11] V. Mitev, I. Malakov, "Analysis of the Quality of Polymer Parts for Automatic Assembly," AIP Conference Proceedings, Volume 3063, Issue 1, 060012, 21 February 2024, International Conference on Engineering Physics, Electronics and Earth Science (EEPES 2023), Kavala, Greece, ISSN 0094243X, ISBN 978-073544856-8, DOI 10.1063/5.0195873

[12] I. Malakov, V. Zaharinov, S. Nikolov, R. Dimitrova, G. Stambolov, "Determining the Influence of Model Parameters on the Choosing of an Optimal Size Range of Pneumatically Actuated Linear Modules for Sprayer Robots," Annals of DAAAM and Proceedings of the International DAAAM Symposium, DAAAM 2022, 33(1), pp. 105-114, DOI: 10.2507/33rd.daaam.proceedings.016

[13] I. Malakov, V. Zaharinov, "Interactive Software System for Multicriteria Choosing of the Structural Variant of Complex Technical Systems," Annals of DAAAM for 2012 & Proceedings of the 23rd International DAAAM Symposium, ISBN 978-3-901509-91-9, ISSN 2304-1382, Editor B[ranko] Katalinic, Published by DAAAM International, Vienna, Austria 2012, pp. 0199-0204.

[14] I. Malakov,V. Zaharinov, S. Nikolov, R. Dimitrova, " Computer-Aided Choosing of an Optimal Structural Variant of a Robot for Extracting Castings from Die Casting Machines," In Actuators, volume 12, issue 9, 2023, September. DOI: 10.3390/act12090363

[15] D. Komarski, D. Diakov, H. Nikolova, V. Vassilev, "Analysis of the Impact of the Central Connecting Element Stiffness on the Accuracy Characteristics of Micro-Positioning Elastic Module with 'Butterfly' Flexures", In 33rd International Scientific Symposium Metrology and Metrology Assurance, MMA, 2023. DOI: 10.1109/MMA59144.2023.10317907

[16] D. Diakov, D. Komarski, "Micro-positioning Module for Angular Orientation Position of the Axis of Rotation Analysis", In 31st International Scientific Symposium Metrology and Metrology Assurance, MMA, 2021, DOI: 10.1109/MMA52675.2021.9610873

[17] D. Diakov, D. Komarski, H. Nikolova, "Optimization of Butterfly Flexures for Angular Positioning", In 31st International Scientific Symposium Metrology and Metrology Assurance, MMA, 2021. DOI: 10.1109/MMA52675.2021.9610833

[18] D. Komarski, D. Diakov, R. Nikolov, "Analysis of the Transfer Curve and the Center of Rotation of Elastic Micro-Positioning Module with Optimized Butterfly Flexures", In 32nd International Scientific Symposium Metrology and Metrology Assurance, MMA, 2022. DOI: 10.1109/MMA55579.2022.9993338

[19] K. Tomczyk, P. Beńko, K. Ostrowska, "Maximum Energy Density for Evaluation of the Dynamic Accuracy of LVDT Sensors Applied in the Energy Industry," Energies, volume 17, issue 22, 2024. DOI: 10.3390/en17225525

[20] K. Tomczyk, K. Ostrowska, J. Sładek, J. Konieczny, " The Levenberg–Marquardt Procedure for Modeling Accelerometers Used in the Energy Industry," Energies, volume 17, issue 23, 2024. DOI: 10.3390/en17236072

[21] B. Gao, W. Shen, L. Zheng, W. Zhang, H. Zhao, "A Review of Key Technologies for Friction Nonlinearity in an Electro-Hydraulic Servo System," Machines, volume 10, issue 7, 2022. DOI: 10.3390/machines10070568

[22] B. Zhang, M. Enyan, R. Junsen, Z. Xinxing, L. Hongyu, " Position Control of Electro-hydraulic Servo System Based on Repetitive Control Strategy," Recent Patents on Mechanical Engineering, volume 17, issue 4, pp. 260-280. DOI: 10.2174/0122127976288436240221060807

[23] P. Wos, R. Dindorf, "Nonlinear Modeling and Parameter Identification for Electro-Hydraulic Servo System," In 2019 20th International Carpathian Control Conference (ICCC), 2019, May. DOI: 10.1109/CarpathianCC.2019.8765947

Environment. Technology. Resources. Rezekne, Latvia
Proceedings of the 16th International Scientific and Practical Conference. 2025. Volume IV, 73-79

Parameter Evaluation and Control in an Electro-Hydraulic System Using an Advanced Least Squares Method

Dimitar Dichev
Department of Mechanical and Precision Engineering
Technical University of Gabrovo
Center of competence "Smart mechatronic, eco-and energy-saving systems and technologies"
Gabrovo, Bulgaria
dichevd@abv.bg

Borislav Georgiev
Department of Mechanical and Precision Engineering
Technical University of Gabrovo
Center of competence "Smart mechatronic, eco-and energy-saving systems and technologies"
Gabrovo, Bulgaria
gborislav@gbg.bg

Iliya Zhelezharov
Department of Mechanical and Precision Engineering
Technical University of Gabrovo
Center of competence "Smart mechatronic, eco-and energy-saving systems and technologies"
Gabrovo, Bulgaria
izhel@tugab.bg

***Abstract*— Electro-hydraulic systems are characterized by high complexity and nonlinearity, caused by the dynamic interactions between the fundamental quantities that determine their operation and control. The present study proposes a method for adaptive parameter estimation using an advanced method of least squares (A-LS) (Advanced Least Squares), applicable to nonlinear dynamical systems. The paper presents a mathematical model describing the dynamics of the electro-hydraulic system, as well as an approach for adaptive parameter estimation using Recursive Least Squares (RLS) in combination with the Stochastic Gradient Method (SGD). The main goal is to minimize errors between measurement results and predicted model values, ensuring high accuracy and stability under variable operating conditions. The results of the simulations show that the use of RLS for angular velocity estimation and SGD for adaptive load torque correction allows for effective noise suppression in measurements and precise tracking of system dynamics. The proposed approach provides a basis for optimizing electro-hydraulic systems through adaptive methods and can be useful for applications requiring high accuracy and reliability.**

Keywords*— Electro-hydraulic system; Recursive least squares; Stochastic gradient descent; dynamic parameter estimation.

I. INTRODUCTION

Electro-hydraulic systems play an essential role in several industrial and engineering applications requiring high accuracy, reliability, and efficiency in motion control [1-5]. These systems combine the advantages of electrical and hydraulic technologies, providing high drive power in compact dimensions and good dynamic performance [6-10]. They are also widely used in robotics, automation, aviation systems, digital program control (CNC), heavy industry, and mobile hydraulics, where precise control of forces and movements is required [11-20].

Among the main advantages of electro-hydraulic systems are a high power-to-weight ratio, the ability to smoothly adjust the movement and a large output force. Additionally, they can operate under extreme loads and are suitable for applications requiring the ability to transmit large forces and power in compact sizes. Another important advantage is the high efficiency of power transmission and the ability to work with several types of loads, including intermittent dynamic loads. These systems can be integrated with advanced control algorithms, such as adaptive and predictive regulators, which further improves their flexibility and energy efficiency [21, 22].

Despite these advantages, electro-hydraulic systems also have significant drawbacks that can limit their accuracy and stability. A major problem is the nonlinearities that arise because of the dynamic interactions between pressure, flow, and load. Factors such as changes in temperature, mechanical backlash and viscosity of the working fluid also contribute to the complex behaviour of the system. In addition, noises appear in the measuring circuits of the system, which can reduce the quality of control and lead to significant errors in the evaluation of parameters. Another important disadvantage is the delay in the dynamic response of the system, which can lead to undesirable transients and instability in case of sudden changes in the load [23, 24].

Online ISSN 2256-070X
https://doi.org/10.17770/etr2025vol4.8417
© 2025 The Author(s). Published by RTU PRESS.
This is an open access article under the Creative Commons Attribution 4.0 International License.

To overcome these shortcomings, various methods of correction and optimization have been proposed. These include the Kalman filter and its advanced versions, including the Extended Kalman Filter (EKF) and the Advanced Kalman Filter (UKF), which can be used to optimally filter measurements and reduce the impact of noise. Another alternative technique is the Wiener filter, which provides optimal linear filtering of the signal in the presence of white noise. In some cases, nonlinear adaptive methods are also applied, such as filters based on the Monte Carlo method (Particle Filters) and methods based on neural networks, which provide greater flexibility when working with dynamically changing systems [25-27].

This article proposes an advanced method for adaptive parameter estimation based on the Least Squares method with recursive correction (RLS) and the stochastic gradient method. Compared to the above methods, RLS offers more efficient processing of parametric estimates in real time and does not require prior noise statistical information, as is required with the Kalman filter. In addition, the stochastic gradient method provides rapid adaptation to changing dynamic external loads without incurring significant computational costs typical of nonlinear filters. The purpose of this method is to minimize errors between measured and predicted values, ensuring higher accuracy and stability under changes in operating conditions. The method combines adaptive algorithms to estimate parameters, considering dynamic influences on the system, and is particularly suitable for applications where external forces and moments change in real time.

This article will present a detailed analysis of the electro-hydraulic system, develop the mathematical model for adaptive parameter assessment and analyse the effectiveness of the proposed methodology through a simulation model.

II. MATERIALS AND METHODS

A. Description of the electro-hydraulic system

The electro-hydraulic system developed in this work is a set of mechanical, hydraulic, and electronic components that work together to provide high-precision motion control. In Fig. 1, its schematic diagram is presented. At the heart of the system is the induction motor 1, whose operation is controlled by frequency control 10. This control allows for a change in the frequency and voltage of the current supplied to the motor, which provides precise control of speed and torque. The induction motor is connected to the hydraulic pump 2, which converts mechanical energy into hydraulic energy, creating flow rate and pressure. These parameters, in turn, determine the operation of the hydraulic motor 4, which converts hydraulic energy back into mechanical energy, driving the output shaft and overcoming the external load 8.

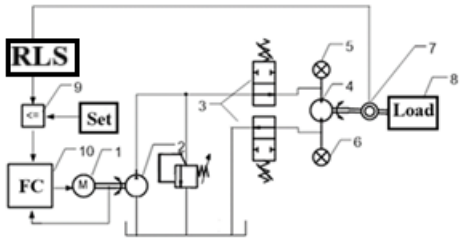

Fig. 1. Schematic diagram of electro-hydraulic drive system.

The system is equipped with measuring sensors that provide information about the change in the main values in the system. Pressure sensors 5 and 6 are installed at the inlet and outlet of the hydraulic motor, which measure the inlet and outlet pressure. In addition, to measure the angular velocity, a tach generator 7 is installed to the shaft of the hydraulic motor. The system also contains ON/OFF valves 3, which control the flow of hydraulic fluid, as well as a tuning unit 9, where the signals from the developed control optimization filter are transmitted.

B. Development of the RLS mathematical model for adaptive parameter estimation

The mathematical model is based on the differential equation describing the dynamics of the electro-hydraulic system:

$$T_{hid}(t) = J_l \cdot \dot{\omega}_l(t) + B_l \cdot \omega_l(t) + T_L(t), \qquad (1)$$

where: $T_{hid}(t)$ - the moment that reaches the shaft of the hydraulic motor; J_l - Inertial moment of the hydraulic motor shaft; B_l - Coefficient of friction in the hydraulic motor; $T_L(t)$ - the external load applied to the shaft of the hydraulic motor.

Equation (1) describes the balance of torques, considering inertial forces, frictional losses, and the influence of external load. This approach is standard for modeling dynamic systems and allows analysing the influence of various parameters on the behaviour of the system.

The torque generated by the hydraulic motor can be determined from the equation.

$$T_{hid}(t) = \frac{V_d}{2\pi} \cdot \Delta P(t) = T_{hid}(t) = \frac{V_d}{2\pi} \cdot [P_{in}(t) - P_{out}(t)], \qquad (2)$$

where V_d - The displacement of the hydraulic motor (the volume of fluid moved per revolution); $P_{in}(t)$ и $P_{out}(t)$ – the inlet and outlet pressure of the hydraulic motor, measured now of time t.

To apply the method for adaptive estimation of parameters based on the method of least squares, it is necessary to bring equation (1) into a discrete form and conform to the structure of the iterative procedure, i.e.

$$\omega_l(k+1) = \omega_l(k) + \Delta t \cdot \frac{V_d}{2\pi \cdot J_l} \cdot [P_{in}(k) - P_{out}(k)] - \Delta t \cdot \frac{B_l}{J_l} \cdot \omega_l(k) - \Delta t \cdot \frac{T_L(k)}{J_l}, \quad (3)$$

The external load $T_L(k)$ it is usually not a constant value, and its accurate prediction of each step of the iterative procedure can provide useful information for the effective control of the electro-hydraulic system. In this work, a method for determining the current values of the external load, based on iterative optimization, is adopted. Since $T_L(k)$ Equation (3), the method for iterative optimization can be based on this dependence, minimizing the difference between the predicted $\omega_l^{pred}(k)$ and the measured angular velocity $\omega_l^{meas}(k)$. The error between the predicted and measured angular velocity is determined by the difference.

$$e(k) = \omega_l^{meas}(k) - \omega_l^{pred}(k), \quad (4)$$

where $\omega_l^{meas}(k)$ - the measured angular velocity in step k; $\omega_l^{pred}(k)$ - the predicted angular velocity from the model.

The aim is to determine this value of $T_L(k)$, where the error $e(k)$ will have a minimum value. To iteratively update $T_L(k)$ In this work, the method of gradient descent was used (SGD), which in this case has the form.

$$T_L(k+1) = T_L(k) - \eta \cdot \frac{\partial E}{\partial T_L}, \quad (5)$$

where η is the coefficient of learning (learning rate), and $E(T_L)$ is determined by the expression.

$$E(T_L) = \frac{1}{2} \cdot \sum_{k=1}^{N} \left[\omega_l^{meas}(k) - \omega_l^{pred}(k)\right]^2 = \frac{1}{2} \cdot \sum_{k=1}^{N} e(k)^2, \quad (6)$$

where $E(T_L)$ - the sum of the squares of the errors and shows how well the moment of the load $E(T_L)$ approach the actual behaviour of the system.

The gradient descent method is preferred in this case over other optimization approaches, as it provides an effective approximation to the optimal solution without the need for prior information about the statistical properties of noise in the system. In addition, gradient descent allows for rapid adaptation to dynamically changing conditions, making it suitable for real-time applications. Compared to methods such as Newtonian optimization, which require the calculation of the second derivative (Hessian matrix), gradient descent is a significantly more computationally efficient approach and can be easily implemented in adaptive algorithms.

The aim is to determine the values of $T_L(k)$, that minimize the function $E(T_L)$. Since the partial derivative $\frac{\partial E}{\partial T_L}$ is a function of the error $e(k)$ It follows that if the error is positive (the predicted speed is less than the measured one), and it is necessary to increase the $T_L(k)$. If the error is negative, the value of the $T_L(k)$. This procedure gradually adjusts the $T_L(k)$, докато грешката стане близка до нула. However, the gradient method does not always guarantee reaching a global minimum. Depending on the initial conditions and characteristics of the error function $E(T_L)$, the algorithm can fall into local minima or have slow convergence, especially if the surface of the error function contains plateau or pronounced minima. To improve convergence, techniques such as adaptive learning factor or the addition of dynamic acceleration in gradient descent are often used in practice to avoid stagnation at negligible local minimums and accelerate reaching the global minimum. In the current study, however, the focus is on the accuracy of load torque estimation, rather than on accelerating convergence. In addition, the adopted adaptive assessment method ensures stable behaviour even in the absence of additional acceleration techniques. It is therefore necessary to determine the gradient in terms of $T_L(k)$, i.e., how the change in the moment created by the external load affects the error. For this purpose, the differentiation rule can be used:

$$\frac{\partial E}{\partial T_L} = \sum_{k=1}^{N} e(k).\frac{\partial e(k)}{\partial T_L}. \quad (7)$$

Since the algorithm being developed works in an iterative procedure, it is more appropriate to use the stochastic gradient method instead of the full gradient, which includes a sum of all iterations (which would be slower and more complex), which updates the parameter step-by-step, using only the current error:

$$T_L(k+1) = T_L(k) - \eta \cdot \frac{\partial e(k)}{\partial T_L(k)} \cdot e(k). \quad (8)$$

The sum in (8) is dropped because the method makes the correction of each iteration using the instantaneous error $e(k)$, instead of waiting for the accumulation of information from all previous steps. This is the main advantage of the Stochastic Gradient Method (SGD) over the classical gradient descent, which uses the average of all errors to update the parameters. Although SGD allows for faster adaptation to current changes in the system and can find an approximation to the optimal solution significantly earlier, it can lead to increased variability in parameter updates. For this reason, the stability of the algorithm depends on the correct choice of the learning factor η. To determine the partial derivative of the $e(k)$ error from the moment created by the load in the kth iteration, the following equation can be used:

$$\frac{\partial e(k)}{\partial T_L(k)} = \frac{\partial}{\partial T_L(k)}\left[\omega_l^{meas}(k) - \omega_l^{pred}(k)\right]. \quad (9)$$

Since $\omega_l^{meas}(k)$ does not depend on $\partial T_L(k)$, the derivative is converted to:

$$\frac{\partial e(k)}{\partial T_L(k)} = -\frac{\partial \omega_l^{pred}(k)}{\partial T_L(k)}. \quad (10)$$

Equation (3) shows that the only term dependent on $\partial T_L(k)$, e $-\Delta t \cdot \frac{T_L(k)}{J_l}$. Therefore:

$$T_L(k+1) = T_L(k) + \eta \cdot \frac{\Delta t}{J_l} \cdot e(k). \quad (11)$$

Formula (11) is the iterative formula for updating the load moment, based on the stochastic gradient method (SGD), which performs a step-by-step update (on each iteration) using only the current error $e(k)$, which makes the algorithm faster and more adaptable. Here we correct $T_L(k)$ at each step, so the mistake $e(k)$ decrease.

An important parameter in gradient descent is the learning coefficient η, which specifies the update step of a moment defining the external load $T_L(k)$ in each iteration. Choosing the appropriate value for this coefficient is essential for the speed and stability of adaptation. If η is too small ($\eta \leq 0.01$), the update of the $T_L(k)$ will be conducted too slowly, which can lead to a significant delay in the algorithm's response to real changes in the system. In such cases, error correction will be insufficiently effective, and the process may require too many iterations to reach an optimal result. If η has too much value ($\eta \geq 0.1$), algorithm will make aggressive adjustments that can lead to variations around the real value of the $T_L(k)$ or even to instability of adaptation. In this case, the load torque will fluctuate unnaturally with each step, and unwanted fluctuations in the system may occur. The experience gained from various applications shows that the initial value of $\eta = 0.05$ is a good compromise between quick adaptation and stability. Depending on the dynamics of the system, this parameter can be further adjusted experimentally to ensure optimal behaviour.

The vector form of the least squares method model, which minimizes errors between measured and predicted values, is as follows:

$$\omega_l(k+1) = \Phi(k) \cdot \theta + \varepsilon(k), \quad (12)$$

where: $\Phi(k)$ is a matrix of regressors; θ is the vector with the parameters of the system; $\varepsilon(k)$ – The error of the model in the kth step.

In this work, in contrast to the classical method of least squares (MLS), which is used to identify constant parameters, we apply MLS for dynamic estimation of the angular velocity of the shaft of a hydraulic motor $\omega_l(k)$ and the moment of external load $T_L(k)$. This is achieved by minimizing error $\varepsilon(k)$, defined as the difference between the measured and predicted angular velocity value:

$$\sum_k \varepsilon^2(k) = \sum_k [\omega_l^{meas}(k+1) - \Phi(k) \cdot \theta]^2. \quad (13)$$

For the display of $\Phi(k)$ and θ, We bring equation (3) to the following form, considering that $T_L(k)$ is evaluated separately by an iterative procedure for the Stochastic Gradient Method (SGD):

$$\omega_l(k+1) = \left(1 - \Delta t \cdot \frac{B_l}{J_l}\right) \cdot \omega_l(k) + \Delta t \cdot \frac{V_d}{2\pi \cdot J_l} \cdot [P_{in}(k) - P_{out}(k)]. \quad (14)$$

The Regressor Matrix $\Phi(k)$ consists of the input values of the model, which determine the dynamics of the system, and serves as the basis for estimating the unknown parameters using the method of least squares. In contrast to the standard applications of the method of least squares, in this study the quantities that are evaluated dynamically are the angular velocity of the hydraulic motor shaft $\omega_l(k)$ and load torque $T_L(k)$, since they change over time and must be precisely defined for the management of the system. In connection with what has been said, the matrix $\Phi(k)$ It can be written as follows:

$$\Phi(k) = [P_{in}(k+1) - P_{out}(k+1) \quad \omega_l^{meas}(k+1)]. \quad (15)$$

In the present work, with sufficient accuracy for real-world applications, we assume that the measured value of angular velocity $\omega_l^{meas}(k)$ is used directly as an input dimension in the model. This decision is because sensor measurements, although subject to some errors, provide more reliable information about the actual dynamics of the system compared to the result of an accumulation of predicted values. The use of measured data prevents the accumulation of errors in the iteration process, which is especially important for the long-term stability of the model. Furthermore, this approach allows the method of least squares to be more precise in estimating angular velocity and load torque, without the need for additional filtering or adaptive algorithms to select optimal values. Therefore, the full form of the matrix (15) will be:

$$\Phi_N(k) = \begin{bmatrix} P_{in}(k+1) - P_{out}(k+1) & \omega_l^{meas}(k+1) \\ P_{in}(k) - P_{out}(k) & \omega_l^{meas}(k) \\ P_{in}(k-1) - P_{out}(k-1) & \omega_l^{meas}(k-1) \\ \vdots & \vdots \\ P_{in}(0) - P_{out}(0) & \omega_l^{meas}(0) \end{bmatrix}. \quad (16)$$

However, in the current recursive algorithm, to minimize computational complexity, we use only the matrix (15).

The Parameter Vector θ contains the constant physical coefficients of the system, which determine the relationship between the input quantities $P_{in}(k) - P_{out}(k)$ and $\omega_l(k)$ in the current iteration and output angular velocity $\omega_l(k+1)$ in the next iteration

$$\theta = \begin{bmatrix} \Delta t \cdot \frac{V_d}{2\pi \cdot J_l} \\ 1 - \Delta t \cdot \frac{B_l}{J_l} \end{bmatrix}. \quad (17)$$

To bring the algorithm to the concept of recursive evaluation of parameters, it is necessary to define the recursive gain factor $K(k)$:

$$K(k) = P(k) \cdot \Phi^T(k) \cdot [\lambda + \Phi(k) \cdot P(k) \cdot \Phi^T(k)]^{-1}, \quad (18)$$

where λ – weight factor (forgetting factor); $P(k)$ – covariance matrix of estimates.

The weighting factor controls the speed of adaptation of the algorithm. Lower values of λ (close to 0.95) give more weight to new measurements, which makes the algorithm more adaptable to changes in system dynamics. Higher values (close to 1) reduce the impact of new data and retain more information than previous estimates, resulting in a smoother correction. Since the processes in the electro-hydraulic system do not change abruptly over time, a value is assumed in this work $\lambda = 0.99$, which provides a good balance between stability and adaptability of the algorithm.

Since the moment created by the external load $T_L(k)$, is determined by a separate stochastic gradient method (SGD), the recursive algorithm (RLS) includes the estimation of angular velocity $\omega_l(k)$ and the pressure difference $P_{in}(k+1) - P_{out}(k+1)$. This allows for more precise adaptive estimation since the dynamics of the system are directly dependent on these two parameters as well.

The use of RLS for $\omega_l(k)$ and SGD for $T_L(k)$ is justified by the different update mechanisms. RLS minimizes accumulated errors, while SGD makes quick corrections step-by-step. The inclusion of $T_L(k)$ in RLS would lead to a conflict between the two methods, which may reduce the effectiveness of adaptive assessment. The vector of the evaluated parameters is:

$$X(k) = \begin{bmatrix} \hat{\omega}_l(k) \\ \Delta\hat{P}(k) \end{bmatrix}, \quad (19)$$

where $\hat{\omega}_l(k) = \omega_l^{pred}(k)$ is the estimation of the angular velocity of the hydraulic motor shaft in the kth step; $\Delta\hat{P}(k)$ is the estimation of the difference between the inlet and outlet pressure of the hydraulic motor in the kth step.

In the adaptive estimation of these parameters, it is necessary to derive a corresponding covariance matrix that defines the uncertainty in the estimates:

$$P(k) = \begin{bmatrix} \sigma_\omega^2 & 0 \\ 0 & \sigma_{\Delta P}^2 \end{bmatrix}, \quad (20)$$

where σ_ω^2 is the variance of errors in angular velocity estimation; $\sigma_{\Delta P}^2$ is the variance of errors in the pressure difference estimate.

Initially, the variances in the $P(k)$ is set with high values, which allows the algorithm flexibility in initial iterations, and subsequently the values are dynamically updated, which leads to a decrease in uncertainty over time.

The recursive formula for updating grades is:

$$X(k+1) = X(k) + K(k) \cdot \delta(k), \quad (21)$$

where the error vector $\delta(k)$ It has the following form:

$$\delta(k) = \begin{bmatrix} \omega_l^{meas}(k+1) - \hat{\omega}_l(k) \\ \Delta P^{meas}(k+1) - \Delta\hat{P}(k) \end{bmatrix}, \quad (22)$$

where $\omega_l^{meas}(k+1)$ is the measured value of the angular velocity in k+1 – iteration; $\Delta P^{meas}(k+1)$ is the measured value of the pressure difference in k+1 – iteration.

After each iteration, the covariance matrix $P(k)$ is updated to consider added information and thus reduce uncertainty in estimates. The update procedure is determined by the matrix equation:

$$P(k+1) = P(k) - K(k) \cdot \Phi(k) \cdot P(k). \quad (23)$$

This adjustment ensures that the algorithm remains adaptable to changes in system dynamics while improving the accuracy of angular velocity and pressure difference estimates.

III. Results and Discussion

A. Evaluation of the operability of the method through a simulation experiment

To evaluate the effectiveness of the proposed adaptive method for parameter estimation, a simulation model has been developed in the MATLAB/Simulink environment. The model includes the electro-hydraulic system from Fig.1 with a dynamically changing load and a mechanism for adaptive estimation of angular velocity and load torque. The presented results illustrate the behaviour of the system under conditions of changing input influences. The estimation of angular velocity is performed using the recursive least squares method (RLS), and the moment of external load is updated using the stochastic gradient method (SGD).

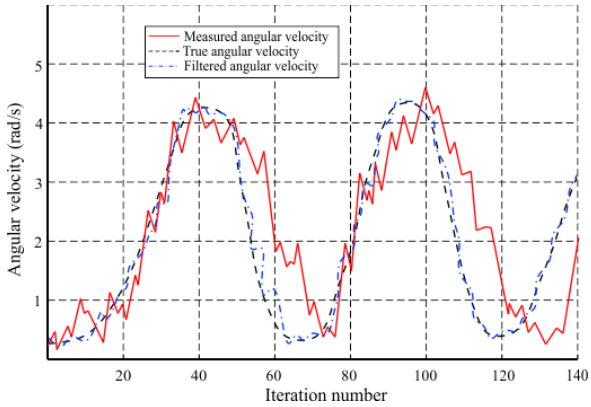

Fig. 2. Comparison of measured, true, and filtered angular velocity estimated by RLS with gradient correction.

In Fig. Figure 2 presents graphically the curves illustrating the measured angular velocity (the red curve), the true angular velocity (the black dotted curve) and the angular velocity estimated by the recursive method of least squares (the blue dotted curve). The graph shows that the measured angular velocity contains significant fluctuations and noise, which makes it difficult to use it directly for control. Despite these fluctuations, the estimation obtained by the recursive method of least squares follows the true angular velocity with high accuracy. This shows that the algorithm effectively eliminates measurement noise and

provides accurate angular velocity determination in real time. The difference between the true and estimated angular velocity is minimal, demonstrating the good convergence of the algorithm. Even with sudden changes in movement, the filtered angular velocity remains stable and follows the dynamics of the system with a small delay.

The results confirm that the proposed methodology provides high accuracy and stability of the estimates, which is essential for the application of the method in electro-hydraulic systems. The successful noise suppression and elimination of parasitic oscillations makes the method suitable for managing dynamic processes where the reliability of assessments is critical.

The dynamics of the estimated load torque $T_L(k)$ is shown in Fig. 3. The curve is obtained using the stochastic gradient method (SGD). The graph shows how the moment created by the external load adapts with each iteration, gradually following the increasing trend of the actual load.

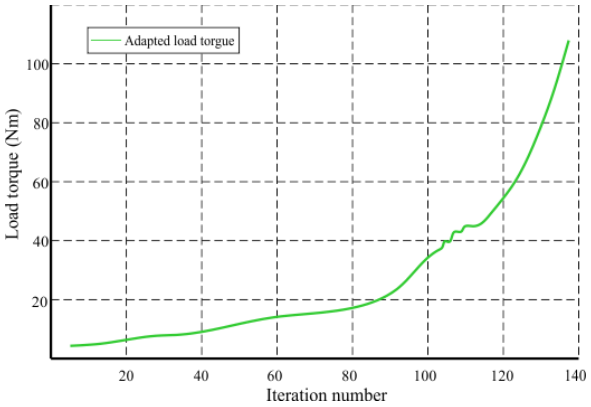

Fig. 3. Adaptive estimation of external load moment by stochastic gradient method (SGD).

In the initial iterations, the load torque is small and changes smoothly, which is the result of the initial uncertainty in the estimates. As the iterations progressed, the algorithm was able to track the change more accurately in load, ensuring a smooth and stable adaptation. At the end of the simulation, an increase in load torque was observed, indicating that the algorithm successfully identified changes in dynamic load.

The absence of significant variations and sharp deviations in the load estimate confirms the stability of the algorithm. This is especially important in applications where the load torque may vary due to external factors, such as changes in operating conditions or external interference.

The results obtained show that the combined use of RLS for angular velocity estimation and SGD for load torque estimation provides reliable and adaptive tracking of system dynamics. This approach allows for rapid adaptation to changing conditions, while maintaining stability and minimizing errors in estimates.

IV. Conclusions

This paper presents an advanced method for estimating parameters in an electro-hydraulic system based on the recursive least squares method (RLS) and the stochastic gradient method (SGD). Through the developed mathematical model and the simulations conducted, it was proved that the proposed methodology provides high accuracy in estimating the angular velocity of the hydraulic motor and the load torque, effectively suppressing noise in measurements.

The results of the simulation experiment confirm that the combined use of RLS and SGD results in reliable adaptation of real-time estimates, which is essential for dynamically changing workloads. The method offers stability and quick response of the system to variations in operating conditions, making it suitable for applications requiring high precision and adaptability.

The proposed approach can be further extended by applying nonlinear optimization techniques, as well as by integrating additional filtering methods to improve immunity to noise and uncertainties in the system.

ACKNOWLEDGMENTS

This research was funded by the European Regional Development Fund under the Operational Program “Scientific Research, Innovation and Digitization for Smart Transformation 2021-2027”, Project CoC “Smart Mechatronics, Eco- and Energy Saving Systems and Technologies”, BG16RFPR002-1.014-0005.

References

[1] A. K. Kumawat, "Control and Modelling of Industrial Electro-Hydraulic Actuation System," in Proc. 2024 2nd Int. Conf. Computer, Communication and Control (IC4), Feb. 2024, doi: 10.1109/IC457434.2024.10486739.

[2] A. Skvorchevsky, "Electronic Load Sensing for Integrating Electro-Hydraulic Mechatronic Actuators with Industry 4.0 and 5.0 Components," in Int. Conf. Reliable Systems Engineering, vol. 762 LNNS, pp. 440-455, Aug. 2023, doi: 10.1007/978-3-031-40628-7_37.

[3] E. Erzan Topçu, "PC-based control and simulation of an electro-hydraulic system," Computer Applications in Engineering Education, vol. 25, no. 5, pp. 706-718, 2017, doi: 10.1002/cae.21831.

[4] J. Li, L. Kong, H. Liang, and W. Li, "Review of development and characteristics research on electro-hydraulic servo system," Recent Patents on Engineering, vol. 18, no. 6, pp. 140-154, 2024, doi: 10.2174/1872212118666230711165517.

[5] S. Z. Mafokwane and D. V. V. Kallon, "Design of Electro-Hydraulic Circuits of Tri-adjustable Automated Heavy-Duty Industrial Handling System," in Proc. Int. Conf. Industrial Engineering and Operations Management, vol. 59, pp. 357-367, 2020.

[6] O. H. Khedr, S. A. Maged, A. K. Al-Oufy, and M. I. Awad, "Developing control systems to improve motion tracking of electro-hydraulic systems subjected to external load," Int. J. Dynamics and Control, vol. 12, no. 3, pp. 761-773, 2024, doi: 10.1007/s40435-023-01228-z.

[7] W. Jiang et al., "A Study on the Electro-Hydraulic Coupling Characteristics of an Electro-Hydraulic Servo Pump Control System," Processes, vol. 10, no. 8, 2022, doi: 10.3390/pr10081539.

[8] K. Tomczyk, P. Beńko, and K. Ostrowska, "Maximum Energy Density for Evaluation of the Dynamic Accuracy of LVDT Sensors Applied in the Energy Industry," Energies, vol. 17, no. 22, 2024, doi: 10.3390/en17225525.

[9] I. Malakov, V. Zaharinov, S. Nikolov, and R. Dimitrova, "Computer-Aided Choosing of an Optimal Structural Variant of a Robot for Extracting Castings from Die Casting Machines," Actuators, vol. 12, no. 9, Sep. 2023, doi: 10.3390/act12090363.

[10] I. Malakov and V. Zaharinov, "Choosing an Optimal Size Range of the Product 'Pipe Clamp'," in Recent Advances in Soft Computing and Cybernetics, R. Matoušek and J. Kůdela, Eds. Cham: Springer, vol. 403, pp. 197-213, 2021, doi: 10.1007/978-3-030-61659-5_17.

[11] V. Mitev and I. Malakov, "Analysis of the Quality of Polymer Parts for Automatic Assembly," AIP Conf. Proc., vol. 3063, no. 1, 060012, Feb. 2024, doi: 10.1063/5.0195873.

[12] I. Malakov and V. Zaharinov, "Interactive Software System for Multicriteria Choosing of the Structural Variant of Complex Technical Systems," in Proc. 23rd Int. DAAAM Symp., Vienna, Austria, 2012, pp. 0199-0204.

[13] I. Malakov et al., "Determining the influence of model parameters on the choosing of an optimal size range of pneumatically actuated linear modules for sprayer robots," in Ann. DAAAM and Proc. Int. DAAAM Symp., vol. 33, no. 1, pp. 105-114, 2022, doi: 10.2507/33rd.daaam.proceedings.016.

[14] Z. Liu et al., "A review on integral evolution of electro-hydraulic actuation in three momentous domains: aerospace, engineering machinery, and robotics," in Proc. 4th Int. Conf. Mechanical Engineering, Intelligent Manufacturing, and Automation Technology (MEMAT), vol. 13082, pp. 141-159, Apr. 2024, doi: 10.1117/12.3026210.

[15] S. Du et al., "Application, and progress of high-efficiency electro-hydrostatic actuator technology with energy recovery: A comprehensive review," Energy Conversion and Management, vol. 321, 2024, doi: 10.1016/j.enconman.2024.119041.

[16] Y. Zhang, "Research and Design of Hydraulic System for CNC Radial Drilling Special Machine Tool," in Advances in Machinery, Materials Science and Engineering Application X, vol. 58, pp. 39-45, 2024, doi: 10.3233/ATDE240601.

[17] D. Komarski, D. Diakov, H. Nikolova, and V. Vassilev, "Analysis of the Impact of the Central Connecting Element Stiffness on the Accuracy Characteristics of Micro-Positioning Elastic Module with 'Butterfly' Flexures," in Proc. 33rd Int. Sci. Symp. Metrology and Metrology Assurance (MMA), 2023, doi: 10.1109/MMA59144.2023.10317907.

[18] D. Diakov and D. Komarski, "Micro-positioning Module for Angular Orientation Position of the Axis of Rotation Analysis," in Proc. 31st Int. Sci. Symp. Metrology and Metrology Assurance (MMA), 2021, doi: 10.1109/MMA52675.2021.9610873.

[19] D. Diakov, D. Komarski, and H. Nikolova, "Optimization of Butterfly Flexures for Angular Positioning," in Proc. 31st Int. Sci. Symp. Metrology and Metrology Assurance (MMA), 2021, doi: 10.1109/MMA52675.2021.9610833.

[20] D. Komarski, D. Diakov, and R. Nikolov, "Analysis of the Transfer Curve and the Center of Rotation of Elastic Micro-Positioning Module with Optimized Butterfly Flexures," in Proc. 32nd Int. Sci. Symp. Metrology and Metrology Assurance (MMA), 2022, doi: 10.1109/MMA55579.2022.9993338.

[21] B. Zhang, M. Enyan, R. Junsen, Z. Xinxing, and L. Hongyu, "Position Control of Electro-hydraulic Servo System Based on Repetitive Control Strategy," Recent Patents on Mechanical Engineering, vol. 17, no. 4, pp. 260-280, doi: 10.2174/0122127976288436240221060807.

[22] K. Tomczyk, K. Ostrowska, J. Sładek, and J. Konieczny, "The Levenberg–Marquardt Procedure for Modeling Accelerometers Used in the Energy Industry," Energies, vol. 17, no. 23, 2024, doi: 10.3390/en17236072.

[23] B. Gao, W. Shen, L. Zheng, W. Zhang, and H. Zhao, "A review of key technologies for friction nonlinearity in an electro-hydraulic servo system," Machines, vol. 10, no. 7, 2022, doi: 10.3390/machines10070568.

[24] J. Li, W. Li, H. Liang, and L. Kong, "A Review of the Research on Electro-hydraulic Load Simulator, and Characteristics with Improvement Methods," Recent Patents on Engineering, vol. 18, no. 3, pp. 45-56, 2024, doi: 10.2174/1872212118666230410102416.

[25] N. Simonsen et al., "Noise attenuation in a secondary controlled electro-hydraulic actuator using an extended Kalman filter," in Proc. Fluid Power Systems Technology, vol. 85239, Oct. 2021, doi: 10.1115/FPMC2021-68658.

[26] W. O. L. Vianna, L. G. de Souza Ribeiro, and T. Yoneyama, "Electrohydraulic servo valve health monitoring using fading extended Kalman filter," in Proc. 2015 IEEE Conf. Prognostics and Health Management (PHM), Jun. 2015, doi: 10.1109/ICPHM.2015.7245033.

[27] L. Lao and P. Chen, "Adaptive Sliding Mode Control of an Electro-Hydraulic Actuator with a Kalman Extended State Observer," IEEE Access, vol. 12, pp. 8970–8982, 2024, doi: 10.1109/ACCESS.2024.3349946.

Environment. Technology. Resources. Rezekne, Latvia
Proceedings of the 16th International Scientific and Practical Conference. 2025. Volume IV, 81-84

Development of Composites Based on Thermosetting Polymers (Epoxy, Polyester and Vinylester Resins) with Cenosphere Fillers in Different Concentrations – 5 wt.%, 10 wt.% and 15 wt.%

Boyan Dochev
Faculty of Mechanical Engineering
Technical University of Sofia, Branch Plovdiv
Plovdiv, Bulgaria
boyan.dochev@gmail.com

Filip Ublekov
Institute of Polymers
Bulgarian Academy of Sciences
Sofia, Bulgaria
fublekov@polymer.bas.bg

Desislava Dimova
Faculty of Mechanical Engineering
Technical University of Sofia, Branch Plovdiv
Plovdiv, Bulgaria
desislava608738@gmail.com

Mihail Zagorski
Faculty of Industrial Technology
Technical University of Sofia
Sofia, Bulgaria
mihail.zagorski.tu@gmail.com

Nikola Tomanov
Faculty of Mechanical Engineering
Technical University of Sofia,
Branch Plovdiv
Plovdiv, Bulgaria
nikotomanov75@gmail.com

***Abstract*—Experiments were conducted to develop lightweight composites based on thermosetting polymers with cenosphere fillers. Cenospheres are rich in Al and Si particles and are known as low-density aluminosilicate CFA microspheres. The production of a polymer-based structural material (composite) with reduced weight and good mechanical properties, in which a waste product polluting the environment is used as a filler, is a current engineering task. Epoxy, polyester and vinylester resins were used, as well as different filler concentrations (cenospheres – 5 wt.%, 10 wt.% and 15 wt.%). The mechanical properties of the developed composites were studied. It was found that the use of cenospheres positively affects the mechanical properties of the vinylester resin, while in the case of other thermosetting plastics an increase in some of the mechanical characteristics was registered.**

***Keywords*—thermosetting polymers, cenospheres, mechanical properties**

I. Introduction

Composite materials are the basis for the development of new efficient products. In industry, polymer-based composites and light alloys are widely used due to their strength and low density. The combination of reduced weight and good mechanical properties make composites the preferred materials for various engineering solutions. They have found wide application in automotive, aerospace, marine and civil engineering.

During the production of electricity from thermal power plants, huge amounts of coal fly ash are generated annually which leads to environmental pollution. Coal fly ash contains heavy metals that can be released upon contact with water [1], minerals such as magnetite, calcite, mullite [2], as well as silica and cristobalite [3]. The furnaces in thermal power plants operate at high temperatures and therefore structural differences are observed in the fly ash particles: plerospheres, ferrospheres and cenospheres (CS) [4]. Plerospheres are particles containing gases, minerals and many smaller particles [5], ferrospheres are spherical particles rich in iron [6], and cenospheres are rich in aluminium and silicon [3]. These Al and Si-rich particles are known as aluminosilicate CFA microspheres [3].

Cenospheres are hollow particles with a spherical shape and their size ranges from 5-500 μm [7], with an average size in the range of 30-350 μm [8, 9]. They have

Online ISSN 2256-070X
https://doi.org/10.17770/etr2025vol4.8431
© 2025 The Author(s). Published by RTU PRESS.
This is an open access article under the Creative Commons Attribution 4.0 International License.

found application in various fields: construction [8], building materials [10], paints and coatings [11], ceramics [12], plastics [13], polymer fillers [14], etc. In [15] the structural, thermal, mechanical and dynamic properties of polypropylene-based composites with cenosphere fillers were investigated. The development of syntactic foam based on high-density polyethylene (HDPE) and cenosphere fillers was presented in [16]. The dielectric properties of a composite of low-density polyethylene (LDPE) and cenospheres were investigated in [17].

The purpose of this study is to study the possibility of developing composites based on thermosetting polymers and cenosphere fillers.

II. MATERIALS AND METHODS

Epoxy, polyester and vinylester resins were used to conduct the experiments. The epoxy system "LETOXIT" is based on epoxy resin for lamination "LETOXIT" PR 227 and hardener "LETOXIT" EM 315. Due to its low viscosity and low surface tension, the used resin system wets the laminating fabrics well, and therefore is used for the production of laminates with glass fibers, carbon or aramid fibers. The manufacturer's prescription was followed for the preparation of the resin system, namely 100:38 mass proportions when mixing (resin:hardener). The polyester resin used is DISTITRON 429 BSX25Q, the hardener is MEKR50 in an amount of 2 wt.%, and the amount of accelerator MEKR used is also 2 wt.%. The vinyl ester resin is DISTITRON VE 100, the hardener is MEKR50 and again the amount used is 2 wt.%.

Cenospheres in amounts of 5 wt.%, 10 wt.% and 15 wt.% with sizes in the range of 50-250 μm, with the main fraction having sizes of 100 μm (Fig. 1), were used to develop the composites.

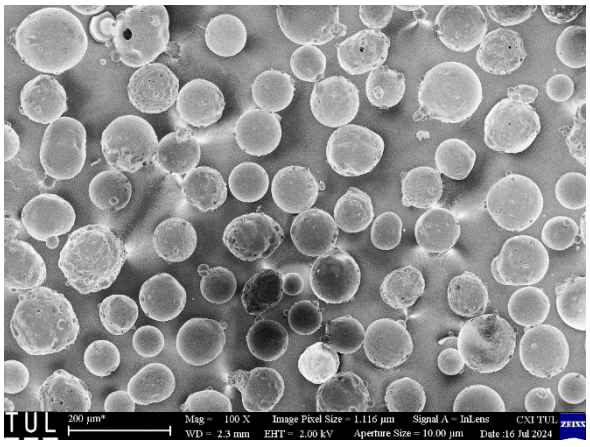

Fig. 1. Image of the cenospheres used.

The composition of the ceramic shell of the cenospheres used was also investigated (Fig. 2 and Fig. 3).

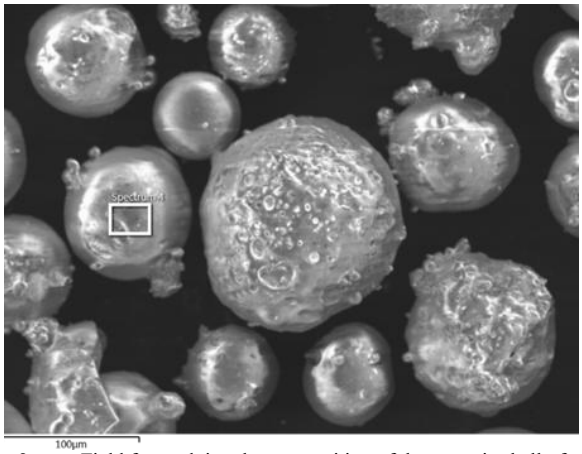

Fig. 2. Field for studying the composition of the ceramic shell of cenospheres

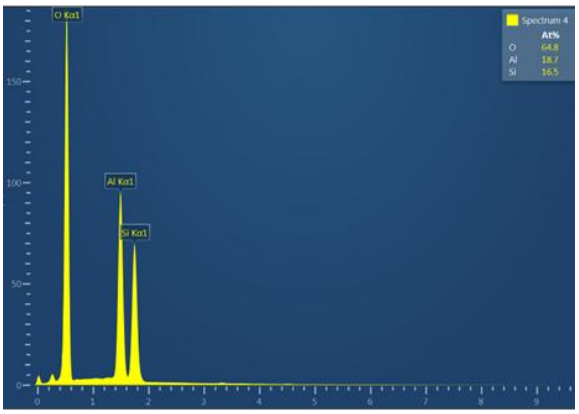

Fig. 3. Chemical composition of the ceramic shell of the used cenospheres.

The results show that the ceramic shell of the used cenospheres consists of silicon-16 at.%, aluminium - 18.7 at.% and oxygen - 64.8 at.%.

The investigated composites based on the thermosetting polymers and aluminosilicate spheres were produced by mechanical stirring at a working temperature of 25ºC (according to the manufacturers' instructions for working with the epoxy resin system). Test specimens were gravity cast for tensile testing and impact toughness testing. Before conducting the mechanical tests, the samples based on epoxy resin were subjected to secondary polymerization at a temperature of 55ºC for 12h. (resin manufacturer's instructions).

The uniaxial tensile test was performed on a Zwick Roell Z050 testing machine, the impact toughness test was performed with an Izod GT-7045-HM device under the following conditions: Izod Impact Test, 1J (10.20 kg.cm), Method - reversed notch, Speed 3.46 m/sec., and the hardness of the composites was measured using the Shore method (scale D - HSD). This method for determining hardness is elastic-dynamic, i.e. the tip is lowered from a certain height and the height of the rebound is used to determine the hardness of the material, using a table showing the value of the hardness versus the rebound value. The measurement was performed using an EQUOTIP hardness tester.

III. Results and discussion

The results of the mechanical tests conducted on the epoxy resin-based composites are shown in Table 1.

Table 1 Results of mechanical tests of epoxy resin-based composite

Cenospheres [wt. %]	Rm [MPa]	A [%]	HSD	E/A (kg.cm/cm^2)
0 wt.%	49	0.8	76.7	1.60
5 wt.%	35.3	0.7	84.7	0.89
10 wt.%	29.2	0.8	87.1	0.88
15 wt.%	26.2	1.7	82.3	0.96

The results obtained show that the pure resin system has the highest values of tensile strength and impact toughness. The addition of 5 wt.% filler leads to a decrease in tensile strength and impact toughness, the elongation at break is like that of the pure polymer, but the hardness of the composite is increased. The highest hardness was measured in the composite with a filler of 10 wt.%, but the tendency to decrease the Rm value is also maintained in it. The impact toughness and the elongation at break are with values identical to the same characteristics as in the composite with 5 wt.% cenospheres. The use of 15 wt.% aluminosilicate spheres as a filler leads to a decrease in the Rm values, the hardness also decreases, but its values are higher compared to those of the pure polymer. A significant increase in the elongation was registered and a tendency to increase the impact toughness value is observed.

The results of the mechanical tests conducted on the polyester resin-based composites are shown in Table 2.

Table 2 Results of mechanical tests of a polyester-based composite

Cenospheres [wt. %]	Rm [MPa]	A [%]	HSD	E/A (kg.cm/cm^2)
0 wt.%	47.8	0.0	79.8	0.32
5 wt.%	29.3	0.0	81.7	0.30
10 wt.%	27.1	0.0	64.8	0.31
15 wt.%	19.8	0.0	55.9	0.26

The results show that the addition of cenospheres to the polyester resin matrix leads to a decrease in both tensile strength and hardness, with only a slight increase in the hardness of the composite being recorded when 5 wt.% filler is used. When 5 wt.% and 10 wt.% cenospheres are used, the impact toughness values of the composite are comparable to the value of the pure resin, and with an increase in the percentage of filler (15 wt.%) the impact toughness decreases.

The results of the mechanical tests conducted on vinylester resin-based composites are shown in Table 3.

Table 3 Results of mechanical tests of a vinylester-based composite

Cenospheres [wt. %]	Rm [MPa]	A [%]	HSD	E/A (kg.cm/cm^2)
0 wt.%	20.5	0.0	75.7	0.375
5 wt.%	33.3	1.3	71.1	0.506
10 wt.%	26	1.7	43.5	0.537
15 wt.%	20	0.7	40	0.443

The results of the studies of composites based on vinylester resin with aluminosilicate sphere filler show a tendency of decreasing hardness values with increasing percentage of filler in the composite. In contrast to the studies with epoxy and polyester resin, with vinylester resin an increase in tensile strength, elongation at break and impact toughness of the composites was registered compared to the same parameters of the pure resin. Only with the composite with 15 wt.% filler was registered a comparable tensile strength compared to the pure polymer.

The experimental results obtained for the studied composites based on the thermosetting polymers with cenosphere fillers are not unambiguous. In the composites with a polyester resin matrix, the amounts of filler used do not positively affect the studied properties. Although the tensile strength and impact toughness of the composites based on epoxy resin are reduced compared to the pure polymer, the filler has a positive effect on the plasticity of the material. The most noticeable positive effect of the different concentrations of cenospheres is registered in the composites based on vinylester resin. A decrease in the hardness of the composites compared to the pure polymer is registered, but the tensile strength and impact toughness are increased. The amounts of filler used have contributed to imparting plasticity to a hard and brittle material. Given that epoxy and vinyl ester resins are commonly used for the production of laminates, expanding the scope of research with reinforcing fibers such as glass fibers, carbon or aramid fibers is appropriate.

IV. Conclusions

Lightweight composites based on thermosetting polymers (epoxy, polyester and vinylester resins) with cenosphere filler in different concentrations – 5 wt.%, 10 wt.% and 15 wt.% have been developed. It has been established that the filler used has a positive effect on the mechanical properties of the vinylester resin, while in the case of other thermosetting plastics an increase in some of the mechanical characteristics has been registered. The obtained results are a prerequisite for expanding the scope of research with the presented composites in order to develop laminates with reinforcing fibers such as glass fibers, carbon or aramid fibers.

The development of lightweight composites with a thermoplastic polymer matrix and aluminosilicate microspheres as filler is the subject of future research.

The development of composites with a polymer matrix and cenosphere filler is a current engineering task. Obtaining new structural composite materials, in which the filler is a waste product and an environmental pollutant (cenospheres), which can be used in mechanical engineering, automotive engineering, aerospace, marine and civil engineering will also have a positive environmental effect.

Acknowledgments: This research is supported by the Bulgarian Ministry of Education and Science under the National Program „Young Scientists and Postdoctoral Students – 2“

REFERENCES

[1] N. B. Kumar,R. Radhika, V. V. Kumar, B. Chakradhar, „Regulatory Requirements for Fly ash Utilisation from Thermal Power Plants in India“, Int. J. Appl. Environ. Sci. 2020, 15, pp. 151–166.

[2] K.Y. Virendra, S. Pallavi, L. Chagan, G. Govindhan, C. Nisha, S. Bijendra, T. Neha, K. Haresh, K. Pankaj, „Synthesis and Characterization of Mullites From Silicoaluminous Fly Ash Waste“, Int. J. Appl. Nanotechnol. Res. IJANR 2020, 5, pp. 10–25.

[3] V.K. Yadav, M.H. Fulekar, „Advances in Methods for Recovery of Ferrous, Alumina, and Silica Nanoparticles from Fly Ash Waste“. Ceramics 2020, 3, pp. 384–420.

[4] C. Nisha, K.Y. Virendra , M. Parth, H. K. Samreen, K. I. Gajendra, R. Suriyaprabha, S. Bijendra, A.K. Yadav, K. R. Raman, „Recovery of Natural Nanostructured Minerals: Ferrospheres, Plerospheres, Cenospheres, and Carbonaceous Particles From Fly Ash“. In Handbook of Research on Emerging Developments and Environmental Impacts of Ecological Chemistry; Gheorghe, D., Ashok, V., Eds.; IGI Global: Hershey, PA, USA, 2020; pp. 450–470.

[5] F. Goodarzi, H. Sanei, „ Plerosphere and its role in reduction of emitted fine fly ash particles from pulverized coal-fired power plants“. Fuel 2009, 88, pp. 382–386.

[6] E. Strzałkowska, „Morphology, chemical and mineralogical composition of magnetic fraction of coal fly ash“. Int. J. Coal Geol. 2021, 240, 103746.

[7] E. Strzałkowska, Z. Adamczyk, $Influence of chemical composition of fly-ash cenospheres on their grains size“. Int. J. Environ. Sci. Technol. 2020, 17, pp. 809–818.

[8] L.N. Ngu, H. Wu, D.K. Zhang, „Characterization of Ash Cenospheres in Fly Ash from Australian Power Stations“. Energy Fuels 2007, 21, pp. 3437–3445.

[9] S. Yoriya, T. Intana, P. Tepsri, „Separation of Cenospheres from Lignite Fly Ash Using Acetone–Water Mixture“. Appl. Sci. 2019, 9, 3792.

[10] H. P. Satpathy, S. K. Patel, A. N. Nayak, „Development of sustainable lightweight concrete using fly ash cenosphere and sintered fly ash aggregate“. Constr. Build. Mater. 2019, 202, pp. 636–655.

[11] A. A. Morquecho, A. C. Valdez, J. A. Quintana, „High temperature thermal barrier coatings from recycled fly ash cenospheres“. Appl. Therm. Eng. 2012, 48, pp. 117–121.

[12] A. Nithyanandam, T. Deivarajan, „Development of fly ash cenosphere-based composite for thermal insulation application“. Int. J. Appl. Ceram. Technol. 2021, 18, pp. 1825–1831.

[13] D. Nakonieczny, M. Antonowicz, Z. Paszenda, „Cenospheres and their application advantages in biomedical engineering—A systematic review“. Rev. Adv. Mater. Sci. 2020, 59, pp. 115–130.

[14] K. Irtiseva, V. Lapkovskis, V. Mironovs, J. Ozolins, V. K. Thakur, G. Goel, J. Baronins, A. Shishkin, „Towards Next-Generation Sustainable Composites Made of Recycled Rubber, Cenospheres, and Biobinder“. Polymers 2021, 13, 574.

[15] A. Das, B. K. Satapathy, „Structural, thermal, mechanical and dynamic mechanical properties of cenosphere filled polypropylene composites“, Materials & Design, Vol. 32, 2011,pp.1477-1484 https://doi.org/10.1016/j.matdes.2010.08.041

[16] B.R. B. Kumar, M. Doddamani, S. E. Zeltmann, N. Gupta, M.R. Ramesh, S. Ramakrishna, „Processing of cenosphere/HDPE syntactic foams using an industrial scale polymer injection molding machine“, Materials & Design, Vol. 92, 2016, pp. 414-423 https://doi.org/10.1016/j.matdes.2015.12.052

[17] J. Sharma, N. Chand, M.N. Bapat, „Effect of cenosphere on dielectric properties of low density polyethylene“, Results in Physics, Vol. 2, 2012, pp. 26-33 https://doi.org/10.1016/j.rinp.2012.03.003

Environment. Technology. Resources. Rezekne, Latvia
Proceedings of the 16th International Scientific and Practical Conference. 2025. Volume IV, 85-90

The Role of the Leader in the Process of Overcoming Communication Barriers in the New Era of Industry 4.0

Svetlana Dimitrakieva
Department of Industrial Management
Technical University of Varna
Varna, Bulgaria
s_dimitrakieva@abv.bg

Marina Marinova-Stoyanova
Department of Industrial Management
Technical University of Varna
Varna, Bulgaria
mpmstoyanova@tu-varna.bg

Zhulieta Mihaylova
Department of Industrial Management
Technical University of Varna
Varna, Bulgaria
zhulieta.mihaylova@tu-varna.bg

***Abstract*— Modern challenges in the new era of Industry 4.0 confront leaders with communication barriers. Barriers are factors that block or negatively change successful communication in teams. They cause stress, which is the result of dynamically developing technologies and advanced automation of processes. Depending on the leader, barriers can be temporary and surmountable, but they can be permanent and more difficult to overcome. The proposed key factors of a leader are closely related to leadership skills in the process of overcoming communication barriers. .Taking into account the specific characteristics of the industry and the growing role of the leader in the process of making management decisions, an algorithm is proposed for successfully overcoming communication barriers in the new era of Industry 4.0. The purpose of the report is to analyze the barriers and systematize the key factors for successful communication in the team and the role of the leader in developing Fig. 1. A model of an algorithm for successfully overcoming communication barriers..**

Keywords*— Communication Barriers, Role of the Leader, Industry 4.0, model of an algorithm for successfully overcoming communication barriers

I. INTRODUCTION

The dynamic changes brought about by technological transformation, digitalization, and automation of production processes lead to shifts in communication methods, which in turn create a growing need for clear communication within teams. The leader's communication plays a crucial role in uniting the team around shared visions and achievable goals.

Communication is the procedure of encoding an purpose into a notification, which is then transmitted through communication channels and decoded by the recipient [1]. A key aspect of managerial communication is the ability to persuade others to act.

In the new era of Industry 4.0, with the increasing influence of artificial intelligence, leaders face challenges related to overcoming new communication barriers in the management process. Communication is one of the essential tools for leaders in managing teams. Interpersonal communication is at the heart of any team's success, but existing barriers related to factors beyond the leaders' control can lead to both positive and negative consequences within the team [2].

The development of Industry 4.0, driven by new technological advancements such as the implementation of information and communication technologies in the production process—e.g., artificial intelligence, digital systems for process monitoring and control, network communications, and large-scale data collection and processing—has necessitated a review of existing communication barriers within teams.

The paper used a qualitative research methodology based on an extensive literature review and critical analysis to explore the key role of leadership in successfully overcoming communication barriers in Industry 4.0.

II. MATERIALS AND METHODS

The study refers to a research methodology based on an extensive review of contemporary literature and critical analysis to systematize the communication barriers and key leadership skills to overcome them in the context of Industry 4.0. Key sources of data include journal publications, research studies, and websites focusing on

Online ISSN 2256-070X
https://doi.org/10.17770/etr2025vol4.8450
© 2025 The Author(s). Published by RTU PRESS.
This is an open access articleunder the CreativeCommonsAttribution 4.0 InternationalLicense.

communication processes, technological developments, and the role of contemporary leadership in the new era of Industry 4.0.

The research process includes systematization and identification of communication barriers, challenges faced by contemporary leaders related to successful overcoming of barriers. The analytical key categories included the nature and types of organizational barriers, the need to improve the skills of the contemporary leader aimed at sustainable industry development.

Personal interview methods were applied with leaders who substantiated the practical issues in the process of interpersonal and cultural communication in teams.Conceptual insights were supported by theoretical frameworks to practical examples and models of management decision making.

This methodological approach helped to develop a theoretical algometric model for successfully overcoming communication barriers in the new era of Industry 4.0.

III. Results and Discussion

Communication barriers are factors that block or significantly alter successful communication. The results of a critical review of the current literature show that about 20% of communication problems that cause problems in Industry 4.0 can be overcome. Awareness and recognition are of paramount importance in the process of overcoming barriers. Successfully overcoming communication barriers leads to an improved organizational environment and optimized work processes in today's reality.

However, organizational readiness to identify significant barriers and successfully overcome them depends entirely on the leadership decisions of leaders. Their role and key skills are the basis for the successful development of any organization in Industry 4.0.

1. Communication barriers in the team

Communication barriers within teams create obstacles in receiving and understanding the messages used by others to convey specific information, ideas, and thoughts. The causes of communication breakdown and the creation of barriers within teams are rooted in individuals' differing attitudes, values, and expectations, which stem from various perceptions, authority, and life status within the team. Barriers are factors that negatively affect successful communication within the team.

Research shows that 20% of these influences can be avoided or successfully resolved by the leader [3]. After conducting analyses, the barriers that affect effective communication in the team in the new era of Industry 4.0 were identified.

A. Personal Barriers.

Personal barriers. A key issue that creates barriers in teams is the informal authority assumed by a team member or the mentorship provided by another person within the team. Status differences related to power and organizational hierarchy, especially in manager-employee relationships, are also a precondition for establishing barriers.

On the other hand, the absence of hierarchy in power differences does not guarantee effective communication. New information technologies offer an alternative way to overcome barriers related to status differences by establishing non-hierarchical work relationships [4].

Interpersonal communication within the team is essential for quality and work relationships in the organization. Leaders who demonstrate empathy and respond to interpersonal communication with employees foster trust and loyal relationships within the team. It turns out that leaders who are direct, dictatorial, and arrogant with employees create barriers, which leads to team unproductivity. Encouraging feedback improves interpersonal communication within the team and prevents barriers [5]. A lack of sincere communication within the team is defined as a barrier that leads to social isolation and inefficiency.

B. Behavioral Barriers.

Behavioral barriers. Behavior related to biases and stereotypes also leads to communication barriers. Appearance and behavior contribute to different stereotypical views among people. Stereotypes arise from various assumptions made by employees within the team [6]. Views are based on bias initiated by specific behavior, appearance, or particular possessions. These barriers lead to communication breakdowns. Leaders must treat every team member equally. Rules and fairness should guide the formation of organizational relationships within the team. Therefore, regardless of viewpoints, appearance, and personality differences among team members, the leader must appreciate all behavioral differences and personality traits of the employees.

C. Cultural Values.

Cultural values and behavior patterns can be confusing communication barriers within the team. People worldwide differ, and these diverse types of cultural stereotypes can be confusing and misleading in intercultural communication. Differences are provoked by international values that influence motivation, leadership, and teamwork in work relationships. Once again, it is the leader’s responsibility to establish, refine, and unify the use of specific words in the communication process and clarify their use within the team.

D. Language Barriers

Language is a key component of communication. Language barriers arise when employees speak different languages or the level of proficiency is different in the relevant language. Barriers also occur when employees

speak the same language but use jargon that is incomprehensible to other team members.

E. Gender Differences.

Communication barriers resulting from gender differences are explained by variations in conversational styles. Men and women have different communication styles. Research shows that women prefer face-to-face communication, as it facilitates direct understanding. It is proven that women provide limited information to team members [7]. In such cases, the leader's role is to clarify the information between parties, rather than allowing free interpretation of the meaning from one's perspective.

2. *A leader's key role for overcoming communication barriers in industry 4.0*

According to Peter Drucker, leadership is the act of pushing human imagination toward higher horizons, elevating the quality of work to higher standards, and developing the human personality beyond its normal limits [8]. There are various definitions of leadership, but one of the most interesting comes from Harry Truman, who described leadership as the ability to get others to do something they don't want to do and make them like it. Regardless of the different definitions, many authors agree that thanks to leadership, people achieve more than they would without a leader, they follow the leader voluntarily, and their efforts are directed toward achieving specific goals.

Leaders in the new era of Industry 4.0 have access to more communication tools than ever before. New technologies lead to restructuring teams and workplaces, which can either encourage or discourage ethical communication. The key factors for overcoming communication barriers in the context of digital transformation in Industry 4.0 have been systematized. As it becomes evident, the leader is at the core of the successful management of any team. As technology advances, the role of communication within the team and its surrounding environment becomes increasingly prominent [9].

A. Clear, Specific, and Systematic Communication.

The leader's role in the team is paramount to effective communication with employees and all stakeholders. According to other authors communication is key to effective crisis management [10]. Leaders must be able to provide clear, specific, and systematic communication to employees, keeping them informed about the organization's state while motivating them and maintaining their motivation.

Leaders must communicate clearly and effectively with the team and other stakeholders. They should be ready to listen to employees' opinions and experiences to make the most effective decisions for the organization and overcome all barriers faced by the Industry 4.0 team [11]. Establishing open and transparent communication with employees and all interested parties reduces uncertainty and builds trust and commitment. Various communication means may be used, including social media, emails, video conferences, and others. It is important to choose the appropriate communication method that is relevant to the needs of team members.

Clear and specific communication. In modern reality of Industry 4.0, leaders must be able to communicate clearly and specifically. They must provide the team with accurate information about the company's condition, as well as the measures that will be taken in a crisis and how it will be overcome [12]. Leaders must be able to answer team members' questions and inform them about the steps taken to resolve the issue.

B. Creating Two-Way Communication.

Creating two-way communication. Leaders' roles should focus on establishing effective two-way communication that allows employees to share their opinions and recommendations. This will help identify problems and generate new ideas. The ability to communicate effectively is important for leaders not only during a crisis but also during the normal functioning of the organization. Leaders should frequently communicate with their team members, informing them about the organization's goals, strategies, and achievements [13]. This will improve the communication culture in the organization and increase employee engagement and motivation

C. Adaptability and Speed.

Adaptability and speed in communication. In the new era of Industry 4.0, change is constant and unpredictable. Leaders must be receptive, adaptable, and swift in delivering the necessary information to the team. This includes encouraging innovation, experimentation, and continuous improvement, where employees feel empowered to take risks and adapt their approach in response to changing conditions [14].

D. Promoting Team Collaboration.

In the process of promoting team collaboration, the leader's role is to guide the team toward cooperation and communication among employees, remove barriers, and encourage the sharing of information and knowledge exchange [15]. By fostering collaboration among employees, leaders successfully guide teams in overcoming barriers in the rapidly changing environment of the new era of Industry 4.0.

E. Resilience and Persistence.

Resilience and persistence are essential to the leader's role in the new era of Industry 4.0, where challenges are inevitable. Through open communication, leaders must ensure their teams' resilience by providing

support, resources, and guidance to help employees cope effectively with stress and uncertainty [16].

F. Balancing Professional and Personal Life.

The leader's role in successfully overcoming barriers is related to creating a balance between the professional and personal life of team members. The leader must provide access to resources and time to encourage employees to take breaks for recharging. Creating a favorable work environment where employees feel comfortable sharing and seeking help when needed leads to successfully overcoming various barriers.

G. Building Collaboration and Communication Channels.

Establishing strategic communication channels with partners and stakeholders leads to increased team trust in the leader and successful goal achievement. Collaboration and communication channels are the key to success in the new era of Industry 4.0. Leaders should build strategic partnerships and relationships with other organizations, stakeholders, and communities to ensure rapid and secure communication during crises [17].

The role of the leader and communication with key partners, suppliers, customers, and stakeholders leads to the creation of sustainable communication channels and the achievement of mutual cooperation [18]. By working together toward common and shared goals, organizations can deal more effectively with uncertainty and create value for everyone involved.

H. Encouraging the team towards continuous improvement.

The leader must encourage the team to continuously improve and learn. Continuous learning in the process of digitalization is essential for the successful development of the team in Industry 4.0, where knowledge and skills become obsolete at an ever-faster pace. Leaders should encourage their team members to pursue lifelong learning and professional development, motivating employees to expand their knowledge, acquire new skills, and adapt to changing technologies and trends [19].

I. Clear, specific, and strategic communication.

Guided by strategic goals and values. In times of uncertainty and ambiguity, the role of the leader is to guide the team through a clear purpose and values, ensuring effective communication, a specific direction, and clarity amid chaos. Leaders must clarify the compelling vision and mission to inspire and motivate employees.

J. Unified communication system.

The leader must create conditions for unified virtual communication and provide technological support to team members. Creating a unified communication system offers employees in the team ample opportunities to tackle challenges.

K. Personal example.

For successful communication, the personal example of the leader is of paramount importance. Demonstrating integrity, empathy, and resilience encourages a team culture of trust, transparency, and ethical behavior, where employees feel valued, respected, and empowered to give their best at work. Openness and honesty towards all employees play a key role in the process of effective communication. In modern conditions, the leader should focus on communication with honesty, clarity, humanity, and responsibility.

L. Technological progress.

With the advancement of technologies, interaction between team members is interrupted. Technological advancements have completely changed how the team interacts. In today's reality, it is possible to communicate with people worldwide online, through text, email, video, or mobile apps, so we may be more connected than ever before with our peers. With the development of artificial intelligence and the presence of robots, the leader's role is increasingly important, and human emotionality is a competitive advantage within the team [20].

The role of leaders is not only to communicate clearly and inspiringly but also to possess emotional intelligence, communicate with care, honesty, and empathy with each team member, and build trust. These unique human qualities of empathy, vulnerability, and authenticity are irreplaceable powerful drivers of influence and inspiration. Team leaders must build communication precision and trust, inspire the team, and attract more followers [21].

Now more than ever, leaders and their teams need the space to think differently so that decisions are based on a range of diverse, critically oriented perspectives. The leader's role is also recognized in encouraging thoughts, opinions, and ideas from the team. Encouraging talent at all levels is a key factor in the new era of Industry 4.0

3. A model of an algorithm for successfully overcoming communication barriers

The analyses and derivations of barriers and key skills are a prerequisite for developing a theoretical model for successfully overcoming emerging communication barriers in the new era of Industry 4.0.

The successful implementation of a model of an algorithm for successfully overcoming communication barriers depends on multiple factors, as well as organizational readiness. The proposed model is visualized in Fig. 1 trust in AI systems and the evolving regulatory landscape. The following subsections present an in-depth discussion of these results, structured around the benefits, applications and barriers to the implementation of AI in management.

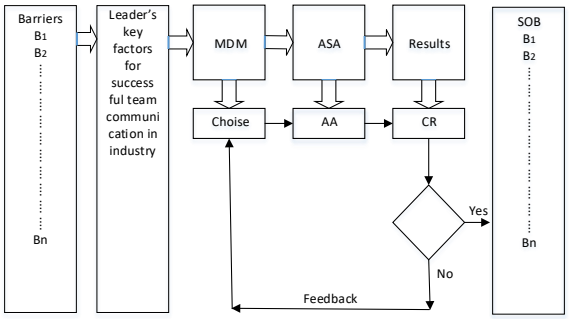

Fig. 1. A model of an algorithm for successfully overcoming communication barriers.

The algorithm is based on two blocks at the input of the algorithm, which are a synthesis of the primary information about the stages in the algorithm of the model for successfully overcoming communication barriers. The first block contains the selected barriers, and the third block identifies the key leadership skills. Based on the key skills, communication barriers that are significant for the industry are selected, after which they move on to the stage of making management decisions (MDM). The goal of the first stage is to make an informed choice (Choice) for a barrier that must be overcome as a priority.

The second stage is related to the implementation of the selected alternatives (ASA), as a result of which the specific alternative is implemented (AA).

In the third stage, the results obtained in the process of overcoming the barriers (Results) are analyzed. The main goal is to implement thorough control of the obtained results (CR).

If the barriers are successfully overcome (SOB), there is a way out of the problem situation and the communication barriers are successfully overcome.

In the process of controlling, deviations or negative results can be identified, which lead to the provision of feedback and a return to the stage of making a management decision. The process proceeds to a phased and sequential implementation of the algorithm set in the model for overcoming communication barriers.

IV. Conclusions

The role of the leader in managing and interacting with team members is a powerful form of communication but requires a new focus to meet contemporary challenges. In the communication process, the leader must create opportunities for every employee to share new ideas and opinions, thereby enhancing the team's effectiveness and success.

Overcoming barriers in the communication process is especially important to enable collaboration and coordination within the team, particularly in crisis situations. Referring to leadership abilities to communicate and lead the team, information, goals, directions, emotions, etc., are shared.

The identified barriers in the new era of Industry 4.0 can help improve communication in crisis management and support both the successful functioning of the team and the benefits for all stakeholders.

Effective leadership in the new era of Industry 4.0 requires adaptive leaders who overcome barriers and build bridges for successful communication, enabling team development amidst constant change and uncertainty. By embracing adaptability, promoting resilience and well-being, leaders promote team communication in the modern reality and stimulate organizational resilience and success. A proposed theoretical model can be applied in organizations to successfully overcome communication barriers. Referring to the challenges and opportunities in the new era of Industry 4.0, by overcoming barriers, leaders successfully guide the team towards long-term growth and prosperity in an ever-changing global economy.

REFERENCES

[1] C. Caldwell, Communication, Meaning, and Identity: Moving Toward Discovery, 978-1536172690, Nova Science Pub Inc, March 1, 2020

[2] P. Pavlov, S. Mikhaleva and L. Pavlova, The European Institutional Response to Global Challenges, https://ejournal.vfu.bg/pdfs/STATIA_e-Journal%20VFU-NOV2021.pdf [14.09.2022], 2021

[3] J. W. Gilsdorf, Organizational Rules on Communication: How Employees Are and Are Not Learning the Ropes", Journal of Business Communication 35, 2023

[4] R. Kapur, Understanding Personal Barriers within the Course of Communication, December 2020

[5] W. E. Donahue, Improving Interpersonal Communication Skills: A Competency-Based Approach that Integrates Communication and Interpersonal Skills, 979-8843865245 August 3, 2022

[6] J. Whitmore, Breaking Down the Barriers to Management Creativity, Manager, The British Journal of Administrative Management, May/June 2002

[7] R.I. Swaab and D. F. Swaab, Sex Differences in the Effects of Visual Contact and Eye Contact in Negotiations", Journal of Experimental Social Psychology 45, 2009

[8] P. Drucker, Drucker's Top Tips to Successful Leadership, 2019

[9] K. E., Siregar, N. Akhter, Digital Leadership in the Era of Industry 4.0: A Comprehensive Literature Review, July 2024

[10] V. N. Murty, K. S. Subramanian, The role of communication in crisis management, International Journal of Human Resource Management and Research (IJHRMR), ISSN(P): 2249-6874; ISSN(E): 2249-7986, Vol. 4, Issue 5, Oct 2014

[11] M. Pohl, One-to-One Process: Practicing consistent two-way communication between employee and supervisor (Organizational ReWilding: Elements of an Exceptional Business), The ReWild Group, 2-2023

[12] A. Kaneko, Team Communication in the Workplace: Interplay of Communication Channels and Performance, Business and Professional Communication Quarterly, 2023

[13] J. Mahadevan, Virtual Team Collaboration A Guide for Individual Team Members, Springer, 2024

[14] M. McKeown, Adaptability: The Art of Winning In An Age of Uncertainty, Published by Kogan Page, First published April 3, 2012

[15] D. Oragui, 14 Effective Ways to Promote Team Collaboration, https://helpjuice.com/blog/team-collaboration, 2022

[16] G. Deep, The power of resilience and flexibility in business leadership: Adapting to change, Magna Scientia Advanced Research and Reviews, 2023

[17] D. Holtzhausen and A. Zerfass, The Routledge Handbook of Strategic Communication, First published by Routledge, 2015

[18] G. Blokdyk, Communication Channel A Complete Guide, Emereo Publishing, 2021

[19] T. Van Weert, M. Kendall, Lifelong Learning in the Digital Age Sustainable for all in a changing world, Kluwer academic publishers New York, Boston, Bordrecht, London, Moscow, 2004

[20] M. Ilchenko, L. Uryvsky, L. Globa, Progress in Advanced Information and Communication Technology and Systems, Springer, 2023

[21] R. Anandan, G. Suseendran, S. Balamurugan, A. Mishra, D. Balaganesh, Human Communication Technology: Internet of Robotic Things and Ubiquitous Computing, Print ISBN:9781119750598, Online ISBN:9781119752165, Scrivener Publishing LLC, 2022

Environment. Technology. Resources. Rezekne, Latvia
Proceedings of the 16th International Scientific and Practical Conference,2025. Volume IV, 91-98

Integrating Artificial Intelligence into the Management Decision-Making Process in the New Era of Industry 4.0

Svetlana Dimitrakieva
Department of Industrial Management
Technical University of Varna
Varna, Bulgaria
s_dimitrakieva@abv.bg

Marina Marinova-Stoyanova
Department of Industrial Management
Technical University of Varna
Varna, Bulgaria
mpmstoyanova@tu-varna.bg

Boris Gramchev
Department of Industrial Management
Technical University of Varna
Varna, Bulgaria
gramchev@gmail.com

***Abstract*— The integration of AI into management decision-making is transforming businesses in the era of Industry 4.0, driven by technologies like IoT, big data, and cloud computing. This study aims to explore the role of AI in enhancing operational efficiency, reducing costs, and fostering innovation in management practices. The working method involves a review of current literature to assess AI's capabilities, benefits, and associated challenges. AI supports faster, data-driven decisions, improving operational performance and allowing for more strategic, creative work. It aids in risk management, supply chain optimization, and identifying market opportunities. However, AI integration presents challenges, such as implementation complexity, expertise needs, data privacy concerns, and the potential impact on jobs. Ethical issues, including accountability and transparency, are crucial for maintaining trust. Despite these challenges, the study concludes that AI's role in reshaping decision-making offers significant potential for businesses to gain a competitive edge and adapt to changing market dynamics.**

Keywords*— *Artificial Intelligence (AI), Decision-Making, Industry 4.0, Management.

I. Introduction

The arrival of Industry 4.0, propelled by the convergence of emerging technologies like the Internet of Things (IoT), big data analytics, cloud computing, and most prominently, Artificial Intelligence (AI), has brought about a new wave of digital transformation in manufacturing and management practices. Above all, AI has become a prime mover of change, revolutionizing how companies approach management decision-making processes, strategy formulation, and operational management. With its potential to handle massive volumes of information, identify patterns, and draw predictive conclusions, AI offers tremendous opportunities to enhance the efficiency of operations, reduce operational costs, and foster innovation. However, the integration of AI in managerial decision-making is accompanied by opportunities along with challenges that need to be understood in order to leverage its complete potential in today's business environment.

The increasing integration of artificial intelligence in management practices highlights the topicality of this study, as businesses worldwide seek to adapt to the demands of Industry 4.0. The purpose of this research is to analyze the opportunities and challenges associated with incorporating AI into managerial decision-making processes and to provide insights into how organizations can strategically leverage AI technologies for enhanced operational performance and innovation.

Industry 4.0 is the ongoing advancement towards automation and data exchange in manufacturing technologies, founded on cyber-physical systems, IoT, cloud computing, and artificial intelligence. Industry 4.0 facilitates the creation of "smart factories" in which machines, systems, and individuals collaborate via networking to enhance production processes and increase efficiency [1]. Artificial intelligence technologies, in particular machine learning, natural language processing, and data mining, have become key drivers of digitalization of management decision-making across various industries including manufacturing, finance, healthcare, and logistics. AI's ability to process high amounts of data in real-time qualifies it as an effective decision-making tool.

It can also facilitate predictive analytics, supply chain optimization, risk assessment, and employee management support [2]. Additionally, artificial intelligence can improve operating efficiencies by automating routine

Online ISSN 2256-070X
https://doi.org/10.17770/etr2025vol4.8451
© 2025 The Author(s). Published by RTU PRESS.
This is an open access article under the CreativeCommonsAttribution 4.0 InternationalLicense.

tasks, thus allowing human resources to concentrate on strategy and innovation initiatives. Nevertheless, the process of such integration involves many challenges. The intricacies in the implementation of artificial intelligence systems, the requirement for expertise personnel, issues regarding data confidentiality, and the possible effect on jobs need cautious consideration [3]. Incorporating AI in managerial decision-making has various benefits. Firstly, AI can make the management decision-making process more effective and efficient.

Classic management decision-making approaches, usually based on narrow information and personal judgment, are no longer sufficient when confronted with intricate and dynamic business contexts. Artificial intelligence, by contrast, can scrutinize enormous datasets of diverse origins, offering decision-makers valuable insights and facilitating fact-based decisions that are more precise and timely [4]. Data-driven management decision-making has the potential to enhance business performance by enhancing operating efficiency, lowering costs, and enhancing profit margins. Furthermore, the predictive nature of artificial intelligence can enable companies to foresee trends, detect impending threats, and make proactive choices. For instance, artificial intelligence algorithms can analyze past datasets for forecasting future demand, automating inventory management and minimizing supply chain disruptions [5]. Similarly, AI can also assist in finding new market opportunities, customer preference, and competitive threats, thereby assisting businesses to keep ahead in the rapidly evolving marketplace.

Additionally, the application of artificial intelligence in management decision-making has various ethical and social implications. The automation of management decision-making brings into question issues related to accountability, transparency, and fairness. For example, when a decision by an artificial intelligence system harms a stakeholder, who is to blame for the ensuing consequences? There needs to be a guarantee that AI systems are transparent and accountable to uphold trust in these systems [6]. In addition, AI's potential to impact employment is also a fundamental concern as automation may displace human labor in certain sectors, generating joblessness and socio-economic disparities [7].

The utilization of artificial intelligence in strategic management decision-making allows organizations not just to improve the operational effectiveness of their activities but also to improve their capacity for innovation and response to shifting market forces. The use of AI in managerial decision-making, nevertheless, is accompanied by several challenges. A first issue is in relation to the sophistication of AI systems along with the immense level of economic resources needed for effective deployment. Creation, training, and upkeep of artificial intelligence models necessitate significant skills and resources that are potentially beyond smaller businesses or those from emerging economies [8]. In addition, companies must make certain that their AI systems are tied to their strategic goals and are well integrated into current processes and technologies.

II. Materials and Methods

This study employs a qualitative research methodology grounded in an extensive literature review and critical thematic analysis to investigate the integration of AI in management decision-making within the context of Industry 4.0. Primary data sources include peer-reviewed academic journals, industry reports, and institutional publications published between 2014 and 2024, with a particular focus on technological adoption, organizational behavior, and AI governance. To ensure academic rigor, literature was selected based on relevance, citation frequency, and credibility of the source, using databases such as Scopus, Web of Science, and Google Scholar.

The research process involved a systematic identification of recurring themes, patterns, and challenges related to AI implementation in managerial practices. Key analytical categories included: organizational resistance, infrastructure and training needs, algorithmic transparency, ethical implications, and future-oriented applications of AI. Particular attention was given to literature discussing the European context, especially in relation to compliance with data governance regulations such as the General Data Protection Regulation (GDPR). Additionally, secondary data were synthesized to illustrate real-world examples and case studies demonstrating both successful and challenged implementations of AI in various industrial sectors. A constructivist lens was applied to interpret how decision-making processes are shaped by socio-technical interactions between humans and AI systems. Conceptual insights were further supported through reference to theoretical frameworks such as socio-technical systems theory and decision support system models. This methodological approach provides a comprehensive understanding of the opportunities, limitations, and strategic implications of integrating AI into management decision-making. The findings serve as a foundation for future empirical research and the development of actionable managerial frameworks.

III. Results and Discussion

The integration of AI in managerial decision-making presents a complex interplay of opportunities and challenges that reflect broader organizational, technological, and ethical dynamics. The findings of this study, derived from a critical analysis of contemporary literature, reveal that AI is progressively reshaping managerial practices across sectors. However, its successful implementation depends on numerous contextual factors, including organizational readiness, trust in AI systems, and the evolving regulatory landscape.

The following subsections present an in-depth discussion of these results, structured around the benefits, applications, and barriers to AI adoption in management.

1. Management Decision-Making Process

Management Decision-making is an important part of managerial functions and is one of the major challenges to managers in today's dynamic, competitive business environment. Management Decision-making is a process consisting of a sequence of steps, beginning with problem or opportunity identification and concluding with the implementation of the decision. Besides, management decision-making is not always a rational activity founded on information but also is influenced by factors such as personal attitudes, organizational culture, and sometimes external factors such as economic crises or regulatory changes.

A. Identifying the Problem or Opportunity.

The initial step in decision making is the identification of the problem or opportunity. If the problem is not stated clearly, then it is hard to select suitable solutions. This step usually involves extensive collection of information regarding both internal and external determinants of the organization. For instance, whenever an organization undergoes a loss of its market, the very first thing is to identify the root causes—whether due to competitors' pressure, quality, or poor marketing strategy [9].This can involve the application of a range of analysis tools, including SWOT analysis—strengths, weaknesses, opportunities, and threats—and PESTEL analysis, considering political, economic, social, technological, environmental, and legal aspects. These frameworks allow for the comprehension of root problems or the determination of new areas to develop.

B. Generating Possible Solutions.

After the identification of the opportunity or problem, the next process is the development of possible solutions. In this process, managers are required to come up with a complete list of alternatives that can solve the problem identified or capitalize on the spotted opportunity. To maximize effectiveness in this process, a variety of techniques such as brainstorming, innovation, and strategic planning need to be applied to enhance the development of ideas without providing initial constraints. A commonly employed method is the strategy of creative thinking, referred to as “design thinking,” which emphasizes the examination of possible solutions via cooperative efforts and inventive processes [10].

C. Evaluating and Analyzing the Possible Solutions.

After the generation of possible solutions, the next process is to evaluate and analyze their effect. This includes gathering additional information, screening costs and benefits, analyzing risks and benefits of each solution, and forecasting possible effects on the company. This typically includes the use of management decision-making tools such as decision analysis methods, such as sensitivity analysis, scenario planning, or financial projections. The selection of the optimal solution is reliant on the capacity of the manager to scrutinize this information and comprehend the implications of every solution for the organization's long-term strategy.

D. Choosing the Solution and Planning for Its Implementation.

After analyzing potential solutions, management moves to the most suitable alternative. This is a vital phase in that the judgments rendered are not just reasonable but also align with the mission, vision, and long-term objectives of the firm. Managers are sometimes required to make compromises between potential alternatives, taking into consideration resources, time constraints, and other operational dynamics. It is necessary that the decision must be well-founded and the objectives well defined. The process of planning to carry out the decision comes afterward once a solution has been chosen, and it involves making specific actions, allocating tasks, and establishing timetables for executing the decision.

E. Executing the Decision.

Implementation of the decision is a step where abstract strategies are converted into actual activities. Effective communication and team management are needed in this step since those involved in the process must know their roles and commitments. Managers are responsible for making sure all the needed resources are available while ensuring employees are aware of their individual roles in the implementation process. In addition, it is important to monitor the implementation process and rectify any discrepancies from the plan if any.

F. Evaluation and Feedback.

Following the implementation of the decision, the second stage entails evaluation and feedback, which is indispensable for enhancing the management decision-making process. Analysis of outcomes gives managers an insight into the extent to which the decision resulted in intended consequences. Internal players (employees, teams) and external players (customers, partners) may be the sources of opportunities for feedback. Using this information for analytical purposes allows for improvements and adjustments in future management decision-making plans, which is important for continuous improvement and the company's capacity to adapt to the constantly evolving business environment.

In contemporary times, artificial intelligence has started playing a more vital role in the management decision-making processes. AI in management decision-making enables the analysis of big data sets in real-time and equips managers with new tools to enhance the efficiency and accuracy of decisions. Predictive models of

artificial intelligence can examine previous trends and forecast future results, thereby providing organizations with an enormous competitive edge [2]. Furthermore, artificial intelligence can automate some of the routine tasks involved in the management decision-making process, freeing managers to attend to strategic matters and human aspects of management.

2. Integrating Artificial Intelligence into the Management Decision-Making Process in the New Era of Industry 4.0

The evolution of industrial segments has shifted to a new level with the push from digital technology advancements and Industry 4.0 emergence. These innovations are revolutionizing a number of sectors, with businesses increasingly using AI in improving their decision-making. In management, the incorporation of artificial intelligence into decision-making presents great potential for enhancing operational efficiency, predictive market trends, and facilitating well-informed decisions in a timely fashion.

A. The Role of Artificial Intelligence in Decision-Making

Artificial Intelligence is a fast-evolving area of research in the computer science discipline that deals with the development of machines and systems that can carry out tasks traditionally demanding human intellectual abilities. These tasks vary from problem-solving, learning, and reasoning to more advanced functions such as management decision-making [11]. As AI technologies continue to evolve, their use in many industries, particularly in business management, has revolutionized conventional management decision-making processes. Artificial intelligence is enabling organizations to make better, faster, and fact-based decisions that relied earlier on human intuition.

AI in management decision-making is extremely valuable as it is able to provide insights to make strategic choices, automate processes, and predictive analytics to forecast the future and make better-informed decisions. Among the capabilities of AI is its ability to manage enormous sets of data—frequently referred to as "big data"—to uncover hidden patterns, connections, and trends. Such above observations can have the potential to shape business strategy, enabling managers to predict shifts in the marketplace, streamline supply chain efficiency, and make superior resource allocation [12]. Furthermore, artificial intelligence could improve the accuracy of predictions through detecting subtle patterns that may evade human analysts.

AI's ability to enhance management decision-making is especially critical in the modern business environment, which is characterized by a rapidly changing business landscape where companies must make timely and well-informed decisions to remain competitive. By integrating AI systems into management operations, firms are capable of making quicker and more informed decisions, which translate into improved performance. AI's predictive capability enables managers to foresee market trends, customer behaviors, and operational outcomes with great precision. For instance, artificial intelligence technologies are capable of assisting organizations in forecasting changes in demand for supply chain management or anticipating customer attrition in marketing campaigns [13]. Such forecasting enables managers to take proactive actions and alter their strategies in advance, rather than respond to problems after they have arisen.

Another important advantage of artificial intelligence in management decision-making is that it can reduce human biases, which tend to be a key element in conventional management decision-making approaches. When it comes to human decision-making, implicit bias like confirmation bias, anchoring bias, and overconfidence can result in incorrect or poor decisions [14]. However, AI-based systems make decisions based on data and algorithms, which diminishes the influence of individual bias. Through the utilization of objective information in decision-making, artificial intelligence has the capability to ensure business decisions are tied to empirical facts and not personal prejudices. This is especially critical in fields where impartiality is paramount, including recruitment, loan approvals, and financial analysis [15].

One of the most significant features of artificial intelligence in decision-making is the capacity to optimize complicated systems through providing insights into trade-offs and various alternative solutions. In the financial industry, for instance, AI can help managers analyze investment opportunities by quantifying risks, returns, and potential fluctuations in the market. Optimization is not only applicable to financial decisions but also to operational, marketing, and strategic planning tasks [16]. By presenting a variety of potential outcomes and their corresponding risks, artificial intelligence enables managers to make more informed decisions that are aligned with the long-term objectives of the organization.

Further, AI has the potential to enhance management decision-making throughout the organization by interacting with other technologies such as the IoT and blockchain. For instance, in supply chain management, AI systems can interact with IoT devices to get real-time data on inventory levels, shipment status, and customer preference. These data can then be processed and analyzed by AI algorithms to optimize supply chain processes so that businesses can meet customer orders while minimizing surplus goods and lowering costs. Integrating AI with IoT and other advanced technologies provides businesses with an end-to-end, data-driven management decision-making approach that is superior to traditional business models [17].

However, the use of artificial intelligence in managerial decision-making is fraught with challenges. Though it may have potential advantages, most organizations exercise restraint in embracing AI-driven decision models in totality, mainly due to apprehension about trust, data security, and ethical implications [6]. Furthermore, managers may find it difficult to integrate AI into organizational frameworks that are in place, as the move towards data-driven management decision-making demands that the organization undergoes a cultural transformation. To optimize the effectiveness of artificial intelligence, it is imperative for organizations to guarantee that their workforce receives appropriate training in utilizing AI technologies, alongside the establishment of robust data governance protocols aimed at safeguarding confidential information [2].

B. The Impact of Industry 4.0 on Management Decision Making

Industry 4.0 is a term that describes the fourth industrial revolution, which is a tipping point where physical and digital technologies converge. It is a revolutionary transformation that is triggered by the amalgamation of smart systems, IoT, robotics, big data analytics, and artificial intelligence in industries such as manufacturing, logistics, and healthcare [17]. The interrelated nature of these technologies has radically reengineered the environment of industrial activity, providing companies with unparalleled opportunities to drive efficiency, foster innovation, and boost competitiveness. Yet, this change has also created new demands that must be met by managers in order to ensure strategic alignment and optimize decision processes.

At the heart of Industry 4.0 is the utilization of networked devices and systems to facilitate the gathering and analysis of vast volumes of real-time data. Smart systems, IoT devices, and sophisticated robotics allow for the gathering of data from an extensive range of sources, including machinery, supply chains, and customer interactions [2]. This information streams in real-time, making it a dynamic and ever-changing landscape that necessitates real-time management decision-making on the part of managers. The velocity, volume, and diversity of information produced by these systems can inundate conventional management frameworks, which normally depend on systematic, linear management decision-making structures and fixed sources of data.

In the modern era, conventional techniques of management decision-making, frequently depending on established workflows and past information, are progressively inadequate. Complexity in Industry 4.0 demands a more dynamic and responsive strategy. Managers, with real-time information at their fingertips, must be in a position to act quickly in the face of quickly altering circumstances. Managers require tools that have the ability to deal with large volumes of information, pull out useful insights, and make practical recommendations. This is where AI-based management decision-making systems come in [16].

The heightened use of data and automation characteristic of Industry 4.0 necessitates the complementing of human judgment with insights obtained from data. Although managers remain central to the formulation of strategic decisions, artificial intelligence alleviates cognitive load by making suggestions predicated on an in-depth examination of the available data. This thus enables managers to concentrate on more complex, strategic activities as AI systems assume control of the more mundane and operational aspects of decision-making. AI also assists in identifying trends and patterns that may not catch the eye of human managers, thereby making more informed and accurate decisions [12].

Nonetheless, the application of artificial intelligence in managerial decision-making also has a number of challenges. Among them is the risk of overdependence on AI systems. Though AI can support management decision-making through the provision of insights and recommendations, it is not able to substitute for human judgment and experience. Managers must be actively involved in the management decision-making process, placing AI-generated insights into the perspective of their organizational objectives and strategic agendas. Furthermore, there are ethical issues on data privacy, transparency, as well as possible bias in AI algorithms that must be dealt with to make sure AI-based management decision-making systems are accountable and just [6].

In addition, the integration of artificial intelligence into management decision-making also necessitates major adjustments in organizational structures and processes. Classical management pyramids may need to be remodeled to make room for more data-oriented methodology. Managers must acquire new competencies and skills to be able to work side-by-side with AI systems and appropriately interpret results produced by such technologies. The implementation of training and development initiatives will be critical in preparing managers to effectively engage with artificial intelligence technologies, as well as in promoting a culture characterized by ongoing learning and innovation throughout the organization [15].

In spite of these challenges, the effect of Industry 4.0 on managerial decision-making is generally beneficial. Through facilitating organizations to tap the potential of real-time data with artificial intelligence technologies, Industry 4.0 improves the capacity of managers to execute decisions that are better informed, responsive, and effective. Incorporating AI in management decision-making not only enhances operational efficacy but also offers a competitive advantage in a progressively dynamic business landscape. The ongoing development of AI technologies is likely to enhance the potential for

increasingly sophisticated decision support tools, enabling them to maintain a competitive advantage and foster ongoing development and innovation [13].

C. Overcoming Challenges in Integrating AI into Management Decision-Making

As already discussed, the use of artificial intelligence in management decision-making has great potential, but a series of hurdles needs to be overcome for proper implementation. Despite the apparent advantages of AI, such as the ability to process large amounts of data, reduce human biases, and provide predictive analytics, many organizations still face considerable challenges in adopting AI-supported systems. Some of these hurdles entail organizational reluctance, infrastructure changes required, alignment with existing procedures, and cultural resistance to change. Among the primary concerns in embracing AI is companies' reluctance to trust AI-driven management decision-making systems. The majority of managers and workers are skeptical about the consistency and accuracy of AI algorithms. Such systems, designed to replicate human decision-making, are believed by some not to be able to entirely replace human judgment. This lack of trust is based on concerns about the potential for artificial intelligence to produce imperfect or flawed decisions based on incomplete, inaccurate, or biased data [6]. There is also the problem of "black box" algorithms, in which the rationale for AI decisions is not always transparent.

The absence of transparency may undermine faith in artificial intelligence systems, especially in sensitive fields like finance, medicine, and law, where the consequences of mistakes may be extensive. Issues of data privacy and security particularly complicate the incorporation of artificial intelligence into management decision-making frameworks. As AI systems are predominantly data-dependent, organizations will have to ensure that they are compliant with data protection regulations, including the General Data Protection Regulation within the European Union. AI systems also carry an inherent risk of exacerbating algorithmic bias, with one possible consequence of generating unfair or discriminatory outcomes [18].

As AI technologies are progressing at a rapid rate, firms must continue to invest in training and reskilling their workforce to keep up with emerging trends and maintain their competitive advantage [12]. The adoption of AI necessitates radical alterations to existing management practices and organizational cultures. Conventional models of decision-making, with their hierarchical and inflexible character, will not automatically accommodate the flexible, data-oriented characteristics of AI. AI utilization in management decision-making calls for a transition to more cooperative, interdisciplinary teams with the capacity to harness AI technology for improved decision-making. But this transformation could be opposed by managers accustomed to conventional top-down models of management decision-making [2]. To avoid this opposition, companies must create an innovative culture in which the application of AI is seen as a choice for enhancing management decision-making processes and not as a menace to established practices.

Leaders should promote cooperation between technical and non-technical departments so that AI systems can be adopted efficiently and in accordance with the objectives of the organization. Additionally, integrating artificial intelligence in management decision-making requires organizations to be flexible and responsive in their approach. Since AI technologies are evolving further with advancements, management decision-making models need to adapt as well. The rapid pace of innovation in the field of AI presents opportunities as well as challenges for organizations in terms of having to be flexible in their management decision-making processes [19].

New AI technologies that are useful can soon become obsolete, so companies must be capable of being adaptive in their approach and take on new technologies as they become available. Companies that do not keep up with the new advancements in AI lose their ground in relation to competitors and lose their competitive advantage [15]. To surmount these obstacles, organizations must be proactive in embracing AI. Organizations must begin by creating trust in AI systems through transparency, rigorous testing, and adequate explanations of how decisions are made.

Furthermore, businesses must invest in the infrastructure necessary to facilitate AI adoption, including data management systems, AI training programs, and employee upskilling. It is also essential to foster a culture of innovation and flexibility, where artificial intelligence is considered a tool that can augment management decision-making processes and enhance business results. By implementing these measures, organizations can break the barriers to AI adoption and unleash the complete potential of artificial intelligence in management decision-making [20.

D. The Future of AI in Management Decision-Making

With the development of artificial intelligence technologies, their potential to transform management decision-making processes grows exponentially. In the coming decade, it is expected that AI will achieve higher levels of sophistication, which will allow it not only to analyze data but also to carry out autonomous decisions in real-time. This breakthrough represents a significant shift in management decision-making methodologies utilized by companies with more precise, efficient, and data-driven processes. To this extent, artificial intelligence holds the promise to revolutionize the role of human managers and pave new avenues for automating management decision-

making processes across industries where speed and accuracy hold vital importance [19].

One of the areas where artificial intelligence will significantly affect is in autonomous management decision-making systems. In fields like finance, where decision speed is of essence, artificial intelligence can be incorporated in systems that automatically execute trading decisions founded on multifaceted analysis of market data. For instance, artificial intelligence programs can process vast volumes of real-time information, such as market trends, news, and social media sentiments, in a bid to forecast market movement and make trades on their own [21]. These AI programs would assist organizations in maximizing operational efficiency, minimizing human errors, and reacting to market forces quicker than human decision-makers. In finance, artificial intelligence is increasingly being utilized in investment and trading decision-making. As AI technologies continue to develop and mature, it is likely that their influence in this field will grow, thus transforming the financial landscape.

Furthermore, AI's ability to handle large amounts of data from various sources will lead to management decision-making that is more tailored and context-specific. AI systems will be better able to consider individual tastes, behaviors, and situational contingencies when making decisions. This will enable managers to tailor their decisions to the specific needs and circumstances of their company, customers, or workers. The application of customized management decision-making will also bring tremendous benefits in areas such as customer relationship management (CRM), where artificial intelligence can be used to analyze customer information with a view to suggesting personalized services or products that align with individual tastes. As AI algorithms become more skilled at understanding and predicting human behaviors, managers will be able to provide more accurate and relevant solutions, leading to enhanced customer satisfaction and loyalty [15].

Apart from enhancing personalization, the future contribution of artificial intelligence in managerial decision-making is also expected to promote integration among various business functions. AI-based tools are expected to support not only strategic management decision-making processes but also be embedded in day-to-day operational tasks, thereby impacting the overall management decision-making process of organizations. Artificial Intelligence has the potential to enhance supply chain management by better demand forecasting, modifying inventories, and detecting disruptions in real time [2]. AI's application across functions of a business enables firms to make better-informed decisions, be more responsive, and incur lower costs, leading to a more responsive and efficient company.

As AI is increasingly a part of decision-making, organizations will have to evolve their management structures and working processes to appropriately accommodate AI tools. Managers will have to learn to understand AI systems, analyze their recommendations, and apply these insights to make their decisions. This needs a shift in perspective, viewing artificial intelligence not as it is replacing human judgment but instead as a useful tool to optimize the management decision-making process and drive organizational prosperity. Further, there is a necessity for managers to collaborate side-by-side with experts in AI and data scientists for the purpose of ensuring that artificial intelligence systems are adopted within the vision and mandate of the organization [2].

Despite the possible benefits of AI in management decision-making, there are several challenges. Among the most significant of these is the ethical considerations of AI decision-making. As AI systems become increasingly autonomous, there is a danger that decisions will be taken without sufficient human oversight, leading to unexpected outcomes. For instance, AI algorithms may take decisions that reinforce existing biases or discriminatory tendencies, especially if they are trained using discriminatory data [6]. To surmount these challenges, organizations will need to develop robust ethical frameworks and ensure that AI systems are designed to promote fairness, transparency, and accountability.

Moreover, as artificial intelligence systems assume an expanding role in management decision-making processes, there will be a heightened necessity for transparency concerning AI-generated decisions. In sectors where AI technologies are responsible for significant decisions—such as healthcare, finance, and legal matters—various stakeholders will increasingly seek clarity regarding the methodologies utilized by AI in forming its conclusions. Consequently, it will be imperative for AI developers to create systems that are both interpretable and explainable, thus enabling decision-makers to comprehend the reasoning underpinning AI-generated recommendations [2].

IV. Conclusions

The incorporation of AI into management decision-making in the Industry 4.0 era presents both significant opportunities and considerable challenges. Theoretically, AI enhances decision-making models by introducing real-time data analysis, predictive capabilities, and evidence-based strategic planning, thus contributing to the development of more dynamic and responsive management theories. Practically, AI enables managers to optimize operational processes, improve supply chain management, assess risks more effectively, and foster innovation by automating routine tasks and uncovering new market opportunities. Despite barriers such as trust issues, infrastructural demands, and resistance to change, the ongoing advancement of AI technologies and the increasing commitment of organizations to digital transformation suggest that AI will become an essential

tool for improving managerial decision-making, driving innovation, and achieving sustainable competitive advantage in a rapidly evolving, data-driven business environment.

REFERENCES

[1] S.Munirathinam, Industry 4.0: Industrial internet of things. Advances in Computers, 117(1), 129-164. https://doi.org/10.1016/bs.adcom.2019.10.010, 2020

[2] E.Brynjolfsson, and A. McAfee,The second machine age: Work, progress, and prosperity in a time of brilliant technologies. W.W. Norton & Company, 2014

[3] M. Chui, J. Manyika, and M. Miremadi, Where machines could replace humans—and where they can't (yet). McKinsey Quarterly, 2016

[4] T. H. Davenport & R. Ronanki, Artificial intelligence for the real world. Harvard Business Review, 96(1), 108-116, 2018

[5] A. Agrawal, J. Gans, and A. Goldfarb, Prediction machines: The simple economics of artificial intelligence. Harvard Press, 2018

[6] C., O'Neil, Weapons of math destruction: How big data increases inequality and threatens democracy. New York. Crown Publishing Group, 2016

[7] C. B. Frey and M. A. Osborn, The future of employment: How susceptible are jobs to computerization? Technological Forecasting and Social Change, 114, 254-280, 2017

[8] G. Westerman, D. Bonnet, &A. McAfee, Leading digital: Turning technology into business transformation. Harvard Press, 2014

[9] H. Mintzberg, Planning on the left side and managing on the right. Harvard Business Review, 54(4), 49-58, 1976

[10] L. P.Vishwakarma, R.K. Singh, R. Mishra and M.Venkatesh, Exploring the motivations behind artificial intelligence adoption for building resilient supply chains: a systematic literature review and future research agenda, Journal of Enterprise Information Management, 37(4), 1374-1398. https://doi.org/10.1108/JEIM-11-2023-0606, 2024

[11] S. Russell, and P. Norvig, Artificial intelligence: A modern approach. Pearson, 2020

[12] J. Bughin, J. Seong, J. Manyika, M. Chui, & R. Joshi, Notes from the AI frontier—Modeling the Impact of AI on the World Economy. Discussion Paper, McKinsey Global Institute, 2018

[13] T. Choi, S. Wallace &Y. Wang, Big Data Analytics in Operations Management. Production and Operations Management, 27(10), 1868-1883. https://doi.org/10.1111/poms.12838, 2018

[14] J. Dastin, Amazon scraps secret AI recruiting tool that showed bias against women. Reuters, 2018

[15] V. Mayer-Schönberger&K. Cukier, Big data: A revolution that will transform how we live, work, and think. Houghton Mifflin Harcourt, 2013

[16] P. Grabovy and N. Siniak, Using AI and big data in decision making: A framework across disciplines. E3S Web of Conferences, 535, 2024

[17] K. Schwab, The Fourth Industrial Revolution. New York. Crown Business, 2017

[18] Z. Yi,, X. Cao, Z. Chen & S. Li, Artificial Intelligence in Accounting and Finance: Challenges and Opportunities. IEEE Access, 11, 129100-129123, https://doi.org/10.1109/ACCESS.2023.3333389, 2023

[19] A. Raja Santhi, and P. Muthuswamy, Industry 5.0 or industry 4.0S? Introduction to industry 4.0 and a peek into the prospective industry 5.0 technologies. International Journal on Interactive Design and Manufacturing, 17, 947–979. https://doi.org/10.1007/s12008-023-01217-8, 2023

[20] Z. Jan, F. Ahamed, W. Mayer, N. Patel, G. Grossmann, M. Stumptner, & A. Kuusk, Artificial intelligence for industry 4.0: Systematic review of applications, challenges, and opportunities, Expert Systems with Applications, Volume 216. https://doi.org/10.1016/j.eswa.2022.119456, 2023

[21] A. Chymis, Artificial Intelligence in the post-COVID-19 era. Homo Virtualis, 3(2), 55–67. https://doi.org/10.12681/homvir.25449, 2020

Environment. Technology. Resources. Rezekne, Latvia
Proceedings of the 16th International Scientific and Practical Conference.2025. Volume IV, 99-104

Nutritional Strategies and Innovative Technologies for Maintaining the Operational Readiness of Military Personnel in Extreme Conditions

Petia Gencheva
Combat Systems and Equipment
Defence Institute "Professor Tsvetan Lazarov"
Sofia, Bulgaria
p.gencheva@di.mod.bg

Iliyan Hutov
Combat Systems and Equipment
Defence Institute "Professor Tsvetan Lazarov"
Sofia, Bulgaria
i.hutov@di.mod.bg

Borislav Genov
Combat Systems and Equipment
Defence Institute "Professor Tsvetan Lazarov"
Sofia, Bulgaria
b.genov@di.mod.bg

***Abstract*—Executing special missions in extreme conditions requires military personnel to maintain optimal physical and mental performance. This necessitates meticulous planning of rations and beverages to provide sufficient energy, hydration, and immune system support. To enhance interoperability among NATO member states, STANAG 2937 was introduced, standardizing the minimum characteristics and quality assurance of individual operational rations for military use. Key requirements defined in STANAG 2937 include nutritional adequacy, stability, durability, and tailored rations for specific conditions. Rations must provide 4000–6000 calories per day in extreme environments, prioritizing carbohydrates for quick energy, followed by fats and proteins. Packaging must ensure durability, ease of transport, and content preservation. Nutritional supplements, such as energy bars, vitamins, and isotonic drinks, are vital for sustaining energy and overall health. Extreme temperatures significantly influence macronutrient needs. In cold climates, higher fat intake (35–40%) supports energy reserves, while proteins preserve muscle mass and aid thermoregulation. Conversely, in hot climates, increased carbohydrate consumption (55–65%) replenishes glycogen and mitigates energy loss. Vitamins and minerals, such as B-complex, vitamin C, and magnesium, are essential for metabolic functions, immune health, and physical endurance.**

Keywords*— *STANAG 2937, operational rations, military nutrition, extreme conditions, macronutrient requirements.

I. INTRODUCTION

Military operations are often conducted in environments where soldiers are exposed to extreme ecological conditions, such as deserts, the Arctic, and high altitudes. Gradual adaptation to these environments facilitates physiological acclimatization. However, military missions are rarely planned with extended acclimatization periods in mind. Recreational mountaineers, outdoor workers in seasonal cold climates, and residents of cold or high-altitude regions have the advantage of planning their activities in such environments. Those accustomed to cold or high-altitude conditions learn how to adjust their clothing and activities to maintain a sustainable lifestyle, regardless of external conditions.

Regardless of climatic challenges, military forces must be supplied with food, weapons, housing, and other logistical support to enable the immediate execution of their missions [1]. Carrying out special missions in extreme environments requires military personnel to maintain optimal physical and mental states. This necessitates precise planning of rations and beverages that provide adequate energy, hydration, and immune system support. To enhance interoperability among NATO member states and standardize the minimum characteristics and quality assurance of individual operational rations, STANAG 2937 was introduced [2]. This standard defines the requirements for operational rations designed for military use.

The article aims to present the regulatory framework described by NATO strategic documents, as well as the requirements for providing food rations for military personnel in a temperate continental climate and extreme conditions.

II. MATERIALS AND METHODS

Nutritional Values: Rations must provide adequate energy intake and a balanced composition of macro- and

Online ISSN 2256-070X
https://doi.org/10.17770/etr2025vol4.8404
© 2025 The Author(s). Published by RTU PRESS.
This is an open access article under the Creative Commons Attribution 4.0 International License.

micronutrients tailored to the needs of military personnel under various operational conditions. In situations of intense physical exertion or extreme climatic conditions, energy requirements can reach 4000–6000 calories per day. Priority is given to carbohydrates as the primary source of quick energy, followed by fats and proteins [4], [5].

Stability and Shelf Life: The products in the rations must be resistant to various climatic conditions and have a long shelf life to ensure food safety and quality during missions [10].

Packaging: Packaging must be durable, easy to open, and suitable for transportation while protecting the contents from contamination and damage.

Specialized Rations: The standard also describes specialized rations for specific conditions, such as extreme climatic environments or prolonged operations, to meet the diverse requirements of different missions.

Quality and Safety: Ensuring the quality and safety of the food is essential, with adherence to established food safety and hygiene standards strongly recommended [3], [10].

Operational Interoperability: The standardization of rations facilitates joint operations among nations, ensuring that military personnel can use and accept rations from other countries without issues [3].

Related documents, such as Allied Medical Publication-1.11 (AMedP-1.11), provide detailed guidelines and information supporting STANAG 2937 to enhance the effective interoperability of individual operational rations during military deployments, exercises, or operations [3].

The above-mentioned requirements and recommendations are designed to ensure that military personnel receive the necessary nutritional support to maintain their effectiveness and health during operations in various environments and conditions.

A. Combat Rations Include the Following Main Components

a) Ready-to-eat foods and beverages – canned meals (with pork, beef, chicken, or lamb, spaghetti, vegetarian menus, meals for individuals of different religious beliefs, etc.), meat and fish preserves, pâtés, packaged confectionery, spices, sauces, powdered drinks, dragees, chewing gum, and more.
- Disposable tableware – plastic spoons, forks, knives, napkins, wet wipes, toothpicks.
- Means for heating food – through chemical reactions or open fire (e.g., solid fuel).
- Water disinfection agents – in liquid or tablet form.

Disposable tableware, food heating means, and water disinfection components may either be included in the combat ration or provided separately.

B. Combat Ration Packaging Types:

- Primary (protective) packaging – in direct contact with food products, protecting them from environmental influences.
- Secondary (grouping) packaging – used to group individual food and non-food components into a single set.
- Tertiary (transport) packaging – used to group individual sets into larger cargo units (boxes, pallets, containers) for easier transport and storage.

C. Classification of Combat Rations

Combat rations can be categorized based on their intended use:

Individual combat rations are designed to provide food for a single soldier and may include food products for one meal (separately for breakfast, lunch, or dinner) or for an entire day (breakfast, lunch, and dinner, packed in one package). They are further divided into general-purpose rations and those for specific situations. General-purpose individual combat rations are the main rations used in a wide range of missions and operations, typically involving moderate physical activity and moderate climatic conditions. The food components of these rations can be consumed cold or hot, with some requiring water for rehydration or heating [2,3].

Table 1 provides information about the main combat rations used by NATO member countries, including the names of different rations and the number of menus within them. Some countries, such as Albania, Iceland, Luxembourg, Montenegro, and others, do not have available information about their combat rations.

TABLE 1. BASIC COMBAT RATIONS IN NATO MEMBER COUNTRIES [2]

No.	Country	Name of Combat Ration	Number of Menus
1.	Albania	No information	
2.	Belgium	Ration de Combat Individuelle Rechauffable, France	14 menus
3.	Bulgaria	Not used	
4.	United Kingdom	12 Hour Operational Ration Pack, 24 Hour Operational Ration Pack	10 menus, 7 menus
5.	Germany	Einmann Packung (EPa)	19 menus
6.	Greece	Special Forces' Ration	
7.	Denmark	Danish Combat Ration (DCR)	1 version
8.	Estonia	24 Hour Combat Ration Pack	14 menus
9.	Iceland	No information	
10.	Spain	Individual Meal Pack (IMP)	6 menus
11.	Italy	Razione Viveri Specialida Combattimento	7 menus
12.	Canada	Individual Meal Pack (IMP)	6 menus
13.	Latvia	Latvia Armed Forces Combat Ration	9 menus
14.	Lithuania	Field ration based on the US Army MRE	10 menus
15.	Luxembourg	No information	
16.	Norway	Feltrasjon	2 types; 7 menus

No.	Country	Name of Combat Ration	Number of Menus
17.	Poland	Zestaw Żywnościowy Indywidualnej Racji Suchej	3 menus
18.	Portugal	Ração Individual de Combate (RIC)	
19.	Romania	Romanian Ration Prototype	
20.	USA	Meal, Ready-to-Eat (MRE)	24 menus
21.	Slovakia	24 Hour Combat Meal, Ready to Eat (PODAP)	5 menus
22.	Slovenia	24 Hour Combat Ration Pack	3 menus
23.	Turkey	Turkish Outdoors 24 Hour Meal	5 menus
24.	Hungary	24 Hour Meal, Ready to Eat	5 menus
25.	France	Ration De Combat Individuelle Réchauffable	14 menus
26.	Netherlands	Gevechtsrantsoen	
27.	Croatia	Croatia Armed Forces 24 Hour Combat Ration	7 menus
28.	Montenegro	No information	
29.	Czech Republic	Bojová Dávka Potravin (BDP)	2 menus

The need for individual meal packs: Individual meal packs for extreme conditions are specifically designed to provide comprehensive nutrition to military personnel in various situations. According to the requirements of STANAG 2937, each pack must contain:

Main Meal: Freeze-dried or dehydrated foods that are easy to prepare and provide sufficient energy [6], [8].

Energy Bars: High-energy foods that quickly replenish energy [8], [9].

Liquid Foods: Packaged in compact and user-friendly containers.

Vitamins and Minerals: Supplements providing essential micronutrients [9].

Beverages: Isotonic or dehydrated powdered drinks [7], [8].

Utensils: Compact and lightweight for convenience.

Disinfectants: Wet wipes or tablets for cleaning hands and surfaces [11].

TABLE 2. NATO STANDARD FOR THE MINIMUM ENERGY VALUE AND NUTRITIONAL COMPOSITION OF THE GENERAL-PURPOSE COMBAT RATION [3]

№	Nutritional l composition of the general-purpose		
	Nutritional Ingredients	*Measure*	*Quantity*
1.	Energy value	kcal	3600
2.	Carbohydrates	g	404
3.	Proteins	g	118
4.	Fats	no more than 35%	
5.	Vitamin A	µg	900
6.	Vitamin B1	mg	1.2
7.	Vitamin B2	mg	1.3
8.	Vitamin B5	mg	6
9.	Vitamin B6	mg	1.3
10.	Vitamin B9	µg	400
11.	Vitamin B12	µg	2.4
12.	Vitamin C	mg	45
13.	Vitamin D	µg	5
14.	Vitamin E	mg	10
15.	Vitamin K	µg	70
16.	Vitamin PP	mg	16
17.	Calcium	mg	1000
18.	Zinc	mg	14
19.	Iron	mg	8
20.	Magnesium	mg	410
21.	Potassium	mg	3800
22.	Sodium	mg	2300
23.	Phosphorus	mg	700
24.	Iodine	µg	150
25.	Selenium	µg	55
26.	Fluoride	mg	4

It is considered that continuous consumption of combat rations meeting the above minimum standards for up to 30 days will not cause nutritional imbalance in the body of soldiers who must be in good physical health at the beginning of the operation. If consumption exceeds 30 days, it is recommended to diversify the daily menu with fresh food products and increase medical monitoring of the soldiers' health condition. According to data from the report "Nutrition Science and Nutritional Standards for Military Operations" by NATO's Research and Technology Organization, of the twelve combat rations studied from NATO member countries, nine have a maximum recommended continuous use period of 30 days. For the combat rations of Australia, the USA, and Slovenia, the recommended periods are 20, 21, and 10 days, respectively. The main reasons for the shorter periods of continuous consumption are the low approval levels of the rations among soldiers and the lack of variety in the menus.

Additionally, Australia points out the reduction of certain valuable vitamins in the rations due to prolonged storage as an important reason [2, 3].

These packs must be lightweight and compact while providing all necessary nutrients and calories to sustain physical and mental endurance.

C. Impact of extreme temperatures on macronutrient requirements for military personnel

Extreme temperatures—both cold and hot—significantly influence metabolic processes and macronutrient needs for military personnel. In cold conditions, the primary priority is maintaining body heat and adequate energy supply. This necessitates increased energy consumption, with diets requiring higher fat content to provide long-term energy reserves. According to Young and Pasiakos (2013), fats should account for up to 35–40% of total energy intake in cold climates, with a preference for sources rich in omega-3 fatty acids due to their anti-inflammatory properties [4]. Meanwhile, proteins play a critical role in preserving muscle mass, essential for thermoregulation and physical performance [5].

In hot climates, military personnel require increased carbohydrate intake, which serves as the primary source of readily available energy. Young and Deuster (2001) note that carbohydrates should constitute 55–65% of daily energy intake in high temperatures to compensate for significant energy expenditure and prevent glycogen depletion [5]. Additionally, proteins should be moderately increased (around 15–20% of energy intake) to support muscle tissue recovery and prevent catabolism.

The importance of a balanced diet adapted to specific climatic conditions is strongly emphasized in the literature. As Young and Pasiakos (2013) state, "Optimizing macronutrient balance is crucial for maintaining physical endurance, cognitive functions, and the health of military personnel in extreme environments" [4].

D. The role of supplements and energy bars

Supplements in military rations, such as energy bars and dehydrated foods, are crucial for reducing load and providing essential energy reserves. Freeze-drying and dehydration are methods that extend shelf life while preserving nutrients. For example, freeze-drying retains 97% of the nutritional value of products while minimizing changes in structure and taste [7]. Additionally, the process simplifies food digestion and preparation [8], [9].

Hydration Beverages: Hydration is essential for military personnel in extreme conditions. The use of isotonic beverages is recommended to replenish electrolyte levels and prevent dehydration. Advanced drying technologies, such as freeze-drying, enable easy storage and use of beverages with high nutritional value [7], [8].

E. The need for water purification systems

In extreme conditions, ensuring access to clean drinking water is critical for the health and operational capabilities of military personnel. Water purification systems, such as ultrafiltration and reverse osmosis, effectively remove contaminants and pathogens. Research highlights that the use of portable water purification systems significantly reduces the risk of waterborne illnesses and ensures a sustainable supply even in the most adverse conditions [11].

These systems incorporate key technologies such as activated carbon, UV sterilization, and integrated portable pumps. Advanced filtration membranes help eliminate bacteria, viruses, and chemical pollutants, ensuring compliance with military-grade water safety standards. Models described by Taylor and Brown (2022) demonstrate how combining efficient filtration technologies with compact designs can provide safe water for drinking and cooking, even under resource-constrained circumstances [12].

Furthermore, modern purification units integrate real-time water quality monitoring sensors, enabling personnel to assess contamination levels and system performance in the field. The development of nanostructured filtration materials has further improved efficiency, enhancing the removal of heavy metals, toxins, and microscopic contaminants. Some advanced military-grade systems also utilize electrochemical disinfection methods, ensuring prolonged water safety without the need for frequent maintenance.

Recent studies emphasize the effectiveness of advanced nanomaterials in water purification. Research published in the *Journal of Water Process Engineering* highlights that nanostructured membranes improve filtration efficiency and enhance the removal of bacteria, viruses, and heavy metals [13].

Ensuring the availability of potable water has long been a critical challenge for military operations, directly impacting the performance of soldiers. Currently, the U.S. Armed Forces rely on large, centralized reverse osmosis (RO) water treatment systems to produce potable water, which must then be distributed to the points of use. However, the logistics of delivering water to remote expeditionary operations are costly, dangerous, and complex. While the Navy and the Department of Defense (DoD) have developed RO desalination systems that scale effectively to platoon-level (45 soldiers), further scaling down to the squad level (13 soldiers) or smaller units presents significant challenges [14].

In addition to scaling issues, RO systems face several drawbacks, including high consumables usage and maintenance and lifespan issues related to the membranes. Given the growing global concern about the availability of potable water for civilian purposes, there has been increasing development of alternative desalination and purification technologies. These include electrochemical methods, such as capacitive deionization, solar-powered thermal processes, and atmospheric water harvesting techniques, which eliminate the need for direct

desalination. These findings underscore the importance of continuous advancements in water purification technologies, ensuring safe and reliable drinking water for military and emergency response teams in extreme conditions[14].

The integration of purification technologies within tactical and logistical planning significantly enhances operational readiness. Whether deployed in arid environments, disaster-stricken regions, or combat zones, military forces can maintain self-sufficiency in water supply. Additionally, the lightweight and modular design of next-generation portable purification devices allows for rapid deployment and adaptability in diverse operational scenarios. Continued research and development in this field ensure that military personnel have access to reliable and high-performance water purification solutions, even in the most challenging conditions.

III. RESULTS AND DISCUSSION

The analysis shows that combat rations used by NATO member states generally comply with the minimum energy and nutritional requirements set by STANAG 2937. However, prolonged use of these rations—beyond 30 days—can result in reduced intake of certain essential vitamins and minerals, as well as a decrease in soldiers' acceptance due to limited menu variety.

Adapting the nutritional composition of rations to environmental conditions is of key importance. In cold climates, increased fat intake supports heat retention and long-term energy supply, while in hot environments, higher carbohydrate intake is necessary to meet energy demands and prevent fatigue. A well-balanced macronutrient ratio enhances physical endurance and operational performance.

Energy bars, freeze-dried meals, and powdered drinks are practical components due to their extended shelf life, compact packaging, and preserved nutritional value. Requirements, as improving taste and variety, are essential for ensuring nutrition during extreme missions of short duration.

Access to clean drinking water remains a critical factor in sustaining military operations. Modern portable purification technologies—such as nanofiltration, UV sterilization, and electrochemical methods—provide reliable solutions for removing contaminants and pathogens, even in extreme environments. Challenges remain in scaling down systems for small tactical units and maintaining filtration efficiency over time.

In conclusion, the effectiveness and health of military personnel in the field depend greatly on appropriate nutrition, hydration, and access to clean water. Continuous innovation and improvement of rations and purification technologies are essential for meeting the demands of diverse operational scenarios.

IV. CONCLUSION

Ensuring the health, combat readiness, and operational efficiency of military personnel in extreme environments demands a holistic strategy that integrates proper nutrition, hydration, and logistical support. Carefully planned and certified food rations and beverages, tailored to meet the unique demands of each operational setting, are essential for maintaining the physical and mental performance of soldiers. Advanced food preservation techniques, such as freeze-drying, enable the production of lightweight, durable, and high-quality supplies, while robust water purification systems effectively address the risks of contaminated water sources.

The inclusion of essential nutritional supplements, including vitamins and minerals, helps meet the physiological needs of military personnel, enhancing their energy metabolism, immune defense, and physical resilience. Furthermore, standardized frameworks like STANAG 2937 ensure interoperability between allied forces, guaranteeing consistent access to the necessary resources across different nations.

With the increasing global concern about safe drinking water, innovations in desalination and purification technologies offer promising solutions to mitigate water scarcity. Techniques such as capacitive deionization, solar-powered thermal processes, and atmospheric water harvesting present viable alternatives to traditional reverse osmosis systems, reducing logistical burdens and increasing operational flexibility.

Incorporating advanced water purification technologies into military logistics enhances self-sufficiency and operational readiness, ensuring that personnel in the most challenging environments have reliable access to clean water. Continued investment in these technologies, along with their integration into combat rations, is crucial for maintaining the safety, effectiveness, and success of military missions, even under the most extreme and resource-limited conditions. By embracing these innovations and adhering to established standards, military forces can successfully navigate the challenges of extreme environments, ensuring mission success without compromising the well-being of their personnel.

ACKNOWLEDGMENT

National Scientific Program – Security and Defence is funding by Ministry of Education and Science of the Republic of Bulgaria in implementation of National Strategy for the Development of Scientific Research 2017-2030 and was adopted by Decision of the Council of Ministers No. 731 of October 21, 2021.

REFERENCES

[1] Institute of Medicine. Nutritional Needs in Cold and High-Altitude Environments: Applications for Military Personnel in Field Operations. Washington, DC: The National Academies Press, 1996. https://nap.nationalacademies.org/read/5197/chapter/1.

[2] Ivaylo Ralev, „Condition and directions for the development of food supply for the bulgarian army in operations“, "Military Academy 'Georgi Stoykov Rakovski', publisher, 2021, ISBN 978-619-7478-64-8.

[3 STANAG 2136. Requirements for Water Potability during Field Operations and in Emergency Situations. NATO Standardization

Office, 2014. https://www.coemed.org/files/stanags/03_AMEDP/AMedP-4.9_EDA_V1_E_2136.pdf.

[4] A. J. Young and S. M. Pasiakos, "Energy balance and macronutrient distribution during military operations in extreme environments," Nutrition Reviews, vol. 71, no. 3, pp. 211-220, Mar. 2013. DOI: 10.1111/nure.12020.

[5] A. J. Young and P. Deuster, "Nutritional strategies to optimize performance during military operations in extreme cold environments," Military Medicine, vol. 166, suppl_3, pp. 71-76, Mar. 2001. DOI: 10.1093/milmed/166.suppl_3.71.

[6] S. Bhatta, T. Stevanovic Janezic, and C. Ratti, "Freeze-Drying of Plant-Based Foods," Foods, vol. 9, no. 1, p. 87, Jan. 2020. DOI: 10.3390/foods9010087.

[7] T. M. Oyinloye and W. B. Yoon, "Effect of Freeze-Drying on Quality and Grinding Process of Food Produce," Processes, vol. 8, no. 3, p. 354, Mar. 2020. DOI: 10.3390/pr8030354.

[8] K. Mostafa, "General Principles of Freeze-Drying," ResearchGate, 2020. [Online]. Available: https://www.researchgate.net/publication/342123456_General_Principles_of_Freeze-Drying.

[9] NATO Standardization Agreement (STANAG) 2560. Evaluation of NATO Medical Treatment Facilities. NATO Standardization Office, 2017. Available: https://coemed.org/files/stanags/03_AMEDP/AMedP-1.6_EDA_V2_E_2560.pdf..

[10] Institute of Medicine. Dietary Reference Intakes for Vitamin C, Vitamin E, Selenium, and Carotenoids. Washington, DC: National Academy Press, 2000. [Online]. Available: https://www.ncbi.nlm.nih.gov/books/NBK225472/

[11] J. Smith and P. Johnson, "Portable Water Purification Systems for Field Operations," Journal of Environmental Safety, vol. 12, no. 4, pp. 234-245, 2021.

[12] K. Taylor and M. Brown, "Advanced Filtration Technologies in Emergency Water Supply," Water Research, vol. 15, no. 3, pp. 128-145, 2022.

[13] Maria Rajkiewicz, „Trends in membrane filtration technology: theory and application“, Chapter, BookChemical and Applied Engineering Materials, 2015, Imprint Apple Academic Press, p. 49, eBook ISBN9780429173110

[14] Paul A. DeSario, Jeffrey W. Long, and Kenan P. Fears, “Technology Assessment of Water Treatment Devices for Small-Scale Production”, OMB No. 0704-0188, DCN: 0543-1045-23.

Environment. Technology. Resources. Rezekne, Latvia
Proceedings of the 16th International Scientific and Practical Conference. 2025. Volume IV, 105-110

Simulation Analysis of Wiener and Low-Pass Filtration in EHS

Borislav Georgiev
Department of Mechanical and Precision Engineering
Techical University of Gabrovo
Center of competence "Smart mechatronic, eco-and energy-saving systems and technologies"
Gabrovo, Bulgaria
gborislav@gbg.bg

***Abstract*— In electro-hydraulic systems (EHS), when using tach generator feedback, we have high-frequency noise due to various sources. Precise control of the speed of the actuator is necessary because the tachometer signal is crucial for closed-loop control. Therefore, accurate measurements are essential. In this paper, an analysis of Wiener filter and low-pass filters used in an electro-hydraulic system with feedback from the speed of the actuator (hydraulic motor) is made.**

Keywords*— Electro-hydraulic systems, Wiener filter, low-pass filters.

I. INTRODUCTION

Electro-hydraulic systems are used in numerous applications and industries due to their efficiency and power. Electro-hydraulic systems provide precision and speed in production in automated assembly lines, aircraft control, robotic surgical systems, wind turbine control systems such as hydraulic blade adjustment mechanisms and many other areas of application [1, 5, 6, 7, 8, 9].

White noise in sensor feedback can cause various problems in the control and regulation of the electro-hydraulic system, and can blur the actual speed values, leading to inaccurate measurements and less precision in system control [2, 3, 4, 20, 23, 24, 25].

Unwanted fluctuations in the control signal may occur, which can lead to system instability and uneven operation. Due to noise, the controller may react incorrectly to changes in feedback, resulting in a delay in response or over-regulation [15, 16, 17].

In systems with adaptive control [10, 11, 12, 22], noise can make it difficult for the controller to learn, resulting in inefficient adaptation to changes in operating conditions. Instability and fluctuations caused by noise can lead to increased wear on hydraulic components, which reduces their lifespan. The overall efficiency of the system may decrease because the controller cannot optimize operation due to incorrect measurements. Finally, poor system regulation caused by noise can lead to an increase in energy consumption, which is economically inefficient.

In conclusion, this can significantly affect the performance and reliability of an electro-hydraulic system [18, 19, 21], highlighting the importance of filtering and signal processing.

II. MATERIALS AND METHODS

A. Description of the electro-hydraulic system

Fig. 1 shows an electro-hydraulic system with hydraulic motor speed control via a pulse width modulator (PWM), consisting of: 1 – PWM, 2 – DC Motor, 3 – Pump, 4 – tach generator, 5 – hydraulic motor and 6 – PID Regulator.

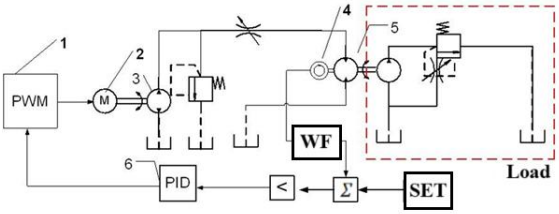

Fig. 1. Frequency response of the Butterworth filter for different filter orders.

The speed of the hydraulic motor is adjusted by PWM via the signal received from the feedback sensor /tach generator/, where the signals from the developed control optimization filter are transmitted and enters the summing device. Then is compared with the signal from the setting device and is processed by the PID regulator.

Online ISSN 2256-070X
https://doi.org/10.17770/etr2025vol4.8415
© 2025 The Author(s). Published by RTU PRESS.
This is an open access article under the Creative Commons Attribution 4.0 International License.

B. Filter comparision

A Wiener filter (WF) is a complex statistical filter that aims to optimally reconstruct a signal from noisy data, while a low-pass filter (L-PF) is a simpler filter that removes high-pass components, often used to smooth out or reduce noise.

TABLE 1 FILTER COMPARISION

Feature	Wiener Filter	Low-Pass Filter
Goal	To optimally estimate an unknown signal from noisy observations.	To attenuate high-frequency components in a signal
Approach	Based on statistical principles, minimizing the mean square error between the estimated and desired signals.	Based on frequency response, attenuating frequencies above a cutoff frequency.
Design	Requires knowledge of the signal and noise power spectra	Primarily determined by the cutoff frequency
Adaptivity	Can adapt to changes in signal and noise characteristics	Fixed unless the cutoff frequency is adjusted
Performance	Can achieve optimal performance in the mean square error sense	Performance depends on the choice of cutoff frequency and the nature of the signal and noise.

It would be good to use WF when optimal signal estimation is crucial, and knowledge of signal and noise statistics is available.

On the other hand, when a simpler approach is sufficient and the main goal is to eliminate high-frequency noise, L-PF are recommended.

In an electro-hydraulic tachometer feedback system, we have high-frequency noise that can come from various sources such as:

a) Tachometer noise: Electronic noise, mechanical vibrations, etc.

b) Hydraulic system noise: Pressure fluctuations, valve switching noise, etc.

c) Environmental noise: Electromagnetic interference, etc.

Precise speed control is required in closed-loop driving, so accurate measurements are essential.

Low pass filter advantages are: Simple, computationally inexpensive, effective in silencing high-frequency noise.

Disadvantages: It can lead to phase shift and slowdown, potentially affecting the stability or performance of the system.

Wiener filter advantages is: Optimally minimizes the mean square error, can adapt to changing noise characteristics.

Disadvantages: Requires knowledge of signal and noise statistics, can be computationally more complex.

For most practical electro-hydraulic systems, a well-designed low-pass filter is often sufficient for easier implementation and adjustment.

It can effectively reduce noise while maintaining reasonable system response. The reduced computational burden has fewer requirements on the control system.

let us look at the following factors in which the Wiener Filter is preferable:

a) Noise characteristics: If the noise is strongly connected or stationary, the Wiener filter can offer better performance.

b) System complexity: If computing resources are plentiful and noise is a significant problem.

C. Principle of operation of the Low-pass filters

a)Butterworth filter

A Butterworth filter is a type of signal processing filter designed to have the flattest frequency response in the passband. It is also known as a maximum amplitude flat filter. It was invented in 1930 by British engineer and physicist Stephen Butterworth in his paper "On the Theory of Filter Amplifiers".

The main characteristic of a Butterworth filter is that it provides a flat frequency response up to a cutoff frequency, after which this response begins to decline. The cutoff frequency is the point at which the signal amplitude decreases by 3 dB. Butterworth filters can be designed with different orders, with higher orders providing a steeper decrease in the frequency response after the cutoff frequency.

Butterworth filters are preferred when it is necessary to provide a smooth frequency response without ripples in the passband.

In design, we aim for a response close to the ideal filter. Finding the exact ideal characteristics is a challenge that requires complex higher-order filters.

If we increase the order of the filter, the number of cascaded stages with the filter also increases. But in practice, we cannot achieve the ideal Butterworth frequency response. Because it produces excessive ripples in the passband.

The Butterworth filter provides a mathematically flat frequency response up to the -3dB cutoff frequency without any ripples. Frequencies above this limit will roll off at a rate of -20 dB in a first-order filter.

If you increase the order of the filter, the rate of roll-off period also increases. And for the second order it is -40 dB. The quality factor for the Butterworth filter is 0.707.

The fig.2 below shows the frequency response of the Butterworth filter for different filter orders.

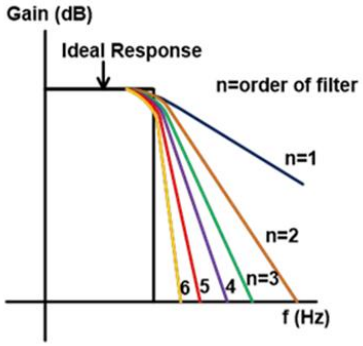

Fig. 2. Frequency response of the Butterworth filter for different filter orders.

The generalized form of frequency response for nth-order Butterworth low-pass filter is:

$$H(j\omega) = \frac{1}{\sqrt{1+\varepsilon^2\left(\frac{\omega}{\omega_C}\right)^{2n}}}, \quad (1)$$

where: n- order of the filter, ω- operating frequency (passband frequency) of circuit,

ω_C- cut-off frequency, ε- maximum passband gain = A_{max}.

The below equation is used to find the value of ε.

$$H_1 = \frac{H_0}{\sqrt{1+\varepsilon^2}}, \quad (2)$$

where: H_1 – minimum passband gains and H_0 – maximum passband gain.

b) Savitzky-Golay filter

The Savitzky-Golay filter (S-GF) is a digital filter used to smooth data while preserving important signal features, such as peaks and valleys. It was developed by Abraham Savitzky and Marcel Golay in 1964 and is also known as the polynomial smoothing filter.

The basic idea of the S-GF is to apply a polynomial fit to subsets of adjacent data points using the linear least squares method. This is achieved by convolution, using convolution coefficients that are applied to all subsets of the data to obtain estimates of the smoothed signal.

The S-GF is particularly useful in data processing where it is important to preserve the high-frequency components of the signal while reducing noise. It is used where it is necessary to smooth data without significant loss of information.

Savitzky-Golay smoothing filters tend to filter out less of the signal's high-frequency content than standard averaging FIR filters. However, they are less successful at rejecting noise when noise levels are particularly high.

In general, filtering consists of replacing each point of a signal by some combination of the signal values contained in a moving window centered at the point, on the assumption that nearby points measure the same underlying value. For example, moving average filters replace each data point with the local average of the surrounding data points. If a given data point has k points to the left and k points to the right, for a total window length of L = 2k + 1, the moving average filter makes the replacement

$$x_s \to \widehat{x_s} = \frac{1}{L}\sum_{r=-k}^{k} x_s + r\,, \quad (3)$$

S-GF generalize this idea by least-squares fitting an nth-order polynomial through the signal values in the window and taking the calculated crucial point of the fitted polynomial curve as the new smoothed data point. For a given point, x_s

$$\begin{bmatrix} x_{s-k} \\ \vdots \\ x_{s-1} \\ x_s \\ x_{s+1} \\ \vdots \\ x_{s+k} \end{bmatrix} =$$

$$\begin{bmatrix} b_0 + b_1(t_s - k\Delta t) + b_2(t_s - k\Delta t)^2 + \cdots + b_n(t_s - k\Delta t)^n \\ \vdots \\ b_0 + b_1(t_s - 1\Delta t) + b_2(t_s - 1\Delta t)^2 + \cdots + b_n(t_s - 1\Delta t)^n \\ b_0 + b_1(t_s - 0\Delta t) + b_2(t_s - 0\Delta t)^2 + \cdots + b_n(t_s - 0\Delta t)^n \\ b_0 + b_1(t_s + 1\Delta t) + b_2(t_s + 1\Delta t)^2 + \cdots + b_n(t_s + 1\Delta t)^n \\ \vdots \\ b_0 + b_1(t_s + k\Delta t) + b_2(t_s + k\Delta t)^2 + \cdots + b_n(t_s + k\Delta t)^n \end{bmatrix}$$

$$= \begin{bmatrix} a_0 + a_1(-k) + a_2(-k)^2 + \cdots + a_n(-k)^n \\ \vdots \\ a_0 + a_1(-1) + a_2(-1)^2 + \cdots + a_n(-1)^n \\ a_0 + a_1(-0) + a_2(-0)^2 + \cdots + a_n(-0)^n \\ a_0 + a_1(1) + a_2(1)^2 + \cdots + a_n(1)^n \\ \vdots \\ a_0 + a_1(k) + a_2(k)^2 + \cdots + a_n(k)^n \end{bmatrix}, \quad (4)$$

or, in terms of matrices,

$$x = \begin{bmatrix} 1 & -k & (-k)^2 & \cdots & (-k)^n \\ \vdots & \vdots & \vdots & \iddots & \vdots \\ 1 & -2 & (-2)^2 & \cdots & (-2)^n \\ 1 & -1 & (-1)^2 & \cdots & (-1)^n \\ 1 & 0 & 0 & \cdots & 0 \\ 1 & 1 & 1^2 & \cdots & 1^n \\ 1 & 2 & 2^2 & \cdots & 2^n \\ \vdots & \vdots & \vdots & \ddots & \vdots \\ 1 & k & k^2 & \cdots & k^n \end{bmatrix} \begin{bmatrix} a_0 \\ \vdots \\ a_n \end{bmatrix} \equiv H_a. \quad (5)$$

To find the Savitzky-Golay estimates, use the pseudoinverse of H to compute a and then premultiply by H:

$$\hat{x} = H(H^T H)^{-1} H^T x = Bx. \quad (6)$$

To avoid ill-conditioning, "sgolay" uses the "qr" function to compute an economy-size decomposition of H as H = QR, in terms of which $B = QQ^T$.

It is necessary to compute B only once. The Savitzky-Golay estimates for most signal points result from convolving the signal with the center row of B. The result is the steady-state portion of the filtered signal. The first k rows of B yield the initial transient, and the final k rows of B yield the final transient.

c) Median filter

The main idea of the median filter (MF) is to run through the signal entry by entry, replacing each entry with the median of the entry and its neighboring entries. The idea is like a moving average filter, which replaces each entry with the arithmetic mean of the entry and its neighbors. The pattern of neighbors is called the "window", which slides, entry by entry, over the entire signal. For one-dimensional signals, the most obvious window is just the first few preceding and following entries, whereas for two-dimensional (or higher-dimensional) data, the window must include all entries within a given radius or ellipsoidal or rectangular region (i.e., the MF is not a separable filter).

Typically, by far most of the computational effort and time is spent on calculating the median of each window. Because the filter must process every entry in the signal, for large signals, the efficiency of this median calculation is a critical factor in determining how fast the algorithm can run. Furthermore, some types of signals use whole number representations: in these cases, histogram medians can be far more efficient because it is simple to update the histogram from window to window, and finding the median of a histogram is not particularly onerous.

D. Principle of operation of the Wiener filter

A Wiener filter is a signal processing method that is used to smooth out superimposed noise data and to optimally recover the original signal. It is suitable for stationary systems where noise and signal have certain statistical characteristics (average value and dispersion). The main purpose of the filter is to minimize the RMS error between the restored signal and the original one.

The formula for the Wiener filter depends on the noise covariance matrix and the signal covariance matrix. Assuming that σ^2 is the dispersion of noise and that R is the autocovariance matrix of the signal, it follows that.

$$W = R(R + \sigma^2 I)^{-1} \tag{7}$$

This matrix can be calculated if the exact statistical characteristics of the noise and signal are known. In practical terms, the calculation of W may require measurements or experimental data to accurately determine parameters. In case we want to include the specific noise from the sensors to measure the parameters of the electro-hydraulic system, we need to model these influences in the specific dynamic conditions of the measurement mode. The autocovariance matrix R It usually represents the internal dynamics of the signal, including the interactions between the different states of the system.

The Disturbance Matrix (noise) σ^2 defines the input noise uncertainty, which, in the case of optimization of electro-hydraulic systems, determines how noise affects the spectral components of the signal and how they are processed to minimize the rms error. This matrix is usually diagonal, with each diagonal field representing the dispersion of the corresponding noise signal. Estimates of states are calculated according to the formula:

$$\hat{\mathrm{x}} = \mathrm{Wy} \tag{8}$$

where $\hat{\mathrm{x}}$ is the vector of the evaluated states.

E. Development of the Wiener filter design

Implementing a Wiener filter alongside a PID controller can effectively enhance signal processing and control system performance by reducing noise and improving signal estimation.

It was developed linear filter used in signal processing to minimize the mean square error between an estimated random process and the desired process. A control loop feedback mechanism that computes an error value based on the difference between a desired setpoint and a measured process variable.

To define the system model let assume we have a desired signal $s(t)$ that is corrupted by noise $n(t)$. Then the observed signal $x(t)$ is:

$$x(t) = s(t) + n(t) \tag{9}$$

The purpose of the Wiener filter is to obtain an estimate of $s(t)$ from $x(t)$. The estimated value $\hat{s}(t)$ is.

$$\hat{s}(t) = H(f).x(t) \tag{10}$$

Here $H(f)$ is the transmission function of the Wiener filter, which is determined by the spectral properties of the signal and noise.

The Wiener filter minimizes the following function:

$$J = E\{(s(t) - \hat{s}(t))^2\} \tag{11}$$

where $E\{.\}$ is the operator of the mathematical expectation.

The goal is to design a filter $H(f)$ that minimizes the mean square error. The transmission function of the Wiener filter in the frequency space is given by:

$$H(f) = \frac{S_s(f)}{S_s(f)+S_n(f)} \tag{12}$$

where $S_s(f)$ is the spectral density of the signal and $S_n(f)$ is the spectral density of noise.

In the simulation, the Wiener filter is implemented by an FIR (Finite Impulse Response) filter that approximates the desired transmission function $H(f)$. In the MATLAB the fir1 function generates an FIR filter that can be set to a certain frequency limit (in this simulation, 0.3 is set).

After filtration (fig.3), the output of the Wiener filter (the filtered signal) is fed to the PID regulator, which

controls the system based on the values obtained. The mathematical model of the PID regulator is:

$$u(t) = K_p e(t) + K_i \int e(t)dt + K_d \frac{de(t)}{dt} \quad (13)$$

where $e(t)$ is the error between the set value and the actual value, $u(t)$ is the output of the PID regulator.

III. RESULTS AND DISCUSSION

To simulate the ongoing processes in the system, the software product Matlab Simulink, Sim hydraulic, Sim Electronic is used.

In Fig.3. shows the signal from the tach generator and the transients of the change in the speed of the hydraulic motor at different through sections of the load throttle valve. The red curve shows the signal filtered by the Wiener filter.

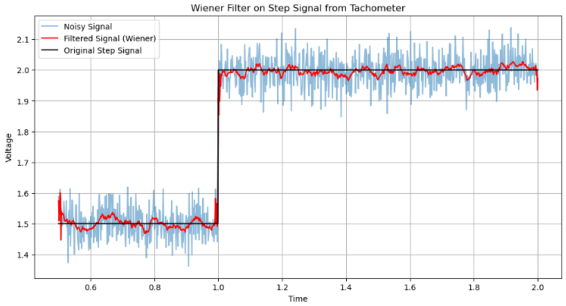

Fig. 3. Signal from the tach generator and the transients of the change in the speed of the hydraulic motor at different through sections of the load throttle valve.

The developed simulation model makes it possible to study the dynamic characteristics of an electro-hydraulic drive system with rotary movement of the actuator. Transients obtained under different loads and input signals allow to analyze the behavior of the system and evaluate the influence of different parameters of setting the analyzed types of filters.

When using a Wiener (see fig.4) filter with an appropriate setting, a significant reduction in the identified error in the system is achieved and the quality of the transient process is improved.

The use of hydraulic and electro-hydraulic systems to drive several machines and assemblies in the industry places different demands on the quality of work and the accuracy of work in static and dynamic modes.

As a result of the simulations and analysis of the electro-hydraulic speed control system of a hydro motor, it can be concluded that the error is greater between the set value and the actual value of the signal from the speed sensor in the low-pass filters compared to the Wiener filter under the same conditions. As can be seen in Fig.4. With the reduction of the load (opening the load throttle) in the first minute of the simulation, the speed response from the tach generator changes ramp wise.

DC motors can be used in a variety of applications in a wide range of prices and sizes. Therefore, the PWM control system of the DC motor driving an unregulated pump is energy efficient and cheaper to implement.

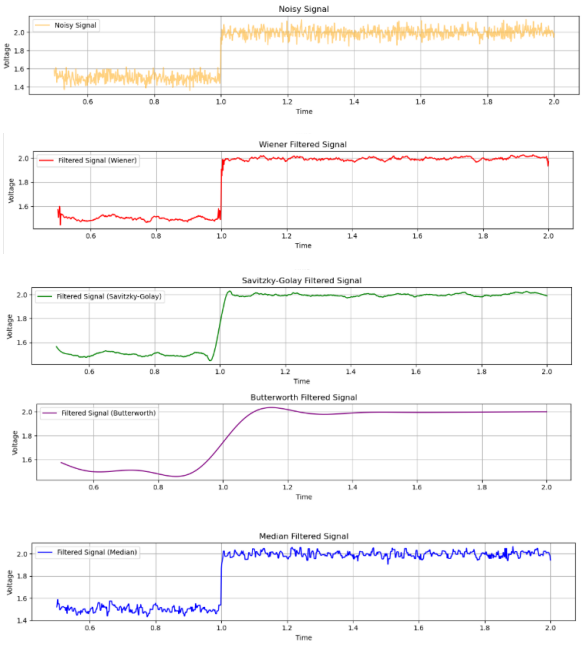

Fig. 4. Comparative presentation of simulated filter results.

The main reason for using pulse width modulation in DC motor regulation is to avoid excessive heat dissipation in linear amplifiers. The problem of dissipation often leads to high heat absorption, because of which forced cooling. PWM amplifiers can significantly reduce this problem because they have much higher power conversion efficiency. In addition, the input signal can be directly received from any digital system without the need for digital-to-analog converters.

IV. CONCLUSIONS

Evaluating the selected filter in a simulation environment can evaluate its performance under various conditions. Evaluating the filter on the actual system and fine-tuning the parameters based on observed performance reduces the time required to implement the system, as potential problems can be identified and resolved.

Simulation and analysis of several types of filters for processing signals with sensor noise in electro-hydraulic systems provide significant benefits, including system optimization, increased reliability, improved signal quality, flexibility, and ease of implementation. These benefits lead to more efficient and reliable systems that can meet the specific requirements of different applications.

The main advantage of the Wiener filter over low-pass filters is its ability to optimize the signal-to-noise ratio (SNR). While low-pass filters reduce the high-frequency components of a signal, they can also reduce useful information and introduce distortion. The Wiener filter, on the other hand, uses the statistical properties of the signal and noise to minimize the mean square error between the filtered and the original signal.

In this way, the Wiener filter can better restore the original signal and preserve the useful information, while reducing noise. This makes it more effective in situations where preserving signal quality is important.

ACKNOWLEDGMENT

This research was funded by the European Regional Development Fund under the Operational Program "Scientific Research, Innovation and Digitization for Smart Transformation 2021-2027", Project CoC "Smart Mechatronics, Eco- and Energy Saving Systems and Technologies", BG16RFPR002-1.014-0005.

REFERENCES

[1] H. C. Pedersen and T. O. Andersen, "Pressure Feedback in Fluid Power Systems—Active Damping Explained and Exemplified," in IEEE Transactions on Control Systems Technology, vol. 26, no. 1, pp. 102-113, Jan. 2018, doi: 10.1109/TCST.2017.2650680

[2] Y. Huang, W. Bao, F. Li and X. Li, "Sparse Time-Frequency Analysis Based on Instantaneous Frequency Estimation and Fault Diagnosis Application," in IEEE Transactions on Instrumentation and Measurement, vol. 71, pp. 1-9, 2022, Art no. 3525509, doi: 10.1109/TIM.2022.3210987.

[3] Y. Jiang, Y. Chen and P. Wang, "An Iterative Adaptive Vold–Kalman Filter for Nonstationary Signal Decomposition in Mechatronic Transmission Fault Diagnosis Under Variable Speed Conditions," in IEEE Transactions on Industrial Informatics, vol. 20, no. 8, pp. 10510-10519, Aug. 2024, doi: 10.1109/TII.2024.3393536.

[4] L. M. Halabi, H. A. G. Al-Kaf and K. -B. Lee, "Efficient Fault Detection for Open Circuit Faults in HANPC Inverters Using Artificial Neural Network for Motor Drive Applications," 2023 IEEE International Symposium on Sensorless Control for Electrical Drives (SLED), Seoul, Korea, Republic of, 2023, pp. 1-6, doi: 10.1109/SLED57582.2023.10261371.

[5] L. An and N. Sepehri, "Hydraulic actuator circuit fault detection using extended Kalman filter," Proceedings of the 2003 American Control Conference, 2003., Denver, CO, USA, 2003, pp. 4261-4266 vol.5, doi: 10.1109/ACC.2003.1240505.

[6] F. Zheng, S. Li, C. Ding, J. Zhao, J. Ruan," Theoretical and Experimental Research on the Cartridge Two-Dimensional (2D) Electro-Hydraulic Servo Valve," Advances in Mechanical Engineering. 2021;13(2). doi:10.1177/1687814021996532

[7] T. Jiang, W. Lu, L. Lu, L. Xu, W. Xi, J. Liu, Y. Zhu, "Inlet Passage Hydraulic Performance Optimization of Coastal Drainage Pump System Based on Machine Learning Algorithms," Journal of Marine Science and Engineering(2025), 13. 274. 10.3390/jmse13020274.

[8] O. Khedr, M. Awad, A Aloufy, S. Maged, " Optimizing Power Consumption and Position Control in an Electro-Hydraulic System with Cylinder Bypass and NN-MPC," Scientific Reports (2024). 14. 10.1038/s41598-024-51318-x.

[9] K. Ormandzhiev, S. Yordanov, G. Mihalev, K. Kostov, "Parametric Optimization of Electrohydraulic Servo System, "E3S Web of Conferences (2020), 207. 04003. 10.1051/e3sconf/202020704003.

[10] D. Dichev, I. Zhelezarov, R. Dicheva, D. Diakov, H. Nikolova, G. Cvetanov, " Algorithm for Estimation and Correction of Dynamic Errors, "XXX International Scientific Symposium "Metrology and Metrology Assurance 2020", September, 2020, Sozopol, Bulgaria, pp. 91-95. DOI: 10.1109/MMA49863.2020.925426111.

[11] D. Dichev, F. Kogia, H. Nikolova, D. Diakov, " A Mathematical Model of the Error of Measuring Instruments for Investigating the Dynamic Characteristics, " Journal of Engineering Science and Technology Review. Volume 11, Issue 6, 2018, pp. 14 -19. DOI: 10.25103/jestr.116.03

[12] D. Dichev, F. Kogia, H. Koev, D. Diakov, " Method of Analysis and Correction of the Error from Nonlinearity of the Measurement Instruments, " Journal of Engineering Science and Technology Review. Volume 9, Issue 6, 2016, pp. 116 -121. DOI: 10.25103/jestr.096.17

[13] D. Dichev, D. Diakov, R. Dicheva, I. Zhelezarov, O. Kupriyanov, "Analysis of Instrumental Errors Influence on the Accuracy of Instruments for Measuring Parameters of Moving Objects," 31st International Scientific Symposium Metrology and Metrology Assurance, MMA 2021, September, 2021, Sozopol, Bulgaria. DOI: 10.1109/MMA52675.2021.9610855

[14] D. Dichev, H. Koev, D. Diakov, N. Panchev, R. Miteva, H. Nikolova, "Automated System for Calibrating Instruments Measuring Parameters of Moving Objects," 59th International Symposium ELMAR, September 18-20 th, 2017, Zadar, Croatia, pp. 219-224. DOI: 10.23919/ELMAR.2017.8124472

[15] C. Conev, T. Karadzhov, Application of the Finite Element Method for the Design of Small Arm Barrels, (2023) Vide. Tehnologija. Resursi - Environment, Technology, Resources, 2, pp. 114-118, DOI: 10.17770/etr2023vol2.7213.

[16] M. Kokalarov, "Predetermination of the Uncertainty Budget and Error Analysis of the Photogrammetric Method in Heavy Machinery" Proceedings of the 30th DAAAM International Symposium, (2019): pp. 0914 - 0920. doi: 10.2507/30th.daaam.proceedings.127;

[17] M. Kokalarov, B. Sakakushev, S. Parvanov "Generalized Methodology for Application of the Photogrammetric Method for Measurement in Heavy Engineering" XXXI Международен научен симпозиум Метрология и метрологично осигуряване (MMA), (2021): pp. 0095-0099. doi: 10.1109/MMA52675.2021.9610966.

[18] S. Guolei, L. Kan, L. Yifan, C. Haoze, L. Mengru and L. Liang, "Analysis of Fluid Pulsation Characteristics and Its Suppression Method Design for One-Side Slide Spool of Counter Balance Valve," 2023 9th International Conference on Fluid Power and Mechatronics (FPM), Lanzhou, China, 2023, pp. 1-10, doi: 10.1109/FPM57590.2023.10565437.

[19] R. R. Chazim, I. Bahiuddin, H. A. Prabhakara, R. S. Nugroho, F. Imaduddin and S. Amri Mazlan, "Field Dependent Force Predictions of a Meandering Valve Based-Magnetorheological Damper Using Multilayer Artificial Neural Networks," 2022 2nd International Conference on Electronic and Electrical Engineering and Intelligent System (ICE3IS), Yogyakarta, Indonesia, 2022, pp. 299-304, doi: 10.1109/ICE3IS56585.2022.10010062.

[20] D. Cristofori, A.Vacca, K. Ariyur, "A Novel Pressure-Feedback Based Adaptive Control Method to Damp Instabilities in Hydraulic Machines," Commercial Vehicles 5(2):586-596, 2012, https://doi.org/10.4271/2012-01-2035.

[21] J. Watton, " Fundamentals of Fluid Power Control". Cambridge University Press; 2009.

[22] D. Diakov, D. Komarski, H. Nikolova, "Optimization of Butterfly Flexures for Angular Positioning", In 31st International Scientific Symposium Metrology and Metrology Assurance, MMA, 2021. DOI: 10.1109/MMA52675.2021.9610833

[23] D. Pulov, T. Karadzhov, Y. Pulova-Ganeva , "A Variant For Using Regression Analysis To Assess The Electromagnetic Environment In An Urban Area, " Environment. Technologies. Resources. Proceedings of the International Scientific and Practical Conference, Rezekne, Latvia, v. 1, p. 200–203, 2023. DOI: 10.17770/etr2023vol1.7185.

[24] D. Pulov, T. Karadzhov, " Optoelectronic Device For Measuring The Power Of Laser Radiation, " Environment. Technologies. Resources. Proceedings of the International Scientific and Practical Conference, Rezekne, Latvia, v. 3, p. 286–290, 2021. DOI: 10.17770/etr2021vol3.6590.

[25] D. Pulov, T. Karadzhov, " Temperature Measurement With Photodiode In Different Operating Modes, " Environment. Technologies. Resources. Proceedings of the International Scientific and Practical Conference, Rezekne, Latvia, v. 3, p. 291–295, 2021. DOI: 10.17770/etr2021vol3.6556.

Environment. Technology. Resources. Rezekne, Latvia
Proceedings of the 16th International Scientific and Practical Conference.2025. Volume IV, 111-115

Experimental Study of the Frequency Characteristics of an Electropneumatic Tracking System with High Speed Pneumatic Valves and PWM Control

Georgi Slavchev Iliev
dept. Power Engineering
Technical University of Gabrovo
Center of competence "Smart mechatronic, eco-and energy-saving systems and technologies"
Gabrovo, Bulgaria
g.iliev@tugab.bg

Hristo Nedev Hristov
dept. Power Engineering
Technical University of Gabrovo
Center of competence "Smart mechatronic, eco-and energy-saving systems and technologies"
Gabrovo, Bulgaria
christo@tugab.bg

Docho Svetlozarov Dimitrov
dept. Power Engineering
Technical University of Gabrovo
Center of competence "Smart mechatronic, eco-and energy-saving systems and technologies"
Gabrovo, Bulgaria
docho5_dim@abv.bg

***Abstract*— This paper describes an experimental study on the frequency characteristics of an electropneumatic tracking system with a high-speed pneumatic on/off valve (HSPV) and Pulse Width Modulation (PWM) control. A demonstration experimental test bench has been developed to analyze the Bode diagrams of magnitude and phase for an electropneumatic tracking system with a double-rod pneumatic cylinder, and the system's critical frequency has been determined. A specialized virtual instrument is used for control and data acquisition. The process control and data processing are performed automatically by a computer and the corresponding NI interface board. The results are presented in graphical form and analysis of the obtained Bode Diagrams was made.**

Keywords — critical frequencies, electropneumatic positioning system, frequency responses, high speed pneumatic valves, PWM control.

I. INTRODUCTION

Electropneumatic tracking systems offer several advantages—they are fast-acting, reliable, and easy to maintain. Traditionally, they are built using a proportional valve or a servo valve, which are high-cost pneumatic control components. However, designing a pneumatic tracking system with high speed pneumatic on/off valves (HSPV) and PWM control enables similar advantages at a lower cost.

The high-speed pneumatic on/off valve (HSPV) is a commonly used and fundamental component in modern digital fluid power control systems. As a key control element, the dynamic characteristics of HSPV influence the response of the entire pneumatic tracking system.

Due to air compressibility, the adverse effects of friction, and low damping properties, pneumatic devices require complex control strategies. Pneumatic actuation systems are widely used in CNC machines, aviation technology, and other applications, where they must meet strict requirements in both static and dynamic operating modes [1],[3],[5].

To analyze electropneumatic tracking systems and design control algorithms, frequency characteristics (amplitude-frequency and phase-frequency) are widely used to describe the system's dynamic properties. Experimental determination of frequency characteristics allows for the development of accurate mathematical models, which can be utilized in system design to achieve specific performance and precision levels [8].

A demonstration research test bench has been developed for real-time control and investigation of an electropneumatic tracking system. This test bench enables the determination of frequency characteristics and the critical frequency range of an electropneumatic tracking system under dynamic conditions.

In many cases, electropneumatic systems must meet requirements not only for precise tracking of input signal

Online ISSN 2256-070X
https://doi.org/10.17770/etr2025vol4.8427
© 2025 The Author(s). Published by RTU PRESS.
This is an open access article under the Creative Commons Attribution 4.0 International License.

variations but also for high response speed [9], [18], [20], [24].

The response speed of an electropneumatic system is characterized by two key parameters:

Response time – The time required for the output signal to match the input signal. Fast systems exhibit minimal response times.

Natural (critical) frequency – indicates the rate at which the electropneumatic system can respond to signal variations per second.

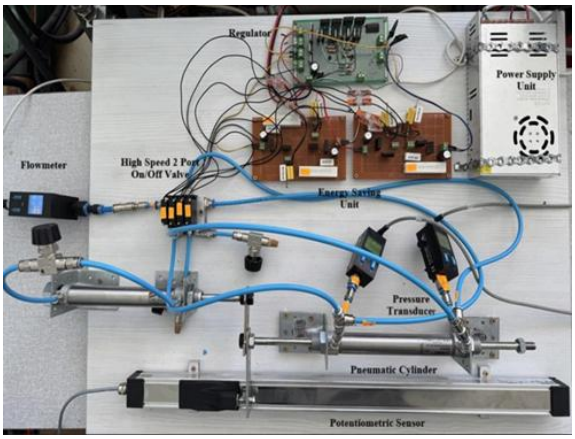

Fig. 1. Demonstration Research Test Stand.

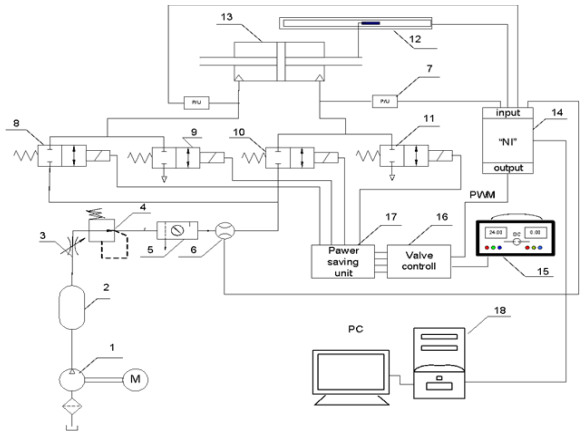

Fig. 2. Schematic Diagram of the High-Speed Pneumatic On/Off Valve with PWM Control

1 - screw compressor; 2 - receiver; 3 – throtle valve; 4 – presure ruducting valve; 5 - air preparation system preparatory; 6 - flowmeter; 7 - pressure transducer, 8, 9, 10, 11 high speed pneumatic on/off valve; 12 - potentiometric sensor, 13 - double-rod pneumatic cylinder, 14 - terminal board (NI); 15 - power supply unit; 16 – Valve Controler, 17 - Power saving unit, 18 – PC,

II. MATERIALS AND METHODS

A. Experiment Description

The demonstration research test stand is shown in Fig. 1. The control of the experimental process, data collection and processing, and data archiving are performed automatically by a computer and an interface board manufactured by National Instruments. For the purposes of this experiment, specialized software—LabVIEW—is used to manage the experimental processes, allowing an unlimited number of real-time measurements and data processing.

The investigated system consists of the following elements: a screw compressor, a high-speed pneumatic on/off valve, a double-rod pneumatic cylinder AIGNEP MJ0250125, and measuring equipment, a regulator, and an energy-saving block [1], [3], [5], [6].

The position control of the pneumatic cylinder with a double-ended rod is implemented using four HSPV- (SX 12 F-AH) valves, operating as follows. When all four valves are closed (Off), the piston remains in the required position. When Valve 1 and Valve 4 are open (On), the piston moves to the left. Similarly, when Valve 2 and Valve 3 are open, the piston moves to the right, thus performing a reciprocating motion (Fig. 2). The solenoid is actuated using PWM technique, with control implemented

through analogue circuits. A virtual instrument for control and dynamic process analysis in the electro-pneumatic tracking system has been developed [8],[13].

The developed virtual instrument enables both the control of the electro-pneumatic tracking system and its real-time analysis by collecting and processing data from displacement, flow rate, and pressure sensors. The virtual instrument generates sinusoidal PWM control signals. The formation of sinusoidal voltage through PWM is an effective way to control the HSPV, allowing smooth modulation depth adjustment. Using PWM significantly improves energy efficiency while maintaining high-quality process control [22], [24].

The variation of the input signal and the displacement of the pneumatic cylinder are recorded using the same virtual instrument. At low input signal frequencies, the piston of the pneumatic cylinder oscillates at the same frequency as the input signal. As the input frequency increases while maintaining the signal amplitude, the oscillation frequency of the cylinder also increases. However, at high frequencies, the pneumatic cylinder can no longer follow the input signal variations, and its oscillation amplitude decreases. The frequency at which this begins to occur is defined as the critical frequency [2], [6], [8].

Natural (critical) frequency – indicates the rate of input signal changes to which the electropneumatic system can respond.

The frequency response of the system is determined by two graphs:

- Amplitude-Frequency Response (AFR)

The ratio of amplitude at measured frequencies to the amplitude at very low frequencies is recorded in decibels (dB) and plotted on a logarithmic scale. An amplitude

ratio of -20 dB means that the amplitude at a given frequency is ten times smaller than the amplitude at low frequencies. Plotting the amplitudes for all measured frequencies yields the amplitude-frequency response [7], [15].

- Phase-Frequency Response (PFR)

The delay of the output signal relative to the input signal is measured in angular degrees. A phase delay of 360° means that the output signal lags by one full cycle. The graphical representation of phase shift as a function of frequency is known as the phase-frequency response.

When the input signal amplitude changes by 10%, the cylinder should move only a small distance. Therefore, it can respond to such input signal changes even at high frequencies. The amplitude and phase characteristics deviate from the horizontal line only at high frequencies. When the input signal amplitude changes by 90%, the distance the pneumatic cylinder needs to travel is nine times greater. It almost does not follow the input signal variations. The amplitude and phase characteristics also deviate from the horizontal line at low frequencies.

- Critical Frequency

The critical frequency value is obtained from the amplitude-frequency response. It is the frequency at which the amplitude drops to 70.7% or -3 dB [2],[6].

The limitations of using HSPV- "SX 12 F-AH (0.15~0.7 MPa) SMC Japan" with PWM control are determined by the maximum pressure specified by the manufacturer.

B. Order of Experiment Execution

1. The selected operating pressure for the experiment is 4 bar (it is possible to conduct the experiment at different pressures).

2. The chosen parameters for the operation of the virtual instruments created for the experiment are configured. A sinusoidal input signal with different amplitudes—0.3 V, 0.5 V, and 0.7 V—and a frequency ranging from 0.7 Hz to 5 Hz is set. The initial position of the electro-pneumatic tracking system is established. After preliminary tests of the control and measurement circuit, the experimental study begins. The obtained results, the input signals, as well as the assigned output signals, are displayed on the screen, recorded, archived, and processed to be presented graphically. After recording is completed, the system returns to its initial position [2].

3. The experiment is repeated as many times as necessary to eliminate errors.

For the experimental study of the frequency characteristics of the pneumatic positioning system, it is assumed that the instruments have significantly smaller time constants than the tested system. In practice, their transient processes occur much faster, and they are considered ideal first-order aperiodic units with time constants significantly smaller than the time constant of the investigated system [2].

III. RESULTS AND DISCUSSION

Figure 3 presents the amplitude-frequency (AFR) and phase-frequency response (PFR) of the pneumatic positioning system at an input signal amplitude of 0.3 V.

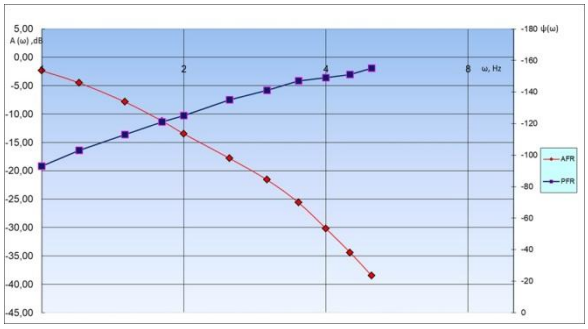

Fig. 3. AFR and PFR at an input signal amplitude of 0.3 V.

Figure 4 presents the AFR and PFR of the pneumatic positioning system at an input signal amplitude of 0.5 V.

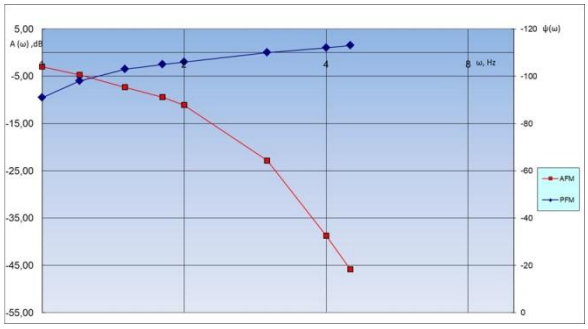

Fig. 4. AFR and PFR at an input signal amplitude of 0.5 V.

Figure 5 presents the AFR and PFR of the pneumatic positioning system at an input signal amplitude of 0.7 V.

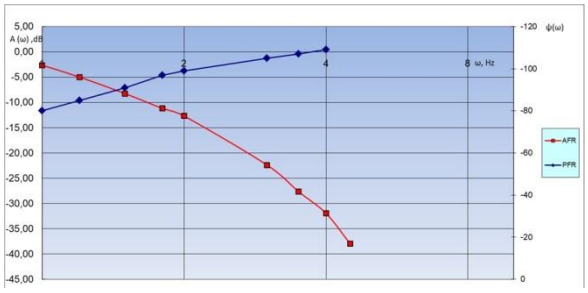

Fig. 5. AFR and PFR at an input signal amplitude of 0.7 V.

Figure 6 presents the AFR of the pneumatic positioning system at input signal amplitudes of 0.3 V, 0.5 V, and 0.7 V.

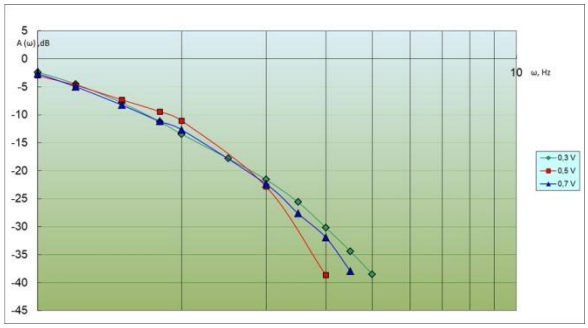

Fig. 6. AFR at input signal amplitudes of 0.3 V, 0.5 V, and 0.7 V

Figure 7 presents the PFR of the pneumatic positioning system at input signal amplitudes of 0.3 V, 0.5 V, and 0.7 V.

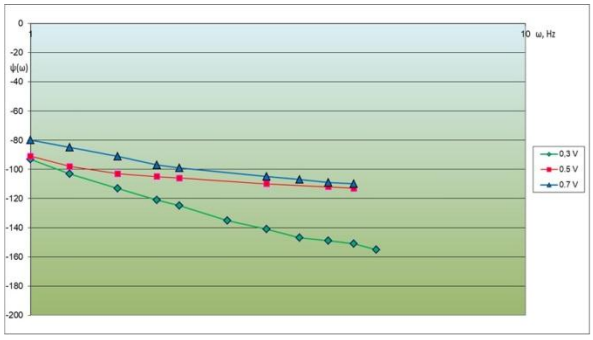

Fig. 7. PFR at input signal amplitudes of 0.3 V, 0.5 V, and 0.7 V.

IV. CONCLUSIONS

The conducted experimental study has yielded frequency characteristics of an electro-pneumatic tracking system with high-speed pneumatic valves (HSPV) and PWM control at different input signal amplitudes—0.3 V, 0.5 V, and 0.7 V. The obtained characteristics confirm the nonlinear nature of the system, as the frequency characteristics vary depending on the amplitude of the input signals.

From the presented characteristics, the system's critical frequency can be determined. It remains within narrow limits for different input signals, ranging from 0.8 Hz to 1.5 Hz, as defined by the PFR at -90°.

V. ACKNOWLEDGMENTS

This research was financially supported by the scientific research activities for Young Scientists and Postdoctoral Researchers as part of the first phase of the National Program "Young Scientists and Postdoctoral Researchers – 2".

This research was funded by the European Regional Development Fund within the OP "Research, Innovation and Digitalization Programme for Intelligent Transformation 2021-2027 ", Project No. BG16RFPR002-1.014-0005 Center of competence "Smart Mechatronics, Eco- and Energy Saving Systems and Technologies"

REFERENCES

[1] G. Iliev and H. Hristov, "Modelling and Simulation of Electropneumatic Positioning System Including the Length of Pneumatic Lines", Environment. Technology. Resources 14th International Scientific and Practical Conference. June 15-16, 2023, Rezekne Academy of Technologies, Rezekne, Latvia, ISSN 1691-5402, vol.3, pp. 106-111, Online IS. https://journals.rta.lv/index.php/ETR/article/view/7186 https://doi.org/10.17770/etr2023vol3.7186

[2] G. Iliev, "Experimental Study Of The Frequency Responses Of Electropneumatic Positioning System", ,Jun.2024, Environment. Technology. Resources 14th International Scientific and Practical Conference. June 15-16, 2023, Rezekne Academy of Technologies, Rezekne, Latvia pp. 90–94, Online ISSN: 2256-070X https://journals.rta.lv/index.php/ETR/article/view/8116' https://doi.org/10.17770/etr2024vol3.8116

[3] G. Iliev, H. Hristov, "Modelling and Simulation of Dynamic Processes of Pneumatic Lines" ENVIRONMENT. TECHNOLOGY. RESOURCES 14th International Scientific and Practical Conference. June 15-16, 2023, Rezekne Academy of Technologies, Rezekne, Latvia, Page 112-118 OnlineISSN:2256-070X https://journals.rta.lv/index.php/ETR/article/view/7190 https://doi.org/10.17770/etr2023vol3.7190

[4] G. Iliev, and H.Hristov, "Experimental Static Frow Characteristics Of Hing Speed On/Off Pneumatic Valves", Mechanics of Machines, 131 YEAR XXXII,№1, ISSN 0861-9727 pp.25-28, 2024

[5] A. Andreev, H. Hristov, G. Iliev, M.Racheva, "Mathematical Model for a Pneumatic Force Actuator System" BGSIAM'15 PROCEEDINGS 10th Annual Meeting of the Bulgarian Section of SIAM, Page 4-6, ISSN 1313-3357, December 21-22, 2015 Sofia

[6] G. Iliev, H. Hristov, A. Anchev, "Experimental study of frequency characteristics of electropneumatic positioning system" RU-Angel Kanchev, Ruse, Bulgaria, Scientific Works, vol. 53. series. 1.2, , pp. 244 – 248, ISSN 1311-3321, 2014

[7] G. Iliev, H. Hristov,A. Anchev, "Experimental study of friction force parameters in a pneumatic cylinder" "UNITECH", Gabrovo, Bulgaria, vol. II, pp 277-280. ISSN 1320-230X, 2012

[8] G.Iliev and H. Hristov,"Speed Control Of Pneumatic Cylinders Using High Speed 2 Port On/Off Valves With Pulse Width Modulation", Environment. Technologies. Resources. Proceedings of the International Scientific and Practical,Conference.3,(Jun.2024),pp.95–100. https://journals.rta.lv/index.php/ETR/article/view/8117 https://doi.org/10.17770/etr2024vol3.8117

[9] A.Whitmore, S. "Frequency response model for branched pneumatic sensing systems" Amer Inst Aeronautics Astronautics; Nov-Dec 2006 Vol. 43, Issue 6, pp.1845-1853 https://arc.aiaa.org/doi/10.2514/1.20759 https://doi.org/10.2514/1.20759

[10] Y. T WANG,and SINGH, R." Frequency-response of a nonlinear pneumatic system" Journal of applied mechanics-transactions of the asme ,Vol. 54, Issue 1, pp.209-214, MAR 1987; https://asmedigitalcollection.asme.org https://doi.org/10.1115/1.3172960

[11] A.Grigaitis, and V. Gelezevicius, A" Electropneumatic Positioning System with an Adaptive Force Controller" Elektronika Ir Elektrotechnika,Issue 7, Page 3-6, 2008.

[12] M. Smaoui and X. Brun, D.Thomasset,"Robust position control of an electropneumatic system using second order sliding mode" IEEE International Symposium on Industrial Electronics; Proceedings Of The Ieee-Isie, Vols 1 And 2 , pp.429-434, 2004.

[13] W. Essmat Abdul-Lateef, Glebov Nikolay Alexeevich, Naseer Hamed Farhoo, Ahmed H. Khdir and Dina H. Shaker. "Modelling and Controlling of position for electro-pneumatic system using Pulse-Width-Modulation (PWM) techniques and Fuzzy Logic controller" IOP Conference Series: Materials Science and Engineering, Volume 765, 1st International Conference of Electromechanical Engineering and its Applications (ICEMEA) 25–26 February 2020, Baghdad, Iraq.

https://iopscience.iop.org/article/10.1088/1757-899X/765/1/012020
DOI 10.1088/1757-899X/765/1/012020

[14] R. Kumar & J. R. B. del Rosario," Design and Simulation of Electro-Pneumatic Motion Sequence Control Using FluidSim" Applied Mechanics and Materials, Vol. 446-447, pp.1146-1150, 2014.
www.scientific.net/AMM.446-447.1146
https://doi.org/10.4028/www.scientific.net/AMM.446-447.1146

[15] Ioannis Tsitsimpelisa, C. James Taylora, Barry Lennoxb, Malcolm J. Joycea. "A review of ground-based robotic systems for the characterization of nuclear environments" Progress in Nuclear Energy . 2019, 111(pp.109–124).
www.elsevier.com/locate/pnucene.

[16] D. Pulov, T. Karadzhov, "Optoelectronic Device for Measuring the Power of Laser Radiation", Environment. Technology. Resources. Rezekne, Latvia, Proceedingsofthe 13th International Scientificand Practical Conference. Vol.3, pp. 286-290, 2021, Online ISSN 2256-070X,
https://journals.rta.lv/index.php/ETR/article/view/6590
https://doi.org/10.17770/etr2021vol3.6590

[17] M. Marino "A Geometrical Synthesis Of Comez Textile Mechanisms Of Finally Removed Possibilities" Environment. Technology. Resources 14th International Scientific and Practical Conference. June 15-16, 2023, Rezekne Academy of Technologies, Rezekne, Latvia, Volume 3, page 168 to 171,
https://journals.rta.lv/index.php/ETR/article/view/7187
https://doi.org/10.17770/etr2023vol3.7187

[18] M. Marinov J. "Synthesis Of Eight Middle Lost Mechanisms Finally Discharged Discreet Positions ",Rezekne Education in Engineering Sciences Vol.2(2024) page 435-439 ,
https://journals.rta.lv/index.php/ETR/article/view/8067
https://doi.org/10.17770/etr2024vol2.8067

[19] M.Shih and M.Ma, "Position control of a pneumatic rodless cylinder using fuzzy PWM control method". Mechatronics 1998; vol.41(2C),pp.241–53.

[20] M. Shih andM. Ma," Position control of a pneumatic rodless cylinder using sliding mode M-D-PWM control the high speed solenoid",JSM E Int J 1998;vol.41(2C):pp.236–41.

[21] M Pipan, N Herakovic," Closed-loop volume flow control algorithm for fast switching pneumatic valves with PWM signal" Control Engineering Practice Volume 70, January 2018,Pages114-120
https://www.sciencedirect.com/science/article/pii/S096706611730240X?via%3Dihub
https://doi.org/10.1016/j.conengprac.2017.10.008

[22] Elif Erzan Topc¸u, _Ibrahim Yu¨ksel , Zeliha Kamıs" Development of electro-pneumatic fast switching valve and investigation of its characteristics" Mechatronics ,Volume 16, Issue 6, July 2006, Pages 365-378
https://www.sciencedirect.com/science/article/pii/S0957415806000250?via%3Dihub
https://doi.org/10.1016/j.mechatronics.2006.01.005

[23] M. Taghizadeh, A. Ghaffari, F. Najafi „Modeling and identification of a solenoid valve for PWM control applications" Comptes Rendus MécaniqueVolume 337, Issue 3, March 2009, Pages 131-140.
https://comptes-rendus.academie-sciences.fr/mecanique/articles/10.1016/j.crme.2009.03.009
https://doi.org/10.1016/j.crme.2009.03.009

[24] B.Zhang, Qi Zhong,Ji-en Ma,Hao-cen Hong, Hui-ming Bao,Yan Shi, Hua-yongYang"Self-correcting PWM control for dynamic performance preservation in high speed on/off valve",Mechatronics, Volume 55, November 2018, Pages 141-150
https://www.sciencedirect.com/science/article/pii/S0957415818301442
https://doi.org/10.1016/j.mechatronics.2018.09.001

Environment. Technology. Resources. Rezekne, Latvia
Proceedings of the 15th International Scientific and Practical Conference.2025. Volume IV, 117-122

Experimental Investigation of Dynamic Processes in an Electropneumatic Positioning System with High Speed Valves and PWM

Georgi Slavchev Iliev
dept. Power Engineering
Technical University of Gabrovo
Center of competence "Smart mechatronic, eco-and energy-saving systems and technologies"
Gabrovo, Bulgaria
g.iliev@tugab.bg

Hristo Nedev Hristov
dept. Power Engineering
Technical University of Gabrovo
Center of competence "Smart mechatronic, eco-and energy-saving systems and technologies"
Gabrovo, Bulgaria
christo@tugab.bg

***Abstract*— This paper presents a demonstration experimental test bench for investigating the dynamic characteristics of an electropneumatic positioning system with High Speed Pneumatic Valves (HSPV) and Pulse Width Modulation (PWM) control. A specialized virtual instrument has been developed for real-time control, data acquisition, and processing. The transient response of the electropneumatic positioning system is examined under various single-step input signals with frequencies ranging from 30 Hz to 70 Hz and varying duty cycles from 30% to 90%. The results are presented graphically, demonstrating that the system exhibits better linear characteristics compared to conventional pneumatic actuation systems.**

Keywords*— dynamic characteristics, electropneumatic positioning system, high speed pneumatic valves, PWM control.

I. INTRODUCTION

Pneumatic actuation systems have been utilized in engineering for many years. In the past, they were primarily used for movement between two positions with end-of-travel switches due to their poor dynamic and nonlinear characteristics [4],[6],[12]. Advancements in technology, electronics, and microprocessor systems have led to a growing adoption of pneumatic actuation systems in the industry. They are widely applied in robotics, aviation, CNC machines, metallurgy, and many other technologies. These systems are environmentally friendly and energy- saving.

In most applications, pneumatic actuation systems are utilized for position control of the pneumatic actuator when using pneumatic servo valves or proportional distributors. However, pneumatic servo valves are expensive, and proportional distributors do not offer the fastest response time due to their deadband sensitivity [1]-[5],[10].

To find an alternative technical solution for the precise positioning of pneumatic actuation systems, switching valves with digital control techniques such as Pulse Width Modulation (PWM) can be used to achieve linear dynamic flow control characteristics with the fastest possible response time and significantly reduced electrical power consumption. Conventional single-stage solenoid on/off valves are bulky and have low dynamic characteristics. These valves make fine positioning control difficult due to the valve's response limitations. Therefore, a high speed switching valve is required to achieve high performance [11], [13], [16], [18], [20].

The primary reason for using PWM control for fast switching is to reduce the valve response time. These valves are characterized by miniaturization of the main overall dimensions of the housing and internal elements, as well as advanced electronics. Many researchers have applied PWM techniques in controlling pneumatic switching valves and have obtained positive results. The PWM signal frequencies used depend on the valve response time and typically range between 20 Hz and 100 Hz. The relationship between pulse width and flow rate has always been considered linear.

The standard equation for flow rate through a pneumatic valve is defined in ISO 6358 (2013) and is used in almost all mathematical models of high speed switching pneumatic valves. As a result, further in-depth research is required to examine the dynamic characteristics of electropneumatic positioning systems with High Speed Pneumatic Valves (HSPV) and PWM control. More accurate mathematical models should be

Online ISSN 2256-070X
https://doi.org/10.17770/etr2025vol4.8430
© 2025 The Author(s). Published by RTU PRESS.
This is an open access article under the Creative Commons Attribution 4.0 International License.

developed to describe the dynamics of position control in electropneumatic positioning systems utilizing HSPV and PWM control [20], [21].

II. MATERIALS AND METHODS

The HSPV used in this study of the dynamic characteristics of the electro-pneumatic positioning system is the SX 12 F-AH (0.15~0.7 MPa) from SMC Japan, with a response time of less than 0.4 ms. Description and Construction of HSPV. The HSPV is designed as an electromagnetic, on-off, 2/2 valve. The plunger consists of a rectangular plate made of magnetic material with a specific geometry. During operation, the coil lifts the plunger, and when deactivated, it returns to its initial position due to pressure (a spring is not involved in the valve's operation). A specialized pneumatic demonstration stand has been developed, as shown in Figure 2, for experimental studies on dynamic processes in pneumatic actuation systems with HSPV.

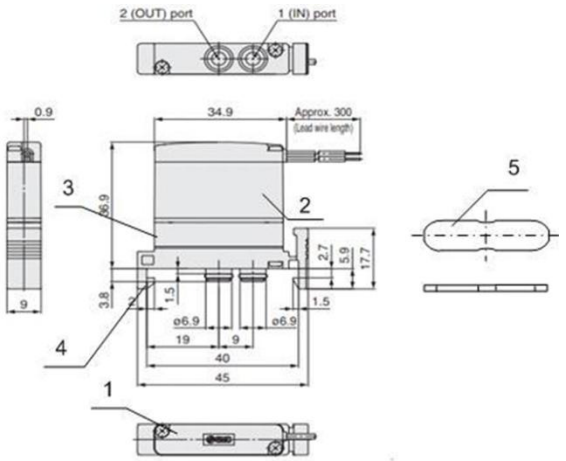

Fig. 1 Illustrates the schematic of the HSPV - SX 12 F-AH, SMC Japan.

1. Cover cap; 2. Upper panel with an electromagnetic coil; 3. Second panel housing the working zone of the plunger; 4. Lower panel with connectors for valve connection, inlet, and outlet; 5. Plunger (plate made of magnetic material).

The stand is equipped with a state-of-the-art data acquisition system (DAQ) and a specialized virtual instrument that allows real-time investigation of transient processes in the electro-pneumatic positioning system with HSPV and PWM control.

The control of the piston position in the pneumatic cylinder with a double-extended rod, "AIGNEP MJ0250125," within the electro-pneumatic system is achieved using four high-speed pneumatic valves, as shown in Figure 1. The operation is schematically illustrated in Figure 2. When all four valves are closed, the piston remains in the desired position. When Valve 1 and Valve 4 are opened, the piston moves forward. Similarly, when Valve 2 and Valve 3 are opened, the piston moves backward. The solenoid is actuated using pulse-width modulation (PWM) control, implemented through analog circuits. A virtual instrument has been created using the "LabVIEW" software for managing and investigating the dynamic processes in the electro-pneumatic positioning system with HSPV and PWM control, along with the corresponding NI interface board [4].

The closing position of the valve is determined by the maximum force generated by the flow acting on the plunger. This maximum force is equal to the force exerted by the static pressure, which in turn can be calculated based on the pressure in the closed state and the surface area over which it acts [21].

The developed virtual instrument enables both the control of the electro-pneumatic tracking system and its real-time investigation by collecting and processing data from sensors measuring displacement, flow rate, and pressure [1],[5],[10].

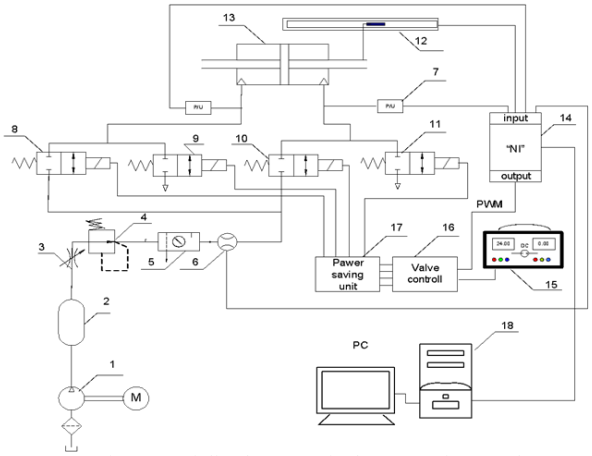

Fig. 2 Specialized pneumatic demonstration stand

1 - screw compressor; 2 - receiver; 3 – throtle valve; 4 – presure ruducting valve; 5 - air preparation system preparatory; 6 - flowmeter; 7 - pressure transducer, 8, 9, 10, 11 high speed pneumatic on/off valve; 12 - potentiometric sensor, 13 - double-rod pneumatic cylinder, 14 - terminal board (NI); 15 - power supply unit; 16 – Valve Controler, 17 - Power saving unit, 18 – PC,

The virtual instrument generates both single-step input signals and sinusoidal pulse-width modulated (PWM) control signals. The formation of single-step signals and sinusoidal voltage through pulse width modulation (PWM) is crucial for effective control of the HSPV, allowing smooth modulation depth adjustment. PWM implementation results in significant energy savings while maintaining high process control quality [4].

The measurement of input signals, piston rod displacement, flow rate, and the pressures in the left and right chambers of the double-rod pneumatic cylinder is recorded using the same virtual instrument. [10], [14], [20], [21].

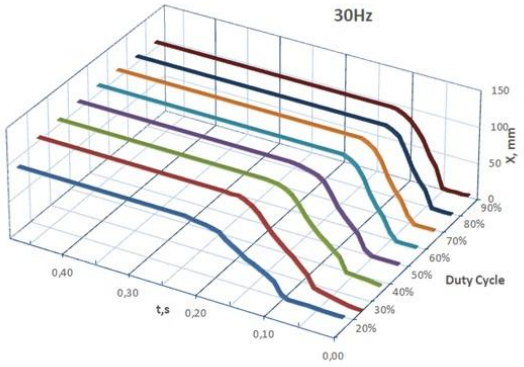

Fig. 3. Displacement of the rod of the pneumatic cylinder at a frequency of 30 Hz and different duty cycle.

Figure 3, 4, 5, 6. Shows experimental transients with PWM at frequencies of 30 Hz and different duty cycles from 30% to 90%.

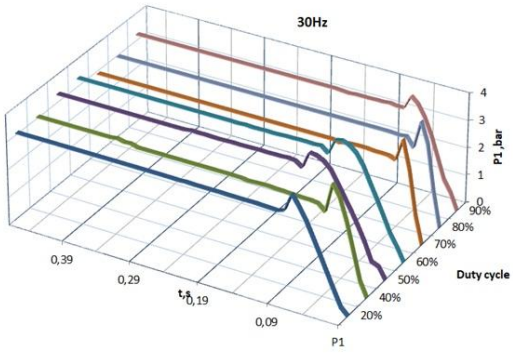

Fig. 4. Pressure drop in the left chamber of the pneumatic cylinder at a frequency of 30 Hz and a different dudy cycle.

When a single-step input signal is applied, the pneumatic cylinder rod moves a precisely defined distance and stops at the set position. The pneumatic cylinder can be controlled with different PWM frequencies and duty cycles.

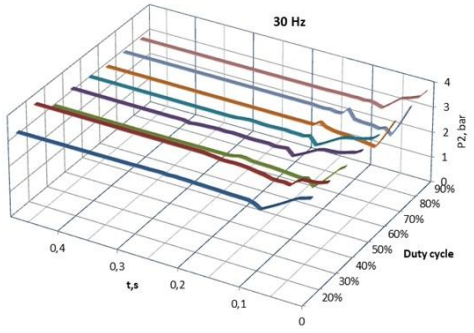

Fig. 5. Pressure washout in the right chamber of the pneumatic cylinder at a frequency of 30 Hz and a different dudy cycle.

Displacement of the rod of the pneumatic cylinder, pressure in the left and right chambers of the cylinder and the flow rate entering the electropneumatic positioning system. The results are shown graphically. The selected operating pressure for the electro-pneumatic positioning system is 4 bar.

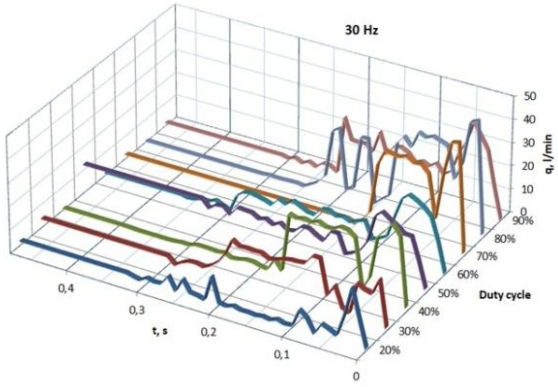

Fig. 6. Variation of the flow rate entering the electropneumatic positioning system.

Figure 7, 8, 9, 10. Shows experimental transients with PWM at frequencies of 50 Hz and different duty cycles from 30% to 90%.

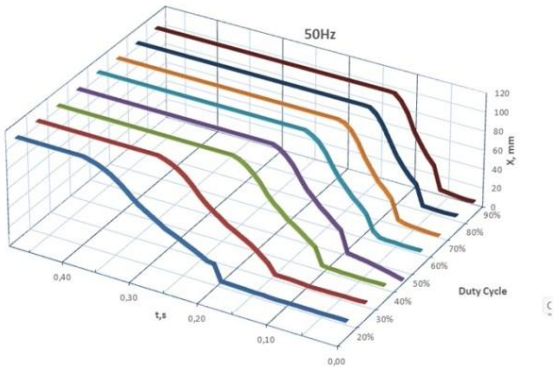

Fig. 7. Displacement of the rod of the pneumatic cylinder at a frequency of 50 Hz and different duty cycle.

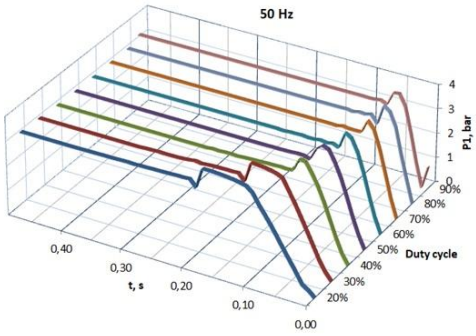

Fig. 8. Pressure drop in the left chamber of the pneumatic cylinder at a frequency of 50 Hz and a different dudy cycle.

Displacement of the rod of the pneumatic cylinder, pressure in the left and right chambers of the cylinder and the flow rate entering the electropneumatic positioning system. The results are shown graphically.

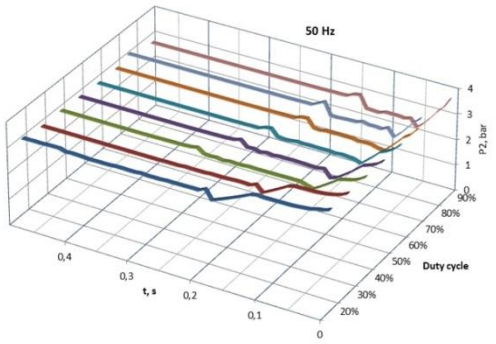

Fig. 9. Pressure washout in the right chamber of the pneumatic cylinder at a frequency of 50 Hz and a different dudy cycle.

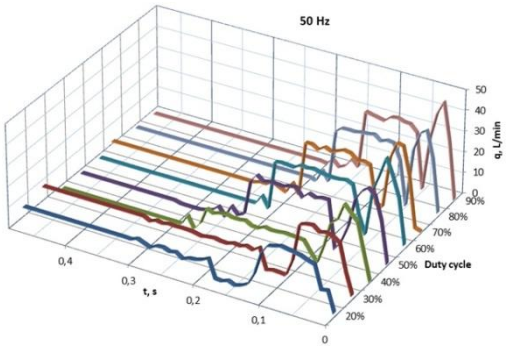

Fig. 10. Variation of the flow rate entering the electropneumatic positioning system.

Figure 11, 12, 13, 14. Shows experimental transients with PWM at frequencies of 50 Hz and different duty cycles from 30% to 90%. Displacement of the rod of the pneumatic cylinder, pressure in the left and right chambers of the cylinder and the flow rate entering the electropneumatic positioning system. The results are shown graphically.

From the resulting transients, at 30 Hz frequency and Duty Cycle change, the following is observed:

At 20% Duty Cycle, there is a time delay of the spent input signal of 0.08 seconds. The rod travel time of the pneumatic cylinder is from 0.08 to 0.22 s for a distance of 70mm. The average speed is 0.50 m/s.

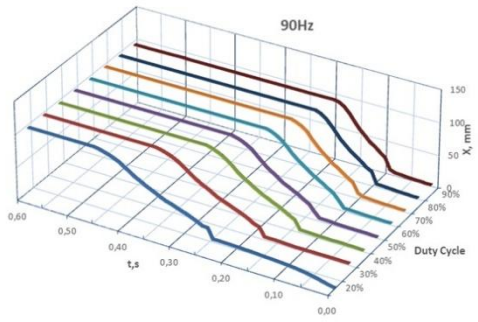

Fig. 11. Displacement of the rod of the pneumatic cylinder at a frequency of 90 Hz and different duty cycle.

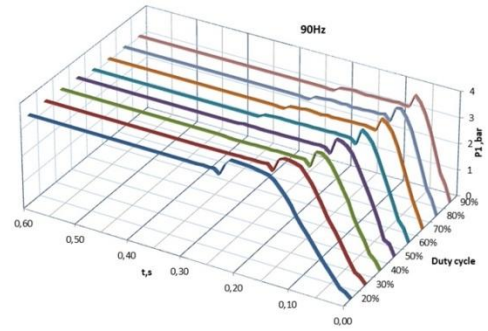

Fig. 12. Pressure drop in the left chamber of the pneumatic cylinder at a frequency of 90 Hz and a different dudy cycle.

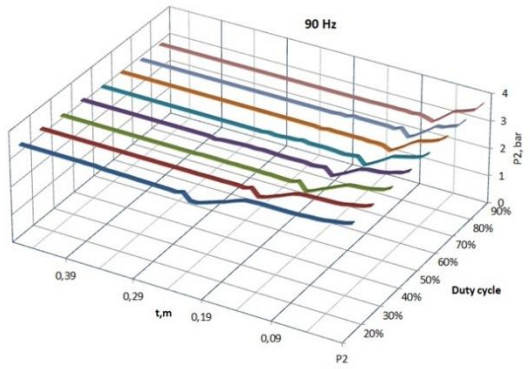

Fig. 13. Pressure washout in the right chamber of the pneumatic cylinder at a frequency of 90 Hz and a different dudy cycle.

At 90% Duty Cycle, the time delay of the spent input signal is 0.08 seconds. The rod travel time of the pneumatic cylinder is in the time range, measured in seconds, of 0.03 to 0.10 for a distance of 70 mm. The average speed is 1.00 m/s.

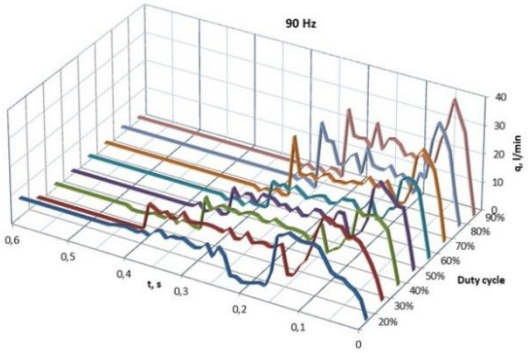

Fig. 14. Variation of the flow rate entering the electropneumatic positioning system.

The measurements and the results obtained in percent fill between 20 and 90% are described in TABLE 1

TABLE 1 EXPERIMENTAL RESULTS AT 30 HZ

Duty Cycle	30 Hz			
	Signal delay time,s	*Move time, S*	*Distance, mm*	*C, m/s*
20%	0.08	0.08-0.22	70	0.500
30%	0.07	0.07-0.19	70	0.583
40 %	0.06	0.06-0.17	70	0.636
50%	0.05	0.05-0.15	70	0.700
60%	0.04	0.04-0.13	70	0.707
70%	0.03	0.03-0.11	70	0.795
80%	0.03	0.03-0.10	70	1.000
90%	0.03	0.03-0.10	70	1.000

TABLE 2 EXPERIMENTAL RESULTS AT 50 HZ

Duty Cycle	50 Hz			
	Signal delay time,s	*Move time, S*	*Distance, mm*	*C, m/s*
20%	0.18	0.18-0.37	70	0.368
30%	0.14	0.14-0.29	70	0.467
40 %	0.10	0.13-0.24	70	0.636
50%	0.08	0.08-0.19	70	0.636
60%	0.07	0.07-0.17	70	0.700
70%	0.06	0.06-0.15	70	0.778
80%	0.05	0.05-0.13	70	0.875
90%	0.05	0.05-0.12	70	0.966

From the resulting transients, at a frequency of 50 Hz and Duty Cycle change, the following is observed:

At 20% Duty Cycle, there is a time delay of the spent input signal of 0.18 seconds. The rod travel time of the pneumatic cylinder is from 0.18 to 0.37s for a distance of 70mm. The average speed is 0.368 m/s.

At 90% Duty Cycle, the time delay of the spent input signal is 0.05 seconds. The rod travel time of the pneumatic cylinder is in the time range, measured in seconds, of 0.05 to 0.13 for a distance of 70mm. The average velocity is 0.966 m/s.

TABLE 3 EXPERIMENTAL RESULTS AT 90 HZ

Duty Cycle	90 Hz			
	Signal delay time,s	*Move time, S*	*Distance, mm*	*C, m/s*
20%	0.24	0.24-0.45	70	0.333
30%	0.17	0.17-0.36	70	0.368
40 %	0.13	0.13-0.28	70	0.467
50%	0.12	0.12-0.26	70	0.500
60%	0.10	0.10-0.23	70	0.538
70%	0.09	0.09-0.21	70	0.538
80%	0.08	0.08-0.18	70	0.700
90%	0.07	0.07-0.17	70	0.700

The measurements and the results obtained in percent fill between 20 and 90% are described in TABLE 2

From the resulting transients, at a frequency of 90 Hz and Duty Cycle change, the following is observed:

At 20% Duty Cycle, there is a time delay of the spent input signal of 0.24 seconds. The rod travel time of the pneumatic cylinder is from 0.24 to 0.45s for a distance of 70mm. The average speed is 0.333 m/s.

At 90% Duty Cycle, the time delay of the spent input signal is 0.07 seconds. The rod travel time of the pneumatic cylinder is in the time range, measured in seconds, of 0.07 to 0.17 for a distance of 70mm. The average speed is 0.70 m/s.

The measurements and the results obtained in percent fill between 20 and 90% are described in TABLE 3.

CONCLUSIONS

The experimental studies on the dynamic characteristics of the electro-pneumatic positioning system with High Speed Pneumatic Valves (HSPV) and Pulse Width Modulation (PWM) control have yielded transient processes—flow rate of the system, pressure in the left and right chambers of the double-rod pneumatic cylinder, and displacement of the cylinder rod—at different input signal values, with frequencies ranging

from 30 Hz to 70 Hz and varying duty cycles from 30% to 90%.

The PWM allows to control the speed of the pneumatic cylinder with a double out rod, as well as to monitor the input signal time (delay time). The pressures in the left and right chambers of the pneumatic cylinder show instantaneous response as well as the flow rate entering the system.

The obtained characteristics confirm the improved linear properties of the electropneumatic positioning system, which allows for its broad application in the industry.

ACKNOWLEDGMENTS

This study was financially supported by the research activities program for young scientists and postdoctoral researchers, as part of the first stage of the National Program "Young Scientists and Postdoctoral Researchers – 2."

This research was funded by the European Regional Development Fund within the OP “Research, Innovation and Digitalization Programme for Intelligent Transformation 2021-2027 ”, Project No. BG16RFPR002-1.014-0005 Center of competence “Smart Mechatronics, Eco- and Energy Saving Systems and Technologies”

REFERENCES

[1] G. Iliev, H.Hristov, “Modelling and Simulation of Electropneumatic Positioning System Including the Length of Pneumatic Lines” ENVIRONMENT. TECHNOLOGY. RESOURCES 14th International Scientific and Practical Conference. June 15-16, 2023, Rezekne Academy of Technologies, Rezekne, Latvia, Page 106-111 ISSN 1691-5402 Online IS. DOI 10.17770/etr2023vol3.7186

[2] G. Iliev, “Experimental Study Of The Frequency Responses Of Electropneumatic Positioning System”, ETR, vol. 3, pp. 90–94, Jun. 2024, DOI: 10.17770/etr2024vol3.8116.

[3] G. Iliev, Hristov H. “Modelling and Simulation of Dynamic Processes of Pneumatic Lines” ENVIRONMENT. TECHNOLOGY. RESOURCES 14th International Scientific and Practical Conference. June 15-16, 2023, Rezekne Academy of Technologies, Rezekne, Latvia, Page 112-118 ISSN 1691-5402 Online IS. DOI 10.17770/etr2023vol3.7190

[4] G.Iliev, and H.Hristov, “Experimental Static Frow Characteristics Of Hing Speed On/Off Pneumatic ValveS” Mechanics of Machines 131 YEAR XXXII,№1,2024 ISSN 0861-9727 pp.25-28

[5] Andrey Andreev, Hristov H., Iliev G., Racheva. M. “Mathematical Model for a Pneumatic Force Actuator System” BGSIAM’15 PROCEEDINGS 10th Annual Meeting of the Bulgarian Section of SIAM. December 21-22, 2015 Sofia. Page 4-6,ISSN 1313-3357.

[6] G.Iliev,. and H.Hristov, Speed Control Of Pneumatic Cylinders Using High Speed 2 Port On/Off Valves With Pulse Width Modulation. ENVIRONMENT. TECHNOLOGIES. RESOURCES. Proceedings of the International Scientific and Practical Conference. 3, Jun. 2024, pp.95–100. DOI:https://doi.org/10.17770/etr2024vol3.8117.

[7] Y. T WANG,and R. SINGH,” Frequency-response of a nonlinear pneumatic system” Journal of applied mechanics-transactions of the asme Volume 54, Issue 1, Page 209-214 MAR 1987; DOI:10.1115/1.3172960.

[8] A.Grigaitis, and V.A.Gelezevicius, ” Electropneumatic Positioning System with an Adaptive Force Controller” ELEKTRONIKA IR ELEKTROTECHNIKA 2008 Issue 7, Page 3-6.

[9] M. Smaoui, X. Brun, and D. Thomasset, “Robust position control of an electropneumatic system using second order sliding mode” IEEE International Symposium on Industrial Electronics 2004; PROCEEDINGS OF THE IEEE-ISIE 2004, VOLS 1 AND 2 , pp.429-434.

[10] X.Brun, S. Sesmat, D. Thomasset, and S. Scavarda, “Study of "Sticking and restarting phenomenon" in electropneumatic positioning systems” Journal of dynamic systems measurement and control-transactions of the asme, volume 127, issue 1, page 173-184; mar 2005; ISSN 0022-0434; DOI:10.1115/1.1858443.

[11] R. Kumar and J. R. B. del Rosario, Design and Simulation of Electro-Pneumatic Motion Sequence Control Using FluidSim: Applied Mechanics and Materials,2014, 446-447, 1146-1150. DOI: 10.4028/ www.scientific.net/AMM.446-447.1146

[12] S.Cajetinac, D.Seslija , S. Aleksandrov and M. Todorovic, PWM Control and Identification of Frequency Characteristics of a Pneumatic Actuator using PLC Controller // ELECTRONICS AND ELECTRICAL ENGINEERING, AUTOMATION, ROBOTIC , SISSN 1392 – 1215, 2012. No 7(123).

[13] I. Tsitsimpelisa, C. J.Taylora, B. Lennoxb, J. Malcolm, J. Joycea. A review of ground-based robotic systems for the characterization of nuclear environments. Progress in Nuclear Energy. 2019, 111 pp.109–124. www.elsevier.com/locate/pnucene.

[14] I. Nikolaev and O. Alipiev "Numerical Method for Determining the Instantaneous Flow Rate of a Three-Rotor Gear Pump With Bilateral Lantern Meshing" 14th International Hybrid Conference for Promoting the Application of Mathematics in Technical and Natural Sciences - AMiTaNS’22, AIP Conference Proceedings, Vol. 2953 (2023): 080009-1...080009-10. doi: 10.1063/5.0178372.

[15] M.C. Shih and M. Ma, Position control of a pneumatic rodless cylinder using fuzzy PWM control method. Mechatronics 1998;41(2C), pp. 241–53.

[16] M.C. Shih and M. Ma, “Position control of a pneumatic rodless cylinder using sliding mode M-D-PWM control the high speed solenoid”.JSM E Int J 1998;41(2C):236–41.

[17] B. Georgiev and T. Karadzhov, “Comparative Analysis Of Geometric Deviations In Contact Measuring Instruments For Control And Laser Contactless Scanning”, ETR, vol. 3, pp. 306–310, Jan. 2024, doi: 10.17770/etr2023vol3.7182.

[18] B. Georgiev and T. Karadzhov, “Investigating The Repeatability Of 3d Printers Using A Multi-Sensor Measurement System”, ETR, vol. 3, pp. 65–69, Jun. 2024, doi: 10.17770/etr2024vol3.8114.

[19] M Pipan, N Herakovic,“ Closed-loop volume flow control algorithm for fast switching pneumatic valves with PWM signal“ Control Engineering Practice Volume 70, January 2018,Pages114-120 https://doi.org/10.1016/j.conengprac.2017.10.008

[20] E. Topc¸ I. Yu¨ksel , Z. Kamıs, “Development of electro-pneumatic fast switching valve and investigation of its characteristics“ Mechatronics ,Volume 16, Issue 6, July 2006, Pages 365-378 https://doi.org/10.1016/j.mechatronics.2006.01.005

[21] M. Taghizadeh, A. Ghaffari, F. Najafi „Modeling and identification of a solenoid valve for PWM control applications“ Comptes Rendus MécaniqueVolume 337, Issue 3, March 2009,pp. 131-140. https://doi.org/10.1016/j.crme.2009.03.009

Environment. Technology. Resources. Rezekne, Latvia
Proceedings of the 16th International Scientific and Practical Conference. 2025. Volume IV, 123-126

A study of the Boilover Phenomenon. Experimental Determination of Mass Burning Rate and Boilover Time

Evgeniy Ivanov
Faculty of Fire Safety and Civil Protection
Academy of the Ministry of Interior
Sofia, Bulgaria
evgivanov@amvr.bg

Stefan Parvanov
Faculty of Fire Safety and Civil Protection
Academy of the Ministry of Interior
Sofia, Bulgaria
sip_81@abv.bg

***Abstract*- The phenomenon of "boilover" a catastrophic event characterized by the explosive ejection of burning liquid from heated storage tanks, poses significant safety risks in industrial settings. This study investigates the critical parameters influencing boilover, such as mass burning rate and time to onset, utilizing a meticulously designed experimental apparatus that simulates real-world conditions on a reduced scale. The experiment setup includes a combustion chamber, precise thermocouple arrays for temperature monitoring, and scaled-down oil storage models to replicate the thermal dynamics observed in actual tanks. By observing the combustion process from its initiation to the critical boilover event, this study not only tracks the progressive temperature changes but also identifies specific precursor signals of impending danger. The research employs a combination of direct observation and sophisticated data analysis techniques to dissect the interactions between the burning fuel and the underlying water layer, crucial for understanding the boilover mechanism. Enhanced by mathematical modeling, the findings propose predictive tools that forecast the timing of boilover, enabling preemptive safety measures. Ultimately, this study aims to refine risk assessment practices and improve preventive strategies, thereby safeguarding lives and property against one of the most dramatic threats in fire safety management when handling and storing flammable liquids.**

Keywords- boilover, experiment, mass burning rate, time to boilover.

I. INTRODUCTION

The occurrence of "boilover" in storage tanks presents significant safety risks within industries handling flammable and combustible liquids, characterized by a sudden, violent ejection of burning fuel from heated storage vessels. This event drastically escalates fire intensity, threatening infrastructure integrity, environmental safety, and posing extreme hazards to emergency responders, including firefighters engaged in suppression and rescue operations [1], [2], [3].

Historical incidents, laboratory experiments, and theoretical analyses underscore the critical necessity of comprehensive research into boilover phenomena to enhance preventive strategies and improve emergency responses.

Boilover typically occurs during fires involving storage tanks containing oils, petroleum products, alternative fuels, or vegetable oils layered atop water, which may accumulate due to condensation, leakage, or firefighting activities. The mechanism involves complex thermal and physical interactions, notably heat transfer from the burning fuel to an underlying water sublayer, creating conditions for explosive vaporization and ejection of fuel [4]. The boilover process occurs in distinct stages, including the steady burning stage, "slop over," "froth over," and the violent "boilover" itself. During steady burning, a hot layer forms and gradually propagates downward into the fuel layer. "Slop over" describes discontinuous frothing releases of fuel, generally from one side of the tank, while "froth over" represents a continuous, less intense release akin to rolling liquid. Finally, "boilover" constitutes the most violent and hazardous stage, characterized by explosive fuel ejection and fireball formation [5].

Several researchers have provided critical insights into these mechanisms. [6] investigated steady-state combustion dynamics of oil slicks on water, establishing foundational thermal transfer relationships widely referenced in boilover studies [7].

In-depth analyses furthered understanding through models predicting boilover onset based on experimental data, emphasizing thermal interactions between fuel layers

Online ISSN 2256-070X
https://doi.org/10.17770/etr2025vol4.8445
© 2025 The Author(s). Published by RTU PRESS.
This is an open access article under the Creative Commons Attribution 4.0 International License.

and water substrates [2]. This paper highlighted specific combustion characteristics of crude oil, detailing the precursors and conditions necessary for boilover occurrence through extensive experimental validation of [3].

Fundamental insights into liquid fuel combustion dynamics and diffusion burning characteristics essential to boilover studies were pioneered by [3], [8] who provided critical empirical data and theoretical models still widely utilized today. The complexities involved in heat propagation through layered liquids, especially heat accumulation in water sublayers, were rigorously addressed through mathematical models employing inverse Stefan problems, greatly enhancing predictive accuracy [9].

Further, [4]provided comprehensive theoretical frameworks on fire dynamics, crucial for conceptualizing boilover phenomena within broader fire safety contexts. [10] complemented this theoretical knowledge by advocating detailed experimental modeling to validate predictive theories effectively, bridging gaps between empirical data and theoretical predictions.

Despite significant advancements, systematic validation of boilover predictive models remains limited, particularly regarding diverse fuel properties and mass burning rate influences. This study aims to address these gaps by systematically quantifying key parameters, such as mass burning rate, temperature gradients, and boilover onset timings under controlled experimental conditions. Ultimately, this research seeks to refine predictive models, enhancing industrial safety protocols and emergency response strategies, significantly mitigating the catastrophic impact of boilover incidents.

II. MATERIALS AND METHODS

The prediction of the time required for the onset of the "boilover" phenomenon in a burning tank containing oil, petroleum products, alternative fuels, and vegetable oils is of utmost importance. This allows firefighters on the scene to be alerted, enabling the timely evacuation of all individuals near the fire. Accurate prediction of the phenomenon's onset time necessitates information about the type and quantity of the stored substance, as well as the presence of water in the tank.

To develop a model for predicting the boilover onset time, it is essential to study the formation and growth of the hot layer. Subsequently, an accurate profile of the heat transfer rate between the hot layer and the underlying fuel must be established, along with the heat transfer from the heated tank walls to the fuel layers beneath the burning one.

Research shows that boilover occurs within seconds after the water layer within the fuel reaches a temperature of 100°C. Therefore, a precise analysis of the temperature interface between the water and fuel layers is a viable method for predicting the phenomenon.

Due to the large size of fuel tanks, heat transfer within them is significant. Consequently, cooling the tank walls has little influence on the formation of the hot layer and, therefore, on the occurrence of boilover.

Materials Used:

- *Combustion Chamber:* A controlled environment where the burning experiments are conducted. This chamber is designed to safely contain the fire and prevent external influences;
- *Oil Storage Tank Models*: Scaled-down versions of real oil storage tanks, typically made from metal, used to simulate real-world scenarios. These models are filled with oil and a layer of water to mimic the conditions found in industrial storage tanks;
- *Thermocouples:* Used to measure temperatures at various points within the tank. These are essential for monitoring the progression of heat through the layers of oil and water.

Methods employed:

- *Experimental Setup*: The experiment involves setting up the scaled-down tank models within the combustion chamber. These tanks are filled with a predetermined ratio of oil and water;
- *Data Collection:* Temperature data collected from the thermocouples are logged continuously through a data acquisition system. This data is crucial for mapping the temperature gradient and for modeling the conditions leading to boilover;
- *Data Analysis*: The collected data (temperature and oil level reading) are analyzed to identify the key thermal dynamics and physical behaviors that precede a boilover event. This analysis helps in refining predictive models for boilover.

The expulsion refers to the spilling of the tank's contents over its entire external surface. The spreading of burning fuel poses significant risks to the environment, equipment, and human safety. In the study [9] reported the formation of a hot zone within the fuel layer (crude oil and kerosene) during the combustion process. The mechanism behind the formation of such a hot zone in the fuel layer examines the process of distillation of fuel components and the heat transfer toward the water sublayer and the tank walls.

Both models are developed in the study of [10]. The reason for selecting lies in their ability to incorporate variable values derived from the experimental setups.

$$t_b = -20.5235 + 557.2043 \frac{H_0}{\sqrt{D}} \quad (1)$$

t_b = Time to boilover occurrence (min).
H_0 = Initial thickness of the fuel layer (m).
D = Diameter of the tank (m).

This model assumes that the time to boilover is influenced by the initial thickness of the fuel layer and the diameter of the tank. It suggests a linear relationship with these variables.

$$t_b = \frac{H_0}{V_{hz}} - k(H_0 + H_w) \quad (2)$$

t_b = Time to boilover occurrence (min).
V_{hz} = Growth rate of the hot zone (m/min).
H_0 = Initial thickness of the fuel layer (m).
H_W = Thickness of the water layer (m).
k = Coefficient, where k=0k = 0k=0 if the fuel temperature is below its ignition temperature, and k=1k = 1k=1 otherwise.

$$V_{hz} = \frac{\Delta h}{\Delta \tau} \quad (3)$$

Δh = distance between the first and the third thermocouple (m).
$\Delta \tau$ = The time between thermocouple three reaching 100 °C and thermocouple one reaching 100 °C (min).

This correlation accounts for the growth rate of the hot zone, the initial thickness of the fuel layer, and the thickness of the water layer beneath the fuel. It also introduces a coefficient that varies depending on whether the fuel temperature is below its ignition temperature.

III. Results and Discussion

During the experimental study of the boilover phenomenon, six experiments were conducted using flammable liquids (diesel fuel, motor oil and sunflower oil) with varying amounts of fuel added to the system. In the initial experiments, the boilover effect was not observed, which can be attributed to insufficient time for the development of a "hot layer" beneath the fuel surface. Additionally, the distillation of the fuel occurred rapidly, predominantly yielding heavier distillates that did not sustain burning effectively.

Fig. 2. Extinguishment due to the insufficient amount of fuel.

As the experiments progressed, more fuel was added to the crucible, increasing the energy within the system. This adjustment facilitated the development of the "hot layer" essential for the onset of boilover. This layer acts as a thermal reservoir, gradually heating the underlying non-flammable layer (typically water), leading to the eventual boilover effect. During the experiments the "boilover" phenomenon was observed with the presence of all its stages.

Fig. 2. Stages of boilover occurrence.

The results from the six experiments and the correlations employed are shown in Table 1. Each experiment investigated variables such as fuel layer thickness, heat wave propagation and the dynamics of temperature distribution leading to „boilover".

TABLE 1 STUDY RESULTS

№	Fuel	Experimental time to boilover	Correlation 1 (min)	Correlation 2 (min)	Heat wave propagation (m/min)	Mass burning rate $\dot{m}$ (g/m²s)	Temperature of boilover occurance
1.	Diesel fuel	*	*	*	*		*
2.	Diesel fuel	*	*	*	*		*
3.	Diesel fuel	16,3	12,68	8,8	0,005 13	0,014	107,6
4.	Motor oil	19,1	17,42	14,29	0,003 36	0,050	172,9 **
5.	Motor oil	21,2	22,17	19,76	0,003 30	0,284	103,9
6.	Non refined sunflo wer oil	24,5	26,91	2,06 **	0,018 5	*	*

"*" – No data
"**" – Large deviation

The results provided critical insights into the mechanisms and predictive models for determining the onset of this phenomenon. Observations confirmed the importance of precise measurements of thermal transfer, which were analyzed using both manual data collection and computational tools like the "Polymonitor" program.

Experiment one was terminated due to an incorrect connection of the thermocouples. Experiment two showed that the "boilover" phenomenon does not occur when the fuel quantity is insufficient, confirming the necessity for a sufficiently energetic "hot layer." Experiments three and four, involving diesel fuel and motor oil, demonstrated violent boilover events, with the presence of all its stages, consistent with previously reported experimental analyses of fuel burning on water layers [10], characterized by sharp temperature rises (107.6 °C and 172.9 °C respectively), as illustrated in Figure 3.

Fig. 3. Boilover phenomenon

These findings show a strong correlation between the mass burning rate and the intensity of the boilover – motor oil displayed significantly higher burning rates (0.050–0.284 g/m²s), which explains the severity of the event.

In experiment five, the excessive fuel volume led to flame smothering during the frothing phase. Experiment six showed a boilover without ignition, highlighting the low flammability of unrefined sunflower oil despite considerable heat accumulation.

Analysis of numerical values from Table 1 indicates that the applied predictive correlations (equations 1 and 2) yielded results closely matching experimental values, particularly in experiments 3-5. Significant deviations, especially with sunflower oil, suggest the need for model adaptation based on the specific physicochemical properties of fuels. The propagation speed of the heat wave (ranging from 0.0033 to 0.0185 m/min) also significantly influenced water layer evaporation dynamics and time to boilover.

IV. CONCLUSIONS

This research focuses on the experimental and theoretical investigation of the "boilover" phenomenon during the combustion of flammable liquids stored above water layers, including diesel fuel, motor oil, and unrefined sunflower oil. The phenomenon, characterized by the sudden and explosive ejection of burning liquid, poses significant fire safety hazards in industrial facilities handling hydrocarbons, alternative fuels, and vegetable oils.

A specially designed experimental setup was developed and validated to simulate real-world storage conditions at a reduced scale. Experiments measured critical parameters such as mass burning rate, heat wave propagation speed, and the time to boilover onset. Data were analyzed using two correlation models and compared against experimental results to assess model accuracy.

Key findings indicated that:

- The mass burning rate and heat wave propagation speed are the primary predictors of boilover onset.
- Higher mass burning rates, particularly observed with motor oil, led to more intense and violent boilover events.
- Fuel properties, such as flammability and thermal behavior, significantly influence the accuracy of predictive models.
- While the models showed good predictive capability for diesel and motor oil, significant deviations were found for unrefined sunflower oil, highlighting the need for model adaptation based on specific fuel characteristics.

Future work will extend the research by scaling the experimental apparatus to larger vessel diameters (up to 150 cm) and studying the impact of turbulent flame regimes on boilover formation. The ultimate goal is to refine risk assessment methodologies and enhance preventive strategies for facilities that store and process flammable liquids.

ACKNOWLEGMENTS

This study is financed by the Bulgarian National Science Fund under contract № КП-06-М67/8/15.12.2022.

REFERENCES

[1] A. Y. Walavalkar и A. K. Kulkarni, „Combustion of water-in-oil emulsion layers supported on water,“ Combustion and Flame, pp. 1001 -1011, 2001.

[2] H. Koseki, „‘Boilover and crude oil fire,“ Journal of Applied Fire Science, pp. 243-272, 1993/94.

[3] V. I. Blinov и G. N. Khudiakov, „The burning of liquid pools,“ DokladyAkademi Nauk SSSR, p. 1094, 1957.

[4] D. Drysdale, „An Introduction to Fire Dynamics,“ в An Introduction to Fire Dynamics, Chichester,, John Wiley & Sons, 2011, pp. 181-223.

[5] B. &. Twardus, „A study of the burning of a slick of crude oil on water,“ Symposium (International) on Combustion, том 19, № 1, pp. 847-854, 1982.

[6] B. &. Twardus, „A study of the burning of a slick of crude oil on water,“ Symposium (International) on Combustion, том 19, № 1, pp. 847-854, 1982.

[7] J. Hristov, J. Arnaldos, E. Planas-Cuchi и J. Casal, „Accidental burning of a fuel layer on a waterbed: a scale analysis of the models predicting the pre-boilover time and tests to published data,“ International Journal of Thermal Sciences, pp. 221-239, 2004.

[8] V. I. Blinov и G. N. Khudiakov, „Diffusion Burning of Liquids,“ Academy of Sciences, Moscow, 1961.

[9] J. Hristov, „An inverse Stefan problem relevant to boilover: Heat balance integral solutions and analysis,“ Thermal Science, том 11, № 2, pp. 141-160, 2007.

[10] D. W. Yang, P. H. Zhang и B. Z. Chen, „Boilover Starting Time of Small-scale Crude Oil Tank,“ Applied Mechanics and Materials, pp. 564-567, 2013.

Environment. Technology. Resources. Rezekne, Latvia
Proceedings of the 16th International Scientific and Practical Conference. 2025. Volume IV, 127-132

Determining the Relationship Between the Parameters Time to Boilover and Mass Burning Rate with the Prevention and Response Strategies in Petroleum Product Storage Tank Fires

Evgeniy Ivanov
Faculty of Fire Safety and Civil Protection
Academy of the Ministry of Interior Sofia, Bulgaria
evgivanov@amvr.bg

Stefan Parvanov
Faculty of Fire Safety and Civil Protection
Academy of the Ministry of Interior Sofia, Bulgaria
sip_81@abv.bg

***Abstract*- The phenomenon of "boilover" in storage tanks containing petroleum products is among the most hazardous events that can occur during large-scale fires. When water is present at the bottom of the tank, the burning hydrocarbon layer may cause a sudden evaporation of the water, followed by a violent ejection of hot liquid and a massive fireball. This scenario poses severe threats to personnel safety, facility integrity, and environmental protection. Given the increasing global demand for petroleum-based fuels and the continued use of large above-ground storage tanks, understanding and mitigating the risks associated with boilover has never been more critical. The primary objective of this study is to clarify how two key parameters - time to boilover and mass burning rate - influence both prevention and response strategies during petroleum product tank fires. The research employs a combination of experimental data analysis and critical literature review to assess how these parameters correlate with the escalation of fire events. The experiments, conducted under controlled laboratory conditions, measured the influence of fuel properties, water layer thickness, and burning surface area on boilover onset and burning intensity. Based on these findings, the study synthesizes the most applied structural (e.g., tank design, insulation, drainage systems) and operational (e.g., cooling tactics, fuel-level monitoring, emergency response timing) fire protection strategies. Emphasis is placed on how real-time assessment of the mass burning rate and the predicted time to boilover can inform decision-making during emergencies. The results show that the earlier identification of critical thresholds significantly enhances the effectiveness of intervention measures. Moreover, certain prevention methods - such as early cooling and drainage - can delay or even prevent boilover if applied in a timely manner. Ultimately, this study bridges the gap between theoretical fire behavior parameters and practical fire safety management, offering a more predictive and data-driven approach to handling storage tank fires.**

Keywords: boilover, prevention and response, mass burning rate, time to boilover.

I. Introduction

Petroleum product storage tanks are essential for industrial operations, yet they present significant fire safety hazards, particularly the phenomenon known as *boilover*. Boilover is a violent event resulting from the rapid vaporization of a water layer beneath a burning fuel, leading to a sudden ejection of hot liquid and a massive fireball [1], [2].

This phenomenon severely threatens personnel safety, environmental integrity, and critical infrastructure.

The increasing storage and industrial use of alternative fuels, edible oils, and essential oils further elevate these risks due to their distinct thermophysical properties compared to traditional petroleum products [3], [4].

Previous studies have categorized boilover into thin-layer and deep-layer events, where thin-layer boilover occurs with fuel layers below 10 mm and deep-layer boilover with thicker fuel deposits [5], [6]. While thin layers can lead to rapid ignition and spread, deep-layer fires can accumulate significant thermal energy, culminating in explosive boilover.

The fundamental works of [6] and [7] established that the development of a "hot zone" within the fuel layer and the heat conduction toward the water layer are critical factors leading to boilover. Subsequent experiments conducted by researchers such as [4] , [8] have emphasized the relevance of the mass burning rate and the temperature

Online ISSN 2256-070X
https://doi.org/10.17770/etr2025vol4.8446
© 2025 The Author(s). Published by RTU PRESS.
This is an open access article under the Creative Commons Attribution 4.0 International License.

gradients within the fuel to predict the onset of this phenomenon.

Despite considerable progress, most existing models focus on one-dimensional heat conduction and neglect the complex multicomponent composition of biofuels and vegetable oils [9], [10].

Moreover, empirical correlations proposed by [2] and experimental observations by researchers like [11] point out the limitations of generalizing data obtained from crude oil fires to other fuels.

This study aims to experimentally and theoretically investigate the relationship between two critical parameters **mass burning rate** and **time to boilover** for various classes of combustible liquids, including petroleum products, biofuels, edible oils, and essential oils. By analyzing the dynamics of heat and mass transfer, as well as the development of the "hot zone" within the fuel layer, this research seeks to create predictive models capable of assessing boilover risks in a wide variety of industrial conditions.

Building upon the experimental work and theoretical models described in prior literature [7], [6], [4], [8], [5] the present research develops an integrated framework linking experimentally determined burning rates and boilover times to preventive and emergency response strategies. Ultimately, the findings aim to contribute to safer storage system designs, improved firefighting protocols, and risk management practices.

II. MATHERIALS AND METHODS

A. Time to boilover

The time to boilover (t_b) represents the interval between the ignition of the fuel and the sudden ejection of hot liquid when the water at the bottom reaches a critical temperature. A simplified conceptual model often used in literature [12] is:

$$t_B = \frac{\rho_1 c_p h_{HC}(T_{HW}-T_a)}{Q_f - \dot{m}\left[\Delta h_v + c_p(T_{0av}-T_a)\right]} \quad (1)$$

where:

ρ_l - fuel density at the temperature T_a (kg/m^3);

C_p- specific fuel temperature T_a (kJ/kg K);

h_{HC} - initial fuel tank thickness before start of fire (m);

$\dot{m}$ - mass burning rate (kg/m^2 s);

Δh_v - temperature for start of evaporation Ta (kJ/kg);

T_a - ambient temperature (K);

T_{HW} - temperature of Heat wave during boilover (K). T_{HW} can be derived from fuel-distillation curves.

In simplified form, the equation has the following form:

$$t_B = \frac{\rho_f c_{p,f} h_f}{\dot{q}_T} \quad (2)$$

where:

ρ_f - density of the fuel;

$c_{p,f}$ - specific heat capacity of the fuel;

h_f - fuel layer thickness;

$\dot{q}_T$ - net heat flux or thermal transfer rate reaching the bottom layers.

B. The mass burning rate

After analyzing literary sources [13] [14] the mass burning rate ($\dot{m}$) can be defined as:

$$\dot{m} = \frac{\frac{dm_f}{dt}}{A} \quad (3)$$

where:

m_f - mass of the fuel;

t - time;

A - surface area of the fuel layer.

The negative sign highlights the reduction in fuel mass over time. A higher $\dot{m}$ implies a more intense fire and a faster buildup of heat within the tank. However, the relationship between $\dot{m}$ and t_b can be influenced by numerous parameters, including fuel composition, moisture content, and tank geometry.

III. RESULTS AND DISCUSSION

The preliminary experimental data used in this study is summarized in Fig. 1. It includes:

- fuel type (diesel fuel, motor oil);
- experimental time to boilover (compared to two correlation-based predictions);
- heat wave propagation rate;
- mass burning rate ($\dot{m}$)
- temperature of boilover occurrence.

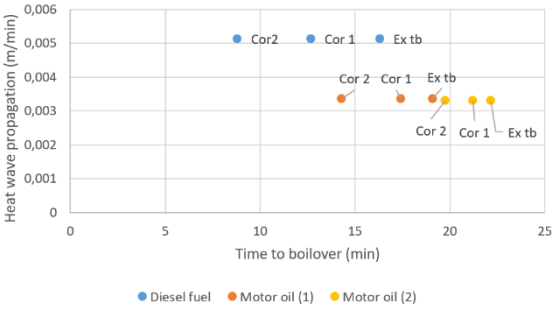

Fig. 1. Preliminary experimental data.

A. Key observations

Drawing on the data presented in Fig. 1, several essential observations emerge regarding the behavior of different fuels and their corresponding boilover dynamics.

a) time to boilover

The experimental time to boilover for Diesel Fuel is measured at 16.3 minutes, whereas Correlation 1 predicts 12.68 minutes and Correlation 2 suggests 8.8 minutes. This discrepancy highlights those experimental conditions (fuel composition, ambient temperature, initial water layer thickness, tank geometry) can lead to significantly different outcomes than theoretical or semi-empirical models. Diesel, being relatively more volatile than heavier oils, can heat up the water layer quicker. However, external factors (e.g., wind, tank insulation, or the formation of a partial foam due to combustion byproducts) may delay the actual onset of boilover compared to simplified models. The first sample of motor oil exhibits a boilover time of 19.1 minutes, which is only moderately higher than the predicted 17.42 minutes (Correlation 1) but substantially longer than 14.29 minutes (Correlation 2). These figures suggest that the fuel's higher viscosity and lower volatility, compared to diesel, slow the overall heat penetration. The second sample shows the longest measured time to boilover at 21.2 minutes, aligning closely with one correlation (22.17 minutes) and slightly exceeding the other (19.76 minutes). The relatively better match might indicate that the correlation used for 22.17 minutes was calibrated to fuels with similar physical properties.

Together, these findings confirm that heavier, more viscous fuels (such as motor oil) may yield a longer time to boilover, yet the margin between experimental and predicted values can vary considerably depending on fuel-specific parameters.

b) discrepancies between experimental and correlation values

In some cases, Correlation 1 is closer to the experimental result (e.g., Diesel at 12.68 vs. 16.3 minutes) than Correlation 2 (8.8 vs. 16.3 minutes). However, for Motor Oil 1 or 2, the reverse scenario can occur.

These discrepancies can arise from assumptions about uniform heat flux, constant burning rate, or simplified water layer behavior in the models. Additionally, minor differences in initial conditions – such as water salinity, micro-emulsions, or tank wall thickness – can lead to significant variability in real experiments.

c) Heat Wave Propagation Speed

Measured at 0.00513 m/min in the diesel fuel layer, indicating a moderate rate of thermal penetration. Although this could cause the water layer to reach boiling in a relatively short timeframe, the actual event (16.3 minutes) was somewhat delayed, possibly due to environmental cooling or partial foam formation on the surface.

Both samples of motor oil exhibit lower heat wave propagation speeds, around 0.0033 m/min, reflecting the higher viscosity of motor oil. This slower progression of the thermal front can postpone boilover onset, which partly explains the longer times to boilover observed experimentally (19.1 and 21.2 minutes). Even with a slower heat wave, if the bottom water layer remains trapped and eventually reaches a critical temperature, the ensuing boilover can still be severe. The longer heat accumulation period may also allow more time for intervention measures – yet, if no intervention occurs, the ultimate boilover event can be dramatic.

d) Mass Burning Rate ($\dot{m}$)

Diesel Fuel: 0.014 g/m²·s

Motor Oil (1): 0.050 g/m²·s

Motor Oil (2): 0.284 g/m²·s

These values reveal significant variability even among "similar" fuels (two samples of motor oil). Such differences highlight the importance of specific fuel characteristics, including the presence of additives, contaminants, or differing moisture content. A higher mass burning rate typically implies more rapid heat release; however, the corresponding time to boilover does not decrease at a strict linear proportion. Factors such as tank geometry, water distribution, and potential surface crusting or partial foam formation can alter the dynamics.

Practical implications of safety measures in petroleum fire scenarios stress the necessity of tailored strategies. The design and establishment of specific safety thresholds involve the creation of an equation to determine the possible fire extinguishing interval based on various dependencies. Each type of petroleum product may require its own calibrated correlation or monitoring approach to ensure that safety protocols are accurate and reflective of the distinct properties of different fuels. This necessitates continuous verification of these safety measures through regular validation against live or pilot-scale testing to prevent reliance on potentially inadequate emergency plans that are based on a single correlation if conditions deviate from those initially assumed.

A multimodal approach is advocated by some fire safety experts, who suggest combining multiple correlations and then comparing real-time data to both, using the most conservative estimate to trigger an early response. Thermal monitoring plays a critical role, especially the deployment of thermocouples at various depths to detect the gradual rise in temperature, which is particularly important for heavier oils. For these fuels, fire crews might gain extra minutes to apply foam or cooling measures before a boilover occurs, emphasizing the importance of robust early detection systems to capitalize on this extended intervention window.

In practice, adaptive foam application strategies require operators to adjust foam concentration and application rates according to the observed burning rate. Heavier fuels might need more robust or sustained foam coverage to effectively manage the fire. Additionally, knowing the variability in burning rates helps emergency planners in allocating resources more efficiently, estimating the quantity of firefighting media needed under worst-case scenarios [15], [16].

Such detailed understanding and adaptable responses are critical in enhancing safety protocols and ensuring preparedness in facing the dynamic challenges of petroleum fires.

B. Strategies for Prevention and Response

Building on these data-driven insights, the strategies for prevention and response to potential petroleum fires are intricately designed to tackle specific challenges through various proactive and reactive measures. The prevention strategies focus on controlling the water layer and constructive measures. Regular drainage is emphasized to minimize water accumulation at the tank's bottom, which is crucial since even a small layer can cause sudden boilover at higher burning rates. Managing water-fuel emulsions is also critical to avoid hidden pockets of water that can rapidly turn into steam. In terms of constructive measures, the use of thermal insulation helps slow down heat conduction to the tank's bottom, potentially extending the time before a boilover occurs. Adjusting tank geometry to include proper drainage and slopes can further reduce water retention, while advanced monitoring systems like real-time thermocouple arrays and mass-loss measurements are employed to predict the onset of a boilover.

A further innovative approach involves the integration of multisensory early warning systems linked to predictive algorithms. These systems combine real-time data from multiple indicators—such as temperature gradients, heat flux, and fuel mass loss—and use calibrated boilover models to trigger automated alerts or activate suppression systems. Such predictive frameworks enable dynamic adaptation of emergency protocols before critical thresholds are reached.

Another preventive strategy includes the implementation of fuel classification protocols based on boilover sensitivity. By categorizing stored liquids according to key physical and thermochemical properties - such as density, heat capacity, boiling point, and water solubility - fire safety engineers can assign specific intervention procedures tailored to each fuel type. This enhances decision-making and response planning, particularly in facilities storing mixed classes of combustible liquids [17].

Additionally, dual drainage systems with automatic thermal activation represent a highly effective structural safeguard. These systems are designed to automatically open secondary drainage channels if the tank bottom temperature exceeds predefined safety thresholds. By rapidly evacuating accumulated water before it reaches a critical evaporation point, this measure helps to prevent boilover in scenarios where manual intervention might be delayed or impossible [8].

Organizational measures are also integral to prevention, with regular personnel training focusing on critical roles such as managing the rate of mass loss and water accumulation. Maintenance and inspection routines ensure that drainage systems, seals, and measurement devices are functioning properly, enhancing overall safety and preparedness.

Response strategies are varied and cater to different emergency scenarios. Foam application is a primary response, reducing oxygen availability and cooling the surface layer, with continuous monitoring required to maintain effective coverage, especially with volatile fuels. Cooling techniques include external water sprays on tank walls to limit downward heat transfer and, more rarely, internal cooling, which carries the risk of water entrapment beneath the hot fuel. Controlled fuel removal strategies, such as lowering the fuel depth, can delay boilover by shortening the heat path, although this requires specific infrastructure and adherence to safety protocols due to the risks involved with transferring hot fuel. Smoke and gas management are critical, as high mass burning rates ($\dot{m}$) can produce large quantities of hazardous combustion products, with ventilation strategies often being limited but potentially supplemented by external cooling and foam. Lastly, effective communication and coordination through an operational center that receives real-time data on $\dot{m}$ and temperature are essential, deciding on the appropriate response measures like foam application or cooling. Evacuation protocols are established to act preemptively if $\dot{m}$ exceeds critical thresholds, ensuring safety and minimizing risk to personnel and infrastructure.

The implementation of the strategies highlights the need for a structured prioritization of prevention and response measures based on their influence on fire dynamics. The following Table 1 categorizes each measure according to its criticality and effectiveness in controlling the two key parameters: time to boilover and mass burning rate. This prioritization framework supports decision-makers in optimizing fire safety protocols by focusing on the most impactful interventions.

TABLE 1: PREVENTION AND RESPONSE MEASURES

Measure	**Priority Level**	**Justification/ Influence**
Real-time thermal monitoring systems	Critical	Enables early detection of approaching boilover through heat gradient tracking.
Predictive alarm systems with multisensory inputs	Critical	Combines thermal, mass loss, and flux data with AI models for early intervention triggers.
Water drainage management	Critical	Eliminates the root cause of boilover by removing water accumulation.
Dual drainage systems with automatic	Critical	Ensures passive drainage during emergencies, reducing reliance

Measure	Priority Level	Justification/ Influence
thermal activation		on human response.
Automated foam application systems	High Importance	Shortens response time and reduces heat flux; especially critical during high ṁ.
Tank cooling systems (external sprays)	High Importance	Limits vertical heat transfer and slows heat wave propagation.
Dynamic firefighting strategies based on mass burning rate (ṁ)	High Importance	Allows scalable foam and cooling tactics according to real-time combustion intensity.
Fuel removal infrastructure for emergency depth reduction	High Importance	Reduces fuel column, delaying heat transmission to the water layer.
Fuel classification protocols based on boilover sensitivity	High Importance	Enables tailored intervention strategies for different liquid fuels based on thermophysical properties.
Floating thermal shields	Supplementary	Reduces surface heat absorption and delays internal heating, but adds operational complexity.
Segmented tank design	Supplementary	Contains spread of burning liquid during partial boilover, applicable to new constructions only.
Drone-based thermographic monitoring	Supplementary	Enhances situational awareness but serves primarily as an auxiliary measure.
Multimodal prediction approach	Supplementary	Improves forecast accuracy but requires high computational input and calibration.
Differentiated evacuation thresholds based on ṁ	High Importance	Facilitates proactive protection of personnel based on measurable
		hazard escalation.
Regular emergency drills for boilover scenarios	High Importance	Builds preparedness and improves coordination under real fire conditions.

IV. Conclusion

In addressing the critical challenges associated with petroleum product storage tank fires, particularly the hazardous phenomenon of boilover, this study highlights the necessity of integrating precise experimental data and robust theoretical frameworks into practical fire safety strategies. The findings underscore the complex relationship between key parameters specifically, the time to boilover and mass burning rate and their implications for effective fire prevention and response.

Experimental results demonstrate significant discrepancies between theoretical predictions and observed outcomes, reinforcing the importance of accounting for fuel-specific properties, environmental conditions, and tank design features in risk assessment models. The variation observed among different fuels emphasizes the need for tailored safety protocols and adaptive intervention strategies, particularly in scenarios involving fuels with distinct thermophysical characteristics, such as diesel and motor oils.

The study identifies critical preventive measures, including effective drainage systems, thermal insulation, and advanced monitoring technologies, which collectively enhance safety by delaying or preventing boilover events. Additionally, dynamic response tactics—such as adaptive foam application, external cooling, and real-time data monitoring—are shown to significantly reduce risks when promptly and appropriately implemented.

Ultimately, this research contributes valuable insights toward the development of comprehensive, predictive, and adaptable fire safety management practices. Continuous validation and refinement of these strategies against experimental data are recommended to ensure their reliability and effectiveness in diverse operational conditions. These steps will significantly strengthen the capacity to safeguard human life, infrastructure integrity, and environmental sustainability in the face of petroleum product storage tank fires.

V. Acknowlegments

This study is financed by the Bulgarian National Science Fund under contract № КП-06-М67/8/15.12.2022.

REFERENCES

[1] J. P. Garo, J. P. Vantelon, S. Gandhi and J. I. Torero, "Determination of the Thermal Efficiency of Pre-boilover Burning of a Slick of Oil on Water," Spill Science & Technology Bulletin, pp. 141-151, 1999.

[2] J. Hristov, J. Arnaldos, E. Planas-Cuchi and J. Casal, "Accidental burning of a fuel layer on a waterbed: a scale analysis of the models predicting the pre-boilover time and tests to published data," International Journal of Thermal Sciences, pp. 221-239, 2004.

[3] H. Koseki, Y. Natsume, Y. Iwata, T. Takahashi and T. Hirano, "Large-scale boilover experiments using crude oil," Fire Safety Journal, pp. 529-535, 2006.

[4] F. Ferrero, M. Muñoz and J. Arnaldos, "Effects of thin-layer boilover on flame geometry and dynamics in large hydrocarbon pool fires," Fuel Processing Technology, pp. 227-235, 2007.

[5] J. L. Torero, S. M. Olenick, J. P. Garo and J. P. Vantelon, "Determination of the Burning Characteristics of a Slick of Oil on Water," Spill Science & Technology Bulletin, pp. 379-390, 2003.

[6] V. I. Blinov and G. N. Khudiakov, "Diffusion Burning of Liquids," Academy of Sciences, Moscow, 1961.

[7] J. P. Garo, J. P. Vantelon and A. C. Fernandez-Pello, "Experimental study of the burning of a liquid fuel spilled on water," Twenty-fifth Symposium (International) on Combustion, pp. 1481-1488, 1994.

[8] LASTFIRE, " Large atmospheric storage tank fires," Resource Protection International, , 2007.

[9] J. M. Chatris, J. Quintela, J. Folch, E. Planas, J. Arnalds and J. Casal, "Experimental study of burning rate in hydrocarbon pool fires," Combustion and Flame, pp. 1373-1383, 2001.

[10] J. P. Garo, J. Vantelon and H. Koseki, "Thin layer boilover - Prediction of its onset and intensity," Combustion Science, pp. 1217-1235, 2006.

[11] H. Koseki and G. W. Mulholland, "The effect of diameter on the burning of crude oil pool fires," Fire Technol 27, pp. 54-65, 1991.

[12] A. L. Henry Persson, "Review of fi re incidents 1951–2003," SP Swedish National Testing and Research Institute, Borås, 2004.

[13] D. Drysdale, "An Introduction to Fire Dynamics," in An Introduction to Fire Dynamics, Chichester,, John Wiley & Sons, 2011, pp. 181-223.

[14] D. W. Yang, P. H. Zhang and B. Z. Chen, "Boilover Starting Time of Small-scale Crude Oil Tank," Applied Mechanics and Materials, pp. 564-567, 2013.

[15] DIRECTIVE 2012/18/EU , On the Control of Major-accident Hazards Involving Dangerous Substances, 2012.

[16] B. A. J. P. P.A.M. Uijt de Haag, The 'Purple Book': Guideline for Quantitative Risk Assessment in the Netherlands, 2005.

[17] L. van Gelderen, In-Situ Burning of Crude Oil on Water: A study on the fire dynamics and fire chemistry in an Arctic context, Technical University of Denmark, 2017.

Environment. Technology. Resources. Rezekne, Latvia
Proceedings of the 16th International Scientific and Practical Conference. 2025. Volume IV, 133-137

Approaches Towards Improving the Safety of Dinitramides as Energetic Materials

Nadejda Jeleva
Combat Systems and Equipment
Defence Institute "Professor Tsvetan Lazarov"
Sofia, Bulgaria
nadjajeleva@gmail.com

Petia Gencheva
Combat Systems and Equipment
Defence Institute "Professor Tsvetan Lazarov"
Sofia, Bulgaria
p.gencheva@di.mod.bg

***Abstract*— In recent years, there has been a resurgence of scientific interest in polynitrogen energetic materials. The considerable number of nitrogen bonds contributes to a high formation heat, and their low carbon and hydrogen content results in a good oxygen balance. The main decomposition product is nitrogen and that turns them into environmental-friendly energetic materials attracting research and investment. Very promising chlorine-free oxidizer is Ammonium dinitramide (ADN). In addition to its excellent performance and low ecological impact, this innovative oxidizer provides tactical advantages by eliminating primary metal oxide smoke and secondary aerosol smoke from condensed water vapor and exhaust products. Mitigating the risk of detection, reduction in corrosive combustion products and low flame temperature define Ammonium dinitramide as high energy eco-propellant and pyrotechnic igniter for rocket fuels. The minimized smoke output and reliable combustion characteristics make it well-suited for high-acceleration tactical missiles and underwater propulsion systems. Nevertheless, the high hygroscopicity of Ammonium dinitramide is a property severely influencing the hazards and safety of this promising energetic. To prevent ADN from absorbing moisture during handling, storage and processing the relative humidity of the environment should be below 55% [1]. Beyond its hygroscopic nature, ADN is also known to be incompatible with isocyanates, leading to spontaneous reactions and decomposition. To address the challenges associated with ADN and facilitate its production and application, the research community employs innovative methods. There are ongoing studies investigating the most efficient ADN particle form. The research discovers the utilisation of different polymers to lay uniform ADN particle coating thus improve the absorption of ambient humidity. This paper presents a summary of recent advancements in ADN improvement methods aimed at enhancing stability. Successful solutions for anti-hygroscopicity method are essential for the future application. Tests are being conducted to enhance the conditions of the ADN synthesis for scalable production.**

Keywords*— *Ammonium dinitramide, Hygroscopicity, Synthesis, Sensitivity.

I. Introduction

Numerous studies with promising results are being published from various geographical regions, competing with the hope of breakthroughs. The advantages of the polynitrogen salts over their atomic-like non-ionic analogues include lower vapor pressure, higher density, and higher thermal stability.

It is extremely important that polynitrogen salts are ecological, "green materials," as the primary product of decomposition is molecular nitrogen. Although it is expected that purely polynitrogen compounds will reach ten times higher detonation pressure and a detonation velocity of 30 km/s, their synthesis and regeneration under atmospheric conditions are problematic. The properties of polynitrogen salts are improved when combined with various cations and anions or because of independent modification of the ionic parts. Progress is being observed in the creation of high-performance polynitrogen salts with improved sensitivity.

II. Materials And Methods

A. Ammonium dinitramide

In 1971, a triazole, called dinitramide $N(NO_2)_2^-$, was created, characterized as an ammonium salt with potential use in rocket fuels. This molecule can be used as a partially oxidizing product of the azide ion, where an oxygen molecule is added to each nitrogen atom. Ammonium nitrate (AN) and ammonium perchlorate (AP) are the most utilized propellant oxidizers. AP has excellent performance characteristics but during the decomposition process releases large amounts of chlorine containing gas with negative influence on ozone layer, formation of acid rain and toxic pollution of soil and water. The aammonium

Online ISSN 2256-070X
https://doi.org/10.17770/etr2025vol4.8400
© 2025 The Author(s). Published by RTU PRESS.
This is an open access article under the Creative Commons Attribution 4.0 International License.

dinitramide (ADN) excelled in performance, reaching explosive heat 3.92 kJ/g and detonation velocity 6000 m/s with charge diameter of 100 mm [2]. Thanks to the low characteristic signal, enthalpy of formation – 1207.4 kJ/kg and high gas yield its application spread from solid propellants to explosives [3]. The mechanical properties, stabilities and detonation performance of hexogen (RDX) and octogen (HMX) are not satisfactory. Another nitramine explosive hexanitrohexaazaisowurtzitane (Cl-20) expresses high mechanical sensitivity that increases its hazard and safety handling. Cl-20 is reporting with impact sensitivity 4 N and friction sensitivity 94 N [4]. Compared with these nitramine explosives ADN is an excellent chlorine-free inorganic oxidizer with high performance and detonation velocity and can be quickly introduced as their replacement.

The use of dinitramide salts in composite solid fuels prevents the formation of chlorine waste products during combustion. These salts have high heat of formation and density. They are promising candidates for high-energy materials with extensive military and civilian applications. Key advantages of these salts include high specific impulse, high combustion speeds, low gas emissions, and attractive prices.
ADN is the best-known dinitramide salt due to its good performance in composite solid fuels. As a natural alternative to AP, ADN is characterized by a lower oxygen balance and lower formation heat than perchlorate, but with better specific impulse and combustion gases that do not contain hydrogen chloride. The drawback is that like other ammonium salts, this salt is hygroscopic, which challenges its use in fuels. Unlike nitramines, ADN burns near the surface with a strong exothermic reaction, contributing to higher heat efficiency by returning it to the deflagrating surface, hence increasing the burning rate.

Various methods are known for obtaining ADN, but it is mainly produced in large quantities from sulfamate salts and nitrating acid. The production process is known as the "one-step reaction" (1) and occurs in a strongly acidic environment, leading primarily to dinitramide acid $HN(NO_2)_2$ [5].

$$[H_2NO_3S]^- + 2NO_2 + H_2O \rightarrow HN(NO_2)_2 + [SO_3\,OH]^- + 2H^+ \quad (1)$$

Dinitramide acid in this acidic environment is unstable and prone to decomposition into AN. For this reason, in 2005, Carin Voerde and Henrik Skifs patented a method for converting dinitramide acid into ADN [6]. The reaction is shown in (2).

$$HN(NO_2)_2 + {NH_4}^+ \rightarrow NH_4 + [N(NO_2)_2]^- + H^+ \quad (2)$$

The resulting ADN has properties that can be compared with AP, as shown in Table 1.

TABLE 1. COMPARISON OF PROPERTIES OF AP AND ADN

Compound	Formula	Density (g/cm^3)	Formation Heat (MJ/kg)	Detonation Velocity (km/s)	Oxygen Balance (%)
AP	NH_4ClO_4	1.90	-2.52	160	34.00
ADN	$NH_4[N(NO_2)_2]$	1.80	-1.22	206	-4.40

ADN is registered under REACH with the number 453-090-2. Assessment tests were conducted by an independent and accredited institute in Switzerland with results determine ammonium dinitramide as non-carcinogenic and non-allergenic. It is not irritating when in contact with skin and eyes but may cause irritation if inhaled. ADN is harmful if ingested. Toxicological studies with 90-day follow-up on the reproductive system of female rats indicate embryotoxicity of ammonium dinitramide. Studies show that it can decompose and form reactive nitrogen metabolites that could be harmful to biological systems. Hepatocyte studies suggest that the compound affects cellular DNA in vitro. Further traditional gene-toxicity tests indicate that it is potentially mutagenic [4].

The form of the synthesized ADN crystals, produced in the standard manner without solvent or cooling, is rod-like or needle-like. These forms are unsuitable as they increase the viciousness of the product. This has led to research for a more suitable crystal form. The preferred form is spherical. This plays an important role in solid fuels since round crystals contribute to higher density of ADN. In 2011, Muskatei proposed a method for shaping the initial crystals by applying a chemical modifier during the crystallization process. This method results in obtaining crystals with a specific size ranging from a few microns to several hundred microns, with a spherical shape. Key parameters to be determined include: the type of solvent, primarily its viscosity to control the crystallization rate and atom integration; temperature cycles affecting solubility; impurity presence; stirring speed, and others [7].

B. Silver Dinitramide

In 2016, a group of scientists synthesized and characterized the structure of silver dinitramide ($AgN(NO_2)_2$) [8]. The aim was to investigate its potential use as an ecological alternative to AP. The thermal decomposition mechanism was studied to track the toxicity of the products and the conditions for activating the process. The thermal decomposition of $AgN(NO_2)_2$ occurs in two stages: the first stage (408-483 K) results in a 21.86% weight loss, and the second stage (483-800 K) results in a 28.24% mass loss. The products of the decomposition include N_2O , $AgNO_3$, NO_2 , O_2 , and Ag. The activation energy was found to be Ea = 66.59 kJ/mol,

with a linear correlation coefficient of $r = 0.9913$, calculated using the Kissinger method. The silver dinitramide shows promise as a high-energy material with potential industrial or military applications. Its advantage over current materials is the elimination of pollution from chlorinated combustion products.

III. Results And Discussion

In 2013, research was published where the viscosity of ADN was lowered using an alcohol solvent such as glycerol or a mixture of alcohols, such as glycerol and 1,4-butanediol. The experiment used a solvent with a viscosity equal to or higher than 0.25 Pa/s, at which spontaneous nucleation occurs. Under these conditions, the crystallization process results in ADN with a high charge level [9].

Other methods for controlling the shaping of ADN crystals are also being explored. Important conditions include product purity and viscosity, considering its melting point of 93°C, which is lower than its decomposition temperature of 124°C.

A. Prilling Tower

In this method, molten AND is sprinkled at the top of a prilling tower. The droplets, moving downward in the cooling tower, meet a counterflow of cooling nitrogen, resulting in granules of AND as depicted in Fig. 1 [10].

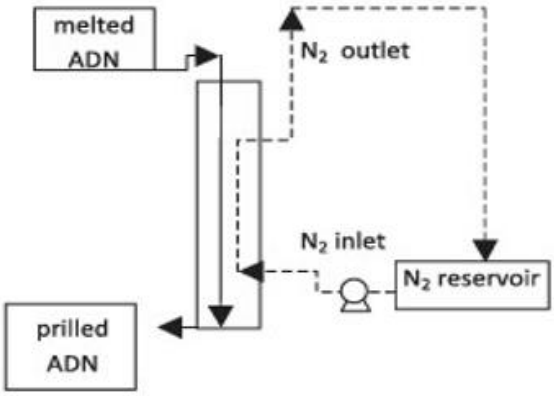

Fig. 1. The schematics of Prilling Tower technique for production of ammonium dinitramide granules.

B. Emulsion Crystallization

High-purity ADN is poured into a reactor with a non-polar liquid. The mixture is stirred constantly to form a homogeneous dispersion. The liquid is heated until the crystals melt, forming an emulsion. Stirring continues until the desired droplet size is achieved. The emulsion is cooled, and the droplets solidify into spherical shapes [11] [12].

C. Spray Crystallization

In this method, molten ADN is sprayed through a nozzle into a container filled with liquid nitrogen. This technique was introduced for ammonium dinitramide in 2005 and further modified in 2006. Its advantage lies in the compactness of the equipment used [5].

D. Microencapsulation

The surface of each particle is coated with a thin polymer layer, typically wax, to protect it from moisture and reaction with hardening agents during transport and storage. However, wax is not suitable for use in rocket propellants, and it must be washed off the surface before further polymer processing.

E. Coacervation

ADN particles are dispersed in an emulsion of ethyl cellulose in cyclohexane. The dispersion continues until the ethyl cellulose particles surround each ADN particle, forming a thin, continuous layer on its surface. The process is induced by pH, temperature, and the addition of a third component. The dispersion is then cooled, and the layer hardens. The processed ADN is separated and dried.

F. Fluidized Bed

In this method, ADN particles are suspended in a chamber with an upward flow of air. The polymer is sprayed into the chamber, either from the bottom or the top. The particles remain suspended until the coating hardens. The process is outlined in Fig. 2 [5]. In 2009 Heintz successfully tests different polymers used as binders in propellants.

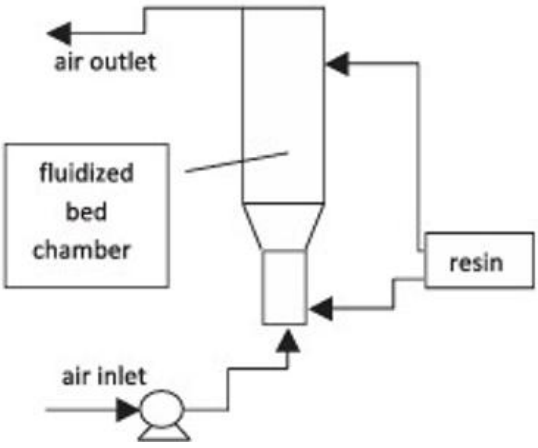

Fig. 2. The schematic of Fluidized Bed process.

G. Supercritical Fluidized Bed

This is a modification of the fluidized bed method, where air is replaced with carbon dioxide, taking advantage of its supercritical properties at moderate temperatures and high pressure. Supercritical fluids exhibit low viscosity (like gases) and high density (like liquids), making them more suitable for this process. However, the chamber walls must be reinforced to withstand the high pressure.

H. Spray Dryer

This method is typically used for smaller particles (<50 microns), where the fluidized bed method is not

applicable. The resin and ADN are dispersed and sprayed into a container, where solvents evaporate, leaving a polymer coating on the surface of each particle. The coated particles harden and are separated from the solvents as shown in Fig. 3.

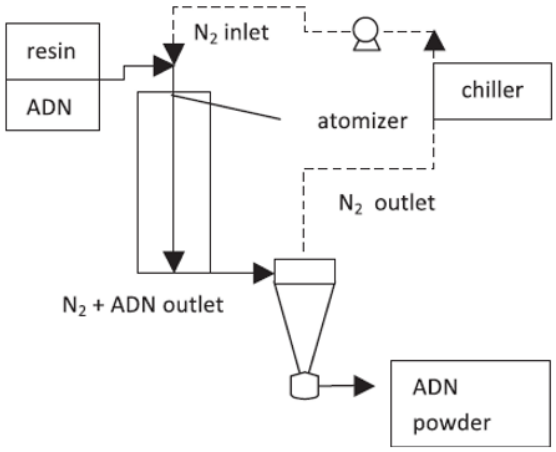

Fig. 3. The spray dryer technique.

I. Prilling and Coating with Ultrasound

This method, researched in 2018, involves forming spherical ADN granules and coating them with a polymer using ultrasound [13]. The polymer mixture includes toluene, graphene, citryl ammonium butyl, Cab-o-sil, and a coating polymer (polystyrene or polybutadiene). The method reduces the working temperature and eliminates melting during the shape transformation process. The resulting product has particle sizes and thermal stability close to those obtained through conventional melting methods. This innovative method could provide an alternative route for producing ADN particles for use in rocket propulsion systems.

Other research published in 2021 combines utilization of ultrasound with power of 70 W, volume ratio of solvent to antisolvent is 1:50 and the antisolvent temperature 20℃ [14]. The conclusion based on the test results is that the volume ratio of solvent to antisolvent is the most important factor in controlling the morphology and particle size of ADN crystals. There is a correlation between the antisolvent temperature and crystal size. The increase in antisolvent temperature leads to gradual increase in crystal size.

J. Co-crystalization technology

Co-crystallization is a supra-molecular method that two or more diverse types of molecules could be placed in one cell with a pre-defined molar ratio and interactions like hydrogen bonds, electrostatic interactions, π-π stacking, van der Waals forces etc. would occur among these molecules initiating co-crystallization. The main driver for co-crystallization mechanism are the interactions. This technology is utilized to amend the oxygen balance, molecular structure, density, improve mechanical properties, decrease sensitivity, increase detonation performance, and enhance thermal stability of energetic materials. Co-crystallization has been used to improve the hygroscopicity of ADN. In 2019, Bellas and Matzger developed an ADN/ PDO (pyrazine-1,4-dioxide) composite using stoichiometric ratio of 2:1. This compound reached excellent physical and energy characteristics, zero oxygen balance, enhanced specific impulse and improved hygroscopicity. The relative humidity at 25°C elevated from 53.5% to 79.5%. However, the melting point of ADN/PDO cocrystal was low of 113℃ [15]. Co-crystallization can improve the hygroscopicity and density of ADN, but attention should be paid to the ligand content since higher values can negatively impact the energy characteristics of the composite. Co-crystallization technology succeeded to improve ADN hygroscopicity, but results lead to a conclusion that the method will not be able to complete the target by its own.

All above methods illustrate various approaches to improving the physical and chemical properties of ADN, as part of ongoing efforts to reduce its hygroscopicity and expand its potential use in rocket propellant systems and explosives.

IV. Conclusions

The replacement of AP with the environmentally friendly and economical ADN results in an increase of the specific impulse of a rocket by 20%, with a 40% decrease in rocket motor weight. In other applications like low characteristic signal propellants, the total specific impulse can be increased by 7%. ADN unveils excellent characteristics paving the road to successful utilization if the obstacles as high hygroscopicity and sensitivity to mechanical stimulation are eliminated. Methods like prilling, surface coating, and co-crystallization prove to be to some degree successful but not enough or not well developed yet to deliver the desired goals. A combination of different technologies might be the future direction for further development in the research field.

Acknowledgement

We would like to thank Defense Institute "Professor Tsvetan Lazarov", Sofia, Bulgaria for giving us the opportunity to present this paper.

References

[1] J. P. Agrawal, *High Energy Materials. Propellants, explosives and pyrotechnics*, Weinheim: WILEY-VCH Verlag GmbH & Co., 2010. [E-book] Available: Wiley e-book.

[2] H. Östmark, A. Helte, S. Karlsson, Ar. Hahma, H. Edvinsson, "Detonation Properties And Reaction Rate Modeling Of Melt Cast Ammonium Dinitramide (ADN)," in *12th International Detonation Symposium*, San Diego, 2002.[Online]. Available: https://www.researchgate.net/publication/237737933. [Accessed 25 11 2024].

[3] R. Meyer, J. Köhler, A.Homburg, *Explosives*, 6th ed., Wiley VCH & Co, 2007. . [E-book] Available: Wiley e-book.

[4] E. W. Schmidt, "Alkyl Perchlorate Esters– Fluorine", *Encyclopedia of Oxidizers*, vol. Volume 1:, De Gruyter, 2022. [E-book] Available: De Gruyter e-book.

[5] M. Y. Nagamachi, "ADN The new oxidizer around the corner for an environmently friendly smokeless propellant", *Journal of Aerospace Technology and Management,* vol. 1, no. 2, pp. 153-160, 12 2009. Available: https://jatm.com.br/jatm/article/view/19/226. . [Accessed 14 02 2024].

[6] C. Voerde, H. Skiefs, "Method of Producing Salts of Dinitramidic Acid", Sweden 2005. [Online]. Available: https://patentscope.wipo.int/search/en/detail.jsf?docId=WO2005070823. [Accessed 28 11 2024].

[7] G.D. Silva, S.C.Rufino, K.Iha, "Green Propellants Oxidizers", *Journal of Aerospace technology and Management,* vol. 5, no. 2, pp. 139-144, 2013. Available: http://dx.doi.org/10.5028/jatm.v5i2.229. [Accessed 14 05 2023].

[8] B. Chen, B. Jin, R. Peng, F. Zhao, J. Yi, H. Guan, X. Bu, J. Zhao, S. Chu, "The thermal decomposition of silverdinitramide $AgN(NO_2)_2$," *Journal of thermal analysis and calorimetry,* 07 2016. Available: https://link.springer.com/article/10.1007/s10973-016-5643-z. [Accessed 08 06 2024].

[9] F. R. J. B. J.-M. Muscatelli, "Method for obtaining ADN crystals through crystallization in a viscous madium", USA Patent 8491736B2, 23 07 2013. Available: https://www.freepatentsonline.com/8491736.html. . [Accessed 06 11 2024].

[10] T. K. Highsmith, C. S. McLeod, R. B. Wardle, R. Hendrickson, "Thermally-Stabilized Prilled Ammonium Dinitramide Particles, And Process For Making The Same", USA Patent US6136115, 24 10 2000. Available: https://patentscope.wipo.int/search/en/detail.jsf?docId=US39243338&_fid=WO1999001408. [Accessed 11 06 2024].

[11] U. Teipel, T. Heintz, H. H. Krause "Crystallization of Spherical Ammonium Dinitramide (ADN) Particles", *Propellants, Explosives, Pyrotechnics,* vol. 25, no. 2, pp. 81-85, 04 2000. Available: https://onlinelibrary.wiley.com/doi/abs/10.1002/%28SICI%291521-4087%28200004%2925%3A2%3C81%3A%3AAID-PREP81%3E3.0.CO%3B2-F. [Accessed 11 06 2024].

[12] T. Heintz, W. Reinhard, C. Birke, K. Leisinger "Particle Size Adjustment Of Spherical Ammoniumdinitramide Particles (Adn-Prills) Produced Byemulsion Crystallization", in *Fraunhofer-Institut für Chemische Technologie (International Annual Conference)* , Karlsruhe, Germany, 2014. Available: https://publica.fraunhofer.de/entities/publication/1ed3b9a1-004b-491d-8e71-3e14ec602ee5. [Accessed 06 11 2024].

[13] A. Rahman, J. Chin, K. How Cheah, "Prilling and Coating of Ammonium Dinitramide using ultrasound", *Aerospace,* vol. 5, no. 1, p. 29, 2018. Available: https://www.researchgate.net/publication/323671074. [Accessed 11 06 2024].

[14] J. Li, , R. Yang, T. Zeng, J. Hu, W. Tang , Z. Liu, L. Gong, "Preparation and growth mechanism of micro spherical ammonium based on ultrasound", *Ultrasonics Sonochemistry,* vol. 78, 08 2021. Available: https://www.researchgate.net/publication/353929835. [Accessed 25 03 2024].

[15] M. K. Bellas, Prof. A. J. Matzger, "Achieving Balanced Energetics through Cocrystallization", *Angewandte Chemie,* vol. 58, no. 48, pp. 17185-17188, 25 November 2019. Available: https://doi.org/10.1002/anie.201908709. [Accessed 29 11 2024].

Environment. Technology. Resources. Rezekne, Latvia
Proceedings of the 16th International Scientific and Practical Conference. 2025. Volume IV, 139-144

System for Testing and Determining the Accuracy of a Mechanical Watch

Tsanko Karadzhov
Department of Mechanical and Precision Engineering
[1]Technical University of Gabrovo
[2]Center of competence "Smart mechatronic, eco-and energy-saving systems and technologies
Gabrovo, Bulgaria
karadjov_s@abv.bg

Borislav Georgiev
Department of Mechanical and Precision Engineering
[1]Technical University of Gabrovo
[2]Center of competence "Smart mechatronic, eco-and energy-saving systems and technologies
Gabrovo, Bulgaria
gborislav@gbg.bg

***Abstract* — This paper presents a new system for measuring the accuracy of mechanical clocks with Swiss Movement. Mechanical watches are complex devices consisting of many miniature components. Even small deviations in accuracy can lead to significant differences in timekeeping. Testing the accuracy of mechanical watches is an important process that ensures their functionality, durability, and value. It helps maintain a high level of precision in timekeeping, which is critical in many aspects of daily life and professional activity. The developed system provides a readily applicable alternative to measure and improve the accuracy of watches using a personal computer and acoustic analyses. The proposed methodology contributes to expanding the possibilities of investigating the dynamic characteristics of mechanical watches.**

Keywords* — *Accuracy, Mechanical watch, Accelerometer, Measurement system.

I. INTRODUCTION

Mechanical watches are inherently less precise than quartz watches [2]. A typical modern mechanical watch exhibits a daily deviation of approximately ±10 seconds, whereas a certified chronometer-grade mechanical watch is tested to run within -4 to +6 seconds per day [7]. In practical terms, this indicates that an ordinary mechanical watch may deviate by several minutes per month, while a chronometer-grade mechanical watch maintains accuracy within 1 or 2 minutes per month [10,11]. In comparison, an average quartz watch shows a greater degree of accuracy, typically exhibiting a daily deviation of approximately ±1 second equivalent to 30 seconds per month.

Mechanical watches, despite the lower accuracy, continue to be preferred both for their complexity, yet combined with engineering precision, and for their reliability [16]. In the context of dynamic processes, the accuracy of these devices is determined by the interaction of multiple factors such as the oscillations of the balance wheel, the influence of the environment and the mechanical characteristics of the components.

II. MATERIALS AND METHODS

A. Components of a Mechanical Watch

The block diagram of a mechanical watch is structured into the following key components – fig. 1.

Power source includes mainspring and barrel. The main spring is the primary energy source of a mechanical watch. It stores mechanical energy when wound manually or automatically. The barrel houses the main spring and regulates its release of power to the gear train. It also provides a consistent force over time.

Gear train transmits the energy from the barrel to the escapement and hands of the watch. It involves a series of gears that step down the speed of the main spring's release. The gear train also drives the hands of the watch, which displays the time.

Escapement is crucial for maintaining consistent time intervals. It allows the gear train to move forward in fixed steps, thus controlling the movement of the hands. It transfers energy to the balance wheel and ensures that the gear train advances at a regulated pace.

Online ISSN 2256-070X
https://doi.org/10.17770/etr2025vol4.8449
© 2025 The Author(s). Published by RTU PRESS.
This is an open access article under the Creative Commons Attribution 4.0 International License.

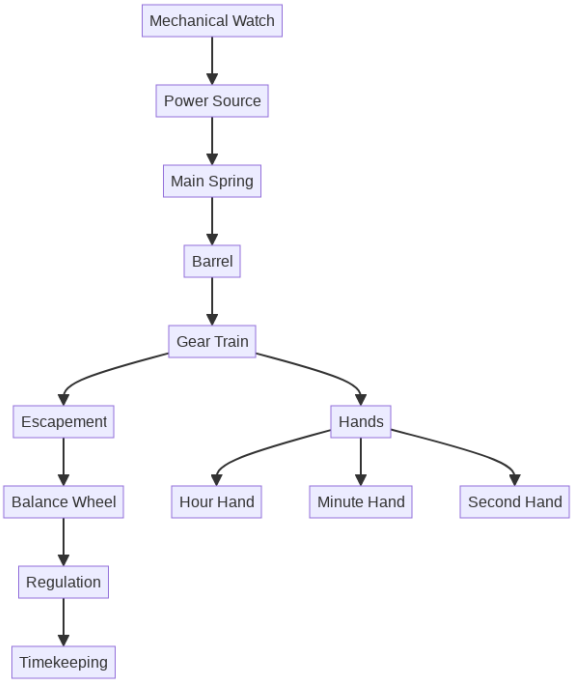

Fig. 1. Block Diagram of the Elements of a Mechanical Watch.

Balance wheel oscillates back and forth, acting as the timekeeping element of the watch. It works alongside escapement to divide time into equal parts [5].

Regulation system adjusts the tension of the balance spring, fine-tuning the rate at which the balance wheel oscillates, thereby ensuring the watch keeps accurate time.

Timekeeping is the outcome of all these processes, displaying accurate time to the user through the watch's hands.

Each component plays a critical role in the mechanical harmony of a traditional watch, resulting in precise and reliable timekeeping.

B. *Balance Spring Oscillation System. Analytical Description of the Movement of the Balance Wheel*

We will focus on the balance spring oscillation system in more detail because the accuracy of the mechanical clock depends on it. The balance wheel of a mechanical watch operates on the principles of harmonic motion, driven by the interplay between the balance wheel itself and the attached hairspring also known as the balance spring.

Oscillatory motion – The balance wheel performs a periodic back-and-forth rotational movement around its pivot. This motion is akin to that of a simple harmonic oscillator, like a pendulum but rotational. The angle of rotation (θ) as a function of time (t) can be described by:

$$\theta = \theta_0 \cos(\omega t + \varphi) \quad (1)$$

where:

θ_0 is the maximum angular displacement,

ω is the angular frequency,

ϕ is the phase constant.

The hairspring provides a restoring torque that is proportional to the angular displacement:

$$\tau = -k\theta \quad (2)$$

where:

τ is the restoring torque,

k is the spring constant of the hairspring.

Angular frequency and period – The balance wheel's natural frequency depends on the spring constant and the moment of inertia (I) of the wheel:

$$\omega = \sqrt{\frac{k}{I}} \quad (3)$$

The period (T) of oscillation, which is crucial for timekeeping, is given by:

$$T = \frac{2\pi}{\omega} = 2\pi\sqrt{\frac{I}{k}} \quad (4)$$

Since the period is independent of the amplitude, the balance wheel is an effective timekeeper. During each oscillation, the escapement provides a small impulse to maintain the amplitude of the balance wheel's motion. Damping is minimal in a well-designed watch, ensuring that the amplitude remains stable over time.

Regulation of timekeeping – The balance wheel's consistent period ensures that each tick of the escapement wheel is uniform, translating to precise movement of the watch's hands. A typical mechanical watch balance wheel oscillates at a rate of 5 to 10 beats per second, often described as 18000 to 36000 beats per hour (BPH).

C. *Energy Transfer Mechanism*

In a mechanical watch, energy transfer and damping are critical for maintaining accurate timekeeping. The process involves the coordinated function of the mainspring, gear train, escapement, and balance wheel – fig. 2. The mainspring stores potential energy when wound. This energy is gradually released to drive the gear train. The gear train multiplier the high torque of the mainspring to a suitable level and delivers it to the escapement.

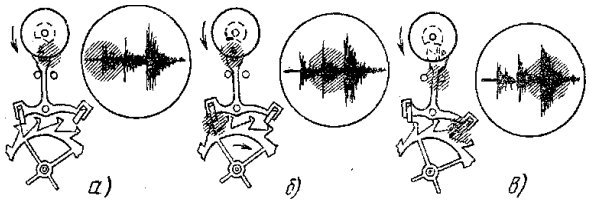

Fig. 2. Schematics of the oscillator beats

The escapement mechanism serves two main purposes – Regulates the release of energy to the balance wheel and converts the continuous motion of the gear train into discrete impulses. The escapement transfers a small amount of energy to the balance wheel with each oscillation, maintaining its motion against damping losses.

The energy transfer can be quantified as:

$$E = \tau . \theta \quad (5)$$

where:

E is the energy transferred,

τ is the torque applied by the escapement [22],

θ is the angular displacement of the balance wheel.

D. Damping in the Balance Wheel System

Damping is the process that dissipates energy from the oscillating system, primarily due to friction – at the pivot points of the balance wheel, air resistance – as the wheel moves through the air, internal friction in the hairspring – especially as it flexes during oscillation.

Damping introduces a resistive torque proportional to the angular velocity ω:

$$\tau_d = -b . \omega \quad (6)$$

where:

τ_d is the damping torque.

b is the damping coefficient

ω is the angular velocity of the balance wheel.

E. Mathematical Model of the Damped Harmonic Oscillator

The balance wheel's motion under damping follows the equation [2]:

$$I \frac{d^2\theta}{dt^2} + b \frac{d\theta}{dt} + k\theta = 0 \quad (7)$$

where:

I is the moment of inertia of the balance wheel.

k is the spring constant of the hairspring.

The solution of this equation for [11] underdamped systems is:

$$\theta(t) = \theta_0 e^{-\frac{b}{2I}t} \csc(\omega_d t + \emptyset) \quad (8)$$

where:

θ_0 is the initial amplitude.

The exponential term represents the decay of the oscillation amplitude over time.

$\omega_d = \sqrt{\frac{k}{I} - \left(\frac{b}{2I}\right)^2}$ is the damped angular frequency.

F. Quality Factor (Q-Factor) of the Oscillator

The quality factor Q measures the efficiency of the oscillation and is defined by [13]:

$$Q = \frac{2\pi E}{\Delta E} \quad (9)$$

where:

E is the energy stored per cycle,

ΔE is the energy lost per cycle due to damping.

A high Q factor indicates minimal energy loss and thus a more precise timekeeping device. Good mechanical watches often achieve Q values above 500 [14].

Insufficient energy transfer leads to a decrease in oscillation amplitude, affecting the escapement's performance. Excessive damping causes a loss of oscillatory energy, potentially stopping the balance wheel. Balanced damping ensures that the balance wheel receives just enough energy to counteract losses, maintaining consistent oscillations. The fine-tuning of energy transfer and damping is essential for the watch's consistent and accurate performance over extended periods.

III. Results and Discussion

A. Factors Affecting Accuracy of Mechanical Watches

Despite careful design and certification, a mechanical watch's accuracy can be influenced by numerous factors. Some are inherent to the mechanism, while others are external influences or related to maintenance. Factors like gravity (position), temperature, magnetism, shocks, and maintenance all play a role in a mechanical watch's accuracy [16]. High-quality watches are engineered and adjusted to minimize these influences – for instance, being adjusted in multiple positions, using anti-magnetic and temperature-compensated materials, and having shock absorbers [8]. Yet even the best mechanical watch is a balance of tiny physical forces, so its rate can never be as unwavering as a quartz oscillator.

Furthermore, the accuracy of a mechanical watch can be influenced by the nonlinearity of the static characteristics of its components. In [3], methods for analyzing and correcting these errors are proposed, along with mathematical models that enable the evaluation and compensation of errors caused by nonlinearity. Together with this, the accuracy of such measurement systems is also affected by instrumental and methodical errors, especially in dynamic measurements. In [19], a method for analyzing these errors and determining their probabilistic characteristics is proposed, which is important for mechanical watch accuracy testing [19].

B. Mechanical watch accuracy measurement devices

Mechanical watch accuracy measurement devices are specialized instruments used to evaluate the performance and accuracy of mechanical watches. These devices analyze key parameters such as rate, amplitude, beat error, and positional variations [6]. Some of the commonly used devices include:

Timegrapher – A timegrapher is a professional instrument that measures the accuracy of mechanical watches by analyzing the sound of the ticking mechanism. It provides key metrics such as *rate* – the deviation in seconds per day (s/d), *amplitude* – the swing range of the balance wheel (typically 270° to 315° is ideal), *beat error* – the difference in time between ticks, indicating if the balance wheel is centered, *lift angle* – specific to the watch's design, affecting amplitude calculations.

Mechanical Watch Timing Machine – These machines measure the watch's performance in various positions (e.g., dial up, dial down, crown up). They simulate the watch's wear and help detect positional accuracy issues.

Vibrograph – A traditional device that measures the watch's vibrations to calculate its accuracy. Though older technology, it is still used in some watchmaking workshops.

Smartphone Apps – Modern smartphone apps, coupled with a microphone adapter, can provide basic accuracy measurements by analyzing the ticking sound of a mechanical watch. Apps like Watch Tuner and Tickoprint offer similar functionalities as professional devices but at a consumer level [9].

These devices cater to diverse needs, ranging from professional watchmakers who require precision instruments to enthusiasts seeking cost-effective methods to assess the accuracy of their timepieces.

C. *Methods for increasing the accuracy of mechanical watch*

Increasing the accuracy of a mechanical watch involves fine-tuning its components and maintaining optimal operating conditions [21]. Here are some methods for increasing the accuracy of mechanical watches:

Regulating the Balance Wheel – The regulator lever can be moved to change the effective length of the hairspring, which affects the rate of oscillation of the balance wheel. If fine tuning needs to be done, this can be done by lengthening or shortening the balance spring.

Temperature Compensation – Balance wheels and hairsprings are made of materials with low thermal expansion help maintain accuracy despite temperature changes or there is another one older method include using bimetallic balance wheels that adjust their diameter with temperature changes [20].

Shock Resistance and Incorporating shock absorbers are systems like Incabloc or Kif that prevent damage to the delicate pivots of the balance wheel, maintaining accuracy even when subjected to shocks.

Optimizing amplitude – Ensuring the balance wheel swings between 270° and 315° to avoid over-rotation or under-rotation. Regular servicing helps maintain the ideal amplitude by reducing mechanical resistance [24].

Testing in various positions – Mechanical watches are typically adjusted in multiple positions (e.g., dial up, crown down) to minimize positional variance. Watchmakers adjust the watch to minimize deviations across different orientations.

Using High-Precision Components – The escapement controls the release of energy and the ticking rate. Enhancing its precision improves the watch's accuracy.

Regular Maintenance – Over time, oils dry out, and dirt accumulates. Regular service ensures all components function smoothly. Components like the mainspring or the escapement may need replacement to restore accuracy [10].

Environmental Control – Modern watches may include anti-magnetic materials to prevent the balance spring from becoming magnetized. Controlling temperature and humidity is necessary because extreme conditions can affect the metal components, altering the watch's accuracy.

Use of advanced technologies like implementing silicon hairsprings which these are less affected by temperature, magnetism, and wear. Use of advanced technologies like implementing silicon hairsprings which these are less affected by temperature, magnetism, and wear. Other advanced technology is the use of high-beat movements which are increasing the frequency of the balance wheel oscillations e.g., 36000 BPH enhances timekeeping stability.

D. *Accuracy Measurement System for Mechanical Watch via LabVIEW*

A LabVIEW measurement system was developed to analyze the acoustic signals from the watch operation – fig. 3. This LabVIEW measurement system is designed for the real-time acquisition, filtering, spectral analysis, and visualization of sound signals [4]. The system utilizes a continuous data acquisition method, processes the data through configurable filters, performs spectral analysis, and displays the data in both time and frequency domains [15]. Below is a detailed step-by-step description of how each component functions and interacts within the system.

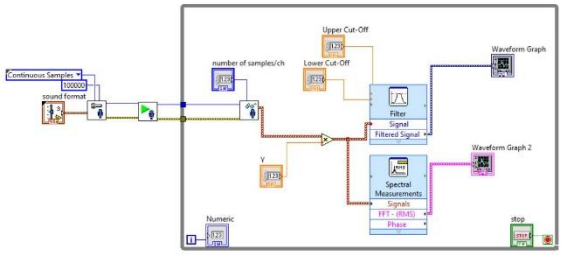

Fig. 3. Block diagram of the measuring system in LabVIEW

The built-in microphone on the laptop was used for the measurement. The system begins by configuring a virtual channel DAQmx for sound input with continuous sampling mode. The sample rate is set to 100,000 samples per channel, ensuring high-resolution data acquisition. Shell sound format is appropriately configured to match the input device specifications [12].

DAQmx Start Task – This VI initializes the acquisition process, enabling the continuous collection of sound data from the input source [17].

DAQmx Read – The DAQmx Read VI captures the waveform data based on the defined sample rate and the number of samples per channel. The captured waveform is output for further processing.

Signal Filtering – Filter VI – Filters are used to remove noise from the signal. The raw signal is processed through a configurable filter (e.g., a bandpass or bandstop filter). The Upper Cut-Off and Lower Cut-Off frequency controls allow the user to define the passband of the filter, removing unwanted frequencies from the signal. The output of the

filter is a Filtered Signal, which is then ready for visualization and analysis.

Time-Domain Visualization – The filtered signal is displayed in real-time on a Waveform Graph, allowing the user to visualize the signal in the time domain. This view is useful for observing how the filtering process affects the raw signal, showing wave shapes and amplitude changes over time.

Spectral Analysis – The filtered signal is also fed into the Spectral Measurements VI for frequency domain analysis. The spectral [18] measurements VI computes the FFT (RMS) (Fast Fourier Transform - Root Mean Square) and Phase of the signal. The FFT provides insight into the frequency components present in the signal, revealing peaks at dominant frequencies and overall spectral distribution. The frequency domain data (FFT) is displayed on a second waveform graph. This graph presents the power spectrum of the signal, showing frequency versus amplitude, which is valuable for identifying specific frequencies present in the sound input. The spectral analysis of the signal in this case has nothing to do with the measurement. It can be used for diagnostics on the work of the mechanical watch.

The addition of the Spectral Measurements VI enhances the system's capability by providing insights into the frequency spectrum of the signal, making it particularly useful for applications in audio analysis, noise reduction, and frequency-specific monitoring. This is necessary to understand the condition of the watch and if you need to service the movement.

This LabVIEW system is a real-time measurement system for sound pulses coming from a mechanical watch, which receives sound data, filters it according to user-defined frequency ranges, and visualizes the processed signal – fig. 4 [23].

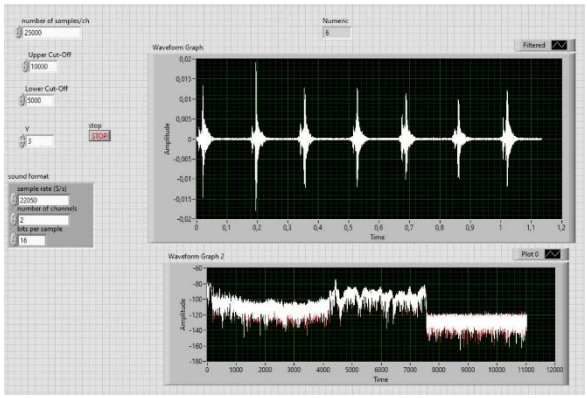

Fig. 4. LabVIEW measurement signal visualization

The data from the measuring system can be transferred to Excel and from there the time between individual pulses can be determined and the clock error calculated for 24 hours [1]. The period on the clock T_i is determined by the impulse in Excel. The absolute error for a time equal to a period is determined by the expression:

$$\Delta T = T_i - T_0 \qquad (10)$$

T_i – measured value for the period,

T_0 – nominal value for the period.

The time for which the clock is ahead or behind in one day is determined by the expression in seconds per 24 hours (s/24h):

$$\omega = 86400\frac{\Delta T}{T} \qquad (11)$$

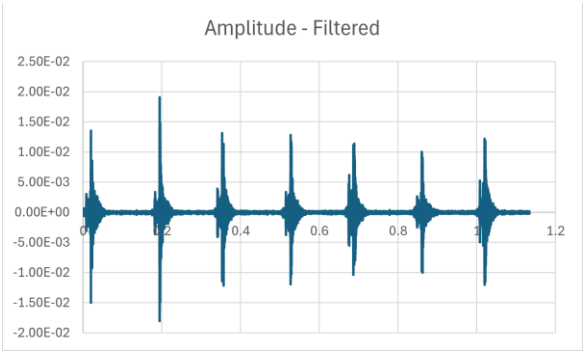

Fig. 5. Measurement signal in Excel

E. Experimental Data and Results

TABLE 1 MEASUREMENT RESULTS

№	Measured error – s/24h		
	Brand watch	*Timegr.*	*LabVIEW*
1	Zaria	+23	+24
2	Poljot	+9	+6
3	Molnija	-10	-8
4	Pobeda	+27	+24
5	Seiko 5	+11	+11
6	Orient	+9	+9
7	Citizen	-3	+1
8	Certina	-5	-7
9	Slava	+11	+9
10	Doxa	+3	+3

The measurements were taken with professional Timegrapher No.1000 and the developed LabVIEW system at temperature 20 °C and at the same watch position.

CONCLUSIONS

The developed system for testing and determining the accuracy of mechanical watches provides a reliable and practical solution for watchmakers and researchers. By leveraging acoustic analysis and the LabVIEW platform, the system offers a cost-effective and efficient alternative to traditional measurement devices such as professional timegraphers. The experimental results demonstrate that the system delivers comparable accuracy, with minimal

deviation between measurements. Moreover, the system's adaptability for real-time analysis and its ease of use makes it a valuable tool for ongoing studies of the dynamic characteristics of mechanical watches.

ACKNOWLEDGMENT

This research was funded by the European Regional Development Fund under the Operational Program "Scientific Research, Innovation and Digitization for Smart Transformation 2021-2027", Project CoC "Smart Mechatronics, Eco- and Energy Saving Systems and Technologies", BG16RFPR002-1.014-0005.

REFERENCES

[1] J. Song, L. Cao, Y. Wang, F. Zhang, Y. Shi, G. Wang, X. Li, and Y. Chen, "A LabVIEW-Based Generalized Experimental Test Platform for Precision Machining Control Algorithms," Processes, vol. 12, p. 2542, 2024, doi: 10.3390/pr12112542.

[2] T. Aihara, C. Kamio, Y. Hara, K. Ito, and K. Jujo, "Dynamic accuracy measurement system for mechanical wristwatch," Precision Engineering, vol. 70, pp. 117–123, 2021, doi: 10.1016/j.precisioneng.2021.01.018.

[3] D. Dichev, F. Kogia, H. Koev, and D. Diakov, "Method of analysis and correction of the error from nonlinearity of the measurement instruments," Journal of Engineering Science and Technology Review, vol. 9, no. 6, pp. 116-121, 2016, doi: 10.25103/jestr.096.17.

[4] S. Su and R. Du, "Signature analysis of mechanical watch movements," Mechanical Systems and Signal Processing, vol. 21, pp. 3189–3200, 2007, doi: 10.1016/j.ymssp.2007.04.006.

[5] B. Zhang, S. Sun, and S. Zhang, "Research on Acoustic Characteristics Measurement by Using LabVIEW," Applied Mechanics and Materials, vols. 644-650, pp. 920-924, 2014, doi: 10.4028/www.scientific.net/AMM.644-650.920.

[6] D. Dichev, H. Koev, T. Bakalova, and P. Louda, "A Gyro-Free System for Measuring the Parameters of Moving Objects," Measurement Science Review, vol. 14, no. 5, pp. 263-269, 2014, doi: 10.2478/msr-2014-0036.

[7] G. Xu, P. Ko, and R. Du, "A study on the precision of mechanical watch movement with Tourbillon," Journal of Sound and Vibration, vol. 330, no. 16, pp. 4019-4028, 2011, doi: 10.1016/j.jsv.2011.03.020.

[8] L. Lazov, E. Teirumnieks, N. Angelov, and E. Teirumnieka, "Proceedings of the 12th International Scientific and Practical Conference," Rezekne, Latvia, vol. III, pp. 134-136, 2019, doi: 10.17770/etr2019vol3.4143.

[9] Measuring Shock and Vibration with Accelerometer Sensors, Dewesoft Test & Measurement. [Online]. Available: https://dewesoft.medium.com/measuring-shock-and-vibration-with-accelerometer-sensors-246b47d8feed [Acceesse: May 24, 2020].

[10] Y.H. Anis, W.L. Cleghorn, and J.K. Mills, "Modal analysis of microgrippers used in assembly of MEMS devices," 2005 International Conference on MEMS, NANO and Smart Systems, Banff, Canada, July, 2005.

[11] D. Dichev, H. Koev, D. Diakov, N. Panchev, R. Miteva, and H. Nikolova, "Automated System for Calibrating Instruments Measuring Parameters of Moving Objects," in Proc. 59th Int. Symp. ELMAR, Zadar, Croatia, 2017, pp. 219-224, doi: 10.23919/ELMAR.2017.8124472.

[12] N. Sato et al., "Novel MEMS Power Generator With Integrated Thermoelectric and Vibrational Devices," in Proc. 13th Int. Conf. Solid-State Sensors, Actuators and Microsystems, Korea, 2005, pp. 295–298.

[13] E. Teirumnieks, L. Lazov, A. Snikeris, and I. Balchev, "Laser marking and engraving of household and industrial plastic products," Journal of Physics: Conference Series, vol. 1859, 2020, doi: 10.1088/1742-6596/1859/1/012016.

[14] N. Robuschi, F. Braghin, A. Corigliano, A. Ghisi, and A. Tasora, "On the dynamics of a high frequency oscillator for mechanical watches," Mechanism and Machine Theory, vol. 117, pp. 276-293, 2017, doi: 10.1016/j.mechmachtheory.2017.07.013.

[15] Y. Fu and R. Du, "A Study on the Dynamics of Swiss Lever Escapement Mechanism," International Symposium on Collaborative Research in Applied Science, Vancouver, Canada, 2005, pp. 8–15.

[16] D. Dichev et al., "A method for correction of dynamic errors when measuring flat surfaces," Sensors, vol. 24, no. 16, 2024, doi: 10.3390/s24165154.

[17] G. Johnson and R. Jennings, LabVIEW Graphical Programming, McGraw-Hill Professional, 2001, ISBN: 0071370013.

[18] R. Bitter, T. Mohiuddin, and M. Nawrocki, LabView, Advanced Programming Techniques, 2nd ed., 2007, eBook ISBN 9781315222097, doi: 10.1201/9780849333255.

[19] L. Lazov, N. Angelov, and E. Teirumnieks, "Influence of pulse duration on the process of laser marking of CT80 carbon tool steel products," Laser Physics, vol. 31, 2021, doi: 10.1088/1555-6611/abe5af.

[20] L. Sigcha et al., "Occupational risk prevention through smartwatches: precision and uncertainty effects of the built-in accelerometer," Sensors, vol. 18, no. 11, p. 3805, 2018.

[21] D. Dichev et al., "Analysis of instrumental errors influence on the accuracy of instruments for measuring parameters of moving objects," in Proc. 31st Int. Sci. Symp. Metrology and Metrology Assurance, Sozopol, Bulgaria, 2021, doi: 10.1109/MMA52675.2021.9610855.

[22] S. Liu, J. Zhang, and Y. Zhang, "A wearable motion capture device able to detect dynamic motion of human limbs," Nat. Commun., vol. 11, p. 5615, 2020, doi: 10.1038/s41467-020-19424-2.

[23] D. Pulov and P. Tsvyatkov, "Optical Systems for Reducing the Divergence of Laser Beams," in Proc. 14th Int. Sci. and Practical Conf. Environment. Technology. Resources., Rezekne, Latvia, 2023, vol. 3, pp. 339–343, doi: 10.17770/etr2023vol3.7217.

[24] G. Aiello, G. La Scalia, M. Vallone, P. Catania, and M. Venticinque, "Real time assessment of hand-arm vibration system based on capacitive MEMS accelerometers," Comput. Electron. Agric., vol. 85, pp. 45–52, 2012.

Environment. Technology. Resources. Rezekne, Latvia
Proceedings of the 16th International Scientific and Practical Conference .2025. Volume IV, 145-149

Research and Modeling of the Finishing Method of Cylindrical Gear Teeth Through Cold Plastic Calibration

Kalin Krumov
Department of Mechanical Engineering and Technology
Technical University of Gabrovo
Gabrovo, Bulgaria
kalin_krasimirov_krumov@abv.bg

Hristo Metev
Department of Mechanical Engineering and Technology
Technical University of Gabrovo
Gabrovo, Bulgaria
hmetev@abv.bg

***Abstract*—The operational performance of gearwheels is largely determined by the accuracy of the parameters and the quality of the working surfaces of the teeth, the requirements for which are constantly increasing. To optimize the machining conditions (increasing productivity, tool durability and the quality of the machined gearwheels), a method for finishing machining by calibration on gear-shaving and thread-rolling machines is proposed in the work. Experimental studies have been conducted to prove the operability of the proposed method. The results obtained have been analyzed and compared with gear-milled gearwheels in terms of kinematic accuracy, smoothness of operation and contact of the teeth. Regression models have been obtained for the accuracy parameters of the teeth before and after processing by calibration and subsequent heat treatment, the analysis of which shows that their size is largely determined by their input values. The results of the studies confirm the assumption of the presence of a correlation between the same accuracy parameters at the input and at the output during processing by calibration and subsequent heat treatment.**

Keywords*—calibration, gear-shaving machines, thread-rolling machines, accuracy.

I. INTRODUCTION

In today's complex environment and in the conditions of Industry 4.0, engineering companies are required to make great efforts to maintain their competitiveness in the domestic and foreign markets and constantly seek solutions for higher efficiency and productivity [1] - [3]. The practice of industrially developed countries has long proven that one of the preferred solutions is the development of progressive methods for processing the surfaces of parts, determining their operational characteristics.

The operational performance of gearwheels is largely determined by the accuracy of the parameters and quality of the working surfaces of the teeth, the requirements for which are constantly increasing. This results from the sharp increase in the peripheral speeds, transmitted power, accuracy, as well as the need for their reliability and durability in production conditions, with optimal metal consumption. This leads to the need of conducting research, related to improving the qualities of gearwheels and gear trains.

One of the directions is to develop progressive methods for finishing gear teeth based on reconstruction of existing universal machines or adding special attachments to them, which can be manufactured and maintained by tool-shops of medium capabilities [4] - [6].

One such method is calibration, in which the teeth are processed by surface plastic deformation, using the property of metals to deform plastically in their cold state [4], [7]. Hardened gear rollers are used as deforming elements, which roll the workpiece with pre-cut teeth. The axes of the machined wheel and the gear rollers are parallel, and the machining is performed with gradual reduction of the center distance between the teeth.

Under the action of the deforming element, the micro-irregularities, resulting from the previous tooth machining are smoothed out, with the metal moving away from the contact point and filling the adjacent recesses. Thus, the size of the micro-roughnesses on the machined surfaces decreases, creating micro-irregularities, qualitatively different from those, resulting from machining by material removal. This method allows to obtain teeth with low roughness and increased ability to retain a continuous oil layer.

Online ISSN 2256-070X
https://doi.org/10.17770/etr2025vol4.8420
© 2025 The Author(s). Published by RTU PRESS.
This is an open access article under the Creative Commons Attribution 4.0 International License.

In calibration there is an opportunity to significantly increase the contact surface, which leads to lower contact stresses and reduced noise when the tooth pair is in operation. The surface metal layers get strengthened and their hardness increases at a certain depth, while the main part of the metal remains with a high impact toughness; residual compressive stresses arise; and, in result, gearwheels with improved strength and operational performance are obtained.

The aim of the present work is to study and model the quality indicators of the teeth of cylindrical gearwheels, machined through calibration in order to substantiate the real possibility for commercial implementation of the calibration method as a method for tooth finishing processing.

II. MATERIALS AND METHODS

The engagement without lateral clearance between the machined gearwheel and the tool in the calibration process is performed along two crossed tangents to the main cylinders of the part and the tool (the engagement lines), one of which starts from the tooth head of the part and passes through the engagement pole to the tooth base, machining one side of the tooth, the driven one. On the reverse side of the tooth, the engagement occurs from the base to the head of the tooth. The sliding motion of the lateral surfaces of the teeth, relative to each other, causes material accumulation (in the direction from the tooth head and base towards the dividing cylinder) on the driven teeth surfaces of the machine part (Fig.1). In result, material compression occurs along the dividing cylinder and, on the reverse side of the tooth, material is removed from the dividing cylinder towards the base and head of the tooth. As a consequence, the outer diameter of the wheel increases.

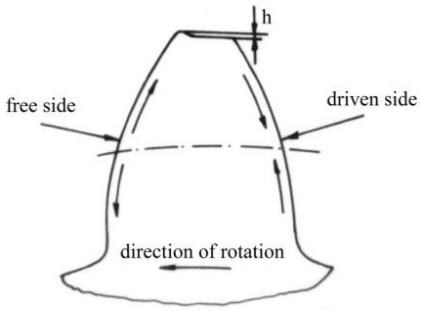

Fig. 1. Material displacement in the process of tooth machining by calibration.

The conditions for implementing the calibration process are related to:

- *The choice of a machine,* which allows: the radial feed of the tool to be limited with great accuracy; synchronous rotation of the calibration gearwheels; a possibility to disengage and center the calibration gearwheels depending on the number of teeth of the workpiece; a possibility to adjust the radial force.
- *The tool material:* with individual for each particular case thermal treatment and accuracy; with high hardness and impact toughness of the working surfaces.
- *The material of the blanks* – the hardness of the workpieces should not be greater than HB 220.

In order to optimize the conditions of machining (to increase productivity, tool durability, and improve the quality of the machined gearwheels) a tool has been proposed and a method for finishing machining by calibration on gear-shaving machines has been implemented by the Department of Mechanical Engineering Equipment and Technologies at the Technical University of Gabrovo.

Experimental studies were conducted by machining 60 gearwheels, made of 41Cr4 steel with a hardness of HRC18, divided into 12 groups of 5, by calibration on a semi-automatic gear-shaving machine 5702B with the following tooth parameters: m = 3mm; z = 52; β_d = 14°04'; b = 25mm.

The tooth parameters were measured before and after processing by calibration:

- to assess the kinematic accuracy – the differential indicators: radial chatter of the gear ring Frr and fluctuation in the base tangent length FVwr;
- to assess the smoothness of operation – the deviation from the tooth profile *ffr;*
- to assess the contact between the teeth - the deviation from the direction of the teeth *Fβr*;
- roughness of the working surfaces;
- surface layer hardness.

The control and measurement of the obtained quality indicators was carried out with: a normometer (with an accuracy of 0.01 mm), a gear tooth measuring machine PFSU 640 (KLINGELBERG - Germany), a TESA Rugosurf 20 profilometer and a "NEQFOT-2" microhardness tester.

The calibrating carbide tools had the following parameters: m = 3 mm; z = 53; accuracy grade - 6 (ENBDS3296), hardened to HRC58...60 and with roughness of the working surfaces Ra = 0,32μm.

The preliminary processing of the teeth before calibration is milling with a worm modular cutter on a 5K310 gear-milling machine.

To establish a rational operating mode, preliminary single-factor experiments were conducted. Based on them, the following were adopted: tool rotation frequency $n = 100\ min^{-1}$, longitudinal feed $V_f = 35\ mm/min$, radial feed $f_p = 0,14;\ 0,04;\ 0,02;\ 0\ mm$ at number of strokes $p = 4$.

III. RESULTS AND DISCUSSION

The obtained results of the measurements, made before (curves 1) and after (curves 2) processing by calibration, are presented graphically in Fig. 2.

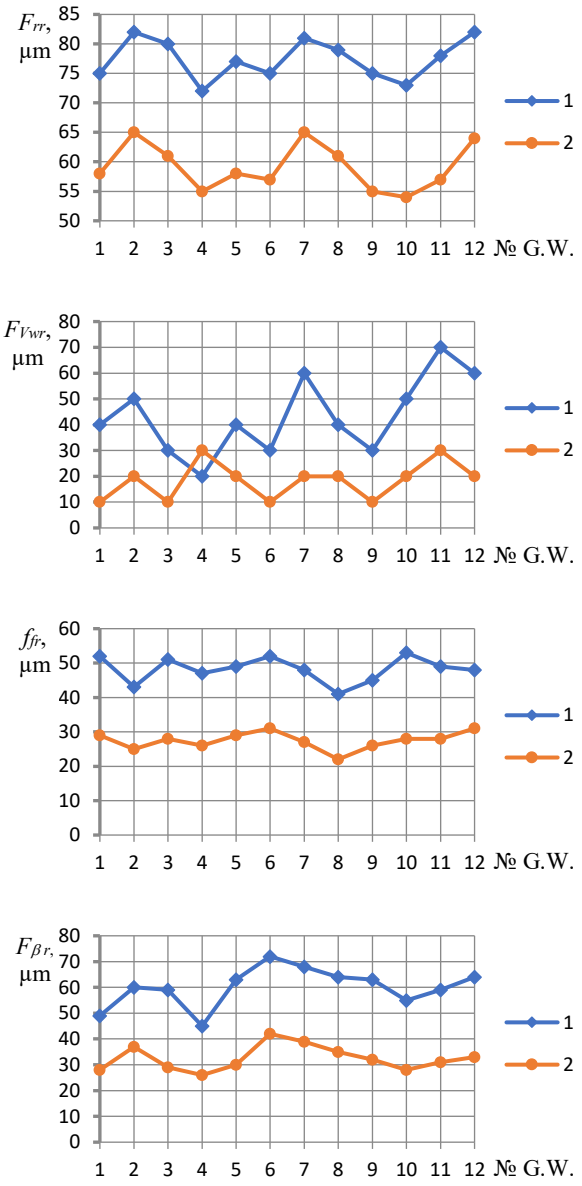

Fig. 2 Results from the experimental studies.

The graphs show that the accuracy of the studied parameters increases by an average of 1.5 to 3 times. To achieve higher accuracy for f_{fr} and $F_{\beta r}$, (Fig. 2), it is necessary to distribute the most of the allowance to the tooth head, since with an increase in f_p, the thickness of the tooth head becomes thinner, which leads to an increase in the deviations f_{fr} and $F_{\beta r}$. If this condition is met, a reduction of f_{fr} and $F_{\beta r}$ from 3 to 6 times can be achieved.

A barrel-like shape is obtained along the direction of the tooth, which is favorable when the axes of the assembled gear train are not parallel. A significant reduction in the roughness is obtained on the lateral surfaces of the teeth (up to $R_a = 0,16$ *µm*, while with shaving the roughness is $R_a = 0,63$ *µm).* The surface hardness of the working surfaces of the teeth also increases, which is favorable for non-heat-treated gearwheels, and subsequent thermal and chemical-thermal treatment results in more uniform phase changes and saturation.

The deformation rate depends on V_f (at a low rate of deformation, the tool acts on the machined surfaces for a longer time and the plastic deformation spreads to a greater depth, making it necessary in practice to work with a higher deformation rate, as this leads to higher productivity).

Productivity increases up to 2 times, since the allowance during calibration is deformed for 3÷4 longitudinal strokes, while in a process of shaving it is removed for 6÷8 strokes.

The durability of the carbide calibrating tools is 6÷8 times greater than the durability of the high-speed steel shavers (the increase in tool durability is explained not only by the carbide design of their teeth, but also by the replacement of the sliding friction during shaving with rolling friction during the process of calibration).

It is not possible to apply a large deformation force when processing teeth by calibration on a shaving semi-automatic machine, as this leads to rapid breakage of the supporting elements of both the mandrel and the machine. Therefore, it is necessary to use four working strokes, setting radial feed for three of them (0,14; 0,04; 0,02 mm/stroke), and the fourth stroke performed without radial feed in order to deform the allowance, remaining from the elastic deformations in the technological system.

The company "Troymash" AD Dryanovo owns a thread-rolling machine UPW-25 x 100 (Germany), which can also be used as a tooth-calibrating one.

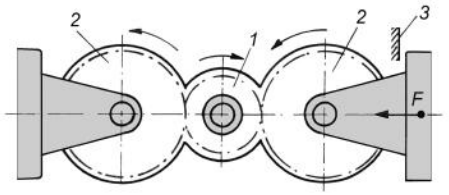

Fig. 3. Scheme of conducting the experimental research.

This machine allows to carry out finishing machining: with two calibrating synchronously rotating gearwheels during radial feed of one gearwheel to the other; with options for sensing and limiting the radial feed of the tool; and with an axial feed of the workpiece for machining the tooth profile across the entire width (Fig. 3). The machine is with a stepless control of the rotation frequency ($50 \div 200 min^{-1}$) and radial force ($\leq 250.10^3$N), and can be switched on to a semi-automatic or automatic cycle of operation with an accuracy of the center distance $\pm 4.10^{-3}$mm.

Experimental studies were carried out on this machine to determine the dependencies between the input values of the different accuracy parameters before calibration, i.e., after tooth milling, and their values at the output of

the processes of calibration and heat treatment. Planetary gearwheels from a planetary reducer for electric hoists, made of C45 steel, with a number of teeth $z = 49$ and module $m = 2,25$ *mm*, were used as objects for research. The accuracy of the gearwheels before and after calibration was evaluated according to the same indicators specified above.

The processing of the experimental data involves two stages. The first stage (preliminary statistical analysis) consists in checking the homogeneity of the samples and the hypothesis of normality of distribution of the studied parameters. The second stage involves finding the mathematical description for the change in gearwheel accuracy after processing their teeth by calibration and heat treatment. Such a description is a polynomial (linear or nonlinear), establishing the relationship between the input and output values of the accuracy parameters. The method of correlation analysis was used to find the model.

The regression model allows to perform a complete statistical analysis of the empirical regression equation. For all studied accuracy parameters, it is established that the correlation between the output and input values is a linear one. Then the regression equation has the form:

$$y = a + bX \qquad (1)$$

Table 1 shows the results, concerning the individual accuracy indicators, as well as the regression equations after calibration for input factors of tooth milling.

TABLE 1 REGRESSION MODELS AND STATISTICAL ANALYSIS AFTER CALIBRATION

Parameter of accuracy	$\bar{X}$	$\bar{Y}$	S_x^2	S_y^2	r_{xy}	Equation of regression
F_{rr}	0,1122	0,0768	0,00148	0,00120	0,845	$\hat{Y}$=0,0086+0,7615X
F_{Vwr}	0,0288	0,0272	0,00249	0,00111	0,766	$\hat{Y}$=0,0125+0,5119X
f_{fr}	0,0577	0,0364	0,00017	0,00002	0,466	$\hat{Y}$=0,0261+0,1799X
$F_{\beta r}$	0,0553	0,0335	0,00017	0,00010	0,630	$\hat{Y}$=0,0067+0,4834X

The regression equations determine the magnitude of the error in the output depending on the error in the input. The coefficient b in these equations shows what part of the error at the input is transferred to the output, and the free member a – the magnitude of the error, obtained during the execution of the given operation. A criterion for the strength of the relationship between the same accuracy parameters before and after calibration is the coefficient of correlation r_{xy}.

The regression analysis shows that the free member in the regression equations for the parameters F_{rr}, F_{Vwr}, f_{fr} and $F_{\beta r}$ is insignificant, i.e., the error, obtained during the execution of the calibration operation is insignificant and can be ignored. Since in all equations the coefficient b is in the range $0<b<1$, from here it follows that for the studied parameters partial correction of the output error occurs. The correction is the smallest for the parameter F_{Vwr}, and the largest – for f_{fr}. In the latter case, an error occurs during the execution of the operation itself, equal to 0,026 mm.

As a result of the plastic deformation, hardening of the working surfaces of the teeth occurs (at a depth of up to 0,05 mm), which results in strengthening the material and increasing its hardness (up to 70.10^8 N/m^2). Greater hardness is obtained on the driven side, where the material is compressed against the dividing cylinder of the gearwheel.

The roughness of the working surfaces of the teeth reaches $R_a = 0,16\mu m$ and is an indicator of the noise and efficiency of the gear trains.

The experiments conducted showed the real possibility to implement finishing machining of gearwheels by cold plastic calibration in manufacturing.

During the heat treatment of the gearwheels after the calibration operation, an increase in the values of the individual parameters is observed, which is also reflected in the regression equations shown in Table 2.

The studies show that after heat treatment the actual dispersion field expands for all studied parameters of accuracy.

TABLE 2 REGRESSION MODELS AND STATISTICAL ANALYSIS AFTER HEAT TREATMENT

Parameter of accuracy	$\bar{X}$	$\bar{Y}$	S_x^2	S_y^2	r_{xy}	Equation of regression
F_{rr}	0,0768	0,0863	0,00120	0,00125	0,981	$\hat{Y}$=0,0094+1,001X
F_{Vwr}	0,0272	0,0505	0,00111	0,00133	0,923	$\hat{Y}$=0,0206+1,101X
f_{fr}	0,0364	0,0413	0,00016	0,00017	0,948	$\hat{Y}$=0,0086+0,9786X
$F_{\beta r}$	0,0335	0,0452	0,0015	0,00145	0,933	$\hat{Y}$=0,0076+1,122X

IV. CONCLUSION

A relationship has been established between the values of the accuracy parameters of the teeth of cylindrical gearwheels before and after processing by calibration and subsequent heat treatment, with the magnitude of all studied accuracy parameters being largely determined by their input values. The results of the research confirm the existence of a correlation between the same accuracy parameters at the input and output when processing by calibration and subsequent heat treatment.

After machining by calibration, the parameters of accuracy for the gear teeth are improved, except for the length of the base tangent.

The obtained regression models allow the tolerance of the accuracy parameters to be distributed between the mechanical and thermal processing and thus to avert waste.

The roughness of the calibrated tooth surfaces is improved by 3 to 6 times.

The hardness of the surface layer increases 1,5 times after calibration, and 2,1 times after subjecting the workpieces to calibration and heat treatment (with the existing technology - shaving and heat treatment by high-

frequency current (HFC) - the hardness of the surface layer increases 1,5 times).

The research shows that calibration can also be applied to finishing the teeth of cylindrical gearwheels.

ACKNOWLEDGMENTS

This research is supported by the Scientific Research Fund of the Technical University of Gabrovo, project "Innovative Technologies and Instrumentation in Mechanical Engineering".

REFERENCES

[1] D. Petrova, B. Vlahova, A. Lengerov, T. Zlateva-Petkova. Improvement of Constructive-Technological Approaches Reducing Innovative Obsolescence of Industrial Technologies in the Context of Industry 4.0, Vide. Tehnologija. Resursi - Environment, Technology, Resources, Proceeding of the 14th International Scientific and Practical Conference, 2023, Volume I, pp. 180-186, Print ISSN 1691-5402, Online ISSN 2256-070X, DOI: https://doi.org/10.17770/etr2023vol1.7238 https://www.scopus.com/authid/detail.uri?authorId=56323816400.

[2] D. Petrova, B. Vlahova, A. Lengerov, T. Zlateva-Petkova. Study of the State of Innovation Development and Obsolescence in the Republic of Bulgaria of Companies from the Mechanical Engineering Sector, Vide. Tehnologija. Resursi - Environment, Technology, Resources, Proceeding of the 14th International Scientific and Practical Conference 2023, Volume I, pp. 187-194, Print ISSN 1691-5402, Online ISSN 2256-070X, DOI: https://doi.org/10.17770/etr2023vol1.7239 https://www.scopus.com/authid/detail.uri?authorId=56323816400

[3] N. Nikolova. Industry 4.0 - development and consequences for sustainable development of Bulgaria, 13th International Scientific and Practical Conference "Environment. Technology. Resources", June 17-18, pp. 245-251, 2021, Academy of Technologies, Rezekne, Latvia,Volume III, ISSN 1691-5402, ISSN 2256-070X.

[4] B. Matev, P. Kunov, Installation for modeling the process of surface plastic deformation (SPD) of gearwheel teeth. International scientific conference, VMEI – Gabrovo, 1990.

[5] Handbook of the Machining Technologist", part 2, State Publishing House "Technika", Sofia, 1990.

[6] Production of gearwheels. Handbook. Under the general editorship of Taits B.A. Moscow, Mashinostroenie Publishing House, 1990.

[7] T. Kuzmanov, Hr. Metev. Technology of mechanical engineering, parts 2,3. Publishing house "EX-PRESS" Ltd. - Gabrovo, 2015, 2016.

Environment. Technology. Resources. Rezekne, Latvia
Proceedings of the 16th International Scientific and Practical Conference. 2025. Volume IV, 151-155

Research of the Surface Roughness During Hard Turning of 42CrMoS4 Steel with a Quick-Change Tool Holder

Georgi Karlovski
Department "Mechanical Engineering and Instrumentation"
Technical University of Gabrovo
Gabrovo, Bulgaria
g_karlovsky@abv.bg

Petko Naydenov
Department of Management
Technical University of Gabrovo
Gabrovo, Bulgaria
petkonaydenov@abv.bg

***Abstract*— This paper presents an analysis of the surface roughness during turning of hardened 42CrMoS4 steel using a quick-change tool holder with innovative design. The experiments used a Swiss-type CNC lathe - GOODWAY SW-20. The process was performed at cutting speed of 130 to 170 m/min, feed of 0.12 to 0.18 mm/tur and cutting depth of 1.5mm. Based on the results obtained, a mathematical model was developed, the graphic interpretation of which is presented in two-dimensional and three-dimensional coordinate systems. The mathematical model was used in the dispersion analysis to determine the influence of speed and feed during turning on the roughness of the machined surface. Graphical relationships are presented for the influence of the controlling factors on roughness.**

Keywords—hardened alloy steels, regression analysis, Swiss type lathes.

I. INTRODUCTION

When solving quality problems, it is important to ensure the accuracy and stability of technological processes, especially those parameters that have a significant functional impact on the performance of manufactured products [1], [2], [3]. Perhaps the most significant event that almost completely changed the world of tools is associated with the emergence and development of powder metallurgy. It created the technology for the production of metal-ceramic hard alloy - carbide [4], [5], [6]. Over the next few decades, a wave of innovations was observed that improved the performance characteristics of carbide tools and expanded their range of applications [7], [8], [9]. Most of the key technologies in the field have already existed for several decades, which is expected to lead to a certain degree of standardization in some product groups and markets. However, the tool manufacturing industry manages to maintain a high level of innovation in most of its areas, which allows for increased competitiveness through savings, increased productivity and capacity, and in some cases, improved quality. In this regard, in recent years, various modifications of quick-change holders have been designed and implemented in production, which have significantly improved the conditions for turning and increased the quality of the machined surfaces [2], [3].

Swiss-type CNC lathes are widely used in various sectors of the industry due to their many advantages over other CNC machines and turning centers. They are automatic lathes with a movable headstock and a guide bushing, designed for precise high-performance machining of complex small-sized parts with a short cycle of the technological process, obtained from bar material in conditions of high-volume production. Their application is especially effective in machining short and thin parts due to their specific design, which allows the cutting tool to perform machining in close proximity to the guide bushing [10], [11]. In this regard, the aim of the present study is to investigate, model and analyze the influence of the elements of the cutting mode (speed and feed) [3], [12], [13] on the roughness of the machined surfaces when turning short axisymmetric parts made of hardened steel 42CrMoS4 using a new design of a quick-change toolholder.

II. MATERIALS AND METHODS

Experimental studies on the influence of the type of tool holder on the roughness of the machined surfaces were conducted when manufacturing parts from alloy steel 42CrMoS4 (1.7227) – Fig. 1 with a hardness of 33-35 HRC and a chemical composition according to Table 1[14,15].

Online ISSN 2256-070X
https://doi.org/10.17770/etr2025vol4.8437
© 2025 The Author(s). Published by RTU PRESS.
This is an open access article under the Creative Commons Attribution 4.0 International License.

TABLE 1 CHEMICAL COMPOSITION OF STEEL 42CRMOS4, %

C	Si	Mn	Ni	Cr	Mo	P	S
0.38-0.45	0.17-0.37	0.50-0.80	≤0.3	0.9-1.2	0.15-0.25	≤0.035	≤0.035

The turning process was carried out on a Swiss CNC lathe, model GOODWAY SW-20. – Fig. 2. In the experiments, an innovative design of a quick-change holder type NX02-K-SV-HCL11– Fig. 3[2] was used, allowing the delivery of coolant directly to the cutting zone, thus significantly reducing local heating at the tip of the cutting tool and improving the chip removal process [16]. In the research process, a carbide insert type VCMT11.03.02 was used.

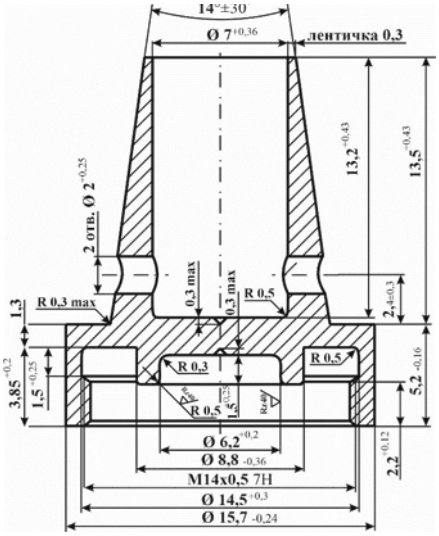

Fig.1. Detail drawing.

Fig. 2. GOODWAY SW-20 system[3], [13]

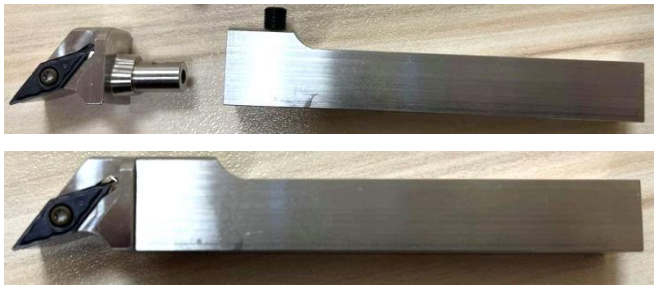

Fig.3. Quick-change holder.

The used quick-change tool holder ensures constant tool geometry:

- front angle – γ= -5°;
- rear angle – α = 0.7°;
- main setting angle – kr = 93°;
- auxiliary setting angle - kr¹ = 32°;
- tool tip radius - rε.= 0.2mm.

The turning process was carried out with the following parameters:

- cutting speed Vc = 130÷170 m/min;
- feed f = 0.12÷0.18 mm/turn;
- cutting depth ap = 1.5mm.

When assessing the roughness, a control size Ø15.7+0.2 was used – Fig. 1, on the surface of the machined parts. The measurements were made with a TESA Rugosurf 20 profilometer according to the methodology described in [17], [16]. The device is compatible with the following standards and regulations: DIN 4762, DIN 4768, DIN 4771, DIN 4775 and DIN 4766-1, ISO 4287; ISO 12085 (BDS 728-79).

In practice, various methods are used for the formation of mathematical models and optimization of technological processes [18], [4], [5]. In this particular case, the regression analysis method was used. When building the mathematical model based on preliminary experiments and literature data, the cutting speed (Vc, m/min) – X1, and the feed rate (f, mm/tur) – X2 were selected as input variables, and the roughness of the machined surfaces – Y1(Ra, μm) was studied as a target function.

The areas of variation of the factors are shown in Table 2.

III. RESULTS AND DISCUSSIONS

The roughness values in – table 3 were determined when turning batches of 550 parts, with measurements made every 50 pieces. The graphical interpretation is presented in Fig. 4. The statistical processing of the experimental results was carried out in accordance with the methodology set out in [18], [5], in the following sequence: ¬ determination of the model coefficients; ¬ determination of the significance of the regression coefficients using Student's t-test ¬ determination of the multiple correlation coefficient R^2 ¬ determination of the significance of multiple coefficients using the Fisher criterion. The results of the study were processed with the QstatLab software and a mathematical model – 1 was obtained, describing with

high accuracy the relationship between the roughness and the cutting mode (Vc m/min and f mm/tur).

TABLE 2 FACTORS AREAS OF VARIATION

Factor levels	X_1,(Vc) m/min	X_2, (f)mm/tur	Coded value
$X_{i0} + \Delta X_i$	170	0,18	+1
X_{i0}	150	0,15	0
$X_{i0} - \Delta X_i$	130	0,12	-1

The graphical interpretation of the model is shown in Figure 5.

$$У=3,4395556+0,30916667X_1+0,147X_2 \quad (1)$$

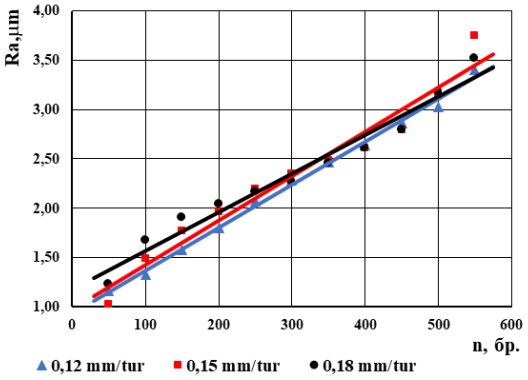

a

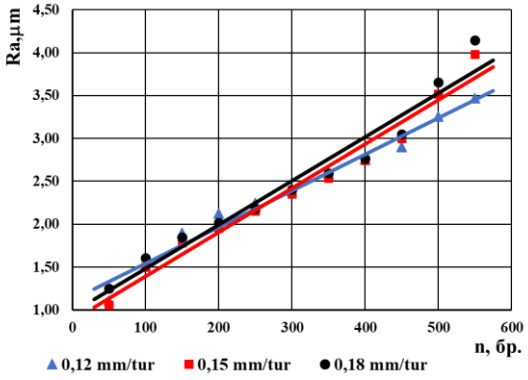

b

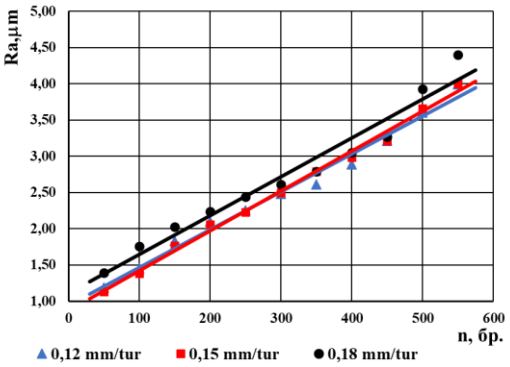

c

Fig.4. Roughness changes on a 550 pcs. batch and feed rate 0,12; 0,15 и 0,18 mm/tur and cutting speed: a - 130 m/min; б - 150 m/min и в - 170 m/min.

TABLE 3. EXPERIMENT PLAN

№	X_0	X_1	X_2	$X_1 X_2$	X_1^2	X_2^2	Y_1
1	+1	+1	+1	+1	+1	+1	3,927
2	+1	-1	+1	-1	+1	+1	3,182
3	+1	+1	-1	-1	+1	+1	3,605
4	+1	-1	-1	+1	+1	+1	3,022
5	+1	+1	0	0	+1	0	3,658
6	+1	-1	0	0	+1	0	3,131
7	+1	0	+1	0	0	+1	3,654
8	+1	0	-1	0	0	+1	3,254
9	+1	0	0	0	0	0	3,523

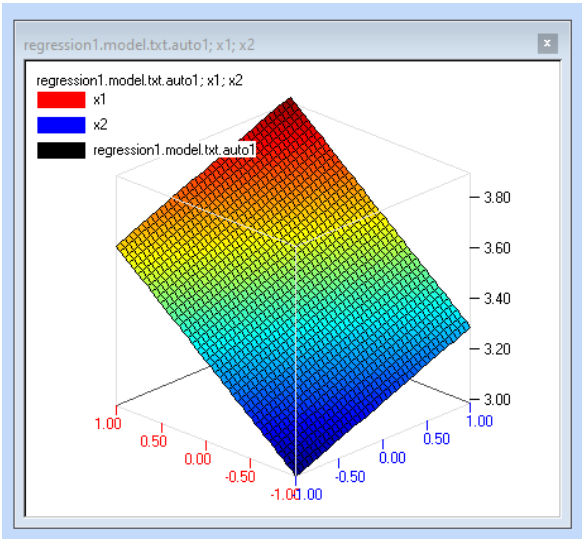

a

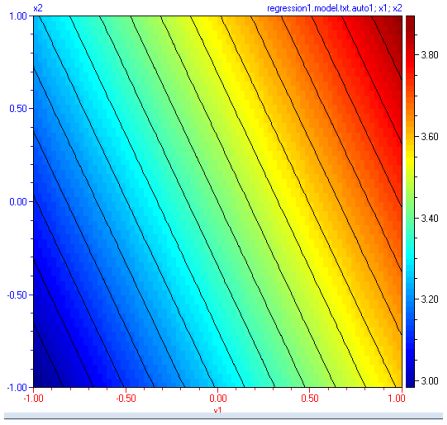

b

Fig.5.Graphical presentation of the mathematical model
a – tridimensional; b – bidimensional.

Based on the obtained model, an analysis of variance (ANOVA) was performed to determine the influence of the controlling factors on the roughness of the machined surface.

A graphical interpretation of this influence is shown on Figure 6.

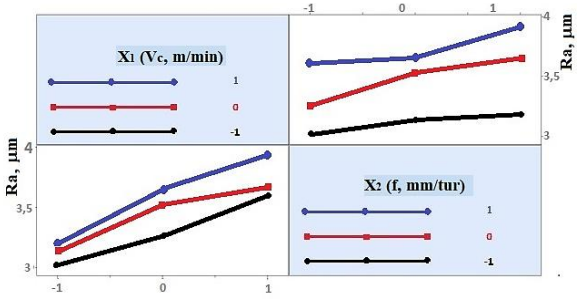

Fig.6. Influence of the factors cutting speed – Vc and feed rate -f to the roughness of the surface.

IV. CONCLUSION

From the studies conducted and the results obtained, the following important conclusions can be formulated:

1. The change in roughness during hard turning of short rotary parts was monitored depending on the cutting speed - Vc = 130÷170 m/min, and the feed - f = 0.12÷0.18 mm/tur, at a constant cutting depth - ap = 1.5mm.

2. Graphical dependences for the change in roughness - Ra, µm, as a function of the cutting speed and feed, for batches of parts from 50 to 550 pieces, were developed.

3. It has been proven that with an increase in the number of processed parts from 50 to 550, the roughness of the size Ø15.7+0.2 increases by 3.5÷4.5 µm.

4. The cutting speed has a more significant influence on the roughness. With its increase from 130 to 170 m/min, the roughness of the machined surfaces when processing batches of 550 parts increases by approximately 1 µm.

5. It has been proven that with a roughness limit of Ra=3.0µm with a cutting speed of 130 m/min, up to 450 parts can be processed regardless of the feed. With an increase in the cutting speed to 170 m/min, while maintaining the roughness requirement, up to 400 parts can be processed.

6. Based on the experimental results, a mathematical model was compiled for the influence of the factors cutting speed and feed on the roughness of the machined surfaces.

7. Graphical dependencies in two- and three-dimensional coordinates of the compiled mathematical model were developed.

8. A dispersion analysis of the mathematical models was performed and graphical dependences for roughness as a function of cutting speed and feed were presented.

REFERENCES

[1] D. Petrova, B. Vlahova, A. Lengerov, Tz. Zlateva-Petkova, “Study of the State of Innovation Development and Obsolescence in the Republic of Bulgaria of Companies from the Mechanical Engineering Sector”, presented at the 14th International Scientific and Practical Conference on Environment, Technology, Resources, ETR 2023, Rezekne, Latvia, June, 2023, Volume I , pp. 187–194.

[2] G. Karlovski, “A System for Quick-change Tool Mounting”, Automation of discrete production, Vol. 5, Sofia, 2023, pp.82÷85.

[3] G. Karlovski, “Application for quick-change holders as a way to increase efficiency in the production of workpieces with CNC machines”, Automation of discrete production, Vol. 5, Sofia, 2023, pp. 86÷90.

[4] I. Mitev, “Determining the diffusion coefficient in simultaneous saturation with boron and carbon austenite alloyed with cooper in powder metallurgy structural materials”, presented at AIP, vol. 2980, 2024, p.060016-1÷060016-7.

[5] I, Mitev, “Optimizing the quantity of liquid phase at the sintering of powder construction materials from system Fe-Cu-Sn” presented at AIP, vol. 2980, 2024, p.060017-1÷060017-7.

[6] I. Miteva, I.Vinev, I.Mitev, “Features of Alloying Matrix of Water-dispersed Iron Powders”, presented at the 13th International Scientific and Practical Conference on Environment, Technology, Resources, ETR 2021, Rezekne, Latvia, Volume 3, 2021, pp.226÷231.

[7] D. Petrova, “Innovative Obsolescence in Mechanical Engineering and Singleness of Indicators”, presented at the 15th International Scientific and Practical Conference on Environment, Technology, Resources, ETR 2024, Rezekne, June 2024, Vol. 3, pp 221 – 224.

[8] D. Petrova, B. Vlahova, A. Lengerov,Tz. Zlateva-Petkova, “Improvement of Constructive-Technological Approaches Reducing Innovative Obsolescence of Industrial Technologies in the Context of Industry 4.0”, presented at the 14th International Scientific and Practical Conference on Environment, Technology, Resources, ETR 2023, Rezekne, Latvia, June, 2023, Volume I, pp. 180–186.

[9] D. Petrova, N. Nikolova, A. Lengerov, “Modeling business process reengineering in the digital era of industry 4.0”, presented at the 11th International Scientific Conference “TechSys 2022” – Engineering, Technologies and Systems, 2022, pp. 070013-1 - 070013-7.

[10] T. Kuzmanov, K. Krumov, Technical preparation of production, EKS-PRESS, Gabrovo, 2013.

[11] Ugrinov P. CNC metal cutting machines. S., "Avangard Prima" Publishing House, 2019.

[12] G. Viktors, E. Gerins, J. Rudzitis, A. Kromanis. "The Effect of the Cutting Parameters on the Machined Surface Roughness", Solid State Phenomena, Vol. 260, 2017, pp. 219-226.

[13] G. Karlovski et al., "Selection of Instrumentation Based on Statistical Analysis",presented at the 32nd International Scientific Symposium "Metrology and Metrology Assurance", MMA 2022, Sozopol, 7-11 September 2022.

[14] M. Nabil, O. Taha, T. Elbitar, I. El Mahallawi. "Thermomechanical processing of 42CrMoS4 steel." Presented at International heat Treatment and Surface Engineering - IHSE 2010. Vol. 4 (2), pp. 87-92.

[15] M. Saez-de-Buruaga, L. Gainza, P. Aristimuno, D. Soler, G. Ortiz-de-Zarate, O. Aizpuru, R. Mielgo, P.J. Arrazola. "FEM modeling of hard turning 42CrMoS4 steel." Presented at the 17th CIRP Conference on Modelling of Machining Operations. 82 (2019), pp. 77–82.

[16] I. Mitev, S. Tsenkulovski, "Local Processing of Non-Metal Materials with Concentrated Energy Flow", presented at the 14th International Scientific and Practical Conference on Environment, Technology, Resources, ETR 2023, Rezekne, Latvia, June, 2023, Volume 3, pp.183÷186.

[17] S. Tsenkulovski, I. Mitev "Influence of the Parameters of the Lasser marking process of the depth of penetration in layer-reinforced composites", presented at the 15th ISPC "Environment Technology Resources", V.Turnovo, Bulgaria, 27 and 28 06.2024, Vol. 3, pp 319-324.

[18] I. Alexandrova, Fundamentals of engineering research. Vasil Aprilov University Publishing House, Gabrovo, 2003.

Environment. Technology. Resources. Rezekne, Latvia
Proceedings of the 16th International Scientific and Practical Conference. 2025 Volume IV, 157-160

Structures for Woven-Like Knitting Fabrics Made on Circular Knitting Machines

Desislava Kovacheva
Department of Industrial Design and Textile Engineering
Technical university of Gabrovo
Gabrovo, Bulgaria
dkovacheva@tugab.bg

Borislav Stoyanov
Department of Industrial Design and Textile Engineering
Technical university of Gabrovo
Gabrovo, Bulgaria
b.stoyanov@tugab.bg

Krasimir Drumev
Department of Industrial Design and Textile Engineering
Technical university of Gabrovo
Gabrovo, Bulgaria
kid@tugab.bg

Ivelin Banev
Department of Industrial Design and Textile Engineering
Technical university of Gabrovo
Gabrovo, Bulgaria
banev830202@gmail.com

Petar Nikolov
Department of Industrial Design and Textile Engineering
Technical university of Gabrovo
Gabrovo, Bulgaria
pet_nik1979@abv.bg

***Abstract* — In this article, options for woven-like knitting structures on a crochet basis are considered worked on circular knitting machines. Technical and technological parameters for their production are described. Nine variants to achieve knitting on type of a double-faced and an interlocking basis have been developed. In both groups, sub-variants with the presence or absence of press elements are proposed. The cylinder and disc rows with two types of needles – short and long are presented in tabular form. The all structures were successfully knitted on the circular knitting machine.**

Keywords* — *low elasticity knitting, round knitted fabric, woven-like knitting structure.

I. INTRODUCTION

Knitted fabrics made with a single-face single-thread knit on linear or circular knitting machines with a single needle bed are easily deformed (stretched) in width and length. This means that the stitches have great freedom of movement. The bending resistance of the thread that formed the stitch is negligible and a large slippage is possible at the contact points where the stitches are joined. In longitudinal stretching, the loops lengthen due to the narrowing of their arcs, and in transverse stretching, the loops widen due to the shortening of their hips [1]-[3].

Single-thread double-face knits can have a completely identical or different appearance on both sides. This depends on the combination of the front and back stitches when knitting. The two types of stitches are arranged in separate stitch columns and in the knitting one or more front stitches alternate with one or more back stitches. Such knits have a high compressibility in width, which is why in a relaxed state two adjacent front stitches (when alternating one front stitch with one back stitch) touch and cover the back stitch knitted between them. As a result, only the front stitches remain visible on both sides of the knitting, with the back stitches being hidden between them. However, when the knitting is stretched, the back stitches between the front stitches are also revealed [4]-[6].

In knitted fabrics made in a smooth double-faced single-thread knit on double-row circular knitting machines, the number of stitches along the width of the fabric is doubled. As a result, a thread of a correspondingly longer length is incorporated into them, which allows for greater stretching of the fabric and from there – of the product made from this fabric. In order to knit the stitches easily, the following general rule must be observed when pulling and shaping them - when a needle begins to push the thread caught by its hook through the old stitch, the opposite needle adjacent to it must already have pushed and pulled its stitch. By following this rule, the goal is to prevent two or more needles from simultaneously being in the position of threading and pulling the thread, because this would make knitting difficult on the one hand, and on the other hand, the thread itself is subjected to tension and friction in a couple of needles, which leads to increased fragility during knitting.

Online ISSN 2256-070X
https://doi.org/10.17770/etr2025vol4.8421
© 2025 The Author(s). Published by RTU PRESS.
This is an open access article under the Creative Commons Attribution 4.0 International License.

Knitting in which the stitches are drawn in and out of the two rows of needles alternately is called sequential knitting. Sequential knitting without welding multiple needles in simultaneous knitting is only done on coarser machines, where the needles are spaced farther apart [7], [8]. As a rule, this knitting principle is applied on linear knitting machines (with a maximum fineness class of E12).

On finer machines, such as modern large-diameter circular knitting machines (with fineness class E16 - E32), sequential knitting is not suitable, since many needles will always be overlapped during the knitting process. As a result, uneven knitting, thread breakage, etc. will result. Therefore, on finer machines, knitting from both rows of needles is done in the so-called distributive way. Knitting in this way is done twice. First, the needles from one row knit their stitches, while the needles from the other row only catch the thread. After a few stitches from the first row of needles have been knitted, the needles from the second row thread and knit their stitches. Since a thread is needed to knit these stitches, and the thread guide has already passed, the thread is taken from the opposite previously knitted stitches, which are pulled out significantly longer for this purpose. In this way, the stitches on both rows of needles are aligned, the thread is distributed equally between them and the knitting becomes more uniform. With this knitting, much denser knits can be obtained than with sequential knitting.

There are two possible needle arrangements on a circular knitting machine:

1) elastic, sometimes called in practice "*crochet*" – when a cylinder needle lies in front of a rib on the disc or opposite – „rib against needle";

2) interlock – when the mutual arrangement of the cylinder and the disc is such that their needle distribution is "needle against needle".

Interlock circular knitting machines are loaded with short and long cylinder needles and with short and long disc /rip/ needles, the normal loading being interlock, i.e. needle against needle. In addition, rip needles /short and long/ can be with low and high heels. In this case, all the channels of the cylinder are the same and the loading is unlimited, while the disc long needles are through one, i.e. the standard loading is "short-long".

Despite this specificity, which largely limits the sampling possibilities, the loop formation process is the same as in other circular knitting machines. It is carried out by both rows of needles and, as already mentioned, the knitting principle is distributive.

To reduce the stretchability of double-faced single-thread knits, it is often necessary to exclude needles in one or both needle beds. The knitted fabrics thus obtained have reduced elasticity and successfully replace a number of woven fabrics.

The term "fabric-like knits" was originally used for plain interlock fabrics made of wool, later it was used for double-face knits with single-face rows, for double pique, for single pique and "texi-pique" structures made of any material suitable for outerwear [9]. The term is also used for colored double relief jacquard and "cloquet" type fabrics. The general name "fabric-like knits" is applicable to cross-knit fabrics made on a double-face or interlock basis, the construction of which is designed to reduce the natural extensibility of the structure [10].

Knitted fabrics for outerwear and sportswear are of particular interest. The development of this part of knitwear production is determined by the following factors: favourable loop structure, properties of the processed material, modern technical solutions in dyeing and finishing, high productivity and small installation area, leading to a small number and low capital investment, expanded sampling capabilities of modern circular knitting machines, etc.

With the mass introduction of high-performance modern circular knitting machines into knitwear production, the question of the optimal use of synthetic and natural raw materials, i.e. their appropriate combination both in share participation and in suitable knitted structures, is relevant. Double-row circular knitting machines have a wide range of options for manufacturing two-component two-layer circular knitted fabrics in fabric-like knits. In two-layer circular knitted fabrics, the inner layer is made of cotton and cotton-type yarns, and the outer layer is made of synthetic textured silks. The fabrics produced by this technology have extremely high hygiene and performance indicators. This group of knits is called fabric-like, due to the alternation of single-face and double-face rows, in which some of the stitches are extended and provide stability in the direction of the stitch column, and the presence of underlays - in the stitch row. The use of synthetic silks also provides good dimensional stability with appropriate finishing.

Characteristic features of these settings are the relatively high material consumption (220 – 300 g/m^2) and residual shrinkage along the stitch column (e.g. up to 12% for PA-s). The increased specific area density is primarily due to the lower classes machines on which these settings are worked (E18 and E20) on the one hand, and the linear density of the raw materials used – cotton 20*tex* and 25*tex*. The high residual shrinkage depends in principle on two factors: the tendency of the hips of the press stitches to open and deform the stitches supporting them and the heat setting of the synthetic component. It should be known that the polyester component is fixed better than the polyamide one.

The aim of this article is to present the possibilities for obtaining some fabric-like knits on a crochet basis, made on circular knitting machines. In this way, it is possible to optimally select an option for the production of knitted fabric according to the specifics of its purpose.

II. MATERIALS AND METHODS

Fig. 1 and Fig. 2 show relatively mass-produced two-layer fabrics in a fabric-like knit on a double-faced base with and without fang elements and alternative knitting of the rip needles. The thread feeding schedule is: the odd systems (first and third) knit with cotton (P) 100%, and the

even ones (second and fourth) – with textured polyamide silk (PA-s).

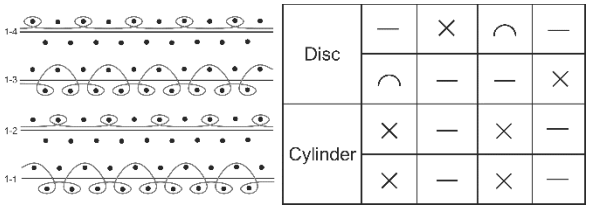

Fig. 1. Fabric-like knit on a double-faced base.

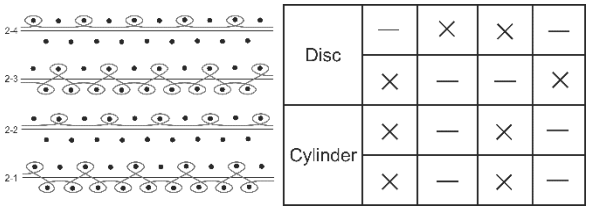

Fig. 2. Fabric-like knit on a double-faced base with fang elements.

Fabric-like knits, in addition to the property of reduced stretchability, also allow for the placement of materials in different planes of the fabric. The so-called two- and more layered effect is obtained. This is due to the presence of single-face and double-face stitch rows, in which the material with a higher linear density is knitted in single-face rows. This specificity of the structure determines a significant improvement in the physiological hygienic qualities that are crucial for sports products. There are two main groups of fabric-like knits: on a double-face crochet base and on a double-face interlock base. Each of these groups has numerous derivatives depending on the ratio of single-face and double-face rows in the repeat, the sequence of knitting the needles and the presence of fang elements. Variation with these parameters affects the performance of the knitted fabric. Taking these influences into account, the following knitting structures were selected for experimentation:

A. On a double-faced basis:

1) with press elements

a) with successively alternating double-faced one-sided half-thinned on the reverse side stitch rows and single-faced reverse stitch rows with successive knitting of the disc needles – Fig. 1.;

b) with successively alternating double-faced one-sided half-thinned stitch rows with alternative knitting of the disc needles – Fig. 2.;

2) without press element:

a) with successively alternating double-faced one-sided half-thinned on the reverse side stitch rows with alternative knitting of the disc needles – Fig. 3.;

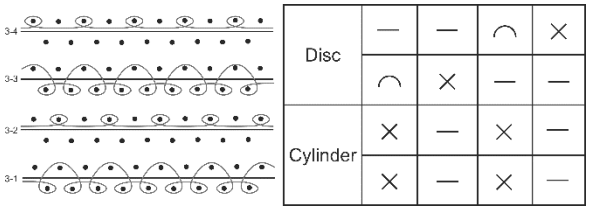

Fig. 3. Fabric-like knit with press elements.

b) with successively alternating double-faced one-sided half-thinned on the reverse side stitch rows and single-faced reverse stitch rows with successive knitting on the disc needles – Fig. 4 and Fig. 5;

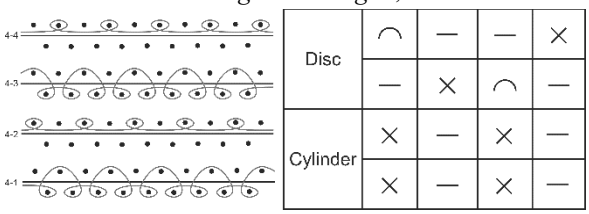

Fig. 4. Fabric-like knit with press elements.

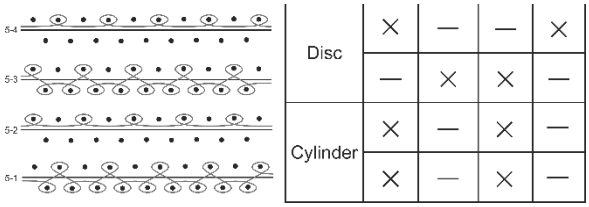

Fig. 5. Fabric-like knit with press elements.

B. On an interlock basis

1) with press elements

a) with alternating interlock rows, semi-raised single-faced reverse rows and one-sided press needles – Fig. 6;

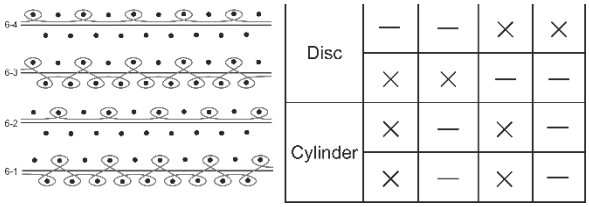

Fig. 6. Fabric-like knit on interlock basis with press elements.

b) with alternating interlock rows, semi-sparse single-faced reverse rows and single-sided press interlock rows with sequential knitting of the disc needles – Fig. 7;

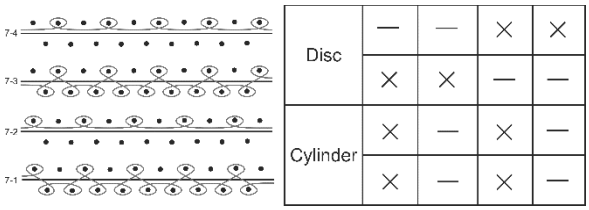

Fig. 7. Fabric-like knit on interlock basis with press elements.

2) without press elements:

a) with alternating interlock rows and half-thinned single-face reverse rows with sequential knitting of the disc needles – Fig. 8;

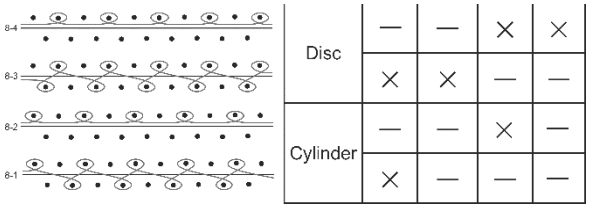

Fig. 8. Fabric-like knit on interlock basis without press elements.

b) alternating two interlock rows and single-faced, reverse, semi-spaced rows – Fig. 9.

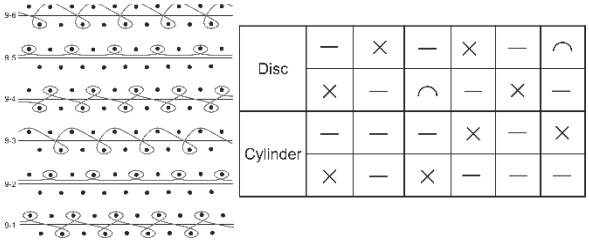

Fig. 9. Fabric-like knit on interlock basis without press elements.

It should be noted that the design of the structural parameters of fabric-like knits, based primarily on geometric models, is inapplicable to these multilayer composite knits. The main reason for this is the simply interaction between the elements of the structure, which determines their shape and mutual arrangement in the repeat.

III. Results and Discussion

The knitted structures shown in Fig. 1 – Fig. 9 were successfully knitted on the circular knitting machine "Multikarat" E20, 30", 48f. Several clarifications should be made for the listed knits. The selected technological equipment allows for easy and convenient sampling, especially when choosing cylinder needles. They can be selected in any order due to the presence of additional selection levers and selectors in the appropriate spacing. The most convenient in this case is the sequential loading of the selectors. In addition, the needles can be raised (working or knitting position), half-raised (press or fan position) or not work. A combination with the capabilities of the selectors and the functions of the individual system is also possible (e.g. conditionally odd ones to knit, and even ones to fang, or in another order). In tabular form, the figures are presented with the cylinder and disk rows with two types of needles – short and long, respectively cylinder and disc. This is the standard arrangement in most circular knitting machines. Regarding the needle arrangement – crochet and interlock: all machines, except for strictly interlock ones, are usually fixed in crochet arrangement. In this position, they can produce both types of knits. This is because the transfer from one needle arrangement to another is associated with precise machine centering, especially when increasing the fineness of the machine.

Acknowledgments

This work was supported by the project НИП2025-11 of Technical university of Gabrovo funded by the Scientific Research Fund.

This research was funded by the European Regional Development Fund under the Operational Program "Scientific Research, Innovation and Digitization for Smart Transformation 2021-2027", Project CoC "Smart Mechatronics, Eco- and Energy Saving Systems and Technologies", BG16RFPR002-1.014-0005.

References

[1] A.Dalidovich, Fundamentals of the Theory of Knitting, Light Industry, Moscow, 1970 (in Russian).

[2] G.Krasii, V. Kersek, V. Gamretskaya, R. Sakharnaya, Reference book on knitting, Technica, Sofia, 1980 (in Bulgarian).

[3] A. Charalambus, Projecting and designing of knitted products, Compass Agency Ltd, Sliven Bulgaria, 2025, ISBN: 978-954-8558-33-4, (in Bulgarian).

[4] D. Spenser, „Knitting Technology", Technology & Engineering, Elsevier, 2014.

[5] S. C. Ray, „Fundamentals and Advances in Knitting Technology", CRC Press, Technology & Engineering, 2012.

[6] C.Estorilio, R. Rodrigues, A. Fagan, C. Cziulik, Conceptual Design Methodology for Knitted Fabrics. In: Canciglieri Junior, O., Noël, F., Rivest, L., Bouras, A. (eds) Product Lifecycle Management. Green and Blue Technologies to Support Smart and Sustainable Organizations. PLM 2021. IFIP Advances in Information and Communication Technology, vol 639. Springer, Cham. 2022.https://doi.org/10.1007/978-3-030-94335-6_4

[7] T. Stoilov, Machines and processes in knitwear production, University Publishing House of TU – Sofia, Sofia, 2008 (in Bulgarian).

[8] S. Jensen, Sequence knitting. Journal of Mathematics and the Arts, 17(1–2),2023, pp. 111–139. https://doi.org/10.1080/17513472.2023.2199375

[9] K. F. Au, „Advances in Knitting Technology", Technology & Engineering, Elsevier, 2011.

[10] EN ISO 8388:2005: Knitted fabrics - types - vocabulary.

Environment. Technology. Resources. Rezekne, Latvia
Proceedings of the 16th International Scientific and Practical Conference. 2025. Volume IV, 161-164

Analytical Determination of Error from Static Adjustment of Boring Heads Cutting Part During Combined Machining of Holes

Angel Lengerov
Technical University of Sofia, Branch Plovdiv
Plovdiv, Bulgaria
anlen@tu-plovdiv.bg

Nadya Arabadzhieva
University of Food Technologies
Plovdiv, Bulgaria
n_arabadzhieva@uft-plovdiv.bg

Konstantin Chukalov
Technical University of Sofia, Branch Plovdiv
Plovdiv, Bulgaria
chukalov@tu-plovdiv.bg

***Abstract*—In the publication is presented analytical studies about an analyze of of boring heads cutting part accuracy for combined tools for machining holes by cutting and burnishing. It was found that the accuracy of the static size of the tool when using triangular and square inserts is determined by tolerances of inserts sides. When using round inserts, static radius error depends only on insert radius error.The conclusions drawn show that by determining appropriate tolerances for elements of fixtures, the specified accuracy of the processed parts is ensured.**

***Keywords*—error, accuracy, boring, holes**

I. Introduction

The accuracy of the dimensions obtained in combined machining by cutting and burnishing of holes from hydro- and pneumatic cylinders largely depends on the accuracy of the cutting elements of the boring tool[1].

Analyzing the accuracy of machining when using tools with square, triangular and round inserts is essential for the process of static adjustment of the technological system in boring and burnishing of holes. [2],[3].Using dimensional analysis to assess the influence of the geometric parameters of the tool on the accuracy, it is possible to minimize errors from combined machining of holes[4]

II. Materials and Methods

The diametrical size of the boring head is determined by the position of the cutting elements. In modern metal-cutting tool designs, soldering of the cutting inserts is increasingly rare, preferring the use of non-returnable, mechanically fixed inserts. In this case, the accuracy of the diametrical size of the tool will be determined by the accuracy of the insert and the accuracy of the position of the socket for its installation [5],[6]

Fig. 1 schematically shows the installation of a square non-returnable insert in the boring head housing and the dimensional chain determining the static radius of the tool A_Σ[7].[8]. By projecting the dimensional chain onto an axis parallel to A_Σ, an expression for determining its size can be obtained.

$$A_\Sigma = A_т + a(sin\chi'_r + cos\chi'_r) + r\ (sin\chi'_r + cos\chi'_r - 1) \quad (1)$$

where: $A_т$ – is the size of the tool body;
a – the width of the insert;
r – the radius of curvature at the tip of the insert;
Assuming that for each individual tool A_T = const from formula (1) the following expression for the static radius error can be obtained:

$$\omega_\Sigma = T_a(sin\chi'_r + cos\chi'_r) + Tr\ (sin\chi'_r + cos\chi'_r - 1) \quad (2)$$

From the dependence (2) it follows that the accuracy of the static size of the tool is determined by the tolerances of the width a and the radius r, as well as by the auxiliary setting angle χ'_r.[9] The degree of influence of these three factors on the accuracy of the tool is different. The influence of the width of the insert and the radius of curvature can be compared by the ratio of their transmission coefficients ξa and ξr[10]:

$$\frac{\xi_a}{\xi r} = \frac{sin\chi'_r + cos\chi'_r - 1}{sin\chi'_r + cos\chi'_r} \quad (3)$$

Online ISSN 2256-070X
https://doi.org/10.17770/etr2025vol4.8403
© 2025 The Author(s). Published by RTU PRESS.
This is an open access article under the Creative Commons Attribution 4.0 International License.

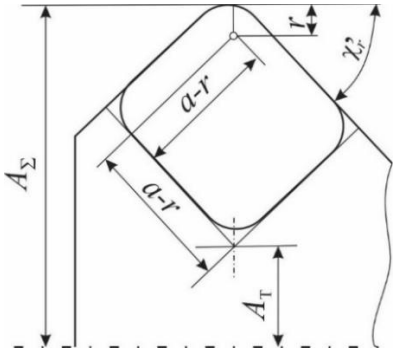

Fig. 1. Dimensioning square insert

The graphical dependence for (ξa)/ξr as a function of the auxiliary setting angle χ_r' is shown in Fig. 2. It can be seen from it that the influence of the radius of curvature error is significantly weaker than that of the width of the insert, reaching its maximum at χ_r' = 45°[11].

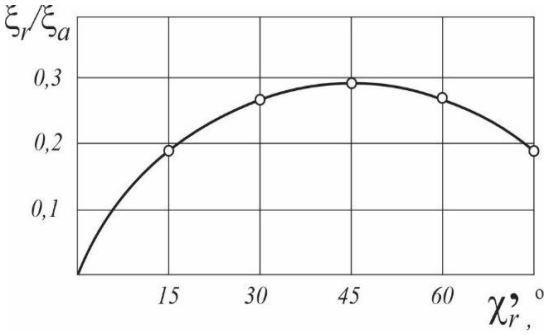

Fig. 2. Dependence of the ratio of the transmission coefficients ξa and ξr on the auxiliary setting angle

To express the influence of the auxiliary setting angle on the accuracy of the tool, it is convenient to rework formula (2) by setting $T_r = kTa$. This yields:

$$\frac{\omega\Sigma}{T_a} = (1+k)\,(sin\chi_r' + cos\chi_r'\ ) - k \qquad (4)$$

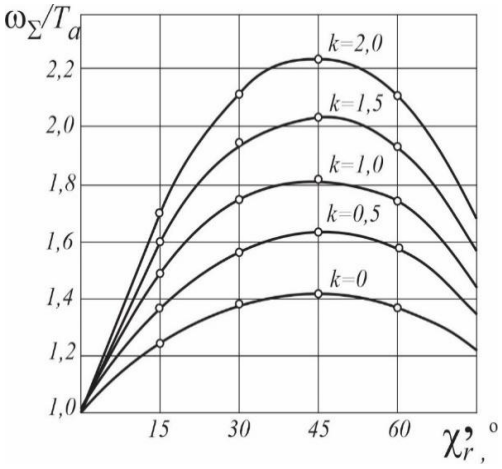

Fig. 3. Dependence of the ratio (ω_Σ)/Ta on the auxiliary setting angle χ_r'

Dependence (4) is presented graphically in Fig. 3. It can be seen that with increasing χ_r' from 0° to 45° the total error of the static radius of the tool grows and reaches its maximum at χ_r'= 45°. The intensity of the increase in the total error is the smallest at Tr=0 and increases with increasing Tr.

An analogous expression for the error of the static radius of the tool can be translated for other shapes of the non-flowable plate.

Fig. 4 shows schematically the establishment of a triangular, and Fig. 5 - of a round insert.

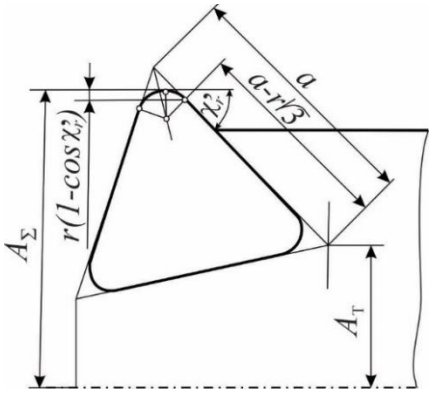

Fig. 4. Dimensioning triangle insert

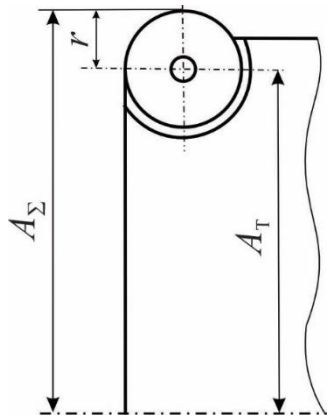

Fig. 5. Dimensioning round insert

The expressions for the static radius of the tool and its error in these two cases will have the form:

For triangle insert

$$A_\Sigma = A_T + a \qquad (5)$$

$$\omega_\Sigma = sin\chi_r' + Tr\,(\sqrt{3}sin\chi_r' + cos\chi_r') \qquad (6)$$

For round insert:

$$A_\Sigma = A_T - r \qquad (7)$$

$$\omega_\Sigma = Tr \qquad (8)$$

For round non-returnable inserts, the static radius error of the tool depends only on the error of the insert radius.

For triangular inserts, as well as for square inserts, the static radius error depends on three parameters: the insert

size a, the radius of curvature r and the auxiliary setting angle χ_r'.

To compare the insert size a and the radius of curvature r, the ratio of their transmission coefficients is used:

$$\frac{\xi r}{\xi_a} = \frac{\sqrt{3}sin\chi_r' + cos\chi_r' - 1}{sin\chi_r'} \quad (9)$$

III. Results and Discussion

Graphically, the dependence (9) is shown in Fig. 6.

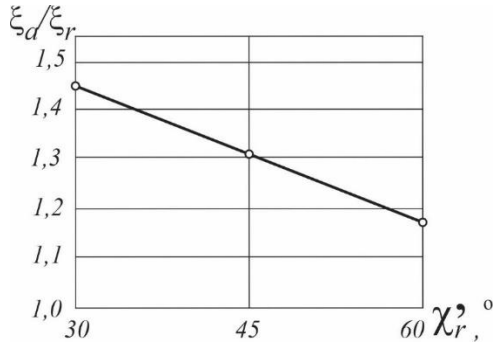

Fig. 6. Dependence of the ratio of the transmission coefficients ξa and ξr on the auxiliary setting angle

The influence of the auxiliary setting angle on the static radius error is expressed by the dependence:

$$\frac{\omega_\Sigma}{T_a} = sin\chi_r' + k\,(\sqrt{3}sin\chi_r' + cos\chi_r' - 1) \quad (10)$$

The dependence (10) is presented graphically in Fig. 7.

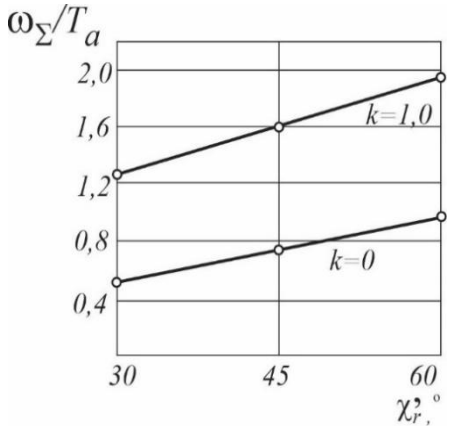

Fig. 7. Dependence of the ratio (ωΣ)/Ta on the auxiliary setting angle χ_r'

With the increase in the auxiliary setting angle χ_r' in the range from 30° to 60°, the error of the static radius of the tool increases. The absolute increase in the error increases r with increasing χ_r' [12,13].

In the course of the technological process, the size of the static radius changes. The factors that influence it are: elastic deformations arising from the cutting force between the support surfaces of the boring head and the insert; thermal deformations; dimensional wear of the cutting insert.

The first two factors are insignificant for the boring heads of the considered class.

The dimensional wear of the tool is a systematic factor that changes the static radius in the course of the technological process. The intensity of its influence can be estimated from the process accuracy diagram. Fig. 8 shows an example of the accuracy diagram of a stable technological process.

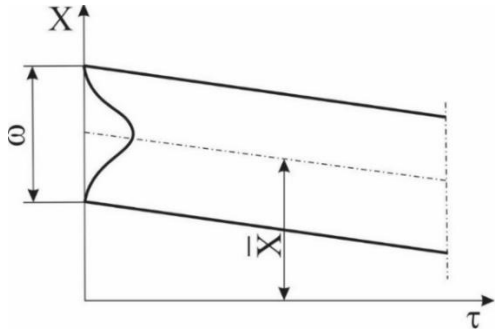

Fig. 8. Accuracy diagram of a stable technological process

The influence of dimensional wear on dimensional formation is expressed by the linear regression equation for the average size of the machined parts:

$$\overline{X} = \tilde{a} + \tilde{b}\tau \quad (11)$$

From equation (11) it follows that for a certain period of time, Δτ, of operation at one setup, the change in the static size of the tool, $\Delta\overline{X}$, as a result of dimensional wear will be:

$$\Delta\overline{X} = \tilde{b}\Delta\tau \quad (12)$$

The error for one part of the batch, $\Delta\overline{X}_{det}$, can be determined by replacing Δτ in formula (12) with the time spent on cutting, Tдет, during its processing.

$$\Delta\overline{X}_{det,} = \tilde{b}.T_{det} \quad (13)$$

IV. Conclusions

Analytical relationships have been obtained to determine the influence of the geometric parameters of cutting carbide inserts with different configurations (triangular, square, round) on the static adjustment during boring. These, together with the magnitude of the dimensional wear of the inserts, can serve as a basis for creating a mathematical model of the accuracy of the combined hole machining process[14].

V. Acknowledgments

This research was funded by the European Regional Development Fund within the OP " Research, Innovation

and Digitalization Programme for Intelligent Transformation 2021-2027 ", Project CoC "Smart Mechatronics, Eco- and Energy Saving Systems and Technologies", No. BG16RFPR002-1.014-0005.

REFERENCES

[1] R. Dwivedi, A. Somatkar and S. Chinchanikar, "Modeling and optimization of roller burnishing of Al6061-T6 process for minimum surface roughness, better microhardness and roundness," Metal Working and Material Science, vol. 26, pp. 52–65, 2024. https://doi.org/10.17212/1994-6309-2024-26.3-52-65

[2] N.-T. Nguyen, H. Le, T. Hoang, V. H. Nguyen and H.-H. Nguyen, "Modeling of milling forces in facing process of aluminum alloy AL7075 using the square inserts", EUREKA: Physics and Engineering, pp. 101–112, 2024. https://doi.org/10.21303/2461-4262.2024.003209

[3] X. Chen et al., "Research on machining technology of stepped boring for intersecting holes in aircraft", Journal of Physics: Conference Series., vol. 2882, p. 012019, 2024. https://doi.org/10.1088/1742-6596/2882/1/012019

[4] K. Skalski, A. Morawski and W. Przybilski, "Analysis of contact elastic-plastic strains during the process of burnishing", International Journal of Mechanical Sciences, vol. 37, no. 5, pp. 461–472, 1995.

[5] M. H. El-Axir and A. A. Ibrahim, "Some surface characteristics due to center rest ball burnishing" , Journal of Materials Processing Technology., vol. 167, pp. 47–53, 2005. https://doi.org/10.1016/j.jmatprotec.2004.09.078

[6] W. Cai, J. Xiang, G. Dong, K.-h. Lai and M. Wiercigroch, "Analytical modelling of parallel multidirectional cutting of slender shafts", International Journal of Mechanical Sciences, 2025. [ttps://doi.org/10.1016/j.ijmecsci.2025.110024

[7] L. Nowakowski, J. Rolek, S. Blasiak and M. Skrzyniarz, "The Influence of Insert Mounting Errors on the Surface Roughness of 1.0503 Steel in Face Milling", Materials, vol. 17, p. 6144, 2024. https://doi.org/10.3390/ma17246144

[8] T.-T. Luyen, H. Kien and D.-T. Nguyen, "A Combined simulation and experimental investigation on tool radius influence on enhancing the formability SPIF process for Al1050 sheet material", International Journal of Modern Physics B, 2024. https://doi.org/10.1142/ S0217979225400247

[9] S. Dyadya, O. Kozlova, P. Tryshyn, D. Yakhno and D. Dziuba, "Influence of Helical Cutting-Edge Angle on End-Milling Stability", Cutting & Tools in Technological System, pp. 86–94, 2024. https://doi.org/10.20998/2078-7405.2024.101.08

[10] A. Jiang, Z. Liu, S. Wang, J. Wen, Y. Li and J. Zhao, "Optimized design of indexable insert drill based on radial cutting force balance", International Journal of Advanced Manufacturing Technology, vol. 128, pp. 1–13, 2023. https://doi.org/10.1007/s00170-023-12063-z

[11] F. Kazemi, C. Song, A. Clare and X. Jin, "A New Cutting Mechanics Model for Improved Shear Angle Prediction in Orthogonal Cutting Process", Journal of Manufacturing Science and Engineering, vol. 147, pp. 1–31, 2024. https://doi.org/10.1115/1.4066976

[12] H. Liu, Z. Meng, L. Han and W. Zhang, "Design of Damping Damping Design of New Boring Head Drive Structure", Mechanical Engineering Science, vol. 5, 2024.//doi.org/10.33142/mes.v5i1.12711

[13] W. Bouzid and J. L. Lebrum, "Influence of finishing by burnishing on surface characteristics", Journal of Materials Engineering and Performance, vol. 12, no. 1, pp. 37–40, 2003.

[14] S. Shvets and V. Astakhov, "Effect of Insert Angles on Cutting Tool Geometry", Journal of Engineering Sciences, vol. 7, pp. A1–A6, 2020. https://doi.org/10.21272/jes.2020.7(2).a1

Environment. Technology. Resources. Rezekne, Latvia
Proceedings of the 16th International Scientific and Practical Conference. 2025 Volume IV, 165-168

Improvement of Dimensional Accuracy Analysis for Assembly of Engineering Parts

Angel Lengerov
Technical University of Sofia, Branch Plovdiv
CoC "Smart Mechatronics, Eco- and Energy Saving Systems and Technologies"
Plovdiv, Bulgaria
anlen@tu-plovdiv.bg

Silvia Salapateva
Technical University of Sofia, Branch Plovdiv
CoC "Smart Mechatronics, Eco- and Energy Saving Systems and Technologies"
Plovdiv, Bulgaria
sisisal@tu-plovdiv.bg

Konstantin Chukalov
Technical University of Sofia, Branch Plovdiv
Plovdiv, Bulgaria
chukalov@tu-plovdiv.bg

***Abstract*—This publication proposes approaches to improve accuracy of assembly of mechanical engineering parts based on the use and application of dimensional analysis. The conclusions drawn show that by determining appropriate tolerances for elements of fixtures, the specified accuracy of the processed parts is ensured.**

***Keywords*—fixture, assembly, accuracy, accuracy analysis.**

I. Introduction

Improving assembly accuracy by improving approaches for fast and accurate orientation of the connected components is an important stage in the fixture design process. The applied approaches regarding the use of dimensional analysis to calculate the error of locating crankshaft-type parts will help reduce the amount of scrap when assembling the journal bearings of a coaxial crankshaft[1]. This makes the goal of this work relevant and contributes to improving the quality and productivity of the technological assembly process. The choice of assembly method and approach is made depending on the specific design features of the product, the size of the production program, the content of the operations and the technical requirements. For the implementation of the study, technological dimensional chains have been compiled, through which the relevant accuracy indicators of the assembly process have been analyzed.

Quality of assembled mechanical engineering parts included in the design of various machine units to a certain extent depends on accuracy of the used fixtures [1]. In a number of cases, the ultimate goal - assembly accuracy is achieved entirely through appropriate design and high-quality manufacture of an assembly fixture [2]. The increased requirements in modern mechanical engineering for the quality of assembled parts impose a new approach to the dimensioning of the elements of technological equipment [3].

This is based on the wider application of dimensional analysis [4]. At present, the determination of dimensional tolerances when designing fixtures is carried out conditionally (depending on experience of the designer). In this way, significant errors are allowed and often lead to unnecessary expenditure of labor, funds and time in technological preparation [5].

II. Materials and Methods

The work presents an approach to improving the accuracy of assembly of mechanical engineering parts, based on the application of dimensional analysis. In it, the accuracy of the elements of the fixtures is regulated, proceeding from the accuracy of the assembled parts [6].

Dimensional analysis is widely used in the design and assembly of special fixtures, regardless of their type and degree of automation [7]. For fixtures intended for fixing and fastening basic parts and assemblies, dimensional analysis is not necessary. They are intended to provide the necessary stability of the parts during the assembly process and are usually not subject to requirements for the accuracy of the position of the fixed part.

For special fixtures for accurate and rapid orientation of assembled parts, the accuracy of their constituent elements is of particular importance [8]. Therefore, the determination of their tolerances must be carried out using dimensional analysis. When using such fixtures, the operator is freed from the need to ensure the mutual position of the assembled parts. This is done automatically by bringing the assembled parts into contact with the supporting and guiding elements of the fixture. In addition, this significantly increases labor productivity. As an

Online ISSN 2256-070X
https://doi.org/10.17770/etr2025vol4.8422
© 2025 The Author(s). Published by RTU PRESS.
This is an open access article under the Creative Commons Attribution 4.0 International License.

example, Fig. 1 shows a fixture for assembling a composite crankshaft [9]. It achieves alignment of the main journals 1 and 4[10]. This shaft can be assembled without a fixture, but the correction of the misalignment of the main journals must be carried out by the adjustment method [11]. The nuts 5 and 7 are slightly unscrewed, the inaccuracy is corrected, they are screwed in again and the displacement is measured. This process can be repeated many times, requiring high qualifications of the adjuster operator, and the process itself is of low productivity. When using the fixture, the position of the main journals is ensured by their single installation in the support prisms, after which nuts 5 and 7 are fastened.

In the design variant of the fixture shown in Fig. 1, the crankshaft is assembled in a vertical position. In this case, the misalignment of the main journals will depend on the accuracy of the dimensions of the fixture.

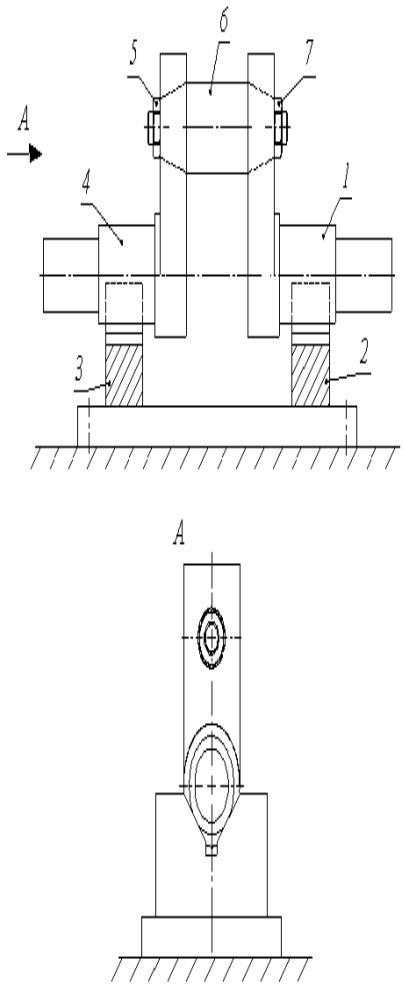

Fig. 1. Device for assembly of crankshaft.

III. RESULTS AND DISCUSSION

In the assembly process, the products are included in technological dimensional chains. In these chains, the achieved accuracy indicators of the assembled products are closing links. Component links are the dimensions of the parts and the inaccuracies and clearances in the joints of the fixtures. Fig. 2 shows the dimensional chain for achieving the alignment of the main journals A_Δ of the crankshaft, assembled using the fixture from Fig. 1. For convenience in creating the chain, here the two prisms are shown one above the other, while maintaining the common base surface of the fixture plate. The dimensional chain is symmetrical, and the component links are:

A_1, A_6 - distance from the axis of the prism to the axis of the pin hole;

A_2, A_5 - clearance between the hole in the prism and the pin;

A_3, A_4 - distance from the base surface to the axis of the pin hole.

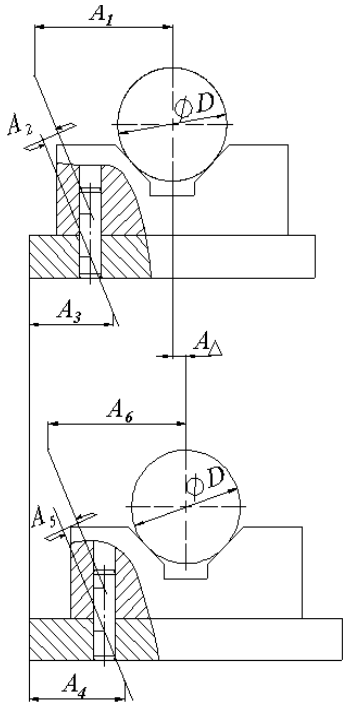

Fig. 2. Dimensional chain.

Depending on the number of units, the method of complete interchangeability is applied (if the number of units is more than 4) [12]. The solution of the straight-line problem is carried out by initially applying the principle of equal tolerances. i.e.

$$T_1 = T_2 = \cdots = T_{n-1} = T_{av.}$$

$$T_{av.} = \frac{T_\Delta}{\sqrt{n-1}} \quad (1)$$

The calculated average value is indicative. The tolerances of the individual units are determined taking into account the accuracy of the technological method of processing and the size of their nominal values. The displacement of the prism relative to the average position as a result of the clearances A_2 and A_5 can occur in both directions, therefore they participate in the dimensional chain with the full value of their tolerance. After the correction, a check is carried out according to the known equation for the tolerance of the closing unit.

$$T_\Delta = \sqrt{\sum_{i=1}^{n-1} T_i^2}\ . \quad (2)$$

A characteristic feature of this design variant, as shown by the composite dimensional chain, is that the misalignment of the main necks A_Δ is influenced only by the structural dimensions and clearances of the fixture. The inconvenience of this type of basing is that the operator must hold the shaft by hand until the nuts are screwed in. The same fixture can be made in another variant, in which the wedge neck is in a horizontal plane and can rest on a solid stop. This will facilitate assembly, since holding by hand is not necessary. In the second variant, the dimensional chain changes and the accuracy of the closing link is influenced by other dimensions of the fixture parts. This can be seen from the diagram constructed in Fig. 3.

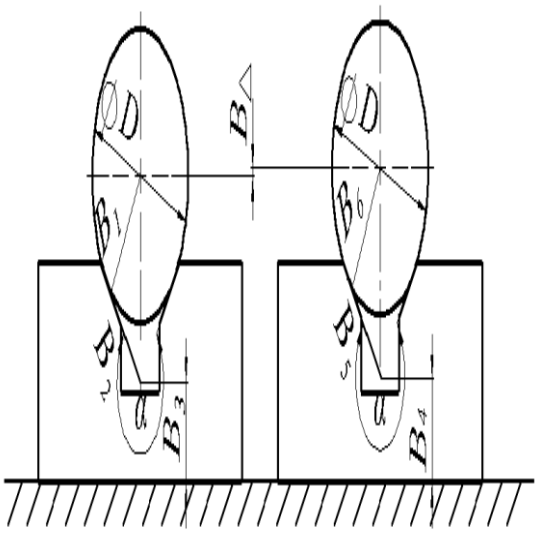

Fig. 3. Second design option.

For convenience in its compilation, the prisms are shifted in a horizontal plane with the upper surface of the plate remaining as a common base. The dimensional chain in this case is also symmetrical. The constituent links are:

B_1, B_6 - radius of the main journal;

B_2, B_5 - distance from the contact point to the top of the prism (the intersection of the two inclined surfaces);

B_3, B_4 - distance from the top of the prism to its base.

For convenience in determining the error of the closing link, only one (left) branch of the dimensional chain can be considered[13]. The value of the nominal value in the left branch B' will be determined by the expression.

$$B'_\Delta = -\frac{D}{2} sin\frac{\alpha}{2} - \frac{D}{2tg\frac{\alpha}{2}} cos\frac{\alpha}{2} - B_3 \quad (3)$$

$$B'_\Delta = -\frac{D}{2}\left(\frac{1}{sin\frac{\alpha}{2}} + 1\right) - B_3 \quad (4)$$

After mathematical transformations of equation (4) based on the theory of dimensional chains, the dimensional error is obtained as:

$$T'_b = \frac{T_D}{2}\left(\frac{1}{sin\frac{\alpha}{2}} + 1\right) + T_3 \quad (5)$$

Since the dimensional chain is symmetrical, the total error of the closing link T_b will be obtained by doubling the T_b:

$$T_b = \frac{T_D}{2}\left(\frac{1}{sin\frac{\alpha}{2}} + 1\right) + 2T_3 \quad (6)$$

From this it can be seen that the error obtained when setting a composite crankshaft in a horizontal position will depend not only on the dimensions of the fixture parts, but also on the tolerance of the diameter of the main journals.

IV. CONCLUSIONS

Based on the analyses and calculations made for the example of assembling a composite crankshaft, it can be seen that dimensional analysis can be used to determine appropriate tolerances for manufacturing the elements of the fixtures. The results of the study can be applied not only in cases of initial assembly of products after the stage of their manufacture, but also in cases of repair. This contributes to the creation of conditions for the implementation of flexibility in assembly operations and control of the technical parameters of the assembly operation of composite crankshafts..In some cases, dimensional analysis helps to justify or reject a given design variant of the fixture. The latter must be carried out under well-defined specific production conditions. It is also necessary to know the technological capabilities for manufacturing the elements of the fixture, the accuracy of the diameter of the main journals and the required requirement for the alignment of the main journals. In individual cases, if the accuracy indicators of the assembly process are unsatisfactory, further processing of individual surfaces of the assembled crankshafts is allowed in order to ensure the necessary dimensional tolerances.

V. ACKNOWLEDGMENTS

This research was funded by the European Regional Development Fund within the OP "Research, Innovation and Digitalization Programme for Intelligent Transformation 2021-2027", Project CoC "Smart Mechatronics, Eco- and Energy Saving Systems and Technologies", No. BG16RFPR002-1.014-0005.

REFERENCES

[1]. A.-K. Onken, F. Meiners and K. Tracht, "Spare parts for selectively assembled linked parts in micro production", Procedia Manufacturing, vol. 19, pp. 82–86, 2018. [Online]. Available: https://doi.org/10.1016/j.promfg.2018.01.012. (Accessed: January 4, 2025).

[2]. K. Hirano, K. Mori and A. Matsubara, "Experimental Characterization of Contact Stiffness for Fixture Design", International Journal of Automation Technology, vol. 19, pp. 15–23, 2025. [Online]. Available: https://doi.org/10.20965/ijat.2025.p0015. (Accessed: January 4, 2025).

[3]. V. Lebedev, G. Prokopec, Y. Korol'kov and A. Shishkina, "Technological assurance of surface quality and operational properties of machine parts", 2024. [Online]. Available: https://doi.org/10.12737/1900534. (Accessed: January 4, 2025).

[4]. F. Zhao, Z. Liu, D. Wang, Q. Huang and S. Chen, "Coupled Study on the Uniformity and Dimensional Accuracy of 316L

Microchannel Roll Forming", 2024. [Online]. Available: https://doi.org/10.21203/rs.3.rs-5292086/v1. (Accessed: January 4, 2025).

[5]. C. U. Jung and V. Nallagatla, "Significant error in significant figures?", Journal of the Korean Physical Society, vol. 78, 2021. [Online]. Available: https://doi.org/10.1007/s40042-020-00027-5. (Accessed: January 10, 2025).

[6]. L. Yin, F. Yang, P. Zhu and Q. Qin, "Research on module partition for remanufacturing parts to be assembled", The South African Journal of Industrial Engineering, vol. 33, pp. 114–125, 2022. [Online]. Available: https://doi.org/10.7166/33-1-2646. (Accessed: January 4, 2025).

[7]. Z. Chen, L. Shen, C. Zhang, C. Li, J. Shou and J. Zhang, "Design of Special Fixture for Welding Assembly of Steel Joints", 2022. [Online]. Available: https://doi.org/10.1007/978-981-19-1309-9_41. (Accessed: January 4, 2025).

[8]. G.Shterev, P.Mitev, ''Automated system for control and management of a machine forautomatic assembly of curtain brackets and hooks'', Metrology and Metrology Assurance, pp.345-347, 2017

[9]. I. Lind, M. Luginbill, T. Nalli and J. Shaktman, "Automated Fixture for Crankshaft Inspection", 2011.

[10]. U. Werner, "Shaft vibrations in induction machines caused by 2x excitation due to elliptical form deviations of the shaft journals", Proc. 19th Int. Congr. Sound Vib. (ICSV), vol. 1, pp. 65–72, 2012.

[11]. K. Qian and Y. Chen, "A gear tooth side clearance adjustment device and measurement method", Journal of Physics: Conference Series, vol. 2913, p. 012011, 2024. [Online]. Available: https://doi.org/10.1088/1742-6596/2913/1/012011. (Accessed: January 4, 2025).

[12]. I. Voyachek, E. Slashchev and D. Malikova, "Feasibility Study of Applying Group Interchangeability Method for Assembly Components of Machines", 2020. [Online]. Available: https://doi.org/10.1007/978-3-030-22063-1_30. (Accessed: January 4, 2025).

Environment. Technology. Resources. Rezekne, Latvia
Proceedings of the 16th International Scientific and Practical Conference. 2025. Volume IV, 169-180

Mechanical and Morphological Properties of PP/PE Composite Fishing Net Ropes

Inga Lasenko
Institute of Mechanical and Biomedical Engineering
Riga Technical University
Riga, Latvia
inga.lasenko@rtu.lv

Andris Martinovs
Engineering Centre, Rezekne Academy of Riga Technical University
Rezekne, Latvia
andris.martinovs@rta.lv

Artūrs Mačanovskis
Institute of Mechanical and Biomedical Engineering
Riga Technical University
Riga, Latvia
arturs.macanovskis@rtu.lv

Arta Viluma-Gudmona
Institute of Mechanical and Biomedical Engineering
Riga Technical University
Riga, Latvia
arta.viluma.gudmona@gmail.com

Sanjay Rajni Vejanand
Institute of Mechanical and Biomedical Engineering
Riga Technical University
Riga, Latvia
sanjay.vejanand@rtu.lv

Sandra Vasilevska
Faculty of Economics and Social Development
Latvia University of Life Sciences and Technologies
Jelgava, Latvia
sandra.vasilevsky@gmail.com

Sai Pavan Kanukuntla
Institute of Mechanical and Biomedical Engineering
Riga Technical University
Riga, Latvia
sai-pavan.kanukuntla@rtu.lv

***Abstract*— This study examined how the extrusion process, which is affected by different thermal settings, and the raw material sources, composed of various polypropylene (PP) and polyethylene (PE) blends with or without calcium carbonate ($CaCO_3$) additives, influence the quality and mechanical properties, such as tensile strength, elongation, and stiffness, of composite ropes for fishing net production. A comparative analysis of extrusion process parameters was conducted among four distinct extruders from the Promatech, Miyachi, Sima, and Ichikawa companies with a focus on their thermal settings, characterized by varying the temperature profiles. The investigation was extended to the utilization of PP derived from different sources and granule compositions, including formulations with $CaCO_3$ additives. In terms of breaking force, the samples with $CaCO_3$ showed an average increase of 5.2% when compared to those without $CaCO_3$. With the addition of $CaCO_3$, the elongation at break increased by an average of 8.7%. The addition of $CaCO_3$, surprisingly, resulted in a slight decrease in stiffness, averaging a decrease of 2.1% when compared to the samples without $CaCO_3$. Most significantly, the addition of $CaCO_3$ resulted in a significant decrease in Young's modulus, with an average reduction of approximately 66.4% compared to the samples without $CaCO_3$. This study reveals substantial differences in rope mechanical quality due to variations in raw materials and extrusion parameters, emphasizing the need for adapting the manufacturing process to consistently produce high-quality composite ropes for knitting fishing nets.**

Keywords*—Polypropylene; polyethylene; calcium carbonate additives; extrusion process parameters; composite ropes.

I. Introduction

Polymers have many applications in various industries, such as textiles [1], [2], packaging [3], automotive [4], aerospace [5], biomedical [6]–[9], and electronics [8], [10]. Some of the common properties of polymers are elasticity [11], [12], toughness, thermal stability, electrical conductivity, optical transparency, and biocompatibility [13], [14]. Composites are a type of materials that consists of a matrix material and reinforcing fibers [15]. Composite ropes are widely used for fishing net production, as they can withstand harsh marine environments and reduce the risk of ghost fishing [16]. Previous research indicates that approximately 2.5% of all fishing equipment is lost annually, encompassing over 78,000 km² of nets, more than 25 million pots and traps, and 740,000 km of longlines. The degradation of oceanic plastic debris, including discarded fishing gear, has significant implications for the health of

Online ISSN 2256-070X
https://doi.org/10.17770/etr2025vol4.8398
© 2025 The Author(s). Published by RTU PRESS.
This is an open access article under the Creative Commons Attribution 4.0 International License.

marine organisms and ecosystems. Marine plastics are hypothesized to serve as vectors for invasive species and pathogens across oceanic environments [17]. Among marine plastic debris, abandoned fishing nets, lines, and ropes are considered the most lethal forms, as they frequently result in the entanglement and subsequent mortality of various aquatic mammals, seabirds, and turtles [18].

The design and material choice of aquaculture nets can have a big impact on the industry's profitability, productivity, and environmental sustainability [19], [20]. The quality of these ropes is influenced by various factors, including the extrusion parameters during the manufacturing process and the characteristics of the raw materials used [21]. Among the different materials used for aquaculture nets, polypropylene (PP) and polyethylene (PE) are the most common and widely used synthetic polymers [22]. In terms of durability, strength, flexibility, buoyancy, UV resistance, and corrosion resistance, PP and PE outperform other materials such as nylon. PP and PE are also relatively inexpensive and simple to manufacture, making them suitable for aquaculture [23]. In particular, the choice of polypropylene (PP) as the primary material for composite ropes [24], as well as the potential inclusion of calcium carbonate ($CaCO_3$) additives, plays a significant role in determining composite ropes' mechanical properties and performance [25], [26].

$CaCO_3$ is specifically added to the granules with the objective of reducing stiffness and ensuring that the final ropes are flexible. This consideration holds particular significance in the context of weaving fishing nets, where flexibility is paramount, and rigid ropes present challenges during the fabrication process (fragile and high volume) [27]. By navigating the intricacies of variations in raw materials and $CaCO_3$ modifications, **this study aimed** to unravel the nuanced impact of these choices on the mechanical properties and suitability of composite ropes for specific applications.

Extrusion parameters, such as temperature settings, impact the structural integrity and flexibility of composite ropes. Different extrusion machines exhibit varying thermal profiles, which may result in variations in rope quality [28]. In this study, four different companies' extruders, Promatech, Miyachi, Sima, and Ichikawa, were compared in terms of their thermal settings.

Problem description: Comparative research has been conducted on the mechanical properties of composite ropes for fishing net production, particularly regarding the impact of extrusion process parameters and raw material variations. Previous studies have often focused on isolated factors, neglecting the complex interplay between extrusion conditions, polymer blends, and additives like $CaCO_3$. Moreover, the relationship between surface morphology and mechanical properties in these specialized composites remains poorly understood. This study aims to address these knowledge gaps by conducting a comprehensive analysis of the effects of diverse extrusion parameters and raw material compositions on the mechanical and surface properties of composite polymer ropes.

Despite theoretical expectations of a uniform rope quality, the existing empirical evidence suggests that differences in raw materials (polymers) and extrusion parameters lead to variations in rope thickness, bulk volume, and stiffness [29]. Currently, there is no standardized assessment on how raw materials and extrusion parameters may affect rope quality, which suggests that the manufacturing process can impact the quality of composite polymer ropes for knitting fishing nets in various ways. There are some standardized assessments for rope quality, such as ISO 9554:20191 [30], which specifies the general characteristics of fiber ropes and their constituent materials. Therefore, it is important to understand how the process parameters influence the quality of composite polymer ropes and ensure their consistency.

Limited comparative research has been conducted on the mechanical properties of composite ropes for fishing net production, particularly regarding the impact of extrusion process parameters and raw material variations. Previous studies have often focused on isolated factors, neglecting the complex interplay between extrusion conditions, polymer blends, and additives like $CaCO_3$. Moreover, the relationship between surface morphology and mechanical properties in these specialized composites remains poorly understood. This study aims to address these knowledge gaps by conducting a comprehensive analysis of the effects of diverse extrusion parameters and raw material compositions on the mechanical and surface properties of composite polymer ropes.

This study presents a comparative analysis of ten types of composite polymer ropes (with the same combination of polymer structures, as well as a variation of calcium carbonate), showing how the process parameters affect the quality of composite polymer ropes and how to adjust the manufacturing process to consistently produce high-quality composite ropes for knitting fishing nets. Understanding the intricate relationship between extrusion parameters and composite polymer raw materials is crucial in achieving the desired rope characteristics (physical and mechanical) and, ultimately, enhancing fishing net production.

II. Materials and Methods

A. Extruder Specifications and Thermal Settings

In this study, four distinct extruders, manufactured by different companies with the trade names Promatech, Miyachi, Sima, and Ichikawa (Table 1), were utilized to produce identical types of composite polymer ropes. Each extruder was characterized by specific thermal settings tailored to optimize both productivity and the quality of the resulting ropes. The thermal parameters for each extruder were meticulously controlled and varied.

TABLE 1 EXTRUDER SPECIFICATIONS

Extruder	Country	Screw Area Temperature (°C)	Outlet Temperature (°C)	Bath Temperature (°C)	Oven Temperature (°C)
Promatech	Italy	215-240	210	110	130
Miyachi	Japan	200-215	190	100	140
Sima	Italy	215-240	200	110	130
Ichikawa	Japan	205-220	205	110	140

B. Raw Material Selection and Utilization

The choice of raw materials influences the composition and characteristics of composite polymer ropes. The selection of distinct raw materials added complexity to the study, as variations in material properties could contribute to differences in the resulting composite ropes. This study strategically employed a diverse range of raw materials, consisting of polypropylene (PP) and polyethylene (PE). The PP was sourced from various companies, and included Capilene®, ©Rompetrol, Mosten® TB002, and Hyosung Topilene F501, each with distinct granules. Polyethylene (PE) granules were exclusively sourced from Orlen Unipetrol RPA (Czech Republic) Company (trademark: PE-HD Liten® TB 49-060) contributing to a standardized granule composition adopted across all ten manufactured ropes.

As described in the aforementioned references, adding $CaCO_3$ of different shapes and concentrations to polypropylene composites has been shown to enhance their mechanical properties. For instance, adding 10 wt% of homopolymer polypropylene (PP) with spherical $CaCO_3$ increased tensile and flexural strengths by 14.5% and 11.8%, respectively. Needle-like $CaCO_3$, at a 30 wt% concentration, resulted in a 20.6% increase in tensile strength and a 25.8% increase in flexural strength. Additionally, lower concentrations of $CaCO_3$, such as 5 wt%, demonstrated tensile and flexural strength enhancements of 12.7% and 8.9%, respectively. These variations highlight the importance of optimizing $CaCO_3$ content and shape to achieve specific mechanical performance targets in polypropylene composites. [31]–[34]. The masterbatch (granules) were composed of 70% polypropylene (PP) and 30% polyethylene (PE), with variations introduced in the 6th, 7th, 9th, and 10th samples through the addition of 5% and 10% $CaCO_3$, respectively (Table 2). The physical, mechanical, and thermal characteristics of the composite polymers utilized in this study are shown in Table 2.

The granule composition, a critical determinant of the mechanical and structural attributes, adhered to a consistent formulation—polypropylene (PP) (CAS Registry Number® 9003-07-0; molecular formula $(C_3H_6)_x$; melting point 158-170 °C; density 0.92 g/cm³) and polyethylene (PE) (CAS Registry Number® 9002-88-4; chemical formula: $(C_2H_4)_n$; flash point: 270 °C; density: 0.962 g/mL at 25 °C; melting point: 92 °C)—except for samples 6, 7, and 10. This deliberate blend sought to capture the synergistic effects of both polymers on the final properties of the composite polymer ropes. PP and PE were obtained from Sigma-Aldrich chemicals (Merck KGaA, Darmstadt, (64287) Germany).

$CaCO_3$ (calcium carbonate 99.95 Suprapur®, CAS 471-34-1, was obtained from Sigma-Aldrich chemicals (Merck KGaA, Darmstadt, (64287) Germany).

TABLE 2 COMPOSITION OF PP AND PE WITH/WITHOUT CACO3 ON EXTRUDER TYPE

No	Type of extruder	Polypropylene (PP) and concentration (%)	Polyethylene (PE) and concentration (%)	$CaCO_3$ (%)
1	Promatech extruder, Promatech Technologies, Crespellano—Bologna, Italy	PP Capilene® E 50 E, Polypropylene Homopolymer, Carmel Olefins Ltd (Israel) **70%**	PE-HD Liten® TB 49-060 Orlen Unipetrol RPA, (Czech Republic) **30%**	-
2	Promatech extruder, Promatech Technologies, Crespellano—Bologna, Italy	PP SS-05:F401 ©Rompetrol Refining SA, (Romania) **70%**	PE-HD Liten® TB 49-060 Orlen Unipetrol RPA, (Czech Republic) **30%**	-
3	Promatech extruder, Promatech Technologies, Crespellano—Bologna, Italy	PP Mosten® TB002, Unipetrol RPA, (Czech Republic) **70%**	PE-HD Liten® TB 49-060 Orlen Unipetrol RPA, (Czech Republic) **30%**	-
4	Miyachi extruder, Miyachi Iron Works, Ltd, Japan	PP Hyosung Topilene F501 (China) **70%**	PE-HD Liten® TB 49-060 Orlen Unipetrol RPA, (Czech Republic) **30%**	-
5	Sima extruder, Sima Headquarters, S.R.L., (MO) Italy	PP Mosten® TB002, Unipetrol RPA, (Czech Republic) **70%**	PE-HD Liten® TB 49-060 Orlen Unipetrol RPA, (Czech Republic) **30%**	-
6	Ichikawa extruder, Ichikawa Iron Works Co. Ltd, Japan	PP Capilene® E 50 E, Polypropylene Homopolymer, Carmel Olefins Ltd (Israel) **66.5%**	PE-HD Liten® TB 49-060 Orlen Unipetrol RPA, (Czech Republic) **28.5%**	5%
7	Ichikawa extruder, Ichikawa Iron Works Co. Ltd, Japan	PP Capilene® E 50 E, Polypropylene Homopolymer, Carmel Olefins Ltd (Israel) **63%**	PE-HD Liten® TB 49-060 Orlen Unipetrol RPA, (Czech Republic) **27%**	10%
8	Ichikawa extruder, Ichikawa Iron Works Co. Ltd, Japan	PP Capilene® E 50 E, Polypropylene Homopolymer, Carmel Olefins Ltd (Israel) **70%**	PE-HD Liten® TB 49-060 Orlen Unipetrol RPA, (Czech Republic) **30%**	-
9	Ichikawa extruder, Ichikawa Iron Works Co. Ltd, Japan	PP Capilene® E 50 E, Polypropylene Homopolymer, Carmel Olefins Ltd (Israel) **65%**	PE-HD Liten® TB 49-060 Orlen Unipetrol RPA, (Czech Republic) **30%**	5%
10	Ichikawa extruder, Ichikawa Iron Works Co. Ltd, Japan	PP Capilene® E 50 E, Polypropylene Homopolymer, Carmel Olefins Ltd (Israel) **70%**	PE-HD Liten® TB 49-060 Orlen Unipetrol RPA, (Czech Republic) **25%**	5%

TABLE 3 PHYSICAL, MECHANICAL, AND THERMAL CHARACTERISTICS OF POLYMER COMPONENTS

Polymer component	Capilene® E 50 E (PP)	SS-05: F401 (PP)	Mosten® TB 002 (PP)	Hyosung Topilene F501 (PP)	Liten® TB 49-060 (PE)
Melt Flow Rate (g/10 min)	1.8	2 - 3.5	2	3.0	0.6
Density (g/cm3)	0.905	0.905 - 0.917	0.902	0.90	0.949
Tensile Strength at Yield (MPa)	32	Min. 30	28	35.3	24
Flexural Modulus (MPa)	1400	Min. 900	1700	1570	1200
Izod Impact Strength (kJ/m2)	4	Min. 2	6.5	3.9	7
Vicat Softening Temperature (°C)	154	Min. 150	155	105	125
Heat deflection Temperature (°C)	96	Min. 45	55	150	80

C. Specimen Description

The commercially available ropes utilized in this study were manufactured using low-power, single-type extruders. Specifically, a one-screw extruders PP&PE FDY - 40 Tex, featuring 2 positions x 10 ends and a production capacity of up to 500 kg/hour, were employed. This equipment is operational at the SIA "MAGISTR" (24 Raina street, LV-5401, Daugavpils, Latvia) enterprise. The selection of this particular manufacturing process and supplier ensures consistency in the rope samples and aligns with industry standards for rope production (EN ISO 10572). Fig. 1 illustrates the comprehensive methodological process, beginning with rope material selection and culminating in comparative analysis (EN ISO 2062). This flowchart delineates the sequential steps of the procedure, providing a visual representation of the study's systematic approach.

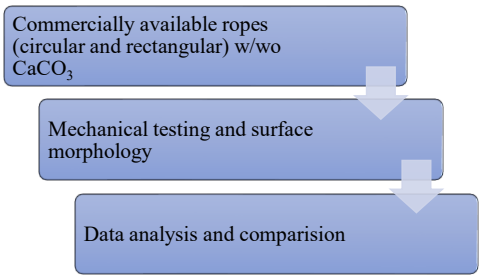

Fig. 1. Flowchart depicting the methodological sequence from initial rope selection to final comparative analysis.

The length of the specimens was measured using a Mitutoyo Strait-Line Tape Measure (Japan), which has a range of 0 – 3 m and two scales, one in metric and one in imperial units. The tape measure has a double coating at the end of the blade, a dual-sided hook, and a finger brake to control the retraction speed. The verification number is G366V22, 15.06.2023. The thickness of the specimens was determined using a Mitutoyo QuantuMike IP65 Digital Micrometer (Japan), which has a discreteness of 0.001 mm and a computer personal calibration at start-up. The digital micrometer has a coarser spindle thread that feeds the spindle by 2 mm per thimble revolution, a carbide measuring face, and a waterproof design. The mass of the specimens was determined using KERN PCB M Laboratory Scales (Germany), which have an accuracy class of II high, a maximum capacity of 200 g, and a discreteness of 0.01 g. The laboratory scales have a large LCD display, a stainless-steel weighing plate, and a shock-proof plastic housing. The calibration certificate number is M0901K22, 15.06.2023. The prepared specimens are shown in Fig. 2 in different shapes, such as circular and rectangular, and their parameters are summarized in Table 4. Figure 2(a) depicts the shape of samples 1–7 with a circular cross-section, whereas Fig2(b) depicts samples 8–10 with a rectangular cross-section.

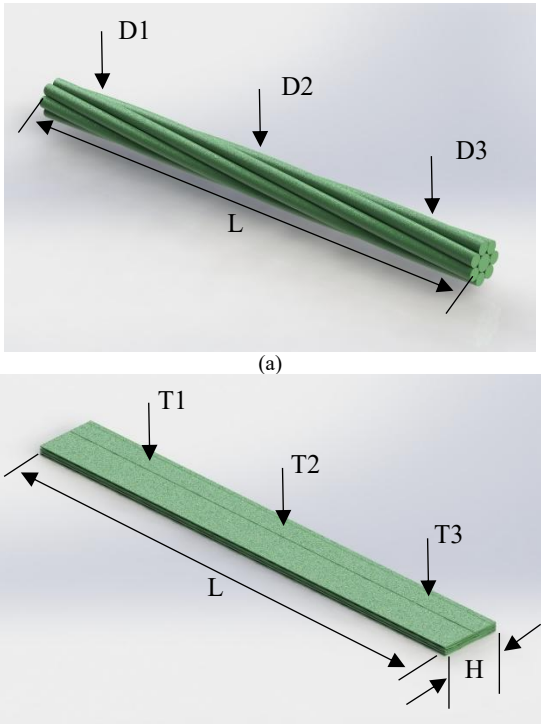

Figure 2. (a) Circular composite polymer rope and (b) rectangular composite polymer rope.

TABLE 4 SPECIMEN PARAMETERS

No.	Average Mass (g)	Initial Length (mm)	Average Thickness (mm)	Average Height (mm)	Average Diameter (mm)
1	0.1	100	-	-	0.416
2	0.103	100	-	-	0.432
3	0.110	100	-	-	0.443
4	0.1	100	-	-	0.420
5	0.11	100	-	-	0.405
6	0.105	100	-	-	0.407
7	0.1	100	-	-	0.401

8	0.031	100	0.353	1.241	-
9	0.034	100	0.430	1.240	-
10	0.032	100	0.294	1.221	-

D. Mechanical Testing: Breaking force and elongation at maximum breaking force

The samples were kept under normal conditions for 24 hours in a controlled environment according to the standard temperature, relative humidity, and pressure specified by ISO 139:19732. The breaking force and elongation at break of individual composite polymer rope specimens were measured using ISO 5079:2020. The physical and mechanical properties of the fiber ropes were measured using ISO 2307:2010. The process parameters for the standard atmospheres for conditioning and testing are shown in Table 5.

TABLE 5 PROCESS PARAMETERS FOR STANDARD ATMOSPHERES FOR CONDITIONING AND TESTING

Parameter	Value	Unit
Temperature	25±10; (21)	°C
Relative humidity	45-80; (W (% RM)) = 60	%
Atmospheric pressure	84.0-106.7; (760)	kPa (mm Hg)
Clamping length	10	cm
Clamping area	5	cm
Pre-load	5	H
Elongation speed	5	mm/s

E. Stiffness and Young's Modulus

The Young's modulus E (Pa) of the specimens was calculated using the following equation [35]:

$$E = \frac{FL}{A\Delta L} \quad \dots (1)$$

where F is the breaking force (N), L is the initial length (mm), A is the cross-sectional area (mm²), and ΔL is the elongation at maximum breaking force (mm). Young's modulus (E) is the material's stiffness and it measures the resistance to deformation under tensile stress [36].

The stiffness modulus k (N/m) of the specimens was calculated by multiplying the Young's modulus (E) by the cross-sectional area (A) and dividing by the initial sample length (L), as follows [35]:

$$k = EA/L \quad \dots (2)$$

The stiffness modulus k is the ratio of the applied force to the displacement caused by it along the same axis.

F. Study of the Samples' Surface Morphology

An Olympus LEXT OLS5000 3D Measuring Laser Microscope (Japan) was used to obtain surface images and 3D relief of the samples, and to measure their roughness. For this study, smooth areas on the sample surface without initial (113-1125 times magnification) visible defects—pores, cracks, or grooves—were selected at a magnification of 2255 times. This microscope allows us to obtain surface optical images and 3D models at 113, 227, 451, 1125, and 2255 times magnification for measuring the dimensions of the surface elements, and determining the surface roughness S_a (arithmetical mean height) (µm), S_z (maximum height) (µm), and S_q (root mean square height) (µm).

ISO 5079:2020

III. RESULTS AND DISCUSSION

A. Breaking force and elongation

The results shown in Table 6 indicate that the composite polymer ropes have different mechanical properties depending on the type. The highest average breaking force was observed for sample 3 (154.85 N), followed by sample 6 (149.11 N) and sample 5 (147.30 N). The lowest average breaking force was observed for sample 1 (73.04 N), followed by sample 4 (116.50 N) and sample 2 (122.12 N). The highest elongation at maximum breaking force was observed for sample 6 (13.28 mm), followed by sample 5 (12.76 mm) and sample 7 (12.20 mm). The lowest elongation at maximum breaking force was observed for sample 1 (5.51 mm), followed by sample 9 (9.99 mm) and sample 4 (8.61 mm). A visual comparative assessment of the test results of breaking force and elongation at maximum breaking force of the ten samples in accordance with ISO 5079:2020 is depicted in Fig. 3 and 4.

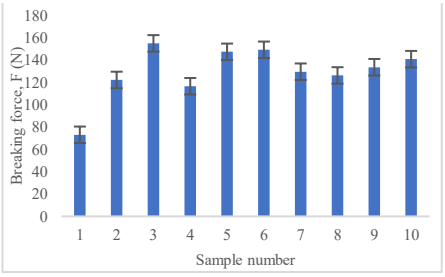

Fig. 3. Comparison graph of the values of breaking force of the ten samples

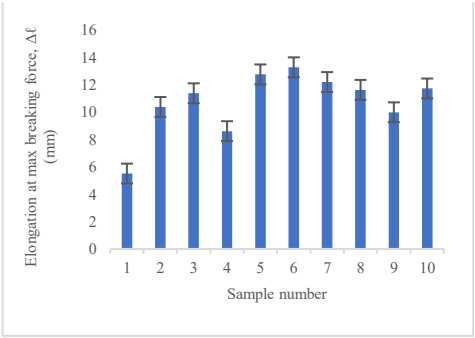

Fig. 4. Comparison graph of the values of elongation at maximum breaking force of the ten samples.

TABLE 6 TEST RESULTS OF BREAKING FORCE AND ELONGATION AT ISO 5079:2020 .KING FORCE

No.	Average Breaking Force, F (N)	Average Elongation at Max. Breaking Force, Δℓ (mm)
1	73.04	5.51
2	122.12	10.38
3	154.85	11.38
4	116.50	8.61
5	147.30	12.76
6	149.11	13.28
7	129.50	12.20

8	126.14	11.63
9	133.51	9.99
10	140.72	11.73

The samples processed through the Prematech and Sima extruders (samples 1, 3, 5, and 8) exhibited higher breaking forces, indicative of enhanced structural integrity. The elevated screw area temperatures and medium-to-hard rope hardness contributed to better molecular alignment and interfacial adhesion. In contrast, the samples processed with the Miyachi and Ichikawa extruders (samples 2, 4, 6, 7, 9, and 10) showed lower breaking forces, suggesting that lower screw area temperatures and softer rope hardness may lead to reduced tensile strength.

The breaking force of 73.05 N observed in sample 1, which was the lowest breaking force observed among all samples, produced by the Prematech extruder with the highest screw area temperature and medium rope hardness, aligns with the general trend. The highest breaking force of 154.85 N was observed in sample 3, which was composed of 30% PE-HD Liten® TB 49-060 and 70% PP Mosten® TB002. These results can be attributed to the specific combination of polymer blend composition and extrusion process parameters employed by both the Prematech and Sima extruders.

The $CaCO_3$ filler content also had a significant effect on the breaking force and elongation of the ropes. The ropes with 5% $CaCO_3$ filler (samples 9 and 10) had relatively a lower average elongation (compared to the sample 6) but samples 6 and 10 had higher breaking force compared to the sample 9. Sample 6, with 5% $CaCO_3$, displayed the highest breaking force (149.11 N) among all samples (excluding sample 3), emphasizing the positive impact of $CaCO_3$ in enhancing the mechanical properties. The average breaking force of the ropes with 5% $CaCO_3$ increased by 14.42 % (compared to the ropes without $CaCO_3$). The average elongation at break of the ropes with 5% $CaCO_3$ increased by 16.18% compared to the ropes without $CaCO_3$. This shows that the $CaCO_3$ filler enhanced the strength and stiffness of the ropes by acting as a reinforcing agent.

The rope with a higher 10% $CaCO_3$ filler content (sample 7) had on 1.34 time average elongation higher (than samples 9 and 10) but on 11.61 time lower breaking force than the ropes with a lower 5% $CaCO_3$ filler content (samples 6, 9 and 10). This shows that the 10% $CaCO_3$ filler (compared to 5% $CaCO_3$) reduced the strength and stiffness of the ropes by acting as a diluent, lowering the polymer content, as well as the interfacial adhesion and molecular orientation of the polymer chains, thereby leading to more flexible and weaker ropes.

B. Stiffness and Young's modulus

Table 7 represents the stiffness and Young's modulus results obtained from mechanical testing, where among all the results, the two best and the two lowest, close in value, were distinguished. The samples with the highest stiffness were observed for: sample 3 ($137.39*10^2$ N/m) and sample 4 (135.67*102 N/m), while the lowest stiffness were noted: for sample 7 ($106.12*10^2$ N/m) and sample 8 ($108.46*10^2$ N/m). Similarly, the highest Young's modulus were observed for: sample 1 (9.8 GPa) and sample 4 (9.725 GPa), and the lowest Young's modulus were observed for: sample 8 (2.478 GPa) and sample 9 (2.499 GPa). A visual comparative assessment of the calculative results of stiffness and Young's modulus in the ten samples in accordance with ISO 2307:2010 is depicted in Fig. 5 and 6.

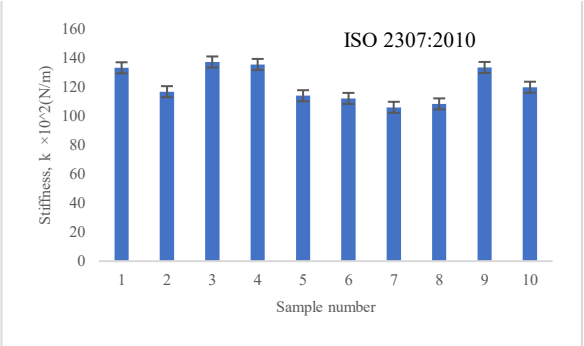

Fig. 5. Comparison graph of the stiffness values of the ten samples.

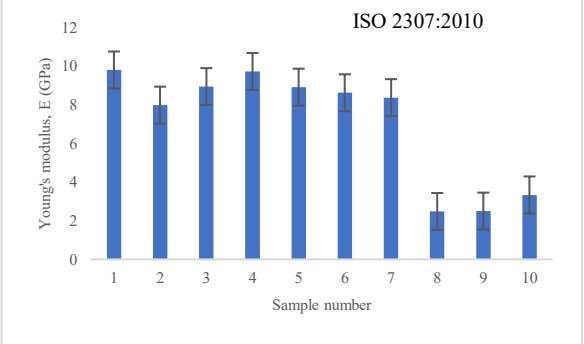

Fig. 6. Comparison graph of Young's modulus values of the ten samples.

TABLE 7. RESULTS OF STIFFNESS AND YOUNG'S MODULUS

No.	Stiffness, *k* (N/m)	Young's modulus, *E* (GPa)
1	$133.36*10^2$	9.8
2	$116.89*10^2$	7.98
3	$137.39*10^2$	8.94
4	$135.67*10^2$	9.725
5	$114.11*10^2$	8.91
6	$112.24*10^2$	8.62
7	$106.12*10^2$	8.369
8	$108.46*10^2$	2.478
9	$133.59*10^2$	2.499
10	$119.96*10^2$	3.335

The Prematech extruder, with a higher screw area temperature and medium rope hardness, resulted in sample 1 having the highest stiffness ($133.36*10^2$ N/m) and Young's modulus (9.8 GPa). The elevated temperatures likely facilitated better molecular alignment, leading to increased stiffness. This aligns with the general understanding that higher processing temperatures

contribute to a more ordered polymer structure [33], resulting in higher stiffness and Young's modulus.

Sample 3, utilizing Mosten® TB002, demonstrated the highest stiffness ($137.39*10^2$ N/m). The unique properties of Mosten® TB002, possibly related to molecular weight or chain architecture, contributed to the observed higher stiffness. This indicates the significance of raw material selection in achieving the adapted mechanical properties in polymer composite ropes.

The samples with higher stiffness and Young's modulus (samples 1, 3, and 4) were produced by the Promatech and Sima extruders, had a higher PP content, and did not have $CaCO_3$ filler. The samples with lower stiffness and Young's modulus (samples 7, 8, 9, and 10) were produced by the Miyachi and Ichikawa extruders, had a lower PP content, and had $CaCO_3$ filler. These results confirm that higher temperature and hardness of the extruders, higher PP content of the blends, and the absence of $CaCO_3$ filler enhanced the stiffness and Young's modulus of the ropes, while lower temperature and hardness of the extruders, lower PP content of the blends, and the presence of $CaCO_3$ filler reduced the stiffness and Young's modulus of the ropes. The obtained result well correlated with [37].

Samples 6, 7, and 9, containing $CaCO_3$, exhibited improved stiffness compared to their counterparts without $CaCO_3$. Sample 6, with 5% $CaCO_3$, demonstrated the highest stiffness ($112.24*10^2$ N/m), indicating that the addition of $CaCO_3$ contributed to the composite rope's stiffness. The positive impact of $CaCO_3$ on stiffness is in line with its role in reducing the overall rigidity of the composite rope, making it more flexible for specific applications. $CaCO_3$ addition, surprisingly, resulted in a modest reduction in stiffness, with $CaCO_3$-containing samples showing an average decrease of 2.1% compared to those without $CaCO_3$. $CaCO_3$ led to a significant reduction in Young's modulus, with the $CaCO_3$-containing samples showing an average reduction of approximately 66.4% compared to samples without $CaCO_3$.

The breaking force of the Ichikawa extruder-produced composite ropes surpassed those observed in prior studies by 51.49% to 54.07%, indicating a significant improvement in mechanical performance. Comparative analysis with prior studies [32], [38], and [39] reveals that sample 6 (66.5% PP, 28.5% PE, 5% $CaCO_3$) exhibits a 54.07% higher breaking force than that reported in a prior study [32] (70% PP, 25% PE, 5% $CaCO_3$). This improvement is attributed to sample 6's higher PP content and lower PE content, enhancing its stiffness, strength, and crystallinity, while a lower $CaCO_3$ content reduces brittleness and stiffness, and improves ductility and impact resistance. Similarly, the elongation at maximum breaking force surpasses that observed in prior studies by 51.85% to 56.32%. Notably, sample 6 displays a 56.32% higher elongation compared to study [32], credited to its lower PP content and higher PE content, thereby promoting its ductility, toughness, and flexibility. Maintaining the same $CaCO_3$ content as study [38] minimized the impact on composite deformation and strain. In contrast, stiffness was 17.04% to 21.88% lower compared with studies [32], [38], and [39]. Specifically, sample 9 (65% PP, 30% PE, 5% $CaCO_3$) exhibited a 21.88% higher stiffness than a prior study [38], attributed to its higher PE and lower $CaCO_3$ content, improving ductility and flexibility. A lower PP content reduced the modulus, strength, and crystallinity, enhancing deformation and strain. Also, it should be noted, Young's modulus was 9.05% to 12.45% lower, with sample 9 displaying a reduction of 12.45% compared to study [40]. This is attributed to sample 9's higher PE and lower $CaCO_3$ content, reducing stiffness, strength, and crystallinity, along with a lower PP content further reducing the modulus and improving deformation and strain.

Lastly, at 5 wt% $CaCO_3$, it is well dispersed in the matrix. However, at a higher ratio, the $CaCO_3$ particle (compared with 10 wt%) tends to gather to form bigger clusters; therefore, these clusters could play as defects, resulting in lower mechanical properties. The interfacial connection and compatibility between PE, PP, and $CaCO_3$ reinforce the mechanical properties of the plastic. This effect could be mostly generated from the formation of β-form crystalline of PP, caused by the synergistic effect between PE and $CaCO_3$ [41], [42].

C. Study of the Surface Morphology of the Samples

Fig. 7 shows the surface structure of the sample 1. These are presented under two different magnifications: (a) 113 times (image area size of 2.57 x 2.57 mkm) and (b) 2255 times (image area size of 128 x 127 mkm). The red squares in (a) show the corresponding location in (b) under higher magnification. The colored scale in (b) shows the height change in mkm on the viewed surface. The measurement of surface roughness was carried out along 30 points on the sample surface (along the transverse line based on the mode indicated in Fig. 7), and the average value is shown in Table 8.

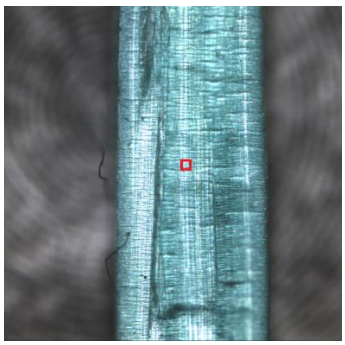

(a)

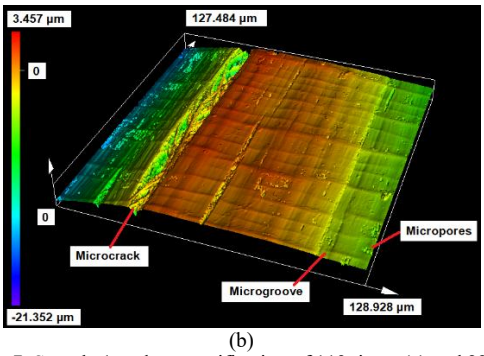

(b)

Fig. 7. Sample 1 under magnification of 113 times (a) and 2255 times (b).

In samples 1 and 4–10, in the longitudinal direction of the fiber, microgrooves can be observed on the surface (in samples 1, 6, and 7, there are possibly also microcracks because they have an uneven surface), with a width and depth of 1–8 µm; in samples 2 and 3, there are practically no microgrooves.

In samples 1–5, in the transverse direction of the fiber, there are ridges (ramps) that are 0.5–2.5 µm high (the surface of all these ridges is smooth); in samples 6–10, there are practically no such ridges.

The surface roughness was measured in a square size of 32 x 32 µm located in the center of the analyzed area (128 x 127 µm) of the sample (Fig. 8). A relatively small area (32 x 32 µm) was used because the surface of the samples is not flat (it is curved). In this case, only the microstructure was studied (the macrostructure with its defects was not taken into account). Surface roughness S_a, S_z, and S_q are shown in Table 8.

The surface of sample 3 has the least number of defects and one of the smallest roughness values. Perhaps for this reason, the breaking force (Table 6) and stiffness (Table 7) are the highest for this sample in comparison with the other nine samples.

It is highly important to know and analyze the surface morphology of a material, primarily due to the performance characteristics of the product (the fishing net).Microscopic abrasive particles (sand, corundum, etc.), which are present in seawater, can become stuck on surface defects (micropores, microgrooves, and microcracks) [43]. During operation, they will accelerate the material's wear process. Additionally, seawater is an "aggressive" environment for the operation of rope materials due to the seawater chemical composition. Six major ions make up > 99% of the salts dissolved in seawater: four cations—sodium (Na^+), magnesium (Mg^{2+}), calcium (Ca^{2+}), and potassium (K^+)—and two anions—chloride (Cl^-) and sulfate (SO_4^{2-}) [44]. These six ions and the five next most common ones make up the major constituents of seawater and comprise 99.99% of dissolved materials; they have a chemical effect on rope materials and accelerate their aging; this leads to the breakdown of the polymer chains (in materials made of polymer fiber) [45]. Aging is faster on surface defects. Both wear and aging processes reduce the lifespan of fishing nets. Therefore, a material with a minimum number of surface defects is optimal. In this investigation, it is sample number 3.

In the comparison of surface values, samples 1, 2, 4, 6, 7, 9, and 10 exhibit moderate surface roughness, indicating a textured surface. The variations observed can be attributed to differences in extruder types, polymer compositions, and the inclusion of $CaCO_3$. In particular, sample 8 deviates from the trend with a higher surface roughness value of 0.324±0.071 µm (S_a). However, it is crucial to note that this result comes with a relative error, emphasizing the necessity of considering measurement uncertainties during surface roughness assessments.

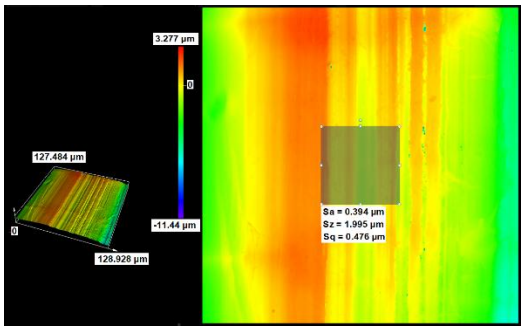

Fig. 8. Example of roughness measurement (sample no. 8).

TABLE 8. RESULTS OF SURFACE ROUGHNESS

No.	Average Roughness Sa (µm)	Average Roughness Sz (µm)	Average Roughness Sq (µm)
1	0.282	6.273	0.366
2	0.227	3.228	0.303
3	0.178	1.104	0.215
4	0.206	4.081	0.318
5	0.228	3.180	0.316
6	0.233	2.592	0.280
7	0.284	2.997	0.361
8	0.324	2.042	0.383
9	0.145	5.905	0.231
10	0.165	4.555	0.206

The relative errors of each measurement were S_a=22%, S_z=20%, and S_q=23%.

The roughness of the rope material may have a positive effect on the adhesion of the fibers in the rope, depending on the type of material, the type of extruder, and the type of additive [46]. Roughness can increase the surface area and the mechanical interlocking of the fibers, which can improve the cohesion and strength of the rope [47]. However, roughness can also introduce defects and irregularities that can reduce the uniformity and quality of the rope [48]. Therefore, the optimal roughness of the rope material depends on the balance between these factors. According to a study conducted at the University of Pittsburgh, surface roughness affects the functional properties of surfaces, including adhesion [49]. Roughness imparts an additional surface area with which an adhesive can make contact when forming a bond. Another study found that there is a clear dependency between the adhesive bond strength and surface roughness [50].

Roughness, micropores, and microcracks primarily affect the strength characteristics (strength and reliability of the sample).

For the first sample, the average roughness index (S_z) is 6.273 μm and the number of micropores (in the study area) is the highest compared to the other nine samples. Therefore, the breaking force (F_1=73.04±2 N) is almost two times lower than that for the other nine samples. However, it is possible the high surface roughness of the filaments (S_a = 0.282±14 mkm, S_z = 6.273±13 mkm, and S_q = 0.366±12 mkm), in combination with the physical and mechanical properties of the composite polymer (PP, PE) (Table 2), has an impact on the stiffness value of the sample, which shows one of the highest values of k_1=133.36*10^2 N/m in comparison to samples 2, 5, 6, 7, 8, and 10 (the average value of which is k_{avg}=112*10^2 N/m). At the same time, Young's modulus (which determines the properties of the material) is also the highest (E_1=9.8 GPa) out of the 10 samples studied. With a slight deviation, the same values of Young's modulus are characteristic of samples 2–7 (Table 5); their values are almost 3.3 times higher than those for samples 8–10.

It is possible that the roughness and strength of a material are influenced by its production conditions (the technical data for the production of the samples on an extruder). For example, with the same combinations of composite materials (comparing the first and eighth samples) but produced on different types of extruders (first sample—Promatech extruder; eighth sample—Ichikawa extruder; Table 1), the breaking force for the eighth sample is 1.73 times higher than that for the first sample, while the roughness (compared using the S_z value) is three times less. It can also be noted that using composite raw materials from different suppliers (for example, first sample: PP Capilene®, PE-HD Liten®; second sample: PP SS-05:F401, PE-HD Liten®; third sample: PP Mosten® TB002, PE-HD Liten® (Table 1)), but with the samples produced on the same type of equipment (Promatech extruder), results in different values of the breaking force, namely, the breaking force increases algebraically (F_1=73.04±2 N; F_2=122.12±2 N; F_3=154.85±3 N), and the elongation at break $\Delta\ell$ increases accordingly (Table 4). This means that under the same production conditions (on the same type of extruder equipment), but using different types of raw materials, we obtain different values for the physical and mechanical parameters of the samples [32], [37], [51].

However, when comparing the stiffness and Young's modulus for samples 1–3, it can be noted that the stiffness of the second sample is significantly lower (k_2=116.89*10^2 N/m) than the average value for the first and third samples (k_{avg}=135.38 *10^2 N/ m). The same pattern is observed for the Young's modulus values (E_2 = 7.98 GPa; for the first and third samples: E_1 = 9.8 GPa and E_3 = 8.94 GPa). Furthermore, during the tactile subjective assessment, it was noted that the second sample was the hardest to the touch compared to the other nine samples. This means that the production of the final products (such as fishing nets) will be significantly difficult (in the process of knitting fibers on textile machines).

The same pattern (during tactile assessment) was observed for the fifth sample (the sample was hard to the touch). The values of roughness, stiffness, and Young's modulus, when compared with the corresponding values for the second and fifth samples, are correlated. However, the values of breaking force and elongation at maximum breaking force of the fifth sample (F_5=147.30±3 N; $\Delta\ell_5$=12.76±0.4 mm) are higher than those for the second sample (F_2=122.12±2 N; $\Delta\ell_2$=10.38±0.2 mm) (Table 4). Obviously, the quality indicators of the fifth sample are influenced by either the type of raw materials (PP Mosten® TB002; PE-HD Liten®) or the type of extruder equipment selected (technological production conditions) (Sima extruder) (Table 1).

Regarding tactile properties, it can be noted that the fourth sample is characterized by high softness compared to the other nine samples. Despite this, the fourth sample is characterized by high stiffness values (k_5=135.67*10^2 N/m) and Young's modulus (E_5=9.725 GPa), compared to the corresponding values for samples 2, 5, 6, 7, 8, and 10, whose average values are k_{avr}=112.96*10^2 N/m and E_{avr}=6.62 GPa (Table 5). However, the average roughness value, which is almost two times higher than that for samples 3, 6, 7, and 8, and the presence of microcracks affect the breaking force (F_4=116.50±1 N) and elongation of the sample ($\Delta\ell_4$=8.61±0.3 mm), whose values are the lowest compared to the other samples (3, 5, 6, 7, 8, 9, and 10).

The inclusion of $CaCO_3$ in the composition of the polymer material (sixth and seventh samples, Table 1) did not affect the roughness indicators of the samples, compared to the eighth sample (without $CaCO_3$). However, the addition of $CaCO_3$ affected the presence of longitudinal microcracks in the sixth and seventh samples. This may be a consequence of insufficient homogeneity of the polymer composite. It should be noted that the addition of $CaCO_3$ to the composition of the polymer (sixth sample) sharply increased the breaking force F_6=149.11±4 N and elongation at maximum breaking force $\Delta\ell_6$=13.28±0.3 mm, compared with the values of the breaking force and elongation at maximum breaking force of the seventh and eight samples: F_7=129.50±2 N; $\Delta\ell_7$=12.20±0.2 mm; F_8=126.14±3 N; $\Delta\ell_8$=11.63±0.4 mm. However, the stiffness values for samples 6, 7, and 8 practically correlate, with k_{avr}=108.94*10^2 N/m, but the value of Young's modulus for the eighth sample (without $CaCO_3$) is 3.4 times lower than for that of the sixth and seventh samples. This proves that the presence of $CaCO_3$ in the composite increases the breaking force, elongation at maximum breaking, stiffness, and elastic modulus, and 5% $CaCO_3$ is preferable to 10% $CaCO_3$, it correlates with [31].

Adding 5% of $CaCO_3$ to the composition of the polymer material in such a way that the percentile amount of either PP or PE is changed (ninth and tenth samples, Table 1) leads to a significant increase in the sample surface roughness (S_z) by almost 2.5 times compared to the

roughness values for samples 6, 7, and 8 (samples 6–10 were produced on the same type of Ichikawa extruder and the same types of raw materials were used), which allows us to compare the roughness values and physical and mechanical characteristics with each other. As shown in the analysis of the surface structure of the ninth and tenth samples, they are characterized by micropores. This may also be the result of insufficient homogenization of the polymers, combined with the addition of 5% $CaCO_3$ to the composite structure. However, with such a percentage combination of PP, PE, and 5% $CaCO_3$ (ninth and tenth samples), the values of the breaking force increase significantly and amount to F_9=133.51±2 N and F_{10}=140.72±3 N compared with the values of the breaking force for samples 6, 7, and 8. There is also an increase in the stiffness of the ninth and tenth samples: k_9=133.59*10^2 N/m and k_{10}=119.96*10^2 N/m compared to samples 6–8, whose average value is k_{avr}=108.94*10^2 N/m. At the same time, the Young's modulus, which characterizes the ability of a material to resist tension, during the elastic deformation of the ninth sample is E_9=2.449 GPa; for the tenth sample, it increases slightly to E_{10}=3.335 GPa.

However, the average value of Young's modulus for the ninth and tenth samples correlates with the value of Young's modulus for the eighth sample (without $CaCO_3$) but is three times lower than for the sixth and seventh samples (E_{avr}=8.49 GPa). If we optimize the choice of the combination of polymer components in the composite based on the breaking force (between the ninth and tenth samples), and then with the percentage of components for the tenth sample (PP 70%; PE 25%; $CaCO_3$ 5%), the breaking force is higher than for the ninth sample. However, the surface roughness of the ninth and tenth samples (when comparing their values with samples 6, 7, and 8) is two times higher; this negatively affects the performance characteristics of products such as fishing nets.

These findings have significant implications for the fishing industry and other sec-tors utilizing composite polymer ropes. By optimizing extrusion parameters, carefully se-lecting raw materials, and judiciously incorporating additives like $CaCO_3$, manufacturers can tailor rope properties to meet specific application requirements. This level of custom-ization could lead to improved performance, longevity, and sustainability of fishing gear and other rope-based products.

Future research directions may include further investigation into the long-term per-formance and durability of composite ropes under various environmental conditions, the exploration of additional additives or surface treatments to enhance specific properties such as UV resistance or biodegradability, and the development of predictive models to streamline the optimization process for new composite rope formulations.

IV. CONCLUSIONS

This study demonstrates that the mechanical properties of composite polymer ropes result from a complex interplay between extrusion process parameters, polymer composition, and the inclusion of calcium carbonate ($CaCO_3$).

The choice of the extruder and its associated parameters proved crucial in determining the rope quality. Notably, the Promatech and Sima extruders, characterized by higher (11.6-17.1%) screw area temperatures and medium-to-hard rope hardness, generally produced ropes with superior breaking forces. These findings highlight the importance of optimizing the processing conditions to achieve the desired mechanical properties in composite ropes.

The incorporation of $CaCO_3$ yielded positive results in terms of flexibility enhancement. The samples containing $CaCO_3$ exhibited an average increase of 14.42% in breakingforce compared to those without, indicating a reinforcement effect that contributed to increased flexibility and energy absorption capacity. However, this study also revealed an optimal $CaCO_3$ content of 5%, beyond which mechanical properties may begin to deteriorate, suggesting a threshold effect for $CaCO_3$ reinforcement.

The selection of raw materials emerged as a significant factor influencing rope properties. The use of Mosten® TB002 in sample 3 resulted in exceptional breaking force (154.85 N) and stiffness (137.39*10^2 N/m), demonstrating the potential for tailoring rope properties through the careful selection of polymer blends.

An analysis of the surface morphology revealed a correlation between surface defects, roughness, and mechanical properties. Sample 3, with the lowest number of surface defects and one of the lowest roughness values, exhibited the highest breaking force and stiffness (137.39*10^2 N/m) among all samples. This finding emphasizes the importance of surface quality in determining the overall performance of composite ropes and suggests that minimizing surface defects could be a key strategy for enhancing rope durability and strength.

This research elucidated important relationships between processing conditions, structural characteristics, and the final properties of composite ropes. These processing–structure–property relationships provide valuable insights for optimizing production processes to achieve the desired rope characteristics.

REFERENCES

[1] B. Baye and T. Tesfaye, "The new generation fibers: a review of high performance and specialty fibers," Polym. Bull., vol. 79, no. 11, pp. 9221–9235, 2022, doi: 10.1007/s00289-021-03966-6.

[2] I. Lasenko, J. V Sanchaniya, S. P. Kanukuntla, A. Viluma-Gudmona, S. Vasilevska, and S. R. Vejanand, "Assessment of Physical and Mechanical Parameters of Spun-Bond Nonwoven Fabric," Polymers, vol. 16, no. 20. 2024. doi: 10.3390/polym16202920.

[3] K. Dharmalingam and R. Anandalakshmi, Polysaccharide-Based Films for Food Packaging Applications. 2019. doi: 10.1007/978-981-32-9804-0_9.

[4] H. Mohammadi, Z. Ahmad, S.A. Mazlan, M.A. Faizal Johari, G. Siebert, M. Petrů, S.S. Rahimian Koloor, "Lightweight Glass Fiber-Reinforced Polymer Composite for Automotive Bumper Applications: A Review," Polymers (Basel)., vol. 15,

no. 1, pp. 1–30, 2023, doi: 10.3390/polym15010193.

[5] V. T. Rathod, J. S. Kumar, and A. Jain, "Polymer and ceramic nanocomposites for aerospace applications," Appl. Nanosci., vol. 7, no. 8, pp. 519–548, 2017, doi: 10.1007/s13204-017-0592-9.

[6] J. Jeevanandam, S. Pan, J. Rodrigues, M. A. Elkodous, and M. K. Danquah, "Medical applications of biopolymer nanofibers," Biomater. Sci., vol. 10, no. 15, pp. 4107–4118, 2022, doi: 10.1039/D2BM00701K.

[7] J.V. Sanchaniya, I. Lasenko, S.-P. Kanukuntala, H. Smogor, A. Viluma-Gudmona, A. Krasnikovs, V. Gobins, I. Tipans, "Mechanical and thermal characteristics of annealed-oriented PAN nanofibers," Polymers (Basel)., 2023, doi: doi.org/10.3390/polym15153287.

[8] J. V. Sanchaniya, I. Lasenko, S. P. Kanukuntla, A. Mannodi, A. Viluma-gudmona, and V. Gobins, "Preparation and Characterization of Non-Crimping Laminated Textile Composites Reinforced with Electrospun Nanofibers," Nanomaterials, vol. 13, no. 13, p. 1949, 2023, doi: 10.3390/nano13131949.

[9] D. Grauda, D. Butkauskas, R Vyšniauskienė, V. Rančelienė, N. Krasņevska, A. Miķelsone, K. Žagata, V. Gobiņš, I. Rashal, D. Rašals,, "Establishment of Biotesting System to Study Features of Innovative Multifunctional Biotextile," Proc. Latv. Acad. Sci. Sect. B Nat. Exact, Appl. Sci., vol. 77, no. 3–4, pp. 186–192, 2023, doi: 10.2478/prolas-2023-0026.

[10] A. D. Mori, A. Karali, E. Daskalakis, R. Hing, P. S. D. Jorge, G. Cooper, G. Blunn, "Poly- ε -Caprolactone 3D-Printed Porous Scaffold in a Femoral Condyle Defect Model Induces Early Osteo-Regeneration," pp. 1–14, 2024.

[11] J. V Sanchaniya and S. Kanukuntla, "Morphology and mechanical properties of PAN nanofiber mat," J. Phys. Conf. Ser., vol. 2423, no. 1, p. 012018, 2023, doi: 10.1088/1742-6596/2423/1/012018.

[12] J. V. Sanchaniya, S.-P. Kanukuntla, S. Simon, and A. Gerina-Ancane, "Analysis of mechanical properties of composite nanofibers constructed on rotating drum and collector plate," 21st Int. Sci. Conf. Eng. Rural Dev. Proc., vol. 21, pp. 737–744, 2022, doi: 10.22616/erdev.2022.21.tf227.

[13] S. Gao, G. Tang, D. Hua, R. Xiong, J. Han, S. Jiang, Q. Zhang, C. Huang, "Stimuli-responsive bio-based polymeric systems and their applications," J. Mater. Chem. B, vol. 7, no. 5, pp. 709–729, 2019, doi: 10.1039/c8tb02491j.

[14] J. V. Sanchaniya, I. Lasenko, V. Gobins, and A. Kobeissi, "A Finite Element Method for Determining the Mechanical Properties of Electrospun Nanofibrous Mats," Polym., vol. 16, no. 6, p. 852, 2024, doi: 10.3390/polym16060852.

[15] J.V. Sanchaniya, I. Lasenko, V. Vijayan, H. Smogor, V. Gobins, A. Kobeissi, D. Goljandin, "A Novel Method to Enhance the Mechanical Properties of Polyacrylonitrile Nanofiber Mats: An Experimental and Numerical Investigation," Polymers (Basel)., vol. 16, no. 7, p. 992, Apr. 2024, doi: 10.3390/polym16070992.

[16] R. Skvorčinskienė, N. Striūgas, R. Navakas, R. Paulauskas, K. Zakarauskas, and L. Vorotinskienė, "Thermal Analysis of Waste Fishing Nets for Polymer Recovery," Waste and Biomass Valorization, vol. 10, no. 12, pp. 3735–3744, 2019, doi: 10.1007/s12649-019-00803-w.

[17] C. Wilcox, N. J. Mallos, G. H. Leonard, A. Rodriguez, and B. D. Hardesty, "Using expert elicitation to estimate the impacts of plastic pollution on marine wildlife," Mar. Policy, vol. 65, pp. 107–114, 2016, doi: 10.1016/j.marpol.2015.10.014.

[18] K. J. Parton, T. S. Galloway, and B. J. Godley, "Global review of shark and ray entanglement in anthropogenic marine debris," Endanger. Species Res., vol. 39, pp. 173–190, 2019, doi: 10.3354/esr00964.

[19] B. H. Hogan, "Net gains in aquaculture net technology," no. June, pp. 5–9, 2020.

[20] B. Qiu, M. Wang, W. Yu, S. Li, W. Zhang, S. Wang, J. Shi, "Environmentally Friendly and Broad – Spectrum Antibacterial Poly (hexamethylene guanidine)– Modified Polypropylene and," 2023.

[21] T. Sato and M. Shishido, "Mechanical and structural properties for recycled thermoplastics from waste fishing ropes," J. Mater. Cycles Waste Manag., vol. 22, no. 5, pp. 1682–1689, 2020, doi: 10.1007/s10163-020-01062-x.

[22] R. Juan, C. Domínguez, N. Robledo, B. Paredes, S. Galera, and R. A. García-Muñoz, "Challenges and opportunities for recycled polyethylene fishing nets: Towards a circular economy," Polymers (Basel)., vol. 13, no. 18, pp. 1–15, 2021, doi: 10.3390/polym13183155.

[23] A. Kozioł, K. G. Paso, and S. Kuciel, "Properties and Recyclability of Abandoned Fishing Net-Based Plastic Debris," Catalysts, vol. 12, no. 9, 2022, doi: 10.3390/catal12090948.

[24] R. Behaviors and A. L. Composites, "Rui Gou," Eff. Differ. Polypropyl. Ammonium Lignosulfonate Contents Cryst. Behav. Rheol. Behav. Mech. Prop. Ethyl. Propyl. Diene Monomer/ Polypropylene/ Ammonium, vol. 14, no. 1, pp. 2079–2096, 2019.

[25] W. Yu, F. Yang, L. Wang, Y. Liu, and J. Shi, "Starch-Based Fishing Composite Fiber and Its Degradation Behavior," Int. J. Polym. Sci., vol. 2020, 2020, doi: 10.1155/2020/9209108.

[26] M. Hyvärinen, R. Jabeen, and T. Kärki, "The modelling of extrusion processes for polymers-A review," Polymers (Basel)., vol. 12, no. 6, 2020, doi: 10.3390/polym12061306.

[27] M. Berihuete-Azorín, O. Lozovskaya, M. Herrero-Otal, and R. Piqué I Huerta, "Fishing Nets and String at the Final Mesolithic and Early Neolithic Site of Zamostje 2, Sergiev Posad (Russia)," Open Archaeol., vol. 9, no. 1, 2023, doi: 10.1515/opar-2022-0283.

[28] D. C. Chen, D. F. Chen, S. M. Huang, and W. J. Shyr, "The Investigation of Key Factors in Polypropylene Extrusion Molding Production Quality," Appl. Sci., vol. 12, no. 10, 2022, doi: 10.3390/app12105122.

[29] L. Yang, S. Li, Y. Li, M. Yang, and Q. Yuan, "Experimental Investigations for Optimizing the Extrusion Parameters on FDM PLA Printed Parts," J. Mater. Eng. Perform., vol. 28, no. 1, pp. 169–182, 2019, doi: 10.1007/s11665-018-3784-x.

[30] M. Ramesh, L. Rajeshkumar, and D. Balaji, "Influence of Process Parameters on the Properties of Additively Manufactured Fiber-Reinforced Polymer Composite Materials: A Review," J. Mater. Eng. Perform., vol. 30, no. 7, pp. 4792–4807, 2021, doi: 10.1007/s11665-021-05832-y.

[31] Y. Peng, M. Musah, B. Via, and X. Wang, "Calcium carbonate particles filled homopolymer polypropylene at different loading levels: Mechanical properties characterization and materials failure analysis," J. Compos. Sci., vol. 5, no. 11, 2021, doi: 10.3390/jcs5110302.

[32] Y. Jing, X. Nai, L. Dang, D. Zhu, Y. Wang, Y. Dong, W. Li, "Reinforcing polypropylene with calcium carbonate of different morphologies and polymorphs," Sci. Eng. Compos. Mater., vol. 25, no. 4, pp. 745–751, 2018, doi: 10.1515/secm-2015-0307.

[33] T. Thenepalli, A. Y. Jun, C. Han, C. Ramakrishna, and J. W. Ahn, "A strategy of precipitated calcium carbonate (CaCO3) fillers for enhancing the mechanical properties of polypropylene polymers," Korean J. Chem. Eng., vol. 32, no. 6, pp. 1009–1022, 2015, doi: 10.1007/s11814-015-0057-3.

[34] N. S. Yousef, "Statistical Study on Additives Used to Improve Mechanical Properties of Polypropylene," Polymers

(Basel)., vol. 14, no. 1, 2022, doi: 10.3390/polym14010179.

[35] J. R. Keaton, "Young's Modulus BT - Encyclopedia of Engineering Geology," P. T. Bobrowsky and B. Marker, Eds. Cham: Springer International Publishing, 2018, pp. 955–956. doi: 10.1007/978-3-319-73568-9_298.

[36] K. Yamamoto, A. Takasaki, and N. Hosoya, "Assessment of Dynamic Young's Modulus and Damping Ratio of Bamboo Fiber Reinforced Polymer Composites using Shock Wave BT - Advances in Mechanism and Machine Science," 2019, pp. 4217–4226.

[37] H.-N. T. Pham and V.-T. Nguyen, "Effect of calcium carbonate on the mechanical properties of polyethylene terephthalate/polypropylene blends with styrene-ethylene/butylene-styrene," J. Mech. Sci. Technol., vol. 34, no. 10, pp. 3925–3930, 2020, doi: 10.1007/s12206-020-2201-1.

[38] P. Castejón, M. Antunes, and D. Arencón, "Development of inorganic particle-filled polypropylene/high density polyethylene membranes via multilayer co-extrusion and stretching," Polymers (Basel)., vol. 13, no. 2, pp. 1–16, 2021, doi: 10.3390/polym13020306.

[39] J. Z. Liang, C. Y. Tang, R. K. Y. Li, and T. T. Wong, "Mechanical properties of polypropylene/CaCC3 composites," Met. Mater., vol. 4, no. 4, pp. 616–619, 1998, doi: 10.1007/BF03026368.

[40] S. Chen, X. Wang, X. Ma, and K. Wang, "Morphology and properties of polypropylene/nano-CaCO3 composites prepared by supercritical carbon dioxide-assisted extrusion," J. Mater. Sci., vol. 51, no. 2, pp. 708–718, 2016, doi: 10.1007/s10853-015-9272-x.

[41] F. Ke, X. Jiang, H. Xu, J. Ji, and Y. Su, "Ternary nano-CaCO 3/poly(ethylene terephthalate) fiber/polypropylene composites: Increased impact strength and reinforcing mechanism," Compos. Sci. Technol., vol. 72, no. 5, pp. 574–579, 2012, doi: 10.1016/j.compscitech.2012.01.001.

[42] J.-I. Weon and H.-J. Sue, "Mechanical properties of talc- and CaCO3-reinforced high-crystallinity polypropylene composites," J. Mater. Sci., vol. 41, no. 8, pp. 2291–2300, 2006, doi: 10.1007/s10853-006-7171-x.

[43] J. P. Duarte, C. E. M. Guilherme, A. H. M. F. T. da Silva, A. C. Mendonça, and F. Tempel Stumpf, "Lifetime prediction of aramid yarns applied to offshore mooring due to purely hydrolytic degradation," Polym. Polym. Compos., vol. 27, no. 8, pp. 518–524, 2019, doi: 10.1177/0967391119851386.

[44] J. K. Edzwald and J. Haarhoff, "Seawater pretreatment for reverse osmosis: Chemistry, contaminants, and coagulation," Water Res., vol. 45, no. 17, pp. 5428–5440, 2011, doi: 10.1016/j.watres.2011.08.014.

[45] H. Xiao, S. Liu, D. Wang, and Y. Chen, "Abrasion–Corrosion Behaviors of Steel–Steel Contact in Seawater Containing Abrasive Particles," Tribol. Trans., vol. 61, no. 1, pp. 12–18, Jan. 2018, doi: 10.1080/10402004.2016.1268227.

[46] G. Han, X. Tao, X. Li, W. Jiang, and W. Zuo, "Study of the Mechanical Properties of Ultra-High Molecular Weight Polyethylene Fiber Rope," J. Eng. Fiber. Fabr., vol. 11, no. 1, p. 155892501601100100, Mar. 2016, doi: 10.1177/155892501601100103.

[47] R. Neppalli, C. Marega, A. Marigo, M.P. Bajgai, H.Y. Kim, S.S. Ray, V. Causin, "Electrospun nylon fibers for the improvement of mechanical properties and for the control of degradation behavior of poly(lactide)-based composites," J. Mater. Res., vol. 27, no. 10, pp. 1399–1409, 2012, doi: 10.1557/jmr.2012.70.

[48] M. Spoerk, J. Gonzalez-Gutierrez, C. Lichal, H. Cajner, G.R. Berger, S. Schuschnigg, L. Cardon, C. Holzer, "Optimisation of the adhesion of polypropylene-based materials during extrusion-based additive manufacturing," Polymers (Basel)., vol. 10, no. 5, 2018, doi: 10.3390/polym10050490.

[49] Abhijeet Gujrati, "Understanding Nanoscale Surface Roughness and its Effect on Macroscale Adhesion," Master Thesis, vol. 27, p. i, 2020.

[50] S. Budhe, A. Ghumatkar, N. Birajdar, and M. D. Banea, "Effect of surface roughness using different adherend materials on the adhesive bond strength," Appl. Adhes. Sci., vol. 3, no. 1, pp. 0–9, 2015, doi: 10.1186/s40563-015-0050-4.

[51] M. D. Roussel, A. R. Guy, L. G. Shaw, and J. E. Cara, "The use of calcium carbonate in polyolefins offers significant improvement in productivity," TAPPI Eur. PLACE Conf., vol. 1, pp. 225–236, 2005.

Environment. Technology. Resources. Rezekne, Latvia
Proceedings of the 16th International Scientific and Practical Conference. 2025. Volume IV, 181-184

Determination of Axial Forces of Tool Elements for Plastically Strengthening Hole Machining

Angel Lengerov
Technical University of Sofia, Branch Plovdiv
CoC "Smart Mechatronics, Eco- and Energy Saving Systems and Technologies"
Plovdiv, Bulgaria
anlen@tu-plovdiv.bg

Nadya Arabadzhieva
University of Food Technologies
Plovdiv, Bulgaria
n_arabadzhieva@uft-plovdiv.bg

Silvia Salapateva
Technical University of Sofia, Branch Plovdiv
CoC "Smart Mechatronics, Eco- and Energy Saving Systems and Technologies"
Plovdiv, Bulgaria
sisisal@tu-plovdiv.bg

***Abstract*—When machining holes by burnishing, there is a direct relationship between the main parameter - the applied force and the geometric elements of the deforming rollers. This relationship can be determined by considering the force balance of the tool during operation. It is determined by the accuracy of the workpiece positioning and tool adjustment, and is expressed in the unevenness of the allowance, both in the transverse and in the proper section of the workpiece. The nature of the errors obtained and their magnitude depend, in addition to the accuracy of the relative position of the workpiece and the tool, on the scheme and operating mode. In order to simplify the analysis, it is necessary to neglect the friction forces during rolling and the magnitude of the elastic recovery of the material after burnishing. The tightness of the deforming elements is formed depending on the prescribed roughness of the surfaces, the type of material being processed and the type of tool. The rate of deformation of the machined holes is limited by the power of the machine and the design features of the deforming separator tool. This publication provides analytical dependencies for determining axial components of the deforming force using roller-ball separator tools for machining holes. Dependencies are derived for determining the optimal number of deforming elements ensuring a given accuracy of machined surfaces.The obtained analytical dependencies allow, under given production conditions, to ensure the necessary quality indicators of processing by changing the number of deforming elements and their radius in the tool design. From the condition for dynamic equilibrium of the support cone, the relationship between the cutting force and the deformation force can be revealed. This is a prerequisite for determining the transmission coefficients of the power chain for the two types of deforming elements - balls and rollers.**

Keywords*— *axial force, strain elements, holes, quality.

I. INTRODUCTION

The method of surfaces finishing of structural steels is based on strain of microroughness of surface layer of metal, which helps to form quality indicators of parts[1].

By means of burnishing in the conditions of force contact interaction of surface with deforming elements, performing a given movement and having a certain shape and geometry, a significant reduction in height of roughness of the cylindrical holes is obtained[2].[3].[4].The hardness of the metal of the deforming elements must be higher than the hardness of the processed metal and the roughness of the deforming surfaces is less than desired roughness of the processed surfaces[5].

During the force interaction in the contact zone between the strain elements and the processed surfaces, high pressure and stresses arise, which cause elastic and plastic deformations in the surface layer of the processed surface, as a result of this impact, the latter changes its roughness, and the surface layer changes its structure, physical-mechanical and chemical properties[6]. The purpose of this article is to determine the necessary axial force to overcome the friction forces of ball and roller deforming elements of combined tools for machining holes. This will allow the creation of methodologies for optimized technological parameters of burnishing process based on the roughness of the machined surfaces. Through a comparative analysis with the application of recommended and computational modes of cutting and burnishing processing, it is possible to obtain results for the efficiency of the process depending on the length of the tool.

Online ISSN 2256-070X
https://doi.org/10.17770/etr2025vol4.8455
© 2025 The Author(s). Published by RTU PRESS.
This is an open access article under the Creative Commons Attribution 4.0 International License.

II. MATERIALS AND METHODS

The analysis of the burnishing process requires a detailed consideration of force balance of the conical deforming rollers and deforming balls in their interaction with other structural elements of the tool and the machined hole[7].

The deforming elements are rollers and balls from standard rolling bearings[8]. The balls have a diameter of ϕ=8mm and ϕ=10mm. The conical rollers have a slope of 2°30' and 3°, and the large diameter is ϕ=6.5 mm and ϕ=8.2 mm with a length of 10 mm and 15 mm, respectively[9]. The radius of curvature at the deforming end of the rollers is ρ=2.5÷3 mm. The angle of the smoothing part φ_1, depending on the roller setting, is recommended to be minimal, and for steel machining it is 20'<φ_1< 50' φ_1=30' is selected. Standard rollers were used due to the difficulty in producing original ones in the conditions of single production by the factories - implementers of such tools.

The quality of the processed surfaces is also influenced by the type of connection of the deforming elements - rigid, elastic and with self-regulation[10]. For this purpose, when studying the operability of the combined tools, various designs were implemented, combined tools for processing holes.

The support cone and the separator of the tools are made of bearing steel with heat treatment to HRC = 62÷64[11]. The remaining elements are mainly made of medium carbon steel, heat treated to HRC = 40.

The deforming elements perform the role of a movable rest and a vibration damper in the system[12]. When working with such tools, a closed system is obtained, in which the energy of self-excited or forced oscillations is dissipated in the system of the cutting part, deforming part, workpiece and to a significant extent the remaining elements of the technological system are excluded.

III. RESULTS AND DISCUSSION

It is known that the friction forces during deformation are determined by the dependence[13]

$$F_{mp} = F_N^{'} tg\varphi_1 = \mu F_N^{'} \tag{1}$$

where $F_N^{'}$ is the radial component of the normal force; μ - the coefficient of sliding friction ($\mu = tg\varphi_1$).

Based on the desire to accurately determine the force factors, the assumption is taken into account that the coefficients of sliding and rolling friction between the deforming rollers and the machined surface - and between the deforming rollers and the support shaft - are not equal to each other, i.e. each of them has a specific, discrete value.

Then it may be written:

$$F_{ов} = F_N^{'} tg\left(\alpha + \varphi_2\right) \tag{2}$$

where α is the angle at the apex of the cone of the deforming rollers; F_N - the normal force to the contact surface between the deforming rollers and the support shaft; $F_N^{'}$ - the radial component of the normal force; F_o - the axial component of the normal force .

The condition for equilibrium of the forces applied along the tool axis has the form

$$F_{ов} - F_{mp} - F_{mp1} = 0 \tag{3}$$

where $F_{ов}$ is the external axial force;

F_{mp} -sliding friction force between the deforming rollers and the processed surface;

F_{mp1} - sliding friction force between the deforming rollers and the separator.

Substituting (1) and (2) into (3), and expressing the external axial force after the corresponding trigonometric transformations:

$$F_{ов} = F_N^{'}\left[\frac{tg\alpha\left(1-\mu\mu_1\right)+\mu+\mu_1}{1-\mu_1 tg\alpha}\right] \tag{4}$$

In dependence (4) the denominator and the term in small brackets would have numerical values extremely close to unity and for this reason they can be ignored, in which case the error will not exceed 0.5%. In such a case, dependence (4) takes the form

$$F_{ов} = F_N^{'}\left[\mu + \mu_1 + tg\alpha\right] \tag{5}$$

Conditions (4) and (5) reflect the process of pure sliding of the deforming roller when entering or leaving the machined hole until the completion of the machining. They also make it possible, during the experimental study of the processes, to indirectly judge the magnitude of the normal deforming force by the magnitude of the axial force. This dependence is also valid for tools with cylindrical rollers, in which case it takes the form.

$$F_{ов} = F_N^{'}\left[\mu + \mu_1\right]. \tag{6}$$

The determination of the forces acting on the deforming element is shown in Fig. 1, *a* - for the deforming element ball, and in Fig. 1, *b* - for the deforming element roller.

From the condition for force equilibrium for deforming elements balls, the following dependencies are obtained:

$$F_c = F_{n1}\sin\frac{\varphi}{2} + F_{n2}\sin\alpha \tag{7}$$

$$F_{n2} = F_{n1}\frac{\cos\frac{\varphi}{2}}{\cos\alpha} \tag{8}$$

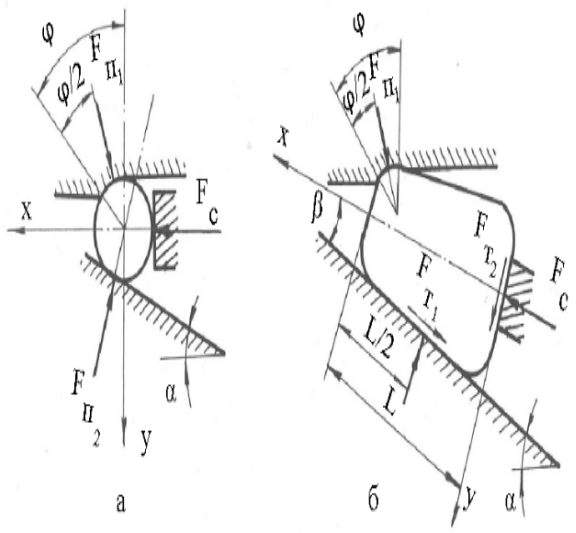

Fig. 1. Loading of the deforming element:a) ball;b) roller.

For deforming elements rollers, the following relationships are obtained:

$$F_c = F_{n1}\sin\left(\alpha-\beta+\frac{\varphi}{2}\right)-F_{n2}\left(\sin\beta+f\cos\beta\right) \quad (9)$$

$$F_{n2} = F_{n1}\frac{\cos\left(\alpha-\beta+\frac{\varphi}{2}\right)-f\sin\left(\alpha-\beta+\frac{\varphi}{2}\right)}{\cos\beta\left(1-f^2\right)-2f\sin\beta} \quad (10)$$

$$F_{n2} = F_{n1}\frac{\cos\psi-f\sin\psi}{\cos\beta\left(1-f^2\right)-2f\sin\beta} \quad (11)$$

$$F_{n2} = F_{n1}\frac{\cos\psi-f\sin\psi}{\cos\beta\left(1-f^2\right)-2f\sin\beta}. \quad (12)$$

From the dynamic equilibrium condition of the support cone, the relationship between the cutting force and the deforming force can be revealed. The loading of the cone is shown in Fig. 2.

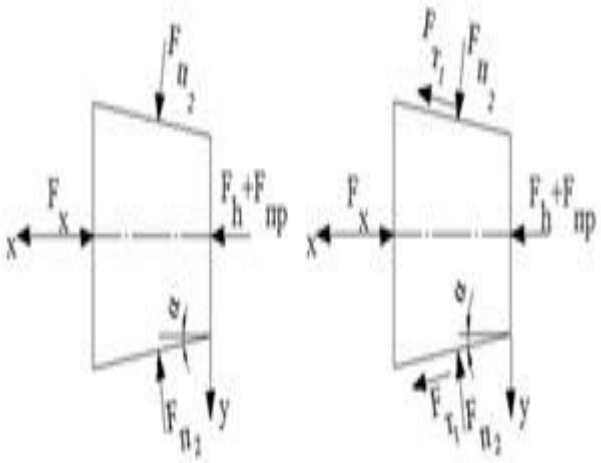

Fig. 2. Loading of the support cone: a) for a ball deforming element; b) for a roller deforming element.

For deforming elements such as balls, this relationship is expressed by the dependence:

$$F_x = zF_{n1}tg\alpha\cos\frac{\varphi}{2}+F_{np}+F_h \quad (13)$$

For deforming elements rollers the dependence has the form:

$$F_x = zF_{n1}\frac{\left(\cos\psi+f\sin\psi\right)\left(\sin\alpha+f\cos\alpha\right)}{\left(1-f^2\right)\cos\beta-2f\sin\beta}+ \quad (14)$$
$$+F_{np}+F_h$$

Here F_{np} is the force from the spring included in the tool;

F_h - the force from the hydraulic system;

z - the number of deforming elements.

From expressions (13) and (14) by differentiation, the transmission coefficients of the power chain can be determined, respectively, for deforming elements balls and rollers:

$$\frac{dF_x}{dF_{n1}} = ztg\alpha.\cos\frac{\varphi}{2} \quad (15)$$

$$\frac{dF_x}{dF_{n1}} = z\frac{\left(\cos\psi+f\sin\psi\right)\left(\sin\alpha+f\cos\alpha\right)}{\left(1-f^2\right)\cos\beta-2f\sin\beta} \quad (16)$$

Dependencies (15) and (16) can be represented in the form:

$$\frac{\partial F_x}{\partial F_{n1}} = K_c z \quad (17)$$

$$\frac{\partial F_x}{\partial F_{n1}} = K_p z \quad (18)$$

where $K_c = tg\alpha.\cos\frac{\varphi}{2}$

$$K_p = \frac{\left(\cos\psi+f\sin\psi\right)\left(\sin\alpha+f\cos\alpha\right)}{\left(1-f^2\right)\cos\beta-2f\sin\beta}.$$

From the expressions of the total differential of the functions (13) and (14), by moving to finite increments of F_x and Fn1, we can write:

$$\Delta F_x = \Delta F_{n1}\frac{\partial F_x}{\partial F_{n1}} \quad (19)$$

The permissible fluctuation of the deforming force can be determined from the condition for ensuring the quality of the surface treated with burnishing [2]:

$q = \left(1,8\div2,1\right)\sigma_s$

Therefore, where we can obtain an expression for the permissible fluctuation of the deforming force:

$$\Delta F_{n1} = 0,3\pi\sigma_s \left(r.\sin\varphi\right)^2 \quad (20)$$

After substituting in (19) the partial derivatives with expressions (17) and (18) and the permissible change of the deforming force in expression (20), we obtain:

$$\Delta F_x = 0,3\pi\sigma_s \sin^2\varphi.r^2.K_c.z \quad (21)$$

$$\Delta F_x = 0,3\pi\sigma_s \sin^2\varphi.r^2.K_p.z \quad (22)$$

From expressions (21) and (22) the condition for ensuring the quality of the processed surface can be obtained:

$$zr^2 = \frac{F_x}{0,3\pi\sigma_s \sin^2\varphi.K_c} \quad (23)$$

$$zr^2 = \frac{F_x}{0,3\pi\sigma_s \sin^2\varphi.K_p} \quad . \quad (24)$$

The obtained dependencies (23) and (24) allow, under given production conditions, to ensure high-quality processing by varying the number of deforming elements and their radius in the tool design[14].[15].

IV. Conclusions

Based on the derived analytical dependencies for determining the axial force during burnishing of cylindrical surfaces with rolling and ball separator tools, it is possible to ensure specified quality indicators of the surfaces. This is achieved by adjusting the number of deforming elements, providing the necessary friction forces during sliding during burnishing of cylindrical rotational surfaces.

V. Acknowledgments

This research was funded by the European Regional Development Fund within the OP " Research, Innovation and Digitalization Programme for Intelligent Transformation 2021-2027", Project CoC "Smart Mechatronics, Eco- and Energy Saving Systems and Technologies", No. BG16RFPR002-1.014-0005.

REFERENCES

[1] G. Singh, "Advanced Finishing Processes for Cylindrical Surface Finishing," 2024. [Online]. Available: https://doi.org/10.1201/9781003327905-9 (Accessed: January 3, 2025).

[2] I. Tatarintsev, V. Kuznetsov, M. Popov and V. Popov, "The Effect of Stick-Slip Friction on the Stability of Nanostructuring Burnishing," Applied Sciences, vol. 14, 2024. [Online]. Available: https://doi.org/10.3390/app142311148 (Accessed: January 3, 2025).

[3] K.Jamkamon and P. Janmanee, "Improving Machining Performance for Deep Hole Drilling in the Electrical Discharge Machining Process Using a Step Cylindrical Electrode," Applied Sciences, vol. 11, p. 2084, 2021. [Online]. Available: https://doi.org/10.3390/app11052084 (Accessed: January 3, 2025).

[4] H. Metev and K. Krumov, "Determination of Accuracy in Finishing Machining Through Surface Plastic Deformation with Account of the Phenomenon of Technological Heredity," in 12th Int. Sci. Conf. TechSys 2023, AIP Conf. Proc., vol. 3078, 2024. [Online]. Available: https://doi.org/10.1063/5.0208291 (Accessed: January 3, 2025).

[5] [O. Tiutkin, A. Radkevych, O. Dubinchyk and V. Kharchenko, "Parametric analysis of a strain state of a soil base strengthened with vertical elements," Mining of Mineral Deposits, vol. 18, pp. 104–112, 2024. [Online]. Available: https://doi.org/10.33271/mining18.02.104 (Accessed: January 3, 2025).

[6] V. Mekheda, "Modeling of elastic plastic deformation of near-surface layers of materials," Vestnik of Samara University. Natural Science Series, vol. 30, pp. 25–34, 2024. [Online]. Available: https://doi.org/10.18287/2541-7525-2024-30-3-25-34 (Accessed: January 3, 2025).

[7] J. Zhao, B. Wang and L. Zhanqiang, "The investigation into burnishing force, burnishing depth and surface morphology in rotary ultrasonic burnishing," 2016. [Online]. Available: https://doi.org/10.3969/j.issn.1000-1093.2016.04.018 (Accessed: January 3, 2025).

[8] Y. Zhao, Y. Zi, Z. Chen, M. Zhang, Y. Zhu and J. Yin, "Power Loss Investigation of Ball Bearings Considering Rolling-Sliding Contacts," International Journal of Mechanical Sciences, vol. 250, 2023. [Online]. Available: https://doi.org/10.1016/j.ijmecsci.2023.108318 (Accessed: January 3, 2025).

[9] N. Sherbutaev, A. Goncharuk, R. Iskhakov and O. Starichkova, "Development of universal mathematical model for calculation of the geometrical parameters of deformation zone during tube rolling using piercing mills with cup-shaped, barrel type and conical rollers," Ferrous Metallurgy, vol. 78, pp. 150–159, 2022. [Online]. Available: https://doi.org/10.32339/0135-5910-2022-2-150-159 (Accessed: January 3, 2025).

[10] G. V. Kustarev, S. A. Pavlov, K. A. Rusinov, A. A. Gusev and N. V. Novotortsev, "The introduction of a rigid body of finite dimensions into an elastic-elastic half-space reinforced on the surface by a deformable plate," Scientific and Technical Bulletin of Bryansk State University, vol. 10, pp. 296–302, 2024. [Online]. Available: https://doi.org/10.22281/2413-9920-2024-10-04-296-302 (Accessed: January 3, 2025).

[11] L. Polyakova, A. Fominyh, V. Karelin and S. Myshkov, "On a Support Function on a Convex Cone," 2022. [Online]. Available: https://doi.org/10.1007/978-3-030-87966-2_77 (Accessed: January 3, 2025).

[12] V. Kochergin, S. Glushkov and D. Abramenkov, "Application of dynamic vibration dampers for vibration protection of bridge structures," The Russian Automobile and Highway Industry Journal, vol. 21, pp. 960–971, 2025. [Online]. Available: https://doi.org/10.26518/2071-7296-2024-21-6-960-971 (Accessed: January 3, 2025).

[13] B. Cheng, B. Dong, S. Chen and J. Xiao, "The effect of process parameters during the insertion phase of robotic friction stir welding on axial force," The International Journal of Advanced Manufacturing Technology, 2025. [Online]. Available: https://doi.org/10.1007/s00170-025-15207-5 (Accessed: January 3, 2025).

[14] S. Slavov and A. Markov, "A Tool for Ball Burnishing with Ability for Wire and Wireless Monitoring of the Deforming Force Values," 2023.

[15] A. Raza and S. Kumar, "A comparative investigation on the surface characteristics of AISI 304 and AISI 1045 steel influenced by turning combined with ball burnishing," Proceedings of the Institution of Mechanical Engineers, Part L: Journal of Materials: Design and Applications, vol. 239, 2024. [Online]. Available: https://doi.org/10.1177/14644207241263793 (Accessed: January 3, 2025).

Environment. Technology. Resources. Rezekne, Latvia
Proceedings of the 16th International Scientific and Practical Conference .2025. Volume IV, 185-188

Investigation of the Trend Between the Results of the Barkhausen Magnetic Noise (MBN) Method with Classical Methods for Ion Nitrided Testing of Steel, BH11

Velichko Machev
University of Transport – Sofia
"Todor Kableshkov"
Sofia, Bulgaria
vmatchev@vtu.bg

Vladimir Kamenov
Technical University - Sofia
Sofia, Bulgaria
vladokamenov@tu-sofia.bg

Stefan Stanev
"University of Transport – Sofia
"Todor Kableshkov"
Sofia, Bulgaria
s-stanev@vtu.bg

Nikolay Tontchev
University of Transport – Sofia
"Todor Kableshkov"
Sofia, Bulgaria
tontchev@vtu.bg

Abstract **- The Barkhausen magnetic noise (MBN) method has emerged as a promising technique for non-destructive measurement of residual stresses, especially in ion nitrided instrumental steels. The study determines the applicability of MBN in comparison to traditional X-ray diffraction (XRD), relative wear resistance and microhardness measurements by focusing on its potential for faster and more reliable evaluations. The comparison is made on MBN speed because it provides a rapid assessment compared to other methods that often require more extensive sample preparation and longer measurement times. MBN does not alter the test material, preserving its integrity for later use. While traditional methods, such as XRD, are surface sensitive, MBN can offer information on subsurface stresses depending on the measurement configuration. The correlation performed, links the study on the one hand to the process logic and on the other hand to microhardness and tribological testing.**

Keywords — Barkhausen magnetic noise (MBN), ion nitrided instrumental steel, residual stress, X-ray diffraction (XRD).

I. Introduction

Chemical-thermal treatment processes are essential for modern industrial applications improving the surface properties of materials. They improve the hardness and wear resistance of materials. Nitride layers derive their outstanding mechanical properties from internal stresses and phase composition, which are tightly controlled in modern plasma processes. By enriching the surface layer with elements such as nitrogen, carbon, or a combination of the two elements the mechanical properties are significantly improved, which by its mechanism is due to an increase in the residual internal surface stresses. The mechanism of formation of nitride layers consist in that nitrogen atoms diffuse into the surface of iron-carbon alloys [1]. The nitrogen atoms penetrate the iron lattice forming different phases depending on the temperature and nitrogen concentration, the γ'-phase Fe_4N possesses, a wall-centered cubic lattice with a nitrogen solubility of 5.7-6.1% at 500-590°C , and the ε-phase $Fe_{2-3}N$ a hexagonal lattice Above 590° C, 4.55-11.1% N. The phase composition has a direct influence on the mechanical properties: the hardness of the ε-phase is of the order of (1 200-1 400 HV) for wear resistance, and the γ'-phase Fe_4N (FCC) guarantees 20-30% higher fatigue strength compared to the base material), corrosion resistance [2].

The ion nitriding process allows precise adjustment of the thickness and composition of the carburized layer, which is crucial for achieving the desired performance characteristics resulting from the different phase composition obtained on the surface. X-ray crystallography is in this respect the most widely used method for the analysis of surface stresses (up to 20 μm depth) by measuring changes in interatomic distances [3,4]. The study [5] is based on the change of magnetic properties under the influence of stresses, and sometimes neutron

Online ISSN 2256-070X
https://doi.org/10.17770/etr2025vol4.8418
© 2025 The Author(s). Published by RTU PRESS.
This is an open access article under the Creative Commons Attribution 4.0 International License.

diffraction is used, allowing the analysis of stresses in bulk materials [6]. As demonstrated in the cited references, different phases in the nitride layers determine different internal stresses dictated by the concentration of the diffusing element. The internal stresses occurring after chemical-thermal treatment are determined by specialized methods that take into account the influence of the phase composition on the mechanical properties of the material. These stresses are critical to the reliability and durability of the workpieces. In the present study an attempt has been made to compare the results obtained, by MBN method and XRD method. The MBN method is based on the phenomenon in which abrupt changes in magnetization occur in ferromagnetic materials due to stress changes known as Barkhausen jumps. This method is sensitive to microstructural changes and residual stress fields in materials, making it suitable for non-destructive evaluation of residual stresses [7,8]. MBN is characterized in that it provides a rapid assessment compared to XRD, which often requires more extensive sample preparation and longer measurement times. It has the advantage of not altering the material under test, preserving its integrity for later use and while traditional methods, such as XRD, are surface sensitive, MBN can offer information on subsurface stresses depending on the measurement configuration [9,10 and 11].

Compared to MBN , XRD is a well-established method for measuring residual stresses, but is associated with certain limitations, among which are longer measurement times and complex setups, which can be a disadvantage in industrial applications requiring rapid evaluations, as well as the need for precise sample preparation, leading to variability and potential errors in the results. In contrast, studies have shown that MBN provides a simpler approach with faster results. For example, studies have shown that the root mean square (RMS) stress of MBN signals is highly sensitive to changes in stress, demonstrating a significant increase under applied loads compared to the minimal changes observed with XRD under similar conditions .Despite its advantages, the MBN method faces challenges accurate quantitative results require careful calibration due to the influence of microstructure along with residual stresses [12]. Simultaneous variation of microstructure and residual stresses can complicate the interpretation of data from different transport applications [13,14,15].

II. MATERIALS AND METHODS

The aim of the study is to demonstrate that the Barkhausen magnetic noise method represents a viable alternative to traditional analysis with classical methods for testing ion nitrided steel. The steel BH11 is taken as an example. One of the tasks of the study is to demonstrate that MBN's ability to give faster results while maintaining non-destructive integrity makes it particularly attractive for industrial applications. Nonetheless, to provide reliable quantitative measurements, calibration and mixed effects challenges must be overcome.

The stages and sequence of work in the study were subject to the methodology described in [16, 17]. Since this methodology was developed for the four parameters, they guarantee, on the one hand, the adequacy of the results subsequently obtained and, on the other hand, the intelligent representation of the solution itself. Following the selection of the object of study, heat-resistant steel BH11/BS4659/, Table 1 shows the chemical composition and Table 2 indicates the range of variation of the main input parameters:

TABLE 1 CHEMICAL COMPOSITION OF STEEL, BH11/BS4659/, [%]

Steel	C	Cr	Mo	Si	Mn	W	V	Ni	Cu	S
BH11	0,38	4,50	1,20	0,91	0,22	–	0,47	0,14	0,11	0,006

After conducting the experiment, the surface microhardness of the nitrided layer-HV0.1, the relative wear resistance of the nitrided layer-KV, the thickness of the bonded zone- δbz., the total diffusion thickness of the nitride layer- δtot. were determined in [16]. All these parameters were implemented by the authors of [16] by standard methodologies.

TABLE 2 RANGE OF VARIATION OF INPUT PARAMETERS

	Process parameter of ion nitriding and pre-heat treatment	Low level		Average value		High level	
		Mode change interval value					
		CODE	***[–1]***	***CODE***	***[0]***	***CODE***	***[+1]***
1	Nitriding temperature *Tnit* [^{o}C] – (X_1)	510		530		550	
2	Ammonia pressure *PNH3* [Pa] – (X_2)	150		300		450	
3	Nitriding time τ [h] – (X_3)	4		7		10	
4	Temperature tempering before nitriding *Ttem* [^{o}C] – (X_4)	600		650		700	

From the experiment set up in this way, eight regimes were analysed on processed ion nitriding samples using both the classical and the recommended methodology of the Barkhausen Magnetic Noise (MBN) method. These modes are described in Table 3.

TABLE 3 TECHNOLOGICAL REGIMES TO BE INVESTIGATED AND ANALYSED

	Zyu	Test mode parameters	Structure

		Tnit [ºC] (X_1)	*PNH3* [Pa] (X_2)	τ [h] (X_3)	*Ttem* [ºC] (X_4)	
1	1	510	150	4	600	γ`
2	9	510	150	4	700	α
3	13	510	150	10	700	γ`
4	5	510	150	10	600	γ'
5	3	510	450	4	600	γ`+ έ
6	4	550	450	4	600	γ’
7	16	550	450	10	700	γ`+έ
8	8	550	450	10	600	γ`

The Barkhausen effect consists in the fact that when a ferromagnetic material is magnetized by an external magnetic field, it is accompanied by numerous jumps in the magnetization. When an external magnetic field is applied, the domain walls move. These movements generate electromagnetic pulses. Magnetic noise characteristics are measured with an inductive receiver with a piezo sensor. To study the Barkhausen effect, a setup was created to measure the non-destructive informational characteristics of magnetic noise emission in ferromagnetic materials. In fig. 1. the basic block diagram of the equipment for measuring EBN is shown

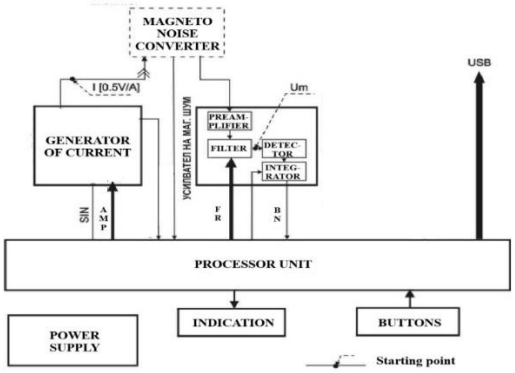

Fig. 1. Block diagram of the device for measuring EBN.

III. RESULTS AND DISCUSSION

The data from the measurements of technological modes presented in Tab. 3 modes are presented in Table 4. Their analysis, however, must be carried out in an integrated way, from all the data presented in the table. Nevertheless, it should be noted that higher values of the noise voltage amplitude are associated with less residual compressive stress. However, this statement can be analyzed, specifically for each of the modes, because from the simultaneous analysis of a class of heat-resistant steels, it turned out that combinations of different alloying elements, have a more significant effect on the internal stresses, than the combinations of the ion nitriding mode parameters [2].

The difference between the first and second mode (Table 4) lies in the recoil temperature, with the internal stresses being smaller at 7000 C, the amplitude of the stress noise, larger, which is evidenced by the microstructure nitride ferrite . When comparing the third with the fourth mode, despite the same structure, nitride austenite and different recoil temperature, in the case larger residual stresses and smaller noise amplitude is associated with the larger diffusion zone. When comparing mode one with mode three, the lower amplitude of the mode one noise stress is due to the minor bonded zone, which is also reflected in the larger hardness.

TABLE 4 RESULTS OF THE MEASUREMENTS OF THE TECHNOLOGICAL MODES UNDER ANALYSIS

	Hv	Ub	Rela-ted zone μm	Diffu-sion zone μm	Struc-ture
1	1131	10.5	1	120	γ’
2	998	17.9	0	110	α
3	1124	15.1	0	120	γ’
4	1225	12.9	1	220	γ’
5	1206	18.7	0	130	γ’+ έ
6	1108	13.6	7	210	γ’
7	1050	20.7	1	220	γ’+έ
8	1097	12.8	9,5	230	γ’

The higher stiffness of the fifth mode (1206) is conditioned with a more stable microstructure, but the smaller thickness of the diffusion zone is the reason for the higher stress amplitude from noise. This is overcome in mode four, which is characterized by a larger diffusion zone, a smaller noise stress amplitude, and a correspondingly larger microhardness.

Everything in Table 4 can be generalized to the seventh and eighth modes, where despite the difference in the 7000C recoil temperature (in the seventh mode), the more stable structure is unable to lower the stress amplitude, which is also reflected in the lower microhardness. Mode seven compared to mode one, despite the smaller diffusion zone, the higher hardness determined in mode seven significantly affects the trend found for the stress amplitude from noise. The same, but to a lesser extent, can be verified by the eighth process mode, where the lower amplitude than the seventh mode corresponding to larger residual stresses is due to the larger widths of the coupled and total diffusion zone as well as the lower recoil temperature.

From this detailed systematic analysis of the complex interactions between different parameters affecting the properties of the nitrided layer, trends can be identified, which, however, are not able to express a precise correlation between all the quantities analysed. Nevertheless, this kind of analysis, besides describing the complexity of the problem, highlights a user-friendly method, the advantages of which focus on the benefits described above.

CONCLUSION

The analysis presents a holistic approach to understanding how different nitriding parameters affect the steel properties due to internal stresses, as accounted for by the Barkhausen magnetic noise (MBN) method, with predetermined results from classical test methods. This combines theoretical justification with practical applications to help the user. The above findings highlight the relationship between the conditions and the material processing, the determined characteristics, with contributions to knowledge in materials science and engineering. The conclusions that follow in this direction:

The high internal residual stresses obtained under certain nitriding conditions (temperature, ammonia pressure, time and temperature of treatment), in addition to the higher hardness, will be associated with a higher relative wear resistance for the BH11 steel, which is guaranteed by the presence of γ'-phase nitride associated with improved wear resistance due to reduced adhesive forces.

It is found for the investigated steel BH11 , that less nitriding time and reduced ammonia pressure can increase the residual stresses , hardness and wear resistance. Conversely, longer processing time and higher chamber pressure also contribute positively on this effect.

The specific machining conditions of BH11 steel yield significant results: after quenching, subsequent tempering as remarkable microhardness, as reported, by the amplitude of the stress from noise occurs at lower tempering temperatures.

In this way, the characteristics of the stress signal provide information about the properties and condition of the material without damaging it.

Define abbreviations and acronyms the first time they are used in the text, even after they have been defined in the abstract. Abbreviations such as IEEE, SI, MKS, CGS, sc, dc, and rms do not have to be defined. Do not use abbreviations in the title or heads unless they are unavoidable.

ACKNOWLEDGMENTS

The authors would like to thank the Todor Kableshkov University of Transport for admitting for consideration and funding, the project "Precision Manufacturing Integration: Development of Educational Materials, on Cutting and Additive Technologies Related to Real-Time Quality Management".

REFERENCES

[1] L. Gontijo, R. Machado, L. Casteletti and P. Nascente. Evaluation of the effect of cooling speed on the layer formation on stainless steel by plasma carbonitriding. Acta Microscopica 12: p. 155-158.

[2] A. Zumbllev, I. Zumbilev, Determining the Residual Stresses in the Nitrided Layers with X-Ray Diffraction Techniques, Proceedings of lnternational Conference on Materials Science & Technology, 25- 29 October, 2009, Pitsburgh, USA, p. 2434-2454.

[3] M. Gelfi, E. Bontempi, R. Roberti, L. E. Depero, X-ray diffraction Debye Ring Analysis for Stress measurement (DRAST): a new method to evaluate residual stresses, Acta Materialia, Vol. 52, Issue 3, 2004, Pages 583-589, ISSN 1359-6454, https://doi.org/10.1016/j.actamat.2003.09.041

[4] Standard Method for Verifying the Alignment of X-ray Diffraction Instrumentation for Residual Stress Measurement, E 915, Annual Book of ASTM Standards, Vol 03.01, ASTM, Philadelphia, 1984, pp. 809-812.

[5] M. Jamesv and J. Cohen, The Measurement of Residual Stresses by X-Ray Diffraction Techniques, Editor(s): H. Herman, Treatise on Materials Science and Technology, Elsevier, Vol. 19, Part A, p. 1-62, ISSN 0161-9160, 1980.

[6] A. Rocha, T. Stroheacker, V. Tomala and T. Hirsch: Microstructure and residual stresses of a plasma-nitrided M2 tool steel, Surface and Coatings Technology, 115, pp. 24-31, 1999.

[7] C. Gür. Review of Residual Stress Measurement by Magnetic Barkhausen Noise Technique. Materials Performance and Characterization, 7, 504-525, 2018.

[8] G. Matzkanin, and C. Gardner(. Measurement of Residual Stress Using Magnetic Barkhausen Noise Analysis, 1975.

[9] T. Kaleli and H. Hizli. Comparison of two procedures for reliable measurement of residual stress in carburized steels by magnetic barkhausen noise method, 2018.

[10] Y. Zhu, Y. Zheng, J. Tan, and J. Zhou. Comparison of longitudinal critically refracted ultrasonic waves and magnetic Barkhausen noise for tensile stress measurement. Insight - Non-Destructive Testing and Condition Monitoring, 2022.

[11] A. Maussymbayeva, V. Yurov, Va Portnov, M. Rabatuly and G. Rakhimova. Assessment of the influence of the surface layer of coals on gas-dynamic phenomena in the coal seam. Naukovyi Visnyk Natsionalnoho Hirnychoho Universytetu, 2024.

[12] H. Dong, X. Liu, Y. Song, B. Wang, S. Chen, and C. He. Quantitative evaluation of residual stress and surface hardness in deep drawn parts based on magnetic Barkhausen noise technology, 2022

[13] D. Dimitrov, K. Lalov, Intelligent rail transport management systems - methodological essence, goals and tasks, ENVIRONMENT. TECHNOLOGIES. RESOURCES. Proceedings of the International Scientific and Practical Conference, vol. 2, p. 83-88, https://doi.org/10.17770/etr2024vol2.8050, 2024.

[14] D.Dimitrov, I. Manche, Methodological and technical aspects of models for digital management of transport systems, ENVIRONMENT. TECHNOLOGIES. RESOURCES. Proceedings of the International Scientific and Practical Conference, vol. 2, p. 79-82, https://doi.org/10.17770/etr2024vol2.8049, 2024.

[15] D. Dimitrov, Digitization and intelligent management systems in transport: an overview of problems and solutions, ENVIRONMENT. TECHNOLOGIES. RESOURCES. Proceedings of the International Scientific and Practical Conference, vol. 2, p. 89-96, https://doi.org/10.17770/etr2024vol2.8048, 2024.

[16] A. Zyumbilev, I. Zyumbilev, Ion nitriding and carbonitriding of steels, p. 325, ISBN:978-619-236-187-7, 2020

[17] N. Tontchev, Z. Cekerevac, Approach and Application in Multicriteria Decision Support in the Field of Materials Science. MEST Journal, (MEST) 2, no. 118-2, 2014

Environment. Technology. Resources. Rezekne, Latvia
Proceedings of the 16th International Scientific and Practical Conference. 2025. Volume IV, 189-193

Computer Grafoanalitic Kinematical Analysis for Four-Bar Linkage Mechanism

Marin Jordanov Marinov
Technical University - Gabrovo
Department of Industrial Design and Textile Engineering
Gabrovo, Bulgaria
marinov@tugab.bg

***Abstract*— In this work, a methodology for calculating a class of lever mechanisms is proposed using a current software product for solving algebraic equations. They are adapted in the environment of the theory of mechanisms, where the main kinematic parameters of the articulated four-link mechanism are presented in graphical form. These parameters are linear and angular velocities and linear and angular accelerations. The work is related to the course in general and mechanical engineering at the Technical University - Gabrovo.**

Keywords* — *computer kinematical analyses, four-bar linkage mechanism, Math Lab.

I. Introduction

The proposed algorithm for the analysis of the most commonly used mechanism allows, in the operating environment of the modern software product Math LAB 2020 for Windows, which has enormous computational capabilities and its graphic images on the monitor allow the reading of information with great accuracy, to accelerate and improve the analysis. The graphic images of the changes in the kinematic quantities (angles of rotation, angular velocities, angular accelerations, etc.) of the links of the mechanism, for one revolution of the input lever, make it possible to easily perform a force analysis of this mechanism. The reliability of the algorithm is established with a detailed solved example.

The analysis is compiled with given: uniform rotation of the leading link 1, the initial angular orientation of this link and the geometric dimensions of all links of the mechanism. The algorithm, as is known [10] and [23] is a finite series of rules, according to which after a finite number of uniquely defined steps a solution to a given problem is obtained, uniquely corresponding to the conditions given in it.

The purpose of the publication is to create a systematic approach for metric synthesis on discrete positions of lever mechanisms using the most commonly used geometric and algebraic methods, through the creation of algorithms and program modules in the Math LAB for Windows environment.

The following main tasks arise from the purpose of the article:

1. Compilation of algorithms for kinematic synthesis of four-link transmission hinge mechanisms using the following methods: the method of symmetries, the method of the maximally contracted evolute, the determinant method, the Alt method, the method using the Freudenstein [1] equation, the method using vector-matrix equations and the analytical-optimization method. The algorithms should be compiled for three, four and five discrete positions.

2. Compilation of algorithms for kinematic analysis of four-link closed kinematic chains, three-link closing parallel chains in the profile of the inserted higher kinematic pair.

3. The values of all sought kinematic parameters should be graphically and analytically reported.

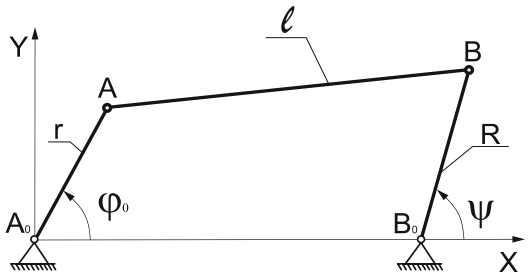

Fig.1 shows a four-bar lever mechanism.

Online ISSN 2256-070X
https://doi.org/10.17770/etr2025vol4.8428
© 2025 The Author(s). Published by RTU PRESS.
This is an open access article under the Creative Commons Attribution 4.0 International License.

II. MATERIALS AND METHODS

II.1 *Conditions and algorithm of analysis*

The algorithm for kinematic analysis is built with the following given conditions: uniform rotation of the leading link, the initial angular orientation of the same link and the geometric dimensions of all links of the mechanism.

The construction of this algorithm is carried out in the following sequence:

1. The input data determined by the analysis conditions (ω, r, l, R, □□, □□, L=A0B0) are entered.

2. The number of positions n of the mechanism at which the analysis will be performed is determined.

3. The step by which the leading link will rotate when moving from one to an adjacent position is determined.

$$h = \frac{2.\pi}{n} \qquad (1)$$

4. The number of positions of the mechanism is chosen as a variable parameter □□□□i □n .

5. Three arrays of values of the angular orientations of the leading link are calculated, each of which is for n–1 positions

$$\begin{aligned} \varphi_k &= \varphi_0 + \varphi_1 + (i-3).h \ , \ k = -1,1,2,...,n-2 \\ \varphi_l &= \varphi_0 + \varphi_1 + (i-2).h \ , \ l = 1,2,...,n-1 \\ \varphi_m &= \varphi_0 + \varphi_1 + (i-3).h \ . \ m = 2,3,...,n \end{aligned} \qquad . (2)$$

6. Three arrays of coordinates XA and three arrays of coordinates YA of the center of the movable hinge A (connecting the leading link to the reel fork) are determined, at n–1 positions of the mechanism.

$$\begin{aligned} X_{Ak} &= r.\cos\varphi_k \ , \ k = -1,1,2,\ldots,n-2 \\ Y_{Ak} &= r.\sin\varphi_k \ , \\ X_{Al} &= r.\cos\varphi_l \ , \ l = 1,2,\ldots,n-1 \\ Y_{Al} &= r.\sin\varphi_l \ , \\ X_{Am} &= r.\cos\varphi_m \ , \ m = 2,3,\ldots,n \\ Y_{Am} &= r.\sin\varphi_m \ , \end{aligned} \qquad (3)$$

7. The six arrays of coordinates of the movable joint B (connecting the crank and the rocker arm) corresponding to the arrays (3) are determined, each of which is respectively for n–1 positions of the mechanism:

$$\begin{aligned} X_{Bk} &= L + R.\cos\psi_k \ , \ k = -1,1,2,...,n-2 \\ Y_{Bk} &= R.\sin\psi_k \ , \\ X_{Bl} &= L + R.\cos\psi_l \ , \ l = 1,2,...,n-1 \\ Y_{Bl} &= R.\sin\psi_l \ , \\ X_{Bm} &= L + R.\cos\psi_m \ , \ m = 2,3,...,n \\ Y_{Bm} &= R.\sin\psi_m \ , \end{aligned} \qquad (4)$$

8. Using the condition for geometric constraint of the crank and the arrays (3) and (4), six arrays of the sinus and cosines of the angular orientations of the rocker □k , □l , □m are determined.

$$\begin{aligned} \sin\psi_k &= \frac{b_k.c_k + a_k.\sqrt{a_k^2 + b_k^2 - c_k^2}}{a_k^2 + b_k^2} \ , \\ \cos\psi_k &= \frac{-a_k.c_k + b_k.\sqrt{a_k^2 + b_k^2 - c_k^2}}{a_k^2 + b_k^2} \ , \\ \sin\psi_l &= \frac{b_l.c_l + a_l.\sqrt{a_l^2 + b_l^2 - c_l^2}}{a_l^2 + b_l^2} \ , \\ \cos\psi_l &= \frac{-a_l.c_l + b_l.\sqrt{a_l^2 + b_l^2 - c_l^2}}{a_l^2 + b_l^2} \ , \\ \sin\psi_m &= \frac{b_m.c_m + a_m.\sqrt{a_m^2 + b_m^2 - c_m^2}}{a_m^2 + b_m^2} \ , \\ \cos\psi_m &= \frac{-a_m.c_m + b_m.\sqrt{a_m^2 + b_m^2 - c_m^2}}{a_m^2 + b_m^2} \ , \end{aligned} \qquad (5)$$

where:

$$\begin{aligned} a_k &= 2.R.(L - X_{Ak}); \ b_k = 2.R.Y_{Ak}; \ c_k = L^2 + r^2 + R^2 + l^2 - 2.L.X_{Ak} \\ a_l &= 2.R.(L - X_{Al}); \ b_l = 2.R.Y_{Al}; \ c_l = L^2 + r^2 + R^2 + l^2 - 2.L.X_{Al} \\ a_m &= 2.R.(L - X_{Am}); \ b_m = 2.R.Y_{Am}; \ c_m = L^2 + r^2 + R^2 + l^2 - 2.L.X_{Am} \end{aligned}$$

9. Three arrays of the angular orientations of the rocker are calculated:

$$\begin{aligned} \psi_k &= 2.\arccos(sign(\sin\psi_k)\sqrt{(0{,}5 + 0{,}5.\cos\psi_k)}) \ , \\ \psi_\ell &= 2.\arccos(sign(\sin\psi_\ell)\sqrt{(0{,}5 + 0{,}5.\cos\psi_\ell)}) \ , \\ \psi_m &= 2.\arccos(sign(\sin\psi_m)\sqrt{(0{,}5 + 0{,}5.\cos\psi_m)}) \ . \end{aligned} \qquad (6)$$

10. By performing two consecutive numerical differentiations, two arrays of numerical values are determined, respectively for the first and second translation functions of the mechanism.

$$\psi'_R = \frac{\psi_m - \psi_k}{2.h} \qquad (7)$$

$$\psi''_R = \frac{\psi_m - 2.\psi_\ell + \psi_k}{h^2} \ . \qquad (8)$$

11. Two arrays of the numerical values of the angular velocity ωR and the angular acceleration εR of the rocker are determined.

$$\omega_R = \psi'_R.\omega \qquad (9)$$

$$\varepsilon_R = \psi''_R.\omega^2 \ . \qquad (10)$$

12. Six arrays of the numerical values of the coordinates of the hinge B are calculated.

$$X_{Bk} = L + R.\cos\psi_k \quad ,$$
$$Y_{Bk} = R.\sin\psi_k \quad ,$$
$$X_{Bl} = L + R.\cos\psi_l \quad ,$$
$$Y_{Bl} = R.\sin\psi_l \quad ,$$
$$X_{Bm} = L + R.\cos\psi_m \quad ,$$
$$Y_{Bm} = R.\sin\psi_m \quad . \qquad (11)$$

13. Six arrays of the numerical values of the sinus and cosines of the angular orientations of the winch are determined

$$\sin\theta_k = \frac{Y_{Bk} - Y_{Ak}}{l} \quad ,$$
$$\cos\theta_k = \frac{X_{Bk} - X_{Ak}}{l} \quad ,$$
$$\sin\theta_l = \frac{Y_{Bl} - Y_{Al}}{l} \quad ,$$
$$\cos\theta_l = \frac{X_{Bl} - X_{Al}}{l} \quad ,$$
$$\sin\theta_m = \frac{Y_{Bm} - Y_{Am}}{l} \quad ,$$
$$\cos\theta_m = \frac{X_{Bm} - X_{Am}}{l} \quad . \qquad (12)$$

14. Three arrays of the numerical values of the angular orientations of the winch are calculated:

$$\theta_k = 2.\arccos(\,sign(\sin\theta_k)\sqrt{(0{,}5 + 0{,}5.\cos\theta_k)}\,) \quad ,$$
$$\theta_\ell = 2.\arccos(\,sign(\sin\theta_\ell)\sqrt{(0{,}5 + 0{,}5.\cos\theta_\ell)}\,) \quad ,$$
$$\theta_m = 2.\arccos(\,sign(\sin\theta_m)\sqrt{(0{,}5 + 0{,}5.\cos\theta_m)}\,) \quad . \qquad (13)$$

15. Two arrays of the numerical values of the first and second derivatives of the angular orientations of the winch are calculated, respectively.

$$\theta_l' = \frac{\theta_m - \theta_k}{2.h} \quad ,$$
$$\theta_l'' = \frac{\theta_m - 2.\theta_\ell + \theta_k}{h^2} \quad . \qquad (14)$$

16. Two arrays of numerical values of the angular velocity and angular acceleration of the object are defined.

$$\omega_R = \theta_l'.\omega \quad ,$$
$$\varepsilon_R = \theta_l''.\omega^2 \quad . \qquad (15)$$

17. Six arrays of numerical values of the coordinates of the center of gravity of the object are calculated. Here this will be done assuming that the object has a constant cross-section.. [3]

$$X_{Sk} = \frac{Y_{Ak} + Y_{Bk}}{2} \quad ,$$
$$Y_{Sk} = \frac{X_{Bk} - X_{Ak}}{2} \quad ,$$
$$X_{Sl} = \frac{Y_{Al} + Y_{Bl}}{2} \quad ,$$
$$Y_{Sl} = \frac{X_{Bl} - X_{Al}}{2} \quad ,$$
$$X_{Sm} = \frac{Y_{Am} + Y_{Bm}}{2} \quad ,$$
$$Y_{Sm} = \frac{X_{Bm} - X_{Am}}{2} \quad . \qquad (16)$$

18. Four arrays of numerical values are defined, two of which are for the velocity projections and two for the acceleration projections of the center of gravity S of the object. [4]

$$V_{Sx} = \frac{X_{Sm} - X_{Sk}}{2.t} \quad ,$$
$$V_{Sy} = \frac{Y_{Sm} - Y_{Sk}}{2.t} \quad ,$$
$$a_{Sx} = \frac{X_{Sm} - X_{Sl} + X_{Sk}}{t^2} \quad ,$$
$$a_{Sy} = \frac{Y_{Sm} - Y_{Sl} + Y_{Sk}}{t^2} \quad . \qquad (17)$$

19. Plot the graphs of the kinematic and geometric parameters of the mechanism as a function of the angular orientation of the leading knee 1.

III. RESULTS AND DISCUSSION

Example: To perform a kinematic analysis of a hinged four-link mechanism given: $\omega=80s^{-1}$, r=60mm, L=120mm, $\varphi_1=0$, $\varphi_0=\pi/6$.

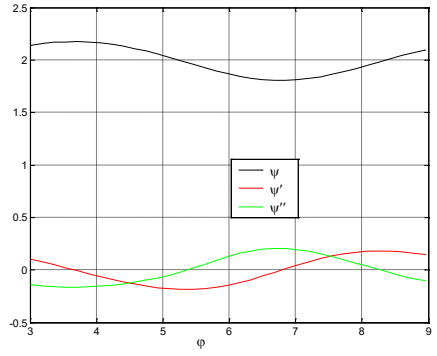

Fig.2 The change in the angle of the third link, as the first and second position functions.

The analysis was performed according to the compiled algorithm.

In Fig.2, the graphs of the position function $\psi_R = \psi_R(\varphi)$, of the first translation function $\psi'_R = \psi'_R(\varphi)$ and of the second translation function $\psi''_R = \psi''_R(\varphi)$ are plotted.

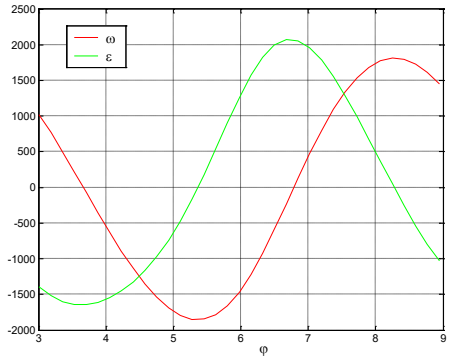

Fig.3 Angular velocity and angular acceleration.

In Fig.3, the graphs of the angular velocity and angular acceleration of link 2 are plotted.

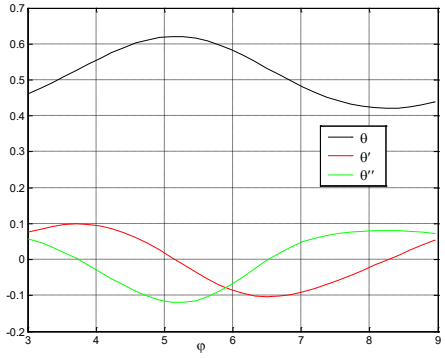

Fig.4 The relative rotation of the second unit

In Fig.4, the graphs of the angular orientations $\theta_I = \theta_I(\varphi)$, $\theta'_I = \theta'_I(\varphi)$ and $\theta''_I = \theta''_I(\varphi)$ are plotted.

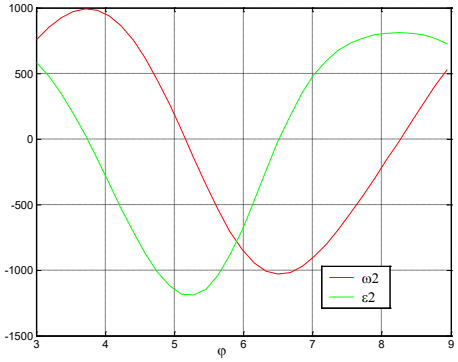

Fig.5 The angular velocity and angular acceleration of the second unit.

Fig.5 shows the graphs of the angular velocity and angular acceleration of the forklift.

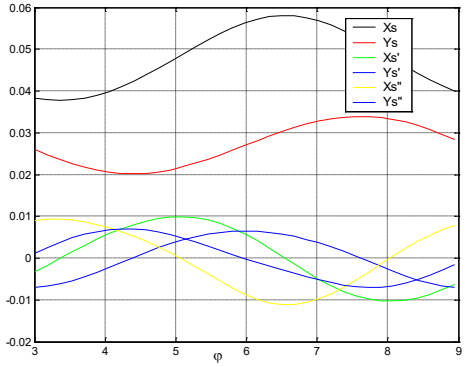

Fig.6 The coordinates of the centers of gravity of units 1, 2 and 3.

Fig.6 shows the graphs Xs= Xs(φ) and Ys= Ys(φ), as well as the first and second translation functions of the two displacements.

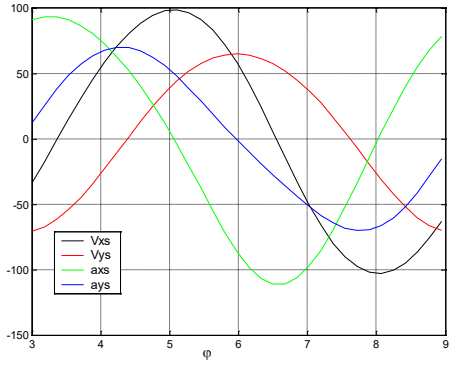

Fig.7. The linear velocities and linear accelerations of the centers of gravity of the initial unit.

Fig.7 shows the graphs of the velocities and accelerations of point S as a function of the rotation of the initial unit 1. [9]

IV. Conclusions

This article is intended for the education of bachelor's and master's students in the field of mechanical engineering and the field of applied analysis of mechanisms and machines for industry.

The purpose of this publication is to raise the level of teaching in the field of the theory of machine mechanisms and automatic lines in industrial production.

The program prepared in the MathLab 2020 environment is very voluminous and therefore only the graphs of the derivative functions (velocities and accelerations) are given.

The development of program modules for synthesis, in an environment of modern software products, allows

for the acceleration of the synthesis process itself, as well as for the analysis of the obtained results.

V. ACKNOWLEDGEMENTS

This paper has been supported by the Gabrovo Technical University research fund, project NIP 2025-13.

VI. REFERENCES

[1] A., Lengerov, D., Petrova and M., Bozhakov, Technological Assurance Of The Milling Process Of Prismatic Channels In Heat Exchange Aluminum Alloys, Vide. Tehnologija. Resursi - Environment, Technology, Resources, Volume 3, Pages 154 – 157, 2024, 15th International Scientific and Practical Conference on Environment. Technology. Resources, ETR 2024, Rezekne 27 June 2024 through 28 June 2024, ISSN 16915402, ISBN 978-171389957-0, DOI 10.17770/etr2024vol3.8163, ISSN 0094243X, 15517616.

[2] D., Petrova, Vlahova, B., Lengerov, A. and Zlateva-Petkova, Improvement of Constructive-Technological Approaches Reducing Innovative Obsolescence of Industrial Technologies in the Context of Industry 4.0, Vide. Tehnologija. Resursi - Environment, Technology, Resources, Proceeding of the 14th International Scientific and Practical Conference, 2023, Volume I, pp. 180–186, Print ISSN 1691-5402, Online ISSN 2256-070X, DOI: https://doi.org/10.17770/etr2023vol1.7238 https://www.scopus.com/authid/detail.uri?authorId=56323816400

[3] D., Petrova, Vlahova, B., Lengerov, A. and Zlateva-Petkova, T., Study of the State of Innovation Development and Obsolescence in the Republic of Bulgaria of Companies from the Mechanical Engineering Sector, Vide. Tehnologija. Resursi - Environment, Technology, Resources, Proceeding of the 14th International Scientific and Practical Conference 2023, Volume I, pp. 187–194, Print ISSN 1691-5402, Online ISSN 2256-070X, DOI: https://doi.org/10.17770/etr2023vol1.7239 https://www.scopus.com/authid/detail.uri?authorId=56323816400

[4] D., Petrova, N., Nikolova and A., Lengerov, Modeling business process reengineering in the digital era of industry 4.0, 11th International Scientific Conference "TechSys 2022" – Engineering, Technologies and Systems, AIP Conf. Proc. 2980,070013-1–070013-7; https://doi.org/10.1063/5.0185275, Published by AIP Publishing. 978-0-7354-4814-8/$30.00, pp. 070013-1 to 070013-7, ISSN 0094243X, 15517616, SJR=0,15.

[5] D. Petrova, N., Nikolova and A., Lengerov, Organizational design of the management system of the reengineered enterprise - Design and implementation, 11th International Scientific Conference "TechSys 2022" – Engineering, Technologies and Systems, AIP Conf. Proc. 2980, 070012-1–070012-8; https://doi.org/10.1063/5.0185274 , Published by AIP Publishing. 978-0-7354-4814-8/$30.00, pp. 070012-1 to 070012-8, ISSN 0094243X, 15517616, SJR=0,15.

[6] D. Petrova, Innovative Obsolescence in Mechanical Engineering and Singleness of Indicators, Vide. Tehnologija. Resursi - Environment, Technology, Resources, Volume 3, Pages 221 – 224, 2024, 15th International Scientific and Practical Conference on Environment. Technology. Resources, ETR 2024, Rezekne 27 June 2024 through 28 June 2024, ISSN 16915402, ISBN 978-171389957-0, DOI 10.17770/etr2024vol3.8123.

[7] G.A. Timofeev, Theory of Mechanisms and Machines, Moskow Uride 2010.

[8] G. Iliev and H. Hristov, "Modelling and simulation ot electropneumatic positioning system including the length of pneumatic lines", ETR, vol. 3, pp. 106–111, Jan. 2024, doi: 10.17770/etr2023vol3.7186.

[9] G. Iliev and H. Hristov, Speed control pneumatic cylinders using high speed 2 port on/off valves with pulse width modulation. environment, technologies, resources. Proceedings of the International Scientific and Practical Conference. 3, (Jun. 2024), 95–100. DOI: doi.org/10.17770/etr2024vol3.8117.

[10] I. I., Artobolevskiy, Theory of Mechanisms and Machines. Science, Moscow, 1967.

[11] J. Uicker, G. Pennok and J. Shigley, Theory of Machines and Mechanisms, Fifth Edition, Oxford University Press 2017.

[12] L.L. Harrisberger, An overview of structural synthesis of three-dimensional mechanisms, constructing science and technology of mechanical engineering, World, Moscow, 1965.

[13] M., Marinov, Synthesis of planar mechanisms by extremely distant discrete positions. Dissertation abstract to get the scientific and educational degree "PhD" - TU Sofia 2002, pp.36.

[14] M.J. Marinov, B.I. Stoychev, D.M. Guteva and M.V. Georgiev, Computer modeling and geometric analysis of Click-Clack mechanisms. "Mechanics of the machines" 2016 booklet 118 pp.35-39.

[15] Michael Stanisic, Mechanisms and machines; Kinematics, Dinamics and synthesis, Stamford 2015.

[16] Myszka David, Machines & Mechanisms: Applied Kinematic Analysis, 2011.

[17] P.T. Stoyanov, Geometric precision synthesis of planar lever mechanisms. "Mechanics of the machines" 2002 p.56 vol. 33.

[18] R.A. Rusev and V.B. Galabov, Structuring of rational planet-lever mechanism for passing the weft through the weaving machines. "Mechanics of machines" 2002 pp.26 booklet 33.

[19] S. Singh, Theory of Machines: Kinematics and Dynamics, Pearson Education, India 2011

[20] S. Stefanov, Theoretical mechanics, statics, kinematics and dynamics, Sofia 2014.

[21] V. B. Bhandari, Design of Machine Elements Fifth Edition, McGraw Hill 2020.

[22] V.B. Galabov, M. J. Marinov and N.B. Nikolov, Synthesis on a guiding MF at two points, respectively phase relation and double midpoint, "Mechanics of machines" 1999, booklet 26.

[23] V.B. Galabov and M. J. Marinov, Synthesis of articulated four-link mechanism by discrete relative positions. "Mechanics of the machines",Varna, 2002.

Environment. Technology. Resources. Rezekne, Latvia
Proceedings of the 16th International Scientific and Practical Conference .2025 Volume IV, 195-199

Research of Electricity Losses in Electric Networks

Misho Matsankov
Faculty of Electronics and Automation, Plovdiv branch
Technical University of Sofia
Sofia, Bulgaria
email: misho.ivanov@abv.bg

***Abstract*—The production, transmission and distribution as well as the consumption of electrical energy are processes that are connected and simultaneous. The processes of transmission and distribution of electrical energy from the place of production to the place of consumption is a process associated with certain losses that can be provoked by various factors. Electrical loads are random in nature, but nevertheless they obey certain cyclicality in weekly, monthly, seasonal and annual aspects. In practice, it is necessary to determine and analyse them with sufficient accuracy. In this paper the error of electric power losses determination in distributed networks applying are analysed. An algorithm for calculate electric power losses with reading shape factor of load curves are made. For electrical networks differently configuration are applied the probability approach and investigate magnitude electric power losses.**

Keywords*— *distributed networks, electricity losses, load curves, shape factor, probability approach.

I. INTRODUCTION

The production, transmission and distribution as well as the consumption of electrical energy are processes that are connected and simultaneous. The processes of transmission and distribution of electrical energy from the place of production to the place of consumption is a process associated with certain losses that can be provoked by various factors.

Power losses and energy losses in distribution networks play a critical role in the overall efficiency of the electricity grid, affecting operational costs, reliability and sustainability of the grid. The introduction of the possibilities of reconfiguration of the electrical networks makes it possible to limit the losses of electrical energy on them [4,6], increase the reliability [1,2,3,4,5]. The use of real data on the power flows in the sections, and on the network as a whole, makes it possible to estimate the losses with greater accuracy and to take measures to limit them [7,8,11,12]. The introduction of a large number of decentralized energy sources in recent years has caused a change in the directions and sizes of the transmitted power on the sections. In a certain sense, a change in the freight schedules. In general, a change in the mode parameters (voltage level in the nodes, magnitude and direction of the transmitted powers, magnitude of short-circuit currents and other) [14] and the quality of the electrical energy [17,18] of the network is induced [9].

In practice, it is necessary to determine and analyse them with sufficient accuracy. Electrical loads are random in nature, but nevertheless they obey certain cyclicality in weekly, monthly, seasonal and annual aspects.

The determination of energy losses ΔW on an annual basis in electrical distribution networks can be carried out in the design stage or the operation process, when the configuration of the network, the lengths and sections of the wires in the individual sections, the transmitted powers on the branches and known loads in the nodes are known. In some isolated cases, there is insufficient information on the specified parameters, data on the annual commodity schedule in the nodes of the network.

Different methods can be applied to determine power losses and energy, each of which has a recommended area of application [13,15]. Their application leads in some cases to determining the result with an error exceeding 10%. Inaccuracy of information is the main difficulty in determining ΔW with sufficient accuracy [13,15].

In practice for approximate calculations of electricity losses with insufficient information, the following dependence is used [13,15,16]:

$$\Delta W = \Delta P_{max}.\tau \qquad (1)$$

Where ΔP_{max} are the active power losses in the maximum load mode; τ - the fictitious duration of power losses [13,15].

Online ISSN 2256-070X
https://doi.org/10.17770/etr2025vol4.8458
© 2025 The Author(s). Published by RTU PRESS.
This is an open access article under the Creative Commons Attribution 4.0 International License.

The losses calculated in this way have a large error, even with a fully known network configuration, lengths and cross-sections of the wires in the sections, since the values τ are determined for a specific freight schedule, which introduces unavoidable inaccuracy.

The aims of the paper is to determine the error in the determination of power losses in distribution networks when applying deterministic methods, to propose an algorithm for the calculation of ΔW in a probabilistic approach with the average values ΔW of the loads in the nodes, in to investigate the magnitude of power losses for power networks with different configurations.

II. MATERIALS AND METHODS

A. Electricity Losses In Radial Networks

The calculation expression for electricity losses contains the effective values of current Ie, active power Pe and reactive power Qe for time T, determined on an annual basis in [10,13,15].

$$\Delta W = 3.I_e^2.R.T.10^{-3} \quad (2)$$

The equation (2) can also be represented as (3).

$$\Delta W = \frac{P_e^2+Q_e^2}{U^2}R.T \quad (3)$$

Where R is the active resistance of the conductors, and U is the nominal voltage of the distribution network.

The effective values I_e, P_e and Q_e, for an annual load schedule of I(t), P(t), Q(t) are determined by the average values of the corresponding regime parameters I_c, P_c and Q_c with (4), (5) and (6), respectively.

$$P_e = K_\Phi.\mathrm{P_c} \quad (4)$$

$$Q_e = L_\Phi.Q_c \quad (5)$$

$$I_e = G_\Phi.I_c \quad (6)$$

Where K_ϕ, L_ϕ, G_ϕ are respectively the coefficients of the shape of the graph of I(t), P(t) and Q(t), which characterize the degree of its unevenness.

If electrical networks with higher nominal voltages are considered, to determine the effective values values I_e, P_e and Q_e, through the average I_c, P_c and Q_c, data on the voltage in the relevant node and the static characteristic of the load, which is known with sufficient accuracy, are used [13].

At a minimum value of $K_\phi = 1$, then $P_e = P_c$ and P(t) = const and the unevenness of the load schedule is minimal. The (7) or (8) follows from equation (2), (4), (5) and (6).

$$\Delta W = 3.10^{-3}.R.T.G_\Phi^2.I_c^2 \quad (7)$$

$$\Delta W = \frac{R.T}{U^2}.\left(K_\Phi^2.P_c^2 + L_\Phi^2.Q_c^2\right) \quad (8)$$

The limits of variation of electrical loads are determined by $\alpha = Pmax_{min}$ and $\beta = Qmax_{min}$.

The maximum value of the shape factor Kf can be determined by $K_{\phi\,\max} = \frac{1+\alpha}{2\sqrt{a}}$ and $L\frac{1+\beta}{2\sqrt{\beta}}_{\phi max}$

For more accurate calculations of $K_{o\phi}^2$, expression (9) is used. the expression for $L_{o\phi}^2$ can be written by the same logic.

$$K_{o\Phi}^2 = \frac{1}{2} + \frac{1}{8.\alpha}.(1+\alpha)^2 = f(\alpha) \quad (9)$$

the allowed error is determined by (10) for $|\delta_\alpha|$ and by a similar approach for $|\delta_\beta|$

$$|\delta_\delta| = \frac{K_{o\Phi}^2-1}{K_{o\Phi}^2} = \frac{(1+\alpha)^2-4.\alpha}{(1+\alpha)^2+4.\alpha} = \varphi(\alpha) \quad (10)$$

B. Determination Of Electricity Losses In Distribution Networks

In electrical networks with a large number of branches and nodes to determine the power loss using a deterministic approach, the is usually used (11).

$$\Delta P = \sum_{k=1}^{N}\frac{(P_k^2+Q_k^2).R_{kk}}{U_k^2} + 2\sum_{j<k}^{1,N}B_{jk}\frac{(P_jP_k+Q_jQ_k).R_{jk}}{U_jU_k}.cos\theta_{jk} - 2\sum_{j,k}^{1,N}\frac{(P_jP_k+Q_jQ_k)}{U_jU_k}.sin\theta_{jk} \quad (11)$$

Where P_k and Q_k are the active and reactive power at the node k-th; U_k – the voltage in the node k-th of the network; ; θ_{jk} - the phase shift (dephasing) between the voltages U_j and U_k in the corresponding node j and k; R_{kk} , R_{jk} - the own and mutual active resistances of the network for the respective nodes j and k;

The use of the statistical approach is more appropriate when determining losses in distribution networks [13]. The input parameters are U_j and U_k; R_{kk}, R_{jk} and θ_{jk}. The average values of the active power P_{kc} and reactive power Q_{kc} are determined and:

$$\Delta P_c = \sum\frac{R_{kk}}{U_{kc}^2}(P_{kc}^2+Q_{kc}^2) + 2\sum\frac{R_{jk}.cos\theta_{jkc}}{U_{jc}U_{kc}}\left(P_{jc}P_{kc} + Q_{jc}Q_{kc}\right) - 2\sum\frac{R_{jk}.cos\theta_{jkc}}{U_{jc}U_{kc}}\left(P_{jc}P_{kc} - Q_{jc}Q_{kc}\right) \quad (12)$$

The load schedules of the nodes captured at the minimum mode P_1 (t) and maximum mode P_n (t), respectively, are the smallest and largest value in the set of realizations of the random process. All other possible cases are included in these limits [13].

Knowing the load distribution law allows one to calculate the missing elements in the set. This law is determined by statistical processing of a given daily commodity chart.

The uniform density distribution has the form shown below:

$$f(P,t)=\begin{cases}\frac{1}{P_n(t)-P_1(t)}, P_1(t)\le P(t)\le P_n(t);\\ 0, P(t)<P_1(t); P(t)>P_n(t).\end{cases} \quad (13)$$

The Individual realizations in the random process are calculated at the boundary values with:

$$P_k(t)=P_1(t)+(k-1)\frac{P_n(t)-P_1(t)}{n-1}$$

$$P_k(t)=P_1(t)+(k-1)\Delta P(t); \quad (14)$$

$$k=1,2,\dots,n; t=1,2,\dots,24/\Delta t$$

Where n is the duration of the random process; Δt - the diskette interval of the load schedule.

The estimation of the coefficient of variation of the load schedule for active power is used in the modeling of the capacities in the nodes.

$$\tilde{v}_P(t)=\frac{\sqrt{\tilde{D}[P(t)]}}{\tilde{M}[P(t)]}. \quad (15)$$

Considering the law of uniform density of load distribution, for the coefficient of variation is obtained:

$$\tilde{v}_P(t)=\frac{\sqrt{n(n-1)}[P_1(t)-P_n(t)]}{\sqrt{3}(n-1)[P_1(t)+P_n(t)]} \quad (16)$$

The rms value of the load is determined by:

$$\tilde{M}[P^2(t)]=\tilde{M}[P(t)]^2+\tilde{D}[P(t)]$$

$$\tilde{M}[P^2(t)]=\tilde{M}[P(t)]^2[1-\tilde{v}_P^2(t)] \quad (17)$$

With the obtained mathematical expressions, the mode parameters in the distribution networks are determined.

Loads are considered to be uncorrelated due to their physical independence:

$$\frac{1}{T}\int_0^T P_jP_k dt=M(P_jP_k)=MP_jMP_k=P_{jc}P_{kc} \quad (18)$$

The dependencies for the reactive fats in the nodes of the distribution network are analogous.

If the coefficients of the shape of the load schedules are used, (9) is transformed into the form (19).

$$\Delta P_c=\Delta P_{oc}+\sum\frac{R_{kk}}{U_{kc}^2}\left[\left(K_{k\phi}^2-1\right)P_{kc}^2+\left(L_{k\phi}^2-1\right)Q_{kc}^2\right] \quad (19)$$

Where the first term of is the main and the second term is the dispersion component of the power losses.

III. RESULTS AND DISCUSSION

The results of the calculations for $K_{o\phi}^2$ and $|\delta_\alpha|$ for radial electrical networks, depending on α are presented in fig.1 and fig.2.

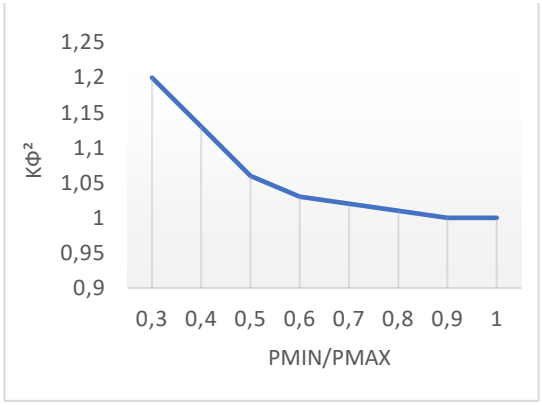

Fig. 1. Dependence of the form factor and limits of variation of electrical loads.

The error |δ| when calculating the electricity losses in radial lines for the real load schedules for a specific load type, it reaches even higher values, especially for industrial loads.

Fig.2 shows that at α<0.4, the error in determining ΔW exceeds 10%. The error is between 5 and 10%. At α>0.52, the error in calculating the power losses remains within the permissible limits

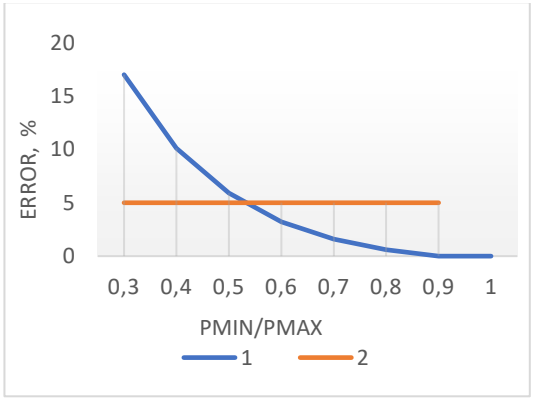

Fig. 2. Dependence of the error and limits of variation of electrical loads - 1 and Limit value - 2.

According to the proposed algorithm, software was developed for determining power losses in a distribution network. The power range in the nodes varies from 2.5 to 4.5 MW, cos φ e in the interval from 0.9 to 0.95. Calculations are carried out for electrical networks with two types of configurations:

- a lightly loaded network with a large total branch length.
- A highly loaded network with a small total branch length.

The average values of power losses in distribution networks are presented in Fig.3. The summarized results of

the calculations show that as the number of nodes increases, the dispersion component of the losses decreases

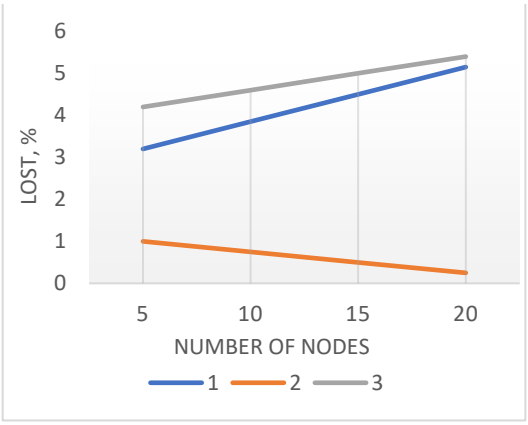

Fig. 3. Average values of power losses in a distribution network: 1 – main component; 2 – dispersion ingredient; 3 – total value.

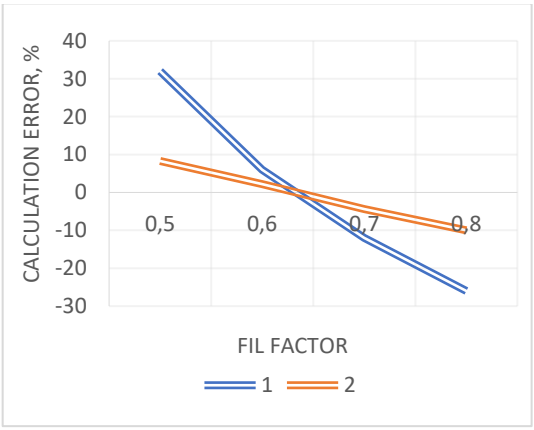

Fig. 4. Error in determining the electricity losses depending on the filling factor: 1 – with the fictitious duration method; 2 – with a probabilistic approach.

Fig. 4 shows the change in electricity losses depending on the load factor of a known load schedule, determined respectively by the fictitious duration method and the probabilistic approach. The error is calculated relative to the case of applying a stepwise load schedule approximation with a very small sampling step.

IV. CONCLUSIONS

The error in the determination of ΔW exceeds 10 % at $\alpha<0.4$. When $0,4<\alpha<0,5$ the error is between 5 and 10%. At $\alpha>0.52$, the error in calculating the electricity losses remains within the permissible limits.

A probabilistic approach to determining electricity losses combined with determining the shape factor of the load schedule is recommended for distribution networks.

From the conducted calculations of power losses in distribution networks, it is found that as the number of distribution network nodes increases, the dispersion component of losses decreases.

When applying the probabilistic approach, the calculation error is within the permissible limits for values of the load factor of the load schedule in the interval from 0.6 to 0.75

V. ACKNOWLEDGMENTS

The author would like to thanks the Research and Development Sector at the Technical University of Sofia, Bulgaria for their financial support.

REFERENCES

[1] N. Tsygulev, V. Khlebnikov, and Y. Voronina, "Specific aspects of calculating electrical energy losses in electricity networks". VIII International Scientific Conference Transport of Siberia – 2020, In IOP Conference Series: Materials Science and Engineering (Vol. 918, No. 1, p. 012156). doi:10.1088/1757-899X/918/1/012156

[2] A. Augugliaro, L. Dusonchet, and E. Riva Sanseverino, "Voltage drop and power losses fast evaluation through equivalent models of feeders for optimal operation of automated distribution networks". European transactions on electrical power, 217-225, 1999 https://doi.org/10.1002/etep.4450090401.

[3] S. W., Wang, C. Y. Hung, and D. C. Lin, "Loop-type feeder models for fast distribution system calculations",10th International Power & Energy Conference (IPEC 2012), pp. 611-615.

[4] T. H. Chen, and S. W.Wang, "Simplified bidirectional-feeder models for distribution-system calculations". IEE Proceedings-Generation, Transmission and Distribution 1995, 142(5), pp. 459-467.

[5] M. Todorovski, "A reduction method for radial distribution feeders: ensuring parity in voltages and losses". IEEE Transactions on Power Systems2024, 39(2), pp. 4759-4762, DOI:10.1109/TPWRS.2024.3351490

[6] T. H. Chen, and S. W. Wang, (1995, November). "Applications of simplified bi-directional feeder models for accelerating the voltage-drop and power-loss calculations", International Conference on Energy Management and Power Delivery EMPD'95 (Vol. 2, pp. 708-713).

[7] A. R., Manito, U. H. Bezerra, T. M. Soares, J. P Vieira, M. V Nunes, M. E. Tostes, and R. C., de Oliveira, "Technical and non - technical losses calculation in distribution grids using a defined equivalent operational impedance". IET Generation, Transmission & Distribution, 13(8), pp. 1315-1323

[8] C. E. M.Rodrigues, M. E de Lima Tostes, U. H Bezerra, T. M. Soares, E. O. de Matos, L. S. Soares Filho, and C. J. da Silva Moura, "Technical Loss Calculation in Distribution Grids Using Equivalent Minimum Order Networks and an Iterative Power Factor Correction Procedure". Energies 2021., 14(3), pp. 1-23

[9] Y. Ma and G. Fu, "Analysis of the Impact of Power Grid Structure and Equipment Types on Distribution Losses", 6th International Conference on Energy, Power and Grid (ICEPG 2024), pp. 775-779,

[10] M. I. Fursanov, A. A. Zalotoy, and V. V. Makarevich, "Calculation of technological consumption (loss) of electricity in modern 0.38–10 kV electrical distribution networks", Energetika. Proceedings of CIS higher education institutions and power engineering associations 2018, 61(5), pp. 408-422, https://doi.org/10.21122/1029-7448-2018-61-5-408-422

[11] M. Junxia, G. Binqing, L. Fuchao, and D. Peidong, "Study on power loss of distribution network with distributed generation and its reactive power optimization problem", International Conference on Power System Technology 2014, pp. 1213-1216

[12] S. Totalov, V. Zlatanova, V. Garbeva, N. Paunkov, P. Katsarova, "Comparative analysis of electrical energy measurement errors with commercial measurement tools", Conference of the Union of Scientists in Bulgaria 2011, vol. B – IX

[13] St. Nedeltcheva, "Electrical networks and systems with decentralized generating sources", TU – Sofia Publishing house, Sofia, April 2018, ISBN 978-619-167-348-3

[14] S. Petrov, "Monitoring of mode parameters in distribution electric networks", Announcements of TU-Sliven №4, 2019, ISSN1312-3920

[15] P. Notov and St., Nedeltcheva, "Electroenergetics", Vol. 2, TU – Sofia Publishing house, Sofia, 2009.

[16] Nedelcheva S., "Application of mathematical models for determining the losses of electricity in CH and HV power lines. Anniversary scientific conference", Conference Sliven'97.

[17] R. Simionov, K. Seymenliyski, G. Georgiev, and other, "Studying the Impact of PV Plants on Power Quality", Communications in Computer and Information Science, DOI:10.1007/978-3-031-23226-8_6

[18] Ordinance No. 3, Ministry of Energy and Energy Resources, Republic of Bulgaria, 2004

Environment. Technology. Resources. Rezekne, Latvia
Proceedings of the 16th International Scientific and Practical Conference, 2025. Volume IV, 201-207

Research of Electrical Generator Model (Stage: Phase Differences Impact on Generation Processes)

Vaidotas Matutis
Faculty of Electronics and Informatics
Vilniaus kolegija | Higher education institution
Vilnius, Lithuania
v.matutis@eif.viko.lt

Loreta Savulioniene
Faculty of Electronics and Informatics)
Vilniaus kolegija | Higher education institution
Vilnius, Lithuania
l.savulioniene@viko.lt

Mantas Vanagas
Faculty of Electronics and Informatics
Vilniaus kolegija | Higher education institution
Vilnius, Lithuania
m.vanagas@eif.viko.lt

Karolis Bojakovas
Faculty of Electronics and Informatics
Vilniaus kolegija | Higher education institution
Vilnius, Lithuania
karolis.bojakovas@stud.viko.lt

Tomas Kasperavicius
Faculty of Electronics and Informatics
Vilniaus kolegija | Higher education institution
Vilnius, Lithuania
t.kasperavicius@eif.viko.lt

Abstract— The article presents the interim results of the ongoing research. At this stage, measurements are being made with a model in which two energy sources are already installed in the impeller with rotated wings. The main purpose of this research is to observe the impact of phase difference in the process of generating electricity and its efficiency by measuring the output power of a rectifier with voltage stabilizing circuits when changing the phase between the two generator sources. In the presence of two electrical energy sources, the voltage generated by these generator sources was measured, as well as the current when changing the phase (the mutual position of the coils relative to each other creates a phase difference in the generated current, and the magnets are connected to each other by a stationary mechanical connection). Methode - the phase change is measured when both sources have a common electrical connection and when both sources do not have a common electrical connection, at that moment they are connected only by the mechanical part. Research determines that when changing the angle between the coils, the phase between the voltage fluctuations generated by both sources' changes. But the angles between the coils does not depend either on the variant of connecting the sources or on the connected load.

Keywords— electricity, electricity generator, regeneration, robotic systems, wind.

I. INTRODUCTION

This article publishes the data of a study that is part of an ongoing study and the initial results of which have already been published in previous publications [6] [7] [9] ... The investigation is ongoing with the consent and cooperation of the owners of the patent [4] in order to fully reveal the possibilities of the patented technology and possible additional effects.

For a start, we would also like to emphasize some of the nuances in the design of the impeller itself, which may not have been so clearly stated in previous publications. A general picture of the impeller currently in use is shown in Fig.1. In it, the cavity into which the magnetic ring is installed is clearly visible.

Online ISSN 2256-070X
https://doi.org/10.17770/etr2025vol4.8443
© 2025 The Author(s). Published by RTU PRESS.
This is an open access article under the Creative Commons Attribution 4.0 International License.

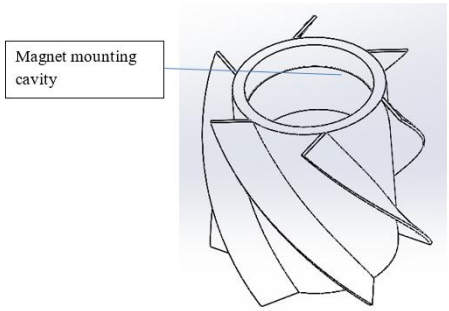

Fig. 1. Impeller used in the experiment.

However, these cavities are even more intelligibly depicted in the form of an impeller greying in Fig.2. In these cavities, magnets are installed in the impeller stationary and rotate together with the impeller. The starting position of the magnets with each other was not specially selected. It hasn't even been determined, so it's random and unchanging. It can be said that magnets are connected to each other by a stationary mechanical connection.

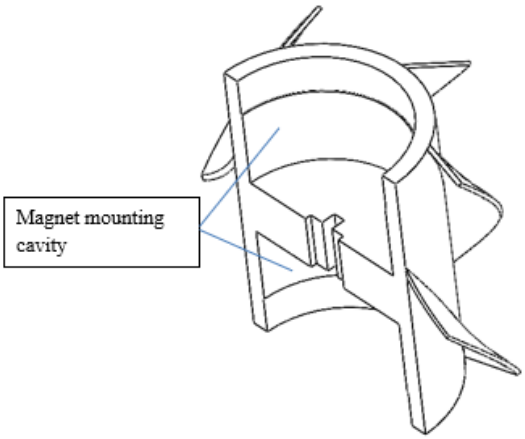

Fig. 2. Greying of the impeller used in the experiment.

The layout and impeller used in the experiment were designed using SolidWorks software, which is convenient to design in, since everything is in one space and it is possible to get an overall picture of the system in a 3D environment. Using a variety of SolidWorks features, it was possible to design a layout and an impeller rotating in it.

In previous experiments [6] [7] [9], it was observed that changing the positions of the coils changes the voltage generated, and changes in the curves observed during their fixation depending on the phase.

At this time, the simulation will not be used, since there is no possibility to make different phases between the reels for the sources and record their changes. Thus, all test results were obtained by measuring the design of the prototype used (experimental results).

II. Materials and Methods

Since two energy sources are installed in the generator's current layout, in such a design we have the opportunity to change the positions of the source coils relative to each other from 0° to 360° degrees. By changing (rotating one coil when the other is fixed) the position of the coil of one of the sources every 20° degrees, changes in the voltage generated by the generator's sources (influence on generation processes) and in the output, when the load using the generated energy is already connected to the generators, will be measured. In order to notice the changes in the energy generated by the sources and how they interact with each other, we will make several different types of measurements. Studies begin with the change of the position (phase) of the coils in different energy sources in the absence of any electrical connection. Both sources work independently and are connected only by magnets installed stationary in the impeller. In this way, it will be observed whether changes in the mechanical position of the coils in the generated energy flow occur due to changes in the mechanical position of the coils. We will use an oscilloscope by connecting it directly to the sources for measurements.

To monitor the voltage generated by the sources and the current at the exit after the load, we will connect both sources to separate diode rectifiers with a voltage stabilizer (Fig.9 or Fig.10) and after voltage equalization we will measure the resulting values of currents and voltages (as if we had two dc sources). As a load after rectifying, we will use an indicative diode and an elementary resistance. We will make measurements by varying the possibilities of connecting these sources. We will connect them in parallel (plus with plus, minus with minus), in series (plus of one source with minus of another source, the remaining contacts for connecting the indicative load) and vice versa (plus of one source with a plus of another source, the remaining contacts for connecting the indicative load).

III. Results and Discussion

As we have already mentioned at the beginning it is measured when there is no electrical connection between the two sources of the generator. At this stage, only the angle of position of the coils is changed, which theoretically should create a shift between the fluctuations of the measured voltage at different sources of the generator. A two-channel oscilloscope was used to capture this difference. Channel A will check one of the power sources, the other channel B will check the other power source. Since it is not possible to make 0° as a reference point by mechanical means at this point, the angle of 0° degree will be conditional.

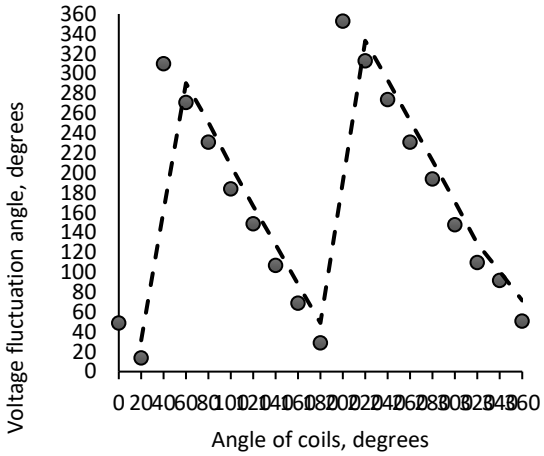

Fig. 3. Dependence of the phase of the electric signal on the angle of the coils.

According to the data presented in the graph (Fig.3), it can be seen that a direct relationship is formed between the angle of position of the coils and the fluctuations of the voltages between the existing sources. At the same time, we can note that the angle of the coils with the angle of voltage fluctuations passes and a displacement of 180° degrees is formed. From the theoretical side, such a phenomenon should have been obtained, since when changing (rotating) the positions of the coils relative to each other, when rotated at an angle of 180° degrees, the coils then simply change places, this can be seen in the drawing of the previously published impeller section [9]. And after turning the angle of 180° degree, the results should repeat and repeat. When analyzing this data and graphs, one should evaluate the human error and inaccuracies in the design of the layout, since access to the exact angle of rotation of the coil is not created. Although with a margin of error, the data corresponded to the forecast results, so increasing the accuracy at this point would not change the results.

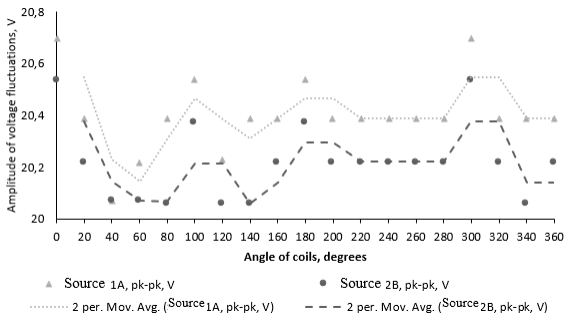

Fig. 4. The dependence of the amplitude of voltage fluctuations on the mutual angle of the coils.

When measuring the changes in the amplitude of voltage fluctuations depending on the angle between the coils (Fig.4), we can see from the results obtained and the graph that the voltage amplitude varies between 20.07 V and 20.54 V.

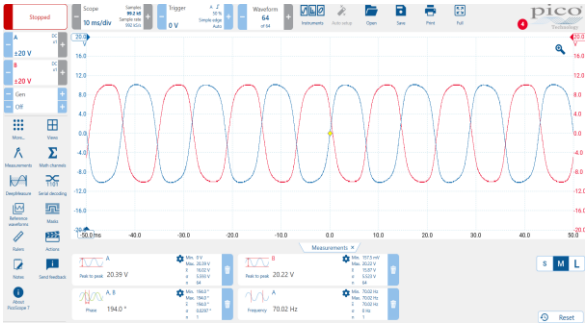

Fig. 5. Oscillogram of amplitudes of voltage fluctuation.

In the oscillogram (Fig.5), we see that in the absence of an electrical connection, the amplitudes of voltage fluctuations in both sources are approximately the same, and at the same time the frequency practically coincides. When changing the angle of position of the coils, one can see the phase shift between the fluctuations in the voltages generated by the sources. It is also noted that during the study, when the load is not connected, distortions in the shape of the signal do not appear. Further, variants of various connections of both sources were studied: parallel, sequential and vice versa. A parallel connection is formed when the wires of the positive pole of both sources are connected together, at the same time the wires of the negative pole of both sources are also connected together. A sequential connection is made when the wire of the positive pole of the first source with the load is connected, the cord of the negative pole with the wire of the positive pole of the second source, and the wire of the second negative pole with the load. The reverse or reverse serial circuit is formed by connecting the wire of the negative pole of the first source with the load, the wire of the positive pole with the wire of the positive pole of the second source, and the wire of the negative pole of the second source with the load thereby closing the circuit.

First of all, it will be studied when no load is connected (the outputs after the diode bridges are open), and the changes in the amplitude of the voltage oscillations generated by the sources depending on the angle of position between the coils will be measured. The results obtained are shown in Fig.6 graph.

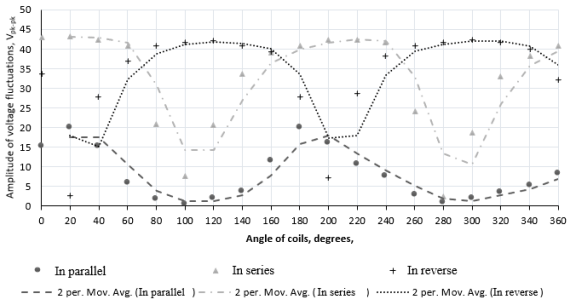

Fig. 6. Change in the voltage amplitude of different connections of two sources from the angle of the coils.

According to the data presented in Fig.6 graph, it can be seen that sequential and vice versa connections cause greater changes in the amplitude of voltage fluctuation compared to a parallel connection. In a sequential connection, the average amplitude of the generated voltage is about 32.42 V, the reverse connection is about 33.94 V, while the parallel one is only 8.08 V. According to the angle between the coils, it can be seen that in the case of a sequential connection, the damping occurs at the position from 80° to 160° degrees and from 240° to 340° degrees, and during the reverse connection at such angles, damping is not formed.

In the graph, we can quite clearly see such an angle of position of the coils with each other, in which the maximum amplitude of the voltage is obtained. That angle depends on the variant of connecting the two sources: if it is a sequential connection, it is the angle at the degree of 20°, at which 42.45 V is obtained; if it is a reverse connection, it is 300° degree, which also yields 42.45 V; in the case of a parallel connection, it is a rotation of 20° degrees at which the maximum amplitude of voltage fluctuations is measured at 19.95 V. Further studies are carried out when a constant load is already connected, to different variants of connections between the two sources. A 24-Ω resistor and a red LED were used to create the load. The resistor acts more as part of the load, and the diode as an indicator that shows or has enough power generated to illuminate the diode (visualization). During the study, using a multimeter, the voltage drop on the load and the unit of current flowing in the circuit is measured. The results of the current measurements are given in Fig.7 graph and the results of the voltage measurements in Fig.8.

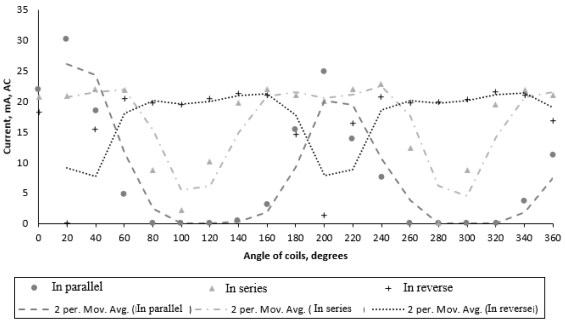

Fig. 7. The dependence of electric current on the angle between the coils under load.

From the graph of the dependence of electric current on the angle of the coils Fig.7 we can see that when changing the angle between the coils, the current at the corresponding points falls. The trend of current elevations and descents is associated with the Fig.6 graph, at the same angles there are changes in the current. Unlike the previous graph, all connections are approximately the same depending on how much current is generated, it is only a fundamental observation that at the moment of parallel connection, small permissible angles are obtained between angles of 200° and 220° degrees compared to other connections, in a sequential connection the maximum current between 160° and 240° degrees is obtained, and in the reverse connection between angles of 80° and 160° degrees. According to this graph, it can be said that the maximum current is obtained under load during a sequential and reverse connection.

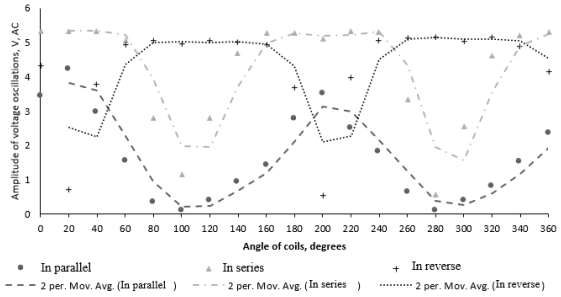

Fig. 8. Dependence of the amplitude of voltage fluctuations on the angle between the coils under load.

When examining graph in Fig.8, it can be seen that the trends observed when comparing the graphs in Fig.7 and in Fig.6 are repeated. The amplitude of voltage oscillation under load varies the same in all cases of connection - π (i.e. 180° degree) in a multiple. It has also been observed that the voltage amplitude settles at 5.35 V at a sequential or reverse circuit, and in the case of a parallel connection, the maximum voltage amplitude grows to only 4.22 V.

Summarizing all three graphs Fig.6, Fig.7 and Fig.8 and the data obtained from the study of the generator's source interconnections, both with and without load, it can be seen that the trends in voltage and current variation are related and repeated every π angle. Depending on the variant of connecting the sources, at the appropriate angles we observe inhibition, and in other cases, an increase in the amplitude of the oscillations. During a sequential connection, inhibitions occur at angles between degrees 80° and 160°, and at angles of 260° and 320° degrees. In the case of parallel connection, damping is observed at the angles between degrees 60° and 180° and at the angles between degrees 240° and 340°. It is noteworthy that during all stages of the study, in the case of a parallel connection, the minimum values of the data were measured in comparison with the sequential or reverse connection variant. During the inverse connection, damping occurs at the angles between degrees 0° and 60°, and at the angles between degrees 180° and 240°. Comparing these connection options, we can see that both with a sequential connection and inverse, the processes take place quite analogously.

Further, for experiments, an electrical connection is already being created between both sources of the generator at the output part. First, diode bridges with voltage regulators are connected separately for each source. Then two connections between them are possible: parallel and sequential.

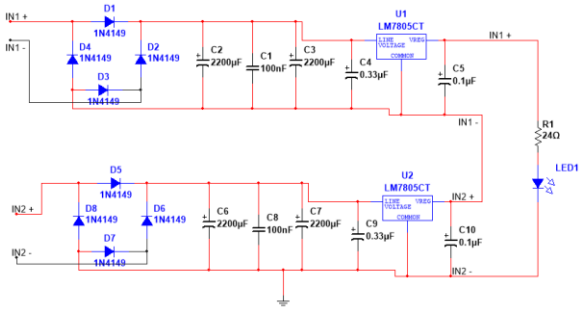

Fig. 9. Principle electrical diagram of the sequential connection of two sources.

To create a sequential connection, it is necessary to connect the wire of the negative pole of the first source with the wire of the positive pole of the second source. The wire of the positive pole of the first source with the load, which is then connected to the negative pole wire of the second source. Such a connection is shown in the figure Fig.9. The essence of this principle is similar to the connection of batteries in series, i.e. to increase the amplitude of the voltage without changing the magnitude of the current. In this way, in theory, the amplitude of the generated voltage oscillations, which falls on the load, should be doubled.

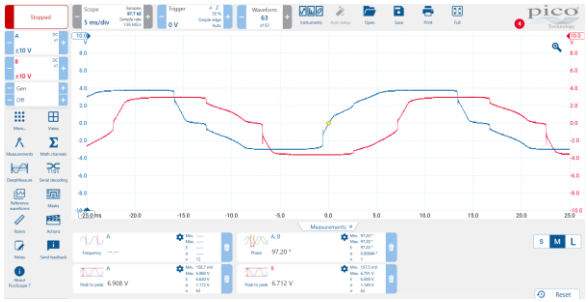

Fig. 10. Oscillogram showing the changes in the generated voltage fluctuations (with diode bridges and load in the presence of a sequential connection).

In order to notice the changes in the load, a resistance of 24 Ω and a red LED (visualization) were used. Using these components, voltage and current are measured at the output. From the resulting oscillogram Fig. 10, one can see the influence of the load on the fluctuations in the generated voltage when the mechanical angle of the position of the coils is formed at about 240 degrees. This means that the load affects the fluctuations in the generated voltage. Next, we will observe how this influence changes at the angles between the different coils. An oscilloscope and a multimeter were used to capture the data, and the data is shown in Fig. 11 graph.

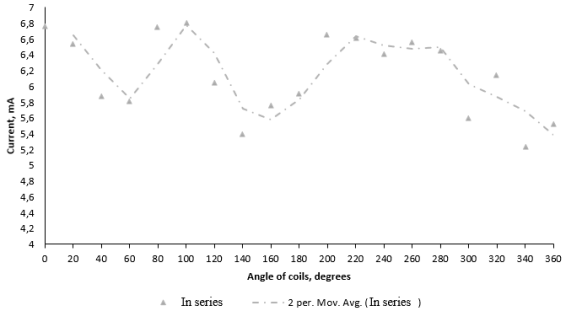

Fig. 11. The dependence of the current of two sources connected in series to the phase.

Fig. 11 shows that the change in current as the position of the coils changes is more than 20% . The current ranges from 5.25 mA to 6.75 mA.

Next, the parallel connection under the bridges with the load will be measured. By analogy with sequential connection, all measurement methods remain the same.

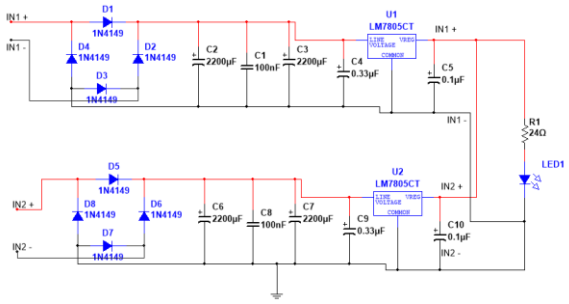

Fig. 12. Principle electrical scheme of parallel connection of two sources.

To make a parallel connection, it is necessary to connect the wires of the positive pole of both sources together and connect to the load. At the same time, the wires of the negative pole of both sources are also connected together and connected to the negative pole of the load. The parallel connection diagram is shown in fig.12.

Fig. 13. Oscillogram showing the changes in the generated voltage fluctuations (with diode bridges and load at parallel circuits).

From the fig.13 graph, it can be seen that the load at parallel (Fig12) connection of sources similarly affects the input signal as in a sequential circuit. In the presented case, the voltage oscillation curve, although more orderly, is also distorted and limited in a similar way to

the positive and negative maximums of the amplitudes of the oscillations. Since we see that changes are formed, further measured at different angles of the coils, the data obtained is shown in the graph below the text (Fig.14).

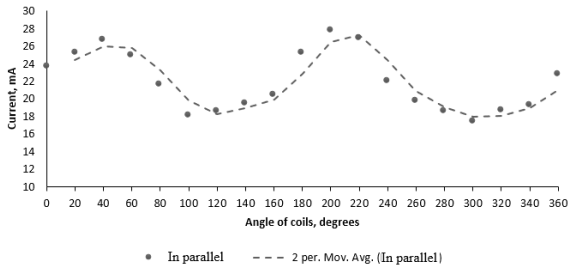

Fig. 14. The dependence of the current generated by two sources connected in parallel on the angle between the coils (with diode bridges and load).

According to the measurement data presented in Fig.14, we can see the observed trend of current change by changing the angle between the coils, at the same angles i.e. at the angles between 180° and 220°, as well as at the angles between 0° and 60° degrees, the maximum value of the measured current is obtained. In comparison with the sequential connection, the current increased three times more. The trend of oscillations between rise and inhibition has been maintained the same – π multiple.

Next, the change in the amplitude of voltage oscillations from the angle between the coils is measured. In the same way as with current measurements, the same circuits are maintained, sequential and parallel.

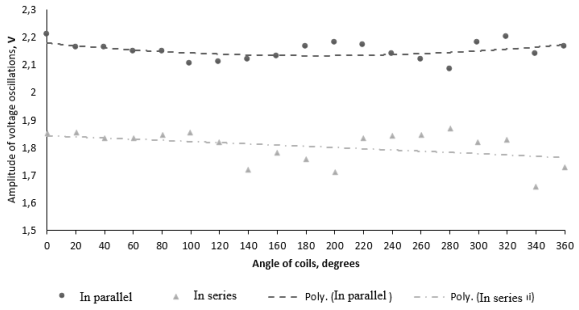

Fig. 15. Curves of the amplitudes of voltage oscillations on the angle of position of the coils at sequential and parallel connections of two sources (with diode bridges and load).

Analyzing the data presented in graph Fig15, we can see that the voltage changes with a slight change in the positions between the coils, the difference is about ~10% in both sequential and parallel connections. Comparing the results of both connection options, at this point we received a little more voltage in the case of parallel connection than in the case of a serial circuit (about 0.4 V more).

Summarizing the presented research results, we can say that the angle of position of the coils with each other influences the process of generating electricity. When changing the angle between the coils, the phase between the voltage fluctuations generated by both sources' changes. It has been observed that the change is a π multiple. Since two energy sources are built in, after testing different combinations of their interconnection during the study, it was observed that inhibition occurs at the angles of the positions of some coils. Inhibition occurs at the same angles between the coils does not depend either on the variant of connecting the sources or on the connected load.

It was also noted that during a parallel connection, a lower power is obtained compared to the variants of sequential and reverse connection.

IV. Conclusions

We can see that the interrelationship of the coils quite significantly influences the process of generation when we have a generator of the presented design with two energy sources.

Effective use of the system of such a design requires appropriate alignment of the positions of the coils with each other;

The method of connecting the generator's two sources also has a fairly significant impact on the generation process itself;

The results of the measurements obtained are further systematized and analyzed in order to identify also the possibilities and trends of increasing the effectiveness of this step.

All the data presented was obtained by conducting experiments in laboratory conditions when the layout was placed on the path of a constant air flow. We tried to create the same air flow for each measurement and select it close to the air flow when the incoming car was driving at a speed of about 50 km / h. Next, it is planned to conduct these experiments in real conditions and at different air flow rates.

References

[1] R. P. Mukund. Wind and solar power systems: design, analysis, and operation. Boca Raton, Taylor & Francis, 2006.

[2] Autorių kolektyvas, informacijos rinkinys „Viskas, ką reikia žinoti apie vėjo energetiką“ [elektroninis išteklius], Vilnius, Lietuvos vėjo elektrinių asociacija, 2020. Prieiga per internetą: https://lvea.lt/wp-content/uploads/2021/01/LVEA_Viskas-ka-reikia-zinoti-apie-vejo-energetika.pdf

[3] L. Augulis, A. Jotautis, D. Rutkūnienė. Fizika: mechanika, termodinamika, elektromagnetizmas: mokomoji knyga [elektroninis išteklius]. Kaunas, Technologija, 2012. [žiūrėta 2014-12-15]. Prieiga per internetą: https://www.ebooks.ktu.lt/eb/656/fizika_mechanika_termodinamika_elektromagnetizmas/

[4] V. Matutis, M. Matutis, Patentinis aprašymas, 2019, Prieiga per internetą: https://worldwide.espacenet.com/patent/search/family/068887188/publication/EP3840192A1?q=EP3840192A1

[5] V. Matutis, L. Savulionienė, P. Šakalys, T. Kasperavičius, Energy Generator Prototypes Development And These Research Integration Into The Educational Process. Society. Integration. Education. Rēzeknes Tehnoloģiju akadēmija, 2022,

DOI: https://doi.org/10.17770/sie2022vol1.6884 (http://journals.ru.lv/index.php/SIE/article/view/6884/5683)

[6] V. Matutis, L. Savulionienė, P. Šakalys, T. Kasperavičius, Research of Power Generator Prototype Development and Integration into Autonomous Robotic Systems. Society. Integration. Education. Rēzeknes Tehnoloģiju akadēmija,, 2021, DOI: https://doi.org/10.17770/sie2021vol5.6453

[7] V. Matutis, L. Savulioniene, T. Kasperavicius, and D. Savulionis, "Electric Generator Model Research (Stage Efficiency Of Electromechanical Part)", ETR, vol. 3, pp. 175–179, Jun. 2024, doi: 10.17770/etr2024vol3.8155.

[8] P. Šakalys, L. Savulionienė, D. Savulionis. Research of robotic systems control methods using motion recognition tools, machine learning and skeletalization algorithms // Sabiedrība. Integrācija. Izglītība = Society. Integration. Education : proceedings of the International Scientific Conference, May 28th-29th, 2021. Rēzekne : Rezekne Academy of Technologies. ISSN 1691-5887. eISSN 2256-0629. 2021, p. 448-458. DOI: 10.17770/sie2021vol5.6451.

[9] V. Matutis, L. Savulioniene, P. Sakalys, and L. Gzegozevske, "Research Of The Principal Model Of The Electric Energy Generator Of The Electric Car (Stage Combination Of Mechanical And Electromechanical Parts)", ETR, vol. 3, pp. 172–175, Jan. 2024, doi: 10.17770/etr2023vol3.7261.

Environment. Technology. Resources. Rezekne, Latvia
Proceedings of the 16th International Scientific and Practical Conference. 2025. Volume IV, 209-215

Automated Groundwater Monitoring System with Real-time Data Collection and Analysis Using LoRa and GSM Technologies

Gulrukh Memonova
Mobile communication technologies
*Tashkent University of Information Technologies named after Muhammad al-Khwarizmi*line
Tashkent, Uzbekistan
memonovagulrux@gmail.com

Peter Schmidt
Department of Applied Informatics
University of Economics in Bratislava
Bratislava, Slovakia
peter.schmidt@euba.sk

Javlon Tursunov
Institute of Multimedia Information and Communication Technologies
Slovak University of Technology in Bratislava,
Bratislava, Slovakia
javlontursunov0817@gmail.com

Guljakhon Gofurova
Information and Computing Center
Railways UZB
Tashkent, Uzbekistan
sherzodguli33@gmail.com

***Abstract* — Groundwater monitoring is crucial, particularly in drought-prone areas. Manual methods are time-consuming, inaccurate and weather-dependent. GSM solutions are costly and energy-intensive with limited network coverage and other currently existing works and methodologies have certain limitations. Taking these, other factors and limitations into consideration when it comes to monitoring underground water, this research presents an innovative automated system using energy-efficient LoRa technology for real-time monitoring, enhancing efficiency and reliability while reducing costs and energy consumption. The main purpose of this study is to develop and validate an innovative automated groundwater monitoring system that employs energy-efficient LoRa technology for real-time data collection and analysis, thereby overcoming the limitations of manual methods and traditional GSM solutions while ensuring enhanced reliability, scalability and cost-effectiveness. Additionally, the main contribution is the development of an innovative system used for underground water monitoring and comparison of effectiveness of LoRa based network with the GSM based network, comparing the effectiveness of this system with different network topologies when it comes to establishing such a system. Star, line and mesh network topologies were deployed to optimize data transmission and energy efficiency, packet loss and latency of these topologies were evaluated, thus enabling innovative continuous and automated groundwater monitoring. Results show the LoRa-based system significantly reduces energy consumption and operational costs compared to GSM with reliable data transmission even in areas with limited mobile coverage. This research and validation demonstrate the feasibility and advantages of integrating LoRa technology with different topologies into groundwater monitoring systems, providing a scalable solution for sustainable water management, especially in water-scarce regions. Wireshark was used to analyze the results in terms of latency, considering the convenience of the different topologies in different scenarios. The Introduction section highlights the topicality of the topic, study purpose and reviews the current state-of-the-art with limitations of existing approaches addressed by this research. The Materials and Methods section details the design and implementation of the system, with the Results and Discussion section presenting our findings. Finally, the Conclusion section discusses the scientific contributions and value of our research and outlines potential areas for further improvement.**

Keywords — *Diver sensor, LoRa, NodeMCU Wi-Fi module, Raspberry Pi.*

I. Introduction

In recent years, water scarcity has emerged as a critical issue impacting various regions around the world, including Uzbekistan. The country, with its arid climate and reliance on agriculture, faces significant challenges due to drought conditions and inefficient water management practices. According to sources, lack of water in central Asian countries is causing an 11 percent decrease in their GDP and according to the UN, countries in this region lose

Online ISSN 2256-070X
https://doi.org/10.17770/etr2025vol4.8412
© 2025 The Author(s). Published by RTU PRESS.
This is an open access article under the Creative Commons Attribution 4.0 International License.

at least $1.75 billion annually due to inconsistent coordination of water use [1]. Apart from that, water coming from Amudarya, one of the two main rivers in Uzbekistan, will decrease dramatically [2]. During the summer months, agricultural crops suffer considerably, exacerbated by the improper planning and execution of irrigation without an adequate understanding of groundwater levels. This situation highlights the urgent need for innovative solutions and research to optimize water usage and enhance agricultural productivity. Research indicates that within the next 20 years, the demand for water in Uzbekistan will substantially increase, while available water resources will sharply decrease, potentially amplifying the current water shortage up to five times, thus categorizing Uzbekistan as a red region in terms of water scarcity [3]. Apart from these sources, there are a lot of sources that will support how dire the situation is.

Groundwater, an essential resource for agriculture, often goes unmonitored due to the limitations of traditional methods. Accurate and timely data on groundwater conditions, such as salinity, temperature, flow speed and water level, can revolutionize water management practices which can help in terms of addressing the above-mentioned water scarcity. However, conventional approaches, including manual monitoring and GSM-based systems, are often energy-intensive, costly and limited by mobile network coverage, especially in remote areas.

Considering this, the primary objective of this research is to design, implement and rigorously evaluate an innovative automated groundwater monitoring system that leverages energy-efficient LoRa technology. By addressing the limitations associated with manual monitoring and conventional GSM approaches, this study aims to provide a robust framework for real-time data acquisition, enhanced network reliability and sustainable water resource management in water-scarce regions. Precisely, this work introduces an advanced groundwater monitoring system leveraging LoRa (Long Range) wireless technology. LoRa offers a low-power, cost-effective solution for long-range communication, making it ideal for remote monitoring applications and real-time groundwater monitoring, thus facilitating informed decision-making for irrigation management. Our system employs a diver device placed at a depth of 150 meters to measure various groundwater parameters. The data collected by the diver is processed by an Arduino, which then transmits the data via LoRa to a central Raspberry Pi. Experiments were carried out with different network topologies—star, line and mesh—to determine the most efficient configuration for data transmission. The data is further relayed to a custom server using a NodeMCU WiFi module for comprehensive analysis and monitoring. Additionally, this research provides insights into which network topologies should be used under different conditions and results of the different topologies in terms of coverage, power consumption, delay and packet loss are compared and represented. Wireshark was used to measure the performance of created different networks based on different topologies and conditions.

The continuation of this section focuses on the most relevant literature and state-of-the-art works aimed at addressing the challenges of groundwater monitoring and management, including various technologies and methodologies that have been proposed and implemented to enhance the accuracy, efficiency, and cost-effectiveness of monitoring groundwater parameters. By analyzing these works, specific research gaps and limitations are identified that are addressed by our research. Prior research on traditional and modern groundwater monitoring systems are explored, highlighting the advantages and drawbacks of different approaches. This includes a review of GSM-based systems, which, despite their widespread use, often suffer from high energy consumption and dependency on mobile network coverage. The adoption of emerging technologies such as LoRa which offers promising solutions for remote and low-power applications, is explored as well. The identification of these gaps in existing research informs the design and implementation of our proposed approach, which is detailed in the section called Materials and Methods. Our work builds on the strengths of previous studies while addressing their shortcomings, particularly in terms of energy efficiency, network reliability, and scalability in diverse environmental conditions. By integrating innovative technologies and comparing different network topologies, our study contributes to the advancement of sustainable groundwater monitoring solutions. In our work, we mainly focus on the Lora module which is like a GSM module to establish wireless communication. Low-power communication has many on-the-shelf choices, but LoRa is one of the best [4][5]. LoRa technology provides a very eye-catching combination of ultra-long distance, low power consumption, and safe data transmission, which can effectively solve the security and stability problems of data communication. In the work done in [6], the authors propose a system utilizing M2M-LoRa technology for monitoring water quality, distribution and pollution control in Smart Village Projects. This system employs LoRa motes and sensors placed in water tanks across 200 locations, allowing continuous monitoring of water quality and levels. The collected data is centrally displayed, facilitating comprehensive control over the water distribution system and enabling the prevention of water wastage and the distribution of polluted water. According to [7], the authors propose using the NuttyFi ESP8266 WiFi board for water level measurement, combining advanced technology with creativity. This system facilitates real-time data transfer and remote monitoring via the Blynk IoT app, allowing users to check water levels globally and control an actuator module. The incorporation of ultrasonic technology enhances the precision and reliability of readings. This system offers a state-of-the-art, user-friendly solution for optimal water management, demonstrating efficient performance with minimal computational costs. The study in [8] developed

an IoT-based automated irrigation system to optimize water usage in agriculture, addressing the critical issue of water scarcity. Temperature and moisture sensors gather data, which is transmitted via a LoRa network to a controller unit for threshold comparison and motor activation or deactivation. The system also utilizes a GSM module to notify users of motor status via SMS and records sensor data and water consumption on Thingspeak for analysis. Research by [9] details a pioneering project by the Department of Fisheries and Aquaculture (DJPB) to model high-density tilapia cultivation, aiming for a stocking density of 25 fish per square meter at 20 ppt salinity. The project's success relies on rigorous water quality management, facilitated by an IoT Smart Water Quality Monitoring System that measures key parameters-temperature, Dissolved Oxygen (DO), pH, salinity, and water volume-providing real-time updates at one-second intervals. The system's initial deployment involves installing 10 units across ponds with surface areas of 4000m² and 2000m².

The authors in [10] designed a LoRa-based IoT network for hydroponic farm monitoring, leveraging IoT advancements for precise wireless data transfer. The system employs various sensors to measure key parameters, with real-time data transmitted via LoRa to a gateway for simultaneous viewing and analysis by authorized users, enhancing monitoring efficiency. This approach capitalizes on LoRa's advantages, including long-distance communication, battery longevity, and noise resistance, making it a superior solution for continuous hydroponic farm oversight.

Based on the work in [11], the authors develop a Fog Server-based irrigation system to enhance smart agriculture by increasing crop yield and reducing water wastage. Their system employs LoRaWAN to relay sensor data to a fog server, using MQTT and Node-Red for micro-service communication. This framework's key advantage is its functionality in areas with intermittent internet connectivity, making it a robust solution for modern agricultural challenges. The findings of [12] present a smart irrigation system utilizing LoRa P2P networks, designed to automate irrigation by learning from expert farmers' experiences. Experimental results indicate the system's high suitability for modern greenhouse agriculture. In [13], the authors developed an Internet-based automation system for plant monitoring, using an Arduino Atmega 328p microcontroller and LoRa 915 MHz to measure water pH, soil pH, and soil moisture, ensuring optimal irrigation in agricultural lands. The system, tested with Pakcoy plants, uses LoRa-integrated water containers to maintain average pH levels, displaying real-time data via the Thingspeak IoT server.

Work done by authors in [14] develops a field management system incorporating a field server and a local wireless network using LoRa to significantly reduce power consumption and maintenance frequency, thus easing agricultural workloads and facilitating knowledge transfer among Japanese farmers. Experimental results demonstrate effective data transmission between the master unit and field server, with a daily power consumption of 75.36 mW, allowing for theoretical continuous operation of up to 995 days which is sufficient for monitoring rice cultivation. The authors in [15] address the challenges of irrigation monitoring over extensive agricultural lands and under extreme weather conditions by developing an IoT-based system using LoRa. They implement a data communication protocol to efficiently manage multi-node data transmission and accommodate new devices, thereby optimizing communication and expanding the reach of irrigation monitoring. In the research done in [16], authors propose an enhanced tropical peatland Fire Weather Index (FWI) system, integrating groundwater level (GWL) data with the drought code (DC) to better predict fire risk. Utilizing a LoRa-based IoT system for data collection in Raja Musa Forest Reserve in Malaysia, the study verifies the system's efficacy by comparing its data with that of METMalaysia, showing a high correlation of 0.8. A robust IoT-based monitoring and control system aimed at addressing water supply challenges in urban residential areas, emphasizing continuous real-time monitoring for efficient water distribution, supply management, and quality control was proposed by authors in the research [17]. The system utilizes a network of physical items equipped with sensors, software, and network connectivity, enabling remote monitoring and control from anywhere, with data uploaded to the cloud via Adafruit for real-time tracking and management facilitated by efficient client-server communication. The next research given in [18] discusses the critical challenges faced by water supply departments due to decreased rainfall, emphasizing the need for robust monitoring and control systems to address issues such as water distribution, interrupted supply and conservation. The proposed IoT-based approach enables continuous and real-time monitoring of water supply, facilitating efficient management through the integration of sensors, software and network connectivity. An innovative approach was described in [19] which integrates sensors and intelligent algorithms to optimize infrastructure efficiency. Powered by an external Arduino board and GSM module, the system monitors water quality, temperature, turbidity, and pH levels, offering enhanced adaptability and connectivity compared to existing WiFi-dependent models. Simulation results validate its effectiveness, highlighting feasibility and potential impact, while an innovative alert feature notifies users of deviations in water quality parameters, enhancing practicality and responsiveness. This research contributes to the discourse on water infrastructure management, offering a forward-thinking approach to resilient and sustainable practices. Most previous works in this domain have utilized pre-existing server solutions, whereas our approach involves the development of our own server, website and monitoring

system from scratch, thus allowing more customization aimed at enhancing efficiency.

II. Materials and Methods

In this section, we outline the detailed methodology and workflow employed in the implementation and evaluation of the underground monitoring system using LoRa technology. The methodology is structured to provide a systematic approach to the setup, deployment, and data transmission of sensor nodes, as well as the establishment of a central gateway for data collection. Following the workflow depicted in Figure 1, we describe the configuration of sensor nodes, their deployment in the field, and the setup of the central gateway. Furthermore, we discuss the implementation of three different LoRa topologies (star, mesh, and line) and their respective advantages and disadvantages. The methodology also covers the data transmission and collection process, including the processing and storage of collected data. Finally, we explain the real-time monitoring and analysis of environmental parameters through a web-based interface.

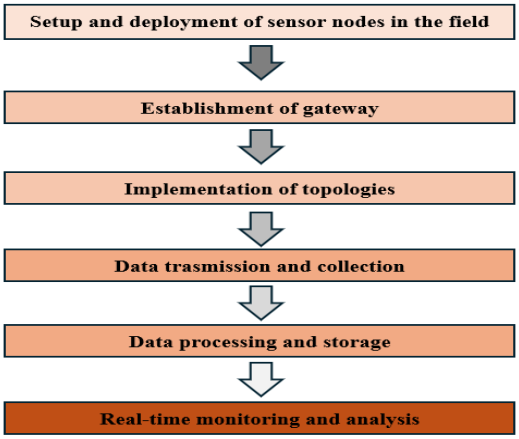

Fig. 1. Workflow.

This comprehensive methodology ensures a clear understanding of the procedures involved in developing and evaluating the underground monitoring system.

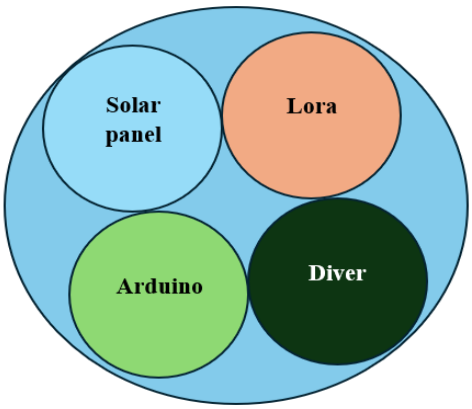

Fig. 1. Node elements.

Each sensor node in the well was meticulously configured to include an Arduino microcontroller, a LoRa device, and a Diver sensor along with a solar panel to power it up (Fig 2).

Fig. 2. Diver sensor.

The Diver sensor was responsible for measuring water level, salinity, and temperature from groundwater up to 150 meters deep (Fig 3).

Fig. 3. The well equipped with a solar panel.

The collected data was processed and transmitted via LoRa communication for further analysis. Solar panels powered the nodes, ensuring autonomous and sustainable operation. Sensor nodes equipped with solar panels were strategically deployed across various locations within the designated area. Each node was installed in the wells to provide comprehensive coverage and collected environmental data, including water level, salinity, and temperature (Fig 4).

A central gateway was established to gather data from the sensor nodes.

Fig. 4. Main components of gateway.

The gateway consisted of a LoRa gateway, a Raspberry Pi, and a GSM module, enabling long-distance data transmission between GSM modules (Fig 5).

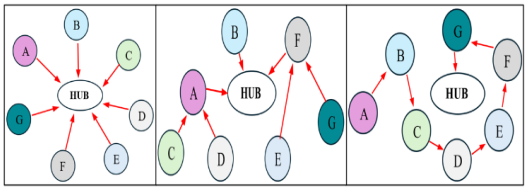

Fig. 5. Star, Mesh and Line topologies (Hub means the gateway)

Three different topologies—star, mesh, and line—were deployed to assess their respective advantages and disadvantages (Fig 6).

Each topology's performance was evaluated in terms of energy consumption, latency, and packet loss. Wireshark, a network protocol analyzer, was used to measure latency and packet loss, and the power consumption of each node was measured as well. The results of each topology are illustrated in the results section.

Sensor nodes transmitted data to the gateway using LoRa communication and the gateway, comprising a LoRa gateway, Raspberry Pi, and GSM device, relayed this data to another secondary Hub equipped with a GSM module for long-distance transmission. This secondary Hub contains GSM and NodeMCU WiFi devices and NodeMCU is connected to an Internet-enabled router and this WiFi module is responsible for sending the data to the server.

Upon receiving data from the gateway, the GSM module relayed the raw data to the Nodemcu WiFi module in the secondary Hub, ensuring it was refined and structured for further analysis. The processed data was then transmitted to the server using Wi-Fi communication via the NodeMCU Wi-Fi module. This module, connected to a Wi-Fi network with internet access, facilitated the swift and reliable transmission of data to the server, where it was securely logged and stored for future reference (Fig 7).

A comprehensive web-based monitoring system was established to visualize and analyse the collected data in real-time.

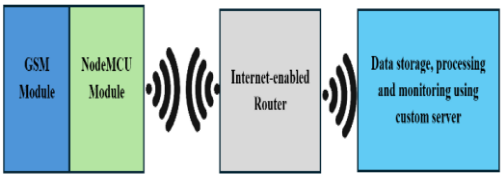

Fig. 6. Sending data to server from secondary Hub.

The web server continuously received data from the NodeMCU Wi-Fi module, accurately logging environmental parameters such as water level, temperature, salinity, and speed of water flow.

The server, along with storing data, processes this data and updates the web interface in real time, providing users with immediate insights into the monitored environment. The user-friendly web interface displays real-time data graphically, showing trends and changes over time. Additionally, it offered detailed historical data, allowing users to review past readings and analyse long-term trends. This setup facilitated easy tracking, comparison of data, and proactive management based on the collected insights.

III. Results and Discussions

This section presents our comparative analysis of This section presents our comparative analysis of three network topologies-star, mesh, and line-in an automated system for monitoring underground water parameters, focusing on energy consumption, latency, and packet loss. The data reveals the efficiency and reliability of each topology, highlighting their respective advantages and disadvantages. Energy consumption, critical for solar-powered nodes, is illustrated in the table below, showing milliampere-hour (mAh) usage for each node and the gateway across the topologies.

TABLE 1. ENERGY CONSUMPTION COMPARISON

Nodes	Star (mAh)	Mesh (mAh)	Line(mAh)
A	30.4	42.1	28.6
B	35.1	50.4	36.9
C	32.6	26.7	48.2
D	33.8	53.3	59.5
E	37.2	22.8	75.3
F	40.5	67.7	90.7
G	39.7	35.9	102.8
Gateway	109.3	92.0	70.6

The energy consumption analysis of different topologies reveals that the star topology exhibits moderate energy consumption, with the gateway consuming the highest energy due to its central role in data collection and transmission. In contrast, the mesh topology shows higher energy consumption in nodes as a result of the multi-hop communication required, but the gateway itself consumes less energy compared to the star topology. The line topology, however, results in the highest energy consumption for most nodes, especially those close to the gateway since they receive and transmit signal at the same time, which highlights the inefficiencies inherent in long linear communication chains. Also, another disadvantage is that if any node does not work, it may lose connectivity, thus losing the data of other nodes that pass through this node.

Latency is a measure of the time taken for data to travel from a node to the gateway. Lower latency is crucial for real-time monitoring applications. The table below presents the latency in milliseconds (ms) for each node across the three topologies.

TABLE 2. LATENCY

Nodes	Star (ms)	Mesh (ms)	Line(ms)
A	30.3	30.3	905.6
B	35.7	35.7	682.2
C	32.6	71.1	460.8
D	25.6	77.5	349.4
E	23.7	83.9	235.9
F	29.8	95.2	128.3
G	30.5	33.8	45.7

The latency analysis indicates that the star topology maintains low latency due to direct communication between nodes and the gateway. Conversely, the mesh

topology generally exhibits higher latency than the star topology as a result of the additional hops required for data transmission. The line topology, however, suffers from significantly higher latency, particularly for nodes further from the gateway, due to the sequential nature of data transmission.

Packet loss is a critical parameter affecting the reliability of data transmission in sensor networks. Lower packet loss indicates more reliable communication. The table below displays the packet loss percentage for each node across the three topologies.

TABLE 3. PACKET LOSS

Nodes	Star (%)	Mesh (%)	Line (%)
A	5.4	13.7	23.8
B	12.8	15.2	19.6
C	7.1	11.5	15.3
D	11.6	16.8	12.7
E	9.3	12.9	9.1
F	4.7	14.3	6.4
G	7.7	17.4	3.2

The packet loss analysis reveals that star topology exhibits the lowest packet loss overall, benefiting from direct communication paths to the gateway. In contrast, the mesh topology shows moderate packet loss, reflecting the complexity and potential interference inherent in multi-hop communications. The line topology, however, experiences the highest packet loss, particularly for nodes further from the gateway, due to its linear communication path.

Star topology offers several advantages, including low latency, low packet loss, and simpler network management. However, it also has disadvantages such as higher energy consumption at the gateway and a potential single point of failure. In contrast, the mesh topology increases network robustness and redundancy but comes with higher energy consumption due to multi-hop communication and increased latency. The line topology, while advantageous for its simple implementation and minimal management, suffers from high latency and packet loss, particularly as the distance from the gateway increases, as well as higher energy consumption. The results highlight the strengths and weaknesses of each topology in terms of energy consumption, latency, and packet loss. The star topology, while exhibiting low latency and packet loss, faces higher energy demands at the gateway. The mesh topology provides robustness and redundancy but suffers from increased latency and energy consumption. The line topology, despite its simplicity, struggles with high latency, packet loss, and energy inefficiencies.

In addition to the above analysis, it is worth noting that our experimental setup presents avenues for further exploration. The observed variations in energy consumption, latency, and packet loss suggest that while the star topology offers optimal performance in terms of latency and reliability, its inherent energy demands at the gateway may require further optimization. Future work could investigate hybrid network configurations or adaptive protocols that dynamically balance the advantages of star, mesh, and line topologies, especially in environments with variable interference or node density. Moreover, exploring additional network topologies—such as ring or cluster-based networks—and integrating machine learning techniques for predictive maintenance and traffic management could further enhance system robustness and scalability. This expanded scope could lead to more comprehensive strategies for automated groundwater monitoring, ensuring that the system remains efficient under diverse operational scenarios and weather conditions. Such research directions will not only refine our current approach but also contribute to the development of next-generation monitoring systems tailored for sustainable water resource management in water-scarce regions.

IV. CONCLUSIONS

In this study, we developed an automated system for monitoring underground water at a depth of 150 meters by integrating diver sensors, Arduino processing, LoRa communication and a custom server for real-time data management. Our experimental evaluation, conducted across seven well nodes using star, mesh, and line network topologies, demonstrated that the star topology yields the lowest latency and packet loss, confirming its superiority for real-time applications. Power consumption measurements revealed that, although the star topology imposes higher energy demands on the gateway, the overall system performance clearly validates the efficiency of the proposed approach. Importantly, our results underscore the feasibility of employing LoRa technology as an effective alternative to conventional GSM-based methods, offering improved power efficiency and reduced operational costs. By comparing multiple network configurations, we proved the versatility and performance benefits of using LoRa across varied deployment scenarios, providing a robust foundation for enhanced decision-making in water resource management. Furthermore, future research could advance this work by exploring hybrid network topologies that integrate the strengths of star, mesh, and line configurations. Such approaches could enable adaptive protocols that dynamically respond to varying interference levels and node densities, thereby further enhancing system reliability and efficiency. These innovations promise to extend the applicability of our monitoring system to even more challenging environments. The insights gained through our research pave the way for the development of more efficient and reliable water resource management strategies, thereby contributing to the sustainable utilization of this vital natural resource.

REFERENCES

[1] “Water shortage may lead to a decrease in GDP of Central Asian countries by 11%,” kun.uz. https://kun.uz/en/51169440 (accessed October. 10, 2024).

[2] "Water of Amudarya may decrease sharply due to Kushtepa canal being built by Taliban," kun.uz. https://kun.uz/en/21230060 (accessed October. 10, 2024).

[3] "Water scarcity in Uzbekistan: Probable drought and escalating environmental challenges," kun.uz. https://kun.uz/en/41497711 (accessed October. 10, 2024).

[4] A. Cano-Ortega and F. Sánchez-Sutil, "Monitoring of the Efficiency and Conditions of Induction Motor Operations by Smart Meter Prototype Based on a LoRa Wireless Network," Electronics, vol. 8, no. 9, p. 1040, Sep. 2019, doi: 10.3390/electronics8091040.

[5] V. K. Sarker, J. P. Queralta, T. N. Gia, H. Tenhunen, and T. Westerlund, "A Survey on LoRa for IoT: Integrating Edge Computing," 2019 Fourth International Conference on Fog and Mobile Edge Computing (FMEC), Jun. 2019, doi: 10.1109/fmec.2019.8795313.

[6] A. M. Manoharan and V. Rathinasabapathy, "Smart Water Quality Monitoring and Metering Using Lora for Smart Villages," 2018 2nd International Conference on Smart Grid and Smart Cities (ICSGSC), Aug. 2018, doi: 10.1109/icsgsc.2018.8541336.

[7] A. Dogra, A. Badhoutiya, B. Goyal, K. Kriplani, A. Juyal, and H. Kaur, "Revolutionizing Water Level Monitoring with the Wi-Fi Board," 2024 11th International Conference on Computing for Sustainable Global Development (INDIACom), Feb. 2024, doi: 10.23919/indiacom61295.2024.10498623.

[8] M. N. Amogha Hegde, M. S. Naik, S. N. Chaitra, M. Madhavi, and A. Ravichandra, "Prediction and Analysis of Water Requirement in Automated Irrigation System using Artificial Neural Network(ANN) and Lora Technology," 2021 IEEE International Conference on Distributed Computing, VLSI, Electrical Circuits and Robotics (DISCOVER), Nov. 2021, doi: 10.1109/discover52564.2021.9663706.

[9] F. B. G. Pratama, F. Hidayatullah, E. L. I. P. Sari, I. K. A. Enriko, F. N. Gustiyana, and A. Luthfi, "Solar-Powered LoRa Wireless Water Quality Monitoring for Saline Tilapia Aquaculture," 2024 International Conference on Green Energy, Computing and Sustainable Technology (GECOST), Jan. 2024, doi: 10.1109/gecost60902.2024.10474710.

[10] S. Rathod, S. Dhanan, S. S. Harsha, S. Choudhary, and S. K. P, "LoRa Technology Based Hydroponic Farm Monitoring System," 2021 2nd International Conference on Smart Electronics and Communication (ICOSEC), Oct. 2021, doi: 10.1109/icosec51865.2021.9591729.

[11] D. Rajasekhar, J. Miao, S. Mishra, S. K. Nayak, and R. Yadav, "Intelligent Irrigation Technique for LoRa Enabled Fog Assisted Smart Agriculture," 2023 IEEE 9th World Forum on Internet of Things (WF-IoT), Oct. 2023, doi: 10.1109/wf-iot58464.2023.10539579.

[12] Y. C. Chang, T. W. Huang, and N. F. Huang, "A Machine Learning Based Smart Irrigation System with LoRa P2P Networks," 2019 20th Asia-Pacific Network Operations and Management Symposium (APNOMS), Sep. 2019, doi: 10.23919/apnoms.2019.8893034.

[13] Puput Dani Prasetyo Adi, Dwi Arman Prasetya, Rahman Arifuddin, Anggraini Puspita Sari, Fransiska Sisilia Mukti, Volvo Sihombing, "Application of IoT-LoRa Technology and Design in irrigation canals to improve the quality of agricultural products in Batu Indonesia," 2021 2nd International Conference On Smart Cities, Automation & Intelligent Computing Systems (ICON-SONICS), Oct. 2021, doi: 10.1109/icon-sonics53103.2021.9617175.

[14] T. Hirata, K. Terada, M. Toyota, Y. Takada, K. Matsumoto, and M. S. Tanaka, "Proposal of a power saving network for rice fields using LoRa," 2017 IEEE 6th Global Conference on Consumer Electronics (GCCE), Oct. 2017, doi: 10.1109/gcce.2017.8229298.

[15] A. Kurniawan, H. Al-Hakim, D. J. Rumala, and I. K. E. Purnama, "LORAPAI: LoRa Routing Protocol for an Agricultural Irrigation System," 2021 International Seminar on Intelligent Technology and Its Applications (ISITIA), Jul. 2021, doi: 10.1109/isitia52817.2021.9502198.

[16] Lu Li, Aduwati Sali, Jiun Terng Liew, Nur Luqman Saleh, Sharifah Mumtazah Syed Ahmad, Azizi Mohd Ali, "Estimation of Ground Water Level (GWL) for Tropical Peatland Forest Using Machine Learning," IEEE Access, vol. 10, pp. 126180–126187, 2022, doi:10.1109/access.2022.3225906.

[17] Sandhya. A. Kulkarni, V. D. Raikar, B. K. Rahul, L. V. Rakshitha, K. Sharanya, and V. Jha, "Intelligent Water Level Monitoring System Using IoT," 2020 IEEE International Symposium on Sustainable Energy, Signal Processing and Cyber Security (iSSSC), Dec. 2020, doi: 10.1109/isssc50941.2020.9358827.

[18] Md. N. Alam, A. Shufian, Md. A. A. Masum, and A. A. Noman, "Efficient Smart Water Management System Using IoT Technology," 2021 International Conference on Automation, Control and Mechatronics for Industry 4.0 (ACMI), Jul. 2021, doi: 10.1109/acmi53878.2021.9528202.

[19] J. Janani, A. Sanjeevi Gandhi, S. Aishwarya, and T. Porselvi, "Smart Water Monitoring with GSM Alerts: An IoT Approach," 2024 IEEE International Students' Conference on Electrical, Electronics and Computer Science (SCEECS), Feb. 2024, doi: 10.1109/sceecs61402.2024.10482084.

Environment. Technology. Resources. Rezekne, Latvia
Proceedings of the 16th International Scientific and Practical Conference. 2025. Volume IV, 217-223

Multi-objective Optimization of Cutting Parameters for CNC Turning 42CrMo4 Hardened Steel Using Utility Function

Hristo Metev
dept. Mechanical engineering and technology
Technical University of Gabrovo
Gabrovo, Bulgaria
hmetev@abv.bg

Irina Aleksandrova
dept. Mechanical engineering and technology
Technical University of Gabrovo
Gabrovo, Bulgaria
irina@tugab.bg

Nikolay Kolev
dept. Mechanical engineering and technology
Technical University of Gabrovo
Gabrovo, Bulgaria
nikikolev@abv.bg

***Abstract*—The optimum turning conditions for 42CrMo4 hardened steel, defined and recommended in the literature, are valid only for certain cutting tools and machine tools. In this paper, an attempt has been made to optimize the cutting parameters for CNC turning with robotic power supply of the machine tool by using a new type of CVD coated replaceable carbide insert as cutting tool. To determine the optimal cutting conditions such as cutting speed, feed and depth of cut, a multi-objective optimization, based on a genetic algorithm, was conducted. The generalized arithmetic mean utility function with weighting coefficients has been chosen as the optimization parameter, which is a complex index characterizing the cutting tool lifetime and production rate in turning. The optimization problem has been solved in the following sequence: 1) a model of the generalized utility function was created, reflecting the complex influence of the turning process parameters; 2) the optimal cutting conditions were determined, under which the generalized utility function has a maximum; 3) Pareto optimal solutions were found, which guarantee the best combination between tool lifetime and production rate in turning.**

Keywords*—multi-objective optimization, generalized utility function, CNC turning, 42CrMo4 hardened steel.

I. INTRODUCTION

Improvement of manufacturing processes for machining, including the turning process, is of paramount importance in modern mechanical engineering. Increasing the production rate of these processes, as well as the toollife of cutting tools and the quality of machined surfaces is guaranteed by the selection of optimal conditions for machining materials with different physical and mechanical properties, using modern optimization methods and algorithms [1], [2].

One of the most commonly used materials for the production of important parts with high strength and hardness (compressor parts, turbine parts, working elements of heavy ground and underground machinery, parts for agricultural machinery) on CNC lathes is the hardened medium-carbon low-alloy steel 42CrMo4+QT. The optimum conditions for its machining by turning as defined and recommended in technical literature are valid only for certain cutting tools and machine tools, as well as for a certain hardness of the machined material. Roughness of machined surfaces, cutting tool lifetime/tool wear, chip formation/chip breaking, production rate, cutting forces and cutting power were used as optimization parameters [3] – [10]. Their optimum values were obtained for different combinations of values of the control factors of the turning process (cutting speed, depth of cut, feed, cutting tool geometry). Both conventional (Taguchi method, Response surface design methodology, Iterative mathematical search technique - linear, non-linear, and dynamic programming techniques) and unconventional (heuristic search technique, metaheuristic search technique - Genetic algorithm (GA), Tabu search (TS), Simulated annealing (SA)) techniques have been used to define them.

The analysis of the results presented in Refs. [1], [2], [11] - [16] shows that the multi-objective optimization of turning process parameters offers a greater amount of information for making a reasoned decision for selecting optimal conditions, and the generalized utility function method is one of the most commonly used multi-objective optimization methods in industry. With this method, researcher can easily determine the optimal parameters in the group of solutions. The generalized utility function has many advantages over other combination methods mainly due to its flexibility, as it allows to simultaneously

Online ISSN 2256-070X
https://doi.org/10.17770/etr2025vol4.8413
© 2025 The Author(s). Published by RTU PRESS.
This is an open access article under the Creative Commons Attribution 4.0 International License.

maximize some of the output quantities and minimize others [1], [15], [16].

In spite of the large number of optimization studies of the turning process, there is no evidence in the literature for defined optimum conditions for machining hardened 42CrMo4 steel on a CNC turning machine with robotic power supply.

This paper presents the results of the multi-objective optimization based on the generalized utility function method of the CNC turning process parameters with robotic power supply of the machine tools, using a new type of CVD-coated replaceable carbide insert as the cutting tool. The optimum values of the cutting conditions (cutting speed, feed and depth of cut) were determined to ensure the best combination between tool life and production rate.

II. MATERIALS AND METHODS

The multi-objective optimization of the hard turning process for 42CrMo4 steel (Table 1 [17]) boils down to determining cutting conditions - cutting speed V_c^* (m/min), feed f^*(mm/rev) and depth of cut a_p^* (mm), that provide a combination between maximum cutting tool lifetime and maximum production rate of process. To solve the optimization problem, the generalized arithmetic mean utility function with weighting coefficients Φ_A is chosen as the optimization parameter. It is a complex indicator determining the turning process parameters - tool lifetime and production rate in turning.

Cutting tool lifetime is determined by the distance L (mm) travelled by the tool on the machined surface, determined when machining a certain number of workpieces in a particular cutting conditions until a technological wear criterion is reached – roughness Ra_k = 2.0 μm. The roughness of the machined surface is measured with a TESA Rugosurf 20 profilometer in accordance with ISO3274, class 1. The production rate of the turning process is evaluated by the machining time t (min), including the main and auxiliary time, to travel the path L in a specific conditions of cutting (defined in the ESPRIT CAM environment).

To determine the tool lifetime and process production rate in turning hardened 42CrMo4 steel depending on the cutting conditions, experimental investigation were conducted on a HARRIS C400 CNC lathe with a Mitsubishi robopro DR800 robotic power supply (Fig. 1). The robotic station provides a repeatability of positioning of ±0,02 mm and an auxiliary time of locating for each workpiece of 23.37 s. A 6% solution of Fuchs Ecocool Mach 300 was used as lubricating coolant.

The machined workpieces have the shape and dimensions shown in Fig. 2.

Processing is carried out with a new type of CVD-coated (TiCN+Al2O3+TiCN+TiN) carbide insert from Iscar with the designation CXMG 12T508-M3P IC8150 [18], fixed onto a tool holder, type PCLXL 2525-12M. Combination of the cutting insert with the tool holder resulted in tool major cutting edge angle $\kappa_r = 95°$, tool minor cutting edge angle $\kappa_r' = 5°$, tool orthogonal rake angle $\gamma_0 = -6°$, tool orthogonal clearance angle $\alpha_0 = 6$ and nose radius 0.8 mm.

The optimization problem is solved in the following sequence:

1) Theoretical and experimental models are constructed for the generalized arithmetic mean utility function with weighting coefficients depending on the control factors of the turning process ($X_1 = V_c$ (m/min) - cutting speed; $X_2 = f$ (mm/rev) - feed; $X_3 = a_p$ (mm) – depth of cut), the general form of which is:

$$\Phi_{Ah} = A_0 + \sum_{i=1}^{n} A_i X_i + \sum_{i=1}^{n} A_{ii} X_i^2 + \sum\sum_{i<j} A_{ij} X_i X_j \ . \quad (1)$$

The models are built based on multifactor experiments to investigate the influence of control factors on the generalized utility function, conducted according to an orthogonal central compositional plan with number of trials $N = 2^n + 2n + 1 = 9$ ($n = 3$ is the number of control factors). The levels of variation of the control factors are presented in Table 2.

TABLE 1 CHEMICAL COMPOSITION AND PHYSICO-MECHANICAL PROPERTIES OF 42CRMO4 STEEL

Chemical composition (Wt%)							
C	***Si***	***Mn***	***Ni***	***Cr***	***Mo***	***P***	***Cu***
0.405	0.239	0.652	0.110	0.894	0.180	0.012	0.227
Hardness – HRC 34.3; Yield strength point $f_y \geq 850$ MPa							

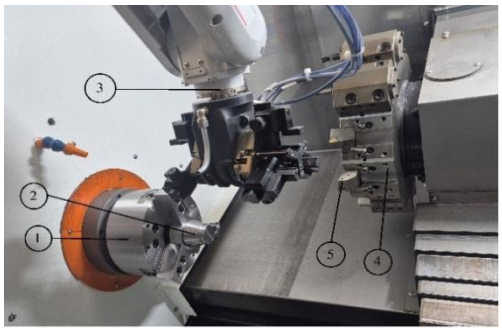

Fig. 1. Workspace of a HARRIS C400 CNC lathe with robotic power supply (1 – chuck; 2- workpiece; 3 - station for robotic power supply Mitsubishi robopro DR800; 4 – turret head; 5 – cutting tool)

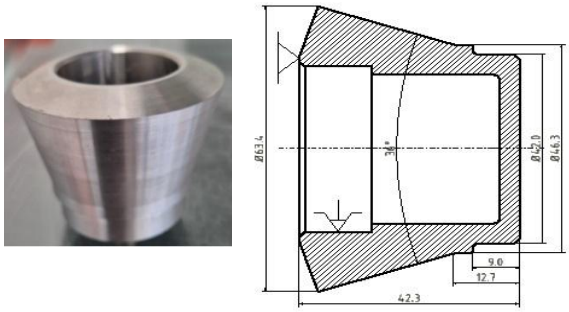

Fig. 2. Machined workpiece

The generalized arithmetic mean utility function with weighting coefficients is determined upon each trial according to the relationship:

$$\Phi_{Ah} = \eta_1 . w_1 + \eta_2 w_2, \qquad (2)$$

where: w_1 and w_2 - weighting coefficients for the parameters cutting tool lifetime and turning process production rate, respectively; η_1 and η_2 - utility coefficients.

The values of the weighting coefficients are respectively: for Φ_{A1} - $w_1 = 0.2$; $w_2 = 0.8$; for Φ_{A2} - $w_1 = 0.8$; $w_2 = 0.2$. In the first case, a higher production rate of the turning process is ensured, and in the second - a greater tool lifetime of the cutting tool.

The utility coefficients η_1 and η_2 are given by the relationships:

$$\eta_1 = \frac{L - L_u}{L_g - L_l} k_L; \qquad \eta_2 = \frac{t - t_u}{t_g - t_l} k_t, \qquad (3)$$

where: $L_g = L_{max}$ and $L_l = L_{min}$ - utility limits of the tool lifetime parameter; $t_g = t_{max}$ and $t_l = t_{min}$ - utility limits of the production rate parameter; $L_u = L_{min}$ and $t_u = t_{max}$ - the most useless results of the investigated tool lifetime and production rate parameters obtained within the factor space; $k_L = +1$; $k_t = -1$ - coefficients accounting for the utility of the increase in the parameter under investigation.

2) The combinations of values of the control factors ($X_1^* = V_c^*, X_2^* = f^*, X_3^* = a_p^*$) in the studied factor space are determined, for which the generalized arithmetic mean utility functions with weighting coefficients Φ_{Ah} have maximum value:

$$\Phi_{Ah}(X_1^*, X_2^*, X_3^*) = (\Phi_{Ah})_{\max} > \Phi_{Ah}(X_1, X_2, X_3)\ . \qquad (4)$$

3) Pareto-optimal solutions are determined that guarantee the best combination between maximum tool lifetime and maximum production rate when turning hardened 42CrMo4 steel on a CNC lathe with robotic power supply.

TABLE 2 FACTOR LEVELS IN THE EXPERIMENTAL DESIGN

Factors		Factor levels		
		-1	0	+1
X_1	V_c (m/min)	180	230	280
X_2	a_p (mm)	2.0	2.5	3.0
X_3	f (mm/rev	0.15	0.2	0.25

III. RESULTS AND DISCUSSION

A. Modelling of Generalized Utility Function

The design of the experiment with the values of the generalized arithmetic mean utility functions with weighting coefficients Φ_{A1} and Φ_{A2} determined according to relation (2), as well as the investigated turning process parameters (path L from the tool along the machined surface to reach roughness $Ra_k = 2.0$ μm and machining time t) are presented in Table 3. In specifying utility functions Φ_{A1} and Φ_{A2}, the values of the most useless result and the utility limits of the turning process parameters are: for tool lifetime - $L_u = 42\,237$ mm; $L_g = 67\,742$ mm; $L_l = 42\,237$ mm; for machining time - $t_u = 427.92$ min; $t_g = 427.92$ min; $t_l = 102.9$ min.

After statistical analysis of the experimental results by applying the regression analysis method and QstatLab software [19], theoretical and experimental models for the generalized arithmetic mean utility functions Φ_{A1} and Φ_{A2} were constructed (Table 4).

The models include only the significant regression coefficients determined according to the condition $\hat{t} > t_{\alpha/2,\nu}$, where $\hat{t}$ and $t_{\alpha/2,\nu}$ are the calculated values of the Student's t-criterion for each of the regression coefficients and the tabular value of the Student's t-criterion, respectively (α=0.05 is the significance level; $\nu = N - k$ is the number of degrees of freedom; k is the number of coefficients in the model).

Regression models are adequate because the condition $\hat{F} > F_{\alpha,\nu_1,\nu_2}$ is met with a 95% confidence probability. The calculated $\hat{F}$ and tabular F_{α,ν_1,ν_2} values of the Fisher criterion (α=0,05; $\nu_1 = k - 1$ and $\nu_2 = N - k$ are degrees of freedom) for each of the regression models are presented in Table 4. Theoretical and experimental models describe with high accuracy the dependencies between generalized utility functions Φ_{A1} and Φ_{A2} and the control factors. The values of the determination coefficients are $\hat{R}^2 = 0.971 - 0.988$ (Table 4).

The influence of cutting conditions on the generalized utility functions Φ_{A1} and Φ_{A2} is presented graphically in Fig. 3. To determine the degree of impact of the control factors on Φ_{A1} and Φ_{A2}, Analysis of Variance (ANOVA) was carried out using QStatLab (version 6.1.1.3) [19]. The ANOVA interaction plots for the generalized utility functions are shown in Fig. 5.

TABLE 3 DESIGN OF THE EXPERIMENT AND GENERALIZED UTILITY FUNCTIONS

Control factors			CNC turning parameters		Utility coefficients		Generalized utility function	
x_1	x_2	x_3	L (mm)	t (min)	η_1	η_2	Φ_{A1}	Φ_{A2}
-1	-1	-1	67 742	427.92	1	0	0.2	0.8
1	-1	-1	65 170	266	0.899	0.498	0.578	0.819
-1	1	-1	47 547	295.17	0.208	0.408	0.368	0.248
1	1	-1	46 312	187.5	0.160	0.74	0.624	0.276
-1	-1	1	61 740	234	0.765	0.597	0.631	0.731
1	-1	1	61 225	148.75	0.744	0.859	0.836	0.767
-1	1	1	42 237	159.6	0	0.826	0.661	0.165
1	1	1	42 360	102.9	0.005	1	0.801	0.204
-1	0	0	52 170	246.67	0.389	0.558	0.524	0.423
1	0	0	51 465	158.17	0.362	0.83	0.736	0.456
0	-1	0	63 455	234.33	0.832	0.596	0.643	0.785
0	1	0	45 077	164.25	0.111	0.811	0.671	0.251
0	0	-1	53 439	265.3	0.265	0.500	0.453	0.312
0	0	1	50 055	147.92	0.307	0.861	0.750	0.418
0	0	0	51 888	190.13	0.378	0.732	0.661	0.449

TABLE 4 THEORETICAL AND EXPERIMENTAL MODELS OF THE GENERALIZED UTILITY FUNCTION AND STATISTICAL CHARACTERISTICS OF THE MODELS

Models	Fisher criterion		$\widehat{R}^2$
	$\widehat{F}$	F_{α,ν_1,ν_2}	
$\Phi_{A1} = -3.2604 + 0.0076.V_c + 0.4815.a_p + 18.061.f - 22.72.f^2 - 0.001.V_c.a_p - 1.095.a_p.f - 0.0145.V_c.f$	163.975	3.787	0.988
$\Phi_{A2} = 3.8723 + 0.0003.V_c + 2.7545.a_p + 6.5171.f + 0.4406.a_p^2 - 17.1429.f^2$	94.011	3.482	0.971

Both analysis of the theoretical and experimental models (Table 4) and the graphics plotted on the basis of them (Fig. 3), as well as the interpretation of ANOVA results (Fig. 4), allow us to draw the following conclusions:

a) The greatest influence on the generalized arithmetic mean utility function Φ_{A1} is caused by the depth of cut, as its increase increases the value of Φ_{A1} from 1.8 to 3 times. The effect of the depth of cut increases when the feed and cutting speed decrease. Speed of cutting also has a significant influence on Φ_{A1}, the increase of which in the studied range leads to an increase in the value of Φ_{A1} up to 2.7 times.

b) The greatest influence on the generalized arithmetic mean utility function Φ_{A2} is exerted by the feed, as its increase increases the value of Φ_{A2} from 3.2 to 3.9 times. The influence of feed increases with increasing the depth of cut and decreasing the cutting speed.

These conclusions show that the cutting conditions have a different impact on the generalized arithmetic mean utility function, which depends on the way it is determined and is related to the different influence of cutting speed, feed and depth of cut on the cutting tool lifetime, defined by the path L (mm), and the turning production rate, estimated by the time t (min). The results of the study conducted by the authors show that the depth of cut has the greatest impact on machining time, and the feed has the greatest influence on the cutting tool lifetime.

B. Definition of Optimum Turning Conditions

The optimization problem for turning 42CrMo4 steel on a CNC lathe with robotic power supply was solved by applying a genetic algorithm and using the QStatLab software product. Optimal cutting conditions (cutting speed V_c^*, feed f^* and depth of cut a_p^*) are those at which the generalized arithmetic mean utility functions Φ_{A1} and Φ_{A2} have a maximum (Table 5).

The determined Pareto-optimal solutions guarantee the best combination of tool lifetime and production rate when turning hardened 42CrMo4 steel on a CNC lathe with robotic power supply. Cutting conditions (V_c^*, a_p^* и f^*) at which the generalized arithmetic mean utility function Φ_{A1} has a maximum, provide higher production rate of the turning process, and those at which the generalized arithmetic mean utility function Φ_{A2} has a maximum - higher lifetime of the cutting tool. Values of the tool path L, determined by way of experimentation as a parameter for assessing its lifetime, and of the machining time t are presented in Table 5.

IV. CONCLUSIONS

In this paper, a new approach for the optimization of the turning process is proposed, which takes into account the specificity of its particular application in the machining of 42CrMo4 steel on a CNC turning machine with robotic power supply, using a cutting tool with a new type of replaceable carbide insert with CVD coating. As an optimization parameter, the generalized mean-arithmetic utility function with weighting coefficients is chosen, being a complex index characterizing the tool lifetime and process production rate.

TABLE 5 OPTIMUM TURNING CONDITIONS

Optimal conditions			CNC turning parameters		Generalized utility function	
V_c^* m/min	a_p^* mm	f^* mm/rev	L mm	t min	Φ_{A1}	Φ_{A2}
280	2.0	0.25	61 543.58	145,96	0.846	-
280	2.0	0.19	63 742.49	200,16	-	0.832

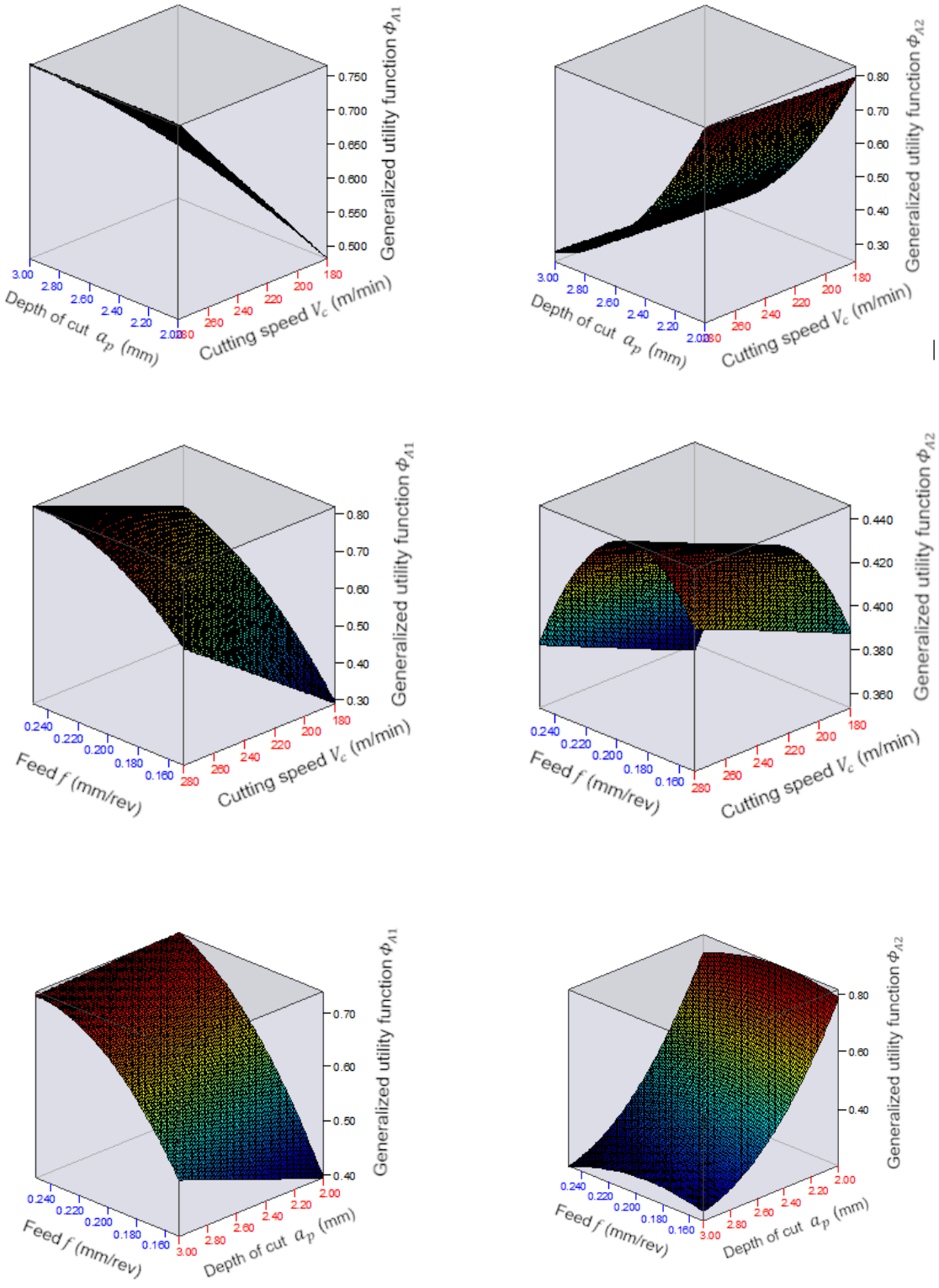

a) b)

Online ISSN 2256-070X
https://doi.org/10.17770/etr2025vol4.8413
© 2025 The Author(s). Published by RTU PRESS.
This is an open access article under the Creative Commons Attribution 4.0 International License.

Fig. 3. Graphical visualization of the generalized utility function models for CNC turning: (a) arithmetic mean generalized utility function Φ_{A1} with weighting coefficients $w_1 = 0.2$; $w_2 = 0.8$; (b) arithmetic mean generalized utility function Φ_{A2} with weighting coefficients $w_1 = 0.8$; $w_2 = 0.2$.

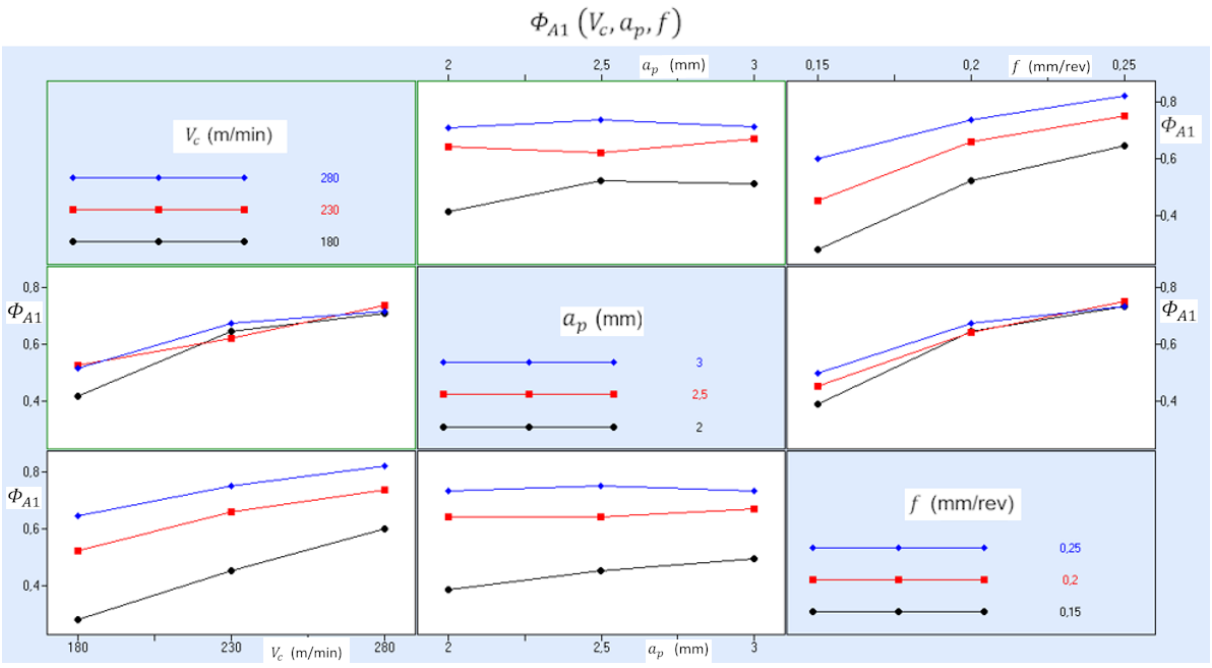

a)

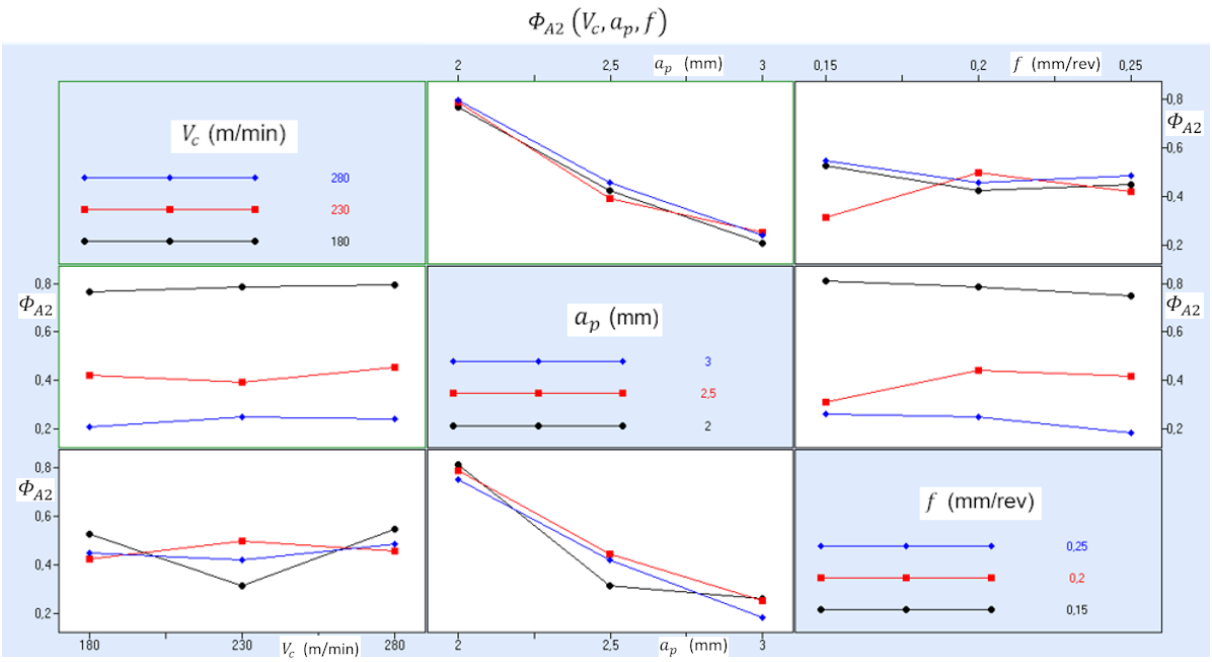

b)

Fig. 4. Interaction plots for the generalized utility function models for CNC turning: (a) arithmetic mean generalized utility function Φ_{A1} with weighting coefficients $w_1 = 0.2$; $w_2 = 0.8$; (b) arithmetic mean generalized utility function Φ_{A2} with weighting coefficients $w_1 = 0.8$; $w_2 = 0.2$.

The following results were obtained:

(1) Theoretical and experimental models have been constructed to determine the generalized utility function, reflecting the complex influence of the control factors of the turning process (cutting speed, cutting depth and feed). Said models are based on the

results of comprehensive investigated of cutting tool lifetime, determined by the path L (mm), and turning production rate, estimated by the time t (min) depending on the cutting conditions.99

(2) By applying the generalized arithmetic mean utility function with weighting coefficients and a genetic algorithm, Pareto-optimal conditions for turning (cutting speed, cutting depth and feed) of hardened steel 42CrMo4 have been determined (Table 5). They provide the best combination of process production rate and cutting tool lifetime compared to the optimum conditions for machining hardened 42CrMo4 steel defined in [3]-[10] .

(3) . The production rate and tool lifetime of machining with the specified optimum cutting conditions (Table 5) with the new type of inserts are comparable to those of machining with CBN inserts [10], with tooling costs approximately three times less.

The results obtained by applying the new optimization approach allow an increasing of the efficiency and control of the turning process of 42CrMo4 steel. They can be used in all machine-building companies for processing parts with high strength and hardness (compressor parts, turbine parts, drive shafts, pump shafts, lathe spindles, working elements of heavy ground and underground machinery, parts for agricultural machinery etc.) from hardened 42CrMo4+QT steel on CNC lathes with robotic power supply. The new type of Iscar CXMG 12T508-M3P IC8150 replaceable carbide inserts used provide high tool lifetime and production rate related to their resistance to cracks, crater wear and flank wear well as adhesion to the substrate.

V. Acknowledgments

This research was funded by the European Regional Development Fund within the OP "Research, Innovation and Digitalization Programme for Intelligent Transformation 2021-2027", Project CoC "Smart Mechatronics, Eco- and Energy Saving Systems and Technologies", No BG16RFPR002-1.014-0005.

References

[1] L Mukherjee and P. K. Ray, "A review of optimization techniques in metal cutting processes." Computers&Industrial Engineering, vol. 50(1-2), pp. 15-34, 2006, https:// doi.org/10.1016/j.cie.2005.10.001

[2] X. Wang, Z. J. Da, A. K. Balaji ,and I. S. Jawahir, "Performance-Based Predictive Models and Optimization Methods for Turning Operations and Applications: Part 3 - Optimum Cutting Conditions and Selection of Cutting Tools." Journal of Manufacturing Processes, vol. 9(1), pp. 61-74, 2007, https://doi.org/10.1016/S1526-6125(07)70108-1.

[3] E. Aslan, N. Camuscu, and B. Bingoren, "Design optimization of cutting parameters when turning hardened AISI 4140 (63 HRC) with Al2O3 + TiCN mixed ceramic tool." Materials & Design, vol. 28, pp. 1618-1622, 2007, https://doi:10.1016/j.matdes.2006.02.006.

[4] H. Akkuş, "Experimental and Statistical Investigation of Ra in Turning of AISI 4140." Sakarya University Journal of Science, vol. 23(5), pp. 775-781, 2019, https://doi.org/10.16984/saufenbilder.490668.

[5] S. R. Das, D. Dhupal, and A. Kumar, "Study of surface roughness and flank wear in hard turning of AISI 4140 steel with coated ceramic inserts." J Mech Sci Technol, vol. 29, pp. 4329–4340, 2015, https://doi.org/10.1007/s12206-015-0931-2.

[6] A.R Motorcu, Y. Isik, A. Kus, and M.C. Cakir, "Analysis of the cutting temperature and surface roughness during the orthogonal machining of AISI 4140 alloy steel via the taguchi method." Materiali in Tehnologije, vol. 50(3), pp. 343-351, 2016.

[7] G. Sharan and R. K. Patel, "Optimization of cutting parameters of turning for hardness of AISI 4140 alloy steel." in ICMPC-2019, Materials Today: Proceedings, vol. 18, pp. 3582–3589, 2019.

[8] B. Hamadi, M.A. Yallese, L. Boulanouar, A Hammoudi, and M. Nouioua. "Evaluation of the cutting performance of PVD, CVD and MTCVD carbide inserts in dry turning of AISI 4140 steel using RSM-based NAMDE optimization." J Braz. Soc. Mech. Sci. Eng. vol. 44, pp. 342+, 2022. https://doi.org/10.1007/s40430-022-03633-5.

[9] Padhan, N.K.Wagri. L. Dash, A. Das, S.R. Das, M. Rafighi, and P. Sharma, "Investigation on Surface Integrity in Hard Turning of AISI 4140 Steel with SPPP-AlTiSiN Coated Carbide Insert under Nano-MQL." Lubricants, vol. 49(11), 2023, https://doi.org/10.3390/lubricants11020049.

[10] I. Meddour, M.A. Yallese, H. Bensouilah, A. Khellaf and M. Elbah, "Prediction of surface roughness and cutting forces using RSM, ANN, and NSGA-II in finish turning of AISI 4140 hardened steel with mixed ceramic tool." Int J Adv Manuf Technol, vol. 97, pp. 1931–1949, (2018), https://doi.org/10.1007/s00170-018-2026-6.

[11] V. S. Konnur, S. S. Kulkarni, S. V. Hiremath, V.S. Kanal, and V.C Nirale, "Analysis of CNC turning parameters and simultaneous optimisation of surface roughness and material removal rate by MOGA for AISI 4340 alloy steel." Advances in Materials and Processing Technologies, 12 Nov 2023, https://doi.org/10.1080/2374068X.2023.2280293.

[12] O. Manav, S. Chinchanikar, and M. Gadge, "Multi-performance optimization in hard turning of AISI 4340 Steel using Swarm Optimization technique", in IConAMMA_2017, Materials Today: Proceedings, vol. 5, pp. 24652–24663, 2018.

[13] R. Q. Sardiñas, M. R. Santana, and E. A. Brindis, "Genetic algorithm-based multi-objective optimization of cutting parameters in turning processes." Particle Engineering Applications of Artificial Intelligence, vol. 19(2), pp. 127-133, 2006, https://doi.org/10.1016/j.engappai.2005.06.007.

[14] S. Chinchanikar and S. K. Choudhury, "Effect of work material hardness and cutting parameters on performance of coated carbide tool when turning hardened steel: An optimization approach." Measurement, vol. 46, pp. 1572-1584, 2013, https://doi.org/10.1016/j.measurement. 2012.11.032.

[15] A. Aleksandrov and I. Aleksandrova, Theory of Experiment, Gabrovo, Bulgaria: Experess, 2012.

[16] S. Kumari, D. Bandhu, A. Kumar, R. K. Yadav, K. Vivekananda, "Application of Utility Function Approach Aggregated with Imperialist Competitive Algorithm for Optimization of Turning Parameters of AISI D2 Steel.“ in Lecture Notes in Intelligent Transportation and Infrastructure, Recent Advances in Mechanical Infrastructure, A. Parwani, P. Ramkumar, Eds. Singapore: Springer, 2020, https://doi.org/10.1007/978-981-32-9971-9_6.

[17] "Overview of 42CrMo4 Steel: Properties and Applications." [Online]. Available: https://ambhe.com/42crmo4-steel/. [Accessed: Feb. 16, 2025].

[18] "ISCAR Cutting Tools - Metal Working Tools." [Online]. Available: https://www.iscar.bg/index.aspx/countryid/38/lang/bg. [Accessed: Feb. 16, 2025].

I. N. Vuchkov and I. I. Vuchkov, Statistical methods of quality control, robust engineering, planning, modeling and optimization, QStatLab, v 5.3, 2009.

Environment. Technology. Resources. Rezekne, Latvia
Proceedings of the 16th International Scientific and Practical Conference. 2025. Volume IV, 225-233

Investigation of the Machinability of 42CrMo4+QT Steel in Tool Turning with Carbide Inserts on CNC Machines with Robotic Power Supply

Hristo Metev
dept. Mechanical engineering and technology
Technical University of Gabrovo
Gabrovo, Bulgaria
hmetev@abv.bg

Irina Aleksandrova
dept. Mechanical engineering and technology
Technical University of Gabrovo
Gabrovo, Bulgaria
irina@tugab.bg

Nikolay Kolev
dept. Mechanical engineering and technology
Technical University of Gabrovo
Gabrovo, Bulgaria
hnikipkolev@abv.bg

***Abstract*—The optimum machining conditions recommended in the literature for one of the most commonly used materials for responsible heavy-duty workpieces in mechanical engineering, 42CrMo4+QT steel, are valid only for certain cutting tools and machine tools. This paper presents the results of an investigation of the machinability of this type of steel on the criteria of cutting tool lifetime and roughness of machined surfaces in turning on CNC machines with robotic power supply. A planned experiment has been carried out as a result of which theoretical and experimental models have been obtained and graphical dependencies, reflecting the influence of cutting speed and feed when working with replaceable carbide inserts from different manufacturers have been constructed. The dependencies allow to predict with sufficient accuracy the tool lifetime of the studied inserts and the roughness of the machined surfaces using cutting conditions in a certain range. The analysis carried out shows that the machinability of 42CrMo4+QT steel depends on the elements of the cutting conditions, with the widest variation in the values of the cutting tool lifetime criterion. The cutting speed has a stronger influence on this criterion. The optimum cutting conditions that guarantee maximum tool lifetimes of the studied inserts and minimum roughness of the machined surfaces ware determined.**

***Keywords*— machinability, modeling tool lifetime, roughness..**

I. Introduction

Steel 42CrMo4+QT is a hardened version of steel 42CrMo4, in which the content of chromium and molybdenum as the main alloying elements contributes to its high strength, durability and wear resistance. This makes it particularly suitable for the manufacture of parts in mechanical engineering, operating in conditions requiring high strength and hardness, such as parts of compressors, turbines, working elements of heavy ground and underground equipment, parts for agricultural machinery, etc. [1], [2]. The optimal conditions for its processing specified and recommended in the literature are valid only for certain cutting tools and metal-cutting machines [3] - [4]. Till now, there is no information on the machinability of this type of steel, using cutting tools with carbide indexable inserts on CNC lathes with robotic power supply.

The aim of the present work is to investigate the influence of cutting speed and feed on the machinability of 42CrMo4+QT steel according to the criteria of cutting tool lifetime and roughness of the machined surfaces when machining with replaceable carbide inserts from different manufacturers on CNC turning machines with robotic power supply, to obtain relevant theoretical and experimental models and to determine the optimal cutting conditions.

II. Materials And Methods

To investigate and model the effect of cutting condition elements on the tool lifetime of carbide inserts and the roughness of the machined surfaces when machining 42CrMoS4-QT steel on CNC lathes with a robotic power supply, a two-factor optimal design experiment was conducted, using an orthogonal central composition design. The number of trails is:

Online ISSN 2256-070X
https://doi.org/10.17770/etr2025vol4.8414
© 2025 The Author(s). Published by RTU PRESS.
This is an open access article under the Creative Commons Attribution 4.0 International License.

$$N = 2^2 + 2.2 + 1 \quad (1)$$

The feed f (mm/rev) and the cutting speed Vc (m/min) were selected as the control factors. The cutting depth was a_p = 1.5 mm.

The machined worpiece (Fig. 1), made of steel 42CrMo4+QT, have hardness HRC=33.8, yield strength point $f_y \geq$ 850 MPa and chemical composition presented in Table 1.

The experiments were conducted on a HARRIS C400 CNC lathe with a FANUC BOXI Raptor Auto Loader robotic feeding station (Fig. 2). Zet Chemie ZET-cut 6040 GTL was used as the coolant.

Replaceable carbide inserts from various manufacturers were used as cutting tools [11] - [13]. The carbide inserts have coatings (Table 2) ensuring high wear resistance.

The inserts were set in a quick-change type toolholder, providing the following geometrical parameters: tool major cutting edge angle $\kappa_r = 95°$, tool minor cutting edge angle $\kappa_r' = 5°$, tool orthogonal rake angle $\gamma_0 = -6°$, tool orthogonal clearance $\alpha_0 = 7°$, nose radius $r_\varepsilon = 0.4$ mm.

TABLE 1 CHEMICAL COMPOSITION OF 42CRMO4 +QT STEEL

Chemical composition (Wt%)							
C	***Si***	***Mn***	***Ni***	***Cr***	***Mo***	***P***	***Cu***
0.405	0.239	0.652	0.110	0.894	0.180	0.012	0.227

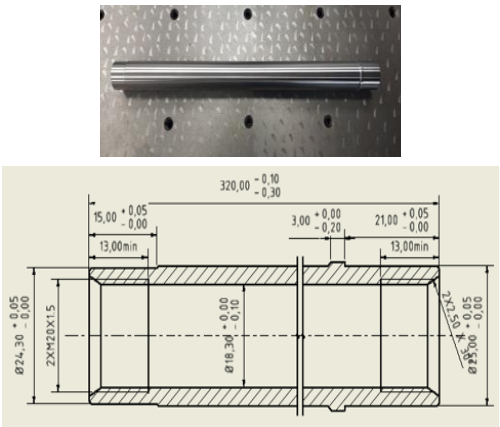

Fig. 1 Machined workpiece

In order to study the tool lifetime and roughness, single-factor experiments were conducted to determine the effect of the number of machined workpieces on roughness at given values of cutting speed and feed (Fig. 3) [14].

Tool lifetime was defined as the number of workpieces machined in a specific cutting conditions, with the roughness of the machined surface Ra=3,0 μm as the wear criterion.

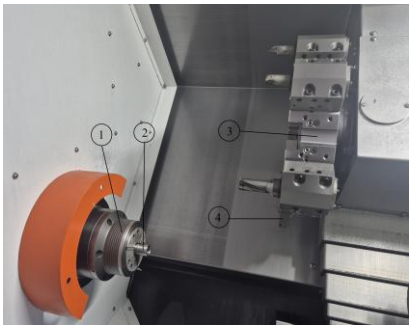

Fig. 2 Workspace of a HARRIS C400 CNC lathe with robotic power supply (1 – chuck; 2 - workpiece; 3 – turret head; 4 – cutting tool)

TABLE 2 CARBIDE REPLACEABLE INSERTS

Insert (ISO 13399)	Manufacturer	Coated
CCMT09T304-F1 TP2501	SECO	CVD: TiN+ Al_2O_3
CCMT09T304-MP	PALBIT	CVD TiN+Al_2O_3+TiCN
CCMT09T304-F3M IC807	ISCAR	PVD: TiAlN+TiN

The roughness was determined for a number of machined workpieces n=50 and a specific cutting conditions and was measured with a TESA Rugosurf 20 profilometer.

Based on preliminary information, a type of model has been adopted:

$$Y_{hp} = B_0 + \sum B_i X_i + \sum B_{ii} X_i^2 + B_{12} X_1 X_2 \quad (2)$$

where: $Y_{1p} = T_p$ – tool lifetime; $Y_{2p} = Ra_p$ - roughness of the machined surfaces; $p = 1, 2, 3$ - number corresponding to the type of insert (Table 2); X_1 = f (mm/rev); X_2= V_c (m/min).

The levels of variation of the control factors are presented in Table 3.

III. RESULTS AND DISCUSSION

The experimental design and experimental data are shown in Table 4.

The processing of the experimental results was carried out in accordance with the methodology set out in [15], in the sequence:

- determining the coefficients of the model;

- significance check of the regression coefficients by Student's t- test at significance level α=0.05;

- calculation of the determination coefficient $\hat{R}^2$;

- significance testing of the multiple coefficient by Fisher's criterion at the significance level α=0.05.

The research results were processed with the software product QstatLab [16], and the resulting models are shown in Table 5.

TABLE 3 LEVELS OF CONTROL FACTORS

Control factors		Factor levels		
Coded	***Natural***	***-1***	***0***	***+1***
x_1	f (mm/rev)	0.12	0.15	0.18
x_2	Vc (m/min)	130	150	170

The models describe with sufficient accuracy the relationship between tool lifetime and roughness and the cutting conditions elements Vc and f. The values of the coefficient of determination $\hat{R}^2$ and the tabulated F^T and calculated $\hat{F}$ value of the Fisher criterion are presented in Table 5. Table 4 presents the determined values of the tool lifetime $\hat{T}_p$ and roughness $\hat{Ra}_p$ of the machined surface in accordance with the constructed theoretical and experimental models (Table 5).

The graphical interpretation of the determined models is shown in Fig. 4.

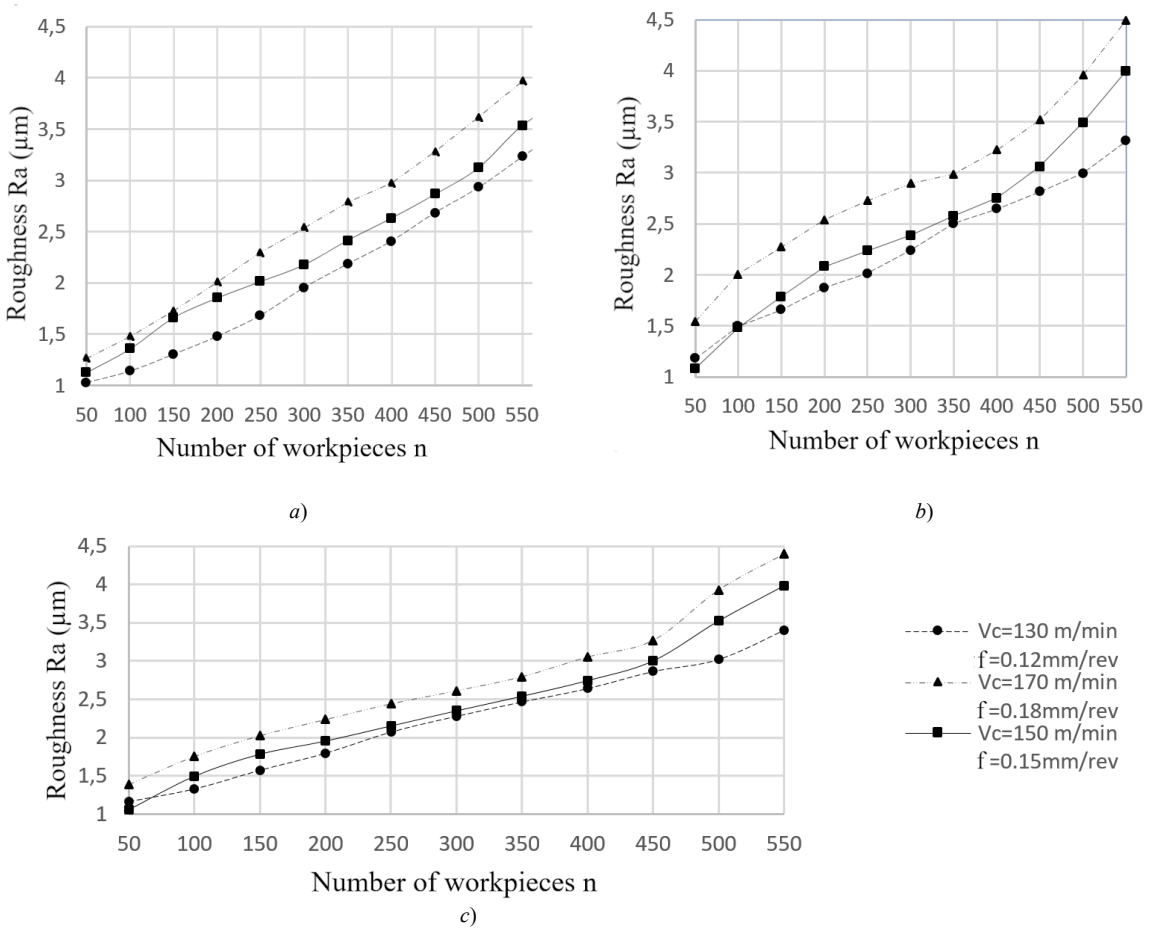

Fig. 3 Variation of roughness depending on the number of machined workpieces in turning with replaceable carbide inserts: *a* - CCMT09T304-F1 TP2501 of a company SECO; *b* - CCMT09T304-MP of a company PALBIT; *c* - CCMT09T304-F3M IC807 of a company ISCAR.

TABLE 4. EXPERIMENTAL DESIGN AND EXPERIMENTAL DATA

No	Cutting conditions		Tool lifetime (number of workpieces)						Roughness, µm					
	f *(mm/rev)*	V_c *(m/min)*	T_1	$\hat{T}_1$	T_2	$\hat{T}_2$	T_3	$\hat{T}_3$	Ra_1	$\hat{Ra}_1$	Ra_2	$\hat{Ra}_2$	Ra_3	$\hat{Ra}_3$
1	0.12	130	510	512	500	501	490	490	1.028	1.032	1.179	1.166	1.168	1.159
2	0.18	130	490	491	475	476	475	474	1.039	1.059	1.254	1.268	1.235	1.230
3	0.12	170	425	426	400	401	420	420	1.176	1.153	1.183	1.174	1.189	1.184
4	0.18	170	405	404	355	356	390	390	1.264	1.241	1.543	1.561	1.389	1.388
5	0.12	150	480	479	455	456	465	463	1.057	1.092	1.087	1.109	1.109	1.122

6	0.18	150	455	457	420	421	440	440	1.132	1.150	1.387	1.354	1.253	1.259
7	0.15	130	505	502	490	488	480	482	1.095	1.046	1.085	1.083	1.032	1.046
8	0.15	170	415	415	380	378	405	405	1.172	1.197	1.243	1.234	1.131	1.137
9	0.15	150	470	468	440	438	450	452	1.127	1.121	1.087	1.098	1.062	1.042

TABLE 5. THEORETICAL AND EXPERIMENTAL MODELS AND STATISTICAL ANALYSIS

Insert	**Theoretical and experimental models**	**Fisher criterion**		$\widehat{R}^2$
		$\widehat{F}$	F^T	
CCMT09T304-F1 TP2501	$T_1 = 285 - 361.111.f + 5.333.V_c - 0.025.V_c^2$	695.476	5.409	0.99617
	$Ra_1 = 0.976 - 2.8109.f + 0,02518.f.V_c$	19.553	5.143	0.82264
CCMT09T304-MP	$T_2 = 469.583 + 666.667.f + 2,25.V_c - 0.0125.V_c^2 - 8.333.f.V_c$	1611.0	6.388	0.99876
	$Ra_2 = 9,3611 - 58,340f - 0,0597V_c + 148,704f^2 + 0,00015.V_c^2 + 0,119f.V_c$	43.696	9.013	0.96388
CCMT09T304-F3M IC807	$T_3 = 188.125 + 548.611.f + 5.271.V_c - 0.0208.V_c^2 - 6.25.f.V_c$	943.533	6.388	0.99788
	$Ra_3 = 8.099 - 55.64.f - 0.043.V_c + 165.37.f^2 + 0.00012.V_c^2 + 0.0554.f.V_c$	58.253	9.013	0.97281

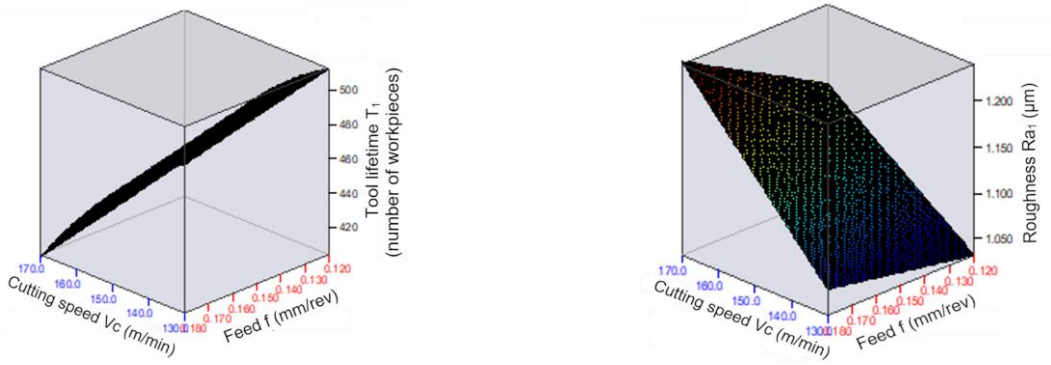

a)

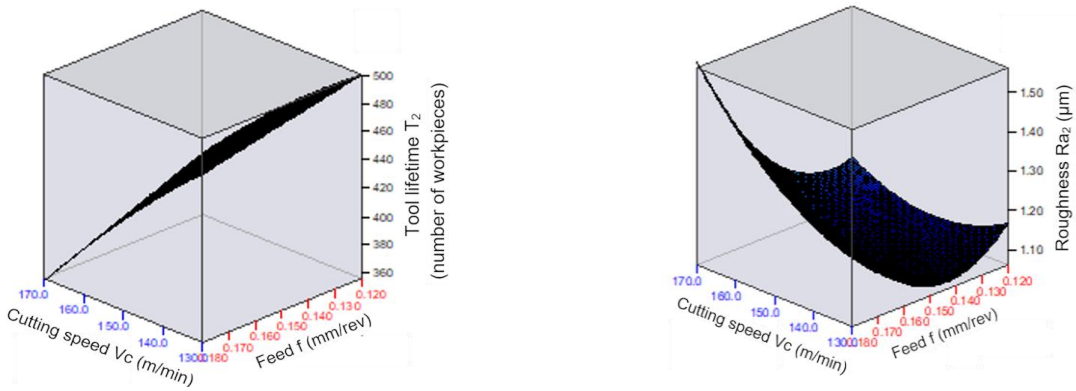

b)

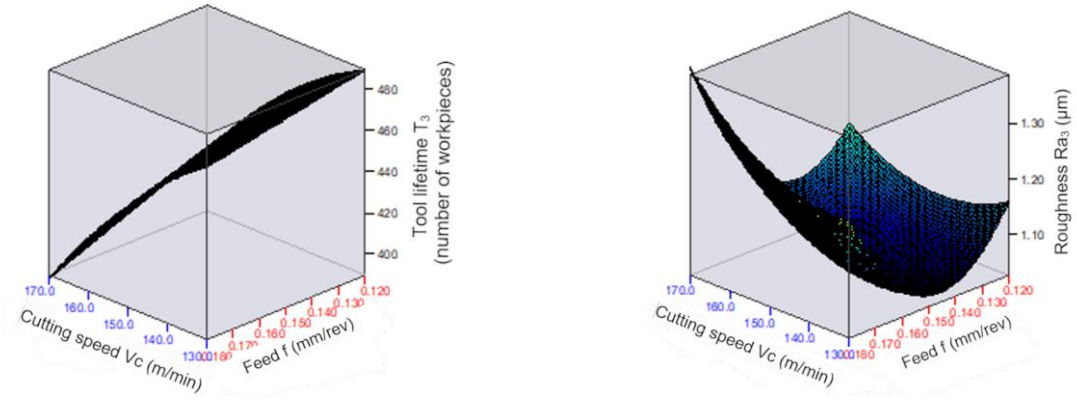

c)

Fig. 4 Graphical dependences of the tool lifetime of the inserts and the roughness of the machined surfaces depending on the feed f (mm/rev) and cutting speed Vc (m/min) (*a* - CCMT09T304-F1 TP2501 of a company SECO; *b* - CCMT09T304-MP of a company PALBIT; *c* - CCMT09T304-F3M IC807 of a company ISCAR)

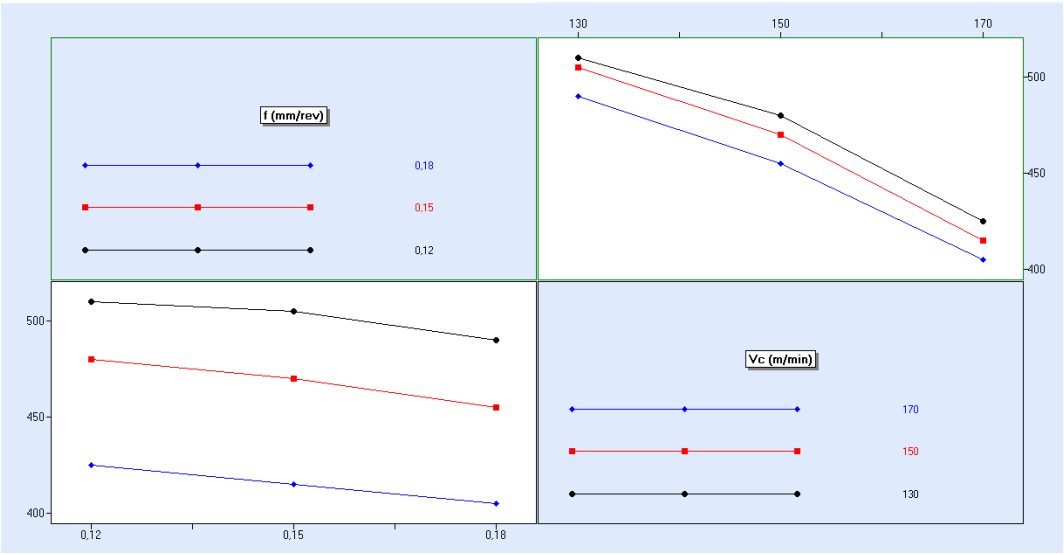

a)

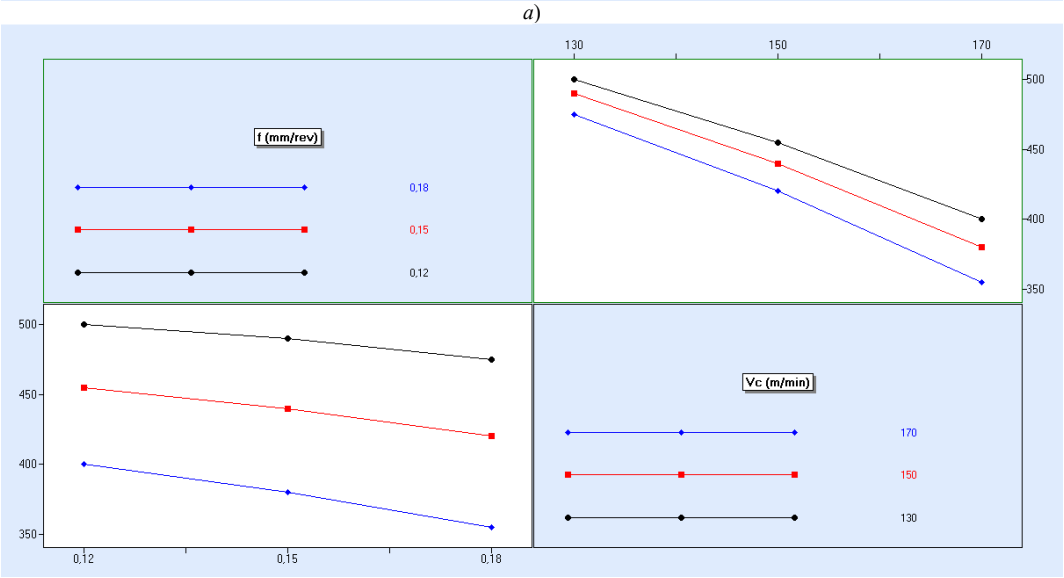

b)

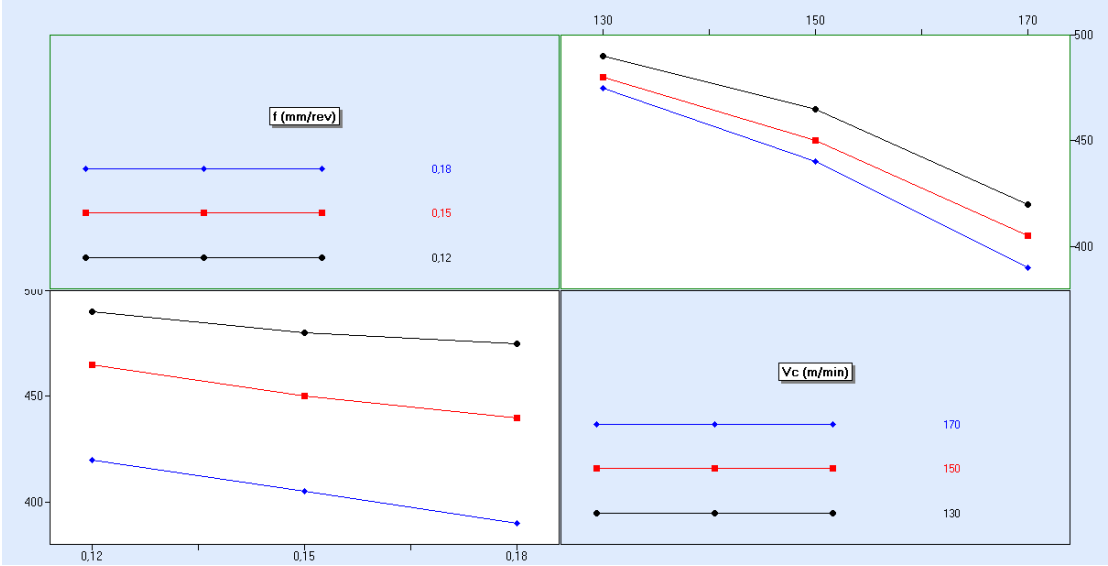

c)

Fig. 5 Visualisation of the influence of the feed f and cutting speed Vc on the tool lifetime of machining with carbide inserts: *a* - CCMT09T304-F1 TP2501 of a company SECO; *b* - CCMT09T304-MP of a company PALBIT; *c* - CCMT09T304-F3M IC807 of a company ISCAR

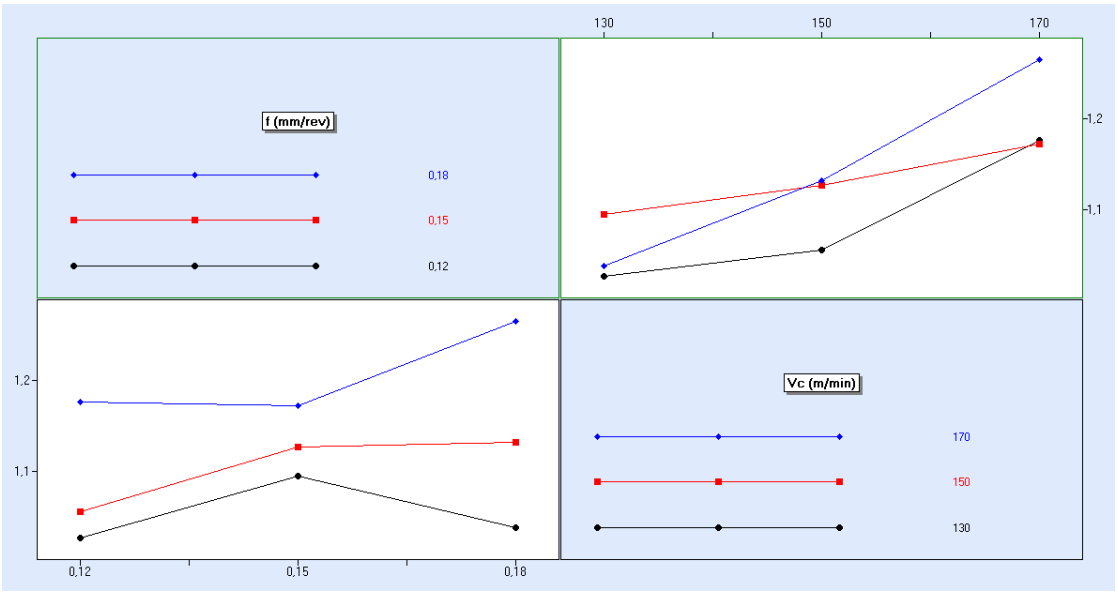

a)

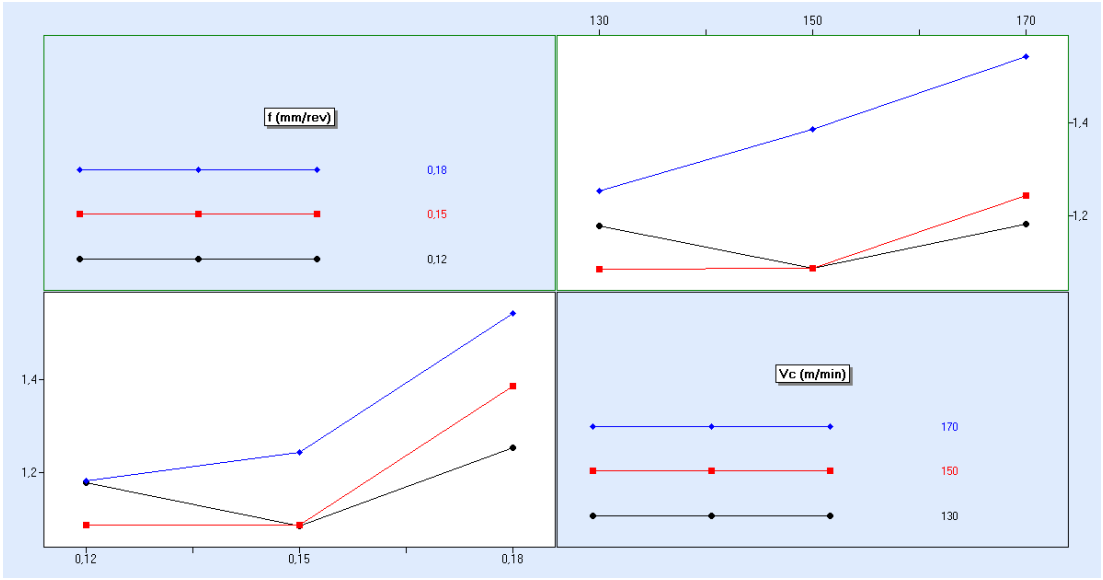

b)

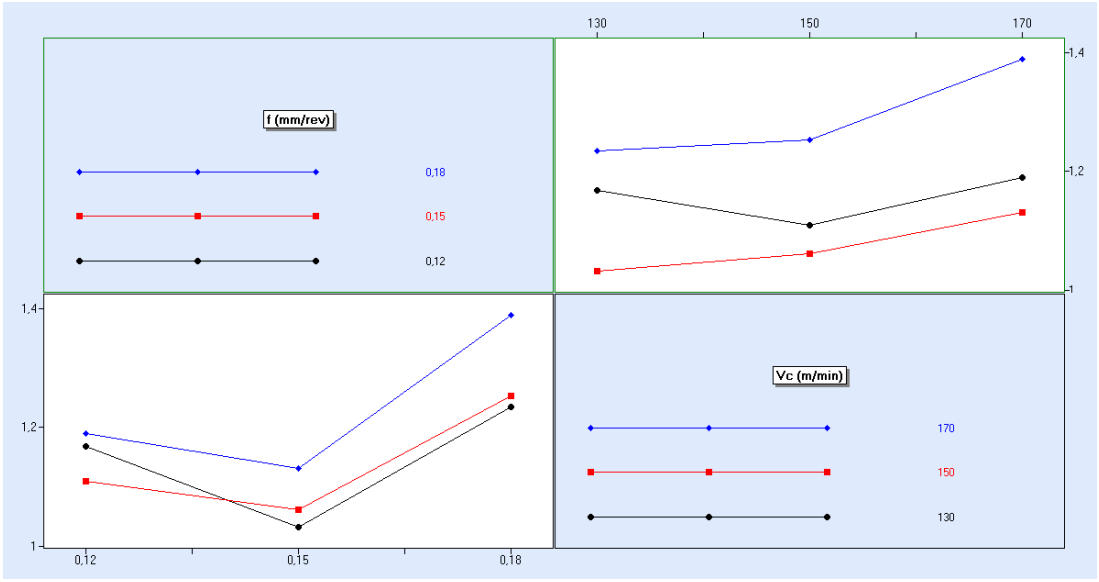

c)

Fig. 6 Visualisation of the influence of the feed f and cutting speed Vc on the roughness of machining with carbide inserts: *a* - CCMT09T304-F1 TP2501 of a company SECO; *b* - CCMT09T304-MP of a company PALBIT*; c* - CCMT09T304-F3M IC807 of a company ISCAR.

Analysis of variance (ANOVA) was performed to determine the influence of the control factors on tool lifetime and roughness. The graphical interpretation of this influence is shown in Fig. 5 and Fig. 6.

The analysis of the obtained theoretical and experimental models and of the graphical dependencies constructed on their basis shows that:

- The machinability of 42CrMo4+QT steel under the criterion cutting tool lifetime depends on the cutting conditions, and with increasing values of Vc and f there is a decrease in tool lifetime, i.e. deterioration in machinability (Table 6). The influence of the cutting speed is stronger, and its variation in the investigated range leads to a variation of the tool lifetime from 19% to 29% for individual inserts. The increase of the feed leads to decrease of the tool lifetime with 5 to 8.4% (Table 7). The highest tool lifetime, respectively the best machinability of 42CrMo4+QT steel according to this criterion was obtained when machining with the inserts CCMT09T304-F1 TP2501 of the company SECO (T = 512 workpieces at feed f_{min} = 0.12 mm/rev and Vc_{min} = 130m/min; T = 404 workpieces at f_{max} = 0.18 mm/rev and Vc_{max} = 170 m/min) (Table 6).

- The evaluation of the machinability by the roughness criterion of the machined surfaces shows that with increasing f and Vc, there is an increase in roughness i.e. a deterioration in machinability (Table 6). According to this criterion the best machinability, i.e. the lowest roughness is obtained when machining with the inserts CCMT09T304-F1 TP2501 of the company SECO (Ra = 1032 µm at f_{min}= 0.12 mm/rev and Vc_{min} = 130 m/min; Ra = 1.241 µm at f_{max} = 0.18 mm/rev and Vc_{max} =

170 m/min) (Table 6). For the CCMT09T304-F1 TP2501 inserts, there is a stronger influence of the cutting speed on the roughness, and for the CCMT09T304-MP and CCMT09T304-F3M IC807 inserts - of the feed on the roughness (Table 7).

The optimization of the cutting conditions elements was carried out by determining the combination of feed rate f (mm/rev) and cutting speed Vc (m/min) at which maximum tool lifetime of the cutting inserts and minimum roughness of the machined surfaces is achieved (Table 8).

TABLE 6 LIMITS OF VARIATION OF THE CRITERIA OVER THE RANGE OF CUTTING CONDITIONS INVESTIGATED

Insert	f_{min} = 0.12 mm/rev Vc_{min} = 130 m/min		f_{max} = 0.18 mm/rev Vc_{max} = 170 m/min	
	***T* (number of workpieces)**	***Ra* (μm)**	***T* (number of workpieces)**	***Ra* (μm)**
CCMT09T304-F1 TP2501	512	1.032	404	1.241
CCMT09T304-MP	501	1.166	356	1.561
CCMT09T304-F3M IC807	490	1.159	390	1.388

TABLE 7 INFLUENCE OF CUTTING CONDITIONS ELEMENTS ON MACHINABILITY CRITERIA, %

Insert	f_{min} = 0.12 mm/rev f_{max} = 0.18 mm/rev		Vc_{min} = 130 m/min Vc_{max} = 170 m/min	
	ΔT	***ΔRa***	***ΔT***	***ΔRa***
CCMT09T304-F1 TP2501	4.9	5.3	20.9	14.4
CCMT09T304-MP	8.4	21.2	29.1	12.9
CCMT09T304-F3M IC807	5.3	11.9	19.0	7.9

TABLE 8 CUTTING CONDITIONS PROVIDING MAXIMUM TOOL LIFETIME AND MINIMUM ROUGHNESS

Insert	Cutting conditions			T (number of work-pieces)	Ra (μm)
	***f* (mm/rev)**	***Vc* (m/min)**	***a_p* mm**		
CCMT09T304-F1 TP2501	0,12	130	1,5	512	1,032
CCMT09T304-MP	0,12	130	1,5	501	1,166
CCMT09T304-F3M IC807	0,12	130	1,5	490	1,159

IV. CONCLUSIONS

The machinability of 42CrMo4+QT steel was investigated on the cutting tool lifetime with replaceable carbide inserts and roughness of machined surfaces when machined on CNC lathes with robotic power supply. As a result of the investigation, the following conclusion can be drawn.

1) Theoretical and experimental models for the tool lifetime of the inserts and the roughness of the machined surfaces as 42CrMo4+QT steel machinability criteria have been built, reflecting the influence of the feed f and the cutting speed Vc.

2) Graphical dependencies have been constructed, with the help of which the tool lifetime of the examined inserts and the roughness of the machined surfaces can be predicted with sufficient accuracy in the cutting conditions in the range f = 0.12 - 0.18 mm/rev and Vc = 130 - 170 m/min.

3) The obtained models and relationships show that the machinability of 42CrMo4+QT steel depends on the elements of the cutting conditions, with the widest variation in the values of the cutting tool lifetime criterion. The cutting speed has a stronger influence on this criterion.

4) With the increase of cutting speed and feed, there is a decrease in tool lifetime and an increase in roughness i.e. deterioration in machinability of 42CrMo4+QT steel. The best machinability is obtained when machining with SECO's CCMT09T304-F1 TP2501 inserts.

5) The optimal cutting conditions were determined which guarantee maximum tool lifetime of the examined inserts and minimum roughness of the machined surfaces (Table 8).

ACKNOWLEDGEMENT

This research was funded by the European Regional Development Fund within the OP "Research, Innovation and Digitalization Programme for Intelligent Transformation 2021-2027", Project CoC "Smart Mechatronics, Eco- and Energy Saving Systems and Technologies", No BG16RFPR002-1.014-0005.

REFERENCES

[1] M. Nabil M., O. Taha, T. Elbitar, and I. El Mahallawi. "Thermomechanical processing of 42CrMoS4 steel." International heat Treatment and Surface Engineering,vol.4(2), 2010, pp. 87-92, https://doi.org/10.1179/174951410X12646901266726.

[2] M. Saez-de-Buruaga, L. Gainza, P. Aristimuno, D. Soler, G. Ortiz-de-Zarate, O. Aizpuru, R. Mielgo, and P.J. Arrazola. "FEM modeling of hard turning 42CrMoS4 steel." Procedia CIRP, vol. 82, ,pp. 77-82. 2019, https://doi.org/10.1016/j.procir.2019.04.059.

[3] E. Aslan, N. Camuscu, and B. Bingoren, "Design optimization of cutting parameters when turning hardened AISI 4140 (63 HRC) with Al2O3 + TiCN mixed ceramic tool." Materials & Design, vol. 28, pp. 1618-1622, 2007, https://doi:10.1016/j.matdes.2006.02.006.

[4] H. Akkuş, "Experimental and Statistical Investigation of Ra in Turning of AISI 4140." Sakarya University Journal of Science, vol. 23(5), pp. 775-781, 2019, https://doi.org/10.16984/saufenbilder.490668.

[5] S. R. Das, D. Dhupal, and A. Kumar, "Study of surface roughness and flank wear in hard turning of AISI 4140 steel with coated ceramic inserts." J Mech Sci Technol, vol. 29, pp. 4329–4340, 2015, https://doi.org/10.1007/s12206-015-0931-2.

[6] A.R, Motorcu, Y. Isik, A. Kus and M.C. Cakir, "Analysis of the cutting temperature and surface roughness during the orthogonal machining of AISI 4140 alloy steel via the taguchi method." Materiali in Tehnologije, vol. 50(3), pp. 343-351, 2016.

[7] G. Sharan and R. K. Patel, "Optimization of cutting parameters of turning for hardness of AISI 4140 alloy steel." in ICMPC-2019, Materials Today: Proceedings, vol. 18, pp. 3582–3589, 2019.

[8] B. Hamadi, M.A. Yallese, L. Boulanouar, A Hammoudi, and M. Nouioua. "Evaluation of the cutting performance of PVD, CVD and MTCVD carbide inserts in dry turning of AISI 4140 steel using RSM-based NAMDE optimization." J Braz. Soc. Mech. Sci. Eng. Vol. 44, pp. 342+, 2022. https://doi.org/10.1007/s40430-022-03633-5.

[9] Padhan, N.K.Wagri. L. Dash, A. Das, S.R. Das, M. Rafighi, and P. Sharma, "Investigation on Surface Integrity in Hard Turning of AISI 4140 Steel with SPPP-AlTiSiN Coated Carbide Insert under Nano-MQL." Lubricants, vol. 49(11), 2023, https://doi.org/10.3390/lubricants11020049.

[10] I. Meddour, M.A. Yallese, H. Bensouilah, A. Khellaf and M. Elbah, "Prediction of surface roughness and cutting forces using RSM, ANN, and NSGA-II in finish turning of AISI 4140 hardened steel with mixed ceramic tool". Int J Adv Manuf Technol, vol. 97, pp. 1931–1949, (2018), https://doi.org/10.1007/s00170-018-2026-6.

[11] "Seco Cutting Tool," [Online]. Available:https://www.secotools.com/article/20857?language=en. [Accessed: Feb. 16, 2025].

[12] "Palbit-Products Cutting" [Online]. Available: https://www.palbit.pt/en/products/cutting/. [Accessed: Feb. 16, 2025].

[13] "Iscar Cutting Tool" [Online]. Available: https://www.iscar.com/eCatalog/Index.aspx. [Accessed: Feb. 16, 2025].

[14] N. Kolev, I. Aleksandrova, H. Metev, "Investigation of roughness in machining of 42CrMo4+QT steel on robot-feed CNC machines", in International Scientific Conference UNITECH 2023: Proceedings, pp. II80 - II85, November 2023.

[15] A. Aleksandrov and I. Aleksandrova, Theory of Experiment, Gabrovo, Bulgaria: Experess, 2012.

[16] I. N. Vuchkov and I. I. Vuchkov, Statistical methods of quality control, robust engineering, planning, modeling and optimization, QStatLab, v 5.3, 2009.

Environment. Technology. Resources. Rezekne, Latvia
Proceedings of the 16th International Scientific and Practical Conference. 2025. Volume IV, 235-238

Influence of the Geometric Eccentricity of a Gear on the Vibrations of a Bevel Gear

Yuliyan Minchev
Department of Mechatronics
Naval Academy N.Vaptsarov, Varna, Bulgaria
Varna, Bulgaria
julminchev@nvna.eu

Ivaylo Minchev
Department of Mechatronics
Naval Academy N.Vaptsarov, Varna, Bulgaria
Varna, Bulgaria
iminchev@nvna.eu

***Abstract*— The influence of geometric eccentricity on the oscillations of bevel gears is studied. A gear train consisting of two "exact" gears with axes offset from the geometric center is considered. A mathematical model is compiled through which the oscillations in the tooth engagement are studied. It is proved that the oscillations in the contact zone are described by the Mathieu equation. It turns out that the geometric eccentricity of bevel gears excites two types of oscillations - forced and parametric. Experimental results from a ship's power system are presented.**

Keywords*— *oscillations, bevel gears, geometric eccentricity, azimuth thrusters.

I. INTRODUCTION

Gear vibration has been the subject of much attention by many authors. The variable stiffness of the gear mesh is a major natural vibration exciter [1][2][3]. It excites two types of vibration [1] :

1. Forced oscillations with a frequency equal to the frequency of stiffness change and multiples of it

$z\omega$, $2z\omega$, $3z\omega$,…

here z is the number of teeth, and ω is the rotation frequency.

2. Parametric oscillations with a frequency equal to half the frequency of stiffness change and multiples of it:

$$\frac{1}{2}z\omega,\ \frac{3}{2}z\omega,\ \frac{6}{2}z\omega,\ \ldots.$$

Vibrations are also caused by technological errors in the manufacture of gears:

- error in the main step [4][5] ;
- profile error [1];
- geometric eccentricity of the gears [1][7] .

II. MATERIALS AND METHODS

The influence of geometric eccentricity on the vibrations of cylindrical gears was studied in [1][7] . In the present work, the influence of geometric eccentricity on the vibrations of bevel gears (Fig. 1) is studied. We will consider a gear consisting of two “exact” gears (Fig. 2) with axes displaced from the geometric center. The centers of the base circles of the wheels are located at the points O' and O'' . The common normal $\tau-\tau$ to the base circles is the normal to the tooth profiles at the contact point. In the presence of eccentricity, the point O' and O'' rotate about the points O_1 and O_2 . This causes a displacement of the line $\tau-\tau$, a displacement of the engagement pole and a change in the gear ratio. For cylindrical gears with geometric eccentricity, this problem was studied in [1] . In Fig. 2 , the centers of rotation of the wheels are marked with O_1 and O_2 . They are displaced at a distance $l_1 = O_1O'$ and $l_2 = O_2O''$ from the geometric centers. From the centers of rotation O_1 and O_2 we draw the normals O_1A_1 and O_2B_1 to the common normal $\tau-\tau$ of the base circles. Therefore, the lines O_1A_1 and O_2B_1 are parallel to the radii of the base circles, respectively.

$$r_1 = O'A',\ r_2 = O''B'$$

For the segments O_1A_1 and O_2B_1 is satisfied

$$\begin{aligned} O_1A_1 &= r_1 + e_1\cos(\varphi_1+\alpha) = r_{O1} \\ O_2B_1 &= r_2 + e_2\cos(\varphi_2-\alpha) = r_{O2} \end{aligned} \quad (1)$$

For the translation relation we get

Online ISSN 2256-070X
https://doi.org/10.17770/etr2025vol4.8434
© 2025 The Author(s). Published by RTU PRESS.
This is an open access article under the Creative Commons Attribution 4.0 International License.

$$i=\frac{\omega_1}{\omega_2}=\frac{r_2+e_2\cos(\varphi_2-\alpha)}{r_1+e_1\cos(\varphi_1+\alpha)}=$$

$$=\frac{r_2}{r_1}.\frac{1+\frac{e_2}{r_2}\cos(\varphi_2-\alpha)}{1+\frac{e_1}{r_1}\cos(\varphi_1+\alpha)}= \quad (2)$$

$$=i_O\frac{1+\lambda_2\cos(\varphi_2-\alpha)}{1+\lambda_1\cos(\varphi_1+\alpha)}$$

Here $i_O=\frac{\omega_1}{\omega_2}=\frac{r_2}{r_1}$ - translational relationship of precisely mounted wheels.

$$\lambda_1=\frac{e_1}{r_1},\lambda_2=\frac{e_2}{r_2} \quad (3)$$

The magnitudes of λ_1 and λ_2 are small. Therefore, the translation relation (2) is of the form(3)

$$i=i_O(1+\varepsilon),$$

Where ε is a small parameter.

After developing (2) in order, we obtain

$$\varepsilon=\lambda_2\cos(\varphi_2-\alpha)-\lambda_1\cos(\varphi_1+\alpha) \quad (4)$$

Here $\varphi_1=\omega_1 t,\varphi_2=\omega_2 t$

We will build a mathematical model of the single-stage bevel gear. The dynamic model is shown in Fig. 3. The gear consists of two gears 1 and 2, mounted on elastic supports with stiffnesses C_1 and C_2 in the direction of the meshing line. The stiffness of the gear mesh is represented by an elastic element with stiffness C also in the direction of the meshing line. The angular coordinates of the wheels 1 and 2 are φ_1 and φ_2, and their vibrational displacements in the direction of the meshing line are denoted by y_1 and y_2. The line $\tau-\tau$ performs small oscillations around an average position, which can be neglected when determining the direction of the axes y_1 and y_2.

The deformation of the tooth occlusion is

(5) $x=r_{O1}\varphi_1+r_{O2}\varphi_2+y_1-y_2$

Based on (3) we present

(6)
$$r_{O1}=r_1\left(1+\lambda_1\cos(\omega_1 t+\alpha)\right)$$
$$r_{O2}=r_2\left(1+\lambda_2\cos(\omega_2 t-\alpha)\right)$$

After applying the Lagrange method, the equations are obtained

$$\begin{vmatrix} I_1\ddot{\varphi}_1+Cxr_{O1}(t)=0 \\ I_2\ddot{\varphi}_2+Cxr_{O2}(t)=0 \\ m_1\ddot{y}_1+C_1y_1+Cx=0 \\ m_2\ddot{y}_2+C_2y_2-Cx=0 \end{vmatrix} \quad (7)$$

In (7) I_1 and I_2 denote the mass moments of inertia of the gears, and m_1 and denote m_2 their masses. Equations (7) represent a system of differential equations with variable coefficients describing the oscillations of eccentrically mounted "precise" bevel gears.

We will study the oscillations in the gear meshing of eccentrically mounted "precision" gears. For this purpose, we assume $y_1\equiv y_2\equiv 0$. From (7) we obtain

$$\begin{vmatrix} I_1\ddot{\varphi}_1+Cxr_{O1}(t)=0 \\ I_2\ddot{\varphi}_2+Cxr_{O2}(t)=0 \end{vmatrix} \quad (8)$$

We substitute (6) into (8) and write (8) in the form:

$$\begin{vmatrix} \ddot{\varphi}_1+\frac{C}{I_1}r_1x+\frac{1}{I_1}xCr_1\lambda_1\cos\psi_1=0 \\ \ddot{\varphi}_2+\frac{C}{I_2}r_2x+\frac{1}{I_2}xCr_2\lambda_2\cos\psi_2=0 \end{vmatrix} \quad (9)$$

Here $\psi_1=\omega_1 t+\alpha$, $\psi_2=\omega_2 t-\alpha$.

With accuracy up to small first-order quantities, we assume

$$x=r_1\varphi_1+r_2\varphi_2 \quad (10)$$

We will multiply the first equation of (9) by r_1, and the second by r_2 and sum them. Thus we get

$$\ddot{x}+\omega_C^2(1+\varepsilon_1\cos\psi_1+\varepsilon_2\cos\psi_2)x=0 \quad (11),$$

where

$$\omega_C^2=C\left(\frac{r_1^2}{I_1}+\frac{r_2^2}{I_2}\right),\ \varepsilon_1=C\frac{r_1^2}{I_1}\lambda_1\frac{1}{\omega_C^2},$$

$$\varepsilon_2=C\frac{r_2^2}{I_1}\lambda_2\frac{1}{\omega_C^2}$$

Equation (11) describes the vibrations in the contact zone in the general case when both wheels have geometric eccentricity.

When the second wheel is exactly $\lambda_2=0$. The vibrations in the contact area are described by the equation:

$$\ddot{x}+\omega_C^2(1+\varepsilon_1\cos\psi_1)x=0 \quad (12)$$

When the first wheel is straight, $\lambda_1=0$ the vibrations in the contact patch are described by the equation

$$\ddot{x}+\omega_C^2(1+\varepsilon_2\cos\psi_2)x=0 \quad (13)$$

We will present (12) and (13) in general form

$$\ddot{x} + \omega_C^2(1 + \varepsilon_i \cos\psi_i)x = 0 \quad (14)$$
$$i = 1,2$$

From (14) we get

$$\frac{d^2x}{d\psi_i^2} + (\lambda_i + \mu_i \cos\psi_i)x = 0\,, \quad (15)$$

Where

$$\lambda_i = \left(\frac{\omega_C}{\omega_i}\right)^2, \mu_i = \left(\frac{\omega_C}{\omega_i}\right)^2 \varepsilon_i$$

This is Mathieu's equation. The equation has two types of solutions,

$$x = A_1 \sin\omega_i t + B_1 \cos\omega_i t + \\ + A_2 \sin 2\omega_i t + B_2 \cos 2\omega_i t... \quad (16)$$

$$x = A_{\frac{1}{2}} \sin\frac{\omega_i}{2} t + B_{\frac{1}{2}} \cos\frac{\omega_i}{2} t + \\ + A_{\frac{3}{2}} \sin\frac{3}{2}\omega_i t + B_{\frac{3}{2}} \cos\frac{3}{2}\omega_i t... \quad (17)$$

Solution (16) defines forced oscillations with a wheel rotation frequency of geometric eccentricity and multiples of it.

Solution (17) defines parametric oscillations with a frequency equal to half the wheel rotation frequency with geometric eccentricity and multiples thereof.

The values of μ_i are small. In such a case, at

$$\lambda_i \approx 1 \text{ and } \lambda_i \approx 4$$

forced oscillations of the type (16) are observed.

At small values of μ_i in the vicinity of

$$\lambda_i \approx \frac{1}{4}, \lambda_i \approx \frac{9}{4}$$

parametric oscillations of the type (17) are observed.

It turns out that the geometric eccentricity of bevel gears excites two types of oscillations:

- forced by the species(16)
- parametric of the type (17)

An analogous result is defined in [1] for spur gears.

Vibrations in the contact area of bevel gears excite radial and axial vibrations of the bearings.

III. RESULTS AND DISCUSSION

We will present experimental results on the vibrations of the driving bevel gear of a main engine of a ship's propulsion system. The ship is a diesel- electric motor . The engine is asynchronous with a power of 1500 kW at 1791 rpm. Fig. 4 presents the spectra of the vibrations of the driving bevel gear in the three directions:

- vertical (Fig. 4-a) - 2,029 mm/s
- horizontal (fig. 4-b)-5.3712 mm/s
- axial (Fig. 4-c) - 3.0698 mm/s

In the vertical and horizontal vibrations, the vibrations with rotational frequency (1791rpm) are dominant. These are forced oscillations. In the axial oscillations, the oscillations with the frequency are dominant $\frac{1}{2}\omega_1 \approx 900 rpm$. These are parametric oscillations. It should be noted that the frequency range in which parametric oscillations are observed is narrow. In this case, the engine is asynchronous, therefore the rotation frequency is practically constant. This creates conditions for the existence of parametric oscillations continuously.

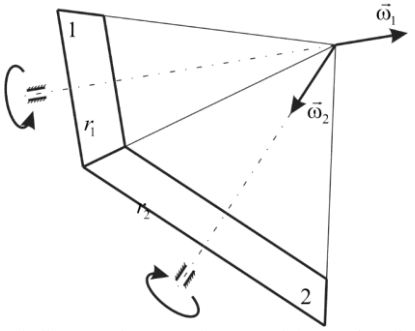

Fig. 1. The influence of geometric eccentricity on the vibrations of bevel gears

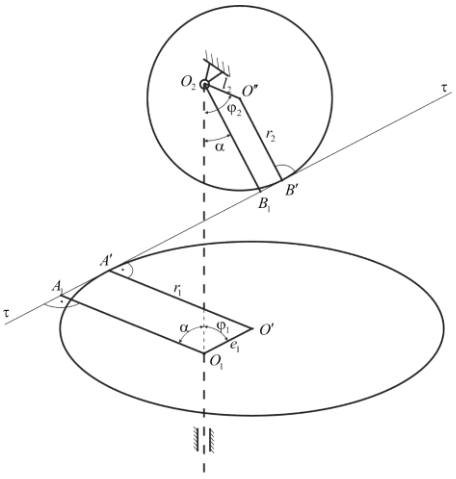

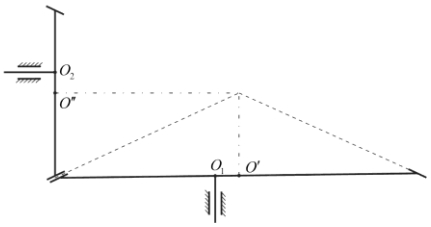

Fig. 2. Gear consisting of two “exact” gears

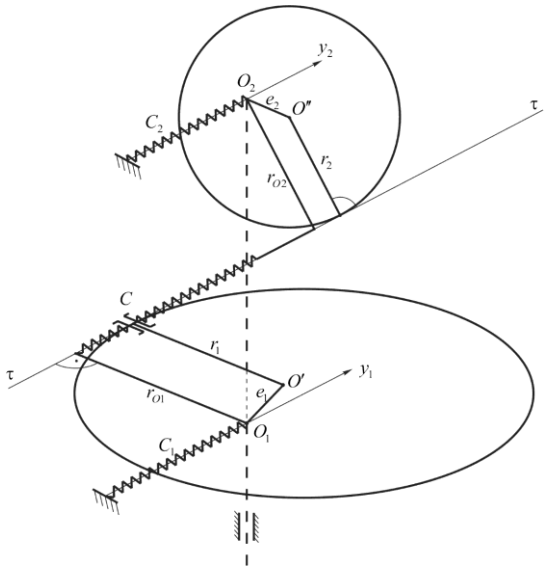

Fig. 3. The dynamic model of the single-stage bevel gear

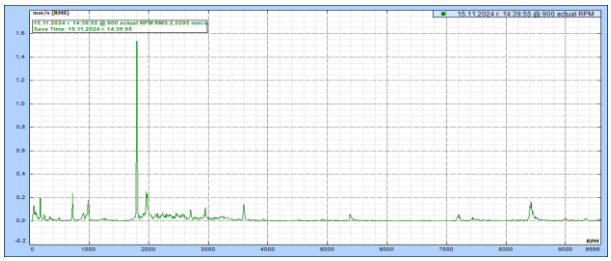

Fig. 4-a. The spectra of the vibrations of the driving bevel gear vertical

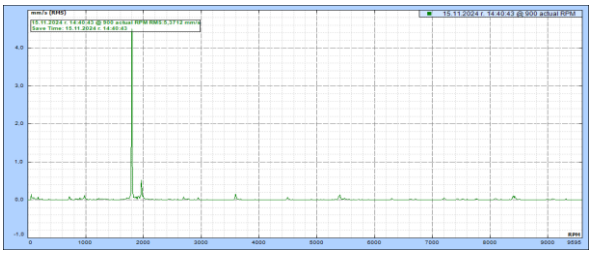

Fig. 4-b. The spectra of the vibrations of the driving bevel gear horizontal

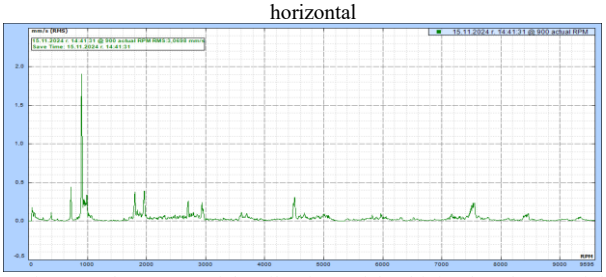

Fig. 4-c. The spectra of the vibrations of the driving bevel gear axial

REFERENCES

[1] N.D.Minchev, V.Grigorov, Vibrodiagnostics of rotary and piston machines. DI Technika 1988. 280pp.

[2] B.M.Abramov, Fluctuating straight teeth toothed wheel . Kharkiv, Ed. Kharkiv University, 1968.

[3] B.G.Belnikolovski, Dynamics of machines with spur gears. Dissertation, Technical University of Sofia , 1998.

[4] N.N. Minchev,Oscillations of a gear mechanism with a cyclic step error, Journal of Machine Mechanics No. 38, pp. 162-166

[5] N.N. Minchev, On the vibrations of gear mechanisms with a step error. Journal of Machine Mechanics No. 37, pp. 17-19

[6] N.N. Minchev, I.N. Minchev, Y.M. Minchev, N. Trizlova, On the vibrations of the gear driving drum rotary kilns. Journal Mechanics of Machines No. 66, pp. 147-151.

[7] N.N.Minchev. Influence of the variable stiffness of the gear mesh on the vibrations of a gear with geometric eccentricity. Journal of Machine Mechanics No. 37, pp. 87-88.

Environment. Technology. Resources. Rezekne, Latvia
Proceedings of the 16th International Scientific and Practical Conference. 2025. Volume IV, 239-243

On the Influence of the Elastic Anisotropy of the Propeller on the Vibrations of Azimuth Thrusters

Yuliyan Minchev
Department of Mechatronics
Naval Academy N.Vaptsarov, Varna, Bulgaria
Varna, Bulgaria
julminchev@nvna.eu

Ivaylo Minchev
Department of Mechatronics
Naval Academy N.Vaptsarov, Varna, Bulgaria
Varna, Bulgaria
iminchev@nvna.eu

***Abstract*— A possibility for excitation of oscillations from the propeller of azimuth thrusters is analyzed.. The shaft is short, cantilever type. The propeller blades create elastic anisotropy of the propeller shaft with respect to the transverse stiffness. The influence of the elastic anisotropy of the propeller shaft on the oscillations of azimuth thrusters is studied . A mathematical model describing the oscillations is proposed, which is reduced to the Mathieu equation. It is proven that the elastic anisotropy of the propeller shaft excites two types of oscillations: forced with a blade frequency and multiples of it, and parametric with a frequency equal to half the blade frequency and multiples of it. Experimental results are presented.**

Keywords*— *propeller, oscillations, elastic anisotropy, azimuth thrusters.

I. INTRODUCTION

The vibrations excited by the propeller are the subject of attention of many researchers. Attention is focused on the hydrodynamic forces. As is known, they depend on the operating conditions of the propeller. (propeller behind the stern or propeller in the nozzle). The propeller is subject to static balancing of the inertial forces, which are a significant exciter of vibrations. A major exciter of vibrations is the hydrodynamic unbalance of the propeller. It is the result of a disturbed geometry of the propeller, which leads to a mismatch of the center of mass of the attached mass of water with the axis of rotation.

The oscillations of the ship's hull excited by the propeller are discussed in [1][2][3][6][7] , with experimental results presented in [3][6] and [7].

II. MATERIALS AND METHODS

In this work, a possibility for excitation of oscillations by the propeller of azimuth thrusters is analyzed . In this case, the propeller shaft is of the cantilever type (Fig. 1). The shaft is short. The propeller blades create elastic anisotropy of the shaft with respect to the transverse stiffness. As is known [4][5], the elastic anisotropy of the crankshaft of the main engines is an exciter of parametric oscillations of the shaft line. Therefore, in this work, the influence of the elastic anisotropy of the propeller shaft on the oscillations of azimuth thrusters is studied . In this case, the elastic anisotropy is due to the shape of the propeller. In the section where there is a blade, the transverse stiffness is greater. Fig. 2 shows a schematic of a shaft with a four-bladed propeller. It is not difficult to see that the transverse stiffness is a function of the angle of rotation φ . Along the x and axes, y the stiffness is maximal, while along the axis z , which corresponds to $\varphi = 45^o$, it is minimal. The transverse stiffness in this case can be approximated by a function of the form

$$C = C_O + C_1 \cos 4\varphi \qquad (1)$$

The minimum stiffness is C_O , and the maximum is $C_O + C_1$.

We will compile a mathematical model describing the oscillations of a cantilevered comb propeller. The propeller is represented as a disk (Fig. 3), which rotates with a constant angular velocity ω . The propeller oscillates in the direction of the axes x and y . In addition, the angular oscillations α and β about the axes x and are also taken into account y . When compiling the mathematical model, we will apply the theorems for changing the amount of motion and the kinetic moment. The kinetic moment of rotation (Fig. 3) is:

$$K = I\omega \qquad (2\text{-a})$$

Parameter I is the mass moment of inertia about the axis of rotation, which is orthogonal to the plane of the disk. The angular momentums α and β (Fig. 3) are:

Online ISSN 2256-070X
https://doi.org/10.17770/etr2025vol4.8435
© 2025 The Author(s). Published by RTU PRESS.
This is an open access article under the Creative Commons Attribution 4.0 International License.

$$K_x = I_x\dot{\alpha}\,, K_y = I_y\dot{\beta} \tag{2-b}$$

Here I_x and I_y are the equatorial mass moments of inertia of the disk with which the propeller is modeled.

As a result of the angular oscillations of the disk about the axes x and y the kinetic moment K of rotation, which is orthogonal to the plane of the disk, there is a projection (Fig. 4) along the fixed axis x:

$$I\omega\alpha \tag{3}$$

And projection(Fig. 4) along the fixed axis y:

$$I\omega\beta \tag{4}$$

Based on (1), (2), (3) and (4) and the graphical interpretation in Fig. 4, the kinetic moments along the axes x and are obtained y:

$$\begin{aligned} K_{OX} &= I_x\dot{\alpha} + I\omega\beta \\ K_{OX} &= I_y\dot{\beta} + I\omega\alpha \end{aligned} \tag{5}$$

We will define the elastic constants of the cantilever shaft [8] . When a displacement is given y (Fig. 5-a) of the free end, an elastic force arises along the axis y:

$$F_{yy} = C_{11}y \tag{6}$$

and moment on x:

$$M_{xy} = C_{21}y \tag{7}$$

When a displacement is set x (Fig. 5) at the free end, an elastic force arises along the axis x:

$$F_{xx} = C_{11}x \tag{8}$$

and moment about axis y:

$$M_{yx} = C_{21}x \tag{9}$$

When defining an angular deformation α (Fig. 5-c) along the axis x, an elastic force arises along the axis y

$$F_{yx} = C_{12}\alpha \tag{10}$$

and axial moment x

$$M_{xx} = C_{22}\alpha \tag{11}$$

When an angular deformation β (Fig. 5-d) is imposed along the axis y, an elastic force arises along the axis x

$$F_{xy} = C_{12}\beta \tag{12}$$

and axial moment y

$$M_{yy} = C_{22}\beta \tag{13}$$

Based on (6), (8), (10) and (12), after applying the momentum change theorem, the differential equations are obtained:

$$\begin{vmatrix} m\ddot{x} + C_{11}x - C_{12}\beta = 0 \\ m\ddot{y} + C_{11}y - C_{12}\alpha = 0 \end{vmatrix} \tag{14}$$

Based on (5), (7), (9), (11) and (13) after applying the theorem for changing the angular momentum, the differential equations are obtained:

$$\begin{vmatrix} I_x\ddot{\alpha} + I\omega\dot{\beta} + C_{21}y - C_{22}\alpha = 0 \\ I_y\ddot{\beta} - I\omega\dot{\alpha} - C_{21}x + C_{22}\beta = 0 \end{vmatrix} \tag{15}$$

Equations (14) and (15) form a system of equations that describe the oscillations of the propeller.

The elastic constants [8] have the form:

$$C_{11} = \frac{12EJ}{l^3}\,,\; C_{12} = \frac{6EJ}{l^2}, C_{22} = \frac{4EIJ}{l} \tag{16}$$

The elastic constants represent the transverse stiffnesses of the cantilever shaft with a comb screw. Due to the elastic anisotropy resulting from the presence of the blades, they are approximated by functions of the form (1)

$$C_{ij} = C_{ij}^o + C_{ij}^1\cos k\varphi \tag{17}$$

We will limit ourselves to considering the oscillations only along the x and axes y, neglecting the angular oscillations. Then from (14) we obtain:

$$\begin{aligned} m\ddot{x} + C_{11}x &= 0 \\ m\ddot{y} + C_{11}y &= 0 \end{aligned} \tag{18}$$

The equations (18) are the same, so we will analyze the oscillations in x. Substituting (17) into (18) we obtain:

$$m\ddot{x} + \left(C_{11}^o + C_{11}{}'\cos k\varphi\right)x = 0 \tag{19}$$

Assuming $\sin k\varphi \approx \sin k\omega t$ we write equation (19) in the form

$$\ddot{x} + \omega_C^2\left(1 + \frac{C_{11}{}'}{C_{11}^o}\cos k\omega t\right)x = 0 \tag{20}$$

Here $\omega_C^2 = \dfrac{C_{11}^o}{m}$

After fitting, $k\omega t = \tau$ equation (20) takes the form

$$\frac{d^2x}{d\tau^2} + \left(\lambda + \mu\cos\tau\right)x = 0\,, \tag{21}$$

Where

$$\lambda = \left(\frac{\omega_C}{k\omega}\right)^2, \mu = \frac{\omega_C^2}{\left(k\omega\right)^2}.\frac{C_{11}^1}{C_{11}^o} = \frac{\lambda C_{11}^1}{C_{11}^o}$$

The resulting differential equation is the well-studied Mathieu equation. The type of the general solution of the equation depends on the values of the parametric λ and μ [9] . For small values of μ at

$$\lambda_1 \approx 1, \lambda_2 \approx 4$$

oscillations are excited with a frequency equal to the frequency of change of the stiffness and multiples of it:

$$\begin{aligned} x = A_1\sin k\omega t + B_1\cos k\omega t + \\ + A_2\sin 2k\omega t + B_2\cos 2k\omega t + \ldots \end{aligned}$$

For small values of μ, when

$$\lambda_1 \approx \frac{1}{4}, \lambda_2 \approx \frac{9}{4}$$

Parametric oscillations are excited with a frequency equal to half the frequency of stiffness change and multiples of it:

$$x = A_{\frac{1}{2}} \sin\frac{k\omega t}{2} + B_{\frac{1}{2}} \cos\frac{k\omega t}{2} +$$

$$+A_{\frac{3}{2}} \sin\frac{3}{2}k\omega t + B_{\frac{3}{2}} \cos\frac{3}{2}k\omega t + \ldots$$

III. RESULTS AND DISCUSSION

The experimental results are from the two azimuth thrusters on a ship with a propeller rotation frequency of 244 *rpm* . The propellers are four-bladed. Forced oscillations with frequencies, $2.4\omega = 1952 rpm$ are observed $4\omega = 976 rpm$.

Fig. 6 presents results for the azimuth thruster - port side, and Fig. 7 for starboard side as shown in Table 1.

TABLE 1

direction	AT. port side	AT. starboard
vertically	Fig. 6-a	Fig. 7-a
horizontally	Fig. 6-b	Fig. 7-b
axial	Fig. 6-c	Fig. 7-c

It should be noted that the oscillations are of low intensity (up to $1,55 mm/s$). Here the qualitative result is essential, confirming the hypothesis of excitation of oscillations as a result of the elastic anisotropy of the propeller shaft with a propeller.

In the case under consideration, the screws are in a nozzle, therefore there is no hydrodynamic exciter of blade frequency oscillations.

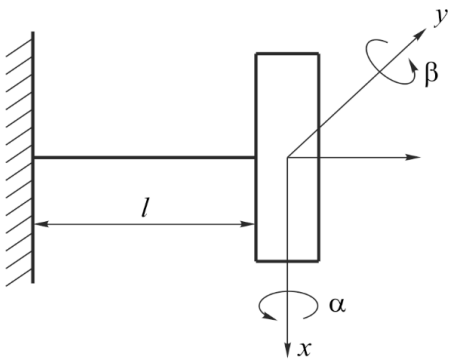

Fig. 1. The propeller shaft is of the cantilever type

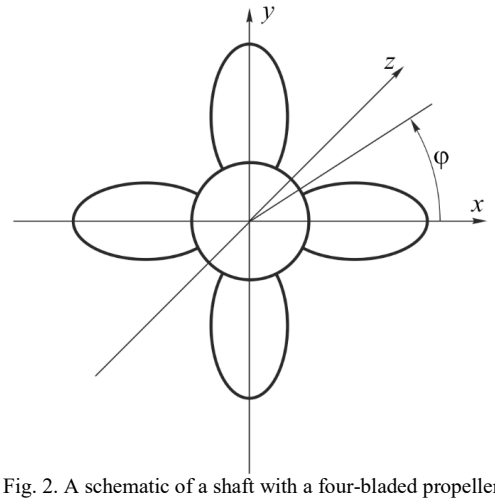

Fig. 2. A schematic of a shaft with a four-bladed propeller

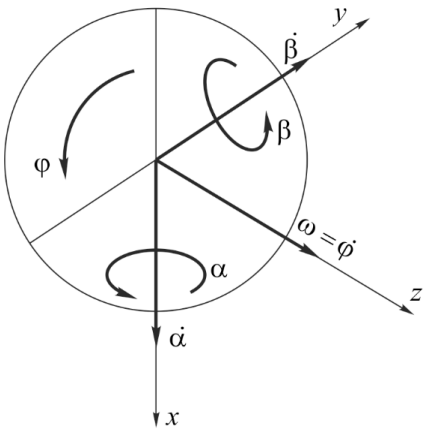

Fig. 3. The propeller is represented as a disk

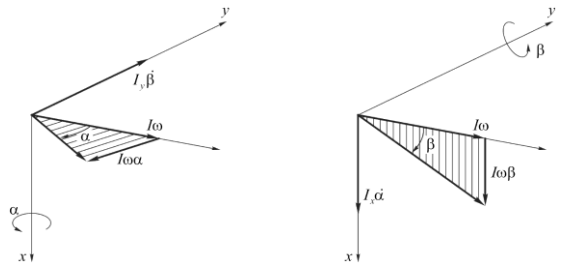

Fig. 4-a. Projection of the kinetic moment along the x and y axes

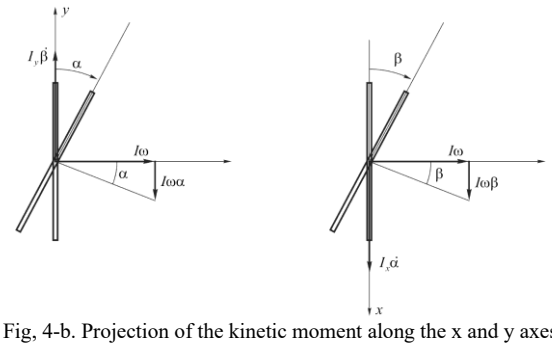

Fig, 4-b. Projection of the kinetic moment along the x and y axes

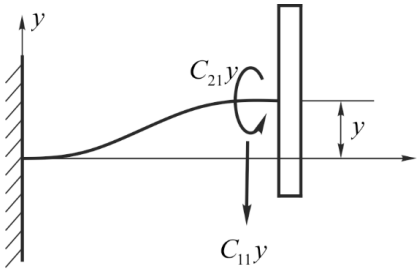

Fig. 5-a. the elastic constants of the cantilever shaft. When specifying a displacement y

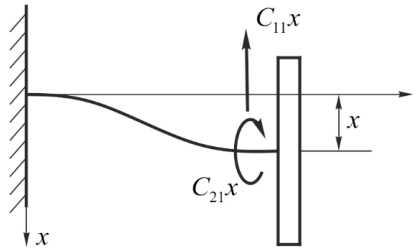

Fig. 5-b the elastic constants of the cantilever shaft. When specifying a displacement x

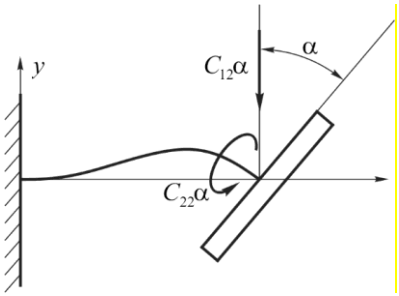

Fig. 5-c the elastic constants of the cantilever shaft. When specifying a displacement α

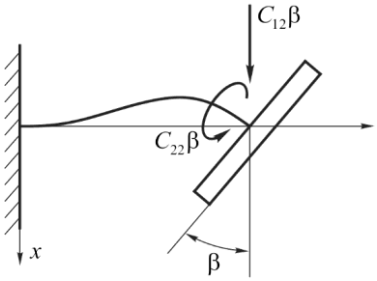

Fig. 5-d. the elastic constants of the cantilever shaft. When specifying a displacement β

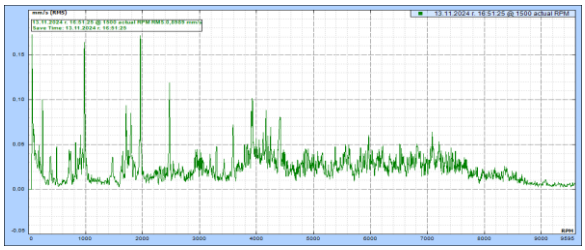

Fig. 6-a. Azimuth thruster oscillation spectrum port side vertical

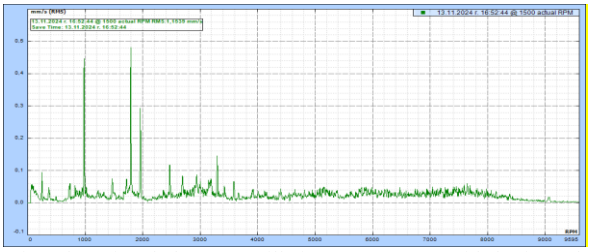

Fig. 6-b. Azimuth thruster oscillation spectrum port side horizontal

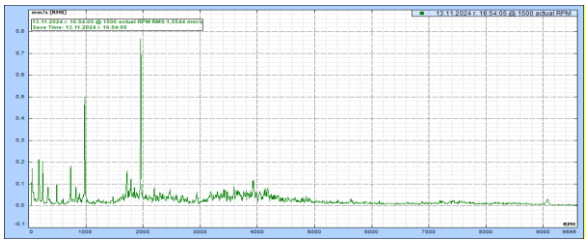

Fig. 6-c. Azimuth thruster oscillation spectrum port side axial

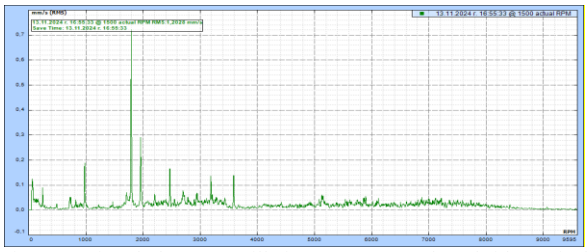

Fig. 7-a Azimuth thruster oscillation spectrum starboard side vertical

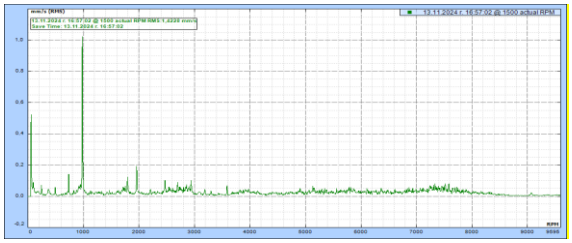

Fig. 7-b Azimuth thruster oscillation spectrum starboard side horizontal

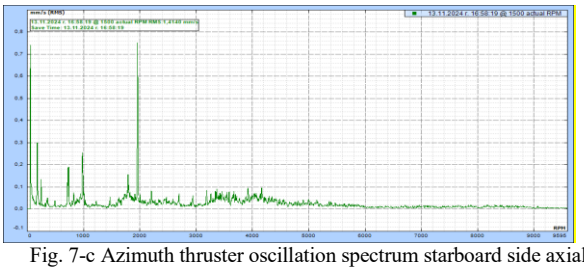

Fig. 7-c Azimuth thruster oscillation spectrum starboard side axial

REFERENCES

[1] N.D.Minchev, Dynamics of ship engines. DVI. Sofia 1983. p. 448.

[2] N.D.Minchev, Hr.Draganchev, Strength and vibrations of ship engines. IK. Galaktika 1992. p. 389.

[3] N.D. Minchev, Y.U. Minchev, I.N. Minchev, On the excitation of ship hull vibrations by the propeller. Journal Mechanics of Machines No. 107, pp. 81-91.

[4] N.N. Minchev, Y.U. Minchev, I.N. Minchev, Transverse vibrations of a ship's shaft line and a ship's engine with

consideration of the elastic anisotropy of the crankshaft. Journal of Machine Mechanics No. 42 pp. 88-100.

[5] N.N. Minchev, Y.U. Minchev, I.N. Minchev, Mechanomathematical modeling of transverse vibrations of a ship shaft line with consideration of the elastic anisotropy of the crankshaft. Journal Mechanics of Machines No. 49, pp. 165-171.

[6] Y.M. Minchev, I.N. Minchev, Mechanomathematical model and experimental results on the excitation of ship hull vibrations by a paddle wheel. Journal Mechanics of Machines No. 126, pp. 158-168.

[7] N.D. Minchev, Y.U. Minchev, I.N. Minchev, On the excitation of ship hull vibrations by the propeller. Journal of Machine Mechanics No. 107, 2014, pp. 81-90.

[8] F.M. Dimentberg, K.T. Shatalov, A.A. Gusarov, The wobbly machine . Ed. Mechanical Engineering , Moscow 1964.

[9] N.D. Minchev V. Grigorov, Vibrodiagnostics of rotary and piston machines. DI "Technika" Sofia 1988. p. 280

Environment. Technology. Resources. Rezekne, Latvia
Proceedings of the 16th International Scientific and Practical Conference. 2025. Volume IV, 245-250

Determing the Compensating Action of Copper After Sintering of Powder Metallurgical Structural Steels

Petko Naydenov
dept. Economics
Technical University of Gabrovo
Gabrovo, Bulgaria
petkonaydenov@abv.bg

***Abstract*— This paper studies the dimensional changes during sintering of steel powders structural materials alloying with a 2,5 percents copper compound. Studied were three types of steel powders – NC 100.24; SC100.26 and ASC 100.29. Carbon concentration in the test pieces is between 0,2 and 0,8 percents, and their density between 6,2 and 7,0 grams per cubic centimeter. Presented are graphical relationships of the dimensional changes depending on the carbon concentration in the tested samples and their density.**

Keywords*— carbon concentration, density, dimensional changes, iron powder, permeability.

I. INTRODUCTION

With the advent of Industry 4.0 in recent years, there is a distinct trend towards increasing the degree of digitization, connectivity, autonomy and intelligence of production processes. Their efficiency, productivity and accuracy are constantly being improved, while at the same time shortening the response times and the processing cycles. Innovative and energy-saving technological processes are taking bigger share in the production of goods and supplies from all branches of industry [1] – [9]. The development of non-conventional technological processes, in addition to their energy-saving advantages, make it possible to obtain new materials that are impossible to obtain by conventional technologies. In this regard, the contribution of powder metallurgy is significant [10] – [14].

The powder metallurgical technology allows obtaining up-to-date construction materials from which details can be made, the chemical composition and mechanical properties of which cannot be achieved by conventional methods. Such elements as copper, phosphorus, tin, etc., which are considered harmful impurities in conventional steels, are widely used in powder metallurgy [11], [15], [16].

Copper is an element that is not used in conventional metallurgy, but has a number of features that favor its use in powder metallurgy. The more important of them are:

- can be obtained in the form of powder by different technologies;
- the obtained copper particles can be of different shapes;
- has easily recoverable oxides;
- high plasticity, which facilitates pressing;
- lower melting temperature than iron, which causes sintering in the presence of a liquid phase, etc. [11], [12], [15].

Along with the mentioned advantages of copper, its addition in powder metallurgical samples leads to significant changes in their linear dimensions [11], [15].

In this regard, the aim of the present study is to track the change in linear dimensions after sintering of iron carbon powder metallurgical structural materials alloyed with 2.5% copper.

II. MATERIALS AND METHODS

In the research process, powder metallurgical samples of three types of iron powders produced by the company "Höganäs" - Sweden - NC100.24, SC 100.26 and ASC 100.29 were developed.

One of the most widespread iron powders obtained by the reduction method in the practice of powder metallurgy production is NC 100.24. The compactability of this brand of iron powder is very good, and thanks to the spongy structure of the particles, their formability is very high. The raw (after pressing) and final (after sintering)

Online ISSN 2256-070X
https://doi.org/10.17770/etr2025vol4.8439
© 2025 The Author(s). Published by RTU PRESS.
This is an open access article under the Creative Commons Attribution 4.0 International License.

strengths of parts from these powders are very high, and the hydrogen concentration in them is low.

The SC 100.26 type iron powder has the best compactability of all the sponge iron powders produced by the company "Höganäs" using the reduction method. This makes it particularly suitable to produce parts with a single pressing, to which there are requirements for higher density. Like the powder of the previous type, SC 100.26 also has a high raw strength, but a slightly higher density. It is used in the production of details that will later be subjected to chemical-thermal treatment.

Iron powder ASC 100.29 is a representative of the group of water-dispersed powders. Now it is the highest quality iron powder produced by the company "Höganäs". It is very clean. It can be compacted with great results, because the particles are almost spherical in shape. This allows, after a single pressing, to achieve a density of 7.2÷7.3g/cm^3. These powders are particularly suitable to produce structural products with high density, as well as for products with certain magnetic characteristics.

The mixture for the samples, in addition to iron powder, contains 0.2÷1.0% standard graphite powders brand UF - 4, with the carbon concentration in the range of 96÷97% and 2.5% electrolytic copper with a particle size of 63μm. The ingredients of the charge are placed in a non-metallic cylinder of a drum mixer with intersecting axes of rotation and 0.8% of the coating substance "Kenolube" is added. The resulting batch is homogenized for 20 minutes.

After mixing, the ingredients of a sample are weighed on electronic scales with accuracy of 0.001g. The mass is determined depending on the pressing effort and the desired density [13], [14]. The weighed powders are placed in the pressing matrix, the dimensions of which are 0.03÷0.07% larger than the dimensions of the sample bodies - ø25 h=20mm. The pressing was carried out bilaterally on a fast-acting press with an effort of 200÷800 MPa. This allows obtaining samples with a density in the interval 6.2÷7.0g/cm^3.

The samples were sintered in a laboratory horizontal muffle furnace with a "Carbolitte" ceramic tube in the presence of dissociated ammonia - NH3. – fig.1.

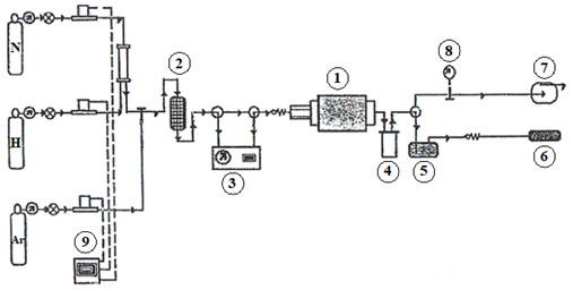

Fig.1. The sintering system;
1 – furnace; 2 - molecular dryer – sieve; 3 – hygrometer SHAW; 4 - separator plasticizer; 5 - oil valve; 6 – lighter; 7 - rotary vacuum pump; 8 - pressure gauge; 9 - computer (software MGF&PC).

The quantitative ratio of nitrogen and hydrogen in the working space of the crucible is 75%H_2 and 25%N_2. The sintering was carried out at a temperature of 1150°C for 1 h controlling the speed of the incoming gas and its dew point.

To prevent oxidation of the samples during the sintering process, closed ladles and backfill (75%Al_2O_3+15%FeMn+10%C) were used. The backfill helps to limit to a minimum the mass loss of the samples because of the oxidation of the iron powders at the high sintering temperatures.

The heating of the samples takes place in two stages:

- First stage - The samples are heated to 800ºC and kept at this temperature in order to separate the plasticizer - fig.1 position 4.
- Second stage - Heating continues at a rate of 10ºC/min until isothermal sintering temperature - 1150°C.

The dimensional changes of the studied samples - Δl, is determined in percentages as a ratio of the dimensions after pressing and after sintering.

III. RESULTS AND DISCUSSION

The experimental results for the three investigated brands of iron powders with different concentrations of carbon in them and density in the range of 6.2÷7.0g/cm^3 are presented in table 1, and their graphic interpretation in fig.2÷4, respectively, for an iron matrix of powders NC100.24; SC 100.26 and ASC 100.29.

TABLE 1 EXPERIMENTAL RESULTS

A

ρ, g/cm^3	**Δ l, %**				
	Fe	***Fe + C***			
		C, %			
		0,2	***0,4***	***0,6***	***0,8***
Iron powder type NC 100.24					
6,2	-0,14	-0,17	-0,13	-0,04	-0,01
6,4	-0,11	-0,15	-0,07	-0,01	+0,02
6,6	-0,09	-0,11	-0,02	+0,01	+0,05
6,8	-0,08	-0,09	0,00	+0,05	+0,07
7,0	-0,07	-0,03	+0,02	+0,08	+0,09
Iron powder type SC 100.26					
6,2	-0,14	-0,11	+0,01	+0,05	+0,08
6,4	-0,12	-0,10	0,00	+0,04	+0,08
6,6	-0,09	-0,09	0.00	+0,04	+0,07
6,8	-0,07	-0,07	-0,01	+0,03	+0,06
7,0	-0,06	-0,05	-0,01	+0,03	+0,06
Iron powder type ASC 100.29					
6,2	-0,21	-0,17	-0,15	-0,7	-0,02
6,4	-0,18	-0,16	-0,13	-0,05	-0,01
6,6	-0,16	-0,14	-0,10	-0,05	-0,01
6,8	-0,13	-0,10	-0,07	-0,03	0,00
7,0	-0,09	-0,08	-0,05	0,00	+0,01

B

ρ, g/cm^3	**Δ l, %**			
	Fe + C + 2,5% Cu			
	C, %			
	0,2	***0,4***	***0,6***	***0,8***
Iron powder type NC 100.24				
6,2	+0,22	+0,21	+0,18	+0,16
6,4	+0,22	+0,19	+0,17	+0,13

6,6	+0,21	+0,19	+0,15	+0,11
6,8	+0,21	0,18	+0,13	+0,09
7,0	+0,20	+0,16	+0,11	+0,08
Iron powder type SC 100.26				
6,2	+0,27	+0,25	+0,24	+0,19
6,4	+0,26	+0,24	+0,23	+0,18
6,6	+0,26	+0,23	+0,22	+0,18
6,8	+0,25	+0,22	+0,21	+0,17
7,0	+0,25	+0,21	+0,19	+0,17
Iron powder type ASC 100.29				
6,2	+0,50	+0,46	+0,37	+0,30
6,4	+0,49	+0,44	+0,35	+0,29
6,6	+0,47	+0,39	+0,32	+0,27
6,8	+0,45	+0,35	+0,30	+0,24
7,0	+0,42	+0,31	+0,29	+0,22

The values obtained during the measurements show that in the samples of pure iron after sintering, the change in the linear dimensions has a negative sign, therefore, a shrinkage of the samples is observed, which is of the order of -0.14÷-0.20% in samples with density 6.20g/cm^3. As the density of the samples increases to 7.00 g/cm^3, the internal porosity of the blanks decreases, and hence the possibility that the blanks undergo a large change in their dimensions during the coalescence of the powder particles. Therefore, in samples with high density, the change in dimensions decreases almost twice and is within the limits of -0.07÷-0.09%.

The addition of carbon to the matrix leads to a decrease in the compressibility of the blanks, but despite this, at a carbon concentration of 0.2%, the tendency for the dimensional change to be in the negative part remains. For samples containing 0.4%C and a density of 6.80g/cm^3 made of iron powder NC100.24, practically no changes in the linear dimensions of the blanks are observed. The same was found for samples of SC 100.26 iron powder with a density of 6.40÷6.60 g/cm^3. For samples made because of iron powder ASC 100.29, linear changes are not observed at a density of 7.00 g/cm3 and 0.6%C, and for samples with 0.8%C, the dimensions of the samples do not change at a density of 6.80 g/cm^3. Therefore, we can draw the conclusion that at low carbon concentrations - 0.2÷0.6%C, powder Fe-C samples decrease in size, like those made of pure iron. When the carbon concentration increases above 0.6%, however, a change in the linear dimensions of the samples is found in a positive direction - towards their growth. The concentration interval in which the powder metallurgical structural details of the Fe-C system will not suffer linear changes, or they will be insignificant - 0.4÷0.6%C.

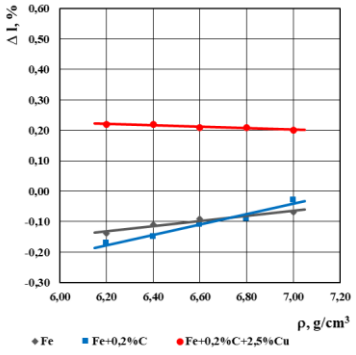

a.

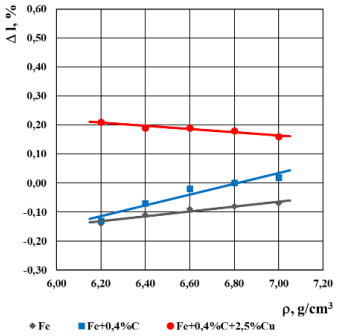

b.

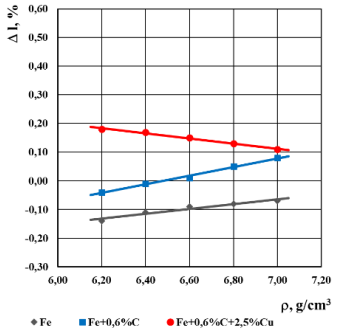

c.

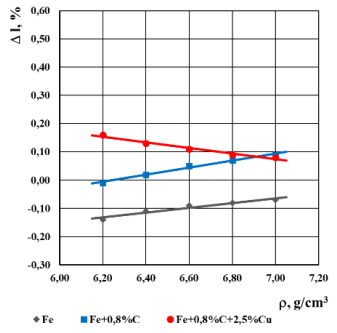

d.

Fig.2. Distribution of values for linear changes depending on density and the carbon concentration of NC 100.24 iron powder samples: a – 0,2%C; b – 0,4%C; c – 0,6%C; d – 0,8%C

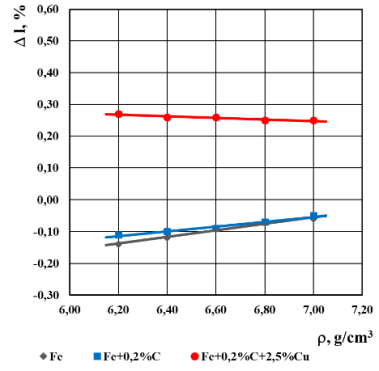

a.

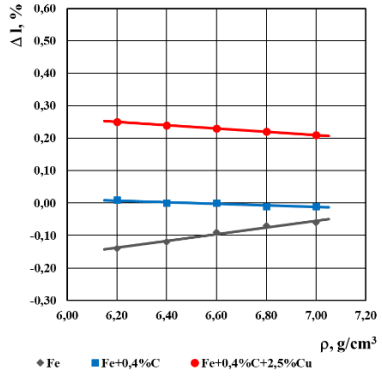

b.

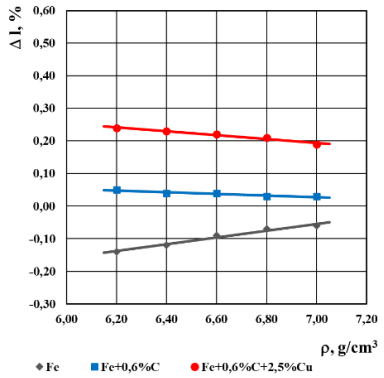

c.

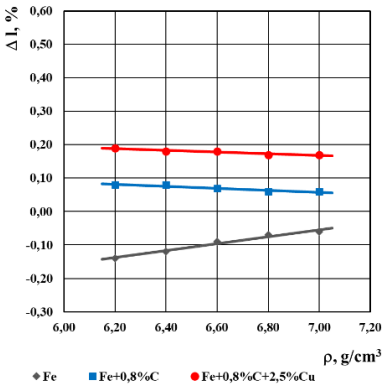

d.

Fig.3. Distribution of the values for the linear changes depending on the density and the carbon concentration of SC 100.26 iron powder samples; a – 0,2%C; b – 0,4%C; c – 0,6%C; d – 0,8%C

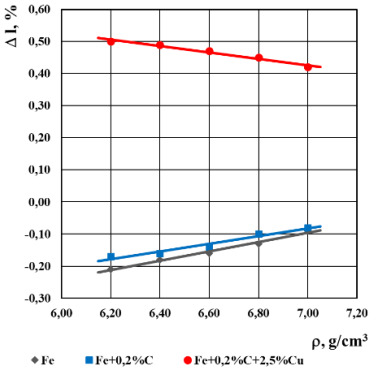

a.

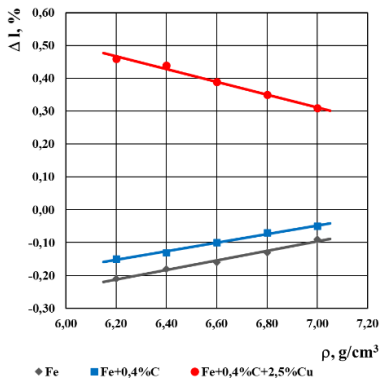

b.

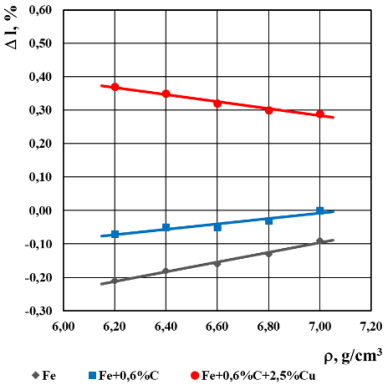

c.

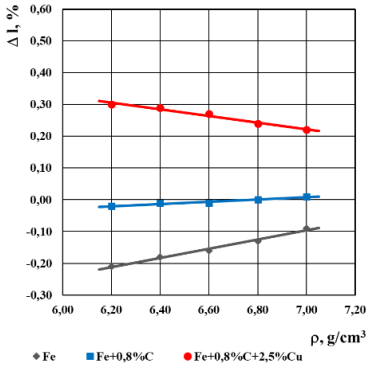

d.

Fig.4. Distribution of the values for the linear changes depending on the density and the carbon concentration of ASC 100.29 iron powder samples a – 0,2%C; b – 0,4%C; c – 0,6%C; d – 0,8%C

Copper is an element that leads to an increase in the size of powder blanks [11], [15], [16]. The copper melted in the sintering process penetrates the boundaries of the iron grains. This copper film replaces the hard boundaries between the grains, resulting in an expansion of the samples. In addition, the penetration of the liquid phase into the polycrystalline system leads to its destruction and its separation into individual grains. This can lead to expansion of the blanks in cases where the torn particles are irregularly shaped and cannot be compacted into the volume that encloses them. The copper in the sintering process dissolves in the iron particles, forming in the matrix an ε-phase (a solid solution of the iron in the copper), which in turn displaces the iron particles and causes an increase in the size of the blanks – fig.5.

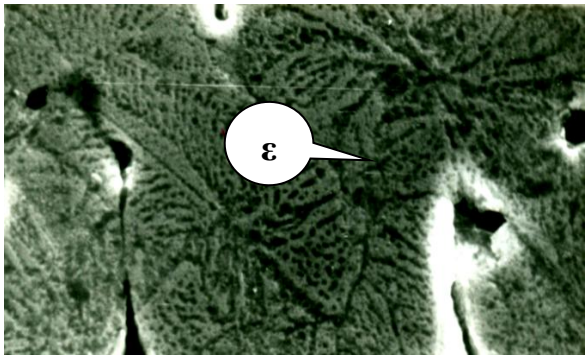

Fig.5. Location of the ε phase along the iron grain boundaries

It is for these reasons that in the samples with a minimum amount of carbon – 0.2%, a significant increase in the size of the blanks is observed, which is not affected by their density. For samples of iron powder NC100.24, this increase is in the range +0.20÷+0.22%, and for those from powder SC 100.26 it is +0.25÷+0.27%. The largest increase was recorded in samples of iron powder ASC 100.29 - +0.40÷+0.50%.

As the carbon concentration increases from 0.2 to 0.8%, a decrease in the size of the blanks is noticed, and those of iron powder NC100.24 undergo a change of +0.06÷+0.12%. In the case of SC 100.26 samples, the change in size growth is in the range of +0.05÷+0.08%, and in the case of ASC 100.29 samples - +0.20%.

This compensating influence of the carbon concentration on the „copper growth“ of the powder billets can be attributed to the fact that the carbon in the iron matrix prevents the penetration of the molten copper on the surface of the iron particles and this reduces its solubility in the iron. In addition, carbon is an element that reduces the diffusion coefficient of copper in iron [10,16] and increases the dihedral angle θ between iron grains and liquid copper – fig.6. This leads to an intensification of the sintering process in the presence of a liquid phase.

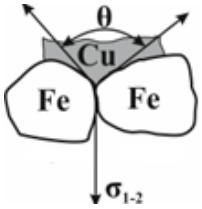

Fig.6. Scheme of the formation of the bilateral angle - θ, of the solid (Fe) / liquid (Cu) phase boundary

All these factors lead to limiting the size growth of copper-alloyed blanks

IV. CONCLUSION

The following more important conclusions can be drawn from the research conducted and the results obtained:

- After sintering of samples of pure iron, the change in linear dimensions has a negative sign, therefore a shrinkage of the blanks is observed, which in samples with a density of 6.20g/cm^3 is of the order of -0.14÷-0.20%;
- As the density of the samples increases from 6.20g/cm^3 to 7.00 g/cm^3, the internal porosity of the blanks decreases, and hence the possibility that the samples undergo a large change in their dimensions during the coalescence of the dust particles.
- The addition of carbon to the matrix leads to a decrease in the compressibility of the blanks, but despite this, at a carbon concentration of 0.2%, the tendency for the change in dimensions to be in the negative part remains.
- In small concentrations - 0.2÷0.6%, carbon leads to a reduction in the dimensions of the samples similar to those of pure iron. At a carbon concentration above 0.6%, however, a change in the linear dimensions of the samples in a positive direction - towards their growth - is found.
- The carbon concentration at which the details of the Fe-C system will not suffer linear changes or they will be insignificant is 0.4÷0.6%.
- During the sintering process, copper dissolves in the iron particles, forming an ε-phase (a solid solution of iron in copper) in the matrix. It displaces the iron particles and causes an increase in the size of the blanks.
- The compensating influence of the carbon concentration on the "copper growth" of the powder billets can be explained by the fact that the carbon in the iron matrix prevents the penetration of the molten copper on the surface of the iron particles and this reduces the solubility in the iron as well.

V.REFERENCES

[1] D. Petrova, B. Vlahova, A. Lengerov,Tz. Zlateva-Petkova, "Improvement of Constructive-Technological Approaches Reducing Innovative Obsolescence of Industrial Technologies in the Context of Industry 4.0", presented at the 14th International Scientific and Practical Conference on Environment, Technology, Resources, ETR 2023, Rezekne, Latvia, June, 2023, Volume I, pp. 180–186.

[2] D. Petrova, B. Vlahova, A. Lengerov, Tz. Zlateva-Petkova, "Study of the State of Innovation Development and Obsolescence in the Republic of Bulgaria of Companies from the Mechanical Engineering Sector", presented at the 14th International Scientific and Practical Conference on Environment, Technology, Resources, ETR 2023, Rezekne, Latvia, June, 2023, Volume I , pp. 187–194.

[3] D. Petrova, N. Nikolova, A. Lengerov, "Modeling business process reengineering in the digital era of industry 4.0", presented at the 11th International Scientific Conference "TechSys 2022" – Engineering, Technologies and Systems, 2022, pp. 070013-1 - 070013-7.

[4] D. Petrova, "Innovative Obsolescence in Mechanical Engineering and Singleness of Indicators", presented at the 15th International Scientific and Practical Conference on Environment, Technology, Resources, ETR 2024, Rezekne, June 2024, Vol. 3, pp 221 – 224.

[5] G. Karlovski et al., "Selection of Instrumentation Based on Statistical Analysis", presented at the 32nd International Scientific Symposium "Metrology and Metrology Assurance", MMA 2022, Sozopol, 7-11 September 2022.

[6] T. Kuzmanov, Hr. Metev, S. Parashkevov, Electrophysical and electrochemical technologies in mechanical engineering, EKS-PRESS, Gabrovo, 2005.

[7] S. Tsenkulovski, I. Mitev "Influence of the Parameters of the Lasser marking process of the depth of penetration in layer-reinforced composites", presented at the 15th ISPC "Environment Technology Resources", V.Turnovo, Bulgaria, 27 and 28 06.2024, Vol. 3, pp 319-324.

[8] I. Mitev, S. Tsenkulovski, "Local Processing of Non-Metal Materials with Concentrated Energy Flow", presented at the 14th International Scientific and Practical Conference on Environment, Technology, Resources, ETR 2023, Rezekne, Latvia, June, 2023, Volume 3, pp.183÷186.

[9] L. Sobotova., "Laser marking as environment technology.", Journal Open Engineering. Available: https://doi.org/10.1515/eng-2017-0030, [Accessed January 15, 2025]

[10] I. Mitev, Unconventional electrotechnological processes, EKS-PRESS, Gabrovo, 2020.

[11] I. Mitev, Copper in two-component powder metallurgical systems, EX-PRESS, Gabrovo, 2019.

[12] I. Miteva, I.Vinev, I.Mitev, "Features of Alloying Matrix of Water-dispersed Iron Powders", presented at the 13th International Scientific and Practical Conference on Environment, Technology, Resources, ETR 2021, Rezekne, Latvia, Volume 3, 2021, pp.226÷231.

[13] I. Miteva, et all., "Influence of the pressing force on the strength properties of sintered materials based on water-dispersed iron powders alloyed with cooper.", IJSTII "Machines technologies Materials", year XV, Issue 1/2021, pp. 34÷37

[14] I. Miteva, et all.**,** "Influence of the pressing force on the mechanical characteristics of an iron matrix of water dispersed powder alloyed with nickel", Journal of the Technical University of Gabrovo, Volume 63, 2021, pp.47÷50.

[15] I. Mitev, "Optimizing the quantity of liquid phase at the sintering of powder construction materials from system Fe-Cu-Sn", presented at AIP Conference, 2024, Vol. 2980, pp.060017-1÷060017-7.

[16] I. Mitev, "Determining the diffusion coefficient in simultaneous saturation with boron and carbon austenite alloyed with cooper in powder metallurgy structural materials", presented at AIP, vol. 2980, 2024, p.060016-1÷060016-7.

Environment. Technology. Resources. Rezekne, Latvia
Proceedings of the 16th International Scientific and Practical Conference. 2025. Volume IV, 251-256

Investment Activity of SMEs in the Furniture Industry in the Republic of Bulgaria

Neli Nikolova
Department "Management"
Technical university of Gabrovo
Gabrovo, Bulgaria
nik_nel@abv.bg

Desislava Petrova
Department "Management"
Technical university of Gabrovo
Gabrovo, Bulgaria
des_petrova@abv.bg

***Abstract*— The article presents data from a survey conducted in 26 furniture companies in the country in the period 2023 - 2024. The aim is to diagnose the main limiting factors affecting their functioning; to obtain information about their investment activity for analysis and assessment of the management of the investment process in SMEs by identifying problem areas. The method used is a questionnaire survey among line and functional managers. Conclusions are formulated about the investment needs of the surveyed enterprises..**

Keywords*— *investment activity, investment projects, furniture SMEs, limiting factors.

I. INTRODUCTION

Investments are an essential factor for the development of any company, and investing is an important activity in the overall business process. In practice, due to the limited capital resources, owners often have to choose one or another sphere of activity, area or object of investment. Making the right investment decisions depends on the knowledge, competences and skills of managers. Making investments to provide new fixed assets has a long-term impact on the production process [1].

Furniture production is one of the traditional economic sectors for Bulgaria with a history that goes back far back in time. The first large furniture factory was established two centuries ago, but long before that, domestic furniture was famous for its quality and skillful workmanship. Our country ranks 21st in Europe in furniture production, with production worth 614 million euros in 2023. The furniture industry in the Republic of Bulgaria is famous for its excellent price/quality ratio, which makes it a preferred partner for Western European companies. Over 85% of production is exported, and according to some analysts, this percentage reaches 90.

The purpose of the study is to obtain information about the investment activity of small and medium-sized enterprises in the country by analyzing the management of the investment process in them, identifying problem areas, and outlining the prospects for sustainable development and higher investment activity [2].

II. MATERIALS AND METHODS

For the purposes of the study, the following approaches and methods were used: literature research and analysis; comparative analysis; graphic and tabular methods. methods of analysis and synthesis, surveys, interviews, statistical methods for analyzing interrelationships. Expert assessments published in numerous specialized publications, scientific reports, macroeconomic analyses, statistical reference books, annual reports, strategies and results of survey studies were also used. The data are from official publications of the Ministry of Finance (MoF), the National Statistical Institute (NSI), the Institute of Market Economy (IME), the Executive Agency for the Promotion of Small and Medium-sized Enterprises (ESME), the Branch Chamber of the Woodworking and Furniture Industry (BCWFI), etc.

According to NSI data, production in Bulgaria related to this sector in Europe and the world has recorded a 25.4% growth. Only three countries on the Old Continent – Bulgaria, Latvia and Italy – have managed to achieve over 25% growth in furniture. Chairs, upholstered furniture with a lot of manual labor, mattresses – these are just some of the industries in which Bulgarian companies have proven themselves. There is specialization in furnishing shops and showrooms of famous brands all over the world. High-class hotels are also being furnished. In some of the production segments, a serious contraction in orders is already being reported. Among the reasons are the lack of raw materials and the increase in the price of materials and energy carriers. Our country is in 19th place in Europe in furniture exports. The main export

Online ISSN 2256-070X
https://doi.org/10.17770/etr2025vol4.8436
© 2025 The Author(s). Published by RTU PRESS.
This is an open access article under the Creative Commons Attribution 4.0 International License.

destinations are Romania, Greece, France, Germany, the Czech Republic, Italy, the Netherlands and the United Kingdom [3].

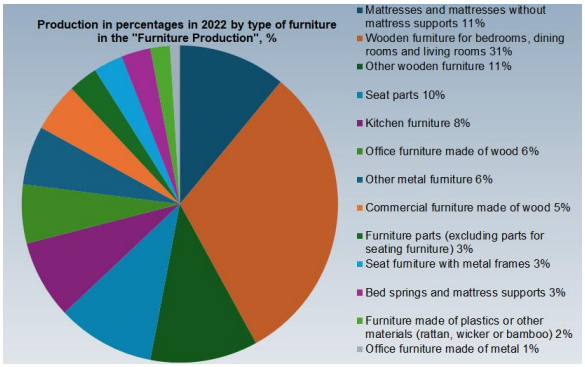

Fig. 1. Production in percentages in 2023 by type of furniture in the "Furniture Production" sector, Source: Chamber of Commerce of Wood and Furniture Industry (CCWFI).

As a type of furniture, the largest share in the manufactured output is made up of bedroom, dining room and living room furniture (31%), mattresses (11%), other wooden furniture (11%), parts for seating furniture (10%), kitchen furniture (8%) and others.

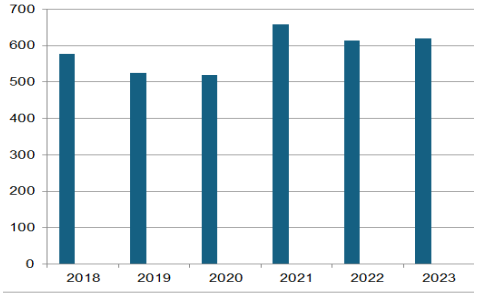

Fig. 2. Furniture production in Bulgaria (2018 – 2023), million EUR, Source: Chamber of Commerce of Wood and Furniture Industry (CCWFI).

In 2023, the employed in the "Furniture Manufacturing" sector accounted for 4.5% of the employed in the manufacturing industry, and the share of their net turnover was about 2% of the net turnover in the industry. The enterprises in the sector are mainly micro (from 0 to 9 employees) and small (from 10 to 49 employees), representing nearly 98% of all enterprises in the sector. The share of medium-sized enterprises (from 50 to 249 employees) is 2%, and of large enterprises (with 250 and more employees) - 0.4%. The employed in micro- and small enterprises occupy a share of 55% (respectively 25.7% for micro- and 29.4% for small enterprises), the share of the employed in medium-sized enterprises is 21.1%, and in large enterprises - 23.7%. Large enterprises account for 36.7% of the net turnover in the sector, medium-sized enterprises account for 23.6%, and micro and small enterprises account for 39.7% [4].

TABLE 1 EMPLOYEES AND NET TURNOVER IN THE "MANUFACTURE OF FURNITURE" SECTOR BY ENTERPRISE GROUPS ACCORDING TO THE NUMBER OF EMPLOYEES IN THEM FOR 2022,SOURCE: EUROSTAT

Indicators	Group of companies					
	0 to 9	10 to 19	20 to 49	50 to 249	250+	Total
Employees, number	5 592	2 774	3 637	4 606	5 172	21 781
Net turnover, million EUR	129,5	84,0	134,9	207,3	321,6	877,3

The following graph shows that the main group for which investments are made in training is the 18-26 year old group. The reason for this is the insufficient adequacy of the curricula and the lack of real practical training of graduates of specialized educational institutions. A problem for companies in the furniture industry is the very low commitment and willingness of employees to participate in training to improve their qualifications or to improve their knowledge and skills [5].

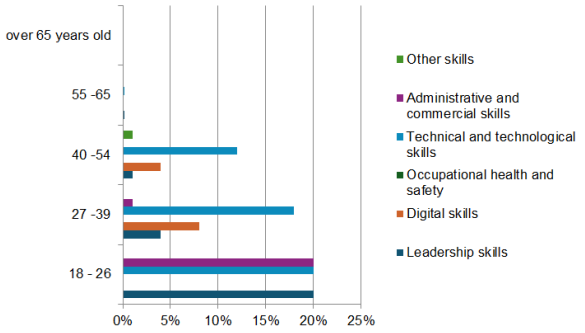

Fig. 3. Personnel training conducted (2022 - 2023) - by age group in percentages - in the "Furniture Production" sector.

The industry has the potential to develop a circular economy. An important direction is the recycling and reuse of materials, associated with appropriate technologies, a lot of investment, time and targeted efforts towards changes in the utilization of materials. Companies from the industry, pressured by high energy prices, are building their own photovoltaic power plants on the roofs of their enterprises in order to cope with the energy crisis and price pressure on their own [6].

More and more companies in the furniture industry are investing in the construction of photovoltaic power plants. According to data from the Chamber of Woodworking and Furniture Industries (CWFI), companies in the industry are turning to such projects to cover their own electricity needs, but also to meet the requirements for transitioning to a circular economy and reducing their carbon footprint. Geopolitical events and the unstable external environment present SMEs in the Bulgarian furniture industry with serious challenges and the need to seek options to cope with the high and unpredictable costs of electricity and gas [7].

Digitalization and automation, improving the qualifications of those employed in the sector will provide prospects in the competitive race. The Bulgarian furniture industry is an example of innovation, modernization, optimization of production and implementation of

robotization, with high-quality production, highly valued in Europe and around the world [8]. However, the industry is struggling with the lack of wood and raw materials. Furniture industry enterprises in Bulgaria employ 50,000 people in small settlements located next to the raw material. The Bulgarian furniture industry is a sector with very serious traditions, which produces mainly for export. Over 80% of furniture production in Bulgaria is mainly directed to Western Europe. One of the advantages of Bulgarian SMEs, which makes them preferred by Western partners, is their exceptional flexibility. They are ready to respond extremely quickly to changing requirements. Value-added production, export development, modernization, adoption of new technologies and the concept of Industry 4.0 – this is the modern image of Bulgarian furniture production [9].

A key stage in achieving the main objective of the report is the application of SWOT analysis, with the help of which the investment climate is outlined in a synthesized form, used to identify the problem areas in the investment management of furniture companies such as [10 - 11]:

- influence of the environment;
- presence of investment activity,
- financing of investments;
- development of investment strategies;
- information and personnel security in the investment process;
- development activity and innovations in companies from the furniture industry.

The analysis of the factors affecting the investment management of furniture companies is structured into three groups, distinguished as follows [12]:

- analysis of external environmental factors with indirect impact;
- analysis of external environmental factors with direct impact;
- internal systemic analysis of enterprises.

TABLE 2 SWOT ANALYSIS OF THE FURNITURE INDUSTRY IN REPUBLIC OF BULGARIA

Opportunities	Threats
▫ attracting foreign investments ▫ taking advantage of the advantages of EU membership ▫ increasing investment in exports ▫ investing in technologies that reduce the use of materials ▫ investing in energy-saving production ▫ investing in reducing the harmful impact of production ▫ investing in personnel training ▫ investing in R&D, interaction between scientific organizations and business ▫ increasing innovation activity	▫ global economic crisis ▫ danger of deflationary pressure ▫ legislative restrictions ▫ political instability ▫ corporate indebtedness ▫ weak investment activity ▫ difficulties with financing investments ▫ mismatch between the demand and supply of labor ▫ strong competitive pressure from foreign companies on the Bulgarian and international markets
Strengths	**Weaknesses**
▫ traditions in production ▫ qualified workforce ▫ sufficient quantities of cheap local raw materials and energy ▫ low labor costs ▫ flexibility and quick response to market needs ▫ good technological equipment in a large part of the enterprises in the sector ▫ branch organization, contacts with international organizations ▫ export orientation of the sector	▫ lack of long-term strategies ▫ strong dependence on a small number of customers (markets) ▫ insufficient knowledge in the field of marketing and management ▫ weak innovation activity ▫ low degree of internationalization, poor knowledge of good practices ▫ insufficient investment in development and personnel ▫ need for product reorientation, use of modern materials and changes in furniture design ▫ insufficient reliable and consistent product quality

TABLE 1 INDICATORS FOR STUDYING THE STRATEGIC MANAGEMENT OF INVESTMENTS IN FURNITURE COMPANIES

Environmental influence	Firms' reaction to changes in the external environment
	Factors limiting the investment activity of firms
Investment	Investment structure
Financing of investments	Investment Financing Structure
	Investment Financing Sources
Investment strategy	Development of investment strategies in companies
	Methods for economic evaluation of investments
	Discount rate
	Risk assessment in investment projects
Information security	Sources of investment ideas
Staffing	Making a decision to invest in companies
	Organization of the investment process
Development/Innovation	Generating ideas for investing in companies

The conducted surveys provide an opportunity for practical verification of the existing problems in investment management, related to the level of competence and training of the management team, the lack of systematicity and strategic orientation in the investment process in furniture companies, and the existence of a relationship between the size of the companies and the way in which their investment management is carried out [13].

III. RESULTS AND DISCUSSION

A survey was conducted in 26 leading small and medium-sized enterprises in the sector, selected by the criterion of volume of production, forming the image of the furniture industry in Bulgaria [14]. The analysis of the

results of the survey was carried out on the basis of summarized information about the companies. A purposive sample of 26 companies in the furniture sector, selected by the criterion of sales volume for the period 2018 - 2023, was observed. Comparisons were made between the answers given by them. The distribution of the companies into three groups, according to their size, is as follows:

- medium (over 100 employees) - 10 pcs.;
- small (between 51 and 100 employees) - 8 pcs.;
- micro (up to 10 employees) - 8 pcs.

The comparison was carried out in order to derive a relationship between the size of the companies and the investment management they conduct. The questions included in the questionnaire at this stage of the study are systematized in the following groups: Main characteristics of the surveyed companies;

- Influence of the environment on the activities of companies;
- Investment activity of furniture companies;
- Management of investments in furniture companies.

Based on the comparative analysis, regularities are derived regarding the management of investments in furniture companies. The reaction of enterprises to the external environment during the period under review is that they rather try to adapt to changes. Only about 1/3 of them express readiness for bolder investment decisions (Fig. 4).

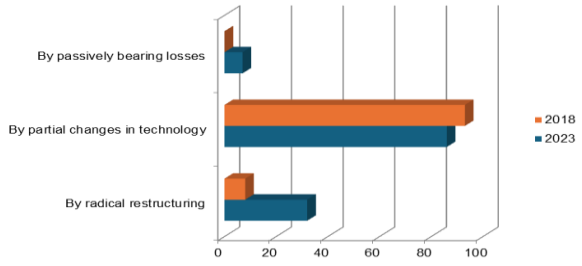

Fig. 4. Reaction to the external environment

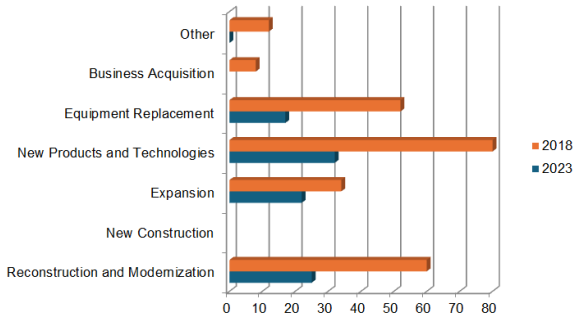

Fig. 5. Investment structure

The structure of investment financing shows that the share of financing with own funds is predominant compared to that of financing with attracted capital (Fig. 6).

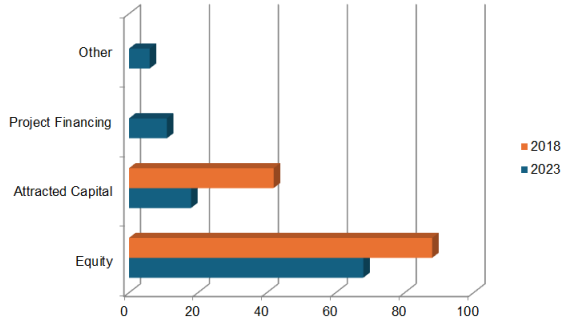

Fig. 6. Financing Structure

The limiting factors for the investment activity of companies are more likely to be associated with internal weaknesses of the companies than with the negative influence of the external environment (Fig. 7).

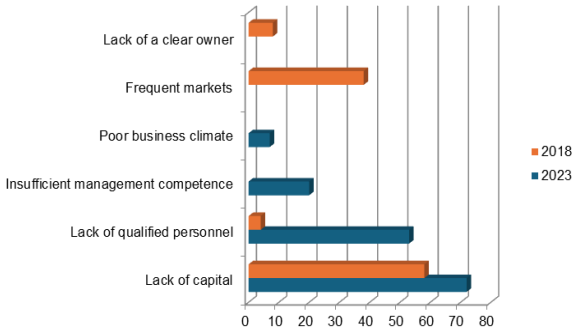

Fig. 7. Factors limiting the investment activity of companies

The results of the analysis show that investment ideas come almost entirely from managers and owners. They are significantly less frequently proposed by middle management in companies (Fig. 8).

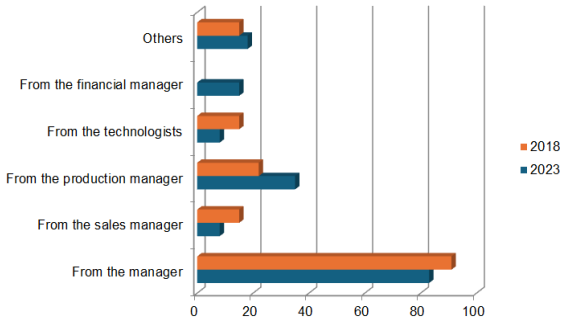

Fig. 8. Comparison of results on the question: who are the generators of ideas for investing in the furniture industry in 2018 and 2023

Regarding the sources of investment ideas:

- in the first place are visits to fairs, exhibitions and scientific conferences;
- in the second place – contacts with customers, distributors, suppliers, etc.;
- in the third place – observations of competitors' activities.

Publications in specialized publications are used much less frequently. The number of companies with their own R&D unit is insignificant (Fig. 9).

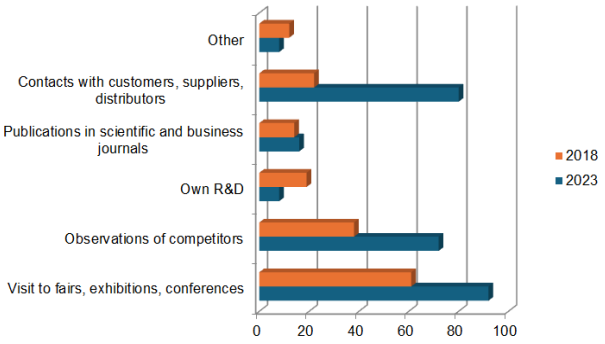

Fig. 9. Sources of investment ideas

Most often, the organization is not assigned to any specific unit in the companies, but is decided for each individual investment case. The results of the analysis show a lack of independent investment units in the furniture companies for the period studied (Fig. 10).

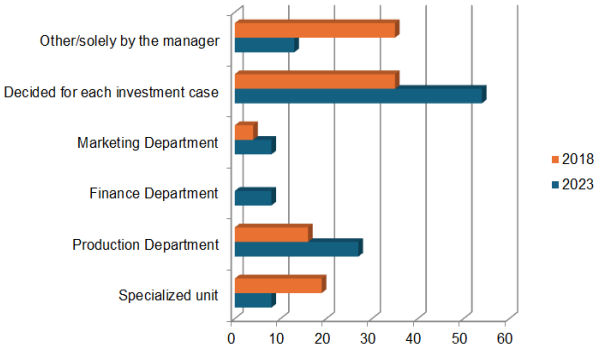

Fig. 10. Which unit organizes the investment process on company

The majority of the surveyed line and functional managers in furniture companies in our country carried out current and follow-up control over the implemented investment projects present on Fig. 11 and Fig. 12.

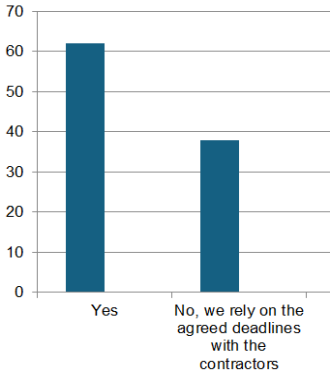

Fig. 11. Control over the progress of investment projects

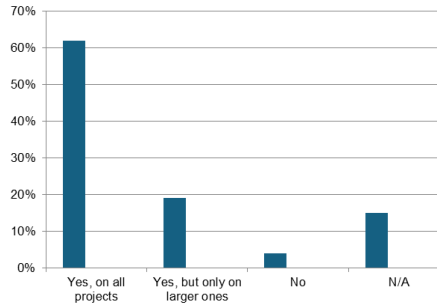

Fig. 12. Post-investment control over projects

IV. CONCLUSIONS

The conducted research shows the presence of serious management gaps and errors in the investment management of furniture companies in each phase of the investment process and in each of the functions performed in the management process - in the planning, organization and control activities. Improving investment management in furniture companies is also related to the need for a more in-depth knowledge of the environment, which requires a wider use of marketing information in the process of making investment decisions. Managers of furniture SMEs encounter difficulties in planning investments, determining their economic efficiency, as well as assessing the risk of investment. There is a need for a wider use of dynamic methods for investment analysis and increasing the burden of risk assessment. One of the permanent tasks of management in companies should be to create opportunities for training specialized personnel through participation in specialized courses; scientific conferences and external training on issues related to investment management. The implementation of investment decisions of strategic importance for enterprises in the furniture industry depends on their future sustainable development. For this reason, it is of utmost importance to:

- Create units or attract specialists in companies with the necessary knowledge and competencies in the investment field;
- Provide broader opportunities for staff participation in the process of generating investment ideas with the assistance of scientific institutes and universities;
- Strengthen ongoing control. For smaller projects, it is appropriate to apply linear schedules, and for more complex ones - network schedules, which cover all stages of the investment process.

REFERENCES

[1] G. Chipriyanova, Atanasov, A., Krasteva-Hristova, R., Environmental Management for Sustainable Business in Chemical Industry in Bulgaria, Vide. Tehnologija. Resursi - Environment, Technology, Resources, Volume 1, Pages 95 – 101, 2024, 15th International Scientific and Practical Conference on Environment. Technology. Resources, ETR 2024, Rezekne, 27 June 2024 through 28 June 2024, Code 201245, Conference Proceedings, ISSN 16915402, ISBN 978-171389957-0, DOI 10.17770/etr2024vol1.7971.

[2] N. Nikolova, Development of a System for Assessment of Digital Professional Suitability in the Company Environment, Vide.

Tehnologija. Resursi - Environment, Technology, Resources, Volume 3, Pages 211 – 216, 2024, 15th International Scientific and Practical Conference on Environment. Technology. Resources, ETR 2024, Rezekne, 27 June 2024 through 28 June 2024, Code 201245, Conference Proceedings, ISSN 16915402, ISBN 978-171389957-0, DOI 10.17770/etr2024vol3.8136.

[3] D. Petrova, An Alternative Approach to Reducing Aging of Innovative Industrial Products in Terms of Industry 4.0, Environment. Technology. Recourses – Proceeding of the 13-th International Scientific and Practical Conference, Rezekne Academy of Technologies, Rezekne, Latvia, 2021, ISSN 1691-5402, Online ISSN 2256-070X, https://doi.org/10.17770/etr2021vol3.6507 p. 274-280, scopus

[4] G. Chipriyanova, Chipriyanov, M., Luchkov, K., Investigation and Analysis of Attitudes Towards the Implementation of Artificial Intelligence in Internal Business Processes, Vide. Tehnologija. Resursi - Environment, Technology, Resources, Volume 2, Pages 61 – 67, 2024, 15th International Scientific and Practical Conference on Environment. Technology. Resources, ETR 2024, Rezekne, 27 June 2024 through 28 June 2024, Code 201245, Conference Proceedings, ISSN 16915402, ISBN 978-171389957-0, DOI 10.17770/etr2024vol2.8032.

[5] N. Nikolova, N., Human Capital in the Changing Work Environment of Industry 4.0, Vide. Tehnologija. Resursi - Environment, Technology, Resources, Open Access, Volume 3, Pages 187 – 193, 2023, 14th International Scientific and Practical Conference on Environment. Technology. Resources, ETR 2023, Rezekne, 15 June 2023 through 16 June 2023, Code 191610, DOI: https://doi.org/10.17770/etr2023vol3.7177

[6] I. Balabanova, Georgiev G., "Image Recognition by FFT, Artificial Intelligence and k-Nearest Neighbors Approach". IOP Publishing, Journal of Physics: Conference Series - EEPES'22, vol. 2339, pp. 1-8, 2022.

[7] D. Petrova, Intelligent, Innovative and Sustainable Industry in Bulgaria – prospects and challenges, Vide I. Tehnologija. Resursi - Environment, Technology, Resources, Proceeding of the 12th International Scientific and Practical Conference „Environment. Technology. Resources", June 20-22, 2019, Rezekne, Latvia, Volume I, pp. 210-215, ISSN 1691-5402 – print, ISSN 2256-070X – online. https://doi.org/10.17770/etr2019vol1.4188

[8] D. Petrova, Vlahova, B., Lengerov, A., Zlateva-Petkova, T., Study of the State of Innovation Development and Obsolescence in the Republic of Bulgaria of Companies from the Mechanical Engineering Sector, Vide. Tehnologija. Resursi - Environment, Technology, Resources, 2023, 1, pp. 187–194, DOI: https://doi.org/10.17770/etr2023vol1.7239 , https://www.scopus.com/authid/detail.uri?authorId=56323816400

[9] N. Nikolova, Entrepreneurial "Blue" Practices for Sustainable Development and Resources Efficiency, 12th Inter-national Scientific and Practical Conference "Environment. Technology. Resources", June 20-22, 2019, Rezekne Academy of Technologies, Rezekne, Latvia, Volume I, 198-203, ISSN 1691-5402, ISSN 2256-070X.

[10] J. Sunbi, Gallina A., Contemporary Management of Innovation: Are We Looking at the Right Things?, USA, 2019.

[11] M. Schillings, Strategic Management of Technological Innovation, Ravi Shankar, Edition: 6, 2019.

[12] S. Mumtaz, A. Alsohaily, Z. Pang, A. Rayes, K. F. Tsang and J. Rodriguez, 'Massive Internet of Things for Industrial Applications: Addressing Wireless IIoT Connectivity Challenges and Ecosystem Fragmentation', IEEE Industrial Electronics Magazine, vol. 11, no. 1, pp. 28-33, March 2017.

[13] H. Klaus, F. Hetzelt, P. Hofmann, A. Blecker and D. Schwaiger, 'Challenges and Solutions for Industry-Grade Secure Connectivity', 2019 International Conference on Networked Systems (NetSys), Munich, Germany, 2019.

[14] G. Chipriyanova, Marinova, M.., Technological Aspects of Accounting Automation System as a Decision Support System, Vide. Tehnologija. Resursi - Environment, Technology, Resources, Open Access, Volume 2, Pages 28 – 33, 2023, 14th International Scientific and Practical Conference on Environment. Technology. Resources, ETR 2023, Rezekne, 15 June 2023 through 16 June 2023, Code 191610, DOI: https://doi.org/10.17770/etr2023vol2.7309 .

Environment. Technology. Resources. Rezekne, Latvia
Proceedings of the 16th International Scientific and Practical Conference. 2025. Volume IV, 257-263

Selection of Materials Using Multicriteria Decision Making. a Case Study on Cellular Materials

Jekaterina Niktina
Riga Technical University
Rīga, Latvia
jekaterina.nikitina@rtu.lv

Viktors Mironovs
Riga Technical University
Rīga, Latvia
viktors.mironovs@rtu.lv

Irina Voronova
Riga Technical University
Rīga, Latvia
irina.voronova@rtu.lv

Vladimirs Šatrevičs
Riga Technical University
Rīga, Latvia
vladimirs.satrevics@rtu.lv

***Abstract*— In recent years, many companies have been striving to transition towards a sustainable, circular economy, focusing on the efficient use of materials and environmental protection. This has become a strategic necessity. One promising approach is the replacement of traditional sheet metals with cellular metal materials, such as perforated metal sheets, expanded metal, welded picket fences, and woven wire mesh. This substitution offers both environmental and economic benefits, while also supporting eco-technological innovations in regional industries. To evaluate the applicability of specific cellular metal materials, several factors must be considered, including the potential for weight reduction, noise reduction, and other environmental impacts. This article presents a multi-criteria decision-making methodology applied to the category of cellular materials, using the example of a perimeter fence in an urban environment. It provides a detailed overview of the types of materials, production methods, and the most significant factors of advantage. The main objective is to highlight the benefits of cellular materials. The primary objective is to highlight the benefits of cellular materials. A group expert assessment method was employed in this study. Findings indicate that perforated metal materials are most popular in properties to Cellular Materials (CMs). However, experts assess that CMs offer unique advantages in construction, design, and environmental sustainability compared to braided or expanded alternatives.**

Keywords* — *Assessment, benefits, cellular materials, circular economy, environmental sustainability, manufacturing efficiency, perforated materials, raw materials.

I. INTRODUCTION

In the industrial world, sustainability is gaining in importance, and it is the main issue in research and development regarding manufacturing. Looking for higher resource efficiency and lightweight components results in a continuously increasing use of parts made by additive manufacturing and cellular materials [1].

Recent technological advances have led to an increased availability of production processes for a wide range of cellular metals and alloys. In contrast to many of the materials available before, cellular metals, which can be produced nowadays, are less expensive, therefore being suited for wide-ranging applications in mass markets [2]. Studies on the application of cellular structures have progressed and have been applied in various fields, including vehicles, aircraft industries, and even military applications [3].

Characteristics of sustainable production are therefore efficient for use of lightweight products made from metal, e.g. cellular metal, by providing cheaper resources, reduced waste generation and pollution and enhanced resilience [4]. The additive manufacturing process is a suitable technology to meet the demand for resource efficiency. Due to the principle of placing material only at locations where it is needed, additive manufacturing reduces the material consumption during manufacturing and the energy consumption during the lifetime of vehicles and aircraft. The localised production minimises transport, and hence emissions are reduced.

Online ISSN 2256-070X
https://doi.org/10.17770/etr2025vol4.8461
© 2025 The Author(s). Published by RTU PRESS.
This is an open access article under the Creative Commons Attribution 4.0 International License.

The property profile exhibited by cellular metals identifies several applications, especially in technologies requiring multifunctionality. Their specific property attributes suggest implementation as: ultralight panels/shells, energy absorbing structures and heat dissipation media, as well as for vibration control. Connections between the properties that govern these performance benefits and the cellular architecture, cell morphology and density have been made. Cellular metals are engineered structures that use significantly less base material by introducing voids in the form of pores or perforations. This not only reduces the overall consumption of materials but also aligns with resource-efficient design strategies [5].

From an ecological-economic standpoint, the adoption of cellular metals contributes to:

- Reduced material extraction and associated environmental degradation, as cellular structures require significantly less raw material compared to solid sheets, which reduces mining and processing impacts [2].
- Lower energy consumption during production, transportation, and operation, due to the lightweight nature and reduced volume of material used [6].
- Enhanced recyclability and reuse potential in product life cycles, as metallic foams and perforated metals can be reprocessed similarly to conventional metals, often with fewer sorting requirements [7].
- Lower production costs over time, particularly in high-volume sectors such as automotive, aerospace, and construction, due to material efficiency and streamlined logistics.
- These outcomes align with regional sustainability goals while promoting green industry development, especially in resource-constrained or environmentally sensitive regions [8].
- The integration of cellular metal technologies within regional industries supports ecotechnological innovation by enabling their use in:
- Renewable energy systems (e.g., heat exchangers, solar collectors) due to high thermal conductivity and lightweight design.
- Building envelopes and facades, improving energy efficiency while reducing structural load.
- Sustainable mobility solutions, where weight reduction contributes to energy savings and emissions reduction [8].

Moreover, the design flexibility of cellular metals allows for local adaptation and supports decentralised manufacturing models, such as additive manufacturing or closed-loop recycling, which enhance regional techno-logical resilience and reduce dependency on global supply chains.

Incorporating cellular metals into regional development strategies reflects a systemic approach to sustainable growth, as it:

- Encourages smart specialisation in green material science, aligning with the EU's Smart Specialisation Strategy (S3), which promotes innovation-led growth tailored to regional strengths, including clean and advanced materials [9].
- Stimulates eco-industrial clusters and innovation hubs, fostering collaboration between research institutions, manufacturing sectors, and clean-tech start-ups — key components of regional resilience and sustainable industrial policy.
- Aligns with regional climate neutrality targets and investments in green infrastructure, as emphasised in the European Green Deal and Just Transition Mechanism, both of which advocate for climate-resilient, low-carbon regional economies supported by eco-innovation and sustainable materials.

These strategies are especially relevant for regions aiming to participate in major policy frameworks such as the European Green Deal, the Just Transition Mechanism, and the UN Sustainable Development Goals. Replacing traditional sheet materials with cellular metal structures—such as perforated or foam metals—offers a strategic advantage in regional development by reducing the use of critical raw materials, lowering environmental impact, and enhancing material efficiency. This shift supports ecological-economic goals by promoting resource conservation, lowering emissions in production and transport, and enabling cost-effective manufacturing. At the same time, it drives ecotechnological innovation, encouraging the development of advanced, sustainable materials and production methods. Integrating such technologies strengthens regional resilience, supports green industrial growth, and aligns with broader goals of the circular economy and climate-neutral development.

Modern construction and mechanical engineering demand new materials that are both lighter and stronger. Among these, cellular materials are gaining prominence.

As for the manufacturing methods of the periodic cellular metal, Wadley et al. [10] - [13] have been conducting research in this field for many years. Specifically, Wadley [13] gave an overview of various cellular metals manufacturing, and subsequently he also introduced various manufacturing processes for the periodic cellular metal, including honeycomb, corrugated topologies, lattice truss structures and so on. The development of new composite CMs is advancing rapidly [14], with their most practical applications emerging in construction and architecture [15].

Particularly noteworthy is the group of materials comprising four main types: wicker, perforated, expanded, and cellular flooring (see Fig. 1), which are produced in the largest volumes.

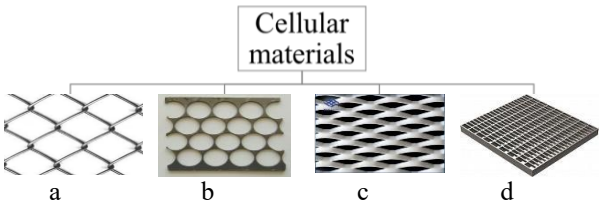

Fig. 1. Types of cellular materials: a) wicker; b) perforated, c) stretched; d) cellular flooring.

They are used in the fabrication of barriers, filters for construction materials, concrete reinforcement, protective screens, and more (see Fig. 2). All these types of cellular materials share a key advantage: they are significantly lighter than solid materials. However, selecting the most suitable material for specific purposes requires evaluating additional factors, such as cost-effectiveness, load resistance, durability, recyclability, and other properties.

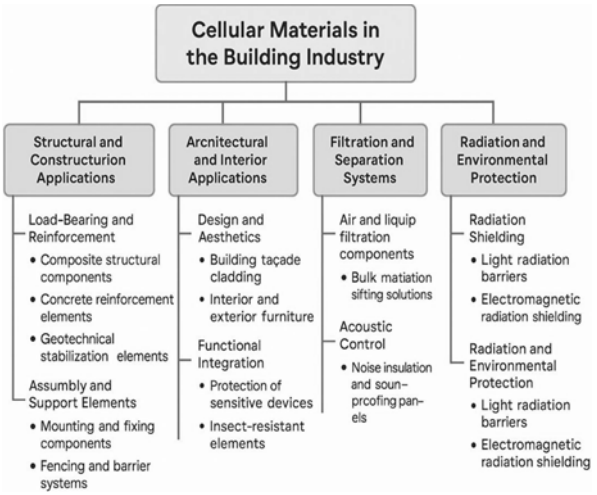

Fig. 2. Main areas of application of cellular materials for the building industry.

On 5 January 2023, the Corporate Sustainability Reporting Directive entered into force. Similar initiatives aiming to contribute to the transition toward a more circular economy are increasingly numerous. Cellular woven structures (CWS) are composed of aluminium or steel wires with diameters typically ranging from 0.5 to 5.0 mm (see Fig. 3). The weaving process results in the formation of cells of various sizes and shapes. For instance, aluminium CWS are frequently utilised in contemporary interior design across a variety of applications. In the construction sector, plaster mesh—constructed from galvanised or PVC-coated wire—finds widespread use. Additionally, CWS are employed in the sifting of loose materials, the filtration of solutions, and are commonly incorporated in the manufacturing of fences, enclosures, and other types of barriers [16].

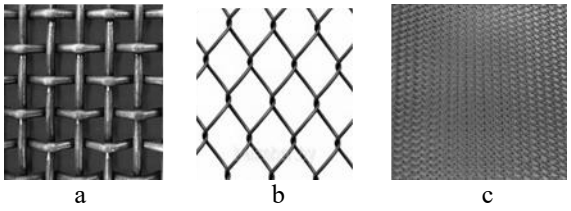

Fig. 3. Metal wire cellular woven structures: for a) interiors; b) fencing; c) damping.

Cellular woven meshes (CWM) are produced from galvanised, non-galvanised, and stainless steel. Galvanised steel mesh is known for its durability and reliability. It has high strength and is resistant to moisture, harsh environments, and temperature fluctuations, making it ideal for use in fences, barriers, and screens (see Fig. 4) [17]. This type of mesh is also used as a sieve to separate fine particles from bulk construction materials. For woven meshes, low-carbon steel wire with a thickness of 0.6 to 2.0 mm is typically used [18], [19].

CWM is widely applied in construction and finishing work, such as reinforcing plaster layers. It is also used for various other tasks, including separating sections of concrete structures during sequential concrete pouring, screening materials (such as limestone or gravel) under foundations, creating drainage layers, filtering bulk construction materials and gaseous mediums, and constructing lightweight barriers [20].

Fig. 4. Cellular woven mesh.

Welded wire meshes are also utilised in construction. The most practical option from a technological perspective is the mesh with square or rectangular openings, produced through the contact welding method (see Fig. 5).

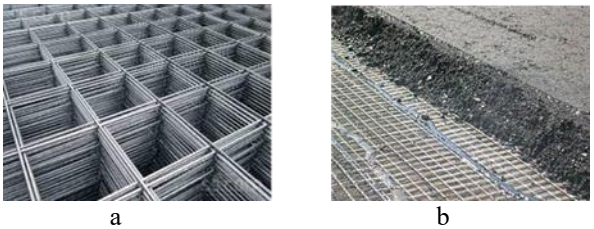

Fig. 5. Welded wire mesh (a) and its use in road construction (b).

The primary applications of CWS include partitions, building facades, and machinery enclosures. From industrial to commercial uses, wire mesh is a versatile metal product with limitless potential. Often overlooked as a facade solution, wire mesh offers numerous advantages and features when used to create screens. These qualities make it a viable construction material [21].

A. Cellular metal materials advantages

The application of cellular metal materials in construction, design, and environmental protection requires numerous benefits and advantages to be selected through the development of materials, and the production and end-user qualities, e.g. against noise, light, and electromagnetic radiation [11].

Another significant advantage of perforated metal materials (PMM) is their capacity to facilitate innovative design solutions [15].

Furthermore, CM has great potential for manufacturing components of ventilation systems [22]. These materials not only ensure reliable ventilation but also protect against insects that may enter through the ventilation openings (see Fig. 6).

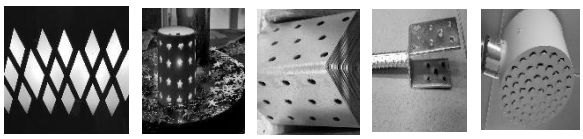

a b c d e

Fig. 6. Applications of PMM in Construction and Architecture: for Fencing (a); in Lighting Fixtures (b); for Structural Support (c, d); in Ventilation Systems (e).

The main methods for producing CM discussed in and shown in Fig. 7 are also important factors when selecting the necessary advantages for companies.

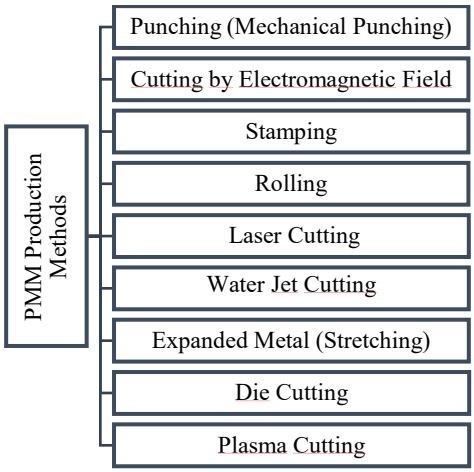

Fig. 7. Basic methods of production.

Cellular metal is widely used for end-user noise reduction, sun protection, and its aesthetic appeal, making it a versatile and effective material in various fields, particularly in construction and architecture [23] - [26]. New configurations, sizes, shapes, materials, compositions, and properties of perforated metal have become significant factors in enhancing the combination of essential characteristics needed across different industrial sectors [25].

II. MATERIALS AND METHODS

Based on a comprehensive literature review, ten universal key factors were identified to evaluate the benefits of using different materials, specifically in terms of their contribution to performance and functionality. These factors provide a framework for understanding how materials offer distinct advantages in various applications. After the literature review authors have selected a list of advantages – factor groups:

1. Radiation Shielding Effectiveness. This factor directly impacts the material's ability to act as a protective shield.

2. Mechanical Strength. This factor evaluates the material's durability and its ability to withstand environmental stresses, making it suitable for use in protective screens that need to resist mechanical wear and tear.

3. Corrosion Resistance. The material's ability to resist degradation from exposure to elements such as moisture, salt, and chemicals [27].

4. Environmental Barrier Properties. The material's ability to function as a comprehensive protective barrier against various environmental factors, including thermal exposure, airborne particulates (such as dust), and gaseous pollutants (such as smoke and industrial emissions).

5. Acoustic Insulation (Noise Reduction). The material's effectiveness in blocking sound transmission, reducing noise pollution, and ensuring the creation of quieter environments.

6. Light Transmission and Visibility. The extent to which the material allows light to pass through while still providing protection. A balance between blocking harmful radiation and maintaining visibility or natural light transmission is crucial, especially in architectural and interior applications.

7. Aesthetic and Design Flexibility. The material's ability to accommodate various design options, including perforation patterns, colours, and finishes, for architectural and decorative purposes. This factor assesses the material's potential for integration into design while maintaining its protective functions.

8. Recyclability and Sustainability. Social, Environmental, and Governance (ESG). The material's potential for recycling after use and its environmental impact throughout its life cycle. This factor includes evaluating the material's resource efficiency, ability to be reused, and minimal environmental degradation during production and disposal.

9. Durability and Long-Term Performance. This includes factors like weather resistance, fatigue under stress, and the material's ability to function effectively over an extended period without significant degradation.

10. Ease of Manufacturing and Installation. The simplicity and efficiency of the manufacturing process and installation. This includes assessing factors such as material handling, required processing steps (e.g., perforation, treatment), ease of installation, and the associated labour costs.

During the last decade a lot of the research efforts have been made to incorporate the vagueness of the initial information for the solution of the complex nature practical problems by multi-criteria decision making (MCDM) methods. There are a lot of the cases when solving multicriteria decision making problems it is necessary to deal with uncertain, imprecise and inconsistent information.

There are many debates about indicators and its interpretation – how to represent and what to represent [14], [18], [28] - [30] Several recent papers have demonstrated high disagreement among existing social, environmental, and governance rankings (e.g., [31], [32]).

However, these factors alone do not provide a comprehensive assessment of the advantages of using CM and could be very subjective in different projects. Also, some factors could be factor groups and consist of numerous sub-elements. It is essential to evaluate additional aspects such as production and delivery costs, corrosion resistance, durability, strength characteristics, and the potential for reuse and recycling.

The selected factors are universal, identified using the method of taxonomy, and can be applied to various cases where choosing the right option, such as the material, is essential. These 10 factors were presented to 10 experts for assessing their relative importance.

The experts have been tasked with comparing the factors that characterise the importance of assessing the benefits of using the material for a fence. The fence will be constructed in the city centre for parking cars, and it should protect the vehicles while also ensuring long-term durability. Additionally, the fence should maintain its primary function of protecting cars and be designed to minimise noise pollution for citizens. It should also offer protection from radiation.

After evaluating the factors, the experts were presented with four materials for a case study to assess their suitability for the fence project. The materials included:

- Cellular woven meshes
- Expanded mesh
- Perforated metal
- Welded mesh

To conduct a cost-benefit analysis, the average price in the Latvian market was included. While prices are not stable and can fluctuate due to various factors, including geopolitical situations, the same analysis method can still be applied. In the event of price changes, the only adjustment needed is to replace the price, and the cost-benefit analysis will provide the final result for selecting the most appropriate material.

III. Results and discussion

The expert method discussed in the literature was utilised to assess the benefits of using cellular metal materials for specific applications. This approach was selected based on the premise that experts, employing robust scientific and technical reasoning, can effectively conduct cost-benefit analyses to evaluate the advantages of CM and other materials.

The required number of experts is estimated based on the hypothesis that expert agreement is 0.5 or more [32].

$$N = (K \cdot P_g)/(T_{ow} + W) = (10 \cdot 0.95)/(0.2 + 0.5) = 14, \quad (1)$$

Where

K - number of assessed factors, K =10;

P_g - probability belief, $P_g = 0.95$;

T_{ow} - tolerable error, $T_{ow} = 0.2$

From 14 experts, 10 experts with a competence of 0.75 and above were selected. The ten experts by using the paired assessment method, evaluated ten factors among themselves and created an ordered series of factors:

F9>F4>F2>F8>F3>F5>F10>F7>F1>F6 (2)

For this series of factors, the authors applied the formula to calculate the relative importance of each factor. This was done using the following formula (1), for each criterion value.

$$\omega\,(F_i) = \omega_i = \frac{2(m - j(F_i) + 1)}{m(m+1)}, \quad (3)$$

Where

$j(F_i)$ - factor Fi position number in a ranking sequence (see Formula 1)

The results of the assessment of the significance of the factors for material assessment are presented in Table 1. A case study was presented to assess the selection of metal materials for protective screens. Experts were then asked to perform a paired comparison between different materials to determine their relative effectiveness using these factors for different materials (Table 1).

TABLE 1 FORMATION OF A GROUP OF EXPERTS BASED ON THE METHOD OF SELF-ASSESSMENT OF EXPERT COMPETENCE (TABLE CREATED BY THE AUTHORS)

Factors		Advantage assessment. Likert				
		Relative score for factors	***Cellular woven meshes***	***Expanded mesh***	***Perforated metal***	***Welded mesh***
F1	Radiation Shielding Effectiveness	0.036	2	3	5	4
F2	Mechanical Strength	0.145	3	4	4	5
F3	Corrosion Resistance	0.109	3	4	5	4
F4	Environmental Barrier Properties	0.164	2	3	5	4

F5	Acoustic Insulation (Noise Reduction)	0.091	2	3	5	2
F6	Light Transmission and Visibility	0.018	5	4	2	4
F7	Aesthetic and Design Flexibility	0.055	3	4	5	3
F8	Recyclability and Sustainability. ESG	0.127	4	4	5	4
F9	Durability and Long-Term Performance	0.182	3	4	5	5
F10	Ease of Manufacturing and Installation	0.073	4	3	2	4

The results of expert assessments regarding the beneficial use of certain materials for different materials are given in Table 2.

TABLE 2 ASSESSMENT OF THE SIGNIFICANCE OF FACTORS BY AN EXPERT GROUP (TABLE CREATED BY THE AUTHORS)

Factors		Assessment of relative advantage			
		Cellular woven meshes	***Expanded mesh***	***Perforated metal***	***Welded mesh***
F1	Radiation Shielding Effectiveness	0.07	0.11	0.18	0.40
F2	Mechanical Strength	0.44	0.58	0.58	0.73
F3	Corrosion Resistance	0.33	0.44	0.55	0.44
F4	Environmental Barrier Properties	0.33	0.49	0.82	0.66
F5	Acoustic Insulation (Noise Reduction)	0.18	0.27	0.46	0.18
F6	Light Transmission and Visibility	0.09	0.07	0.04	0.07
F7	Aesthetic and Design Flexibility	0.17	0.22	0.28	0.17
F8	Recyclability and Sustainability. ESG	0.51	0.51	0.64	0.51
F9	Durability and Long-Term Performance	0.55	0.73	0.91	0.91
F10	Ease of Manufacturing and Installation	0.29	0.22	0.15	0.29
	Total	2.95	3.64	4.58	4.09
	Relative advantage of certain material (Benefit, B)	0.19	0.24	0.30	0.27
	Advantage Rankings	IV	III	I	II

As we can conclude, perforated material receives priority, while the most important factors are F9 (Durability and performance; 0.182); F4 (Environmental Barrier; 0.164); F2 (Mechanical Strength; 0.145) and F8 (Recyclability and Sustainability, ESG; 0.127).

At the end, it is necessary to give an example of approximate cost-benefit analysis based on recent material prices (Table 3). Cost (C) is defined as the relative share of the cost of a material in a group of four materials being analysed.

Experts estimate that currently, the benefits of using PMM in construction, design, and environmental protection surpass those of woven and stretched materials, but other materials could be giving a similar cost-benefit advantage.

TABLE 3 RESULTS OF THE COST-BENEFIT ANALYSIS (TABLE CREATED BY THE AUTHORS)

Material	Benefit (B)	Cost, EUR/m^2	C	C/B	Rank
Cellular woven meshes (1)	0.19	130	0.19	1.01	II
Expanded mesh (2)	0.24	200	0.29	0.83	IV
Perforated metal (3)	0.30	210	0.30	0.99	III
Welded mesh (4)	0.27	150	0.22	1.24	I

IV. CONCLUSIONS

Following the evaluation of cellular metal materials for the specific application, the results indicate that perforated metal materials demonstrate the most advantageous properties among CMs. In construction, design, and environmental protection, woven and stretched/expanded metal materials are the most comparable alternatives to PMM, highlighting the unique advantages of PMM in these fields.

Experts estimate that the benefits of using PMM in construction, design, and environmental protection are most factors outweigh those of woven and stretched materials.

Nonetheless, PMM requires additional labour costs relative to solid sheet metal; its overall cost is 10-20% lower, with non-ferrous metals seeing reductions of up to 30%. Other mesh materials could bring a similar cost-benefit advantage. This cost efficiency positions PMM as a financially viable option for various applications from the cost-benefit perspective.

Furthermore, it is important to mention the expert evaluation method used. For the specific case of a perimeter fence, an analysis of responses from 10 experts using the group assessment methodology led to the selection of the cellular material option in the form of a welded picket fence. This method is simple, dynamic and effective for addressing specific technical solution choices in construction and mechanical engineering. The method is also applicable to a wide range of materials and is particularly useful for critical raw materials, whose limited availability requires careful selection for specific applications. The efficient choice for their application is essential, especially to ensure sustainability and optimise their use.

The decreasing costs of PMM are driven by increasing production volumes and the effective recycling of production waste, which minimises losses. These factors contribute to the sustainability and economic attractiveness of PMM in the market.

The findings suggest that PMM not only offers economic benefits but also supports sustainable practices in construction and design. As the demand for innovative materials continues to grow, PMM is well-positioned to meet both performance and environmental standards, making it a valuable asset in modern construction methodologies.

References

[1] I. I. Dani, W.G. Drossel, N. Milaev, H. Korn, C. Hannemann, J. Hohlfeld, R. Wertheim, “Sustainability of industrial components using additive manufacturing and foam materials,” Procedia Manuf., vol. 43, pp. 10–17, 2020, doi: 10.1016/j.promfg.2020.02.102.

[2] J. Banhart, “Manufacture, characterisation and application of cellular metals and metal foams,” Prog. Mater. Sci., vol. 46, no. 6, pp. 559–632, 2001, doi: 10.1016/S0079-6425(00)00002-5.

[3] R. Setiawan, A. I. Komara, and B. Budiwantoro, “Numerical and experimental investigation of aluminum double arrowhead cellular

structure manufactured using sheet metal forming," Results Eng., vol. 26, 2025, doi: 10.1016/j.rineng.2025.104667.

[4] Q. Zuo, K. He, H. Mao, X. Dang, and R. Du, "Manufacturing process and mechanical properties of a novel periodic cellular metal with closed cubic structure," Mater. Des., vol. 153, pp. 242–258, 2018, doi: 10.1016/j.matdes.2018.05.011.

[5] A. G. Evans, J. W. Hutchinson, and M. F. Ashby, "Cellular metals," Curr. Opin. Solid State Mater. Sci., vol. 3, no. 3, pp. 288–303, 1998, doi: 10.1016/S1359-0286(98)80105-8.

[6] European Commission, "Critical raw materials resilience: Charting a path towards greater security and sustainability." [Online]. Available: https://ec.europa.eu/docsroom/documents/42849[Accessed April 15, 2025].

[7] United Nations Development Programme, "Transforming our world: The 2030 agenda for sustainable development." 2015, [Online]. Available: https://sdgs.un.org/2030agend[Accessed April 15, 2025].

[8] European Commission, "The European Green Deal," 2019, [Online]. Available: https://ec.europa.eu/info/strategy/priorities-2019-2024/european-green-deal_en[Accessed April 15, 2025].

[9] K. Morgan, "Smart Specialisation: Opportunities and Challenges for Regional Innovation Policy," Reg. Stud., vol. 49, no. 3, pp. 480–482, 2015, doi: 10.1080/00343404.2015.1007572.

[10] H. Ruiz, P. Cobo, T. Dupont, B. Martin, and P. Leclaire, "Acoustic properties of plates with unevenly distributed macroperforations backed by woven meshes," J. Acoust. Soc. Am., vol. 132, no. 5, pp. 3138–3147, 2012, doi: 10.1121/1.4754520.

[11] X. Li, Q. Wu, L. Kang, and B. Liu, "Design of multiple parallel-arranged perforated panel absorbers for low frequency sound absorption," Materials (Basel)., vol. 12, no. 13, 2019, doi: 10.3390/ma12132099.

[12] M. Mironovs, V.; Lisicins, "Perforated metal materials and their use possibilities," RTU Publ. House, 2015.

[13] G. W. Kooistra and H. N. G. Wadley, "Lattice truss structures from expanded metal sheet," Mater. Des., vol. 28, no. 2, pp. 507–514, 2007, doi: 10.1016/j.matdes.2005.08.013.

[14] Z. Wang, "Recent advances in novel metallic honeycomb structure," Compos. Part B Eng., vol. 166, pp. 731–741, 2019, doi: 10.1016/j.compositesb.2019.02.011.

[15] V. Mironovs, A. Tatarinov, and S. Gorbacova, "Expanding Application of Perforated Metal Materials in Construction and Architecture," IOP Conf. Ser. Mater. Sci. Eng., vol. 251, p. 012027, Oct. 2017, doi: 10.1088/1757-899X/251/1/012027.

[16] A. Shishkin, T. Koppel, V. Mironov, I. Hussainova, J. Locs, and H. Haldre, "Microwave Reflectance and Transmittance Properties of Conductive Composite Materials," Energy Procedia, vol. 113, pp. 354–361, May 2017, doi: 10.1016/j.egypro.2017.04.006.

[17] M. C. S. de Abreu, F. N. H. Ferreira, J. F. Proença, and D. Ceglia, "Collaboration in achieving sustainable solutions in the textile industry," J. Bus. Ind. Mark, vol. 36, no. 9, pp. 1614–1626, Oct. 2021, doi: 10.1108/JBIM-01-2020-0041.

[18] Z. Zhao, Y. Peles, and M. K. Jensen, "Properties of plain weave metallic wire mesh screens," Int. J. Heat Mass Transf., vol. 57, no. 2, pp. 690–697, Feb. 2013, doi: 10.1016/j.ijheatmasstransfer.2012.10.055.

[19] J. Yip and S. P. Ng, "Study of three-dimensional spacer fabrics: Physical and mechanical properties," J. Mater. Process. Technol., vol. 206, no. 1–3, pp. 359–364, Sep. 2008, doi: 10.1016/j.jmatprotec.2007.12.073.

[20] A. G. Evans, J. W. Hutchinson, and M. F. Ashby, "Cellular metals," Curr. Opin. Solid State Mater. Sci., vol. 3, no. 3, pp. 288–303, Jun. 1998, doi: 10.1016/S1359-0286(98)80105-8.

[21] C. Wang, K. Shankar, and A. Fien, "Finite element simulation of impact response of wire mesh screens," EPJ Web Conf., vol. 94, p. 04033, Sep. 2015, doi: 10.1051/epjconf/20159404033.

[22] M. K. Sharma, S. Preet, J. Mathur, A. Chowdhury, and S. Mathur, "Thermal performance analysis of naturally ventilated and perforated sheet based double skin facade system for hot summer conditions," Int. J. Vent., vol. 21, no. 4, pp. 263–283, Oct. 2022, doi: 10.1080/14733315.2021.1901003.

[23] G. W. Kooistra and H. N. G. Wadley, "Lattice truss structures from expanded metal sheet," Mater. Des., vol. 28, no. 2, pp. 507–514, Jan. 2007, doi: 10.1016/j.matdes.2005.08.013.

[24] G. Martínez, E. Casanova, and C. Graciano, "Failure response of expanded metal meshes subject to transversal impact," Lat. Am. J. Solids Struct., vol. 20, no. 7, 2023, doi: 10.1590/1679-78257585.

[25] G. Martínez, C. Graciano, and P. Teixeira, "Energy absorption of axially crushed expanded metal tubes," Thin-Walled Struct., vol. 71, pp. 134–146, 2013, doi: 10.1016/j.tws.2013.05.003.

[26] C. Graciano, G. Martínez, and D. Smith, "Experimental investigation on the axial collapse of expanded metal tubes," Thin-Walled Struct., vol. 47, no. 8–9, pp. 953–961, Aug. 2009, doi: 10.1016/j.tws.2009.02.002.

[27] M. D. Nouri, H. Hatami, and A. G. Jahromi, "Experimental and numerical investigation of expanded metal tube absorber under axial impact loading," Struct. Eng. Mech., vol. 54, no. 6, pp. 1245–1266, Jun. 2015, doi: 10.12989/sem.2015.54.6.1245.

[28] E. D. G. Fraser, A. J. Dougill, W. E. Mabee, M. Reed, and P. McAlpine, "Bottom up and top down: Analysis of participatory processes for sustainability indicator identification as a pathway to community empowerment and sustainable environmental management," J. Environ. Manage., vol. 78, no. 2, pp. 114–127, 2006, doi: 10.1016/j.jenvman.2005.04.009.

[29] A. De Pascale, R. Arbolino, K. Szopik-Depczyńska, M. Limosani, and G. Ioppolo, "A systematic review for measuring circular economy: The 61 indicators," J. Clean. Prod., vol. 281, 2021, doi: 10.1016/j.jclepro.2020.124942.

[30] S. Harris, M. Martin, and D. Diener, "Circularity for circularity's sake? Scoping review of assessment methods for environmental performance in the circular economy." Sustain. Prod. Consum., vol. 26, pp. 172–186, 2021, doi: 10.1016/j.spc.2020.09.018.

[31] I. Voronova and V. Shatrevich, "Sectoral risk assessment: a case of the Latvian forestry sector," Jun. 2020. doi: 10.3846/bm.2020.621.

[32] A. Efimenko, I. Zlobin, A. Avilov, and A. Markov, "Application of expert evaluation method for realization of tasks in construction industry," E3S Web Conf., vol. 91, 2019, doi: 10.1051/e3sconf/20199108034.

Environment. Technology. Resources. Rezekne, Latvia
Proceedings of the 16th International Scientific and Practical Conference. 2025. Volume IV, 265-269

Properties Assessment of Perforated Metal Plates for Medical Use

Marija Osipova
Mechanical and Biomedical Engineering Institute
Riga Technical University
Riga, Latvia
marija.osipova@edu.rtu.lv

Viktors Mironovs
Mechanical and Biomedical Engineering Institute
Riga Technical University
Riga, Latvia
viktors.mironovs@rtu.lv

Antons Pacejs
Rezekne Academy of Riga Technical University
Rezekne, Latvia
antons.pacejs@rta.lv

Aleksejs Tatarinovs
Institute of Electronics and Computer Science
Riga, Latvia
aleksejs.tatarinovs@edi.lv

Jānis Lungevics
Mechanical and Biomedical Engineering Institute
Riga Technical University
Riga, Latvia
janis.lungevics@rtu.lv

Vjacheslavs Zemchenkovs
Mechanical and Biomedical Engineering Institute
Riga Technical University
Riga, Latvia
v.zemchenkov@gmail.com

***Abstract*—Thin-walled and sheet materials with regular through holes (perforation) have wide practical application in various fields, including in medicine for the manufacture of implants, trays for placing and storing cutting instruments, sterilization of consumables. Perforated metal materials (PMM), primarily made of titanium and stainless steel, are of the most attention to specialists in the field of medical engineering, since they are characterized by lower weight, high strength and biomechanical compatibility. The mechanical characteristics of PMM are determined by the initial properties of the material, the dimensions of the sheet or tape, the shape and total area of the perforation. If selected correctly, dimensions and area of the perforations can provide optimal flexibility and plasticity with a significant reduction in the weight of the implant. This paper presents properties of perforated plates made of stainless steel, obtained by non-destructive methods. In particular, the dependences of the Lamb wave velocities at different frequencies on the specific total area of the plate's perforation are shown. The data of elastic properties dependences on the perforation area. The data of microscopic studies of changes in the quality of holes obtained by laser cutting are also presented.**

Keywords— implants, laser cutting, non-destructive methods, perforated metal materials.

I. Introduction

Metallic materials with a perforated structure, with regular or irregular perforations (through-holes), have a wide range of practical applications in medicine. They are used for manufacturing dental implants, trays for storing and organizing surgical instruments, and for sterilizing disposable medical supplies (Fig. 1) [1] – [3].

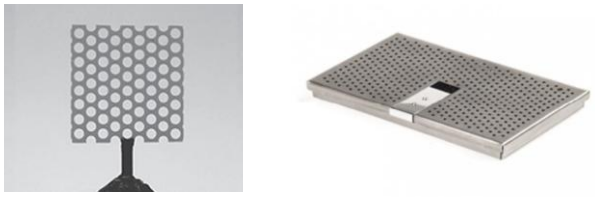

Fig. 1. Variations of perforated materials use in medical applications: dental joint implant and sterilization tray.

Metallic materials, such as titanium and stainless steel, are of the high interest to specialists in medical engineering. Those materials are preferred due to their lower weight, high strength, and superior biocompatibility compared to other materials [4], [5]. In implant manufacturing, PMMs provide enhanced strength while maintaining a low weight (Fig. 2).

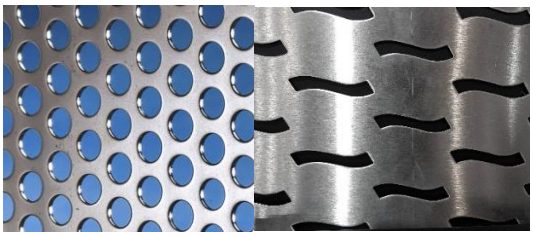

Fig. 2. Types of perforation in metal constructions.

Modern prosthetic limbs are also frequently made from PMMs, which reduces their weight and enhances patient

Online ISSN 2256-070X
https://doi.org/10.17770/etr2025vol4.8453
© 2025 The Author(s). Published by RTU PRESS.
This is an open access article under the Creative Commons Attribution 4.0 International License.

comfort. Perforation holes vary in size and shape. An important parameter of a product made from perforated material is the total perforation area, as well as the relative arrangement of the holes [6]. Circular perforations provide a high hole density and good ventilation [7], [8]. Studies show that perforation parameters significantly affect the mechanical properties of perforated elements [9]. It has been established that implants with high mechanical strength bear most of the load, leading to atrophy of the surrounding bone tissue and a decrease in its density around the implant, a phenomenon known as stress shielding effects [10] – [13]. Therefore, it is crucial to reduce the elastic properties, such as Young's modulus of materials and elements used in orthopaedic implants [3]. PMMs with Young's modulus close to the elastic-plastic properties of human bone (Young's modulus: 10–30 GPa, depending on the bone type) ensure better load distribution between the implant and the surrounding bone, reducing stress shielding effects and ensure better load distribution between the orthopaedic implant and the bone, reducing the risk of bone degradation [14], [15]. Effective control of these properties through material selection and manufacturing technologies, such as the use of alloys with modified microstructures, porous or powder-based material structures, and the application of PMMs, enhances osteointegration and improves implant functionality [10], [11]. Various technological methods are used for manufacturing PMMs, including stamping, waterjet cutting, plasma cutting, and laser cutting [16], [17]. Laser cutting enables the production of components with more complex perforation patterns and smaller hole sizes [6]. In this process, which is used for manufacturing medical devices, important factors include surface roughness and deviations in hole profile.

II. Materials and Methods

For experimental studies, plates made of stainless steel SS304 were manufactured using the laser cutting method (Fig. 3). The main objective of this work was to investigate the properties of perforated steel plates, including elastic properties, perforation accuracy, and ultrasound propagation velocities, in order to determine the impact of perforations on these characteristics.

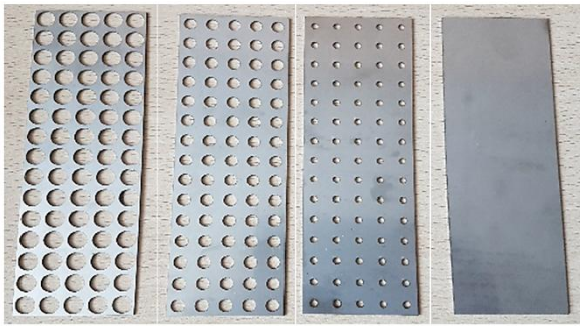

Fig. 3. Perforated stainless steel SS304 plates. Length: 140 mm, width: 25 mm, thickness: 1 mm. Hole diameter: 3 to 8 mm. Total perforation area: 0% to 50%.

A. Elastic properties determination.

The determination of the elastic properties of perforated metal plates was conducted through non-destructive methods, laser vibrometry using the Polytec PSV-500 system. Laser vibrometry is a method of determining the dynamic properties of the sample - the resonant frequencies, which in turn are needed to determine the elastic properties [18] – [20]. In the control software, the excitation frequency range was configured from 0 to 10 kHz, encompassing the resonance frequencies of the plates. The surface of each plate was systematically scanned along its length and width to capture a detailed representation of its vibrations. The obtained resonance frequency values were used in the corresponding equations to determine the Young's modulus of the plates. Each perforated stainless steel SS304 sample underwent testing using the laser vibrometry method. Following each test, the fundamental bending frequency was recorded. Table 1 presents the collected data on the fundamental bending frequencies for all tested samples. The Young's modulus E of the samples was calculated using the fundamental bending frequency f_b with the following formula:

$$E = 0.9465 \times m \times \frac{f_b^2}{b} \times \left(\frac{l}{h}\right)^3 \times T \qquad (1)$$

where the geometric parameters required for calculating the Young's modulus of the tested samples included thickness h, length l, and width b, while the physical parameter considered was mass (m). The correction factor T (applicable for $l/h > 20$) was computed using the following equation:

$$T = 1 + 6.585 \left(\frac{h}{l}\right)^2 \qquad (2)$$

Young's modulus E of the tested samples was determined using experimentally obtained fundamental bending frequencies, applying the equations (1) and (2) as referenced in [21], [22]. For these calculations, key geometric parameters, including length, width, and thickness — were precisely measured with a caliper, while the sample weight was recorded using a scale. The data used for calculating Young's modulus of perforated stainless steel 304 plates are presented in Table 1.

TABLE 1. Physical, geometric, experimental, and computed data of perforated stainless steel SS304L samples.

Sample №	***Weight (g)***	***Fundamental bending frequency (kHz)***	***Correction factor T***	***Perforated plates Young's modulus (GPa)***
1	57.838	236.875	1.000293	207.6171
2	53.690	226.75	1.000293	176.4166
3	43.634	207.875	1.000293	120.4983
4	27.687	178.375	1.000293	56.2987

B. Lamb wave velocities at different frequencies determination.

Ultrasonic measurements were carried out using the surface profiling method using a pair of transducers, a transmitter and a receiver. One of the transducers was fixed on the surface of the plate, and the other moved linearly along the surface, with the ultrasonic signals being recorded step by step. The propagation velocity of the ultrasonic wave was measured by the shift of the first extremum of the received signal and calculated as a linear approximation of the ratio of the increment in the distance between the transducers to the increment in time. The measurements were carried out using three pairs of transducers with operating frequencies of 60, 150 and 450 kHz. To amplify the signal at a given operating frequency of the emitter, the excitation pulse was a 2-period tone-burst at this carrier frequency. To weaken the reflected signals from the ends of the plates and prevent their interference with the direct propagation signal, the plates were dampened at the edges with plasticine. Silicone-based acoustic gel was used as contact lubricant.

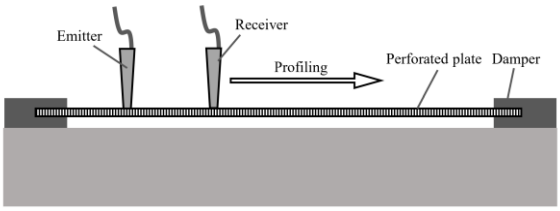

Fig. 4. Layout of ultrasonic measurements on the perforated plate.

C. Accuracy of the perforation determination.

To assess the accuracy of the perforations, equipment from the Japanese company MITUTOYO was used. Profile evaluation was also conducted through macro- and microscopic analysis. The Quick Vision QV-X302T1L-E optical measurement system was employed to assess the diameter deviation of perforations in SS304 stainless steel plates. The perforations, with nominal diameters of 3 mm, 5.5 mm, and 8 mm, were measured using the system's high-resolution camera and advanced image processing software. The measurement procedure involved placing the perforated plate on the motorized stage of the Quick Vision system. The stage was adjusted to align the perforations with the camera's field of view. The system's autofocus function was utilized to ensure sharp imaging of the perforation edges. For each perforation, the diameter was measured at multiple points along the circumference to account for potential ellipticity or irregularity. The software calculated the average diameter and compared it to the nominal diameter, determining the deviation. The results were recorded with a resolution of 0.1 µm. The Quick Vision QV-X302T1L-E system provided repeatable and precise measurements, enabling the quantification of diameter deviations for quality control and compliance with specified tolerances (Fig. 5). The data were exported for further statistical analysis to evaluate the consistency of perforation dimensions across the plates.

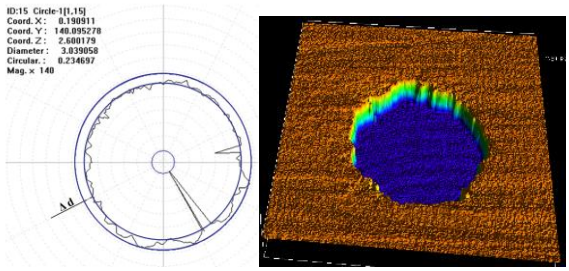

Fig. 5. Perforation profile with 3 mm diameter in SS304 steel plate and enlarged perforation 3D profile.

III. RESULTS AND DISCUSSION

A. Elastic properties measurements.

On Figure 3 is shown a plot, that presents the dependence of Young's modulus of perforated stainless steel SS304 plates on the perforation area for plates. The plot indicates a decrease in Young's modulus of perforated plates as the perforation area increases.

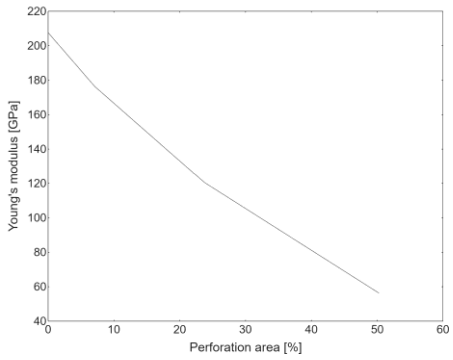

Fig. 6. Dependence of Young's modulus of perforated SS304 stainless steel plates on perforation (perforated plates dimensions of Length: 140 mm, width: 25 mm, thickness: 1 mm. Hole diameter: 3 to 8 mm. Total perforation area: 0% to 50%).

As the perforation area is 0%, the Young's modulus of perforated plate is 207.617 GPa. With an increase of perforation area to 7.07 %, the decreasing trend continues, and the Young's modulus of perforated plate reaches 176.417 GPa. When the perforation area increases to 23.76 %, the Young's modulus of perforated plate decreases further to 120.498 GPa. The most significant reduction in all parameters occurs at a perforation area of 50.27 %, where the Young's modulus of perforated plate falls to 56.299 GPa. Summarizing the Young's modulus there is a

gradual decrease in Young's modulus (about a 151.318 GPa difference). Considering the Young's modulus of human bone, which ranges from 10 to 30 GPa, the sample with the highest perforation area 50.27 %, has a Young's modulus of perforated plate is 56.299 GPa, which is still higher than the Young's modulus of human bone. Therefore, further research into SS304 stainless steel plates with perforation areas greater than 50.27 % would be necessary to reduce the Young's modulus closer to that of human bone.

B. Ultrasonic measurements.

Using surface profiling of plates, we obtained ultrasound propagation velocities in the range from 1080 to 2800 m/s. This is several times lower than the velocity of the longitudinal wave in steel, where its tabular value is about 6300 m/s in volume. In addition, a pronounced dependence of the velocity on frequency was obtained. From this we concluded that the measured values of the velocity refer to an asymmetrical zero-order Lamb wave or a flexural wave. For this wave, the propagation velocity depends on the ratio of the plate thickness to the ultrasonic wavelength, and therefore, for the same plate thickness, on the frequency.

As the degree of perforation increased from 0 to 50.27 %, the velocity of the flexural wave decreased consistently. Figure 7 illustrates the dual dependence of the ultrasound velocity on both the frequency and the degree of perforation.

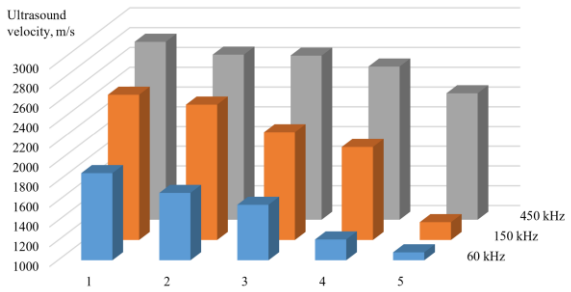

Fig. 7. Changes in ultrasound velocity in perforated plates depending on the specific degree of perforation (1 - 0; 2 - 7.1%, 3 - 12.6%, 4 - 23.8%, 5 - 50.3%) for three ultrasound frequencies (60, 150 and 450 kHz).

At the same time, the degree of dependencies is different at different frequencies and at different sections of perforation increment. So, at a high frequency of 450 kHz, the graph of the speed dependence on the degree of perforation is flat, at a low frequency of 60 kHz it is steep, and at an intermediate frequency of 150 kHz it is flat at a low degree of perforation and steep at a high degree. This can be explained by the fact that at high frequency the ultrasonic wave tends to bypass the perforation and spread over a solid area, while at low frequency it makes the plate vibrate. Thus, the ultrasound velocities at different frequencies can be used as indicators of the properties of the plate material and the integral rigidity of the plate, considering the perforation. By applying advanced data analysis methods in the future and larger databases, it becomes possible to differentially evaluate the factors of plate thickness, its material properties and the degree of perforation.

C. Perforations accuracy measurements.

Measurements of the hole profile in steel plates produced by laser cutting revealed a slight increase in profile deviations as the hole diameter increased. At the same time, no changes in hole profile deviations along the length of the plate were observed. Figure 8 illustrates the variation in circularity of perforations along the length of SS304 stainless steel plates for three different hole diameters (3 mm, 5.5 mm, and 8 mm). The x-axis represents the plate length (0 to 140 mm), while the y-axis shows the circularity of the perforations. The results indicate that for 3 mm perforations, circularity fluctuates significantly along the plate length, with values ranging from 0.06 to 0.14, suggesting greater variability in profile accuracy. In contrast, 5.5 mm and 8 mm perforations exhibit more stable circularity values, remaining within a narrower range (approximately 0.035 to 0.06). The lower circularity deviations in larger perforations indicate improved hole profile consistency. A notable trend is the higher circularity variability for 3 mm perforations, particularly at the beginning and end of the plate. This could be attributed to process-related effects such as thermal influence, laser power fluctuations, or cutting path instabilities. The 5.5 mm and 8 mm perforations remain relatively stable along the entire plate length, indicating that larger holes maintain better geometric precision.

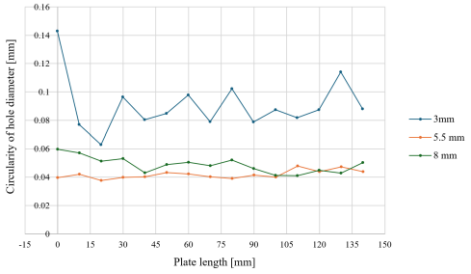

Fig. 8. Dependence of circularity of perforated SS304 stainless steel plates on plate lenght (perforated plates dimensions - length: 140 mm, width: 25 mm, thickness: 1 mm. Hole diameter: 3 to 8 mm).

This data indicate that increasing the perforation area in stainless steel plates significantly alters their mechanical and acoustic properties. However, it should be noted that the study was limited to a specific material (SS304) and a particular range of perforation areas. Further research is needed to assess whether similar trends occur in titanium-based or other biomedical alloys. Previous studies have primarily focused on the mechanical properties of metal constructions with circular holes, in civil engineering

applications, while their potential for medical use remained largely understudied [23]. This work presents a comparative analysis of key elastic parameters for perforated metal constructions, for medical orthopedic implants, to decrease the stress-shielding effect.

CONCLUSIONS

The study investigated the properties of perforated stainless steel SS304 plates, focusing on their elastic properties, perforation accuracy, and ultrasound propagation velocities. Using non-destructive methods, including laser vibrometry, the research determined that the Young's modulus of the plates decreases as the perforation area increases, with a significant reduction observed at a 50.27 % perforation area. This reduction in Young's modulus suggests potential for better load distribution in medical implants, reducing stress shielding effects.

Additionally, the study found that ultrasound velocity related to the propagation of Lamb wave in plate decreases with increased perforation, indicating changes in the entire rigidity of the plate under the influence of perforation.

The accuracy of perforations was assessed, revealing that medium-sized holes (5.5 mm) have the most stable circularity, while smaller and larger holes show higher deviations.

ACKNOWLEDGMENTS

This work has been supported by the Latvian Council of Science LZP FLPP no. LZP -2021/1-0290, Comprehensive assessment of the condition of bone and muscle tissue using quantitative ultrasound (BoMUS)". We would like to thank students A. Sirotkina (Riga Technical University) for active participation.

REFERENCES

[1] L. Kroes, "Creating More Efficiency and Patient Safety by Changing Processes and Contents of Instrument Trays," M.S. thesis, University of Twente, Enschede, The Netherlands, 2009.

[2] Wexler Surgical, "Wexler metal sterilization tray single level with silicone brackets," Available online: https://www.wexlersurgical.com/wexler-metal-sterilization-tray-single-level-wsilicone-brackets-105quotx215quotx25quot-266x533x63cm-p-1464.html (accessed Oct. 1, 2024).

[3] M. Dewidar, A. Khalil, and J. K. Lim, "Processing and mechanical properties of porous 316L stainless steel for biomedical applications," Trans. Nonferrous Met. Soc., vol. 17, pp. 1–4, 2007.

[4] A. L. Nuwirth, B. S. Ashley, W. M. Hardaker, and N. P. Sheth, "Biomedical applications of metals," in Metals in Biomedical Applications, M. Rai, A. P. Ingle, and S. Medici, Eds. Cham, Switzerland: Springer International Publishing, 2018, pp. 3–95.

[5] H. T. Swee, Engineering Materials for Biomedical Application, Hackensack, NJ, USA: World Scientific Publishing Co., 2004, pp. 4–29.

[6] V. Mironovs and M. Lisicins, Perforated Metal Materials and Their Use Possibilities, Riga, Latvia: RTU Publishing House, 2015, pp. 15–152.

[7] V. Mironovs, J. Kuzmina, D. Serdjuks, Y. Usherenko, and M. Lisicins, "Sustainable lifecycle of perforated metal materials," Materials, vol. 3012, pp. 1–8, 2023.

[8] S. C. Baik, K. H. Oh, and D. N. Lee, "Analysis of the deformation of a perforated sheet under uniaxial tension," J. Mater. Process. Technol., vol. 58, pp. 1–6, 1996.

[9] C. Ziemian, M. McClintock, and R. T. Ziemian, "Torsional strength of aluminum shapes—circular and rectangular solids," Eng. Proc., vol. 43, pp. 2–4, 2023.

[10] M. M. Shahzamanian, R. Banerjee, N. B. Dahotre, A. R. Srinivasa, and J. N. Reddy, "Analysis of stress shielding reduction in bone fracture fixation implant using functionally graded materials," Compos. Struct., vol. 321, pp. 1–4, 2023.

[11] M. Niinomi and M. Nakai, "Titanium-based biomaterials for preventing stress shielding between implant devices and bone," Int. J. Biomater., vol. 2011, no. 836587, pp. 1–10, 2011.

[12] K. Yaqoob, I. Amjad, M. A. M. Awan, U. Liaqat, M. Zahoor, and M. Kashif, "Novel method for the production of titanium foams to reduce stress shielding in implants," ACS Omega, vol. 8, pp. 1–9, 2023.

[13] R. J. Narayan, Ed., Materials for Medical Devices, 1st ed. Materials Park, OH, USA: ASM International, 2012.

[14] E. Wintermantel, J. Mayer, T. N. Goehring, and S. Aqida, "Composites for biomedical applications," Ref. Modul. Mater. Sci. Mater. Eng., vol. 2, pp. 2–3, 2016.

[15] D. F. William, Handbook of Biomaterial Properties, 2nd ed. New York, NY, USA: Springer, 2016, pp. 153–154.

[16] R. Chiba, R. Nakamura, and Y. Suga, "Forming-limit strains of perforated steel sheets under biaxial stress state," J. Mater. Design Appl., vol. 233, no. 11, pp. 2401–2415, 2019.

[17] Y. Wang, X. Liao, J. Lu, and J. Ma, "Optimization method of sheet metal laser cutting process parameters under heat influence," Machines, vol. 12, no. 3, p. 206, 2024.

[18] A. Krasnikovs, O. Kononova, A. Machanovskis, V. Zaharevskis, P. Akishins, and S. Ruchevskis, "Characterization of mechanical properties by inverse technique for composite reinforced by knitted fabric. Part 2. Experimental evaluation of mechanical properties by frequency eigenvalues method," J. Vibroeng., vol. 14, no. 2, pp. 691–698, 2012.

[19] M. Wesolowski, E. Barkanov, S. Rucevskis, A. Chate, and G. La Delfa, "Characterization of elastic properties of laminated composites by non-destructive techniques," in Proc. ICCM Int. Conf. Compos. Mater., 2009, pp. 5–7.

[20] E. Barkanov, M. Wesolowski, P. Akishin, and M. Mihovski, "Techniques for non-destructive material properties characterization," in Non-destructive Testing and Repair of Pipelines, E. N. Barkanov, A. Dumitrescu, and I. A. Parinov, Eds. Cham, Switzerland: Springer, 2018, pp. 194–203.

[21] G. Pickett, "Elastic properties of materials," Proc. ASTM, vol. 45, p. 846, 1945.

[22] ASTM Standard E 1876-07, Standard Test Method for Dynamic Young's Modulus, Shear Modulus, and Poisson's Ratio by Impulse Excitation of Vibration, ASTM International, 2007.

[23] C. Ziemian, M. McClintock, and R. T. Ziemian, "Torsional strength of aluminum shapes—circular and rectangular solids," Eng. Proc., vol. 43, pp. 2–4, 2023.

Environment. Technology. Resources. Rezekne, Latvia
Proceedings of the 15th International Scientific and Practical Conference. 2025. Volume IV, 271-276

Mathematical Model for Calculating the Dispersion Flow Rate of Decontamination Solutions for Chemical and Radiological Agents When Sprayed from Nozzles

Nikolay Iliyanov Padarev
„V. Levski" National Military University
Faculty of Security and Defence
Veliko Tarnovo, Bulgaria
nipadarev@gmail.com

***Abstract*—The mathematical model for calculating the flow rate of fluids when dispersed from nozzles is based on the principles of fluid mechanics, using equations for the velocity of the fluid and the effects of nozzle diameter, pressure, and the dynamic properties of the fluid (density, viscosity). The model includes calculations of the flow rate based on the theoretical exit velocity from the nozzle, along with corrections for pressure losses associated with friction and turbulence. The Reynolds number is used to assess the flow characteristics (laminar or turbulent), which is crucial for optimizing the fluid dispersion. In MATLAB, various plots are generated to show the dependencies between the flow rate, nozzle diameter, and pressure, enabling a deeper understanding of the fluid behaviour during dispersion. The model is applicable to different types of fluids, including solutions with surfactants and hypochlorites, used for disinfection purposes.**

Keywords*— *decontamination, fluid dispersion, CBRN devices, dynamic properties of the fluid, spraying systems.

I. Introduction

The development of Chemical, Biological, Radiological, and Nuclear (CBRN) machine decontamination systems is a critical aspect of military, emergency response, and industrial safety. These systems are designed to neutralize, remove, or contain hazardous contaminants from military vehicles, equipment, and infrastructure after exposure to CBRN threats. The advancement of CBRN decontamination technologies has been driven by the increasing risks posed by chemical warfare, bioterrorism, radiological threats, and nuclear incidents. [1] - [10]

Modern decontamination efforts focus on speed, efficiency, material compatibility, and environmental safety. These systems use a variety of chemical agents, physical cleaning methods, and advanced materials to ensure thorough decontamination while minimizing damage to sensitive equipment.

Innovations in dispersing solutions for the decontamination of nuclear, chemical, and biological (NBC) agents are essential to improving response capabilities in defence, emergency response, and industrial safety. [11] - [13]

Current methods are slow and resource-intensive: Many decontamination processes require large amounts of water, chemicals, or time to be effective. Innovations in dispersing solutions can significantly reduce response time and improve efficiency. Speed is crucial to minimizing casualties and environmental contamination, especially in high-risk areas such as military operations or urban centres. New solutions allow faster targeted decontamination without excessive liquid waste or secondary contamination. Many chemical-based decontaminants are toxic, corrosive, or leave harmful residues that further contaminate the environment. [14]

Traditional decontamination requires high-pressure water systems that generate hazardous runoff. Modern autonomous spraying systems, drones, and robotic decontamination units reduce the need for human operators to enter contaminated areas.

Wearable decontamination solutions (e.g., self-decontaminating fabrics) provide real-time protection.

Online ISSN 2256-070X
https://doi.org/10.17770/etr2025vol4.8425
© 2025 The Author(s). Published by RTU PRESS.
This is an open access article under the Creative Commons Attribution 4.0 International License.

Traditional decontamination equipment is bulky and difficult to transport.

Advanced dispersing solutions (e.g., lightweight decontamination sprays, self-activating gels) enhance mobility. Decontaminants must work on a variety of surfaces (e.g., vehicles, weapons, infrastructure, sensitive electronic components). Innovations allow for more even distribution and effectiveness on porous and non-porous surfaces.

Advanced dispersing solutions can neutralize chemical, biological, and radiological threats simultaneously, reducing the need for multiple systems.

The flow rate (Q) of fluids when sprayed from nozzles can be calculated using fluid dynamics formulas that account for the nozzle diameter, the pressure of the fluid, the density of the fluid, and the efficiency coefficients.

Basic Formula (1) for Calculating the Flow Rate:

$$Q = C_d * A * \sqrt{\frac{2*\Delta P}{\rho}} \quad (1)$$

Where:

- Q – flow rate of the fluid, in m³/s or l/s;
- C_d – discharge coefficient (dimensionless value, usually between 0.6 and 0.9 depending on the nozzle);
- A – cross-sectional area of the nozzle opening, in m²;
- ρ – density of the fluid, in kg/m³;
- ΔP – pressure difference, in Pa. This is the difference between the pressure of the fluid before the nozzle and the atmospheric pressure. [15]

Discharge Coefficient (C_d) reflects the efficiency of the nozzle in converting pressure energy into kinetic energy. It varies depending on the nozzle design and condition. Nozzle Diameter of the nozzle significantly impacts the flow rate. Larger nozzles allow more fluid to pass through, increasing the flow rate. The pressure difference is the force driving the fluid through the nozzle. It's the difference between the pressure inside the pipe or reservoir and the pressure at the nozzle exit. Higher pressure differences result in higher flow rates. The density of the fluid affects its ability to flow. Higher-density fluids require more energy to move through the nozzle.

For round nozzles (2) [16]:

$$A = \pi * \frac{d^2}{4} \quad (2)$$

Where d – diameter of the nozzle opening, in meters.

Spraying nozzles can have different shapes, which affect the discharge coefficient (C_d). When creating a mathematical model for a specific case, the value of C_d that is provided in the manufacturer's documentation should be used. If the fluid is viscous, instead of the standard formula, correction factors should be applied to account for the fluid's viscosity.

If there is more than one nozzle, as is common in machines used for the decontamination of nuclear, chemical, and biological agents, the total flow rate (Q_{total}) is calculated using the following formula (Formula 3):

$$Q_{total} = N * Q \quad (3)$$

Where:

- N – the number of nozzles.
- Q – the flow rate per nozzle (as calculated using the formula previously mentioned).
- Q_{total} – the total flow rate for the system.

This approach helps account for multiple nozzles and gives a comprehensive understanding of the system's performance, ensuring that the total volume of fluid required for the decontamination process is accurately calculated. The flow rate from a nozzle is directly influenced by the nozzle diameter, the pressure driving the fluid, the density of the fluid, and the efficiency of the nozzle (C_d). For accurate calculations, each of these factors should be considered, as they impact the volume of fluid sprayed over time.

To calculate the flow rate of a fluid being sprayed from a nozzle, we can use Torricelli's equation and empirical coefficients. The general formula for the flow rate $Q_{through}$ a nozzle is given by the following formula (Formula 4):

$$Q = C_d * A\sqrt{2 * g * h} \quad (4)$$

Where:

- Q – the flow rate (m³/s or l/s)
- C_d – the discharge coefficient (dimensionless), which accounts for the efficiency of the nozzle
- A – cross-sectional area of the nozzle (m²)
- ΔP – pressure difference (Pa), which is the difference between the pressure before the nozzle and the atmospheric pressure
- ρ – density of the fluid (kg/m³)

This formula is derived from Torricelli's law, which is based on the principles of fluid dynamics. It assumes that the flow of the fluid is caused by the pressure difference between the inlet and the nozzle outlet, and the velocity of the fluid is related to the square root of the pressure difference. This formula considers both the pressure difference and the fluid density, along with the nozzle's characteristics (size and discharge coefficient), to calculate how much fluid will pass through the nozzle in each time.[15]

The model is based on Bernoulli's equation, considering:

- Hydrodynamic losses (friction, discharge coefficient)
- Flow regime
- Nozzle friction – modelled using the Darcy-Weisbach equation
- Viscous losses – accounted for through the Reynolds number and empirical turbulence models
- Cavitation and vapor pressure are not included in the model. If the pressure drops below the liquid's vapor pressure, cavitation may occur, leading to a decrease in flow rate. However, this is not characteristic of the developed model.

II. Materials and Methods

A. Deactivating solutions based on surfactants

Surfactants are used to neutralize and remove hazardous substances such as chemical, biological, or radioactive contaminants. They work by emulsifying, dissolving, or breaking down harmful agents, making them less dangerous and easier to wash away.

These solutions typically contain:

- Anionic, non-ionic, or cationic surfactants – help degrade contaminants.
- Oxidizers – such as sodium hypochlorite (NaClO) or hydrogen peroxide (H_2O_2), which break down toxic substances.
- Buffer systems – maintain an optimal pH for neutralization.
- Complexing agents – help bind heavy metals.

Some deactivating substances used for military purposes include:

- DS2 solution – military standard for decontamination. DS2 is a highly alkaline solution with strong solvent and emulsifying properties.
- Oxidizing mixtures based on sodium percarbonate.
- Solutions with Triton X-100 or Tween-80 – used in laboratories. Triton X-100 and Tween-80 are widely used non-ionic surfactants with applications in research, pharmaceuticals, and industrial settings.

They are primarily used for solubilization, emulsification, and protein stabilization.

B. Decontamination Solutions Based on Hypochlorite

Decontamination is the process of neutralizing and breaking down toxic chemical agents (CWAs) like mustard gas (HD), sarin (GB), VX, and other nerve agents. Solutions based on sodium hypochlorite (NaOCl) or calcium hypochlorite ($Ca(OCl)_2$) are commonly used for decontamination, as hypochlorites act as strong oxidizers that break down the molecules of toxic agents. Known hypochlorite-based solutions include: Alkaline Hypochlorite Solutions and Calcium Hypochlorite ($Ca(OCl)_2$) Solution – "Bleaching Lime".

Table 1 shows the main differences between the two solutions.

TABLE 1 Comparison of the Two Solutions

Property	NaOCl Solution	$Ca(OCl)_2$ Solution
Decontamination of VX, HD	Yes	Yes
Decontamination of biological agents	Partial	Yes
Stability during storage	High	Low
Corrosiveness	Moderate	High
Application on equipment	Suitable	Limited

III. Results and Discussion

A. Definition of Input Parameters:

- Nozzle dimensions, d or l;
- Fluid characteristics ρ, μ;
- Pressures: P_{in}, P_{out}.

B. Flow Rate Calculation (Theoretical and Actual):

- Calculate the theoretical velocity $V_{theoretical}$;
- Compute the Reynolds number to determine the flow regime.
- Identify the flow regime (laminar or turbulent) and determine the friction factor, f.
- Calculate frictional losses.
- Adjust the actual flow rate based on the calculated losses.

C. Specific Effects of Solutions on the Model

a) Surfactants

- Reduce surface tension – can affect the dispersion process
- Change viscosity (μ) – increased viscosity can lead to higher pressure losses
- Affect the Reynolds number (Re) – increased viscosity reduces the Reynolds number (Re), which can alter the flow regime

b) Hypochlorite Solutions

- Higher density (ρ) compared to pure water (~1100–1200 kg/m³)
- Can cause corrosion, increasing nozzle roughness
- Chemical activity can change the discharge coefficient due to interaction with the walls

D. How do we adapt the mathematical model?

- To account for these factors, we make the following modifications in the model - Adjusting the Reynolds number
- The Reynolds number changes because, the density of hypochlorite solutions is higher
- The viscosity of surfactant solutions may be higher

E. Visualization:

- Plot of flow rate vs. nozzle diameter.
- Plot of flow rate vs. inlet pressure.
- Plot of Reynolds number.

With this mathematical model, we can accurately predict the flow rate under different conditions.

The following modifications have been made to the model:

- We corrected the Reynolds number.

The Reynolds number changes because the density of hypochlorite solutions is higher. The viscosity of surfactant solutions may be greater. [15], [16]

$$R_e = \frac{\rho_{solution} * V * d}{\mu_{solution}} \quad (5)$$

Where:

- $\rho_{solution}$ is the density of the solution, kg/m³.
- V is the velocity of the fluid or solution, m/s.
- d is the diameter of the pipe or characteristic length, m.
- $\mu_{solution}$ is the dynamic viscosity of the solution, Pa.s or N.s/m^2.
- Re is the Reynolds number.

We have adjusted the discharge coefficient (Cd), as it depends on the properties of the liquid. Typically:

- Pure water – Cd ≈ 0.98
- Viscous surfactant solutions – Cd ≈ 0.92 – 0.96
- • Hypochlorite solutions – Cd ≈ 0.90 – 0.94 [15]

We introduce the corrected formula (6):

$C_d = C_{d\ whater} - \Delta C_{d\ viscosity} - \Delta C_{d\ corrosion}$ (6)

$\Delta C_{d\ viscosity}$ – decreases at high μ;

$\Delta C_{d\ corrosion}$ – decreases with a damaged surface.

The flow rate of the liquid passing through a nozzle increases with the nozzle diameter. This is because a larger diameter increases the cross-sectional area available for the liquid to pass through, allowing a greater volume of liquid to flow through the nozzle per unit time. The relationship is linear, meaning that as the nozzle diameter increases, the flow rate also increases.

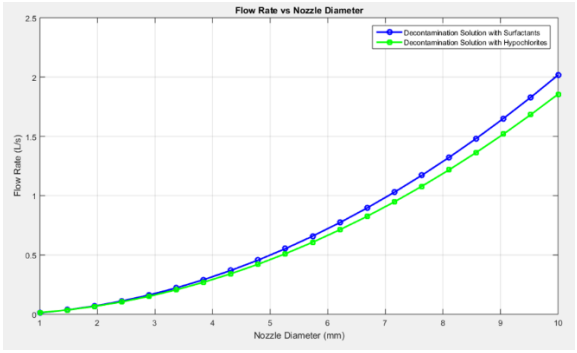

Fig. 1. Flow rate of decontamination solutions versus nozzle diameter.

For disinfection solutions containing surfactants and hypochlorite solutions, the flow rate increases in a similar manner. However, the actual volume of liquid passing through the nozzle will differ due to variations in the density and viscosity of the two solution types. Larger nozzles enable a higher flow rate, which is crucial for applications requiring rapid disinfection of large surfaces or volumes.

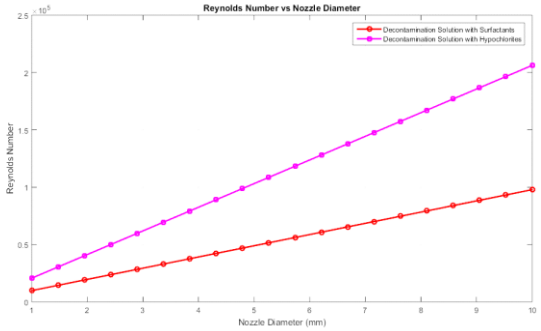

Fig. 2. Flow rate of decontamination solutions versus inlet pressure.

Increasing the inlet pressure will raise the flow rate, but to a lesser extent than increasing the nozzle diameter. Higher inlet pressure results in a greater liquid flow rate, which is beneficial for applications requiring faster dispersion of disinfectant solutions. However, the effect of pressure increase on flow rate is limited compared to the impact of nozzle diameter. This is due to the quadratic relationship between flow rate and pressure.

Since surfactant solutions typically have a higher density than hypochlorite solutions, their flow rate may be lower under the same pressure conditions.

The Reynolds number (R_e) measures the turbulence of the flow. It increases with the nozzle diameter because a larger diameter leads to a consistent increase in flow rate, which can cause the transition from laminar to turbulent flow. As the nozzle diameter increases, the Reynolds number also rises, indicating the potential transition from laminar to turbulent flow.

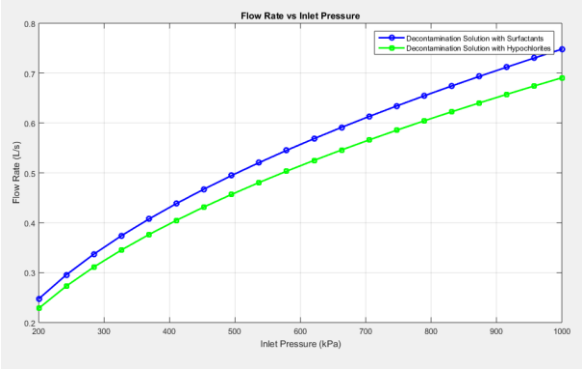

Fig. 3. The relationship between the Reynolds number and the nozzle diameter.

For surfactant solutions, which have a higher viscosity, the Reynolds number will be lower than for hypochlorite solutions, which have a lower viscosity. This suggests that higher pressure or larger nozzles may be necessary for surfactant solutions to achieve turbulent flow.

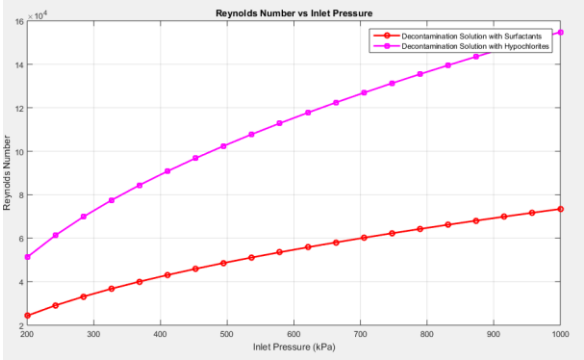

Fig. 4. Relationship between the Reynolds number and the inlet pressure.

The Reynolds number increases with rising pressure. Higher pressure leads to an increased flow velocity, which in turn enhances turbulence. As the inlet pressure increases, the flow becomes more turbulent for all liquids, which is crucial for effective spraying and disinfection.

Surfactant solutions will transition to turbulent flow at lower pressures compared to hypochlorite solutions because surfactants have higher density and viscosity.

IV. Conclusion

Increasing the nozzle diameter leads to a higher flow rate, which is important for effective dispersion of the liquid. Increasing the inlet pressure also raises the flow rate, but its effect is less significant compared to increasing the nozzle diameter. The Reynolds number indicates the transition from laminar to turbulent flow. For more viscous liquids (surfactants), higher pressure or a larger nozzle diameter is required to achieve turbulent flow. Surfactant solutions will require more effort for effective dispersion compared to hypochlorite solutions due to their higher density and viscosity. These relationships and conclusions can be useful for optimizing disinfection processes in industrial applications involving chemical or radiological substances.

V. Acknowledgements

This research is supported National Science Program „Security and Defense”, adopted with RMS No. 731 of 21.10.2021 and according to Agreement No. D01-74/19.05.2022.

VI. Disclosure of Interests

The author has no competing interests.

References

[1] N. Dolchinkov, "Construction of a system for monitoring the pollution of water bodies with waste," Environment. Technology. Resources., Rezekne, Latvia, Proc. 15th Int. Sci. Pract. Conf., vol. 1, pp. 136–141, 2024. DOI: https://doi.org/10.17770/etr2024vol1.7989

[2] N. Dolchinkov, N. Nichev, and Y. Boyanova, "Uranium mines in Bulgaria - Analysis of the state 30 years after their closure," Environment. Technology. Resources., Proc. 15th Int. Sci. Pract. Conf., vol. 1, pp. 123–129, 2024. DOI: https://doi.org/10.17770/etr2024vol1.8002

[3] S. Vambol, M. Alqahtani, N. Dolchinkov, M. Ilyas, S. Yeremenko, V. Sydorenko, and O. Dzhulai, "Investigation of the transfer radioactive contamination from the Chernobyl zone and its impact on radiation in the environment," Ecological Engineering & Environmental Technology, vol. 25, no. 12, pp. 70–84, 2024. DOI: https://doi.org/10.12912/27197050/193261

[4] N. Tonchev, V. Georgiev, N. Hristov, and Y. Kirilov, "Characterization of the 'determination by displacement' approach – defmot with an emphasis on the analysis of multifactorial models," Academic Journal, vol. 12, no. 1, 2023.

[5] N. Tontchev and St. Ivanov, "Madmml - visual multiple criteria approach and decision support system," Transport `05, vol. 19–23, 2005.

[6] P. Koprinkova-Hristova and N. Tontchev, "Echo State Networks for multi-dimensional data clustering," in Artificial Neural Networks and Machine Learning – ICANN ’12, 2012, pp. 571–578.

[7] I. Minevski, Risk in the Transportation of Dangerous Goods by Land Transport, V.T.: Publishing House of the National University of the Republic of Bulgaria, 2018. ISBN: 978-954-753-271-7

[8] N. Tontchev and E. Yankov, "Multi-criteria support for decision-making by shifting restrictions," Int. Sci. Conf. Mathematical Modeling, no. 1, 2017.

[9] Н. Николов, „RDD – мръсни бомби“, Сборник доклади от Годишна университетска научна конференция, том 4, НВУ „В. Левски“, 2021, с. 193–197.

[10] R. Marinov, "Model of management of processes and phenomena’s in the military security system," Environment. Technology. Resources., Proc. 15th Int. Sci. Pract. Conf., vol. IV, pp. 173–177, 2024. DOI: https://doi.org/10.17770/etr2024vol4.8188

[11] Innovative Technologies for Cleaning the Environment: Air, Water and Soil, 14th Int. Seminar on Nuclear War and Planetary Emergencies. World Scientific Publishing, 1993.

[12] Technological Innovations in Sensing and Detection of Chemical, Biological, Radiological, Nuclear Threats and Ecological Terrorism. Netherlands: Springer Netherlands, 2012.

[13] Functional Nanostructures and Sensors for CBRN Defence and Environmental Safety and Security. Netherlands: Springer Netherlands, 2020.

[14] F. Sabath, CBRN Protection: Managing the Threat of Chemical, Biological, Radioactive and Nuclear Weapons. Germany: Wiley-VCH, 2013.

[15] P. K. Kundu and I. M. Cohen, Fluid Mechanics, 4th ed. Elsevier Academic Press, 2004.

[16] O. Reynolds, "On the dynamical similarity of flow in tubes and the criteria for the transition between laminar and turbulent flow," Philosophical Transactions of the Royal Society A: Mathematical, Physical and Engineering Sciences, 1883, pp. 935–982.

Environment. Technology. Resources. Rezekne, Latvia
Proceedings of the 16th International Scientific and Practical Conference. 2025. Volume IV, 277-281

Wind Tunnel Study of Aerodynamic Characteristics of Wing with Arc Shaped Wingtips

Stanimir Penchev
Department of Transport and Aircraft Equipment and Technologies
Technical Univercity of Sofia, Plovdiv Branch
Plovdiv, Bulgaria
spenchev@tu-plovdiv.bg

Hristian Panayotov
Department of Transport and Aircraft Equipment and Technologies
Technical Univercity of Sofia, Plovdiv Branch
Plovdiv, Bulgaria
hristian@tu-plovdiv.bg

***Abstract*— Wingtips devices like winglets and other types are created and intended to improve aerodynamic efficiency of aircraft based on minimizing induced end vortex drag. Investigation of aerodynamic characteristics of these devices at low Reynolds numbers is the aim of the study. In present study the models of basic straight tapered wing and wing with arc shaped wingtips are examined. For this purpose the basic model is equipped with replaceable tips with different geometry. The measurements are performed in low - speed wind tunnel at Reynolds number of around 100000. The analysis of the collected data shows that the best aerodynamic characteristics have configuration with 45 degrees dihedral at the tips of the wing. The results can be used in the conceptual design of small unmanned aerial vehicles (UAV) to improve their performance such as range and endurance.**

Keywords*— *aerodynamic efficiency, drag, lift, wingtip design.

I. INTRODUCTION

Wingtip devices are designed to improve the aerodynamic efficiency of aircraft by increasing lift, reducing drag, and decreasing the intensity of tip vortices. They have many variations and can be divided into three main groups - in the plane of the wing, flat, at an angle to the plane of the wing, and with a nonplanar shape [1]. These devices increase the effective aspect ratio of the wing and reduce induced loses, but on the other hand they also increase parasite drag. Another drawback is the increased mass of the wing due to augmented bending moment. The main task in the design process is to choose an aerodynamic layout that will allow for the realization of better flight performance. There are different types of wingtip devices [2] and the more common ones are shown in Fig. 1.

Wind tunnel studies are one of the most widely used methods for determining the aerodynamic characteristics of wingtip devices [3] – [6]. Results of studies on a wing with elliptical winglets [7], multi-element winglet systems [8], [9], and also a wing–grid tips with several elements and a semicircular planform [10] have been published. The data from these experiments show a significant increase in lift curve slope and maximum lift to drag ratio.

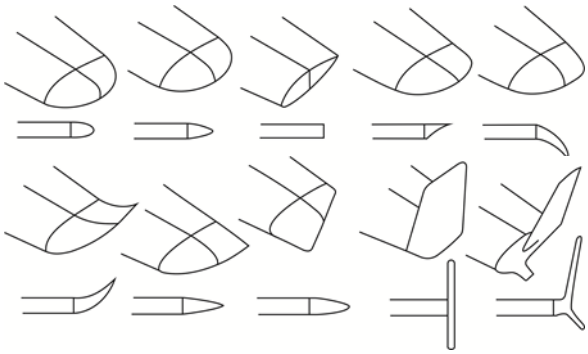

Fig. 1. Common view of wingtips devices.

The article presents a comparative wind tunnel study of the aerodynamic characteristics of models with a trapezoidal wing and winglet configurations at low Reynolds numbers. The research was carried out at the Laboratory of Aerodynamics in the Plovdiv branch of the Technical University of Sofia. Based on the results of the experiments, a comparison of aerodynamic characteristics of the different configurations was made.

Online ISSN 2256-070X
https://doi.org/10.17770/etr2025vol4.8444
© 2025 The Author(s). Published by RTU PRESS.
This is an open access article under the Creative Commons Attribution 4.0 International License.

II. MATERIALS AND METHODS

A. Model details

The wind tunnel model consists of several parts - cylindrical body, two half – wing consoles and replaceable tips. This design allows obtaining many variants with a minimum number of manufactured parts.

The unswept base wing has a trapezoidal shape in plane, with a wing span of 400 mm, root chord 60 mm, tip chord 40 mm, mean geometric chord 50 mm, taper ratio 0.67, aspect ratio 8, reference wing area 0.02 m^2, without geometric twist. The cross-sections of the wing and the wingtip devices are made of airfoil NACA0012. The diameter of the body is 53.5 mm and the length is 384 mm.

The wingtips have arc-shaped form as shown in Fig. 2. The trailing edge of wing model (t.e.) is straight and leading edge (l.e.) has increased sweep angle. The cant angle is denoted as θ.

The releasable parts of wind tunnel model are made by the rapid prototyping technology Fused Deposition Modelling (FDM), which uses polymers (mainly ABS) suitable for both prototypes and final products. The obtained details are appropriate both for conducting functional tests and for use as final products. They have a good appearance, which can be subjected to further processing. Before the test, the manufactured details are additionally processed in order to improve their surface quality and obtain the necessary smoothness.

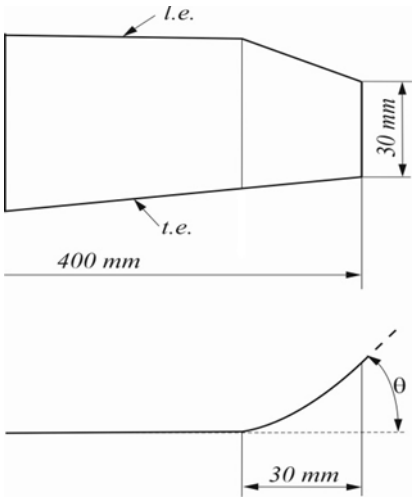

Fig. 2. Schematic diagram of the winglet design.

Additional pre-fabricated aerodynamic surfaces have been mounted to the half - wing consoles of the multiple - part model and thus various configurations have been obtained. The use of symmetrical profiles and the absence of geometric twist allows for easier arrangement. 3-D models in the SolidWorks software package have been developed (Fig. 3).

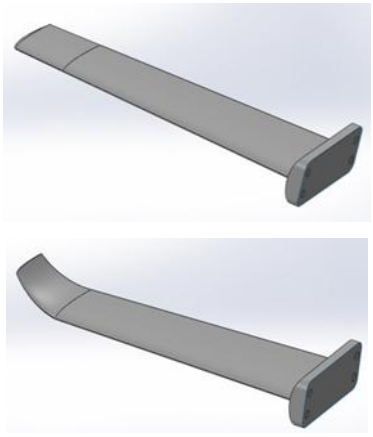

Fig. 3. 3-D representation of half - wing models.

Three different values and two directions for the cant angle are used. Negative values have the wingtips pointing downwards (Table 1).

TABLE 1 DATA FOR THE TEST MODELS

Test models	**Data**	
	Cant angle θ	***Designation***
Base wing	0°	base wing
Wing with winglets	15°	arc15p
	30°	arc30p
	45°	arc45p
	-15°	arc15n
	-30°	arc30n
	-45°	arc45n

B. Wind tunnel and instrumentation

A low-speed closed circuit wind tunnel of 600 mm x400 mm rectangular open test section and 1000 mm long is used for carrying out the experiments (Fig. 4). The wind tunnel can be operated at a maximum air speed of 50 m/s and has a capacity for setting an angle of attack from -10° to 20°. Detailed data on the design and characteristics of the test facility are given in [11].

Internal strain gage aerodynamic balances [12] measure directly the forces and moments in the coordinate system of the balances: axial force ***X***, normal force ***Z*** and pitch moment ***M***.

Fig. 4. Aircraft model mounted in the wind tunnel test section.

During the experiment, the following is carried out: automated control of the model's movement according to a set program; automated output of information with strain gauges, a flow temperature sensor, sensors for measuring the total pressure and the differential pressure; data processing and visualization.

III. RESULTS AND DISCUSSION

The conditions under which the wind tunnel tests were carried out were a constant flow speed of 25 m/s and a change in the angle of attack from 2° to 12° with a step of 1°. These conditions correspond to Reynolds numbers around 100000, calculated using the base wing mean chord. The effective Reynolds number according to [13] is 180000. The experiments determined the aerodynamic forces and the moment in the plane of symmetry of the model – lift, drag and pitch moment. The origin of the related coordinate system of the model coincides with the origin of the root chord of the wing. The obtained results are adjusted by introducing a correction for the downwash angle in the test section [11]. The lift force coefficient C_L, drag force coefficient C_D and pitch moment coefficient C_m are calculated.

The data presented in Fig. 5 and Fig. 6 shows the same values of stall angles of attack and negligible variation for maximum lift coefficients. The lift curve slope is less than that of the base wing.

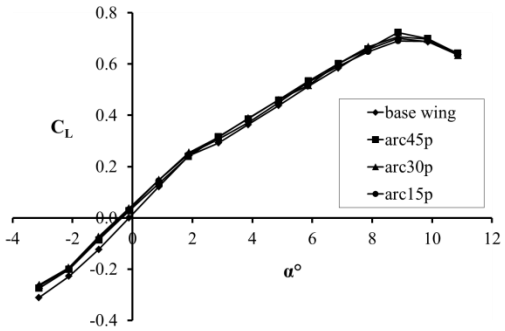

Fig. 5. Lift coefficient vs. angle of attack.

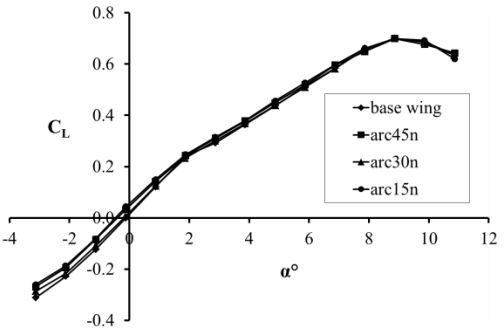

Fig. 6. Lift coefficient vs. angle of attack.

The minimum drag coefficients (Fig. 7) are almost the same and lower than those of the base wing. One of the reasons for this is that the same reference wing area, equal to that, of the base wing, is used for the aerodynamic performance calculation.

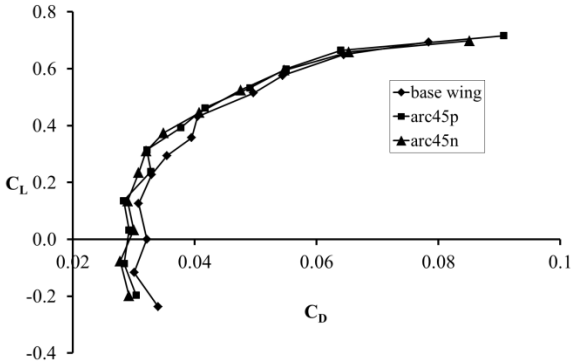

Fig. 7. Drag polar for selected configurations.

There is practically no change in the pitch moment for different configurations – Fig. 8.

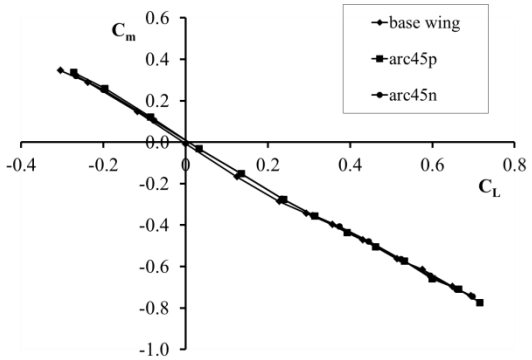

Fig. 8. Pitch moment coefficient for selected configurations.

At a maximum lift to drag ratio, the minimum required thrust for level flight is obtained, i.e., the maximum endurance with the other things being equal. To evaluate the aerodynamic efficiency at angles of attack smaller and larger than the most advantageous one, the coefficients ***C1*** and ***C2*** were calculated.

$$C1 = \frac{C_L^{1.5}}{C_D} \quad (1)$$

$$C2 = \frac{C_L^{0.5}}{C_D} \quad (2)$$

The maximum values of these coefficients correspond to the modes of minimum required power for level flight and maximum flight range [14]. Under the first of these modes, the angle of attack is larger than the most advantageous one, while under the second it is smaller and respectively lift coefficient. The calculation of these quantities and the comparison of their values with the values for the base wing will allow evaluating the

possibilities of increasing the flight performance for aircrafts, using the studied aerodynamic characteristics.

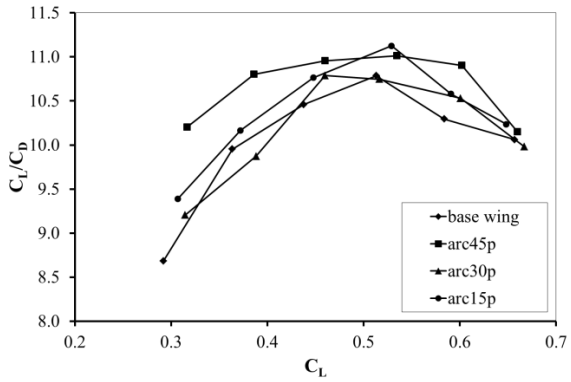

Fig. 9. Lift to Drag ratio vs. lift coefficient.

The change in the lift to drag ratio is smoother and, in the range of C_L from 0.3 to 0.7, it has higher values for configurations with ±45° cant angle compared to the base wing. At lift coefficient of around 0.5 the maximum values are observed. The increase is less than 4% compared to the baseline model.

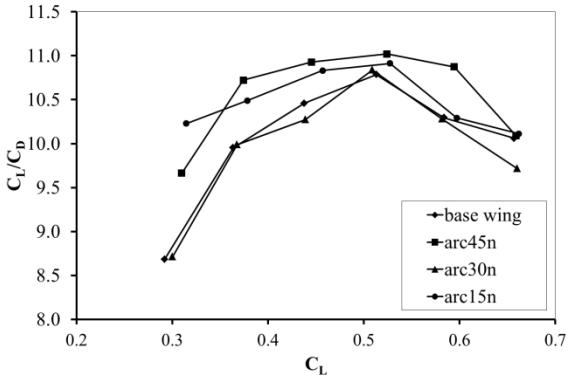

Fig. 10. Lift – to - Drag ratio vs. lift coefficient.

The change in the coefficients ***C1*** and ***C2*** (Fig. 11 and Fig. 12) is more significant. At lift coefficient of around 0.65 the maximum values of coefficients ***C1*** are observed and the increase is about 4%. The maximum values of the coefficient ***C2*** have the highest rise compared to the base wing. For configurations with ±45° cant angle the increase is up to 8%. The lift coefficient for these conditions has values slightly above 0.3.

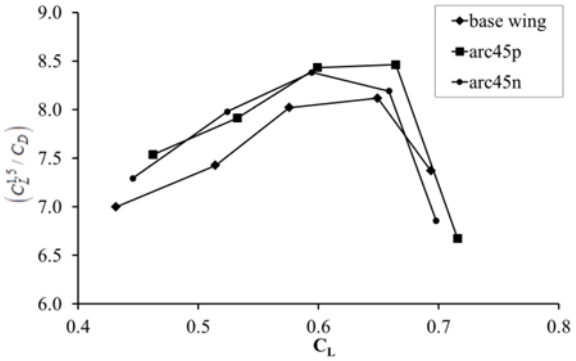

Fig. 11. Variation of coefficient ***C1*** vs. lift coefficient.

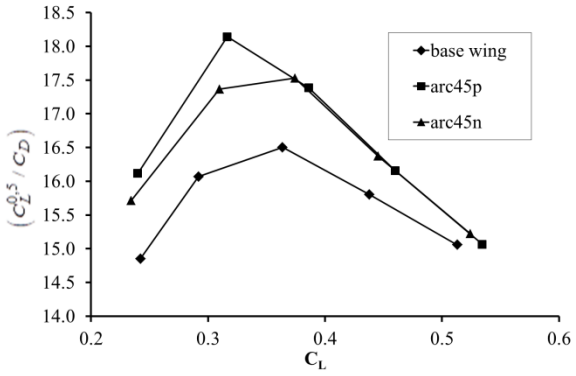

Fig. 12. Variation of coefficient ***C2*** vs. lift coefficient.

Table 2 presents the calculated values of the aerodynamic characteristics for the studied configurations. Lift curve slope is estimated for positive lift coefficients in the linear range. The stall angle of attack for all configurations is around 9°.

TABLE 2 SUMMARY RESULTS

Test models	**Aerodynamic characteristics**				
	C_{Lmax}	$C_{L\alpha}$	$(C_L/C_D)_{max}$	***C1***	***C2***
base wing	0.70	4.30	10.65	8.11	16.21
arc15p	0.69	4.24	11.13	8.24	16.95
arc30p	0.71	4.16	10.78	8.19	16.41
arc45p	0.72	4.47	11.08	8.46	17.44
arc15n	0.70	4.23	10.93	7.91	16.60
arc30n	0.70	4.28	10.84	7.95	16.47
arc45n	0.70	4.33	11.02	8.38	17.52

IV. CONCLUSIONS

Based on the research conducted and the results obtained, the following main conclusions can be drawn:

- The winglet models with ±45° cant angle have increased lift to drag ratio, minimum power and maximum range coefficients;
- It cannot be clearly determined whether configurations with positive or negative dihedral have better characteristics;
- The results show that winglet models have a greater increase in aerodynamic efficiency at low angles of attack.

The latter observation is interesting from an aerodynamic point of view and needs further investigation. To clear up the influence of the winglet's dihedral, further studies for models with a cant angle of 60 to 90 are required.

The results of the research can be used to create computational models to study the influence of geometric parameters such as twist, chord distribution, etc., and achieve an optimal winglet design. Another application of the obtained experimental data is in the development process of small UAVs.

ACKNOWLEDGMENTS

The authors would like to thank the European Regional Development Fund under the Operational Program "Scientific Research, Innovation and Digitization for Smart Transformation 2021-2027", Project CoC "Smart Mechatronics, Eco- and Energy Saving Systems and Technologies", BG16RFPR002-1.014-0005 for funding the publication.

REFERENCES

[1] S. Penchev, Study of aerodynamic characteristics of wings with wingtip devices, Technical University – Sofia, Sofia, Bulgaria, Ph. D. thesis, 2018.

[2] D. P. Raymer, Aircraft Design: A Conceptual Approach, Washington DC: AIAA Education Series, 2012.

[3] M. I. Inam, M. Mashud, A Nahian and S. M. S. Selim, Induced drag reduction for modern aircraft without increasing the span of the wing by using winglet. International journal of mechanical and mechatronics, vol. 10, pp. 49-53, 2010.

[4] V. R. Nikolic, Planform variations and aerodynamic efficiency of movable tip strakes, Journal of Aircraft, vol. 44(1), pp. 340-343, 2007.

[5] V. R. Nikolic, Effect of leading-edge form on performance of wing-movable tip strake configurations, Journal of Aircraft, vol. 44(5), pp. 1749-1753, 2007.

[6] M. F. Reeder, W. Allen, J. M. Phillips and R. Dimmick, Wind-tunnel measurements of the E-8C modeled with and without winglets, Journal of Aircraft, vol. 45(1), pp. 345-348, 2008.

[7] P. R. Arora, A. Hossain, P. Edi, A. A. Jaafar, T. S. Younis and M. Saleem, Drag reduction in aircraft model using elliptical winglet. Journal-The Institution of Engineers, vol. 66(4), pp. 1-8, 2005.

[8] M. Berens, Potential of multi-winglet systems to improve aircraft performance, Technical University Berlin, Berlin, Germany, Ph.D. thesis, 2008.

[9] F. M. Catalano and H. D. Ceron-Munoz, Experimental analysis of aerodynamic characteristics of adaptive multi-winglets, Proceedings of the Institution of Mechanical Engineers, Part G: Journal of Aerospace Engineering, vol. 220(3), pp. 209-215, June 2006, https://doi.org/10.1243/09544100JAERO22.

[10] A.Hossain, A. Rahman, A. Iqbal, M. Ariffin and M. Mazian, Drag analysis of an aircraft wing model with and without bird feather like winglet, International Journal of Aerospace and Mechanical Engineering, vol. 6(1), pp. 8-13. 2012.

[11] H. Panayotov, S. Penchev and Kolibarov, Experimental study of canard UAV aerodynamics, In MATEC Web of Conferences, vol. 133, EDP Sciences, 2017. https://doi.org/10.1051/matecconf/201713301002

[12] C. Britcher and D. Landman, Wind Tunnel Test Techniques, Academic Press, 2023.

[13] H. Panayotov, S. Penchev and M. Zikyamov, Experimental study of turbulence in the test section of wind tunnel, Environment. Technology. Resources., 15th International Scientific and Practical Conference, Rezekne, Latvia, Jun. 2024, vol. 3, pp. 217–220, https://doi.org/10.17770/etr2024vol3.8118.

[14] E. Torenbeek, H. Wittenberg, Flight physics. Essentials of aeronautical disciplines and technology with historical notes. London: Springer, 2009.

Environment. Technology. Resources. Rezekne, Latvia
Proceedings of the 16th International Scientific and Practical Conference. 2025. Volume IV, 283-288

Wind Tunnel Investigation of Wake Characteristics of a Wing with Winglets

Stanimir Penchev
Department of Transport and Aeronautical Engineering
Technical Univercity of Sofia, Plovdiv Branch
Plovdiv, Bulgaria
spenchev@tu-plovdiv.bg

Hristian Panayotov
Department of Transport and Aeronautical Engineering
Technical Univercity of Sofia, Plovdiv Branch
Plovdiv, Bulgaria
hristian@tu-plovdiv.bg

Martin Zikyamov
Department of Transport and Aeronautical Engineering
Technical Univercity of Sofia, Plovdiv Branch
Plovdiv, Bulgaria
martinzikyamov@gmail.com

***Abstract*— Aircraft performance such as range and endurance is highly dependent on induced and vortex drag. There is a close relationship between wake structure and aerodynamic performance. In the present paper the velocity field behind the model of wing with winglet is studied. The methodology and equipment for the study in low speed wind tunnel ULAK – 1 are presented. The pressure field is obtained using a five-hole pressure probe which is positioned in a cross plane at 300 mm behind the wing trailing edge. Acquired experimental data are used to calculate cross flow velocity and vorticity fields at an angle of attack of 6 degrees - around maximum lift to drag ratio. The results are compared to the data of the model with planar wing. During the subsequent processing coefficients of lift and induced drag can be obtained.**

Keywords—experimental study, five – hole pressure probe, velocity field, vorticity.

I. INTRODUCTION

In experimental studies conducted in wind tunnels, methods utilizing flow parameter data in a control area around the object of interest are commonly employed [1] – [3]. This approach facilitates the determination of the components of aerodynamic drag - namely profile drag, induced drag, and wave drag and allows for an assessment of how the design parameters of the model influence these components [4].

One study [5] examined the vortex wake of a transport aircraft model featuring a wing with a winglet and two engines mounted on pylons at mid-wing, using a constant temperature anemometry for measurements across seven planes. The processed data revealed the velocity distribution, the axial component of the vorticity (perpendicular to the measurement plane), and the turbulence intensity, while also establishing the vortex structures in the wake near the model.

Another research [6] explored the effect of the winglet's dihedral angle on the velocity distribution and wake characteristics of a wing model. This investigation utilized a spatial velocity probe with seven measurement openings to capture the velocity field [7], [8]. The wing airfoil tested was NACA 0015, and experiments were conducted at a Reynolds number of 185,000. Results indicated a reduction in the maximum velocity projection in the measurement plane, a decrease in vorticity, and diminished induced drag when employing a wing with a winglet compared to a baseline wing.

In yet another study [9], the equipment, methodology, and findings from an experimental investigation into the near wake of a rectangular wing were presented. A pressure sensor was employed to directly ascertain the velocity circulation in the measurement area, with a grid measurement step of 2 mm. The formation and development of the trailing vortices were also examined [10].

Additionally, equipment that utilizes optical [11] – [13] or ultrasonic measurement methods has been deployed to assess flow parameters in the test section of the wind tunnel. A study [14] investigating the flow in the wake of a rectangular wing shaped with NACA 0012 airfoil was carried out using Particle Image Velocimetry (PIV), a modern optical method increasingly gaining traction. Findings from this study indicated that the flow velocity within the core of the trailing vortex varied according to an exponential law.

The techniques for determining aerodynamic characteristics based on wake parameters are among those utilized in the analysis of wings equipped with wingtip devices and play a crucial role in enhancing the understanding of flow dynamics and evaluating the contributions to induced drag.

Online ISSN 2256-070X
https://doi.org/10.17770/etr2025vol4.8452
© 2025 The Author(s). Published by RTU PRESS.
This is an open access article under the Creative Commons Attribution 4.0 International License.

This publication introduce the equipment and methodological background of a developed system designed to measure flow parameters within the test section of the wind tunnel at the Laboratory of Aerodynamics in the Plovdiv branch of the Technical University of Sofia. The studies are centred on the assessment of the pressure field using a five-hole pressure probe. Following the analysis of the experimental data, characteristics of the velocity field were obtained. Measurement results for two configurations- a wing with a winglet and a planar wing at an angle of attack of 6° are presented, along with an overview of the equipment's capabilities for determining the aerodynamic characteristics of a lifting surface using alternative methods.

II. Materials and Methods

A. System for Determining Flow Parameters

An experimental setup was designed and constructed to determine the flow parameters (static pressure, total pressure, magnitude, and direction of velocity) in the test section of a wind tunnel.

The main components of the developed laboratory setup include:

- A low-speed wind tunnel with an open test section [14].
- A model positioning mechanism (α-β mechanism).
- A two-coordinate stand for the movement and positioning of a spatial five-hole velocity probe.
- A servo drive equipped with stepper motors and CNC control.
- A module for measuring total pressure, velocity, and flow angles, utilizing a spatial velocity probe and five 24PC differential pressure sensors.
- Measuring and control equipment based on a personal computer, utilizing NI cDAQ – 9174, NI 9237, and NI USB – 6211 modules.
- Specialized software for processing measurement results in the LabVIEW environment.

This setup allows for comprehensive analysis of airflow characteristics within the wind tunnel.

The main component of the system is a two-coordinate stand designed for the movement and positioning of a spatial velocity measuring probe within the test section of the aerodynamic wind tunnel (AWT). The moving plane is oriented perpendicular to the direction of the undisturbed flow, with the object of study positioned in front of it (Fig. 1).

A pressure receiver, connected to a stepper servo drive, can be moved to provide various movement profiles and speeds. The software allows for setting a single position or executing a predefined movement profile.

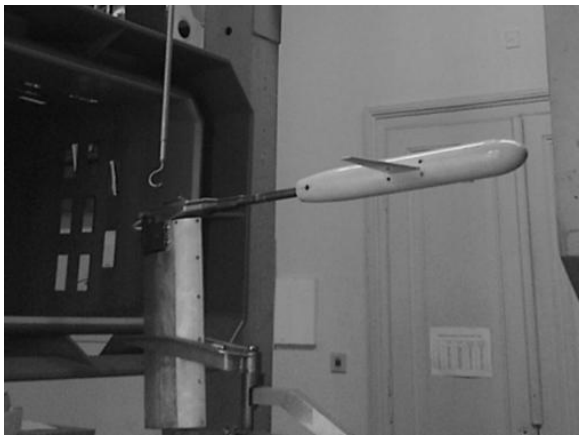

Fig. 1. Location of the model and the velocity measuring probe in the test section of the wind tunnel.

The mechanical part employs ball screw pairs, cylindrical guides, and ball bushings. The movement range along the horizontal z-axis extends from 0 to 650 mm, while the vertical y-axis ranges from 0 to 400 mm. This configuration enables measurement of flow parameters at all points across the cross-section of the test area, with a displacement speed of up to 1000 mm/min. The position of the probe within the plane is measured using ELPT position sensors. During experiment, the following parameters are measured: atmospheric pressure (p_a), overpressure in the fore chamber of the AWT (p_f), pressure readings from the spatial velocity probe ($p_1 – p_5$), and model positioning, which includes angles of attack (α) and sideslip (β). All measured values are recorded in a file. Control of the system is managed through NI cDAQ – 9174, NI 9237, and NI USB – 6211 modules, utilizing software developed in the LabVIEW environment.

The model is attached to the positioning mechanism within the test section of the AWT and is set to the appropriate angles of attack and slip by sending control signals from the NI USB–6211 module. Since the spatial velocity probe remains in a fixed position, a device has been developed to adjust the model's distance from this plane.

The software enables the automation of measurements during experiments. To achieve this, the specified movement profile of the pressure probe is executed through digital programming control of the coordinate stand. A software module is in place to read and record measurement results, synchronized with the coordinate stand’s movements via the ELPT position sensors. Pressure readings are taken at predetermined steps along the movement trajectory set previously in the software.

The graphical user interface of the software module (Fig. 2) provides real-time information regarding the position of the pressure probe, pressure values, average flow velocity in the test section, and atmospheric pressure. These quantities are recorded in a file and vary based on the coordinates in the displacement plane yOz. The system allows for continuous measurement of pressures p_1 - p_5, as well as measurements taken upon reaching specific positions within the plane.

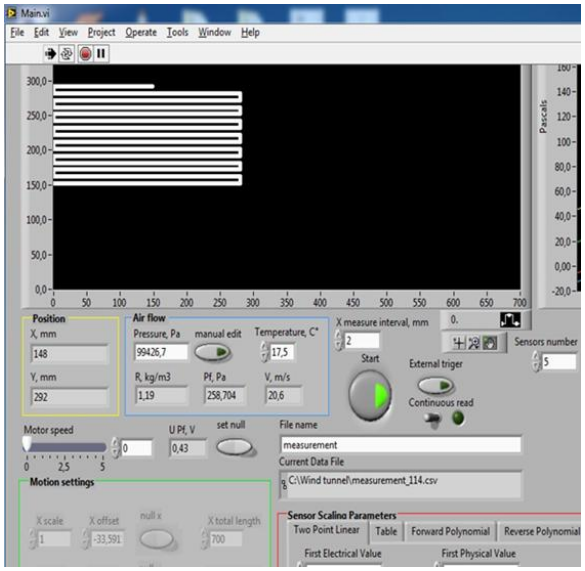

Fig. 2. Software module panel.

The system utilizes a spatial velocity probe with a spherical head and five pressure holes (Fig. 3): a central (p_1), two lateral holes in the vertical plane (p_2, p_3), and two lateral holes in the horizontal plane (p_4, p_5). The diameter of the sphere is 3.5 mm, and the design angle is 45°. To determine the velocity components V_x, V_y, and V_z, it is essential to calibrate the pressure probe [16], [17]. This calibration process involves obtaining functions of the pressure coefficients based on the flow angles α and β within both the horizontal and vertical planes.

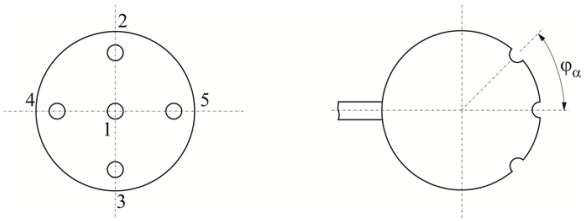

Fig. 3. Layout of the pressure receiver holes.

These coefficients are calculated as follows:

$$C_{p,\alpha} = \frac{p_2 - p_3}{p_1 - \overline{p}} = f(\alpha, \beta) \quad (1)$$

$$C_{p,\beta} = \frac{p_4 - p_5}{p_1 - \overline{p}} = f(\alpha, \beta) \quad (2)$$

$$C_{p,t} = \frac{p_1 - p_t}{p_1 - \overline{p}} = f(\alpha, \beta) \quad (3)$$

$$C_{p,st} = \frac{p_1 - p_{st}}{p_1 - \overline{p}} = f(\alpha, \beta) \quad (4)$$

In the dependencies (1) – (4), p_t и p_{st} represent the total and static pressures of the undisturbed flow, respectively, while $\overline{p}$ - denotes the arithmetic mean value of the pressures p_2 – p_5. The measured quantities are obtained at the nodes of a rectangular grid defined by the coordinates y and z in the measurement plane.

The processing of the experimental results follows this sequence:

1. For each position (z, y), the pressure coefficients $C_{p,\alpha}$ and $C_{p,\beta}$ are determined from the measured pressures $p_1 - p_5$ using dependencies (1) – (4).

2. Utilizing calibration dependencies and the determined pressure coefficients, the local flow angles α and β in the measurement plane are established.

3. The velocity V and its components in the measurement plane are calculated using the established relationships.

$$V = \sqrt{\frac{2}{\rho}(p_1 - \overline{p})(1 - C_{p,t} + C_{p,st})} \quad (5)$$

$$V_x = V \cos\alpha \,.\, \cos\beta \quad (6)$$

$$V_y = V \sin\alpha \,.\, \cos\beta \quad (7)$$

$$V_z = V \sin\beta \quad (8)$$

4. The velocity field in the measurement plane is represented graphically, allowing for the determination of the format and location of the vortex wake.

5. Next, the radius of the trailing vortex core and the distance from its center to the plane of symmetry of the model are measured. To identify these characteristics of the wake, the distribution of horizontal and vertical velocity projections within the measurement plane are analyzed. The data is extracted from the graphical representation in areas where there is a quantities transition from maximum positive to maximum negative values of the velocity projections.

6. The axial component of the vorticity ζ_x is defined:

$$\zeta_x = \frac{\partial V_z}{\partial y} - \frac{\partial V_y}{\partial z} \quad (9)$$

The results obtained can be used to determine the lift and induced drag coefficients.

B. Processing of Experimental Data

When studying the characteristics of the airflow past the wing, the velocity components' distribution is measured in a specific plane. Typically, the measurement points are arranged in a rectangular, structured grid, which may have constant or varying intervals in both coordinates. The vorticity of the vortex layer is represented by the circulation of the velocity around the corresponding cell in the computational grid (Fig. 4).

$$\zeta_{k+1/2,j+1/2} = \Gamma_{k+1/2,j+1/2} / \Delta y \Delta z \qquad (10)$$

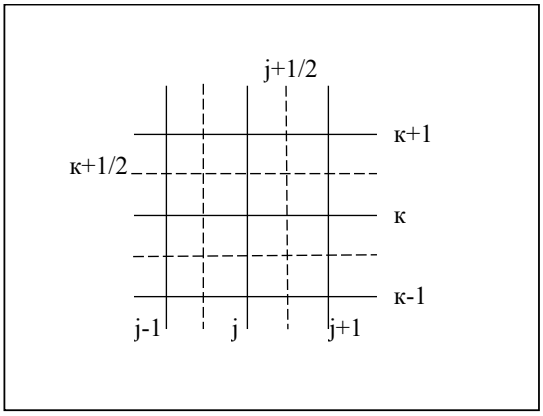

Fig. 4. Scheme of the Computational Grid

In the expression above, ***Δy*** and ***Δz*** denote the grid intervals in the vertical and horizontal directions, respectively. The circulation of velocity around a given computational cell is calculated as follows [18].

$$\begin{aligned} \Gamma_{k+1/2,\,j+1/2} &= 0,5(V_{y_{k,j}} + V_{y_{k+1,j}}).\Delta y + \\ &+0,5(V_{z_{k+1,j}} + V_{z_{k+1,j+1}}).\Delta z - \\ &-0,5(V_{y_{k,j+1}} + V_{y_{k+1,j+1}}).\Delta y - \\ &-0,5(V_{z_{k,j+1}} + V_{z_{k+1,j+1}}).\Delta z \end{aligned} \qquad (11)$$

C. Geometric Characteristics of the Models

The models used in the wind tunnel research are fabricated using Fused Deposition Modeling (FDM) rapid prototyping technology, employing polymers like ABS that are suitable for both prototypes and final products. Before testing, the manufactured parts undergo additional processing to enhance the quality of their surfaces and achieve the required smoothness.

The configuration of the test model is determined by how it is attached in the test section of the AWT. The model features a cylindrical body with a rounded front end and two half wing consoles (Fig. 1). The base planar wing has a trapezoidal shape with a span of 400 mm, a root chord of 60 mm, a tip chord of 40 mm, a mean geometric chord of 50 mm, a taper ratio of 1.5, and an aspect ratio of 8. The wing gross area is 0.02 m², without geometric twist. The cross-sections of both the wing and winglet are constructed from the same airfoils - NACA0012. The model body has a diameter of 56.5 mm and a length of 384 mm.

In the wing with winglet model, the leading edge sweep is increased at the end of the cantilever by 15% of the half-span. The winglet measures 20 mm in length, with chords of 30 mm at the root and 15 mm at the tip, and features a dihedral of 75° (Fig. 5).

Fig. 5. Wing tip shape with winglet

III. Results and Discussion

Experiments were conducted using two different wing models. Flow parameter studies were performed with a flow velocity of 20 m/s and a wing angle of attack (***α***) of 6°. Measurements were taken in a plane located 300 mm behind the trailing edge of the wingtip: specifically in the wake area behind the right half of the wing. The measurement step was set at 10 mm. The following charts present the results of the velocity projections, which help outline and characterize the vortex wake.

In Fig. 6 – Fig. 9, the coordinates of the measurement points have been recalculated so that the position of the base planar wing is at the level of y = 0 mm, and the model's plane of symmetry coincides with the coordinates ***z*** = 0 mm. Additionally, dimensionless coordinates are employed, using the half-span (***l/2***) of the planar wing as a parameter.

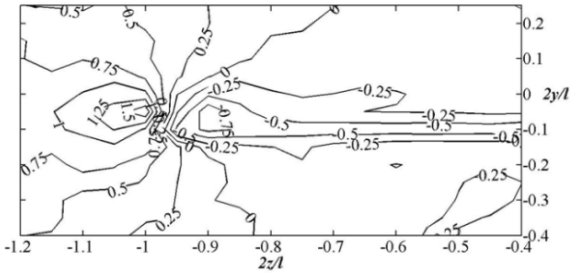

Fig. 6. Distribution of the velocity vertical projection V_y for a planar wing.

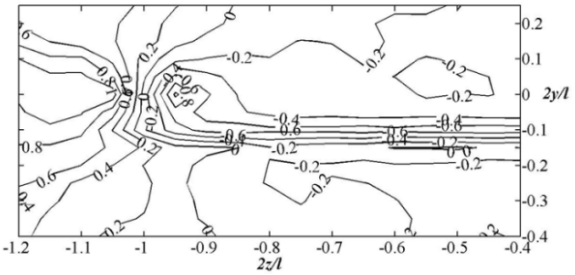

Fig. 7. Distribution of the velocity vertical projection V_y for a wing with winglets.

The presented data clearly demonstrate the differences in flow behind the two research models. For the wing with the winglet, the wake exhibits a pronounced spatial character. The end vortex zone is positioned higher and is located further from the model's plane of symmetry.

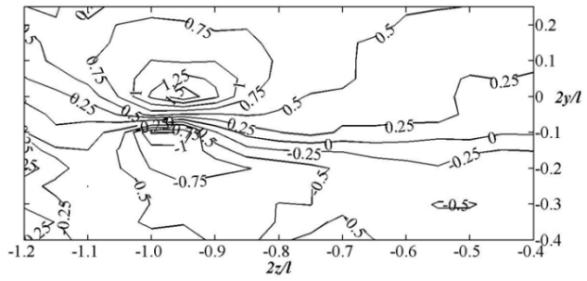

Fig. 8. Distribution of the velocity horizontal projection V_z for a planar wing.

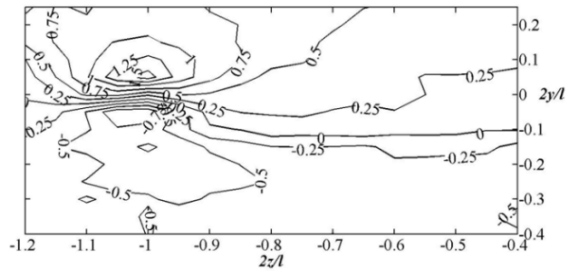

Fig. 9. Distribution of the velocity horizontal projection V_z for a wing with winglets.

Using methods and dependencies (10) and (11), the velocity field results for both the base wing and the model featuring the winglet were processed. The distribution of vorticity in the wake for both wing types was obtained (Fig. 10 and Fig. 11).

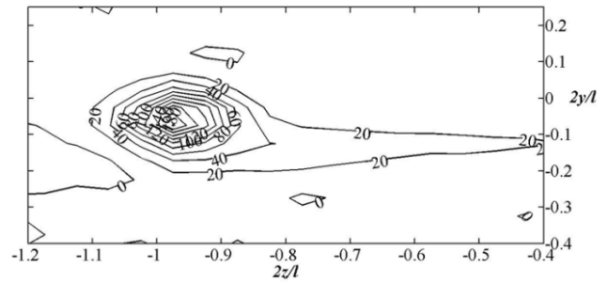

Fig. 10. Distribution of vorticity ζx for the base wing.

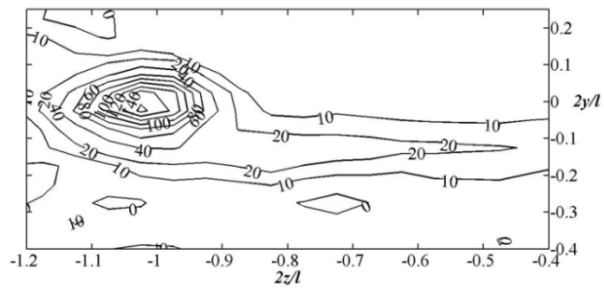

Fig. 11. Distribution of vorticity ζx for a wing with winglets model.

When analyzing the results presented in Fig.10 and Fig. 11, it is observed that the vorticity reaches a larger maximum value for the planar wing. In contrast, the vorticity distribution for the wing equipped with a winglet is more uniform. The vortex wake occupies a larger area, and the center of the formed end vortices are positioned farther from the plane of symmetry. There are established theoretical models that describe aerodynamic characteristics based on the circulation of the flow velocity in the wake, the radius of the vortex core, and the distance between the centers of the end vortices [19]. According to these models, an increase in the distance between the end vortices corresponds to an increase in lift and a decrease in the induced drag of the wing. When evaluating different wing models, these results are supported by studies of integral aerodynamic characteristics [20], which indicate an increase in lift-to-angle of attack ratio, as well as an improved lift-to-drag ratio.

IV. Conclusions

The equipment and methodological framework outlined in this publication provide an opportunity to enhance research at the Laboratory of Aerodynamics in the Plovdiv Branch of the Technical University of Sofia. The experimental data can also be utilized to determine the lift force and components of aerodynamic drag. Visualization and quantitative assessment of the flow velocity field are crucial for process to design an aircraft and specifically assessing the aerodynamic efficiency of various wingtip devices. This is an essential area for further research development. Additionally, combining these methods with others, such as Particle Image Velocimetry (PIV), could improve existing vortex wake models and aid in the development of new ones.

Acknowledgments

The authors would like to thank the European Regional Development Fund under the Operational Program “Scientific Research, Innovation and Digitization for Smart Transformation 2021-2027”, Project CoC “Smart Mechatronics, Eco- and Energy Saving Systems and Technologies”, BG16RFPR002-1.014-0005 for the financial support of the experiments and to the National Program "Young Scientists and Postdoctoral Fellows - 2" at the Technical University of Sofia for funding the publication.

References

[1] D. D. Chao and C.P. van Dam, Wing drag prediction and decomposition, J. of Aircraft, vol. 43(1), pp. 82-90. 2006.

[2] A. C. de Bruin and F. Ganzevles, Data analysis of wake survey tests behind swim model in dnw-lst and dnw-llf wind tunnels, National Aerospace Laboratory NLR, Tech. Rep. NLR-TR-2001-201, 2001.

[3] M. Lanzetta, B. Mele and R. Tognaccini, Advances in aerodynamic drag extraction by far-field methods, J. of Aircraft, vol. 52(6), pp. 1873-1886. 2015.

[4] Y. Deng, Y. Zhang and H. Chen. Drag prediction and decomposition of a real aircraft based on middle-field and far-field methods, 7th European conference for aeronautics and space sciences (EUCASS), 2017, DOI: 10.13009/EUCASS2017-380

[5] A. Alexander and C. Breitsamter, Transport aircraft wake influenced by a large winglet and winglet flaps, J. of Aircraft, vol. 45(2), pp. 686-699, 2008.

[6] P. Gerontakos and T. Lee, Effects of winglet dihedral on a tip vortex, J. of Aircraft, vol. 43(1), pp. 117-124, 2006.

[7] D. Birch, T. Lee, F. Mokhtarian and F. Kafyeke, Structure and induced drag of a tip vortex, J. of aircraft, vol. 41(6), pp. 1138-1145, 2004.

[8] T. Lee and L.S. Ko, Vortex wake generated behind a forward swept wing, J. of aircraft, vol. 46(2), pp. 717-721, 2009.

[9] G. Lombardi and P. Skinner, Wing-tip vortex in near field: an experimental study, J. of aircraft, Vol. 42(5), pp. 1366-1368, 2005.

[10] M. Giuni, Formation and early development of wingtip vortices, Ph.D. thesis, University of Glasgow, Glasgow, Scotland, 2013.

[11] O. A. Elsayed, Experimental investigation of plain- and flapped-wing tip vortices, J. of Aircraft, vol. 46(1), pp. 254-262, 2009.

[12] S. Kaplan and A. Altman, Wake vorticity measurements for low aspect ratio wings at low Reynolds number, J. of Aircraft, vol. 44(1), pp.241-251, 2007.

[13] C. Britcher and D. Landman, Wind Tunnel Test Techniques, Academic Press, 2023.

[14] H. Zhang, Y. Zhou and J. Whitelaw, Near field wingtip vortices and exponential vortex solution, J. of Aircraft, vol. 43(2), pp. 445-449, 2006.

[15] H. Panayotov, S. Penchev and M. Zikyamov, Experimental study of turbulence in the test section of wind tunnel, Environment. Technology. Resources., 15th International Scientific and Practical Conference, Rezekne, Latvia, Jun. 2024, vol. 3, pp. 217–220, https://doi.org/10.17770/etr2024vol3.8118.

[16] G. Brune, Quantitative low-speed wake surveys, J. of aircraft, vol. 31(2), pp. 249-255, 1994.

[17] J. Diebold and M. Bragg, Study of a swept wing with leading-edge ice using a wake survey technique, 51st AIAA Aerospace Sciences Meeting including the New Horizons Forum and Aerospace Exposition, Grapevine, Texas, USA, 07-10 January, 2013, AIAA 2013-0245.

[18] M. Giles and R. Cummings, Wake integration for three-dimensional flowfield computations: theoretical development, J. of aircraft, vol. 36(2), pp. 357-365, 1999.

[19] S. Penchev, Application of various vortex models for determination of wing induced drag, MTM Journal, Issue 8-9, pp. 57-60, 2008, ISSN 1313 – 0226.

[20] S. Penchev, Wind tunnel study of wing with winglets,, Thermal Engineering,.vol. 11(1), pp. 37-40, 2016.

Environment. Technology. Resources. Rezekne, Latvia
Proceedings of the 16th International Scientific and Practical Conference .2025 Volume IV, 289-296

Classification of Micromechanical Elements and Fabrication of Beam-type Micromechanical Elements

Desislava Petrova
Department "Management"
Technical university of Gabrovo
Gabrovo, Bulgaria
des_petrova@abv.bg

***Abstract*—This article presents the developed classification of micromechanical elements, as well as the calculations and fabrication of micromechanical elements of the beam type, using the theory of elasticity and the Finite Element Method (FEM). The principle of etching a conventional angle and partial etching of freely vibrating components is considered. The technical model of the clamped beam, physical and mathematical modeling, as well as simulation and verification of correctness are described. The relationship between the design and entry into the database of the automated design system "MICROSYS 25" of microsystem engineering products is presented.**

Keywords*— *classification of micromechanical elements (MMEs), design, modeling.

I. INTRODUCTION

Digital skills and competences have an important role in increasing the possibilities of adaptation of human capital to the changing requirements of jobs and the labor market in the conditions of Industry 4.0. [1 - 3].

The creation of any Microtechnology product (micromechanical component - MMC, Micromechanical element - MME, microcomponents - MC, sensors, etc.) is reduced to the construction of two systems of connections, relating to: the design of the Microsystems Technology product itself and the production process of its manufacture [4 - 7].

It is necessary that the connections in the production process (PP) be constructed in strict accordance with the system of connections contained in the design of the product itself, i.e. the technological process (TP) inherits the system of sets of the two types of connections characteristic of the design - a system of connections in the design of the product and that in the production process of the product, which is presented in Fig. 1.

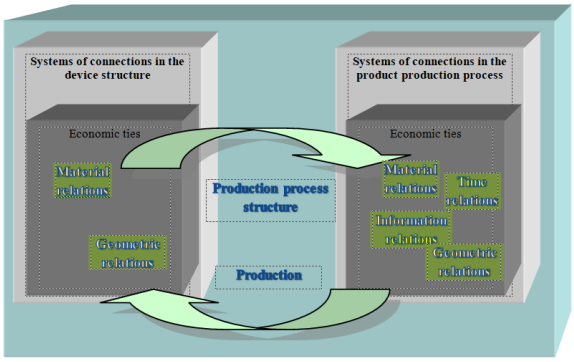

Fig. 1. General system of the sets of connections of the product design (MMK) and the production process [3 -6]

The system of connections that make up the product (MMC) can be considered strictly deterministic, while the production process is a very complex probabilistic system, belonging to the category of cybernetic control systems [8].

Considering the production process of making the product (MMC) as a manifestation of the overall system of sets, technology and studies these connections in order to solve the problem of ensuring the required quality at a given productivity and minimal expenditure of time, labor, energy and materials.

A microsystem can be defined as any element, device or system built from a certain number of Microcomponents (MCs). A generally accepted model of a microsystem is the model of a standard control system, shown in chapter one, Fig. 2. (generally accepted model of a microsystem). Most of the developed microsystems have this structure and can be constructed from components manufactured using different technologies on different substrates, but connected together in the form of

Online ISSN 2256-070X
https://doi.org/10.17770/etr2025vol4.8396
© 2025 The Author(s). Published by RTU PRESS.
This is an open access article under the Creative Commons Attribution 4.0 International License.

a hybrid microsystem. Another possibility is for all components of the system to be manufactured on a common substrate, using an appropriate technology in the form of a monolithic (integrated) microsystem [9 - 12].

Each microsystem consists of one or more components from the three classes shown in fig. 2:

- Microsensors – detect changes in the system's environment;
- Intelligent components – make decisions based on changes determined by the sensors [13];
- Executive micromechanisms (actuators) – through them the system changes the parameters of the environment.

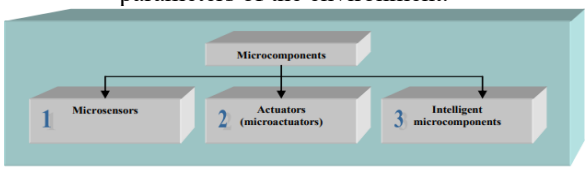

Fig. 2. Classification of Microcomponents (MCs)

The object of classification is two of the classes of microcomponents: microsensors and actuators, as well as MME included in their construction.

In the practice of AP, there are two methods for classifying design objects [14 - 16]:

- Hierarchical - the specified set of objects is divided into subordinate sets.
- Faceted - the specified set of objects is divided into independent sets for different classification features.

In the automated system for the design of MMEs and products from the MST "MICROSIS 25" the faceted method of classification is used. The choice is based on the fact that the classifiers developed in this way have the ability to be constantly supplemented with new elements and this does not violate their structure.

The purpose of the article is:

- To present the developed classification of micromechanical elements, as well as the calculations and fabrication of micromechanical elements of the beam type, using the theory of elasticity and the Finite Element Method (FEM) [17 - 19];
- To consider the principle of etching a conventional angle and partial etching of freely vibrating components [20];
- To describe the technical model of the clamped beam, the physical and mathematical modeling, as well as the simulation and verification of correctness.

II. Materials and Methods

Classification of microcomponents (MCs) – systematization and presentation in tabular form for more convenient work

Sensor – an element or device for converting a physical, chemical or biological measured quantity "m" into an equivalent signal "s", most often electrical, and this signal is a function of the measured quantity:

$$s = f(m) \tag{1}$$

The executive mechanism (actuator) is an element that converts the electrical quantity into a physical, chemical or biological quantity [21].

This dependence represents a conversion characteristic and is a generalized theoretical form of the specific physical laws that govern the operation of individual sensors. The main parameter of the sensors is their differential sensitivity "S", which is defined as the ratio between the change in the output and the change in the input quantity:

$$s = \frac{ds}{dm} \tag{2}$$

The classification of microsensors (MSs) is based on the following main classification features:

- According to the nature of the received output signal: Active sensors and Passive sensors.
- According to the position relative to the sensed object: Non-contact sensors and Contact sensors.

Non-contact sensors are divided according to the type of signal from the sensed element into: Electromechanical and Electromagnetic.

Contact sensors are divided according to:

- Type of impact Responsive: to touch; to sliding; to effort.
- The method of converting the applied force to the sensor into: Perceiving the force as a mechanical displacement of the sensor; and Perceiving the force as a deformation of the sensitive element.

The classification of executive micromechanisms is based on the following groups:

- Microactuators – divided into: Electrostatic; Magnetic; Multiplying and reducing; Piezoelectric; Magnetostrictive;
- Positioning and locating: Positioning; Gripping; Fastening.
- Microoptical: Microscanners; Microspectrome-ters.
- Thermal;
- Hydraulic and pneumatic;

- Biomedical: Micromanipulators; Microstimula-tors; Surgical microinstruments.

MMEs are listed as basic structures for microcomponents in Table 1. The emphasis is on the most common elements as basic structures in sensors, actuators and microsystems. The MMEs listed in the table are embedded in the developed classification.

TABLE 1 MMES AS BASIC STRUCTURES FOR MC

Micromechanical Elements (MMEs)	**Microcomponents (MCs)**
	Measurement of mechanical quantities:
Membranes, Plates	Force, torque, speed – acceleration sensors
Beams	Measuring heads for atomic force microscopy
Pyramid combs, V-shaped combs	-
Protruding structures, micro masses	Functions for propulsion and transmission, respectively control of energy flows
Micro nozzles, fluid channels	Microvalves, pumps
3D, partially movable structures	Inkjet printer heads
Linear and multidimensional displacement units	Electromechanical transducers (piezoelements, actuators for digital devices and video cameras)
Spring convex systems	Thermomechanical converters (bimetallic), micromotors, microgears
Gears	Moments broadcast
Needle supports	A set of them in a pressure sensor, raster probes for measuring temperature, the meaning of carrying a moment

The classification of MME has been developed and is divided into four levels of hierarchy:

- First level – type of MME;
- Second level – main characteristics of MME;
- Third level – method of attachment of MME;
- Fourth level – geometry of MME.

Fabrication of micromechanical beam-type elements

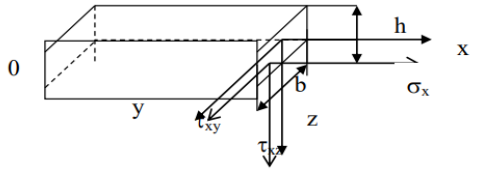

Fig. 3. Stresses expressing external forces on a beam

For their description, the theory of elasticity and FEM are used, which is particularly suitable for application in computer methods for calculation and simulation. A microcomponent of the beam type, located in the coordinate system x, y, z, is shown schematically in Figure 3.

After matching the geometry equations with the imposed constraints, they take the form:

$$\begin{cases} \varepsilon_x = \frac{\partial u}{\partial x}; \gamma_{xy} = \frac{\partial u}{\partial y} + \frac{\partial v}{\partial x} \\ \varepsilon_y = \frac{\partial v}{\partial y}; y_{yz} = \frac{\partial v}{\partial z} + \frac{\partial w}{\partial y} = 0 \\ \varepsilon_z = \frac{\partial w}{\partial z} = 0; y_{zx} = \frac{\partial w}{\partial x} + \frac{\partial u}{\partial z} = 0 \end{cases} \quad (3)$$

Since the linear strain ε_z is equal to zero, it follows that the normal stress σ_z and the directional cone μ_z are also equal to zero. From this it follows that $\mu_x = \mu_y = \mu$.

The functional dependence between the individual quantities takes the form:

$$\begin{cases} \varepsilon_x = \frac{1}{E}(\sigma_x - \mu\sigma_y) \\ \varepsilon_y = \frac{1}{E}(\sigma_y - \mu\sigma_x) \\ \gamma_{xy} = \frac{2(1+\mu)}{E}\tau_{xy} \end{cases} \quad (4)$$

The same relationship, but resolved in terms of voltages, is:

$$\begin{cases} \sigma_b = \frac{E}{1-\mu}(\varepsilon_b + \mu\varepsilon_b) \\ \sigma_b = \frac{E}{1-\mu^2}(\varepsilon_b + \mu\varepsilon_b) \\ \tau_{bb} = \frac{E}{2(1+\mu)}\gamma_{bb} \end{cases} \quad (5)$$

After integrating we obtain:

$$\begin{cases} v(x,y,z) = -z\frac{\partial w(x,y)}{\partial y} + v_0(x,y) \\ u(x,y,z) = -z\frac{\partial w(x,y)}{\partial x} + u_0(x,y) \end{cases} \quad (6)$$

Since $u_0(x,y)$ and $v_0(x,y)$ are unknown integration functions that are determined by the condition for non-deformability of the midline, then:

$$\begin{cases} u(x,y,0) = 0 \\ v(x,y,0) = 0 \end{cases} \quad (7)$$

Substituting z = 0 into the system, we get:

$$\begin{cases} u_0(x,y) = 0 \\ v_0(x,y) = 0 \end{cases} \quad (8)$$

Finally for the system we get:

$$\begin{cases} u(x,y,z) = -z\frac{\partial w(x,y)}{\partial x} \\ v(x,y,z) = -z\frac{\partial w(x,y)}{\partial y} \end{cases} \quad (9)$$

After substitution we get:

$$\begin{cases} \varepsilon_x = -z\dfrac{\partial^2 w}{\partial x^2} \\ \varepsilon_y = -z\dfrac{\partial^2 w}{\partial y^2} \\ \gamma_{xy} = -2z\dfrac{\partial^2 w}{\partial x \partial y} \end{cases} \quad (10)$$

Substituting the deformations into the physics equations for the principal stresses, we obtain:

$$\begin{cases} \sigma_x = -\frac{E_z}{1-\mu^2}\left(\frac{\partial^2 w}{\partial x^2} + \mu\frac{\partial^2 w}{\partial y^2}\right) \\ \sigma_y = -\frac{E}{1-\mu^2}\left(\frac{\partial^2 w}{\partial y^2} + \mu\frac{\partial^2 w}{\partial x^2}\right) \\ \gamma_{xy} = -\frac{E_z(1-\mu)}{(1-\mu^2)}\cdot\frac{\partial^2 w}{\partial x \partial y} \end{cases} \quad (11)$$

So far, we have obtained formulas for the principal stresses. It is necessary to obtain the secondary stresses using the same function w(x,y). The equations from statics are used:

$$\begin{cases} \frac{\partial \tau_{zx}}{\partial z} = -\left(\frac{\partial \sigma_x}{\partial x} + \frac{\partial \tau_{yx}}{\partial y}\right) \\ \frac{\partial \tau_{zy}}{\partial z} = -\left(\frac{\partial \tau_{xy}}{\partial x} + \frac{\partial \sigma_y}{\partial y}\right) \\ \frac{\partial \sigma_z}{\partial z} = -\left(\frac{\partial \tau_{xz}}{\partial x} + \frac{\partial \tau_{yz}}{\partial y}\right) \end{cases} \quad (12)$$

Substituting the expressions for σ_x, σ_y and $\tau_{xy} = \tau_{yz}$, performing the indicated differentiation operations and integrating once with respect to the parameter z, we obtain:

$$\begin{cases} \tau_{zx} = \tau_{xz} = \frac{Ez^2}{2(1-\mu^2)}\cdot\frac{\partial}{\partial x}\nabla^2 w + f_1(x,y) \\ \tau_{zy} = \tau_{yz} = \frac{Ez^2}{2(1-\mu^2)}\cdot\frac{\partial}{\partial y}\nabla^2 w + f_2(x,y) \end{cases} \quad (13)$$

where $f_1(x,y)$, $f_2(x,y)$ are the unknown integration functions, and ∇ is the Laplace operator.

$$\nabla^2 = \frac{\partial^2}{\partial x^2} + \frac{\partial^2}{\partial y^2} \quad (14)$$

The determination of the integration functions is carried out from the boundary conditions, or at z = +h/2 , $\tau_{zx} = 0$, $\tau_{zy} = 0$.

$$\begin{cases} f_1(x,y) = -\frac{Eh^2}{8(1-\mu^2)}\cdot\frac{\partial}{\partial x}\nabla^2 w \\ f_2(x,y) = -\frac{Eh^2}{8(1-\mu^2)}\cdot\frac{\partial}{\partial y}\nabla^2 w \end{cases} \quad (15)$$

From here for the stiffness we get:

$$F = \frac{Eh^3}{12(1-\mu^2)} \quad (16)$$

Determination of bending moment:

$$M_y dy = \int_{-\frac{h}{2}}^{+\frac{h}{2}} z\sigma_x dy dz = dy\int_{-\frac{h}{2}}^{+\frac{h}{2}} z\sigma_x dz \quad (17)$$

According to the analogue principle, it can be used and used for other purposes. It finally works:

$$\begin{cases} M_y = -F\left(\frac{\partial^2 w}{\partial x^2} + \mu\frac{\partial^2 w}{\partial y^2}\right) \\ M_x = -F\left(\frac{\partial^2 w}{\partial y^2} + \mu\frac{\partial^2 w}{\partial x^2}\right) \\ M_{xy} = M_{yx} = -F(1-\mu)\frac{\partial^2 w}{\partial x \partial y} \end{cases} \quad (18)$$

The stresses as a function of internal forces are:

$$\begin{cases} \sigma_x = \frac{M_y}{J}z \\ \sigma_y = \frac{M_x}{J}z \\ \tau_{xy} = \frac{M_{xy}}{J}z \end{cases} \quad (19)$$

where the moment of inertia is $J = \frac{h^3}{12}$

Strength verification is performed using the IVth strength theory.

$$\sigma_{equivalent}^{IV} = \sqrt{\sigma_1^2 + \sigma_2^2 - \sigma_1\sigma_2} \quad (20)$$

Clamped beams, bent beams or freely suspended elements made of resistive insulating layers (SiC, Si_3N_4, SiO_2) or silicon are suitable as basic structures for acceleration sensors, resonators or thermal insulation of functional elements. They are produced from silicon wafers by etching at conventional angles.

Figure 4 shows a structured resistive layer of Si3N4 (silicon nitride) on a U-shaped cutout for obtaining an MME beam type. Its edges are parallel to the intersection lines of the (111)-plane. Anisotropically acting solutions remove material perpendicular to the surface layer in the (100)-plane direction. The etching process is carried out by removing in the (411)-plane direction.

The etching rates of silicon planes with larger etching coefficients are highly dependent on the production conditions (temperature, concentration, presence of cations, addition of alcohol, stirring of the solution, etc.).

The etching time t is obtained by assuming the condition that for the complete release of a beam-type element in the (411)-front direction starting from the conventional angles at which the base x (Fig. 3.) lies opposite:

$$t = \frac{x}{\ddot{A}R_{(411)}} = \frac{x}{[u.\ddot{A}R_{(100)}]} \quad (21)$$

where: ÄR(411) is the etching rate in the (411)-plane direction; ÄR(100) is the etching rate in the (100)-plane direction.

Then the etching depth (d) is:

$$d = t.\ddot{A}R_{(100)} \quad (22)$$

Silicon beam structures can be fabricated using stop layers using the following methods: bromine doping by ion implantation, epitaxy or diffusion, electrochemical or chemical etching.

The clamped beam is mainly subjected to bending. It is fabricated by etching at conventional angles. Silicon beam structures can be fabricated using stop layers – bromine doping, by ion implantation, epitaxy or diffusion, electrochemical or chemical etching [22, 23].

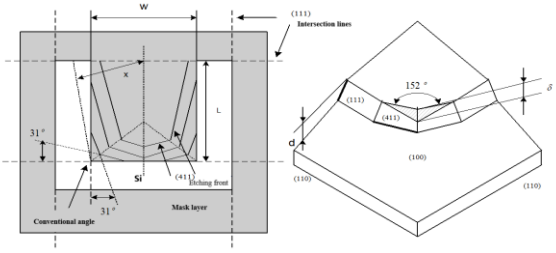

Fig. 4. Principle of conventional corner etching and partial etching of freely vibrating components

In the "Project" category on CAD system "MICROSYS 25" there is the goal setting, current status, statistical data, results.

In the "Development" category, there is the name and date of development, data on their properties and structure – geometric dimensions, material-specific characteristics or system characteristics [24].

In the "Technology" category, the technology for manufacturing MMC is described. For the current example with a clamped beam – by etching the conventional corners or with stop layers for Si structures – beam type, by doping with bromine, by ion implantation, epitaxy or diffusion, electrochemical or chemical etching [25].

In the "Production" category on CAD system "MICROSYS 25", there is the data on the production and quality assurance of the components – product name, serial number and date of production.

In the "Modeling" category on CAD system "MICROSYS 25"– description of the validity area, quality, modeling method – by theorist based on physical laws determined by studying the behavior of the system as a result of numerous measurements. The parameters used in modeling are replaced as characterizing data in the database (DB). Such are, for example: moment of inertia, spring constant, resonant frequency, damping coefficient, etc.

In the "Simulation" category are the results of the simulations performed, the simulation model used and the type of simulation.

III. Results and Discussion

Technical model (Fig. 5) – tensioned beam:

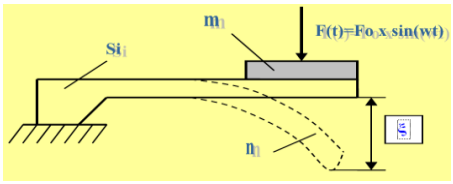

Fig. 5 Technical model of the tensioned beam ξ

Physical modeling – the tensioned beam is presented in Fig. 6.

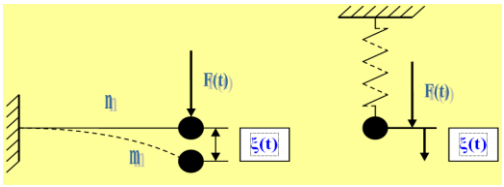

Fig. 6 Physical model of the tensioned beam

Mathematical modeling – represents an equivalent electrical circuit. Shown in Figure 7.

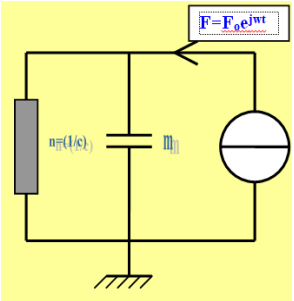

Fig. 7 Mathematical model of the tensioned beam

Simulation:

- Mathematical modeling solutions [26 - 28];

$$B(w) = \frac{\zeta(w)}{F(w)} = n.\frac{1}{\left(1-\frac{w}{w_0}\right)}.{w_0}^2 = \frac{1}{(m.n)} \qquad (23)$$

- Analysis of the solution found and graphical interpretation – fig. 10.

Verification of correctness (proof) – Fig. 8 and Fig. 9.

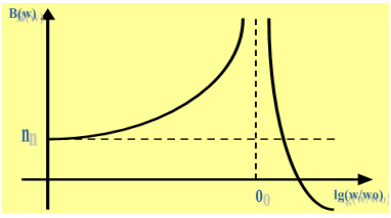

Fig. 8. Graphic of the solution of the tensioned beam model

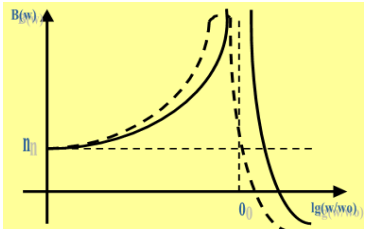

Fig. 9. Verification

The physical model is modified, which is then compiled from the corresponding mathematical model – Fig. 10.

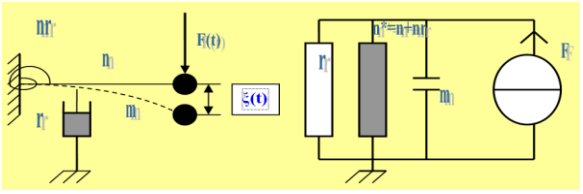

Fig. 10 Modified model of the tensioned beam model

Solution:

$$B(w) = \frac{\zeta(w)}{F(w)} = n.\frac{1}{\left\{1+\left[j.\frac{1}{Q}.\frac{w}{w_0{}^{*2}}\right]-\left(\frac{w}{w_0{}^{*2}}\right)^2\right\}} \quad (24)$$

$$w_0{}^{*2} = \frac{1}{(m.n^*)}$$

$$Q = \frac{1}{w_0{}^{*2}.n.r}$$

Where:

B – magnetic induction;

m – mass;

F – force;

Q – resonant quality factor;

n – susceptibility;

r – frictional resistance;

j – imaginary part;

w – circular frequency;

w_o – resonant frequency;

ξ – displacement;

F_o – excitation force;

nr – torsional elasticity;

b – width;

z – resistance;

z_w – wave resistance;

W – step response;

t – time.

An example of a model of a beam loaded in bending (Fig. 11) can be represented by the following types of models:

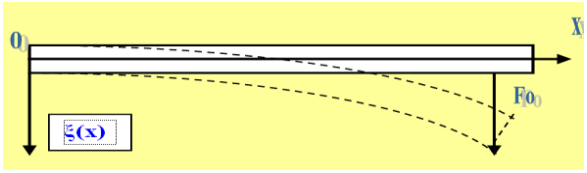

Fig. 11 Diagram of a beam under bending load

Differential equation of a beam under bending load:

$$EI\xi(x)^{III} = 0 \quad (25)$$

$$\xi(0) = 0 \quad (26)$$

$$\xi^{I}(0) = 0 \quad (27)$$

$$\xi^{II}(0) = 0 \quad (28)$$

$$-Ei\xi^{III} = 0 \quad (29)$$

Where: E is the modulus of elasticity;

I – surface moment of inertia;

i – current;

ξ – displacement.

Mesh model of a beam loaded in bending (Fig. 12 and 13).

$$n = \frac{l^3}{12.E.I} \quad (30)$$

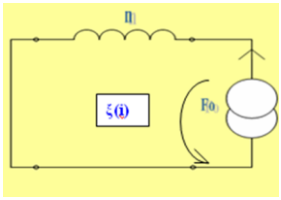

Fig. 12 Network model

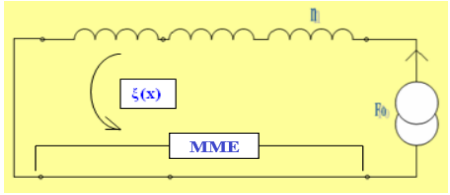

Fig. 13 Final network model

Finite element method – Fig. 14

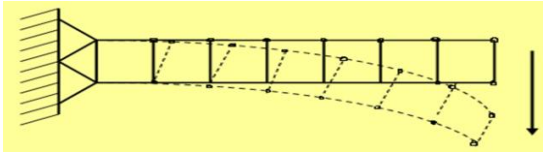

Fig. 14 End elements of a tensioned beam loaded in bending.

Thus, from a project to a final product, by sequentially going step by step through the categories in the CAD system "MICROSYS 25" database, taking into account the classification of microcomponents. The development of MMC consists of many technological methods, united in a certain technological sequence. The project needs relevant technologies, not technological dependencies.

The most common case in engineering practice is loading the beam in the xz plane with concentrated forces and moments or distributed forces with intensity $q(x)=q_z(x)$. In this case, the differential dependencies take the form [29]:

$$\frac{dQ}{dx} = -q(x) \tag{31}$$

$$\frac{dM}{dx} = Q(x) \tag{32}$$

Where $Q = Q_z$, $M = M_y$, $q = q_z$. In formulas for simplicity of writing, the indices of Q, M, and q are omitted, since there is no danger of making an error.

When differentiating the second dependence of with respect to x again, we obtain [30]:

$$\frac{d^2M}{dx} = \frac{dQ(x)}{dx} = -q(x) \tag{33}$$

$$M'' = -q(x) \tag{34}$$

The flow of the technology simulation is shown in Fig. 15.

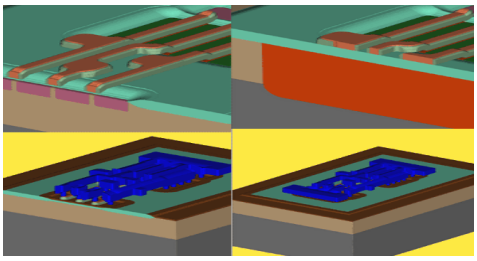

Fig. 15 Simulation of technology of a tensioned beam loaded in bending

The choice of the type of analysis and the geometry of the finite elements depend on the problem statement. When choosing 3D elements or 2D elements, the difference in the obtained result is minimal. In many cases, it is possible to reduce the dimensions without causing serious changes in the accuracy of the result. Many simulation tasks result in a symmetrical geometry. Then it is possible to present only a part of the detail, for example half or a quarter of it. This reduction of dimensions saves significant calculation time, so the deviation in the result can be ignored. In order to visualize the results of the simulation, a program called Post-Processor is used. With the help of this program, the result can be visualized both in numerical and graphical form. Another option when visualizing the results is the ability to animate the deformation. The program allows saving the results for the purpose of further processing and research.

IV. Conclusions

The developed classification of micromechanical elements is presented, as well as the calculations and fabrication of micromechanical elements of the beam type, using the theory of elasticity and the Finite Element Method (FEM);

The principle of etching a conventional angle and partial etching of freely oscillating components is considered;

The technical model of the clamped beam, physical and mathematical modeling, as well as simulation and verification of correctness are described.

An analysis-summary of the existing classifications of microcomponents is carried out: microsensors and executive micromecha-nisms (actuators), micromechanical elements and basic technologies in microtechnology, using known classification features.

References

[1] N. Kolev; Aleksandrova I, Metev H. Modeling and Optimiza-tion of Tool Life When Machining 42CrMo4+QT Steel on Swiss-Type CNC Lathes. In: 33rd International Scientific Symposium Metrology and Metrology Assurance, MMA 2023, Conference Proceedings, Sozopol 7-11 September 2023,Code 194604, DOI: 10.1109/MMA59144.2023.1031792, ISB N: 979-835033810-2.

[2] N. Nikolova, Development of a System for Assessment of Digital Professional Suitability in the Company Environment, Vide. Tehnologija. Resursi - Environment, Technology, Resources, Volume 3, Pages 211 – 216, 2024, 15th International Scientific and Practical Conference on Environment. Technology. Resources, ETR 2024, Rezekne, 27 June 2024 through 28 June 2024, Code 201245, Conference Proceedings, ISSN 16915402, ISBN 978-171389957-0, DOI 10.17770/etr2024vol3.8136.

[3] N. Nikolova, N., Human Capital in the Changing Work Environment of Industry 4.0, Vide. Tehnologija. Resursi - Environment, Technology, Resources, Open Access, Volume 3, Pages 187 – 193, 2023, 14th International Scientific and Practical Conference on Environment. Technology. Resources, ETR 2023, Rezekne, 15 June 2023 through 16 June 2023, Code 191610, DOI: https://doi.org/10.17770/etr2023vol3.7177

[4] D. Petrova., Doctor tezis, Database for automated design of micromechanical components for microsystems engineering products, Gabrovo, 2008

[5] D. Petrova, Intelligent, Innovative and Sustainable Industry in Bulgaria – prospects and challenges, Vide I. Tehnologija. Resursi - Environment, Technology, Resources, Proceeding of the 12th International Scientific and Practical Conference „Environment. Technology. Resources", June 20-22, 2019, Rezekne, Latvia, Volume I, pp. 210-215, ISSN 1691-5402 – print, ISSN 2256-070X – online. https://doi.org/10.17770/etr2019vol1.4188

[6] D. Petrova, An Alternative Approach to Reducing Aging of Innovative Industrial Products in Terms of Industry 4.0, Environment. Technology. Recourses – Proceeding of the 13-th International Scientific and Practical Conference, Rezekne Academy of Technologies, Rezekne, Latvia, 2021, ISSN 1691-5402, Online ISSN 2256-070X, https://doi.org/10.17770/etr2021vol3.6507 p. 274-280, scopus

[7] D. Petrova, Vlahova, B., Lengerov, A., Zlateva-Petkova, T., Study of the State of Innovation Development and Obsolescence in the Republic of Bulgaria of Companies from the Mechanical Engineering Sector, Vide. Tehnologija. Resursi - Environment,

Technology, Resources, 2023, 1, pp. 187–194, DOI: https://doi.org/10.17770/etr2023vol1.7239 , https://www.scopus.com/authid/detail.uri?authorId=56323816400

[8] I. Ahmad, T. Kumar, M. Liyanage, J. Okwuibe, M. Ylianttila and A. Gurtov, 'Overview of 5G Security Challenges and Solutions', IEEE Communications Standards Magazine, vol. 2, no. 1, pp. 36-43, March 2018.

[9] H. Metev, T. Kuzmanov, Manufacturing Technologies (part IV), Technological processes for CNC machines, „EX-PRESS“Ltd. – Gabrovo, Gabrovo, 2007.

[10] H. Metev, Krumov K. Determination of inaccuracy by milling taking into account the phenomenon of technological heredity. In: 9th International scientific conference "TechSys 2020" – Engineering, technologies and systems, Plovdiv, 2020. IOP Conf. Series: Materials Science and Engineering 2020; 878(1), 012049. doi:10.1088/1757-899X/878/1/012049.

[11] H. Metev, Krumov K, Vlahova B. Economic Aspects Of The Modular Tools. In: 11th International Scientific Conference “TechSys 2022” - Engineering, Technologies and Systems, Technical University of Sofia, Plovdiv Branch, 26-28 May 2022. (AIP Conf. Proc. 2980, 2024). DOI: 10.1063/5.0184231, ISBN: 978-073544814-8.

[12] H. Metev, Krumov K. Determination of Accuracy in Finishing Machining Trough Surface Plastic Deformation with Account of the Phenomenon of Technological Heredity. In: 12th International scientific conference “TechSys 2023”- Engineering, Technologies and Systems, Technical University of Sofia, Plovdiv Branch, 18-20 May 2023 (AIP Conf. Proc. 3078, 2024). DOI: 10.1063/5.0208291, ISSN: 0094243X.

[13] H. Klaus, F. Hetzelt, P. Hofmann, A. Blecker and D. Schwaiger, 'Challenges and Solutions for Industry-Grade Secure Connectivity', 2019 International Conference on Networked Systems (NetSys), Munich, Germany, 2019.

[14] M. Marinov Jordanov, Vector-Matrix Computer Method for Drafting Circling-Point Curves and Centering-Point Curves of Burmester, Vide. Tehnologija. Resursi - Environment, Technology, Resources, Volume 2, Pages 440 – 443, 2024, 15th International Scientific and Practical Conference on Environment. Technology. Resources, ETR 2024, Rezekne, 27 June 2024 through 28 June 2024, Code 201245, Conference Proceedings, ISSN 16915402, ISBN 978-171389957-0, DOI 10.17770/etr2024vol2.8072.

[15] M. Marinov, Jordanov, Synthesis of Eight Middle Lost Mechanisms Finally Discharged Discreet Positions, Vide. Tehnologija. Resursi - Environment, Technology, Resources, Volume 2, Pages 435 – 439, 2024, 15th International Scientific and Practical Conference on Environment. Technology. Resources, ETR 2024, Rezekne, 27 June 2024 through 28 June 2024, Code 201245, Conference Proceedings, ISSN 16915402, ISBN 978-171389957-0, DOI 10.17770/etr2024vol2.8067.

[16] M. Marinov, A Geometrical synthesis of comez textile machanisms of finally removed possibilities, Environment. Technology. Resources. Rezekne, Latvia Proceedings of the 14th International Scientific and Practical Conference. Volume 3, pp. 168-171, ISSN 1691-5402.

[17] M. Schillings, Strategic Management of Technological Innovation, Ravi Shankar, Edition: 6, 2019.

[18] M. Sain, Y. J. Kang and H. J. Lee, 'Survey on security in Internet of Things: State of the art and challenges', 19th International Conference on Advanced Communication Technology (ICACT), Bongpyeong, 2017.

[19] N. Kolev; Aleksandrova I, Metev H. Modeling and Optimiza-tion of Tool Life When Machining 42CrMo4+QT Steel on Swiss-Type CNC Lathes. In: 33rd International Scientific Symposium Metrology and Metrology Assurance, MMA 2023, Conference Proceedings, Sozopol 7-11 September 2023,Code 194604, DOI: 10.1109/MMA59144.2023.1031792, ISB N: 979-835033810-2.

[20] S. Mumtaz, A. Alsohaily, Z. Pang, A. Rayes, K. F. Tsang and J. Rodriguez, 'Massive Internet of Things for Industrial Applications: Addressing Wireless IIoT Connectivity Challenges and Ecosystem Fragmentation', IEEE Industrial Electronics Magazine, vol. 11, no. 1, pp. 28-33, March 2017.

[21] J. Sunbi, Gallina A., Contemporary Management of Innovation: Are We Looking at the Right Things?, USA, 2019.

[22] I. Mitev, Optimizing the quantity of liquid phase at the sintering of powder construction materials from system Fe-Cu-Sn, 11th International Scientific Conference “TechSys 2022” – Engineering, Technologies and Systems, AIP Conf. Proc. 2980, https://doi.org/10.1063/5.0184238 , Published by AIP Publishing. 978-0-7354-4814-8/$30.00, pp. 060017-1 to 060017-7.

[23] I. Mitev, Determining the diffusion coefficient in simultaneous saturation with boron and carbon of austenite alloyed with cooper in powder metallurgy structural materials, 11th International Scientific Conference “TechSys 2022” – Engineering, Technologies and Systems, AIP Conf. Proc. 2980, 060016-1–060016-8; https://doi.org/10.1063/5.0184239 , Published by AIP Publishing. 978-0-7354-4814-8/$30.00, pp. 060016-1 to 060016-8.

[24] T. Kuzmanov, K., H. Metev, I. Tsvyatkova. Morphological method application to designing modular sectional tools systems. International scientific conference UNITECH’03, Gabrovo, Bulgaria 2003, vol.1. pp. 544-546. ISBN 954-683-167-0.

[25] S.Tsenkulovski, Mitev, I., Influence of the Parameters of the Laser Marking Process on the Depth of Penetration in Layer-reinforced Composites, Vide. Tehnologija. Resursi - Environment, Technology, Resources, Volume 3, Pages 319 – 324, 2024, 15th International Scientific and Practical Conference on Environment. Technology. Resources, ETR 2024, Rezekne, 27 June 2024 through 28 June 2024, Code 201245, Conference Proceedings, ISSN 16915402, ISBN 978-171389957-0, DOI 10.17770/etr2024vol3.8147.

[26] G. Chipriyanova, Atanasov, A., Krasteva-Hristova, R., Environmental Management for Sustainable Business in Chemical Industry in Bulgaria, Vide. Tehnologija. Resursi - Environment, Technology, Resources, Volume 1, Pages 95 – 101, 2024, 15th International Scientific and Practical Conference on Environment. Technology. Resources, ETR 2024, Rezekne, 27 June 2024 through 28 June 2024, Code 201245, Conference Proceedings, ISSN 16915402, ISBN 978-171389957-0, DOI 10.17770/etr2024vol1.7971.

[27] G. Chipriyanova, Chipriyanov, M., Luchkov, K., Investigation and Analysis of Attitudes Towards the Implementation of Artificial Intelligence in Internal Business Processes, Vide. Tehnologija. Resursi - Environment, Technology, Resources, Volume 2, Pages 61 – 67, 2024, 15th International Scientific and Practical Conference on Environment. Technology. Resources, ETR 2024, Rezekne, 27 June 2024 through 28 June 2024, Code 201245, Conference Proceedings, ISSN 16915402, ISBN 978-171389957-0, DOI 10.17770/etr2024vol2.8032.

[28] G. Chipriyanova, Marinova, M.., Technological Aspects of Accounting Automation System as a Decision Support System, Vide. Tehnologija. Resursi - Environment, Technology, Resources, Open Access, Volume 2, Pages 28 – 33, 2023, 14th International Scientific and Practical Conference on Environment. Technology. Resources, ETR 2023, Rezekne, 15 June 2023 through 16 June 2023, Code 191610, DOI: https://doi.org/10.17770/etr2023vol2.7309 .

[29] A. Kocilovii, I R.K. Madsteriakova – 4 izd., prerab. Idop., Spravochnik tehnologa-mashinostroitelia – Tom 2, Moskva, Mashinostroenia, 1985.

[30] An. Lengerov, “Algorithmic model of technical and economic calculation of optimal technological process “Manufacturing Technologies (part XI), 2016, vol.26. pp. 94-96. ISSN 1312-8612.

Environment. Technology. Resources. Rezekne, Latvia
Proceedings of the 16th International Scientific and Practical Conference. 2025. Volume IV, 297-304

Innovative Development and Competitiveness of the Industrial Sector in Bulgaria

Desislava Petrova
Department "Management"
Technical university of Gabrovo
Gabrovo, Bulgaria
des_petrova@abv.bg

Neli Nikolova
Department "Management"
Technical university of Gabrovo
Gabrovo, Bulgaria
nik_nel@abv.bg

***Abstract*— This article presents methods for assessing the innovative development and compe-titiveness of the industrial sector in the Republic of Bulgaria. Guidelines and recommendations for their acceleration are indicated. A cross-section of the Bulga-rian industry is also made, assessing the innovative acceleration of the technologies used.**

***Keywords*— Competitiveness, Industrial sector, Innovative development.**

I. INTRODUCTION

The processes we have witnessed in recent years have one common feature – the speed of ongoing changes, the transfer of knowledge, the competiti-veness of individual industries and productions on a global scale, the innovative obsolescence of techno-logies. A partial analysis of Key Enabling Techno-logies and their influence on the innovative deve-lopment of industry in the Republic of Bulgaria has been made, which is presented in Table 1. A key factor in the future will be innovative obsolescence and the timely response of companies.

In this paper, we present our analysis of the six KETs, presented in Figure 1 and Table 1, that are of para-mount importance for Europe's technological sove-reignty in the future. For each presented KET, we provide a definition, describe its main uses and its importance and potential for Europe, with respect to technological sovereignty, and social and economic impact. In this context, we will also outline the main challenges and requirements along the technological value chain. All information reflected in this chapter is based on desktop research and interviews with experts from industry and academia. Throughout this chapter we also present five different case studies that use or build on one or more KETs.

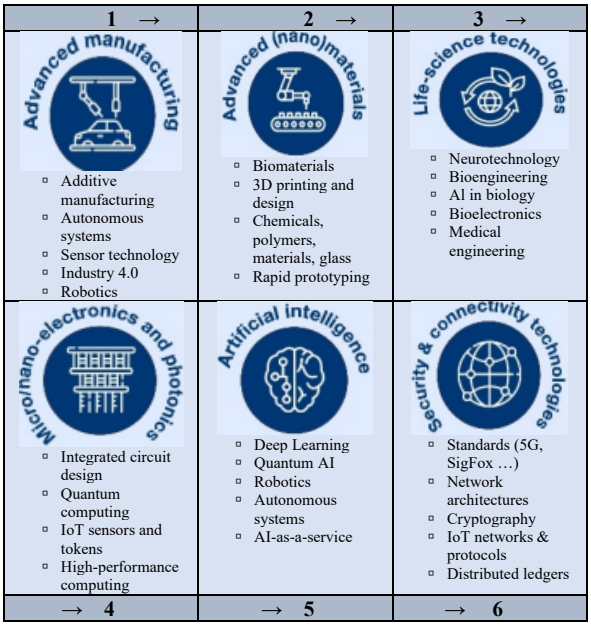

Fig. 1. Key Enabling Technologies (KETs) by 2024

TABLE 1 KEY ENABLING TECHNOLOGIES

KETS		Examples	Societal Challenges	Missions
Production Technologies	**Advanced Manufactu-ring Technologies**	Smart, high performance, high precision and additive manufacturing and processes, Robotics, Process Industry, Green Propulsion Technologies, Integrated Bio-refineries	**ENVIRO MENT**	**Missions …**
	Advanced Materials and Nano-technologies	High performance, smarts sustainable materials, Nanomaterial's,	**ENERGY**	

Online ISSN 2256-070X
https://doi.org/10.17770/etr2025vol4.8397
© 2025 The Author(s). Published by RTU PRESS.
This is an open access article under the Creative Commons Attribution 4.0 International License.

		Nanotechnology, Biomaterials, 2D Materials, Light Weight Technologies, New Chemistry		
	Life-Science Technologies	Industrial Biotechnology, High throughput biology, Automation for biology, Synthetic biology, Genomics (Genome Engineering/Synthetic Genomes) Cell & tissue engineering, Biologisation of manufacturing, Biosensors, Bio Activators, Bio Actuators, Lab on a Chip, New Chemistry, Neurotechnologies	**MOBILITY**	
Digital Technologies	**Micro-/Nano-electronics and Photonics**	IoT, Smart/Intelligent sensors, Quantum technology, Supercomputing (high power, high performance, neuro-computing, beyond CMOS), Displays (LCD, Plasma) & Lighting (LED, OLED), Photonics integrated circuits and Biophotonics	**HEALTH & WELLBEING**	**Missions …**
	Artificial Intelligence	Data generation and handling, Big data analytics, Machine learning and deep learning, Smart Robots, Virtual agents, Software Technologies, Decision making technologies	**FOOD & NUTRITION**	
Cyber Technologies	**Security and Connecti-vity**	Secure and Authenticated Communication, Avoiding identity thief, Data protection and privacy, IoT, Data/Connectivity Safety and Security, Human-Machine Interfaces, Hunan-Computer/ Robot Interaction, 5G, Baseband/processor platforms	**SECU-RITY** / **PRIVA-CY**	**Missions …**
		e-Governance, e-Administration, e-Voting, Cyber-Physical Systems, e-Safety and e-Security, Technology Assessment, Blockchain	**INCLU-SION & EQUALITY**	

II. MATERIALS AND METHODS

After conducting a SWOT analysis of the innovative development of industry in the Republic of Bulgaria based on data from the National Statistical Institute and on-site research on key elements (technology, efficiency and regulators), we decided to conduct an analysis on the following key elements: Advanced manufacturing, Materials, Life-science technologies, Micro/nano-electronics and Photonics, AI. We define European technological sovereignty as the ability for Europe to develop, provide, protect, and retain critical technologies required for the welfare of European citizens and prosperity of businesses, and the ability to act and decide independently in a globalised environment [11, 12]. This definition encompasses three key elements:

- Technological – the development of European R&D competencies by maintaining a strong knowledge base, strong industry, and strong networks in the critical technologies [14, 15];
- Economic – the achievement and preservation of a position of leadership in KETs, the ability to turn R&D into market products, and having access to a diversity of resources along the value chain with the aim of reducing dependence on third countries;
- Regulatory – the development of adequate policies and standards to influence global regulation, standards, and practices that reflect European values.

Advanced manufacturing describes the use of innovative technologies and methodologies in the manufacturing domains to improve existing products or create new ones. The main ambition is to enhance the output of manufacturing through improved and more efficient processes as well as high-performance production facilitated by digitalisation, i.e. production and manufacturing activities that build on data, computational results, automation, or sensing. Thus, advanced manufacturing and related technologies can boost productivity by increasing flexibility and making it viable for more and more manufacturers to offer highly customised products to customers. In addition, manufacturers can produce in smaller batches for specific customers or more easily adjust their production to design changes [22]. Advanced manufacturing encompasses different topics and applications, including but not limited to:

- Additive Manufacturing;
- Industry 4.0 concepts;
- Industrial-IoT;
- Manufacturing process optimization;
- Sensor technology;
- Interconnectivity between factories and manufacturing sites;
- 5G and 6G;
- Intelligent robotics;
- Autonomous systems;
- UAV technology
- Telecommunications;
- Operating systems for various nodes.

The applications of this KET target all manufacturing processes and domains. Given the current challenges of EU Member States in terms of declining population, increased automation in production and manufacturing

could help address labour shortages expected in the coming decades. Furthermore, processes in factories and production should be further optimised and improved to increase the competitiveness of the European economy. This KET will increase the overall quality of products as well as the responsiveness to market changes, allowing manufacturers to quickly adapt their manufacturing processes to the market situation. The necessary time to market, as well as unit quantities, can be reduced, so manufacturers could have a competitive advantage compared to manufacturers using solely traditional manufacturing methods. Advanced Manufacturing also allows manufacturers to produce high-quality goods made to buyers exact specifications.

Efficient processes and production facilitated by digitalisation require interconnectivity between factories, exchange of relevant data sets, using sensor networks to gather necessary manufacturing data, and using new technologies (e.g. Augmented or Virtual Reality) to train new workers. Workers need to acquire specialised digital and technical skills to be able to make use of the full potential of advanced manufacturing. Our research and the interviews we conducted indicate, however, that there is still a struggle within the established industrial community to understand the overall expected benefits of advanced manufacturing in the manufacturing domain, leading to disadvantages in the context of remaining competitive on the market. Advanced manufacturing will pose a challenge to the job market, as some jobs will be at risk due to automation, e.g. in the context of 'predictive maintenance' or assembly lines. A gradual introduction of ICT in traditional manufacturing can minimise the negative impact while maximising the expected positive aspects. This should be combined with corresponding trainings in order to meet the required skill levels of the workers [18, 19, 20].

Materials impact humans in almost every single aspect of life and have a huge impact on the environment, economy and society in general. This KET includes the research on advanced smart materials for the fabrication and production of a new generation of products. Generally speaking, advanced materials refer to materials (e.g. polymers, metals and alloys, glass, ceramics, composites, etc.) with new or improved properties that increase their performance over conventional products and processes. Advanced materials can facilitate the transition to more sustainable technologies with improved characteristics and enhanced performance. This is strongly aligned with Europe's goals in the context of the European Green Deal and industrial strategy [22].

R&D in this area will enable advanced processes and products to be provided by the European industries while reducing the negative environmental impact and positively influence European societies. Advanced materials in the automotive sector will directly lead to reduced emissions having a positive impact on Europe's goal towards a sustainable future, which is directly related to the European Green Deal. According to the US Office of Energy Efficiency & Renewable Energy: 'Advanced materials are essential for boosting the fuel economy of modern automobiles while maintaining safety and performance. Because it takes less energy to accelerate a lighter object than a heavier one, lightweight materials offer great potential for increasing vehicle efficiency. A 10% reduction in vehicle weight can result in a 6% - 8% fuel economy improvement.

Future advancements in material-related research will increase the competitiveness of European products and companies on the global stage (e.g. automotive, aero-space industry, energy sector, etc.) thereby also creating new jobs in the corresponding industries. Main challenges and requirements along the technological value chain Similar to advanced manufacturing, securing access to necessary raw and processed materials is of utmost importance for the development of this KET. The transition towards a sustainable circular economy has the potential to help overcome the resource challenge. It will maintain the value of products and used raw materials for as long as possible, while at the same time minimising the generation of waste. Since materials are so fundamental for the global economy, they have a heavy impact on supply and value chains. The main challenge is to focus on flexible and lean supply chains thereby enabling rapid prototyping and faster adjustments to market changes facilitated by digital enablers and other relevant developments. Europe should try to shape a viable path towards the creation of technological eco-systems that are socially and economically just. Improved technological ecosystems would lead to new jobs for the European economy. However, these jobs will require specialised digital skills that are currently in shortage.

In general, ***life-science technologies*** can be seen as an intersection of engineering and life sciences dealing with the technical use of findings related to life science, especially in the interrelation of biology, automation and digitalisation. On the one hand, the profound understanding of the functioning of living systems enables the production of new or improved products as well as processes for e.g. the pharmaceutical/chemical industries or for environmental technology [10]. On the other hand, knowledge related to engineering is needed to integrate biological systems into technical processes (e.g. the production of pharmaceutical ingredients in sufficient quantity and quality). The Covid-19 pandemic has shown that the sufficient production of high-quality vaccines is a very complex task, influenced by many different stakeholders and dependent on different raw materials, reinforcing the importance of this KET with respect to technological sovereignty. This is strongly aligned with Europe's goals in the context of Horizon Europe (especially in the health cluster).

Based on the most promising use case scenarios in the context of life-science technologies, Europe can transition to a resilient and healthier European society in terms of new medical achievements and applications such as optimised pandemic responses, innovative products based on conducted research or technological implementations. For example, lab-on-a-chip is

envisioned to facilitate automation and high-throughput screening which is especially relevant in the context of the Covid-19 pandemic. The positive impacts are not limited to health only, they can also be expected in the domains of agriculture, medicine, pharmaceuticals and food science [13].

Life-science technologies use specialised raw materials (such as lipids, cells) for research and for high-quality and high-quantity production. Similar to other KETs, here we observe a strong dependence on non-European suppliers, which became especially acute during the Covid-19 pandemic. For example, appropriate trade agreements and diversified supply chains are required to address pricing policy, price pressure, and other challenges.

The ***micro/nano-electronics and photonics*** relate to all types of digital and computing technologies in the magnitude of high-performance computing and communication based on micro/nanoelectronics. The major goal of micro/nano-electronics is to improve the performance of electronics, while at the same time reducing their size, weight and/or power requirements. Thus, micro/nano-electronics play a fundamental role in further digitalisation or technological advancements in general. The micro/nano-electronics and photonics also relate to computing based on photonic principles – i.e. optical/photonic computing - that use photons produced by lasers or diodes for computational aspects, in order to provide an alternative computing approach with improved characteristics related to bandwidth, signal loss, etc. compared to traditional computing [16, 17].

Micro/nano-electronics play a fundamental role in many different application domains in our everyday life as well as in support of other KETs. Their range of application is enormous: smartphones, laptops, automotive, aviation, robotics, industrial automation, health, medicine, lab on chip, sensor networks, additive manufacturing, smart cities, logistics, pandemic prevention and more. Advancements related to micro/nano-electronics directly influence the lives of every European citizen and are of paramount importance in order to stay competitive on the global market. In addition, a special focus should also be put on the future application of quantum technology, in order to maintain and improve the competitiveness of the European industry and society. Furthermore, the overall digitalisation pushed by such technologies is a game changer on a global scale.

The highly specialised domain of micro/nano-electronics and photonics require highly educated researchers and industrial experts, who are in deficit in Europe. In addition, the supply and value chains in these domains often encompass non-European suppliers and know-how carriers, and European research results are mostly commercialised in third countries. The dependency on nonEuropean manufacturers puts Europe in a weaker position in the global geo-political competition. The main challenges are, therefore, to bring back some of these supply/value chain parts and know-how to Europe and to foster a new generation of experts, who not only have the potential for research-related breakthroughs but also for the commercialisation of research, strengthening the position of Europe. Quantum computing hardware is experiencing challenges on the fundamental-science level, i.e. instability of the basic computing units (qubits), which compute results that are still heavily influenced by noise and are hence imprecise. Targeted research on fault-tolerant computing is required to reduce error rates [8, 9].

AI is the science and engineering of developing intelligent systems which perform tasks that typically require human intelligence. It comprises intelligent decision making based on automated choices, which are obtained by algorithms processing predefined rules or analysing large amounts of data, learning the decision models and applying these models in particular situations. Modern AI-based algorithms and systems are mainly driven by huge amounts of data. The superordinate goal is to detect patterns in the available data, which are later used during the decision-making process. Therefore, the increasing availability of data and the tremendous advances in computing power are key drivers of the current success and boom of AI [4].

Large amounts of data are available over IoT platforms and Open/ Big/ Commercial Data Platforms across the EU. Utilizing such data sets and processing them with state-of-the-art AI techniques will lead to new products, optimised processes and improved industrial processes in many domains. It will increase the quality of life across Europe. AI has the potential to revolutionise manufacturing by improving or automating many industrial processes. This can help to counteract the shortage of skilled labour and strengthen European industry. AI can also be used for predictive maintenance to increase the lifetime and reliability of industrial facilities and production lines. The use of AI in the field of mobility and autonomous driving holds enormous potential for Europe. It can help to reform the European car industry by developing new technologies and business models to make this industry more sustainable and future-proof. In mobility, AI can disrupt the traffic and public transport sector in many European cities. Automation and intelligent transport systems can reduce costs and enable the implementation of cleaner transport systems. The high amount of traffic in many European cities can be reduced through the additional demand-oriented usage of shared selfdriving cars. These actions will result in a sustainable reduction in environmental pollution and noise levels. In the long-term, this will increase the quality of life and make European cities more attractive to live in. AI has a great socio-economic potential. AI can be used to develop new business models and help to counteract the shortage of skilled labour. AI can be applied in the medical sector and healthcare systems which will result in an increase in the quality of life. For example, AI can be used to develop new medications and treatment therapies, to improve diagnostics and prevention of diseases and to support trained medical professionals. Finally, AI can contribute

to the mitigation of climate change through intelligent energy and waste management and automated analysis of climate data.

III. Results and Discussion

For the purpose of the discussion, we have presented some of the results obtained, which are summarized and graphically illustrated in the following figures, including a comparison in the time period 2019 - 2023 for the industry in Bulgaria and data for the EU are presented.

Since AI algorithms are driven by data, the availability, quality, and integrity of datasets is one of the most challenging requirements associated with AI. Availability of data to all EU citizens through Open Data portals, Geo-Information Systems, IoT networks, and various one-stop-shop platforms is critical. The use of AI in safety-critical areas such as manufacturing, medicine, energy management, or autonomous driving means that safety and functionality must be ensured at all times. Explainability, accountability, and transparency of AI-based algorithms and applications is another crucial challenge, which has not yet been solved and must be a focus of further research. Black-box AI systems cause uncertainties in automated decision-making and entail not only security risks but also legal challenges. Explainability and transparency are also basic requirements for the standardisation and certification of AI algorithms and applications – which is another significant challenge. Standardisation and certification should ensure both the quality and dependability of AI systems as well as their compliance with the EU's ethical requirements. This is an area where the EU has the potential to take a leading role internationally. The recruitment of highly skilled researchers and workers experienced in mathematics, stochastics, and computer science needs to be ensured and the current brain drain reversed. Europe struggles to attract and retain international talent, and European companies (especially SMEs) suffer from the lack of financial resources to establish internal teams of experienced AI experts, which currently prevents businesses from using AI for business model innovation. The emerging cloud-based AI-as-a-Service (AIaaS) helps to address this challenge as it requires less experienced personnel and therefore gives SMEs a fair chance to use AI.

The security and connectivity technologies are a fundamental enabler and building block for other KETs and for digital transformation. These technologies are ubiquitous due to the ongoing digitalisation and growing deployment of IoT devices.

Technologies based on this KET will lead to increased connectivity, digitalisation, and cybersecurity in Europe and result in a larger set of optimised processes, increased quality of life, and better services for European citizens. Therefore, the use and further development of these technologies support the EU strategies towards advanced Connectivity for a European Gigabit Society and Cybersecurity.

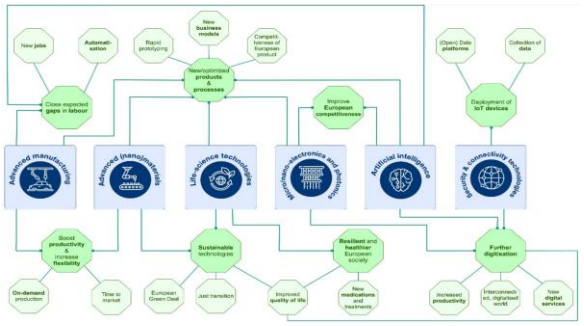

Fig. 2. Positive impacts and light green indicates

Specifically, this KET will enable the development of new, better, and more secure digital services with high quality for European citizens. These can increase quality of life and will additionally enhance the attractiveness of Europe by accelerating digitalisation. Security and connectivity technologies will intensify and speed up the deployment of IoT devices, which will also boost the development of (open) IoT platforms. This wide-spread roll-out of IoT devices will enable the autonomous and secure collection of data on a larger scale.

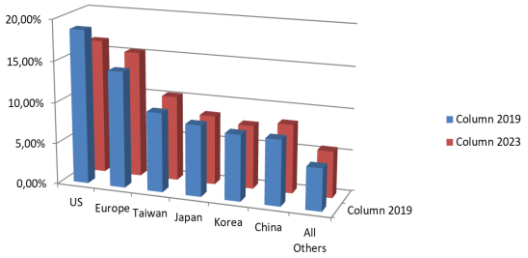

Fig. 3. Evolution of R&D intensity in 2019 (blue) and 2023 (red) in the semi-conductor industry

Such a strategy would itself consist of a multitude of actions, some of which we have proposed for various areas relevant to the development and deployment of KETs in Europe. These actions aim to address economic and technology elements of technological sovereignty. Specifically, we have grouped additional policy options around the four identified challenges.

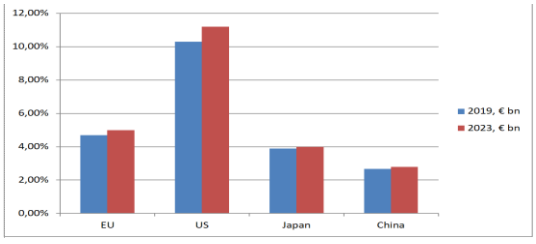

Fig. 4. R&D investment growth of the top 2 500 companies, in %, 2019-2023

Although European countries strive to achieve a common goal - to make Europe the most competitive knowledge-based economy, and although they work together to build a common research area, both the approaches to shaping science and technology policy

applied at the national level and the registered achievements from its implementation remain extremely diverse, due to cultural differences.

In Bulgaria, in mid-2024, the European Innovation Center and the sociological agency "Vitosha Research" surveyed 1053 manufacturing enterprises in order to establish their technological potential and their need for new technologies.

Manufacturing enterprises have the largest share (just over 40%), followed by those providing services with 38%. The study also covers 61 engineering and 5 research organizations, as well as one technology incubator. According to the form of ownership, the largest number of private enterprises (889 or 84%), owned by local individuals. They are followed by enterprises with state or municipal ownership (4.3%). The same number (35 or 3.3%) are enterprises with mixed ownership (state and private or private by Bulgarian and foreign persons). The smallest share are enterprises with entirely foreign ownership – only 26 or 2.5% [1, 2, 3].

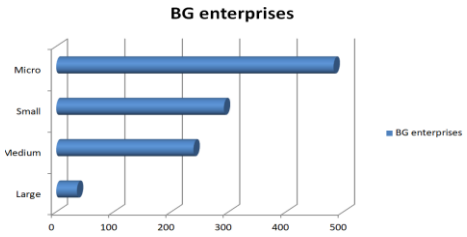

Fig. 5. The distribution of enterprises according to the total number of employees

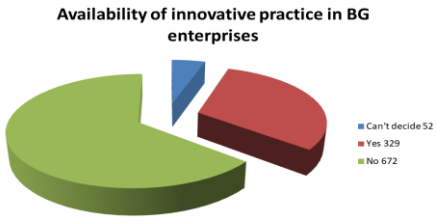

Fig. 6. Availability of innovative practice in Bulgarian company

These results correspond to the specified operational planning horizon with a horizon of up to 6 months – 330 (31%) enterprises, up to 1 year – 394 (37%), 145 enterprises have a planning horizon of up to 3 years, 54 – up to 5 years, and only 28 indicate that they carry out planning activities up to and over 10 years. This gives them the opportunity to use the results of technological forecasting. It is also known that the implementation of innovative activity requires an analysis of technological development trends in the relevant area and the setting of strategic goals, which, on the other hand, is associated with a greater long-term planning [5, 6].

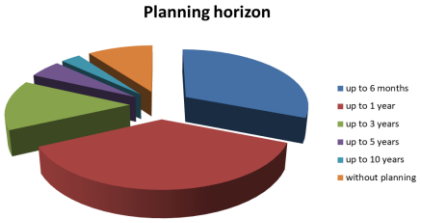

Fig. 7. Distribution of Bulgarian companies according to the adopted planning horizon

Bulgarian enterprises have their own explanation for the reasons that make it more or less difficult for them to implement innovation policy and plan it. As holding factors with the greatest impact on innovation activity, they point out: the lack of appropriate sources of financing, lack of incentives from the state, high economic risk, high costs, organizational obstacles, lack of qualified personnel, lack of markets, the COVID crisis, the wars in Ukraine and the Middle East, as well as the delay in the process of joining the Eurozone.

Bulgaria stands out from other EU countries in two sectors – IT and manufacturing. In these sectors, Bulgarians have the highest shares of people wanting to start a business – 15%, compared to an EU average of 13% in the IT sector and 8% compared to an EU average of 4% in the Manufacturing sector. In 2023, a new trend is observed in the entrepreneurial ecosystem, namely the focus on smaller settlements outside the traditional top-5 cities (Sofia, Plovdiv, Varna, Burgas and Ruse), and in particular where there are no universities or limited outsourced training at established universities. Innovation networks in Bulgaria, including new business associations, international business networks and academic networks, are increasing their intensity and interconnectedness. The Bulgarian Enterprise Europe Network continues to be among the leaders in Europe, with activity indicators above the EU average despite the lack of a national co-financing mechanism, which exists in one form or another in all other EU member states. Financing Research and development (R&D) spending in Bulgaria reached BGN 1,266 million (according to the latest available data for 2022), which represents an increase of nearly 18% compared to the previous year. However, as a relative share, R&D spending accounts for only 0.75% of GDP – a decrease of 0.02 pp on an annual basis, a significant retreat from the "record" 2015. Enterprises carry out more than two-thirds of R&D spending in the country (68%) [7]. The total amount of business investments in research and development amounted to BGN 858 million, which is an increase of 21% on an annual basis. The achieved increase allows business to maintain the share of R&D spending in GDP at a level of 0.51%, which, however, remains significantly below the peak values of 2015. The share of R&D expenditure in GDP of the Higher Education sector has also remained unchanged – 0.05%, which is a result of an increase in the amount spent by higher education institutions on science and technology transfer by 14% on a year-on-year basis. The exception is the Public Sector, where there is a decrease in the share of R&D expenditure

in GDP by 2 pp to 0.19%. The amount spent on scientific research development by public research organizations is BGN 322 million, with a year-on-year growth of nearly 11%.

IV. CONCLUSIONS

In conclusion, the EU can combine its academic, technological, and industrial strengths with a high-quality digital infrastructure and a regulatory framework based on its fundamental ethical and moral values to act as a forerunner in innovation in the data economy and its related AI-based applications, as envisaged in the European strategy on artificial intelligence. In 2023, the European economy improves its innovation potential. The growth (change in the value of the Innovation Index on average for the EU-27) for the last seven-year period is 8.5%, and for the last one year – 0.51%. However, the gap of the European Union economy from the USA, China and Japan remains significant and worrying, especially against the background of a series of global and regional crises and challenges. The reasons for this comparative lag are mainly rooted in the EU's inability to fully use the scale of its common market, to concentrate public and private resources effectively in scientific research and innovation, and to create companies capable of competing on a global level. These limitations were particularly evident in the EU's inability to rapidly increase the capacity of its defense industry and to help Ukraine counter Russian aggression. Given the long-term deterioration of the security environment at the EU borders, the long-term development of the community will increasingly depend on the ability of economies to collectively create and sustain technologies and innovations that are ahead of their main strategic competitors, Russia and China. In addition, this is a necessary condition for the EU's long-term goal of strategic autonomy and geopolitical weight to be achieved.

Bulgaria recorded the most significant improve-ment in its innovation performance on a year-on-year basis within the EU-27 – nearly 14%, followed by the Czech Republic (11%) and Poland (8%). However, the country's higher innovation index values over the past year are not enough to make up for the gap with the EU average. Bulgaria remains in the penultimate place in the group of emerging innovators (ahead of Romania) at 46.7% compared to the EU-27 average and even below the group's average performance of 54%. In 2023, Bulgaria recorded the most significant improvement in the following areas compared to 2016, selected as the baseline in the latest report of the European Innovation Scoreboard: share of inno-vative enterprises that interact with partners with-in the innovation process (growth of 51.8%); increased number of joint publications between representatives of the public and private sectors; process innovations with growth of 45% and share of innovative enterprises with product innovations (82.2%); employment in innovative enterprises (growth of nearly 41%); emissions of fine dust particles from industry, as well as development of technologies rela-ted to reducing the negative environmental footprint, in respect of which Bulgaria recorded positions equal to the EU-27 average. Thanks to the strongly deve-loping ICT sector, Bulgaria recorded a more tangible approach to the average European levels in the indicators of the number of specialists in the field of ICT (83%) and export of knowledge-intensive servi-ces (75%). According to the European Regional Inno-vation Scoreboard, all Bulgarian regions fall into the last group of emerging innovators. The only indi-cation that the South-West Planning Region (SWP) is doing relatively better than the national average is the positive sign (+) added to the category. The lack of (significant) progress for Bulgaria demonstrated in the European Innovation Scoreboard and the additional analysis at regional level are also confirmed by the data of the Global Innovation Index for 2023. In the company of 132 countries, Bulgaria drops four positions year-on-year to 38th place. Measured by the index values, the difference is 0.5 points in the direction of decline (or an innovation index of 39, which is the lowest for the country in more than 10 years). However, within the EU, Bulga-ria ranks 22nd, ahead of Poland, Greece, Croatia, Slovakia and Romania. In the group of countries with high average income per capita, Bulgaria ranks third, one position lower than in 2022, after China (12th overall) and Malaysia (36th overall). Technological and scientific product Bulgaria ranks 24th within the EU-27 with 45 patent applications to the European Patent Office (EPO) (2 more than in 2021), ahead of Cyprus, Croatia and Latvia. In terms of the number of patent applications per 1 million people (6.6 patents), Bulgaria is ahead only of Romania (2.4 patents). For comparison, patent applications to the EPO origin-nating from Sweden are 481.8 per 1 million people (1st in the EU-27), and from Slovenia – 58.4 (1st among the countries of Central and Eastern Europe). Only 22 patents were granted to Bulgarian companies and organizations by the European Patent Office (EPO) (1 less than in 2021), which puts us only ahead of Cyprus and Lithuania. In 2022, the patents issued by the Patent Office of the Republic of Bulgaria (PORB) to Bulgarian patent holders were 87, which is less than half of their number in the previous year. A decrease in the number of patents granted is present in all institutional sectors.

In the future, research will be focused on innovative obsolescence of technologies and its management through alternative solutions.

REFERENCES

[1] D. Petrova, Intelligent, Innovative and Sustainable Industry in Bulgaria – prospects and challenges, Vide I. Tehnologija. Resursi - Environment, Technology, Resources, Proceeding of the 12th ISPC „Environment. Technology. Resources", June 20-22, 2019, Rezekne, Latvia, Volume I, pp. 210-215, ISSN 1691-5402 – print, ISSN 2256-070X – online. https://doi.org/10.17770/etr2019vol1.4188

[2] D. Petrova, An Alternative Approach to Reducing Aging of Innovative Industrial Products in Terms of Industry 4.0, Environment. Technology. Recourses – Proceeding of the 13-th ISPC, Rezekne Academy of Technologies, Rezekne, Latvia, 2021, ISSN 1691-5402, Online ISSN 2256-070X, https://doi.org/10.17770/etr2021vol3.6507 p. 274-280, scopus

[3] D. Petrova, Vlahova, B., Lengerov, A., Zlateva-Petkova, T., Study of the State of Innovation Development and Obsolescence in the Republic of Bulgaria of Companies from the Mechanical Engineering Sector, Vide. Tehnologija. Resursi - Environment, Technology, Resources, 2023, 1, pp. 187–194, DOI: https://doi.org/10.17770/etr2023vol1.7239 , https://www.scopus.com/authid/detail.uri?authorId=56323816400

[4] I. Balabanova, Georgiev G., "Image Recognition by FFT, Artificial Intelligence and k-Nearest Neighbors Approach". IOP Publishing, Journal of Physics: Conference Series - EEPES'22, vol. 2339, pp. 1-8, 2022.

[5] G. Chipriyanova, Atanasov, A., Krasteva-Hristova, R., Environmental Management for Sustainable Business in Chemical Industry in Bulgaria, Vide. Tehnologija. Resursi - Environment, Technology, Resources, Volume 1, Pages 95 – 101, 2024, ETR 2024, Rezekne, 27 June 2024 through 28 June 2024, Conference Proceedings, ISSN 16915402, ISBN 978-171389957-0, DOI 10.17770/etr2024vol1.7971.

[6] G. Chipriyanova, Chipriyanov, M., Luchkov, K., Investigation and Analysis of Attitudes Towards the Implementation of Artificial Intelligence in Internal Business Processes, Vide. Tehnologija. Resursi - Environment, Technology, Resources, Volume 2, Pages 61 – 67, 2024, ETR 2024, Rezekne, 27 June 2024 through 28 June 2024, Code 201245, Conference Proceedings, ISSN 16915402, ISBN 978-171389957-0, DOI 10.17770/etr2024vol2.8032.

[7] G. Chipriyanova, Marinova, M.., Technological Aspects of Accounting Automation System as a Decision Support System, Vide. Tehnologija. Resursi - Environment, Technology, Resources, Open Access, Volume 2, Pages 28 – 33, 2023, Environment. Technology. Resources, ETR 2023, Rezekne, 15 June 2023 through 16 June 2023, Code 191610, DOI: https://doi.org/10.17770/etr2023vol2.7309 .

[8] H. Klaus, F. Hetzelt, P. Hofmann, A. Blecker and D. Schwaiger, 'Challenges and Solutions for Industry-Grade Secure Connectivity', 2019 International Conference on Networked Systems (NetSys), Munich, Germany, 2019.

[9] Hr. Metev, T. Kuzmanov, Manufacturing Technologies (part IV), Technological processes for CNC machines, „EX-PRESS"Ltd. – Gabrovo, Gabrovo, 2007.

[10] I. Ahmad, T. Kumar, M. Liyanage, J. Okwuibe, M. Ylianttila and A. Gurtov, 'Overview of 5G Security Challenges and Solutions', IEEE Communications Standards Magazine, vol. 2, no. 1, pp. 36-43, March 2018.

[11] I. Mitev, Optimizing the quantity of liquid phase at the sintering of powder construction materials from system Fe-Cu-Sn, 11th International Scientific Conference "TechSys 2022" – Engineering, Technologies and Systems, AIP Conf. Proc. 2980, https://doi.org/10.1063/5.0184238 , Published by AIP Publishing. 978-0-7354-4814-8/$30.00, pp. 060017-1 to 060017-7.

[12] I. Mitev, Determining the diffusion coefficient in simultaneous saturation with boron and carbon of austenite alloyed with cooper in powder metallurgy structural materials, 11th International Scientific Conference "TechSys 2022" – Engineering, Technologies and Systems, AIP Conf. Proc. 2980, 060016-1–060016-8; https://doi.org/10.1063/5.0184239, Published by AIP Publishing. 978-0-7354-4814-8/$30.00, pp. 060016-1 to 060016-8.

[13] J. Sunbi, Gallina A., Contemporary Management of Innovation: Are We Looking at the Right Things?, USA, 2019.

[14] M. Marinov Jordanov, Vector-Matrix Computer Method for Drafting Circling-Point Curves and Centering-Point Curves of Burmester, Vide. Tehnologija. Resursi - Environment, Technology, Resources, Volume 2, Pages 440 – 443, 2024, Environment. Technology. Resources, ETR 2024, Rezekne, 27 June 2024 through 28 June 2024, Conference Proceedings, ISSN 16915402, ISBN 978-171389957-0, DOI 10.17770/etr2024vol2.8072.

[15] M. Marinov, Jordanov, Synthesis of Eight Middle Lost Mechanisms Finally Discharged Discreet Positions, Vide. Tehnologija. Resursi - Environment, Technology, Resources, Volume 2, Pages 435 – 439, 2024, Environment. Technology. Resources, ETR 2024, Rezekne, 27 June 2024 through 28 June 2024, Conference Proceedings, ISSN 16915402, ISBN 978-171389957-0, DOI 10.17770/etr2024vol2.8067.

[16] M. Schillings, Strategic Management of Technological Innovation, Ravi Shankar, Edition: 6, 2019.

[17] M. Sain, Y. J. Kang and H. J. Lee, 'Survey on security in Internet of Things: State of the art and challenges', 19th International Conference on Advanced Communication Technology (ICACT), Bongpyeong, 2017.

[18] N. Nikolova, Development of a System for Assessment of Digital Professional Suitability in the Company Environment, Vide. Tehnologija. Resursi - Environment, Technology, Resources, Volume 3, Pages 211 – 216, 2024, ETR 2024, Rezekne, 27 June 2024 through 28 June 2024, Code 201245, Conference Proceedings, ISSN 16915402, ISBN 978-171389957-0, DOI 10.17770/etr2024vol3.8136.

[19] N. Nikolova, N., Human Capital in the Changing Work Environment of Industry 4.0, Vide. Tehnologija. Resursi - Environment, Technology, Resources, Volume 3, Pages 187 – 193, 2023, Environment. Technology. Resources, ETR 2023, Rezekne, 15 June 2023 through 16 June 2023, Code 191610, DOI: https://doi.org/10.17770/etr2023vol3.7177

[20] N. Nikolova, Entrepreneurial "Blue" Practices for Sustainable Development and Resources Efficiency, "Environment. Technology. Resources", June 20-22, 2019, Rezekne Academy of Technologies, Rezekne, Latvia, Volume I, 198-203, ISSN 1691-5402, ISSN 2256-070X.

[21] S. Mumtaz, A. Alsohaily, Z. Pang, A. Rayes, K. F. Tsang and J. Rodriguez, 'Massive Internet of Things for Industrial Applications: Addressing Wireless IIoT Connectivity Challenges and Ecosystem Fragmentation', IEEE Industrial Electronics Magazine, vol. 11, no. 1, pp. 28-33, March 2017.

[22] S.Tsenkulovski, Mitev, I., Influence of the Parameters of the Laser Marking Process on the Depth of Penetration in Layer-reinforced Composites, Vide. Tehnologija. Resursi - Environment, Technology, Resources, Volume 3, Pages 319 – 324, 2024, Environment. Technology. Resources, ETR 2024, Rezekne, 27 June 2024 through 28 June 2024, Conference Proceedings, ISSN 16915402, ISBN 978-171389957-0, DOI 10.17770/etr2024vol3.8147.

Environment. Technology. Resources. Rezekne, Latvia
Proceedings of the 16th International Scientific and Practical Conference. 2025. Volume IV, 305-308

Modern Risk Analysis in the Planning and Implementation of Modernization Projects in Railway Infrastructure

Irena Petrova
Department of Technology, Organization and Management of Transport
Todor Kableshkov University of Transport
Sofia, Bulgaria
ipetrova@vtu.bg

***Abstract*—The implementation of modernization projects in railway infrastructure is accompanied by a number of risks that affect their successful implementation within the planned budget and time. In general, risks are considered as technical, financial, environmental and social. The identification and management of these risks is essential for the successful implementation of the project within the set scope, and this has an impact on the provision of modern and safe rail transport. Modern approaches to detailed planning and risk assessment, as well as the implementation of new monitoring technologies contribute to successful transport projects. The modern approach to risk management devotes a special role to public participation. The goal is to minimize social tension and achieve a better understanding of projects on the part of the population. This study analyzes and improves risk management methods for planning and implementing railway infrastructure modernization projects.**

Keywords — risk management, railway projects, risk assessment, probability of occurrence.

I. INTRODUCTION

Most railway projects have a long planning and implementation period, involving many subcontractors, different interests, a large budget, which makes them vulnerable to a large number of risks. Different sources can lead to this large-scale group of risks. It can be financial reasons, design changes, safety problems, environmental factors, political instability. The larger the projects, the more important risk management becomes for the success of the project. Emerging problems in railway projects usually affect the state.

By definition, projects are a unique activity limited within a certain budget and time, which explains the accompanying risks. There are no risk-free projects. For the successful implementation of the project, early identification of possible risks and their management by minimizing or eliminating them is necessary. Risk avoidance would lead to stagnation, to lagging behind others. "If a project does not involve any risk... Don't do it. Risk and reward go hand in hand," write American project management experts Tom de Marco and Timothy Lister. Risk is a consequence of one or more causes, as a result of which one or more events occur and inevitably accompanies any project. Risk management as a process always starts with identifying and managing potential risks. A missed risk can jeopardize the project, which requires risk management to be applied throughout the entire life cycle [1].

II. MATERIALS AND METHODS

Risk accompanies future events that may affect the scope, schedule and budget of the project. Risk refers to problems that have not arisen that have a negative impact and can also happen to positive opportunities that do not lead to danger.

In general, risks are classified into two large groups: general risks and specific risks. The general risks relate to political, social, economic and legal processes over which the parties to the project cannot exert influence. These factors influence the choice of the project to be implemented and the amount of funding. The types of risk in the management of transport projects are presented in Table 1. [2][3].

Online ISSN 2256-070X
https://doi.org/10.17770/etr2025vol4.8440
© 2025 The Author(s). Published by RTU PRESS.
This is an open access article under the Creative Commons Attribution 4.0 International License.

TABLE 1 TYPES OF RISK

	Types of risk	**These include:**
General risks	Political risks	Government policy Tax regime; Foreign Economic Policy; Concession; Etc.
	Trading risks	Currency regime; Inflation; Interest rate.
	Legal risks	Change in laws and legal acts.
Specific risks	Development risks	Licenses and permits; Tenders; Delay in project planning; Problems with contracts.
	Construction risks	Construction delays; Problems with construction and installation works; Overspending; Debt risk,
	Operating costs	Technical risks; Demand; Delivery; Management; Fire; Flood; Zemetrenie; Damage to facilities; Financing of the project' Etc.

Financial and regulatory risks are leading factors for the success of a construction project. Financial uncertainty in most cases is the result of fluctuations in the prices of materials and labor. Dynamic price changes lead to inaccurate project budget forecasts. Regulatory risks are related to frequently changing laws and regulations [4].

A particularly relevant risk factor that affects all areas of the economy is the shortage of qualified labor. The shortage of labor can be at all levels – workers, technicians, managers [5].

The occurrence of an unforeseen risk leads to a negative, demotivating impact on the project team. To reduce risk, regular employee and manager training, automation, collaborative work platforms, breaking the project into small pieces, and using agile management methodologies are recommended [6].

The success of railway projects depends on the project team. Unskilled team members are usually the cause of overscheduling, reduced productivity, and more [7].

The risk associated with the protection of the confidentiality of information assets related to the project should not be overlooked [8].

A. Risk management

Risk management is a management policy including procedures and practices for risk analysis and control [9][10].

The project risk management model based on statistical data has been developed in two steps. The first stage includes the collection of data from surveys, project documentation and their preliminary processing (cleaning). In the second stage, the data is analyzed with multiple regression analysis. Regression analysis examines the linear correlation between multiple dependent and independent variables, which makes it extremely suitable for risk assessment in the project [11].

Risk management in railway infrastructure projects is a process involving specific management activities. The goal is to anticipate the possible obstacles and the projects to continue their implementation while remaining within the planned budget and duration. For the successful implementation of the project, it is necessary to implement a risk management process throughout the entire life cycle.

The following methods shall be used to assess the likelihood of risk:

a) probabilistic methods – using Gaussian distribution;

b) scenario methods – the implementation of the project is described through various scenarios;

c) statistical methods – using statistical data, the main statistical parameters are calculated, including average, variance and probable distribution;

d) expert methods – by filling in questionnaires, the probability of occurrence of the risk event in the project is assessed;

e) Insurance risks – If the project is unable to ensure its implementation in the event of a risk event, it is necessary to apply insurance measures for risk management;

f) inventory planning – by setting aside funds for unforeseen expenses;

g) Sustainable methods – use estimates that are not always optimal, but retain their reliability when deviating from the expected distribution patterns. These assessments are called stable in theory [12].

Every project should have a risk management plan. The use of appropriate software to create a risk management plan facilitates the monitoring of the processes for the implementation of identification, assessment, mitigation and monitoring activities. It must also include a contingency plan.

The risk management plan describes the activities in four steps:

a) Risk identification – using data from similar projects, potential risks that may affect the implementation are assessed;

b) Risk assessment methodology – ranking risks based on their probability and level of impact. A risk assessment matrix may be used.

c) Designation of risk management officers – for each project risk, there must be a responsible person who monitors and responds if necessary [13].

d) Risk register – contains information about all identified risks, their description and impact measures.

e) Risk mitigation – creating a plan to mitigate risk and mitigate its impact.

To identify hazards in railway projects, it is recommended to use the HAZOR (Hazard and Operability Analysis) method. It is used during the design period and in the process of operation. Considers risk events as a deviation from the norms for design, construction and operation [14].

Not all risk quantification studies go through the sequence of steps, often limited to the identification of hazards, especially when reliable data are lacking [15].

B. Risk assessment methodology

In the ISO/IEC 31010 standard "Risk management" – Methods for risk assessment, 31 methods of risk assessment are considered. A combination of several methods suitable for different stages is recommended [16].

The following methods are applied for risk assessment: mathematical statistics, numerical methods, probability theory, graph theory, machine learning and artificial intelligence, decision tree, critical point, environmental risk analysis, cost-benefit analysis [17].

The risk assessment includes two variables. One variable is a quantitative assessment of the probability of the occurrence of the risk, and the other represents its consequences. A five-point scale is used to assess the likelihood of risk occurrence. Table 2 provides the scale for assessing the likelihood of occurrence of risk.

TABLE 2 PROBABILITY OF RISK OCCURRENCE

P – Probability of occurrence of risk	Scale
Almost unbelievable	1
Unlikely	2
Probable occurrence	3
Highly likely occurrence	4
Common	5

This scale is used in combination with a risk impact assessment to build a risk analysis matrix. By multiplying the probability of occurrence and the severity of the impact, an overall risk rating is obtained, which supports the decision-making process for risk mitigation or management. The scale can be adapted depending on the specifics of the project by expanding the categories.

Estimates of possible risk effects are presented in Table 3.

TABLE 3 POSSIBLE CONSEQUENCES OF RISK

Consequence C	Importance of the possible consequences of risk
2	No significant effect
4	Small effect
6	Medium effect
8	Critical effect
10	A catastrophic effect. Project failure.

The general formula for calculating risk that is applied in engineering systems and project management is [18].

$$R = P * C, \quad (1)$$

Where:

R – risk

P – probability

C – consequence.

Table 4 presents the calculated risk values according to Formula 1 and a scale for the level of significance for the project.

TABLE 4 RISK VALUE

Designation	Risk level	Risk level
R1	Very low risk	$R \leq 10$
R2	Low risk	$11 \leq R \leq 20$
R3	Moderate risk	$21 \leq R \leq 30$
R4	High risk	$31 \leq R \leq 40$
R5	Veri high risk	$31 \leq R \leq 40$

The considered risk assessment method is the most used in European transport projects. After categorizing the risks, management managers are appointed.

For quantitative risk assessment, three-step and five-step matrices are often used, using formula (1) for calculation. An important point in risk assessment is the determination of an acceptable risk. It refers to risks with minimal impact on the implementation of the project [19].

III. RESULTS AND DISCUSSION

Risk management in railway projects is a task of strategic and operational planning aimed at identifying, analyzing, controlling and minimizing threats that could adversely affect the technical, time, financial or safety implementation of the project. Due to the high degree of complexity, the long life cycle and the important role of the railway infrastructure, it is necessary to apply a systematic approach to risk management.

A methodology for risk assessment should be short and clearly spelled out. There should be no opportunity to interpret what to do and how to do it.

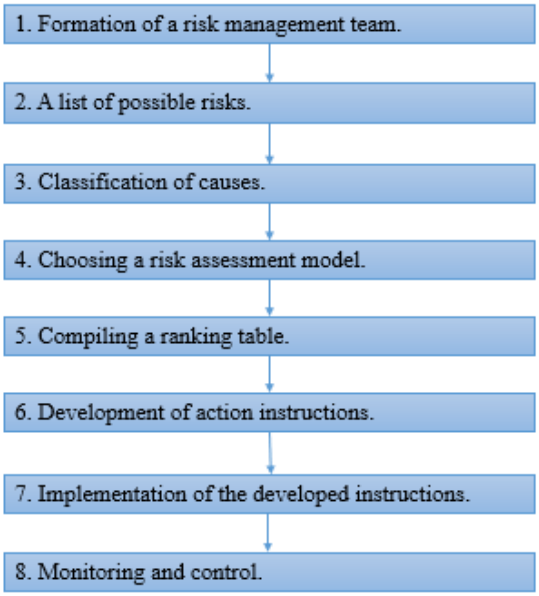

Fig. 1. Risk management methodology

Based on the methodology, project risks are simulated in terms of delay, cost and quality.

Figure 1 presents a methodology for risk management for railway projects. It identifies, analyzes, assesses risks and provides an action plan to achieve the project objectives.

In conclusion, the presented methodology provides a robust framework for effective risk management in railway projects. Through a combination of theoretical principles and practical tools, it contributes to higher safety and efficiency in the implementation of railway infrastructure projects.

IV. Conclusions

This study examines articles and standards published in the last five years. The conclusion is that the topic of risk management in the design and implementation of railway projects was poorly considered during the period.

The future of risk management in rail projects lies in the use of artificial intelligence (AI) in the risk identification process and impact assessment procedures. By analyzing historical data from multiple similar projects, AI can predict potential risks and minimize human error.

IV. References

[1] B. Winfried, "Risikomanagement: Projektrisiken managan statt verdranagen," 2023. [Online]. Available: https://organisationsberatung.net/risikomanagement/. [Accessed 23 02 2025].

[2] T. Daskalova, Management of Infrastructure Projects, Sofia: UNWE Publishing Complex, 2022.

[3] S. Tzvetkova, "Risk Management in the Development of Transport Projects," *Engineering, Business, Environmental Science,* no. DOI:10.37708/EP. SWU. V8I2.14; ID: 229615875, 2020.

[4] J. Singh, "Risk Assessment and mitigation in Construction Building Projects," *Constuction and Building Materials Engineering,* no. 2581-6454, https://www.researchgate.net/publication/388642957, pp. 14-23, 2025.

[5] A. A. Vighio, "Risk Assessment of High and Low Budget Construction Projects," *International Research Journal of Modernization in Engineering Technology and Science,* no. e-ISSN: 2582-5208, DOI: 10.56726/IRJMETS43387, 2023.

[6] K. K. O. Ş. İdil Çalık, "Life Cycle Risk Management for Improving Labor Productivity in Construction Projects in Türkiye," *Buildings,* no. DOI: 10.3390/buildings15030484, 2025.

[7] S. K. A. J. Elnaz Safapour, "Effective Project Management Principles and Strategies in Transportation Infrastructure Projects," *Conference: Creative Construction Conference,* no. DOI: 10.3311/CCC2020-064, 2020.

[8] G. B. M. L. E. B. Karin Bernsmed, "An evaluation of practitioners' perceptions of a security risk assessment methodology in air traffic management projects," *Journal of Air Transport Management,* vol. 102, no. 0969-6997, https://doi.org/10.1016/j.jairtraman.2022.102223, 2022.

[9] M. Stefanova, Risk Management in Complex Systems (on the Example of the Railway System of Bulgaria), Sofia: abstract, 2017.

[10] J. Mancheva, Lecture Notes on 'Project Risk Management', Sofia: University of Architecture, Civil Engineering and Geodesy, 2020.

[11] B. Zhao, "Construction of an Assessment Model for Project Risk," *Highlights in Business, Economics and Management,* vol. 42, 2024.

[12] B. Titarenko, "Risk assessment for construstion projects of transport infrastructure objects," in *IOP Conf. Series: Earth and Enviromental Science*, Chicago, doi :10.1088/1755-1315/90/1/012057, 2017.

[13] P. Landau, "Now to Make a Risk Management Plan," ProjectManager, 26 09 2024. [Online]. Available: https://www.projectmanager.com/blog/risk-management-plan. [Accessed 24 02 2025].

[14] D. ". k.g. infrastructure", Safety procedure PB 2.09. Methodology for determination. Risk Assessment and Management, Sofia, 2021.

[15] D. B. K. B. S. M. M. N. M. Maxime Rigaud. Jürgen Bückers, "The Methodology of Risk Quantification Research," *Environmental Health,* no. https://doi.org/10.1186/s12940-023-01039-x, 2024.

[16] "БДС EN IEC 31010:2019, Risk management - Risk assessment techniques," 14 11 2019. [Online]. Available: https://bds-bg.org/bg/project/show/bds:proj:105683. [Accessed 22 02 2025].

[17] P. Burdyak, "Model of risk management in rail transport," *International Scientific Siberian Transport Forum - TransSiberia 2023,* vol. 402, no. https://doi.org/10.1051/e3sconf/202340206017, p. E3S Web of Conf., 2023.

[18] B. Galev, D. D. E. H. N. G. B. Galev, Safety and Health at Work in Transport, Sofia: ISBN – 978–954–12–0145–9, Todor Kableshkov University of Transport, 2008.

[19] V. Bozhkov, "On the Risk Assessment Process as Part of the Understanding of External Control," *Audit,* no. https://www.ides.bg/media/1774/03-2020-vasil-bozhkov.pdf, 2020.

Environment. Technology. Resources. Rezekne, Latvia
Proceedings of the 16th International Scientific and Practical Conference. 2025. Volume IV, 309-314

Algorithm and Flowchart for Geometric Modeling of Microcomponents Based on the CAD System "MICROSYS 25"

Desislava Petrova
Department "Management"
Technical university of Gabrovo
Gabrovo, Bulgaria
des_petrova@abv.bg

Tsanka Zlateva-Petkova
Department "Management"
Technical university of Gabrovo*)*
Gabrovo, Bulgaria
tszlateva@abv.bg

Angel Lengerov
Department Mechanical engineering and technologies
Technical university of Sofia, Branch Plovdiv
CoC – "Smart-Mechatronics, Eco- and Energy Saving Systems and Technologies"
Plovdiv, Bulgaria
anlengerov@abv.bg

***Abstract*—The article presents the general system of sets of connections of the design of the product and the production process. An algorithm and a flowchart for geometric modeling of the automated system "MICROSYS 25" for microsystems equipment products and a flowchart of an algorithm for selecting a technological process (TP) of the automated system have been developed.**

Keywords— automated system, microsystems engineering, technological design.

I. INTRODUCTION

The main task of automated structural design is the implementation of a principle structural scheme of the designed object and preparation of documentation. The tasks solved in this process can be divided into two groups [1, 2]. One - structural design solves the determination of the geometric parameters of the structure, and these are the tasks of geometric design. The second group of tasks - to synthesize the structure (typology) of the structure, taking into account the functional characteristics of the object, and these are the tasks of topological design. In addition to them, the tasks of structural design also include checking (analysis) of the qualities of the resulting structural solution. Geometric design includes the tasks of geometric modeling, geometric synthesis and design documentation, topological design includes the tasks of layout, placement and routing.

The object of the specialized automated design system "MICROSYS 25" is the development of the database of the modules "structural design" and "technological design", as well as the relationship between them in. The product is considered not as a mechanical connection of different types of objects (elements and components) or as a random community of heterogeneous and independent phenomena occurring in it, but as something holistic, representing a single organic whole of interconnected objects, ensuring the manifestation of numerous mutually conditioned relationships between different phenomena [3].

Thanks to this type of connectivity and conditioning of objects and phenomena, a specific product is formed, which functions in a characteristic and unique way. Thus, the issue of connections and their mutual conditioning becomes important both in the process of designing the product (MMC, MME, MC, etc.), and in the process of its production, because it is the structure and properties of the connections that determine the quality and value of the product, the level of production intensity and its efficiency.

The creation or construction of the product is reduced to the construction of a system of two mutually conditioned sets of connections - material and geometric [4, 5].

For the materialization of each construction, an appropriate PP must be created, representing a new system of five mutually conditioned sets of connections of:

- material properties;
- geometry (topology);
- information;
- time and

Online ISSN 2256-070X
https://doi.org/10.17770/etr2025vol4.8441
© 2025 The Author(s). Published by RTU PRESS.
This is an open access article under the Creative Commons Attribution 4.0 International License.

- economic sets of connections

The mutual dependence between the sets of material properties and dimensional relationships is necessary in the production process in order to create an analogous system of relationships in the product and to define its quality [6]. The set of information relationships is necessary for the management of the production process, and it is carried out in time and at the expense of living and material labor (a set of economic relationships).

The creation of each product (MMC, MME, MC, sensor, etc.) is reduced to the construction of two systems of relationships, relating to: the design of the product (MMC) and the production process of its manufacture.

It is necessary that the relationships in the PP be constructed in strict accordance with the system of relationships contained in the design of the product, i.e. TP inherits the system of sets of the two types of relationships characteristic of the design, which must be included in the new more complex system (Fig. 1).

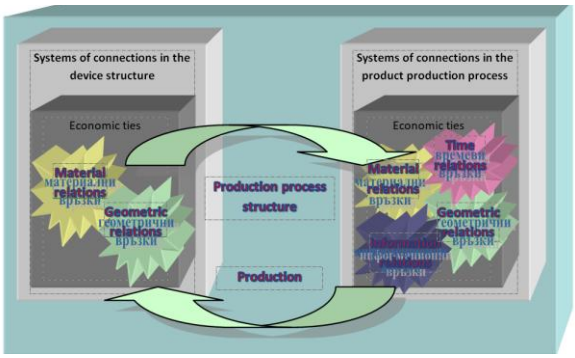

Fig. 1. General system of the sets of connections of the product design (MMK) and the production process

The system of connections constituting the product (micromechanical components - MMC) can be considered strictly deterministic, while the production process is a complex probabilistic system belonging to the category of cybernetic control systems [7].

Considering the production process of manufacturing the product (micromechanical components - MMC) as a manifestation of the overall system of sets, technology and studies these connections in order to solve the problem of ensuring the required quality at a given productivity and minimal expenditure of time, labor, energy and materials [8, 9, 10].

II. Materials and Methods

A. Algorithm for geometric modeling of micromechanical elements (MME) for the system for automated design of components of microsystems technology

For geometric modeling of MME included in the construction of microcomponents, two main methods of structural design are used:

- Variant geometric modeling - its use is determined by the fact that the system will design variants of geometrically similar MME. This requires the components and the MMEs that make them up to be classified into groups according to structural and technological features. The concept of variant geometric modeling consists in the development of groups of geometrically similar MME. For each group, a geometric parametric model is developed, which contains all the features of the elements of the corresponding group. Each designed MME is coded and refers to a microcomponent, in the construction of which the designed MME is included. Microcomponents are also divided into groups and a structural parametric model is created for each of them. Each designed microcomponent (MC) is coded. In variant geometric modeling, there are two possible solutions. If there is a geometric model in the DB that completely matches that of the designed MME, only the dimensions of the specified parameters of the element are entered and they are saved in the DB as a ready-made solution. If the geometry of the designed MME does not match any geometric model from the DB, the closest model is selected. The necessary corrections are entered and it is saved in the DB as a new geometric model of the MME. The dimensions are entered for the specific designed MME and it is saved in the DB as a ready-made solution [11, 12, 13, 14].
- Generative geometric modeling – if there is no geometric model in the DB that fully or partially matches the designed MME, then its geometry is designed, the parameters of this model are determined and it is saved in the DB as a new solution of a group of designed MMEs. The dimensions of the specific designed element are entered and the data are saved in the DB as a ready-made solution [15, 16].

Algorithm of a submodule for geometric modeling of a structural design module of the "MICROSYS 25" system:

1. In the table "Ready-made solutions of MME" from the database, a ready-made solution of MME is searched. If such a solution is found, go to item 15. If no ready-made solution is found, go to item 2.
2. From the table "Microcomponents" (MC) from the database, a component is selected in the construction of which the designed MME is included.
3. From the table "Micromechanical elements" (MME) from the database, the type of the designed MME is selected.
4. In the table "Geometric models of MME" from the database, a ready-made geometric model of the designed MME is searched. If a ready-made geometric model is found, go to item 5. If no such MME model is found, go to item 8.
5. Generation of a unique variant number with values for the parameters of the designed MME.
6. Entering the variant with values for the geometric parameters of the designed MME.

7. Recording the values in the table "Variants with values for MME parameters" from the database. Proceed to item 15.
8. Creating the geometric model of the designed MME.
9. Defining and entering the parameters describing the designed MME.
10. Generating a unique number for the geometric model of the designed MME.
11. Recording the created model in the table "Geometric models of MME" of the database.
12. Generating a unique number for the variant with values for the MME parameters.
13. Entering the variant with values for the geometric parameters of the designed MME.
14. Recording the values in the table "Variants with values for MME parameters" of the database.
15. Proceeding to the submodule "Engineering analysis".

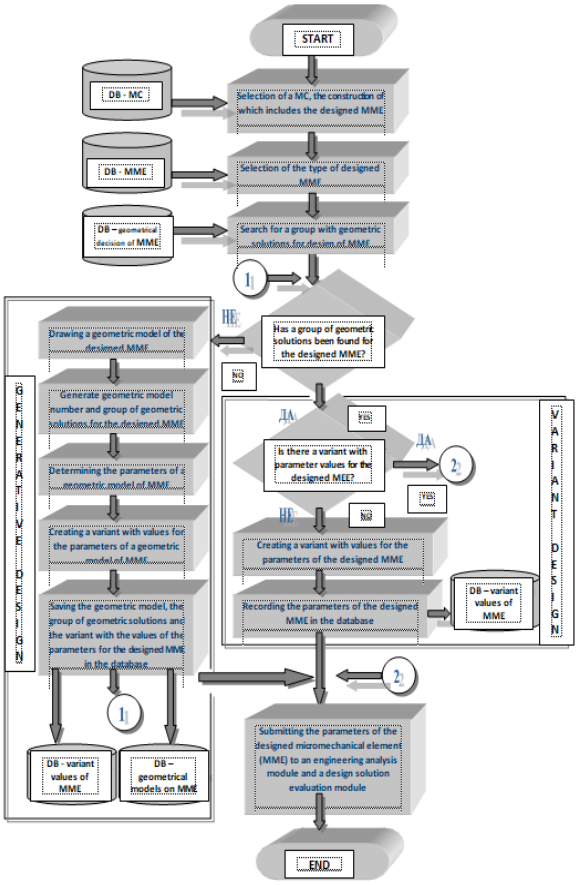

Fig. 2. Block diagram of the geometric modeling algorithm from the automated system "MICROSYS 25"

B. Algorithm for selecting a technological process of the "MICROSYS 25" system

Two design approaches are used in Automated process design on Technological Process (APTP) – variant and generative. The basis of the variant design method is the unification of objects and processes, by using the methods of typical TP and group processing. The generative method provides automated synthesis of an individual TP [17, 18, 19]. The revised algorithm for automated technological design of MME includes the variant design approach. This choice is determined by the specifics of production in microtechnics – mass production using group technology [20]. Variant design is based on the fact that for each group of micromechanical elements, typical technological processes (TTP) are developed for different processing methods. The choice of a specific type of TP is determined by the degree of suitability of this TP for the specifically designed MME.

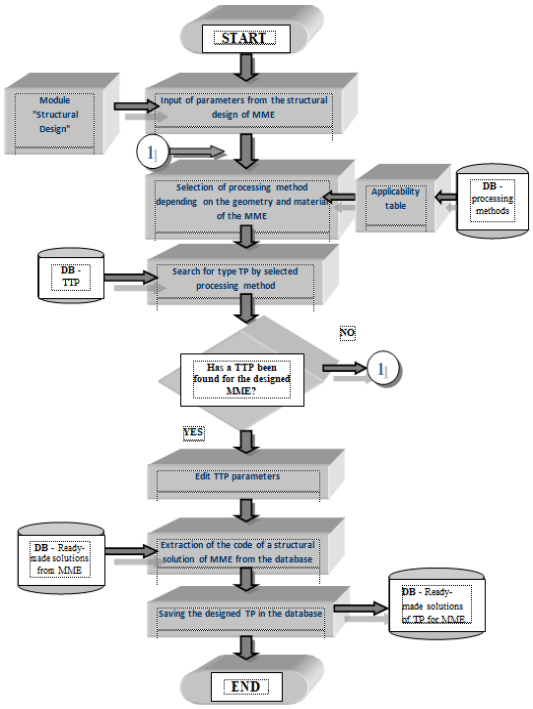

Fig. 3. Flowchart of the algorithm for selecting a technological process (TP) of the automated system "MICROSYS 25"

The algorithm of the module for selecting a technological process of the "MICROSIS" system works in the following sequence:

1. In the table "Ready-made solutions of TP" from the DB, a ready-made project of TP for the designed MME is searched. If such a solution is found, go to item 8. If no ready-made solution is found, go to item 2.
2. From the "Constructive design" module, the parameters of the designed MME are transferred - geometric description, dimensions, technical requirements, material.
3. Selection of a processing method from those possible for the specific MME according to the criteria of geometric features and material.
4. In the table "Typical TP" of the DB, a search is made to see if there is a TTP for the specific MME. If such a solution does not exist, go to item 3. to select a new processing method.
5. Editing the TTP parameters for the specific MME.

6. From the table “Ready-made solutions of MME” of the DB, the code of the MME for which the TP is being designed is extracted.
7. In the table "Ready-made solutions of TP" of the DB, the data for the designed TP are recorded.
8. Transition to the submodule "TP Evaluation".
9. Economic efficiency of the technological process [21, 22, 23].

The block diagram of the algorithm for selecting TP is shown in Fig. 3.

III. Results and Discussion

Figure 2 shows the optimized block diagram of the geometric modeling algorithm. To create the geometric model of a designed MME, it is necessary to use a software product that must have the following characteristics:

- Ability for 3D modeling of objects.
- Ability to enter dimensions as parameters.
- Ability to correct an already designed object.
- Ability to automatically generate drawings.
- Ability to exchange data with other systems through standardized graphic file formats.
- The models must be directly used for structural analysis or other applications.

In microtechnology, repeated operations are used to structure layers, which implement the main processes (basic technologies) and are presented in Figure 4 and Figure 5, but can also be classified as follows:

A) Deposition of layers on a substrate or a previous layer:

- Physical methods for manufacturing elements by applying thin layers using the methods of vacuum evaporation and sputtering;
- Chemical methods for gas-phase deposition of polycrystalline silicon and amorphous layers;
- Epitaxy - deposition of a single-crystal layer;
- Electrodeposition of galvanic and chemical coatings;
- Methods for applying thick layers.

B) Modification of the surface layer of the substrate, as well as of an already finished layer, so that a new layer with other physical properties, different from the initial state, is formed:

- Thermal oxidation;
- Diffusion;
- Ion implantation.

C) Structuring of a protective layer – production of a protective layer by lithography as a mask for the next etching operation and LIGA (combined lithographic - galvanic) method [24, 25].

D) Methods for microstructuring by mechanical micromachining [26].

E) Removal of layers by etching the areas of the substrate free from the mask, respectively the areas of the layer.

F) Methods for processing by high-energy sources:

- Electron beam processing;
- Laser beam processing;
- Plasma jet processing.

The technological processes and methods of shaping and shaping, as well as surface (layer) shaping and shaping are illustrated below in Fig.4 and Fig. 5.

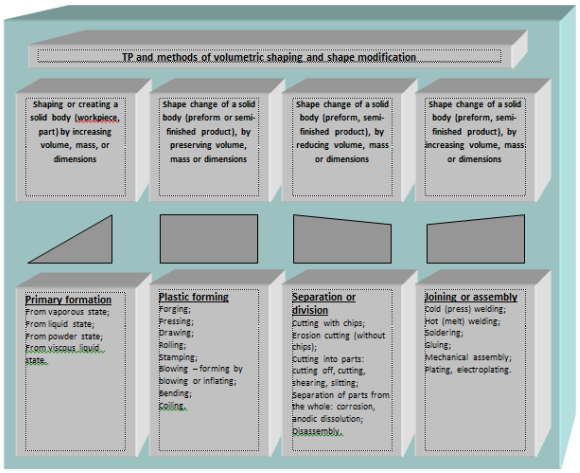

Fig. 4. TP and volumetric forming methods

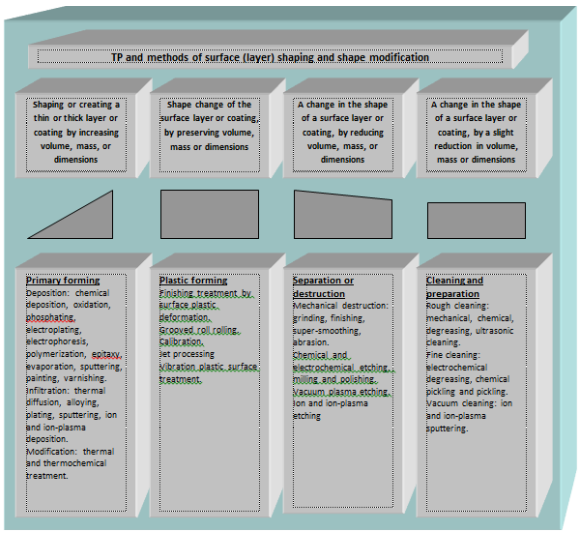

Fig. 5. TP and methods of surface (layer) forming

IV. Conclusions

An algorithm has been developed for the modules for “Geometric Modeling” and “Constructive Design” of the CAD system “MICROSYS 25”, according to which the geometric modeling of MME from MT is best performed using a variant or generative method.

The “Choice of a technological process” from the module “Technological Design” of the specialized

automated system "MICROSYS 25" has been implemented using a variant method of designing technological processes.

Classifications of microcomponents – microsensors, executive micromechanisms and MME, using the facet method, have been further developed, summarized and presented in tabular form (convenient for further work and processing). The tables serve to build the design database of the CAD system "MICROSYS 25".

The design of the design and technological database of the CAD system "MICROSYS 25" has been implemented, and their relational models have been presented.

The automated system for the design of MMK for products from MT "MICROSYS 25" has not completed the design cycle, since computational software is required, therefore the CAD/CAM system is not completed, but is open for further development.

ACKNOWLEDGMENTS

This research was funded by the European Regional Development Fund within the OP "Research, Innovation and Digitalization Programme for Intelligent Transformation 2021-2027", Project CoC "Smart Mechatronics, Eco- and Energy Saving Systems and Technologies", No. BG16RFPR002-1.014-0005.

REFERENCES

[1] Hr. Metev, T. Kuzmanov, Manufacturing Technologies (part IV), Technological processes for CNC machines, „EX-PRESS"Ltd. – Gabrovo, Gabrovo, 2007.

[2] T. Kuzmanov, K., H. Metev, I. Tsvyatkova. Morphological method application to designing modular sectional tools systems. International scientific conference UNITECH'03, Gabrovo, Bulgaria 2003, vol.1. pp. 544-546. ISBN 954-683-167-0

[3] D. Petrova., Doctor tezis, Database for automated design of micromechanical components for microsystems engineering products, Gabrovo, 2008

[4] A. Kocilovii, I R.K. Madsteriakova – 4 izd., prerab. Idop., Spravochnik tehnologa-mashinostroitelia – Tom 2, Moskva, Mashinostroenia, 1985.

[5] An. Lengerov, "Algorithmic model of technical and economic calculation of optimal technological process "Manufacturing Technologies (part XI), 2016, vol.26. pp. 94-96. ISSN 1312-8612.

[6] H. Klaus, F. Hetzelt, P. Hofmann, A. Blecker and D. Schwaiger, 'Challenges and Solutions for Industry-Grade Secure Connectivity', 2019 International Conference on Networked Systems (NetSys), Munich, Germany, 2019.

[7] I. Balabanova, G.Georgiev, "Image Recognition by FFT, Artificial Intelligence and k-Nearest Neighbors Approach". IOP Publishing, Journal of Physics: Conference Series - EEPES'22, vol. 2339, pp. 1-8, 2022.

[8] N. Nikolova, Development of a System for Assessment of Digital Professional Suitability in the Company Environment, Vide. Tehnologija. Resursi - Environment, Technology, Resources, Volume 3, Pages 211 – 216, 2024, 15th International Scientific and Practical Conference on Environment. Technology. Resources, ETR 2024, Rezekne, 27 June 2024 through 28 June 2024, Code 201245, Conference Proceedings, ISSN 16915402, ISBN 978-171389957-0, DOI 10.17770/etr2024vol3.8136.

[9] N. Nikolova, Human Capital in the Changing Work Environment of Industry 4.0, Vide. Tehnologija. Resursi - Environment, Technology, Resources, Open Access, Volume 3, Pages 187 – 193, 2023, 14th International Scientific and Practical Conference on Environment. Technology. Resources, ETR 2023, Rezekne, 15 June 2023 through 16 June 2023, Code 191610, DOI: https://doi.org/10.17770/etr2023vol3.7177

[10] N. Nikolova, Entrepreneurial "Blue" Practices for Sustainable Development and Resources Efficiency, 12th Inter-national Scientific and Practical Conference "Environment. Technology. Resources", June 20-22, 2019, Rezekne Academy of Technologies, Rezekne, Latvia, Volume I, 198-203, ISSN 1691-5402, ISSN 2256-070X.

[11] I. Mitev, Determining the diffusion coefficient in simultaneous saturation with boron and carbon of austenite alloyed with cooper in powder metallurgy structural materials, 11th International Scientific Conference "TechSys 2022" – Engineering, Technologies and Systems, AIP Conf. Proc. 2980, 060016-1–060016-8; https://doi.org/10.1063/5.0184239 , Published by AIP Publishing. 978-0-7354-4814-8/$30.00, pp. 060016-1 to 060016-8.

[12] J. Sunbi, A. Gallina, Contemporary Management of Innovation: Are We Looking at the Right Things?, USA, 2019.

[13] M. Schillings, Strategic Management of Technological Innovation, Ravi Shankar, Edition: 6, 2019.

[14] M. Sain, Y. J. Kang and H. J. Lee, 'Survey on security in Internet of Things: State of the art and challenges', 19th International Conference on Advanced Communication Technology (ICACT), Bongpyeong, 2017.

[15] M. Marinov Jordanov, Vector-Matrix Computer Method for Drafting Circling-Point Curves and Centering-Point Curves of Burmester, Vide. Tehnologija. Resursi - Environment, Technology, Resources, Volume 2, Pages 440 – 443, 2024, 15th International Scientific and Practical Conference on Environment. Technology. Resources, ETR 2024, Rezekne, 27 June 2024 through 28 June 2024, Code 201245, Conference Proceedings, ISSN 16915402, ISBN 978-171389957-0, DOI 10.17770/etr2024vol2.8072.

[16] M. Marinov, Jordanov, Synthesis of Eight Middle Lost Mechanisms Finally Discharged Discreet Positions, Vide. Tehnologija. Resursi - Environment, Technology, Resources, Volume 2, Pages 435 – 439, 2024, 15th International Scientific and Practical Conference on Environment. Technology. Resources, ETR 2024, Rezekne, 27 June 2024 through 28 June 2024, Code 201245, Conference Proceedings, ISSN 16915402, ISBN 978-171389957-0, DOI 10.17770/etr2024vol2.8067.

[17] D. Petrova, Intelligent, Innovative and Sustainable Industry in Bulgaria – prospects and challenges, Vide I. Tehnologija. Resursi - Environment, Technology, Resources, Proceeding of the 12th International Scientific and Practical Conference „Environment. Technology. Resources", June 20-22, 2019, Rezekne, Latvia, Volume I, pp. 210-215, ISSN 1691-5402 – print, ISSN 2256-070X – online. https://doi.org/10.17770/etr2019vol1.4188

[18] D. Petrova, An Alternative Approach to Reducing Aging of Innovative Industrial Products in Terms of Industry 4.0, Environment. Technology. Recourses – Proceeding of the 13-th International Scientific and Practical Conference, Rezekne Academy of Technologies, Rezekne, Latvia, 2021, ISSN 1691-5402, Online ISSN 2256-070X, https://doi.org/10.17770/etr2021vol3.6507 p. 274-280, scopus

[19] D. Petrova, B. Vlahova, A. Lengerov, T. Zlateva-Petkova, Study of the State of Innovation Development and Obsolescence in the Republic of Bulgaria of Companies from the Mechanical Engineering Sector, Vide. Tehnologija. Resursi - Environment, Technology, Resources, 2023, 1, pp. 187–194, DOI: https://doi.org/10.17770/etr2023vol1.7239 , https://www.scopus.com/authid/detail.uri?authorId=56323816400

[20] S. Mumtaz, A. Alsohaily, Z. Pang, A. Rayes, K. F. Tsang and J. Rodriguez, 'Massive Internet of Things for Industrial Applications: Addressing Wireless IIoT Connectivity Challenges and Ecosystem Fragmentation', IEEE Industrial Electronics Magazine, vol. 11, no. 1, pp. 28-33, March 2017.

[21] G. Chipriyanova, A. Atanasov, R. Krasteva-Hristova, Environmental Management for Sustainable Business in Chemical Industry in Bulgaria, Vide. Tehnologija. Resursi - Environment, Technology, Resources, Volume 1, Pages 95 – 101, 2024, 15th International Scientific and Practical Conference on Environment. Technology. Resources, ETR 2024, Rezekne, 27 June 2024 through 28 June 2024, Code 201245, Conference Proceedings, ISSN 16915402, ISBN 978-171389957-0, DOI 10.17770/etr2024vol1.7971.

[22] G. Chipriyanova, M. Chipriyanov, K. Luchkov, Investigation and Analysis of Attitudes Towards the Implementation of Artificial Intelligence in Internal Business Processes, Vide. Tehnologija. Resursi - Environment, Technology, Resources, Volume 2, Pages 61 – 67, 2024, 15th International Scientific and Practical Conference on Environment. Technology. Resources, ETR 2024, Rezekne, 27 June 2024 through 28 June 2024, Code 201245, Conference Proceedings, ISSN 16915402, ISBN 978-171389957-0, DOI 10.17770/etr2024vol2.8032.

[23] G. Chipriyanova, M. Marinova, Technological Aspects of Accounting Automation System as a Decision Support System, Vide. Tehnologija. Resursi - Environment, Technology, Resources, Open Access, Volume 2, Pages 28 – 33, 2023, 14th International Scientific and Practical Conference on Environment. Technology. Resources, ETR 2023, Rezekne, 15 June 2023 through 16 June 2023, Code 191610, DOI: https://doi.org/10.17770/etr2023vol2.7309 .

[24] I. Ahmad, T. Kumar, M. Liyanage, J. Okwuibe, M. Ylianttila and A. Gurtov, 'Overview of 5G Security Challenges and Solutions', IEEE Communications Standards Magazine, vol. 2, no. 1, pp. 36-43, March 2018.

[25] I. Mitev, Optimizing the quantity of liquid phase at the sintering of powder construction materials from system Fe-Cu-Sn, 11th International Scientific Conference “TechSys 2022” – Engineering, Technologies and Systems, AIP Conf. Proc. 2980, https://doi.org/10.1063/5.0184238 , Published by AIP Publishing. 978-0-7354-4814-8/$30.00, pp. 060017-1 to 060017-7.

[26] S.Tsenkulovski, I. Mitev, Influence of the Parameters of the Laser Marking Process on the Depth of Penetration in Layer-reinforced Composites, Vide. Tehnologija. Resursi - Environment, Technology, Resources, Volume 3, Pages 319 – 324, 2024, 15th International Scientific and Practical Conference on Environment. Technology. Resources, ETR 2024, Rezekne, 27 June 2024 through 28 June 2024, Code 201245, Conference Proceedings, ISSN 16915402, ISBN 978-171389957-0, DOI 10.17770/etr2024vol3.8147.

Environment. Technology. Resources. Rezekne, Latvia
Proceedings of the 16th International Scientific and Practical Conference. 2025. Volume IV, 315-321

Methodology for Variant and Generative Design of Microcomponents Based on the CAD System "MICROSYS 25"

Desislava Petrova
Department "Management"
Technical university of Gabrovo
Gabrovo, Bulgaria
des_petrova@abv.bg

Tsanka Zlateva-Petkova
Department "Management"
Technical university of Gabrovo)
Gabrovo, Bulgaria
tszlateva@abv.bg

Angel Lengerov
Department Mechanical engineering and technologies
Technical university of Sofia, Branch Plovdiv
CoC – "Smart-Mechatronics, Eco- and Energy Saving Systems and Technologies"
Plovdiv, Bulgaria
anlengerov@abv.bg

***Abstract*— Microsystems engineering (MSE) is becoming increasingly important for the future technical and economic development of the world. The global market for microsystems products is experiencing tremendous growth, with countries such as the USA, Japan and Germany reaching high levels of development and technological development. It is currently a strategic direction that determines the development of human civilization and completely changes the appearance of manufactured products in the 21st century. Microengineering concerns technolo-gies and the practical implementation of three-dimensional structures and elements based on them with dimensions in the order of micrometers (μm). One of its main goals is to integrate microelectronic circuitry with micromechanical three-dimensional structures, by implementing complex integrated complexes called microsystems (MS). The purpose of this report is to present the developed methodology for variant and generative design of the specialized automated system for designing products from Microsystems Engineering "MICROSYS 25". The developed standard technolo-gical process for the production of flat circular membranes with double-sided plugs, by double-sided anisotropic etching, is illustrated. The recording of the generated information and a standard technological process in the relational database of an automated system is presented. The further development of the "MICROSYS 25" project is the development of multiple technological processes for micromechanical elements and components and their recording in the library database and thus optimizing the process of developing new technological processes.**

Keywords*— automated system, microsystems engineering, technological design.

I. Introduction

The specific characteristics of MSs compared to traditional (macrosystems - MS) are based mainly on their size [3]. When choosing a method for automated design of MSs, the methods of their production and operation are taken into account. Group technologies are usually used for the production of microsystems. When applying such technologies, a large number of elements are processed simultaneously, while manual intervention is not necessary or is insignificant. The production equipment used is expensive, since high accuracy requirements are imposed. It is economically advantageous to produce microsystems in large quantities. Microsystem technology is unsuitable for the production of prototypes, because the scheme of mass production using group technology is violated. Unlike traditional systems, the possibility of repair in microsystems is limited. Therefore, the main goal in development is to obtain a fully functioning system at the first implementation. The development of microsystems production is aimed at reducing the cost of materials and equipment, the number of technological operations and improving their functional properties (accuracy, operating range, sensitivity, etc.) while simultaneously increasing reliability. With the increasing complexity of microsystems, the design stage plays an increasingly important role in the production process. The developed automated system "MICROSYS 25" covers all stages of design – geometric modeling, engineering analysis and determination of a technological process for

Online ISSN 2256-070X
https://doi.org/10.17770/etr2025vol4.8442
© 2025 The Author(s). Published by RTU PRESS.
This is an open access article under the Creative Commons Attribution 4.0 International License.

manufacturing. The object of design is micromechanical functional elements, which are the smallest units of microsystems.

For the Automated Design (AD) of components and Technological Processes (TP) for them in the "MICROSYS 25" system, two main design approaches are used:

- Variant design;
- Generative design.

The algorithm for generative design is described in detail in "Algorithm and flowchart for geometric modeling of microcomponents based on the CAD system "MICROSYS 25"" [3]. The basis of variant design is the unification of components and functional elements and the basic technologies for their production. It is expressed through the use of TTP and group processing methods. Group technology is a production concept in which the existing similarities of the designed objects and TP are identified and used in order to obtain advantages in their design and production by uniting them in groups.

For the implementation of variant design of micromechanical functional elements, a classification and coding system has been developed, with components and functional elements (FE) divided into groups [3]. The criteria for separation are the similar constructive and technological features of FE, according to the sequence of their processing and the assignment of a given FE to a specific microcomponent (MC) – microsensor or executive micromechanism (microactuator).

The facet classification method was used, in which the set of components and FEs were divided into independent sets. Monocodes with a hierarchical tree structure were used for coding. The meaning of each position depends on the meaning of the previous position. This method of coding allows coding a large amount of information using a limited set of symbols and the ability to update the classifiers [1, 2].

The following classifiers were developed [3]:

- MC in electromechanical microsystems - microsensors and microactuators are systematized in detail.
- Micromechanical functional elements, divided into groups of beams, plates, membranes, pyramidal and V-shaped combs, blades, needle supports, 3D-partially movable microstructures, etc. The groups are subdivided into subgroups according to the geometric features of the FE.

Technological processes in microtechnology (MT) are divided into the following main groups:

- Methods for applying layers on a substrate or a previous layer [4];
- Methods for modifying and structuring the surface layer of the substrate [11];
- Structuring by micromachining;
- Radiation processing methods.

A classification [3] has been developed based on information about:

- MC – types, principle of operation, application;
- FE – design parameters, standard technologies for their production;
- TP – principles of processes, schemes and parameters, equipment, application.

According to the block diagram of the algorithm for geometric design of micromechanical functional elements of the "MICROSYS 25" system, a ready-made geometric model corresponding to the designed functional element is searched from the database [3]. If such a model exists, only the specific geometric parameters and material are entered, then engineering analysis is performed. If a ready-made model does not exist, geometric modeling of FE is performed and its recording in the database as a ready-made model for subsequent design of other FEs with the same geometry is performed. After conducting the engineering analysis, technological design is performed. A standard technology for the production of the designed FE is searched in the database. When such a technology is found, it is edited, and technological documentation is output depending on the FE parameters. If there is no standard technology for the designed FE, we proceed to generative design.

For each group of functional elements, a common TP is developed, which is called the standard technology. Table 1. shows a standard technology for manufacturing round membranes with double-sided stoppers by anisotropic etching, with dimensions in μm and the membrane colored in gray.

TABLE 1 TYPICAL TECHNOLOGICAL PROCESS FOR MANUFACTURING FLAT CIRCULAR MEMBRANES WITH DOUBLE-SIDED STOPPERS BY DOUBLE-SIDED ANISOTROPIC ETCHING

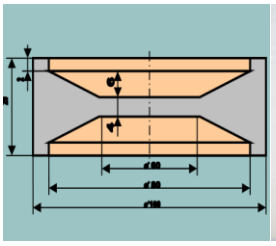

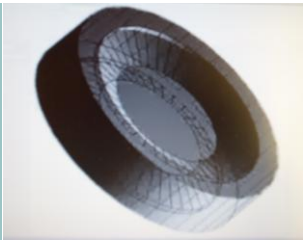

No.	Operation scheme	Operation code	Name of the operation
1	2	3	4
1	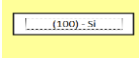		Preparing the substrate
2	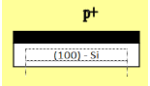	2.1.2.1 2.1.2.1.1 2.1.2.2.1	Doping: Building an etch-stop layer by doping with the chemical element boron (B) 1. By general diffusion for sizes 1÷25 μm (for boron) 2. By general ion implantation – for sizes up to 1 μm (for boron)
3	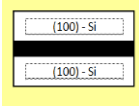	1.1.3 1.1.3.1 1.1.3.2 1.1.3.3	Epitaxy: Building an epitaxial p-Si layer 1. Gas phase epitaxy for sizes 4÷17 μm 2. Solution epitaxy – for sizes 2.4μm 3. Molecular beam epitaxy – for

			sizes below 1 μm
4		2.1.1 2.1.1.1 2.1.1.2	Oxidation: 1. Liquid thermal oxidation 2. Dry thermal oxidation
5	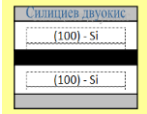	2.2.1 2.2.1.0.0.1	Photolithography: Surface preparation, washing and drying.
6	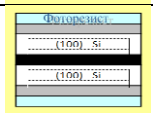	2.2.1 2.2.1.0.0.2	Photolithography: Deposition of photoresist
7	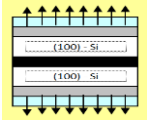	2.2.1 2.2.1.0.0.3	Photolithography: Drying – removing the solvent and bringing the photoresist into a solid insoluble phase
8	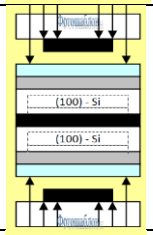	2.2.1 2.2.1.0.0.4	Photolithography: Photopattern alignment (photo template) and exposure – the positive resist under the influence of light passes into an insoluble phase
9		2.2.1 2.2.1.0.0.5	Photolithography: Developing the photoresist – washing in solvent to remove the exposed resist
10	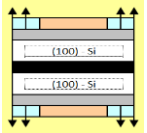	2.2.1 2.2.1.0.0.6	Photolithography: Fixing – hardening of the resist and removal of solvent residues
11	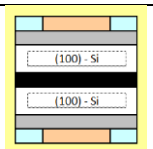	2.2.1 2.2.1.0.0.7	Photolithography: Local Etching – Through a Photoresist Mask 1. Liquid Local Etching 2. Dry Local Etching
12	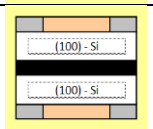	2.2.1 2.2.1.0.0.8	Photolithography: Photoresist Removal – "Stripping" 1. In boiling H_2SO_4 2. Gas and ionic
13	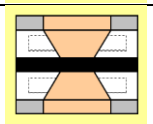	2.3 2.3.1 2.3.2.	Double-sided anisotropic etching 1. Liquid chemical anisotropic etching 2. Dry anisotropic etching
1	2	3	4

II. Materials and Methods

The automated system "MICROSYS" is for structural and technological design of MME. Its variant design algorithm has been tested using examples from the classifiers of components and technological processes for them. The database built on the basis of the classifiers allows "MICROSYS 25" to be used as an information - reference system or catalog system for the selection of functional MME, through its visualization modules [12, 13].

Membrane fabrication

Membranes are most often produced from resist etched layers that are deposited and structured on a substrate before anisotropic deep etching. As such, mask layers made of SiC, Si_3N_4, SiO_2 or doped stop layers are used [11]. Membranes can be double-sidedly located on the substrate or attached layers to supports. Figure 4 shows a silicon oxynitride membrane, which is coated on the front, front side of the substrate by through-etching of the same on the reverse side. Therefore, as a rule, double-sided polished substrates are used, which are coated on the reverse side with a mask layer. The mask layer and the membrane layer can be made of the same material, so that the coating of the front and back sides in a CVD (chemical) reactor can be carried out in successive operations [14, 15]. The profile holes in the back mask layer determine the sagging and positioning of the membrane on the front side. The decisive parameter here is the thickness of the substrate and the deviations from it must be minimal. If the membrane must take the correct position relative to the movable structures on the front side, double-sided development is used in the structuring by lithography.

The production of the front side of the membrane is possible by etching, by obtaining an etched ridge. The membrane shown in Figure 1 (b) is suspended on four supports and is a basic structure for applying, for example, functional layers of a sensor, which must have good thermal insulation to the periphery. When designing the profile openings, the design rules (h>c) are observed.

The etching of closed membranes on the reverse side can be carried out in a single dose, with which the intended structures on the front side (e.g. metallization) are protected before the etching bath. In this way, On-Chip - the integration of microelectronic circuits with micromechanical membrane structures is achieved.

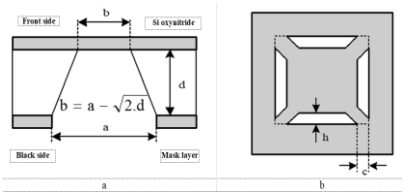

Fig. 1. Etching of membranes:

a) on the reverse side; b) on the front side, under etching condition h>c

The mechanical stresses in membrane-type structures are an essential prerequisite for carrying out the production process and the deformation is assumed as an output value in the mathematical model for description [10]. A sandwich-type structure is often used (for example, from LPCVD - Si_3N_4 and TEOS - SiO_2 - layers), in which tensile and compressive stresses are combined with an appropriate choice of layer thickness. The silicon oxynitride layers used in the PECVD process can be produced by optimizing the process parameters (gas pressure, gas mixing, power). Table 2. shows the process parameters for coating 1μm Si_3N_4.

TABLE 2 PROCESS PARAMETERS FOR COATING A SILICON SUBSTRATE

Power, W	100 to 13,56 MHz
Gas pressure, mTor	650 ÷ 800
Substrate temperature, ˚C	300
Gas temperature, ˚C	250
Gas mixture	80SiH_4 / 80NH_3 / 1000N_2

The type of membrane material and thickness depend on complex factors. Very thin membranes (0.1 – 1 μm) with low thermal conductivity (~1W/mK) are obtained by PECVD and LPCVD methods from amorphous SiC, Si_3N_4, SiO_2 layers, if the aim is to achieve thermal insulation of the functional layers. Silicon membranes with a thickness of ~10 μm can be obtained by epitaxy and embedded stop-etch layers – basic structures for piezoresistive pressure sensors [10].

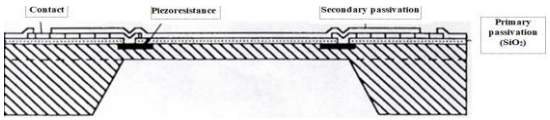

Fig. 2. Piezoresistive silicon pressure sensor.

TABLE 3 PROCESS SEQUENCE FOR MEMBRANE FABRICATION

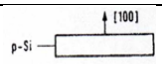	Substrate
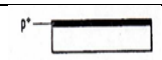	Establishment of etch-stop layer by boron doping
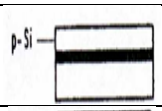	Establishment of epitaxial p-Si layer
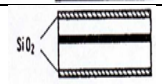	Oxidation
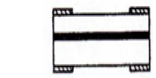	Photolithography and trench opening
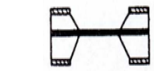	Double-sided anisotropic etching

III. RESULTS AND DISCUSSION

Preferable options for graphic images and photographs are: 300 dpi resolution, 8 bits per pixel, grayscale.

A piezoresistive pressure sensor with a silicon membrane made by anisotropic etching on the reverse side of a silicon substrate is designed. The dimensions of the membrane are radius r = 2 mm; thickness b = 0.004 mm; pressure p = 0.1 N/mm^2.

The physicomechanical characteristics of the silicon (Si) material are: modulus of elasticity E = 1.9 . 10^{11}Pa, μ = 2,4.

The deformation of the membrane is considered in the linear region – δ_{max}= ½ b, i.e. the boundary conditions of the load are determined.

When designing the structural parameters according to FEM, the membrane is considered as a firmly fixed thin elastic plate loaded with a distributed load p = 0.1 N/mm^2.

The mathematical description of a membrane is given by the membrane differential equation. It is derived by the Prantl analogy. The method of analogies is widely used in structural mechanics and in the theory of elasticity. The torsion function φ(x,y) is defined by the Poinson differential equation:

$$\frac{\delta^2\varphi}{\delta X^2}+\frac{\delta^2\varphi}{\delta Y^2}=-2G\nu \quad (1)$$

Where: δ is the angle of twist, rad; 2G – the multiple of the angle of twist, taken with a negative sign, rad.

Equation (1) is valid subject to the following boundary condition for displacement:

$$\varphi(s)=0 \quad (2)$$

From the equilibrium problem of an ideal membrane it is known that the vertical displacement ω(x,y) of an arbitrary point of it is determined by integrating the differential equation:

$$\frac{\delta^2\omega}{\delta X^2}+\frac{\delta^2\omega}{\delta Y^2}=-\frac{q}{H} \quad (3)$$

Where: q is the distributed load acting on the membrane, N/mm^2; at the boundary condition:

$$\omega(s)=0 \quad (4)$$

The comparison of the differential equations and boundary conditions of the two problems shows that if we load the membrane with a distributed load q = 2HGδ, the function ω(x, y) will coincide with φ (x,y). In this way, the abstractly introduced function φ(x,y) becomes concrete and illustrative [16, 17].

The differential equation of the membrane (3) describes the mathematical model of the membrane deformation. FEM is used to solve a specific differential equation. According to it, the membrane is assumed to be an elastic plate, in which the bending stresses caused by the transverse forces are negligibly small compared to the tensile stresses lying in the midplane, which are large. In this method, the membrane is considered as a type of plate, i.e. it belongs to plates with a small thickness [20].

The differential equation of a thin elastic plate, which is from the second group of plate elements derived by FEM, is not of interest to us, because the membrane belongs to the third group of plate elements. It is derived by considering a thin elastic plate loaded with a distributed load q = q (x, y), acting along the z axis. The displacement function is ω = ω(x, y), which describes the deformation of the plate. After certain derivations and transformations, the desired differential equation is obtained:

$$\frac{\delta^4\omega}{\delta X^4} + 2\frac{\delta^4\omega}{\delta X^2\delta Y^2} + \frac{\delta^4\omega}{\delta Y^4} = \frac{q(X,Y)}{F} \quad (5)$$

The boundary conditions of the load must be determined. For this purpose, the possible stresses that satisfy the linearity condition will be determined. It is assumed that the membrane is firmly fixed.

It is known from the theory that in order to increase the accuracy of the solution obtained by FEM, it is necessary to apply a dense finite element mesh in the loaded area of the model under study. Since this area is not always known in advance, in practice, second and subsequent analyses are carried out in order to denser the mesh in the loaded areas and the results obtained for each subsequent analysis, after correcting the mesh, do not differ significantly within the required accuracy [18, 19].

The determination of the equivalent stresses of brittle materials, such as silicon (Si), is done using Moore's strength theory in a three-dimensional stressed state.

Moore's strength theory differs fundamentally from classical theories. It is based on the logical systematization of the results of the necessary experiments, and not on hypotheses regarding criteria for the occurrence of a dangerous state [6, 7].

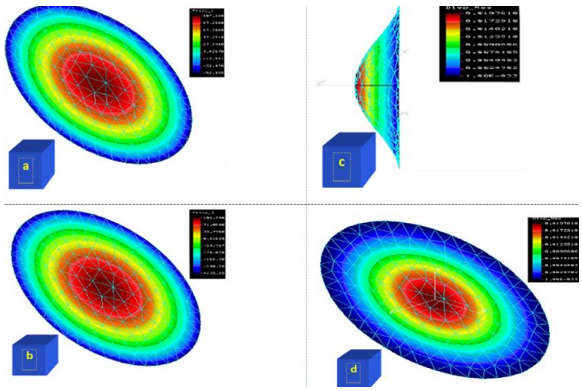

Fig. 3.

a) Principal normal stress σ_1, MPa; b) Principal normal stress σ_3, MPa; c) Distribution of total displacements, mm; d) Distribution of total displacements along the z axis, mm.

$$\sigma^{IV}_{equivalent} = \sigma_1 - k\sigma_3, MPa \quad (6)$$

$$\sigma_1 > \sigma_2 > \sigma_3 \quad (7)$$

The equivalent stresses are determined using formula (6).

From figure 3a, the axial stress is determined σ_1=107,220 MPa, and from figure 3b, the corresponding tangential stress σ_3=106,340 MPa.

The coefficient k is equal to 0.15.

$$\sigma^{IV}_{equivalent} = \sigma_1 - k\sigma_3 = 107{,}220 - 0{,}15.106{,}340 = 91{,}27, MPa \quad (8)$$

$$\sigma^{IV}_{equivalent} = 91{,}27\ MPa < \sigma_{allowable} = 120 MPa$$

From the results obtained, it follows that the equivalent stress is less than the allowable for the material. From theory it is known that tensile or compressive stresses (in this case tensile) are less than 5% of the bending stresses.

Figure 2 shows a piezoresistive pressure sensor with a silicon membrane fabricated by anisotropic etching of the reverse side of the silicon substrate. The strongest piezoresistive effect is observed at the location of maximum membrane deformation. Stoppers prepared by diffusion or ion implantation are used to form the active structure of the sensor. The silicon p-layer doped with a high boron content (concentration of boron impurities 5.10^{19} cm^{-3}) is etched much more. This possibility has been applied in the manufacture of the membrane, and by using etching processes at the protruding edges, bridge structures can also be obtained. Membranes with a small distance from the substrate surface can be made using surface layer mechanics methods. The most common material used is polysilicon with a structuring, subsequently removed by selective etching, sublayer of SiO_2 or PSG, which requires holes for access of the solution. This means that membranes without holes (profile cutouts) cannot be manufactured using this method. In addition to the polysilicon-based method, many variants with other materials for the layer have already been developed, for example SiO_2 layers under SOI substrates [8, 9].

Finally, let us present the following example of a typical technological process for the manufacture of a micromechanical element (MME)

Fig. 4 shows a MME flat membrane and a TP for its manufacture. Based on this TP, an example of a TTP for the manufacture of a group of flat round membranes with one-sided stoppers according to the MME classifier has been developed. The membrane in Fig. 4 is an element of a microcomponent (MC) piezoresistive pressure sensor.

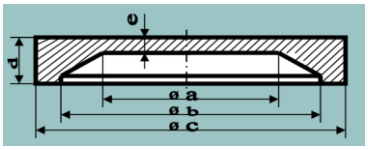

Fig. 4. Flat round membrane with one-sided stoppers

TABLE 4 TYPICAL TECHNOLOGICAL PROCESS FOR MANUFACTURING FLAT ROUND MEMBRANES WITH ONE-SIDED STOPPERS

No.	Operation scheme	Operation code	Name of the operation
1	2	3	4
1	(100) - Si		Preparing the substrate
2	p+ (100) - Si	2.1.2.1 2.1.2.1.1 2.1.2.2.1	Doping: Establishment of an etch-stop layer by doping with boron 1. By general diffusion 2. By ion implantation
3	Силициев двуокис (100) - Si	2.1.1 2.1.1.1 2.1.1.2	Oxidation: 1.Thermal oxidation 2. Anodic oxidation

4	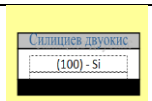	2.2.1 2.2.1.0.0.1	Photolithography: Surface preparation – washing and drying
4	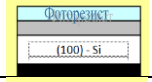	2.2.1 2.2.1.0.0.2	Photolithography: Deposition of photoresist
4	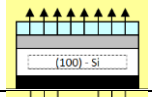	2.2.1 2.2.1.0.0.3	Photolithography: Drying – removing the solvent and bringing the photoresist into a solid insoluble phase
4	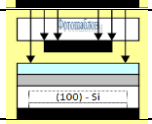	2.2.1 2.2.1.0.0.4	Photolithography: Combining the photopattern and exposing the positive resist under the influence of light passing into an insoluble phase
4	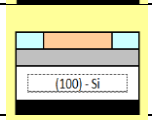	2.2.1 2.2.1.0.0.5	Photolithography: Developing the photoresist – washing in solvent to remove the exposed resist
4	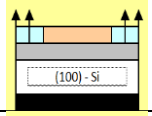	2.2.1 2.2.1.0.0.6	Photolithography: Fixing – hardening of the resist and removal of solvent residues
4	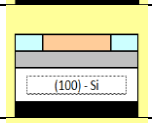	2.2.1 2.2.1.0.0.7	Photolithography: Local Etching – Through a Photoresist Mask 1. Liquid Local Etching 2. Dry Local Etching
8	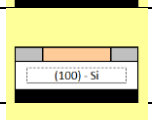	2.2.1 2.2.1.0.0.8	Photolithography: Photoresist Removal – "Stripping" 1. In boiling H_2SO_4 2. Gas and ionic
5	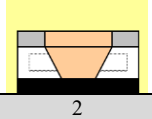	2.3 2.3.1 2.3.2	Local anisotropic etching 1. Liquid chemical anisotropic etching 2. Dry anisotropic etching
1	2	3	4

IV. CONCLUSIONS

- A methodology for variant and generative design has been developed.
- A typical technological process for the production of flat round membranes with double-sided stoppers by double-sided anisotropic etching is presented and illustrated.
- A typical technological process for the production of flat round membranes with single-sided stoppers by double-sided anisotropic etching is presented.
- The recording of the generated information and a typical technological process in the database of an automated system for the design of microsystems equipment products "MICROSYS 25" is presented.

ACKNOWLEDGMENTS

This research was funded by the European Regional Development Fund within the OP "Research, Innovation and Digitalization Programme for Intelligent Transformation 2021-2027", Project CoC "Smart Mechatronics, Eco- and Energy Saving Systems and Technologies", No. BG16RFPR002-1.014-0005.

REFERENCES

[1] A. Kocilovii, I R.K. Madsteriakova – 4 izd., prerab. Idop., Spravochnik tehnologa-mashinostroitelia – Tom 2, Moskva, Mashinostroenia, 1985.

[2] An. Lengerov, "Algorithmic model of technical and economic calculation of optimal technological process "Manufacturing Technologies (part XI), 2016, vol.26. pp. 94-96. ISSN 1312-8612.

[3] D. Petrova., Doctor tezis, Database for automated design of micromechanical components for microsystems engineering products, Gabrovo, 2008

[4] D. Petrova, Intelligent, Innovative and Sustainable Industry in Bulgaria – prospects and challenges, Vide I. Tehnologija. Resursi - Environment, Technology, Resources, Proceeding of the 12th International Scientific and Practical Conference „Environment. Technology. Resources", June 20-22, 2019, Rezekne, Latvia, Volume I, pp. 210-215, ISSN 1691-5402 – print, ISSN 2256-070X – online. https://doi.org/10.17770/etr2019vol1.4188

[5] D. Petrova, An Alternative Approach to Reducing Aging of Innovative Industrial Products in Terms of Industry 4.0, Environment. Technology. Recourses – Proceeding of the 13-th International Scientific and Practical Conference, Rezekne Academy of Technologies, Rezekne, Latvia, 2021, ISSN 1691-5402, Online ISSN 2256-070X, https://doi.org/10.17770/etr2021vol3.6507 p. 274-280, scopus

[6] D. Petrova, Vlahova, B., Lengerov, A., Zlateva-Petkova, T., Study of the State of Innovation Development and Obsolescence in the Republic of Bulgaria of Companies from the Mechanical Engineering Sector, Vide. Tehnologija. Resursi - Environment, Technology, Resources, 2023, 1, pp. 187–194, DOI: https://doi.org/10.17770/etr2023vol1.7239 , https://www.scopus.com/authid/detail.uri?authorId=56323816400

[7] I. Balabanova, Georgiev G., "Image Recognition by FFT, Artificial Intelligence and k-Nearest Neighbors Approach". IOP Publishing, Journal of Physics: Conference Series - EEPES'22, vol. 2339, pp. 1-8, 2022.

[8] H. Klaus, F. Hetzelt, P. Hofmann, A. Blecker and D. Schwaiger, 'Challenges and Solutions for Industry-Grade Secure Connectivity', 2019 International Conference on Networked Systems (NetSys), Munich, Germany, 2019.

[9] Hr. Metev, T. Kuzmanov, Manufacturing Technologies (part IV), Technological processes for CNC machines, „EX-PRESS"Ltd. – Gabrovo, Gabrovo, 2007.

[10] I. Mitev, Optimizing the quantity of liquid phase at the sintering of powder construction materials from system Fe-Cu-Sn, 11th International Scientific Conference "TechSys 2022" – Engineering, Technologies and Systems, AIP Conf. Proc. 2980, https://doi.org/10.1063/5.0184238 , Published by AIP Publishing. 978-0-7354-4814-8/$30.00, pp. 060017-1 to 060017-7.

[11] I. Mitev, Determining the diffusion coefficient in simultaneous saturation with boron and carbon of austenite alloyed with cooper in powder metallurgy structural materials, 11th International Scientific Conference "TechSys 2022" – Engineering, Technologies and Systems, AIP Conf. Proc. 2980, 060016-1–060016-8; https://doi.org/10.1063/5.0184239 , Published by AIP Publishing. 978-0-7354-4814-8/$30.00, pp. 060016-1 to 060016-8.

[12] J. Sunbi, Gallina A., Contemporary Management of Innovation: Are We Looking at the Right Things?, USA, 2019.

[13] M. Marinov Jordanov, Vector-Matrix Computer Method for Drafting Circling-Point Curves and Centering-Point Curves of Burmester, Vide. Tehnologija. Resursi - Environment, Technology, Resources, Volume 2, Pages 440 – 443, 2024, 15th International Scientific and Practical Conference on Environment. Technology. Resources, ETR 2024, Rezekne, 27 June 2024 through 28 June 2024, Code 201245, Conference Proceedings, ISSN 16915402, ISBN 978-171389957-0, DOI 10.17770/etr2024vol2.8072.

[14] M. Marinov, Jordanov, Synthesis of Eight Middle Lost Mechanisms Finally Discharged Discreet Positions, Vide.

Tehnologija. Resursi - Environment, Technology, Resources, Volume 2, Pages 435 – 439, 2024, 15th International Scientific and Practical Conference on Environment. Technology. Resources, ETR 2024, Rezekne, 27 June 2024 through 28 June 2024, Code 201245, Conference Proceedings, ISSN 16915402, ISBN 978-171389957-0, DOI 10.17770/etr2024vol2.8067.

[15] M. Schillings, Strategic Management of Technological Innovation, Ravi Shankar, Edition: 6, 2019.

[16] M. Sain, Y. J. Kang and H. J. Lee, 'Survey on security in Internet of Things: State of the art and challenges', 19th International Conference on Advanced Communication Technology (ICACT), Bongpyeong, 2017.

[17] N. Nikolova, Development of a System for Assessment of Digital Professional Suitability in the Company Environment, Vide. Tehnologija. Resursi - Environment, Technology, Resources, Volume 3, Pages 211 – 216, 2024, 15th International Scientific and Practical Conference on Environment. Technology. Resources, ETR 2024, Rezekne, 27 June 2024 through 28 June 2024, Code 201245, Conference Proceedings, ISSN 16915402, ISBN 978-171389957-0, DOI 10.17770/etr2024vol3.8136.

[18] S. Mumtaz, A. Alsohaily, Z. Pang, A. Rayes, K. F. Tsang and J. Rodriguez, 'Massive Internet of Things for Industrial Applications: Addressing Wireless IIoT Connectivity Challenges and Ecosystem Fragmentation', IEEE Industrial Electronics Magazine, vol. 11, no. 1, pp. 28-33, March 2017.

[19] S.Tsenkulovski, Mitev, I., Influence of the Parameters of the Laser Marking Process on the Depth of Penetration in Layer-reinforced Composites, Vide. Tehnologija. Resursi - Environment, Technology, Resources, Volume 3, Pages 319 – 324, 2024, 15th International Scientific and Practical Conference on Environment. Technology. Resources, ETR 2024, Rezekne, 27 June 2024 through 28 June 2024, Code 201245, Conference Proceedings, ISSN 16915402, ISBN 978-171389957-0, DOI 10.17770/etr2024vol3.8147.

[20] T. Kuzmanov, K., H. Metev, I. Tsvyatkova. Morphological method application to designing modular sectional tools systems. International scientific conference UNITECH'03, Gabrovo, Bulgaria 2003, vol.1. pp. 544-546. ISBN 954-683-1

Environment. Technology. Resources. Rezekne, Latvia
Proceedings of the 16th International Scientific and Practical Conference, 2025. Volume IV, 323-327

Application of Alternative Approaches for Innovative Technology Obsolencence in Bulgarian Engineering Companies

Desislava Petrova
Department Management
Technical university of Gabrovo
Gabrovo, Bulgaria
des_petrova@abv.bg

***Abstract*—The purpose of the present work is to present a study of the developed methods of alternative solutions in the assessment of innovation obsolescence in 15 engineering companies in Bulgaria, using the questionnaire method. First, the technology and organization of innovation obsolescence is assessed for each investigated enterprise separately. Second assessment of resources for innovation development. Third manifestation of innovation obsolescence by phases and fourth - Manifestation of obsolescence in individual innovation stages for each investigated enterprise separately, based on planned obsolescence.**

***Keywords*—alternative solutions, innovative obsolescence, questionnaire.**

I. INTRODUCTION

During the transition from the twentieth to the twenty-first century, there is an unprecedented accumulation of new knowledge in world history [1, 2, 3, 4]. This time coincides with the development of information and telecommunication technologies (ITT), with the creation of hitherto unknown opportunities for the use of arrays of new knowledge. The innovation activity is developed in all priority directions, incl. management, engineering, telecommunications. Scientific knowledge has been applied in new technological developments and is a powerful generator of economic growth at the macro and microeconomic level [5, 6]. The purpose of this article is to present a survey conducted among 15 enterprises in the mechanical engineering sector in the Republic of Bulgaria. For this purpose, a Questionnaire was developed, which was field-tested and shows the innovation obsolescence with the help of the alternatives for its assessment.

As part of what is new in science, the current dissertation "Alternative solutions against the rapid innovative obsolescence of technologies in mechanical engineering" is a current development. The dissertation deals with the main problems, tools and approaches for innovation management. An analytical study of the impact of innovative aging on technology has been made [7]. A methodology for selection of alternative solutions against rapid innovative aging has been developed, applying an integrated approach to modelling aging itself - innovative and programmatic, and proposed for application known - a method for determining the degree of innovation; method for innovation activity; method for innovative aging and method for alternative solutions. The developed algorithm for connection and symbiosis between the methods achieved the desired result. The prerequisites for the application of the methodological statement for selection of alternative solutions are defined. Approbation of the methodological position in 15 Bulgarian enterprises in real production conditions was made. It has been unequivocally proven that innovative aging is a regularity and that it takes precedence over physical wear and tear. An alternative approach to choosing solutions to reduce the harmful effects of rapid innovative aging is proposed. All this proves the relevance of the development and the possibilities for application in SMEs in the Republic of Bulgaria [8, 9].

For this purpose, an object (enterprise) was chosen for the experiment. As an approbation of the methodological setting in real production conditions, a selection of 15 small, medium and large machine-building enterprises in the Republic of Bulgaria was made [10, 11].

The testing methodology (experiment) includes:

1. Technology and organization of innovation development and innovation obsolescence for each group of investigated enterprises (small, medium, large);
2. Resources for innovation development for each investigated enterprise separately;
3. Manifestation of innovation obsolescence by phases for each investigated enterprise separately;
4. Manifestation of obsolescence in the individual innovation stages for each investigated enterprise separately.

The obtained data are summarized and presented in tabular form.

Online ISSN 2256-070X
https://doi.org/10.17770/etr2025vol4.8462
© 2025 The Author(s). Published by RTU PRESS.
This is an open access article under the Creative Commons Attribution 4.0 International License.

II. Materials and Methods

Technology and organization of innovation development and innovation obsolescence for each group of investigated enterprises (small, medium, large) - Table 1.

Table 1 Innovation Development Technology And Organization, Innovation Obsolescence

Does the enterprise have a programmed development of innovation activity and innovation obsolescence, including	**YES**	**NO**
Programmed innovative development and innovative obsolescence of technologies and production products	+	
Development of new (innovative) products	+	
Other innovative solutions	+	
Does the enterprise have a strategy for development activities, including:	**YES**	**NO**
Own design and construction office.	+	
Comprehensive product design development.	+	
Product design.	+	
Control over the product manufacturing stages.	+	
Shortened time from idea to product reaching the consumer.	+	
Is there a strategy for personnel development, including:	**YES**	**NO**
Maintaining the qualification level of the staff.	+	
Involvement of all personnel in the formation the construction and implementation of the company's innovation strategy.	+	
Leveraging staff knowledge to radically improve innovation processes.	+	
Using the advantages of multifaceted knowledge of problems to expand the innovative capabilities of the company.	+	
Is there a marketing strategy.	+	
A market strategy to target	**YES**	**NO**
Improving operational and innovation efficiency.	+	
Promotes customer loyalty to innovative products.	+	
Rapid response to customer needs for innovative solutions.	+	
Encourages effective use of market opportunities to offer innovative products.	+	
Competitively acceptable prices of the innovative products intended for the market.	+	
Reduction of innovation risk.		+
Quality incl.	**YES**	**NO**
ISO certification level.	+	

Resources for innovation development for each investigated enterprise separately – Table 2.

Table 2 Resources For Innovation Development For Each Investigated Enterprise

What resources for innovation development does the company have, including	**YES**	**NO**
Material, including available equipment and technologies	+	
Temporary (carrying out modernization, delivery of new high-performance equipment, new technologies, etc.)	+	
Cash (on hand, bank, loan, programs, etc.)	+	
Information resources available, attraction, etc.	+	
Using the Internet and searching and analyzing information	+	
Do you use the following internet practices?	**YES**	**NO**
Virtual distribution of information related to technology and work organization;	+	
Internet coordination of various activities, technologies, constructions, transports, as well as joint implementation of assembly work;		+
Directories for storing technological and constructive novelties (innovations);	+	
Online procurement with innovation suppliers and consumers.	+	
Technologies in virtual and real time;		+
Customer service and innovation websites.	+	
Search and analyze information	**YES**	**NO**
Research on a regular basis the opinion of users about innovative products and the individualization of the technological product.	+	
Monitoring the actions and tactics of competitors regarding innovative designs.	+	
Forecasting sales of innovative products and anticipating changes in consumer preferences;	+	
Using market research and research on novelties;	+	
Regular monitoring of publications related to innovations in the company's sector of activity;	+	
Conducting strategic innovation intelligence;	+	
Search for additional sources of information.	+	
Human Resources	+	
Human resource management is targeted on hiring creative people, including:	**YES**	**NO**
Highly qualified staff with experience and seniority;	+	
Multifaceted competence.		+
Development opportunities for associates at all levels, including:	**YES**	**NO**
Create effective communications;	+	
Monitoring the satisfaction of all associates.		+
Creative management, including	**YES**	**NO**
Encouraging people who introduce innovations and changes;	+	
Participation in training programs;	+	
Stimulation of innovative proposals;	+	
Guaranteeing interesting work;	+	
Development of staff skills.	+	

Manifestation of innovation obsolescence by phases for each investigated enterprise separately on Table 3.

TABLE 3 MANIFESTATION OF INNOVATION OBSOLESCENCE

In production phase.	YES	NO
Programmed obsolescence;	+	
No programmed obsolescence.	+	
In the post-production phase (Operation).	**YES**	**NO**
Programmed obsolescence;	+	
No programmed obsolescence.	+	
Solutions for programmed aging.	**YES**	**NO**
Are alternative solutions taken?		+

Questionnaire. To study the manifestation of innovation obsolescence and alternative solutions to eliminate its harmful consequences.

(Answer YES or NO)

1. Mechanical engineering company for: "MONEK - SOUTH" JSC, Kardzhali, production of mining and beneficiation and metallurgical equipment, mining and drilling tools, spare parts, rubber products, repair and related engineering activities.
2. Own construction unit. YES
3. Do they use alternative solutions. YES
4. Do they apply programmed obsolescence. NO
3. If it was used, in which of the innovation phases was it used; idea, design, production, service. IDEA, DESIGN, PRODUCTION. NO
4. What are the results; good, average, no positive results and benefits. GOOD
5. Other opinions and suggestions. ……
Conducted the survey: ……. Date……..

Each of the 15 companies was surveyed and based on the data received, the following tables were systematized: Table 1, Table 2, Table 3, Table 4, Table 5, Table 6 and Table 7. The data in this case are for "MONEK - SOUTH ” JSC, town of Kardzhali [11 - 16].

III. RESULTS AND DISCUSSION

Manifestation of obsolescence in the individual innovation stages for each investigated enterprise separately.

Note: Planned obsolescence is taken as a base.

Conceptual stage - on Table 4, but design stage -on Table 5.

TABLE 4 CONCEPTUAL STAGE

№	Activities	Time Hours %	Deviations – time increase/ decrease in hours %
1	Generating ideas	100	-5
2	Methods of generating ideas	100	-5
3	Methods for evaluation and selection of ideas	100	0
4	Criteria for evaluating ideas	100	+3
5	A selection of ideas	100	0
6	Technical assignment	100	0

TABLE 5 DESIGN STAGE

№	Activities	Time Hours %	Deviations – time increase/ decrease in hours %
1	Idea solutions - marketing	100	-8
2	Work solutions - marketing	100	+4
3	Choosing a design approach	100	0
4	Choice of 2D or 3D methods	100	+10
5	Combining the stages - KI	100	-10
6	Simulation, models, virtual reality	100	-2

Production stage is present on Table 6.

TABLE 6 PRODUCTION STAGE

№	Activities	Time Hours %	Deviations – time increase/ decrease in hours %
1	Technical training	100	-20
2	Production (phases: preparatory, processing, assembly)	100	+1
3	Testing, control, storage	100	10

After production stage (service) - present on Table 7.

TABLE 7 AFTER PRODUCTION STAGE

№	Activities	Time Hours %	Deviations – time increase/ decrease in hours %
1	Service - monitoring, registration	100	-20
2	Feedback	100	-20

The survey card developed for the purpose is as follows:

A summary of the study is in Table 8 [17, 18].

TABLE 8 A SUMMARY OF THE STUDY

Company name		N_n	S_m	M_m	L	AR
1	2	3	4	5	6	7
1	"MONEK-YUG" JSC, Mining equipment	100	1	0,20	20	Outsourcing
2	"DINAMO SLIVEN" JSC El. engines etc.	100	1	0,15	15	Outsourcing, applications
3	"LIEBHER-HAUSGERETE MARITSA EOOD Refrigerators, freezers	70/100	2	0,50	50	Modules, programmed obsolescence
4	"VITTE AUTOMOTIVE BULGARIA" LTD Locking systems	50/80/100	3	0,80	80	Programmed obsolescence, software applications
5	"TRANSVAGON" JSC Freight cars	100	1	0,20	20	Outsourcing
6	SKYMONT" OOD Equipment for the mining, chemical industry	100	1	0,30	30	Outsourcing, modules, applications
7	"ZMM-SLIVEN" JSC Mechanical engineering, equipment	100	1	0,20	20	Outsourcing
8	"TEREM-IVAYLO" EOOD Military equipment	100	1	0,40	40	Modules, applications
9	"HEM" JSC Apparatus for energy, etc.	100	1	0,30	30	Modules
10	"MADARA AGRO" LTD Agricultural machinery	100	1	0,30	30	Modules
11	"HYDROPLASTFORM" LTD Canning industry equipment	100	1	0,2	20	Outsourcing
12	"FABKO" LTD Lathes, mills	100	1	0,10	10	Outsourcing
13	"ALPEN AND SONS" LTD Tool equipment	100	1	0,20	20	Outsourcing
14	"DARM" Ltd	100	1	0,40	40	Modules,
	Punches, pointed forms, etc.					applications
15	"DIANGELI" ET Measuring tools	100	1	0,30	30	Applications

Note: Nn - Degree of innovation (J_{ino}), % Basic product; Sm - Innovation activity (S) Number Basic product; Mm/L – Innovative aging (M), % Basic product; AR - Alternative solutions (AR) 1. Programmed obsolescence 2. Modular constructions 3. Outsourcing

IV. CONCLUSIONS

A methodology was developed and tested in 15 engineering enterprises.

A questionnaire was developed.

An analytical study of the state of innovation development and innovation obsolescence in the selected engineering companies was carried out. On this basis, it has been established that innovation obsolescence has priority over physical obsolescence.

The applied alternative approach for choosing solutions to reduce the harmful impact of rapid innovation obsolescence has been tested in these enterprises. The obtained results prove its practical and theoretical significance and applicability.

Analytical results show that between innovative and "programmed" obsolescence we have both a mutual relationship and a different functional significance. One is a regularity, and the other can be an alternative to rapid innovation obsolescence.

REFERENCES

[1] S.Berger, Making in America: From Innovation to Market, USA, 2013.

[2] S.Dais, Industrie 4.0 –Anstoli, Vision, Vorgehen. In: Bauernhansl, Th., ten Hompel, M., Vogel-Heuser, B.(Hrsg.): Industrie 4.0 in Produktion, Automatisierung und Logistik. Anwendung – Technologien – Migration, Wiesbaden: Sprin-ger, Fachmedien, 2014, p. 628.

[3] M. Schillings, Strategic Management of Technological Innovation, Ravi Shankar, Edition: 6, 2019.

[4] J. Sunbi, A. Gallina, Contemporary Management of Innovation: Are We Looking at the Right Things?, USA, 2019.

[5] N. Nikolova, , Intellectual Capital Management used for Optimizing the Activities of Modern Small and Medium Enterprises/Companies. 4th International Conference Economics and Management-Based on New Technologies, EMoNT 2014, 12-15 June 2014, Vrnjačka Banja, Serbia., pp.258-262, ISBN 978-86-6075-045-9.

[6] N.Nikolova, Human Capital in the Changing Work Environment of Industry 4.0, Vide. Tehnologija. Resursi - Environment, Technology, Resources, Open Access, Volume 3, Pages 187 – 193, 2023, 14th International Scientific and Practical Conference on Environment. Technology. Resources, ETR 2023, Rezekne, 15 June 2023 through 16 June 2023, Code 191610, DOI: https://doi.org/10.17770/etr2023vol3.7177

[7] M. Chipriyanov, and M. Andonovska, Specific character of the media as business organizations and models for analysing the values created by them. // Business Management, 2022 (1), p. 5-16, Retrieved from www.scopus.com

[8] D. Petrova, Analysis of SMEs in Bulgaria – Assessment of Their Innovation Activities, Rezekne 2013, Latvia, Rezekne Higher

Education Institution, Faculty of Engineering, Scientific Institute for Regional Studies, Environment. Technology. Resources, Proceedings of the 9th International Scientific and Practical Conference June 20-22, 2013, Volume 3, ISSN 1691-5402: pp.46-49.

[9] D. Petrova, Analysis of Trends and Opportunities for Technological Development of Bulgarian Enterprises, Proceedings of the International Conference Danube Black Sea, 3E – Energy, Environment & Efficiency, September 18-21, 2013 Galati, Romania, ISBN, pp. 413-417.

[10] D. Damianov, Modern alternatives to rapid innovative aging, Scientific Bulletins of NTS in Mechanical Engineering, Year XXVI, Vol. 3/224, ISSN 1310–3946, 27 ISTC "ADP 2018", June 2018, pp. 278-283.

[11] S. Demirova, Alternative Of Innovative Aging In SMEs By Lowering The Product Cost Price, Journalijar, Vol 5, Issue 08, 2017, pp.1244-1252, DOI: 10.21474/IJAR01/5178, ISSN: 2320-5407.

[12] I. Balabanova, G. Georgiev, "Image Recognition by FFT, Artificial Intelligence and k-Nearest Neighbors Approach". IOP Publishing, Journal of Physics: Conference Series - EEPES'22, vol. 2339, pp. 1-8, 2022.

[13] I. Mitev, Optimizing the quantity of liquid phase at the sintering of powder construction materials from system Fe-Cu-Sn, 11th International Scientific Conference "TechSys 2022" – Engineering, Technologies and Systems, AIP Conf. Proc. 2980, https://doi.org/10.1063/5.0184238 , Published by AIP Publishing. 978-0-7354-4814-8/$30.00, pp. 060017-1 to 060017-7.

[14] I.Mitev, Determining the diffusion coefficient in simultaneous saturation with boron and carbon of austenite alloyed with cooper in powder metallurgy structural materials, 11th International Scientific Conference "TechSys 2022" – Engineering, Technologies and Systems, AIP Conf. Proc. 2980, 060016-1–060016-8; https://doi.org/10.1063/5.0184239 , Published by AIP Publishing. 978-0-7354-4814-8/$30.00, pp. 060016-1 to 060016-8.

[15] D.Petrova, Analysis of SMEs in Bulgaria – Assessment of Their Innovation Activities, Rezekne 2013, Latvia, Rezekne Higher Education Institution, Faculty of Engineering, Scientific Institute for Regional Studies, Environment. Technology. Resources, Proceedings of the 9th International Scientific and Practical Conference June 20-22, 2013, Volume 3, ISSN 1691-5402: 46-49.

[16] D. Petrova, Analysis of Trends and Opportunities for Technological Development of Bulgarian Enterprises, Proceedings of the International Conference Danube Black Sea, 3E – Energy, Environment & Efficiency, September 18-21, 2013 Galati, Romania, ISBN, pp. 413-417.

[17] D. Petrova, Intelligent, Innovative and Sustainable Industry in Bulgaria – prospects and challenges, Vide I. Tehnologija. Resursi - Environment, Technology, Resources, Proceeding of the 12th International Scientific and Practical Conference „Environment. Technology. Resources", June 20-22, 2019, Rezekne, Latvia, Volume I, pp. 210-215, ISSN 1691-5402 – print, ISSN 2256-070X. https://doi.org/10.17770/etr2019vol1.4188

[18] D.Petrova, An Alternative Approach to Reducing Aging of Innovative Industrial Products in Terms of Industry 4.0, Environment. Technology. Recourses – Proceeding of the 13-th International Scientific and Practical Conference, Rezekne Academy of Technologies, Rezekne, Latvia, 2021, ISSN 1691-5402, Online ISSN 2256-070X, pp. 274-280.
https://doi.org/10.17770/etr2021vol3.6507

Environment. Technology. Resources. Rezekne, Latvia
Proceedings of the 16th International Scientific and Practical Conference. 2025. Volume IV, 329-335

Passive Athermalization of Lenses for LWIR Spectral Range

Dimcho Pulov
Department of Mechanical and Precision Engineering
Technical University of Gabrovo
National Center of Excellence Mechatronics and Clean Tecnologies
Gabrovo, Bulgaria
pulov@tugab.bg

Petar Tsvyatkov
Department of Mechanical and Precision Engineering
Technical University of Gabrovo
Gabrovo, Bulgaria
p.cviatkov@tugab.bg

***Abstract*— This paper investigates the possibility of passive athermalization of objectives for the long-wave infrared (LWIR) region of the spectrum. The main scientific problem is the difficulty in designing an athermalized objectives without the use of aspherical and diffractive surfaces and with the availability of a limited number of optical materials. A design methodology is applied, the focus of which is the use of materials with a negative thermal coefficient of refractive index and with specific values of the refractive index and Abbe number. The results obtained show that the designed objectives are thermally stable in a wide temperature range and have the ability to work with medium-format FPA microbolometric arrays.**

Keywords—LWIR spectrum, optical design, passive athermalization, IR optical materials

I. INTRODUCTION

In can order to fulfill their intended purpose, modern IR thermal cameras must meet high requirements in terms of their resolution, sensitivity and reliability when operating in various environmental conditions. The propagation medium of the radiation can strongly affect the optical radiation by generally weakening the optical radiation and reducing the contrast in the image. Most often, this environment is the Earth's atmosphere, and its optical characteristics depend on such factors as pressure, humidity, and temperature. Modern thermal imaging cameras must be able to operate with ambient temperature variations from -40 to +60 degrees. Moreover, the quality of performance of such IR systems must be stable across the entire temperature range [1], [2].

When the temperature changes, the design parameters of the optical system change. As a result, the path of the rays and the focal length of the lens change, which leads to an increase in the geometrical spot and a shift of the focusing plane from the plane of the photoreceiver matrix. It is obtained temperature defocusing of the image, deterioration of image quality, and instability in the operation of the entire IR system [3], [4].

Temperature defocusing is particularly important for lenses operating in the LWIR spectrum because optical materials for the LWIR spectrum have a higher refractive index n and a higher gradient of the refractive index with respect to temperature change $^{dn}/_{dt}$ compared to materials for the visible region of the spectrum [5] - [8]. For this reason, it is necessary for such lenses to be athermalized, i.e. to compensate for the influence of temperature on the stability of its operation. For this reason, it is necessary for such lenses to be athermalized, i.e. to be compensated for the influence of temperature on the stability of its operation.

Several methods exist for athermalizing lenses:

- Passive optical method. It consists of a suitable selection of optical materials for the lenses (matched to the housing material) and subsequent optimization of the optical scheme [9] - [11]. A separate variation of this method is the use of diffractive optical elements and diffractive and aspherical surfaces [12] - [15]. With this method, the lenses construction is simple, lightweight, and reliable because it has no additional moving elements. However, it implies the use of diverse and expensive optical materials and technologies.
- Passive mechanical method. It consists of adding to the objective structure several movable mechanical elements (spacer rings), which are made of different materials and have a linear expansion coefficient respectively greater and smaller than that of the lenses [2], [5]. Moving these elements

Online ISSN 2256-070X
https://doi.org/10.17770/etr2025vol4.8448
© 2025 The Author(s). Published by RTU PRESS.
This is an open access article under the Creative Commons Attribution 4.0 International License.

compensates for thermal defocusing [16] - [18]. With this method, high focusing accuracy is possible due to the wide range of linear expansion coefficients of different materials. However, the application of this method leads to an increase in the mass and dimensions of the lenses, sealing problems may arise, and their reliability is lower.

- Active electromechanical method. It consists of adding to the design of the lens an electromechanical drive system that moves one or several optical elements longitudinally [1], [2]. Due to the high accuracy of the servomotors used, this method is the most precise for compensating for thermal defocusing under all existing temperature gradients [19] - [21]. The need to use servomotor and moving mechanical elements determines the complexity, increase in mass and dimensions, and lower reliability of this method. This method is justified for application only for complex multi-lens lenses, in which there is already an integrated electric drive for moving the components (e.g. zoom lenses).

A comparison has been made between the different athermalization methods and the most important characteristics of the lenses in Table 1.

TABLE 1 ATHERMALIZATION METHODS

	Optical passive	**Mechanical passive**	**Electro mechanical active**
Constant FOV	yes	yes	yes
Variable FOV	no	yes	yes
Zoom	no	yes	yes
Reliability	Very good	Good	Depends on components used
Mass and dimensions	Small	Medium	Big
Stability to external influences	Very good	Good	Affected by vibrations
Power supply	no	no	yes
Price	Low	Medium	High

It can be seen from Table 1 that when designing compact IR lenses, the passive optical method for athermalization is the most preferred.

There are known solutions related to the application of the passive optical method. Most often these are graphoanalytic solutions. It is proposed in [22] that optical materials for individual lenses should be chosen so that their Abbe number ν and Thermal glass constant T are proportional. This method is convenient and suitable in the presence of a large number of optical materials which to choose from. With a limited number of optical materials available, this method is difficult to realising and does not always lead to result. In [23] - [28], methods for passive athermalization of lenses are proposed, based on the use of various nomograms for the selection of suitable optical materials. For all of them, a graph is drawn, on the axes of which different combinations of the dependencies between Abbe number ν and Thermal glass constant T for different optical materials are plotted. Different authors give different geometric criteria for the correct choice. These are convenient and relatively simple solutions. Their common disadvantage is that they give one specific solution and do not take into account all possible combinations of optical materials. Furthermore, a solution for a multi-component optical system cannot be found by this method.

In [29] - [33], lenses for thermal cameras are considered, the optical scheme of which includes diffractive optical elements or diffractive and aspherical surfaces. These are very promising methods that allow the development of high-quality objectives composed of a small number of individual lenses, even with a limited number of optical materials. Their common disadvantage is that these are technologically more difficult and expensive solutions. Furthermore, the energy transmission at the end of the diffractive optical element decreases.

It can be summarized that the issue of correcting defocusing caused by (arising as a consequence of) temperature gradients during the operation of IR imaging devices is a relevant issue, especially in cases of a limited number of optical materials and without the use of complex electromechanical moving devices. All of this argues the development of this work, the goal of which is to design a passively athermalized LWIR lens for the thermal region of the spectrum.

II. MATERIALS AND METHODS

A. Temperature defocusing and conditions of athermalization

Let the optical system be given with its design parameters *r, t, n* (Fig. 1). When the temperature changes by a value of Δt, they change as follows:

- the refractive indexn_i n of the element with number i becomes $n_i + dn_i = n_i + \beta\Delta t$, where $\beta = \frac{dn_i}{dt}$ is thermal coefficient of refractive index;

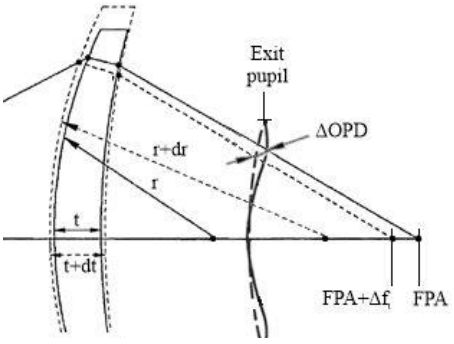

Fig. 1. Lens with thermal deformation.

- the radius r_i of the surface with number i becomes $r_i + dr_i = r_i + \alpha_{L_i}\,\Delta t$, where α_{L_i} is thermal expansion coefficient of lens material;
- the thickness t_i of the optical element with number i becomes $t_i + dt_i = t_i + \alpha_{L_i}\,\Delta t$;
- size of airspase with number i becomes $t_i + dt_i = t_i + \alpha_H\,\Delta t$, where α_H e thermal expansion coefficient of housing material.

As a result of these changes in the design parameters, a temperature defocusing Δf_t occurs, which for a objective composed of m thin lenses can be determined by the expression:

$$\Delta f_t = -f\left(\frac{\sum_{i=1}^{m} T_i\phi_i}{\phi} + \alpha_H\right)\Delta t \qquad (1)$$

where:

- f is the focal length of the entire objective;
- ϕ_i is the optical power of the element with number i, $i = 1 \div m$;
- ϕ is the optical power of the entire objective;
- $T_i = \frac{dn_i/dt}{n_i - 1} - \alpha_{L_i}$ is thermal glass constant.

An IR lens, in addition to being athermalized, must have constant optical power and small chromatic aberrations in the working spectral range. In such a case, the condition for athermalization can be written as:

$$\begin{cases} \phi_1 + \phi_2 + \cdots + \phi_m = \phi \\ \frac{\phi_1}{v_1} + \frac{\phi_2}{v_2} + \cdots + \frac{\phi_m}{v_m} = 0 \\ T_1\phi_1 + T_2\phi_2 + \cdots + T_m\phi_m = -\alpha_H\phi \end{cases} \qquad (2)$$

where: v_i is the Abbe number in the spectral range $(8 \div 12)$ μm of the lens with number i , $i = 1 \div m$.

B. Optical materials and photoreceivers for LWIR range of the spectrum

There are a relatively limited number of optical materials that are transparent in the infrared spectrum. They can be classified into three groups:

• infrared semiconductor crystals and optical ceramics – Ge, Si, GaAs, ZnSe, ZnS etc.;

• chalcogenide glasses – Amtir, Gasir, IRG, IKS, IG etc.;

• alkali metal halides – e.g. KRS-5, AgCl, CsBr, NaCl, KBr, CsI etc.

For correcting temperature aberrations, the most important meaning are the temperature and optical characteristics of optical and non-optical materials: thermal glass constant T_i ; thermal coefficient of refractive index β ; thermal expansion coefficient α_{L_i}, thermal expansion coefficient of housing material α_H.

The analysis of IR materials shows that the coefficient α_{L_i} varies from 5 [K^{-1}] for GaAs to 61 [K^{-1}] for KRS5. The β coefficient varies from -236 [K^{-1}] for GaAs to 396 [K^{-1}] for KRS5 [2], [4], [6], [11]. These high values of α_{L_i} and β imply high and unacceptable values of the temperature defocusing in non-thermalized lenses. There is a group of IR materials with a negative value of β coefficient. This means that when the temperature changes, the refractive index will change in the opposite direction compared to the change in the physical parameters of the corresponding optical element. In such a case, it is possible to design a lens in which the temperature defocusing caused by the change in the radii and thicknesses of the optical elements will be compensated by an opposing temperature defocusing caused by the change in the refractive index of the material. Thermal expansion coefficient of the most common housing materials changes from 1,3.10^{-6} [K^{-1}] for Invar to 23,6.10^{-6} [K^{-1}] for Aluminum.

The dimensional characteristics of the lens (focal length and angular field) depend on the physical dimensions of the photoreceivers used. Furthermore, image quality requirements depend on the pixel size of the photoreceiver. Modern uncooled microbolometric matrix have a format from 120 × 160 to 768 × 1024 pixels and a pixel size 17 μm or 25 μm.

C. Passively athermalized lens design methodology

Passive athermalization of a lens implies the selection of optical materials in which temperature defocusing is minimized and the resulting deterioration in image quality is permissible. Optical path difference (OPD) is used as a criterion for evaluating the quality of the lens. The change in temperature by Δt causes change in OPD, which is determined by the expression

$$\Delta OPD = -\frac{Tf'}{(2F/\#)^2}\Delta t \qquad (3)$$

The Strehl ratio for diffraction limited lenses should be $Str. \geq 0{,}8$ and then according to the Marechal criterion

$$\Delta OPD \leq 0{,}071\lambda \qquad (4)$$

Good athermalization of a lens in the LWIR range of the spectrum will be obtained when using a combination of the following types of optical materials:

- materials with both a high refractive index and a high Abbe number;
- materials with $\beta < 0$
- materials with low Abbe number.

The analysis conducted so far allows us to propose the following methodology for selecting materials for passive athermalization of a refractive objective (Fig. 2). It is possible to achieve good athermalization with 3 lenses (triplet) for relatively simpler optical systems. If to the objective has higher requirements for its geometric and energy resolution and 3 lenses are not sufficient to correct its field aberrations, then additional lenses need to be added to correct them.

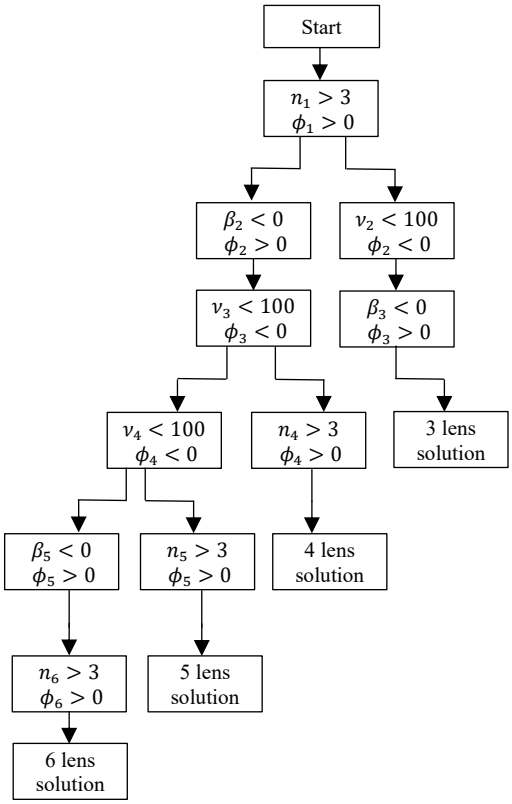

Fig. 2. Block diagram for selection of materials for passive athermalization of an IR lens.

For objective of 3-lens.

- The first lens is positive and made of a material with a higher refractive index.
- The second lens is negative and made of a material with a low Abbe number.
- The third lens is positive and is made of a material with $\beta < 0$.

For a objective of more than 3 lenses.

- The first lens is positive and made of a material with a higher refractive index.
- The second lens is positive and made of a material with $\beta < 0$.
- The third lens is negative and is made of a material with a relatively lower Abbe number.
- The fourth lens can be positive or negative. If it is positive, it is made of a material with a high refractive index. If it is negative, it is made of a material with a relatively lower Abbe number.
- The fifth lens is positive and is made of a material with $\beta < 0$ or a material with a higher refractive index.
- The sixth lens is positive and is made of a material with a high refractive index.
- Lenses with high optical power must be made of a material in which the influence on the temperature defocusing of the β coefficient is greater.

In the proposed methodology, the second and third lenses work as optical compensators of temperature deformation. The second lens – at the expense of the negative value of the coefficient β, and the third lens – at the expense of the negative optical power. The other lenses serve to maintain the set focal length f and to fulfil the condition for image quality.

Lens variants are shown for which the selection of materials was made according to the proposed methodology in Table 2.

TABLE 2 ATHERMALIZED LENS VARIANTS

Lenses and optical materials	**Optical powers**	**Optical system layout**
Lens 1 Ge/ZnSe/KRS5	+/-/+	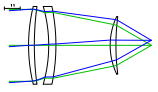
Lens 2 Ge/KRS5/ZnSe/Ge	+/+/-/+	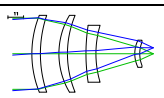
Lens 3 GaAs/KRS5/ZnS/GaAs	+/+/-/+	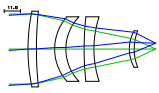
Lens 4 GaAs/AgCl/ZnS/ZnS/GaAs	+/+/-/-/+	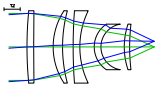

Table 3 shows the optical and thermo-optical characteristics of the materials used.

III. RESULTS AND DISCUSSION

The dimensional characteristics of the lens were determined: 60 mm, focal length F/1.2 and angular field 8°. Using the methodology proposed in item II, five athermal objectives consisting of 3, 4 and 5 lenses were designed. All lenses are spherical and have no diffractive surfaces. The housing material is aluminum. Optics software for layout and optimization OSLO was used and the lenses were optimized using the Marechal criterion for the root mean square of the wave aberration. To evaluate the image quality of the designed lenses, the root mean square of OPD_{RMS} was determined within the entire field of view using the expression

$$OPD_{RMS} = \sqrt{\frac{\sum_{i=1}^{m}(OPD_i - \overline{OPD})^2}{m-1}} \quad (5)$$

where:

- OPD_i is the optical path difference between the off-axial ray number i and the axial ray;
- $\overline{OPD}$ is the arithmetic mean of the optical path difference between the off-axis rays and the on-axis ray; the optical power of the element i, $i = 1 \div m$;
- m is the number of off-axis rays.

TABLE 3 OPTICAL AND THERMO-OPTICAL CHARACTERISTICS OF THE MATERIALS USED

IR Materials	**n, average value**	**Abbe number ν**	**Thermal refractive index coefficient β .10^{-6}, [K^{-1}]**	**Thermal expansion coefficient α_L.10^{-6}, [K^{-1}]**
lens materials				
Ge	4,02	869,13	398,3	5,7
GaAs	3,29	108,09	186	5
ZnSe	2,42	57,18	61,6	7,1
ZnS	2,24	25,46	40,3	6,6
KRS-5	2,37	164,90	-236	61
AgCl	1,98	168,5	-61	32,4
CsBr	1,66	132,6	-78,4	47.2
housing materials				
Aluminum	housing material			23,6

Table 4 shows the values of OPD_{RMS} the designed lenses. As can be seen, all lenses except Lens1 fulfil condition (1). The reason for this is that Lens1 is a lens composed of 3 lenses, the materials of which are such that the temperature defocusing is minimal. Due to the small number of variable parameters, simultaneous correction of temperature and field aberrations for the entire field of view is not possible. All other lenses are composed of more lenses (3 or 4). They are athermalized and their image quality is close to diffraction.

TABLE 4 ANALYSIS ON THE DESIGNED LENSES

Lenses	***OPD$_{RMS}$***	**Ensquared Energy (25x25) µm, % on axis/full field**			
		Temperature, °C			
		-40	**-20**	**40**	**60**
Lens 1 Ge/ZnSe/KRS5	0,074λ	49 8	54 8	68 10	72 12
Lens 2 Ge/KRS5/ZnSe/Ge	0,065λ	75 64	77 67	80 75	81 75
Lens 3 GaAs/KRS5/ZnS/GaAs	0,072λ	67 75	70 76	77 73	77 71
Lens 4 GaAs/AgCl/ZnS/ZnS/GaAs	0,046λ	58 59	57 59	57 58	56 58

To assess the degree of correction of the temperature defocusing, the energy concentration function and the Modulation Transfer Function (MTF) of the lenses at different operating temperatures and angular fields were used. Fig. 3 shows the MTF graphs of the designed lenses for four temperatures $(-40, -20, +40, +60)°C$. The maximum spatial frequency for which the MTF is determined is20 mm^{-1}, which corresponds to the Nyquist frequency for a microbolometric matrix with a pixel size of $25\mu m$. Table 4 shows the values of the energy concentration in a square of size $(25x25)\mu m$ for these 4 operating temperatures.

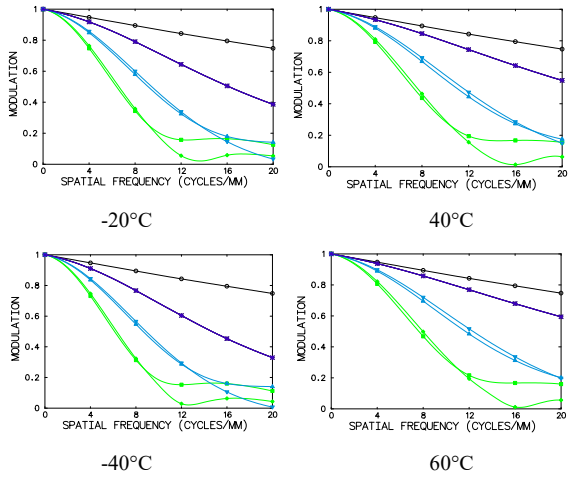

Lens 1

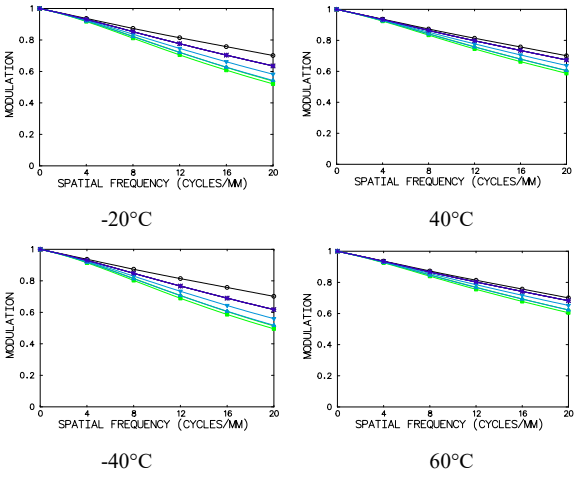

Lens 2

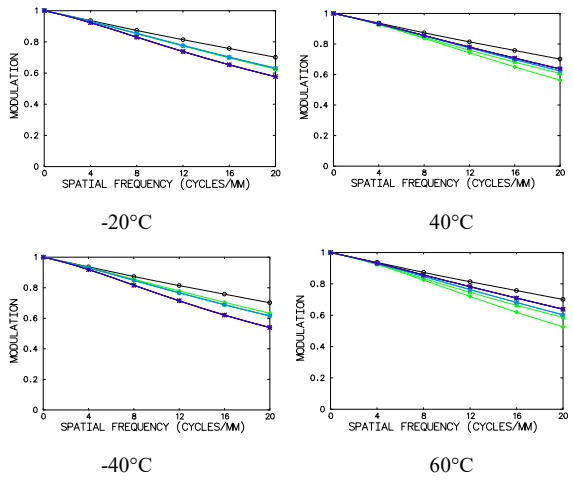

Lens 3

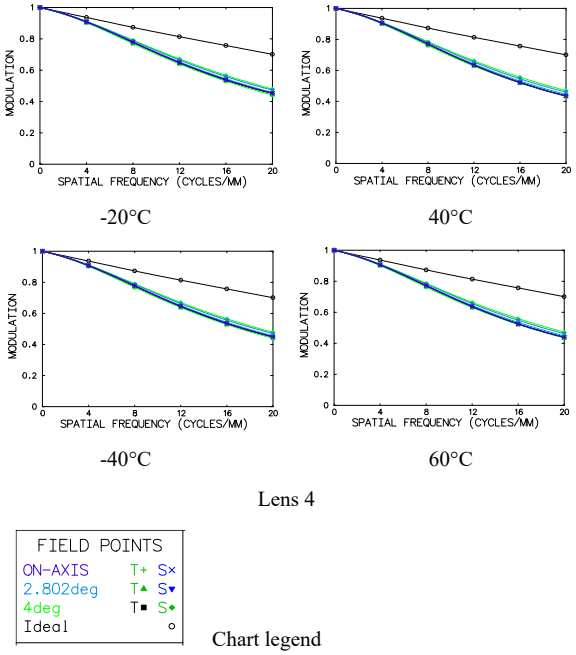

Fig. 3. MTF of lenses for different temperatures.

From Table 4 it can be seen that:

- for all lenses (except Lens 1) the energy concentration on the pixel of the microbolometric matrix is high – from about 50% to slightly over 70%;
- for all lenses the energy concentration is relatively constant for all operating temperatures;
- the operation of Lens 4 from the point of view of temperature change is the most stable, because in it the energy concentration is constant both with temperature change and for the entire field of view (deviations no more than 3%).

From Fig. 3 it can be seen that the MTF for the Nyquist frequency of most lenses is between 0.5 and 0.6, which means that they are diffraction-limited systems. The exceptions are Lens 1 for off-axis rays and partially Lens 4. The MTF of the lenses for different temperatures are very close, which indicates their high degree of athermalization.

The results obtained allow the use of the designed lenses with medium format microbolometric matrix at temperatures from -40 to +60 degrees.

IV. Conclusions

The influence of temperature on the design and optical parameters of IR lenses has been analyzed. The conditions for correcting the temperature defocusing have been formulated.

A methodology for the design of a passively athermalized LWIR objective has been developed. The essence of the methodology is the use of optical materials with different values of the refractive index and Abbe number. A mandatory condition is that at least one of the materials has a negative thermal coefficient of refractive index, i.e., it must be an alkali halide.

Optical schemes have been developed and the optical powers of objectives with 3, 4 and 5 lenses have been determined. Athermal diffraction-limited objectives for the LWIR region of the spectrum have been designed, which have subsequently been optimized using the Marechal criterion. The image quality has been assessed by the root-mean-square value of the OPD. The degree of correction of the temperature defocus has been assessed using the energy concentration function and MTF.

It has been found that an objective composed of 3 lenses cannot be simultaneously athermalized and meet the requirements for image quality over the entire field of view. The objectives with 4 and 5 lenses are diffraction-limited and athermalized over the entire field of view. They have stable characteristics when working with FPA microbolometric matrix with a pixel size of $(25x25)\mu m$ and a format of (320x240).

Acknowledgment

This research was funded by the European Regional Development Fund within the OP "Research, Innovation and Digitalization Programme for Intelligent Transformation 2021-2027", Project No. BG16RFPR002-1.014-0006 National Center of Excellence Mechatronics and Clean Tecnologies.

References

[1] P. Rogers, "Athermalization of IR Optical Systems", Proc. of SPIE, Vol.10260, 1991. doi: 10.1117/12.48455

[2] T. H. Jamison, "Athermalization of optical instruments from the optomechanical viewpoint", Optical Design, Vol. CR43, pp. 131—159, 1992, doi: 10.1117/12.61105

[3] J. Tejada, "Passive Athermalization: Maintaining Uniform Temperature Fluctuations", Photonics Handbook, Optical Design, 2006, pp. 341–345, May 2006.

[4] J. Rayces and L. Lebich, "Thermal compensation of infrared achromatic objectives with three optical materials", Proc. of SPIE, Vol. 1354, pp. 752 – 759, 1990.

[5] V. Povey, "Athermalisation Techniques in Infra Red Systems", Proc. of SPIE, Vol. 0655, pp. 142–153, 1986, doi: 10.1117/12.938420

[6] A.R. Hilton, Chalcogenide glasses for infrared optics. NY: The McGraw-Hill Education; 2009.

[7] H.M, Hassan, TA-E Eldessouky and M. Medhat, "Compact athermalized LWIR objective lens", J Opt 2023, 52(1), pp. 261-268. doi: 10.1007/s12596-022-00892-2.

[8] O. N. Balatsenko and L. N. Arkhipova, "Environmentally stabilized thermal-imaging optical systems," Journal of Optical Technology. 90(9), pp. 491-497, 2023, doi: 10.1364/JOT.90.000491

[9] G.E. Romanova and G. Pyś, "Research of aberration properties and passive athermalization of optical systems for infrared region", Pro SPIE 2015, 9626: 96260H. doi: 10.1117/12.2191119.

[10] V. M. Tiagur, O. K. Kucherenko and A. V. Muraviov, "Passive optical athermalization of an IR three-lens achromat", J. Opt. Technol, Vol. 81, pp. 199–203, 2014, doi: 10.1364/JOT.81.000199

[11] K. Schwertz, A. Bublitz and S. W. Sparrold, "Advantages of using engineered chalcogenide glass for color corrected, passively athermalized LWIR imaging systems", Proc. of SPIE, Vol. 8353, 2012, doi: 10.1117/12.919430

[12] I.A. Levin, “Thermo-optical aberrations of radially symmetric diffractive optical elements”, Computer Optics 2016, 40(1): 51-6. doi: 10.18287/2412-6179-2016-40-1-51-56

[13] G.I, Greisukh, S.T. Bobrov and S.A. Stepanov, “Optics of diffractive and gradient-index elements and systems”, Bellingham: SPIE Press; 1997.

[14] G.P. Behrmann and J.P. Bowen, “Influence of temperature on diffractive lens performance”, Applied Optics 1993, 32(14): 2483-2489.

[15] Liu Rui-qi, Chen Xing-ming and Zhao Jia-qi, “Applied Research of Diffractive Optical Elements in IR Imaging Systems”,[J]. Infrared Technology, 31(6), pp. 327-330, 2009. doi: 10.3969/j.issn.1001-8891.2009.06.005

[16] D. Dichev, D. Diakov, I. Zhelezarov, S. Valkov, M. Ormanova, R. Dicheva and O. Kupriyanov, “A method for correction of dynamic errors when measuring flat surfaces”, Sensors, volume 24, issue 16, 2024. doi: 10.3390/s24165154

[17] D. Dichev, D. Diakov, R. Dicheva, I. Zhelezarov and O. Kupriyanov, “Analysis of instrumental errors influence on the accuracy of instruments for measuring parameters of moving objects”, 31st International Scientific Symposium Metrology and Metrology Assurance, MMA 2021, September, 2021, Sozopol, Bulgaria. doi: 10.1109/MMA52675.2021.9610855

[18] B. Georgiev and Ts. Karadzhov, “Investigating the repeatability of 3d printers using a multi-sensor measurement system”, Environment. Technologies. Resources. Proceedings of the International Scientific and Practical Conference, Rezekne, Latvia, v. 3, p. 65–69, 2024. doi: 10.17770/etr2024vol3.8114.

[19] B. Georgiev and Ts. Karadzhov, “Comparative analysis of geometric deviations in contact measuring instruments for control and laser contactless scanning”, Environment. Technologies. Resources. Proceedings of the International Scientific and Practical Conference, Rezekne, Latvia, v. 3, p. 306–310, 2024. doi: 10.17770/etr2023vol3.7182.

[20] D. Dichev, H. Koev, D. Diakov, N. Panchev, R. Miteva and H. Nikolova, “Automated System for Calibrating Instruments Measuring Parameters of Moving Objects”, 59th International Symposium ELMAR, September 18-20 th, 2017, Zadar, Croatia, pp. 219-224. doi: 10.23919/ELMAR.2017.8124472

[21] D. Dichev, H. Koev, T. Bakalova and P. Louda, “A Gyro-Free System for Measuring the Parameters of Moving Objects”, Measurement Science Review, volume 14, issue 5, 2014, pp. 263-269. doi: 10.2478/msr-2014-0036

[22] D.S. Volosov, “Photographic Optics. Theory, Principles of Design, Optical Characteristics”. Moscow, Iskusstvo Publ., 1978, 543 p.

[23] Y. Tamagava, S. Wakabayashi and T. Tajime, “New design method for athermalized optical systems”, Proc. SPIE, V. 1752, pp. 232–238, 1992, doi: 10.1117/12.130734

[24] K. Schwertz, D. Dillon and S. W. Sparrold, “Graphically selecting optical components and housing material for color correction and passive athermalization”, Proc. of SPIE, Vol. 8486, 2012, doi: 10.1117/12.930968

[25] Y. Tamagava, “Multilens system design with an athermal chart”, Applied Optics, V. 33., pp. 8009–8013, 1994, doi: 10.1364/ao.33.008009

[26] L. Lazov, E. Teirumnieks, N. Angelov and E. Teirumnieka, “Methodology for automatic determination of contrast of laser marking for different materials”, Environment. Technology. Resources. Rezekne, Latvia, Proceedings of the 12th International Scientific and Practical Conference, 2019, Volume III, 134-136, doi: 10.17770/etr2019vol3.4143

[27] S.E. Ivanov and G.E. Romanova, “Calculation of heat-stabilized achromatic IR-lenses using a graphic method for choice of optical materials”, Journal of Instrument Engineering, Vol. 60, issue 3, pp. 256–262, 2017, doi: 10.17586/0021-3454-2017-60-3-256-262

[28] S.E. Ivanov and G.E. Romanova, "Optical material selection method for an apochromatic athermalized optical system," Journal of Optical Technology. 83(12), 729-733 (2016). doi: 10.1364/JOT.83.000729

[29] G.I. Greisukh, I.A. Levin and O.A. Zakharov, “Diffractive elements in thermal imaging monofocal dual-band objectives: design and technological aspects”, Computer Optics, 48(2), pp. 210- 21, 2024. doi: 10.18287/2412-6179-CO-1336.

[30] V. Laborde, J. Loicq, J. Hastanin and S. Habraken, “Multilayer diffractive optical element material selection method based on transmission, total internal reflection, and thickness”, Appl Opt, 61(25), pp. 7415-7423, 2022. doi: 10.1364/AO.465999

[31] I. Draganov, L. Lazov, E. Teirumnieks and N. Angelov, “Numerical modeling and simulation for laser beam welding of ultrafine-grained aluminium”, Published, 2021, Laser Physics, Volume 31, 066001 IOP Publishing, doi:10.1088/1555-6611/abf5d3

[32] A.S. Garshin and K.A. Andreev, “Design of athermalized infrared lenses involving diffractive optical elements”, Scientific and Technical Journal of Information Technologies, Mechanics and Optics, 2018, vol. 18, no. 6, pp. 961–967 (in Russian). doi: 10.17586/2226-1494-2018-18-6-961-967

[33] J. Wang and C. Vue, “Athermalization and thermal characteristics of multilayer diffractive optical elements”, Applied Optics, vol. 54, no 33, pp. 9665–9670, 2015. doi: 10.1364/AO.54.009665

Environment. Technology. Resources. Rezekne, Latvia
Proceedings of the 16th International Scientific and Practical Conference, 2025. Volume IV, 337-343

Proper Orthogonal Decomposition Technique for Dimensional Reduction for Numerical Snapshot Matrix

Rajeev Ralla
Institute of Mechanical and Biomedical Engineering
Riga Technical University
Riga, Latvia
rajeev.ralla@edu.rtu.lv

Karunamoorthy Rengasamy Kannathasan
Institute of Mechanical and Biomedical Engineering
Riga Technical University
Riga, Latvia
karunamoorthy.rengasamy-kannathasan@rtu.lv

Ilgar Jafarli
Institute of Mechanical and Biomedical Engineering
Riga Technical University
Riga, Latvia
ilgar.jafarli@rtu.lv

Abstract*— Computational fluid dynamics (CFD) simulations generate huge datasets with many variables such as Velocity and Pressure at nodes, elements, and time steps. It is challenging and expensive to analysis large datasets and storage, developing applications over the large datasets required additional computational resources and storage volume. To addresses this problem, we have employed data reduction technique for the reduction of the complexity and utilize its computational resources. Reduced Order Modelling emerged technique leading dimensional reduction yet preserving dominant features, patterns and discarding less significant features. Focusing on developing the Reduced Order Models (ROM) for data compression, we implemented Proper Orthogonal Decomposition (POD) technique for dimensionality reduction. Proper Orthogonal Decomposition (POD) is widely used for building efficient Reduced Order Model (ROM) in CFD simulations, enabling effective dimensionality reduction while preserving key flow characteristics. POD extracts the high-energy structures from the flow field, representing dominant patterns through POD modes that contributes to the overall dynamics. Dimensional reduction is achieved by truncating lower-energy modes based on rank, retaining only the most significant features. In this paper we conducted numerical simulation flow over the convex shape object cantered in the flow path, with parametric velocity ranging 25 -300 m/s and density 900 - 2000 kg/m2 of the water. The solution matrix is extracted and total volume was 8.83 MB. After computing POD modes and captured five most energetic modes (Rank = 5) and truncated other modes. The resulting ROM took 4.42 MB achieving a data volume saving of 4.41 MB (8.83 - 4.42 MB). when compared with volume consumptions over the single full numerical simulation (482 MB) to ROM (4.2 MB) is 477.8 MB and percentage occupation for the ROM is only 0.87% which is less than 1% of the original size of full simulation. This study also explores effective techniques for generating and truncating POD-based ROM. It also demonstrates the use of EZyRB-based ROM combined with Radial Basis Function (RBF) interpolation is applied to the POD coefficients using EZyRB library allows fast reconstruction of flow fields without running Full Order Model (FOM) to predict system responses for new parameter values, density 1232 kg/m2 and velocity 152 m/s we successfully reconstructed the flow field using ROM without conducting FOM. These new parameter values were projecting onto the original spatial domain for the visualization and comparing results with Ansys Fluent FOM. Highlighting the efficiency and effectiveness of ROM in parametric interpolation with lower dimensions and provides an intuitive approach for developing digital models that accurately represent physical systems with significantly reduced the computational volume and resources.

Keywords*— CFD, Data Reduction, EZyRB, POD, Radial Based Function, ROM.

I. Introduction

High fidelity CFD simulations are essential for analyzing fluid flow behavior over an object in applications like aerospace and biomedical field, often requires significant computational resources and results huge datasets [1], [2]. These datasets are not only difficult to store and manage, but also practically infeasible to work with the machine learning models since data sets contains millions of nodal points in spatial and field variables. Interpretation or manipulation of these datasets, sometimes required additional libraries, which can make real time analysis difficult. Reduction of this data set dimensionality will reduces the data store capacity, facilitate faster

Online ISSN 2256-070X
https://doi.org/10.17770/etr2025vol4.8447
© 2025 The Author(s). Published by RTU PRESS.
This is an open access article under the Creative Commons Attribution 4.0 International License.

computation. In many industrial and research applications, parametric simulations are repeatedly conducted to evaluate system performances. This highlights the demand for Model reduction techniques and interpolation methods to handle unseen variables, aiming to lower the computational cost and data volume [3]. This paper addresses the advantages of developing Reduced Order Model (ROM) and integrating with interpolation techniques to fasten the simulations without conducting Full Order Model (FOM) [4]. A data-driven technique is required to reduce complexity while preserving the high accuracy of the original data. Proper Orthogonal Decomposition (POD), forms the basis of Reduced Order Modeling [3]-[5]. When developing ROMs, generating data is the key step, and various methods can be employed. The snapshot method, or solution matrix of the simulated system is commonly used [4]-[6]. POD technique plays a major role, by decomposing the solution datasets and finding spatial structures [7] that captures the variance in a dataset typically identify the flow features during the transient simulation of the flow. EZyRB is a Python based open library for the developing ROM and RBF for the interpolation [8], [9]. EZyRB based ROM process typically in three steps 1. Data generation from CFD simulation high fidelity dataset. 2. POD extracting the dominant features and preserve. 3. RBF interpolation method can be used to predict the solution matrix for the new parameters. The purpose of following these steps is to develop the ROM and enhancing predictive models by reducing the complexity of dataset, while retaining key flow features. Developing a bridge by accessing the ROM models to other techniques like optimization and predicting modeling [10]-[11]. A comparative study between the FOM and ROM to demonstrate the reduction in storage capacity and runtime simulation making it valuable tool for reducing computational resources.

II. Materials and Methods

A. Method of Generating Datasets

The numerical snapshot [6] is a combination of spatial points, grid numbers and various parameters of interests such as velocity, pressure, and turbulence in matrix format. Typically, data generated from a series of snapshots, known as the snapshot method, is stored in Excel format. However, using Python, this data can be efficiently stored in arrays or matrices (e.g., NumPy arrays), enabling easy manipulation and processing without relying on Excel, thus improving computational efficiency. Where high resolution photos are taken, and each pixel are considered as grid points or elements. The core ideal behind developing the ROMs to preserve the physical system in a digital format. During ROM development, the data is typically organized as a series of rows and columns, representing different parameters or time steps. This approach provides a clear picture of the transformation of row and columns helping to understand the reduction of data points during implementation. Solution data is derived from the flow over a convex shaped solid body in middle of the rectangular fluid domain of length of 135 mm and height of 60 mm.

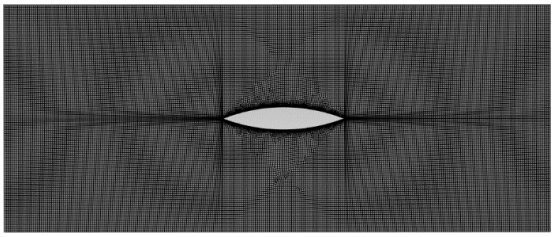

Fig. 1. Mesh Generation of Fluid Domain.

The mesh consists of a total of 38580 nodes, each node carrying the values of the velocities and pressure across the domain. A series of steady simulations are conducted using ANSYS Fluent, varying both density and velocity of fluid to analyze their effects on pressure and velocity distribution over a convex shape. The simulation data is carefully exported containing node numbers, spatial coordinates in the x and y directions, along with the relevant variables of interest.

TABLE 1 DATASET

Node number (Id)	x-coordinate (mm)	y-coordinate (mm)
10709	0.063636	0.019036
23525	0.0094683	0.033570
34025	0.0229060	0.052042

TABLE 2 DATASET TWO

x-velocity (m/s)	y-velocity (m/s)	total pressure (Pa)
55.85	-2.802	1605.152
50.00	-0.006	1604.587
50.26	-0.060	1610.362

The above table shows randomly selected data values from solution exported data points. Total data matrix consists of 38580 rows and 6 columns (38580,6), consuming 2.6MB storage. Similar, way we can extract 10 solution datasets with same number of nodes, each corresponding to different velocities and fluid densities.

TABLE 3 DENSITY AND VELOCITY

Density kg/m2	900	1000	1100	1200	1250
Velocity m/s	25	50	80	100	135

TABLE 4 DENSITY AND VELOCITY TWO

Density kg/m2	1300	1400	1500	1750	2000
Velocity m/s	150	200	225	250	300

The datasets comprise of 10 individual simulations solution data points, each with a shape of (38580, 6), resulting in a total storage of 26 MB. Each dataset is

flattened according to the parameters, the shape of flatten data (1 row x 115740 columns). The snapshot matrix or FOM is the collection and arrangement of these parameters, resulting in the shape of (10 row x 115740 columns), containing a total of 1157400 data points and occupying 8.83 MB of storage. This structure provides a detailed representation of the spatial data points.

B. Method of Dimensional Reduction

Dimensional reduction displays the approximation of high-fidelity data here snapshot matrix data points of shape (10, 1157400) points projecting into lower dimensional space which captures most of the essential features of snapshot matrix. Understanding the modes that captures most of the features and truncated the remaining modes by ranks which has lower performances easy to store data and increase in computational efficiency. The original snapshot matrix took 8.83MB storage by applying data reduction techniques, we can compare storage capacity. POD method is used to reduce the dimensionality of snapshot matrix, can ensure the accurately represents the system. Memory efficiency and high-fidelity data combination enables the handling of larger datasets still maintain precision in simulations and analyses. Single Value Decomposition (SVD) is a matrix decomposition tool to perform POD, POD method captures the important modes which has maximum variance, and the modes are orthogonal. Capturing the orthogonal matrix using the SVD decomposition of the snapshot matrix (m × n) where m is the number of snapshots and n is the number of spatial points in this case.

$$Snapshotmatrix\ _X\ = U\Sigma V^T \quad (1)$$

$U \in \mathbb{R}^{mxm}$ contain the left singular vector matrix U of shape m × m only contain the time depended on structures.

$\Sigma \in \mathbb{R}^{nxn}$ is a diagonal matrix n × n with singular values σ_i are the energy modes, POD utilizes this energy of the modes for the data compression or dimensionality reduction.

$V^T \in \mathbb{R}^{nxn}$ contains the right singular vectors matrix, V^T which consist of n × n spatial modes.

In a diagonal matrix, contains real and non-negative values in the diagonals, and zeros are present outside the diagonal. Singular values are arranged in descending order, from higher to lower. Truncated SVD based on ranks or modes, where the highest singular values are preserved, and the lower ones are discarded. If the singular values capture the higher singular values in first 3 or 4 singular values capturing the 99% of the physical system variance, truncating the matrix to rank 3 or mode 3 can effectively reduce dimensionality of the matrix, preserving the most significant modes and eliminating the less important ones.

$$Trancated_{snapshotmatrix_{X_r}} =$$

$$= U_r\Sigma_r{V^T}_r \quad (2)$$

$U_r \in \mathbb{R}^{mxr}$ contains the left singular vectors matrix of shape (m, r) reduction based on rank columns.

$\Sigma_r \in \mathbb{R}^{rxr}$ is a diagonal matrix r × r with singular values σ_r becomes a square matrix size based on rank. Since most energy modes are captured in initial singular values and remaining off diagonal values with lower impact in collection can be neglected, Consequently, truncating the smaller singular values leads to a reduction in the size of the diagonal matrix, effectively lowering the rank and reducing the dimensionality of the system while retaining the most significant features.

${V^T}_r \in \mathbb{R}^{rxn}$ contains the right singular vectors matrix of ${V^T}_r$ of shape of n × n, it plays a major role to project the reduced truncated matrix back to the original space and is aligned with the columns of the original matrix.

Truncated_snapshotmatrix_ X_r , provides an approximation of the original matrix on the low-rank space. Each component in the matrix decomposition has significant dimensionality reduction based on the rank r. The truncated left singular vectors and diagonal matrix $U_r\Sigma_r$, represent the transformation that projects data onto the low-rank subspace, with dimensions corresponding to the row of the original matrix. Truncated right singular vector ${V^T}_r$ correspond to the dimension of the column of the original matrix are used to reproject the low-rank space back onto the original space, reconstructing an approximation of the original matrix.

The coefficient matrix plays a crucial role in interpolation, as it is associated with right singular vectors and diagonal matrix. Coefficient matrix $\mathsf{C} \in \mathbb{R}^{rxn}$ contains parametric coefficients, reflexes the contribution of modes to the original data. It establishes the mapping between the input parameters and reduction model, leading to effective interpolation to predict solution for the unknown parameter values.

$$Coefficients_matrix = C = \Sigma_r{V^T}_r \quad (3)$$

For developing ROM, EZyRB [12], Pandas [13] and NumPy [14] Python-based libraries are used by converting to flattened data matrix to reduced order modeling. EZyRB: Easy Reduced Basis Method package divides the workflow into two sections. Section 1. Data generation and construction of data base based on the parameters and develop dimensional reduction using POD.

Section 2. Surrogate model construction on the parametric data using RBF interpolation for mapping between parameters and coefficients matrix for the fast and smooth approximation for the new parameters [15].

The following algorithm is used POD values extraction from the snapshot matrix and modes for visualization and followed by the truncation.

```
# pod
Rank = 5 # Retain 5 dominant modes
pod = POD (method='svd', rank=Rank)
pod.fit(snapshots_matrix)
reduced_snapshots          =          pod.
transform(snapshots_matrix)
#----------------------------------------
----------------------------
print     ("Singular     values:",     pod.
singular_values)
# Calculate the total variance
total     variance     =     np.sum     (pod.
singular_values**2)
# Calculate the explained variance for each
mode
Explained_variance          =          pod.
singular_values**2 / total_variance
# Calculate and print cumulative explained
variance
cumulative_variance          =          np.
cumsum(explained_variance)
print  ("Cumulative  Explained  Variance:",
cumulative_variance)
```

Extracting Singular values, Cumulative explained variance and explained variance along with additional POD shapes [16] and modes are vital for making decisions for the additional truncation required for retaining or removing additional modes.

The original shape of the matrix (10, 115740), with 10 parametric snapshots. The POD modes shape (10, 5) retains 5 significant modes. These modes are retained and projected back onto the original spatial points, resulting in a reduced snapshot of 5 modes over 115740 spatial points, resulting in a reduced snapshot that reconstructs modes on the original space.

TABLE 5 SINGULAR VALUES

Mode =5	Singular values	Explained variables per mode	Cumulative Explained Variance
1	2.23e+10	9.99e-01	0.99996171
2	1.37e+08	3.80e-05	0.99999977
3	7.05e+06	9.97e-08	0.99999987
4	5.94e+06	7.07e-08	0.99999994
5	5.50e+06	6.06e-08	1

From the above table, Mode1 has the higher singular values if 2.23e10 and explained variance 9.99e-01 the first mode almost captures the 99.9% of variance in the data, which become significant in capturing. Followed by the mode 2 singular value 1.37e+8 and explained variance 3.80e-5 very small remains some variance captured still not significant as mode l but remains explaining small fraction of variance. Mode 3 and beyond singular value continuous to decreases and minimal variance changes. cumulative explained variance shows the total percentage variance explained by the modes by 5 cumulative variances reached 1 says 100% variance are explained within 5 modes. Considering the adding modes beyond mode 5, occupies extra space still retain all the variance captured within mode 5.

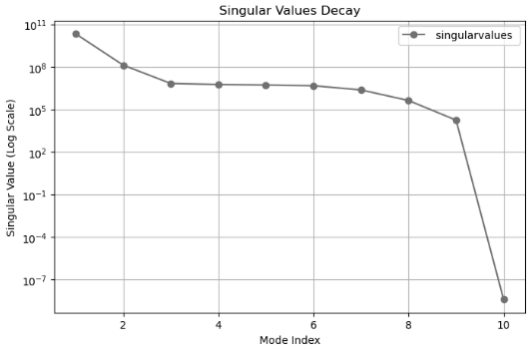

Fig. 2. Singular Values of the 10 snapshots.

From the above graph, we can see all 10 modes of the snapshot matrix dataset. After fifth mode, the singular values are decrease drastically, indicating their participation to capturing the variance is negligible.

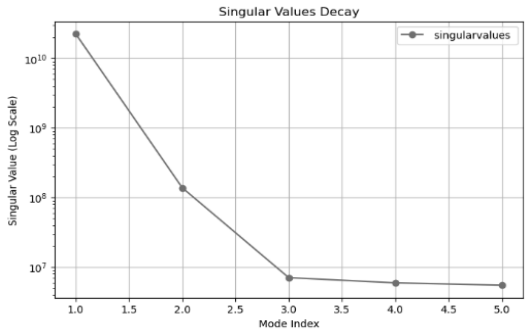

Fig. 3. Rank=5 Truncated Singular Values.

After mode 5 we can truncate for the data reduction this will justify truncation based on the singular values. Data storage capacity, the original data snapshot matrix required 8.83 MB storage capacity, ROM storage: 4.42 MB almost the half of the size and Storage Difference: 4.41 MB space is saved. This lightweight data set easy to handle and manipulation.

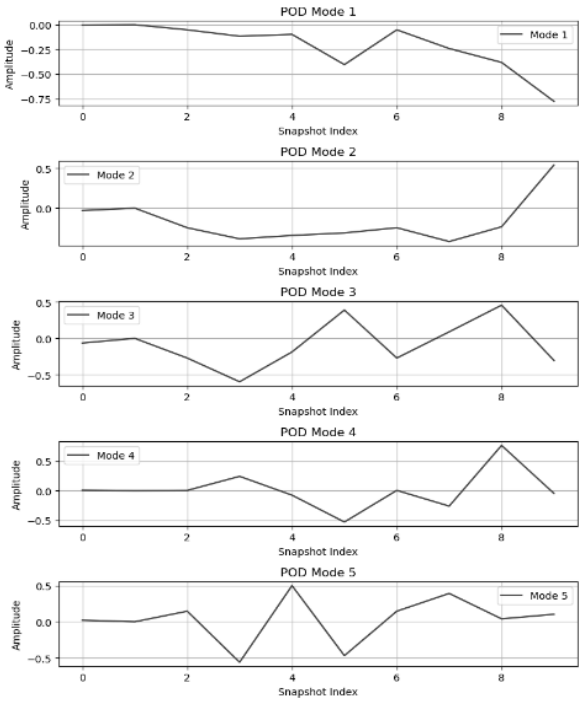

Fig. 4. POD Modes Rank = 5.

POD modes [17] represent the dominant features or spatial structure in the snapshot matrix, highlighting the most significant flow features. The x-axis represents the snapshot index, corresponding to 10 snapshots captured under various parameters. The y-axis value or amplitude, indicates the strong contribution of variance at different snapshots (spatial location or flow region) in the flow region. Amplitude of mode 1 exhibits smoothly and transitioning into negative value indicating an opposite influence this case high to low pressure in certain regions of the spatial domain.

Mode 2, amplitude start with 0 and moves towards positive value by the final snapshot index. This mode likely captures he spatial distribution of pressure or development of flow features over time. Modes 3 and 4 exhibit fluctuations, associated with transient effects or turbulent features which as smaller effects in the flow [18]. Higher-order modes primarily capture the small variation in the flow or secondary features. By truncation based on the amplitude avoiding the more oscillating amplitudes or focusing on dominant flow structure.

C. Interpolation

The EZyRB package enhances computational efficiency by incorporating the RBF [16] enabling rapid solution approximate for new parameters avoiding the need to compute full model simulation. This significantly reduces computational cost while maintaining accuracy. The following code demonstrates how to implement this approach:

```
from ezyrb import RBF
from ezyrb import Database
  rbf = RBF (kernel='gaussian', smooth=0,
                epsilon=1)
       rbf. Fit (parameters_matrix,
            reduced_snapshots)
         print (rbf. interpolator)
 new_parameters = np. array ([1232, 152]])
                # value
        newparameter_values = rbf.
          predict(new_parameters)
      print (predicted_values. shape)
    reshaped_values = predicted_values.
        flatten (). reshape (-1, 3)
```

RBF is commonly used for interpolation between known parameters using snapshot data points. The algorithm presented utilizes a Gaussian kernel [11], where the RBF compute's function values based on the distance from the center, ensuring smooth and accurate approximations.

$$\varphi(r) = e^{-\epsilon r^2} \quad (4)$$

where:
$r = \|x - c\|$ from the point x to center c
ϵ is a positive parameter that controls the width of the Gaussian function, ϵ =1 from the above code.

In the RBF framework, the center points represent the parametric locations where the solution matrix is constructed. POD is then applied to reduce data complexity. Each parameter corresponds to functional values, or snapshot data points, which depend on the parameter matrix, ensuring efficient representation of the system's behavior. RBF interpolation utilizes the snapshot data to construct a predictive model allowing for the estimation of functional values or generating new snapshots for unseen input parameters within the defined domain or parameter matrix range. The given new parameter values (1232, 152) for density and velocity of the water. After interpolation produces a new snapshot with a flattened shape of (1, 115740). This single row representation retains all the variables velocity in x, y direction and total pressure. The final step to recreate the spatial points for the visualization. Deflattening the data points, arrange the columns according to original data shape (38580, 6) and projecting onto the original nodes restore the visual representation of the ROM, closely approximates the original system.

These are comparative results between commercial software Ansys Fluent with the EZyRB package for the new parameters in terms of storage. The FOM from the Fluent took 482 MB of storage including mesh and solution data. The EZyRB based ROM model took 4.2MB of storage capacity.

1. Volume Occupation Difference (in MB)

$$\text{Difference} = \text{Full Model size} - \text{ROM Model size} = 482\ \text{MB} - 4.2\ \text{MB} = 477.8\ \text{MB}$$

2. Percentage occupation of ROM compared Full Model

$$\text{Percentage Occupation} = \left(\frac{ROM\ Model\ size}{Full\ Model\ size}\right) * 100 \quad (5)$$
$$= \left(\frac{4.2}{482}\right) * 100 \ = 0.87\%$$

ROM only occupies 0.87% of the FOM storage capacity. It reduced the storage capacity by approximately 99.13% to the FOM.

III. Results and Discussion

Reconstructed pressure for new parameters density 1232 kg/m^2 and velocity 152 m/s.

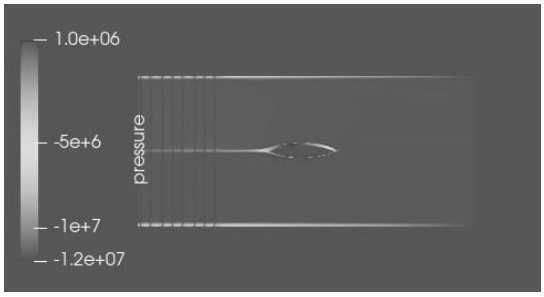

Fig. 5. Reconstructed Pressure Values in spatial points.

TABLE 6 PRESSURE VALUES

Max	Min
1.0e+06 Pa	-1.2e+7 Pa

Ansys Fluent FOM simulation for the new parameter's density 1232 kg/m^2 and velocity 152 m/s.

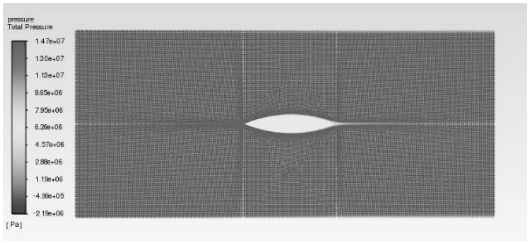

Fig. 6. FOM Simulation for the Pressure.

TABLE 7 PRESSURE VALUES

Max	Min
1.47e+07 Pa	-2.19e+6 Pa

Reconstructed model x-velocity direction

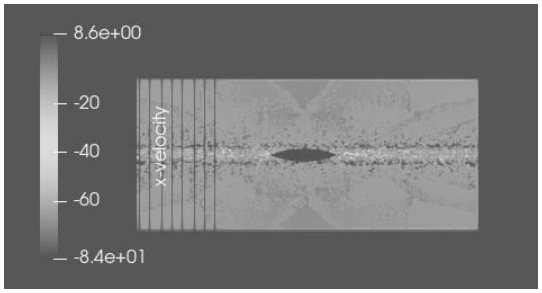

Fig. 7. Reconstructed x-velocity in spatial points.

TABLE 6 RECONSTRUCTED X-VELOCITY

Max	Min
1.47e+07 Pa	-2.19e+6 Pa

Ansys FOM simulation of the x-velocity direction

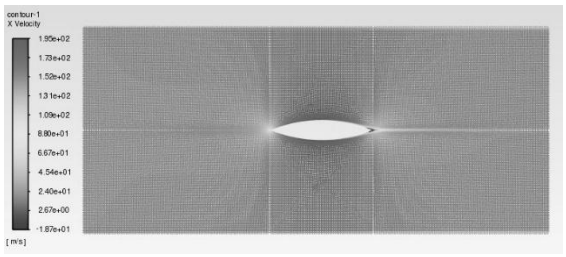

Fig. 8. FOM of x-velocity.

TABLE 7 FOM X-VELOCITY

Max	Min
1.47e+07 Pa	-2.19e+6 Pa

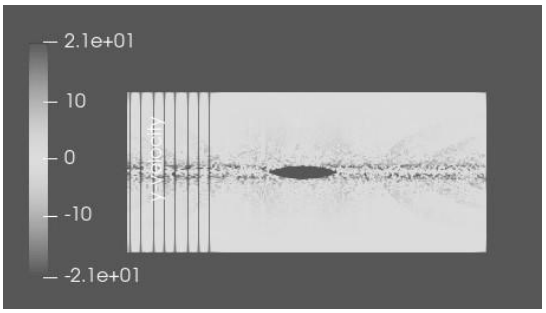

Fig. 9. Reconstructed Y- Velocity.

TABLE 8 RECONSTRUCTED Y-VELOCITY

Max	Min
1.47e+07 Pa	-2.19e+6 Pa

Ansys FOM simulation y velocity direction

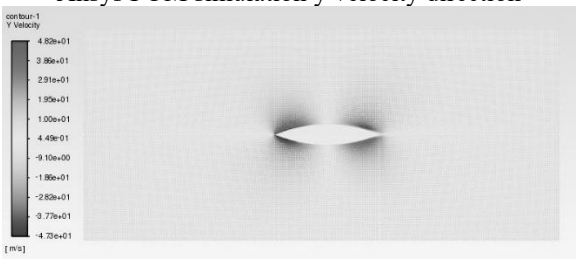

Fig. 10. FOM of Y- velocity.

TABLE 9 FOM Y-VELOCITY

Max	Min
1.47e+07 Pa	-2.19e+6 Pa

ROM captured the majority features and truncated small-scale fluctuations. In contrast, the FOM simulation

captures all the features, these changes significantly in the overall results. Reconstructed pressure has slightly deviated results compare to the FOM. Reconstructed pressure, x-velocity and y-velocity and compare with FOM, ROM, Pressure max value 1.0e+06 Pa and FOM 1.47e+07 Pa and the percentage difference is approximately 38.0%. ROM, velocities in x- direction has 8.6e+00 m/s and FOM 1.95e+02 m/s and the percentage difference is approximately 183.2%. y-direction 2.1e+01 m/s and FOM 4.82e+01 m/s and the percentage difference is approximately 78.6%, this effect demonstrates the truncation overall effective features are captured for preservation and perform multiple simulations with various parameters without going for FOM simulation other.

IV. COUNCLUSION

The Reduced Order Model (ROM) captures effectively the most dominant features while reducing the storage. Solution matrix occupied 8.83 MB storage capacity, but ROM took 4.42MB nearly half of its size. Percentage occupation of ROM compared Full Model is 0.87% of storage capacity. Reduction of the computational complexity with less storage capacity yet providing the approximate results without simulating FOM. ROM approach beneficial in applications required rapid evaluations, such as optimization and faster iterations. ROM can integrated with various machine learning techniques for predictive models making them a valuable tool for multidisciplinary optimization and digital twin applications. The presented approach enables the fastening the prediction of flow behavior using reduced models. We can extent this approach over the 3-dimensional data sets typically 3d simulations such as UAV design simulations, ventilation system and turbomachinery flow. By compressing high dimensional 3D spatial and flow field variables into lower dimensions space capturing the dominant features, enabling the interpolation can perform seamlessly and allow for reconstruct the parametric scenario on full scale and project original space. This reduces the time consumption unlike full order model and reduction in data volume. The reduced order model (ROM) enables faster iteration in optimization, system performance evaluation and decision making, become valuable tool for storage.

REFERENCES

[1] P. L. J. L. &. B. G. Holmes, Turbulence, Coherent Structures, Dynamical Systems and Symmetry., United Kingdom.: Cambridge University Press., 2012

[2] J. Reddy, An introduction to the finite element method, McGraw-Hill, 2006. T. Jordan and P. A. Taylor, Hacktivism and Cyberwars: Rebels with a cause? London: Routledge, 2004.

[3] S. L. &. K. J. N. Brunton, Data-Driven Science and Engineering: Machine Learning, Dynamical Systems, and Control., Cambridge, UK: Cambridge University Press., 2019.

[4] P. G. S. &. W. K. Benner, "A survey of projection-based model reduction methods for parametric dynamical systems," SIAM Review, vol. 57, no. 4, pp. 483-531, 2015.

[5] T. &. R. G. Taddei, "Model order reduction based on data: A survey of existing approaches and new. perspectives.," Advances in Computational Mathematics, vol. 3, no. 47, pp. 1-34, 2021.

[6] L. Sirovich, "Turbulence and the dynamics of coherent structures.," Quarterly of Applied Mathematics, vol. 3, no. 45, pp. 561-571, 1987.

[7] G. H. P. &. L. J. L. Berkooz, "The proper orthogonal decomposition in the analysis of turbulent flows.," Annual Review of Fluid Mechanics, vol. 25, pp. 539-575, 1993.

[8] J. &. B. P. Salmist, "EZyRB: A Python-based library for Reduced Order Modeling with Radial Basis Function Interpolation," Computational Mechanics, vol. 68, pp. 343-367., 2021.

[9] J. S. &. U. M. Hesthaven, Introduction to Reduced Order Modeling for Computational Fluid Dynamics., Society for Industrial and Applied Mathematics, 2016.

[10] K. &. D. S. Taira, "Data-driven methods for model reduction and flow analysis: Insights from EZyRB and other ROM techniques.," Journal of Fluid Mechanics, vol. 894, pp. 1-30., 2020.

[11] X. &. H. L. Ma, "Efficient interpolation methods for reduced order models using Radial Basis Functions," Computers & Fluids, vol. 186, pp. 123-132., 2019.

[12] J. N. K. Steven L. Brunton, Data Driven Science & Engineering., Washington : Brunton & Kutz, 2017.

[13] E. Contributors, "EZyRB Documentation," 1 april 2021. [Online]. Available: https://mathlab.github.io/EZyRB/. [Accessed 13 march 2025].

[14] T. P. D. Team, "Pandas Documentation," [Online]. Available: https://pandas.pydata.org/docs/user_guide/reshaping.html. [Accessed 13 March 2025].

[15] T. N. Developers, "NumPy Documentation," 14 october 2022. [Online]. Available: https://numpy.org/doc/. [Accessed 13 march 2025].

[16] M. T. a. G. R. Nicola Demo, "EZyRB: Easy Reduced Basis Method," The Journal of Open Source Software, vol. lll, no. 24, p. 662, 2018.

[17] S. Volkwein, Proper Orthogonal Decomposition: Theory and Reduced-Order Modelling, Konstanz: Lecture Note (August 27, 2013), 2013.

[18] P. M. L. R. T. Regert, "Investigation of the Link between Physics and POD Modes," RTO-MP-AVT-124, no. 4, pp. 11- 2, 2005.

Environment. Technology. Resources. Rezekne, Latvia
Proceedings of the 16th International Scientific and Practical Conference. 2025. Volume IV, 345-350

Trends in the Development of the Tractor and Combine Fleet in Latvia

Adolfs Rucins
Latvia University of Life Sciences and Technologies
Jelgava, Latvia
adolfs.rucins@lbtu.lv

Dainis Viesturs
Latvia University of Life Sciences and Technologies
Jelgava, Latvia
dainis.viesturs@lbtu.lv

***Abstract*— The article contains an analysis of the results of research of the development of the tractor and combine fleet in Latvia in 2014-2023. The age structure and technical condition of the tractor fleet have been determined. More than 100 thousand tractors and 9.5 thousand combines are registered in the country. More than 100 thousand tractors and 9.5 thousand combines are registered in Latvia. 32.2% of tractors are in good technical condition, 71% of tractors are over 30 years old, only 10.8% fall into the age group of up to 15 years, which is usually considered the depreciation period. Combine harvester fleet is in a similar technical condition. The current registration procedure of the tractor equipment - without excluding the obsolete and worn-out equipment from the register - does not provide an impartial impression of the technical condition of the tractor equipment fleet, the performance of the fleet and the energy supply to agriculture. During the period an average of 462 new tractors with a power exceeding 100 HP and 130 new harvesters were purchased annually. Using the available registry data about the capacity and year of registration of tractors and combines, the total capacity of the fleet by year was calculated. To ensure depreciation of the tractor equipment that has been in operation for more than 15 years, the calculated capacity has been reduced by 15%, but increased by 10%, which approximately corresponds to the area, cultivated by the equipment that is more than 15 years old. The calculated total capacity is compared with the cultivated area in the corresponding year. It has been established that during the period the total capacity of the tractor fleet has increased by 35%, and the sown area by 13%, so the increase in capacity significantly outpaces the increase in the sown area, which allows the work to be carried out in shorter agrotechnical terms. The capacity of the combine harvester fleet has also increased similarly. It is expected that the total capacity of the tractor equipment will continue to grow at a similar pace. Since the growth rate of the sown areas will decrease in the future, the issue of the amount of subsidies for the purchase of the new tractor equipment is debatable.**

Keywords*— *engine capacity, fleet of tractors and grain combine harvesters, sown area.

I. INTRODUCTION

The area of the agricultural and arable land in Latvia is increasing annually at the expense of recovery of the overgrown areas, and, consequently, the area sown with agricultural crops. Thus, in the period 2014-2023, the area of land, used for agriculture increased by 5.3%, while the sown area increased by 13.0%, and at the end of the period it was 1303.0 thousand ha. Of the sown areas of agricultural crops, the fastest growth is for cereals, rapeseed and legumes - during the mentioned period their total area increased by 33.3%, and in 2023 it was 1022.4 ha [1]. The production of several other types of crops is also growing. It is important that the crop production accounted for almost two-thirds (65.5%) of the total value of the final agricultural goods, produced in the country in 2022 [2]. Production is gradually concentrating on larger farms; in 2022 there were 580 farms in Latvia with a cereal and rapeseed sown areas of over 300 ha, an increase of 25% since 2014 [1]. Such intensification of production requires also an appropriate increase in the performance of the tractor and combine fleet as an important means of production. Many scientists have focused on research of the structure of the tractor and combine fleets, labour costs, performance, optimal operating modes, fuel consumption, and other characteristics. In a survey of farmers in the EU countries [3] it was found that in the period of time from 2014 to 2020 they would like to invest the largest amount of investments (40.3 %) into machinery, and of the total investment into machines, 39.2% into the purchase of tractors. The age structure of the tractor and combine fleet in Estonia, the operating and repair costs, depending on the age and brand of tractors, are discussed in studies [4] and [5]. The research of the fuel consumption, performance, and costs of the up-to-date combine harvesters has been conducted by the authors of [6] and [7], finding that the combine harvesters with higher capacity are more economically profitable. The authors of publication [8] in their turn, conducted experiments in 13 fields throughout Italy for four years, and then, by collecting and analysing

Online ISSN 2256-070X
https://doi.org/10.17770/etr2025vol4.8419
© 2025 The Author(s). Published by RTU PRESS.
This is an open access article under the Creative Commons Attribution 4.0 International License.

the extensive material, developed an innovative method for determining the operating costs of the machinery. The characteristics of the Polish farms and tractor fleet are presented in articles [9,10], where it is stated that in 2018 the average farm area was 9.8 ha and the average tractor power was 45.3 kW, and there are also shown changes in these indicators by region and year. The authors of study [11] have identified the most popular brands of tractors and combines in the Czech Republic, the age structure of the machine fleet; and they have also determined the cyclical nature of the number of machines, sold over the years. The efficiency of the combine depending on the harvested area during a three-year period is examined in the work [12]. The authors of [13], compiling data about 90 combines in Lithuania and Latvia, find that in 2016-2018 a combine harvester has worked, on average, only 219.4 ± 13.3 hours per year, using two-thirds of the time for direct work. The age structure of the Latvian tractor fleet, its technical condition, and the energy supply of farms of various sizes are discussed in publication [14].

Methods for determination of the operating and repair costs of tractors are analysed in publication [15]. A methodology for the calculation of the fuel, consumed by tractors in different load modes, is presented in study [16]. The working capabilities and performance of combine harvesters, depending on the type of crop being harvested and grain moisture in Danish conditions, were analysed in [17]. The number of days, suitable for harvesting cereals, changes in the grain moisture during the harvesting period, and harvesting costs depending on these parameters in the Stockholm region over a 30-year period, are analysed in a study [18]. It was found that the average moisture content of the harvested grain in August was 19%. In turn, the authors of [19] have developed a method how to determine the It was found that the average moisture content of grain, harvested in August, was 19%. In turn, the authors of [19] have developed a method how to determine the residual value of a used combine.

The studies reviewed are topical; however, they are addressed to issues, such as the prevalence of a specific type of machines, the performance of the age structures, the losses of grain, the fuel consumption, CO2 emissions, and other operational parameters. Yet these studies do not consider the issue of the performance and adequacy of the total tractor and combine fleet of a larger region or country for timely completion of the field work in a context with the increase in the sown area and production volume, mentioned at the beginning of the chapter. Therefore, it would be appropriate to assess whether the development of the tractor and combine fleet is adequate for timely completion of the increased volumes of the field work. This issue has been partly analysed by the author of study [11], finding that insufficient capacity of the combine fleet is by 50% more expensive than excess capacity. Several authors [14, 20] believe that the criterion for the assessment of the adequacy of the performance of a fleet of tractors and combines may be the ratio of the total power of the engines in their fleet to the cultivated area, or specific power kW ha^{-1}, but the increase in the total power of the fleet should outpace the increase in the sown area and harvested area, respectively. To determine these indicators, it is necessary to find out the capacity of each registered tractor and combine harvester, the age structure of their fleet, technical condition, the most common brands, as well as the sown area and the harvested area in each year of the period.

The aim of this study is to determine the dynamics of the growth of the total and specific capacity of the tractor and combine fleet over a ten-year period and, in comparison with the dynamics of the growth of the sown area and the harvested area, to assess the adequacy of the total capacity of the fleet for timely processing of these areas.

By analysis of the obtained data one can predict a possibility of timely completion of work and the need for renewal of the technical fleet.

II. MATERIALS AND METHODS

Intensive modernization of the machine fleet started after Latvia joined the EU in 2004. Due to the availability of structural funds, the purchase of modern tractors and combine harvesters increased essentially. The trade in machines, manufactured in the Commonwealth of Independent States (CIS), had practically ceased at the beginning of the 2000s, with the exception of the Belarus tractors, manufactured in Belarus and certified in accordance with the EU requirements, which were sold in Latvia until 2022. The purchase of new tractors by year is shown in Table 1. As it is evident, 4,617 new tractors have been purchased over the past ten years, or an average of almost 462 new tractors per year. In the table there are compiled data only of tractors with a power of over 100 HP because the tractors with a lower power of the companies, shown in the table, are practically not purchased for agriculture (except for Belarus), and, in addition, on the farms producing goods, tractors with a lower power are used only for auxiliary work.

TABLE 1 PURCHASE OF NEW TRACTORS DURING A TEN-YEAR PERIOD

Brand of the tractor	2014	2015	2016	2017	2018	2019	2020	2021	2022	2023	Total
John Deere	28	57	105	113	91	70	62	74	110	83	793
Valtra	41	51	62	78	84	83	64	71	112	96	742
Claas	14	33	41	61	89	84	86	117	111	102	738
Belarus	91	70	69	78	89	88	19	24	3	-	531
New Holland	53	21	20	81	67	48	55	47	64	69	525
Case IH	13	20	31	42	50	39	40	50	49	51	385
Fendt	6	18	23	28	36	18	30	26	51	36	272
Massey Ferguson	11	28	30	36	29	37	34	16	34	16	271
Deutz-Fahr	4	14	16	33	39	27	31	27	22	16	229

Brand of the tractor	2014	2015	2016	2017	2018	2019	2020	2021	2022	2023	Total
Others over 100 hp	5	4	7	11	11	18	17	14	18	25	132
Total	266	316	404	561	585	512	438	466	574	494	4617

As evident, the most popular tractors, manufactured in the EU countries, are John Deere, Valtra and Claas, which account for approximately half of the total number purchased. Meanwhile, the purchase of new combines by year is shown in Table 2.

TABLE 2 PURCHASE OF NEW COMBINES DURING A TEN-YEAR PERIOD

Brand of the combine	2014	2015	2016	2017	2018	2019	2020	2021	2022	2023	Total
Claas	71	26	34	46	55	58	29	47	61	64	491
New Holland	33	45	28	41	46	31	25	26	60	41	376
John Deere	10	23	13	26	28	17	9	6	20	22	174
Case IH	8	1	5	6	14	6	8	5	23	10	86
Fendt	-	1	2	5	6	4	1	1	5	4	29
Deutz-Fahr	-	1	2	9	6	3	2	1	2	1	27
Massey Ferguson			1	3	4	5	3	1	-	1	18
Others	7	8	4	6	7	12	10	13	5	2	84
Total	129	104	89	142	166	136	87	100	176	145	1285

As it is evident, 1285 new combines would be purchased during ten years, or, an average, 130 per year, of which 88% are from four brands – Claas, New Holland, John Deere, and Case IH. Tractor machinery purchases by year depend mainly on the amount of subsidies granted.

In the register of the State Technical Supervision Agency (STSA) [21], data can be found on the registration of tractors and combines by year, technical condition in the relevant year, number of vehicles purchased each year, make, model and engine power. By processing these data with statistical methods the age structure and technical condition of this fleet of vehicles have been determined. Using the data from the STSA register and Tables 1 and 2, the total capacity of all the new tractors and combine harvesters of the same brand were initially calculated by year, then, by summing the capacity of all the brands, the total capacity of the tractor and combine fleet in the relevant year.Similar calculations were made for the used equipment, purchased in the relevant years. It is assumem in the calculations that the depreciation period of this equipment is 15 years and that all he tractors, purchased since 2014, are in operation. The total capacity of the fleet has been reduced by 7.5% to allow for replacement (depreciation) of worn-out equipment, and increased by 10%, which could roughly characterize the performance of a large number (approximately 77000) of aging equipment manufactured in the CIS countries, which is over 30 years old, ion the register. In order to be able to carry out the field work in a timely manner, the increase in the total power of tractors should outpace the increase in sown areas, and the increase in the total power of combine harvesters should outpace the increase in the area to be harvested.

Data about the sown area and the harvested area can be obtained from statistical reports [1]. An anticipated increase in total capacity, compared to the area to be processed, means the possibility of shortening the work period [22]. In turn, by relating the total capacity of the fleet to the area to be processed, the specific capacity of the machine fleet is obtained. As mentioned, several authors [14, 20] propose using specific capacity as a criterion for the assessmen of the sufficiency of a fleet's performance. By analysis of the obtained data one can judge about the sufficiency of the pace of renewal of the machine fleet.

III. RESULTS AND DISCUSSION

The total number of registered tractors and combine harvesters is increasing every year, as an average of 460 new tractors and 128 combines were purchased every year; but the existing registration procedure also allows for a large number of worn-out units of equipment to be in the register; this procedure does not impose any obligations or liabilities on the owner. According to STSA data [21] at the end of 2023 there were registered 103,706 tractors and 9,573 combines.

The distribution of the registered tractors by age group is shown in Figure 1, while that of combines is shown in Figure 2.

As obvious from Figures 1 and 2, 67 - 71% of the equipment is older than 30 years, the majority in this age group are obsolete MTZ, T-40, T-25 and similar low-power brnds of tractors and SK-5, Yenisei and Don combine harvesters, manufactured before 1994. The performance of these machines is negligible, some of them are used on small homestead farms or on larger farms for auxiliary work. The performance of this group and other tractors and combines with high wear and tear has been calculated using a methodologically based 10% increase in the total power. The age group up to 15 years, which is most often assumed to be the depreciation period of the

machinery, includes 10.8% or 11,200 tractors and 20.1% or 1,925 combines. Taking into account the sown area [1], the area to be cultivated by one tractor in the age group up to 15 years in 2023 was 116.5 ha, while the area to be harvested by one combine harvester of this group was 530 ha. The equipment of this group in a set of up-to-date inventory, ensures the production of the greatest part of goods. The existing registration procedure – without excluding the obsolete equipment from the register – does not provide an objective picture of agricultural energy supply and makes it difficult to compare the characteristics of the Latvian machinery fleet with the data from Estonia, Poland, the Czech Republic [5], [10], [11], and other countries.

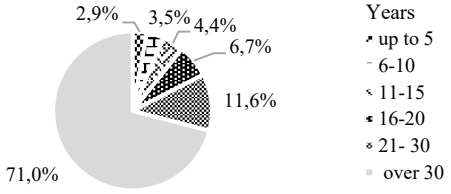

Fig. 1. Distribution of registered tractors by age groups.

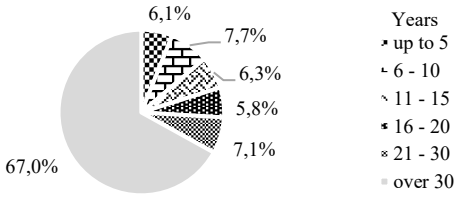

Fig. 2. Distribution of registered combine harvesters by age groups.

As a result of the current registration procedure, the number of tractors has already exceeded 100 thousand. As a result, the average age of the fleet is increasing and the technical condition is deteriorating, creating a false impression about the energy security of agricultural. In 2023 there were 32.2% of registered tractors in technical order, including 90.6% in the age group 1–5 years, and 18.9% in the age group over 30 years. A similar situation is with combines - in 2023, 36.9% were in good technical condition, including 95.3% in the age group 1 - 5 years, but 15.5% - in the age group over 30 years. These indicators have not changed significantly over the past ten years. An average of 32.2 – 36.9% of tractors and combines in good technical condition for the age group distribution, shown in Figures 1 and 2, are considered as a good indicator.

Along with the age structure and technical condition of the fleet, the performance of the fleet is characterized by the total power of its engines. In accordance with the methodology this indicator should be viewed together with the area sown with agricultural crops in the corresponding year. Changes in the total capacity of the tractor fleet, the area sown with agricultural crops, and the specific capacity over a ten-year period are shown in Figure 3.

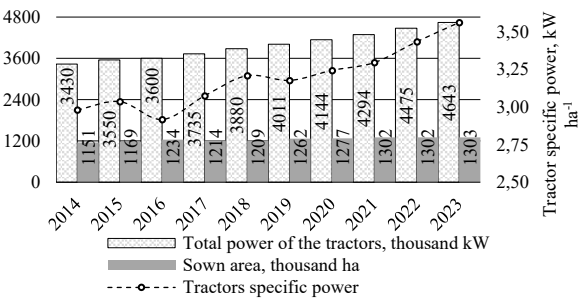

Fig. 3. Changes in the total capacity, specific capacity and sown area of agricultural crops of the tractor fleet in 2014-2023.

The sown area increased by 13% during the period, and at the end of the period it was 1,303 thousand ha, while the total capacity of the tractor fleet increased by 35%. This can be explained by the relatively intensive purchase of new tractors during the period (an average of 462 per year) and the increase in the average power of the purchased tractors. An anticipated increase in the total capacity, compared to the increase in the sown areas, allows the work to be completed in shorter agrotechnical terms, which is important under increasingly extreme climatic conditions. Several authors [14], [20] use specific power as an indicator, characterizing the energy supply of agriculture, which is obtained by dividing the total power of the tractor fleet by the area, sown with agricultural crops in the corresponding year. This indicator has increased from 3.0 to 3.6 kW ha^{-1} during the period (see Fig. 2). The indicator is relatively high, as a previous study [14] found that in Latvia, depending on the size of the farm, it is 1.3 - 4.1 kW ha^{-1}. It decreases as the farm area increases, as the equipment is used more intensively on larger farms. In turn, the authors of article [20] points out that in the European countries this indicator, depending on the size of the farm, is 1.1 - 8.1 kW ha^{-1}. High energy supply allows for shorter deadlines of work but, at the same time, it increases the cost of the product.

But Figure 4 reflects changes in the total capacity, harvested area and total yield of the combine fleet over a ten-year period. As one can see, the harvested area increased by 35% during the period, and at the end of the period it was 1022 thousand ha, while the total capacity of the fleet of combine harvesters ncreased by 70%. Such an increase can be explained by increased purchase of new combines during the period, as well as by the increase in the average capacity of a new combine from 355 kW ha^{-1} at the beginning of the period to 410 kW ha^{-1} at the end. Taking into account the development trends in he combine production [23], it is expected that the increase in capacity will continue. However, the performance of the combine harvesters is also affected by the increase in the total harvest, which increased by approximately 1.2 times at the end of the period, compared to the beginning. The impact of the agrobiological characteristics of cereals upon the performance of the combine harvesters has been discussed in several articles [24], [25]. Using the results of study [25], it can be roughly estimated that a 20% increase in the

total yield reduces the combine performance by 7-8%, i.e., the previously calculated total capacity as a performance criterion at the end of the period should be reduced by 7.5%. After adjustment the total capacity in 2023 was 825.1 thousand kW, an increase of 1.70 times, compared to 2014, which also exceeds the increase in the harvested areas, which increased 1.35 times during this period.

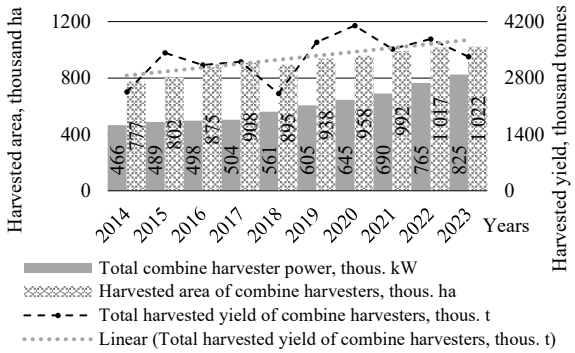

Fig. 4. Changes in the total capacity, harvested area and total yield of the fleet of combines in 2014-2023.

When evaluating these results together with publication [14], which examines the development of the fleet of tractors since 2007, one can conclude that the growth rates of the sown areas are gradually decreasing but the growth rates of the capacity of the total fleet of tractor and combines are increasing. In its turn, the trend, identified in publication [3] – to invest intensively in the purchase of new tractors – indicates that the growth in the total capacity of the tractor fleet will continue. The authors of publication [23] state that the engine power of the new combine harvesters will continue to increase, and thus the total power of the combine harvester fleet will also increase. However, the amount of the land used for agriculture is not increasing, so the intensity of the increase in the arable land will continue to decrease, as its use is limited by the requirements of several EU directives, in addition to the local conditions. Therefore there is no ground for intensive increase in the performance or total capacity of the fleet of tractors and combine harvesters, as it has occurred before; this process can be regulated by the amount of subsidies for the purchase of the aforementioned equipment.

IV. CONCLUSIONS

The age group up to 15 years includes 10.8% of tractors and 20.1% of combines, 78.9 and 83.8% of them are in technical condition, respectively. The equipment of this group, complete with modern inventory, ensures the production of the majority of goods.

The existing procedure of registration of the tractor equipment –without excluding the obsolete and worn-out tractors and combines from the register – does not provide an impartial picture of the technical condition of the fleet, its performance and the energy supply of agriculture.

The anticipated increase in the total capacity of the tractor equipment fleet, compared to the increase in the sown area, increases its performance, compensates for the increase in the sown area and total harvest, and allows work to be completed in shorter agrotechnical terms.

Since the total capacity of the tractor equipment fleet is expected to increase at approximately the same pace as before but the growth rate of the sown areas will decrease, there is debatable the issue of the amount of subsidies for the purchase of new tractors and combines.

REFERENCES

[1] LR Centrālā statistikas biroja materiāli 2014...2023. g. (Materials of the Central Statistic Bureau of Latvia 2014…2023). (In Latvian). Available at: https://data.stat.gov.lv/pxweb/lv/OSP_PUB/ [Accessed March 19, 2025]

[2] Latvian agriculture 2022. Annual report of the Ministry of Agriculture, 2023 5-6 pp. (Latvijas lauksaimniecība 2022. Zemkopības ministrijas gada ziņojums). (In Latvian). Available at: https://www.zm.gov.lv/lv/media/12006/download?attachment [Accessed March 19, 2025]

[3] M. Lefebvre, K. De Cuyper et. al. European Farmers Intentions to Invest in 2014-2020: Survey Results. JRC90441, JRC Working Papers, 2014. Joint Research Centre,100. Available at: https://publications.jrc.ec.europa.eu/repository/handle/JRC90441 [Accessed March 19, 2025]

[4] J. Olt, U. Traat. The maintenance costs of Estonian tractor-fleet. Proceedings of 10th International Conference "Engineering for Rural Development", Latvia, Jelgava, University of Agriculture, 2011, pp. 196-200. Available at: https://www.iitf.lbtu.lv/conference/proceedings2011/Papers/036_Traat.pdf [Accessed March 19, 2025]

[5] J. Olt, R. Ilves, A. Kuut Overview of developments of cereal harvester fleet in Estonia. Proceedings 18th International Conference "Engineering for Rural Development", Latvia, Jelgava, University of Agriculture, 2019, pp. 179-184. https://www.iitf.lbtu.lv/conference/proceedings2019/Papers/N230.pdf [Accessed March 19, 2025] DOI:10.22616/ERDev2019.18.N230

[6] J. Masek, P. Novak, T. Pavlicek Evaluation of combine harvester fuel consumption and operation costs. Proceedings of 14th International Conference "Engineering for Rural Development", Latvia, Jelgava, University of Agriculture, 2015, pp. 78- 83. https://www.iitf.lbtu.lv/conference/proceedings2015/Papers/013_Masek.pdf https://doi.org/10.17221/98/2017-RAE [Accessed March 19, 2025]

[7] L. Benes, P. Novak et. al. John Deere combine harvesters fuel consumption and operation costs. Proceedings of 13th International Conference "Engineering for Rural Development", Latvia, Jelgava, University of Agriculture, 2014, pp. 13-17. https://www.iitf.lbtu.lv/conference/proceedings2014/Papers/02_Benes_L.pdf [Accessed March 19, 2025]

[8] M. Guerrieri, M. Fedrizzi et.al. An innovative multivariate tool for fuel consumption and costs estimation of agricultural operations. Spanish Journal of Agricultural Research 14(4), e0209, 11 ges (2016) eISSN: 2171-9292. http://dx.doi.org/10.5424/sjar/2016144-9490 [Accessed March 19, 2025]

[9] J. Barwicki, S. Gach, S. Ivanovs Proper utilization of soil structure for crops today and conservation for future generations. Proceedings of 11th International Conference "Engineering for Rural Development", Latvia, Jelgava, University of Agriculture, 2012, pp. 10-15. https://www.iitf.lbtu.lv/conference/proceedings2012/Papers/001_Barwicki_J.pdf [Accessed March 19, 2025]

[10] E. Lorencowicz, J. Uziak. Regional structure of tractor market in Poland. Agricultural Engineering 2020, vol. 24 No. 3 pp. 51-62. ISSN 2 0 8 3 -1 5 8 7; DOI: 10.1515/agriceng-2020-0026

[11] J. Masek, P. Novak. Overview of combine harvester and tractor structure on farms in the Czech Republic. Proceedings of 17th International Conference "Engineering for Rural Development", Latvia, Jelgava, University of Agriculture, 2018, pp. 240 - 245. DOI: 10.22616/ERDev2018.17.N282

[12] M. Pristavka, K. Krištof, P. Findura. Reliability monitoring of grain harvester. Agronomy Research, vol. 15 (3), 2017, pp. 817-829. (PDF) Reliability monitoring of grain harvester [Accessed March 19, 2025]

[13] D. Savickas, D. Steponavičius et. al. Combine harvester fuel consumption and air pollution reduction. Water Air Soil Pollution (2020) 231: 95. https://doi.org/10.1007/s11270-020-4466-5 [Accessed March 19, 2025]

[14] N. Kopiks, D. Viesturs, V. Valainis The Fleet of Tractors on the Farms of Latvia, Its Structure and Energy Intensity. Proceedings of 14th International Scientific Conference "Engineering for Rural Development", Jelgava, 2015, pp.84-87. https://www.iitf.lbtu.lv/conference/proceedings2015/Papers/014_Kopiks.pdf [Accessed March 19, 2025]

[15] I. Galiev, C. Khafizov et al., Optimization of tractor operation level. Proceedings of 20th International Conference "Engineering for Rural Development", Latvia, Jelgava, University of Agriculture, 2021, pp. 38-42. International Scientific Conference Engineering for Rural Development 2021 [Accessed March 19, 2025]

[16] R.D. Grisso, M. Kocher, D. Vaughan. Predicting tractor fuel consumption. Applied Engineering in Agriculture. 20(5), 2004, 553-561. (doi: 10.13031/2013.17455) (PDF) Predicting Tractor Fuel Consumption [Accessed March 19, 2025]

[17] C. G. Sørensen. Workability and Machinery Sizing for Combine Harvesting. Agricultural Engineering International: The CIGR e-journal September 2003, pp. 1-19. https://www.researchgate.net/publication/280316072 [Accessed March 19, 2025]

[18] A. de Toro, C. Gunnarsson et.al. Cereal harvesting – strategies and costs under variable weather conditions. Biosystems Engineering, Volume 111, Issue 4, April 2012, pp. 429-439. https://doi.org/10.1016/j.biosystemseng.2012.01.010 [Accessed March 19, 2025]

[19] I. Herranz-Matey, L. Ruiz-Garcia Agricultural Combine Remaining Value Forecasting Methodology and Model (and Derived Tool). Agriculture 2023, 13, 894. https://doi.org/10.3390/agriculture13040894 [Accessed March 19, 2025]

[20] J. Pawlak, G. Pelizzi, M. Fiala On the Development of Agricultural Mechanization to Ensure a Long-Term World Food Supply. Agriculture Engineering International: the CIGR Journal of Scientific Research and Development. Invited Overview Paper. Vol. IV. June, 2002, pp. 1- 21. (PDF) On the development of agricultural mechanization to ensure a long-term world food supply [Accessed March 19, 2025]

[21] Valsts Tehniskās uzraudzības aģentūra (VTUA) State Technical Supervision Agency (STSA) Database: Registration data of agricultural machinery in the Republic of Latvia. (In Latvian). Available at: https://data.gov.lv/dati/lv/dataset/traktortehnikas-registracijas-dati-latvijas-republika [Accessed March 19, 2025]

[22] A. Rucins., D. Viesturs Trends in development of grain combine harvester fleet in Latvia. Proceedings of 23th International Conference "Engineering for Rural Development", Latvia, Jelgava, University of Agriculture, 2024, pp. 149-154. DOI: 10.22616/ERDev.2024.23.TF033 https://www.iitf.lbtu.lv/conference/proceedings2024/Papers/TF033.pdf [Accessed March 19, 2025]

[23] Trends in threshing crop harvesting process technology: 'combine harvesters – increased power density and work quality. - October 12, 2023, (DLG). At Agritechnica 2023. Available at: https://www.agritechnika.com [Accessed March 19, 2025]

[24] L. Špokas, V. Adamčuk et al. The experimental research of combine harvesters. Research in Agricultural Engineering, Vol. 62, 2016 (3): 106–112. doi: 10.17221/16/2015-RAE The experimental research of combine harvesters [Accessed March 19, 2025]

[25] I M. Kuzmich, I L. Rogovskii et. al. Research of passage capacity of combine harvesters depending on agrobiological state of bread mass. AGRITECH- IV-20 IOP Conf. Series: Earth and Environmental Science 677 (2021) 052002. DOI:10.1088/1755-1315/677/5/052002 Research of passage capacity of combine harvesters depending on agrobiological state of bread mass - IOPscience [Accessed March 19, 2025]

Environment. Technology. Resources. Rezekne, Latvia
Proceedings of the 16th International Scientific and Practical Conference. 2025. Volume IV, 351-356

Investigation of the Influence of Parameters in 3D Printing of Nylon CF15 Carbon on Linear Strain During Tensile Creep

Sabi Sabev
Technical University of Sofia,
Branch Plovdiv, Bulgaria
sabi_sabev@tu-plovdiv.bg

Valeri Bakardzhiev
Technical University of Sofia,
Branch Plovdiv, Bulgaria
bakardzhiev@tu-plovdiv.bg

Konstantin Chukalov
Technical University of Sofia,
Branch Plovdiv, Bulgaria
chukalov@tu-plovdiv.bg

***Abstract*—The aim of this article is to investigate influence of 3 printing parameters on linear strain during tensile creep at a constant temperature of 40° on Nylon Carbon samples. To refine the experimental results, a planned experiment was carried out with variables - printing temperature, filament thickness and printing speed. 20 standardized samples were produced with different printing parameters. The experimental results were processed using statistical processing software in order to obtain a regression mathematical model describing relationship between 3d printing parameters and tensile creep. The tests were performed using a dead load of 50 kg for a period of 2 hours. The equipment used for the purposes of the article is calibrated with a high accuracy. The test conditions defined in the ASTM D6992 standard in terms of atmospheric conditions and humidity were met.**

Keywords—mechanical properties, optimization, 3D printing, regression analysis, tensile creep, nylon carbon.

I. Introduction

Creep is a process of slow increase under the action of a load, it is characteristic of many materials - metals, plastics, ceramics, glasses, etc [1]. Creep testing aims to analyze the behavior of materials at high temperature under the action of significant mechanical stresses below the yield strength. There is tensile creep, compressive creep, and flexural creep [2]. The purpose of creep tests is to determine the deformation under certain atmospheric conditions and to prevent destruction. Most often, the test is performed at a constant temperature[3]. There are many standards for creep of materials such as ASTM E139, ASTM D2290, ASTM D2291, and ASTM D2294, etc. Creep is a process that is not fully scientifically understood. Unlike metals, plastics are prone to creep at low temperatures[4]. That is why creep resistance is a key characteristic for plastics. The rate of deformation increases at higher temperatures and higher static loads. When the load is removed,dimensions of samples are not restored[5]. When the plastic deformation limit is exceeded, failure occurs. The use of more and more plastics as structural elements also increases the need to study creep resistance.

II. Materials and Methods

Nylon CF15 carbon is characterized by high strength, stiffness, thermal and chemical resistance. It is recommended for structures that are frequently loaded[6]. This material contains carbon fibers with a length of 100 µm in order to improve mechanical properties. Nylon CF 15 carbon is not recommended for the food and medical industry. The material is used as a structural material for bearings, reinforced parts, gears, etc[7].

20 samples were printed according to a preliminary plan drawn up in Minitab using the cental composition design, fig.1[8]. The printing parameters and data are:

- Material Nylon CF15 Carbon
- 3d printing speed: 100 - 600mm/s
- Extruding temperature: 235 -265ºC
- Bed temperature: 105ºC
- Layer height: 0,15 – 0,4mm
- Infill: 100%
- Printing time :13- 16 minutes

The samples are manufactured using a 3d printer Adventurer 5M Pro.

Online ISSN 2256-070X
https://doi.org/10.17770/etr2025vol4.8407
© 2025 The Author(s). Published by RTU PRESS.
This is an open access article under the Creative Commons Attribution 4.0 International License.

Fig. 1. Manufactured spicemens.

The test was performed on a calibrated laboratory stand for creep of plastics. During the test, all requirements according to the ASTM D6992 standard regarding atmospheric conditions, humidity, preparation of the samples before the test were met. In all tests, the condition was met that the actual temperature was within ±1° degree of the set temperature. The laboratory stand is double-sloted and allows testing of 2 samples simultaneously. The samples have technological holes for hanging, a sample ready for testing is shown in Fig. 2

Fig. 2. Installment of a sample.

The jaws are matched to the material being tested to prevent slippage during the experiments. Standardized tensile creep test specimens according to ASTM D 638 were used,the selected thickness is 6mm,fig.3[9].

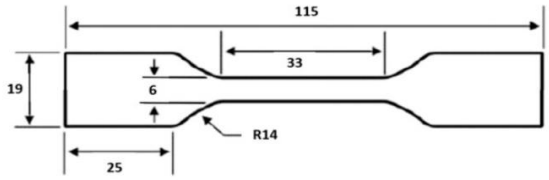

Fig. 3. Dimensions of tensile creep specimens

The mechanical gripping system is technically stable and does not allow the specimen displacements,fig.4

Fig. 4. Gripping testing samples.

After each test, the archived data is checked for sudden large elongations that would compromise the test results. The selected test parameters are static load-50 kg, constant temperature 40°, test duration 120 minutes. The complete set of the stand is shown in Fig.5.

Fig. 5. Used tensile creep stand.

III. RESULTS AND DISCUSSION

Table 1 presents the results of the translated experiments with 20 printed samples.

TABLE 1 TEST RESULTS

№	Deformation [mm]	Temteratute [ºC]	Speed [mm/s]	Layer [mm]
i	Y	X_1	X_2	X_3
1	2,43	241	201	0,20
2	2,33	259	201	0,20
3	2,44	241	499	0,20
4	1,78	259	499	0,20
5	1,42	241	201	0,35
6	1,60	259	201	0,35
7	1,58	241	499	0,35
8	1,26	259	499	0,35
9	2,44	235	350	0,28
10	1,70	265	350	0,28
11	1,38	250	100	0,28
12	1,56	250	600	0,28
13	2,14	250	350	0,15
14	2,12	250	350	0,40
15	2,70	250	350	0,28
16	1,78	250	350	0,28
17	1,90	250	350	0,28
18	1,98	250	350	0,28
19	1,76	250	350	0,28
20	1,98	250	350	0,28

From the measured values shown in Table 1, using Minitab we determine the following parameters[10]:

Range -in which the sample values vary:

$$R = Xi_{max} - Xi_{min} = 1.44 \quad (1)$$

The standard deviation provides information about the deviation of the values in the sample from the arithmetic mean[11]:

$$S = \sqrt{\frac{\sum(X_i - \bar{X})^2}{n-1}} = 0{,}4 \quad (2)$$

The coefficient of variation expresses the dispersion in percentages[12]:

$$V = \frac{S}{\bar{X}} \cdot 100 = 21{,}14\% \quad (3)$$

From the obtained value of the coefficient of variation, we can say that the sample is relatively homogeneous.

The asymmetry coefficient can be represented by the following equation:

$$A_s = \frac{m_3}{S^3} = 0{,}29 \quad (4)$$

Where:

S- standard deviation;

m_3- third central moment

$$m_3 = \frac{\sum(X_i - \bar{X})^3}{n} \quad (5)$$

The coefficient of kurtosis is determined by the equation:

$$E_x = \frac{m_4}{S^4} - 3 = -0{,}3 \quad (6)$$

Where:

m_4- fourth central moment

$$m_4 = \frac{\sum(X_i - \bar{X})^4}{n} \quad (7)$$

The kurtosis result is Ex = -0,3

Although the above conclusions have been made, a regression multivariate statistical analysis should be performed to determine how factors in this case, printing temperature, layer height, and printing speed, affect material creep[13],[14].

Linear in form multiple regression models can be estimated using full models in which all factors are included[15]. General regression equation is:

$$Y = b_0 + b_1X_1 + b_2X_2 + b_3X_3 + \varepsilon \quad (8)$$

Multiple linear regression analysis was performed in Minitab; the results are presented in Table 2.

TABLE 2 SUMMARY OF OBTAINED REGRESSION ANALYZE

Term	Coef	SE Coef	95% CI	T-Value	P-Value	VIF
Layer	-2,66	1,50	(-5,83; 0,51)	-1,77	0,094	20,79
Speed	-0,000063	0,000752	(-0,001651; 0,001524)	-0,08	0,934	9,06
Temp.	0,01065	0,00198	(0,00646; 0,01483)	5,37	0,000	28,57

The interval estimates of the parameters at 95% guaranteed probability are calculated as follow below:

$$\begin{gathered} -5{,}83 \le b_0 \le 0 \\ -0{,}001651 \le b_1 \le 0 \\ 0{,}00646 \le b_2 \le 0{,}01483 \end{gathered} \quad (9)$$

To determine which coefficient is statistically significant, the value in the P-value field is taken. If P-value ≤ α, the null hypothesis is rejected and the coefficient is statistically significant[16].

If P-value ≥ α, the null hypothesis is accepted and the corresponding coefficient is statistically insignificant. Table 3 shows that only the coefficient b2 is statistically insignificant.

TABLE 3 MODEL SUMMARY

S	R-sq	R-sq(adj)	PRESS	R-sq(pred)	AICc	BIC
0,41	96,17%	95,50%	4,09615	94,64%	28,97	30,29

TABLE 4 CORRELATIONS

	DEF	Temp.	Speed
Temp.	-0,329		
Speed	-0,064	0,000	
Layer	-0,483	0,000	-0,000

Table 4 shows the results of the correlation analysis to assess the relationships between factor and the variable[17].It may be concluded that the relationship between the layer height and creep of the material is significant. The relationship between the printing temperature and creep of the material is moderate. However, the relationship between the printing speed and the creep of the material is insignificant. Table 3 shows the coefficient of determination R-sq of the model. From it, we can conclude that 96.17% of the values of the printing temperature, printing speed and layer height directly affect the creep of the specimen.

TABLE 5 ANALYSIS OF VARIANCE

Source	DF	Seq SS	Contri-bution	Adj SS	Seq MS	F-Value	P-Value
Regression	3	73,4539	96,17%	73,4539	24,4846	142,32	0,000
Layer	1	66,7431	87,38%	0,5401	66,7431	387,95	0,000
Speed	1	1,7481	2,29%	0,0012	1,7481	10,16	0,005
Tem	1	4,9627	6,50%	4,9627	4,9627	28,85	0,000
Error	17	2,9247	3,83%	2,9247	0,1720		
Lack-of-Fit	12	2,3196	3,04%	2,3196	0,1933	1,60	0,317
Pure Error	5	0,6051	0,79%	0,6051	0,1210		
Total	20	76,3786	100,00%				

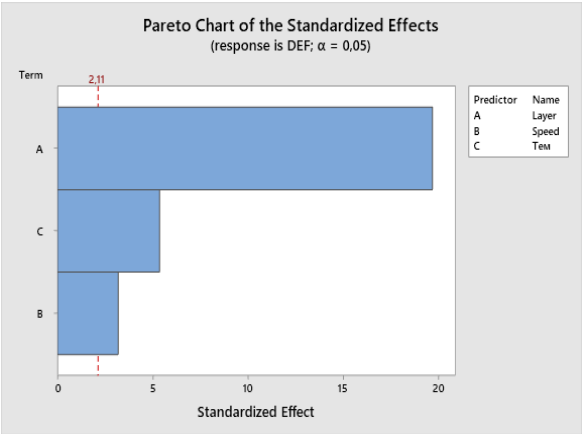

Fig. 6. Pareto chart of the standartized effects

Table 5 shows the influence of each of the factors on the variable, as we can conclude from the above conclusions, the layer height has the strongest influence with approximately 87.38% of the factor values, the second most influential is the printing temperature with 6.50% of the factor values, and the printing speed has a negligible influence with 2.29% of the factor values,fig.6.

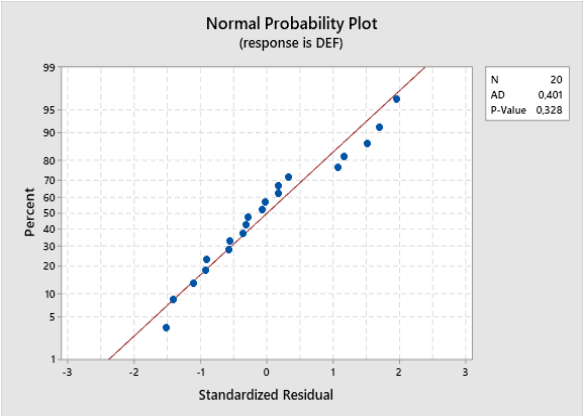

Fig. 7. Normal probability plot

The Anderson-Darling (AD) statistical test was used, which measures how well the data follow the chosen distribution[18]. The test was also used to determine the adequacy of the model. The AD test confirmed the normal distribution of the standardized residuals. The calculated AD value of 0.401 is less than the critical value of 0.704 for the sample of 20 observations and the associated p-value of 0.328 of the AD statistic is significantly above the 0.05 level. The lower value of AD compared to the critical value and the P-value $\geq\alpha$, confirm a normal probability distribution of the residuals,fig.7.

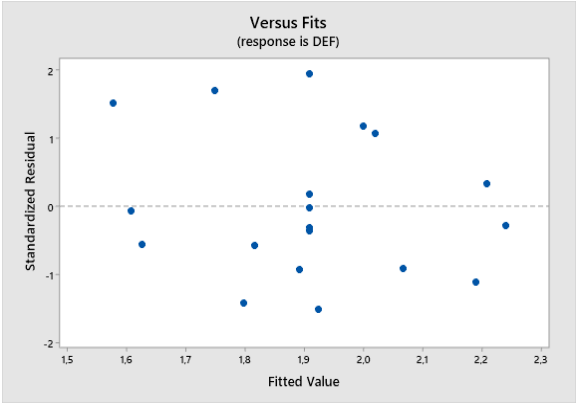

Fig. 8. Versus fits

The standardized residual is equal to the value of the residual divided by an estimate of its standard deviation. These residuals are useful because raw residuals may not be good indicators of bias in the regression model[19]. It is clear that there are no gross errors in this regression model. The analysis of the residuals does not indicate a violation of the assumptions of the regression analysis. From Fig. 8. it is seen that all residuals are in the interval ±2. Therefore, it can be concluded that the regression modelis adequate by these two checks.

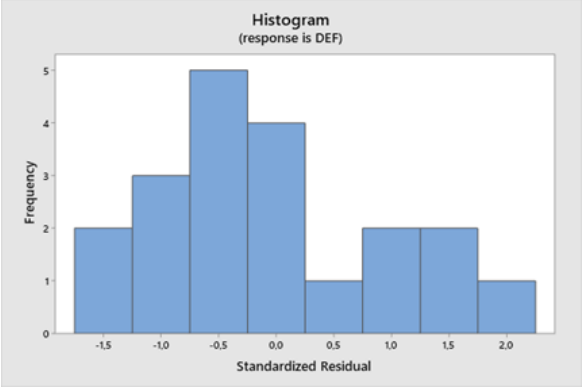

Fig. 9. Standartized residuals

From the calculated empirical values of the coefficients of asymmetry and kurtosis, and what is shown in the figure, we can state that with a sample size of 20 samples, the distribution of the results is asymmetric with a right-extended shoulder and reduced kurtosis, fig. 9.

Figure 10 shows a correlogram of the dependence between the factors and the dependent variable. It is clearly seen that the dependence is linear.

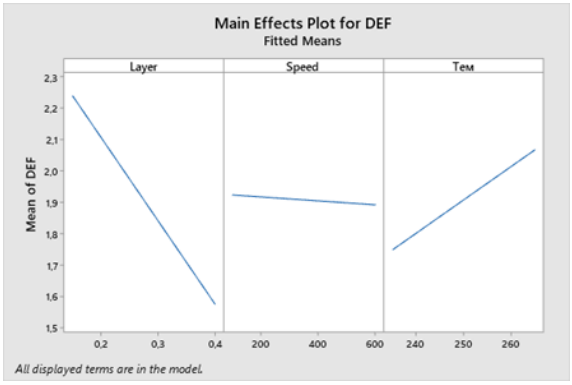

Fig. 10. Main effects plot for deformation.

From Figure 10 we can conclude that as the layer height increases, the creep of the material decreases. At the print speed, the creep change remains relatively constant because the factor does not directly affect the creep. At the printing temperature factor, when we increase the temperature, the creep of the material increases.

Based on the model, a one-parameter optimization of the objective function was performed. The goal of this analysis is 1.5 mm deformation and determining the printing modes. 5 alternative solutions were created with composite desirable 1 close to 1.Response Optimization: DEFORMATION,tab.6

TABLE 6 PARAMETERS

Response	Goal	Lower	Target	Upper	Weight	Impo-rtance
DEF.	Target	1,26	1,5	2,7	1	1

TABLE 7 SOLUTIONS

Solution	Layer	Speed	Tem	DEF Fit	Composite Desirability
1	0,36	600	235	1,50	1,00
2	0,37	100	235	1,50	1,00
3	0,36	600	235	1,50	1,00
4	0,37	100	235	1,50	0,99
5	0,40	600	265	1,72	0,81

TABLE 8 MULTIPLE RESPONSE PREDICTION

Variable	Setting
Layer	0,362384
Speed	600
Тем	235

Response	Fit	SE Fit	95% CI	95% PI
DEF.	1,500	0,270	(0,930; 2,070)	(0,456; 2,544)

From table 7 it can be seen that at 1.5mm tensile creep we have 5 solutions. From the last table 8 we can conclude that the standard error is 0.27 and the variable in the confidence interval:

$$0.93 \leq Y \ll 2.07 \qquad (10)$$

The following figure 11 graphically presents the results of the optimization of the objective function.

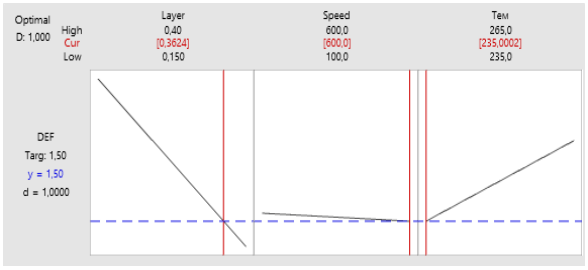

Fig. 11. Results of optimization

The contour plots (fig.12) show the resulting relationships by pair of variables relative to the resulting variable – creep elongation.

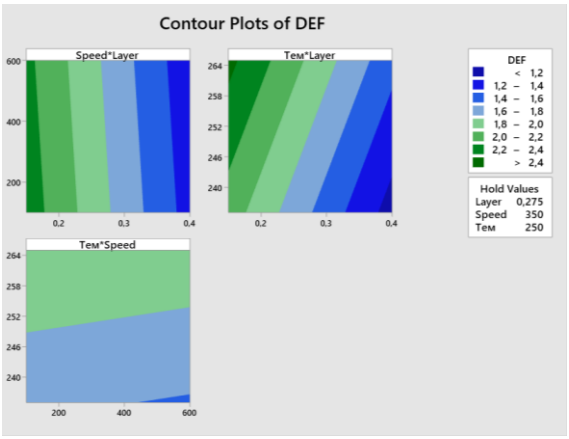

Fig. 12. Contour plots of deformation

Overall, the tensile creep results of Nylon CF 15 Carbon showed high creep resistance compared to bulk PLA,ABS,Nylon and proved that the material can be considered as a promising structural material[20]. The experimental results showed a small dispersion, which validates them.

IV. Conclusions

From the results and their analysis, the following conclusions may be drawn:

1. This study shows with a high degree of probability of 96.17% how height printed layer, the printing temperature and printing speed affect the tensile creep of the Nylon CF15 Carbon material.

2. The study proves with a high degree of probability that there is a strong relationship between the tensile creep and the height of the printed layer. In order to achieve high creep resistance, we need to increase the layer height as much as possible.

3. This study shows that the printing speed does not directly affect the tensile creep, therefore we can print the material at high speeds in order to shorten the printing time and increase productivity.

4. We may conclude that the material should be printed at a lower temperature to increase the tensile strength. It should be borne in mind that printing temperatures lower than 235ºC can clog the nozzle because the material contains carbon particles.

5. As a result of the optimization of the regression model, we can state that for a tensile creep of 1.5mm with a standard error of 0.27%, the layer height should be 0.36mm, the printing temperature 235ºC and the printing speed 600mm/s.

V. Acknowledgments

This research was funded by the European Regional Development Fund within the OP " Research, Innovation and Digitalization Programme for Intelligent Transformation 2021-2027 ", Project CoC "Smart Mechatronics, Eco- and Energy Saving Systems and Technologies", No. BG16RFPR002-1.014-0005.

REFERENCES

[1] S. Ghosh, "Analysis of Creep Deformation", 2024. [Online]. Available: https://doi.org/10.20944/preprints202412.1894.v1. (Accessed: January 3, 2025).

[2] M. Fischbach and K. Weinberg, "Effect of Physical Aging on the Flexural Creep in 3D Printed Thermoplastic", 2023. [Online]. Available: https://doi.org/10.1007/978-3-031-39070-8_7. (Accessed: January 3, 2025).

[3] S. Weaver, "The Creep Curve and Stability of Steels at Constant Stress and Temperature", Journal of Fluids Engineering, vol. 58, pp. 745–751, 2023. [Online]. Available: https://doi.org/10.1115/1.4020383. (Accessed: January 3, 2025).

[4] M. Podrezov, D. Verbylo, I. Danylenko, I. Yevich, I. Tolochyn and I. Tsyganenko, "Creep of low-plastic heat-resistant materials in bending", Uspihi Materialoznavstva, pp. 58–74, 2023. [Online]. Available: https://doi.org/10.15407/materials2023.06.058. (Accessed: January 3, 2025).

[5] M. Sayre, "Plastic Behavior in the Light of Creep and Elastic Recovery Phenomena", Journal of Fluids Engineering, vol. 56, pp. 559–561, 2023. [Online]. Available: https://doi.org/10.1115/1.4019809. (Accessed: January 3, 2025).

[6] I. Christodoulou, V. Alexopoulou and A. Markopoulos, "An Experimental Investigation of the Mechanical Properties of Fused Filament Fabricated Nylon-Carbon Fiber Composites", Cutting & Tools in Technological System, pp. 148–167, 2024. [Online]. Available: https://doi.org/10.20998/2078-7405.2024.100.11. (Accessed: January 3, 2025).

[7] Z. Gan, H. Cao, Y. Yan and Z. Li, "Preparation and properties of carbon fiber-Ni/nylon 66 composites", Acta Materiae Compositae Sinica, vol. 34, pp. 945–951, 2017. [Online]. Available: https://doi.org/10.13801/j.cnki.fhclxb.20160706.003. (Accessed: January 3, 2025).

[8] A. Dar, P. Yadav and N. Aswani, "Optimizing processes and products: The role of DOE", Insight - Statistics, vol. 7, pp. 1–18, 2024. [Online]. Available: https://doi.org/10.18282/i-s644. (Accessed: January 3, 2025).

[9] Y. AbouelNour, N. Rakauskas, G. Naquila and N. Gupta, "Tensile testing data of additive manufactured ASTM D638 standard specimens with embedded internal geometrical features", Scientific Data, vol. 11, 2024. [Online]. Available: https://doi.org/10.1038/s41597-024-03369-y. (Accessed: January 3, 2025).

[10] R. Pontes, L. Tovar and M. Tirelli, "Range-oriented design and operation," 2025. [Online]. Available: https://doi.org/10.1016/B978-0-323-90977-8.00005-4. (Accessed: January 3, 2025).

[11] V. Cvetkov, "Entropy, Observations and Some Standard Deviations", 2024. [Online]. Available: https://doi.org/10.5281/zenodo.1453153. (Accessed: January 3, 2025).

[12] G. Auricchio, P. Giudici and G. Toscani, "How to measure multidimensional variation?", 2024. [Online]. Available: https://doi.org/10.48550/arXiv.2411.19529. (Accessed: January 3, 2025).

[13] F. Kronthaler, "The Multiple Regression Analysis," 2024. [Online]. Available: https://doi.org/10.1007/978-3-662-69107-6_20. (Accessed: January 3, 2025).

[14] H. Mahajan, O. Gule and A. Malpure, "Design and Optimization of 3D Printing Process Parameters", 2024.

[15] S. Chipeva and V. Boshankov, Introduction to Econometry, 2015.

[16] N. Zhou, O. Blaha and D. Zelterman, "Distributions and Their Approximations for p-Values", 2024. [Online]. Available: https://doi.org/10.1007/978-3-031-65937-9_16. (Accessed: January 3, 2025).

[17] H. Risan, A. Al-Azzawi and F. Al-Zwainy, "Correlation", 2025. [Online]. Available: https://doi.org/10.1016/B978-0-443-27362-9.00011-2. (Accessed: January 3, 2025).

[18] H. Coronel-Brizio, A. Hernandez-Montoya, M. Rodríguez-Achach and H. Tapia-McClung, "Anderson-Darling and Watson tests for the geometric distribution with estimated probability of success", PLOS ONE, vol. 19, 2024. [Online]. Available: https://doi.org/10.1371/journal.pone.0315855. (Accessed: January 3, 2025).

[19] X. Qu, "Exact Moments of Residuals of Independence", Mathematics, vol. 12, p. 3987, 2024. [Online]. Available: https://doi.org/10.3390/math12243987. (Accessed: January 3, 2025).

[20] A. Palaniappan, R. Krishnan, P. Vasanaperumal and K. Rajendiran, "Analysis of the Mechanical Characteristics and Properties of a Carbon Fiber–Nylon Composite Influence of the Factors of the Fused Deposition Modeling", Journal of Materials Engineering and Performance, vol. 33, 2024. [Online]. Available: https://doi.org/10.1007/s11665-024-10150-0. (Accessed: January 3, 2025).

Environment. Technology. Resources. Rezekne, Latvia
Proceedings of the 16th International Scientific and Practical Conference. 2025. Volume IV, 357-361

Design and Manufactoring of a Laboratory Stand for Testing Accelerated Tensile Creep of Plastics According to ASTM D6992

Sabi Sabev
Technical University of Sofia,
Branch Plovdiv
Plovdiv, Bulgaria
sabi_sabev@tu-plovdiv.bg

Konstantin Chukalov
Technical University of Sofia,
Branch Plovdiv
Plovdiv, Bulgaria
chukalov@tu-plovdiv.bg

***Abstract*—The article discusses stages of design and manufacturing of a laboratory stand for accelerated tensile creep of plastics according to ASTM D6992. All components necessary for accurate operation of the laboratory stand will be examined: jaws, deadweight system,loading weights, linear strain measurement system and control, test temperature control and monitoring, test data storage and management. The aim of the article is to create flexible systems that allow the stand to be used for other similar test standards and materials. The main task in the design and manufacturing of the stand is to create reliable equipment with a high accuracy degree, automated loading of a control program, as well asability to store a large volume of data for the purpose of creating a database and comparing test results. The mathematical model for calculating equivalent years is directly integrated for easier processing of experimental results. The stand is designed and manufactured for testing 2 samples simultaneously , which facilitates comparison of data from different polymer blends.The stand is calibrated according to its three main quantities - linear strain, temperature and deadweights.The calibration results are presented to assess accuracy of the laboratory stand systems. The stand fully meets the requirements defined according to ASTM D6992. The accuracy of the calibrated quantities allows precise calculations of accelerated creep data on a wide range of materials. Design and manufacturing steps may also be used with other standardized and non-standardized creep tensile testing methods of plastics, as well as other laboratory equipment needs with similar systems and goals.**

Keywords — creep, lab equipment, test methods, design equipment, stepped isothermal method, plastic tests, tensile creep test.

I. Introduction

Creep is a process of slow increase in plastic strain over time at constant temperature and force loading[1]. The loading is carried out in the elastic strain zone[2]. Depending on used test standards , the exam can end without failure or with failure. The test is extremely relevant for heat-resistant materials and characterizes durability of selected material[3].Creep is characterized by 3 stages - undetermined creep, determined creep and creep with a constantly increasing speed[4].The increasing strain at a constant load at a certain temperature is expressed graphically with so-called creep curves. Depending on the applied temperature, there are low-temperature and high-temperature creep [5].There is not enough data to establish the entire creep process of materials, which makes research related to the process very relevant. Creep testing of materials is a long-term method, the duration of which depends on the functional purpose of the structure - it may reach up to 10,000 hours[6].

In practice, there are also theoretical calculations of strain by creating mathematical models based on sample data[7]. Creep testing of materials is widely used for various types of materials - polymers, metals, etc[8]..

Plastics are widely used in automotive, mechanical engineering, construction, etc., and the requirements for their characteristics are increasing. Plastics are tested experimentally for tensile, creep, impact toughness, compression, bending, etc[9]. The test specimens differ depending on used standards.

II. Materials and Methods

Based on the ASTM D6992 standard, the test stand was designed and manufactured to test plastic films for accelerated creep[10]. The requirements of the accelerated creep standard are:[11]:

- The jaws should not allow slippage or excessive stress on test specimens

Online ISSN 2256-070X
https://doi.org/10.17770/etr2025vol4.8408
© 2025 The Author(s). Published by RTU PRESS.
This is an open access article under the Creative Commons Attribution 4.0 International License.

- The universal machine should be equipped with a dead-weight system
- Measurement and control strain values
- Time measurement
- •Temperature measurement and control, temperature hysteresis should be less than 2 degrees;
- •Guaranteeing standardized atmospheric testing conditions
- Management and storage of experimental data.

The designed two identical sets of jaws are for testing two samples with a width of 80 to 100 mm and a sample thickness of maximum 3 mm, a length of up to 250 mm. The jaws contain 3 holes for samples gripping so that it does not buckle or bend and one for gripping to base. All holes are 8.5 mm in diameter. The samples are intended to be gripped with 3 standardized M8 bolts. The lower jaw is designed on one side to grip the sample, and on the other to grip the deadweight systems. The jaw thickness is 6 mm.

The entire mechanical system is freely hanging, hooked at the upper end. The mechanical system consists of 3 clamps, two sets of jaws, a sample, a spacer and a deadweight system. The mechanical system is accompanied by a linear strain measuring system.

The loading system consists of a deadweight mount weighing 2.5 kg. The axis is designed for standard weights of 2.5 kg, 5 kg and 10 kg and can be loaded up to 80 kg.The selected maximum weight is sufficient for a wide range of plastics. For materials with higher creep resistance, the width of the specimens can be reduced.

The measuring system consists of incremental lines with a resolution of 5 microns and a displacement speed of 100 mm/s. The attachment to the mechanical system is carried out using standard ball joints.

To ensure atmospheric conditions during the test, the chamber is insulated except for ceiling. The lab stand door is designed for observing the samples during the test, for this purpose it has a transparent double glazing. To ensure uniform temperature distribution, the stand has two centrifugal fans with a power of 20 watts. Two conical air ducts are used for turbulent air movement. To maintain the temperature,two heaters with a power of 500 watts, controlled by a solid stage relay, are used. To maintain the temperature in the range of ± 0.2 degrees,classic pit control is used. The entire stand with all adjacent systems is shown in a CAD model in fig. 1.

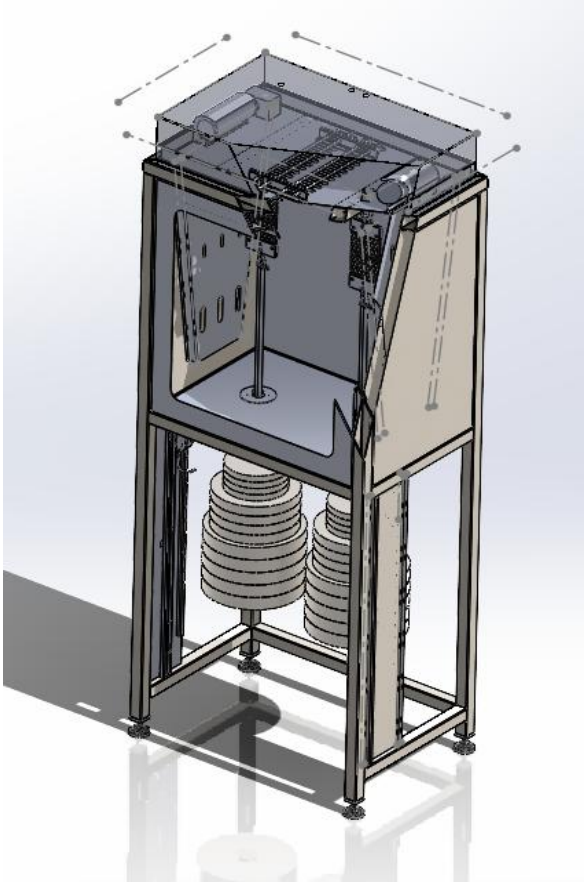

Fig. 1. CAD model of the designed stand.

For measuring the test duration, storing and managing the data, an industrial PLC controller and an HMI panel are used (Fig. 2)[12]. The processed data are recorded in two places - on an SD card and a USB flash drive to prevent the loss of experimental data. In case of a temporary power outage, a UPS with a capacity of 1600 VA is provided. When operating at full power of the stand (1100 watts), this is enough to power the stand for 20 minutes.

Fig. 2. HMI - GT2107-WTSD and PLS-FX5U-32MT/ESS.

The interactive interface provides the ability to store five preset programs. This way, the most frequently used test programs can be quickly launched. There is an option to re-adjust the preset programs for greater flexibility of the laboratory equipment.The home screen contains the following features,fig.3,4:

- Start and stop the program
- Select the test program

- Select language
- Date and time
- Real-time temperature and strain measurement.
- Remaining time until the end of the test
- Consumed electricity power
- Indication of data recording in the flash drive and SD card on parallel..
- Graph of linear strain and equivalent years

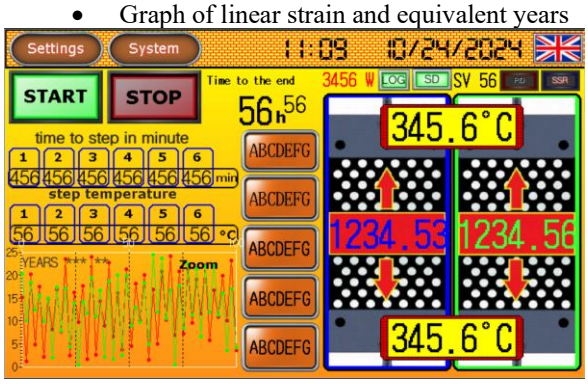

Fig. 3. Home screan.

Fig. 4. Measured linear strain.

Fig. 5 shows the set up test programs screen.Each program may consists of 6 temperature steps, dwelling time and sample length,used for further calculation of elongations in percentages. According ASTM D6992, the minimum duration of each step is 10,000 seconds, and the minimum duration of the entire test is 60,000 seconds. The set up of test programs is as flexible as possible, while at the same time facilitating creation and management of large databases[13]. Data storage and management is very important, as it allows comparison of different plastic blends, as well as results from different test parameters[14]. The graphical presentation of data facilitates the comparison of experimental samples in real time.

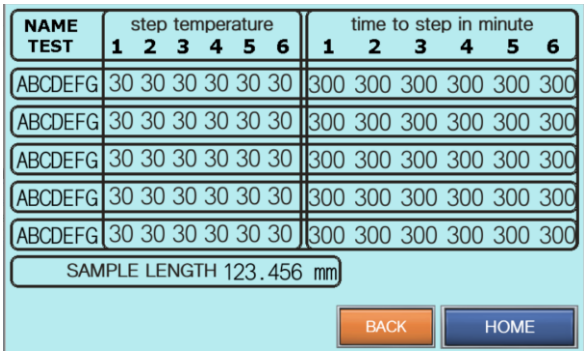

Fig. 5. Test programs set up.

In the system menu fig.6, the recorded data every 5 minutes for the deformation, the actual temperature, time and date are displayed.

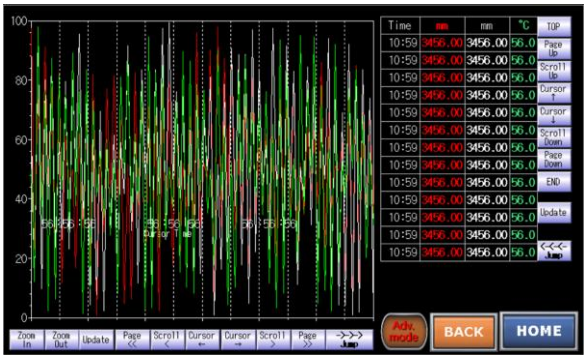

Fig. 6. System menu.

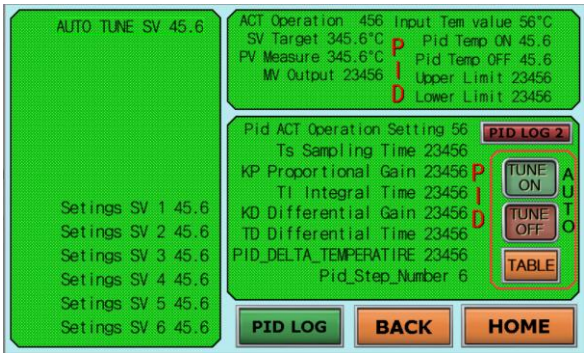

Fig. 7. PID control.

The system is equipped with PID control system and has the ability to auto-tune at any given step. The functional purpose of using a PID control system is to receive input data from the temperature sensors, calculate the difference between the actual and desired setpoint, and adjust the outputs. PID control is most often used for the following variables-voltage,speed, temperature,flow rate, pressure, etc[15].Temperature is a fundamental parameter and its accurate adjustment leads to adequate experimental results.The auto-tuning data is automatically recorded in the menu shown in Fig. 8, and there is also the ability to manually adjust the control parameters

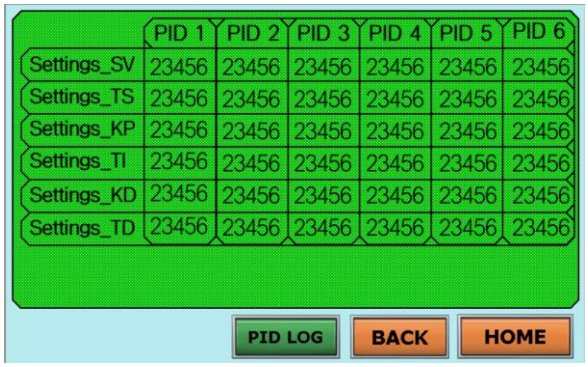

Fig. 8. Auto-tuned data.

The control system allows for monitoring of PID control every five minutes,so the system ensure correct tests.

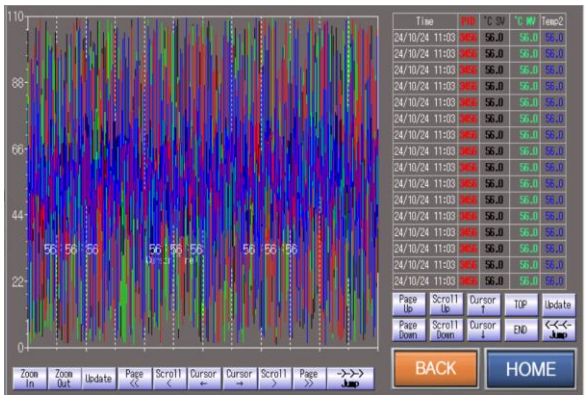

Fig. 9. PID control monitoring.

III. Results and Discussion

The laboratory stand for accelerated tensile creep of plastics was designed and manufactured,fig.10. The stand was tested with various blend plastics in order to validate the performance of its systems. No critical deviations were observed,the temperature is in the range $\pm 1^0$ from the nominal value both in short-term and long-term tests..All requirements of the standard ASTM D6992 have been met, while at the same time the designed and manufactured stand has flexible systems that allow testing of plastics with different force and temperature conditions.Within the scope of the applied specification is possible other gripping systems to be used. At the same time, the information system on the stand allows storage, comparison and management of a large volume of data, which is beneficial for engineering practice. All requirements for reliability, accuracy, and stability of the technical system have been met. In addition to creep testing, the stand can also be used for static load tests. The stand can be used for all types of creep testing defined in the standard, as well as for similar creep tests according to other standards. The stand is made according to all safety standards for electrical and electronic equipment. The autonomous power supply allows the stand to operate for some time during temporary power outages.

Fig. 10. Manufactured stand.

The stand was calibrated by accredited laboratory for its three main quantities - linear strain, temperature and deadweights.The weights were purchased calibrated[16].The results of the calibration of the linear strain are presented in a tab. 1.

TABLE.1 LINEAR STRAIN CALIBRATION RESULTS IN MM

Nominal value	Deviation	Uncertainly,U
0	0	0,02
50	+0,04	0,03
100	+0,06	0,03
200	+0,1	0.05
300	+0,13	0.05
400	+0,15	0.05
500	+0,16	0.05

The results of the temperature calibration are presented in a table 2.

TAB.2 TEMPERATURE CALIBRATION RESULTS

Stand temperature, C^0	35	40
Real temperature, C^0	34,97	39,65
Uncertainly,U, C^0	0,3	0,3

The reported expanded uncertainly of measurement is stated as the standard uncertainly,multiplied by the coverage factor k=2,which for the normal contribution corresponds for the coverage probability of 95%. The stand

meets and even exceeds the requirements set out in the standard.

IV. Conclusions

The stand meets the high requirements for laboratory equipment - reliability, ease of use, automated setup and data logging, the ability to store a large volume of test results. The stand allows flexible operating conditions with a large range of measured linear strains, relatively high test temperature and load range, suitable for heavily loaded plastic structures. The design of the stand can be upgraded with the addition of a system for measuring dynamic loads (for example, cyclic fatigue tensile-compression) by designing a system for additional modules - a strain gauge sensor and a servo system. The main limitation of the stand is the temperature range of the tested material. The stand cover with the adjacent fans is designed as a subsystem that can be replaced with high-temperature fans, which will allow for the measurement of high-temperature creep. The stand can be used for close to standard test conditions, as well as for non-standard tests. The evaluations from the calibration of the stand showed excellent results.

V. Acknowledgments

This research was funded by the European Regional Development Fund within the OP " Research, Innovation and Digitalization Programme for Intelligent Transformation 2021-2027 ", Project CoC "Smart Mechatronics, Eco- and Energy Saving Systems and Technologies", No. BG16RFPR002-1.014-0005.

REFERENCES

[1] Sourangshu, "Analysis of Creep Deformation," 2024. [Online]. Available: https://doi.org/10.20944/preprints202412.1894.v1. [Accessed: January 13, 2025].

[2] Z. Yang, Q. Meng, Z. Fang and X. Zhang, "Supply Chain Elastic Strain", Mathematics, vol. 12, p. 1788, 2024. [Online]. Available: https://doi.org/10.3390/math12121788. [Accessed: January 13, 2025].

[3] Z. Wang, Y. Li, S. Yasin, C. Zheng, P. Hu, L. Zhang and J. Shi, "Preparation and Properties of the Low-Cost Heat-Resistant Rubber Material for Trenchless Rehabilitation of Thermal Pipelines," 2024. [Online]. Available: https://doi.org/10.1115/PVP2024-123175. [Accessed: January 13, 2025].

[4] V. Dacol and E. Caetano, "Modelling the Three-Stage of Creep," 2022. [Online]. Available: https://doi.org/10.1007/978-3-030-76465-4_7. [Accessed: January 13, 2025].

[5] T. Hanes, R. Stephens, J. Siefert and I. Perrin, "Creep Crack Growth on High and Low Creep Ductility Grade 91 Steel," pp. 316–327, 2024. [Online]. Available: https://doi.org/10.31399/asm.cp.am-epri-2024p0316. [Accessed: January 13, 2025].

[6] R. Sandström, "Basic Analytical Modeling of Creep Strain Curves", Materials, vol. 16, p. 3542, 2023. [Online]. Available: https://doi.org/10.3390/ma16093542. [Accessed: January 10, 2025].

[7] A. Iskakbayev, B. Teltayev, Y. Aitbayev and A. Zhaisanbayev, "Accelerated Creep of Asphalt Concrete at Medium Temperatures", Applied Sciences, vol. 14, p. 9393, 2024. [Online]. Available: https://doi.org/10.3390/app14209393. [Accessed: January 10, 2025].

[8] L. Su, S. Wu, G. Fu, W. Zhu, X. Zhang and B. Liang, "Creep characterisation and microstructural analysis of municipal solid waste incineration fly ash geopolymer backfill", Scientific Reports, vol. 14, 2024. [Online]. Available: https://doi.org/10.1038/s41598-024-81426-7. [Accessed: January 10, 2025].

[9] N. Lynch-Aird, J. Woodhouse and C. Barlow, "Plastic Creep Constraint in Nylon Instrument Strings", Materials, vol. 18, p. 223, 2025. [Online]. Available: https://doi.org/10.3390/ma18020223. [Accessed: January 10, 2025].

[10] W. Liu and S. Zhang, "Accelerated creep model based on the law of energy conservation and analysis of creep parameters", Mechanics of Time-Dependent Materials, vol. 28, 2023. [Online]. Available: https://doi.org/10.1007/s11043-023-09628-6. [Accessed: January 10, 2025].

[11] M. A. Hossain, R. Mach, J. Pellicotte and C. Stewart, "Calibration of CDM-Based Creep Constitutive Model Using Accelerated Creep Test (ACT) Data," 2020. [Online]. Available: https://doi.org/10.1115/GT2020-16017. [Accessed: January 10, 2025].

[12] S. Deng, "The Application of PLC in Industry Fields", Highlights in Science, Engineering and Technology, vol. 114, pp. 168–172, 2024. [Online]. Available: https://doi.org/10.54097/28d22249. [Accessed: January 10, 2025].

[13] H. Liu, "Optimization and performance improvement of distributed data storage in hybrid storage systems", World Journal of Advanced Engineering Technology and Sciences, vol. 13, pp. 459–467, 2024. [Online]. Available: https://doi.org/10.30574/wjaets.2024.13.1.0443. [Accessed: January 10, 2025].

[14] S. Cestari, P. Rodrigues, A. Ribeiro, C. Castro, V. Cruz, A. Torres, N. Ramos and A. Machado, "Compatibilizer Efficiency in Enhancing Marine Plastic Waste Valorization Through Simulated Recycled Plastic Blends," *Polymers*, vol. 16, p. 3441, 2024. [Online]. Available: https://doi.org/10.3390/polym16233441. [Accessed: January 10, 2025].

[15] H. Jiang, "Overview and development of PID control", Applied and Computational Engineering, vol. 66, pp. 187–191, 2024. [Online]. Available: https://doi.org/10.54254/2755-2721/66/20240946. [Accessed: January 10, 2025].

[16] J. Militky, D. Křemenáková and M. Venkataraman, "Calibration," 2024. [Online]. Available: https://doi.org/10.1007/978-981-97-6607-9_7. [Accessed: January 10, 2025].

Environment. Technology. Resources. Rezekne, Latvia
Proceedings of the 16th International Scientific and Practical Conference. 2025. Volume IV, 363-367

Dynamic Algorithm for Dimensional Sub-Tuning in Turning

Silviya Salapateva
Faculty of Mechanical Engineering
Technical University of Sofia, Plovdiv Branch,
Center of competence "Smart mechatronic, eco-and energy-saving systems and technologies"
Plovdiv, Bulgaria,
sisisal@tu-plovdiv.bg

Radostina Mihova
Faculty of Mechanical Engineering
Technical University of Sofia, Plovdiv Branch,
Plovdiv, Bulgaria
ralexmihova@gmail.com

***Abstract*— One of the possibilities for increasing the accuracy when machining a series of parts with a single dimensional adjustment (automatic obtaining of dimensions) is to perform more frequent dimensional sub-tuning. There is a possibility to increase the accuracy of machining through dimensional sub-tuning if working with a complete set of data about the dimensions of the machined parts, and not with small current samples. This opportunity arises from the widespread introduction of computer technology for the purposes of managing the technological processes. The article examines the possibilities for determining the moment for dimensional sub-tuning by using computer analysis of information about the dimensions of the machined parts in real time.**

Keywords*— Mechanical engineering, dimension sub-tuning, CNC machine tool.

I. Introduction

One of the possibilities for increasing the accuracy when machining a series of parts with a single dimensional adjustment (automatic obtaining of dimensions) is to perform more frequent dimensional sub-tuning. A borderline case is the continuous automatic dimension sub-tuning to compensate for the influence of systematic factors, which change according to a known law [1]. This possibility is practicable in mass and large-scale serial production, when the processes ae well studied and their statistical features are known, including the parameters of the laws of change of systematic factors. In practice, the method of dimension sub-tuning, using control charts, has found wider application. Of the known charts, the tolerance field is used most efficiently and to the fullest, when working with the statistical estimates of the average size value $\bar{X}$ and mean square root deviation S [2, 3]. In this case small current samples are used, for each of which these statistical estimates are calculated. When their value goes outside the control limits, the process is interrupted and dimension sub-tuning is performed. A condition for applying this method is to have the dispersion ω of the dimensions from random factors (instantaneous dispersion field) relatively small. Compared to the dimension tolerance T, the condition $T > 2\omega$ must be met. This determines the application of the method in fine mechanical processing while limiting its use in clean processing, where the scattering, caused by random factors, is greater.

II. Materials and Methods

There is a possibility to increase the accuracy of machining by dimension sub-tuning, if working with full information about the dimensions of the machine parts, rather than with small current samples. This possibility arises from the widespread introduction of computer technology for the purposes of controlling the technological processes.

When using small current samples, due to their small volume, larger values of the statistical estimates for the instantaneous dispersion field are obtained and thence, larger values of the sub-tuning impulse (the change in the adjusted size) as well. Thus, the total dispersion field is increased.

Using complete information about the dimensions of the machined parts, the change in the average dimension value can be tracked in real time by a regression equation, which represents it as a function of the number of machined parts. For most cases this relationship is a linear regression equation of the type:

$$\bar{X}_n = b_{0n} + b_{1n} n \text{ , } (n = 3, 4, 5, \ldots), \qquad (1)$$

where $\bar{X}_n$ is the average dimension value from the regression equation of the part with a serial number n; b_{0n}

Online ISSN 2256-070X
https://doi.org/10.17770/etr2025vol4.8423
© 2025 The Author(s). Published by RTU PRESS.
This is an open access article under the Creative Commons Attribution 4.0 International License.

and b_{1n} are statistical coefficients in the regression equation.

A series of regression equations is obtained for the first 3, first 4, first 5 etc. machined parts. As the number of machined parts increases, the confidence interval of the regression equation narrows and, respectively, the accuracy of the estimate for the average value increases [3, 4].

A question arises as to how many parts to limit the sample volume, in order to achieve a specific accuracy of the process. There are two possible approaches to solving this problem:

1. Analytical – based on the relative estimate of the change in the average size value with respect to the size tolerance;
2. Statistical – by setting the relative error of the average value at a certain confidence probability.

The analytical method is based on the fluctuation of the angular coefficient $\tilde{b}_n$ in the regression equation:

$$b_{13} \neq b_{14} \neq b_{15} \neq \ldots$$

At the beginning, when the data accumulation starts, the angular coefficient fluctuates strongly. This phenomenon can be named plane precession of the regression equation. When the number of machined parts (sample volume) increases, the fluctuation of the angular coefficient decreases, i.e., the precession damps out.

Fig. 1 graphically represents the precession damping as a real process in clean step turning and under the following conditions [5]: nominal dimension of the part D = 58 mm, tolerance T = 0,046 mm; upper limit deviation ES = 0; lower limit deviation EI = -0,046; positioning error ω_p = 9,74 μm; measurement error $\omega_{изм}$ = 5 μm; instantaneous field of dimension dispersion ω = 30 μm; permissible tool wear h_{Dmax} = 60 μm; sample volume for dimension adjustment n_0 = 3.

The assumed permissible error of dimension adjustment, which is 10% of the dimension tolerance T., can serve as a criterion for sufficient damping of the precession. Therefore, if the difference in the ends of two consecutive regression equations is less than 10%, it can be assumed that the precession has damped out within acceptable limits:

$$[\varepsilon] = 0{,}1T. \qquad (2)$$

If the difference $\Delta\bar{A}_n$ between two sequential values of the average dimension, determined by the regression equations, is less than 0,1T, it can be considered that the precession has slowed down sufficiently.

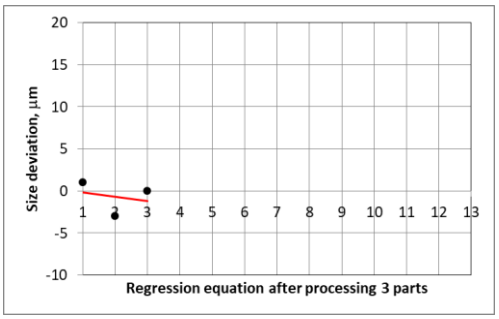

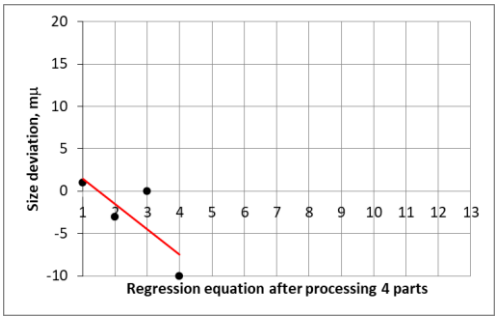

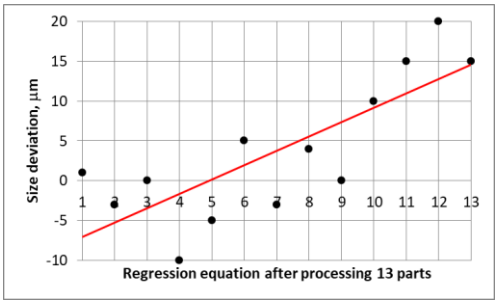

а) regression equation

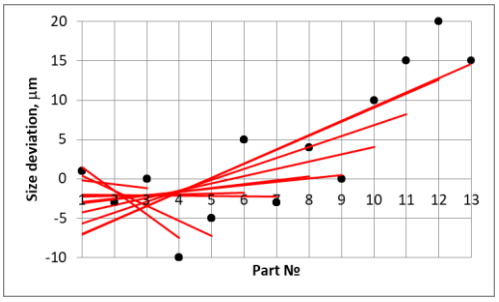

б) dimensioning vector

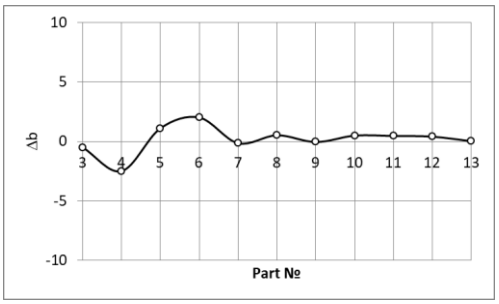

в) precession damping

Fig. 1. Dynamics of the sizing process

However, to use the last regression equation, in which the precession damping is established, to make a decision for performing sub-tuning, this equation must also be adequate.

The adequacy check is performed using the Fisher criterion. The critical value for the Fisher test F is chosen for degrees of freedom $k_1 = k_2 = n_j - 1$ and significance level $\alpha = 0{,}05$.

If the regression equation is not adequate, then the next part is machined and the checks for precession damping and adequacy are repeated. The procedure continues until both conditions are simultaneously satisfied.

Hence, the number of parts n, at which it is possible to interrupt the process of machining and perform sub-tuning, will be determined by the condition:

$$\Delta\bar{A}_n = b_{0(n-1)} - b_{0n} + (n-1)b_{1(n-1)} - nb_{1n} \le 0{,}1T \quad (3)$$

With the statistical method the sample volume is determined iteratively by the condition [6]:

$$n = \left(\frac{t_{\gamma,k} . S . 100}{\Delta_{\gamma,k} . \bar{X}} \right)^2, \quad (4)$$

where $t_{\gamma,k}$ is the Student's t-statistic at confidence probability γ and degrees of freedom $k = n - 1$; $\Delta_{\gamma,k}$ is the relative error in the average value in %.

III. Results and discusion

To compare the two methods for determining the sample volume, an experimental study was conducted by means of performing clean boring of a batch of cylindrical bushings made of steel 35.

The clean boring was performed with a boring bar cantilevered in the turret of a CNC lathe under the following conditions: machine - CNC lathe LT580; machined material - steel BDS EN 10083-2 C35, hot-rolled pipe ∅40/7; diameter of the machined hole D = 29,0 mm; size tolerance T = 50 μm; diameter of the cutting tool – 20 mm; length of the cantilever part of the tool L = 100 mm; hard-alloy plate made of P15, type TPUN 110302; main tool setting angle $\chi_r = 90°$; cutting speed V_c = 120 m/min; feed f = 0,05 mm/rev; average cutting depth a_p = 0,3 mm; measuring instrument – internal gauge with a measuring clock with a division value of 0,001 mm.

The experimental scheme is presented in Fig 2.

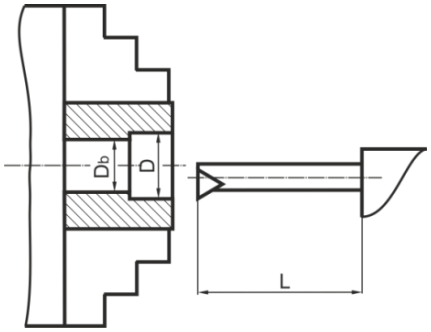

Fig. 2. Experimental scheme (Db – diameter of the workpiece; D – diameter of the machine part)

The analytical method for determining the sample volume was applied initially. A series of workpieces are machined with a single dimension adjustment. The resulting dimensions are measured and entered into a personal computer for statistical processing. After the third, fourth, fifth etc. machined parts, the regression equations are determined and the check (2) is performed. In case of sufficient damping of the precession, the change in the adjusted dimension is determined:

$$\Delta\bar{A}_n = \bar{X}_n - \bar{X}_3, \quad (5)$$

If the difference (4) is statistically significant, then dimension sub-tuning is performed with a magnitude $\Delta\bar{A}_n$ to compensate for the systematic error. If the difference (5) is statistically insignificant, the work continues until reaching significance. Then sub-tuning is performed with the reached difference.

After the dimension sub-tuning, new accumulation of data begins, and similar statistical processing follows, as with the first group of parts. The obtained results are given in Table 1 and graphically represented by the scatter diagram in Fig.3.

Table 1 Results of clean boring of a batch of cylindrical bushings using an analytical method for dimensional sub-tuning

№ of the part	Size, mm	№ of the part	Size, mm	№ of the part	Size, mm
1	29,30	17	29,33	33	29,21
2	29,20	18	29,26	34	29,13
3	29,28	19	29,18	35	29,29
4	29,29	20	29,29	36	29,21
5	29,20	21	29,17	37	29,24
6	29,25	22	29,11	38	29,29
7	29,24	23	29,30	39	29,17
8	29,25	24	29,26	40	29,24
9	29,24	25	29,28	41	29,10
10	29,31	26	29,17	41	29,14
11	29,26	27	29,10	43	29,30
12	29,16	28	29,20	44	29,27
13	29,26	29	29,26	45	29,31
14	29,16	30	29,10	46	29,15
15	29,33	31	29,23	47	29,25
16	29,21	32	29,26		

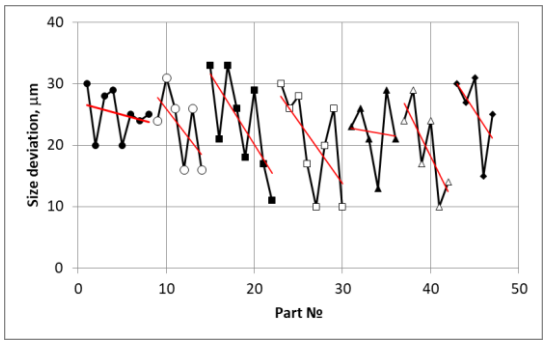

Fig. 3. Scatter diagram of the process of clean boring of a batch of cylindrical bushings with the application of an analytical method for dimension sub-tuning

Six adjustments were made. The following results were obtained from the statistical processing of the data:

- the variances of the six groups (samples) relative to the regression equation are homogeneous. The average dispersion is D_{cp} = 29,5 µm^2, the mean square root deviation is S_{cp} = 5,4 µm and the instantaneous dispersion field is ω_{cp} = 26 µm;
- the average size of the sub-tuning impulse is $\Delta\bar{A}_n = 10,3$ µm;
- the total dispersion field with probabilistic addition of the errors will be:

$$\omega_\Sigma = \sqrt{\omega_{cp}^2 + 3(\Delta\bar{A}_n)^2 + \omega_p^2} = 32\,\mu m. \qquad (6)$$

The diametric processing error of the sub-tuning impulse for the LT580, determined experimentally, is ω_p = 9,74 µm.

When determining the sample volume by the statistical method for the same experimental conditions and statistical estimate of the dispersion, using the methodology, given in [6], at a 10% error in the average value, n = 23 parts is obtained. Therefore, with the accuracy, set this way, the dimension sub-tuning must be carried out after having 23 parts machined. If the work continues until reaching up this number of machined parts, with the dimension deviations measured during the process of boring (Table 2), the scatter diagram, shown in Fig. 4, is obtained.

TABLE 2 RESULTS OF CLEAN BORING OF A BATCH OF CYLINDRICAL BUSHINGS USING A STATISTICAL METHOD FOR DIMENSIONAL SUB-TUNING

№ of the part	Size, mm	№ of the part	Size, mm	№ of the part	Size, mm
1	29,54	9	29,37	17	29,36
2	29,44	10	29,44	18	29,29
3	29,52	11	29,39	19	29,19
4	29,53	12	29,29	20	29,32
5	29,44	13	29,39	21	29,20
6	29,41	14	29,29	22	29,14
7	29,48	15	29,36	23	29,25
8	29,47	16	29,24		

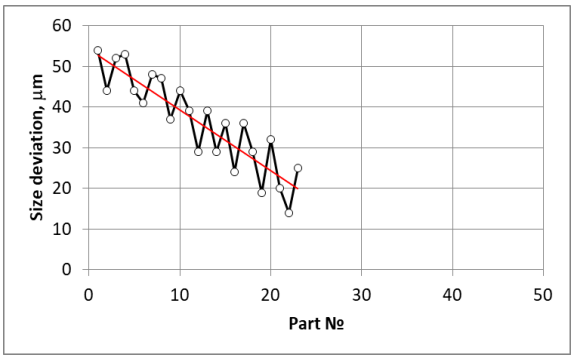

Fig. 4. Scatter diagram of the process of clean boring of a batch of cylindrical bushings with the application of a statistical method for dimensional sub-tuning

In this case, for the sub-tuning impulse it is obtained $\Delta\bar{A}_n = 33,5$ µm.

The total dispersion field determined by formula (5) is respectively ω_Σ = 64 µm.

Hence, when determining the sample volume statistically, twice as much error of machining is obtained for the specific case. Furthermore, the total dispersion field is greater than the dimension tolerance. Therefore, it is impossible to achieve the set accuracy of the average dimension value within the limits of the tolerance, which is a condition for making a sub-tuning decision.

IV. CONCLUSIONS

The conducted analysis allows to conclude that the proposed analytical approach for determining the moment for sub-tuning achieves significantly higher accuracy of the machined parts than if the number of parts between two sub-tunings is determined statistically. By applying this method, a total dispersing field comparable in size to the instantaneous one is obtained.

Consequently, dynamic dimension sub-tuning, based on the results of computer processing of the information about the dimensions of the machined parts in real time, is applicable and effective both for processes with small and with large dimension dispersion, caused by random factors.

V. ACKNOWLEDGMENTS

This research was funded by the European Regional Development Fund within the OP "Research, Innovation and Digitalization Programme for Intelligent Transformation 2021-2027", Project N° BG16RFPR002-1.014-0005 Center of competence "Smart Mechatronics, Eco-and Energy Saving Systems and Technologies".

REFERENCES

[1] Z. Driss, Mechanical Engineering Technologies and Applications Vol.1, e-book, DOI: 10.2174/9789814998185121010l, 2021.

[2] P. Leong, A Guide To Statistical Methods In Research With Cases & Applications: A Research Guidebook, Publisher: Independently published, April 6, 2021.

[3] T. Iyengar, M. Prasad, S. Ranganatham and B. Gandhi, Computer Oriented Statistical Methods, Publisher: S Chand Publishing, 2023.

[4] M. Chandra, Statistical Quality Control, Publisher: Taylor & Francis Inc, 2020.

[5] S. Salapateva, "Technological research for active control in CNC turning" dissertation, Technical University – Sofia, Plovdiv, Bulgaria, 2005.

[6] Bulgarian State Standard "Statistical Methods for Control - General Provisions", Quality Committee at the Council of Ministers of the Republic of Bulgaria, Sofia, 1986

Environment. Technology. Resources. Rezekne, Latvia
Proceedings of the 16th International Scientific and Practical Conference. 2025. Volume IV, 369-373

Cutting Modes in Multi-Pass Turning on CNC Lathes

Silviya Salapateva
Faculty of Mechanical Engineering
Technical University of Sofia, Plovdiv Branch,
Center of competence "Smart mechatronic, eco- and energy-saving systems and technologies"
Plovdiv, Bulgaria
sisisal@tu-plovdiv.bg

Angel Lengerov
Faculty of Mechanical Engineering
Technical University of Sofia, Plovdiv Branch,
Center of competence "Smart mechatronic, eco- and energy-saving systems and technologies"
Plovdiv, Bulgaria
alengerov@tu-plovdiv.bg

***Abstract*— Rolled workpieces are widely used when turning on CNC lathes. The difference between the dimensions and shape of the workpiece and the machine part in these cases is significant and it is necessary to remove the excess of material with the least possible loss of time. This is achieved by means of sequential execution of the work steps (passes) with the corresponding program cycles. Determining the number of passes and the corresponding cutting mode is an optimization problem, which is the subject of the present work.**

***Keywords*— machine building, CNC lathes, cutting modes**

I. INTRODUCTION

In order to achieve high efficiency in labor (high productivity), rough machining is normally performed in one work step, provided that the machine power and the strength of the technological system do not limit this possibility. With CNC machine tools, when rolled workpieces are used, the possibility of single-pass machining is determined not only by the abovementioned limitations, but also by the significant difference between the shape of the target machine part and the blank, which in most cases makes the allowance variable in size. Different schemes for removing the allowance are applied for the differently shaped rotatory profile surfaces, with the machining being carried out in multi-pass. Examples of organizing typical cycles for these cases are given in the specialized literature [1, 2]. Recommended tools and cutting modes are given by the manufacturers of cutting tools for turning [3].

The analysis of the recommended rough turning modes shows that in almost all cases the feed f_n per revolution of the workpiece is less than the depth of cutting a_p. On the one hand, this is determined by the relatively large cutting depth in rough turning and, on the other hand, by the desire to achieve a small height of the micro-roughness on the machined surface. While the latter is essential and important for the process of clean machining, either final or prior to finishing, in multi-pass rough machining the target function is productivity, not accuracy. In this sense, it is of interest to expand the range of research toward cases where the feed approaches or exceeds the depth of cut. Similar studies are reflected in publications [4, 5].

The aim of this study is to make more specific certain elements of the known analyses and complement them with solutions for productivity optimization of multi-pass roughing.

II. MATERIALS AND METHODS

Machining productivity, as a target function for optimizing the cutting mode, is usually represented by means of the basic (machine) time:

$$T_o = \frac{l_{px}}{\nu_f}, \text{ min}$$

or by the volume of the removed metal per unit of time:

$$w = a_p f_n \nu_c, \text{ cm}^3/\text{min},$$

where l_{px} is the length of the working pass in mm; ν_f – the speed of the feed drive in mm/min; a_p – the depth of cut in mm; f_n – the feed per revolution of the part in mm; ν_c – the cutting speed (of the main drive) in mm/min.

In the case of multi-pass machining on a CNC lathe, in addition to the time for the working passes $T_{px,,}$ the machine time should also include the time for the auxiliary strokes T_{cx}, without which it is impossible to accomplish the program cycle. An essential point in solving the optimization problem is determining the optimal number of working and auxiliary passes, which ensure the least machine time for the operation, and their corresponding operating mode. In this case the machine time formula will have the form:

$$T_o = T_м = T_{px} + T_{cx} \text{ min}, \quad (1)$$

Online ISSN 2256-070X
https://doi.org/10.17770/etr2025vol4.8424
© 2025 The Author(s). Published by RTU PRESS.
This is an open access article under the Creative Commons Attribution 4.0 International License.

$$T_o = \frac{1}{\nu_f}\sum_{i=1}^{n_{px}} l_{px\,i} + \frac{1}{\nu_{cx}}\sum_{i=1}^{n_{cx}} l_{cx\,i} \ \ \text{min},$$

where l_{cx} is the length of the auxiliary pass in mm; ν_{cx} – the speed of the auxiliary movement in mm/min; n_{px} – number of working passes; n_{cx} – number of auxiliary strokes.

In multi-pass cycles, when $n_{px} = n_{cx}$ and $l_{px} = l_{cx}$, formula (1) will have the form:

$$T_o = \sum_{i=1}^{n_{px}} l_{px\,i}\left(\frac{1}{\nu_f} + \frac{1}{\nu_{cx}}\right) \text{ min}. \qquad (2)$$

The optimization problem is solved by satisfying the system of constraints [6]:

1. *Regarding tool durability*

$$\nu_c(T) \le \frac{C_\nu K_\nu}{T^m a_p^{x_\nu} f_n^{y_\nu}} \text{ m/min}, \qquad (3)$$

where the constant, correction factor and exponents are selected from specialized reference books [7].

The limit, concerning the cutting speed, can also be determined by using the recommendations of the leading companies in tool manufacturing. For example, for rough machining of medium-carbon steel 45 by a P25 hard-alloy plate, the recommended cutting speed in accordance with the feed at a tool durability of 15 is given in Table 1.

TABLE 1 RECOMMENDED CUTTING SPEEDS [3]

f_n, mm	0,2	0,4	0,6	0,8
$\nu_{c,15}$, m/min	375	290	240	205

In case the tool life is greater than 15 min, the speed is adjusted by a coefficient, presented in Table 2.

TABLE 2 DURABILITY CORRECTION FACTOR [3]

T, min	15	20	25	30	60
$k_{\nu c}$	1	0,95	0,9	0,87	0,75

2. *Regarding cutting power*

$$P_c \le P_e\eta, \qquad (4)$$

where P_c is the cutting power; P_e – the electric motor power for the main drive in kW; η - efficiency coefficient of the main drive chain.

On the other hand [3]:

$$P_c = \frac{\nu_c a_p f_n k_{c;0,4}}{60.1000}\left(\frac{0,4}{f_n \sin\kappa_r}\right)^{0,29}, \qquad (5)$$

where $k_{c;0,4}$ is the coefficient of relative cutting resistance for a chip with a thickness of 0,4 mm in N/mm^2; κ_r – main angle of knife setting.

Solving (4) and (5) together, yields for ν_c:

$$\nu_c(P) = \frac{60.1000 P_e \eta}{a_p f_n k_{c;0,4}}\left(\frac{0,4}{f_n \sin\kappa_r}\right)^{-0,29} \text{ m/min}. \qquad (6)$$

3. *Regarding the permissible height of the surface roughness*

$$\left[R_z\right] \ge \varphi(f_n, r_\varepsilon, \kappa_r, \kappa_r') \text{ mm}, \qquad (7)$$

where κ_r' is the auxiliary angle of knife setting; $r\varepsilon$ is the radius of rounding at the tip of the knife in mm.

4. *Regarding the permissible cutting depth*

It is selected according to the type of the plate and the material under machining, following the recommendations, given by the cutting tool manufacturer.

The following equalities also apply to the optimization model:

1. *Of the number of working passes*

$$n_{px} = \frac{z}{a_p} \text{ (integer number)}, \qquad (8)$$

where z is the roughing allowance in mm.

2. *Of the chip cross-section*

$$S_c = a_p f_n - S_{Rz}, \qquad (9)$$

where S_{Rz} is the roughness cross-section in mm^2.

The roughness cross-section in formula (9) is likely to have a significant impact on the chip cross-section and cutting force only when $f_n > a_p$. Otherwise, it is ignored.

Examples of determining the function on the right-hand side of inequality (7), are shown in Fig. 1.

For a sharp-pointed knife (with a small radius of curvature at the tip), the cross-section of the roughness according to Figure 1a is obtained as:

$$S_{Rz} = \frac{0,5 f_n^2}{\frac{1}{\text{tg}\kappa_r} + \frac{1}{\text{tg}\kappa_r'}}. \qquad (10)$$

The roughness height is accordingly:

$$R_z = \frac{f_n}{\frac{1}{\text{tg}\kappa_r} + \frac{1}{\text{tg}\kappa_r'}}. \qquad (11)$$

For a round plate, according to Fig.1b, it is obtained:

$$S_{Rz} = R f_n\left(1 - 0,5\cos\frac{\alpha}{2}\right) - \pi R^2 \frac{\alpha}{360}. \qquad (12)$$

It is seen from Fig. 1 that it is necessary to impose a constraint on the feed magnitude. There is a limit, at which the height of the roughness reaches the depth of cut ($R_z = a_p$). In this case, the machining loses its meaning, because it does not create a new cylindrical surface, but forms a screw channel. This case is presented in Figure 2.

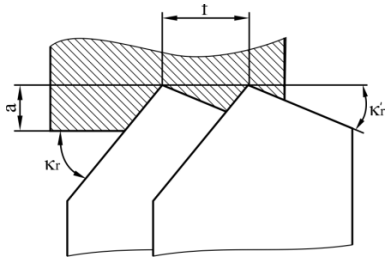

a. in turning by a sharp pointed knife

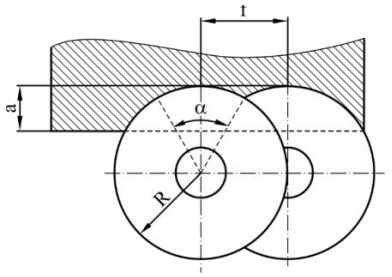

b. in turning by a knife with a round plate

Fig. 1. Roughness cross-section.

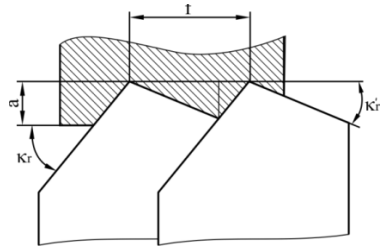

a. when turning with a sharp pointed knife

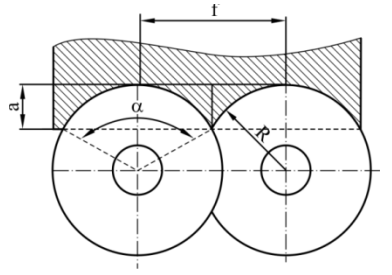

b. when turning by a knife with a round plate

Fig. 2. Limit feed.

The roughness height is accordingly:

$$R_z = R\left(1-\cos\frac{\alpha}{2}\right), \qquad (13)$$

where R is the radius of the round plate in mm.

$$\alpha = 2\arcsin\left(\frac{f_n}{2R}\right). \qquad (14)$$

Similar formulas for the height and cross-section of the roughness can be derived for other types of geometry of the knife's cutting part.

If a condition is set that the limit roughness height is $R_{z,lim} = 0{,}1a_p$, which in practice means that the cutting depth for clean turning must be greater than this height ($a_{p\ clean} > 0{,}1\ a_{p\ rough}$), for the limit feed in the considered examples it will be obtained:

- with a sharp pointed knife:

$$f_{n,lim} = 0{,}1a_p\left(\frac{1}{tg\kappa_r}+\frac{1}{tg\kappa_r'}\right); \qquad (15)$$

- with a round plate:

$$f_{n,lim} = 0{,}2\sqrt{20a_pR-a_p^2}\,. \qquad (16)$$

For example, when a square hard-alloy plate is used, with $\kappa_r = 75^o$, $\kappa'_r = 15^o$, the following feed will be obtained: $f_{n,lim} = 0{,}4a_p$. That is, the limit feed is less than the depth of cut.

For working with round plates at R = 8 mm and $a_p = 2$ mm, from formula (16) it is obtained that $f_{n,lim} = 3{,}55$ mm, i.e., in this case the limit feed is greater than the cutting depth.

It is indicative for both examples that the cross-section of the roughness is relatively small and can be taken into account when determining the cutting force and power.

For rough turning with high feed, it is appropriate to work with purposefully designed hard-alloy plates [7]. Their geometry and recommended cutting modes are listed in the manufacturer's catalog.

III. RESULTS AND DISCUSION

A. Optimization model

The conditions of the optimization problem, considered so far, show that the solution must be sought when working with a large volume of statistical data, obtained experimentally and presented tabularly. The possible approach for this case is numerical optimization. The variable parameter of the mode is the cutting depth (the number of working passes) with the machine time being the target function and the constraints and conditions of the optimization problem described by inequalities and equalities.

The numerical optimization algorithm will contain the following stages and procedures:

1. Selection of a metal cutting tool for roughing

The initial conditions are the type and quality of the material to be machined and the geometric shape of the machined surface. The selection is made based on information, provided by the selected cutting tool manufacturer.

2. Determining the domain of definition for the problem solution

In this case the limiting values of the cutting depth and feed must be defined, since they outline the domain for searching for the solution, leading to the least machine time.

The manufacturer's recommendations for $a_{p\ max}$, $a_{p\ min}$ and the corresponding $f_{n\ min}$, $f_{n\ max}$ are used as initial conditions.

3. Selection of a multi-pass cycle for roughing

The cycle is determined by the geometric shape of the machined surface and the selected tool.

4. Establishing the specific (partial) equation for the target function with the selected multi-pass machining cycle.

5. Scanning the optimization area and finding T_o, min.

Application example: Step turning of a semi-open cylindrical section

Example implementation is shown in Fig.3.

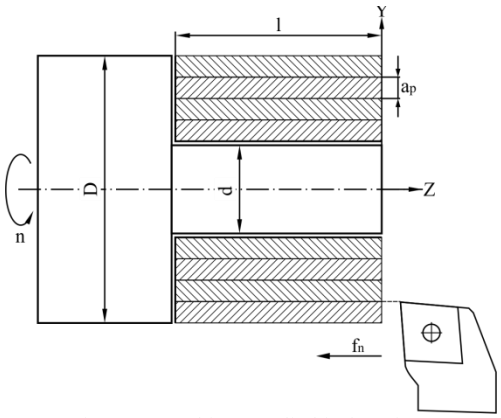

Fig. 3. Multi-pass cylindrical turning .

B. Description of the algorithm

1. The material under machining is medium carbon unhardened steel 45 with a hardness HB of 150 units. The target part is cylindrical in shape with step dimensions D = 100 mm; d = 70 mm; l = 100 mm.

According to [7], the appropriate rough turning tool is made of hard alloy GC4025 (P25), with a rhomboid metal-ceramic plate CNMG120412, having a tip radius r_ε = 1,2 mm; $\kappa_r = 95^o$, $\kappa'_r = 5^o$. The length of the side of the plate is 12 mm.

2. Domain of definition for the problem solution:

a) The manufacturer's recommendation for the pair $a_{p\ max}$, $f_{n\ min}$: $a_{p\ max}$ = 5 mm, $f_{n\ min}$ = 0,2 mm will be used as an initial condition.

b) The recommended in Table 1 cutting speed is $\nu_{c,15}$ = 375 m/min. For a tool durability of 25 min, the correction factor is 0,9 and for the speed it is obtained $\nu_{c,25} = 0{,}9\nu_{c,15}$ = 337,5 m/min.

c) Checking for a power limit at Pe = 6.5 kW, η = 0.8 and $k_{c;0,4}$= 2100 N/mm^2 according to formula (6):

$$\nu_c \le \frac{60.1000.6,5.0,8}{5.0,2.2100}\left(\frac{0,4}{0,2\sin 95^o}\right)^{-0,29}, \text{ m/min.}$$

$$\nu_c = 182 \text{ m/min.}$$

Hence, the cutting speed must be 182 m/min.

d) Determining the limit $a_{p\ min}$, $f_{n\ max}$. The recommended minimum cutting depth for rough turning with the selected tool is $a_{p\ min}$ = 0,5 mm.

The recommended maximum feed value at r_ε = 1,2 mm is from 0,5 to 1 mm. It is assumed that $f_{n\ max}$ = 1 mm.

The recommended cutting speed for this feed value is $\nu_{c,25}$ = 167 m/min.

From formula (6) for the cutting speed it is obtained:

$$\nu_c \le \frac{60.1000.6,5.0,8}{0,5.1.2100}\left(\frac{0,4}{0,2\sin 95^o}\right)^{-0,29}, \text{ m/min.}$$

ν_c = 363,7 m/min.

Consequently, the cutting speed must be 167 m/min.

Finally, for the definition of the domain it is obtained:

$a_{p\ max}$ = 5 mm, $f_{n\ min}$ = 0,2 mm, ν_c = 182 m/min;

$a_{p\ min}$ = 0,5 mm, $f_{n\ max}$ = 1 mm, ν_c = 167 m/min.

3. Selecting a multi-pass cycle for roughing

The cycle is presented in Figure 3.

4. Establishing the specific (partial) equation for the target function with the selected multi-pass cycle of machining

Formula (2) is used to determine the machine time, and the number of working passes is determined by formula (8).

For each of the listed feeds per workpiece revolution f_n,, the minute feed f_o will be different for the sequential working passes, since the diameter of the machined surface changes. At ν_c = const the frequency of rotation will increase from the diameter of the workpiece to the diameter of the machine part and so will f_o accordingly. To simplify the solution in this case, the average feed $\overline{f}_o$ can be used:

$$\overline{f}_o = n_{cp} f_n, \text{ where } n_{cp} = \frac{2000\nu_c}{\pi(D+d)}. \qquad (17)$$

Thus, the machine time for the working passes is obtained:

$$T_{px} = \frac{il_{px}}{\overline{f}_o}. \qquad (18)$$

5. Scanning of the workspace will be performed at variable values of the cutting depth a_p = 0,5; 1,0; 1,5; 2,0; 2,5; 3,0 mm and for the feed per revolution of the part, respectively f = 0,25; 0,50; 0,75; 1,00 mm.

The cutting speed will be determined by the manufacturer's recommendation, presented in Table 1 and will be corrected for a tool durability of 25 min, according to Table 2, with a limit on the machine's power according to formula (6).

Multi-pass machining is performed at the specified speed ν_c = const.

The obtained results for the cutting speed are presented in Table 3.

TABLE 3 CUTTING SPEED ACCORDING TO TOOL LIFE (IN NUMERATOR) AND ALLOWABLE BY MACHINE POWER (IN DENOMINATOR)

a_p, mm	f_p, mm			
	0,25	**0,50**	**0,75**	**1,0**
0,5	315 1036	235 634	190 475	167 387
1,0	315 518	235 317	190 239	167 194
1,5	315 348	235 211	190 158	167 129
2,0	315 259	235 159	190 119	167 97
2,5	315 207	235 127	190 95	167 77
3,0	315 173	235 106	190 79	167 65

Of the two speeds, the lower one is selected for operation.

The results for the machine time are presented in Table 4. The speed of the auxiliary movement is assumed to be ν_{cx} = 6000 mm/min.

TABLE 4 CUTTING SPEED ν_c (IN NUMERATOR) AND MACHINE TIME $T_м$ (IN DENOMINATOR)

a_p, mm	i, number of passes	f_n, mm			
		0,25	**0,50**	**0,75**	**1,0**
0,5	**30**	315 10,67	235 7,31	190 6,12	167 5,29
1,0	**15**	315 5,33	235 3,66	190 3,06	167 2,65
1,5	**10**	315 3,56	211 2,70	158 2,42	129 2,42
2,0	**8**	259 3,43	159 2,82	119 2,53	97 2,33
2,5	**6**	207 3,19	127 2,62	95 2,35	77 2,18
3,0	**5**	173 3,17	106 2,60	79 2,34	65 2,14

To illustrate the analysis, some typical results are presented in Figure 4.

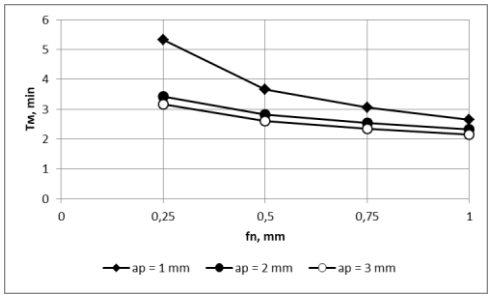

Fig. 4. Machine time.

With the proposed algorithm and methodology for numerical analysis, possibilities for optimizing the cutting mode in multi-pass machining of other types of rotary profile surfaces can be considered.

IV. CONCLUSIONS

The presented analysis for optimizing the cutting modes in multi-pass turning on CNC machine tools allows to draw the following conclusions:

1. The developed algorithm and methodology for numerical analysis make it possible to find cutting modes, ensuring maximum productivity in multi-pass roughing of rotary profile surfaces by turning.

2. For rough turning, it is advisable to use tools, purposefully designed by the tool manufacturers, and providing the possibility to work with large feeds at relatively slight roughness of the machined surface.

3. The cutting speed for small cross-sections of the cut layer is limited by the durability of the tool, and for larger cross-sections - by the permissible cutting power.

4. After reaching a limit in the cross-section of the cut layer, at which the cutting power reaches the permissible value, maximum productivity is achieved for the specific conditions of machining. Further increase in the cross-section by means of the feed does not lead to an increase in productivity. This is confirmed by the considered example and the results, presented in Table 4 and Figure 4.

5. The previous conclusion gives reason to recommend the introduction of adaptive power control in multi-pass rough turning, which will ensure self-programming of the number of working passes while achieving maximum productivity for the set cutting power.

6. Among all cutting modes, providing approximately the same productivity, it is advisable to prefer those, in which the tool durability will be greater.

ACKNOWLEDGMENTS

This research was funded by the European Regional Development Fund within the OP “Research, Innovation and Digitalization Programme for Intelligent Transformation 2021-2027”, Project Nº BG16RFPR002-1.014-0005 Center of competence “Smart Mechatronics, Eco-and Energy Saving Systems and Technologies”.

REFERENCES

[1] T. Kuzmanov, V. Georgiev, H. Metev, Technological processes for CNC machine tools, Publisher: Eks-Pres”, Gabrovo, 2007.

[2] K. Kumar, Chikes Rabjan, J. Davim, CNC Programming for Machining (Materials Forming, Machining and Tribology), Publisher: Springer Nature Switzerland, 2020.

[3] www.sandvikcoromant.org

[4] N. Yemelyanov, I. Yemelyanova, V. Zubenko, “Improving Machining Accuracy Of Cnc Machines With Innovative Design Methods”, IOP Conference Series Materials Science and Engineering, DOI:10.1088/1757-899X/327/4/042028, 2018.

[5] V. Georgiev, S. Salapateva, “Increasing productivity in CNC turning”, Notices of the Technical University in Plovdiv, vol.10, pp.101-107, 2023.

[6] D. Stephenson, J. Agapiou, Metal Cutting Theory and Practice, Publisher: CRC Press, 2019.

[7] A. Averchenkov, B. Bazrov, et al., Handbook of a mechanical engineer in 2 volumes, Publishing House: Mashinostroenie, Moscow, 2023.

Environment. Technology. Resources. Rezekne, Latvia
Proceedings of the 16th International Scientific and Practical Conference.2025. Volume IV, 375-382

Effect of Infill Pattern Design on Tensile Strength of Fused Deposition Modelled Specimens

Jaymin Vrajlal Sanchaniya
Institute of Mechanical and Biomedical Engineering
Riga Technical University
Riga, Latvia
Jaymin.Sanchaniya@rtu.lv

Karunamoorthy Rengasamy Kannathasan
Institute of Mechanical and Biomedical Engineering
Riga Technical University
Riga, Latvia
karunamoorthy.rengasamy-kannathasan@rtu.lv

Sanjay Rajni Vejanand
Institute of Mechanical and Biomedical Engineering
Riga Technical University
Riga, Latvia
sanjay.vejanand@rtu.lv

Jay Joshi
Institute of Mechanical and Biomedical Engineering
Riga Technical University
Riga, Latvia
jay-ashokkumar.joshi@edu.rtu.lv

Inga Lasenko
Institute of Mechanical and Biomedical Engineering
Riga Technical University
Riga, Latvia
inga.lasenko@rtu.lv

***Abstract*—Deep knowledge of the connections between additive manufacturing design elements and the mechanical qualities of additive manufactured products becomes essential as the adoption of technology expands. Research analyses how the arrangement of material inside the printed object affects the tensile strength in specimens made through fused deposition modelling. The evaluation of 18 different infill patterns occurred through standardised tests, while technicians maintained identical processing parameters that included print temperature and both layer height and print speed. The test specimens underwent tensile testing for mechanical analysis. The test results indicate that the concentric pattern delivers maximum elastic modulus values at 1078 MPa, as well as a maximum tensile strength of 26.4 MPa which exceeds other patterns by 12-62% for modulus and 24-98% for strength. The elongation-at-break measurement of 10.5% is the best result for this pattern because it offers 10-338% more flexibility than competing structures. The elastic modulus (665 MPa) and the tensile strength (13.3 MPa) of the lightning pattern are the minimum among all tested patterns. The study also evaluated mass efficiency through strength-to-mass ratio calculations, with the concentric pattern achieving the highest value of 29.7 MPa/g, demonstrating superior weight-normalised mechanical performance alongside its absolute strength advantages. The study provides essential data on the performance-mechanical relationship of infill patterns that allow improvements to additive manufacturing processes to enhance structural integrity. These important results provide guidance for designers working on products that need particular mechanical characteristics.**

Keywords*— Infill pattern, additive manufacturing, tensile test, fused filament fabrication.

I. Introduction

Additive manufacturing technologies gained speed in development to produce complex structural components with minimal waste while managing small production runs efficiently [1]. The technological progress has triggered worldwide research efforts to use polymers across all dimensional scales from nanoscale to macroscale manufacturing of components [2]–[7]. The adoption of additive manufacturing technologies grows rapidly within different industries where notable advancements occur in automotive [8], aerospace [9], biomedical [10], construction [11], [12] and healthcare applications [13] which extend to dental usage and surgical requirements, orthopaedic implant production, tissue engineering work and pharmaceutical manufacturing [14].

Fused filament fabrication (FFF) represents a cost-friendly and flexible manufacturing method which dominates the production of polymeric, composite, and multimaterial components through 3D printing. FFF technology supports a wide range of thermoplastics beyond acrylonitrile butadiene styrene (ABS), polylactic acid (PLA) [15], polycarbonate (PC) [16] and polyamide (PA) [17] which are the most frequently used plastics. Thermoplastic polyurethane (TPU) [18] along with Polyethylene (PE) [19] and Polypropylene (PP) belong to the elastomer category of materials while polyglycolic acid

Online ISSN 2256-070X
https://doi.org/10.17770/etr2025vol4.8409
© 2025 The Author(s). Published by RTU PRESS.
This is an open access article under the Creative Commons Attribution 4.0 International License.

(PGA) and polycaprolactone (PCL) fall under the polyesters group, and the advanced engineering polymers group includes polyoxymethylene (POM), polyetheretherketone (PEEK), polyetherimide (PEI), polyphenylene sulphide (PPS), polysulfone (PSU) polyvinylidene fluoride (PVDF) [20].

The weight efficiency of 3D printed components represents another critical aspect of the optimisation of the FFF process that receives insufficient research attention. When mechanical performance is evaluated relative to material usage through metrics such as strength-to-mass ratios, the true practical value of different infill patterns becomes apparent. This consideration becomes particularly relevant in applications where lightweight, yet strong components are required, such as in aerospace and portable biomedical devices. The comparative analysis of weight efficiency metrics complements traditional mechanical testing by revealing which patterns deliver optimal performance per unit mass.

Various design parameters determine the mechanical behaviour of parts created through 3D printing such as extrusion temperature, build plate temperature, printing speed, extrusion speed, print orientation, layer thickness, raster angle, width and air gaps, nozzle diameter, ambient temperature and humidity, and infill pattern with density [21]–[25]. The influence of infill patterns on mechanical strength receives less research attention than other FFF process parameters, including layer thickness and raster width and orientation.

The analysis of infill patterns in previous research focused on limited options, but the available patterns continue to grow to cover various applications [26]–[29]. Analysis of infill patterns consists of rectilinear, honeycomb, Hilbert curve, octagram, star-shaped, and triangular arrangements. Standardised research does not exist to evaluate the 18 different fill patterns that exist today. This research fills the current knowledge gap by performing a systematic pattern-by-pattern comparison of all 18 infill designs using PLA material, which reveals crucial findings about FFF-manufactured component performance and pattern selection.

II. Materials and Methodology

The test samples used commercial filaments (Prusa Research a.s., Czech Republic) that had 1.75 mm diameter. The specimens followed the dimensioning requirements of ISO 527-5A and received printing on a Prusa Mini machine that used a glass fibre build plate.

The production of complete test specimens using PLA relied on the conditions and parameters presented in Table 1 for the consistency of the FFF process. The drying process at 40 °C for one hour (using eSUN eBOX Lite) was designed to remove moisture and prevent potential manufacturing problems in both the print quality and the mechanical characteristics of the material.

Table 1 Summary of FFF Process Conditions and Parameters

Printing specifications	Value, description
Filament (Ø 1.75 mm)	PLA
3D printer	Prusa Mini
Printer chamber	Semi-open
Nozzle diameter (mm)	0.4
Build plate	Glass fibre
Extrusion temperature (°C)	230
Built plate temperature (°C)	65
Print speed (mm/s)	25
Layer thickness (mm)	0.1
Shell thickness (mm)	0.1 mm
Infill density (%)	40

A layer thickness of 0.1 mm was selected as an optimal compromise between structural integrity [20], mechanical performance, and production efficiency. The width of the infill line (raster) was automatically configured by PrusaSlicer to approximately 0.35 mm when using a 0.4 mm diameter nozzle. All printed samples featured patterned infills encapsulated within a 0.1 mm thickness.

While maintaining all other parameters constant, 18 distinct infill patterns with the mentioned designation: Rectilinear (S1), Aligned Rectilinear (S2), Grid (S3), Triangles (S4), Stars (S5), Cubic (S6), Line (S7), Concentric (S8), Honeycomb (S9), 3D Honeycomb (S10), Gyroid (S11), Hilbert curve (S12), Archimedean Chords (S13), Octagram Spiral (S14), Adaptive Cubic (S15), Support Cubic (S16), Lightning (S17) and Zig Zag (S18). Figure 1 illustrates all of the 18 fill patterns used in this study.

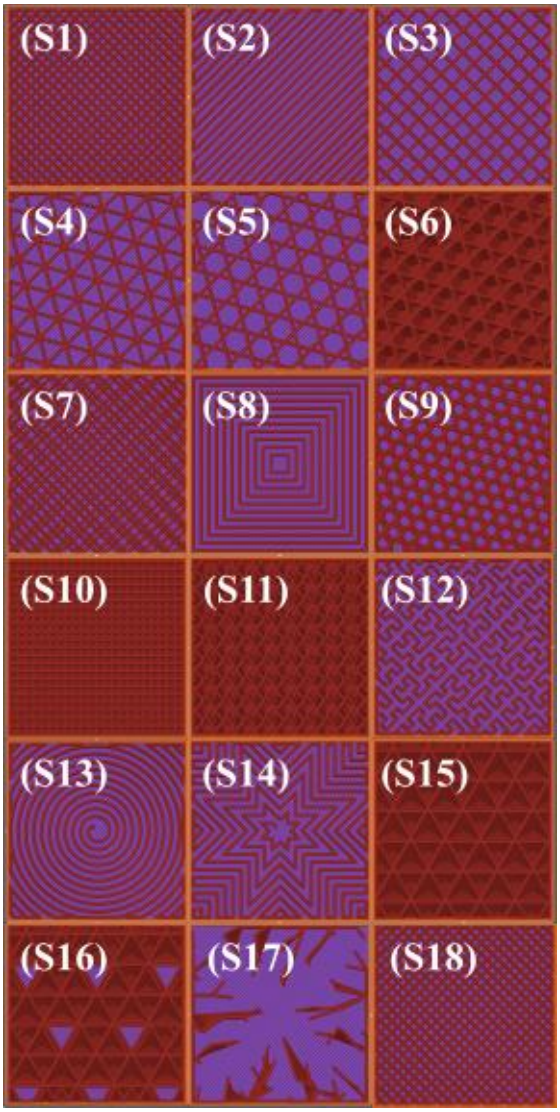

Fig. 1. Visualization of the eighteen infill patterns tested in this study: Rectilinear (S1), Aligned Rectilinear (S2), Grid (S3), Triangles (S4), Stars (S5), Cubic (S6), Line (S7), Concentric (S8), Honeycomb (S9), 3D Honeycomb (S10), Gyroid (S11), Hilbert curve (S12), Archimedean Chords (S13), Octagram Spiral (S14), Adaptive Cubic (S15), Support Cubic (S16), Lightning (S17) and Zig Zag (S18).

Tensile testing of 90 specimens used five replicate samples for each infill pattern design. The experimental tests were executed on a Mecmesin Multi-Test 2.5-i tensile testing machine from PPT Group UK Ltd. (traded as Mecmesin, based in Slinfold, UK) provided with a 250 N sensor. All test conditions received a 1 mm/min uniaxial tensile loading rate as a standardised delivery speed.

Figure 2 illustrates one group of prepared specimens manufactured according to the specified standards.

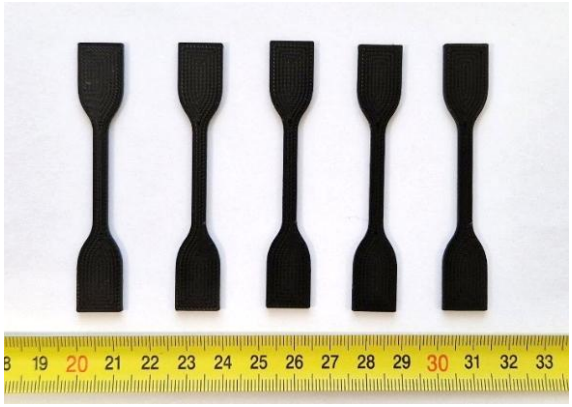

Fig. 2. ISO 527-5A compliant tensile test specimens produced by FFF.

Standardised testing procedures allowed researchers to obtain accurate measurements of mechanical properties, which included elastic modulus along with the ultimate tensile strength and elongation at break. The method provided standardised procedures for valid comparison testing of different fill structures by controlling experimental factors, which are shown in Table 1. Before testing, the specimens were kept under controlled ambient conditions to avoid environmental factors (temperature 23 °C ± 1, relative humidity 30-50%, standard atmospheric pressure: 1 atm) that could alter the results. Mass measurements were performed using a high-precision KERN ABT 5NM scale, which boasts a maximum capacity of 100 g and a precision of 0.000001 g, thus ensuring accurate and reliable results.

III. Results and Discussion

A. Tensile Behaviour of Different Infill Patterns

Tests of 18 different infilled sample arrangements showed substantial variations in their mechanical properties through tensile experiments. Representative stress-strain curves exist for each designation of the infill pattern (S1-S18) which demonstrates different uniaxial loading behaviours as shown in Figure 3.

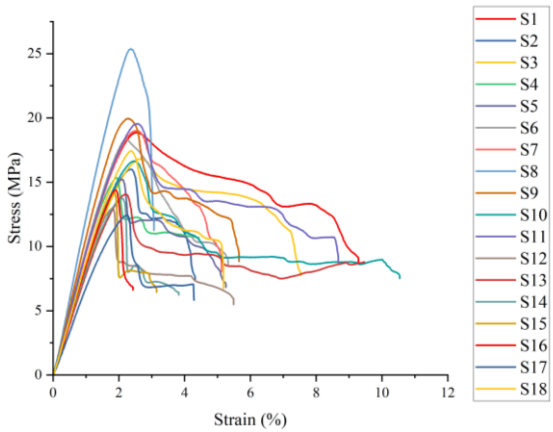

Fig. 3. Representative stress-strain curves for 18-different infill patterns (S1-S18).

The stress-strain curves show elastic behaviour as their first stage and then exhibit yielding before entering the plastic deformation portion. There is a substantial range of elastic modulus combined with maximum tensile strength and elongation at break differences between the tested infill patterns. Patterns S1, S8, and S11 displayed stress peaks that resulted in stepwise failures, while patterns S10 and S13 showed sustained stretching abilities before failure occurred.

S8 showed the strongest mechanical results through its 1078 ± 45 MPa elastic modulus and 26.4 ± 2.3 MPa ultimate tensile strength. Pattern architecture advances stress distribution because its circular loop design spreads tensile loads evenly throughout the entire structure. The tensile loading direction of the material in the deposit promotes beneficial strain patterns throughout the sample area.

The total results of the tensile test demonstrated the lightning pattern (S17) was the weakest arrangement since it contained the lowest elastic modulus (665 ± 61 MPa) coupled with the weakest tensile strength (13.3 ± 1.9 MPa). The lightning pattern displays critical weaknesses that lead to a substantial reduction in elastic modulus (38% less than the concentric pattern) and ultimate tensile strength (50% weaker than the concentric pattern). Material reduction takes priority at the expense of structural integrity in this design. Experiment results shows that the randomly created non-uniform path format within the print structure introduces serious weaknesses, which deteriorate when exposed to tensile forces.

Mass measurements revealed significant variations between the different infill pattern configurations. The lightest specimen was the lightning pattern (S17) at 0.661 g, while the honeycomb pattern (S9) produced the heaviest specimens at 0.974 g, representing a 47% difference in material usage. This weight variation directly impacts the practical application of these patterns, particularly in weight-sensitive contexts.

Regarded as one of the best performers, the 3D honeycomb pattern (S10) achieved an outstanding elongation at a break value of 10.5 ± 1.4% which exceeded all other pattern configurations with respect to flexibility and failure deformation capacity. Multiple layers of interconnected cells in the structure enable progressive deformation, for which ductility improves significantly.

All tested infill patterns received a full analysis of mechanical properties in Table 2 using elastic modulus, ultimate tensile strength, and elongation at break measurements.

The elastic modulus measurements spanned from 665 ± 61 MPa, to 1078 ± 45 MPa while showing a total difference of 62% between the tested patterns. The maximum tensile strength measured between 13.3 ± 1.9 MPa and 26.4 ± 2.3 MPa and created a 98% difference between the lowest and highest values. The ductility performance demonstrated the largest variation because the elongation at break results reached between 2.4% and 10.5%, resulting in a 338% difference between the patterns.

TABLE 2 SUMMARRY OF MECHANICAL PROPERTIES AND WEIGHT FOR 18 INFILL PATTERNS

No.	Pattern Type	Elastic Modulus, E MPa	Ultimate Tensile Strength, σ_{max} MPa	Elongation at Break, Strain ε %	Mass (g)	S:M ratio (MPa/g)
S1	Recti-linear	930 ± 84	20.1 ± 1.1	9.3 ± 1.8	0.893	22.5
S2	Aligned Recti-linear	795 ± 80	17.2 ± 2.3	4.3 ± 0.6	0.884	19.4
S3	Grid	850 ± 52	17.7 ± 1.2	7.5 ± 0.8	0.842	21.0
S4	Triangles	912 ± 82	16.8 ± 0.9	4.5 ± 0.3	0.871	19.2
S5	Stars	837 ± 46	16.2 ± 1.5	5.2 ± 0.9	0.847	19.1
S6	Cubic	942 ± 85	19.2 ± 1.7	5.3 ± 0.7	0.865	22.2
S7	Line	948 ± 76	20.1 ± 1.9	5.1 ± 0.4	0.884	22.74
S8	Concen-tric	1078 ± 45	26.4 ± 2.3	3.0 ± 0.3	0.889	29.7
S9	Honeycomb	971 ± 67	21.1 ± 3.1	5.6 ± 0.9	0.974	21.6
S10	3D honey-comb	892 ± 98	17.7 ± 2.3	10.5 ± 1.4	0.887	19.9
S11	Gyroid	915 ± 57	20.4 ± 1.2	8.7 ± 0.9	0.854	23.8
S12	Hilbert Curve	851 ± 65	14.0 ± 1.1	5.5 ± 0.6	0.898	15.5
S13	Archimedean Chords	730 ± 92	15.3 ± 2.7	9.5 ± 1.6	0.879	17.4
S14	Octagram Spiral	785 ± 81	14.9 ± 1.1	3.8 ± 0.6	0.885	16.8
S15	Adaptive Cubic	820 ± 73	15.2 ± 1.7	3.1 ± 0.2	0.757	20.1
S16	Support Cubic	790 ± 55	15.3 ± 1.5	2.4 ± 0.2	0.760	20.1
S17	Lightning	665 ± 61	13.3 ± 1.9	4.3 ± 0.5	0.661	20.1
S18	Zig Zag	837 ± 74	18.5 ± 1.1	5.1 ± 1	0.869	21.3

The rectilinear pattern (S1) maintained balanced mechanical properties that featured moderate strength of 20.1 ± 1.1 MPa alongside good elongation capacity of 9.3 ± 1.8%. The orthogonal design of this pattern combines strong tensile resistance with sufficient ductility properties. The gyroid pattern (S11) exhibited balanced performance characteristics because it showed a strength of 20.4 ± 1.2 MPa in addition to an elongation of 8.7 ± 0.9% elongation.

The representative sample in Figure 4 shows failure that occurred within the gauge length thus validating the testing methodology.

Fig. 4. Representative fractured tensile sample showing stress concentration in the centre region.

Each fracture surface showed distinct characteristics related to the patterns used in the infill. Massive plastic deformation occurred before failure on fracture surfaces which appeared irregular due to flexible patterns (3D honeycomb, Archimedean chords) while specimens with rigid patterns (concentric, rectilinear) presented neat fracture surfaces with minor necking.

B. Pattern-Specific Performance Analysis

The mechanical response depends heavily on the way the materials get arranged during the printing process. Patterns featuring continuous filament alignment parallel to the tensile force direction (concentric-S8 and rectilinear aligned-S2) produced better tensile strength than patterns having mainly perpendicular or angular material distributions [30], [31].

A continuous circular path in the concentric pattern (S8) provides outstanding performance by aligning materials with tensile loading and minimising interlayer bond weakness which results in tensile strength of 26.4 ± 2.3 MPa [32]. The structural alignment system distributes stresses across all components until failure occurs at all points simultaneously [33].

The 3D honeycomb structure (S10) achieves its high elongation of 10.5% because its three-dimensional configuration allows the material to stretch progressively between multiple layers [34]. The geometric arrangement allows the pattern to function by deforming locally until it reaches failure but avoids complete failure and enables substantial plastic deformation before total separation [35].

The lightning pattern (S17) and support cubic (S16) showcase the worst mechanical performance because their nonuniform material distribution patterns lead to a low strength value of 13.3 ± 1.9 MPa and minimal elongation capability of 2.4% [36]. The structural weaknesses within these patterns stem from their design choice of material reduction and functional needs, which overrides mechanical performance [37].

The grid pattern (S3) achieved moderate success in all mechanical testing results (850 ± 52 MPa modulus, 17.7 ± 2.3 MPa strength, 7.5% elongation) because it optimises mechanical behaviour without surpassing any particular requirement.

When analysing mechanical performance relative to material usage, the concentric pattern (S8) demonstrated exceptional efficiency with a strength-to-mass ratio of 29.7 MPa/g. This represents a 92% improvement over the least efficient pattern, the Hilbert curve (S12), which achieved only 15.5 MPa/g. The gyroid pattern (S11) also performed admirably in weight-normalised terms with an S:M ratio of 23.8 MPa/g, highlighting its potential for applications where both strength and weight considerations are critical.

C. Relationship Between Pattern Design and Mechanical Properties

The results show multiple key connections that exist between the designed infill pattern features and the mechanical outcomes.

- The mechanical strength of specimen produced via FFF increased when parallel material paths were used as concentric (S8) or rectilinear patterns (S1) [38], [39].
- Ductility and elongation improved when using three-dimensional interconnected structures which include the 3D honeycomb (S10) and gyroid patterns (S11) [40].
- The perpendicular material orientation in the cubic (S6) and lightning patterns (S17) reduced mechanical strength and stiffness to a significant extent [41].
- Mechanical performance improved independently of geometric complexity because the simple concentric pattern exceeded both the Hilbert curve (S12) and octagram spiral designs (S14) [42].
- The weight efficiency varied substantially between the patterns, with the concentric pattern (S8) achieving the highest strength-to-mass ratio of 29.7 MPa/g, while patterns with complex geometries such as the Hilbert curve (S12) showed lower efficiency at 15.5 MPa/g despite using similar amounts of material.

The mechanical properties of 3D printed objects depend mainly on three factors, including material orientation compared to structural stress [43], the uninterrupted nature of the printing path [44] as well as the complete network of printed material throughout the component [45]. The mechanical properties of the optimised factors improved in every design independently of the dimensional complexity [46].

The study presents thorough performance assessments of infill patterns, but readers should note its underlying restrictions. The study results only apply to the design of the standardised test specimen design used for this research. The relative performance between patterns can change with different component aspects along with dimension variations due to scaling effects and geometry-based stress distributions.

The mechanical properties remain valid only for PLA material processed under the described conditions. Materials with distinctive crystallinity levels and different molecular weights and additive components may show different relative performances of the infill patterns. Different infill patterns may show changes in their relative performance levels due to environmental factors which include ambient temperature, humidity, and ageing effects.

Standard tensile testing occurs at 1 mm/min strain rate and ambient temperature to generate comparable results yet fails to replicate dynamic loading conditions or high temperatures and creep effects. Future studies which will examine performance under different loading conditions.

Despite certain limitations, the extensive study of 18 unique infill patterns gives engineers valuable tools to select appropriate patterns that maximise component performance according to specific use requirements.

IV. CONCLUSION

The extensive research analysed 18 infill patterns which produced substantial differences in the mechanical characteristics of FDM-printed PLA specimens. The concentric pattern (S8) exhibited superior structural properties because it achieved the highest elastic modulus at 1078 ± 45 MPa along with the ultimate tensile strength at 26.4 ± 2.3 MPa, yet the 3D honeycomb pattern showed remarkable elongation capabilities at 10.5%. The research findings demonstrate that pattern shapes affect mechanical characteristics through path alignment internation and interconnecting forms that enhance performance.

Beyond absolute mechanical performance, the study also revealed significant variations in mass efficiency in all the tested patterns. The concentric pattern not only exhibited superior mechanical properties, but also demonstrated the highest strength-to-mass ratio at 29.7 MPa/g, which represents a critical metric for weight-sensitive applications. This efficiency parameter provides designers with an additional selection criterion when optimising components for specific use cases where both strength and weight considerations are paramount. Substantial variations in S:M ratios—ranging from 15.5 to 29.7 MPa / g, highlight the importance of pattern selection for weight-efficient design in additive manufacturing.

Pattern selection emerges as a vital design parameter for additive manufacturing because it leads to significant variations in performance levels that reach up to 62% in modulus and 98% in strength and 338% in elongation. Research provides quantitative engineering recommendations which allow designers to enhance component performance by matching infill patterns to application needs, thus improving procedures and structural robustness in 3D-printed parts.

V. ACKNOWLEDGEMENTS

This work has been supported by postdoctoral grant No RTU-ZG-2024/1-0048 under the EU Recovery and Resilience Facility funded project No. 5.2.1.1.i.0/2/24/I/CFLA/003 “Implementation of consolidation and management changes at Riga Technical University, Liepaja University, Rezekne Academy of Technology, Latvian Maritime Academy and Liepaja Maritime College for the progress towards excellence in higher education, science, and innovation”.

REFERENCES

[1] S. Salifu, D. Desai, O. Ogunbiyi, and K. Mwale, “Recent development in the additive manufacturing of polymer-based composites for automotive structures—a review,” *Int. J. Adv. Manuf. Technol.*, vol. 119, no. 11, pp. 6877–6891, 2022, doi: 10.1007/s00170-021-08569-z.

[2] J. V. Sanchaniya *et al.*, “A Novel Method to Enhance the Mechanical Properties of Polyacrylonitrile Nanofiber Mats: An Experimental and Numerical Investigation,” *Polymers (Basel).*, vol. 16, no. 7, p. 992, Apr. 2024, doi: 10.3390/polym16070992.

[3] J. V. Sanchaniya, I. Lasenko, V. Gobins, and A. Kobeissi, “A Finite Element Method for Determining the Mechanical Properties of Electrospun Nanofibrous Mats,” *Polym.*, vol. 16, no. 6, p. 852, 2024, doi: 10.3390/polym16060852.

[4] J. V. Sanchaniya *et al.*, “Mechanical and Thermal Characterization of Annealed Oriented PAN Nanofibers,” *Polymers (Basel).*, vol. 15, no. 15, 2023, doi: 10.3390/polym15153287.

[5] J. V. Sanchaniya, I. Lasenko, S. P. Kanukuntla, A. Mannodi, A. Viluma-gudmona, and V. Gobins, “Preparation and Characterization of Non-Crimping Laminated Textile Composites Reinforced with Electrospun Nanofibers,” *Nanomaterials*, vol. 13, no. 13, p. 1949, 2023, doi: 10.3390/nano13131949.

[6] K. R. Kannasthan, A. Krasnikovs, and A. Macanovskis, “Ingredients Degradation in Steel Fiber Reinforced Concrete after Thermal Loading,” *Vide. Tehnol. Resur. - Environ. Technol. Resour.*, vol. 3, pp. 124–128, 2023, doi: 10.17770/etr2023vol3.7228.

[7] O. Kononova, V. Lusis, A. Galushchak, A. Krasnikovs, and A. Macanovskis, “Numerical modeling of fiber pull-out micromechanics in concrete matrix composites,” *J. Vibroengineering*, vol. 14, no. 4, pp. 1852–1861, 2012.

[8] J. C. Vasco, “Chapter 16 - Additive manufacturing for the automotive industry,” in *Handbooks in Advanced Manufacturing*, J. Pou, A. Riveiro, and J. P. B. T.-A. M. Davim, Eds. Elsevier, 2021, pp. 505–530. doi: https://doi.org/10.1016/B978-0-12-818411-0.00010-0.

[9] B. Blakey-Milner *et al.*, “Metal additive manufacturing in aerospace: A review,” *Mater. Des.*, vol. 209, p. 110008, 2021, doi: https://doi.org/10.1016/j.matdes.2021.110008.

[10] R. Kumar, M. Kumar, and J. S. Chohan, “The role of additive manufacturing for biomedical applications: A critical review,” *J. Manuf. Process.*, vol. 64, pp. 828–850, 2021, doi: https://doi.org/10.1016/j.jmapro.2021.02.022.

[11] A. Macanovskis, A. Krasnikovs, O. Kononova, and A. Lukasenoks, “Mechanical Behavior of Polymeric Synthetic Fiber in the Concrete,” *Procedia Eng.*, vol. 172, pp. 673–680, 2017, doi: 10.1016/j.proeng.2017.02.079.

[12] V. Lusis, K. K. Annamaneni, and A. Krasnikovs, "Concrete Reinforced by Hybrid Mix of Short Fibers under Bending," *Fibers*, vol. 10, no. 2, p. 11, Jan. 2022, doi: 10.3390/fib10020011.

[13] E. Rezvani Ghomi, F. Khosravi, R. E. Neisiany, S. Singh, and S. Ramakrishna, "Future of additive manufacturing in healthcare," *Curr. Opin. Biomed. Eng.*, vol. 17, p. 100255, 2021, doi: https://doi.org/10.1016/j.cobme.2020.100255.

[14] C. I. Gioumouxouzis, C. Karavasili, and D. G. Fatouros, "Recent advances in pharmaceutical dosage forms and devices using additive manufacturing technologies," *Drug Discov. Today*, vol. 24, no. 2, pp. 636–643, 2019, doi: https://doi.org/10.1016/j.drudis.2018.11.019.

[15] R. S. Odera and C. I. Idumah, "Novel advancements in additive manufacturing of PLA: A review," *Polym. Eng. Sci.*, vol. 63, no. 10, pp. 3189–3208, 2023, doi: 10.1002/pen.26450.

[16] K. Bulanda *et al.*, "Polymer Composites Based on Polycarbonate (PC) Applied to Additive Manufacturing Using Melted and Extruded Manufacturing (MEM) Technology," *Polymers*, vol. 13, no. 15. 2021. doi: 10.3390/polym13152455.

[17] J. M. Jafferson and D. Chatterjee, "A review on polymeric materials in additive manufacturing," *Mater. Today Proc.*, vol. 46, pp. 1349–1365, 2021, doi: https://doi.org/10.1016/j.matpr.2021.02.485.

[18] S. M. Desai, R. Y. Sonawane, and A. P. More, "Thermoplastic polyurethane for three-dimensional printing applications: A review," *Polym. Adv. Technol.*, vol. 34, no. 7, pp. 2061–2082, 2023, doi: 10.1002/pat.6041.

[19] F. Christakopoulos, P. M. H. van Heugten, and T. A. Tervoort, "Additive Manufacturing of Polyolefins," *Polymers*, vol. 14, no. 23. 2022. doi: 10.3390/polym14235147.

[20] F. N. Mullaveettil, R. Dauksevicius, and Y. Wakjira, "Strength and elastic properties of 3D printed PVDF-based parts for lightweight biomedical applications," *J. Mech. Behav. Biomed. Mater.*, vol. 120, no. March, p. 104603, 2021, doi: 10.1016/j.jmbbm.2021.104603.

[21] M. Golab, S. Massey, and J. Moultrie, "How generalisable are material extrusion additive manufacturing parameter optimisation studies? A systematic review," *Heliyon*, vol. 8, no. 11, p. e11592, 2022, doi: 10.1016/j.heliyon.2022.e11592.

[22] J. Beniak, M. Holdy, P. Križan, and M. Matúš, "Research on parameters optimization for the Additive Manufacturing process," *Transp. Res. Procedia*, vol. 40, pp. 144–149, 2019, doi: https://doi.org/10.1016/j.trpro.2019.07.024.

[23] K. Walia, A. Khan, and P. Breedon, "Polymer-Based Additive Manufacturing: Process Optimisation for Low-Cost Industrial Robotics Manufacture," *Polymers*, vol. 13, no. 16. 2021. doi: 10.3390/polym13162809.

[24] I. Baturynska, O. Semeniuta, and K. Martinsen, "Optimization of Process Parameters for Powder Bed Fusion Additive Manufacturing by Combination of Machine Learning and Finite Element Method: A Conceptual Framework," *Procedia CIRP*, vol. 67, pp. 227–232, 2018, doi: https://doi.org/10.1016/j.procir.2017.12.204.

[25] N. Mohan, P. Senthil, S. Vinodh, and N. Jayanth, "A review on composite materials and process parameters optimisation for the fused deposition modelling process," *Virtual Phys. Prototyp.*, vol. 12, no. 1, pp. 47–59, Jan. 2017, doi: 10.1080/17452759.2016.1274490.

[26] S. F. Khan, H. Zakaria, Y. L. Chong, M. A. M. Saad, and K. Basaruddin, "Effect of infill on tensile and flexural strength of 3D printed PLA parts," *IOP Conf. Ser. Mater. Sci. Eng.*, vol. 429, no. 1, 2018, doi: 10.1088/1757-899X/429/1/012101.

[27] P. K. Mishra, P. Senthil, S. Adarsh, and M. S. Anoop, "An investigation to study the combined effect of different infill pattern and infill density on the impact strength of 3D printed polylactic acid parts," *Compos. Commun.*, vol. 24, p. 100605, 2021, doi: https://doi.org/10.1016/j.coco.2020.100605.

[28] N. S. Hmeidat, B. Brown, X. Jia, N. Vermaak, and B. Compton, "Effects of infill patterns on the strength and stiffness of 3D printed topologically optimized geometries," *Rapid Prototyp. J.*, vol. 27, no. 8, pp. 1467–1479, Jan. 2021, doi: 10.1108/RPJ-11-2019-0290.

[29] M. Lalegani Dezaki, M. K. Ariffin, A. Serjouei, A. Zolfagharian, S. Hatami, and M. Bodaghi, "Influence of Infill Patterns Generated by CAD and FDM 3D Printer on Surface Roughness and Tensile Strength Properties," *Applied Sciences*, vol. 11, no. 16. 2021. doi: 10.3390/app11167272.

[30] F. A. Kucherov, E. G. Gordeev, A. S. Kashin, and V. P. Ananikov, "Three-Dimensional Printing with Biomass-Derived PEF for Carbon-Neutral Manufacturing," *Angew. Chemie - Int. Ed.*, vol. 56, no. 50, pp. 15931–15935, 2017, doi: 10.1002/anie.201708528.

[31] J. M. Chacón, M. A. Caminero, E. García-Plaza, and P. J. Núñez, "Additive manufacturing of PLA structures using fused deposition modelling: Effect of process parameters on mechanical properties and their optimal selection," *Mater. Des.*, vol. 124, pp. 143–157, 2017, doi: https://doi.org/10.1016/j.matdes.2017.03.065.

[32] V. Mazzanti, L. Malagutti, and F. Mollica, "FDM 3D Printing of Polymers Containing Natural Fillers: A Review of their Mechanical Properties," *Polymers*, vol. 11, no. 7. 2019. doi: 10.3390/polym11071094.

[33] G. Dong, G. Wijaya, Y. Tang, and Y. F. Zhao, "Optimizing process parameters of fused deposition modeling by Taguchi method for the fabrication of lattice structures," *Addit. Manuf.*, vol. 19, pp. 62–72, 2018, doi: https://doi.org/10.1016/j.addma.2017.11.004.

[34] J.-Y. Lee, J. An, and C. K. Chua, "Fundamentals and applications of 3D printing for novel materials," *Appl. Mater. Today*, vol. 7, pp. 120–133, 2017, doi: https://doi.org/10.1016/j.apmt.2017.02.004.

[35] G. D. Goh, Y. L. Yap, S. Agarwala, and W. Y. Yeong, "Recent Progress in Additive Manufacturing of Fiber Reinforced Polymer Composite," *Adv. Mater. Technol.*, vol. 4, no. 1, pp. 1–22, 2019, doi: 10.1002/admt.201800271.

[36] A. Cattenone, S. Morganti, G. Alaimo, and F. Auricchio, "Finite Element Analysis of Additive Manufacturing Based on Fused Deposition Modeling: Distortions Prediction and Comparison With Experimental Data," *J. Manuf. Sci. Eng.*, vol. 141, no. 1, Nov. 2018, doi: 10.1115/1.4041626.

[37] T. J. Hoskins, K. D. Dearn, and S. N. Kukureka, "Mechanical performance of PEEK produced by additive manufacturing," *Polym. Test.*, vol. 70, pp. 511–519, 2018, doi: https://doi.org/10.1016/j.polymertesting.2018.08.008.

[38] A. Rodríguez-Panes, J. Claver, and A. M. Camacho, "The Influence of Manufacturing Parameters on the Mechanical Behaviour of PLA and ABS Pieces Manufactured by FDM: A Comparative Analysis," *Materials*, vol. 11, no. 8. 2018. doi: 10.3390/ma11081333.

[39] M. Moradi, A. Aminzadeh, D. Rahmatabadi, and A. Hakimi, "Experimental investigation on mechanical characterization of 3D printed PLA produced by fused deposition modeling (FDM)," *Mater. Res. Express*, vol. 8, no. 3, 2021, doi: 10.1088/2053-1591/abe8f3.

[40] L. Yang, O. Harrysson, H. West, and D. Cormier, "Mechanical properties of 3D re-entrant honeycomb auxetic structures realized via additive manufacturing," *Int. J. Solids Struct.*, vol. 69–70, pp. 475–490, 2015, doi: https://doi.org/10.1016/j.ijsolstr.2015.05.005.

[41] M. Domingo-Espin, J. M. Puigoriol-Forcada, A.-A. Garcia-Granada, J. Llumà, S. Borros, and G. Reyes, "Mechanical property characterization and simulation of fused deposition modeling Polycarbonate parts," *Mater. Des.*, vol. 83, pp. 670–677, 2015, doi: https://doi.org/10.1016/j.matdes.2015.06.074.

[42] L. M. Galantucci, I. Bodi, J. Kacani, and F. Lavecchia, "Analysis of Dimensional Performance for a 3D Open-source Printer Based on Fused Deposition Modeling Technique," *Procedia CIRP*, vol. 28, pp. 82–87, 2015, doi: https://doi.org/10.1016/j.procir.2015.04.014.

[43] T. Yao, Z. Deng, K. Zhang, and S. Li, "A method to predict the ultimate tensile strength of 3D printing polylactic acid (PLA) materials with different printing orientations," *Compos. Part B Eng.*, vol. 163, pp. 393–402, 2019, doi: https://doi.org/10.1016/j.compositesb.2019.01.025.

[44] R. J. Zaldivar, D. B. Witkin, T. McLouth, D. N. Patel, K. Schmitt, and J. P. Nokes, "Influence of processing and orientation print effects on the mechanical and thermal behavior of 3D-Printed ULTEM® 9085 Material," *Addit. Manuf.*, vol. 13, pp. 71–80, 2017, doi:

https://doi.org/10.1016/j.addma.2016.11.007.

[45] M. K. Thompson *et al.*, "Design for Additive Manufacturing: Trends, opportunities, considerations, and constraints," *CIRP Ann.*, vol. 65, no. 2, pp. 737–760, 2016, doi: https://doi.org/10.1016/j.cirp.2016.05.004.

[46] I. Chiulan, A. N. Frone, C. Brandabur, and D. M. Panaitescu, "Recent Advances in 3D Printing of Aliphatic Polyesters," *Bioengineering*, vol. 5, no. 1. 2018. doi: 10.3390/bioengineering5010002.

Environment. Technology. Resources. Rezekne, Latvia
Proceedings of the 16th International Scientific and Practical Conference.2025 Volume IV, 383-387

Strengthening Interfacial Bonding in Nanofibre Laminated Textile Composites

Jaymin Vrajlal Sanchaniya
Institute of Mechanical and Biomedical Engineering
Riga Technical University
Riga, Latvia
Jaymin.Sanchaniya@rtu.lv

Ilze Liepiņlauska
Faculty of Engineering
Rezekne Academy of Technologies
Rēzekne, Latvia
ilze.liepinlauska@rta.lv

Andris Skromulis
Faculty of Engineering
Rezekne Academy of Technologies
Rēzekne, Latvia
andris.skromulis@inbox.lv

Inga Lasenko
Institute of Mechanical and Biomedical Engineering
Riga Technical University
Riga, Latvia
inga.lasenko@rtu.lv

Karunamoorthy Rengasamy Kannathasan
Institute of Mechanical and Biomedical Engineering
Riga Technical University
Riga, Latvia
karunamoorthy.rengasamy-kannathasan@rtu.lv

Sanjay Rajni Vejanand
Institute of Mechanical and Biomedical Engineering
Riga Technical University
Riga, Latvia
sanjay.vejanand@rtu.lv

Liena Poiša
Faculty of Engineering
Rezekne Academy of Technologies
Rēzekne, Latvia
lienapoisa@inbox.lv

***Abstract*—Textiles that use electrospun nanofibre membranes (ENMs) in laminated configurations recently achieved substantial progress in three application areas, including robotic skins, electronic sensors, and medical textiles. Research evaluates nanofibre-laminated textile bonding strength by using multiple experimental methods. The study presents the development of three different textile composites in which polyacrylonitrile (PAN) polymer was treated with electrospinning on fabric through various adhesive techniques. The testing evaluates the different nanofibre-fabric bonding methods using T-peel tests to determine their effectiveness. The direct electrospinning methods used to produce laminated textiles led to negligible or no attachment between fabric materials and ENMs. The electrospinning process led to initial ENM layer adhesion when an adhesion agent was incorporated during the process. The tested composite achieved a 60% higher strength after using adhesive pressure to create it. Research findings show that applying an adhesive agent with pressure between textile materials and ENMs produces optimal interfacial adhesion during the fabrication of laminated textile composites.**

***Keywords*—laminated composites, nanofibres, textiles, T-peel test.**

I. Introduction

Researchers have observed a significant growth in studies on textiles with diverse applications which now include the development of electronic skins for wearable electronic devices [1], [2]. Wearable health monitors and multifunctional robotic skins that replicate the properties of human skin belong to the group of innovative devices that constitute important progress in smart textile technology [3], [4].

The medical field has adopted nanofibres as highly promising materials because they provide excellent benefits for wound dressing applications [5], [6], drug delivery systems [7], [8], and tissue engineering scaffolds [9]. The nanofibre mat with porous structure display several beneficial properties such as a high surface-to-volume ratio combined with minimal weight and flexibility, which allows them to seamlessly integrate with textile technologies [10], [11].

Online ISSN 2256-070X
https://doi.org/10.17770/etr2025vol4.8454
© 2025 The Author(s). Published by RTU PRESS.
This is an open access article under the Creative Commons Attribution 4.0 International License.

The combination of textile materials with nanofibres leads to laminated composite structures through research-developed integration methods. These laminated composite textiles offer multiple advantages from their two constituent materials for applications ranging from stretchable fabric skin to low-force sensors [1], noncrimping textiles [12], acoustic applications [13] and self-powered sensing textiles [14], [15] in diverse technological fields.

Composite materials depend on the level of bonding of the reinforcement elements with the matrix for both performance quality and durability [16], [17]. The interface holds an exceptional importance in nanofibre mats integrated with textile substrates, as it determines stress transfer capabilities and affects overall mechanical characteristics [18], [19]. In laminated composite textiles, robust interfacial bonding is essential, as slippage may compromise the structural integrity of nanofibre mats, which consequently deteriorates the functionality of the composite materials [20], [21].

Research on textiles strengthened through the addition of nanofibre mats has primarily examined mechanical performance and utilisation, yet provides only a limited understanding of the basis for textile-nanofibre mat bonding. The production of nanofibre mats has incorporated three different strategies: direct electrospinning onto textiles as well as pre-electrospinning with adhesive glue and weaving textile yarns. Current methodologies successfully achieve their intended objectives; however, the interfacial strength between textile substrates and nanofibre mats remains a significant knowledge gap in contemporary research.

This study implements established methods from the literature and tests a new method for developing nanofibre-reinforced laminated textiles. This investigation contributes novel insights through its systematic approach to developing three laminated composite textiles, followed by comprehensive T-peel testing and thorough examination of the component adhesive bonding strength. The methodology generates significant empirical data that advances the understanding of interfacial bonding in nanofibre-reinforced textile composites.

II. Materials and Methods

A. Materials

The fabrication of laminated textile composites reinforced with electrospun polyacrylonitrile (PAN) nanofibres required several key materials. The electrospun nanofibres were produced using polyacrylonitrile powder and N,N-dimethylformamide. Polyacrylonitrile, with an average molecular weight of 150,000 (typical) and CAS number 25014-41-9, was sourced from Sigma-Aldrich chemicals (Merck KGaA, Darmstadt, 64287, Germany). N, N-dimethylformamide (DMF), an ACS reagent (solvent) with 99.8% purity and CAS number 68-12-2, was purchased similarly from Sigma-Aldrich chemicals.

The woven fabric used in this investigation was model 21502/45_PN, featuring plain interlacing with a width of 150±1.5 centimetres and a weight of 150±17 grammes per square metre. The fabric structure comprised warp and weft components constructed of 28 Tex linen. This material was obtained from AB 'Linas', S. Kerbedzio Street 23, LT-35114 Panevezys, Lithuania. The fabric adhesive used was a solvent-free formulation, Art. 639820, obtained from Gutermann GmbH, situated at Landstrasse 1, DE-79261 Gutach-Besigau, Germany.

B. Fabrication of nanofibre laminated fabric composites

The fabrication process began with the preparation of the PAN solution, by which PAN powder was incorporated into the DMF solvent at a concentration of 10% wt / wt. This mixture underwent continuous agitation for 8 hours utilising a Thermo Scientific™ Cimarec+™ Stirring Hotplate (USA) at 80°C, with ambient conditions maintained at 22±1°C and 60% relative humidity. The stirring speed was regulated at 800 rpm. Subsequently, the solution was kept at room temperature for 1 hour to facilitate the elimination of air bubbles and achieve solution stability, similarly as mentioned in [22].

The textile compound required exact trimming of the fabric in specific dimensions that corresponded to the circumference of the drum (30 cm by 45 cm) with the weft direction as the longer edge. The RC-5000 rotating drum collector with dimensions of 140 mm in in diameter by 300 mm length from Shenzhen Tongli Tech Co Ltd., Shenzhen, China received this fabric material. The precise application of the fabric adhesive was carried out on the substrate (~210 g/m²) by hand methods following the principles while weight measurements determined the amount of adhesive before and after application.

The electrospinning of PAN nanofibres was conducted at 22±1°C utilising a Fisherbrand™ Single Syringe Pump system (Danbury, CT 06811, USA) in conjunction with the prepared rotating drum assembly. The apparatus used a 10-ml plastic syringe (lure lock) fitted with an 18 Ga needle. The operational parameters encompassed a 20 kV voltage potential, a flow rate of 1 ml / h, and an 18 cm separation between the tip of the syringe and drum collector centre. The drum collector maintained a constant rotational velocity of 1200 rpm (approximate tangential velocity of 8.8 m/s).

Before the T-peel test, all specimens underwent conditioning at 22±1°C and relative humidity below 60% for 48 hours, according to ISO 139:1973 (Textiles—Standard atmospheres for conditioning and testing). To facilitate the collection of PAN nanofibre mats, aluminium foil (45 cm × 5 cm, 35 µm thickness) sourced from Vireo.de, Merseburg (06217), Germany, was placed on the adhesive layer, thereby enabling subsequent collection of nanofibre collection whilst preventing direct interaction between adhesive and nanofibre components.

C. T-peel test of nanofibre laminated fabric composites:

The T-peel test followed ASTM D1876 (Standard Test Method for Peel Resistance of Adhesives - T-Peel Test). The test specimens were cut precisely along the fibre orientation to obtain dimensions of 25 millimetres wide and

100 millimetres long. The PPT Group UK Ltd (as Mecmesin) Multi-Test 2.5-i tensile testing machine measured the adhesive strength with its 25 N sensor. The testing machine adjusted its elongation speed to 100 mm/min following ASTM D1876 standards. Figure 1 presents a visual representation of the samples prepared for the T-peel test, where L denotes the adhesive length of the sample, W represents the specimen width, and l indicates the distance between the grips.

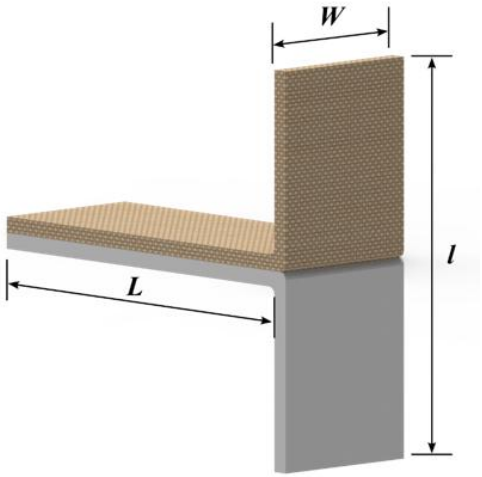

Fig.1. Illustration of the T-peel test specimen.

The investigation comprised three distinct groups of specimens. The first group, designated as S1, consisted of samples in which nanofibres were directly electrospun onto the fabric substrate. The second group, denoted S2, incorporated specimens where adhesive was applied to the fabric prior to the electrospinning process, with nanofibres subsequently deposited directly on the adhesive-treated fabric. The third group, classified as S3, used nanofibres initially collected on aluminium foil, which were subsequently adhered to the fabric using an equivalent amount of adhesive glue. These samples were subjected to pressure application (~600 N/m²) for a duration of 24 hours to ensure optimal bonding.

III. Results and Discussion

The S1 group of samples, which consisted of nanofibres electrospun directly onto the fabric, demonstrated no adhesion between the fabric and the electrospun nanofibres. Figure 2 illustrates the sample from the S1 group after 24 hours at room temperature.

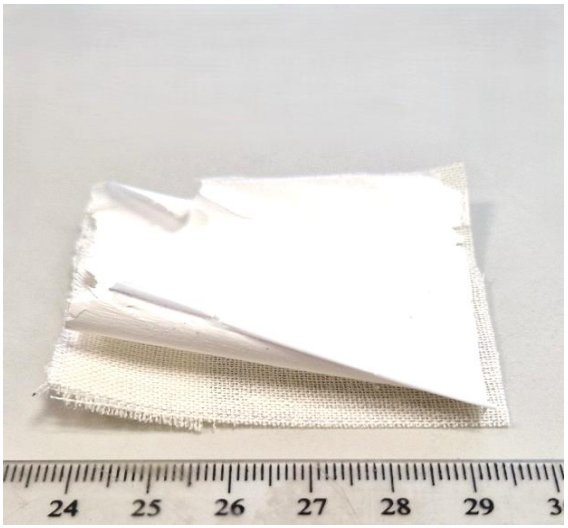

Fig. 2. S1 group sample after 24 hours of exposure to room temperature.

The samples collected from groups S2 and S3 did not lose cohesive properties. Groups S2 and S3 used adhesive materials that led to their stability but in group S1 the electrospun nanofibres reached the collector while staying solid and wrapped it without sticking to the fabric.

Opposite phenomena was observed by [13], which could be attributed to the collection of nanofibres at a reduced distance and their deposition onto the textile in a semi-solid state, as evidenced by the presence of beads in the morphology. Nevertheless, in both this investigation and other published work, the adhesive strength between textile substrates and nanofibre mats remains largely unexplored.

The test results of the T-peel experiments demonstrate that the bond strength between interfacial layers shows different levels for the S2 and S3 samples (Fig. 3). S3 specimens fabricated consisting of pre-collected nanofibres and adhesive application under pressure treatment exhibited high bonding strength through their peak force of 4.3 ± 0.1 N followed by stable bonding at 3.13 ± 0.13 N. The bonding strength of the S2 specimens showed reduced performance when adhesive was applied before direct electrospinning because the initial peak force reached 2.7 ± 0.1 N and then stabilised at 2.16 ± 0.1 N.

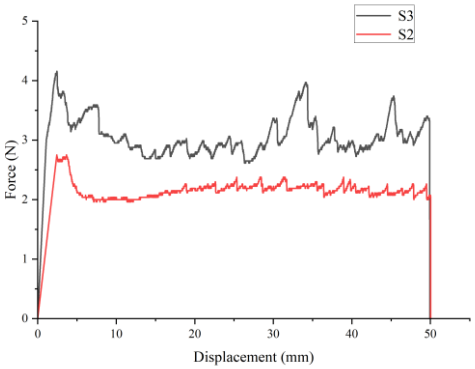

Fig. 3. Representative force displacement curves from T-peel testing of the nanofibre-laminated textiles of groups S2 and S3.

Peak load peel strength measurement for S3 samples produced 172 ± 4 N/m while the steady-state delamination phase exhibited 125.2 ± 5.2 N/m. The peel strength measurements for the S2 samples reached peak values of 108 ± 4 N / m, after which they showed steady-state delamination at 86.4 ± 4 N/m. The pressure-assisted bonding approach creates interfaces that demonstrate a strength at least 60% greater than that of electrospinning onto adhesive-treated fabric under direct conditions.

Both force-displacement curves exhibit characteristic serrated patterns because of the way nanofibre-fabric interfaces fail progressively across the woven structure surface. S3 sample shows maximum force variability because they have more nanofibres properly bound to the fabric base. These cyclic variations in the measurements align with the fabric weaves because the nanofibres establish contact with the natural peaks and valleys on the textile surface.

Laboratory tests on the specimens after failure display additional information on failure behaviours (Figure 4). The S3 specimens maintained better fibres on the fabric surface which confirms that the interfacial bonding achieved superior results. The pressure treatment used during the fabrication improved overall bonding between the nanofibre mat and the fabric structures because it allowed deeper adhesive penetration. The adherence to fabric surfaces turned out to be weaker in the S2 specimens as compared to the S3 because direct electrospinning on the adhesive-treated fabric creates suboptimal fibre-matrix interaction.

Fig. 4. Specimens from group S3 after T-peel testing.

The S3 fabrication method produced superior peak force results of approximately 60% compared to S2 because effective processing parameters enable strong interfacial bonding. The enhancement stems from two important characteristics: the uniform pressure distribution during bonding and the protective effect aluminium foil provides to nanofibre mats before adhesive application.

The total strength measurements between the S2 and S3 test samples have essential value for improving manufacturing methods of nanofibre-laminated textile composites. The pressure-assisted bonding technique (S3) proves advantageous for applications that require strong interfacial strength due to its particular importance in wearable electronic devices and medical textiles.

The steady-force plateau following the initial peak in both specimen types creates favourable conditions for long-term performance calculations in real-life applications. The pressure-assisted bonding approach enables the S3 samples to maintain a steady force level of 3.13 ± 0.13 N as the displacement increases, indicating that the method produces a well-distributed robust bond throughout the entire surface of the composite. Uniform structure is of particular importance for strain sensors and protective clothing because they need consistent textile performance. A similar phenomenon of adhesive-assisted bonding was demonstrated in other textile composite applications [12]. However, while direct comparison of adhesive strength values is not possible since they were not measured in previous studies, similar bonding strategies have been successfully employed for different purposes. For example, in hybrid textile composites, adhesive bonding has been shown to enhance structural integration and mechanical properties, though through different mechanisms and for different applications.

The structural integrity of nanofibres in S3 specimens showed significant improvement with pressure-assisted bonding, demonstrating preservation of the structure of the nanofibre network. This structural preservation plays a vital role in maintaining composite functionality across all performance domains, including electrical functionality and mechanical properties. The observed failure mechanism exhibited progressive detachment of the nanofibres rather than sudden delamination, indicating an energy-absorbing process that contributes to the durability of the product.

IV. Conclusions

The paper analysed the interfacial bond strength of a nanofibre laminated textile composite through three separate fabrication techniques. The experimental results from direct electrospinning failed to establish a meaningful bond between fabric and nanofibre mat (S1). The application of adhesive before electrospinning in Method S2 produced the strongest bond with a peak peel strength of 108 ± 4 N/m. Pressure-assisted bonding of pre-collected nanofibres (S3) served as the most successful method by achieving a peak peel strength of 172 ± 4 N/m, which exceeded the S2 method by 60%.

The results obtained enable fundamental understanding for better manufacturing methods of nanofibre-laminated textile composites. The bonding process developed in this study presents a dependable method to create strong interfacial bonds that is crucial for applications in wearable electronics, in addition to medical textiles and other advanced textile applications requiring superior mechanical reliability. In future, researchers could optimise pressure settings alongside studies on the longevity of the interface in different environmental situations.

V. Acknowledgement

JVS was supported by postdoctoral grant No RTU-ZG-2024/1-0048 under the EU RRF project No 5.2.1.1.i.0/2/24/I/CFLA/003. This work has been supported by research and development grant No RTU-PA-2024/1-0091 under the EU Recovery and Resilience Facility funded project No. 5.2.1.1.i.0/2/24/I/CFLA/003 "Implementation of consolidation and management changes at Riga Technical University, Liepaja University, Rezekne Academy of Technology, Latvian Maritime Academy and Liepaja Maritime College for the progress towards excellence in higher education, science, and innovation".

References

[1] X. You, J. He, N. Nan, X. Sun, K. Qi, Y. Zhou, W. Shao, F.Liu and S. Cui, "Stretchable capacitive fabric electronic skin woven by electrospun nanofiber coated yarns for detecting tactile and multimodal mechanical stimuli," J. Mater. Chem. C, vol. 6, no. 47, pp. 12981–12991, 2018, doi: 10.1039/C8TC03631D

[2] H. Jin, Md O. G. Nayeem, Md O. G. Nayeem, S. Lee, N. Matsuhisa, D.Inoue, T. Yokota, D. Hashizume and T. Someya, "Highly durable nanofiber-reinforced elastic conductors for skin-tight electronic textiles," ACS Nano, vol. 13, no. 7, pp. 7905–7912, 2019, doi: 10.1021/acsnano.9b02297

[3] J. S. Meena, S. Bin Choi, S.-B. Jung, and J.-W. Kim, "Electronic textiles: new age of wearable technology for healthcare and fitness solutions," Mater. Today Bio, vol. 19, no. December 2022, p. 100565, 2023, doi: 10.1016/j.mtbio.2023.100565

[4] B. Baye and T. Tesfaye, "The new generation fibers: a review of high performance and specialty fibers," Polym. Bull., vol. 79, no. 11, pp. 9221–9235, 2022, doi: 10.1007/s00289-021-03966-6

[5] G. Anusiya and R. Jaiganesh, "A review on fabrication methods of nanofibers and a special focus on application of cellulose nanofibers," Carbohydr. Polym. Technol. Appl., vol. 4, no. November, p. 100262, 2022, doi: 10.1016/j.carpta.2022.100262

[6] E. J. Jang, R. Patel, and M. Patel, "Electrospinning Nanofibers as a Dressing to Treat Diabetic Wounds," Pharmaceutics, vol. 15, no. 4, 2023, doi: 10.3390/pharmaceutics15041144

[7] E. R. Radu, S. I. Voicu, and V. K. Thankur, "Polymeric membranes for biomedical applications," Polymers (Basel)., vol. 15, no. 3, pp. 1–28, 2023, doi: https://doi.org/10.3390/polym15030619

[8] S. Baek, H. Park, Y. Park, H. Kang, and D. Lee, "Development of a lidocaine-loaded alginate/CMC/PEO electrospun nanofiber film and application as an anti-adhesion barrier," Polymers (Basel)., vol. 12, no. 3, 2020, doi: 10.3390/polym12030618

[9] L. Bauer, L. Brandstäter , M. Letmate, M. Palachandran, F. O. Wadehn,C. Wolfschmidt, T. Grothe, U. Güth and A. Ehrmann, "Electrospinning for the Modification of 3D Objects for the Potential Use in Tissue Engineering," Technologies, vol. 10, no. 3, 2022, doi: 10.3390/technologies10030066

[10] J. V. Sanchaniya, I. Lasenko, V. Gobins, and A. Kobeissi, "A Finite Element Method for Determining the Mechanical Properties of Electrospun Nanofibrous Mats," Polym., vol. 16, no. 6, p. 852, 2024, doi: 10.3390/polym16060852

[11] J. V. Sanchaniya, I. Lasenko, V. Vijayan, H. Smogor, V. Gobins, A.Kobeissi and D. Goljandin, "A Novel Method to Enhance the Mechanical Properties of Polyacrylonitrile Nanofiber Mats: An Experimental and Numerical Investigation," Polymers (Basel)., vol. 16, no. 7, p. 992, Apr. 2024, doi: 10.3390/polym16070992

[12] J. V. Sanchaniya, I. Lasenko, S. P. Kanukuntla, A. Mannodi, A. Viluma-gudmona, and V. Gobins, "Preparation and Characterization of Non-Crimping Laminated Textile Composites Reinforced with Electrospun Nanofibers," Nanomaterials, vol. 13, no. 13, p. 1949, 2023, doi: 10.3390/nano13131949

[13] M. Kucukali-Ozturk, E. Ozden-Yenigun, B. Nergis, and C. Candan, "Nanofiber-enhanced lightweight composite textiles for acoustic applications," J. Ind. Text., vol. 46, no. 7, pp. 1498–1510, 2017, doi: 10.1177/1528083715622427

[14] X. Guan, B. Xu, M. Wu, T. Jing, Y. Yang, and Y. Gao, "Breathable, washable and wearable woven-structured triboelectric nanogenerators utilizing electrospun nanofibers for biomechanical energy harvesting and self-powered sensing," Nano Energy, vol. 80, no. July 2020, p. 105549, 2021, doi: 10.1016/j.nanoen.2020.105549

[15] L. Liu, W. Xu, Y. Ding, S. Agarwal, A. Greiner, and G. Duan, "A review of smart electrospun fibers toward textiles," Compos. Commun., vol. 22, no. August, p. 100506, 2020, doi: 10.1016/j.coco.2020.100506

[16] S. Budhe, M. D. Banea, S. de Barros, and L. F. M. da Silva, "An updated review of adhesively bonded joints in composite materials," Int. J. Adhes. Adhes., vol. 72, no. October 2016, pp. 30–42, 2017, doi: 10.1016/j.ijadhadh.2016.10.010

[17] R. Hsissou, R. Seghiri, Z. Benzekri, M. Hilali, M. Rafik, and A. Elharfi, "Polymer composite materials: A comprehensive review," Compos. Struct., vol. 262, no. December 2020, pp. 0–3, 2021, doi: 10.1016/j.compstruct.2021.113640

[18] I. Lasenko, J. V.Sanchaniya, S. P. Kanukuntla, Y. Ladani, A. Viluma-Gudmona, O.Kononova, V. Lusis, I. Tipans and T. Selga, "The mechanical properties of nanocomposites reinforced with PA6 electrospun nanofibers," Polymers (Basel)., vol. 15, no. 3, 2023, doi: 10.3390/polym15030673

[19] K. M. F. Hasan, P. G. Horváth, and T. Alpár, "Potential fabric-reinforced composites: a comprehensive review," J. Mater. Sci., vol. 56, no. 26, pp. 14381–14415, 2021, doi: 10.1007/s10853-021-06177-6

[20] F. Adekunle and A. F. M. Seyam, "The Effect of Adhesive Quantity on Adhesion Quality and Mechanical Characteristics of Woven Kevlar Fabric-Reinforced Laminated Structures," J. Compos. Sci., vol. 8, no. 12, 2024, doi: 10.3390/jcs8120505

[21] Y. Zhou, M. Fan, and L. Chen, "Interface and bonding mechanisms of plant fibre composites: An overview," Compos. Part B Eng., vol. 101, pp. 31–45, 2016, doi: 10.1016/j.compositesb.2016.06.055

[22] J. V.Sanchaniya, I. Lasenko, S. P. Kanukuntla, H. Smogor, A. Viluma-Gudmona, A.Krasnikovs, I. Tipans and V.Gobins, "Mechanical and Thermal Characterization of Annealed Oriented PAN Nanofibers," Polymers (Basel)., vol. 15, no. 15, 2023, doi: 10.3390/polym15153287

Environment. Technology. Resources. Rezekne, Latvia
Proceedings of the 16th International Scientific and Practical Conference.2025. Volume IV, 389-392

Generalized Nets and Their Application in the Management of a Recording Studio

Liliya Staneva
Faculty of Technical Sciences
Prof. Asen Zlatarov University of Burgas
Burgas, Bulgaria
anestieva@mail.bg

Yuliyan Petrov
Technical College
Prof. Asen Zlatarov University of Burgas
Burgas, Bulgaria
yulipetrov@abv.bg

***Abstract*- Generalized nets, introduced by Academician Krassimir Atanassov [1], represent an established methodology for modeling and analyzing complex systems. This article explores their potential application in the management of recording studios, focusing on the optimization of recording, processing, and production workflows. The study highlights how generalized nets can enhance coordination between different operational units within a studio, ensuring efficient time and resource management. Recording studios operate as dynamic systems that require seamless integration of diverse technological and organizational components. Decision-making in such an environment must account for scheduling constraints, resource allocation, and task prioritization. By applying the principles of generalized nets, a structured approach to managing these processes can be established, including modeling key workflows, predicting potential challenges, and improving the distribution of human and technical resources.**

Keywords*- *Generalized Nets, Recording Studio, Optimization, Process Management, Petri Nets Theory

I. Introduction

The article examines several key applications of Generalized Nets [1], [2], [3] in the environment of recording studios. These include:

- Modeling the workflow – assisting in structuring the production phases such as recording, mixing, mastering, and distribution;
- Optimization of scheduling – synchronizing recording sessions with the availability of performers;
- Automation of technical processes – managing sound effects and audio filters efficiently;
- Resource monitoring – ensuring the optimal utilization of studio spaces, equipment, and software.

By simulating this net, studio managers can anticipate inefficiencies in the workflow and implement corrective measures. Additionally, the study presents a case in which a recording studio works with multiple artists simultaneously, demonstrating how Generalized Net [6], [7] can be used to visualize and optimize session allocation. The analysis indicates that applying these models leads to improved operational efficiency and higher production quality.

A generalized model for optimizing workflows in a recording studio is proposed, aiming to support the analysis and planning of production stages. The developed net model represents a structured scheme of the workflow, designed to assist in optimizing production processes. In practical applications, specific management details may vary significantly depending on the studio, team, and type of projects. [11], [12]

The purpose of the article is not to prescribe a single working model for all studios but rather to provide a tool that can identify weaknesses, assist in resource planning, and enable experimentation with simulations before making actual changes.

II. Materials and Methods

A generalized net model of the processes in a recording studio has been developed, introducing a set of transitions $A = \{Z_1, Z_2, Z_3, Z_4, Z_5, Z_6\}$, which describe the following processes:

Z_1 = ”Checking for available recording studio”

Z_2 = “Recording in progress”

Z_3 = “Recording completed”

Z_4 = “Mixing in progress”

Online ISSN 2256-070X
https://doi.org/10.17770/etr2025vol4.8429
© 2025 The Author(s). Published by RTU PRESS.
This is an open access article under the Creative Commons Attribution 4.0 International License.

Z_5 = "Mastering in progress"

Z_6 ="Final product"

Each transition can have m input and n output positions, where $m \geq 1$ and $n \geq 1$. The input positions for transition Z are denoted as $l'_1, \ldots, l'_i, \ldots, l'_m$, while the output positions are labeled as $l''_1, \ldots, l''_j, \ldots, l''_n$. An input position that does not receive an arc is considered an entry point of the net, while an output position with no outgoing arc is considered an exit. In the network positions, tokens can be present and move from input to output positions of the transitions. In Generalized Nets, tokens represent information units that pass through the system transitions and carry characteristic data about the process state. When the input positions contain a sufficient number of tokens and the specified transition time occurs, the tokens from the input positions become eligible to move to the output positions. This movement of tokens from input to output positions is called transition activation.

Initially, the tokens entering the net through the input positions have initial characteristics. With each transition within the net, they acquire new characteristics, making each token unique with its own history.

The net model has been created using GNDraw, a software tool designed for the graphical modeling of Generalized Nets Fig. 1.

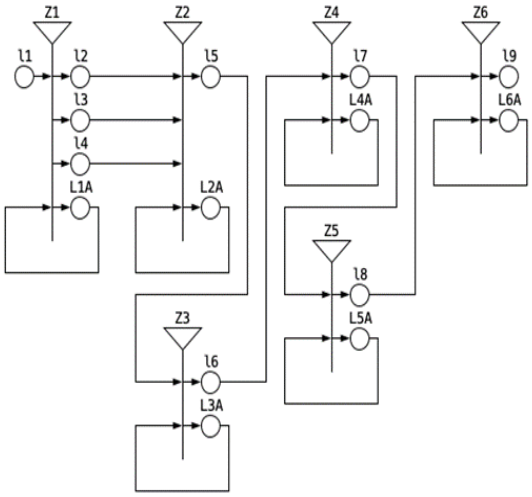

Fig. 1. Graphical representation of a Generalized Net for managing processes in a recording studio, created using GNDraw

The transitions are described as follows:

$Z_1 = \langle\{l_1, L_{1A}\}, \{l_2, l_3, l_4, L_{1A}\}, R_1, M_1 \wedge (l_1) \vee (L_{1A})\rangle$

$R_{1=}$		l_2	l_3	l_4	L_{1A}
	l_1	$false$	$false$	$false$	$true$
	L_{1A}	$W_{1A,2}$	$W_{1A,3}$	$W_{1A,4}$	$true$

$W_{1A,2}$ – "A free recording studio is available"

$W_{1A,3}$, $W_{1A,4}$ – "he necessary conditions for creating a sound recording are available"

The prerequisite is the availability of a free studio space. After the transition is activated, the core moves to the "Recording in Process" position, with a current characteristic corresponding to the type of recording – vocals, string instruments, or drums. Once this condition is met, the incoming core from position l_1 enters position L_{1A}. After the transition, the cores l_2, l_3, l_4 exiting from position L_{1A} are assigned the current characteristics "vocal recording", "string instrument recording", and "drum and keyboard recording".

$Z_2 = \langle\{l_2, l_3, l_4, L_{2A}\}, \{l_5, L_{2A}\}, R_2, M_2 \wedge (l_2, l_3, l_4) \vee (L_{2A})\rangle$

$R_{2=}$		l_5	L_{2A}
	l_2	$false$	$true$
	l_3	$false$	$true$
	l_4	$false$	$true$
	L_{2A}	$W_{2A,5}$	$true$

$W_{2A,5}$ = "The cores l_2, l_3, l_4 are available for the start of the recording"

The incoming cores from positions l_2, l_3, l_4 enter L_{2A}. After the transition, the cores merge into a single core l_5 with the current characteristic "the recordings are ready."

$Z_3 = \langle\{l_5, L_{3A}\}, \{l_6, L_{3A}\}, R_3, M_3 \wedge (l_5) \vee (L_{3A})\rangle$

$R_{3=}$		l_6	L_{3A}
	l_5	$false$	$true$
	L_{3A}	$W_{3A,6}$	$true$

$W_{3A,6}$ = "The recordings are complete"

The incoming core l_5 enters position L_{3A}. After the transition, the core exiting to position l_6 takes the current characteristic "records entering for mixing."

$Z_4 = \langle\{l_6, L_{4A}\}, \{l_7, L_{4A}\}, R_4, M_4 \wedge (l_6) \vee (L_{4A})\rangle$

$R_{4=}$		l_7	L_{4A}
	l_6	$false$	$true$
	L_{4A}	$W_{4A,7}$	$true$

$W_{4A,7}$ = "Processes individual sound recordings (vocals, drums, guitars)"

The incoming core l_6 enters position L_{4A}. After activating the transition, the exiting core l_7 assumes the current characteristic "mixed recordings".

$Z_5 = \langle\{l_7, L_{5A}\}, \{l_8, L_{5A}\}, R_5, M_5 \wedge (l_7) \vee (L_{5A})\rangle$

$R_{5=}$		l_8	L_{5A}
	l_7	$false$	$true$

L_{5A}	$W_{5A,8}$	$true$

$W_{5A,8}$= "focuses on the overall sound balance"

The incoming core l_7 enters position L_{5A}. After activating the transition, the exiting core l_8 assumes the current characteristic "the entire mix is optimized and balanced."

$$Z_6 = \langle\{l_8, L_{6A}\}, \{l_9, L_{6A}\}, R_6, M_6 \wedge (l_9) \vee (L_{6A})\rangle$$

$R_{6=}$

	l_9	L_{6A}
l_8	$false$	$true$
L_{6A}	$W_{6A,9}$	$true$

$W_{6A,9}$= "the sound recording is ready for release"

The incoming core l_8 enters position L_{6A}. After the transition is activated, the exiting core l_9 assumes the current characteristic "the mix processing is complete."

The possibilities for integrating artificial intelligence (AI) [4], [5] in the management of recording studios through neural net represent a significant advancement in process automation. AI can be used for:

- Automated resource allocation – intelligent algorithms can analyze the studio's workload and dynamically propose optimal schedules for recording, mixing, and mastering.
- Sound and quality analysis – AI-based tools can monitor audio quality in real time and automatically suggest corrections to the mix or mastering levels.
- Prediction of delays and optimization – through machine learning, the system can forecast potential issues in the workflow and propose preventive measures.
- Voice and text commands – AI assistants can facilitate the work of sound engineers by executing commands to change mixer settings or activate specific effects.

The integration of artificial intelligence in the management of recording studios will lead to higher efficiency, reduced errors, and optimized time expenditures. In the future, these technologies will enable the creation of fully autonomous studio environments, where AI will manage the entire production process with minimal human intervention.

III. Results and Discussion

The workflow in a recording studio is simulated using the stages described in a generalized net [8], [13],[14]. Time data necessary for each process involved in creating a musical product (song) is provided (Table 1).

Table 1 Workflow in a Recording Studio

Project	Project 1	Project 2	Project 3	Project 4	Project 5
Free Studio Check	13	0	19	6	51
Recording in Progress	20	15	25	11	64
Recording Completed	138	126	154	144	179
Mixing in Progress	178	184	182	191	213
Mastering in Progress	264	254	300	277	258
Finished Product	321	319	334	317	341

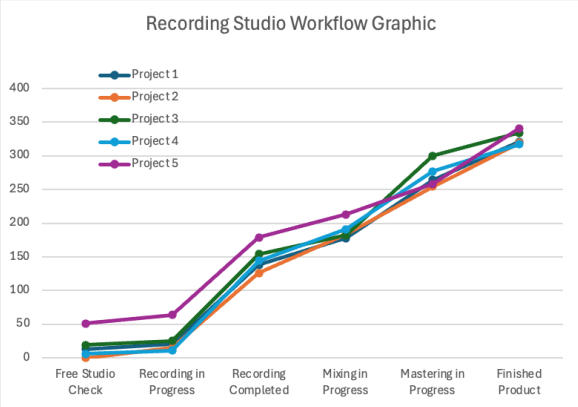

Fig. 2. Analysis of the Studio's Workload by Process Stages

The first chart (Fig. 2) shows the time distribution of projects by stage. It visualizes how each project moves through the different stages over time, allowing the identification of potential "bottlenecks" where multiple projects overlap in the same process. [9], [10]

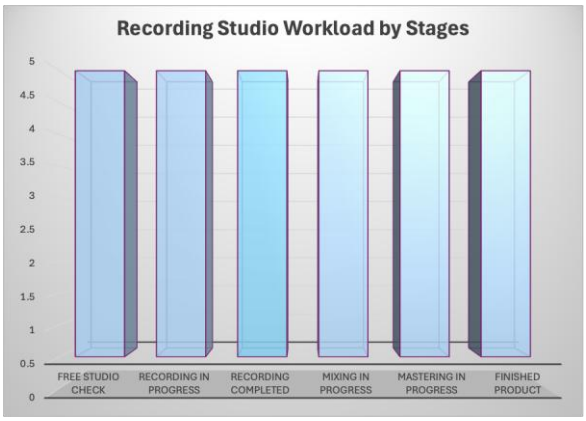

Fig. 3. Time Distribution of Projects by Stages in the Recording Studio

The second chart (Fig. 3) analyzes the studio's workload by stage, showing how many projects are active in each stage. If a stage (for example, mixing) is overloaded, it may indicate that additional resources or a better time allocation is needed. To address this issue, it is necessary to optimize the schedules so that mixing and mastering do not take as much time. To reduce this load,

more engineers or studio resources can be added to distribute the workload. When mixing and mastering take too much time, parallel processes or automated AI solutions can be introduced; in the future, artificial intelligence might be used to analyze the workload in real time and make automatic adjustments. This will allow faster processing of recording projects without any loss in quality. In the next phase of the research on this problem, an algorithm for an automated recording studio schedule may be proposed. [15], [16]

IV. Conclusions

Generalized nets can provide a useful tool for analyzing and optimizing standard production processes in a recording studio. However, managing a studio in real conditions is often considerably more flexible and dynamic, involving human factors, unforeseen changes, and the parallel execution of tasks. Therefore, the model should be viewed as an optimization tool. In the future, these models could be integrated with artificial intelligence systems for more automated management and workload prediction in a studio. The publication applies the use of generalized nets to manage and optimize processes in a recording studio. Most research in this area has focused on industrial and technical systems, but here they are applied in a creative and technological environment.

V. Acknowledgments

In this section, we would like to thank all of our loved ones for their support and motivation throughout the process of our scientific research. This publication is funded by the fund "Support for Publishing Publications in Journals with Impact Factor (IF) and Impact Rank (SJR)" of Prof. Asen Zlatarov University of Burgas, Republic of Bulgaria.

References

[1] K. T. Atanassov, Generalized nets. Singapore: World cientific, 1991.

[2] J. D. Reiss, “Intelligent Systems for Mixing Audio,” J. Audio Eng. Soc., vol. 59, no. 10, pp. 744–749, 2011.

[3] G. Hristova, “Generalized Net Model of Editing Process in a Publishing House,” Scientific Atlas, no. 9, 2024. ISSN: 2738-7518.

[4] H. A. Nimr, “Defuzzification of the outputs of fuzzy controllers,” presented at the 5th Int. Conf. on Fuzzy Systems, Cairo, Egypt, 1996.

[5] T. Murata, “Petri nets: Properties, analysis and applications,” Proc. IEEE, vol. 77, no. 4, pp. 541–580, Apr. 1989.

[6] K. Jensen, Coloured Petri Nets: Basic Concepts, Analysis Methods and Practical Use. Berlin: Springer, 1997.

[7] V. Slavova and K. Atanasov, “A generalized net for modeling working memory and language processing,” in Proc. 7th Int. Conf. Cognitive Modeling in Linguistics, vol. 9, pp. 90–101, 2004.

[8] K. Atanassov, G. Gluhchev, S. Hadjitodorov, A. Shannon, and V. Vasilev, “Generalized nets in image processing and pattern recognition,” in Proc. 6th Int. Workshop on Generalized Nets, Sofia, vol. 17, pp. 47–60, Dec. 2005.

[9] D. Denev and Ts. Tsankov, “A Survey of Data Quality in Digital Processing of Acoustic Signals,” in 2022 Int. Conf. on Communications, Information, Electronic and Energy Systems (CIEES), Veliko Tarnovo, Bulgaria. IEEE, 2022. ISBN: 978-1-6654-9149-5. [Online]. Available: https://doi.org/10.1109/CIEES55704.2022.9990685

[10] D. Denev and A. Docheva, “Software Processing of Audio Signals in Digital Audio Workstation Studio One Through Effect Plugins,” in Proc. Conf. with Int. Participation MATTEH 2024, vol. 2, Communication and Computer Technologies, ISSN: 1314-3921.

[11] D. Denev, “Music Scoring for Film Using Fruity Loops Studio,” Annual of Konstantin Preslavski Univ. of Shumen, vol. XI E, 2021. ISSN: 1311-834X.

[12] D. Denev and Ts. Tsankov, “Synthesis and analysis of linear, discrete and time-invariant systems, used in the field of communications, using MATLAB and signal processing toolbox,” J. Scientific and Applied Research, vol. 22, pp. 72–80, 2022. ISSN: 1314-6289.

[13] K. Atanassov, “The Foreign Object Principle and its generalized net interpretation,” in Proc. 1st Int. Workshop on Generalized Nets, Sofia, vol. 9, pp. 34–36, July 2000.

[14] K. Atanassov and H. Aladjov, “A generalized net for machine learning of the process of mathematical problems solving: on an example with a Smarandache problem,” Smarandache Notions Journal, vol. 12, pp. 338–344, 2001.

[15] S. Fidanova, K. Atanassov, L. Kirilov, V. Slavova, and V. Ivanov, “Generalized Net Model of the Consequences of Earthquake,” in Int. Symp. on Bioinformatics and Biomedicine, Cham: Springer Nature Switzerland, 2022, pp. 281–292.

[16] M. Lubich, V. Papazov, E. Popov, R. Georgieva, D. Dmitrenko, B. Bojkov et al., “A Generalized Net Model of the Prostate Gland’s Functioning,” Mathematics, vol. 10, no. 3, p. 479, 2022.

Environment. Technology. Resources. Rezekne, Latvia
Proceedings of the 16th International Scientific and Practical Conference. 2025. Volume IV, 393-397

Flood Risk Assessment and Management Under Directive 2007/60/EU: Geodetic Approaches and Digital Technologies for Effective Prevention

Ani Stefanova
Department of Applied Geodesy Faculty of Geodesy
University of Architecture, Civil Engineering and Geodesy
Sofia, Bulgaria
stefanova_fgs@uacg.bg

***Abstract*-This article analyses the application of Directive 2007/60/EU on flood risk assessment and management, mainly focusing on the preliminary risk assessment and the methods for identifying and classifying areas with significant potential flood risk. It examines also various criteria and techniques for designing flood threat and risk maps as well as flood risk management plans. Special attention is directed at geodetic activities in the stage of preliminary studies in flood prevention, including digital terrain model of river valleys and creation of cross sections for hydraulic studies. It emphasizes the importance of the accuracy of digital topographic models and cross sections for successful flood management. The article proposes a systematic approach to effective flood risk management using geodetic and digital technologies in compliance with the European standards and Regulations.**

Keywords- cross sections, digital terrain model, European Directive, flood prevention, geodetic works.

I. INTRODUCTION

One of the main factors for floods (Fig. 1) in a certain territory is the inability to process unusually large amounts of water ("high tides") due to intense rainfall, melting snow, destruction of embankments, break of a dam wall or human activity through certain "critical" places of water currents.

Flood prevention includes measures such as research, design, construction works and constant monitoring of the relevant territory.

In the middle of the previous decade, the applied flood prevention measures were established as not sufficient and it was necessary to redirect to comprehensive flood risk management in the conditions of "coexistence" with floods. This is a serious problem that needs a solution.

Fig. 1. Flooded Vidin, Bulgaria - 1942

The main goal and task are to reduce future risk through research, assessment and impact on all factors influencing the flood occurrence and the significance of their consequences to human health, economic activity and environment.

As a solution to the identified problem, a comprehensive approach to flood risk management is introduced with Directive 2007/60/EU [1] – the European Floods Directive.

II. MATERIALS AND METHODS

The flood risk assessment for Bulgaria follows Directive 2007/60/EU, using a unified methodology under the Water Act. It includes geodetic surveys, hydraulic modeling with Chézy and Manning formulas, and digital terrain models from photogrammetry and laser scanning. One-dimensional (1D) and two-dimensional (2D) models estimate flood depths and velocities, while GIS and AutoCAD data ensure accuracy. These methods support precise flood hazard mapping and risk management planning.

Online ISSN 2256-070X
https://doi.org/10.17770/etr2025vol4.8402
© 2025 The Author(s). Published by RTU PRESS.
This is an open access article under the Creative Commons Attribution 4.0 International License.

A. Directive 2007/60/EU for flood risk assessmentand management

Flood risk assessment and management for the Republic of Bulgaria is subject to the European Floods Directive [1] which has been in force since 26.11.2007 and was transposed into the national legislation with the Amendment of the Water Act in August 2010.

The Directive [1] requires member states to implement a long-term planning approach to flood risk reduction in three stages:

- Preliminary flood risk assessment;
- Flood hazard and risk maps;
- Flood risk management plans.

a) Preliminary flood risk assessment

The main task of the preliminary flood risk assessment is to assess the potential future flood risk in the basin management area in terms of human health, economic activity, environment and cultural and historical heritage.

The ultimate goal is to identify areas with a significant potential flood risk or significant likelihood of potential flood risk, based on the preliminary assessment.

According to the Water Act, the preliminary flood risk assessment in Bulgaria is done using a unified methodology [1].

Methodological guidelines have been developed with a detailed description of the necessary work stages and recommendations for their implementation.

The methodological instructions are structured in three separate parts:

- Part A – Preparation for development of methodological guidelines.
- Part B – Methodological guidelines for preliminary flood risk assessment.
- Part C – Methodological guidelines for development of flood hazard and risk maps.

The criteria and methods for determining and classifying risk and identifying areas with significant potential flood risk [1] are listed and described below.

- Horizontal distance criterion (Fig. 2) – the horizontal distance between a site and a nearby river can be used to approximate the flood threat.

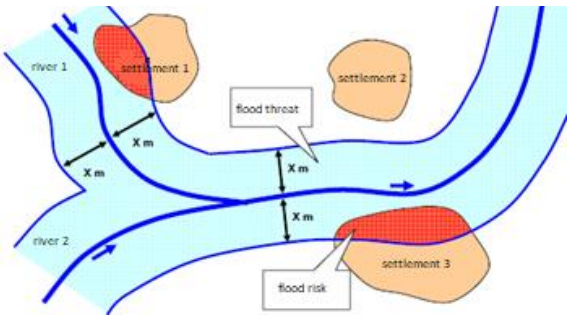

Fig. 2. Schematic draft of horizontal distance criterion

- Criterion for vertical distance (Fig. 3) – it is assumed that there is a constant depth of flooding starting from the lowest point of the river valley.

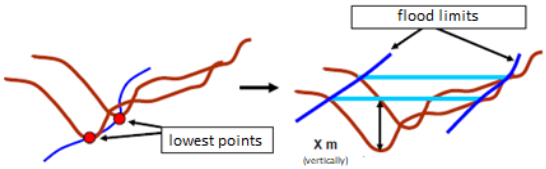

Fig. 3. Approach in applying vertical distance criterion.

- Method for calculating the normal depth – when both hydrology and the influence of topography on flood runoff conditions must be taken into account simultaneously, a simplified hydraulic approximation of the flooded depths calculated for steady movement/steady current conditions can be used. When calculating the normal depth, the Chézy formula (2) and the Manning formula (3) are applied to calculate the Chézy coefficient:

$$Q=V_mA \quad (1)$$

$$V_m = C\sqrt{RI} \quad (2)$$

$$C = \frac{1}{n}R^{1/6} \quad (3)$$

Gauckler-Manning formula:

$$v_m = \frac{1}{n}R^{2/3}I^{1/2} \quad (4)$$

$$R = A/U \quad (5)$$

where: Q – runoff [m^3/s]; v_m – average current velocity [m/s]; A – cross section area [m^2]; C – speed coefficient [$m^{1/2}s$]; R – hydraulic radius [m]; I – water surface slope; n – Manning's roughness coefficient; U – wet perimeter.

- Method of using 1D model for calculating river sections – first, cross sections profiles must be extracted from the digital terrain model (Fig. 4). Based on them, the hydraulic 1D model is created which helps for assessment of depths and water levels in the studied area with set water quantities/runoff values.

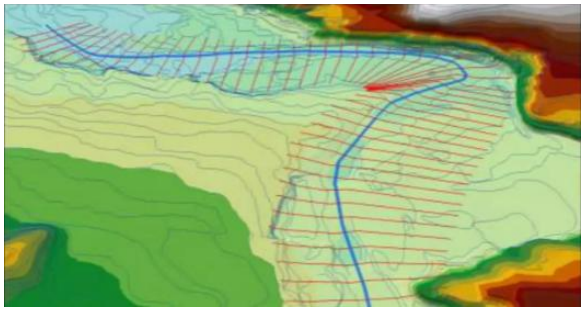

Fig. 4. Determination/extraction of cross section profiles for hydraulic calculations from a digital terrain model

- Method of using 2D - river models - when complex current conditions are present.

- Method of using a hydrological model based on a calculated Raster network for 2D – calculation of the surface runoff.

b) Preparation of flood hazard and risk maps [1]

Map making activities include:

- Geodetic measurements;
- Hydrological and hydraulic calculations and flood threat assessment;
- Processing and analysis of data for potentially affected sites and flood risk assessment;
- Creation of databases with intermediate and final results;
- Preparation of digital maps.

Flood hazard maps (Fig. 5) are for low, medium and high probability of flood occurrence. The Directive regulates the average probability of occurrence – 1%.

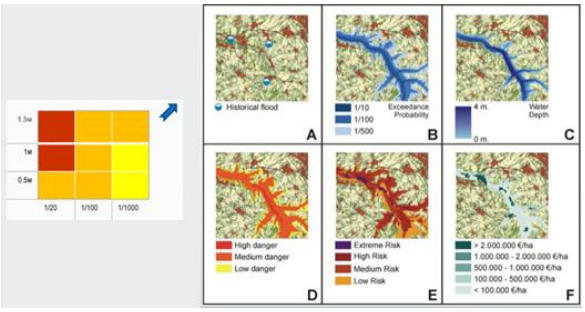

Fig. 5. Flood threat and risk maps: A – map of past floods; B, C – flood threat maps; E, D – flood risk maps; F – flood hazard map

c) Preparation of a flood risk management plans

The development of a flood risk management plan has been assigned to the Director of the Basin Directorate.

Flood risk management plans focus on:

- prevention
- protection
- preparedness
- forecasts and early warning system for flood risk.

B. Geodetic works in preliminary surveys for flood prevention

Geodetic works are part of complex activities related to flood prevention and damage assessment when high tides pass through potentially dangerous river valleys.

During the preliminary surveys, the following geodetic works [2] are carried out:

- Assessment (surveying) of the actual technical characteristics of artificial water sites – reservoirs, protective embankments, corrected spans, bridges, etc.;
- Defining the capabilities of existing reservoirs for high tides accumulation – updating "ponded volumes" curve, "flooded areas" curve, degree of reservoir filling with sediments;
- Geodetic surveying of riverbeds and protective facilities in the corrected river spans;
- Identifying "critical" points in past events;
- Creation of a digital topographic model of the river valley and its flooded areas.

C. Creation of cross-section profiles for hydraulic research

It is necessary that the cross-section profiles in the area of the facilities are representative of the river span with a density that allows for sufficient calculation of energy losses when the water current passes through the bright span of the facility.

The profiles are located in such a way that the energy gradient, the water surface slopes and the nature of the bottom in the inter-profile spaces are practically constant.

Cross-section profiles [2] are laid in:

- places with sharp changes in the river width;
- all major curves in the river bed;
- places where the current velocity changes abruptly, for example in the beginning and in the end of river rapids;
- the beginning and the end of river embankments (Fig. 6);

Fig. 6. Example of location of points for measuring a river profile [4]

- places or in proximity to existing permanent control cross section profiles;
- places of tributaries confluence which contribute to the main river runoff. Profiles are located (on the main current) immediately before and after the points of tributary confluence as well as along the tributary itself, immediately before the place of confluence;
- places before, after and in the span of bridge passages.

USACE (United State Army Corp of Engineers) recommends the following maximum distances between profiles [5]:

- 800m, for wide flooded areas and water surface slopes less than 0.38 ‰;

- 540m, for slopes less than 0.57 ‰;

- 360m, for slopes bigger than 0.57 ‰.

The location and range of the profiles are defined and marked in GIS format. The cross-section profiles are presented in AutoCAD format and the measured points are presented in ArcGIS database in horizontal coordinate system ATRS89 or WGS84. Also, the height data must be presented in the EVRS2007 height system and in the Baltic height system. The coordinates of the profile points are also presented in the 1970-year coordinate system.

D. Digital topographic model of a river valley

In the general case of computer modeling of river valleys aiming to determine the boundaries of flooded areas when passing high tides, the digital terrain model covers the watershed basin of the entire river system - the main river and all tributaries with significant contribution to the total river runoff [2].

The necessary information for creation of digital topographic model is obtained from:

- Airborne laser scanning (Fig. 7);

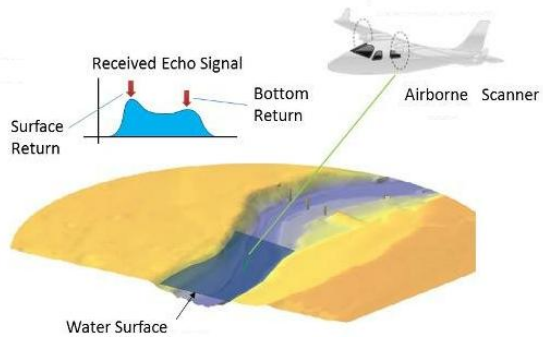

Fig. 7. Laser scanning

- Geodetic surveying of hydrotechnical facilities;

- Cross section profiles of the river bed (Fig. 8);

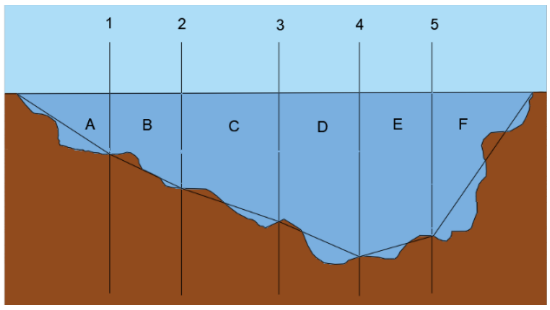

Fig. 8. Scheme of cross section river profiles

- From existing or specially performed topographic, hydrographic, photogrammetric or other types of remote measurements.

- Existing topographic maps (Fig. 9);

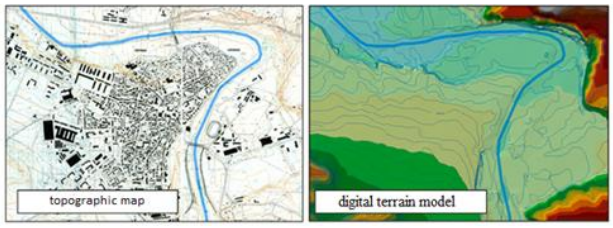

Fig. 9. Digital terrain model built on the basis of an existing topographic map [3]

E. Accuracy of cross section profiles and digital topografic models

In Bulgaria, there are no specific standards for the accuracy of geodetic works for the needs of hydraulic modeling. Only the Technical Specification of the Basin Directorate [6] mentions that the minimum horizontal accuracy of measuring points from cross section profiles is 25cm and the vertical accuracy is 10cm but these accuracies are not justified.

When performing such tasks, geodesists are guided by the specific technical specifications, the available source materials and tools as well as their own professional experience.

The following presentation shows the accuracy requirements determined in a study conducted in the 1990s by the Hydraulics Center of the US Army Corps of Engineers [5], supplemented with considerations regarding the possibility of their application in our country [2].

The main criterion for the impact of errors from the geometry profiles on hydraulic modeling was considered to be the corresponding error in the height of the high tide at a given span of the river valley with an appropriately selected velocity coefficient of the modeled water current.

Based on the research, the following conclusions were drawn:

- In areas where the velocity coefficient is determined with high reliability, the impact of errors in the heights of the cross-section profiles over the height of the model water surface is insignificant;

- The depths in the riverbeds along the profile line must be measured with an accuracy no less than 15 cm, i.e. directly using hydroacoustic equipment.

- Height errors when surveying profiles passing facilities (embankments, road, railway slopes, etc.) must not exceed 15cm. Profiles can be extracted directly from photogrammetric stereo models and in areas with dense vegetation by measuring via GPS in RTK mode or with a total station;

- With a given accuracy of the model high tide height – between 5 and 15cm with a sufficiently reliably

determined velocity coefficient, the allowable error in the heights of the cross-section profiles does not exceed 0.65m. With such accuracy, the profiles can be extracted directly from a stereophotogrammetric model prepared for topography mapping with 2m basic section. In relation to the conditions in Bulgaria, this means that for plain areas, digital terrain models, respectively profiles can be built using Large-scale Topographic Maps (LSTM) in scale 1:5000. In areas with hilly, semi-mountainous and mountainous topography where LSTM does not provide the necessary accuracy in depicting the area, it is necessary to conduct new photogrammetric or lidar measurements ensuring the specified accuracy.

The choice of 15 cm as the accuracy threshold in geodetic measurements for hydraulic modeling is based on both practical considerations and the findings from the Hydraulics Center of the US Army Corps of Engineers. Their study demonstrated that a 15 cm error margin in cross-section profile measurements does not significantly affect the accuracy of hydraulic modeling, particularly when the flow velocity coefficient is well-determined. This threshold aligns with the accuracy capabilities of commonly used surveying equipment, making it a practical standard in hydraulic modeling practices, ensuring sufficient precision without unnecessarily complicating the process.

III. Results and discussion

The flood risk assessment in Bulgaria, conducted under Directive 2007/60/EU, has enabled the identification of areas with significant flood risk through a structured methodology. The application of horizontal and vertical distance criteria, combined with hydraulic modeling, has provided reliable estimates of flood-prone areas. The use of 1D and 2D hydraulic models has improved accuracy in determining water depths and velocities, especially in complex terrain. Digital terrain models (DTMs) derived from geodetic surveys, airborne laser scanning, and photogrammetric data have enhanced the precision of flood hazard and risk maps. Despite the lack of specific national accuracy standards, the integration of USACE guidelines has ensured reliable data collection, particularly in geodetic measurements for hydraulic modeling. The results support effective flood risk management by enabling targeted prevention, protection, and preparedness measures, though further refinement of accuracy standards and methodologies could enhance predictive capabilities.

IV. Conclusion

The implementation of Directive 2007/60/EU and the integration of geodetic works into the flood risk assessment and management process provides a comprehensive approach to protecting society and natural resources. This complex process requires cooperation between different institutions and specialists to ensure maximum efficacy and sustainability of flood prevention and management measures.

ACKNOWLEDGEMENTS

I would like to express my gratitude to the Basin Directorate for providing essential data and methodological guidance for this study. Special thanks to the experts and institutions whose research and recommendations have contributed to improving flood risk assessment and management in Bulgaria.

REFERENCES

[1] Directive 2007/60/EU on flood risk assessment and management, 2007.

[2] T. Kostadinov, D. Ognianov and R. Aneva, Geodetic works for flood protection in potentially dangerous river valleys, International Anniversary Scientific and Applied Conference, UACEG, 2012.

[3] Preliminary flood risk assessment in the main river basins of the Republic of Bulgaria - methodology for flood risk assessment according to the requirements of Directive 60/2007/EU, Part B, Methodological guidelines for preliminary flood risk assessment, Sofia, 2011.

[4] Report on the assessment of potential future floods in the Danube region and identification of indicative flood risk areas, Sofia, 2012.

[5] River Engineering Hydraulic and Channel Stabilization Survey. EM 1110-2-1003. Charter 17. United States Army Corp of Engineers. 2002.

[6] Technical specifications "Preparation of flood hazard maps and flood risk maps for the Danube River Basin Management Region". Programme "Environment" 2007-2013" 2014.

Environment. Technology. Resources. Rezekne, Latvia
Proceedings of the 16th International Scientific and Practical Conference, 2025. Volume IV, 399-406

Agile Leadership Unveiled: Essential Traits

Julija Steinhart
Business Management
BA School of Business and Finance
Riga, Latvia
julja.steinhart@gmx.ch

***Abstract*— The expectation on becoming agile is rising. Businesses implement agile values in the last 20 years, especially in the software and product development, and in the fast-changing and often unforeseen environment, agility may sound as a solution to fast adaptation and flexibility. At the hard of this adaptability lies the agile leader, driving the organizational resilience and innovation. While micro and macro levels of corporate hierarchy have been widely studied, meso level and hierarchical interplay between individual and leader are so far being neglected. The aim of this study is to spot key attributes that define agile leadership excellence. To achieve this aim, a qualitative study based on interviews has been performed. In total, 40 Chief Technology Officers (CTO) who apply agile values and methods in their daily businesses have been interviewed during July-August 2024. In addition, a systematic literature review and bibliometric analysis have been applied to elaborate on academic research in this field. The bibliometric analysis is based on a literature review of publications obtained from Scopus using an inclusive search strategy. To visualize the data, Bibliometrix and VOSviewer have been used. This article aims to enhance research on agile leadership by identifying key traits of agile leader to manage complexity, reciprocate team capabilities and enhance outcome. By examining these traits, author is uncovering the role of leader regarding all stakeholders. The study comes with the conclusion and recommendations for both business and academia.**

Keywords*— *Agile leadership, agility, traits, trends, business

I. Introduction

To survive as a corporation nowadays a fundamental transformation to become more agile is being crucial. The corporation is viewed as living systems that is stable and dynamic at the same time. According to De Smet [1], the transformation of every corporation starts with its leadership that drive successful change while adopting new mindsets and capabilities.

As per meta-analysis performed by Porkodi [2], agile leader impacts efficiency, employee performance, team effectiveness and various organizational outcomes. How to achieve agility and what is meant by that towards leadership practices is an important topic for contemporary research. Agile leadership deployment is impacting also internal processes while offering the opportunities for employees to feel part of the broader decision-making process according to Rialti et. Filieri [3]. Leaders are catalysts for change, identifying rearrangements in the outside environment and adapting business structures accordingly as has been stated by Malik et al. [4].

Consequently, agile values lived by leaders as role models may become not only a challenge but a stimulant for organizational transformation.

Several authors contributed to the study of agile leadership and highlighted its importance for businesses; however, our knowledge on the role of agile leader and its characteristics is still very limited. Especially, there is a lack of understanding on the leadership styles that are most suitable for the C-level management. Understanding the specific actions must take and personal attributes of senior management to ensure strategic development of businesses in the specific industry is equally important.

To address these research gaps, this study investigates the role of emergent leadership style, agile leadership in banking industry. Rigby et al. assert that product-oriented businesses can adopt an agile test-and-learn approach to foster incremental thinking across the company. However, this approach remains challenging for service-oriented businesses like banking [5]. In addition to agile leader incremental, author is building up and expanding three core principles of agile practices defined by Denning. Several authors confirms that agile leadership differs from traditional leadership styles. Thus, with this study, author attempt to answer the following research question:

RQ: What are the main traits and characteristics of agile leader?

To answer this research question and achieve the aim of this study, a qualitative study of an interpretive nature to be considered [6]. The typical leadership study is usually assessed thru a questionnaire that is filled in by subordinates or supervisory, however as stated by Hunter et al [7], since leadership is a process and typical leadership study often fails to consider the situation. Further research also was proving that assessments thru questionnaire can be substantially biased as shown by Hansbrough et al [8]. In addition to that, leadership questionnaires tend to be too generic as

Online ISSN 2256-070X
https://doi.org/10.17770/etr2025vol4.8456
© 2025 The Author(s). Published by RTU PRESS
This is an open access article under the Creative Commons Attribution 4.0 International License.

shown by Yukl [9]. Taking the above into account, author has decided to proceed with the structured interview given that these are established and more context sensitive as confirmed by Liden et Antonakis [10] and Zaccaro et al. [11].

A systematic literature review, a commonly used bibliometric methodology, has been conducted to assess the literature on agile leadership and its role within a specific industry, providing a comprehensive overview of existing research in the specific field as Kraus has shown it [12].

The search period analysed was from July to Augst 2024. Data has been extracted from Scopus in June 2024 to conduct bibliometric analysis to map dominant knowledge gaps in the literature on agile leadership and agile leader. By leveraging the systematic nature of bibliometric methods, tis study pinpoints key areas of research and highlights the underexplored topics on future investigation of leadership characteristics, also independent of leadership styles. This analysis is based on structured method to quantitatively review the volume and evolution of research on agile leadership. The bibliometric analysis also facilitated summarizing the current state of knowledge as proposed by Bolbot [13]. This was summarised from a bibliometric perspective using Scopus and VOSviewer.

The aim of the study is review and integrate situational and context-based parameters into a conceptual framing of agile leader traits. This includes broader scope of leader attributes such as social skills, values and inter-personal capabilities

In that sense, the article is divided into four sections: i) this introduction, ii) tools and methods, iii) results and discussion and v) discussions and final remarks.

II. MATERIALS AND METHODS

A. Tools and data synthesis

Author processed with two-step approach while initially working with the bibliometric analysis to establish the research body and, consequently, while preparing, conducting and assessing the interview results.

The bibliometric analysis on agile leadership has been performed by using Scopus, a leading academic database with extensive research data coverage as well as open-access content [14]. Bibliometric overview provided an understanding on previous research contributions and gaps related to specific leadership style such as agile leadership.

SCOPUS has been used to keep the dataset consistent relying to one database only, ensuring the findings remain comparable. Data from different databases may content biased variations.

Especially the possibility to filter and refine results by specification has been important for usability of Scopus search. To keep align with business practices on agility and considering the introduction of Agile Manifesto in 2001, the search period has been chosen accordingly. For the period of 2001-2024, 706 relevant articles were retrieved on the 'agile leader' and 988 relevant articles on 'agile leadership' and this data has been analysed using bibliometric approach. Out of these only 114 publications have been touching on the criteria *"agile AND (leader OR leadership) AND (traits OR characteristics)"*. None of these has established traits model as main premise of research gap. Titles, keywords and abstracts have been reviewed to make sure that they are consistent with the specified search and to avoid result overlap on both search criteria's (leader and leadership). Hence, manual data cleaning has been performed on the identified results to make sure the data extracted is stable and accurate. Following, a detailed analysis has been conducted on 110 articles that fully met the search criteria, using precise systematic techniques. To proceed with data synthesis and prepare the interview questions, methodical and exacting techniques have been used.

Filters have been set for the language, access type, research period, document type, publication stage.

B. Methods

a) Data selection

The initial collection of the data has been performed based on data within Scopus database and enriched with visualization to graphically represent the bibliometric maps as confirmed by Eck & Waltman [15]. In addition, the research has been formalized while combining both qualitative and quantitative components as identified by Syhyda [16].

It was supplemented by findings from Nielsen [17], that bibliometric analysis identifies emerging trends while building on various statistical methods to analyse large data set.

While analysing the extracted dataset of 114 publications in total, keyword analysis has been performed to understand dependencies and identify coherency of leader characteristics. Hence, co-occurrence within the network of relationships between keywords has been conducted.

A double combination of the pre-defined words has been used within Scopus search ("agile leadership" and "agile leader") for the assessment of the overall results in the first part of this article. Based on applied dataset, further analysis has been conducted based on bibliometrix and overlap visualization in VOSviewer. As a result significant co-occurrences have been identified. On top, cluster analysis was conducted to identify data patterns and findings have been summarized in this article.

Since the defined dataset has been extracted for the period of 2001-2024, this article is based on the analysis covering the specific period and may not reflect most current publications. Since the analysis of author is based during this stage of research on keyword analysis only, a comprehensive examination of sentences and context has been not covered in a full extent. Author, however, bearing this dependency in mind, mitigated the limitation while using VOSviewer to visualize trend analysis.

b) Structured inteview

Based on the initital colleaction of data regard agile leadership characteristics and traits, structured interview questions have been established.

Interviewing is a commongly used research method that allows researchers to explore how individuals subjectively interpret social phenomena around them as been confirmed by Kvale . Thus, interviews allow participants to share their emorions, biases, opinions and attitudes towards organisational contexts.

In comparison to quantitative research that focuses on examining cause-and-effect relationships, qualitative interview uncover how individuals value their social experiences and offers holistic understanding of unexplored phenomena beyond predefined hypotheses and variable relationships as identified by Denzin & Licnoln [18].

Based on the above epistemological stances adopted by researchers, author aligned with the relational nature of private and professional experience of the interviewee, engaged with

them while deepening or rephrazing questions and evaluations as well interpreted interviewees subjective core part within the interview process.

Main aim of interviews was to expand the research practice and establish body of knowledge confirmed by management experiences. The established approached mitigate the biase of approaching leaders that are not in scope of the research question. With other words, the one who are holding C-level position but not fall under the definition of being agile leader or are not applicate agile principes, or rather ones who are make use of agility but not holding leader position.

Before approaching C-level leaders, author created an overview of 236 banks and its management in Switzerland based on data from Statista [19]. Following, CTO (Chief technology officer) position holders have been identified. It must be mentioned that Swiss banking sector is quite fragmented and in addition to large international banks, there are also 24 cantonal banks and 59 institutions in total are rather small banks with up to 200 employees and offering retail banking solutions. Hence, for the research 46 CTOs have been approached with request on interview. Out of these, 46 CTOs confirmed their participation, leading to 40 successful interviews in total. 6 CTOs declined due to timeslot overlaps or business reasons.

In total, 32 questions have been established based on identified elements applied to agile leader within bibliometric analysis, these have been split into 3 categories: stakeholder focus, empowered ownership, collaborative excellence.

Prior each interview, specific personal data has been collected with each interviewee such as size of bank CTO is working with, years of professional experience, years in the leadership position, highest educational qualification, gender.

Each interview has been conducted on site and longed for 30-45 minutes each, leading to approx. 1500 minutes being analysed during the post-interview assessment.

Concluding on the above main parts, the research has been determined with the findings as well as practical and research implications.

III. Results and Discussions on Agile Leader Traits

A. Systematic literature evaluation based on Scopus dataset

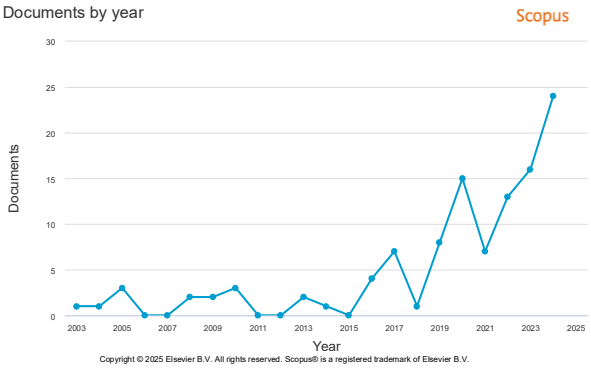

Fig. 1. Number of *publications* and citations on agile leadership traits (2001-2024) [20]

As part of the bibliometric analysis, citations and publication trends have been assessed. The assessment of documents has been ongoing since 2003, with an average of 2 to 3 documents per year. Since 2016, there has been a linear growth in the number of documents, reaching up to 25 documents per year. However, there was a notable drawdown in 2021. Despite this dip, the overall trend indicates a significant increase in document assessments over the years.

General trends indicate a relatively low level of interest in agile leadership traits during the early research years (2012-2017), with a significant surge in publications beginning in 2018. This trend may be attributed to the concept of "governance through goals" and the heightened pressure exerted by Sustainable Development Goals on companies, as noted by Biermann [19]. From 2012 to 2023, the number of published works on this topic has increased elevenfold.

Regarding citation trends, it, in general, proceeding similarly to the publication trends, showing exponential growth since 2012.

A clear correlation trend between published and cited publications is observed.

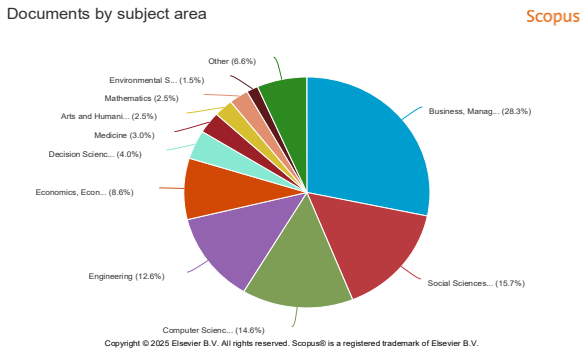

Fig. 2. Number of *publications* and citations on agile leadership traits (2001-2024) [20]

Bibliometric results summarizing raw data output out of Scopus dataset for the research area are presented in Fig 2. Research fields in the Scopus dataset were used to determine the subject areas. The ranking results show that the research area is carried out in several scientific disciplines. Looking at the results, the top 5 fields have been identified: business, management, and accounting (28.3%), social sciences (15.7%), computer science (14.6%), engineering (12.6%), and economics, econometrics, and finance (8.6%). Since a publication may cover and refer to more than one field, there are more results than publications in total. An evaluation of disciplines and source groups revealed that the most popular research topic is sustainable development. Nevertheless, a strong fragmentation of subject areas should have been mentioned.

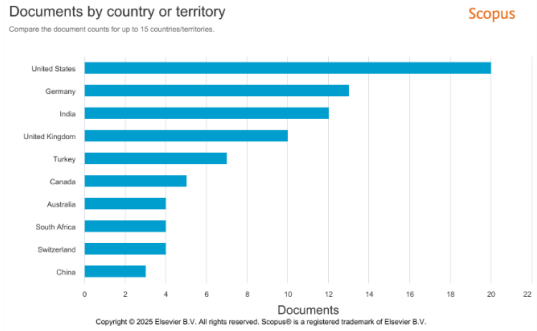

Fig. 3. Number of publications and citations by country or territory on agile leadership traits (2001-2024) [20]

The evaluation of countries confirms this trend, with the United States on position 1, being the most active in terms of publications, representing 22 publications (19.64%) in total. Germany secures the second position with 18 publications (16.07%), followed by India with 16 publications (14.29%). The United Kingdom ranks fourth with 14 publications (12.5%), and Turkey holds the fifth position with 12 publications (10.71%). Other notable contributors are Canada with 10 publications (8.93%), Australia with 8 publications (7.14%), South Africa with 6 publications (5.36%), Switzerland with 4 publications (3.57%), and China with 2 publications (1.79%). An analysis of the countries' publication distribution suggests a relatively balanced pattern, with contributions spread across multiple nations.

B. Fundamental notion, Research trends and Scientific Discussions on agile leader / leadership traits

Keyword analysis may be performed to outline the emerging trends and pivotal networks which supports visual exploration as suggested by Zhu [21] and Cheng [22].

Fig. 4 represents the results of a keyword cluster analysis of the 749 keywords used in the publications by authors since 2001. In total, these keywords were identified and analysed, 48 meeting the thresholds of 3 minimum number of co- occurrences, subsequently treated within keyword analysis from 2012 until 2023.

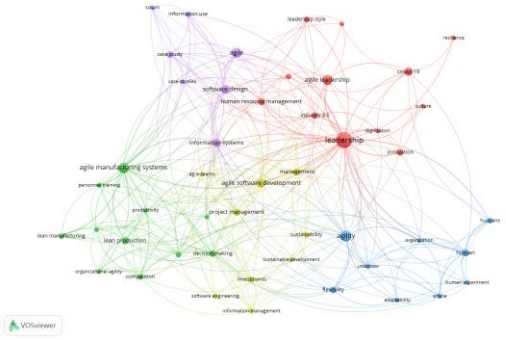

Fig. 4. Five main research clusters (based on most frequently used keywords) [20]

As presented in Fig. 4, five clusters have been identified, showing relations of agile leadership, organizational agility, and software development practices, with key thematic areas emerging as follows:

Cluster 1 (Red): Leadership and Transformation — This cluster focuses on agile leadership traits, leadership styles, digital transformation, innovation, resilience, and the role of human resource management in Industry 4.0 contexts.

Cluster 2 (Green): Operational Agility and Competitive Performance — This cluster emphasizes operational efficiency, lean manufacturing, organizational agility, competition, decision-making, and personnel training as drivers for improving productivity and adapting to dynamic markets.

Cluster 3 (Blue): Human and Organizational Adaptability — The focus here is on agility from a human perspective, exploring adaptability, flexibility, human resource involvement, and organizational behavior within agile environments.

Cluster 4 (Purple): Agile Development and Project Management — This cluster highlights agile software development, project management, software engineering, information management, and sustainability in the context of investments and sustainable development.

Cluster 5 (Yellow): Agile Methods and Case-based Research — This cluster is centered on agile methodologies, scrum practices, software design, and empirical research using case studies to develop and refine agile information systems.

The author has analyzed further and established an overview of research trends with the main objective to understand the evolving relationship between agile practices and organizational performance.

In general, the keywords with the highest occurrences have been analyzed, showing leadership (31), agility (14), agile manufacturing systems (13), agile leadership (12), and agile (12) as the most frequently mentioned terms. This finding provides the opportunity to investigate associations related to agile leadership and organizational performance further, as well as to understand the evolving scientific discourse on agile methodologies and sustainable development.

Table I shows the main keyword clusters generated by VOSviewer. In addition to that, it also shows the number of items that build the cluster: cluster red representing 11 items, cluster green representing 11 items, cluster blue representing 9 items, cluster purple representing 9 items, and cluster yellow representing 7 items accordingly.

TABLE 1. THE MOST IMPORTANT KEYWORD CLUSTERS OBTAINED WITH THE VOSVIEWER.

Cluster (items)	Keywords in a VOSviewer Network
Cluster Red (11)	agile leadership, Culture, digital transformation, digitization, human resource management, industry 4.0, innovation leadership, leadership style, leadership styles, resilience
Cluster Green (11)	agile manufacturing systems, commerce, competition, decision making, lean manufacturing, lean production, organizational agility, organizations personnel, training productivity, societies and institutions
Cluster Blue (9)	adaptability, agility, article, flexibility, human, human experiment, humans, interview organization
Cluster Yellow (9)	agile software development, agile teams, information management, investments management, project management, software engineering, sustainability, sustainable development
Cluster Purple (7)	Agile, case study, case-studies, information systems, information use, scrum, software design

C. EFA Discussion

Factor Loads	**1**	**2**	**3**	**4**	**5**	**6**	**7**	**1 - Com-monal-ity**
I continuously pay attention to excellence and good results					0.556			0.3257
I set clear expectations for team performance.	0.802							0.2030
I track and measure customer satisfaction and use this feedback in order to Improving products/services have an impact on my efforts has a positive impact on the overall performance of the team.	0.751							0.2449
I regularly moderate retrospectives, in order to continuously improve the team's performance, I take steps to resolve any discrepancies between the team members and deliver highquality results, I set high standards for the	0.513		0.317		0.574			0.0614
quality of our work and expect us to exceed these standards, I give our teams clear and	0.360			-0.379	0.326			0.3727
in order to achieve a high quality of work, I make sure that the team focused on the provision of quality work.	0.331	0.399						0.5425
I am transparent with stakeholders when it comes to		0.499			0.391			0.3650
Challenges or setbacks that could have an impact on expectations. I involve stakeholders in the		0.482						0.6232
expectation formation process and include their feedback. I manage the expectations of the					0.354		0.582	0.3987
stakeholders through direct communication.							0.994	0.0366
I attach great importance to personal conversations				0.901				0.2074
If I am not afraid to talk directly to myself about failures, I provide the team members with the resources and support to			0.376	0.488				0.4616
that they need to organize themselves and thus contribute to the team's success.			0.467	0.560				0.2318
I promote a culture of Responsibility and Personal responsibility by being a role model with my own actions.				0.409				0.4261
I balance the autonomy well with collaboration within team members.	0.489							0.4481
I promote the exchange of knowledge between team members.						0.445		0.5052
I always promote cooperation with different stakeholders.						0.972		0.0829
I create meaning and purpose in the team.						0.504		0.4318
I acknowledge and reward Team members who are responsible for take over their work and show responsibility.		0.661						0.3898
I ensure the timely recognition of successes.		0.433		0.379				0.4060
I clearly communicate the future direction of organizational development.	0.548							0.4372
I welcome changed requirements, even in the late Phase	-0.300		0.613					0.5315
I balance well between short-term goals and long-term strategy.		0.624						0.5400
I adapt to changing circumstances during the project and change the strategies accordingly		0.667						0.4878
I promote continuous learning and development.		0.345		0.410				0.5441
When making decisions, I take the needs and preferences of the Putting customers first	-0.416	0.452	0.405					0.4170
I ensure that our products/services meet or exceed our customers' expectations.			0.459	-0.328			0.382	0.4147
Factor Loads	**1**	**2**	**3**	**4**	**5**	**6**	**7**	**1 - Com-monal-ity**
I encourage the team to collect feedback from customers and use it to Improving our products/services.			0.769					0.2768
I promote cooperation in the team in order to identify and respond to customer needs	0.363		0.570					0.3858
I enable the team to make decisions that prioritize the value and satisfaction of the customer.			0.417		-0.390			0.4169

Note. "Factorization of the main axis" extraction was used together with an "Oblimin" rotation

Fig. 5. EFA Page

The exploratory factor analysis (EFA) assessed is based on survey data collected from Chief Technology Officers (CTOs) in the Swiss banking sector, as part of a qualitative and quantitative investigation into agile leadership traits. A total of 40 survey responses were analyzed, representing a diverse range of banks, including both large international institutions and smaller regional banks. The survey comprised 32 items designed to assess various leadership behaviors aligned with agile principles.

The factor analysis was conducted using the principal axis factoring method, which is suitable for identifying latent constructs within datasets that may not exhibit normal distribution and appropriate for studies within banking sector as per Rodriguez- Calderon [23]. An oblimin rotation has been applied, allowing for bootstrapping correlations between factors, which aligns with the understanding that agile leadership traits are often interconnected to figure out personality traits as per Branca et al [24]. Items with factor loadings below 0.3 were removed to ensure the robustness and clarity of the identified factors.

This analysis resulted in the extraction of seven distinct factors, representing core dimensions of agile leadership. These factors reflect different but complementary aspects of leadership personality that contribute sustainably to team and organizational agility, resilience as well as performance. The results of the factor analysis are integrated with qualitative insights from interviews with banking CTOs and a systematic literature review.

a) Factor 1: Performance-oriented leadership

This factor underscores the importance of setting clear performance expectations and measuring outcomes according to Granger et al [25] Agile leaders scoring high on this factor focus on establishing performance benchmarks and tracking key performance indicators, ensuring that teams underpin success criteria and work toward delivering measurable results. Such leaders foster a culture of accountability and drive continuous improvement through regular feedback loops and assessment of customer satisfaction and work quality. Performance-oriented leadership is vital in agile settings due to increase autonomy of a team, necessitating clear goals and performance feedback to maintain alignment. Key survey questions related to this factor included: 'I set clear expectations for team performance.' and 'I track and measure customer satisfaction.'

b) Factor 2: Directive clarity

Directive clarity leads to a leader's ability to reduce ambiguity by providing explicit goals and ensuring that team members understand their roles and responsibilities. Due to dynamics of agile environments, often confusion on expectations appears. Leaders exhibiting directive clarity prevent misalignment by articulating precise objectives and establishing structured processes. While agile principles emphasize flexibility and adaptability, clarity serves as an anchor, ensuring that teams pivot within a shared understanding of their core objectives. Key survey questions related to this factor included: 'I give our teams clear and concrete goals.' and 'I create clear responsibilities and accountabilities.'

c) Factor 3: Embracing change

Change-embracing leaders demonstrate a proactive attitude toward shifting requirements and evolving project scopes according to Jun et Lee [26]. Leaders view changes as opportunities rather than disruptions, fostering a mindset that promotes innovation and responsiveness. This factor aligns closely with the agile manifesto's core value of welcoming changing requirements, even late in development. Leaders remain flexible and adaptive, enabling rapid iterations and adjustments based on emerging insights or market demands. Key survey questions related to this factor included: 'I welcome changing requirements, even in late project stages.' and 'I adapt our plans flexibly to new insights.'

d) Factor 4: Relationship-oriented communication

Core basis of agility is communication as per Hummel et al [27]. Relationship-oriented leaders prioritize building strong interpersonal connections with their stakeholders and within their teams. Hence, open dialogue, personal conversations and trust through transparency are initial. In agile settings, cross-functional collaboration is essential, and the ability to nurture effective communication channels reduces misunderstandings and strengthens team cohesion. Leaders excelling in this dimension create a safe environment where team members feel valued and heard. Key survey questions related to this factor included: 'I place great value on personal conversations and open exchange.' and 'I promote transparent communication in our team.'

e) Factor 5: Excellence and quality focus

A focus on excellence and quality distinguishes leaders committed to delivering high-standard outcomes. This factor reflects a leader's dedication to continuously monitoring work quality, refining processes, and striving for superior performance. Agile methodologies emphasize iterative development and regular feedback loops, making quality assurance a critical component. Leaders emphasizing quality focus instill a culture where teams take pride in their outputs, minimizing defects and enhancing customer satisfaction. Key survey questions related to this factor included: 'I continuously strive for excellence and good results.' and 'I regularly review the quality of our work results.'

f) Factor 6: Knowledge sharing and synergy

This factor emphasizes the collective intelligence within agile teams. Leaders championing this factor ensure free information flow, enabling team members to make informed decisions. The culture of learning and knowledge exchange is promoted, which is especially valuable in agile environments where cross-disciplinary collaboration drives innovation. By fostering team synergy, leaders enhance problem-solving capacity and ensure that teams leverage their collective expertise. Key survey questions related to this factor included: 'I encourage knowledge exchange between team members.' and 'I ensure all team members have access to key information.'

g) Factor 7: Stakeholder engagement

Lastly, stakeholder engagement has been identified as completing factor. Leaders actively involve stakeholders in decision-making processes, gather feedback and manage expectations while creating transparency. Agile leaders understand that value delivery extends beyond internal teams to clients and partners. Maintaining a dialogue with stakeholders ensures that team efforts remain customer-centric and responsive to evolving needs, ultimately fostering trust and enhancing long-term partnerships. Key survey questions related to this factor included: 'I involve stakeholders in the expectation-setting process.' and 'I regularly seek feedback from stakeholders.'

The above identified seven factors derived from the EFA analysis offer a comprehensive framework to understanding the multifaceted nature of agile leadership and contribute sustainably

to further studies. Performance-oriented leadership, directive clarity, change embracing, relationship-oriented communication, excellence and quality focus, knowledge sharing and team synergy, and stakeholder engagement collectively form the foundation of personality traits of the agile leader. By cultivating these dimensions, leaders can better navigate the complexities of agile environments, empowering teams to thrive amidst uncertainty and driving sustainable organizational success.

IV. FINAL REMARKS

This article explored current research body and practically proven personality traits of agile leader. The article shows biases and enlarges research as well provided proposals for further studies.

It aligned the observations in publications on agile leader since creation of Agile Manifesto in 2001. Interest on agility and agile leadership has been absolved since then in academia.

Notably, 110 articles have been analysed to distinguish research trends, keyword analysis while using VOSviewer. Further research could be performed considering all limitations mentioned, foremost the research period of the article being 2001-2024.

In summary, bibliometric analysis primarily examines past publications; however, it also highlights general research trends and interests that can shape future studies on agile leadership and its traits. This study reveals insights on specific client-centric industry.

The contributions of this paper are multifaceted:

Firstly, a comprehensive synthesis of current knowledge on agile leader has been established, offering a valuable reference professionals, academics and decision-makers within banking industry.

Secondly, by revealing several angles on agile leadership, building on systematic literature review and analysis of survey of CTOs while applying EFA, seven factors has been discovered.

This multifaceted analysis emerged trends and identified personality traits of agile leader in practice.

Further studies of 7 factors identified with EFA could significantly enlarge the research body on agile leader. Future research could investigate the interplay between these factors and explore how agile leadership traits evolve across diverse industries. On a business side, integrating these factors into leadership development programs may offer practical pathways for organizations seeking to enhance their agility and striving for agile leadership.

In addition, empirical validation of these factors across different organizational contexts and situational contingencies could enhance the generalizability of the established framework. Understanding the dependencies which specific agile leadership traits are most effective would offer valuable insights for both practitioners and researchers.

In addition, development of quantitative scales to measure these seven factors may enable more rigorous testing and facilitate benchmarking of agile leadership capabilities across industries.

Hence, future studies, building upon the limitations and findings of this study, are poised to delve deeper into studies on agile leader in several industries by exploring real cases. This may lead to further robust and comprehensive research outcomes.

Declarations. The manuscript has not been previously published, submitted or uploaded to any archive or pre-print server. Any tables or figures displayed in the manuscript are of authors own creation, and she holds the copyright for these materials. The author has no relevant financial or non-financial interests to disclose.

Author is a PhD Scholar at BA School of Business and Finance, Latvia. She is researching in the field of agile leadership and sustainable organizational performance as well as private banking. ORCID ID: https://orcid.org/0000-0001-6012-7749

REFERENCES

[1] A. De Smet Michael Lurie Andrew St George, "Leading agile transformation: The new capabilities leaders need to build 21st-century organizations," Oct. 2018. Accessed: Feb. 16, 2025. [Online]. Available: https://www.mckinsey.com/~/media/mckinsey/business%20functions/people%20and%20organizational%20performance/our%20insights/leading%20agile%20transformation%20the%20new%20capabilities%20leaders%20need%20to%20build/leading-agile-transformation-the-new-capabilities-leaders-need-to-build-21st-century-organizations.pdf

[2] S. Porkodi, "The effectiveness of agile leadership in practice: A comprehensive meta-analysis of empirical studies on organizational outcomes," *Journal of Entrepreneurship, Management and Innovation*, vol. 20, no. 2, pp. 117–138, 2024, doi: 10.7341/20242026.

[3] R. Rialti and R. Filieri, "Leaders, let's get agile! Observing agile leadership in successful digital transformation projects," *Bus Horiz*, vol. 67, no. 4, pp. 439–452, Jul. 2024, doi: 10.1016/j.bushor.2024.04.003.

[4] M. Malik, M. M. Raziq, N. Sarwar, and A. Tariq, "Digital Leadership, Business Model Innovation and Organizational Change: Role of Leader in Steering Digital Transformation," *Benchmarking An International Journal*, Apr. 2024.

[5] D. Rigby, J. Sutherland, and A. Noble, "Agile Project Management Agile at Scale," May 2018. Accessed: Feb. 17, 2025. [Online]. Available: https://hbr.org/2018/05/agile-at-scale?destination=/leadership…--4d5eacf81caf039be22f2498dcaa6928ff7dc723%26page%3D11&page=24

[6] J. M. Paes, L. F. Scavarda, P. Ceryno, and E. Machado, "Human technology organizational dimensions for sustainable logistics: a context mechanism outcome model," *Brazilian Journal of Operations and Production Management*, vol. 19, no. 2, 2022, doi: 10.14488/BJOPM.2022.002.

[7] S. T. Hunter, K. E. Bedell-Avers, and M. D. Mumford, "The typical leadership study: Assumptions, implications, and potential remedies," *Leadersh Q*, vol. 18, no. 5, pp. 435–446, Oct. 2007, doi: 10.1016/J.LEAQUA.2007.07.001.

[8] T. K. Hansbrough, R. G. Lord, and B. Schyns, "Reconsidering the accuracy of follower leadership ratings," *Leadersh Q*, vol. 26, no. 2, pp. 220–237, Apr. 2015, doi: 10.1016/J.LEAQUA.2014.11.006.

[9] G. Yukl, "An evaluation of conceptual weaknesses in transformational and charismatic leadership theories," *Leadersh Q*, vol. 10, no. 2, pp. 285–305, Jun. 1999, doi: 10.1016/S1048-9843(99)00013-2.

[10] R. C. Liden and J. Antonakis, "Considering context in psychological leadership research," *Human Relations*, vol. 62, no. 11, pp. 1587–1605, Sep. 2009, doi: 10.1177/0018726709346374.

[11] S. J. Zaccaro, J. P. Green, S. Dubrow, and M. J. Kolze, "Leader individual differences, situational parameters, and leadership outcomes: A comprehensive review and integration," *Leadersh Q*, vol. 29, no. 1, pp. 2–43, Feb. 2018, doi: 10.1016/J.LEAQUA.2017.10.003.

[12] S. Kraus, M. Breier, and S. Dasí-Rodríguez, "The art of crafting a systematic literature review in entrepreneurship research," *International Entrepreneurship and Management Journal*, vol. 16, no. 3, 2020, doi: 10.1007/s11365-020-00635-4.

[13] V. Bolbot, K. Kulkarni, P. Brunou, O. V. Banda, and M. Musharraf, "Developments and research directions in maritime cybersecurity: A systematic literature review and bibliometric analysis," *International Journal of Critical Infrastructure Protection*, vol. 39, p. 100571, 2022, doi: https://doi.org/10.1016/j.ijcip.2022.100571.

[14] "Scopus." Accessed: Aug. 15, 2023. [Online]. Available: https://www.elsevier.com/solutions/scopus/how-scopus-works/content

[15] N. J. van Eck and L. Waltman, "Software survey: VOSviewer, a computer program for bibliometric mapping," *Scientometrics*, vol. 84, no. 2, pp. 523–538, 2010, doi: 10.1007/S11192-009-0146-3.

[16] L. Syhyda, L. Saher, M. Gasior, N. Sygyda, N. Artyukhova, and S. Skrzypek-Ahmed, "Investigating the Role of Innovation in Inclusive and Sustainable Development in Ukraine and South Korea," *Sustainability 2023, Vol. 15, Page 11195*, vol. 15, no. 14, p. 11195, Jul. 2023, doi: 10.3390/SU151411195.

[17] S. B. Nielsen, S. Lemire, I. Bourgeois, and L. A. Fierro, "Mapping the evaluation capacity building landscape: A bibliometric analysis of scholarly communities and themes," *Eval Program Plann*, vol. 99, 2023, doi: 10.1016/j.evalprogplan.2023.102318.

[18] B. Chapter, "Ch. 2: A History of Qualitative Inquiry in Social and Educational Research," *The Sage Handbook of Qualitative Research*, no. 1, pp. 36–65, 2018, Accessed: May 01, 2025. [Online]. Available: https://uk.sagepub.com/en-gb/eur/the-sage-handbook-of-qualitative-research/book242504

[19] Statista.com, "Anzahl Banken Schweiz bis 2023 | Statista." Accessed: Feb. 16, 2025. [Online]. Available: https://de.statista.com/statistik/daten/studie/441277/umfrage/anzahl-der-bankinstitute-in-der-schweiz/

[20] scopus.com, "Scopus - Analyze search results | Signed in." Accessed: Feb. 17, 2025. [Online]. Available: https://www.scopus.com/term/analyzer.uri?sort=plf-f&src=s&sid=f9785dfb8c5980120f1957daa988edb1&sot=a&sdt=a&sl=84&s=TITLE-ABS-KEY%28agile+AND+leadership+AND+traits%29+AND+PUBYEAR+%3e+2000+AND+PUBYEAR+%3c+2025&origin=resultslist&count=10&analyzeResults=Analyze+results

[21] J. Zhu and W. Hua, "Visualizing the knowledge domain of sustainable development research between 1987 and 2015: a bibliometric analysis," *Scientometrics*, vol. 110, no. 2, pp. 893–914, 2017, doi: 10.1007/s11192-016-2187-8.

[22] F.-F. Cheng, Y.-W. Huang, H.-C. Yu, and C.-S. Wu, "Mapping knowledge structure by keyword co-occurrence and social network analysis: Evidence from Library Hi Tech between 2006 and 2017," *Library Hi Tech*, vol. 36, no. 4, pp. 636–650, 2018, doi: 10.1108/LHT-01-2018-0004.

[23] C. E. López-Rodríguez and L. F. Rodríguez-Calderón, "Acceptance and Use of Technology: The Influence on Consumption in the Colombian Banking Sector[Aceptación e uso da tecnoloxía: a influencia no consumo no sector bancario colombiano][Aceptación y uso de la tecnología: la influencia en el consumo en el sector bancario colombiano]," *Revista Galega de Economia*, vol. 33, no. 3, p. 9714, Dec. 2024, doi: 10.15304/rge.33.3.9714.

[24] E. Branca, M. Intenza, and F. Doni, "Startup entrepreneurs' personality traits and resilience: unveiling the interplay of prior experience," *International Entrepreneurship and Management Journal*, vol. 21, no. 1, p. 2, Dec. 2025, doi: 10.1007/s11365-024-01023-y.

[25] "Transformational Performance-Based Leadership: Addressing Non-Routine Adaptive Challenges - Ivey Business Journal." Accessed: Feb. 18, 2025. [Online]. Available: https://iveybusinessjournal.com/publication/transformational-performance-based-leadership-addressing-non-routine-adaptive-challenges/

[26] K. Jun and J. Lee, "Transformational Leadership and Followers' Innovative Behavior: Roles of Commitment to Change and Organizational Support for Creativity," *Behavioral sciences (Basel, Switzerland)*, vol. 13, no. 4, Apr. 2023, doi: 10.3390/BS13040320.

[27] M. Hummel, C. Rosenkranz, and R. Holten, "The role of communication in agile systems development: An analysis of the state of the art," *Business and Information Systems Engineering*, vol. 5, no. 5, pp. 343–355, Jul. 2013, doi: 10.1007/S12599-013-0282-4/METRICS.

Environment. Technology. Resources. Rezekne, Latvia
Proceedings of the 16th International Scientific and Practical Conference. 2025. Volume IV, 407-411

Modeling the Penetration Depth During Laser Marking of Layered Reinforced Composites with a Polymer Matrix

Simeon Tsenkulovski
Dep. "Mechanical Engineering and Instrumentation"
Technical university of Gabrovo
Gabrovo, Bulgaria
s.tsenkulovski@advanced-technology.eu

Petko Naydenov
Department of Management
Technical University of Gabrovo
Gabrovo, Bulgaria
petkonaydenov@abv.bg

***Abstract*— The paper studies the penetration depth of the laser radiation during marking of layered reinforced composite materials with a polymer matrix. The generated radiation is from Fiber laser – RFFL-P-502B. The study of the marking depth was carried out on a measuring microscope using Insize ISD-V150/V250/ V300 software. To derive the mathematical model of the process, a cybernetic scheme with two input factors and one objective function was used. The output power of the laser radiation – P=5÷45W and the marking speed – V=50÷250 mm/s were selected as input quantities. The penetration depth – δ[μm] was the objective function. Based on the derived mathematical models, graphical dependencies in two and three coordinate systems are presented. A dispersion analysis was conducted based on mathematical models and graphical relationships are presented for the influence of the laser beam power and marking speed on the depth of the marking stroke.**

Keywords*— *dispersion analysis, fiber laser, llayered composites, marking depth.

I. INTRODUCTION

The ever-increasing dynamics of change is one of the few constant characteristics of the reality surrounding us. Technological innovations in industry are continuous and comprehensive. The developing directions of "Industry 4.0" lead to the dynamic development of unconventional electrical technologies, powder metallurgy and other energy-saving technological processes [1] - [4]. New electrothermal technologies enable the processing of new materials (essential for the development of the electrical industry, electronics, medicine and other sectors of the economy) with increased operational properties, extended life and increased reliability. The laser marking process as part of electrophysical technologies is massively entering the production of metal products and tools, semiconductor devices, glass and ceramic products [5] - [7]. In recent years, it has also become increasingly widespread in marking non-metallic materials used in industry, as an alternative to traditional marking methods [8] - [12]. This is an innovative method that differs greatly from marking in any other way, without the use of consumables, no chemicals, no ink ribbons or other materials are needed. When laser systems are used for marking, the surfaces of the products are processed extremely accurately, qualitatively, quickly and with clear contours by the laser beam. Laser marking is a non-contact effect on the structure of the processed material, the result of which is obtaining a permanent contrast image. Information can be applied to the surface of the product with this method in the form of inscriptions, identification symbols (letters and numbers), bar codes – fig.1.a, matrix codes (2D) – fig.1.b, special characters, serial numbers, images, decoration, etc.

a. b.
Fig.1. Marking codes: a – matrix; b – 2D.

In practice, with the help of a laser, it is possible to very easily create an arbitrary image of one's own design. The quality of this image is directly dependent on both the type of workpiece being processed and a number of technological factors affecting the contrast of the image, as well as the type of laser source used. The purpose of the present study is to determine the penetration depth during laser marking of layer-reinforced composites with a

Online ISSN 2256-070X
https://doi.org/10.17770/etr2025vol4.8438
© 2025 The Author(s). Published by RTU PRESS.
This is an open access article under the Creative Commons Attribution 4.0 International License.

polymer matrix. Based on the experimental results obtained, mathematical models of the technological process are developed and a dispersion analysis is performed for the influence of the input variables (laser radiation power and marking speed) on the objective function (marking depth).

II. MATERIALS AND METHODS

In this study, two types of samples of textolite and glass textolite were used. The textolite samples are 10mm thick – Fig. 2.a and mechanical characteristics according to DIN 7753/ PFCC 202, and IEC 60893 Hgw 2082. The textolite is a composite material based on phenolic laminate with cotton fabric. Due to the higher density of the cotton fabric, the composite has good dielectric and mechanical properties, The glass textolite samples are type PTGC 201 with a thickness of 10mm – Fig. 2.b and mechanical characteristics according to IEC/EN 60893-3-1. This is a glass fiber phenolic laminate, in which glass fibers or glass fabrics are used as a filler. Epoxy resin is used as a binder. To increase the vibration and chemical resistance of the material, some of the glass fibers have been replaced with polyester fibers.

a. b.

Fig.2. Marked samples: a – textolite and b – glass-textolite.

The marking of the samples was done using a laser installation – Fig. 3,a, based on Fiber lazer – RFFL-P-502B. Its main technological characteristics are presented in Table 1.

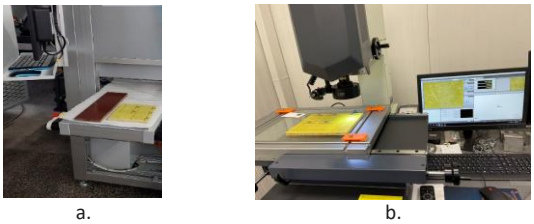

a. b.

Fig. 3 Equipment, a – marking, b - measuring

TABLE 1. CHARACTERISTICS OF THE LASER INSTALLATION

№	Items	Unit	Standard Value	Variation Step
1.	Output Power	w	5÷50	25
2.	Frequency	kHz	50÷100	25
3.	Marking Speed	mm/s	1÷2000	1000
4.	Defocusing	+/- from the focal length		
5.	Focal spot	μm	37÷42	1

The depth of the marking was examined using a measuring microscope – Fig. 3.b, using Insize ISD-V150/V250/V300 software.

III. RESULTS AND DISCUSSION

The main technological parameters in laser marking of layered composite materials on a polymer basis are the marking speed and the output power of the laser unit. To derive the mathematical model of the process, a cybernetic scheme with two input factors and one objective function was used. The input factors and the factor space were selected on the basis of preliminary experiments [6], [10] and analysis of literature sources [7], [14], [15]. In it, the output power of the laser radiation – X1, and the marking speed – X2 were selected as input quantities. As objective functions, the penetration depth – Y1 for glass-textolite samples and - Y2 for textolite samples was studied. The studies were conducted at constant values of: θ the frequency of the laser pulse – f = 50kHz; θ the inclination of the raster – α = 0º; θ defocus – S = 0mm; θ marking repeatability – R = 1. θ wavelength – λ= 1064 nm; θ focal spot diameter - df = 40μm The main levels and ranges of variation of the input quantities are presented in Table 2.

TABLE 2. FACTORS VARIATION

Factors levels	**X_1, P, W**	**X_2, V, mm/s**	**Coded value**
$X_{i0} + \Delta X_i$	45	250	+1
X_{i0}	25	150	0
$X_{i0} - \Delta X_i$	5	50	-1

At the values fixed in Table 2, marking strokes were made, and their depth was measured. The results obtained are plotted in the experimental plan - Table 3.

TABLE 3 EXPERIMENT PLANS

№	X_0	X_1	X_2	X_1X_2	X_1^2	X_2^2	Y_1	Y_2
1	+1	+1	+1	+1	+1	+1	281	182
2	+1	-1	+1	-1	+1	+1	31	18
3	+1	+1	-1	-1	+1	+1	1440	818
4	+1	-1	-1	+1	+1	+1	160	91
5	+1	+1	0	0	+1	0	469	273
6	+1	-1	0	0	+1	0	52	30
7	+1	0	+1	0	0	+1	156	91
8	+1	0	-1	0	0	+1	800	455
9	+1	0	0	0	0	0	260	152

The processing of the obtained results for the investigated objective function – Y1, leads to the determination of a linear regression equation of type 1, and for Y2 – 2

$$Y_1 = b_o + b_1x_1 + b_2x_2 + b_{12}x_1x_2 \quad (1)$$

$$Y_2 = b_o + b_1x_1 + b_2x_2 + b_{12}x_1x_2 + b_{11}x_1x_1 \quad (2)$$

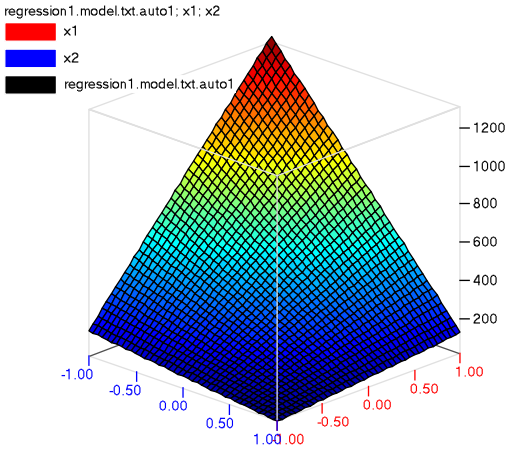

a.

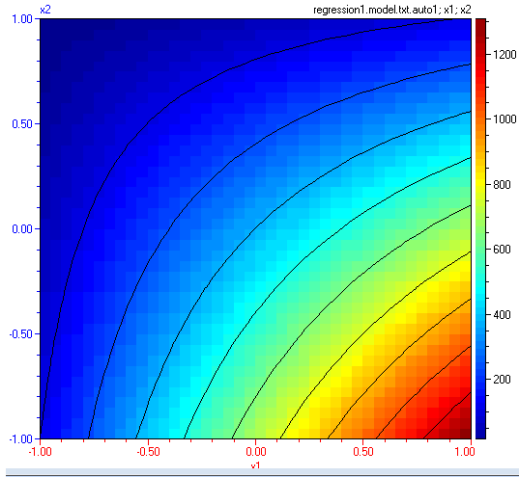

b.

Fig.4.Graphic presentation of $Y_1 = f(X_1, X_2)$
a- tridimensional; б – bidimensional

The coefficients of the regression equation are calculated by 3, 4 and 5 [7], [14], [15]. The obtained values are shown in Table 4.

$$b_0 = d_1 \sum_{u=1}^{N} x_{0u}Y_u + d_2 \sum_{i=1}^{m} \sum_{u=1}^{N} x_{iu}^2 Y_u \quad (3)$$

$$b_i = d_3 \sum_{u=1}^{N} x_{iu}Y_u \quad (4)$$

$$b_{ij} = d_4 \sum_{u=1}^{N} (x_i x_j)_u Y_u \quad (5)$$

TABLE 4 REGRESSION COEFFICIENTS

b	b_0	b_1	b_2	b_{12}	b_{11}
Y_1	405,444	324,500	-322,00	-257,50	-
Y_2	232,667	189,000	-178,83	-140,75	2,667

Based on the obtained values in Table 4, the regression equations for glass textolite and textolite, respectively, 6 and 7, have been derived.

$$Y_1 = 405,444 + 324,500X_1 - 322,000X_2 - 257,500X_1X_2 \quad (6)$$
$$Y_2 = 232,667 + 189,000X_1 - 178,833X_2 - 140,750X_1X_2 + 2,667X_1X_1 \quad (7)$$

Fig. 4 and Fig. 5 present the graphical dependencies of the derived regression equations in three-dimensional and two-dimensional coordinates.

When conducting the analysis of variance of the obtained mathematical models, the computer program AnoVA was used. Its results for the penetration depth for glass-textolite samples are presented in Fig. 6, and for textolite samples in Fig. 7.

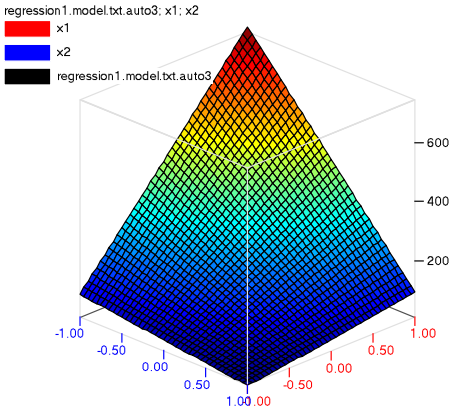

a.

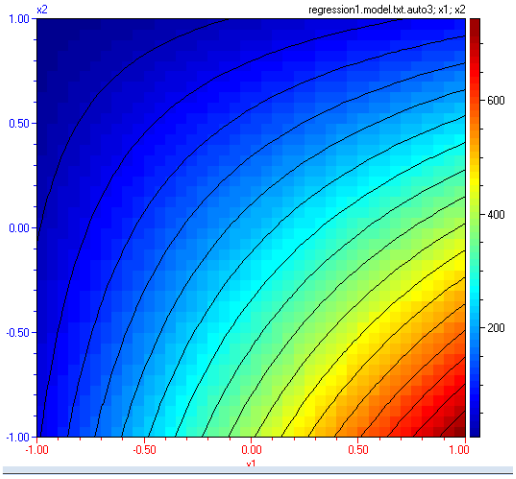

b.

Fig.5.Graphic presentation of Y2 = f (X1, X2).a- tridimensional, b – bidimensional

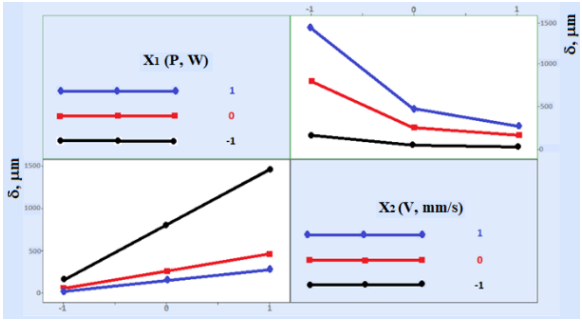

Fig.6.Dispersions analysis of $У_1 = f(X_1, X_2)$.

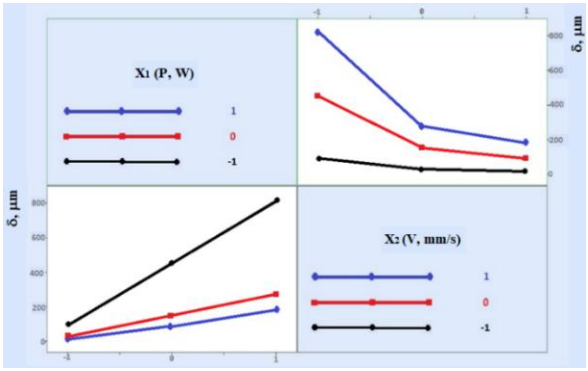

Fig.7.Dispersion analysis of $У_2 = f(X_1, X_2)$

IV. CONCLUSIONS

From the conducted research and the results obtained, we can formulate the following more important conclusions:

- The penetration depth during laser marking of layered reinforced composite materials with a polymer matrix (textolite and glass-textolite) with a thickness of 10mm was studied.
- When building the mathematical models, the laser radiation power – P = 5÷45W, and the marking speed – V = 50÷250 mm/s were selected as input factors. The laser beam penetration depth – δ,µm was studied as an objective function.
- The regression equations for the studied objective functions were derived and checked for adequacy. Graphical dependencies in two and three coordinate systems of the objective functions were constructed depending on the laser radiation power – P, W and the marking speed – V, mm/s.
- Based on dispersion analysis, graphical dependences for the change in the marking depth depending on the power of the laser radiation and the marking speed have been derived. From them, with a sufficient degree of accuracy, the penetration depth of the radiation - δ,µm, in the two studied composite materials can be determined.
- It has been proven that the maximum marking depth is achieved at the studied maximum power - 45 W and minimum marking speed - 50 mm/s. For glass textolite samples it is about 1500 µm, and for textolite samples it is about 800 µm

REFERENCES

[1] D. Petrova, B. Vlahova, A. Lengerov,Tz. Zlateva-Petkova, "Improvement of Constructive-Technological Approaches Reducing Innovative Obsolescence of Industrial Technologies in the Context of Industry 4.0", presented at the 14th International Scientific and Practical Conference on Environment, Technology, Resources, ETR 2023, Rezekne, Latvia, June, 2023, Volume I, pp. 180–186.

[2] D. Petrova, B. Vlahova, A. Lengerov, Tz. Zlateva-Petkova, "Study of the State of Innovation Development and Obsolescence in the Republic of Bulgaria of Companies from the Mechanical Engineering Sector", presented at the 14th International Scientific and Practical Conference on Environment, Technology, Resources, ETR 2023, Rezekne, Latvia, June, 2023, Volume I , pp. 187–194.

[3] D. Petrova, N. Nikolova, A. Lengerov, "Modeling business process reengineering in the digital era of industry 4.0", presented at the 11th International Scientific Conference "TechSys 2022" – Engineering, Technologies and Systems, 2022, pp. 070013-1 - 070013-7.

[4] D. Petrova, "Innovative Obsolescence in Mechanical Engineering and Singleness of Indicators", presented at the 15th International Scientific and Practical Conference on Environment, Technology, Resources, ETR 2024, Rezekne, June 2024, Vol. 3, pp 221 – 224.

[5] G. Karlovski et al., "Selection of Instrumentation Based on Statistical Analysis", presented at the 32nd International Scientific Symposium "Metrology and Metrology Assurance", MMA 2022, Sozopol, 7-11 September 2022.

[6] S. Tsenkulovski, I. Mitev "Influence of the Parameters of the Lasser marking process of the depth of penetration in layer-reinforced composites", presented at the 15th ISPC "Environment Technology Resources", V.Turnovo, Bulgaria, 27 and 28 06.2024, Vol. 3, pp 319-324.

[7] I. Mitev, "Determining the diffusion coefficient in simultaneous saturation with boron and carbon austenite alloyed with cooper in powder metallurgy structural materials", presented at AIP, vol. 2980, 2024, p.060016-1÷060016-7.

[8] L. Lazov, Hr. Deneva, P. Narica, Laser Marking Methods, Rezekne Higher Education Institution (Rēzeknes Augstskola), Rezekne ,2015.

[9] C. Leone C et al., "Wood engraving by Q-switched diodepumped frequency-doubled Nd:YAG green laser.", Optics and Lasers in Engineering, 2009, Vol. 47(1), pp. 161–168.

[10] I. Mitev, S. Tsenkulovski, "Local Processing of Non-Metal Materials with Concentrated Energy Flow", presented at the 14th International Scientific and Practical Conference on Environment, Technology, Resources, ETR 2023, Rezekne, Latvia, June, 2023, Volume 3, pp.183÷186.

[11] J. Peter et al., "Parametric analysis of Nd: YAG laser marking on ceramics." International Journal of Manufacturing Technologies and Management, 2011, Vol. 24(1-4), pp. 124–138.

[12] A. Petutschnigg et al., "Laser treatment of wood surfaces for ski cores: an experimental parameter study.", Advances in Material Science and Engineering, 2013, vol.11, pp. 1-7.
[13] Y. Shin et al., "Pit and rim formation during laser marking of acrylonitrile butadiene styrene plastic.", Journal of Laser Applications, 2005, Vol. 17(4), pp. 243–246.
[14] I. Alexandrova, Fundamentals of engineering research, Vasil Aprilov University Publishing House, Gabrovo, 2003.
[15] I, Mitev, "Optimizing the quantity of liquid phase at the sintering of powder construction materials from system Fe-Cu-Sn" presented at AIP, vol. 2980, 2024, p.060017-1÷060017-7.

Environment. Technology. Resources. Rezekne, Latvia
Proceedings of the 16th International Scientific and Practical Conference. 2025. Volume IV, 413-417

Determining the Relative Importance of Indicators of Suburban Public Transport Comfort by the Method of Geometric Mean Fuzzy-AHP

Mirena Todorova
Faculty of Transport Management
Todor Kableshkov University of Transport
Sofia, Bulgaria
mtodorova@vtu.bg

Kostadin Trifonov
Faculty of Transport Management
Todor Kableshkov University of Transport
Plovdiv, Bulgaria
ktrifonov@vtu.bg

***Abstract*—Nowadays to commute by train and bus in a number of countries is preferred by population for certain distances such as suburban trips. The comfort level of passengers while travelling by public suburban transport is a combination of physical and psychological factors. In order to analyze how comfort affects the choice of transport on a global scale, a number of studies have been carried out. The indicators affecting passenger comfort include the personal space, vehicle environment, level of service, etc. Commuters with different professions and travelling purposes have different notions of comfort. Comfort influences on the choice of transport mode and because of that the main objective is to determine the criteria, which passengers apply to evaluate its level. Multi-criteria decision making is the field that deals with evaluation of indicators or situations according to multiple conflicting criteria. The methods taking into account the presence of subjective elements in passengers' preferences for decision-making have been analyzed considering Analytical Hierarchy Process (AHP) and fuzzy-AHP, which is a structured technique for organizing and analyzing complex solutions based on mathematics and psychology. Using the chosen method, multi-criteria decision has been made to determine the relative importance of indicators by geometric mean fuzzy-AHP. The opinions of practitioners, researchers, managers are considered analogously to the relative importance of indicators. A survey has been developed and conducted with commuters to find out the indicators affecting assessment of comfort and quality of public transport. The study made by a group of experts to evaluate the indicators of comfort has applied the derived geometric mean fuzzy-AHP to determine the relative importance of measurement criteria. The results of study would help to increase the comfort offered and attract more passengers to railway suburban transport taking into account the level of indicators and possibilities of their improvement.**

Keywords* — *geometric mean fuzzy-AHP, comfort, passenger public transport

I. Introduction

The modernization of the railway network nowadays is a result of technological development and introduction of modern rail traffic management systems such as the ERTMS (European Rail Traffic Management System). At the same time it is necessary to meet the increasing demands of passengers for comfort when traveling by rail. Passenger comfort is determined by a combination of physical and psychological factors. A comfortable environment in railway carriages would lead to higher consumption of offered service. That means that the provision of comfort is one of the necessary measures to attract more passengers. In cases where the problem of attracting passengers to a given transport mode is considered, a Logit model is applied [1][2]. It uses the specific cost of transport including the cost of trip, its change, regularity and comfort available. While the first three indicator can be easily determined, to define the offered comfort is a complex issue and depends on the conditions provided to passengers and their personal understandings of what comfort is.

In modern society comfort is a term that refers not only to living conditions, but also to learning, working, traveling, and utilization of all public goods. Moving by train as one of the oldest forms of transport is experiencing a renaissance. In a number of countries rail transport has become increasingly preferred especially at certain distances. If a year ago the accent was put on freight rail transport, nowadays the attention is focused on passengers, speed and comfort.

In the 1970s some studies established an index system affecting passenger comfort and tried to obtain the results

Online ISSN 2256-070X
https://doi.org/10.17770/etr2025vol4.8394
© 2025 The Author(s). Published by RTU PRESS.
This is an open access article under the Creative Commons Attribution 4.0 International License.

of assessment by surveys or other methods. A number of factors were introduced to characterize passenger comfort including temperature, ventilation, lighting, photostimulation, length of trip, etc. Comfort is evaluated also by personal space, travel time, vehicle environment and level of service [3]. One should take into account that passengers with different professions and purposes to travel have different notions of comfort. So, the comfort rating model can be created only by dividing the entire rating coefficient into two parts: objective and subjective factors.

Multi-criteria decision making is the field that deals with evaluation of indicators or situations according to multiple conflicting criteria [4]. The authors of [5] have studied six groups of indicators such as cost, travel time, transport quality, transport means, transport services and social benefits for selection and evaluation of different routes using the fuzzy analytic hierarchy process (FAHP) and the theory of artificial neural network (ANN).

To define the optimal multimodal transport route [6][7][8] by examining criteria such as travel cost, transportation time and transport risk factors, Analytical Hierarchy Process (AHP) and Zero-One Goal Programming (ZOGP) are used. Due to analyzing the passenger preferences and decision-making for choosing a transport mode, the examined indicators determining the comfort offered by public transport have a subjective element. In this case the publications present how analytical hierarchy process (AHP) and the fuzzy logic analytical hierarchy process (FAHP) [9][10] are applied as structured techniques for organizing and analyzing complex decisions based on mathematics and psychology. That is why FAHP will be used to find out the weight of indicators determining comfort when choosing a mode of transport.

II. Materials and methods

In decision making theory, the analytic hierarchy process (AHP) is a mathematically based technique for organizing and analyzing complex decisions developed by Saaty [10][11][12][13]. This method is used to calculate qualified priorities of a given set of alternatives by a scale based on decision maker's judgement. It emphasizes on the importance of decision maker's intuitive judgments and consistency in comparing alternatives in decision-making process. The strength of this approach is that it organizes tangible and intangible factors in a systematic way and offers simple structuring of problems and a possibility of decision making. The relevance of using AHP is based on the fact that this technique allows involvement of individuals in decision making based on evaluating not only numerical, but also intangible factors [14] [15] [16].

When using FAHP, the problem is presented in a hierarchical structure through conditional elements (experts, criteria, subcriteria and alternatives). The specific goal is to be able to assess the weights of examined indicators using the opinion of a group of experts. The experts are selected by specialists as their number should be between 5 and 10. Each expert has to rate the competence of other participating experts and the examined criteria (according to a selected scale) using triangular fuzzy numbers [17]. The solution for determining the weight of indicators is derived using the geometric mean FAHP. The geometric mean is considered an appropriate rule for aggregating individual judgments. The main reason is that the geometric mean method can preserve the reciprocal property in a combined pairwise comparison matrix. The main steps in FAHP are as follows:

- Assessment of the importance of alternatives made consistently (for each level of the hierarchy) using pairwise comparison;

Experts make their selection in the form of assessment for each alternative under examination. The importance of indicators is individually measured by each expert. Pairwise comparison matrices with triangular fuzzy elements are used to derive the weights from a matrix and calculate the sequence of information about the preferences of decision makers.

It is why these pairwise comparison matrices should be created for each expert separately. They are the expert's assessment of the selected indicators relative to each other. To construct such matrices, it is necessary to compare the assessments of different indicators and determine the values according to triangular fuzzy numbers. The matrix should be structured in the following way [18]:

$$X = \{x_{ij}\} = \begin{bmatrix} 1,1,1 & (l_{12}, m_{12}, u_{12}) & \dots & (l_{1n}, m_{1n}, u_{1n}) \\ (u_{12}^{-1}, m_{12}^{-1}, l_{12}^{-1}) & 1,1,1 & \dots & (l_{2n}, m_{2n}, u_{2n}) \\ \dots & \dots & \dots & \dots \\ (u_{1n}^{-1}, m_{1n}^{-1}, l_{1n}^{-1}) & (u_{2n}^{-1}, m_{2n}^{-1}, l_{2n}^{-1}) & \dots & 1,1,1 \end{bmatrix} \quad (1)$$

To find the priority features of main indicators, the fuzzy values for each indicator are determined using the following formulas derived from formula 1:

$$\begin{bmatrix} \left(\sqrt[k]{\left(\sqcap_{j=1}^{k} l_{1j}\right)}, \sqrt[k]{\left(\sqcap_{j=1}^{k} m_{1j}\right)}, \sqrt[k]{\left(\sqcap_{j=1}^{k} u_{1j}\right)} \right) \\ \left(\sqrt[k]{\left(\sqcap_{j=1}^{k} l_{2j}\right)}, \sqrt[k]{\left(\sqcap_{j=1}^{k} m_{2j}\right)}, \sqrt[k]{\left(\sqcap_{j=1}^{k} u_{2j}\right)} \right) \\ \dots \\ \left(\sqrt[k]{\left(\sqcap_{j=1}^{k} l_{nj}\right)}, \sqrt[k]{\left(\sqcap_{j=1}^{k} m_{nj}\right)}, \sqrt[k]{\left(\sqcap_{j=1}^{k} u_{nj}\right)} \right) \\ \sum_{i=1}^{n} \sqrt[k]{\left(\sqcap_{j=1}^{k} l_{ij}\right)}, \sum_{i=1}^{n} \sqrt[k]{\left(\sqcap_{j=1}^{k} m_{ij}\right)}, \sum_{i=1}^{n} \sqrt[k]{\left(\sqcap_{j=1}^{k} u_{ij}\right)} \end{bmatrix}$$

$$= \begin{bmatrix} \text{Average } (l_1^{\sim}, m_1^{\sim}, u_1^{\sim}) \\ \text{Average } (l_2^{\sim}, m_2^{\sim}, u_2^{\sim}) \\ \dots \\ \text{Average}(l_n^{\sim}, m_n^{\sim}, u_n^{\sim}) \end{bmatrix} = \begin{bmatrix} M_1 \\ M_2 \\ \dots \\ M_n \end{bmatrix} =$$

$$= \begin{bmatrix} \frac{M_1}{\sum_{i=1}^{n} M_i} \\ \frac{M_2}{\sum_{i=1}^{n} M} \\ \dots \\ \frac{M_n}{\sum_{i=1}^{n} M} \end{bmatrix} = \begin{bmatrix} W_1 \\ W_2 \\ \dots \\ W_n \end{bmatrix} \quad (2)$$

Thus weight vectors Wi for different factors and subfactors have been obtained. Then it is necessary to determine the consistency index using comparison matrix **A** [19]. If the result is completely consistent, then **A** (before normalization) has the following property:

$$A.\bar{\omega} = \begin{bmatrix} 1 & \frac{w_1}{w_2} & \frac{w_1}{w_3} & \dots.\dots. & \frac{w_1}{w_n} \\ \frac{w_2}{w_1} & 1 & \frac{w_2}{w_3} & \dots.\dots. & \frac{w_2}{w_n} \\ & & \dots\dots\dots & & \\ \frac{w_i}{w_1} & \frac{w_i}{w_2} & \frac{w_i}{w_3} & \dots.\dots. & \frac{w_i}{w_n} \\ & & \dots.\dots & & \\ \frac{w_n}{w_1} & \frac{w_n}{w_2} & \frac{w_n}{w_3} & \dots.\dots. & 1 \end{bmatrix} \cdot \begin{bmatrix} w_1 \\ w_2 \\ \dots\dots\dots \\ w_i \\ \dots.\dots \\ w_n \end{bmatrix} = \lambda_{max}.\bar{\omega} \quad (3)$$

where $\bar{\omega}$ is the eigenvector of λ_{max}. In [20] it is proved that A is of perfect consistency if $\lambda_{max} = n$ or $\lambda_{max} \geq n$. Therefore it is determined according to [21].

$$\lambda_{max} = \frac{\sum_{i=1}^{n} \lambda_i}{n} \quad (4)$$

$$\lambda_i = \left\{ \sum_{j=1}^{n} \left(\frac{l_{ij} + m_{ij} + u_{ij}}{3} . w_j \right) \right\} / M_i \quad (5)$$

Then consistency ratio CR is determined by dividing the value of consistency index (CI) with the value of random index (RI). The value of the consistency index (CI) is derived from equation (6), and the size of RI is taken from *Table* [22] depending on the number of indicators "n":

$$\text{CI} = \frac{\lambda_{max} - n}{n-1} \quad (6)$$

Depending on the size of CR, it can be proceeded to accept the ranking of alternatives, since the solutions are relatively consistent. The authors of most references assume that the value of CR <= 0.10 but the value of CR < 0.2 in source [23] is assumed to be maximally tolerant, so it is used in this specific study.

- The general and local priorities of compared indicators are evaluated sequentially (for each level of the hierarchy).

In cases where indicators with corresponding subfactors are defined, they are evaluated for each level separately. Then each element in the level adds its weighted values and its general or global priority is obtained.

- Determining the weights of experts and the final weights of indicators

The weights for experts is determined in a similar way as in this case n=k=t is equal to number "t" of participating experts. After that a matrix is compiled where the weight of each indicator is determined as a weighted average.

III. Results and Discussion

One of the methods for collecting information about the real situation of traveling in public suburban transport is to conduct a survey. The survey related to this study was carried out completely online by using Google Forms, which provided feedback from passengers travelling in public suburban transport in regard with their assessment of comfort and service. The information collected was used to summarize seven indicators (I) of comfortable travel [22]: I1 – hygiene in the vehicle, I2 – air conditioning, I3 – passenger space, I4 – level of service by staff, I5 – digital services, I6 – connections with other modes of public transport, I7 – adherence to the schedule.

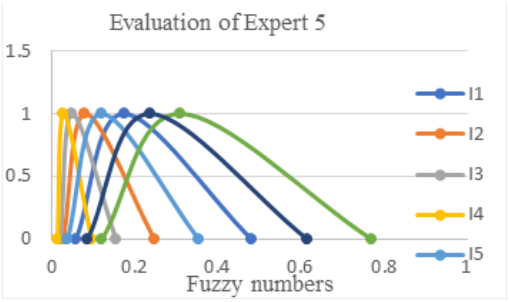

Figure 1. Presentation of evaluation of indicators by Expert 5 as fuzzy numbers.

The selected indicators were evaluated by a group of five experts (E) occupying various positions in management and organization of passenger traffic and having over twenty years of experience (Fig. 1).

Having presented the evaluation of each expert as a matrix of fuzzy numbers, a computational procedure was developed in Excel from MS Office package to determine the weights of indicators using the formulas derived for average geometric FAHP and the assessment of CR adequacy (Table 1).

TABLE 1. MATRIX OF THE EVALUATIONS OF EXPERT 5 AND THE FINAL RESULT

Evaluation	I1	I2	I3	I4	I5	I6	I7	W_i	λ_i
I1	1,1,1	1,3,5	2,4,6	3,5,7	1,2,4	1/5,1/3,1	¼,1/2,1	0.17	7.37
I2	1/5,1/3,1	1,1,1	1,2,4	1,3,5	¼,1/2.1	1/7,1/5.1/3	1/6,1/4,1/2	0.08	7.12
I3	1/6,1/4,1/2	¼,1/2,1	1,1,1	1,2,4	1/5.1/3.1	1/8,1/6,1/4	1/7,1/5,1/3	0.05	7.91
I4	1/7,1/5,1/3	1/5.1/3.1	¼.1/2.1	1,1,1	1/6.1/4.1/2	1/9.1/7,1/5	1/8,1/6,1/4	0.04	6.27
I5	¼,1/2,1	1,2,4	1,3,5	2,4,6	1,1,1	1/6,1/4,1/2	1/5,1/3,1	0.12	6.49
I6	1,3,5	3,5,7	4,6,8	5,7,9	2,4,6	1,1,1	1,2,4	0.29	7.48
I7	1,2,4	2,4,6	3,5,7	4,6,8	1,3,5	¼,1/2,1	1,1,1	0.25	7.24

With the number of indicators n=7, the following indices are obtained: CI = 0.021, RI=1.32 and CR=0.016. The value of CR shows us that we can accept the assessment of the indicators. To obtain the final value, the weight of each indicator has to be determined as a weighted average (Table 2).

TABLE 2 FINAL VALUES OF THE WEIGHTS OF INDICATORS

	E1	E2	E3	E4	E5	Weight I
I1	0.14	0.19	0.21	0.30	0.17	0.19
I2	0.06	0.04	0.08	0.10	0.08	0.07
I3	0.03	0.09	0.08	0.05	0.05	0.06
I4	0.14	0.19	0.14	0.30	0.04	0.16
I5	0.06	0.09	0.21	0.03	0.12	0.10
I6	0.28	0.19	0.08	0.045	0.29	0.19
I7	0.28	0.19	0.21	0.18	0.25	0.23
Evaluation of Experts	0.29	0.16	0.20	0.16	0.19	
						1

IV. CONCLUSIONS

In the recent years the ticket prices in railway transport have been lower for ordinary and suburban trains than the prices for coaches to the same destination and much less than expenses when travelling by car. Despite that there has been a constant outflow of passengers using railway transport, and because of that it is important to determine the indicators that affect comfort of passengers [22][24]. The study has given priority to accuracy of keeping timetables of vehicles on routes – 22.9% but it is due mainly to the number of repairs and rehabilitations of track sections as well as to frequent damages of rolling stock (locomotives or carriages).

The percentage of other factors acting on comfort are as follows: providing "Connections with other types of public transport" – 18.95%, "Hygiene in vehicles" – 19.43%, "Level of service by staff" – 15.6%, availability of air conditioning in rolling stock – 7.2%, provision of space for a passenger – 5.8% and "Digital services" – 5.76%. By determining the weight of indicators, we can assess the level of comfort depending on the type of rolling stock, accurate keeping to traffic schedule and urban mobility, and last but not least the courtesy of service staff (of different carriers).

The model developed to determine the weight of indicators using FAHP geometric mean is completely original and reflects the mathematical formalization of adopted systematic approach of decomposition and synthesis. The mathematical formula for aggregating individual assessments in FAHP has been derived using geometric mean and consistency ratio CR. The described method for determining the comfort indicators allows to determine their weight without returning them for re-evaluation by experts. Although the indicators and their weights have changed over the years, the method developed with Excel files makes the process of factor determination more rapid. The use of Artificial Intelligence (AI) [25] would facilitate not only the speed, but also accuracy with determining the indicators.

Analyzing the results obtained, it is possible to influence on the transport flows attracting more passengers to a given mode of transport by improving the services offered and the indicators that are of lower value. Using a Logit model, it is possible to investigate the distribution of passengers to a given destination depending on the change in comfort indicators or the specific price elements of each transport mode.

V. ACKNOWLEDGMENTS

The authors express their gratitude to the University of Transport „Todor Kableskov", Sofia, Bulgaria for the funding in accordance with the development of the scientific potential of teachers, young scientists and doctoral students, within which the research presented in this article was carried out.

REFERENCES

[1] M.Todorova, Choice of passenger transport mode using Logit model, 23nd International Symposium EURO - Zel 2015 "Recent Challenges for European Railways", 2015, INBS 978-80-263-0936-9, pp.216-223

[2] K.Trifonov, „Research of the competitiveness of the mass passenger transport", Scientific Journal „Mechanics, Transport,

Communications“, 3/2019, art. 1787, [Online]. Available: https://mtc-aj.com/library/1787.pdf

[3] D.J. Oborne and M.J.Clarke, Questionnaire surveys of passenger comfort, Appl Ergon 6(2):pp.97–103, (1975)

[4] S. D. Stoilova, A multi-criteria selection of the transport plan of intercity passenger trains, IOP Conference Series: Materials Science and Engineering, Volume 664, 11th International Scientific Conference on Aeronautics, DOI 10.1088/1757-899X/664/1/012031,URL:https://iopscience.iop.org/article/10.1088/1757-899X/664/1/012031

[5] Qu L., Chen Y. A Hybrid MCDM Method for Route Selection of Multimodal Transportation Network. In: Sun, F., Zhang, J., Tan, Y., Cao, J., Yu, W. (eds) Advances in Neural Networks - ISNN 2008. ISNN 2008. Lecture Notes in Computer Science, vol. 5263, 2008, Springer, Berlin, Heidelberg. DOI: 10.1007/978-3-540-87732-5_42.

[6] M. Oudani, A combined multi-objective multi criteria approach for blockchain-based synchromodal transportation. Computers & Industrial Engineering, vol.176, 2023, DOI: 10.1016/j.cie.2023.108996

[7] Huang W , Shuai B. A methodology for calculating the passenger comfort benefits of railway travel, Journal of Modern Transportation 26(1), 2018, URL: https://link.springer.com/article/10.1007/s40534-018-0157-y

[8] P. Stoyanova, Routing UrbanTransport Network With Weighing Arcs Fuzzy Numbers And Application In Emergency Medical Aid, International Conference on Technics, Technologies and Education 2016 , ICTTE 2016, ARTTE Vol. 5, No. 1, 2017 DOI: 10.15547/artte.2017.01.002

[9] K.Karagaozov and P.Stoyanova, Traffic assignment in transportation network with Fuzzy weight arcs, Scientific Journal „Mechanics, Transport, Communications“, 3/ 2015, art. 1144.

https://mtc-aj.com/library/1144.pdf

[10] Saaty, T.L., Relative Measurement and Its Generalization in Decision Making Why Pairwise Comparisons are Central in Mathematics for the Measurement of Intangible Factors The Analytic Hierarchy/Network Process, Rev. R. Acad. Cien. Serie A. Mat. 102, pp.251–318, 2008, URL: https://doi.org/10.1007/BF03191825

[11] T. L. Saaty, The Analytic hierarchy process, McGraw-Hill, New York, 1980

[12] T. L. Saaty, Fundamental of Decision Making & Priority Theory with the Analytical Hierarchy Process, RWS Publication, Pittsburgh, 1994

[13] T. L. Saaty and K. P. Kearns, Analytical Planning:The Organization of System, ISBN 978-0-08-032599-6, 1985, DOI: https://doi.org/10.1016/C2013-0-03782-6

[14] K. Shaw, R. Shankar, S. S. Yadav and L. S. Thakur, Supplier selection using fuzzy AHP and fuzzy multi-objective linear programming for developing low carbon supply chain. Expert Systems with Applications, 39(9), pp.8182-8192, 2012

[15] M. K. Sagar and D. Singh, Supplier selection criteria: Study of automobile sector in India. International Journal of Engineering Research and Development, 4(4), pp.34-39, 2012

[16] M.Sevkli, S. C.Lenny Koh, S. Zaim, M.Demirbag and E.Tatoglu, An application of data envelopment analytic hierarchy process for supplier selection: a case study of BEKO in Turkey. International Journal of Production Research, 45(9), 1973-2003, 2007

[17] T.N. Prakash, Land Suitability Analysis for Agricultural Crops: A Fuzzy Multicriteria Decision Making Approach. International Institute for Geo-Information Science and Earth Observation Enschede, 1-68, 2003,

URL:http://www.iirs.gov.in/iirs/sites/default/files/StudentThesis/final_thesis_prakash.pdf

[18] P.Agarwal, M.Sahai, V.Mishra, M.Bag and V. Singh, A review of multi-criteria decision making techniques for supplier evaluation and selection. International Journal of Industrial Engineering Computations, 2(4), 801-810, 2011

[19] A. Mendoza, E. Santiago and A.R. Ravindran, A three-phase multicriteria method to the supplier selection problem, International Journal of Industrial Engineering,15(2),pp.195-210, 2008

[20] T. L. Saaty, Decision-Making with the AHP: Why is the Principal Eigenvector Necessary, European Journal of Operations Research, 145(1), pp. 85–91, 2003, URL: https://www.sciencedirect.com/science/article/abs/pii/S0377221702002278

[21] A. Stam and P. D. Silva, Stochastic Judgments in the AHP: The Measurement of Rank Reversal Probabilities, Decision Sciences Journal, June, 2007, URL: https://pure.iiasa.ac.at/id/eprint/4111/1/WP-94-101.pdf

[22] K.Trifonov, Determining the indicators influencing the comfort of traveling by public transport, Scientific Journal „Mechanics, Transport, Communications“, 3/2021, art. 2087, https://mtc-aj.com/library/2087.pdf

[23] D.Dimitrov and I.Petrova, Approach for multicriterial evaluation and selection of railway infrastructure projects, Scientific Journal „Mechanics, Transport, Communications“, art. 2086, 3/ 2021,

https://mtc-aj.com/library/2086.pdf

[24] L.G. Richards, I.D. Jacobson and A.R. Kuhlthau, What the passenger contributes to passenger comfort, PMID: 15677263, Appl Ergon 9(3): pp.137–142, 1978)URL: https://doi.org/10.1016/0003-6870(78)90003-0

[25] Petrova I., Applied methodological essence of project management in transport through artificial intelligence, Environment. Technology. Resources. Rezekne, Latvia Proceedings of the 15th International Scientific and Practical Conference. 2024, Online ISSN 2256-070X, https://doi.org/10.17770/etr2024vol2.8047

Environment. Technology. Resources. Rezekne, Latvia
Proceedings of the 16th International Scientific and Practical Conference, 2025. Volume IV, 419-423

Modeling the Technology of the Varna Ferry Complex Operation Using the Queueing Theory

Mirena Todorova
Faculty of Transport Management
Todor Kableshkov University of Transport
Sofia, Bulgaria
mtodorova@vtu.bg

Mihail Rangelov
Faculty of Transport Management
Todor Kableshkov University of Transport
Sofia, Bulgaria
mrangelov@vtu.bg

ABSTRACT - The article focuses on the analysis and optimization of the technological process at the Ferry Complex for freight transportation, connecting maritime and railway transport. A key feature of this complex is the presence of railway networks with different track gauges, which necessitates specialized operations such as bogie exchange and additional shunting activities, leading to specific challenges in managing technological operations. To optimize technological operations or the required infrastructure at the terminal yards, mathematical modeling and simulations are considered. These simulations include optimization algorithms for resource allocation, heuristic and metaheuristic approaches for the distribution of freight flows, and bogie exchange. The simulations allow for the assessment of the impact of changes in technological processes and support decision-making to improve the complex's performance, as well as its infrastructure, depending on the volume of freight flows, including hazardous materials cargo. The Ferry Terminal is modeled as a complex system, composed of various interacting technological subsystems, which are formalized as queueing systems. This approach allows for the use of well-known analytical formulas from Queueing Theory to represent the technological process. Formulas are derived to determine the duration of technological operations depending on the type of cargo (hazardous or not), the dwell time of the wagons in the complex, and the number of requests per subsystem. This enables the optimization of the technical equipment at the terminal, based on the size of the processed wagon flow. The model is developed for the Varna Ferry Complex, which handles a large volume of freight and involves specific logistics processes related to the handling of freight wagons. The complex includes a bogie exchange facility where wagons undergo the process of replacing running gear to meet the requirements of different track gauges. The technological operations are formalized, evaluated, and various subsystem parameters are determined. As a result, depending on the size of the wagon flow, the technological process or technical equipment of the complex can be optimized. Modernization and optimization of the complex will lead to improved capacity and competitiveness, providing greater flexibility and efficiency in freight handling.

Keywords – ferry complex, mathematical modelling, queueing theory

I. INTRODUCTION

The Ferry Complex Varna (FBK-Varna) holds a strategic geographical position on the Bulgarian Black Sea coast, making it a key logistics hub for freight transport between Europe and the Black Sea basin countries. Located at the crossroads of Asia and Europe, the complex plays an essential role in regional and international trade, enabling combined sea and land freight transport [1].

In recent years, there has been anincreasing trend in freight transport across the Black Sea, driven by global economic processes and regional efforts to improve transport connectivity. Despite the challenges posed by the military conflict in Ukraine, the anticipated stabilization of the region is expected to lead to the restoration of the ferry connection between FBK-Varna and Odessa—a historically significant transport artery that has handled substantial freight volumes.

To address the expected growth in freight traffic and ensure efficient resource management [2][3] at FBK-Varna, the application of scientific methods for analyzing and optimizing operational processes is necessary [4][5]. In this context, queuing theory (QT) offers a powerful tool for modeling the technological operations within the ferry complex [6][7][8][9].

This paper determines the dwell time of railway wagons at FBK-Varna based on the chosen operational technology and the development of an analytical simulation model based on QT. The study provides valuable insights into optimizing transport flows, reducing cargo dwell time, and improving the overall logistical efficiency of the complex. By utilizing QT, service

Online ISSN 2256-070X
https://doi.org/10.17770/etr2025vol4.8395
© 2025 The Author(s). Published by RTU PRESS.
This is an open access article under the Creative Commons Attribution 4.0 International License.

parameters can be analyzed, system load forecasts can be made, and strategies for process efficiency improvement can be proposed [10][11][12].

In order to develop a model of the ferry complex, the freight flows that passed through the complex over the last six years were studied [1] and the operating technology was examined, taking into account the specifics of the station [13].

II. MATERIALS AND METHODS

The ferry complex can be viewed as a queuing system consisting of several subsystems.

To model the ferry complex, a subsystem approach is used, aiming to determine the wagon dwell time and the required technical equipment based on the magnitude of handled wagon flows. The layout follows a fully sequential scheme—reception yard, shunting facility for train decomposition and composition, a bogie exchange facility with tracks for different rail gauge widths, a pre-ferry yard with broad-gauge tracks, and movable bridges for ferry loading and unloading [13]. This sequential layout and the representation of the station as a QT system facilitate the modeling, as depicted in Fig. 1.

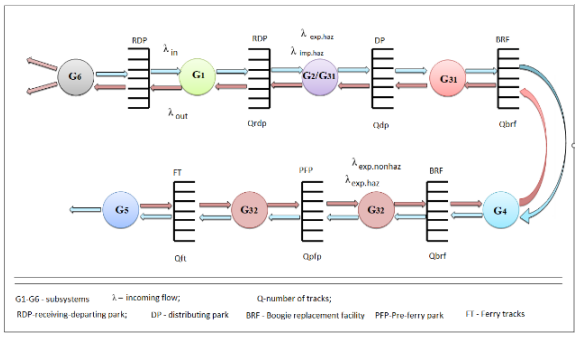

Fig.1 Structural diagram of the Ferry Complex - Varna as a QT system

Depending on the activity being performed, the station consists of six subsystems and each of them is characterized by an input flow λ_{Gi}; service intensity μ_{Gi} , service devices S_{Gi}, service time t_{Gi}^{ser}; probability of expected service P_{Wi}, expected service time W_{Gi} and number of requests in the system n_{Gi} [14][15][16]. In order to determine the stay of the wagons in the station, the processing and expected processing times for the different subsystems must be determined [6][17]. The six technological subsystems G_i involved are:

- Subsystem G_1 - technological system for processing freight trains upon arrival and departure. Freight trains are accepted on the tracks in the POP, the train locomotive is uncoupled, commercial and technical inspection are performed, documents are processed and prepared for decomposition. The same is done when accepting wagons (import). They are prepared for departure. In addition to the operations described, a full test of the brake system is performed on the composed train. The special feature of the station, as well as all the border stations, is that customs checks and document processing are also performed. This subsystem is multi-channel, because there may be more than one brigade for servicing trains, but the number of brigades depends on the size of the served wagon flows for export to the ferry and for import in the opposite direction. Therefore, we assume that subsystem G1 is M/G/s (Poisson input flow/random service time/s service devices). The incoming flow of trains for one day (24 hours) in the subsystem is determined by:

$$\lambda=\lambda_{imp}+\lambda_{exp}=\frac{N_{imp}+N_{exp}}{24}, \quad (1)$$

where: $\lambda_{imp}, \lambda_{exp}$ is the intensity of incoming flow;

$N_{imp}+N_{exp}$ – is the train from import and export

And the service time of the trains is determined by:

$$t_{G_1}^{ser}=\frac{\lambda_{imp}t_{imp}+\lambda_{exp}t_{exp}}{\lambda_{G_1}}\frac{24}{24-T_{const}}, \quad (2)$$

The service intensity is determined by:

$$\mu_{G_i}=\frac{1}{t_{G_i}^{ser}} \text{ [trains/hour]} \quad (3)$$

Waiting time in queue in subsystem M/G/1:

$$W_{M/G/s}=\frac{Pw(1+v_{in}^2)}{2.S.\mu(1-\chi)}, \text{ [h/train]} \quad (4)$$

Where $$\chi=\frac{\lambda_{G_1}}{\mu_{G_i}.s} \quad (5)$$

The total waiting time of one request in subsystem G1 is sum of waiting times in queue and service time:

$$t_{G1}=W_{G_1}+t_{G_1}^{ser}, \text{ [h/train]} \quad (6)$$

- Subsystem G_2/G_{31} - operations of decomposing, composing and shunting with wagons with bogies with standard gauge. The shunting device for decomposing and composing is one, but the servicing shunting locomotives are two, because parallel operations of the shunting device and servicing the workshop for changing bogies can be performed. This system is single-channeled, determined by the number of shunting devices. The incoming flow into the train system for 1 day is determined by the formulas:

$$\lambda_{haz}=\lambda_{import}^{haz.}+\lambda_{export}^{haz} \quad (7)$$

$$\lambda_{nonhaz}=\lambda_{import}^{nonhaz}+\lambda_{export}^{nonhaz.}, \quad (8)$$

where haz/nonhaz – determines the cargo type (hazardous or non-hazardous)

The train service time for 1 day (24 hours) $t_{G2/G31}^{q}$ is determined:

$$t_{G2/G31}^{ser} = \frac{\lambda_{imp}t_{comp}+\lambda_{exp}t_{decomp}+\lambda_{haz}t_{load}+\lambda_{nonhaz}t_{load}}{\lambda_{imp}+\lambda_{exp}} * \frac{24}{24-T_{inc}}, \text{ [h/train]} \quad (9)$$

$$W_{G2/31} = \frac{\rho^2(\upsilon_{inc.}^2+\upsilon_{q.}^2)}{2\mu(1-\rho)(1-(1-\rho)\upsilon_{inc.})}, \text{ [h/train]} \quad (10)$$

- Subsystem G_{32} – shunting operations with wagons with wide gauge bogies. The subsystem includes shunting operations, such as feeding the wagons to the boogie replacement facility (BRF) and the specialized track for changing the bogies; pulling the wagons with the changed bogies into the Pre-ferry park (PFP); unloading and loading operations of ferry ships. There are two locomotives in this subsystem and two shunting brigades work, due to the specifics of the loading and unloading activity: when unloading the ships – first the wagons are pulled from the middle track, then the wagons are pulled from the two symmetrically located tracks simultaneously with the help of two shunting locomotives and finally the remaining two tracks again simultaneously. The reverse process is done similarly. This system is multi-channel and depends on the locomotives used, which cannot be less than two. Therefore, we assume that the G_{32} subsystem is M/G/s (Using same formulas as for G1).

- Subsystem G_4 – changing the bogies of the wagons, which are prepared for loading on the ship or for movement on the railway line. The bogies of the wagons with dangerous goods are changed on a specialized track for changing bogies, by feeding three wagons at a time. The remaining wagons with goods are fed ten wagons at a time. This subsystem is the most interesting, because there is a specialization of the tracks depending on the type of cargo, but the service brigade is now one. That is why it will be considered as a single-channel one with servicing priority requests, which are dangerous goods.

$$W_{haz} = \frac{\rho_{haz}^2(v_{ibx}^2+v_{ioo}^2)}{2.\mu(1-\rho_{haz}).[1-(1-\rho_{haz})v_{bx}]} \text{ [h/train]} \quad (11)$$

$$W_{nonhaz} = \frac{\rho_{haz}^2(v_{ibx}^2+v_{ioo}^2)}{2.\mu(1-\rho_{haz})(1-\rho_{nonhaz}).[1-(1-\rho_{haz})v_{bx}]} \quad (12)$$

$$W_{G4} = W_{haz} + W_{nonhaz} \text{ [h/train]} \quad (13)$$

✓ Subsystem G_5 - technological system for sending a train from a ferry, by sailing the loaded ship by sea. The peculiarity is that these transports are at a large time interval depending on a relatively constant scheduled movement of the ferry. Only the waiting time for departure will be considered, because the loading and unloading of ships as service time is taken into account in subsystem G4. The system will be considered as a single-channel with service intensity depending on the capacity of the ships and the intervals of their arrival. The subsystem is assumed to be M/M/1 and the waiting time for service is:

$$W_{G5} = \frac{\rho}{\mu(1-\rho)}, \text{ [h/train]} \quad (14)$$

- Subsystem G_6 - technological system for sending wagon traffic along the railway network of the individual [d] adjacent sections. It consists of [d] technological systems. For each section, moving transit trains will have priority and the waiting time for departure to the railway network will be determined by the formulas for G_4.

The stay of wagons at the station is determined as the sum of the processing and waiting times for service

$$T_{ferri} = \sum_{i-1}^{6}(t_{i.proc} + t_{i.proc.q}) \quad (15)$$

III. Results and Discussion

The model was applied to a realistic freight flow forecast for 2025 and the following input data: statistical data on the duration of technological operations, two shunting locomotives for each gauge, priority service for wagons with dangerous goods in the bogie change shop (G4), ferries with a capacity of 5 tracks of 10 wagons arriving regularly every day. The specific consideration does not take into account the delays of the ferries due to schedule disruptions due to bad weather or other reasons. The volumes of the incoming flow are for 1 year M = 9689 wagons, of which:

A. M_{imp} = 5 997 wagons:

a) average number of wagons in the composition– $m_{c\ import}$ = 10;

b) 76% wagons with non-hazardous cargo – $M_{imp\ nonhaz}$ = 4 558;

c) 24% wagons with hazardous cargo - $M_{imp\ haz}$ = 1 439.

B. M_{exp} = 3 692:

C.

a) average number of wagons in the composition – $m_{c\ export}$ = 17;

b) 76% wagons with non-hazardous cargo – $M_{export\ nonhaz}$ = 2 806;

c) 24% wagons with hazardous cargo – $M_{exp\ haz}$ = 1 439.

We determine the input parameters for the station in the number of trains per day:

$$N = \frac{M}{365m_c}, tr/day \quad (16)$$

$$N_{imp} = \frac{M_{import}}{365m_{c\ import}} = 1{,}64\ tr/day,$$

$$N_{exp} = \frac{M_{exportc}}{365m_{c\ export}} = 0{,}60\ tr/day,$$

$$N = N_{import} + N_{export} = 2{,}24\ tr/day,$$

Dimensioning of subsystem G1 – subsystem for processing trains by arrival and departure

- The incoming flow of trains for 1 day (24 hours) in the system (7):

$$\lambda = \lambda_{imp} + \lambda_{exp} = \frac{N_{imp} + N_{exp}}{24},$$

where:

λ_{imp}; λ_{exp} – intensity of incoming flow for import and export.

$$\lambda_{imp} = \frac{N_{imp}}{24} = 0{,}07 \text{ train/day};$$

$$\lambda_{exp} = \frac{N_{exp}}{24} = 0{,}03\ train/day,$$

$$\lambda_{G1} = 0{,}093\ train/hour,$$

- the time for servicing trains for 1 day (24 hours) in the system $\overline{t}_{G1}^{\,q} = 6{,}89\ h/train$ by the formulas (2):

$$\overline{t}_{G1} = \frac{\lambda_{imp} t_{imp} + \lambda_{exp} t_{exp}}{\lambda_{G1}} * \frac{24}{24 - T_{const}}, \text{ h/train}$$

where:
T_{const} = 2,20 h.;
t_{imp} = 5,75 h;
t_{exp} = 7,517 h;

We determine the intensity of service (3)

$$\mu_i = \frac{1}{\overline{t}_{Gi}^{\,ser}} = 0{,}144, \text{ train/h}$$

Number of service brigades S = 1. and the probability that the arriving train will wait for service $P_w = \chi = 0{,}648$. Waiting time in queue (4):

W_{G1} =2,42 h/train

The total waiting time of one request in subsystem G1 (6):

t_{G1} =9,31 h/train

In the same way we determine the parameters for the remaining subsystems and the results are given in Table1.

TABLE 1 TIMES IN SMO

	G_1	$G_{2/31}$	G_{32}	G_4	G_5	G_6
t_{ser}	6.89	4.69	5.63	2.13	2.50	0.80
W	2.42	1.99	2.89	7.70	12.84	5.11
t_{Gi}	9.31	6.67	8.52	9.83	15.34	5.91

In cases where we determine the dwell time of export wagons, the times in subsystems G1, G2, G3, G4, and G6 are summed. However, for import wagons, subsystem G6 is replaced by subsystem G5. Export wagons stay at the station is 49.68 hours and imported wagons remain at the station is 40.25 hours.

IV. Conclusion

The Ferry Complex in Varna can be considered a queuing system due to its complex operations, high volume of serviced clients and cargo, and sophisticated infrastructure that ensures effective and coordinated service. Using mathematical modeling and creating a QT model allows for simulating different scenarios involving unexpected changes in cargo flow type and volume, identifying bottlenecks under increased freight traffic.

Model validation showed that the total dwell time for export wagons before departure from Varna Ferry Terminal is approximately 50 hours per wagon, while import wagons remain for 41 hours per wagon. This aligns with reality since trains can be dispatched inland when a complete trainset is ready, whereas export wagon dispatch depends on ferry availability and sea transport conditions.

The longest process is the bogie exchange for hazardous cargo wagons, as only three wagons at a time can be processed on the specialized track due to safety regulations, compared to ten wagons for other types of cargo.

Applying the model for different volumes helps determine the required number of shunting locomotives and crews to ensure proper freight flow management. The model also provides recommendations for improving the complex's throughput and necessary infrastructure.

ACKNOWLEDGMENT

The authors express gratitude to the University of Transport "Todor Kableshkov," Sofia, Bulgaria, for funding the research project, "Models for Optimizing Technological Processes and Determining Infrastructure Element Capacities," within which this study was conducted.

REFERENCES

[1] M. Rangelov, M. Todorova and S. Ananiev, Study of freight flows passing through the Ferry Complex – Varna for the period 2017-2022. Scientific Journal "Mechanics, Transport, Communications", 3/2023, art.2369, 2023, [Accessed: 25 November 2023], Available: https://mtc-aj.com/library/2369.pdf

[2] A. Borisov, Optimization of transport processes in a logistics chain for serving freight flows at local, regional, and national levels. Scientific Journal "Mechanics, Transport, Communications", 3/2016, art.1277, 2016, [Accessed: 14 September 2016], Available: https://mtc-aj.com/library/1277.pdf

[3] T. Emunds and N. Nießen, To build or not to build: A queueing-based approach to timetable independent railway junction infrastructure dimensioning. Electrical Engineering and Systems Science: Systems and Control, [Accessed 20 Sep 2023], Available: https://doi.org/10.48550/arXiv.2309.14351

[4] V. Velyova. Study and Comparative Analysis of The Models for Traffic Safety Prediction. 22th International Scientific And Technical Conference On Transport, Road-Building, Agricultural, Hoisting & Hauling And Military Technics And Technologies -

Trans&MotAuto'14. 23.-24.06.2014,Varna, Bulgaria, ISSUE 9 (158)/ 2014, 2014.

[5] Zl. Trendafilov, Application of simulation-and-analytical models of resource planning and locomotive scheduling, 22nd International Symposium, June 2014, Žilina, Slovakia, University of Žilina, 2014.

[6] Y. Tasev and K. Karagyozov, Guidelines for course and diploma project design on the structure, technology, and design of railway stations and nodes. Technical University Sofia, 1983.

[7] Qi Yi, T. Tao, Qun Zhao and M. Azimi, A new method for estimating truck queue length at marine terminal gates. [Accessed Feb 26, 2025] Available: https://rosap.ntl.bts.gov/view/dot/58268

[8] A. Azab, A. Karam and A. Eltawil, A simulation-based optimization approach for external trucks appointment scheduling in container terminals. International Journal of Modelling and Simulation, Volume 40, 2020 - Issue 5, pp.321-338, [Accessed 19 May 2019], Available: https://doi.org/10.1080/02286203.2019.1615261

[9] N. Grubisic, T. Krljan, L. Maglić and S. Vilke, The microsimulation model for assessing the impact of inbound traffic flows for container terminals located near city centers. Sustainability, 12(22), 9478., 2020 [Accessed: 14 November 2020] Available: https://doi.org/10.3390/su12229478

[10] E. Ozkan, S. Nas and N. Guler, Capacity analysis of Ro-Ro terminals by using simulation modeling method. The Asian Journal of Shipping and Logistics, 32(3), 139-147., 2016, [Accessed 2016], Available: https://doi.org/10.1016/j.ajsl.2016.09.002

[11] G. Chen and Z. Yang, Methods for estimating vehicle queues at a marine terminal: A computational comparison. International Journal of Applied Mathematics and Computer Science, 24(3), 611-619. DOI: 10.2478/amcs-2014-0044. [Accessed: 2014], Available: https://sciendo.com/pdf/10.2478/amcs-2014-0044

[12] Q. Pham, N. Huynh and Y. Xie, Estimating Truck Queuing Time at Marine Terminal Gates. Transportation Research Record: Journal of the Transportation Research Board, 2222, pp. 43-53, 2011. [Accessed 01.01 2011], Available: https://doi.org/10.3141/2222-06

[13] M. Rangelov and M. Todorova, Analysis of the work technology and technical equipment of the Ferry Complex – Varna and selection of a method for its modeling, Scientific Journal "Mechanics, Transport, Communication", Sofia, Bulgaria, 3/2024, art.2543, 2024. [Accessed: 14 September 2024], Available: https://mtc-aj.com/library/2543.pdf

[14] M.Todorova, Technological design of a passenger railway complex. Sofia: ISBN 978-619-91163-2-6, 2020.

[15] K. Karagyozov and P. Stoyanova, Analytical-simulation approach for resource planning in service systems as a mass service system with a non-stationary input process. XIII International Scientific Conference Management and Engineering '15, June 21-24, Sozopol, Bulgaria, Sofia: Technical University, 2015.

[16] R. Mitrev, Analysis and design of mass service systems. Sofia: Technika, 2018.

[17] S. Agnihotri, Application of queuing theory in traffic management system. International Journal of Engineering Research and Technology, 5(6), 1-5, 2016. [Accessed: 2017], Available: http://publications.anveshanaindia.com/wp-content/uploads/2017/07/Application-of-Queuing-Theory-in-Traffic-Management-System.pdf

Environment. Technology. Resources. Rezekne, Latvia
Proceedings of the 16th International Scientific and Practical Conference. 2025. Volume IV, 425-430

Rhetorical Devices in Advertising Slogans: A Competitiveness Viewpoint

Tsvetelina Vladimirova
Marketing and Strategic Planning
University of National and World Economy
Sofia, Bulgaria
lina_vladimirova@unwe.bg

Hristo Kaktrandjiev
Marketing and Strategic Planning
University of National and World Economy
Sofia, Bulgaria
katrandjiev@unwe.bg

Noncho Dimitrov
National and Regional Security
University of National and World Economy
Sofia, Bulgaria
noncho_dimitrov@unwe.bg

***Abstract*—Due to increasing amount of competition as well as a colossal amount of information people come across, nowadays are needed such advertisements that leave a strong impression on potential customers. Previous research has suggested rhetoric can be used to make ads more competitive. The aim of this report is to comment on the usage, as well as the effectiveness of rhetorical figures in advertising. A sample of 815 advertising slogans was gathered from various Bulgarian media. The slogans were analyzed for the presence or absence of rhetorical figures. The results of the study indicate that rhetorical devices are frequently employed when creating advertising slogans. The most commonly used rhetorical figures are metaphor, epithet and appeal. The product categories in which rhetorical devices are most frequently applied are Foods, Beverages and Fashion. The retailing sector is the only one in which fewer than half of the examined slogans rely on the usage of rhetoric. To assess the effectiveness of rhetoric in advertising, an online survey was developed. Three hundred respondents participated. They were asked to evaluate three pairs of advertising slogans. In each of these pairs, the first slogan was taken in its original form - containing a rhetorical device. The second slogan was transformed in such a manner that the rhetorical figure was removed, while the meaning of the slogan was preserved. The respondents had to assess the slogans according to seven criteria. According to the results of this study, the usage of rhetorical figures increases slogans' perceived persuasiveness, creativity, pleasantness, comprehensibility and memorability. The employment of rhetorical devices increase the competitiveness of advertising communication.**

Keywords - advertising slogans, rhetorical figures

I. INTRODUCTION

Never before have people been exposed to such a constant stream of advertising as we witness today. Advertising messages are all around us - on television, radio, newspapers and online where millions of us spend most of our time.

With the advancement of technology, companies will have an increasingly sophisticated and precise arsenal of instruments with which to reach consumers.

However, this rapid process of digitization poses some risks. Every day people are faced with such a colossal amount of information that they often fail to comprehend it.

Advertisements can be easily avoided by potential users. The skepticism that users feel towards advertisements makes them uninterested in them. [1]

Today, more than ever before, advertisements which can easily capture the minds of consumers and leave an impression on them for as long as possible are needed.

A relatively quick, easy, and cost-effective way to achieve this objective is to apply the methods of rhetoric to advertising slogans.

Previous research on the topic can be divided into two broad groups: publications which explore the use of rhetoric in advertising and those which attempt to measure the impact of rhetorical figures in advertising.

The present study aims to examine the impact of rhetorical figures in Bulgarian advertising slogans.

The research goal of this paper is to determine whether the application of rhetorical devices to advertising slogans makes the advertising slogan more competitive. To achieve this goal, seven criteria which make the slogan more competitive have been chosen to be examined.

II. MATERIALS AND METHODS

The research methodology consists of five phases.

A. Phase One

Online ISSN 2256-070X
https://doi.org/10.17770/etr2025vol4.8426
© 2025 The Author(s). Published by RTU PRESS.
This is an open access article under the Creative Commons Attribution 4.0 International License.

The first phase involves building a database of slogans. The slogans were accumulated from the following traditional and digital media: television, newspapers and magazines, radio, billboards and advertising panels, the Internet, social networks.

B. Phase Two

The second phase is the grouping of slogans by product categories. After collecting the slogans, they were distributed into ten different product categories: Food, Beverages, Cosmetics, Fashion, Technology, Automobiles, Medicine and Pharmacy, Retailing, Tourism and Catering, Financial Services and Others.

C. Phase Three

The third phase is content analysis. It consists of the following steps:

- Analysis of the length of the slogans - the average length of the slogans as a whole as well as by product category is calculated

- Ratio of slogans in Bulgarian and in a foreign language - the ratio of slogans in Bulgarian and in a foreign language by product category is determined. Conclusions about the usage of foreign language in Bulgarian advertising are drawn.

D. Phase Four

The next phase of the research methodology includes a detailed rhetorical analysis of advertising slogans:

- The type of rhetorical figures used in Bulgarian advertising is determined; conclusions are made about which tools of rhetoric are preferred as a whole by advertising specialists.

- A rhetorical profile is outlined for each product category:

- The percentage of advertising slogans which use figurative language is determined.

E. Phase Five

The next phase of the research methodology is the development of a questionnaire which aims to gauge the attitudes of respondents towards slogans with and without rhetorical figures.

The sample size of the survey is 300 respondents. 50,7 % of the respondents are female and 49,3 % - male.

The data was collected from 08.10.2022 until 11.11.2022.

The dimensions on the basis of which the slogans are evaluated are adapted from previous studies such as [2], [3], [4], [5]. Respondents are asked to give their assessment of two versions of the same advertising slogan. In the first version, the slogan is presented in the way it appears in the original advertisement from which it was taken - containing a rhetorical figure. In the second version, the rhetorical figure is removed, but the meaning of the slogan is kept.

The first pair respondents are asked to evaluate is:

Slogan 1.1: Вода от сърцето на Родопите (BG) vs Slogan 1.2: Вода от Родопите (BG).

Slogan 1.1: Water from the heart of the Rhodope (EN) vs Slogan 1.2: Water from the Rhodope (EN)

The second pair respondents are asked to evaluate is:

- Slogan 2.1: Кредит на мига (BG) vs Slogan 2.2: Кредит веднага (BG)
- Slogan 2.1: Credit on the spot (EN) vs Slogan 2.2: Credit immediately (EN).

The third pair of respondents are asked to evaluate is:

- Slogan 3.1: Пералнята живее по-дълго с Калгон (BG) vs Slogan 3.2: Пералнята работи по-дълго с Калгон (BG)
- Slogan 3.1: Credit on the spot (EN) vs Slogan 2.2: Credit immediately (EN).

Respondents are asked to rate the slogans according to the following criteria: Originality, Creativity, Persuasiveness, Comprehensibility, Likability, Memorability, Degree to which the slogan incites a purchase.

The lowest grade they can rate a slogan is one and the highest - seven.

III. RESULTS AND DISCUSSION

A. Linguistic Characteristics of Slogans

The linguistic characteristics of the analyzed slogans are examined by product categories.

The highest percentage of advertising messages in a language other than Bulgarian was recorded in the Tourism and Hospitality sector (38.96%). This is not surprising, considering that tourism slogans are aimed not only at the local population, but at guests of the country as well, who may not speak Bulgarian.

In second place is the field of fashion (34.54%), and in third place with a significantly lower percentage is the product category Beverages (20.40%).

Advertising specialists least often use slogans in a foreign language when they aim to promote products and services in the field of medicine and pharmacy 3.80 %. Slogans which advertise financial services rarely use a language different than Bulgarian as well. This can be explained with the higher level of complexity these two product categories possess.

B. Rhetorical Analysis of Slogans

A rhetorical analysis of advertising slogans is conducted. The relative share of slogans with and without

rhetorical figures in the Bulgarian advertising space as a whole, as well as by product categories, is calculated.

The majority of slogans - 63.43% contain at least one rhetorical device. It can be concluded that marketers frequently use the tools of rhetoric in the Bulgarian advertising space.

The relative shares of rhetorical figures in different product categories are examined (Table I).

TABLE I: RELATIVE SHARES OF RHETORICAL FIGURES BY PRODUCT CATEGORY

Product Category	**Slogans with a rhetorical figures**
Foods	83.88 %
Beverages	83.67 %
Fashion	61.82 %
Cosmetics	72.22 %
Technology	59.70 %
Automobiles	71.43 %
Medicine and Pharmacy	63.80 %
Tourism and Hospitality	61.03 %
Financial Services	61.53 %
Retailing	46.29 %
Other	50.79 %

Advertising specialists use rhetorical tools most often when promoting food (83.88%) and beverages (83.88%).

About 60% of the analyzed slogans use figures of speech in the following sectors: Fashion (61.82%), Technology (59.70%), Medicine and Pharmacy (63.80%), Tourism and Hospitality (61.03%), and Financial Services (61.53%). A lower share is observed in the Other product category (50.79%).

The field of retailing is the only one in which less than 50% of the slogans contain a rhetorical figure.

The relative shares of different rhetorical figures in Bulgarian advertising slogans are examined (Table 2).

The most common tool of rhetoric is metaphor. This regularity confirms the observations made in previous studies about the fundamental role of metaphor in advertising [6], [7].

The appeal (21.47%) and the epithet (10.30%) rank second and third in terms of representation in advertising messages in our country. Other common rhetorical figures are exclamation, hyperbole, and gradation.

Synecdoche, oxymoron and pun can be found extremely rarely in the advertising space in Bulgaria (0.49%).

Epistrophe and neologism are present in only 0.36% of slogans.

In the next phase of the study, 300 respondents are asked to compare the three pairs of slogans.

TABLE II RELATIVE SHARES OF DIFFERENT RHETORICAL FIGURES

Type of rhetorical figure	**Relative Share**
Metaphor	44,90 %
Appeal	21,47 %
Epithet	10,30 %
Exclamation	7,11 %
Hyperbole	3,92 %
Gradation	2,57 %
Rhetorical question	2,45 %
Antithesis	2,33 %
Anaphora	1,84 %
Personification	1,84 %
Parallelism	1,59 %
Comparison	1,47 %
Rhyme	1,10 %
Application	0,98 %
Synechdoche	0,49 %
Oxymoron	0,49 %
Pun	0,49 %
Epiphora	0,36 %
Neologism	0,36 %

C. Comparison Between the Average Scores of Slogans

Comparison between the average scores for Slogans 1.1: "Water from the heart of the Rhodope Mountain" and Slogan 1.2: "Water from the Rhodope Maountain".

In regards to originality, the mean score for Slogan 1.1 is 5,56. The mean score for Slogan 1.2 is 3,27. A difference of 2,29 is observed. The level of significance is 0,000, therefore we accept the Alternative Hypothesis (H1).

When comparing Creativity, the mean score for Slogan 1.1 is 5,48, while the mean score for Slogan 1.2 is 2,97. The difference between the two mean scores is 2,51. The level of significance is 0,000, therefore we accept the Alternative Hypothesis (H1).

In regards to persuasiveness, the mean score for Slogan 1.1 is 5,61. The mean score for Slogan 1.2 is 3,35. A difference of 2,26 is noted. The level of significance is 0,000, therefore we accept the Alternative Hypothesis (H1).

When comparing comprehensibility, the mean score for Slogan 1.1 is 5,68, while the mean score for Slogan 1.2 is 3,32 The difference between the two mean scores is 2,51. The level of significance is 0,000, therefore we accept the Alternative Hypothesis (H1).

In regards to pleasantness, the mean score for Slogan 1.1 is 5,87. The mean score for Slogan 1.2 is 3,32. A difference of 2,55 is detected. The level of significance is 0,000, therefore we accept the Alternative Hypothesis (H1).

With reference to memorability, the mean score for Slogan 1.1 is 5,69, while the mean score for Slogan 1.2 is 3,42 The difference between the two mean scores is 2,27.

The level of significance is 0,000, therefore we accept the Alternative Hypothesis (H1).

When comparing the degree to which the slogan incites a purchase, the mean score for Slogan 1.1 is 5,49, while the mean score for Slogan 1.2 is 3,10. The difference between the two mean scores is 2,39. The level of significance is 0,000, therefore we accept the Alternative Hypothesis (H1).

The largest difference between the mean score for Slogan 1.1 and Slogan 1.2 can be observed in regards to memorability. When fast moving consumer goods are being advertised, the usage of rhetorical figures has the biggest impact on how well the slogan is being memorized.

The smallest difference between the mean score for Slogan 1.1 and Slogan 1.2 can be seen in relation to persuasiveness. When promoting fast moving consumer goods, advertising specialists should keep in mind that applying the tools of rhetoric has the smallest effect on how persuasive a slogan is.

The T-criterion of Wilcoxon test is preformed and it shows that all the differences for all seven criteria are statistically significant. All the differences point favourably towards Slogan 1.1.

The differences between the ratings of Slogan 1.1 and 1.2 are large enough to argue that the usage of rhetorical figures makes Slogan 1.1 was rated as more original, more creative, persuasive, understandable, pleasant, memorable, and encouraging to purchase.

Therefore, it can be argued that the employment of rhetorical figures makes advertising slogans more competitive on the basis of all seven criteria which were chosen for this study.

Slogan 2.1 and Slogan 2.2 are compared in the same manner.

Comparison between the average scores for Slogans 2.1: "Credit on the spot" and Slogan 2.2: "Credit immediately".

In regards to originality, the mean score for Slogan 2.1 is 4,99. The mean score for Slogan 2.2 is 3,27. A difference of 2,29 is observed. The level of significance is 0,000, therefore we accept the Alternative Hypothesis (H1).

When comparing Creativity, the mean score for Slogan 2.1 is 4,85, while the mean score for Slogan 2.2 is 3,57. The difference between the two mean scores is 1,28. The level of significance is 0,000, therefore we accept the Alternative Hypothesis (H1).

In regards to persuasiveness, the mean score for Slogan 2.1 is 5,03. The mean score for Slogan 2.2 is 4,03. A difference of 1,00 is noted. The level of significance is 0,000, therefore we accept the Alternative Hypothesis (H1).

When comparing comprehensibility, the mean score for Slogan 2.1 is 5,08, while the mean score for Slogan 2.2 is 5,49 The difference between the two mean scores is -0,41. The level of significance is 0,000, therefore we accept the Alternative Hypothesis (H1).

In regards to pleasantness, the mean score for Slogan 2.1 is 4,65. The mean score for Slogan 2.2 is 3,85. A difference of 0,80 is detected. The level of significance is 0,000, therefore we accept the Alternative Hypothesis (H1).

With reference to memorability, the mean score for Slogan 2.1 is 4,86, while the mean score for Slogan 2.2 is 3,96 The difference between the two mean scores is 0,90. The level of significance is 0,000, therefore we accept the Alternative Hypothesis (H1).

When comparing the degree to which the slogan incites a purchase, the mean score for Slogan 2.1 is 4,68, while the mean score for Slogan 2.2 is 3,84. The difference between the two mean scores is 0,84. The level of significance is 0,000, therefore we accept the Alternative Hypothesis (H1).

The largest difference between the mean score for Slogan 2.1 and Slogan 2.2 can be observed in regards to originality. When financial services are being advertised, the usage of rhetorical figures has the biggest impact on how original the slogan is perceived to be.

The smallest difference between the mean score for Slogan 2.1 and Slogan 2.2 can be seen in relation to comprehensibility. When promoting financial services, advertising specialists should keep in mind that applying the tools of rhetoric has the smallest effect on how comprehensive a slogan is. It is important to note that, according to the results of the study, rhetorical figures make the slogan less understandable.

The T-criterion of Wilcoxon test is preformed and it shows that all the differences for all seven criteria are statistically significant.

The differences between the scores for Slogan 2.1 and 2.2 are large enough to conclude that slogans which use figurative language are perceived as more original, creative, persuasive, pleasant, memorable, and inciting to purchase.

For all criteria, except for comprehensibility, the difference is in favor of the first slogan which contains figurative language. The use of rhetorical figures has its price when advertising financial services - it makes the advertisement less understandable to people.

The usage of rhetorical figures increases the competitiveness of advertising slogans in the sphere of financial services for all criteria, with the exception of comprehensibility.

Slogan 3.1 and Slogan 3.2 are compared in the same manner.

Comparison between the average scores for Slogans 3.1: "The washing machine lives longer with Calgon" and Slogan 3.2: "The washing machine works longer with Calgon".

In regards to originality, the mean score for Slogan 2.1 is 5,91. The mean score for Slogan 2.2 is 3,54. A difference of 2,37 is observed. The level of significance is 0,000, therefore we accept the Alternative Hypothesis (H1).

When comparing Creativity, the mean score for Slogan 2.1 is 5,76, while the mean score for Slogan 2.2 is 3,34. The difference between the two mean scores is 2,42. The level of significance is 0,000, therefore we accept the Alternative Hypothesis (H1).

In regards to persuasiveness, the mean score for Slogan 2.1 is 5,70. The mean score for Slogan 2.2 is 3,66. A difference of 2,04 is noted. The level of significance is 0,000, therefore we accept the Alternative Hypothesis (H1).

When comparing comprehensibility, the mean score for Slogan 2.1 is 5,74, while the mean score for Slogan 2.2 is 5,26 The difference between the two mean scores is 0,48. The level of significance is 0,000, therefore we accept the Alternative Hypothesis (H1).

In regards to pleasantness, the mean score for Slogan 2.1 is 5,72. The mean score for Slogan 2.2 is 3,41. A difference of 2,31 is detected. The level of significance is 0,000, therefore we accept the Alternative Hypothesis (H1).

With reference to memorability, the mean score for Slogan 2.1 is 5,90, while the mean score for Slogan 2.2 is 3,38 The difference between the two mean scores is 2,52. The level of significance is 0,000, therefore we accept the Alternative Hypothesis (H1).

When comparing the degree to which the slogan incites a purchase, the mean score for Slogan 2.1 is 5,77, while the mean score for Slogan 2.2 is 3,28. The difference between the two mean scores is 2,49. The level of significance is 0,000, therefore we accept the Alternative Hypothesis (H1).

The largest difference between the mean score for Slogan 2.1 and Slogan 2.2 can be observed in regards to memorability. When everyday life products are being advertised, the usage of rhetorical figures has the biggest impact on how well the slogan is remembered.

The smallest difference between the mean score for Slogan 2.1 and Slogan 2.2 can be seen in relation to comprehensibility. When promoting products for everyday life, advertising specialists should keep in mind that applying the tools of rhetoric has the smallest effect on the degree to which a slogan is understood. It is important to note that, according to the results of the study, rhetorical figures make the slogan more understandable.

The T-criterion of Wilcoxon test is preformed and it shows that all the differences for all seven criteria are statistically significant.

All differences are statistically significant and in favor of the first slogan, which uses figurative language. With the help of rhetorical tools, advertisements become more original, creative, persuasive, enjoyable, memorable and, last but not least, more inciting to purchase.

It can be argued that rhetorical figures prove to be an amplifier of slogans' competitiveness in regards to all seven criteria chosen for this study.

IV. CONCLUSIONS

Rhetorical figures have a beneficial effect when advertising fast-moving consumer goods, financial services and household goods.

Through the usage of rhetorical figures advertising slogans in the field of fast-moving consumer goods, such as mineral water, prove to be original, creative, persuasive, enjoyable, memorable and, last but not least, more inciting to purchase when compared to slogans without rhetorical figures.

By applying the tools of rhetoric, advertising slogans in the financial services sector turn out to have increased originality, creativity, persuasiveness, enjoyment, memorability and incentive to purchase.

It is important to note that when the object of advertising is products and services in the field of finance, the use of rhetorical devices makes the slogan less understandable.

Rhetorical figures make advertising slogans for everyday usage products more original, creative, persuasive, enjoyable, memorable and more inciting to purchase.

In summary, it can be said that according to the results of our study, rhetorical devices increase the competitiveness of advertising slogans.

A direction for future research would be to develop an index for competitiveness of advertising slogans. Each of the criteria according to which competitiveness is being measured would receive a weight and the index would be measured.

V. ACKNOWLEDGMENTS

This conference paper is written within a Scientific research project „НИД НИ-2/2024/А“, financed by the University of National and World Economy, Sofia, Bulgaria.

REFERENCES

[1] S. Tripathi, V. Jain, J. Pandey, A. Merchant and A. Ambika, "When Consumers Tune Out Advertising Messages," Journal of Advertising Research., vol. 62, no. 1, pp. 3-17, 2022.

[2] M. Toncar and J. Munch, "Consumer responses to tropes in print advertising," Journal of Advertising, vol. 30(, no. 1, pp. 55-65, 2001.

[3] E. F. Mcquarrie and D. G. Mick, "Visual Rhetoric in Advertising: Text‐Interpretive, Experimental, and Reader‐Response Analyses," Journal of Consumer Research, vol. 26, no. 1, pp. 37-54, 1999.

[4] G. Tom and A. Eves, "The use of rhetorical devices in advertising," Journal of Advertising Research, vol. 15, no. 3, p. 39–43, 1999.

[5] S. H. Ang and E. A. C. Lim, "The influence of metaphors and product type on brand personality perceptions and attitudes," Journal of Advertising, vol. 35, no. 2, p. 39–53, 2006.

[6] Х. Кафтанджиев, „Най-ефективната креативна стратегия в рекламата – тази на визуалната (иконичната) метафора„“ ProGrafica„ № 1, pp. 20-25, 2010.

[7] R. O. Fabrize, "Combining Visual and Textual Rhetorical Figures in Advertising," in American Marketing Association Winter Educators' Conference, 2010.

Environment. Technology. Resources. Rezekne, Latvia
Proceedings of the 16th International Scientific and Practical Conference.2025. Volume IV, 431-437

Impact of Light Intensity and Luminaire Type on Basil Yield: Insights from a Hydroponic Urban Agriculture System

Linda Valkovska
Hydroponics
SIA Broccoli
Birzule, Latvia
valkovska3@gmail.com

Amélie Canon
SIA Broccoli
Liège, Belgium
liecanon2002@gmail.com

Anta Sparinska
Bulduri Biotechnology Centre
Bulduri Technical school
Jūrmala, Latvia
anta.sparinska@bulduri.lv

Olivier dal Zuffo
Hydroponics
SIA Broccoli
Birzule, Latvia
olivier@broccoli-global.com

Ansis Avotins
Institute of Industrial Electronics, Electrical Engineering and Energy
Riga Technical University
Riga, Latvia
ansis.avotins@rtu.lv

Martins Marcinkevics
Institute of Industrial Electronics, Electrical Engineering and Energy
Riga Technical University
Riga, Latvia
martins.marcinkevics@rtu.lv

***Abstract*— This study investigates the impact of different artificial lighting systems on the growth and yield of basil (*Ocimum basilicum L.*) within a controlled hydroponic environment. Aimed at comparing the effectiveness of several luminaire types, the research is identifying the optimal lighting conditions that enhance plant growth and productivity in an urban agriculture setting. The experiment was conducted in a 40" HQ shipping container using a Nutrient Film Technique (NFT) system. Basil plants were grown under five different luminaire types (A, B, C, D, E) at varying light intensities (200, 230, 250, 260, and 275 µmol/m²/s) with 3 repetitions. Plant growth parameters, including weight, green plant part length, and total yield per square meter, were measured from 11 plants per growth board (55 plants in each test) after a cultivation period of 27 days post-transplantation. The findings demonstrated significant variations in plant yield and growth characteristics across the different lighting setups. Luminaire C consistently provided the highest yields, particularly at the 260 µmol/m²/s intensity, suggesting its lighting configuration offers optimal conditions for basil production. In contrast, Luminaires D and B showed lower yields, indicating less favourable growth environments under their specific lighting conditions. Statistical analysis revealed that there were observable trends in yield enhancement under specific lamps. Additionally, the study highlighted variations in plant uniformity. In terms of plant uniformity, the standard deviations in length and weight were lowest under Luminaire B, emphasizing its potential for producing uniform crops, a crucial factor in commercial horticulture. The study underscores the critical role of selecting appropriate lighting technologies to maximize plant growth in controlled environment agriculture. By identifying the most effective luminaire types and light intensities, the research contributes valuable insights toward optimizing urban agricultural practices and enhancing the sustainability of food production systems.**

***Keywords*— basil, hydroponics, luminaires**

I. INTRODUCTION

Controlled-environment agriculture (CEA) systems, such as vertical farms and container-based operations, are emerging as vital tools to meet the growing global demand for food. These systems offer precise control over environmental variables, enabling year-round crop cultivation independent of external climate conditions. However, the success of CEA heavily depends on optimizing these controlled parameters, with lighting being one of the most critical factors. Artificial lighting directly influences photosynthesis, plant morphology, and yield, making it essential to select the most suitable light sources for maximizing plant growth.

In indoor cultivation, the spectrum, intensity, and uniformity of lighting play a crucial role in plant development. Studies such as [1] have demonstrated that the ratio of red to blue light can significantly impact the growth and nutraceutical content of plants. Furthermore, [2] highlighted that manipulating the light spectrum using LEDs can optimize growth rates and improve the nutritional quality of crops. This is especially relevant in controlled environments where natural sunlight is limited

Online ISSN 2256-070X
https://doi.org/10.17770/etr2025vol4.8399
© 2025 The Author(s). Published by RTU PRESS.
This is an open access article under the Creative Commons Attribution 4.0 International License.

or absent. [3] noted that improving photosynthetic efficiency through optimal lighting is a key challenge for modern agriculture, particularly for fast-growing crops like basil, parsley, and chives.

Hydroponics, a soil-less cultivation method utilizing nutrient-rich water solutions, has become a vital approach in urban agriculture, particularly for aromatic herbs in Europe [4]. As global food demand continues to rise and arable land becomes increasingly scarce, hydroponic systems especially in closed environments like vertical farms and container-based setups are gaining prominence for their efficient use of resources, reduced water consumption, and minimized pest issues [5], [6]. These systems enable year-round crop production by incorporating Controlled-Environment Agriculture (CEA) principles, allowing for precise regulation of light, temperature, humidity, and nutrient delivery [7]. As a result, hydroponics is increasingly viewed as a sustainable solution for urban food production [8].

One critical factor influencing the success of hydroponic cultivation is light quality, which significantly impacts plant growth, morphology, and yield [9]. Container-based growing systems, commonly used for aromatic herbs, provide numerous advantages in urban contexts [10]. They enable optimal space utilization, which is a crucial benefit in cities where land is limited and expensive [11]. Vertical farming, for example, allows multiple crop layers to be cultivated within a compact area, significantly boosting yield per square meter [12]. Moreover, these systems facilitate precise monitoring and control of environmental parameters, reducing the risk of pest infestations and disease—common issues in traditional soil-based agriculture [5]. Such control over growing conditions supports the fine-tuning of factors like light intensity and nutrient delivery, contributing to enhanced crop productivity and quality [13].

Additionally, the use of container-based systems offers flexibility in production cycles [14]. Farmers can quickly rotate or replace crops in response to market demands, ensuring a steady supply of fresh produce with superior flavor and nutritional profiles [15]. The proximity of these systems to urban centers further reduces transportation costs and carbon emissions, aligning with the growing consumer demand for locally sourced, sustainable food [16].

This literature review will delve into the influence of light quality on hydroponically grown herbs, evaluate the ideal growth conditions for each species, and discuss the challenges of achieving uniform growth in controlled environments [17]. Understanding these dynamics is essential for optimizing hydroponic systems to support sustainable urban agriculture [18].

The Importance of Light Quality in Hydroponics

The effectiveness of photosynthesis depends heavily on light quality, defined by the spectrum of wavelengths emitted by light sources. Key photosynthetic pigments, mainly chlorophyll a and b, absorb particular wavelengths mostly within the blue range (400-500 nm) and red range (600-700 nm) regions [19]. Research by [20] demonstrated that a red-to-blue light ratio of 3:1 can significantly enhance plant growth, yielding a 25% increase in biomass for lettuce and a 30% increase for basil compared to other light ratios. This highlights the necessity of optimizing light ratios tailored to specific crops.

Light Emitting Diodes (LEDs) have revolutionized horticultural lighting due to their efficiency, longevity, and customizable spectra. For instance, [2] found that utilizing a tailored LED spectrum (60% red, 40% blue) enhanced lettuce growth rates by 40% and increased leaf chlorophyll content by 30% compared to fluorescent lighting. Furthermore, [21] noted that LED systems can reduce energy consumption by up to 75% compared to traditional high-pressure sodium (HPS) lights, making them a more sustainable choice for growers.

In addition to light quality, light intensity and uniformity are critical for plant development. Additionally, research by [22] indicated that uneven light distribution could lead to growth discrepancies, with plants receiving optimal light growing 30% larger than those in shaded areas. Several studies have aimed to compare the effectiveness of different artificial lighting systems. For instance, [23] evaluated the growth of basil and lettuce under high-pressure sodium (HPS), fluorescent, and LED systems. The study found that LED lighting resulted in a 60% increase in growth rates and a 20% increase in nutrient content compared to HPS systems. Furthermore, the energy savings from using LEDs were quantified at 50% less electricity compared to traditional HPS systems for the same light output, demonstrating both economic and environmental benefits.

Growth Conditions and Light Sensitivity of Aromatic Herbs

Aromatic herbs, such as basil (*Ocimum basilicum*), have unique growth requirements influenced by light quality and environmental conditions. Understanding these needs is crucial for maximizing growth and nutritional quality, particularly in controlled environment agriculture (CEA).

Basil is a fast-growing herb highly sensitive to light quality. Research by [24] indicates that basil plants exposed to a light spectrum rich in red wavelengths (around 620-660 nm) exhibit enhanced leaf area and chlorophyll concentration, leading to biomass increases of up to 35% compared to those grown under lower red-light conditions. [25] found that specific LED lighting (80% red, 20% blue) significantly improved the essential oil content of basil, enhancing its flavor profile and market value. Optimal growth conditions for basil include temperatures of 18-30 °C, relative humidity of 50-70%, and a nutrient solution pH of 5.5 to 6.5 [26].

The intersection of plant growth and nutritional quality is critical in CEA. [1] highlighted that manipulating light spectra can enhance both biomass production and the

nutraceutical profiles of crops. For instance, basil grown under LEDs with a tailored spectrum exhibited a 35% increase in phenolic compounds compared to those grown under standard fluorescent lighting [25]. This dual focus on yield and nutritional quality is essential for maximizing the benefits of hydroponics in controlled environments, particularly in urban agriculture, where space and resources are limited.

Basil thrives under higher red-light ratios, whereas chives perform best under increased blue light levels, showing a preference for a spectrum comprising 70% blue and 30% red light [27]. Additionally, parsley prefers slightly cooler temperatures (15-21 °C) compared to basil (18-30 °C) [26], [28]. Cilantro's growth can be adversely affected by high temperatures, with optimal growth occurring at 20-25 °C [29]. This variability presents challenges in creating an optimal growing environment that simultaneously meets the diverse needs of these herbs. Strategies to mitigate these challenges may include zoning the growing area by crop type or employing adjustable lighting systems that cater to the specific requirements of each herb.

Despite advancements in hydroponic systems and lighting technologies, challenges remain. Integrating energy-efficient lighting solutions while maintaining optimal growth conditions is a significant hurdle. The high initial costs of advanced LED systems can pose barriers for small-scale producers [10]. Moreover, the long-term effects of continuous exposure to artificial lighting on plant health and productivity are still not fully understood. Future research should focus on conducting long-term studies to evaluate the sustained effects of different lighting systems on plant health and yield over multiple growth cycles. Additionally, exploring the synergistic effects of combined environmental factors (e.g., temperature, humidity) alongside light spectrum will help optimize overall plant performance in closed systems. Finally, assessing the economic feasibility of advanced lighting systems in various hydroponic setups, particularly in terms of energy costs and return on investment, will be critical for widespread adoption.

II. Materials and Methods

The growth characteristics of basil (*Ocimum basilicum*) were investigated within a climate-controlled 40" HQ shipping container retrofitted for urban agriculture. The study utilized a hydroponic Nutrient Film Technique (NFT) system, strategically arranged over a 60 m² area segmented into growing and nursery sections. The nursery section was positioned at a height of 30 cm above the ground, optimized for early-stage plant development.

Basil was seeded into peat pellets (25mm, Jiffy Products S.L. Ltd). Seeding densities were adjusted to species-specific requirements: 4–7 seeds per pellet for basil, these seedlings were uniformly cultivated under controlled conditions temperature, light exposure, day/night intervals, and humidity levels for a 45-day period in the nursery shelves.

Post-nursery, basil plants were transplanted into the main hydroponic NFT system at a density of 63 plants per square meter. This system maintained precise control over environmental parameters to ensure optimal plant growth:

pH and EC: Automatically adjusted within the ranges of 5.8–6.6 and 1.7–2.5, respectively.

Ventilation: Wind blowers activated every 20 minutes, providing 10-minute wind cycles to simulate natural conditions.

Humidity and Temperature: Regulated between 65-85% and 22-24 °C by an HVAC system.

CO2 Enrichment: Levels maintained at 800–1000 ppm via automated CO2 tank systems.

Lighting: Five different luminaire types were utilized: A, B, C, D, E. The main difference between each of the used luminaires is the spectral composition of an emitted light (Fig. 1.). Lamps A and D mostly utilize only red and blue light, which results in a dark pink spectrum. Lamp E includes more green light than the two previously stated lamps, which results in a lighter pink spectrum, but Lamps B and C include a full wavelength band with a peak in the green light region, thus resulting in a white light spectrum.

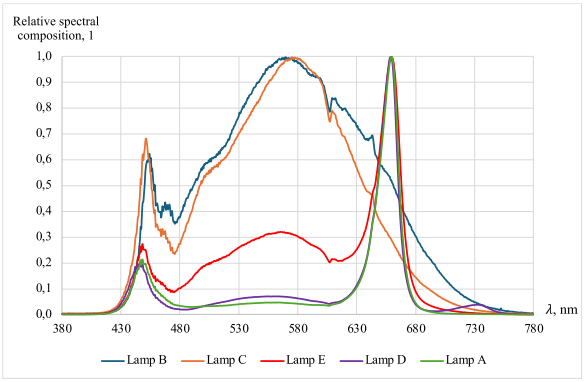

Fig. 1. Relative spectral composition of all 5 used luminaires

Light intensity, controlled via the Control Panel for luminaire A and the "Casambi" app for luminaires B, C, D, and E, was consistently set across all units for each test, ranging from 200 to 275 µmol/m²/s at the centre of each shelf.

The effectiveness of the lighting systems was assessed 27 days post-transplantation by measuring various growth parameters of 11 previous selected plants per square meter of each grow board (see Figure 2). Measurements included:

Plant Dimensions: Total plant length, green part length, and root length.

Biomass: Total plant mass, green part mass, and root mass.

Yield: Calculated per square meter to evaluate the productivity under each lighting condition.

All plants were sourced from identical seed stock and germinated under equivalent conditions to ensure uniformity. Data collection was synchronized, conducted

by the same researcher using standardized methods to guarantee comparability.

Results were analysed to determine the impact of different light treatments on plant growth and yield. Graphical representations of yield across varying light intensities for each luminaire type were prepared facilitating a visual assessment alongside statistical evaluations to discern significant differences and trends.

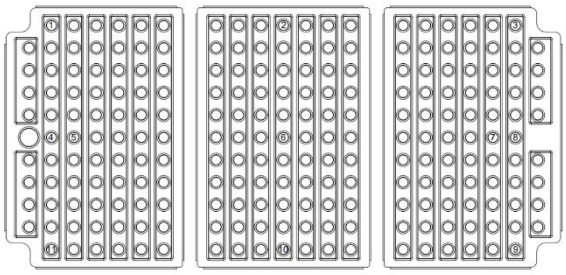

Fig. 2. Marked plants per grow board.

To summarize, in all of the comparative shelves, the plants growing under different luminaire types were sourced from the same seed stock, and the seeds germinated in the same conditions and same time. All of the seedlings were transplanted from the nursery to the hydroponic NFT system at the same time and all of the measurements, and data collection at the harvest were done at the same time, with the same instruments and by the same responsible person. To be able to ensure that data is comparable.

III. Results and Discussion

The study assessed the yield responses of *Ocimum basilicum* subjected to five distinct luminaire types (labeled A through E) across a gradient of light intensities (200, 230, 250, 260, and 275 µmol/m²/s). The experimental design incorporated measurements from 11 individual plants per growth board to ascertain the average weight for each grouping (see table 1). Subsequently, the standard deviation was computed for these values to quantify variability within each sample set. Furthermore, the average length of the green plant part was determined along with its corresponding standard deviation, providing insights into growth uniformity across treatments. Ultimately, the total yield per square meter was calculated, encapsulating the overall productivity of the hydroponic system under each lighting condition.

TABLE 1 MEAN VALUES OF MEASURED PLANTS PER GROWTH BOARD

Luminaire	Measurements					
	Mean weight	***St. dev***	***Mean length***	***St. dev***	***Yield g/m2***	***Light intensity µmol/m²/s***
A	7,1	3,0	30,5	3,1	825,0	
B	5,59	1,84	28,73	3,19	615	200
C	6,64	2,38	28,18	3,43	626	
D	x	x	x	x	x	
E	x	x	x	x	x	
A	7,55	3,2	26,36	2,46	983	230
B	9,27	2,05	27,64	2,23	1082	
C	9,18	4	27,82	2,21	1234	
D	9,73	2,6	29,73	2,14	1004	
E	8,36	3,36	26,91	2,68	987	
A	7,09	3,52	27	4,08	836,75	250
B	7,5	2,76	26,18	3,88	865	
C	9,23	4,37	30,14	3,68	983	
D	7,02	2,95	27,8	3,36	904	
E	4,36	1,64	23,85	3,37	565	
A	2,91	1,16	17,09	3,12	444	275
B	4,73	2,14	18,82	2,69	603	
C	5,18	1,4	24,55	3,11	657	
D	5,27	4,09	23,55	4,64	667	
E	2,09	0,9	19	4,53	430	
A	5	1,41	29,55	1,23	455	260
B	4,27	2,38	27,27	2,38	320	
C	8,45	3,73	28	5,24	561	
D	10,27	8,13	28,09	1,98	522	
E	4,27	1,42	21,91	3,6	238	

The bar graph titled "Effect of Lamp Type on Yield (Labeled by Letters)" presents the average yields of *Ocimum basilicum* achieved under five distinct lighting

conditions, identified as A, B, C, D, and E. Each bar signifies the average yield measured per square meter for each respective luminaire during the experimental evaluation. Notably, Lamp Type C demonstrates the

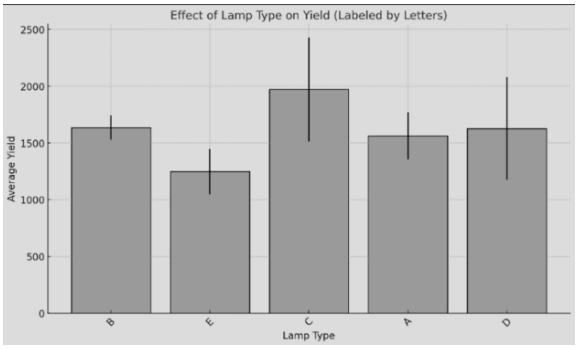

Fig. 3. Effect of Lamp Type on Yield (Labeled by Letters).

highest average yield, which suggests its lighting conditions characterized by a full wavelength band with a peak in the green light region are most conducive for basil growth. This result aligns with findings from [1], who demonstrated that manipulation of light spectra can significantly enhance plant biomass and nutraceutical profiles, supporting the efficacy of targeted spectral optimization in controlled environments.

In contrast, Lamp Type B, despite having a similar full-spectrum output, shows the lowest yield, indicating that other factors, such as spectral balance, may be suboptimal and could benefit from adjustments to enhance growth.

Lamps A and D, which primarily emit red and blue light, creating a dark pink spectrum, may influence plant growth differently due to the absence of a broader spectral range. Similarly, Lamp E, which includes more green light than A and D and produces a lighter pink spectrum, could contribute to a distinct growth response.

Furthermore, the error bars in the graph, representing the standard deviation of yields, highlight variability in plant responses. This variability is more pronounced with Lamp Types C and D, indicating a broader range of yield outcomes that could be attributed to individual plant sensitivities to the provided light spectrum or slight variations in local growing conditions. These differences in yield consistency are critical for understanding each lamp's effectiveness and reliability.

The trends indicate how different lamps perform under varying light intensities (200 to 275) (Fig.2.). Lamp C demonstrates the highest yield at a light intensity of 260, while other lamps like Lamp B and Lamp A exhibit more consistent performance across intensities. These insights can guide the optimization of light setups for maximum yield under specific conditions. Lamp C shows the most dramatic increase in yield with rising light intensity, peaking at 260 before experiencing a decline at 275.This phenomenon corresponds to previous studies, such as [9], suggesting that plants experience a peak efficiency at certain intensities, beyond which additional light becomes counterproductive or even detrimental to growth. This indicates its optimal performance at this specific intensity. Lamp D and Lamp E exhibit more variable performance, with sharp increases or decreases at specific intensities. These trends highlight the potential sensitivity of these lamps to changes in light conditions.

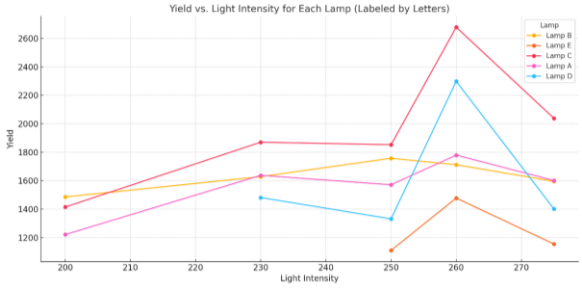

Fig. 4. Yield vs. Light intensity for each lamp.

Lamp B and Lamp A demonstrate more consistent performance across the range of light intensities, with gradual changes in yield. Moreover, lamps primarily emitting red and blue wavelengths (Lamp Types A and D) were observed to produce intermediate yields. These findings support earlier conclusions by [24], [30] which found that red and blue light strongly influence plant morphogenesis and phytochemical profiles but may not necessarily optimize biomass production compared to fuller-spectrum lights.

The comparison emphasizes that light intensity significantly impacts yield, but the optimal intensity varies depending on the lamp. This analysis provides actionable insights for optimizing light setups in controlled environments, helping to maximize yield by choosing the right lamp and light intensity combination.

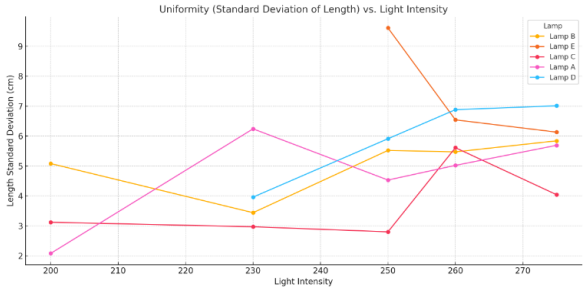

Fig. 5. Uniformity vs. Light intensity

Uniformity, measured as the standard deviation of plant lengths and weights, offered insights into the consistency of plant growth under each lighting condition (Fig.3.): At 230 µmol/m²/s, Lumianire B showed the lowest standard deviation in plant lengths and weights, indicating high uniformity and consistent growth outcomes. In contrast, Luminaire D and E displayed higher variability, particularly at 275 µmol/m²/s, where the plants exhibited greater discrepancies in growth parameters, possibly indicating less ideal lighting conditions for uniform

growth. This finding aligns with observations by [22], who noted that excessive or improperly distributed artificial lighting can lead to uneven plant growth, thereby complicating management and reducing marketability.

These results suggest that while higher light intensities can drive greater yields, they may also introduce variability in plant growth, affecting overall crop uniformity and potentially marketability in commercial operations.

Statistical analyses reinforced these observations: A moderate positive correlation between light intensity and yield (r = 0.25) was observed across all luminaires, underscoring the importance of optimized light management. Notably, lamps with a full-spectrum output, such as Lamp Types B and C, provided a more balanced light composition, which may have contributed to better overall growth conditions. However, despite this broader spectrum, Lamp B exhibited the lowest yield, suggesting that factors beyond spectrum alone, such as light intensity or spectral ratios, play a role in plant development.

A strong correlation between plant weight and yield (r =0.85) indicates that healthier, heavier plants generally produced more biomass, a key factor for commercial basil production. This finding aligns with the spectral influence, as Lamp Type C, which provided a full-spectrum light with a peak in the green region, supported the highest average yield, potentially due to its balanced wavelengths enhancing photosynthetic efficiency. In contrast, Lamps A and D, which primarily emit red and blue light and create a dark pink spectrum, may have promoted specific growth responses but did not necessarily maximize overall biomass production.

Plant length had a weaker correlation with yield (r = 0.13), suggesting that sheer plant size is not the primary determinant of yield. Instead, physiological health, leaf area, or light absorption efficiency factors influenced by spectral composition may be more critical. The presence of more green light in Lamp E's spectrum compared to A and D could have contributed to differences in light penetration and absorption, potentially influencing plant morphology.

However, the observed differences in spectral composition and plant responses highlight the need for further investigation into optimizing light quality for commercial basil production. The variability seen in yield outcomes, particularly with certain lamps, suggests that refining spectral ratios or intensity settings could enhance consistency and maximize production efficiency.

IV. Conclusion

Lamp C, which provides a full-spectrum light with a peak in the green region, resulted in the highest average yield, particularly at 260 µmol/m²/s. This suggests that a balanced light spectrum enhances photosynthetic efficiency and promotes basil biomass production. Lamps A and D, which primarily emit red and blue light, produced lower yields, indicating that the absence of a broader spectral range may limit overall biomass accumulation. A moderate positive correlation (r = 0.25) between light intensity and yield was observed, reinforcing the importance of optimizing light management.

Yield peaked at 260 µmol/m²/s under Lamp C but declined at 275 µmol/m²/s, suggesting that excessive intensity might not further enhance growth.

A strong correlation (r = 0.85) between plant weight and yield was identified, confirming that heavier plants produce more biomass, an essential metric for commercial basil cultivation.

Plant length had a weaker correlation with yield (r = 0.13), suggesting that size alone is not a critical determinant of productivity. Instead, factors like leaf area, light absorption efficiency, and physiological health play more significant roles.

However, the variability in plant responses suggests that further refinements in spectral ratios and intensity levels could improve consistency and optimize yield efficiency.

The study reinforces the importance of selecting the appropriate lighting technologies for hydroponic systems, as spectral composition and intensity significantly influence yield and uniformity.

The findings support the use of full-spectrum lighting, particularly with a peak in green light, to enhance biomass production in basil cultivation.

Further studies are recommended to explore the long-term impacts of these lighting conditions on secondary metabolite production and overall plant health.

V. Acknowledgments

Publication is created with support of the Latvian Rural Development Program "Cooperation", call 16.1 project Nr. 22-00-A01612-000018, "Application of 3D photogrammetry and introduction of innovations promoting energy efficiency to ensure more optimal environmental conditions in vertical agriculture".

REFERENCES

[1] C. Piovene, A. Maggio, and R. P. Barbagallo, "Manipulation of light spectra enhances plant biomass and nutraceutical profile of basil (Ocimum basilicum L.)," Scientific Reports, vol. 5, p. 11952, 2015. https://doi.org/10.1038/srep11952

[2] A. Sæbø, R. Rognan, and A. Abrahamsen, "The effects of different LED light spectra on growth and quality of lettuce," Acta Horticulturae, vol. 609, pp. 129–136, 2003. https://doi.org/10.17660/ActaHortic.2003.609.12

[3] E. H. Murchie and K. K. Niyogi, "Manipulation of photoprotection to improve plant photosynthesis," Plant Physiology, vol. 155, no. 1, pp. 86–92, 2011.

[4] H. M. Resh, Hydroponic Food Production: A Definitive Guidebook for the Advanced Home Gardener and the Commercial Hydroponic Grower, 7th ed. Boca Raton, FL: CRC Press, 2012.

[5] T. Kozai, G. Niu, and M. Takagaki, Plant Factory: An Indoor Vertical Farming System for Efficient Quality Food Production. San Diego, CA: Academic Press, 2016. https://doi.org/10.1016/C2014-0-04689-0

[6] K. Al-Kodmany, "The vertical farm: A review of developments and implications for the vertical city," Buildings, vol. 8, no. 2, p. 24, 2018. https://doi.org/10.3390/buildings8020024

[7] D. Touliatos, I. C. Dodd, and M. McAinsh, "Vertical farming increases lettuce yield per unit area compared to conventional horizontal hydroponics," Food and Energy Security, vol. 5, no. 3, pp. 184–191, 2016.

[8] J. Germer, J. Sauerborn, F. Asch, J. de Boer, J. Schreiber, and G. Weber, "Skyfarming: An ecological innovation to enhance global food security," Journal für Verbraucherschutz und Lebensmittelsicherheit, vol. 6, no. 2, pp. 237–251, 2011. https://doi.org/10.1007/s00003-011-0691-6

[9] E. Kaiser, T. Ouzounis, H. Giday, R. Schipper, E. Heuvelink, and L. F. M. Marcelis, "Adding blue to red supplemental light increases biomass and yield of greenhouse-grown tomatoes, but only to an optimum," Frontiers in Plant Science, vol. 9, p. 2002, 2019. https://doi.org/10.3389/fpls.2018.02002

[10] H. Bai, Y. Guo, and Y. Zhang, "Prospects for the development of containerized vegetable production in urban agriculture," Horticultural Plant Journal, vol. 6, no. 2, pp. 111–119, 2020.: https://doi.org/10.1016/j.hpj.2019.12.003

[11] M. Al-Chalabi, "Vertical farming: Skyscraper sustainability?" Sustainable Cities and Society, vol. 18, pp. 74–77, 2015. https://doi.org/10.1016/j.scs.2015.06.003

[12] K. Benke and B. Tomkins, "Future food-production systems: Vertical farming and controlled-environment agriculture," Sustainability: Science, Practice, and Policy, vol. 13, no. 1, pp. 13–26, 2017. https://doi.org/10.1080/15487733.2017.1394054

[13] C. Kubota and M. Kroggel, "Controlled environment strategies for tipburn management in greenhouse strawberry production," Acta Horticulturae, vol. 1156, pp. 529–536, 2017.

[14] C. Graham, J. Palmer, and G. Edwards-Jones, "The local food sector: Development and economic impact in the urban context," Urban Forestry & Urban Greening, vol. 39, pp. 64–71, 2019. https://doi.org/10.1016/j.ufug.2019.01.002

[15] E. Appolloni, G. Pennisi, and F. Orsini, "Sustainable production of baby leaf vegetables through hydroponics and light-emitting diodes," Sustainability, vol. 13, no. 3, p. 1163, 2021. https://doi.org/10.3390/su13031163

[16] D. Despommier, "The vertical farm: Controlled environment agriculture carried out in tall buildings would create a sustainable urban food supply," Journal of Consumer Protection and Food Safety, vol. 5, pp. 233–236, 2010. https://doi.org/10.1007/s00003-010-0654-3

[17] G. D. Massa, H. H. Kim, R. M. Wheeler, and C. A. Mitchell, "Plant productivity in response to LED lighting," HortScience, vol. 43, no. 7, pp. 1951–1956, 2008.

[18] S. Van Delden, M. SharathKumar, M. Butturini, L. Graamans, E. Heuvelink, M. Kacira et al., "Current status and future challenges in implementing and upscaling vertical farming systems," Nature Food, vol. 2, pp. 944–956, 2021.

[19] Z. Wang, Y. Li, and J. Lu, "Photosynthesis and plant growth under different light quality in hydroponics," Plant Physiology and Biochemistry, vol. 115, pp. 299–307, 2017. https://doi.org/10.1016/j.plaphy.2017.04.017

[20] G. D. Goins, N. C. Yorio, and C. S. Brown, "Photomorphogenic response of lettuce to red and blue light ratios," HortScience, vol. 34, no. 3, pp. 551–554, 1999. https://doi.org/10.21273/HORTSCI.34.3.551

[21] R. C. Morrow, "LED lighting in horticulture," HortTechnology, vol. 18, no. 4, pp. 491–495, 2008. https://doi.org/10.21273/HORTTECH.18.4.491

[22] Z. Jiang, J. Liu, and J. Xu, "Effects of light distribution on the growth of basil in hydroponic systems," Journal of Horticultural Science and Biotechnology, vol. 94, no. 1, pp. 123–129, 2019. https://doi.org/10.1080/14620316.2018.1473718

[23] S. López, M. Medina, and J. Álvarez, "Growth of basil and lettuce under different artificial lighting systems: An evaluation of high-pressure sodium, fluorescent, and LED lighting," Plants, vol. 10, no. 5, p. 1007, 2021. https://doi.org/10.3390/plants10051007

[24] H. Zhang, H. Zhang, and Y. Zhang, "Effects of light spectrum on the growth of basil," Frontiers in Plant Science, vol. 9, p. 223, 2018. https://doi.org/10.3389/fpls.2018.00223

[25] D. A. Kopsell, J. K. Kopsell, and W. M. Randle, "Effects of LED light quality on the growth and essential oil composition of basil," HortTechnology, vol. 24, no. 3, pp. 364–370, 2014.: https://doi.org/10.21273/HORTTECH.24.3.364

[26] E. Heuvelink, "Crop production in controlled environments," in Controlled Environment Agriculture, G. C. van der Meer and E. Heuvelink, Eds., Wageningen: Wageningen Academic Publishers, 1999, pp. 211–239.

[27] Y. Liu, Y. Zhan, and L. Wang, "The effect of light quality on growth and development of chives (Allium schoenoprasum L.) in hydroponics," Horticulture Research, vol. 7, no. 1, pp. 1–10, 2020. https://doi.org/10.1038/s41438-020-0263-2

[28] A. Sinha, S. Sinha, and C. Chatterjee, "The effects of environmental factors on the growth and yield of flat-leaf parsley (Petroselinum crispum var. Neapolitanum)," Agricultural Science, vol. 6, no. 4, pp. 477–485, 2015.: https://doi.org/10.4236/as.2015.64047

[29] P. Kumar, M. Singh, and R. Kaur, "Influence of different environmental factors on the growth and essential oil content of coriander (Coriandrum sativum L.)," International Journal of Chemical Studies, vol. 3, no. 6, pp. 39–45, 2015. [Online]. Available: https://www.chemijournal.com/archives/2015/vol3issue6/PartB/3-6-9.pdf

[30] M. Ashraf, N. A. Akram, F. Al-Qurainy, and M. R. Foolad, "Drought tolerance: Roles of organic osmolytes, growth regulators, and mineral nutrients," Advances in Agronomy, vol. 161, pp. 123–171, 2019.

Environment. Technology. Resources. Rezekne, Latvia
Proceedings of the 16th International Scientific and Practical Conference, 2025. Volume IV, 439-443

Rationality of Using Pneumatic Looseners of Vibration Action on Plow Bodies

Serhii Yermakov
Kamyanets-Podilskyi Instrument Applied College of Construction, Architecture and Design
Kamianets-Podilskyi, Ukraine
dakgps@pdatu.edu.ua

Taras Hutsol
Department of Agricultural Engineering
Odesa State Agrarian University,
Odesa, Ukraine

Oleksandr Hovorov
Faculty of Engineering and Technology
Higher educational institution «Podillia State University»,
Kamianets-Podilskyi, Ukraine

Pavlo Potapskyi
Faculty of Energy and Information Technologies,
Higher educational institution «Podillia State University»,
Kamianets-Podilskyi, Ukraine

Serhii Oleksiyko
Affiliated Unit "Khotyn Vocational College of Higher Educational Institution "Podillia State University"
Khotyn, Ukraine

***Abstract*— In modern agriculture, more and more attention is paid to the problems of energy consumption during deep tillage operations. One of the ways to solve this problem is the use of vibrations to facilitate the work of working bodies and reduce the traction resistance of the unit in general. This paper presents one possible implementation of this idea for a plowing unit. The proposed design improvement in this study involves developing a mechanism to induce vibrations in plow bodies. The theoretical basis is the establishment of general laws governing the effect of vibrations on traction resistance. Ensuring vibrations is offered by installing additional pneumatic vibration dampers in the blades on each plough body. This idea is protected by the patent of Ukraine. In order to establish the effect of vibrations on traction resistance, the Goryachkin's rational formula. was adapted in the work. The effect of vibrations in this formula was accounted for by modifying specific parameters based on scientific research on their influence on the coefficient of friction (f_0) and specific traction resistance (K). The theoretical dependence of traction resistance on the speed of movement of the unit for a plough with and without the use of pneumatic looseners is presented in the work. The graphs indicate that the use of oscillating looseners reduces the traction resistance of the plow by 19...23% in the speed range of 0.5…2.5 m/s. The results of these studies are completely correlated with the data from other studies and can be used to clarify and improve methods of calculating vibratory plough.**

Keywords*— plough, pneumatic hammer, pneumatic soil loosener, plough body, traction resistance, coefficient of friction, vibration.

I. Introduction

As a rule, technological operations related to soil tillage account for up to 40% of total production costs. Therefore, improving soil cultivation technology is a crucial priority.

With the rapid advancement of science and technology, resource conservation must be accompanied by a fundamentally new approach to improving soil tillage quality. In the scientific community, two main approaches to energy resource conservation in soil cultivation have been identified:

- reducing traction resistance;
- developing wide-grip combined machines.

We consider reducing the traction resistance of tillage machines to be the most effective solution, as the development of wide-grip combined machines inevitably leads to increased traction resistance.

A review of scientific studies indicates several possible ways to reduce the traction resistance of tillage machines [1-4]:

- optimizing tool design and reducing weight;
- improving the geometry of working bodies;
- reducing soil friction on working surfaces (e.g., replacing sliding surfaces with rolling surfaces or introducing oscillations in working bodies).

The key challenge in improving tillage machines, including combined models, is reducing traction resistance

Online ISSN 2256-070X
https://doi.org/10.17770/etr2025vol4.8401
© 2025 The Author(s). Published by RTU PRESS.
This is an open access article under the Creative Commons Attribution 4.0 International License.

without significantly complicating the design. Researchers focus particularly on the use of vibration in soil cultivation, one of the most energy-intensive operations in modern agriculture.

The application of vibration and impulse technology provides a new perspective on energy concentration over time and its more efficient use in soil tillage operations.

II. Materials and methods

This research was conducted as part of the scientific project of the educational and research laboratory "DAK GPS" at Higher Education Institution "Podillia State University" [5-7]. This paper aims to develop a mechanism for generating vibrations in plough bodies and to establish the general theoretical relationship between the oscillatory action of vibratory looseners and the traction resistance of the unit.

The necessity of improving existing technical solutions was substantiated by analyzing the challenges associated with deep soil tillage and the limitations of currently available equipment. The design of a plough body equipped with pneumatic vibratory looseners was based on this analysis, incorporating the best available solutions while identifying and addressing their shortcomings.

The variation in the required traction force with changing ploughing conditions should logically follow from a comprehensive and precise theory that accounts for the complex processes involved in plough operation.

According to Loveykin V.S., Chovniuk Yu.V., and Dyachenko L.A. [8], the formulas for calculating the traction resistance of vibrating ploughs should be refined and improved based on the well-known three-term Goryachkin formula:

$$P = f_0 G + K a b + \varepsilon a b \upsilon^2, \quad (1)$$

where P –traction resistance of the tillage implement, H;

f_0 – proportionality factor, which depends on the overall friction coefficient; according to V.P. Goryachkin f_0 =0.5 for stubble, f_0 =1.0 for clover;

G – weight of the machine, N;

K – specific resistance of the plough; K =20000 N/m^2 on the lungs; K =30,000 N/m^2 on average; K =40000-50000 N/m^2 on heavy soils;

a, b – width of capture and depth of processing, m;

ε – coefficient, which takes into account the geometric parameters and frictional properties of the working bodies of the soil tillage machine, ε=1500-2000 N*s^2/m^2;

υ – unit movement speed, m/s.

Goryachkin's rational formula can be seen as an initial attempt to outline key factors before establishing a precise pattern, reflecting the physical relationships between the main parameters of the ploughing process and the overall resistance encountered during operation. However, it does not explicitly account for the influence of various factors on plough traction resistance, including vibration effects, friction forces between field boards and the furrow wall, the vertical component of soil reaction on the plough bodies, resistance forces acting during soil layer separation from the bottom and furrow wall, as well as the thickness of the ploughshare blades.

III. Results and discussion

Based on the analysis of existing soil treatment technologies, an improved plough body design is proposed, in which soil loosening precedes its compression and displacement. This is achieved through the use of compressed air from the tractor's pneumatic system, which is an integral part of its design but remains underutilized due to the absence of direct compressed air consumers.

The improved plough body 6 (Fig. 1) includes a rack 7 with a shelf 8 fixed to it with a front part and a field board 10. A soil loosener - a pneumatic hammer 12 (patent of Ukraine №107117) is additionally installed on the ploughshare 9.

Plough bodies 6 with pneumatic hammers 12 are fixed on the frame 5 of the plough and are connected to the air distribution mechanism 11 with the help of flexible pneumatic lines 4, and through the common pneumatic line 3 and the mechanism 2 of the pneumatic control of the level of loosening are connected to the standard pneumatic system 1 of the tractor.

During the movement of the tractor with the plough, with the pneumatic control mechanism 11 turned on, the working bodies of the pneumatic hammers 12 of all bodies 8, making a reciprocating movement along the path of the tractor, will loosen the soil of any categories with vibration shocks, reducing the resistance to its destruction by ploughshares. As a result, the total resistance to the plough unit's movement decreases, reducing the load on the tractor's engine and ensuring stable operation at nominal speed and optimal load conditions.

Initial assessment of the trinomial Goryachkin's allows us to make some assumptions. The first term of the formula expresses the "dead resistance", which is determined when pulling the ploughs in an open furrow, therefore, under the influence of vibrations, this resistance will obviously decrease. The second term expresses the resistance caused by the deformation of the soil layers [9; 10] and depends on the specific resistance K, which will also be affected by the action of vibrations. The third component of the total resistance is related to the provision of kinetic energy to the soil layers particles depending on the speed of the plough [9]. As noted by V.S.Loveykin. for a vibratory plough that works at a traditional speed (v=1.2...1.4 m/s), this third term of the formula is relatively small (~5% of the total traction resistance), so the traction force of the vibratory plough changes slightly with a change in the speed of the vibratory plough [8].

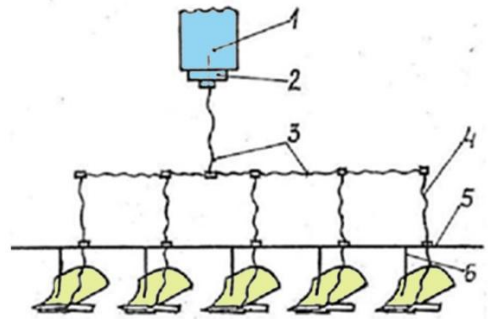

a)

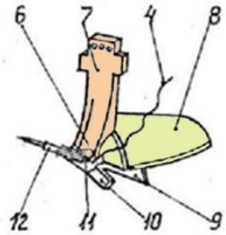

b)

Fig. 1. Scheme of a plough with pneumatic soil looseners: a) general; b) plough body; 1 – tractor pneumatic system; 2 – a mechanism for controlling the degree of loosening of the soil; 3 – common pneumoline; 4 – pneumoline of the plough body; 5 – frame; 6 – plough body; 7 – rack; 8 – shelf; 9 – ploughshare; 10 – field board; 11 – air distribution mechanism; 12 – pneumatic hammer.

Thus, to assess the influence of vibrations on plough operation, it is first of all important to trace their influence on the f0 and K indicators and on the total traction resistance. These indicators are established mainly by research and their results are described in many works.

Various researchers have proven that vibrations are an effective way to reduce traction when the volume of disturbed soil increases. In particular, X. Dong et al. [11] proved that at the vibration frequency of 6.7 and 8.3 Hz, the required traction force of the soil loosener was stable and significantly reduced, which can improve the soil loosening efficiency and reduce the harmful vibration on the tractor. Odey Simon and others. [12] estimated the traction resistance of a vibrating deep loosener and a non-vibrating operation at a depth of 0.35 m for a vibrating deep loosener to be 6.9% - 17% less than for a non-vibrating one. Xirui's experiments also confirmed that the deep loosener using oscillating equipment requires 16-28% less traction resistance compared to traditional ones [13].

Bulgakov V.M., Sviren M.O. and others. experimentally established that when using vibrations in plough, the friction of the soil sliding along the ploughshare and the shelf is significantly reduced, which is the main component in the overall amount of traction resistance [14; 15]. The sticking of working organs also decreases. On light and medium soils, the traction resistance is reduced by 20–30%, and on particularly heavy soils by more than 50% (at optimal vibration modes).

Many researchers have noted that excessive tillage depth not only increases energy consumption and reduces earthmoving efficiency but also accelerates wear and damage to machinery under harsh conditions. This problem can be solved by bionics and vibration techniques [16-18]. Research in a field experiment with deep tillage by Yang M. [19] showed that the soil resistance gradually decreased with increasing vibration frequency. The use of vibrations of the working bodies allowed not only to reduce the resistance, but also to reduce the total energy consumption: the rate of reduction of the resistance reached 14.2–21.2%, and the total energy consumption was reduced by 11.2–16.5%. According to Vasylenko V.V., under the influence of vibration, the soil friction coefficient changes from f = 0.61 (without vibration) to f = 0.50 (with vibration of the friction surface). According to their conclusions, vibration can reduce the coefficient of friction by 18% [20]. Loveykin V.S. etc. note that due to vibrations, this indicator decreases to f = 0.3 for stubble (from 0.5 in Goryachkin V.P.) and to f = 0.5...0.54 for clover (1.0 in Goryachkin V.P.), that is, by 40–45% [8].

Based on the given data for modeling the traction resistance of the plough according to the Goryachkin's formula we will use f0 =0.5 without vibrations and f0 =0.3 with vibrations (stubble), and specific resistance K =50000 N/m2 and K =40000 N/m2 with vibrations (loamy soils), respectively. Other components of the Goryachkin's formula we will accept as permanent. G=1100N, b=5*0.35=1.75 m, (five-furrow plough); ε=1500 N*s2/m2.

The graph of the dependence of the traction resistance on the movement speed v will be repeated three times at the processing depth a = 0.25; 0.30; 0.35 m. The range of the variable υ is assumed to be 0.5–2.5 m/s.

As a result, we will get a graph (Fig. 2), which clearly shows the positive influence of vibrations on the total traction resistance of the plough.

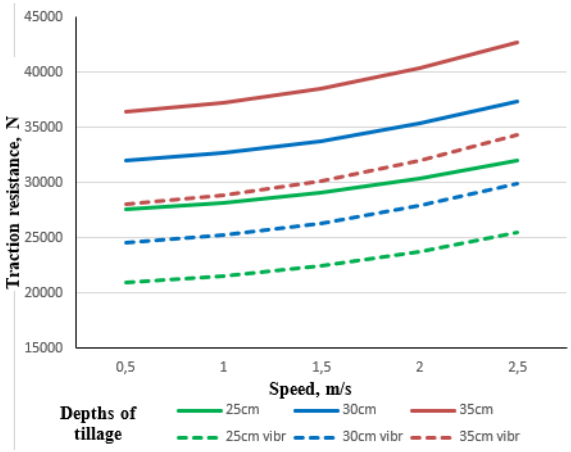

Fig. 2. Dependence of the traction resistance on the speed of movement at different depths of tillage: ——— theoretical curves without vibrations; — — — theoretical curves with a vibration exciter.

The graph depicting the dependence of traction resistance on speed at different tillage depths for traditional and vibratory ploughs generally aligns in shape and values with similar graphs presented by other researchers. [9; 10; 20; 21]. In all these sources, the graphs of the dependence of traction resistance on speed are increasing and slightly concave, as in our case.

Analyzing the graphs for the effectiveness of vibrations, it can be noted that the use of vibrations reduces the theoretically calculated traction resistance of the plough in the range of speeds of 0.5–2.5 m/s by 19–23%. Moreover, at lower speeds, the influence of vibrations is more important: a reduction in traction resistance by 22-23% at a speed of 0.5 m/s and by 19-20% at 2.5 m/s.

If we compare these numbers with the data provided by other scientists, we will have a decrease in traction resistance due to the action of vibration according to data from Simon O. is 17%, Xirui - 16–18%, Bulgakov V.M., Sviren M.O. – 20-30% [14], Yang M. - 14.2–21.2% [19], Vasylenko V.V., Afonychev – 18% [20]. These values correlate well with the obtained theoretical curves.

IV. Conclusions

The application of the proposed plough body with a pneumatic soil loosener in plough units is both promising and environmentally friendly. Reducing overall movement resistance will increase the unit's speed and, consequently, its productivity. Optimizing the diesel engine's speed and load modes will enhance its operational efficiency and economic performance. Additionally, utilizing compressed air from the tractor's pneumatic system to power the pneumatic hammers will stabilize its load.

As a result, fluctuations and maximum deviations in soil resistance will decrease, improving the reliability and durability of both the plough bodies and the plough as a whole. Furthermore, working conditions will improve by eliminating the need to modify the plough for heavy soils, such as removing the rear body.

A comparison of theoretical results indicates a significant reduction in traction resistance for tillage implements equipped with vibrating working bodies compared to conventional ones. The developed model of tillage tool operation allows for the assessment of vibration looseners' effectiveness in reducing traction resistance. This conclusion is supported by graphs that align with similar findings in other studies.

Implementing vibrating working bodies in tillage tools will help minimize agricultural machinery operating costs. The use of vibrations reduces the theoretically calculated traction resistance of the plough within the speed range of 0.5–2.5 m/s by 19–23%. Moreover, at lower speeds, the influence of vibrations is more pronounced: reducing traction resistance by 22–23% at 0.5 m/s and by 19–20% at 2.5 m/s.

The results obtained in the work can further serve to clarify and improve existing engineering methods for calculating the main characteristics and parameters of vibratory ploughs, both at the stages of their design / construction, and in real operation modes.

References

[1] V. P. Horjachkyn, Sobranie sochinenij v 3-x tomax, 1965, vol. 1, 720 p.; vol. 2, 459 p.; vol. 3, 512 p.

[2] V. V. Adamchuk, H. L. Baranov, and O. S. Baranovs'kyi, Suchasni tendencii rozvytku sil'skogospodars'koi tekhniky, Kyiv: Ahrarna nauka, 2004, 396 p.

[3] B. Szabo, F. Barnes, and S. Sture, "Effectiveness of vibrating bulldozer and plow blades on draft force reduction," Transactions of the ASAE, vol. 41, no. 2, pp. 283–290, 1998.

[4] M. Korchak, "Problems of field contamination when growing energy corn as monoculture," E3S Web of Conferences, vol. 154, 2020, Art. no. 01009. https://doi.org/10.1051/e3sconf/202015401009

[5] S. Yermakov, T. Hutsol, V. Devin, S. Oleksiyko, and P. Potapskyi, "The effectiveness of cognitive digressions in classes of general technical disciplines in institutions of higher education of agro-technical direction," Engineering for Rural Development, Jelgava, May 25–27, 2022, pp. 460–465. https://doi.org/10.22616/ERDev.2022.21.TF154

[6] V. Devin, S. Yermakov, O. Gorbovy, V. Pidlisnyj, and A. Semenov, "Research on Working Bodies of Hammer Crushers Employing the Finite Element Method," Vide. Tehnologija. Resursi - Environment. Technologies. Resources, vol. 3, Rezekne, Latvia, 2023, pp. 65–68. https://doi.org/10.17770/etr2023vol3.7197

[7] S. Yermakov, T. Hutsol, I. Garasymchuk, P. Fedirko, and V. Dubik, "Study of the unloading and selection process of energy willow cuttings for the creation of a planting machine," Environment. Technologies. Resources, vol. 3, Rezekne, Latvia, 2023, pp. 271–275. https://doi.org/10.17770/etr2023vol3.7199

[8] V. S. Loviekin, Yu. V. Chovniuk, and L. A. Dyachenko, "Dynamičnyj analiz tjahovoho oporu vybropluhiv," Vibratsii v tekhnitsi ta tekhnolohiiakh, no. 3(67), pp. 112–115, 2012.

[9] D. H. Vojtiuk, Sil's'kogospodars'ki mashyny: osnovy teorii ta rozrakhunku, Sumy: VTD Universytets'ka knyha, 2008, 543 p.

[10] P. M. Zajika, Teoriia sil's'kogospodars'kykh mashyn. T. 1 (4.1). Mashyny ta znariad'dia dlia obrobky hruntu, Kharkiv: Oko, 444 p.

[11] X. Dong, H. Zheng, C. Su, Y. Li, J. Song, and J. Wang, "Test and analysis of vibration characteristics of vibration subsoiler," INMATEH. Agricultural Engineering, vol. 68, no. 3, pp. 906–917, 2022. https://doi.org/10.35633/inmateh-68-90

[12] Patent 1197117 Ukraine, Korpus pluha z pnevmatychnym rozpushyvachem hruntu, 2016, Biul. № 10, p. 5.

[13] S. Yermakov, A. Rud, and M. Vusatyi, "The distribution of cash expenses for the creation of bioenergy willow plantations in Ukraine," Vide. Tehnologija. Resursi - Environment. Technologies. Resources, vol. 1, Rezekne, Latvia, 2023, pp. 74–80. https://doi.org/10.17770/etr2023vol1.7191

[14] V. M. Bulgakov, M. O. Sviren', and R. V. Kisil'ov, "Doslidzhennia vybraziinykh protsesiv pry osnovnomu obrobci hruntu," Naukovyi visnyk Tavriiskoho derzhavnoho ahrotekhnolohichnoho universytetu, vol. 5, no. 1, pp. 3–13, 2015.

[15] V. M. Bulgakov, M. O. Sviren', I. P. Palamarchuk, et al., Vybraziini mashyny sil's'kogospodars'koho vyrobnytstva: Monohrafiia, Kirovohrad: KOD, 2012, 512 p.

[16] J. Sun, Y. Wang, Y. Ma, J. Tong, and Z. Zhang, "DEM simulation of bionic subsoilers (tillage depth > 40 cm) with drag reduction and lower soil disturbance characteristics," Advances in Engineering Software, vol. 119, pp. 30–37, 2018. https://doi.org/10.1016/j.advengsoft.2018.02.001

[17] X. Ma, S. Wang, and H. Wang, "Vibration soil crushing mechanism of self-excited vibration subsoiler in coastal area," Journal of Coastal Research, vol. 103, pp. 426–430, 2020. https://doi.org/10.2112/SI103-087.1

[18] J. Li, X. Jiang, Y. Ma, J. Tong, and B. Hu, "Bionic design of a potato digging shovel with drag reduction based on the discrete

element method (DEM) in clay soil," Applied Sciences, vol. 10, 7096, 2020. https://doi.org/10.3390/app10207096

[19] M. Yang, X. Sun, X. Deng, Z. Lu, and T. Wang, "Extrapolation of tractor traction resistance load spectrum and compilation of loading spectrum based on optimal threshold selection using a genetic algorithm," Agriculture, vol. 13, no. 6, 1133, 2023. https://doi.org/10.3390/agriculture13061133

[20] V. V. Vasilenko and S. V. Vasilenko, "Effect of vibration on resistance force of plough," Advances in Engineering Research, vol. 151, pp. 779–783, 2018.

[21] D. H. Vojtiuk, Sil's'kogospodars'ki mashyny. Osnovy teorii ta rozrakhunku, Kyiv: Vyshcha osvita, 2005, 464 p.

[22] A. Tryhuba, T. Hutsol, I. Tryhuba, et al., "Risk assessment of investments in projects of production of raw materials for bioethanol," Processes, vol. 9, no. 1, 12, 2021. https://doi.org/10.3390/pr9010012

[23] I. V. Holovach, I. P. Palamarchuk, and M. O. Sviren', "Minimal'no dopustyma chastota kolyvan' vibraziynogo vykopuyuchogo robochoho orhanu," Vibratsii v tekhnitsi ta tekhnolohiiakh, no. 4(68), pp. 35–41, 2012.

[24] M. Korchak, S. Yermakov, T. Hutsol, L. Burko, and W. Tulej, "Features of weediness of the field by root residues of corn," Vide. Tehnologija. Resursi - Environment, Technology, Resources, vol. 1, pp. 122–126, 2021. https://doi.org/10.17770/etr2021vol1.6541

Environment. Technology. Resources. Rezekne, Latvia
Proceedings of the 16th International Scientific and Practical Conference. 2025. Volume IV, 445-449

Research Into the Possibility of Creating a Wi-Fi Radar for Detecting Moving Flying Targets in the Nearby Area of Protected Objects

Yosif Yosifov
Faculty "Atillery, AD and CIS"
National Military University Vasil Levski
Veliko Tarnovo, Bulgaria
yvyosifov@nvu.bg

***Abstract*— Nowadays, there are much researches on the creation of passive coherent radar systems for detecting aircraft in the airspace. One of them is the use of systems based on Wi Fi signals for detecting a moving target. This paper research the possibility of detecting and determining the parameters of flying targets using Wi Fi radar in nearby area of protected objects. An analysis of the potential capabilities of such a system has been carried out. The conclusion is that the development of such a system is possible for close distances to the protected object.**

***Keywords*— bistatic passive radar, Wi Fi.**

I. INTRODUCTION

Nowadays we are witnessing a great spread of unmanned aerial vehicles. Many people have them for entertainment purposes because they are easily accessible in price, and they can see things from a bird's eye view. There are enthusiasts who make their own unmanned aerial vehicles. There are also those who violate legal restrictions. There is a problem of protecting critical infrastructure objects that are protected from the entry of unmanned aerial vehicles, although legal software does not allow this, there are ways to hack the software. Proof of this is the entry of an unmanned aerial vehicle at Sofia Airport on February 7, 2025 [1] as a result, there are delays to 6 flights and the possibility of a much more serious incident.

In such a case, there is a need for timely detection of aircraft and establishing the moment of entry into the boundaries of the given object. One way to establish this is through radars that can detect the target and determine its parameters. To protect objects from such an entry, reconnaissance at long distances is not necessary, as is the case with most radar systems, but a short distance beyond the borders of the object with sufficient resolution in distance and angular coordinates is enough. There are many literary sources [3], [4], [7], [8], [9], [10] that study the methods for creating passive radars. Most Wi-Fi-based systems are used to detect people due to the low power of the transmitter and the small detection distance. The idea of the study is to examine whether it is possible to achieve this using a Wi-Fi semi-passive or pseudo-passive bistatic coherent radar for detecting drones at close distances to a protected object (although the research conducted is applicable to any bistatic radar with similar parameters). The research is related to small amateur aircraft, and their classification is discussed in [2].

The paper is organized as follows. First, a review of radar systems with advantages and disadvantages is made. Then, potential abilities for detecting targets in a bistatic Wi-Fi radar are considered. After that, result and discussion. At the end there is conclusions and acknowledgments.

II. MATERIALS AND METHODS

There are two options for building a radar system to monitor the area near an object and the moment of the target entering the territory of the protected object:

A. The first option is to build an active radar. Its advantages are the ability to determine the signal parameters, such as power, frequency retuning, signal formation, etc. Disadvantages: such a system may be quite expensive to purchase.

B. The second option of a radar system and probably cheaper is to build it as a passive radar, which uses a foreign transmitter to detect and determine the coordinates of the target. Several options for such radars are possible, such as those of the radio broadcasting system, TV broadcasting, Satellite communications, GSM communication, Wi Fi communications. The geometry of a bistatic passive radar system has the form shown in "Fig. 1"

Online ISSN 2256-070X
https://doi.org/10.17770/etr2025vol4.8459
© 2025 The Author(s). Published by RTU PRESS.
This is an open access article under the Creative Commons Attribution 4.0 International License.

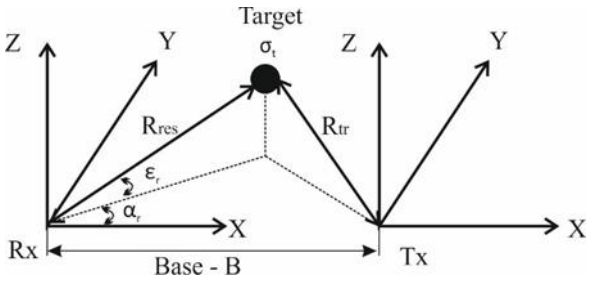

Fig. 1. Geometry of bistatic passive radar.

These systems extract information about the object from the delay time of the signal from the target relative to the direct channel of the transmitted signal. The receiver used in most literature sources [7], [8], [9], [10], [11], [12], [13], [14], [15] uses Software Defined Radio, through which signal processing and spectral analysis are performed.

The signal sources for passive radars can be different and their advantages and disadvantages are discussed below:

a) Analog broadcasting - nowadays TV broadcasting in most countries of the world is digital but passive radars can use radio analogue broadcasting if the country has. Advantages is a high power of the transmitted signal through which targets can be detected at a long distance. Analogue broadcasting has one main disadvantage [3] low resolution depending on the signal spectrum in the context of the transmitted information (music, speech, etc.).

b) Digital TV [3], [7] (DVB-T, DVB-T2) can be used to solve the problem. Advantages: much better resolution compared to the analogue transmitter, low level of side-sheets in the correlation function, independence of the signal spectrum from the message. Disadvantages: lower power than that of analogue television, which reduces the detection distance of especially small targets. Influence of the relief on the detection zone at a distance from the protected object.

c) GSM system [3], [10] – if near the protected object there are base stations of mobile operators, their use is possible for detecting flying objects near the area of the protected object. Advantages: good resolution than analogue broadcast, operation on different frequency bands of the transmitter. Disadvantages – low transmitter power, which significantly reduces the surveillance area, no ability to determine the location and parameters of the transmitter, low accessibility.

d) Wi Fi systems [3], [8], [9] – ability to detect objects at short distances. Disadvantages – low transmitter power, which significantly limits the surveillance area, big side lobes on ambiguity function low range resolution. Advantages if a pseudo-passive system is used (own transmitter with a suitable amplifier) possibility of determining the location of the transmitter for the best resolution. Possibility of manipulating the signal emitted by the transmitter for the purpose of better resolution. From the transmitters examined it is seen that for any conditions (relief, distance of the object from the transmitter) for detecting targets in the area near a given object it is possible to use your own Wi Fi transmitter with a suitable amplifier to increase the power.

In this study, the protected object area is understood as the region that is prohibited for flights of unmanned aerial vehicles. In Bulgaria, these zones are updated every 15 minutes and are provided by the Directorate General "Civil Aviation Administration". They contain information about the coordinates of the object area and restrictions. Looking at the interactive map of the no-fly zones for unmanned aerial vehicles [16], it is seen that there are zones of different sizes and shapes. The flight height in the zones is limited to 150 m or below, but in Bulgaria it is forbidden for unmanned aerial vehicles to fly above this height.

For simplicity, under the protected object area in this article an idealized zone in the shape of a rectangular parallelepiped lying on the ground surface is assumed, its base is flat with a length of 2500 meters by a width of 2000 meters and a height of 200 meters. The transmitter and receiver of the bistatic radar are located equidistantly from the center of the rectangular base in a line along its longitudinal axis. To perform the task, it is not necessary to know anything about the flights of unmanned aerial vehicles outside the area. It is important to detect entry into the zone and monitor drone flights inside the area. In this case, a bistatic range of about 3000 meters is assumed to be sufficient for detection, which is sufficient to cover the dimensions of the object.

In the next part, the potential capabilities of this system are examined and analysed.

First of them is the range and minimal power to detect target.

The operating range of a monostatic coherent radar is determined according to [5], [6].

$$R^4 = \frac{P_{tr}G_{tr}\sigma_t G_{res}\lambda^2 \Delta f T_{acc}}{4\pi^3 q_{min} P_n} \quad (1)$$

Where: R – the maximum detection range of the radar, P_{tr} – the transmitter power, G_{tr} – the directional coefficient of the transmitter antenna, σ_t – the effective reflecting surface of the target, G_{res} – the directional coefficient of the receiver antenna, λ – wavelength, Δf – the receiver passband, T_{acc} – the time for coherent signal accumulation, q_{min} – the required minimum signal-to-noise ratio, P_n – the noise power at the receiver input.

In the bistatic geometry of passive radar Tx and Rx are not in the same position. According to this the distance between Tx and target (R_{tr}) and Rx and target (R_{res}) need to be distributed. In this case, we can assume that $R = \sqrt{R_{tr}R_{res}}$. Then we can assume that $P_{resmin}=q_{min}P_n$ is a minimal power at the receiver input that can be distinguished from the receiver. In this case (1) can be written for bistatic geometry as [4]:

$$(R_{tr}R_{res})^2 = \frac{P_{tr}G_{tr}\sigma_t G_{res}\lambda^2 \Delta f T_{acc}}{4\pi^3 P_{res_{min}}} \quad (2)$$

Solving (2) for P_{resmin} we will get information about what power we will need for the receiver to find the target.

$$P_{res_{min}} = \frac{P_{tr}G_{tr}\sigma_t G_{res}\lambda^2 \Delta f T_{acc}}{4\pi^3 (R_{tr}R_{res})^2} \quad (3)$$

(3) shows the minimum required value of the receiver input power in an idealized space to achieve the maximum value of the radar range, with several factors affecting wave propagation eliminated.

Next of the potential capabilities is range resolution. The potential range resolution Δr of passive radar is calculated according to [3].

$$\Delta r = \frac{c}{2\Delta f_0}\left(\frac{r_\Sigma^2 - 2r_\Sigma cos\alpha_r cos\varepsilon_r + B^2}{(r_\Sigma - Bcos\alpha_r cos\varepsilon_r)^2}\right) = \\ = \Delta R\alpha \quad (4)$$

Where: c- speed of light, Δf_0 – width of the spectrum of the signal from the transmitter, $r_\Sigma = R_{tr} + R_{res}$ – the total distance between Tx, target and Rx, B – the length of base of bistatic radar, α_r – azimuth of the target, ε_r – elevation angle to the target, $\Delta R = \frac{c}{2\Delta f_0}$ – the resolution of a monostatic radar with same parameters of the signal, $\alpha = \frac{r_\Sigma^2 - 2r_\Sigma cos\alpha_r cos\varepsilon_r + B^2}{(r_\Sigma - Bcos\alpha_r cos\varepsilon_r)^2}$ – coefficient by which the resolution of the bistatic radar is reduced.

Analyzing (4) we can see that the resolution of the bistatic radar in the best-case approaches and becomes equal to the range resolution of the monostatic radar. The lowest resolution will be when the target lies on the base of a bistatic radar on the ground surface, in which case Δr tends to ∞.

The last is how much power in the target channel we will have from transmitter.

One of the major problems in a passive radar is to detect the weak signals from the targets against the strong signal coming directly from the transmitter. To estimate the impact of the direct channel on target detection, the equation given in [3] is used. Its calculation is given by the expression:

$$\frac{P_{direct}}{P_t} = 10lg\frac{4\pi(R_{tr}R_{res})^2}{B\sigma_t}\eta, [dB] \quad (5)$$

Where: η – coefficient of energy leaked from the side lobes of the directional antenna. P_{direct} – the power coming directly from the transmitter, P_t – power coming from the target.

III. Results and Discussion

It is necessary to clarify that the results obtained in this study do not apply only to Wi-Fi systems but are applicable to any bistatic radar with similar parameters such as frequency (respectively wavelength), bandwidth, etc.

The result of (3) for P_{resmin} of different values of $\sqrt{R_{tr}R_{res}}$, σt and T_{acc} are given in Fig. 2. Where for the P_{resmin} in [dBm] is used the equation:

$$P_{res_{min}} = 10\text{lg}\left(\frac{P_{res_{min}}}{10^{-3}}\right), [\text{dBm}] \quad (6)$$

The following values were used to obtain the graphs. In Bulgaria, the maximum power for Wi-Fi transmitter is limited to 2 W, therefore it is accepted P_{tr}=2W. The bistatic radar will use one isotropic antenna for transmitter and one directional antenna with a gain of 20 dBm therefore G_{tr}=1, G_{res}=100. The parameters of the signal are λ=0,125 m and Δf=20 MHz.

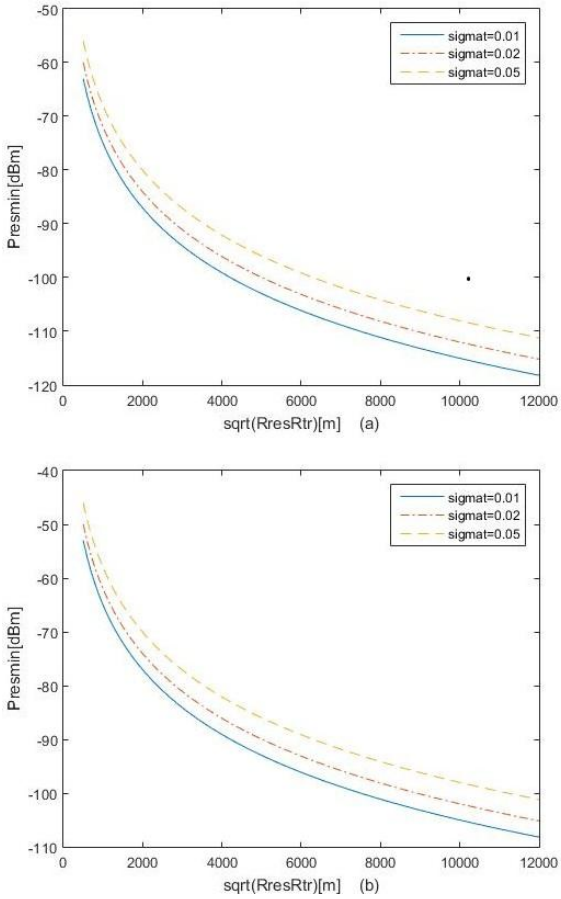

Fig. 2. Minimal power to detect target for T_{acc}=0.1 [s] a) and T_{acc}=1 [s] b)

The result in Fig. 2 show that it will be no easy to detect small, unmanned aircrafts with σ_t=0.01 m^2 with increasing bistatic operating distance. For distance $\sqrt{R_{tr}R_{res}} = 3000\ m$ and T_{acc}=0.1 s the value of P_{resmin}≈ -94 dBm which is not small, but it is possible because there are SDR systems that have more than (-115 dBm) for width of the spectrum of the signal 20 MHz.

According to the results in Fig.2 we can conclude that a much greater range of the bistatic radar than 3000 m can

be achieved. But the solution of (3) for idealized space, where the influence of the ground surface and other losses factors for on the radar observation is neglected. The real one will be less than the calculated one and can be established experimentally for different real area.

Results for Δr from (4) are given in Fig. 3 for different values of r_{Σ}, α_r and B for ε_r=0. The obtained results are for a target moving perpendicular to the middle of the base and located from 100 to 1m respectively from the base. Analyzing (4) and the results for Δr and the coefficient α, it can be concluded that it depends strongly on the position of the target relative to base (B). Its value increases when approaching the base and has the smallest value at the extension of the base.

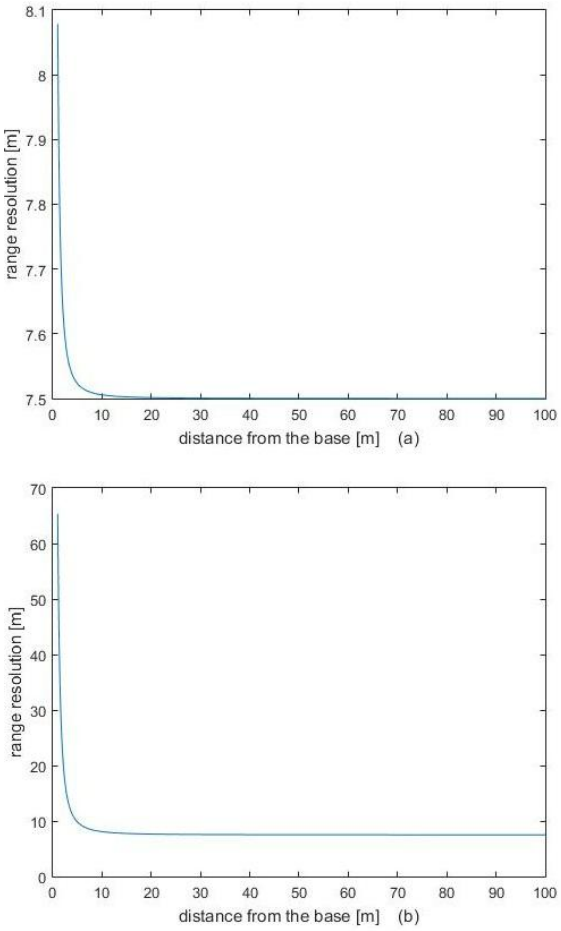

Fig. 3. Range resolution for B=100 [m] a) and B=1000 [m] b).

The potentially largest resolution of the bistatic radar is ΔR which for Δf=20 MHz is 7.5 meters.

In this case, it can be concluded that it is better from the point of view of obtaining better distance resolution to have a smaller distance between the receiver and the transmitter.

From (5) it can be concluded that the energy in the target channel is inversely proportional to the distance between the transmitter and the receiver and does not depend on the power radiated by the transmitter. Direct channel to target signal ratio is given in Fig. 4 for different values of B.

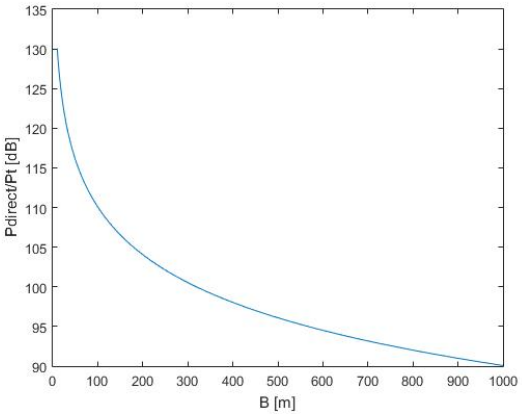

Fig. 4. Direct channel to target signal ratio.

The solution from (5) for η=0.01, σt=0.01 m2, $\sqrt{R_{tr}R_{res}} = 3000\ m.$, B=1000m, B=100m and B=10m is obtained approximately 90 dB, 110 dB and 130 dB respectively. This level of energy leaked from the side lobes is not small and usually various filters are used to suppress it on the target channel [3], [8]. In this case the Base need to be between 100 and 1000m so that it can be more reduced with filters direct channel to target signal ratio.

The conducted studies on the operating range, range resolution and direct channel to target signal ratio of a coherent bistatic pseudo-passive Wi-Fi radar show that it could fulfill the task of detecting the entry of a small unmanned aerial vehicle into the idealized protected area. However, for larger and different sized areas, more bistatic or multistatic radar systems will be needed, which will lead to an increase in the cost of the radar system for monitoring the area. For more accurate results, it is necessary to conduct a practical experiment with coherent bistatic Wi Fi radar and different sized targets in real areas of the area with different relief.

IV. Conclusions

In the paper results of theoretically potential capabilities on passive coherent Wi Fi radar are analysed. The result shows that coherent pseudo passive radar can be used in close distances for detecting unmanned small aerial vehicles for idealized area of protected object. The research conducted in this paper is the basis for beginning practical studies to detect the entry of unmanned aerial vehicles into a protected area.

Acknowledgments

This paper is supported by the National Scientific Program "Security and Defense", approved with Decision № 171/21.10.2021 of the Ministry Council of Republic of Bulgaria.

REFERENCES

[1] "Rule-Breaking Drone at Sofia Airport - More Dangerous Than Expected," Sofia:BNT news, Feb. 10, 2025 [Online] Available: https://bntnews.bg/news/rule-breaking-drone-at-sofia-airport-more-dangerous-than-expected-1326286news.html [Accessed Feb. 24, 2025]

[2] G. Georgiev, S. Parvanov and G Kozarev, "Techniques to protect key objects from unmanned aerial vehicles," Proceedings of University of Ruse - 2022, volume 61, book 3.2., pp. 207-216 (in Bulgarian), ISSN 1311-3321 (print), ISSN 2535-1028 (CD-ROM), ISSN 2603-4123 (on-line).

[3] A. V. Barhatov, V. I. Veremyev, E. N. Vorobiev, A. A. Konovalov, D. A. Kovalev, V. M. Kutuzov and V. N. Mihaylov, Passivnaya kogerentnaya radiolokatsiya. St. Petersburg: St. Petersburg State University of Economics Press, 2016, (in Russian), ISBN 978-5-7629-1921-0

[4] H. Griffits, "Bistatics: Introduction and historical background", NATO STO-EN-SET 133-01 [Online] Available: https://www.sto.nato.int/publications/STO%20Educational%20Notes/RTO-EN-SET-133/EN-SET-133-01.pdf [Accessed Feb. 23, 2025]

[5] P. A. Bakulev, A. V. Bruhansky, G. A. Volkova, G. G. Javadov and A. A. Sosnovsky, Sbornik zadach po kursu "Radiolokatsionnyye sistemy". M: Radiotekhnika, 2007, , (in Russian), ISBN 978-5-88070-146-9

[6] M. I. Skolnik "Radar Handbook" McGraw-Hill Professional; 2edition January 1, 1990

[7] T. Petio, L. Dudas and R. Seller, "DVB-T Based Passive Radar", Proceedings of the 24th IEEE International Conference Radioelektronika, 15-16 April 2014, Slovakia. [Online] Available: https://www.researchgate.net/profile/Tamas-Peto/publication/269301995_DVB-T_based_passive_radar/links/559ac23f08ae793d1382152e/DVB-T-based-passive-radar.pdf?__cf_chl_tk=Bhd1VMs.JA0GpaIjE01a1RJ4KGzn_rGm9eV.dfdowJE-1743190428-1.0.1.1-_IyipM2YVwKvgydYXX4PBPONWvWz2wyO4w3SplNWllw [Accessed Feb. 23, 2025]. https://doi.org/10.1109/Radioelek.2014.6828433

[8] W. Li, M. J. Bocus, C. Tang, S. Vishwakarma, R. J. Piechocki, K. Woodbridge, K. Chetty, "A Taxonomy of WiFi Sensing: CSI vs Passive WiFi Radar," 2020 IEEE Globecom Workshops, 7-11 Dec. 2020, Taiwan [Online] Available: https://discovery.ucl.ac.uk/id/eprint/10110406/1/Li(2020)_A%20Taxonomy%20of%20WiFi%20Sensing%20CSI%20vs%20Passive%20WiFi.pdf [Accessed Feb. 23, 2025] https://doi.org/10.1109/GCWkshps50303.2020.9367546

[9] W. Li, R. J. Piechocki, K. Woodbridge, C. Tang, K. Chetty, "Passive WiFi radar for human sensing using a stand-alone access point," IEEE Transactions on Geoscience and Remote Sensing, Vol. 59, Issue 3 , pp. 1986-1998,25 Feb 2021, [Online] Available: https://ieeexplore.ieee.org/document/9140020 [Accessed Feb. 23, 2025] https://doi.org/10.1109/TGRS.2020.3006387

[10] A. M. Ashleibta, A Taha, M. A. Khan, W. Taylor, A. Tahir, A. Zoha, Q. H. Abbasi and M.A. Imran, "5g-enabled contactless multi-user presence and activity detection for independent assisted living," Sci. Rep. 11:17590–17615, September 2021 [Online] Available: https://www.researchgate.net/publication/354329979_5G-enabled_contactless_multi-user_presence_and_activity_detection_for_independent_assisted_living [Accessed Feb. 23, 2025] http://dx.doi.org/10.1038/s41598-021-96689-7

[11] M. Nedelchev, "Analysis of the interaction of network functions in 4G and 5G networks through software defined radio,"In Proc. Yearbook of "Vasil Levski" National Military University, Part I, 2019, pp. 5-11 (in Bulgarian) ISSN 1312 6148

[12] M. Nedelchev , "An overview of spectrum sensing techniques," Yearbook of "Vasil Levski" National Military University 2019 Part I, pp 13-19 (in Bulgarian) ISSN 1312 6148

[13] Iv. Tsvetkova, R. Bogdanov, M. Nedelchev, "An approach for computer aided designation of frequency channels," Proceedings of University of Ruse - 2021, volume 60, book 3.2., pp. 163-170 (in Bulgarian), ISSN 1311-3321 (print), ISSN 2535-1028 (CD-ROM), ISSN 2603-4123 (on-line).

[14] T. Ignatova, M. Nedelchev, and M. Bedzheva, "Contemporary approaches for effective radio spectrum utilization," Proceedings of University of Ruse - 2022, volume 61, book 3.2., pp. 161-166 (in Bulgarian), ISSN 1311-3321 (print), ISSN 2535-1028 (CD-ROM), ISSN 2603-4123 (on-line).

[15] B. Bedzhev and D. Dimitrov, "A model of signal processing in software defined radio communication systems," Proceedings of the 2023 IEEE International Conference on Information Technologies (InfoTech-2023), 20-21 September 2023, Bulgaria.

[16] Directorate General "Civil Aviation Administration", "Geographical areas of BLS - interactive map," Directorate General "Civil Aviation Administration", Febr. 2025, [Online] Available: https://www.caa.bg/en/node/7062 [Accessed Feb. 23, 2025]

IV
LASER TECHNOLOGIES

Environment. Technology. Resources. Rezekne, Latvia
Proceedings of the 16th International Scientific and Practical Conference. 2025. Volume IV, 453-457

Potential Laser Processing Parameters for Obtaining Milk Repelling Surface on Stainless Steel (AISI 316L)

Arturs Abolins
Rezekne Academy of Riga Technical University
Rezekne, Latvija
artur.abolinsh@inbox.lv

***Abstract*—In the previous authors review article it was confirmed, that the use of hydrophobic surfaces in the food industry is becoming more frequent, and new technologies for creating such surfaces are being developed. Among many available and developing technologies, further authors research is linked with laser radiation made hydrophobic surface on food grade stainless steel (AISI 316L). Many articles were found where researchers proved efficiency of laser made hydrophobic surface interaction with water, but none found where such surface interact with milk. Since milk is a water suspension of different substances (mostly animal fat and proteins), it is much complex fluid, that requires special handling for its processing and preserving. It follows from this, that milk has slightly different physical properties, that can affect its interaction with different hydrophobic surfaces. As no data was found about such interaction, this article main aim is to check free accessible laser processing parameters for obtaining water hydrophobic surface on stainless steel and find out if these parameters are usable for further research, but with milk. First experiments already have shown promising results and may be a start point for searching of most suitable laser processing parameters, in order to get most efficient milk repelling surface on stainless steel.**

Keywords*— *Milk repelling surface, laser treatment, stainless steel, food industry.

I. Introduction

Use of hydrophobic surfaces in food industry is getting wiser due to its useful effects. As reviewed in authors previous article, nowadays most common way to obtain food safe hydrophobic surface is by applying coat of natural wax. This wax surface no only repels water and solutions, but also oil and emulsions. Also, high temperature durability, allows to use wax-based coatings for interaction with hot beverages (tea or coffee), that is why this method is mostly used in single use paper cups or dishes [1], [2]. Other methods are being researched and developed too, since wax coatings require continuous replacement and still can contaminate product that is in contact with it [3].

Passive repelling surfaces, where effect is obtained by base material itself, but with modified surface structure. No regular resurfacing is required, which cuts down maintenance costs and excludes risk of product contamination. These surface structure modifications commonly are obtained by chemical, electrochemical etching or mechanical treatment. These methods still require resources and special tools, as laser treatment gives more controllable and better-quality surfaces. Laser made water and oil repelling or attracting structures on different material structures are current day field of new research and discoveries. [4]

Since water and machine oil are most common fluids used in different machines, engines and transmissions, most researches are made in these fields. Other fluid substances, such as milk and alcohol, are left aside, since food industry are more keen on traditional processing technologies [5]. Willing to explore unknown grounds, author started own research on milk repelling stainless steel surface, that could be obtained by laser processing [6].

As milk is water suspension with animal fats and proteins, it is complex fluid that requires special handling in order to process and preserve it. Also, milk has different physical properties and it may influence on its interaction with hydrophobic surfaces, differing it from regular water. All this must be taken in account, to guarantee that milk remains safe and unchanged after interacting with repelling surface, no contamination is allowed. These requirements may be reason, why up to this day, no more detailed

Online ISSN 2256-070X
https://doi.org/10.17770/etr2025vol4.8386
© 2025 The Author(s). Published by RTU PRESS.
This is an open access article under the Creative Commons Attribution 4.0 International License.

researches were made to figure out if laser treated hydrophobic stainless-steel surface could even be used for milk processing or storage. [7]

First step in these research series, is checking if already known laser treatment parameters for obtaining hydrophobic surface on stainless steel are applicable for milk. Several articles were examined where researchers obtained hydrophobic surface on stainless steel using laser systems, that are similar to authors available ones. Multiple surface samples were made, that was visually tested for its hydrophobic properties not only with water, but also with milk "Table 1 - 2".

TABLE 1

Laser processing parameters used for obtaining hydrophobic surface on AISI 316L stainless steel (1)			
Parameter	***Reference***		
	[8]	[9]	[10]
Pulse power	3 W	0.22 mJ	10 W
Spot size	50 µm	30 µm	n/a
Scan distance	50 µm	50 µm	60 µm
Scan speed	600 mm/s	150 mm/s	500 mm/s
Pulse time	120 ns	40 ns	50 ns
Rate	50 kHz	25 kHz	20 kHz
Water contact angle	160°	169°	158°

TABLE 2

Laser processing parameters used for obtaining hydrophobic surface on AISI 316L stainless steel (2)			
Parameter	***Reference***		
	[11]	Test sample 1	Test sample 2
Pulse power	20 W	5 W	16 W
Spot size	21 µm	n/a	n/a
Scan distance	100 µm	10 µm	70 µm
Scan speed	150 mm/s	200 mm/s	10 mm/s
Pulse time	220 ns	30 ns	50 ns
Rate	25 kHz	80 kHz	200 kHz
Water contact angle	>150°	>150°	>150°

II. MATERIALS AND METHODS

For surface treatment, diode-pumped, q-switched fiber laser ROFIN PowerLine F20 Varia with auto focus platform was used. Large roll of 0.5 mm thick AISI 316L stainless steel was laser cut (Suntop ST-FC1390) in smaller 50x50 mm blank pieces. Test pieces remain their original surface finish, as there were no deep scratches and corrosion signs. Using Rofin laser system own software, required treatment parameters were specified in treatment area of 5x5 mm. Several test surface samples were made using not only data from articles "Table 1 - 2", but also making own discovered parameters (polished surface effect) "Fig. 1".

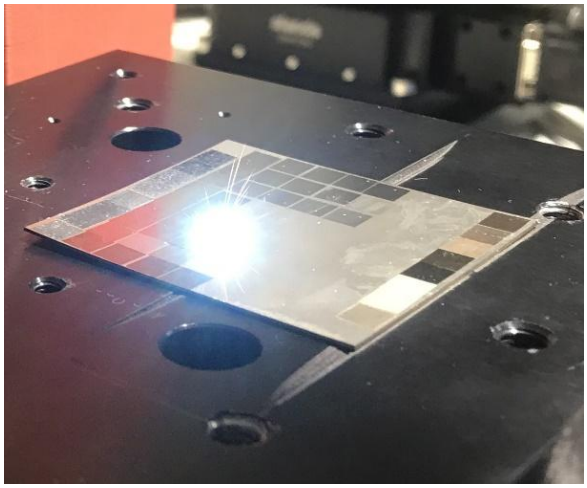

Fig. 1. Laser processing of AISI 316L stainless steel blank piece.

Each modified surface area was tested by placing 20 microlitre drinking water or 3,5% fat pasteurised cow milk droplet using precise laboratory pipette (Gilson-pipetman p100) and visually examined for hydrophobic effect "Fig. 2".

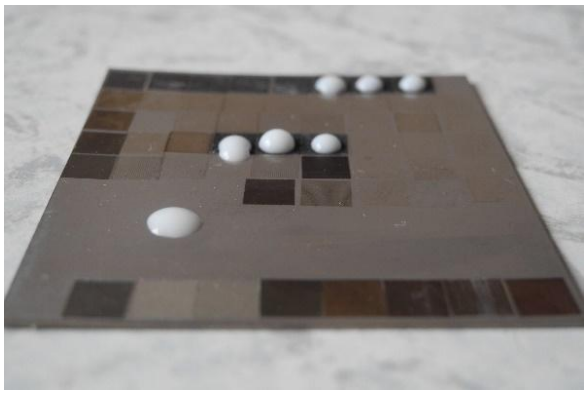

Fig. 2. Laser processing of AISI 316L stainless steel blank piece.

Droplet placing test was regularly repeated for each day for 14-day period in order, to check time-changing effects. After each visual examination, samples were cleaned with dish soap and water, and later dried in air, only first few times paper towel was used to soak moisture.

For gained surface analysis, 3d measuring laser microscope Olympus Lext OLS5000 was used. Microscope system provided not only high-quality colour picture, but also created 3d map of surface, where software calculated its roughness "Fig. 4".

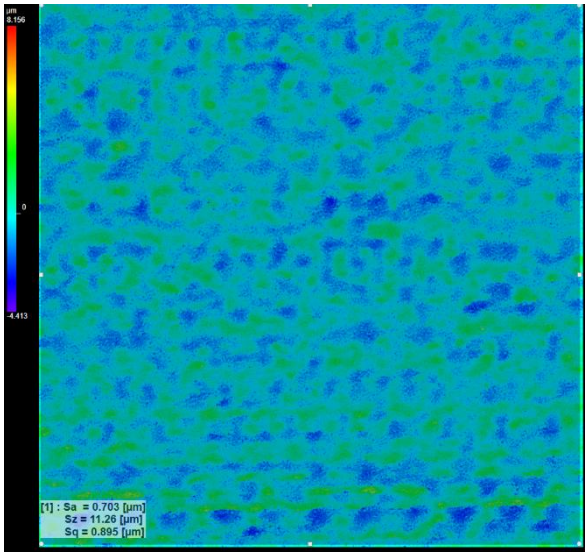

Fig. 3. Laser made hydrophobic surface "heat map" and software calculated roughness parameters.

III. Results and Discussion

In other author articles provided laser processing parameters have indeed proved, that they are usable for obtaining hydrophobic surfaces on stainless steel. All test surface samples have similar visual appearance as non-reflective dark surface with clearly visible rough structure. During first 2 days of water and milk droplet placing, test surfaces have shown super-hydrophilic effect (Contact angle <10°), attracting fluid and immediately spreading it across whole area. With each next day, hydrophilic effect started shift to more hydrophobic, and remaining unchanged after day 7 "Fig. 4" [12].

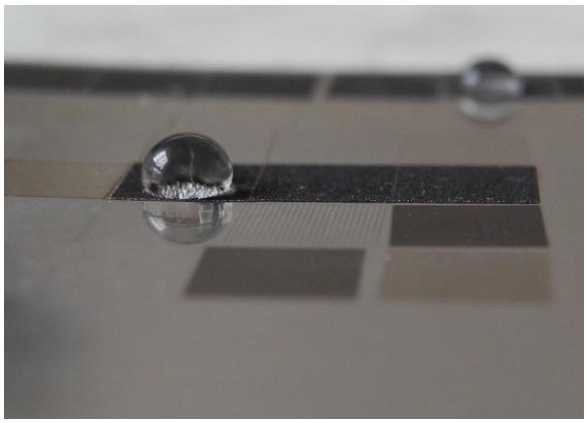

Fig. 4. Water droplet on laser made hydrophobic surface.

Unfortunately, other article mentioned laser processing parameters did not provide identical results, as there was no super-hydrophobic effect observed (Contact angle >150°). Test surfaces have shown better hydrophobic effect (Contact angle 90°-150°) with water droplets, meantime milk clearly performed less hydrophobic "Fig. 5". Such results could be explained by differences in laser systems and used material itself as well.

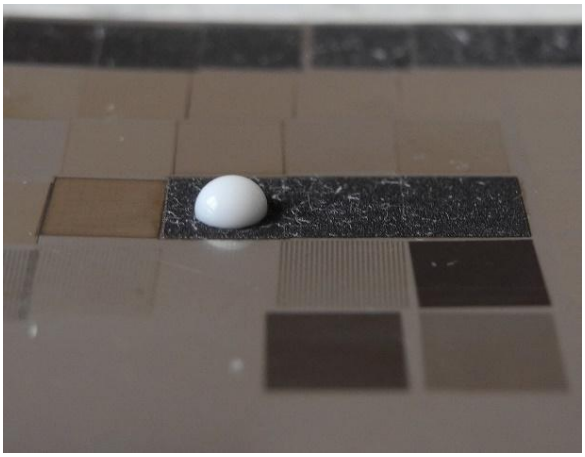

Fig. 5. Milk droplet on laser made hydrophobic surface.

Despite achieving more less desired result – laser made hydrophobic surface on stainless steel, further handling of test samples have shown certain disadvantages, that may exclude such surface structure use in food industry. Main problem appears, as test surface is wiped with any kind of organic material (paper, cloth or even fingertip) leaves residue stuck in hydrophobic structure, technically working as sandpaper "Fig. 6".

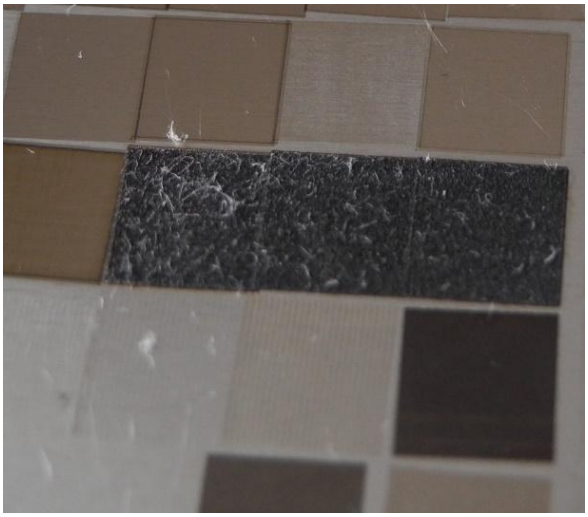

Fig. 6. Organic material residue on laser made hydrophobic surface.

Other unwanted effect was observed as milk droplet leaves stain areal even after it was washed away with sufficient amount of water, meaning that some milk solids tend to stuck inside hydrophobic structure itself "Fig. 7".

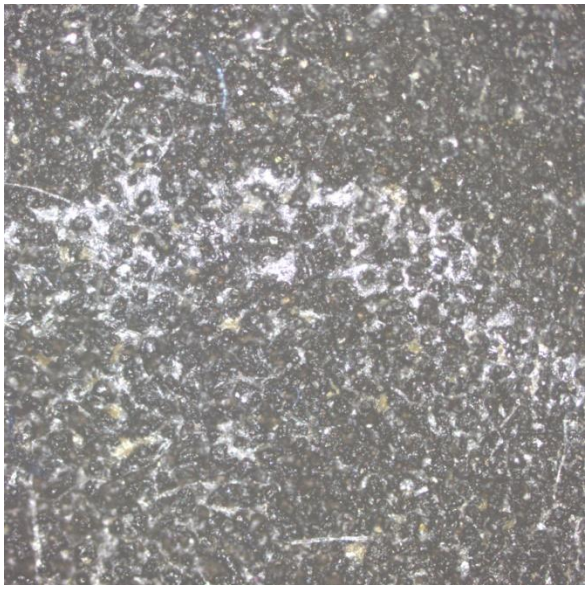

Fig. 7. Milk solids (white) in laser made hydrophobic surface structure.

Such effects are not acceptable from microbiological safety side, as any potential conditions that could contribute to pathogen microflora growth must be avoided [13], [14]. This behaviour could be explained by surface structure geometry, that resembles mountains with peaks, making surface abrasive "Fig.8" [15].

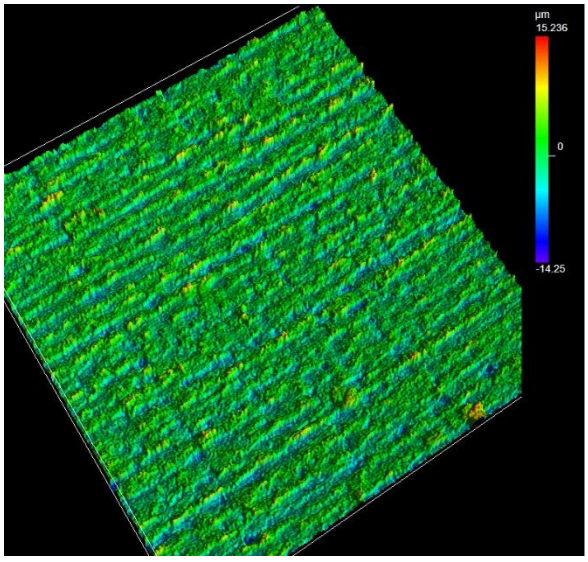

Fig. 8. Laser made hydrophobic surface structure under microscope.

Other laser processing parameters were tested out in order to create and test polished effect surface on stainless steel, as polished surfaces provide quite sufficient microbiological safety, as there are less chances for residue to attach. Test polish effect surfaces "Fig. 9" provide almost no hydrophobic properties, but shows better results, leaving none visible milk stains after surface washing with water [16].

Fig. 9. Comparison of laser "polished" (left) and untreated surface (right).

Direct comparison of laser made hydrophobic and laser "polished" surfaces clearly show their difference in roughness "Fig. 10":

- Laser "polished" surface
  - Sa – 1.073 µm
  - Sz – 21.448 µm
  - Sa – 1,382 µm
- Laser made hydrophobic surface
  - Sa – 8.416 µm
  - Sz – 106.774 µm
  - Sa – 10,664 µm

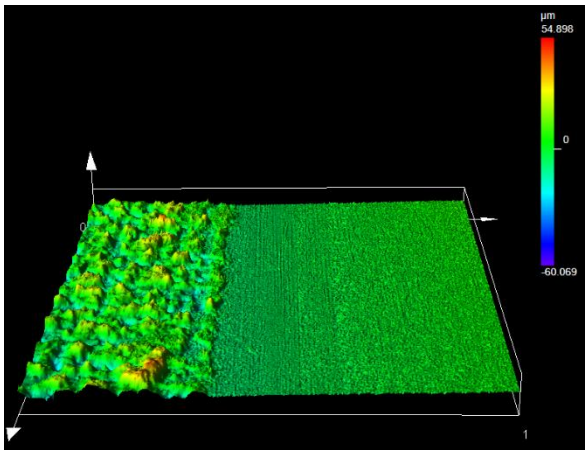

Fig. 10. Microscopic structure comparison of laser "polished" (right) and laser made hydrophobic surfaces (right).

IV. Conclusions

Theoretical use of laser made hydrophobic surfaces on stainless steel is very perspective for food industry, but as this research shows, there are many requirements that must be considered in order to provide microbiological safety. Worlds many decades long experience in food processing equipment production and use proves, that polished

surfaces provide sufficient safety and cleanliness. Nowadays laser processing can provide high quality surface polishing of stainless steel, so this way of technology should be considered for future development and use.

Also, there still may be possibility to achieve both smooth and hydrophobic surface on stainless steel, but by creating dimpled structure, that would be made and tested in future researches [17].

Finally, from personal experience, it is clear, that in laser processing it is quite problematical to achieve identical results if different laser systems are used. Each equipment unit requires its own corrections in processing parameters in order to achieve desired results. Processed material composition and its pre-processed surface finish also influences end result and may require some corrections in parameters.

REFERENCES

[1] I. Ostrov, I. Polishchuk, M. Shemesh, B. Pokroy, Superhydrophobic Wax Coatings for Prevention of Biofilm Establishment in Dairy Food. ACS Applied Bio Materials. 2019, 2, 11, pp. 4932–4940.

[2] M.Ruzi, N.Celik, M.s.Onses, Superhydrophobic coatings for food packaging applications: A review. Food Packaging and Shelf Life. Volume 32, June 2022, 100823.

[3] M.M. Frota, A.L.A.Mattos, K.W.E. Miranda, H.N. Cheng, A.Biswas, M.S.R. Bastos, Superhydrophobic systems in food science and technology: Concepts, trends, challenges, and technological innovations. Applied Food Research. Volume 2, Issue 2, December 2022, 100213.

[4] G.G.Vacas, F.Comino, O.R.Alabanda, Evaluation of the effectiveness and durability of commercial non-stick coatings. Journal of Food Engineering. Volume 370, June 2024, 111959.

[5] A.Pendurthi, S.Movafaghi, W.Wang, S.Shadman, A.P Yalin , A.K Kota, Fabrication of Nanostructured Omniphobic and Superomniphobic Surfaces with Inexpensive CO2 Laser Engraver. ACS Applied Materials & Interfaces. July 2017. 9(31).

[6] A.Abolins, LASER RADIATION MADE HYDROPHOBIC SURFACE ON STAINLESS STEEL FOR FOOD INDUSTRY, A REVIEW. Environment. Technology. Resources. Proceedings of the 15th International Scientific and Practical Conference. Volume 3. June 2024. pp. 358-362.

[7] C. Ramesh, R.C.Chandan, A.Kilara, N.P.Shah, Dairy Processing and Quality Assurance. Second edition. 2016.

[8] J.Zhu, J.Wu, One-step fabrication of an anti-corrosion superhydrophobic surface on stainless steel. Materials Research Express, Volume 7, Number 7, 076404.

[9] U.Trdan, M.Hočevar, P.Gregorčič, Transition from superhydrophilic to superhydrophobic state of laser textured stainless steel surface and its effect on corrosion resistance. Corrosion Science. Volume 123, July 2017, pp. 21-26.

[10] Z.Yang, X.Liu, Y.Tian, A contrastive investigation on anticorrosive performance of laser-induced super-hydrophobic and oil-infused slippery coatings. Progress in Organic Coatings. Volume 138, January 2020, 105313.

[11] V.D.Ta, A.Dunn, T.J. Wasley, J.Li, R.W. Kay, J.Stringer, P.J. Smith, E.Esenturk, C.Connaughton, J.D. Shephard, Laser textured superhydrophobic surfaces and their applications for homogeneous spot deposition. Applied Surface Science. Volume 365, March 2016, pp. 153-159.

[12] U.Trdan, M.Hočevar, P.Gregorčič, Transition from superhydrophilic to superhydrophobic state of laser textured stainless steel surface and its effect on corrosion resistance. Corrosion Science. Volume 123, July 2017, pp 21-26.

[13] E.Radu, A.Dima, E.M. Dobrota, A.M. Badea, D.Ø.Madsen, C.Dobrin, S.Stanciu, Global trends and research hotspots on HACCP and modern quality management systems in the food industry. Heliyon. Volume 9, Issue 7, July 2023, e18232.

[14] A.Amorim, V.L.Silva, P.J.A. Sobral, Food Processing: An overview on links between safety, security, supply chains, and NOVA classification. Cleaner and Circular Bioeconomy. Volume 5, August 2023, 100047.

[15] Y.Wan, X.Wang, C.Zhang, J. Xu, Durable self-cleaning hydrophobic surface of hollow cylindrical stainless steel with controllable adhesion prepared by nanosecond laser. Vacuum. Volume 205, November 2022, 111422.

[16] C.D.Giorgi, V.Furlan, A.G.Demir, E.Tallarita, G.Candiani, B.Previtali, Laser Micro-polishing of Stainless Steel for Antibacterial Surface Applications. Procedia CIRP. Volume 49, 2016., pp. 88-93.

[17] A.Peter, A.H.A. Lutey, S.Faas, L.Romoli, V.Onuseit, T.Graf, Direct laser interference patterning of stainless steel by ultrashort pulses for antibacterial surfaces. Optics & Laser Technology. Volume 123, March 2020, 105954Thomson ISI, EndNote 7. [CD-ROM]. Berkeley, Ca.: ISI ResearchSoft, 2003.

Environment. Technology. Resources. Rezekne, Latvia
Proceedings of the 16th International Scientific and Practical Conference. 2025. Volume IV, 459-465

Numerical Experiments for the Laser Marking by Oxidation, Melting and Evaporation of AISI 304 Stainless Steel Samples

Nikolay Angelov
Department of Mathematics, Informatics and Natural Sciences
Technical University of Gabrovo
Gabrovo, Bulgaria
angelov_np@abv.bg

Lyubomir Lazov
Rezekne Academy of Riga Technical University
Rezekne, Latvia
lyubomir.lazov@rta.lv

Erika Teirumnieka
Rezekne Academy of Riga Technical University
Rezekne, Latvia
erika.teirumnieka@rta.lv

Artis Teilans
Rezekne Academy of Riga Technical University
Rezekne, Latvia
artis.teilans@rta.lv

Arturs Abolinss
Rezekne Academy of Riga Technical University
Rezekne, Latvia
artur.abolinsh@inbox.lv

***Abstract*— Theoretical numerical calculations and numerical experiments with the Temperaturfeld3D software were carried out for laser marking with a fiber laser of AISI 304 stainless steel samples. The theoretical numerical experiments are based on the interrelation of the quantities affecting the technological process, obtained from the heat conduction equation and the heat balance equation. Temperaturfeld3D is a specialized software for laser technological processes, which are characterized by small zones of influence. Temperature fields were obtained for different values of power density and speed. Graphs of the dependences of the critical power densities of melting and evaporation on the speed were constructed using both methods. Preliminary working intervals of the power density were determined for the studied speeds for laser marking by oxidation, melting and evaporation. The results obtained using both methods were compared and analysed in view of the capabilities and advantages of each of these methods.**

Keywords*— Numerical calculation, numerical experiments, laser marking, Temperaturfeld3D, AISI 304 stainless steel, power density, speed.

I. INTRODUCTION

Laser marking is a widely used technological process for creating high-quality markings on the surfaces of industrial products made of various materials, including AISI 304 stainless steel [1] – [5]. In recent decades, it has been continuously expanding its positions and gradually displacing other marking methods due to its advantages: non-contact technology, high quality, high precision, flexibility, high process efficiency, environmentally friendly process.

A number of factors influence the quality of marking [6] – [9]. For each specific case, different materials, laser sources and marking methods should be investigated to optimize the technological process. Numerical or real experiments can be performed, as well as a combination of both methods of investigation.

Some authors have investigated the laser marking process of steel through numerical experiments:

The article [10] focuses on enhancing the laser marking process for creating submillimeter-sized 2D codes on 50CrVA stainless steel. Through numerical simulations, the study examines temperature distributions during laser marking, identifying that temperature variations in the depth direction and oxidation levels in the irradiated area significantly influence the contrast of the 2D codes. The research determines optimal laser parameters, including an average laser power threshold of 3.0 W and a frequency of 100 kHz, for producing identifiable submillimeter 2D codes, aligning well with simulation results. Additionally, increasing the number of laser pulses enhances both the contrast and uniformity of the Data Matrix code modules. To improve corrosion resistance, the study finds that applying a transparent polyurethane coating effectively protects the marked codes. Finally, the research successfully demonstrates the marking of submillimeter 2D codes on cylindrical tools with a diameter of 1 mm. Overall,

Online ISSN 2256-070X
https://doi.org/10.17770/etr2025vol4.8393
© 2025 The Author(s). Published by RTU PRESS.
This is an open access article under the Creative Commons Attribution 4.0 International License.

the study provides a theoretical foundation and experimental approach for identifying small parts through high-quality, corrosion-resistant submillimeter laser-marked codes.

The article [11] presents the results of several numerical experiments aimed at enhancing laser marking processes on tool steel and electronic components. Utilizing specialized software developed in MATLAB, the study simulates laser marking using CuBr and Nd:YAG lasers, focusing on three different pulse durations. The numerical calculations are based on parameters derived from real-world experiments. While the article's does not detail specific findings, it emphasizes the use of simulation models to optimize laser marking techniques.

In the paper [12], the authors present the development of a proof-of-concept software designed to simulate the geometry of engraved surfaces and estimate the depth and width of engraved grooves based on associated laser parameters. The study utilizes COMSOL Multiphysics to model a moving laser beam as a heat source traversing materials such as steel, aluminum, copper, and brass. By simulating the interaction between the laser beam, operating in TEM01 mode, and these materials, the research determines the resulting temperature distributions. A key aspect of the simulation involves using COMSOL's moving mesh mode to represent material removal, which occurs when the material's temperature surpasses its vaporization point due to high-intensity laser exposure. The simulation results were validated through experimental tests, demonstrating the model's effectiveness in predicting engraving outcomes. This approach offers potential benefits in reducing setup time and material costs for laser engraving processes, especially when working with new or expensive materials.

In article [13], the authors use a mathematical model of the technological process of marking on the surface of metal products using a pulsed laser. Using the model, they obtain the optimal technological parameters for laser marking of symbols on the surface of steel products, taking into account the physical properties of the marked material. The resulting technological modes are suitable for automotive, aircraft, railway transport and for marking serial products in mechanical engineering.

The article [14] presents the development of a three-dimensional finite element method (FEM) simulation model for the nanosecond pulsed laser engraving process. The primary objective of this model is to predict the final marking area geometry of the workpiece and optimize the engraving process.

From the literature review, it can be concluded that the process of laser marking of steels has not been studied in sufficient volume, as is also true for AISI 304 steel, one of the most commonly used stainless steels in industry and households.

The aim of the publication is to investigate the technological process of laser marking with a fiber laser on AISI 304 stainless steel through theoretical numerical calculations and numerical experiments using the Temperaturfeld3D software, obtaining preliminary operating ranges of power density for different speeds using both methods and comparing the capabilities of these methods for the studied process.

II. MATERIAL AND METHODS

A. Material

AISI 304 is distinguished by its excellent corrosion resistance, very good weldability and very good mechanical properties. These are the reasons that make it one of the most widely used grades of stainless steel. Its applications are in the automotive industry, the food industry, the medical and pharmaceutical industry, construction and architecture, the chemical and petrochemical industries, and the aerospace industry. The chemical composition of the steel is presented in Table 1. It is a low-carbon steel with alloying elements chromium and nickel. Table 2 gives some basic parameters of the steel. It has low values of the coefficients of thermal conductivity and thermal diffusivity.

TABLE 1 CHEMICAL COMPOSITION OF AISI STAINLESS STEEL

Element	**Content, %**	**Element**	**Content, %**
C	< 0.08	Si	< 1.0
Cr	18.0 – 20.0	P	< 0.045
Ni	8.0 – 10.5	S	< 0.03
Mn	< 2.0	Fe	Balance

TABLE 2 BASIC PARAMETERS OF AISI 304 STAINLESS STEEL

Parameter	**Value**
Absorption capacity A	0.40
Coefficient of thermal conductivity k, W/(kg.K)	16.2
Density ρ, kg/m^3	7850
Specific heat capacity c, J/(kg.K)	500
Coefficient of thermal diffusivity a, m^2/s	4.72×10^{-6}
Melting point temperature T_m, K	1700
Vaporization temperature T_v, K	2950
Latent heat of melting L_m, kJ/kg	266
Latent heat of evaporation L_v, kJ/kg	6500

B. Laser system

Numerical experiments were performed for a laser technology system with a fiber laser. It has very good repeatability, very high positioning accuracy and the ability to move the laser beam in a very wide range. Fiber laser has radiation with a wavelength in the infrared region. It has extremely high beam quality and high efficiency. Table 3 gives the main parameters of the laser system.

TABLE 3 SOME PARAMETERS OF LASER SYSTEM FOR MARKING

Parameter	**Value**
Wavelength λ, nm	1064

Power *P*, W	20
Diameter of work spot *d*, μm	30
Efficiency, %	40
Speed, mm/s	< 6000
Positioning accuracy, μm	2.5

C. Software

To perform the numerical experiments, the Temperaturfeld3D program is used. It is the working environment for calculating temperature fields with a wide range of input parameters and options for analyzing and storing the calculated results. After selecting the dynamic model (suitable for the laser marking process), the main window opens (see Fig. 1). From it, the user has access to the three main sections of the software – input/output, model parameters, calculation.

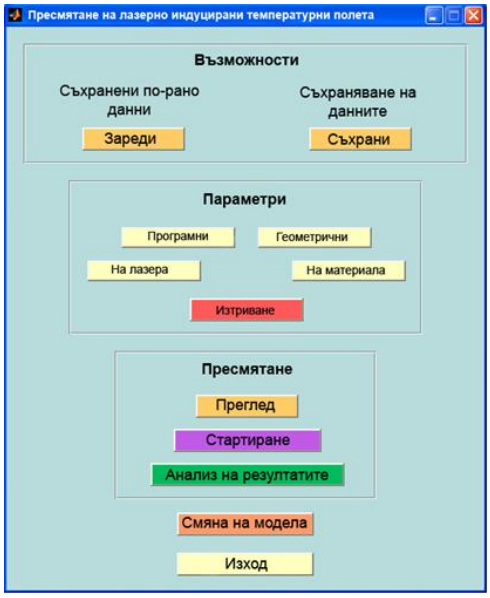

Fig. 1. Main window of the Temperaturfeld3D program.

Input data includes: program parameters, geometric parameters, laser parameters, and material parameters.

After starting and performing the calculations to obtain the temperature fields in the impact zone, the output results are obtained, which include: maximum temperature profile, temperature profile of the material at a given time, temperature dependence on time, temperature change in the depth of the material, animation of the entire process, approximation of the results.

D. Metods

The determination of preliminary operating ranges of power density for different speeds for the laser marking process can be performed both by numerical calculations with expressions giving the relationship between the quantities affecting the process and by numerical experiments with specialized software for studying the process. The obtained results are compared and thus it can be determined which of the two methods is more suitable for these studies.

- Theoretical numerical calculations

Power density and speed are the main parameters affecting the laser marking process of steel. From the heat conduction equation and the heat balance equation, a relationship can be obtained between power density, speed and temperature in the impact zone.

For the critical power density of melting, the formula is obtained

$$q_{scm} = \frac{(1+s)k(T_m - T_0)}{2A}\sqrt{\frac{\pi v}{ad}} \qquad (1)$$

where k is the thermal conductivity coefficient, a – thermal diffusivity coefficient, A – absorption capacity, d – diameter of the working spot, T_0 – initial temperature, $s = \frac{L_m}{c(T_m - T_0)}$ (2) is a parameter, L_m – specific heat of melting, c – specific heat capacity.

The formula for the critical power density of evaporation is

$$q_{scv} = \frac{(1+s')k(T_v - T_0)}{2A}\sqrt{\frac{\pi v}{ad}} \qquad (3)$$

where $s' = \frac{L_m + L_v}{c(T_m - T_0)}$ (4) is a parameter, L_v – specific heat of evaporation.

The determination of the intervals of change of the power density for oxidation, melting and evaporation occurs in three stages:

- Calculation of the critical power density of melting q_{scm} and evaporation q_{scv}.

The values of the critical power densities of melting for different speeds are determined by formulas (1) and (2), with the speed changing in a interval from 10 mm/s to 100 mm/s. The values of the critical evaporation power densities for different speeds are determined by formulas (3) and (4). Graphs of the dependences of the critical power density of melting on speed and the critical power density of evaporation on speed are drawn.

2) Determination of the maximum power density q_{smax} for the laser used.

The maximum power density q_{smax} is calculated using the formula

$$q_{smax} = \frac{4P_{max}}{\pi d^2} \qquad (5)$$

where P_{max} is the maximum power of the laser.

3) Determination of the preliminary power density intervals for oxidation, melting and evaporation for the selected laser and material

The results are presented in a suitable table. The first column shows different speeds, the second column contains the power density intervals for oxidation, the third column for melting, the fourth for evaporation. The third and fourth columns show the power density intervals. These intervals are clearly shown in the graphical images. The oxidation zone is below the graph of the dependence of the critical melting power density on the speed. The melting zone is between the two graphs. The evaporation

zone is above the graph of the dependence of the critical power density of evaporation on the velocity and is limited from above by the maximum laser power density.

- Numerical experiments with the program Temperaturfeld3D

In order to obtain the preliminary operating intervals of power density for different speeds for laser marking by oxidation, melting and evaporation, a series of numerical experiments were carried out with the Temperaturfeld3D program. The difference in this case compared to the calculations using the above formulas is the consideration of the temperature change during the process of some input parameters such as absorption capacity, coefficient of thermal conductivity and density of the material.

Numerical experiments are performed in several stages:

- Obtaining the temperature dependence of power density for different speeds

Through numerical experiments, the temperature fields in the impact zone are obtained for different power densities and speeds (a total of 80 calculations with the Temperatutfeld3d program). From each temperature field, the maximum temperature of the material surface is determined. Graphs of the temperature dependence on the power density are drawn for different speeds. From these, the critical power densities of melting and evaporation are determined for each of the studied speeds;

- Drawing graphs of the dependence of the critical power density of melting and evaporation on the speed;
- Determination of preliminary working intervals for the laser marking process by oxidation, melting and evaporation.

- Comparing the results obtained by the two methods

On one coordinate system, the graphs of the dependence of the critical power density of melting on the speed, obtained from the results of numerical calculations and numerical experiments, are drawn. On another coordinate system, the graphs of the dependence of the critical power density of evaporation on the speed, obtained from the results of numerical calculations and numerical experiments, are drawn. The results obtained by the two methods are analysed and compared.

III. Results and Discussion

Numerical calculations and numerical experiments were carried out according to the presented methodology.

A. Theoretical numerical calculations

Numerical calculations were performed to determine the critical power density of melting and evaporation for different speeds according to formulas (1) – (4). The speed varied in the range from 10 mm/s to 100 mm/s in increments of 10 mm/s. From the results obtained, graphs of the dependences of the critical power densities of melting and evaporationon speeds were constructed (see Fig. 2). The following conclusions can be drawn from them:

- A nonlinear dependence of the two critical power densities on the speed is obtained, as the critical power densities increase with increasing speed;
- The critical power density of melting varies from 0.058×10^{10} W/m^2 to 0.185×10^{10} W/m^2 for the entire studied speed interval. The critical power density of evaporation varies from 0.690×10^{10} W/m^2 to 1.544×10^{10} W/m^2 for the entire studied speed interval;
- Three zones are observed:

zone (1) – corresponds to oxidation of the material;
zone (2) – corresponds to melting of the material;
zone (3) – corresponds to evaporation of the material.

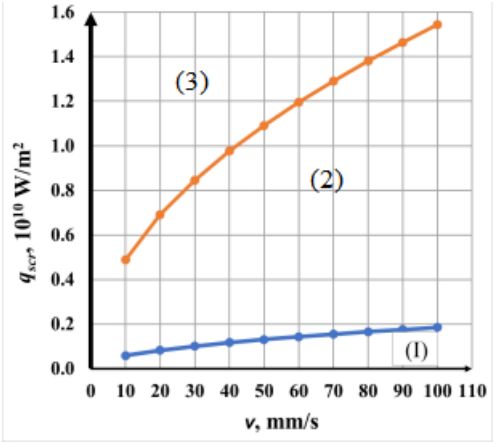

Fig. 2. Graphs of the dependence of the critical power density of melting (blue graph) and evaporation (orange graph) on the speed.

For the maximum power density according to formula (5) it was obtained $P_{max} = 2.831\times10^{10}$ W/m^2.

Based on the obtained calculation results, preliminary operating intervals of power density for different speeds for laser marking by oxidation, melting and evaporation were obtained (see Table 4).

TABLE 4 PRELIMINARY OPERATING INTERVALS OF POWER DENSITY FOR DIFFERENT SPEEDS FOR THE LASER MARKING PROCESS

v, mm/s	**q_s, W/m^2**		
	Oxidation	*Melting*	*Evaporation*
10	$< 0.058\times10^{10}$	0.058×10^{10} – 0.488×10^{10}	0.488×10^{10} – 2.831×10^{10}
20	$< 0.083\times10^{10}$	0.083×10^{10} – 0.690×10^{10}	0.690×10^{10} – 2.831×10^{10}
30	$< 0.101\times10^{10}$	0.101×10^{10} – 0.846×10^{10}	0.846×10^{10} – 2.831×10^{10}
40	$< 0.117\times10^{10}$	0.117×10^{10} – 0.976×10^{10}	0.976×10^{10} – 2.831×10^{10}
50	$< 0.131\times10^{10}$	0.131×10^{10} – 1.092×10^{10}	1.092×10^{10} – 2.831×10^{10}
60	$< 0.143\times10^{10}$	0.143×10^{10} – 1.196×10^{10}	1.196×10^{10} – 2.831×10^{10}

v, mm/s	q_s, W/m²		
	Oxidation	*Melting*	*Evaporation*
70	$< 0.155\times10^{10}$	$0.155\times10^{10} – 1.292\times10^{10}$	$1.292\times10^{10} – 2.831\times10^{10}$
80	$< 0.165\times10^{10}$	$0.165\times10^{10} – 1.381\times10^{10}$	$1.381\times10^{10} – 2.831\times10^{10}$
90	$< 0.175\times10^{10}$	$0.175\times10^{10} – 1.465\times10^{10}$	$1.465\times10^{10} – 2.831\times10^{10}$
100	$< 0.185\times10^{10}$	$0.185\times10^{10} – 1.544\times10^{10}$	$1.544\times10^{10} – 2.831\times10^{10}$

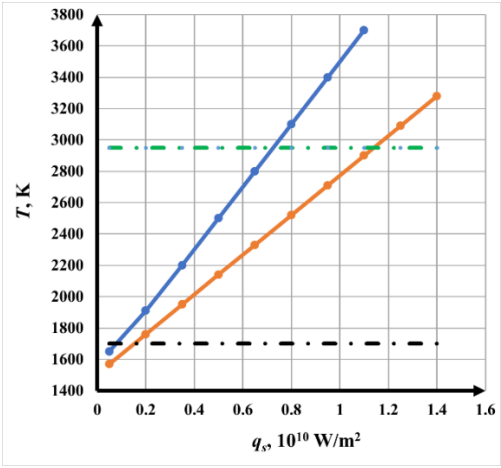

Fig. 3. Graphs of the dependence of temperature on power density for speeds: 30 mm/s – blue graph and 70 mm/s – orange graph.

B. -Numerical experiments with the program Temperaturfeld3D

A series of numerical experiments were performed to study the process of laser marking of AISI 304 stainless steel samples with a fiber laser. Temperature fields in the impact zone were obtained for different power densities and different speeds. The speed varied in the interval from 10 mm/s to 100 mm/s with a step of 10 mm/s. The temperature dependences on the power density for different speeds were obtained. The Figure 3 shows two graphs of the temperature dependence on the power density for speeds: 30 mm/s – blue graph and 70 mm/s – orange graph. From the constructed graphs, the critical power density of melting for speeds 30 mm/s and 70 mm/s is determined from the intersection points of the black line with the blue and orange lines. From the intersection points of the green line with the blue and orange lines, the critical power densities of evaporation for these speeds are obtained. In a similar manner, the critical power densities of melting and evaporation are determined for the remaining studied velocities.

At the next stage, graphs of the dependence of the critical power density of melting and evaporationon the speed were drawn (see Fig. 4). From the analysis of the graphs it follows:

- With increasing speed, the critical power densities increase, as the dependence is nonlinear;
- The critical melting power density changes from 0.056×10^{10} W/m² to 0.174×10^{10} W/m² for the entire studied speed interval. The critical power density of evaporation changes from 0.468×10^{10} W/m² to 1.451×10^{10} W/m² for the entire studied speed interval;
- The same three zones are observed for the laser marking process as in the results of numerical calculations.

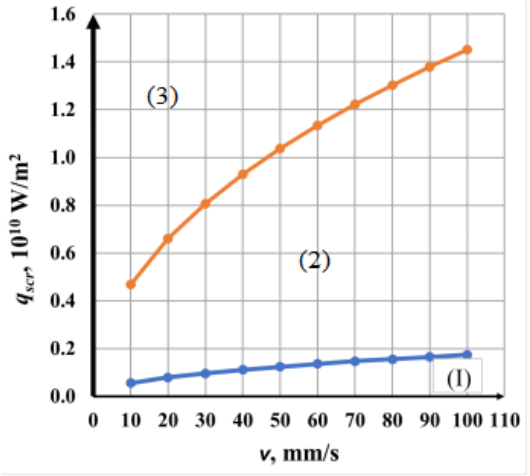

Fig. 4. Graphs of the dependence of the critical power density of melting (blue graph) and evaporation (orange graph) on the speed

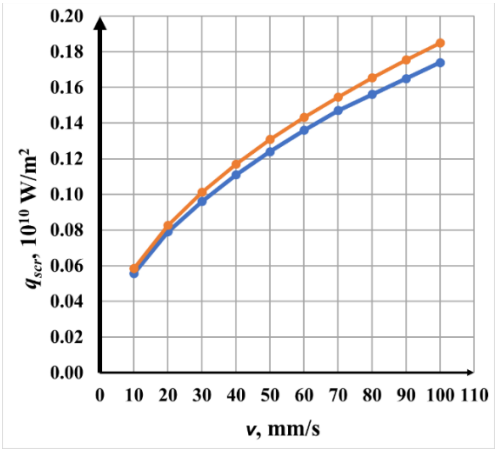

Fig. 5. Graphs of the dependence of the critical melting power density on the speed: blue graph – from numerical experiments and orange graph – from numerical calculations

The obtained preliminary operating intervals of power density for different speeds for laser marking by oxidation, melting and evaporation are presented in Table 5.

TABLE 5 PRELIMINARY OPERATING POWER DENSITY INTERVALS FOR DIFFERENT SPEEDS FOR THE LASER MARKING PROCESS

v, mm/s	q_s, W/m^2		
	Oxidation	*Melting*	*Evaporation*
10	$< 0.056\times10^{10}$	0.056×10^{10} – 0.468×10^{10}	0.468×10^{10} – 2.831×10^{10}
20	$< 0.079\times10^{10}$	0.079×10^{10} – 0.660×10^{10}	0.660×10^{10} – 2.831×10^{10}
30	$< 0.096\times10^{10}$	0.096×10^{10} – 0.807×10^{10}	0.807×10^{10} – 2.831×10^{10}
40	$< 0.111\times10^{10}$	0.111×10^{10} – 0.930×10^{10}	0.930×10^{10} – 2.831×10^{10}
50	$< 0.124\times10^{10}$	0.124×10^{10} – 1.037×10^{10}	1.037×10^{10} – 2.831×10^{10}
60	$< 0.136\times10^{10}$	0.136×10^{10} – 1.134×10^{10}	1.134×10^{10} – 2.831×10^{10}
70	$< 0.147\times10^{10}$	0.147×10^{10} – 1.222×10^{10}	1.222×10^{10} – 2.831×10^{10}
80	$< 0.156\times10^{10}$	0.156×10^{10} – 1.303×10^{10}	1.303×10^{10} – 2.831×10^{10}
90	$< 0.165\times10^{10}$	0.165×10^{10} – 1.380×10^{10}	1.380×10^{10} – 2.831×10^{10}
100	$< 0.174\times10^{10}$	0.174×10^{10} – 1.451×10^{10}	1.451×10^{10} – 2.831×10^{10}

C. Comparing the results obtained by the two methods

According to the methodology, graphs of the dependence of the critical power density of melting on the speed (see Fig. 5) are drawn, obtained from the results of theoretical numerical calculations (orange graph) and numerical experiments with the Temperaturfeld3D program (blue graph). It can be seen that for the numerical calculations the values of the critical power density are about 4.0 – 6.0 % higher than those from the numerical experiments. The graphs of the dependence of the critical power density of evaporation on the speed are presented in Fig. 6. Again, the values of the critical power density of evaporation from the numerical calculations are higher than those from the numerical experiments, differing by about 4.2 – 6.0 %. The explanation is that in the Temperaturfeld3D program the temperature dependence of some parameters is set. For example, as is known, with increasing temperature the absorption capacity of metals and alloys increases, in particular the investigated AISI 304 stainless steel.

It should be noted that achieving the results with numerical experiments using the Temperaturfeld3D program requires a lot of time. A large number of numerical experiments are carried out (at least 80 experiments as noted in the methodology) and the obtained temperature fields are analyzed, a large number of graphs are drawn and analyzed until the preliminary working intervals of the power density for laser marking by oxidation, melting and evaporation are obtained. To obtain the same preliminary working intervals using theoretical numerical calculations, a small number of calculations are made according to the formulas from the theory. These calculations can be automated using a calculator created, for example, in the Excel program. Two graphs are drawn and analyzed in one coordinate system. Therefore, in this case, the time to obtain the final results is several times less.

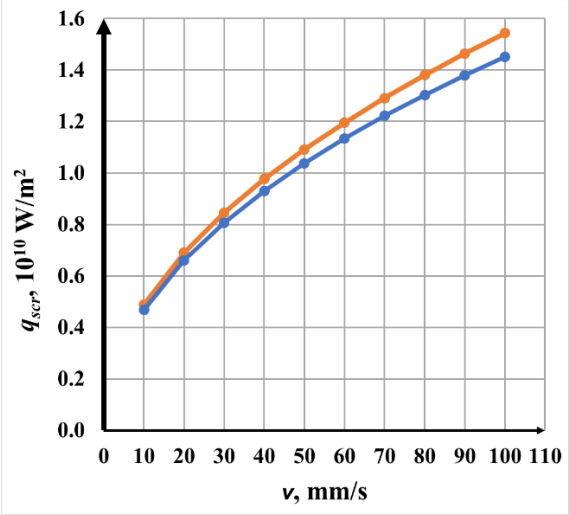

Fig. 6. Graphs of the dependence of the critical power density of evaporation on the speed: blue graph – from numerical experiments and orange graph – from numerical calculations

The accuracy of the results obtained with the Temperaturfeld3D program is slightly higher (4.0 – 6.0 % difference in the obtained results). Both proposed methods have a place in the research for obtaining the preliminary working intervals of the power density for different speeds, but the method with numerical calculations is more direct and saves a lot of time for the researchers.

IV. CONCLUSIONS

This study investigated the laser marking of AISI 304 stainless steel through oxidation, melting, and evaporation using theoretical numerical calculations and numerical experiments conducted with Temperaturfeld3D software. By analysing the interrelation of key process parameters derived from the heat conduction and heat balance equations, the study provided insights into the thermal behaviour of the material under different laser power densities and scanning speeds.

The following results were achieved:

- temperature fields were obtained for different power densities and speeds;
- graphs of the dependence of the critical power density of melting and evaporation on the speed were constructed by both methods;
- preliminary working intervals of the power density were determined for the studied speeds for laser marking by oxidation, melting and evaporation by both research methods.

The comparison between theoretical calculations and numerical simulations highlighted the strengths and limitations of each method, demonstrating their complementary roles in predicting process outcomes.

Overall, this study demonstrates the effectiveness of using FEM-based simulation models to predict and enhance the laser marking process. The results contribute to a deeper understanding of laser-material interactions in stainless steel marking processes, providing valuable guidelines for optimizing laser parameters. Future research could focus on experimental validation of the findings and further refinement of numerical models to improve accuracy and applicability in industrial settings.

REFERENCES

[1] B. Gu, Review: 40 years of laser-marking industrial applications, Lasers and Applications in Science and Engineering, 2006, San Jose, California, United States, Proceedings, Volume 6106, Photon Processing in Microelectronics and Photonics V, 610601, 2006, https://doi.org/10.1117/12.640838

[2] L. Morawiski, S. Swillo and A. Kosanda, Application of Laser Barcode Technology to Sheet Metal Parts Identification, Scientific paper of Silesian University of Technology, Organization and Management Series, No. 162, 2022, http://dx.doi.org/10.29119/1641-3466.2022.162.27

[3] T. Kyrychok, O. Nazarenko and O. Korotenko, Eds., Determining the influence of technological parameters of the laser processing of plastic cards edges on improving their wear resistance, Eastern-European Journal of Enterprise Technologies, Vol. 6, No. 1 (132), 2024, DOI: 10.15587/1729-4061.2024.317448

[4] C. Patel, A. Patel and R. Patel, A Review on Laser Marking Process for Different Materials, IJSRD - International Journal for Scientific Research & Development| Vol. 5, Issue 1, 2017,| ISSN (online): 2321-0613

[5] R. Hamid, A. Marjan, H. Heikki and S. Antti, Color Laser Marking: Repeatability, Stability and Resistance Against Mechanical, Chemical and Environmental Effects, IEEE Access, 2020, DOI: 10.1109/ACCESS.2020.3040744

[6] A. Schkutowa and T. Frick, Laser color marking of stainless steel – Investigation of the fluence dependent and thermal mechanisms in generating laser induced surface modifications, 13th CIRP Conference on Photonic Technologies, 15-19 September 2024, Fürth, Germany, Procedia CIRP 124, 661–664, 2024

[7] E. Amara and H. Fadhela, Experimental investigations on fiber laser color marking of steels, Applied Surface Science, 351, May 2015, DOI:10.1016/j.apsusc.2015.05.095

[8] L. Sobotova and M. Badida, Laser marking as environment technology, Open Engineering, ol. 7, No. 1, pp. 303-316, 2017, https://doi.org/10.1515/eng-2017-0030

[9] Y. Geng, J. Li and C. Lu, Experimental and numerical investigations on color stability of laser color marking, Optics and Lasers in Engineering, Volume 159, 107225, December 2022, https://doi.org/10.1016/j.optlaseng.2022.107225

[10] X. Li, L. Yang and B. Changz, Eds., Simulation and process optimization for laser marking of submillimetre rasterizing 2D code on stainless steel, International Journal of Modern Physics B, Vol. 34, No. 28, 2050266, pp. 1-18, 2020, DOI: 10.1142/S0217979220502665

[11] L. Lazov and N. Angelov Petrov, Optimization of laser marking with the help of simulation models, Turkish Journal of Physics, 37(1):145-150, January 2013, DOI: 10.3906/fiz-1202-4

[12] H. Karbasi, COMSOL Assisted Simulation of Laser Engraving, Engineering, Materials Science, Physics , Proceedings of the COMSOL Conference 2010 Boston, pp. 1-10, 2010

[13] O. Ganzulenko and A. Petkova, Simulation and approbation of the marking laser process on metal materials, IOP Publishing, Journal of Physics: Conference Series 1753, 012016, 2021, DOI:10.1088/1742-6596/1753/1/012016

[14] E. Nikolidakis and A. Antoniadis, FEM modeling simulation of laser engraving, The International Journal of Advanced Manufacturing Technology, 105:3489–3498, 2019, https://doi.org/10.1007/s00170-019-04603-3

Environment. Technology. Resources. Rezekne, Latvia
Proceedings of the 16th International Scientific and Practical Conference. 2025. Volume IV, 467-474

A New Approach to Developing Gamma-ray Laser

Yordan Katsarov
Department of Aviation Equipment and Technologies
Georgi Benkovski Bulgarian Air Force Academy
Dolna Mitropoliya, Bulgaria
yordankatsarov@gmail.com

***Abstract*—A laser can greatly increase its power if the radiation comes from the atomic nucleus. The reason is that gamma rays, which are in the high-energy electromagnetic spectrum, come by their nature from the transition between excited to lower nuclear levels, as opposed to electromagnetic waves produced by atoms. The subject of this work is the development of a gamma laser (Graser). The first step is to excite the nuclei of certain isotopes to a higher-energy nuclear state. The excitation method used here is bombarding the nuclei with neutrons. Some isomeric nuclei, known as metastable, can remain excited for a relatively long time, which is what one is looking for. When an external source stimulates these excited nuclei, they can release their stored energy via gamma rays. The emitted gamma rays are modified to produce a coherent laser beam. This work traces the century-long achievement in the field of laser creation after numerous successful solutions and passing through the recoilless Mössbauer emission from the solid crystal lattice. However, scientists have not been able to create a Grasser due to controversial conditions. This article presents a new method, somewhat unconventional, designed to solve the so-called "Graser dilemma". This can be done by shifting the crystal lattice during the neutron bombarding. The technology has the potential to create extremely powerful lasers that can be used in various applications, including laser weapons.**

***Keywords*— gamma-ray, laser, nuclei, power.**

I. INTRODUCTION

The "laser" originates as an acronym for "Light Amplification by Stimulated Emission of Radiation.", and presents a device that emits light through a process of optical amplification on the stimulated emission of electromagnetic radiation. A gamma-ray laser "Graser" is a theoretical device that would produce a coherent beam of gamma rays, much like how a regular laser produces coherent light. Gamma rays are electromagnetic radiation of the highest energy and shortest wavelength, arising from nuclear transitions rather than electronic transitions in atoms. The difficulty of Graser development makes it a major scientific and technological challenge. This subject combines principles of quantum electronics, nuclear and optical spectroscopy, and materials science with advanced engineering techniques. The majority of proposals would use bombarding electrons or neutrons as the main pump, interacting with neutrons and generating excited states.

This work explores the theoretical and experimental principles necessary for developing a Graser. The main difference with this kind of laser is that gamma rays come from the nucleus, contrary to the familiar electromagnetic spectrum coming from electron transitions in the atom. Scientists, largely, are copying the idea from an atomic laser. Similar to how excited electrons in an atom transition to a higher energy level by absorbing a photon of energy, and vice versa emit a photon when descending to a lower energy level, energy levels exist in the nucleus of an atom, and they are responsible for the emission of high-energy photons - called gamma rays. The quest for more powerful lasers inevitably leads to exploring nuclear transitions as a basis for laser technology.

Albert Einstein's 1917 paper, 'On the Quantum Theory of Radiation,' marked the first step in the creation of a laser [1]. In this groundbreaking work, Einstein introduced the concept of stimulated emission, which later became the theoretical foundation for developing lasers. However, the first successful device came in 1953. Charles Townes and his colleagues [2], [3] at Columbia University created the first “maser” - which stands for “Microwave Amplification by Stimulated Emission of Radiation”. The key point was to organize atoms to emit waves in perfect harmony, achieving coherence in space and time. They essentially turned Einstein's theoretical concept of stimulated emission into a practical reality. The next step is the first laser built by Theodore Maiman [4], [5], [6] at Hughes Research Laboratories, based on theoretical work by Charles Townes and Arthur Schawlow and the optical amplifier patented by Gordon Gould.

Online ISSN 2256-070X
https://doi.org/10.17770/etr2025vol4.8388
© 2025 The Author(s). Published by RTU PRESS.
This is an open access article under the Creative Commons Attribution 4.0 International License.

Discussing the achievements of Graser's development, one has to mention many of the problems facing the Grasser study have been resolved over the years. The question of obtaining a sufficient concentration of resonant excited isomeric nuclear states for collective stimulated emission to occur turns on the broadening of the gamma-ray spectral line [7]. Of the two forms of broadening, the homogeneous broadening is the result of the lifetime of the isomeric state: the shorter the lifetime, the more broadened the line [8] - [12]. This raises the question of finding long-lived isomers. Inhomogeneous broadening comprises all mechanisms by which the homogeneously broadened line is spread over the spectrum [13]. The most familiar inhomogeneous broadening is Doppler recoil broadening from the thermal motion of molecules in the solid containing the excited isomer and recoil from gamma-ray emission, in which the emission spectrum is both shifted and broadened. The problem has been solved by Mössbauer [14] – [16]. The Mössbauer effect gave recoilless radiation exhibits a sharp line on top of the Doppler-broadened background that is only slightly shifted from the center of the background. With the inhomogeneous background removed, and reaching a sharp line, it would seem that there are conditions for gain [17] – [21]. Nevertheless, other difficulties that would degrade gain are the unexcited states that would resonantly absorb the radiation, opaque impurities, and loss in propagation through the crystal in which the active nuclei are embedded [22]. Much of the latter can be overcome by clever matrix crystal alignment [23] to exploit the transparency provided by the Borrmann effect [24], [25], [19], [20]. Another difficulty, i.e., “Graser's dilemma”, is that the properties that should allow for gain and those that would allow for sufficient nuclear inversion density seem incompatible [26]. The time required to activate, separate, concentrate, and crystallize an appreciable number of excited nuclei by conventional radiochemistry is at least a few seconds. To ensure the inversion persists, the lifetime of the excited state must be considerably longer. The heating caused by neutron pumping the inversion *in situ* is incompatible with maintaining the Mössbauer effect. Heating may be reduced by two-stage neutron-gamma pumping in which neutron capture occurs in a parent-doped converter, where it generates Mössbauer radiation that is then absorbed by ground-state nuclei in the Graser [27], [28]. Two-stage pumping of multiple levels offers multiple advantages. Another approach is to use nuclear transitions driven by collective electron oscillations [29], [30]. The scheme would employ a triad of isomeric states: a long-lived storage state, in addition to an upper and lower lasing state. The storage state would be energetically close to the short-lived upper lasing state but separated by a forbidden transition involving one-quantum unit of spin angular momentum. The Graser would be enabled by a very intense optical laser to saturate the forbidden transition. A "complete" chart of nuclides likely contains a very large number of isomeric states, and the existence of such a triad seems likely, but it has yet to be found [31], [32]. Nonlinearities can result in both spatial and temporal harmonics in the near field at the nucleus, [33], [34] opening the range of possibilities for rapid transfer from the storage state to the upper lasing state using other kinds of triads involving transition energies at multiples of the optical laser quantum energy and higher multipolarities.

The first phase of Graser research, emphasizing the use of crystallized radiochemical prepared isomers, ended when the Graser dilemma and the inertia of resonance were encountered. After years of hiatus, it became apparent that these difficulties might be circumvented by the impulsive pumping of short-lived isomers, by rapid separation of isomers of intermediate lifetimes, or by artificial control of the linewidth in long-lived isomers. In the ensuing second phase, it has become apparent that (1) it is not possible to achieve gain on Doppler-broadened gamma-ray lines, i.e., the Mossbauer effect is an essential feature; (2) it is not possible to pump a Graser directly in situ since the only radiation that would not inevitably destroy the Mossbauer host cannot be generated in adequate intensity from known sources; (3) line narrowing will be extremely difficult and complicated, and there are reasons to suspect, that it may have only limited advantages. These negative conclusions of the second phase are offset, however, by hopes raised by recent rapid progress in several technologies, viz., laser-based isotope separation, atomic beam hyperfine spectroscopy, nuclear polarization, production of defect-free solids, and the generation of coherent radiation in the soft-x-ray region. Mainly Widmann’s work and some others, in atomic beam hyperfine spectroscopy has demonstrated the feasibility of isomer-selective optical pumping and separation of isomers based on magnetic moments - in weak currents [35] - [37]. Optical pumping offers the hope that a population of separately pumped nuclei can be not only rapidly concentrated, implanted, and annealed but also polarized to eliminate lower-state absorption. One is convinced that an intermediate concentration step must separate the pumping and lasing stages so that the best hope for the future lies in rapid separation and careful deposition in a host. Unfortunately, properties that should enable amplification and those that would permit obtaining nuclear inversion densities sufficient for lasing are not, at present, compatible. The resonance cross section is so reduced by line broadening, in the case of long-lived transitions, that amplification is not possible; on the other hand, the intense pumping needed to invert isomers with lifetimes in the Mossbauer range may overheat, damage, or even destroy the solid that must support recoilless emission. The proposals reviewed in this article are suggestions for overcoming these difficulties.

II. Materials and Methods

A. Theoretical Formalism

a) Parameters of nuclei

The diameter of the nucleus is about 10,000 times smaller than the diameter of the atom itself. Here is shown, in Table 1, the size of nuclei and the scale of electromagnetic waves, in Table 2. As we can see γ-rays, the wavelength range starts from 0,01nm.

TABLE 1 SIZE COMPARISON FOR NUCLEI.

Unit	Symbol	Length in Meters
Meter	m	1 x 10^0 m
Millimeter	mm	1 x 10^{-3} m
Micrometer	μm	1 x 10^{-6} m
Nanometer	nm	1 x 10^{-9} m
Picometer	pm	1 x 10^{-12} m
Femtometer	fm	1 x 10^{-15} m
Atomic Nucleus		1 x 10^{-15} m

TABLE 2 ELECTROMAGNETIC SPECTRUM ORDER.

Type of Radiation	Wavelen gtRange	Frequency Range	Coman Sources
Radio Waves	> 1 mm	< 300 GHz	Radio, TV, cell phones
Microwaves	1 mm – 1 m	300 GHz - 300 MHz	Microwave ovens, radar
Infrared	700nm-1mm	430 THz - 300 GHz	Heat lamps, remote controls
Visible Light	400nm-700nm	750 THz - 430 THz	Sun, light bulbs
Ultraviolet	10nm-400nm	30 PHz – 750 THz	Sun, black lights
X-ray	0,01nm-10nm	30 EHz – 30 PHz	X-ray machines, some stars
Gamma Rays	<0,01nm	> 30 EHz	Radioactive decay, nuclear reactions

Theoretically, there is no a low border for gamma rays. The highest energy gamma rays observed so far come from astronomical sources, like the Cygnus X-3 micro quasar. To calculate their wavelength, we can use the formula:

$$\lambda = \frac{hc}{E} \quad (1)$$

where: λ is the wavelength,
h is Planck's constant (6.626×10^{-34} Js),
c is the speed of light (3×10^8 m/s),
E is the energy.

For a gamma ray from Cygnus X-3 with an energy of 100 TeV (100×10^{12} eV): $\lambda \approx 1.24\times10^{-20}$ meters

b) Basic formulas for Photon or γ-ray

$$h\nu = E_2 - E_1 \quad (2)$$

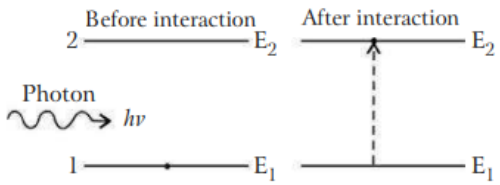

Fig. 1. Induced or stimulated absorption. Source: Physical Optics and Lasers by R.K. Agrawal

where: ν is the frequency corresponding to the energy difference.

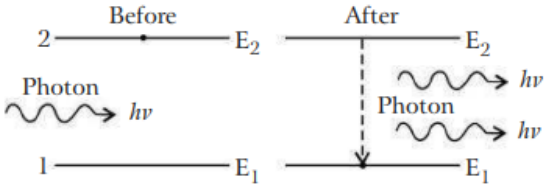

Fig. 2. Stimulated or induced emission. Source: Physical Optics and Lasers by R.K. Agrawal

c) Relation between Spontaneous and Induced Emission

$$A_{21}/B_{21} = 8\pi h\nu^3/c^3 \quad (3)$$

d) Einstein coefficients

A_{21} the probability per unit time of spontaneous emission from the energy state E_2 to the lower energy state E_1.
B_{12} the probability per unit time of induced (stimulated) absorption from $E_1$to E_2.
B_{21} the probability per unit time of induced (stimulated) emission from $E_2$to E_1.

e) Symmetry of Induced Processes:

$$B_{21} = B_{12} \quad (4)$$

f) Population of Energy States

The number of atoms/nuclei in each energy state is given by the Boltzmann distribution:

$$\frac{N_2}{N_1} = \exp\left(-\frac{E_2}{E_1}\right) = \exp\left(-\frac{h\nu}{Tk_B}\right) \quad (5)$$

where: N_1 and N_2 number of atoms/nuclei in states E_1 and E_2, respectively
k_B Boltzmann's constant
T absolute temperature

g) Population Inversion

The establishment of a situation in which the number of nuclei in a higher energy state is greater than that in a lower energy state is called the population inversion.

h) The total linewidth

$$\Gamma = \frac{1}{\tau} \quad (6)$$

where: Γ total linewidth (in radians per second)
τ lifetime of the excited state (in seconds)

The line-broadening factor is therefore crucial. Its maximum possible value of unity occurs only when the transition is purely radiative 2-nd to a ground state. If there are no other contributors to the line breadth, then we say that the line is "homogeneously broadened" by branching, internal conversion, and lower-state decay but is of

"natural" width. In spectroscopy, linewidth is often characterized by the Full Width at Half Maximum (FWHM), which measures the width of the spectral line at half of its maximum intensity:

$$\Delta\nu = \frac{\Gamma}{2\pi} \tag{7}$$

where: $\Delta\nu$ linewidth in hertz (Hz)

i) Doppler-recoil broadening

Because of the random thermal motion of molecules and recoil of the nucleus from photon emission, the emission spectrum is both shifted, on average by:

$$\Delta\nu = 5.32 \text{ x} 10^{-4} \frac{E'}{\mathrm{M}} \quad \text{eV} \tag{8}$$

$$\Gamma_D = 3.3\left(\frac{E'\mu_e}{\mathrm{M}}\right)^{\frac{1}{2}} \quad \text{eV} \tag{9}$$

where: $\Delta\nu$ average frequency shift.
E' photon energy in electronvolts (eV).
M mass of the emitting nucleus or molecule in atomic mass units (u)
μ_e Effective mass related to electron mass.
Γ_D Doppler linewidth.
v_{rms} Root-mean-square thermal velocity in the direction of emission.

This broadening, known succinctly as the "Doppler breadth," simplifies to:

$$\Gamma_D \approx E'\left(\frac{v_{rms}}{c}\right) \tag{10}$$

In the optical region, the recoil shift $\Delta\nu$ is small compared with the Doppler-recoil width and can be neglected.

B. Definitions

a) Nuclear isomers

Refer to nuclei with the same number of protons and neutrons but in different energy states due to varying configurations of nucleons.

b) Metastable States

These isomers exist in excited states with relatively long half-lives (from nanoseconds to years) before decaying to lower energy states. They're denoted with an "m" (e.g., ^{99m}Tc for Technetium-99m).

c) Energy Transitions

When they decay to lower energy states, they emit gamma radiation.

d) Induced transition cross-section

For a transition between two energy levels E_1 *and* E_2:

$$\sigma_{12} = \frac{h\nu}{c} B_{12}, \qquad \sigma_{21} = \frac{h\nu}{c} B_{21}, \tag{11}$$

σ_{12} cross-section for stimulated absorption.

e) Gain Medium

The induced emission cross-section helps determine the gain coefficient g of a laser medium:

$$\mathrm{g} = N_2\sigma_{21} - N_2\sigma_{12} \tag{12}$$

f) Recoilless transitions - The Mossbauer effect

For isomers in solids that show the Mössbauer effect, the gamma-ray emission spectrum exhibits a sharp component superimposed upon the Doppler-broadened background. Often this "recoilless" radiation is essentially of natural width, relatively intense, and only slightly, if at all, displaced from the energy of the nuclear transition. It is manifested by strong resonance absorption of radiation from excited states in one solid by ground states of the same nuclide in a second solid.

The resonance cross-sections, measured in Mössbauer spectroscopy, often are found to be far greater than the nonresonant absorption cross-section, particularly when the recoilless line is near the natural width. In nuclear isomers and Mössbauer spectroscopy, cross-sections for gamma-ray-induced transitions are key to interpreting experimental results.

g) Phonon

At their core, phonons are quantized units of lattice vibrations in crystalline solids. Think of them as the particle-like representations of sound and heat waves moving through a material at the atomic level. Just as photons are the quantized units of electromagnetic waves (light), phonons are the quantized modes of vibrations in a rigid crystal lattice.

h) Debye temperature

$$\Theta_D = \frac{\hbar\omega_D}{k_B} \tag{13}$$

where: $\hbar$ is the reduced Planck constant,
ω_D is the Debye frequency (the maximum phonon frequency),
k_B is the Boltzmann constant.

C. The energy definitions

a) Nuclear Transition.

A nuclear transition refers to the change in energy levels within an atomic nucleus. This can involve the emission or absorption of gamma rays.

b) Displacement energy

The energy required to displace an atom from its lattice position in a crystal. While important for understanding material stability and radiation damage, it is not directly related to the lasing process in a graser.

c) Transferred Energy.

The energy difference between the initial and final nuclear states defines the energy of the emitted or absorbed gamma ray.

D. Methods

The Mössbauer effect is susceptible to thermal vibrations within the crystal lattice. When neutron-pumping is used to achieve population inversion *in situ*, the process introduces significant heating due to the interaction of neutrons with the nuclei, leading to excitations that subsequently decay and deposit energy into the lattice. This increase in temperature enhances phonon activity - essentially, the vibrations of atoms in the lattice, which can disrupt the recoil-free conditions necessary for the Mössbauer effect.

A simplified visualization to illustrate the process:

Neutron-Pumping → Nuclear Excitations → Energy Release into Lattice
↓
Increased Lattice Temperature
↓
Enhanced Phonon Activity (Vibrations)
↓
Reduction of Recoil-Free Gamma-Ray Emission (Mössbauer Effect Compromised)

The core issue is that the Mössbauer effect relies on the emitter and absorber nuclei being part of a solid lattice with minimal thermal motion to ensure recoil-free emission and absorption of gamma rays. Elevated temperatures introduce Doppler broadening and decrease the probability of recoil-free events, thus hindering the effect.

To mitigate this incompatibility, several approaches are considered:

a) Cryogenic Cooling

Implementing efficient cooling systems to maintain the lattice at low temperatures can reduce phonon interactions. Cooling the system to temperatures well below the Debye temperature of the material can help preserve the recoil-free fraction.

b) Material Selection

Choosing materials with higher Debye temperatures increases the range of temperatures over which the Mössbauer effect remains observable. Isotopes embedded in hosts with stiff lattices can sustain lower phonon activity even when some heating occurs (fig.3).

c) Pulse Techniques

Utilizing pulsed neutron sources with low-duty cycles might allow the lattice to dissipate heat between pulses, reducing overall thermal buildup

	Isomeric transition			Mössbauer parameters				Photon cross sections, *b*		Production reaction		
Nuclide	Transition energy	Half-life	Type	Internal conversion coefficient	Recoil energy meV	Debye[b] temp. K	No-phonon fraction $f(T=0)$	Removal[c]	Resonant[d]	Type	Parent	Half-life
^{57}Fe	14.4	97.8 ns	*M*1	8.2	2.0	490	0.93	5.5(3)	1.2(6)	EC	^{57}Co	267 d
	136.5	8.7 ns	*E*2	0.14	175		0.002	1.9(1)	2.3(2)	β	^{57}Mn	1.6 m
^{67}Zn	93.3	9.3 μs	*E*2	0.89	70	327	0.024	5.9(1)	3.6(3)	EC	^{67}Ga	78 h
										β	^{67}Cu	59 h
^{73}Ge	13.3	2.75 μs	*E*2	1100	1.3	370	0.94	1.5(4)	1.2(4)	EC	^{73}As	80 d[e]
	68.3	2.9 μs	*M*1	0.8	34		0.19	1.7(2)	5.6(4)	β	^{73}Ga	49 h
^{83}Kr	9.4	147 ns	*M*1	19.6	0.57	72	0.87	8.5(3)	1.2(6)	EC	^{83}Rb	86 d
^{107}Ag[f]	93.1	44.3 s	*E*3	20	43	225	0.035	3.2(2)	4.6(2)	EC	^{107}Cd	6.7 h
^{119}Sn	23.9	17.9 ns	*M*1	5.2	2.6	210	0.81	2.6(3)	5.6(5)	EC	^{119}Sb	38 h
^{151}Eu	21.5	9.7 ns	*M*1	28.6	1.66	195	0.86		1.6(5)	EC	^{151}Gd	120 d
										β	^{151}Sm	90 y
^{155}Gd	60.0	0.19 ns	*M*1 + *E*2	8.7	12		0.33	3.0(3)	2.3(4)	EC	^{155}Tb	5.6 d
	86.5	6.3 ns	*E*1	0.43	26	195	0.10	1.2(3)	2.2(4)	β	^{155}Eu	5.0 y
	105.3	1.2 ns	*E*1	0.26	38		0.032	7.6(2)	5.6(3)			
^{161}Dy	25.7	28.2 ns	*E*1	2.9	2.2		0.83	6.5(3)	7.9(5)	β	^{161}Tb	6.9 d
	43.8	0.8 ns	*M*2	4.3	6.4	210	0.59	1.6(3)	1.4(5)	EC	^{161}Ho	2.4 h
	74.6	3.3 ns	*E*1	0.65	19		0.22	1.9(3)	5.7(4)			
^{181}Ta	6.2	6.8 μs	*E*1	82	0.11	240	0.99	9.7(4)	7.6(5)	EC	^{181}W	121 d
	136.3	40 ps	*M*1 + *E*2	1.8	55		0.02	5.6(2)	8.6(2)	β	^{181}Hf	42 d
^{191}Ir	82.4	4.0 ns	*M*1	10.7	19	420	0.45	2.6(3)	1.4(4)	β	^{191}Os	15.4 d
	129.4	89 ps	*M*1	2.9	47		0.14	7.8(2)	5.3(3)	EC	^{191}Pt	2.8 d
^{237}Np	59.5	68.2 ns	*E*1	1.1	8.0	200	0.50	2.8(3)	1.6(5)	β	^{237}Pu	6.8 d
										EC	^{237}U	4.5 d
											^{241}Am	460 y

Fig. 3. Lists several isotopes that emit recoilless radiation when in solid hosts. Source: Baldwin et al, (1981)

III. RESULTS AND DISCUSSION

The present work proposes a combination of neutron beams for the excitation of metastable nuclei in the correct crystal lattice to ensure recoil-free Mössbauer emission and, by ensuring such emission, prevent the broadening of the resonant nuclear line, which is crucial for maintaining coherence. However, the challenge lies in selecting the right metastable nuclei and creating the ideal crystal environment. The choice of Europium-151 (^{151}Eu) can offer the conditions we need (fig.3). The half-life of ^{151}Eu is approximately 4.62×10^{18} years. This incredibly long half-life means that ^{151}Eu is nearly stable. ^{151}Eu is a compelling choice when delving into the Mössbauer effect and the pursuit of coherent gamma emission. Its nuclear properties make it suitable for emitting and absorbing gammarays without recoil, which is .essential for maintaining the sharp resonance lines one strives for. The 21.5 keV nuclear transition of ^{151}Eu has relatively low energy, which facilitates the Mössbauer effect at accessible temperatures. By embedding ^{151}Eu atoms into a carefully selected crystal lattice, one can minimize the recoil during gamma emission and absorption. The lattice acts as a collective mass that absorbs the recoil momentum, preserving the energy precision needed for coherence. One of the intriguing challenges with ^{151}Eu is its natural abundance and isotopic purity. Since Europium naturally occurs as two stable isotopes - ^{151}Eu and ^{153}Eu - enriching samples with a higher concentration of ^{151}Eu can enhance the effectiveness of one‘s experimental setup. Isotopic enrichment ensures that a larger proportion of the nuclei participate in the Mössbauer resonance, improving the overall efficiency of recoilless emission.

Creating the appropriate crystal lattice is another hurdle. The lattice must be capable of absorbing the recoil energy completely, which often requires ultra-low temperatures to minimize lattice vibrations - phonons - that can disrupt the process. Quantum engineering at this scale pushes the boundaries of materials science. The choice of host lattice is also crucial. The crystal structure must not only accommodate Europium ions but also possess suitable vibrational properties to suppress phonon interactions that could broaden the resonance line. For our case, the compound E u_2 Ca F_2 (Europium Calcium Fluoride) has been chosen. It is known for its interesting lattice dynamics and structural phase transitions. It can exist in multiple phases, including cubic, trigonal, and monoclinic, depending on temperature and pressure. The cubic phase is particularly stable at ambient conditions, which might be beneficial for maintaining a consistent crystal lattice. Eu_2CaF_2, on the other hand, has a fluorite structure, which is a face-centered cubic (fcc) lattice. This structure is known for its high transparency and low phonon energy, which are advantageous for optical applications. The incorporation of Europium into the CaF_2 lattice can introduce new optical properties, making it my choice for gamma-ray laser.

In exploring the excitation of nuclei with neutrons to produce gamma rays, one is treading a fine line between effectively stimulating the desired nuclear transitions and inadvertently damaging the crystal lattice. The "border of overheating the crystal" refers to the threshold at which neutron irradiation begins to disrupt the crystal structure and undermines the conditions necessary for recoilless emission. When neutrons interact with a crystal lattice, they can transfer significant energy to the atoms within the material.

The key point in the present work is the suggestion that even if the transferred energy exceeds the displacement energy of the atoms, under the right combination of circumstances, the Graser can be achieved:

- Estimating the displacement energy of atoms in E u_2 Ca F_2 involves considering the individual contributions of Fluorine, Calcium, and Europium ions within the crystal lattice. I use the computational method of density functional theory (DFT) to provide quantum mechanical modeling of atomic interactions at finite temperatures and estimate:

  Fluorine Ions: ~25–40 eV
  Calcium Ions: ~30–50 eV
  Europium Ions: ~50–80 eV

- The common estimation to avoid overheating the crystal, usually essential to optimize the neutron flux and energy, is not helping in our case. Usually for neutron energy, one uses thermal or cold neutrons (with energies in the meV = 10^{-3} eV range) to reduce the risk of displacing lattice atoms.
- One knows lower-energy neutrons may have a lower probability of inducing the desired nuclear transitions. However, flux density should be limited the neutron flux minimizes the number of interactions that could lead to lattice damage. It's a balance between enough interactions to excite the nuclei and prevent excessive collisions that harm the lattice.
- Additionally, irradiation time should be shorter to reduce cumulative damage. Pulsed neutron sources should deliver neutrons in bursts, allowing the lattice to dissipate energy between pulses. Pulsed neutron sources with low-duty cycles allow lattices to dissipate heat between pulses, reducing overall thermal buildup.
- Low-temperature operations should further reduce lattice vibrations, enhancing the Mössbauer effect.

Online ISSN 2256-070X
https://doi.org/10.17770/etr2025vol4.8388
© 2025 The Author(s). Published by RTU PRESS.
This is an open access article under the Creative Commons Attribution 4.0 International License.

Cryogenic cooling of the systems to maintain the lattice at low temperatures will reduce phonon interactions. Cooling the system to temperatures well below the Debye temperature of the material will help preserve the recoil-free fraction.

- Exploring external influences such as magnetic and electric fields might offer additional control over the nuclear states of ^{151}Eu. Hyperfine interactions can split the nucleus energy levels, allowing for more precise tuning of the resonance conditions. This added control could be an instrument for additional rising energy and achieving coherence.

One needs energy in the range of keV or MeV to achieve the necessary nuclear transitions and coherence. When discussing Grasers on the base of ^{151}Eu, the energy levels are typically in the keV range. This range is achievable for our case, for instance, the 21.5 keV nuclear transition for ^{151}Eu is a good example of energy levels involved in gamma-ray applications. However, the Graser dilemma is still present, i.e. the neutron beam energy ~22 keV is significantly higher than the displacement threshold energy 50–80 eV. This means that a single neutron with this energy has more than enough energy to displace an atom from its lattice site.

The new method invented here to develop Graser and overthrow Graser's dilemma is “to burn the lattice.” One must stop worrying about damaging the crystal lattice but sacrifice it and consider it a temporary consumable. The “burn” symbolically means that one should leave a high-energy neutron (for example, 22 keV) to destroy/burn the lattice, simultaneously exciting the metastable nuclei (in this case ^{151}Eu). Furthermore, to ensure the continued existence of the Grasser body, a mechanism for moving and constantly feeding a new crystal lattice at the same location where the beam of nuclei hits the lattice must be added. The creation of an excited state, population inversion, and emission of coherent waves will be possible by means of a pulsed beam and only for the exact location and moment. At the next moment, this will happen with the new part of the incoming crystal. Precise adjustments of location and time are mandatory for the process to have an effect.

IV. Conclusions

The quest for a gamma-ray laser resembles that for controlled nuclear fusion in many ways. Neither goal seems to forego any fundamental principle, both offer enormous rewards for success, both present challenging problems in many disciplines, and both have been maddeningly elusive, and both have been pursued for many years. In each, just when one approach has failed, another concept emerges, and the search is renewed. The nuclei that will play an important role in fusion are known; in Graser, where nuclear parameters play a much more important role, there are still no clear candidates.

The theoretical calculations and consideration of the present work suggest the possible development of Graser. It is on the base of the metastable isotope of ^{151}Eu embedded in the crystal lattice as Eu_2CaF_2, a chemical compound that subsequently guarantees recoil-free Mössbauer scattering and prevents the broadening of the Doppler recoil and, in turn, ensures coherence of the laser beam. However, to make Graser possible, one should optimize the neutron flux and energy. On the first impression, the bombarding neutron flux mustn’t exceed energy up to 80 eV, which is the low border of displacement energy for ^{151}Eu, to prevent overheating and damage. On other hand, energies in the area of 80 eV could not be enough to excite the nucleus and create the “population inversion” desired for a coherent beam. The solution is that one can use the energy of the neutron flux at approximately 21.5 keV desired to excite the nuclei and produce a laser beam, however, at the price of destroying the crystal lattice. This new method of "burning and constantly feeding with new crystal“, with embedded metastable nuclei circumvents the Grasser dilemma and practically opens a new way to develop Grasser.

It doesn't matter that the model seems expensive, destroying the hard-to-produce lattice with rare metastable isotopes is quite a waste, but Graser's achievement seems possible. Further research could reduce the heavy losses by finding other chemical elements and/or reducing the lattice burn-up rate.

Using Grasers with energies in this range for defensive purposes could revolutionize areas such as advanced shielding and energy transfer systems.

Acknowledgments

I thank Prof. Mitko Gaydarov, the supervisor of my doctoral studies, as well as Prof. Anton Antonov, and the entire team from the nuclear laboratory at the Institute for Nuclear Research and Nuclear Energy of the Bulgarian Academy of Sciences for the useful discussion.

References

[1] A. Einstein, On the Quantum Theory of Radiation. Physik Zeitschr. JJ3, 121-128, 1917.

[2] J. Gordon, H. Zeiger and C.Townes, Molecular Microwave Oscillator and New Hyperfine Structure in the Microwave Spectrum of NH3: Phys. Rev. 95, 282, 1954.

[3] J. Gordon, H. Zeiger, and C. Townes, The Maser - New Type of Microwave Amplifier, Frequency Standard, and Spectrometer. Phys. Rev. 99, 1264, 1955.

[4] T. Maiman, Stimulated Optical Radiation in Ruby. Nature, 187(4736), 493–494, 1960.

[5] T. Maiman, Spectroscopy and Stimulated Emission in Ruby. Phys. Rev. 123, 1151 – 1157, 1961.

[6] T. Maiman, Stimulated Optical Radiation in Ruby. Essentials of Lasers, 134–136, 1969.

[7] G. Baldwin, Is There a High Frequency Limit to Laser Action? Laser Interaction and Related Plasma Phenomena. Vol. 3B. pp. 875–888, 1974.

[8] V. Vali and W. Vali, Induced gamma y-ray emission. Proceedings of the IEEE. 51 (1): 182–184, 1963.

[9] V. Letokhov, On the problem of the nuclear-transition gamma-laser. Journal of Experimental and Theoretical Physics. 37 (5): 787–793, 1973.

[10] P. Kamenov and T. Bonchev, On the possibility of realizing a gamma laser with long-living isomer nuclei. Bolgarskaia Akademiia Nauk, Doklady. 28 (9): 1175–1177, 1975.

[11] Yu. Il'inskii and R. Khokhlov, On the possibility of observation of stimulated gamma radiation. Soviet Physics Uspekhi. 16 (4): 565–567, 1974.

[12] Yu. Il'inskii and R. Khokhlov, Possibility of creating a gamma-laser. Radiophysics and Quantum Electronics. 19 (6): 561–567, 1976.

[13] G. Baldwin, On the Feasibility of Grasers. Laser Interaction and Related Plasma Phenomena. Vol. 4A. pp. 249–257, 1977.

[14] R. Mössbauer, Kernresonanzfluoreszenz von Gammastrahlung in Ir191. Zeitschrift für Physik A (in German). 151 (2): 124–143, 1958.

[15] H. Frauenfelder, The Mössbauer Effect. W. A. Benjamin. LCCN 61018181, 1962.

[16] A. Andreev, Yu. Il'inskii, and R. Khokhlov, Role of collective and induced processes in the generation of Mössbauer gamma radiation. Journal of Experimental and Theoretical Physics. 46 (4): 682–684, 1977.

[17] I. Terhune and G. Baldwin, Nuclear superradiance in solids. Physical Review Letters. 14 (15): 589–591, 1965.

[18] G. Baldwin, Bibliography of GRASER research. Los Alamos Scientific Laboratory Report LA-7783-MS, 1979.

[19] A. Andreev and Yu. Il'inskii, Amplification in a gamma laser when the Bragg condition is satisfied. Journal of Experimental and Theoretical Physics. 41 (3): 403–405, 1975.

[20] A. Andreev, Yu. Il'inskii, Possible use of the Borrmann effect in the gamma laser. Journal of Experimental and Theoretical Physics. 43 (5): 893–896, 1976.

[21] D. Marcuse, Line Broadening in Recoil-Free Gamma-Ray Resonance Absorption. Physical Review, 131(3), 1631–1639, 1963

[22] Yu. Il'inskii and R. Khokhlov, On the possibility of observation of stimulated gamma radiation. Soviet Physics Uspekhi. 16 (4): 565–567, 1974.

[23] G. Baldwin and J. Solem, Recoilless gamma-ray lasers. Reviews of Modern Physics. 69 (4): 1085–1117, 1997.

[24] G. Borrmann, Über Extinktionsdiagramme der Röntgenstrahlen von Quarz. Physikalische Zeitschrift. 42: 157–162, 1941.

[25] Yu. Kagan, Use of the anomalous passage effect to obtain stimulated emission of gamma quanta in a crystal. JETP Letters. 20 (1): 11–12, 1974.

[26] G. Baldwin and J. Solem, Kinetics of neutron-burst pumped gamma-ray lasers. Laser Physics. 5 (2): 326–335, 1995.

[27] V. Gol'danskii, Yu. Kagan and V. Namiot, Two-stage pumping of Mössbauer gamma-ray lasers. JETP Letters. 18 (1): 34–35, 1973.

[28] V. Gol'danskii and Yu. Kagan, The possibility of creating a nuclear gamma laser. Journal of Experimental and Theoretical Physics. 37 (1): 49, 1973.

[29] J. Solem and L. Biedenharn, Primer on coupling collective electronic oscillations to nuclei. Los Alamos National Laboratory Report LA-10878, 1987.

[30] L. Biedeharn, G. Baldwin and K. Boer, Nuclear excitation by laser-driven coherent outer shell electron oscillations. Proceedings of the First International Laser Science Conference, Dallas, TX, November 18–22, 1985. Stwalley, W. C.; Lapp, M.; Eds. Vol. 146. pp. 52–53, 1986.

[31] G.Baldwin and J. Solem, Recoilless gamma-ray lasers. Reviews of Modern Physics. 69 (4): 1085–1117, 1997.

[32] J. Solem, L. Biedenharn and G. Rinker, Calculation of harmonic radiation from atoms subjected to strong laser fields and the possibility of nuclear excitation. Journal of the Optical Society of America A. 4: 53, 1987.

[33] J. Solem and L. Biedenharn, Laser coupling to nuclei via collective electronic oscillations: A simple heuristic model study. Journal of Quantitative Spectroscopy and Radiative Transfer. 40 (6): 707–712, 1988.

[34] J. Solem, Theorem relating spatial and temporal harmonics for nuclear interlevel transfer driven by collective electronic oscillation. Journal of Quantitative Spectroscopy and Radiative Transfer. 40 (6): 713–715, 1988.

[35] E. Widmann, for the ASACUSA Cusp Collaboration. Hyperfine Spectroscopy of Antihydrogen, Hydrogen, and Deuterium. Phys. Part. Nuclei **53**, 790–794 (2022). https://doi.org/10.1134/S1063779622040141

[36] A. Andreev, Atomic Spectroscopy - Introduction to the Theory of Hyperfine Structure. Springer, Book, Electronic (ISBN: 978-0-387-28469-9), 2006.

[37] W. G. Jin, T. Horiguchi, M. Wakasugi, et al. Systematic study of isotope shifts and hyperfine structures in YbI by atomic-beam laser spectroscopy. Hyperfine Interact 74, 310, 1992. https://doi.org/10.1007/BF02398640

Environment. Technology. Resources. Rezekne, Latvia
Proceedings of the 16th International Scientific and Practical Conference. 2025. Volume IV, 475-480

Optimization of Parameters for White and Dark Laser Marking of Copper and Brass Products

Lyubomir Lazov
Rezekne Academy of Riga Technical University
Rezekne, Latvia
lyubomir.lazov@rta.lv

Risham Singh Ghalot
Rezekne Academy of Riga Technical University
singhrisham93@gmail.com

Nikolay Angelov
Department of Mathematics Informatics and Natural Sciences
Technical University of Gabrovo
Gabrovo, Bulgaria
angelov.np@abv.bg

***Abstract*— This publication examines two principal techniques of fibre laser marking on copper and brass substrates, focusing on the achievement of both dark and white (light) markings. It investigates the effects of marking speed, power density, frequency, and raster pitch on marking contrast. The study identifies the power density threshold that distinguishes between light and dark markings, determining the experimental critical power density for melting at varying speeds for both materials. It also compares experimental values with theoretical predictions of critical melting power density. The findings offer practical recommendations for optimizing laser parameters to achieve high-contrast markings, thereby enhancing traceability and quality control in industrial applications involving copper and brass components.**

***Keywords*— Brass, Contrast, Copper, Fibre Laser, Laser Marking, Power Density, Raster Step, Speed.**

I. Introduction

Laser marking has become an essential technology for the permanent labelling and traceability of metal components across various industries, including electronics, automotive, military production, medical device industry, and aerospace. The ability to create both light and dark markings on copper and brass is particularly valuable for enhancing product identification and quality control. Dark markings provide high contrast for easy visual recognition, while light markings offer subtle, durable labels suitable for automated registration. The capability to achieve both marking types on a single sample opens new possibilities in manufacturing processes.

However, laser marking of copper and brass presents significant challenges due to their high reflectivity and thermal conductivity. These properties make it difficult to achieve consistent contrast and precise control over the marking process [1] – [7]. High reflectivity reduces the absorption of laser energy, with much of it being dissipated into space, while high thermal conductivity of materials leads to heat transfer outside the impact zone, which can lead to the creation of a larger heat-affected zone and deterioration of the marking quality [8] – [10]. These factors complicate the task of achieving the desired marking result and determining the necessary values of power density, marking speed, frequency and raster step.

Several studies have explored laser marking of copper and brass, focusing on aspects such as surface oxidation, microstructure changes, and the influence of laser parameters on marking quality.

In the paper [10], the study is about the influence of speed, raster pitch and power on the roughness and microhardness of the marked areas of copper samples. The experiments were conducted with a fibre laser and a copper bromide laser. The laser power, scan speed and raster pitch were varied to determine their effect on the obtained microhardness and surface roughness. From the experimental data, the speed dependences of the roughness and microhardness for three degrees and two pulse durations for the fibre laser were obtained. The dependence of the roughness and microhardness on the raster pitch for both types of lasers is also shown.

In the paper [11], the authors investigated the influence of pulse duration, power density, speed and linear density of pulses on the depth of marking on brass alloy 260 samples using a fibre laser. They also obtained results on the influence of speed and pulse duration on the path width in laser marking.

In the publication [12], the authors investigate the role of power density of melting and evaporation and speed to realize several laser technological processes on copper samples for a fibre laser and a CuBr laser. A methodology has been developed to determine preliminary operating intervals of power density for different speeds for the laser marking, laser ablation and laser texturing processes. From

Online ISSN 2256-070X
https://doi.org/10.17770/etr2025vol4.8390
© 2025 The Author(s). Published by RTU PRESS.
This is an open access article under the Creative Commons Attribution 4.0 International License.

theoretical calculations, graphics of the dependences of the critical power density of melting and evaporation on the speed were drawn. Areas where oxidation, melting or evaporation occur were defined. Comparing the theoretical results and the obtained experimental results shows a very good convergence between them for both laser sources.

Researchers have investigated methods for enhancing contrast and durability, but the transition between light and dark markings, as well as the critical melting power density, have not been studied. While theoretical models exist for predicting melting thresholds, experimental validation across different marking speeds and materials has not been reported in other studies.

This article aims to address these gaps by systematically studying the influence of key laser parameters on marking contrast for copper and brass. The purpose is to determine the experimental critical melting power density for different speeds, compare these values with theoretical predictions, and provide practical guidelines for achieving high-contrast laser markings. The findings contribute to refining laser marking techniques, ultimately enhancing the reliability and versatility of marking processes for industrial applications.

II. Materials and Methods

The research conducted is aimed at simultaneously obtaining light and dark laser marking on copper and brass samples. They are implemented with a fibre laser system.

A. Materials

Copper (Cu) is a metal with exceptional high electrical & thermal conductivity, favourable resistance to corrosion (forms a protective oxide layer), great malleability and ductility, and marvellous antimicrobial properties. These properties contribute to its widespread use in industry like - electrical & electronics, defence, construction, transportation, renewable energy facilities, healthcare sanitation, etc.

Whereas brass (CuZn) is a copper-zinc alloy with superb corrosion resistance, excellent malleability & ductility, satisfactory electrical conductivity, and high wear resistance. It has wide applications in the military industry, architecture, jewellery, plumbing parts manufacturing, musical instruments, sculptures, decorations, etc.

B. Laser System

The used laser system is from the ROFIN (Submerged in Coherent.inc) laser manufacturer. The model used is ROFIN powerline F20 laser system. The technical parameters of the laser system are as follows in the Table 1.

TABLE 1 PARAMETERS OF FIBRE LASER SYSTEM USED IN THE RESEARCH.

Parameters	Denotations	Values	Units
Wavelength	λ	1064	nm
Power	P	20	W
Beam Diameter	d	30	µm
Frequency	ν	20 - 50	kHz
Pulse Duration	τ	4 - 200	ns
Scan Speed	v	1 - 20000	mm/s
Pulse Energy	E_p	0.1 - 1	mJ
Focus	f	184	mm

A laser technological system with a fibre laser (see Fig. 1) operating in the near infrared region and in pulsed mode was used. The pulse duration varies over a wide range, and the high frequency provides a large overlap of the pulses in the direction of the laser beam. The laser system is characterized by high positioning accuracy and good repeatability. The laser beam can be moved at a speed varying within very wide limits [13] – [15].

Fig. 1. ROFIN 20 W fibre laser system at Laser Institute of Rezekne Academy of Technology.

B. Experimental Methods

The experiments aim to investigate the influence of speed v and power density q_s factors on obtaining dark and white (light) marking with a fibre laser on copper and brass samples. The frequency and raster step are kept constant for each of the experiments.

To obtain dark and light marking on copper and brass, matrices were designed to conduct the experiments.

- Study of the influence of speed and power density for obtaining dark and light marking on copper

For copper, the matrix consists of processing areas with dimensions 10 mm × 10 mm arranged in 6 rows and 8 columns, with each area corresponding to a different marking speed v and power density q_s (Fig. 2). Copper samples are prepared and fibre laser marking of these 48 areas is performed. After laser marking of the samples, the contrast k_x^* for each marked area is determined.

Contrast k_x^* measurement could be defined as the visual variation of brightness of the laser processed and un-processed area of the substrate. The contrast k_x^* in percent (%) is determined on the reference scale in the relative units or in percent. On the grey scale of the bitmap, each image can be represented as a number between 0 (black) and 255 (white). A reference number N_f is determined with 'Adobe Photoshop' for the image of the surface around the marked area. For a specific grey scale mark image, by means of comparison (when merging it with a reference image), the

corresponding N_x value is measured. The contrast k_x^* is determined by linear interpolation from the expression (1):

$$k_x^* = \frac{N_f - N_x}{N_f} \times 100\% \quad (1)$$

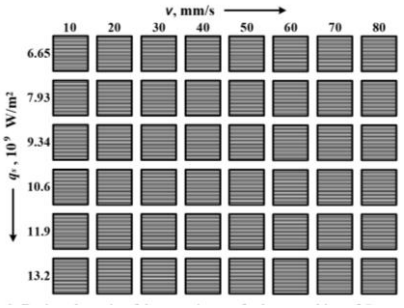

Fig. 2. Designed matrix of the experiments for laser marking of copper samples.

- Study of the influence of speed and power density on obtaining dark and light marking on brass

For brass, the matrix is made of processing areas 5 mm × 5 mm with 3 rows and 7 columns, similar as earlier, with different values of speed v and power density q_s for each area (Fig. 3). Then, marking is performed and the contrast k_x^* of the 21 areas is determined.

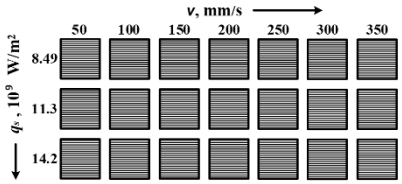

Fig. 3. Designed matrix of the experiments for laser marking of CuZn samples.

- Drawing contrast versus speed graphs and determining critical melting power density for different speeds

For the copper samples, the next step in the study is to plot contrast k_x^* versus speed v for different power densities q_s for light and dark markings. The contrast k_x^* variation intervals for both markings are obtained. The critical power density q_{sc} for melting q_{scm} for different speeds v are determined from the results.

For the brass samples, the contrast k_x^* variation intervals for both types of markings are obtained. The next step is to determine the critical power density q_{sc} for melting q_{scm} for different speeds v.

- Comparison of experimental and theoretical values of critical power density of melting

To compare the experimental q_{scme} and theoretical q_{scmt} values of the critical power density for melting q_{scm}, it is necessary to calculate the theoretical value. It is obtained by the formula (2):

$$q_{scm} = \frac{(1+s)k(T_m - T_0)}{2A}\sqrt{\frac{\pi v}{ad}} \quad (2)$$

where the parameter s is given by the expression $s = \frac{L_m}{c(T_m - T_0)}$, T_m – melting point, T_0 – initial temperature (ambient temperature), A – absorptive capacity, v – speed, a – coefficient of thermal conductivity, d – diameter of the working spot.

III. Results and Discussion

After analysing the marked areas, we found that there is a clear boundary indicating the transition between dark and light marking for different technological parameters – marking speed v, laser power density q_s, raster step Δx and frequency ν. This led us to the idea that the critical power densities q_{sc} for different speeds v at constant values of the other parameters for the selected materials and the technological laser system with a fibre laser can be experimentally determined.

A. Experiments with Copper Samples

According to the designed matrix, laser marking of copper samples was performed. They are for six power densities: $q_{s1} = 6.65 \times 10^9$ W/m^2, $q_{s2} = 7.93 \times 10^9$ W/m^2, $q_{s3} = 9.34 \times 10^9$ W/m^2, $q_{s4} = 10.6 \times 10^9$ W/m^2, $q_{s5} = 11.9 \times 10^9$ W/m^2, and $q_{s6} = 13.2 \times 10^9$ W/m^2, with the speed v varying in the range from 10 mm/s to 80 mm/s in 10 mm/s increments. The parameters that were kept constant during the experiments were: frequency $\nu = 20$ kHz and raster step $\Delta x = 10$ µm. The marked areas are presented in Fig. 4.

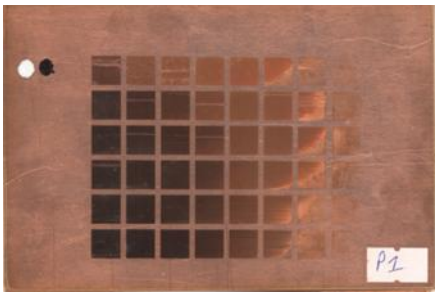

Fig. 4. General view of marked areas on a copper sample.

From the obtained experimental results, graphs of the dependence of contrast k_x^* on speed v for different power densities for dark marking (Fig. 5) and light marking (Fig. 6) are plotted. From them, the following conclusions can be made:

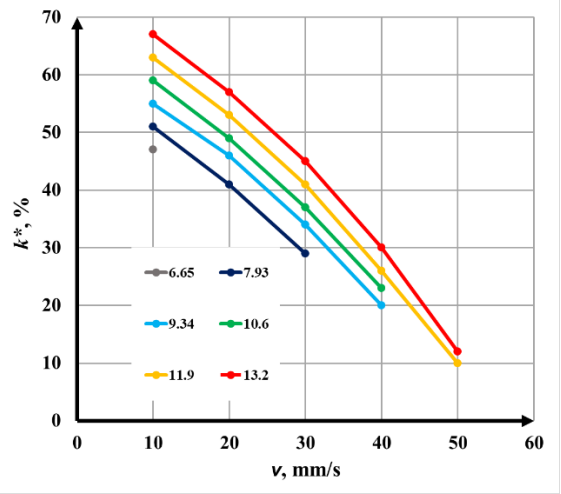

Fig. 5. Graphs of the dependence of contrast on speed for dark marking.

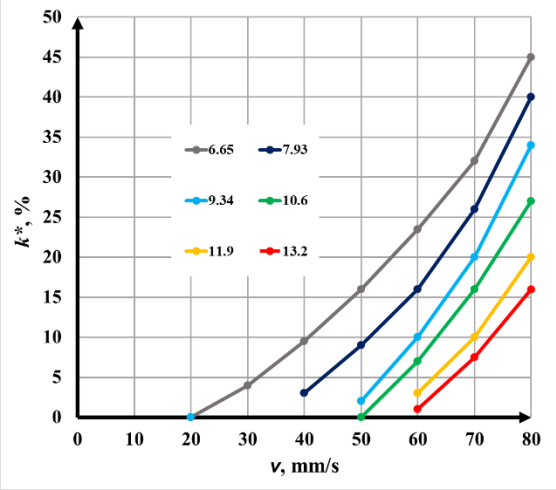

Fig. 6. Graphs of the dependence of contrast on speed for white (light) marking.

- When obtaining a dark marking, the contrast k_x^* varies within the following limits: from 51% to 29% when varying the speed v from 10 mm/s to 30 mm/s and a power density of q_{s2} = 7.93 × 10^9 W/m^2; from 55% to 20% when varying the speed v from 10 mm/s to 40 mm/s and a power density of q_{s3} = 9.34 × 10^9 W/m^2; from 59% to 23% when varying the speed v from 10 mm/s to 40 mm/s and a power density of q_{s4} = 10.6 × 10^9 W/m^2; from 63% to 10% when varying the speed v from 10 mm/s to 50 mm/s and power density of q_{s5} = 11.9 × 10^9 W/m^2 and from 67% to 12% when varying the speed v from 10 mm/s to 50 mm/s and power density of q_{s6} = 13.2 × 10^9 W/m^2.

- For the specified parameters, raster marking is implemented by melting, with the contrast k_x^* changing due to the different roughness of the marked areas [10].

- The following operating speed v intervals were obtained for the visual perception of the dark marking:

- from 10 mm/s to 15 mm/s for q_{s3} = 9.34 × 10^9 W/m^2.
- from 10 mm/s to 18 mm/s for q_{s4} = 10.6 × 10^9 W/m^2.
- from 10 mm/s to 24 mm/s for q_{s5} = 11.9 × 10^9 W/m^2.
- from 10 mm/s to 26 mm/s for q_{s6} = 13.2 × 10^9 W/m^2.

- When receiving a light marking, the contrast k_x^* changes: from 0% to 45% when the speed v varies from 20 mm/s to 80 mm/s and the power density is q_{s1} = 6.65 × 109 W/m2; from 3% to 40% when the speed v varies from 40 mm/s to 80 mm/s and the power density is q_{s2} = 7.93 × 109 W/m2; from 2% to 34% when the speed v varies from 50 mm/s to 80 mm/s and the power density is q_{s3} = 9.34 × 109 W/m2; from 0% to 27% when the speed v varies from 50 mm/s to 80 mm/s and the power density is q_{s4} = 10.6 × 109 W/m2; from 3% to 20% when varying the speed v from 60 mm/s to 80 mm/s and power density is q_{s5} = 11.9 × 109 W/m2 and from 1% to 16% when varying the speed v from 60 mm/s to 80 mm/s and power density is q_{s6} = 13.2 × 109 W/m2.

- This case can be explained by the fact that the resulting laser marking is probably due to oxidation, as the marked surface is lighter than the unmarked surface (the base).

- The following operating speed v intervals were obtained when automatically registering the light marking:

- from 55 mm/s to 80 mm/s for q_{s1} = 6.65 × 10^9 W/m^2.
- from 64 mm/s to 80 mm/s for q_{s2} = 7.93 × 10^9 W/m^2.
- from 70 mm/s to 80 mm/s for q_{s3} = 9.34 × 10^9 W/m^2.
- from 74 mm/s to 80 mm/s for q_{s4} = 10.6 × 10^9 W/m^2.

- The simultaneous obtaining of dark and light marking on one sample allowed us to determine the limit for obtaining laser marking by melting or by oxidation for the selected parameters of the study for fibre laser and material copper, i.e. to determine the experimental critical power density q_{sc} for different speeds v. The results are presented in Table 2. The theoretical values of the critical power density q_{sc} were calculated by formula (2). The comparison between the two values showed that the theoretical values are higher than the experimental ones for the interval of studied speeds v. This result is explained by the fact that the change in the characteristics of copper with increasing temperature during the implementation of the process was not considered in the theoretical calculations.

TABLE 2 EXPERIMENTAL AND THEORETICAL CRITICAL POWER DENSITY FOR MELTING FOR DIFFERENT RATES FOR CU SAMPLES.

v, mm/s	q_{scme}, W/m^2	q_{scmt}, W/m^2
20	6.65 × 10^9	6.79 × 10^9
31	7.93 × 10^9	8.45 × 10^9
43	9.34 × 10^9	9.67 × 10^9
50	10.6 × 10^9	11.3 × 10^9
54	11.9 × 10^9	12.4 × 10^9
58	13.2 × 10^9	13.6 × 10^9

B. Experiments with Brass Samples

The brass samples were exposed to the environment for a long time and had an oxide layer. Their background is changed in this way, which darkens. Experiments were conducted for raster laser marking of a brass sample for three power densities: q_{s7} = 8.49 × 10^9 W/m^2, q_{s8} = 11.3 × 10^9 W/m^2, and q_{s9} = 14.4 × 10^9 W/m^2. The speed v varied from 50 mm/s to 350 mm/s in 50 mm/s increments. The parameters that were kept constant during the experiments were: frequency ν = 100 kHz and raster step Δx = 30 µm. A panoramic photograph of the marked areas is given in Fig. 7. The contrast k_x^* of the marking was determined for each marked square.

Fig. 7. General view of marked areas on a sample of brass.

After analysing the obtained results, the following was established:

- For a power density of q_{s7} = 8.49 × 10^9 W/m^2, a bright marking is obtained for the speed v interval studied as the contrast k_x^* varies from 12% to 75%, and no dark marking is observed. For a power density of q_{s8} = 11.3 × 10^9 W/m^2, a dark marking is available for a speed v of 50 mm/s as the contrast k_x^* is 25%, and a bright marking is obtained for a speed v of 100 mm/s to 350 mm/s as the contrast k_x^* varies from 0 to 43%. For a power density of q_{s9} = 14.4 × 10^9 W/m^2, a dark mark is obtained for a speed v of 50 mm/s to 100 mm/s as the contrast k_x^* varies from 35% to 14%, and a bright mark is obtained for a speed v of 150 mm/s to 350 mm/s as the contrast k_x^* varies from 0 to 27%.

- The dark marking was obtained by removing the oxide layer and subsequent melting of the material (see marked area in left part of Fig. 7). The laser marking process by melting was implemented.

- The light marking was obtained by removing the oxide layer. In these experiments, a light marking is present in most of the investigated speed v interval. It is explained by the fact that a lower power density (lower absorbed energy, respectively) is required to remove the thin oxide layer from the brass sample in the impact zone. At this raster step, the scanning overlap coefficient has a value of 0 ($k_{soc} = 1 - \frac{\Delta x}{d}$), i.e. there is no overlap, as in raster marking the paths touch each other. In addition, the used frequency of 100 kHz gives a lower pulse energy ($E_p = \frac{P}{\nu}$). The combination of high-speed v, low power density, low pulse energy and zero scanning overlap coefficient do not allow the melting of the brass sample after removing the oxide layer.

- Again, as with the copper sample, simultaneous dark and light markings were obtained on the brass sample. This allowed the determination of the critical power density for melting q_{scm} for two speeds v. The experimental and theoretical results are given in Table 3. Comparing the theoretical values of the critical power density q_{sc} with the experimental ones for both speeds v shows that the theoretical values are higher than the experimental ones.

Experimental determination of critical power densities q_{sc} provides guidance for determining the power density q_s and speed v intervals when conducting research for a specific marking method, for example by oxidation, layer removal (nickel-plated, galvanized, etc. sample) and melting. This shortens the time from the research process to the implementation in production of the laser marking process on products.

TABLE 3 EXPERIMENTAL AND THEORETICAL CRITICAL POWER DENSITY FOR MELTING FOR DIFFERENT RATES FOR CUZN SAMPLES.

v, mm/s	q_{scme}, W/m^2	q_{scmt}, W/m^2
100	11.3 × 10^9	11.7 × 10^9
150	14.4 × 10^9	14.2 × 10^9

C. QR Code marking on Copper and Brass Samples

Quick Response (QR) codes with dimensions ranging between 3 mm to 4 mm were obtained on copper & brass samples with dark and light markings through the optimal research results. The values of the parameters are as follows:

a) QR codes on copper surface (Fig. 8)

- For dark marking, the power density is q_{s5} = 11.9 × 10^9 W/m^2, v = 20 mm/s and ν = 20 kHz.
- For light marking, the power density is q_{s5} = 11.9 × 10^9 W/m^2, v = 80 mm/s and ν = 20 kHz.
- A laser marked QR code of size 3.5 mm, in light marking, was scannable with an electronic device.

Fig. 8. Obtained QR codes on copper surface – starting from left end, white (light) and dark marking, respectively.

b) QR codes on brass surface (Fig. 9)

- For dark marking, the power density is q_{s9} = 14.4 × 10^9 W/m^2, v = 50 mm/s and ν = 100 kHz.

- For grey marking, the power density is q_{s8} = 11.3 × 10^9 W/m^2, v = 50 mm/s and ν = 100 kHz.
- For light marking, the power density is q_{s7} = 8.49 × 10^9 W/m^2, v = 200 mm/s and ν = 100 kHz.
- A laser marked QR code of size 3.8 mm, in light marking, was scannable with an electronic device.

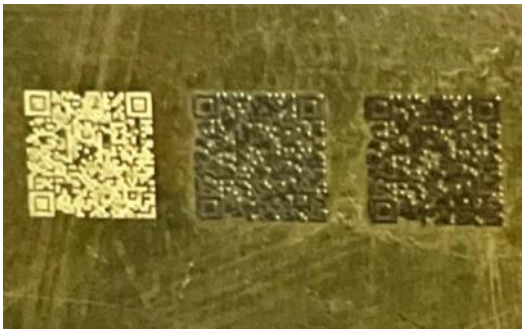

Fig. 9. Obtained QR codes on brass surface – starting from left end, white (light), grey (middle) and dark (right end) marking, respectively.

IV. Conclusions

This publication concerns the influence of some technological parameters for obtaining dark and light marking with a fibre laser simultaneously on one sample for the materials copper and brass. The influence of marking speed, power density, frequency and raster pitch on the contrast k_x^* of the marking is studied. The following results have been achieved:

- Working speed intervals for different power densities for obtaining dark and light marking on copper samples have been determined.
- Working speed intervals for different power densities for obtaining dark and light marking on brass samples have been determined.
- The experimental value of the critical melting power density for different speeds for the two materials has been determined based on finding the limit for obtaining light or dark marking.
- A comparison has been made between the experimental and theoretical values of the critical power density of melting for different speeds.
- Light and dark markings of QR codes have been obtained using optimal technological parameters from the studies.

These results will help to deepen the knowledge of the laser marking process of copper and brass products and the application of these two types of marking in production conditions.

References

[1] N. G. Henriksen, O. Z. Andersen, M. S. Jellesen, T. L. Christiansen and M. A. Somers, "Influence of Laser Marking on Microstructure and Corrosion Performance of Martensitic Stainless-Steel Surfaces for Biomedical Applications, " HTM Journal of Heat Treatment and Materials, vol. 77, no. 3, pp. 177-196, 2022, https://doi.org/10.1515/htm-2022-1010

[2] A. Syakila, M. Jamaludin, M. Quazi, M. Aiman and A. Arslan, Eds., Effect of Laser Parameters on Colour Marking of Ti6Al4V Titanium Alloy, 7th International Conference on Mechanical Engineering Research 2023 (ICMER 2023), Journal of Physics: Conference Series 2688 (2024) 012009, 2024, DOI: 10.1088/1742-6596/2688/1/01200910

[3] K. Kanev, P. Gnatyuk and V. Gnatyuk, "Laser Marking in Digital Encoding of Surfaces," Advanced Materials Research, Vol. 222, pp 78-81, 2021, doi:10.4028/www.scientific.net/AMR.222.78

[4] L. Morawiński, S. Świłło and A. Kocań, Eds., Application of Laser Barcode Technology to Sheet Metal Parts Identification, Scientific Papers of Silesian University of Technology, Organization and Management Series, No. 162, pp. 501-516, 2022, http://dx.doi.org/10.29119/1641-3466.2022.162.27

[5] L. Sobotova and M. Badida, "Laser marking as environment technology, " Open Engineering, 7(1), pp. 303-316, November 2017, DOI: https://doi.org/10.1515/eng-2017-0030

[6] C. Leone, E. Bassoli, S. Genna and A. Gatto, "Experimental investigation and optimization of laser direct part marking of Inconel 718," Optics and Lasers in Engineering, Vol. 111, pp. 154-166, 2018, https://doi.org/10.1016/j.optlaseng.2018.08.004

[7] C. Velotti, A. Astarita, C. Leone, S. Genna, F. Minutolo and A. Squillace, Eds., Laser marking of titanium coating for aerospace applications, Procedia CIRP, Vol. 41, pp. 975-980, 2016, https://doi.org/10.1016/j.procir.2016.01.006

[8] V. Jurčs, E. Yankov, N. Angelov, A. Pacejs and I. Adijāns, Eds., Influence of Technological Parameters on Laser Marking Process of Copper Surfaces, Environment. Technology. Resources. Rezekne, Latvia Proceedings of the 15th International Scientific and Practical Conference. Volume III, pp. 393-398, DOI: https://doi.org/10.17770/etr2024vol3.8179

[9] J. Hlinka and Z. Weltsch, Eds., Analysis of Laser Treated Copper Surfaces, Periodica Polytechnica Transportation Engineering, 47(2), pp. 140-145, 2018, DOI: 10.3311/PPtr.11561

[10] R. Ghalot, l. Lazov, E. Yankov, N. Angelov, "Investigation of the Change in Roughness and Microhardness during Laser Surface Texturing of Copper Samples by Changing the Process Parameters, " Coatings, 13, no. 11, 1970, 2023, https://doi.org/10.3390/coatings13111970

[11] D. Klavins, L. Lazov, A. Pacejs, R. Revalds and E. Zaicevs, Eds., Research of Laser Marking and Engraving on Brass Alloy 260, Proceedings of the 12th International Scientific and Practical Conference: Environment. Technology. Resources, 2019, DOI:10.17770/etr2019vol3.4167

[12] R. Ghalot, L. Lazov, N. Angelov and E. Teirumnieks, Eds., Determination of Preliminary Operating Intervals of Power density for Laser Technological Processes on Copper Samples, Environment Technology Resources: Proceedings of the 15th International Scientific and Practical Conference, Rezekne, 2024, https://doi.org/10.17770/etr2024vol3.8180

[13] "Coherent," [Online]. Available: www.coherent.com. [Accessed 2020].

[14] M. Zervas and C. Codemard, "High Power Fiber Lasers: A Review, " IEEE Journal of Selected Topics in Quantum Electronics, vol. 20, no. 5, 0904123, 2014, DOI: 10.1109/JSTQE.2014.2321279

[15] Duarte F., Tuneable Laser Applications, 3rd ed., CRC Press, 2016, pages 452, ISBN:9781482261073.

Environment. Technology. Resources. Rezekne, Latvia
Proceedings of the 16th International Scientific and Practical Conference. 2025. Volume IV, 481-488

Determination of Preliminary Operating Power Density Ranges for Some Laser Technological Processes on AISI 316 Stainless Steel

Lyubomir Lazov
Rezekne Academy of Riga Technical University
Rezekne, Latvia
lyubomir.lazov@rta.lv

Nikolay Angelov
Department of Mathematics, Informatics and Natural Sciences Technical University of Gabrovo
Gabrovo, Bulgaria
angelov_np@abv.bg

Erika Teirumnieka
Rezekne Academy of Riga Technical University
Rezekne, Latvia
erika.teirumnieka@rta.lv

Artis Teilans
Rezekne Academy of Riga Technical University
Rezekne, Latvia
artis.teilans@rta.lv

Ritvars Revalds
Rezekne Academy of Riga Technical University
Rezekne, Latvia
ritvars.revalds@rta.lv

***Abstract*—Determination of preliminary operating intervals of power density is the first step in optimizing laser technological processes for AISI 316 stainless steel. The study focuses on the laser technological processes of laser marking, laser cutting, and laser welding. Based on the heat conduction equation and the heat balance equation, calculations were performed to determine the critical power density of melting and vaporization at various speeds for the three processes, taking into account the optical and thermo-physical parameters of the material. The results were graphically presented, analyzed, and summarized. Preliminary operating intervals were determined for laser marking through oxidation, melting, and vaporization, as well as for laser cutting and laser welding at different speeds. Our experimental results, along with results from other authors, showed good agreement with the theoretically defined power density intervals for all three technological processes.**

Keywords – Numerical calculations, laser processes, power density, speed.

I. Introduction

In the last few decades, laser technologies have developed very successfully and are constantly expanding their positions in the industry, gradually displacing a number of traditional technologies [1]. Laser systems are used in production for marking, engraving, cutting, welding, drilling holes, hardening, strengthening, sintering, coating, scribing, etc. [2] - [7]. The optimization of such processes is very complex because research is required for different types of materials, types of lasers used, and laser processing methods. For each specific case, real and numerical experiments are conducted to study the influence of the main parameters on the process in order to obtain the required quality of the products and obtain working intervals of these parameters. Both real and numerical experiments have their advantages and place in the research process for laser technologies:

Real experiments provide insight into laser-material interactions and help improve the optimization of laser technological processes. They allow the observation of key physical phenomena, such as the formation of an oxide layer, melt or channels due to evaporation in the impact zone, the generation of splashes and ridges around the impact zone. They also allow direct measurements to be made of the size of the heat affected zone (HAZ), the depth, width and shape of the channels formed during evaporation, the thickness of the oxide layer, the depth and shape of the melt, the surface roughness, the microhardness, and other possible characteristics of the treated area [8] - [10]. Experiments reveal potential safety issues such as the release of harmful substances, harmful fumes and splashes. Many laser processes include real-time monitoring systems (e.g. thermal cameras, pyrometers or high-speed cameras). These measuring instruments provide valuable feedback during experiments that can be used to dynamically adjust parameters and optimize performance. Practical testing ensures that the desired quality standards are met in real applications.

Numerical experiments are a powerful tool for optimizing laser technology processes. They allow for cost-effective, time-efficient, and detailed analysis of process

Online ISSN 2256-070X
https://doi.org/10.17770/etr2025vol4.8391
© 2025 The Author(s). Published by RTU PRESS.
This is an open access article under the Creative Commons Attribution 4.0 International License.

parameters and material behaviour. They are highly cost-effective as they eliminate the need for expensive materials, equipment setup, and physical trial-and-error testing. Energy consumption is minimized as many iterations can be performed virtually. They allow testing of new ideas and projects without significant financial investments. In addition, there is a high time efficiency. Simulations allow for systematic variation, analysis and rapid evaluation of various parameters such as laser power, speed, defocus, repetition rate, pulse duration, etc. compared to physical testing [11] - [12]. They provide detailed insight into laser-material interactions such as temperature field distribution and heat transfer, melting and evaporation dynamics, stress and strain during thermal cycling. Numerical experiments provide good predictive capabilities, such as temperature gradients and heat-affected zones (HAZ), material penetration depths, and melting and vaporization thresholds. It is important to provide a safe testing environment when using numerical experiments, avoiding the health risks to researchers associated with working with high-power lasers or hazardous materials.

It is clear that a combined approach of numerical and real experiments provides better opportunities for optimizing laser technological processes [13]. Numerical experiments allow for fast, cost-effective parameter exploration, while real experiments ensure practical feasibility, accuracy and validation of numerical experiments. Together, they create the opportunity for faster optimization and provide reliable, high-quality and efficient results for industrial applications.

In particular, laser technological processes are widely used in industry for marking, welding and cutting steel products. Research on these laser technological processes is constantly developing and enriching, as there are always enough unexplored areas. The quantities and parameters that influence these processes are different, but can be summarized in three groups related to: the properties of the material (optical and thermo-physical), the laser parameters and the parameters of the technological process. For the three processes, power density and speed are very important, as they are of great importance for delivering the necessary energy to the impact zone during their implementation.

The purpose of this study is to determine preliminary operating ranges of power density for different speeds through numerical calculations for the laser technological processes of marking, welding and cutting for AISI 316 steel (1.4404, 10X17H13M2) and their comparison with real experimental studies for these processes.

II. Materials and methods

A. Material

The research is on an austenitic stainless steel AISI 316, which is widely used in industry. It is characterized by high resistance to acids such as sulphuric acid, acetic acid and citric acid, good tensile strength and ductility, excellent weldability with or without filler materials. It uses welded structures operating in highly aggressive environments, designed for long service life at high temperatures. It has a number of marine applications due to its ability to withstand corrosion in salt water, for example, boat fittings and fasteners, marine architecture components such as railings and ladders, submarine parts and shipbuilding. It is suitable for handling aggressive chemicals and is used to make chemical storage tanks, heat exchangers, pumps and valves in chemical processing systems, components for oil and gas extraction. It is also used for the needs of the food industry in the manufacture of brewing and dairy equipment, food processing machinery, cooking equipment and utensils; in the medical and pharmaceutical industries for the manufacture of surgical instruments, medical implants, pharmaceutical manufacturing equipment; architectural applications; power generation facilities; aerospace industry; automotive industry; water purification systems, etc. The chemical composition of the steel is presented in Table 1. It has a high content of chromium, nickel and molybdenum, which significantly increases its corrosion resistance and mechanically robust. It is necessary to emphasize the importance of molybdenum, which contributes to this steel having significant corrosion resistance in environments that are especially rich in chlorides, and in marine environments.

TABLE 1 CHEMICAL COMPOSITION OF AISI 304 STAINLESS STEEL

Element	**Content, %**	**Element**	**Content, %**
C	0.07	Si	< 1.00
Cr	16.50 – 18.50	P	< 0.05
Ni	10.00 – 13.00	S	< 0.02
Mo	2.00 – 2.50	Cu	< 0.30
Mn	< 2.00	Fe	Balance

Some parameters of AISI 316 steel are given in Table 2. It has relatively small values of thermal conductivity and thermal diffusivity coefficients. The heat is retained close to the heat source, which is beneficial in laser welding, laser cutting and laser marking, as this results in a very small heat affected zone (HAZ) ensuring minimal impact on material properties outside the processed area and is very important for machining precision.

TABLE 2 BASIC PARAMETERS OF AISI 316 STAINLESS STEEL

Parameter	**Value**
Absorption capacity A	0.45
Coefficient of thermal conductivity k, W/(kg.K)	16.3
Density ρ, kg/m^3	7970
Specific heat capacity c, J/(kg.K)	510
Coefficient of thermal diffusivity a, m^2/s	4.01×10^{-6}
Melting point temperature T_m, K	1660
Vaporization temperature T_v, K	3084
Latent heat of melting L_m, kJ/kg	273
Latent heat of evaporation L_v, kJ/kg	7450

B. Laser Systems

The calculations apply to laser technology systems that are used in real production.

Laser technology system for marking is with fiber laser, which is a modern laser operating in the near infrared region. The basic parameters of the laser system are given in Table 3. This laser operates in pulsed mode and has a high frequency and pulse duration in the nanosecond range. It has very high beam quality and high efficiency. The laser system is characterized by high positioning accuracy and a high degree of repeatability.

TABLE 3 SOME PARAMETERS OF LASER SYSTEM FOR MARKING

Parameter	**Value**
Wavelength λ, nm	1064
Power P, W	20
Frequency v, kHz	20 – 50
Pulse duration τ,ns	4 – 200
Pulse energy E_p, mJ	0.1 – 1.0
Pulse power P_p, kW	2.5 – 10
Diameter of work spot d, μm	30
Efficiency, %	40

The laser technological system for welding is with an Nd:YAG laser. This is a solid-state laser emitting in the near infrared region. It operates in pulsed mode. The parameters of the laser system are presented in Table 4. The laser has a low frequency (up to 100 Hz) and a long pulse duration. This makes the laser system suitable for the laser welding process. The positioning accuracy and repeatability of the system are of low values.

TABLE 4 SOME PARAMETERS OF LASER SYSTEM FOR WELDING

Parameter	**Value**
Wavelength λ, nm	1064
Power P, W	500
Frequency v, Hz	1 – 100
Pulse duration τ,ms	1 – 15
Diameter of work spot d, μm	200
Efficiency, %	40

The laser technological system for cutting is with a fiber laser. This is a laser emitting in the near infrared region. It operates in continuous mode. The parameters of the laser system are presented in Table 5. The positioning accuracy of the laser system is high.

TABLE 5 SOME PARAMETERS OF LASER SYSTEM FOR CUTTING

Parameter	**Value**
Wavelength λ, nm	1064
Operating mode	cw
Power P, W	1000
Diameter of work spot d, μm	100
Efficiency, %	40

C. Methods

As noted, speed v and power density q_s are the most important parameters affecting laser technological processes of marking, cutting and welding.

The impact time on the product and the energy absorbed by the material in the impact zone depend on the speed v. The speed requirements are contradictory: on the one hand, the speed must be high in order to reduce the time required to perform the operation and therefore achieve greater efficiency in the production of the product; on the other hand, it must be relatively low in order to absorb the required amount of energy and reach the required temperature for the implementation of the technological process. Considering the other parameters influencing the processes, it is necessary to find a balance between these conflicting requirements and obtain optimal parameters to achieve high product quality.

The power density q_s of the laser radiation is one of the main parameters that determine the changes in the structure or aggregate state of the material in the impact zone. It must be sufficient to absorb the necessary energy in the material and to obtain oxidation, melting or evaporation depending on the technological process. There is a relationship between the power density q_s, the velocity v and the heating temperature T in the impact zone. For a temperature below the melting point, the formula is used

$$q_s = \frac{k(T - T_0)}{2A}\sqrt{\frac{\pi v}{ad}} \qquad (1)$$

where k is the thermal conductivity coefficient, a – thermal diffusivity coefficient, A – absorption capacity, d – diameter of the working spot, T_0 – initial temperature.

In determining the preliminary operating power density ranges for different speeds, the critical melting and evaporation power densities are used. The formulas are obtained by applying the heat conduction equation and the heat balance equation.

For the critical power density of melting, the formula is obtained

$$q_{scm} = \frac{(1+s)k(T_m - T_0)}{2A}\sqrt{\frac{\pi v}{ad}} \qquad (2)$$

where $s = \frac{L_m}{c(T_m - T_0)}$ (3) is a parameter, L_m – specific heat of melting, c – specific heat capacity.

The formula for the critical power density of evaporation is

$$q_{scv} = \frac{(1+s')k(T_v - T_0)}{2A}\sqrt{\frac{\pi v}{ad}} \qquad (4)$$

where $s' = \frac{L_m + L_v}{c(T_m - T_0)}$ (5) is a parameter, L_v – specific heat of evaporation.

The determination of the intervals of change of the power density for oxidation, melting and evaporation occurs in three stages:

1) Calculation of the critical power density of melting q_{scm} and evaporation q_{scv}.

The values of the critical power densities during melting for different speeds are determined by formula (2),

with the speed changing in a certain interval depending on the technological process. The values of the critical evaporation power densities for different speeds are determined by formula (4). Graphs of the dependences of the critical melting power density on speed and the critical evaporation power density on speed are drawn.

2) Determination of the maximum power density q_{smax} for the laser used.

The maximum power density qsmax is calculated using the formula

$$q_{smax} = \frac{4P_{max}}{\pi d^2} \qquad (6)$$

where P_{max} is the maximum power of the laser.

A separate calculation is made for each laser.

3) Determination of the preliminary power density intervals for oxidation, melting and evaporation for the selected laser and material

The results are presented in a suitable table. The first column shows different speeds, the second column contains the power density intervals for oxidation, the third column for melting, the fourth for evaporation. The third and fourth columns show the power density range. These intervals are clearly shown in the graphical images. The oxidation region is below the graph of the dependence of the critical melting power density on the speed. The melting region is between the two graphs. The evaporation region is above the graph of the dependence of the critical power density of evaporation on the velocity and is limited from above by the maximum laser power density.

Some of our experimental results and the results of other authors are plotted on the graphical images and analyzed for consistency with the theoretical results.

III. Results and Discussion

A. Determining preliminary power density operating intervals for the laser marking process

To determine the critical power density of melting, the parameters from Tables 1, 2 and 3 were used. According to formulas (1) and (2), the critical power density of melting was determined for different speeds for AISI 316 stainless steel. The speed was varied from 10 mm/s to 100 mm/s in 10 mm/s increment. The critical power density of evaporation for different speeds was determined from formulas (3) and (4) as the speed was again varied from 10 mm/s to 100 mm/s in 10 mm/s increments. The results are presented graphically in Figure 1. From the analysis of the graphs it follows:

- With increasing speed, there is a nonlinear increase in the critical power density;
- The critical power density of melting varies from 0.063×10^{10} W/m^2 to 0.198×10^{10} W/m^2 for the studied speed interval;
- The critical power density of evaporation varies from 0.590×10^{10} W/m^2 to 1.867×10^{10} W/m^2 for the studied speed interval. The values of the critical power density of evaporation are about 9.50 times higher than those of the critical power density of melting for the corresponding speed. This is because the vaporization temperature of steel is higher than its melting point. Furthermore, the latent heat of vaporization is significantly higher than the latent heat of melting;
- The curve of critical power density of evaporation is much steeper than the curve of critical power density of melting.

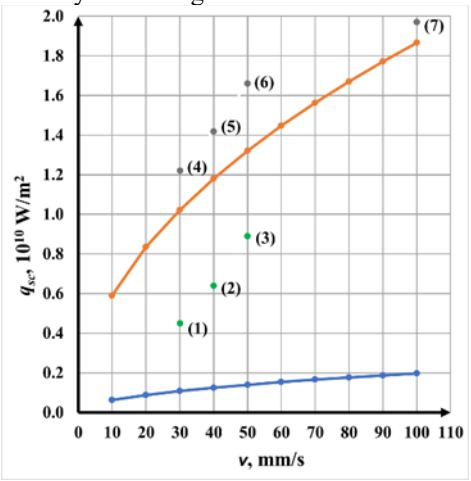

Fig. 1. Graphs of the dependence of the critical power density of melting and evaporation on the speed for AISI 316 steel for the laser marking process.

According to formula (6), the maximum value of the power density of the used laser $q_{smax} = 2.831\times10^{10}$ W/m^2 was determined.

From the obtained results, the preliminary operating intervals of power density for different speeds for AISI 316 steel for the laser marking process by oxidation, melting and evaporation have been determined. The results are presented in Table 6.

TABLE 6 PRELIMINARY OPERATING POWER DENSITY INTERVALS FOR DIFFERENT SPEEDS FOR THE LASER CUTTING PROCESS

***v*, mm/s**	**q_s, W/m^2**		
	Oxidation	***Melting***	***Evaporation***
10	$< 0.063\times10^{10}$	$0.063\times10^{10} - 0.590\times10^{10}$	$0.590\times10^{10} - 2.831\times10^{10}$

v, mm/s	q_s, W/m^2		
	Oxidation	***Melting***	***Evaporation***
20	$< 0.089\times10^{10}$	$0.089\times10^{10} – 0.835\times10^{10}$	$0.835\times10^{10} – 2.831\times10^{10}$
30	$< 0.108\times10^{10}$	$0.108\times10^{10} – 1.022\times10^{10}$	$1.022\times10^{10} – 2.831\times10^{10}$
40	$< 0.125\times10^{10}$	$0.125\times10^{10} – 1.181\times10^{10}$	$1.181\times10^{10} – 2.831\times10^{10}$
50	$< 0.140\times10^{10}$	$0.140\times10^{10} – 1.320\times10^{10}$	$1.320\times10^{10} – 2.831\times10^{10}$
60	$< 0.153\times10^{10}$	$0.153\times10^{10} – 1.446\times10^{10}$	$1.446\times10^{10} – 2.831\times10^{10}$
70	$< 0.166\times10^{10}$	$0.166\times10^{10} – 1.562\times10^{10}$	$1.562\times10^{10} – 0.590\times10^{10}$
80	$< 0.177\times10^{10}$	$0.177\times10^{10} – 1.660\times10^{10}$	$1.660\times10^{10} – 2.831\times10^{10}$
90	$< 0.188\times10^{10}$	$0.188\times10^{10} – 1.771\times10^{10}$	$1.771\times10^{10} – 2.831\times10^{10}$
100	$< 0.198\times10^{10}$	$0.198\times10^{10} – 1.867\times10^{10}$	$1.867\times10^{10} – 2.831\times10^{10}$

We conducted experimental studies on the process of laser marking of AISI 316 stainless steel samples with a fiber laser. Experimental results are presented with green and gray dots in Fig. 1, marked with numbers. These are the parameters that relate to the obtained markings:

for laser marking by melting

Areas are marked with: (1) – $q_s = 0.45\times10^{10}$ W/m^2 and $v = 30$ mm/s, (2) – $q_s = 0.64\times10^{10}$ W/m^2 and $v = 40$ mm/s, and (3) – $q_s = 0.89\times10^{10}$ W/m^2 and $v = 50$ mm/s. The markings are of high contrast, which ranges from 72 % to 67 %.

A good correlation is observed between the experimental values of these regions and the theoretically obtained melting zone located between the two plots in Fig. 1. All green dots are located in this zone.

for laser marking by evaporation

Areas are marked with: (4) – $q_s = 1.22\times10^{10}$ W/m^2 and $v = 30$ mm/s, (5) – $q_s = 1.42\times10^{10}$ W/m^2 and $v = 40$ mm/s, and (6) – $q_s = 1.66\times10^{10}$ W/m^2 and $v = 50$ mm/s. The markings are of high contrast, which ranges from 81 % to 75 %.

All these gray points in Fig. 1 are located above the graph of the theoretical dependence of the critical power density of evaporation on the speed for the studied steel. The experimental data and the preliminary operating intervals of power density for different speeds are consistent.

Some authors also obtain values of power density and speed parameters, which are consistent with the obtained preliminary operating intervals of power density. In the publication of [14], the authors implement laser marking by evaporation with a contrast of the marked area of 79 % at $q_s = 1.97\times10^{10}$ W/m^2 and $v = 100$ mm/s, which corresponds to point number (7) in Fig. 1. The experiments were performed with a fiber laser and for steel 75, which has similar characteristics to those of AISI 316 steel. In article [15], the authors obtain experimental results that are consistent with preliminary operating intervals of power density.

B. Determination of preliminary operating intervals of power density for the laser cutting process

To determine the critical power density of melting and evaporation for AISI 316 stainless steel, the parameters from Tables 1, 2 and 5 were used. Again, as in marking, formulas (1), (2), (3) and (4) are used, with the speed varying from 10 mm/s to 100 mm/s in steps of 10 mm/s. From the obtained numerical calculations, graphs of the dependence of the critical power density of melting and evaporation on the speed for the studied steel for laser cutting were constructed. The following conclusions can be drawn from the graphs:

- A nonlinear increase in the critical power density with increasing speed is observed for the laser cutting process;
- The critical power density of melting is in the interval from 0.034×10^{10} W/m^2 to 0.108×10^{10} W/m^2 for a velocity change from 10 mm/s to 100 mm/s. The critical power density of evaporation varies from 0.323×10^{10} W/m^2 to 1.022×10^{10} W/m^2 for the investigated velocity interval. Again, the critical power density of evaporation is significantly higher;
- The rate of change of the critical power density of evaporation is 7.77×10^7 (W/m^2)/(mm/s), while for

the critical power density of melting it is 0.822×10^7 (W/m^2)/(mm/s).

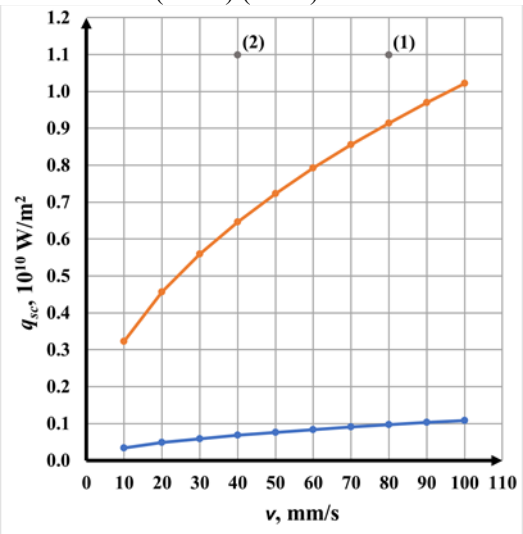

Fig. 2. Graphs of the dependence of the critical power density of melting and evaporation on the speed for AISI 316 steel for the laser cutting process

According to formula (6), the maximum value of the power density of the used laser $q_{smax} = 12.74\times10^{11}$ W/m^2 was determined.

From the obtained results, the preliminary operating intervals of power density for different speeds for AISI 316 steel for the laser cutting process have been determined. The results are presented in Table 7.

TABLE 7 PRELIMINARY OPERATING POWER DENSITY INTERVALS FOR DIFFERENT SPEEDS FOR THE LASER CUTTING PROCESS

v, mm/s	q_s, W/m^2
10	$0.323\times10^{10} - 12.74\times10^{11}$
20	$0.457\times10^{10} - 12.74\times10^{11}$
30	$0.560\times10^{10} - 12.74\times10^{11}$
40	$0.647\times10^{10} - 12.74\times10^{11}$
50	$0.723\times10^{10} - 12.74\times10^{11}$
60	$0.792\times10^{10} - 12.74\times10^{11}$
70	$0.856\times10^{10} - 12.74\times10^{11}$
80	$0.915\times10^{10} - 12.74\times10^{11}$
90	$0.970\times10^{10} - 12.74\times10^{11}$
100	$1.022\times10^{10} - 12.74\times10^{11}$

In the paper [16], the authors investigated the effect of speed at different power densities for cutting AISI 316 steel samples with a fiber laser. The following results were obtained: cutting a 3 mm thick sample with $q_s = 1.11\times10^{10}$ W/m^2 and $v = 80$ mm/s (see point (1) of Fig. 2), and cutting a 4 mm thick sample with $q_s = 1.11\times10^{10}$ W/m^2 and $v = 40$ mm/s (see point (2) of Fig. 2). They are located above the theoretical graph of the dependence of the critical power density of evaporation on speed and laser cutting by evaporation is realized.

C. Determination of preliminary operating intervals of power density for the laser welding process

In the numerical calculations for the laser welding process of AISI 316 stainless steel, the parameters from Tables 1, 2 and 4 were used. Again, as in the other two processes, formulas (1), (2), (3) and (4) were used, with the speed varying from 30 mm/s to 300 mm/s in steps of 10 mm/s. From the obtained numerical calculations, graphs of the dependence of the critical power density of melting and evaporation on the speed for the studied steel for laser welding were constructed. From the analysis of the graphs, the following conclusions can be drawn:

- A nonlinear increase in the critical power density with increasing speed is observed for the laser welding process;
- The critical power density of melting is in the interval from 0.042×10^{10} W/m^2 to 0.133×10^{10} W/m^2 for the speed range from 30 mm/s to 300 mm/s. The critical power density of evaporation varies from 0.396×10^{10} W/m^2 to 1.252×10^{10} W/m^2 for the studied speed interval;
- The rate of change of the critical power density of evaporation is 3.17×10^7 (W/m^2)/(mm/s), while for the critical power density of melting it is 0.337×10^7 (W/m^2)/(mm/s).

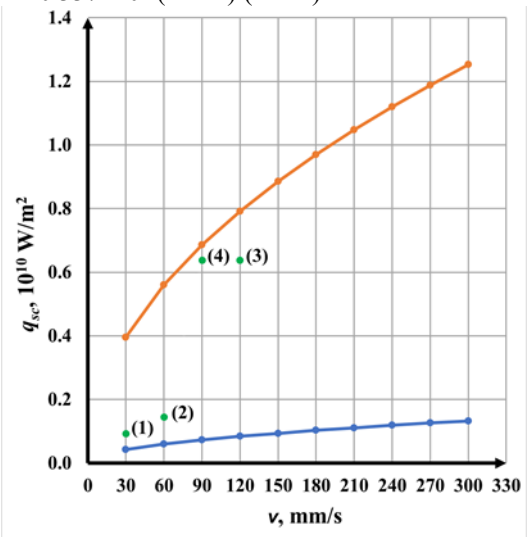

Fig. 3. Graphs of the dependence of the critical power density of melting and evaporation on the speed for AISI 316 steel for the laser welding process

According to formula (6), the maximum value of the power density of the used laser $q_{smax} = 1.592\times10^{10}$ W/m^2 was determined.

From the obtained results, the preliminary operating intervals of power density for different speeds for AISI 316 steel for the laser welding process have been determined. The results are presented in Table 8.

TABLE 8 PRELIMINARY OPERATING POWER DENSITY INTERVALS FOR DIFFERENT SPEEDS FOR THE LASER WELDING PROCESS

v, mm/s	q_s, W/m^2
30	$0.042\times10^{10} – 0.396\times10^{10}$
60	$0.050\times10^{10} – 0.560\times10^{10}$
90	$0.073\times10^{10} – 0.686\times10^{10}$
120	$0.084\times10^{10} – 0.792\times10^{10}$
150	$0.094\times10^{10} – 0.886\times10^{10}$
180	$0.103\times10^{10} – 0.970\times10^{10}$
210	$0.111\times10^{10} – 1.048\times10^{10}$
240	$0.119\times10^{10} – 1.120\times10^{10}$
270	$0.126\times10^{10} – 1.188\times10^{10}$
300	$0.133\times10^{10} – 1.252\times10^{10}$

We conducted experimental studies with a laser system with a diode laser “DF 025” with a wavelength of 808 nm, operating in cw mode. We obtained high-quality laser welding with the following parameters: speed 30 mm/s and power density 9.36×10^8 W/m^2 (see point (1) of Fig. 3) and speed 60 mm/s and power density 14.5×10^8 W/m^2 (see point (2) of Fig. 3). As can be seen from Fig. 3, these points are located between the two curves, which corresponds to a region in which the material is melted. Therefore, there is a complete correspondence between theoretical and experimental results.

In [17], the author Renald Schedewy investigated the laser welding process with a fiber laser on structural steel. The results he obtained were: a weld depth of 2.5 mm at 6.37×10^9 W/m^2 and a speed of 120 mm/s (see point (3) of Fig. 3) and a weld depth of 2.9 mm at 6.37×10^9 W/m^2 and a speed of 90 mm/s (see point (4) of Fig. 3).

IV. CONCLUSIONS

The conducted researches have established the following results:

- Preliminary working intervals of power density were determined for different speeds for different marking methods: by oxidation, which requires lower power density; by melting, which operates at a relatively high power density; by evaporation, which requires even higher power density;
- Preliminary working intervals of power density were determined for different speeds for laser cutting;
- Preliminary working intervals of power density were determined for different speeds for laser welding;
- Consistency of the obtained theoretical results with our and other authors' experimental results was obtained.

The research is a first stage of the optimization of these technological processes on AISI 316 stainless steel. They should continue with experimental and theoretical studies on frequency, pulse duration, effective energy, defocus, etc. The results are of assistance to designers and operators of laser technological systems.

REFERENCES

[1] W. Khan, R. Yasmin, H. Akbar, Eds., Laser Technology: Bridging Historical Milestones and Modern Applications in Science, Industry, and Sustainability, Global Scientific and Academic Research Journal of Multidisciplinary Studies, 2025, pp. 70-84, DOI: 10.5281/zenodo.14770605

[2] M. Chau, "An Overview Study on the Laser Technology and Applications in the Mechanical and Machine Manufacturing Industry," Journal of Mechanical Engineering Research and Developments, 42(5):16-20, August 2019, DOI: 10.26480/jmerd.05.2019.16.20

[3] L. Legres, C. Chamot, M. Varna, A. Janin, "The Laser Technology: New Trends in Biology and Medicine," Journal of Modern Physics, 5(05): 267-279, March 2014, DOI: 10.4236/jmp.2014.55037

[4] A. Stepanov, E. Saukkonen, H. Piilia, Possibilities of laser processing of paper materials, 15th Nordic Laser Materials Processing Conference, Nolamp 15, 25-27 August 2015, Lappeenranta, Finland, Physics Procedia, 78: 138 – 146, 2015, DOI: 10.1016/j.phpro.2015.11.026

[5] T. Ness, "Applications and Advantages of Fiber Laser Technology in the Automotive and Aerospace Industries," International Photonics and Optoelectronics Meetings OSA Technical Digest (online), (Optica Publishing Group, , paper MTh3A.2, 2012, https://doi.org/10.1364/LTST.2012.MTh3A.2

[6] X. Zhang, L. Zhou and G. Feng, "Laser technologies in manufacturing functional materials and applications of machine learning-assisted design and fabrication, " Advanced Composites and Hybrid Materials, 8:76, 2025, https://doi.org/10.1007/s42114-024-01154-4

[7] K. Zhou, S. Sang, C. Wang and Y. Zhou, "Principle, Application and Development Trend of Laser Cleaning, " MMEAT-2022, Journal of Physics: Conference Series, 2383, 012075, 2022, DOI: 10.1088/1742-6596/2383/1/012075

[8] M. Kutsuna and S. Marya, Research and development of laser technology in materials processing, Proceedings of SPIE - The International Society for Optical Engineering, March 2003, 4831:104-109, 2003, DOI:10.1117/12.497939

[9] X. Wang, J. Takács J., G. Krallics and A. Szilagyi, "Experimental research on laser-material interaction, " Periodica Polytechnica Transportation Engineering 28(1), January 2001, https://www.researchgate.net/publication/242194826_Experimental_research_on_laser-material_interaction

[10] M. Pandey and B. Doloi, "Experimental Studies on Laser Marking Characteristics of Stainless Steel 304, " Advances in Modern Machining Processes, 173-184, December 2022, DOI: 10.1007/978-981-19-7150-1_15

[11] O. Ganzulenko and A. Petkova, "Simulation and approbation of the marking laser process on metal materials, " Journal of Physics

Conference Series, 1753(1):012016, February 2021, DOI:10.1088/1742-6596/1753/1/012016

[12] S. Tsirkas, P. Papanikos and T. Kermanidis, "Numerical Simulation of the Laser Welding Process in Butt-Joint Specimens, " Journal of Materials Processing Technology, 134(1):59-69, March 2003, DOI:10.1016/S0924-0136(02)00921-4

[13] G. Rodrigues, J. Pencinovsky, M. Cuypers and J. Duflou, "Theoretical and experimental aspects of laser cutting with a direct diode laser, " Optics and Lasers in Engineering, 61:31–38, October 2014, DOI: 10.1016/j.optlaseng.2014.04.013

[14] P. Tsvyatkov, E. Yankov, L. Lazov and E. Teirumnieks, Investigation of the Influence of Technological Parameters of Laser Marking on the Degree of Contrast, Environment. Technology. Resources. Rezekne, Latvia, Proceedings of the 14th International Scientific and Practical Conference, Volume 3, 370-374, 2024, DOI:10.17770/etr2023vol3.7319

[15] L. Lazov, E. Teirumnieks, Ts. Karadzhov and N. Angelov, "Influence of power density and frequency of the process of laser marking of steel products, " Infrared Physics & Technology, Volume 116, 103783, August 2021, DOI: https://doi.org/10.1016/j.infrared.2021.103783

[16] A. Wetzig, P. Herwig and J. Hauptmann, "Latest Developments of Laser Cutting, " Paper 103, pp. 1-10, https://publica-rest.fraunhofer.de/server/api/core/bitstreams/5e759d65-3018-40c3-94b3-e1409babad52/content

[17] Fraunhofer – Institut fur Werkstoff und Strahltechnik, Jahresbericht 2009, Dresden, 2009, https://www.JB_IWS_2009_de%20(2).pdf

Environment. Technology. Resources. Rezekne, Latvia
Proceedings of the 16th International Scientific and Practical Conference 2025. Volume IV, 489-495

The Impact of CO_2 Laser Treatment on Graphene-Modified KM2-440 Ballistic Kevlar Fabric and Its Property Changes

Jēkabs Lapa
Riga Technical University
Rezekne Academy
Rēzekne, Latvia
jekabs.lapa@gmail.com

Imants Adijāns
Riga Technical University
Rezekne Academy
Rēzekne, Latvia
imants.adijans@rta.lv

Silvija Kukle
Riga Technical University
Riga, Latvia
Silvija.Kukle@rtu.lv

Lyubomir Lazov
Riga Technical University
Rezekne Academy
Rēzekne, Latvia
lyubomir.lazov@rta.lv

Ieva Baķe
Riga Technical University
Riga, Latvia
Ieva.Bake@rtu.lv

Uģis Briedis
Riga Technical University
Riga, Latvia
uģis.briedis@rtu.lv

***Abstract* — This study investigates the laser marking of graphene-modified KM2-440 ballistic Kevlar fabric, exploring how different laser parameters affect its properties. A 1x4 matrix was marked on the fabric using the SUNTOP ST-CC9060 laser system, with each square measuring 30 mm in length and 40 mm in width. Our adjustments to the laser marking parameters encompassed variations in speed and power. Specifically, the speed ranged from 100 mm/s to 150 mm/s, while the power varied between 8.5% and 8.8%. A constant step size (Δx) of 0.08 mm was maintained for all markings. These parameter variations were studied to assess their impact on the fabric's mechanical properties, surface roughness, and durability. Advanced testing methods, including the Olympus LEXT OLS5000 3D Measuring Laser Microscope, were employed to examine the correlation between laser marking parameters and the changes in the fabric's ballistic performance. The findings provide significant insights into the effects of laser processing on the structural integrity and performance of graphene-modified Kevlar fabrics. This research not only contributes to optimizing laser marking parameters for enhanced fabric durability but also offers valuable knowledge on how graphene incorporation affects the ballistic characteristics of Kevlar in the context of laser treatment.**

Keywords* — *laser marking, ballistic Kevlar fabric, graphene-modified,* CO_2 *Laser, laser parameters, mechanical properties, surface roughness.

1. Introduction

In the rapidly advancing field of materials processing, laser technologies have emerged as powerful tools for modifying and enhancing material properties [1]. Over the past decades, lasers have revolutionized traditional processing techniques, offering unparalleled precision, efficiency, and adaptability across various industries, including aerospace, defense, and protective material engineering[2]. Among the numerous laser applications, laser marking and surface modification have gained increasing attention due to their potential to improve material durability [3], mechanical properties, and functional performance.

Recent research has demonstrated the effectiveness of laser treatment in modifying polymeric and composite materials [4], making it a promising approach for enhancing ballistic textiles. CO_2 lasers, in particular, have been widely used for surface structuring and controlled material ablation, leading to alterations in mechanical, thermal, and optical properties [5, 6].

In comparison to conventional mechanical treatments, laser processing offers a contactless, highly controllable, and non-destructive method for modifying ballistic fabrics while preserving their flexibility and structural integrity [7].

Online ISSN 2256-070X
https://doi.org/10.17770/etr2025vol4.8389
© 2025 The Author(s). Published by RTU PRESS.
This is an open access article under the Creative Commons Attribution 4.0 International License.

The integration of graphene into Kevlar-based fabrics represents a novel advancement in the development of next-generation ballistic materials [7]. Graphene, due to its exceptional mechanical strength, electrical conductivity, and thermal stability, has been explored as a reinforcement material in composite applications [8]. However, the challenge remains in effectively incorporating graphene into ballistic Kevlar fabrics while maintaining uniform dispersion and adhesion to the fiber structure [8]. Laser-assisted processing has emerged as a potential technique for enhancing the interaction between graphene and Kevlar fabrics, improving overall material performance.

Current studies on laser-treated graphene-reinforced composites [9] have predominantly focused on metals and rigid polymer structures, with limited research on Kevlar-based ballistic fabrics. The impact of CO_2 laser marking [10] on the microstructural and mechanical properties of graphene-modified KM2-440 ballistic Kevlar fabric remains largely unexplored. By understanding how laser parameters such as power and scanning speed affect the fabric's structural integrity [11], surface roughness, and durability, this study seeks to bridge the knowledge gap in laser-assisted modification of ballistic materials [12].

The objective of this research is to investigate the effects of CO_2 laser processing on graphene-modified KM2-440 ballistic Kevlar fabric, analyzing how different laser parameters influence material properties. A 1×4 matrix was laser-marked using the SUNTOP ST-CC9060 laser system, with varying power (8.5%–8.8%) and scanning speed (100 mm/s–150 mm/s), while maintaining a constant step size of 0.08 mm. To evaluate the laser-induced modifications, advanced characterization techniques, including the Olympus LEXT OLS5000 3D Measuring Laser Microscope, were utilized to assess surface roughness, microstructural changes, and potential improvements in ballistic performance.

The findings of this study will contribute to the development of more durable and impact-resistant ballistic materials [13], advancing protective equipment design for military and law enforcement applications [14, 15]. By optimizing laser processing parameters, this research aims to enhance the structural stability and longevity of graphene-enhanced Kevlar fabrics, ultimately leading to stronger, lighter, and more effective protective armor equipment.

II. Materials and Methods

A. Materials Characteristics

This study focused on an experimental examination a graphene-modified para-aramid ballistic fabric.

The technological limitations of laser processing are primarily influenced by the anticipated effects of the process and the inherent structural characteristics of the material being processed [19], alongside the varying properties of both the substrate and the material itself [19]. The fundamental structural component of Kevlar® consists of a backbone composed of para-oriented benzene rings [19], which facilitates the formation of rod like molecular structures, subsequently leading to the formation of liquid crystalline polymers [19].

Kevlar® KM2+ high modulus fibres woven plain weave fabric style 310 is used (Producer SAATI, Italy). 440 dtex thread density 14 cm^{-1} in warp and weft direction. Fabric thickness 0.17mm, areal density 128 g/m2. The longitudinal Young's modulus of the Kevlar® KM2 fibre is 84.62±4.18 GPa, the ultimate strength of 3.88±0.40 GPa with a failure strain of 4.52%±0.37% and diameter measured using a scanning electronic microscope 12 μm [18] The physical dimensions of the specimen were 100 × 100 mm, with a single-layer thickness of approximately 0.30 mm.

Prior to experimentation, the Kevlar fabric underwent a thorough surface cleaning procedure, including soaking in acetone (2 hours), washing and drying, to eliminate any surface contaminants and finishing agents [7]. This ensured optimal adhesion of the graphene layer to the fabric surface. Subsequently, graphene nanoplatelets were introduced by fabric dip-coating and followed thermal consolidation [7, 8]. This technique was followed by thermal curing at 60°C for 1 hour to promote strong chemical bonding between the graphene coating and the Kevlar fabric surface [7], thereby enhancing the mechanical and electrical properties of the fabric [7, 8].

B. Laser setup

The laser setup used in the experiments was based on the CO_2 Suntop ST-CC9060 system, as shown in Figure 1. Operating with a wavelength of 10640 nm, this continuous-wave (CW) laser system is capable of reaching a maximum power of 100 W. The laser's workspace spans 900 x 600 mm, providing a large area for operation. The precision of the system is maintained at 0.02 mm, ensuring high accuracy during the process. The scan speed of the laser can be adjusted from 0 to 1000 mm/s, depending on the specific needs of the experiment. A water-cooling system was employed to maintain the laser's optimal operating temperature. The laser is classified as Class 4 for safety, requiring proper precautions during use.

It supports data formats including Dxf, bmp, and ai for flexible input options. The total power consumption of the system is 1500 W, ensuring sufficient energy for its high-performance capabilities.

Fig. 1. CO_2 SUNTOP ST-CC9060.

Specification for SUNTOP ST-CC9060 is shown in Table I.

TABLE I. PARAMETERS OF SUNTOP ST-CC9060

Parameter	Magnitude, Unit
Wavelength (*λ*)	10640 nm
Max. Power (*P*)	100 W
Operation mode	CW
Workspace	900 x 600 mm
Precision	0,02 mm
Scan speed	0 – 1000mm/s
Laser Safty Class	4
Cooling system	Water cooling
Data formats	Dxf, bmp, ai
Total power	1500 W

C. Microscope setup

To analyze the surface properties and modifications of the Kevlar KM2-440 ballistic fabric specimens, a 3D laser microscope, specifically the Olympus LEXT OLS5000, was employed, as shown in Figure 2. The microscope operated at a magnification of 451x, ensuring a measurement precision of 0.4 µm. The key technical specifications included a numerical aperture (N.A.) of 0.6, a working distance (W.D.) of 1 mm, a focal depth of 1.8 µm, and a focusing spot diameter of 0.82 µm. The device was capable of measuring an area of 640 × 640 µm, allowing for detailed surface analysis of the Kevlar fabric.

Fig. 2. Olympus LEXT OLS5000 3D Measuring Laser Microscope.

E. Experimental Method

Laser marking was conducted on a Graphene-Modified KM2-440 Ballistic Kevlar Fabric sample with dimensions of [180 x 50 mm] using a CO_2 SUNTOP ST-CC9060 laser. The sample surface remained in its original state without additional cleaning or treatment prior to marking. The marking process involved the creation of a single matrix comprising four rows and one marking.

The laser marking parameters were meticulously adjusted, incorporating a speed of 150 mm/s, power ranging from 8.5% to 8.8%, and a constant step size (Δx) of 0.08 mm for all markings. Specifically, for the first marking, power (P) was set to 8.8%, speed (V) to 150 mm/s, and step size (Δx) to 0.08 mm; for the second marking, P = 8.5%, V = 150 mm/s; for the third marking, P = 8.8%, V = 100 mm/s; and for the fourth marking, P = 8.5%, V = 100 mm/s. The experiments were conducted under ambient conditions without the use of assist gases. The laser marking of the Graphene-Modified KM2-440 Ballistic Kevlar Fabric plate was performed by varying two critical parameters: power (P) in watts and scanning speed (V) in mm/s. Figure 3 illustrates the marking schematics utilized in the experiments.

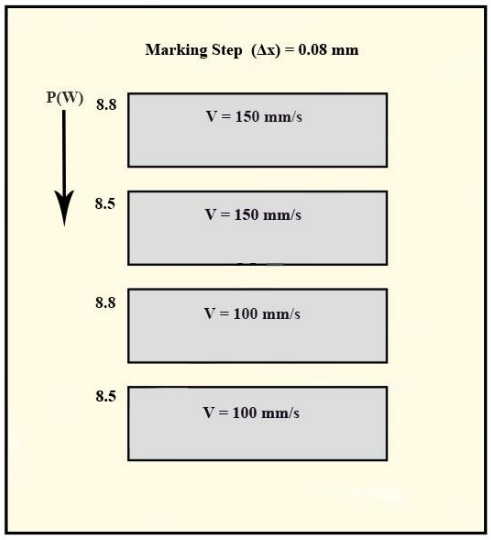

Fig. 3. Laser marking schematics of GRAPHENE-MODIFIED KM2-440 BALLISTIC KEVLAR FABRIC.

In this study, a single matrix was employed, consisting of four rows and one marking, as detailed in Table II. No variations in frequency were introduced. This approach facilitates a comprehensive investigation of the laser marking process, with a particular emphasis on the influence of speed and power settings while maintaining a consistent pulse duration.

TABLE II. CO_2 LASER MARKING PARAMETERS FOR GRAPHENE-MODIFIED KM2-440 BALLISTIC KEVLAR FABRIC

Parameter	Magnitude, Unit
Step size *(Δx)*	0,08 mm
Output Power (*P*)	8.8\8.5\8.8\8.5 %
Scanning Speed (*v*)	150\150\100\100 mm/s
Square Size	30×40 mm

Equation (1) was used to convert the laser power from % to W.

$$P(W) = \frac{P(\%) * P_{max}}{100\%} \quad (1)$$

The computed laser power values, derived from the corresponding percentage settings, are systematically presented in Table III to illustrate the precise power outputs utilized in the experimental process. Additionally, the table includes the corresponding speed values to provide a comprehensive overview of the relationship between power and speed.

TABLE III. POWER AND SPEED CHART

	Test 1	**Test 2**	**Test 3**	**Test 4**
***P* (W)**	8.8	8.5	8.8	8.5
V(mm/s)	150	150	100	100

The contrast factor (K_X) is determined as a percentage value, representing the difference between the unmarked and laser-marked areas [16].

The volume of (K_X) requires assessing the volume of the unmarked region, denoted as (N_f) [17], while the value (N_X) is obtained directly from the laser-marked region. The equation used for this computation is given as follows in Equation (2):

$$K_X = \frac{N_F - N_X}{N_F} \times 100\% \quad (2)$$

To analyze the difference between measured points, a three-dimensional space-based approach is employed. The total difference for the laser-marked region (N_X) is calculated using equation (3):

$$N_x = \sqrt{(\Delta L_x)^2 + (\Delta a_x)^2 + (\Delta b_x)^2} \quad (3)$$

Similarly, the total difference for the unmarked region, (N_f), is expressed in equation (4):

$$N_f = \sqrt{(\Delta L_f)^2 + (\Delta a_f)^2 + (\Delta b_f)^2} \quad (4)$$

In these equations, ΔL, Δa, and Δb represent specific measured variations in the material's response. These values are obtained through analytical evaluation, ensuring precise differentiation between the marked and unmarked areas.

To maintain consistency in contrast assessment, absolute values (K_X)are applied to prevent negative contrast values from affecting result interpretation.

III. RESULTS AND DISCUSSIONS

Surface roughness measurements (Sq, in µm) were conducted on samples processed using varying laser parameters, alongside an unmarked reference surface. Each condition was evaluated at five measurement points to assess surface structure and the influence of processing parameters. The resulting data, including roughness, standard deviation, and percentage change relative to the unmarked surface, are presented in Table IV.

TABLE IV. SURFACE ROUGHNESS SUMMARY (SQ, SD, % CHANGE)

Condition	**Roughness (µm)**	**Std Dev (µm)**	**Change vs Unmarked (%)**
8.8% – 150 mm/s	6.12	0.62	+1.09
8.5% – 150 mm/s	6.20	0.88	+2.39
8.8% – 100 mm/s	5.78	0.69	-4.57
8.5% – 100 mm/s	6.82	0.44	+12.67
Unmarked surface	6.05	0.74	0.00

The unmarked surface exhibited roughness of 6.057 µm, with a standard deviation of 0.746 µm, representing the natural baseline texture of the material without any laser-induced modification.

Among the laser-marked samples:

- At 8.8% power and 150 mm/s, the mean roughness was 6.123 µm, showing a 1.09% increase compared to the unmarked surface.
- At 8.5% power and 150 mm/s, the roughness increased further to 6.201 µm (+2.39%), suggesting that even a slight reduction in power at a constant speed may lead to more significant surface alteration.
- At 8.8% power and 100 mm/s, the roughness decreased to 5.780 µm, a −4.57% change compared to the unmarked baseline. This indicates that slower scanning speed at the same power level may result in a smoother surface morphology.

The most significant increase in roughness was observed at 8.5% power and 100 mm/s, where the surface reached 6.824 µm, corresponding to a 12.67% increase over the unmarked surface. This condition appears to result in the most pronounced topographical modification shown in Figure 4.

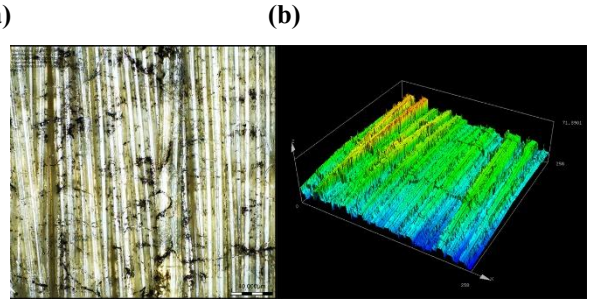

Fig. 4. Surface Morphology of Laser-Marked Graphene-Modified KM2-440 Ballistic Kevlar Fabric at 8.5% Power and 100 mm/s Scanning Speed Showing the Most Pronounced Increase in Surface Roughness Compared to the Unmarked Material.

These findings demonstrate that both laser power and scanning speed are critical roles in determining the final surface characteristics. Notably, the combination of lower power and slower speed have pointed to the highest roughness values, likely due to increased thermal interaction intervals and greater energy deposition per unit area. Conversely, higher power combined with slower scanning speed did not always result in greater roughness, pointing to non-linear relationship influenced by factors such as material absorption threshold and heat dissipation.

Variations in standard deviation across the tested conditions reflect differences in surface consistency. For instance, the 8.5% – 150 mm/s condition exhibited the highest variability, with a standard deviation of 0.882 µm, indicating less consistency in surface texture across the measurement points. In contrast, the 8.5% – 100 mm/s sample showed the most consistent surface, with a lower standard deviation of 0.446 µm, indicating a more homogeneous and consistent surface texture.

In conclusion, the results show that even relatively small changes in laser processing parameters such as slight variations in power or scanning speed—can lead to measurable differences in surface roughness and texture. These differences may significantly affect surface functionality, particularly in materials like Kevlar where surface performance is critical. Therefore, precise control and optimization of laser parameters are essential for ensuring repeatable and application-specific surface properties in laser-marked graphene-modified ballistic materials.

In addition to changes in surface roughness, laser marking also alters the optical properties of the material, particularly surface contrast. Contrast is a factor for the visual detection and readability of the marked features, especially in applications requiring high traceability or optical scanning shown in Figure 5.

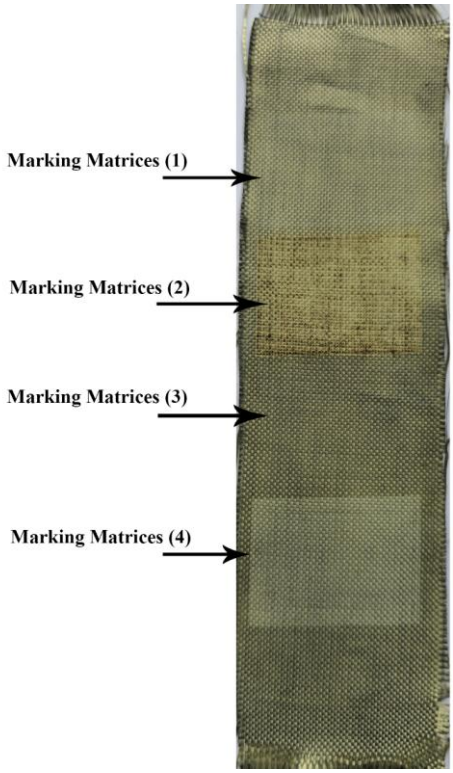

Fig. 5. Laser-Marked Graphene-Modified KM2-440 Kevlar Fabric Showing Four Distinct Marking Matrices (1) – (4).

The image shows a graphene-modified KM2-440 Kevlar fabric with four laser-marked regions labeled (1) through (4). The photo was taken using 8K-resolution camera, clearly capturing the contrast between the marked areas and the surrounding unmarked surface. These visible differences allow for visual evaluation of how laser processing parameters affect surface appearance and marking visibility.

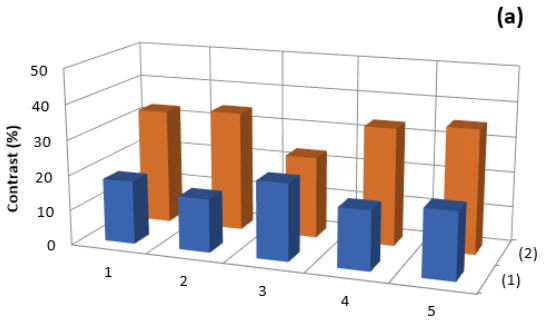

Fig. 6. Contrast Response at Multiple Surface Points on Laser-Marked Matrices (1) and (2).

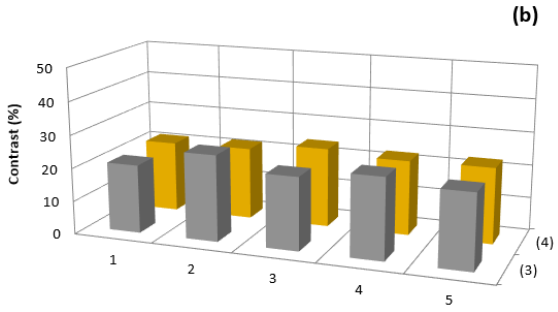

Fig. 7. Contrast Response at Multiple Surface Points on Laser-Marked Matrices (3) and (4).

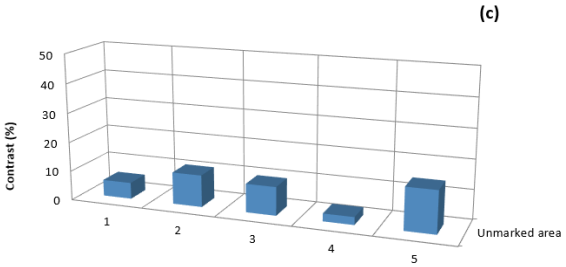

Fig. 8. Contrast Response at Multiple Surface Points on Unmarked Area.

To further evaluate the visual impact of laser processing, contrast levels were analyzed at five distinct surface points across four laser-marked matrices shown in Figure 5, as well as on the unmarked reference area. The calculated contrast values revealed clear differences between treated and untreated zones, indicating that laser parameters significantly influence surface visibility and markings.

The unmarked region exhibited a mean contrast of 33.30%, serving as the baseline for comparison. Among the laser-marked matrices, Matrix (2) shown in Figure 5 demonstrated the highest mean contrast at 50.23%, corresponding to a 50.84% increase over the unmarked surface. This result suggests that the parameter combination used for matrices (2) produced the most optically distinctive surface modification shown in Figure 9.

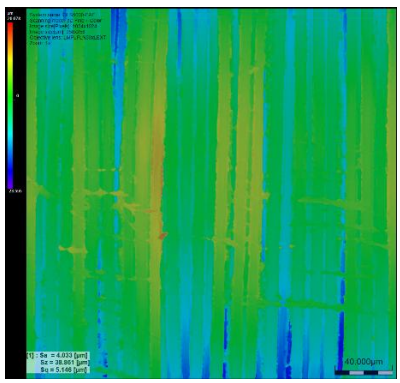

Fig. 9. High-Contrast Surface Modification on Graphene-Modified Kevlar (Matrix 2).

Microscopic examination of Matrix (2) (Figure 9) revealed significant surface alterations, including localized melting and the fusion between the graphene coating and the KM2-440 ballistic Kevlar fabric.

This suggests that the high energy density applied in this region enhanced the interaction between the coating and the substrate, contributing to the observed increase in contrast and altered surface morphology.

The contrast improvements are likely attributable to thermally induced effects, such as microstructural rearrangement, which influence light absorption and reflectivity. These changes highlight the role of thermal interaction in defining the optical response of laser-treated surfaces.

Matrix (1) exhibited a moderate mean contrast of 40.26%, corresponding to a 20.90% increase over the unmarked region. Matrices (3) and (4) showed similar contrast values of 43.88% and 43.45%, equating to 31.77% and 30.48% increases, respectively. These results confirm consistent contrast enhancement across all marked zones, though the effect was most pronounced in Matrix (2).

IV. Conclusions

In this study, we investigated how CO_2 laser treatment affects surface roughness and contrast in graphene-modified KM2-440 ballistic Kevlar fabric. The findings revealed that laser power and scanning speed can significantly alter the fabric's surface characteristics, particularly at low laser power outputs. The highest increase in surface roughness, specifically 12.67%, was observed at a laser power setting of 8.5% combined with a scanning speed of 100 mm/s. These results highlight the importance of precise laser parameter optimization, as excessive laser power can damage the surface structure of fabric-based materials.

References

[1] X. Zhang, Y. Liu, and Z. Wang, "Microstructure and properties of laser cladding CoCrNi-based medium-entropy alloy enhanced by Nb," Journal of Materials Research and Technology, vol. 14, no. 3, pp. 1234-1245, Feb. 2025, doi: 10.1016/j.jmrt.2025.02.100.

[2] S. A. Ahmed, M. Mohsin, and S. M. Z. Ali, "Survey and technological analysis of laser and its defense applications," Defence Technology, vol. 16, no. 1, pp. 1-12, Jan. 2020, doi: 10.1016/j.dt.2020.02.012.

[3] Ł. Łacho, "Recent Advances in Laser Surface Hardening: Techniques, Modeling Approaches, and Industrial Applications," Crystals, vol. 14, no. 8, pp. 726, Aug. 2024, doi: 10.3390/cryst14080726.

[4] S. J. Lim, J. Cheon, and M. Kim, "Effect of laser surface treatments on a thermoplastic PA 6/carbon composite to enhance the bonding strength," Composites A: Applied Science and Manufacturing, vol. 137, pp. 105989, Jun. 2020, doi: 10.1016/j.compositesa.2020.105989.

[5] K. Czyż, J. Marczak, R. Major, A. Mzyk, A. Rycyk, A. Sarzyński, and M. Strzelec, "Selected laser methods for surface structuring of biocompatible diamond-like carbon

layers," Diamond and Related Materials, vol. 68, pp. 44-52, Mar. 2016, doi: 10.1016/j.diamond.2016.01.013.

[6] S. Ravi-Kumar, B. Lies, H. Lyu, and H. Qin, "Laser Ablation of Polymers: A Review," Procedia Manufacturing, vol. 39, pp. 601-608, 2019, doi: 10.1016/j.promfg.2019.06.155.

[7] Kukle, S., Bake, I., & Abele, L. (2024). Graphene-containing para aramid fabric coating via surfactant assisted exfoliation of graphite. Materials Today: Proceedings, 97, 44-51. https://doi.org/10.1016/j.matpr.2023.09.131.

[8] L. Li, M. Zhou, L. Jin, L. Liu, Y. Mo, X. Li, Z. Mo, Z. Liu, S. You, and H. Zhu, "Research Progress of the Liquid-Phase Exfoliation and Stable Dispersion Mechanism and Method of Graphene," Frontiers in Materials, vol. 6, pp. 325, Jun. 2019, doi: 10.3389/fmats.2019.00325.

[9] L. Groo, J. Nasser, L. Zhang, K. Steinke, D. Inman, and H. Sodano, "Laser induced graphene in fiberglass-reinforced composites for strain and damage sensing," Composites Science and Technology, vol. 196, pp. 108367, Jan. 2020, doi: 10.1016/j.compscitech.2020.108367.

[10] M. Ueda, Y. Saitoh, H. Hachisuka, H. Ishigaki, Y. Gokoh, and H. Mantani, "Studies on CO2 laser marking," Applied Surface Science, vol. 42, no. 2, pp. 121-126, Dec. 1990, doi: 10.1016/0143-8166(90)90020-A.

[11] D. Simson and S. Kanmani Subbu, "Effect of Process Parameters on Surface Integrity of LPBF Ti6Al4V," Procedia CIRP, vol. 108, pp. 698-703, Mar. 2022, doi: 10.1016/j.procir.2022.03.111.

[12] S. Wu, P. Sikdar, and G. S. Bhat, "Recent progress in developing ballistic and anti-impact materials: Nanotechnology and main approaches," Defence Technology, vol. 18, no. 6, pp. 1301-1310, Jun. 2022, doi: 10.1016/j.dt.2022.06.007.

[13] S. Wu, P. Sikdar, and G.S. Bhat, Recent progress in developing ballistic and anti-impact materials: Nanotechnology and main approaches. Defence Technology, 2023, 21, pp. 33-61. https://doi.org/10.1016/j.dt.2022.06.007

[14] W. Zou, Recent advancements in ballistic protection - a review. Journal of Student Research, 13(1), 2024. https://doi.org/10.47611/jsrhs.v13i1.5936

[15] J. Shi, H. Li, F. Xu, and X. Tao, Materials in advanced design of personal protective equipment: A review. Materials Today Advances,2021, 12, 100171. https://doi.org/10.1016/j.mtadv.2021.100171

[16] L. Lyubomir, N. Pavels and D. Hristina, "Laser Marking Methods", Technology. Resources, 2015, Volume I, 108-115, pp. 109-112., 2015.

[17] K. McLAREN, XIII—The Development of the CIE 1976 (L* a* b*) Uniform Colour Space and Colour-difference Formula, vol. 92, Journal of the Society of Dyers and Colourists, 1976, pp. 338-341.

[18] B. Sanborn, A. M. Dileonardi, and T. Weerasooriya, "Tensile properties of Dyneema SK76 single fibers at multiple loading rates using a direct gripping method," Journal of Dynamic Behavior of Materials, vol. 1, no. 1, pp. 4-14, Mar. 2014, doi: 10.1007/s40870-014-0001-3.

[19] S. J. Picken, D. Sikkema, H. Boerstoel, and S. Van der Zwaag, "Liquid crystal main-chain polymers for high-performance fibre applications," Liquid Crystals, vol. 38, no. 11-12, pp. 1591-1605, Nov. 2011, doi: 10.1080/02678292.2011.624367.

Environment. Technology. Resources. Rezekne, Latvia
Proceedings of the 16th International Scientific and Practical Conference. 2025. Volume IV, 497-501

Comparative Analysis of the Effectiveness of the Application of UAV and Conventional Ground Equipment for Plant Protection Measures in Sunflower Cultivation

Pavlina Mihaylova
dept. "Economics"
Agricultural University – Plovdiv
Plovdiv, Bulgaria
p_mihaylova@au-plovdiv.bg
ORCID: 0009-001-7432-6455

Yulia Varadinova
dept. "Technology, Organization and Management of Transport"
University of Transport "Todor Kableshkov"
Sofia, Bulgaria
jvaradinova@vtu.bg

Georgi Komitov
dept. "Agricultural Mechanization"
Agricultural University – Plovdiv
Plovdiv, Bulgaria
gkomitov@au-plovdiv.bg
ORCID: 0000-0002-4701-4499

***Abstract*— The use of various means of transport for plant protection measures in agriculture is not new. Its application increases productivity and reduces the cost of growing a variety of products. Conventional ground transport vehicles are self-propelled sprayers or those attached to agricultural tractors. The sprayed solution is stored in a container until it is applied or prepared on site. Inconveniences are created by the transfer of a large amount of detergent, its movement on uneven terrain, the processing of small and specific fields, the change of the working solution, etc. An alternative option is the use of unmanned vehicles – ground or in the air. They have their advantages and disadvantages. Their use is related to the implementation of a number of regulatory documents. However, they give autonomy to producers and enter more and more widely in agriculture. This article aims to compare the costs of using different means of transport as energy sources used for plant protection measures. As an example, when obtaining quantitative values, a sunflower crop typical for the country was used. In addition to standard costs, an attempt has been made to compare the carbon footprints of the use of different means of transport. The sensor part is made of standard soil moisture sensors, and the control part is entrusted to a single-board computer with the ability to control via a wireless network.**

Keywords — agricultural machinery, means of transport, UAV, costs, carbon footprint.

I. INTRODUCTION

Sunflower is one of the most economically important field crops grown in Bulgaria [1]. The popularity of sunflower is growing due to its numerous positive qualities. In addition to the known nutritional qualities, it has the ability to react to various environmental factors, has a shortened development cycle, and is resistant to dry environments. All this makes it attractive for production by a number of farmers [2,3].

The implementation of plant protection measures aims to prevent the destructive losses of pests, weeds and diseases of agricultural crops [4]. Practices to combat them include distancing the host, destroying or reducing the pest or weed, improving resistance and direct protection of plants [4,5]. Known plant protection practices applied against diseases, cultural practices, physical, biological and chemical control are part of the applied pest and weed control methods [4,5].

Plant protection measures are part of the production costs of a farm [6]. The data from these events in many cases support product providers or administrations to improve policy development, administrative decisions or market efficiency. A number of farmers are also using the data to improve the economic performance of their farms. Apart from this, they are able to analyse and compare their activities with the leaders in the region and make informed decisions about future actions [5,6].

This article aims to compare the use of different machines for plant protection measures, thus separating the separate values of operating costs, additional costs and product costs. The obtained values for the machines used will be compared and recommendations for their use will be given depending on the size of the farm.

Online ISSN 2256-070X
https://doi.org/10.17770/etr2025vol4.8387
© 2025 The Author(s). Published by RTU PRESS.
This is an open access article under the Creative Commons Attribution 4.0 International License.

II. MATERIALS AND METHODS

The comparative study was carried out in the land of the village of Biser, Harmanli Municipality. The fields that were cultivated were sown with sunflower by ET "Rossi-Zlatka Koleva". The fields were selected with almost identical conditions and uniformly distant access from the plant. The specified time for moving the machine to the field and back from the base is 0.333 h.

Fig. 1. General appearance of the Pantera 4502 self-propelled sprayer.

There are three machines used for plant protection measures. One is a self-propelled sprayer AMAZONE Pantera 4502 (Fig. 1) [7]. The spraying range is 24 m. The sprayer is equipped with a tank of 4800 l, the spray speed is 3.06 m/s. Fuel consumption is determined when performing plant protection operations 6 l/ha. When moving from the base and back, a flow rate of 19.2 l/h is determined.

Fig. 2. General view of the greenhouse.

The second machine for plant protection measures is the AMAZONE UG2200 sprayer [8]. The working width of the sprayer is 24 m, and the capacity of the detergent tank is 2400 l. The sprayer is used in a machine-tractor unit together with a CLAAS Arion 520 tractor [9]. During the operation of the unit, a consumption of 10 l/h was reported, a spray speed of 2.2 m/s. When moving, the unit reported a consumption of 22 l/h.

Fig. 3. XAG P40 drone when spraying sunflower.

The third plant protection machine used in the current experiment is the UAV XAG P40 (Fig. 3) [10]. The capacity of the detergent tank is 22 l, and the flight time is 0.197 h. The speed of the operations performed is 5 m/s, and the transport to the loading site is fixed at 7 m/s. The working width of spraying from the drone is 4.5 m. In this way, minimal overlap and optimal operation of the drone are guaranteed.

The reported time for charging and returning to the breakpoint is 0.033 h. When the battery is connected to the charging unit, it starts automatically and stops when the battery is fully charged. A flow meter is installed on the fuel line, which reads 0.58 litres per battery charge. The movement of the drone to the field is carried out by pickup and is reported as additional costs, and movement from the base to each field and return.

The price of fuel is averaged and reported according to [11] as of 17.04.2024, diesel is €1.43, and gasoline is €1.38. The fuel consumed by the self-propelled sprayer and the tractor are recorded with flow meters to fuel, after reworking their fuel system according to [12].

The reported cleaning time of the machines after each operation is 0.333 h. For UAV, this time is 0.167 h, because the detergent capacity is 22 l.

According to the adopted methodology, the hourly rate of the workers operating and maintaining the machines (tractor driver) is 6 €/h, of the UAV pilot and the agronomist is 10 /h. This operation is performed by the agronomist for 0.083 h or 0.83 €.

The machines are set to the specified working speed and the time for each operation is recorded by a XINJIE XJ-011 stopwatch, with an accuracy of 1/100 s.

The labour for each operation LO is calculated by the dependence (1):

$$LO = TO.HW \quad (1)$$

In (1) TO is time to operation, measured in hours and HW is the hourly rate of the worker, evaluated in €/h.

Two plant protection measures were carried out with products authorized for use in the EU. According to EU regulations, these products are a second professional category – it requires a specialist who has a certificate for working with plant protection products. The products are

used once. Two treatments are required on each field – one for each product.

One event was held for perennial and annual cereal weeds with the product Tornado 5EK, at the beginning of April at a rate of 2.0 l/ha. More than 14 economically important weeds have been controlled. The product has been applied in the 3-5 leaf phase of the weed. The price of the product is 9.72 €/l.

The other plant protection product with which the event was carried out was MAZA 4SL [13,15]. The product was applied in the third ten days of April at a rate of 1.25 l/ha and a price of 29.67 €/l. The product was applied in phase 4-6 leaf of the weed and controlled over 24 economically important weeds.

The cost of products or fuels is defined as the product of the amount of product or fuel consumed (in litres) and the corresponding cost per litre.

On average, the value of each indicator is defined as the sum of the individual values for the different fields.

The total values of the area costs are determined as a quotient of the total costs and the sum of the area of cultivation.

III. Results and discussion

The results of the experiments are shown in Table 1-5 and figure 4. The indications in the tables are as follows: F is number of fields, A is the area of the fields, FC – fuel consumption, P 1 and P 2 – plant protection products, T – time to operation, L – labor for operation.

In Table 1 contains the data from the experiment using the XAG P40 plant protection drone.

TABLE 1 Experimental data from plant protection measures with XAG P40 drone

F	A, ha	FC, l	P 1, l	P 2, l	T, h	L, €
1	4.38	2.32	8.76	5.48	0.691	6.91
2	2.43	1.16	4.86	3.04	0.35	3.5
3	1.61	0.58	3.22	2.01	0.197	1.97

Extremely low fuel consumption (FC) is noticeable. This is due to the fact that the generator turns on automatically when the battery is plugged into it and turns off when the battery is charged. It is noticeable that four charges of the drone's battery are required. The fuel consumed to charge the batteries is 2.32 l when processing field 1 and 0.58 l when processing field 3 (F). The consumed plant protection products (P 1 and P 2) are according to the manufacturer's norm. It was found that the time for spraying with a drone in larger areas increases with the times for loading and flying to the place of interruption of the operation. Accordingly, the areas treated with the drone per hour decrease. This reduction for the current experiment is 1.84 ha. The operation of the drone in the air depends on various factors, with the strongest influence being the amount of product consumed, the shape of the field and weather conditions. The operational time (T) of the drone in field 1 is 0.691 h, and in field 3 it is 0.197 h per treatment. In all machines for plant protection measures, the times are repeated for each field when processing with different products and therefore in the primary data it is given only for the performance of one operation.

In each working machine, the operating speed of movement and the amount of sprayed solution per ha can be set. A work computer in each machine monitors the correct implementation of the set process parameters.

The cost of labour to carry out the individual operations is impressive because of the high hourly rate of labour. This is due to the need for qualified personnel for ground and air operations. At the same time, these personnel have the necessary qualifications to work with category 2 products. The labour costs (L) of processing the individual fields in operations carried out with a field 1 drone are €6.91, and for field 3 are €1.97.

The experimental data from the plant protection measures carried out with the self-propelled sprayer AMAZONE Pantera 4502 are shown in Table 2. The increased fuel consumption (FC) and the minimum time for operations are impressive. The highest consumption was found in the largest field 1 – 31.2 l. Due to the large volume of the product tank, the fields are processed without additional loading. There are no differences in the time for performing individual operations. The cost of labour (L) to perform operations here is much lower, due to the specific category of labour of operators. In field 1, the cost of labour is 1.18 €, and in field 3 it is 0.22 €.

TABLE 2 Experimental data from plant protection measures with AMAZONE Pantera 4502

F	A, ha	FC, l	P 1, l	P 2, l	T, h	L, €
1	5.2	31.2	10.2	6.5	0.197	1.18
2	3.68	22.08	7.36	4.6	0.139	0.83
3	0.96	5.76	1.92	1.2	0.036	0.22

The analysis of the data from the implementation of plant protection measures with the UG 2200 sprayer shows the highest fuel consumption again at field 1 - 61 l (Table 3). The lowest consumption was found at field 3 - 12.1 l. An increase in the fuel consumption of the machine-tractor unit by almost twice compared to the self-propelled sprayer and the huge difference compared to the drone is impressive. This difference is due to the specifics of the individual machines. to charge the batteries, while the UG 2200 sprayer is dependent on the power machine. It has its own specifics and is universally applicable, while other machines for plant protection measures are strictly specific and cannot be used for any other purpose. As for the cost of labour to perform individual operations, there is a slight increase compared to the self-propelled sprayer. This finding can be explained by the lower productivity of this machine compared to the self-propelled sprayer. The labour cost of using the UG 2200 sprayer is lower than that of using a don, due to the shorter processing time and lower hourly cost of the operator's labour. The highest cost of

labour is in field 1 of €1.92 and the lowest in field 3 of €0.36.

TABLE 3 EXPERIMENTAL DATA FROM PLANT PROTECTION MEASURES WITH AMAZONE UG 2200

F	A, ha	FC, l	P 1, l	P 2, l	T, h	L, €
1	6.1	61	12.2	7.63	0.32	1.92
2	2.97	29.7	5.94	3.71	0.16	0.96
3	1.21	12.1	2.42	1.51	0.06	0.36

The average values from the experiments of plant protection measures in sunflower cultivation are shown in Table 4.1 and Table 4.2. Table 4.1 presents the data on fuel consumption (FC) in euros for the operation (O) and the additional costs (A) of moving the machines. It also gives the price in euros of plant protection products (PC). There is a lower operating cost when using a drone compared to conventional sprayers. This is due to the lower costs of carrying out operations and the lower value of additional costs, such as transporting the machines to the fields and cleaning the tanks for plant protection products. Conventional machines use the independent movement of machines to the field, while drones rely on small vehicles with low fuel consumption. Reducing fuel costs will reduce the carbon footprint generated by sunflower production. The cost of plant protection products depends solely on the consumption rate of the product per ha. The differences in costs found in this column are due to the different area of the fields.

TABLE 4.1 AVERAGE VALUES OF THE CONDUCTED EXPERIMENTS

Machine	A, ha	F C, €		P C, €	
		O	A	P 1	P 2
XAG P40	8.42	11.21	4.99	163.68	312.43
Pantera 4502	9.84	168.85	54.86	189.35	364.94
UG 2200	10.28	294.00	62.86	199.84	381.26

TABLE 4.2 AVERAGE VALUES OF THE LABOR COST

Machine	A, ha	Labor cost, €	
		O	A
XAG P40	8.42	24.76	24.99
Pantera 4502	9.84	4.46	17.98
UG 2200	10.28	6.48	17.98

Table 4.2 shows the data on labour costs when performing the operations. In terms of labour costs, higher costs, both operational (O) and additional (A), are noticeable when using a drone.

The higher costs are due to the higher qualification of drone operators and the longer duration of drone operations. The drone operator is also a vehicle driver and moves the drone to the fields, while his hourly labour rate is higher.

TABLE 5 COMPARATIVE ANALYSIS OF THE RESULTS OF THE EXPERIMENT

Machine	Total cost, €	Total cost per area, €/ha
XAG P40	542.06	64.38
Pantera 4502	800.44	81.35
UG 2200	962.42	93.62

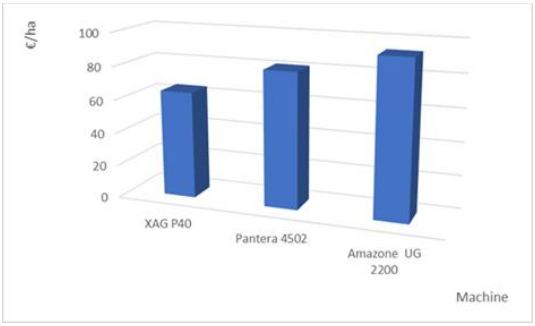

Fig. 4. Consumption per ha when growing sunflower crops.

The analysis of Table 5 and Fig. 4 shows that the cost per ha of growing sunflower crops is the lowest when using a drone and the highest when using a sprayer in a machine-tractor unit. These costs are respectively €64.38 and €93.62.

Using a self-propelled sprayer would reduce these costs by €12.27. With the total cost of growing sunflowers, the use of a drone will cost €540.06 for the current study. According to it, the total cost of using a self-propelled sprayer is €800.44, and for a sprayer in a machine-tractor unit, it is €962.42.

IV. CONCLUSIONS

The lowest costs in growing sunflower crops are obtained when using a plant protection UAV. With it, the fuel costs are to charge the batteries and move it to the fields. However, the use of the drone is limited to small fields and irregularly shaped fields, due to the limited volume of its tank for plant protection products and due to the need to constantly charge the batteries. On this basis, the operating time and the cost of skilled labour increases.

The use of self-propelled plant protection machines significantly shortens the time for carrying out events. Labour costs are minimal, but there are increased fuel costs. It is used in very large fields with large areas close to each other. With self-propelled plant protection machines, the constant additional filling of the plant protection tank is not necessary.

Sprayers, which are part of a machine-tractor unit, are a suitable option for carrying out plant protection measures for medium and small farms, where the high costs of growing sunflower crops are compensated by the lack of an additional expensive self-propelled plant protection machine or UAV.

REFERENCES

[1] N. Neshev, D. Balabanova, M. Yanev and A. Mitkov, Is the plant biostimulant application ameliorative for herbicide-damaged

sunflower hybrids?, Industrial Crops and Products, 182, DOI: 114926. 10.1016/j.indcrop.2022.114926, 2022.

[2] F. Fernández-Luqueño, F. López-Valdez, M. Miranda-Arámbula, M. Rosas-Morales, N. Pariona and R. Espinoza-Zapata, An Introduction to the Sunflower Crop, Sunflowers, chapter 1, Nova Science Publishers, ISBN: 978-1-63117-347-9, 2014.

[3] R. Andrew, N. Kane, G. Baute, C. Grassa and L. Rieseberg, Recent nonhybrid origin of sunflower ecotypes in a novel habitat, Mol Ecol 22(3), 2013,pp. 799-813.

[4] I. Yildirim, Plant Protection Practises and Their Impact on Environment, Journal of Central European Green Innovation, 11 DOI:10.33038/jcegi.3399, 2023, pp. 25-38.

[5] R. Oliveira, U. Antuniassi, A. Mota, and R. Chechetto, Potential of adjuvants to reduce drift in agricultural spraying, Engenharia Agrícola, Vol. 34, DOI: 10.1590/S0100-69162013000500010, 2013, pp. 986-992.

[6] Global Strategy to Improve Agricultural and Rural Statistics, Handbook on Agricultural Cost of Production Statistics, Handbook and Guidelines, Rome, 2016.

[7] Amazone pantera self-propelled sprayer, MI6390, AMAZONEN-WERKE H. DREYER GmbH & Co. KG, 09.2017.

[8] Amazone UG special/super, MI5501, AMAZONEN-WERKE H. DREYER GmbH & Co. KG, 11.2015.

[9] CLAAS Arion 600-500, New standarts up to 180 hp, 331012130909 KK Be 0110, CLAAS UK, 2014.

[10] P40 Agricultural drone. User manual, V. 1.4, Guangzhou Xaircraft Technology CO., LTD, 2022.

[11] Fuel price in Bulgaria https://bg.fuelo.net/calendar/month/2024/04 [Accessed: March 1, 2025]

[12] E. Kehayov, K. Pigoznis, G. Stanchev and G. Komitov, Determination of greenhouse gases emitted by machine-tractor unit by fuel consumption, 5th International Conference on Communications, Information, Electronic and Energy Systems (CIEES), DOI: 10.1109/CIEES62939.2024.10811183, V. Tarnovo, 2024.

[13] List of agricultural products and active substance, https://preparati.info/preparat/TORNADO/279. [Accessed: February 15, 2025].

[14] Tornado 5EK, https://zenithcropsciences.com/wp-content/uploads/2018/01/LABEL_TORNADO-5-EC.pdf. Accessed: April 04, 2025].

[15] Maza 4% SL, Information safety form, V 1.0/BG, 12/03/2018.

Environment. Technology. Resources. Rezekne, Latvia
Proceedings of the 16th International Scientific and Practical Conference. 2025. Volume IV, 503-510

Laser Surface Transformation Hardening with High-Power Diode Lasers

Normunds Teirumnieks
Bulgaria University of Transport
„Technique and construction technologies in transport" Faculty
Sofia, Bulgaria
normunds.teirumnieks@gmail.com

Lyubomir Lazov
Engineering Center
Rezekne Academy of Riga Technical University
Rezekne, Latvia
lyubomir.lazov@rta.lv

Emil Yankov
Engineering Center
Rezekne Academy of Riga Technical University
Rezekne, Latvia
emil.yankov@rta.lv

Edmunds Teirumnieks
Engineering Center
Rezekne Academy of Riga Technical University
Rezekne, Latvia
edmunds.teirumnieks@rtu.lv

Prodan Prodanov
Center of competence; Smart mechatronic, eco-and energy-saving systems and technologies; Faculty of Electrical
Engineering and Electronic
Technical University of Gabrovo,
Gabrovo, Bulgaria
pprodanov@tugab.bg

Artis Teilans
Engineering Center
Rezekne Academy of Riga Technical University
Rezekne, Latvia
artis.teilans@rtu.lv

***Abstract*—Laser Surface Hardening (LSH) is an advanced technique applicable to a wide range of metals and alloys in modern industrial manufacturing, including the automotive sector. Among the various laser types used for hardening, CO_2, solid-state Nd: YAG, and fibre lasers have traditionally been the most common. However, with the development of high-power diode lasers (HPDLs), these have increasingly gained prominence in this field. In the LSH process, high-intensity laser radiation is focused on a localized area, rapidly heating and hardening the material's surface. The steep temperature gradients resulting from rapid heating and cooling induce structural transformations within the treated area. Additionally, the phase transformation from austenite to martensite occurs without the need for external cooling, simplifying the process. This review paper outlines the fundamental principles of laser hardening and its advantages over conventional hardening techniques. Key process parameters and influencing factors are discussed, along with a comparative analysis of LSH against other hardening methods. Furthermore, an overview of experimental research in this area is provided, with a particular focus on HPDL-based hardening. Various methods for analysing and evaluating laser-treated surfaces are also examined.**

***Keywords*— Austenite, High-Power Diode Laser, Laser surface hardening, Martensite, Phase Transformation.**

I. Introduction

Since its inception in the 1970s, laser technology has undergone rapid and exponential growth, with several scientific laboratories, researchers and scientists around the world working in this field today [1]. This growth is due to the unique properties of different types of laser sources, which are essential for modern industrial technologies. These properties include coherence, monochromaticity, high energy density in the processing area and a wide range of laser wavelengths, spanning from the ultraviolet to the infrared region of the electromagnetic spectrum. A prerequisite for this diversity is the different active media (gas, liquid, semiconductor and solid materials) for generating laser radiation with different wavelengths, output power levels and applications. The most used lasers in industry are CO_2, Nd: YAG, fibre lasers and diode lasers [1] – [4]. This diversity and these advantages form the basis for various industrial applications of laser technology, including machining, cutting, welding, drilling, ablation and marking/texturing (Fig. 1).

Surface modification methods such as laser texturing, laser hardening and laser cladding have found wide application in mechanical engineering, medical technology, aeronautics and military applications in recent years. It is well known that various techniques are also used by researchers to improve surface properties such as surface

Online ISSN 2256-070X
https://doi.org/10.17770/etr2025vol4.8392
© 2025 The Author(s). Published by RTU PRESS.
This is an open access article under the Creative Commons Attribution 4.0 International License.

hardness, wettability, friction and wear resistance for laser surface treatment. With the advent of Industry 4.0, laser hardening technology is expanding and developing in new ways, including the use of artificial intelligence (AI).

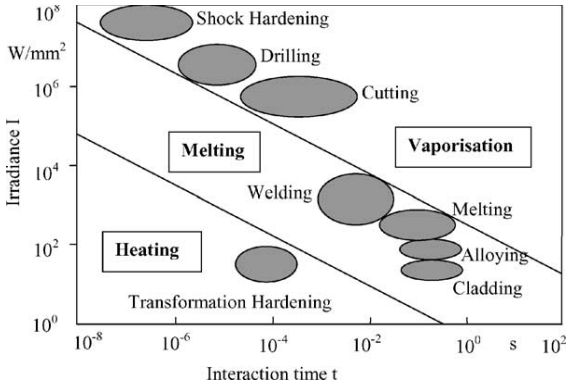

Fig.1. Possible industrial applications of lasers at different interactions of laser radiation with matter [5].

Laser surface hardening, an innovative technology, has become established because the process produces a hardened, wear-resistant outer layer without affecting the desired bulk properties such as toughness and ductility. Compared to other techniques such as induction, arc and flame hardening, the laser hardening process is characterized by short hardening times, easy automation and the ability to harden any part with complex geometry.

Surface hardening is essential for enhancing the performance and functionality of metal products across a wide range of industries. The use of laser technology to modify surface properties has unlocked significant potential for improving mechanical strength, wear resistance, corrosion protection, and even biocompatibility [6].

Recent advancements in laser hardening methods, particularly in surface engineering, have broadened the scope of applications. These innovations have yielded remarkable practical results and paved the way for exciting new possibilities in industrial and technological applications [7] – [13].

Modern high-power semiconductor lasers, due to their unique characteristics such as small size, high efficiency, are today an important factor in surface hardening technology. Laser hardening technology is increasingly being adopted in various industrial sectors including automotive, aerospace, defence and renewable energy systems such as wind turbines, etc. [14] [15].

The stable and successful development of laser surface treatments, including laser hardening, is based on several key advantages they offer compared to conventional technologies [16] – [22]:

- Precise temporal and spatial distribution of directed electromagnetic (laser) energy in the processing area.
- Energy-efficient and material-efficient processes.
- Flexibility to control and manage processing parameters - such as laser power, beam size, and laser scanning speed - to achieve the desired surface and subsurface characteristics.
- High-speed processing and high productivity.
- Minimal heat-affected area (HAZ) and distortion.
- Capability to achieve unique surface properties and a fine microstructure in depth.
- Environmentally friendly, green technology.

II. MATERIALS AND METHODS

Laser hardening is a surface treatment process in which a moving laser beam rapidly heats the laser-affected area above the critical solid-state transformation temperature but below the melting temperature, where the ferrite-to-austenite phase transformation occurs. As illustrated in Fig. 2, the material adjacent to the laser absorption area acts as a heat sink, rapidly cooling the surface through thermal conduction. This effect enables self-hardening, facilitating the transformation of austenite into martensite. As a result, the laser hardening process creates hard, wear-resistant regions on the metal surface while preserving mechanical properties such as strength and ductility [23] – [24].

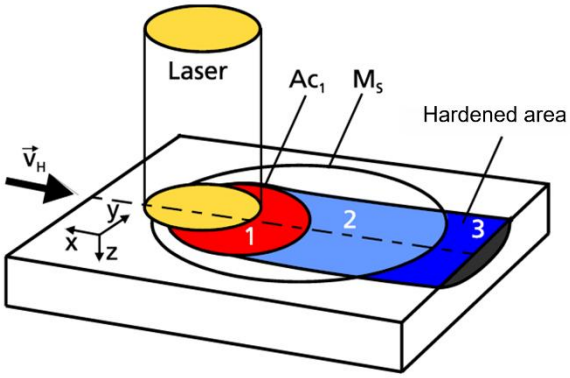

Fig.2. Principle scheme of laser hardening: V_H - the speed at which the laser beam moves; area (1) austenite structure; area (2) - austenite is supercooled; area (3) martensitic structure formation.

Austenite forms from an aggregate structure of pearlite-ferrite in hypoeutectoid steel or pearlite-cementite in hypereutectoid steel. During the heating phase, the body-cantered cubic (BCC) structure of α-iron transforms into the face-cantered cubic (FCC) structure of γ-iron.

In equilibrium transformation, austenite begins to form at temperature Ac_1 (723°C) in carbon steel and completes at the Ac_3 line (A_{CM}), as shown in Fig. 3 [25]. Due to the high heating rate in laser hardening, the transformation curve may shift significantly from the equilibrium state, causing the Ac_3 line to move toward higher temperatures. To achieve sufficient homogenization of austenite above the Ac_3 (A_{CM}) temperature, process parameters are typically adjusted to attain high peak temperatures. However, since a short thermal cycle can lead to insufficient carbon diffusion, the degree of carbon homogenization in the parent material significantly affects the carbon distribution within the martensite and the resulting hardness profile [26].

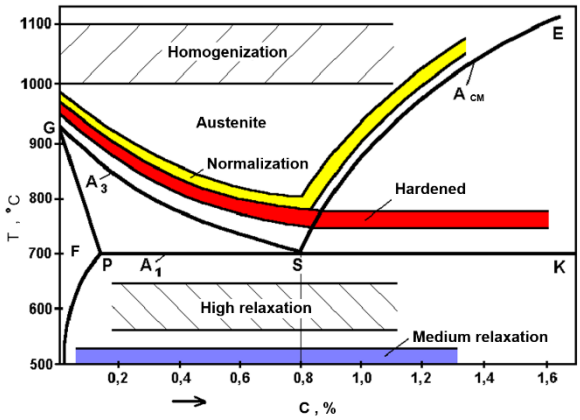

Fig.3.Diagram of surface hardening of steel [25]

Martensitic structure formation occurs exclusively through rapid cooling of austenite, necessitating that the material reaches the austenitization temperature during the heating phase. The thermal cycle in laser surface hardening is much shorter than in bulk hardening, as heating to the austenitization temperature takes place within fractions of a second. Consequently, the heated area must remain above the austenitization temperature long enough for carbon diffusion and austenite homogenization to occur, while ensuring that the surface temperature stays below the material's melting point [27].

Characteristics of HPDLs

The properties of modern high-power diode lasers (HPDLs) make them particularly suitable for use in the technological hardening process. This is due to the following characteristics that this type of lasers has Fig. 4.

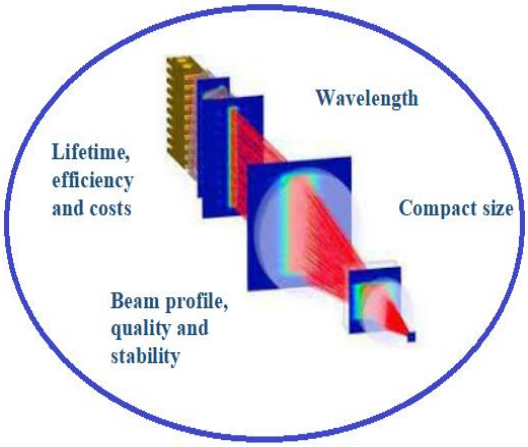

Fig.4. Specific properties of high-power diode lasers (HPDLs) that make them useful for the laser hardening process.

The wavelength λ of the laser radiation generated by most industrial HPDLs is between 800 and 940 nm. These wavelengths λ for most lasers in this range have a lower reflectivity than the surface of the processed metals (see. Fig. 5) Due to their shorter wavelength λ, this type of lasers has a significantly higher degree of absorption already at the start of the laser interaction with the substance.

For example, comparisons of HPDL λ = 800 nm with CO2 lasers λ = 10.6 µm and Nd: YAG lasers λ = 1.06 µm show a significantly higher absorption rate of approximately 1.2 – 13 % when processing various metals [29].

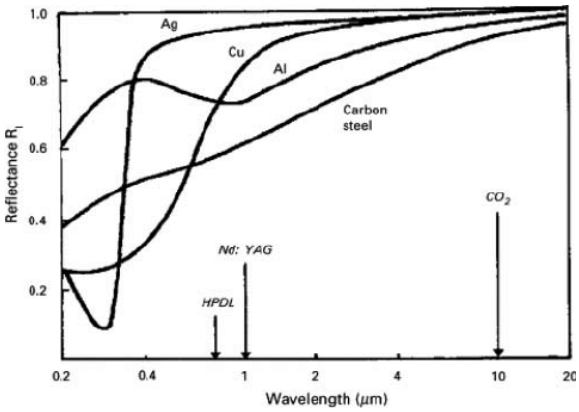

Fig.5. Reflectivity as a function of wavelength for various materials.[28].

According to analyses by World Star Tech - industry-leading laser, the typical laser diode lifetime is between 25,000 and 50,000 operating hours, which is a good indicator of an industrial laser system. The maintenance and operating costs of HPDL are also less than those of competing laser types.

According to analyses by World Star Tech, a leading laser manufacturer, the typical diode life is between 25,000 and 50,000 operating hours, which is a good indicator for an industrial laser system. The maintenance and operating costs of HPDLs are also lower than those of CO_2 and Nd: YAG lasers. While for these lasers the maintenance period varies between 1000 and 200 hours, HPDLs are virtually maintenance-free [30].

The diode laser is the most efficient of all laser types, its typical electrical to optical efficiency is 50 – 65 %, as compared to 10 – 15 % for CO_2, 4 – 5 % for Nd: YAG (arc-pumped) lasers, and 13 – 15 % for Nd: YAG diode-pumped lasers [31] – [33]. The capital costs of HPDLs are also currently lower than CO_2 and Nd: YAG lasers of equivalent power (see Fig. 6).

Due to the nature of the design and their compact size, HPDLs can be relatively easily integrated into conventional machining centres or on robot arms. This is mainly due to the reduced cooling requirements of diode lasers compared to other types of lasers, i.e. HPDLs are significantly more compact than CO_2 and Nd: YAG lasers [30].

The beam profile of an HPDL is typically a rectangular spot due to the nature of the beam and the laser generation process. The typical beam quality of, for example, a 4 kW high-power diode laser (HPDL) when collimated with fibres is about 20 – 30 mm/mrad. HPDLs with specialized beam shaping optics can reach 4 – 10 mm/mrad, but this comes at the expense of a higher cost. One of the main differences between HPDL systems and other laser sources is the number of laser beams generated at the output. In CO_2

and Nd: YAG active medium laser systems, only one beam is generated at the output. In this type of laser, small variations in the excitation time of the laser active medium lead to intensity fluctuations, visible as uneven peaks in the beam profile. In the HPDL system, we have many superimposed laser beams, which compensates for fluctuations in the individual beams, giving the combined beam exceptional modal stability [34].

III. FACTORS INFLUENCING THE PROCESS

The production of a martensitic structure requires a temperature-dependent transformation of the crystal structure of the steel, which redistributes the carbon content during the thermal cycle. Since martensite is obtained exclusively by rapid cooling of austenite, the austenitization temperature must be reached already in the heating phase. The thermal cycle in laser surface hardening is much shorter than that of bulk hardening, heating to the austenitization temperature occurs in fractions of a second. A specific feature here is that the heated area must be maintained above the austenitization temperature for a relatively long enough period to allow carbon diffusion and homogenization of the austenite. The heated surface must be maintained below the melting point of the material [23], [27].

The realization of this extremely complex process depends on the interrelationship between three groups of factors shown in Fig. 6. The factors related to the laser source, the technological process, and the optical and thermophysical properties of the material as a function of the temperature and wavelength of the laser radiation.

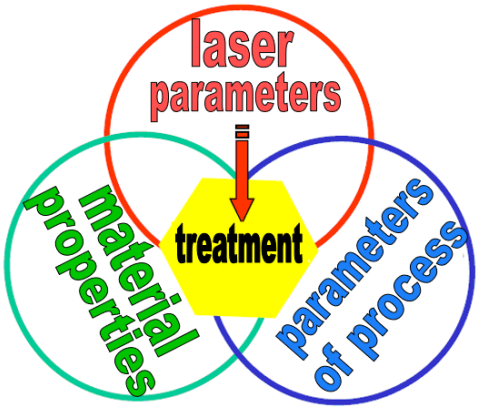

Fig.6. The factors influencing the process of transformation hardening under laser treatment.

A. Wavelength

Fig. 5 provides a clear comparison of the absorption characteristics of different metals as a function of wavelength. The graph shows that CO_2 laser treatment (λ = 10.6 µm) has relatively low efficiency, with absorption rates of approximately 2 – 5 %. To mitigate this limitation during hardening, a special coating is often applied to the surface before treatment to enhance laser energy absorption [35], [36].

B. Laser Power and Laser Power Density

Studies have shown that the laser power required for surface hardening varies from a few watts to several kilowatts, depending on the material type and processing speed. The laser power density used in hardening typically ranges from 10^3 to 10^5 W/cm² [37], which is relatively low compared to other laser-based processing techniques (see Fig. 7).

For steels with high hardenability, a lower laser power density combined with a longer interaction time is recommended to achieve a uniform hardened layer with significant depth. In contrast, for steels with low hardenability, a higher laser power density and shorter interaction time are preferred to ensure the rapid cooling necessary for martensite formation, albeit at the cost of a shallower hardened layer [38], [39].

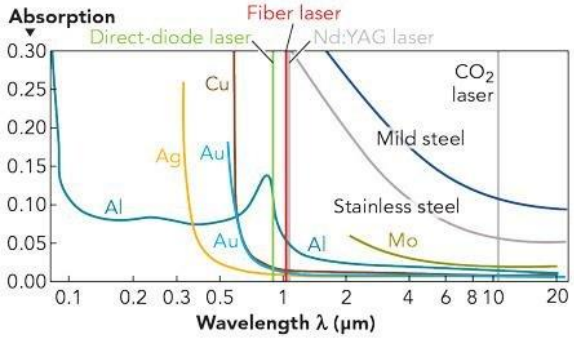

Fig.7. Radiation of laser absorbed varies the wavelength for different metals [40].

C. Different Laser Beam Geometry and Power distribution

Distribution The shape of the heated area in the material usually resembles the function of the intensity distribution in the cross section after the exit of the focusing optics. For example, if the power distribution is Gaussian, then such an effect usually creates a hemispherical hardened area in the material. When working with a rectangular laser beam formed by the optics, a uniform power distribution is created on the surface of the material, and the hardened section also has a rectangular shape with rounded edges. For a given power density and traverse speed, there is an optimal range of beam widths that can produce a large, hardened width without surface melting [41].

A variety of optical solutions can be used to meet specific customized requirements in the practice of laser hardening. Many engineering solutions in design use rotationally symmetric laser beams, which are created by defocusing optics. Shaping optics are also used to provide various shapes of hardened sections with desired high coverage levels (see Fig. 8)

The aspect ratio (ratio of width to length) can be varied to obtain the desired thermal cycle and cross-sectional geometry. A high aspect ratio results in a fast thermal cycle and a wide hardened track. Uniform power distribution across the beam profile includes maximum depth of hardening, depth uniformity, and degree of coverage. Ring and Gaussian beam profiles minimize distortion, but the latter can cause melting in the centre.

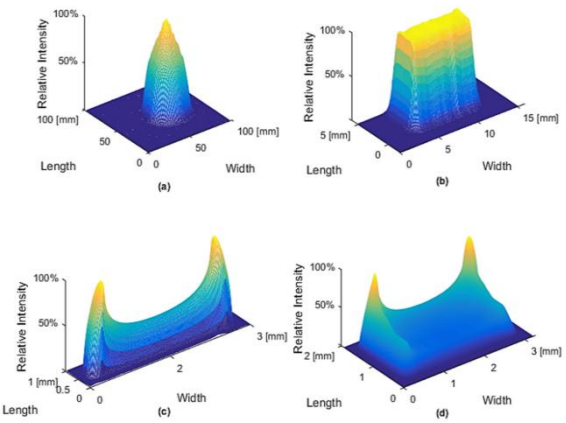

Fig. 8. For laser hardening, four intensity profiles are commonly used. The defocused round top-hat profile (a); the rectangular top-hat profile (b); the intensity profile generated by a harmonic oscillation of a scanning mirror (c) as well as the optimized intensity profile which was calculated by Burger [42].

The optimal power distribution across the heating pattern should include a leading edge with high power density, with power decreasing toward the trailing edge. This is beneficial to the hardening process because it provides a thermal cycle with sufficient time for microstructural homogenization, while also providing a cooling rate high enough to form martensite. This model also minimizes the energy required per unit volume of hardened section [43], [44].

D. Process Parameters in Laser Hardening

a) PROCESS SPEED: The laser irradiation time is inversely proportional to the speed of travel over the material surface. A laser power density in the range of 10^3–10^5 W/cm², with a typical interaction time of 0.1–0.3 seconds, can produce a martensite structure in steel. The speed is a critical parameter that is finely adjusted to achieve the desired hardening depth and homogeneity of the treated surface. Knowing the laser spot diameter and the travel speed, the interaction time can be easily calculated. Additionally, by understanding the power density and exposure time, the hardening process can be accurately modelled and optimized [45].

b) PROCESS GAS: During laser hardening, surface oxidation can significantly increase the absorption of laser energy. This effect was observed by the authors [46] when comparing the hardening of steel in argon and air. Argon and nitrogen are commonly used as process gases. The gas is typically directed at the material surface at a flow rate of approximately 20 L/min through either a coaxial or external nozzle [36], [37]. The process gas serves two primary functions in laser transformation hardening:

- Protection against oxidation – Prevents excessive absorption, which could lead to overheating or melting.
- Optical system protection – Shields the laser optics from contamination during processing.

IV. Results and Discussion

Analysis of laser hardened area is essential for assessing the efficiency and overall effectiveness of the technological process. By studying the microstructural and tribological properties of engineered surfaces, valuable insights can be obtained into the relationship between structural and functional [47]. These insights inform solutions aimed at optimizing the laser hardening process. This section highlights the main characterization methods used to evaluate this innovative technology and allows for comparison with conventional techniques (Fig. 9 and Fig. 10).

A. Micro-structural analysis

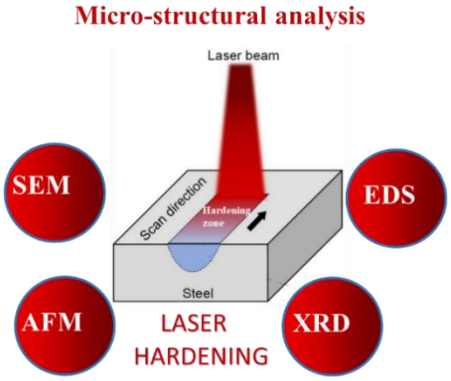

Fig. 9. Different methods for micro-structural analysis of laser transformation hardened area.

Scanning Electron Microscopy (SEM) and Energy-Dispersive Spectroscopy (EDS) Analysis

Scanning electron microscopy (SEM) is a widely used technique for surface microstructural analysis, offering high-resolution images that reveal details of grain structures and phase transitions in the hardened area. To further enhance the analysis, energy-dispersive X-ray spectroscopy (EDS) can be integrated with SEM, allowing the investigation of the elemental composition in the laser-treated surface. This powerful combination provides a comprehensive set of tools for in-depth analysis of laser-treated area. SEM provides important morphological information, helping to understand the relationship between microstructure and material properties. EDS complements this by identifying and quantifying the elemental composition, which is particularly valuable for optimizing post-laser cooling processes in the treatment area. Together, these techniques provide a holistic understanding of the morphology, composition, and overall characteristics of samples after laser treatment, offering insights that are essential for refining and optimizing the laser hardening process [48].

X-ray Diffraction (XRD) Analysis

X-ray diffraction (XRD) is a vital tool for analysing the phase composition and crystallographic structure of the laser-treated area. By examining the diffraction patterns produced by X-ray radiation, detailed insights into the

crystal lattice and atomic arrangement within the treated surface are obtained. XRD enables the identification of phases present in surface-modified layers and provides an evaluation of their structural characteristics.

Through XRD analysis, the crystal structures in the laser-treated area and their relative proportions can be determined. By comparing the diffraction patterns with established crystallographic databases, the specific phases formed during the laser treatment process are identified. Additionally, XRD offers valuable information on structural defects, residual stress, and the quality of crystal growth in the laser-hardened area.

This data is essential for understanding the relationship between surface structure and physical properties, providing a foundation for optimizing the laser surface hardening process to achieve enhanced material performance [49].

Atomic Force Microscopy Analysis

Atomic Force Microscopy (AFM) is a powerful tool for analysing surface topography at the nanoscale. It operates by using a sharp probe that scans the surface and measures the forces between the probe tip and the sample, generating high-resolution topographic images. This methodology is particularly effective in quantifying changes in surface characteristics, such as roughness, following laser processing.

Complementary modes of Atomic Force Microscopy, such as Kelvin Probe Force Microscopy (SKPM) and Magnetic Force Microscopy (MFM), can also be employed. These modes provide additional information about surface potential and magnetic properties, respectively. AFM is widely used in various fields of scientific research and industry. By measuring surface characteristics at the nanoscale, it offers essential insights into material surface properties, helps assess quality, and ultimately contributes to optimizing processes like laser hardening [50] – [52].

B. Analyses of mechanical and tribological characteristics

Surface profilometry

It plays a crucial role in various industries, including automotive, aerospace, and microelectronics, specifically roughness measurement. It is effectively applied in scenarios where precise control of surface properties is essential. Surface profilometry is a technique used to measure surface roughness and evaluate variations in the height of a sample. Most devices employ either a stylus or optical methods (often using a laser beam) to scan the surface and record the profile.

This technique provides quantitative data on parameters such as average roughness (*Ra*), maximum height (*Rz*), and area roughness (*Rq*). Surface profilometry is widely utilized for surface quality control and the optimization of various processes in surface engineering, including laser hardening [54] – [55].

Hardness testing

Several common hardness tests are used in practice, all of which measure the resistance of a material to indentation or penetration. These include the Rockwell hardness test, the Vickers hardness test, and the Brinell hardness test, each employing specific techniques to measure indentation and determine the material's hardness.

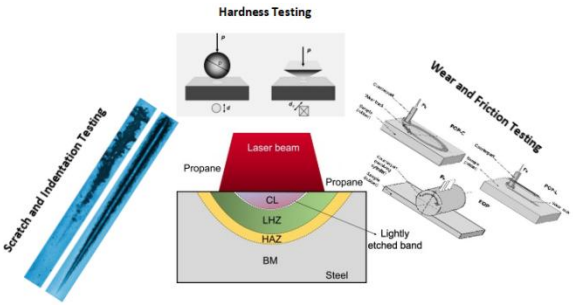

Fig. 10. Types of methods for mechanical and tribological analysis of laser hardened area

The information obtained from these measurements is particularly important in laser surface hardening, as it aids in optimizing the process's technological parameters. This ensures the desired wear resistance and durability of components subjected to mechanical stress [56] – [58].

Scratch and indentation testing

Measurements obtained through scratch and indentation testing of laser-hardened surfaces help evaluate a material's ability to resist wear, withstand mechanical stress, and maintain its functional properties. These tests can determine critical properties such as hardness, modulus of elasticity, bond strength, and resistance to deformation. The data gathered provides valuable insight into the mechanical integrity and performance of the laser-hardening process [59].

Wear and friction testing

To evaluate the tribological performance of surface-engineered areas after laser surface hardening, it is essential to conduct wear and friction tests. Techniques such as pin-on-disk, ball-on-disk, and reciprocating sliding tests are commonly used to simulate contact and sliding conditions under real-world scenarios. These tests provide valuable information on parameters such as wear rate, friction coefficient, and surface resistance. Wear and friction testing allows researchers to assess the performance and durability of surface-engineered materials under various operating conditions. By quantifying wear rate, friction coefficient, and surface damage, these tests facilitate comparative analysis of different laser processing techniques and surface modifications. This, in turn, helps optimize the laser hardening process, achieving the desired engineering outcomes of enhanced wear resistance, reduced friction, and extended surface life [60] – [62].

V. CONCLUSIONS

1. Laser Surface Transformation Hardening (LSTH), particularly when implemented with High-Power Diode Lasers (HPDLs), has proven to be a transformative technique in modern materials engineering. The study

highlights the significant advantages HPDLs offer over traditional hardening technologies, including precise energy control, minimal thermal distortion, high processing speed, and energy efficiency. These attributes not only improve the surface hardness and wear resistance of treated components but also maintain the base material's toughness and ductility—an essential factor in sectors such as automotive, aerospace, and heavy engineering.

2. The experimental and analytical evaluations discussed in this review affirm that HPDLs are highly suitable for the treatment of 42CrMo4 steel and similar alloys. The results show that appropriate tuning of process parameters such as laser power density, beam profile, and traverse speed can result in a uniform martensitic layer with excellent mechanical properties and microstructural uniformity.

3. Additionally, the integration of advanced characterization techniques—including SEM/EDS, XRD, AFM, and various tribological tests—has enabled a deeper understanding of the process–structure–property relationships in laser-hardened surfaces. These methods not only confirm the microstructural transformations but also support optimization efforts for industrial-scale implementation.

4. Overall, this research reinforces the value of HPDLs as a practical and sustainable solution for surface engineering in high-performance applications. Future directions may include further automation, the use of AI for process monitoring, and expansion into dual-use technologies where structural durability and multifunctionality are paramount.

VI. ACKNOWLEDGMENTS

Optimization of the Laser Hardening Process Using Kilowatt Diode Lasers for the Treatment of 42CrMo4 Steel in the Automotive Industry. Project Nr. RTU-PA-2024/1-0023.

Part of this research was funded was funded by the European Regional Development Fund under the Operational Program "Scientific Research, Innovation and Digitization for Smart Transformation 2021-2027", Project CoC "Smart Mechatronics, Eco- and Energy Saving Systems and Technologies", BG16RFPR002-1.014-0005.

REFERENCES

[1] T.H. Maiman, Stimulated optical radiation in ruby, (1960).

[2] Laser Materials Processing, 1st ed.; Bass, M. (Ed.) Elsevier Science: Amsterdam, The Netherlands, 1983; Volume 3, ISBN 9780444601322.

[3] Guarino, S.; Barletta, M.; Afilal, A. High Power Diode Laser (HPDL) surface hardening of low carbon steel: Fatigue life improvement analysis. J. Manuf. Process. 2017, 28, 266–271.

[4] Nemova, G. Brief Review of Recent Developments in Fiber Lasers. Appl. Sci. 2024, 14, 2323.

[5] L. Li, The advances and characteristics of high-power diode laser materials processing, Opt. Lasers Eng. 34 (2000) 231–253.

[6] Bons, S.; Seifert, M.; Brenner, B.; Beyer, E. Laser beam hardening—an energy-efficient heat treatment? In Proceedings of the 28th International Congress on Laser Applications and Electro-Optics, Orlando, FL, USA, 2–5 November 2009; Laser Inst. of America: Orlando, FL, USA, 2009; pp. 219–224.

[7] Casalino, G.; Giorleo, L.; Capello, E.; Segui, V.J. Laser irradiation after machining to recover deformation induced by surface laser hardening. In Proceedings of the Third International Conference of the Society for Manufacturing Engineering: MESIC-09, Alcoy, Spain, 17–19 June 2009.

[8] Kennedy, E.; Byrne, G.; Collins, D.N. A review of the use of high-power diode lasers in surface hardening. J. Mater. Proc. Tech. 2004, 155–156, 1855–1860.

[9] Tan, C.Y.; Wen, C.; Ang, H.Q. Influence of laser parameters on microstructures and surface properties in laser surface modification of biomedical magnesium alloys. J. Magnes. Alloy 2024, 12, 72–97.

[10] Tan, S.; Weng, F.; Sui, S.; Chew, Y.; Bi, G. Progress and prospects in laser additive manufacturing of key materials for aircraft engines. Int. J. Mach. Tools Prod. 2021, 170, 103804.

[11] Homberg, D.; Weiss, W. PID control of laser surface hardening of steel. IEEE Trans. Control System Tech. 2006, 14, 896–904.

[12] Lasota, I.; Protsenko, V.; Matyushkin, A.; Kuznetsov, M.; Gook, S. Laser surface hardening of engine camshaft cams. Mater. Today Proc. 2020, 30, 478–482.

[13] Wang, X.; Lu, Q.; Zhang, P.; Yang, H.; Shi, H.; Sun, T.; Zhou, K.; Chen, K. Review of the simulation of selective laser melting of AlSi10Mg. Opt. Laser Technologies. 2024, 174, 110500.

[14] Li, L. The progress and characteristics of high-power diode laser materials processing. Laser Mater. Proc. 2000, 34, 231–253.

[15] Kennedy, E.; Byrne, G.; Collins, DN A review of the use of high-power diode lasers in surface hardening. J. Mater. Proc. Tech. 2004, 155–156, 1855–1860.

[16] Li, W.-B.; Easterling, K.E. Residual stresses in laser transformation hardened steel. Surf. Eng. 1986, 2, 43–48.

[17] Patwa, R.; Shin, Y.C. Predictive modeling of laser hardening of AISI5150H steels. Int. J. Mach. Tools Manuf. 2007,47, 307–320.

[18] Moradi, M.; Fallah, M.M.; Jamshidi Nasab, S. Experimental Study of Surface Hardening of AISI 420 Martensitic Stainless Steel

[19] Using High Power Diode Laser. Trans. Indian Inst. Met. 2018, 71, 2043–2050.

[20] Maharjan, N.; Zhou, W.; Zhou, Y.; Guan, Y.; Wu, N. Comparative study of laser surface hardening of 50CrMo4 steel using continuous-wave laser and pulsed lasers with ms, ns, ps and fs pulse duration. Surf. Coat. Technol. 2019, 366, 311–320.

[21] Maharjan, N.; Zhou,W.;Wu, N. Direct laser hardening of AISI 1020 steel under controlled gas atmosphere. Surf. Coat. Technol., 2020, 385, 125399.

[22] Frerichs, F.; Lu, Y.; Lübben, T.; Radel, T. Process signature for laser hardening. Metals 2021, 11, 465.

[23] Steen, W. M. (2003). Laser Material Processing, 3rd Edition. Springer-Verlag, London. 408p.

[24] Davis, J. R. (2002). Surface Hardening of Steels: Understanding the Basics, ASM International, Materials Park (OH). 364 p.

[25] Annealing Thermal Cycles, What is Thermal Annealing - Definition - Material Properties 3.03.2025

[26] Brooks, C. R. (1992). Principles of the Austenitization of Steels. Springer, London. 232p.

[27] Thelning, K-E. (1984). Steel and Its Heat Treatment, 2nd Edition.Butterworth-Heinemann, London. 704p.

[28] J.F. Ready, Ready, J. F. (1997). Industrial Application of Lasers, 2nd Edition. Academic Press, London. 599p.

[29] Ehlers, H.J. Herfurth, S. Heinemann, Hardening and welding with high power diode lasers, Proc. SPIE 3945 (2000) 63–70.

[30] P. Loosen, G. Treusch, C.R. Haas, U. Gardenier, M. Weck, V. Sinnhoff, St. Kasperowski, R. vor dem Esche, High-power diodelasers and their direct industrial applications, Proc. SPIE 2382 (1995) 79–88.

[31] Laser Institute of America, Handbook of Laser Materials Processing, Magnolia Publishing Inc., 2001.

[32] L. Li, The advances and characteristics of high-power diode laser materials processing, Opt. Lasers Eng. 34 (2000) 231–253.

[33] H. Hugel, New solid-state laser and their application potentials, Opt. Lasers Eng. 34 (2000) 213–229.

[34] M. Haag, T. Rudlaff, Assessment of different high power diode lasers for materials processing, Proc. SPIE 3097 (1997) 583–591.

[35] Pantsar H. (2005). Models for Diode Laser Transformation Hardening of Steels: [D]. Lappeenranta: Lappeenranta University of Technology.

[36] Grum, J. (2007). Comparison of different techniques of laser surface hardening.Journal of Achievements in Materials and Manufacturing Engineering, 24 (1), 17-25.

[37] Ion, J. C. (2002). Laser transformation hardening. Surf. Eng., 18 (1), 14-31.

[38] Dossett, J. L. and Boyer, H. E. (2006). Practical Heat Treating, 2nd Edition. ASM International, Metals Park (OH). 296p.

[39] Grum, J. Steel Heat Treatment: Equipment and Process Design (edited by Totten, G. E.), 2nd Edition. Ch. 6, 443-447. (2006). CRC Press, New York.

[40] Gong H, Klinger J, Damazyn K, Li X, Huang S. A novel procedure for statistical inference and verification of gene regulatory subnetwork. BMC Bioinformatics. 2015;16 Suppl 7(Suppl 7):S7. doi: 10.1186/1471-2105-16-S7-S7.

[41] Na, S. J. and Yang, Y. S. (1987). Prediction of laser surface hardening zone by using the finite difference method. Proc. of the Int. Conf. on 'Laser Advanced Materials Processing-Science and Applications (LAMP '87)', (May 21-23), Osaka, Japan, Paper 5A02.

[42] Fritz Klocke, Martin Schulz, Stefan Gräfe, Optimization of the Laser Hardening Process by Adapting the Intensity Distribution to Generate a Top-hat Temperature Distribution Using Freeform Optics, Coatings 2017, 7(6), 77; https://doi.org/10.3390/coatings7060077

[43] Baumann, M., Krause, V., Bergweiler, G., Flaischerowitz, M. and Banik, J. (2012), Local heat treatment of high strength steels with zoom-optics and 10kW-diode laser. Proc. of SPIE on 'High Power Laser Materials Processing: Lasers, Beam Delivery, Diagnostics, and Applications', (January 21-26), San Francisco, USA, Paper 82390J.

[44] Laskin, A. and Laskin, V. (2012). Applying of refractive beam shapers of circular symmetry to generate non-circular shapes of homogenized laser beams. Proc. Of SPIE on 'Laser Resonators and Beam Control XIII', (January 22-25), San Francisco, USA, Paper 79130J.

[45] Bradley, J. R. (1988). A simplified correlation between laser processing parameters and hardened depth in steels. Journal of Physics D: Applied Physics, 21 (5), 834-837.

[46] Pantsar H. (2005). Models for Diode Laser Transformation Hardening of Steels: [D]. Lappeenranta: Lappeenranta University of Technology.

[47] Panwar, A.S.; Singh, A.; Sehgal, S. Materials characterization techniques in engineering applications: a review. Mater. Today Proc. 2020, 28, 1932–1937.

[48] Fritz Klocke, Martin Schulz, Stefan Gräfe, Optimization of the Laser Hardening Process by Adapting the Intensity Distribution to Generate a Top-hat Temperature Distribution Using Freeform Optics, Coatings 2017, 7(6), 77, doi.org/10.3390/coatings7060077

[49] Obergfell, Katja, Schulze, Volker, Löhe, Detlef and Vöhringer, Otmar. "Application of X-Ray Diffraction Analysis on Microstructural Investigations of Laser-Hardened Steel Surfaces" International Journal of Materials Research, vol. 92, no. 3, 2001, pp. 265-269. https://doi.org/10.3139/ijmr-2001-0053

[50] Leonardo Orazi, A. Rota, Barbara ReggianiExperimental investigation on a novel approach for laser surface hardening modelling, International Journal of Mechanical and Materials Engineering, 2021, 16(1):2, DOI: 10.1186/s40712-020-00124-0

[51] Moisés Meza Pariona, Viviane Teleginski, Kelly dos Santos, et al.,AFM study of the effects of laser surface remelting on the morphology of Al–Fe aerospace alloys, Materials Characterization, Volume 74, 2012, Pages 64-76, ISSN 1044-5803, https://doi.org/10.1016/j.matchar.2012.08.01

[52] Omar Fadhil Abdullah,Orass Abdulhadi Hussein, Emad Toma Karash, The Laser Surface Treatment Effective on Structural Properties for Invar Alloy (Fe-Ni) Type Prepared by Powder Technology, Key Engineering Materials 844:97-103, 2020

[53] Tonietto, L., Gonzaga, L., Veronez, M.R. et al. New Method for Evaluating Surface Roughness Parameters Acquired by Laser Scanning. Sci Rep 9, 15038 (2019). https://doi.org/10.1038/s41598-019-51545-7

[54] EL Ghadoui, M., Mouchtachi, A. & Majdoul, R. Intelligent surface roughness measurement using deep learning and computer vision: a promising approach for manufacturing quality control. Int J Adv Manuf Technol 129, 3261–3268 (2023). https://doi.org/10.1007/s00170-023-12457-z

[55] Koç, E., Zeybek, S., Kısasöz, B.Ö. et al. Estimation of surface roughness in selective laser sintering using computational models. Int J Adv Manuf Technol 123, 3033–3045 (2022). https://doi.org/10.1007/s00170-022-10406-w

[56] Noureddine Barka, Sasan Sattarpanah Karganroudi, Rachid Fakir, Patrick Thibeault, Vincent Blériot Feujofack Kemda, Effects of Laser Hardening Process Parameters on Hardness Profile of 4340 Steel Spline—An Experimental Approach, Coatings 2020, 10(4),342; https://doi.org/10.3390/coatings10040342

[57] Barka N, Sattarpanah Karganroudi S, Fakir R, Thibeault P, Feujofack Kemda VB. Effects of Laser Hardening Process Parameters on Hardness Profile of 4340 Steel Spline—An Experimental Approach. Coatings. 2020; 10(4):342. https://doi.org/10.3390/coatings10040342

[58] Erdem, M.; Altuğ, M.; Karabulut, M. Investigation of mechanical, microstructural, and machining properties of AISI 420 martensitic stainless steel welded by laser welding. Int. J. Adv. Manuf. Technol. 2016, 85, 481–492.

[59] Broitman, E., Indentation Hardness Measurements at Macro-, Micro-, and Nanoscale: A Critical Overview. *Tribol Lett* 65, 23 (2017). https://doi.org/10.1007/s11249-016-0805-5

[60] Maziar Ramezani, Zaidi Mohd Ripin, Tim Pasang, Cho-Pei Jiang, Cho-Pei Jiang, Surface Engineering of Metals: Techniques, Characterizations and Applications, Metals 2023, 13(7), 1299; https://doi.org/10.3390/met13071299

[61] Su, Y.L.; Kao, W.H.; Chang, G.Y. Tribological, Anti-corrosion, and Electrical Conductivity Properties of CrCx Coatings Deposited on Stainless Steel 316L and Used as Metal Bipolar Plates for Fuel Cells. J. Mater. Eng. Perform. 2023, 32, 3739–3754.

[62] Panwar, A.S.; Singh, A.; Sehgal, S. Material characterization techniques in engineering applications: A review. Mater. Today Proc. 2020, 28, 1932–1937.